

TH 77-20446

N77-18161

NASA CR-145105

**REPRODUCIBLE COPY
(FACILITY CASEFILE COPY)**

**THE INFLUENCE OF FORWARD FLIGHT ON
PROPELLER NOISE**

By

B. Magliozzi

Prepared under Contract No. NAS1-13015

By

Hamilton Standard
Div. of United Technologies Inc.
Windsor Locks, Conn.

for

NASA

National Aeronautics and
Space Administration



NASA CR-145105

**THE INFLUENCE OF FORWARD FLIGHT ON
PROPELLER NOISE**

By

B. Magliozzi

Prepared under Contract No. NAS1-13015

By

Hamilton Standard
Div. of United Technologies Inc.
Windsor Locks, Conn.

for



National Aeronautics and
Space Administration

1. Report No. NASA CR-145105		2. Government Accession No.		3. Recipient's Catalog No.	
4. Title and Subtitle The Influence of Forward Flight on Propeller Noise				5. Report Date February 1977	
				6. Performing Organization Code	
				8. Performing Organization Report No.	
7. Author(s) B. Magliozzi					
9. Performing Organization Name and Address Hamilton Standard, Division of United Technologies Windsor Locks, Connecticut 06096				10. Work Unit No. (TRAIS)	
				11. Contract or Grant No. NAS1-13015	
12. Sponsoring Agency Name and Address National Aeronautics and Space Administration Washington, D.C. 20546				13. Type of Report and Period Covered Contractor Report	
				14. Sponsoring Agency Code	
15. Supplementary Notes					
16. Abstract <p>The results of an experimental program are reported which show the effect of flight on blade surface pressures and propeller noise. It was found that there were significant differences in blade surface pressures and far-field noise between static and flight conditions. The static data showed many high-intensity, tone-like peaks whereas the flight data was generally free from tones. The turbulence ingested by the propeller operating statically was dominated by long, thin eddies. In flight the scale of the turbulence was greatly reduced from that observed statically.</p> <p>From diagnosis of the propeller noise sources, it was concluded that statically the low-frequency tones were primarily steady loading noise with some contribution from thickness noise while the mid-frequency tones and broadband noise were unsteady loading noise. In flight, the tone noise was found to be due to thickness and steady loading. The source of in-flight broadband noise could not be identified, but is probably a combination of propeller self-noise, engine noise, air frame noise, and atmospheric turbulence interaction noise.</p>					
17. Key Words Propeller Noise Inflow Turbulence Interaction Unsteady Blade Loading Blade Surface Pressure Measurement				18. Distribution Statement	
19. Security Classif. (of this report) Unclassified		20. Security Classif. (of this page) Unclassified		21. No. of Pages 22. Price	

TABLE OF CONTENTS

SUMMARY	1
INTRODUCTION	3
APPARATUS AND METHODS	7
<u>Test Aircraft</u>	7
<u>Test Site</u>	7
<u>Instrumentation</u>	7
Blade Surface Pressures	7
Acoustic Measurement Systems	9
Hot Wire Anemometer	10
Other Aircraft Instrumentation	10
Aircraft Data Recording System	10
Calibration	11
<u>Atmospheric Conditions</u>	12
<u>Test Procedure</u>	12
Flyover Tests	12
Taxi Tests	12
Static Tests	13
DATA REDUCTION	15
<u>Pressure Data</u>	15
Time History Plots	15
Narrow-Band Frequency Analyses	15
Statistical Properties	16
Alternate Procedures for Statistical Properties	17
<u>Acoustic Data</u>	18
1/3 Octave Band Analyses	18
Narrow-Band Frequency Analyses	18
<u>Hot-Wire Anemometer Data</u>	19
<u>Aircraft Operating Conditions</u>	19

DISCUSSION OF RESULTS	20
<u>Transient Conditions (Take-Offs)</u>	20
Blade Surface Pressure Data	20
Wing-Tip Microphone Data	21
<u>Static Propeller Operating Conditions</u>	22
Blade Surface Pressure Data	22
Acoustic Data	26
<u>Flight Conditions</u>	27
Blade Surface Pressure Data	27
Acoustic Data	29
Hot-Wire Anemometer Data	29
<u>Comparison of Flight and Static Data</u>	30
Blade Surface Pressures	30
Acoustic Data	31
<u>Comparison of Measurements With Theory</u>	32
Background	32
Propeller Noise Diagnosis	33
Calculation of Unsteady Blade Loading Noise	34
CONCLUSIONS	37
APPENDIX A - BLADE SURFACE PRESSURE TIME HISTORY PLOTS	141
APPENDIX B - BLADE SURFACE PRESSURE NARROW-BAND SPECTRUM PLOTS	175
APPENDIX C - BLADE SURFACE PRESSURE STATISTICAL PROPERTIES	377
APPENDIX D - FAR-FIELD NOISE 1/3 OCTAVE BAND DATA TABULATIONS	415
APPENDIX E - WING-TIP MICROPHONE DATA NARROW-BAND SPECTRUM PLOTS	443
APPENDIX F - HOT-WIRE ANEMOMETER STATISTICAL PROPERTIES	493
REFERENCES	513

SUMMARY

In this program, one blade of one propeller of a light STOL transport aircraft was modified to accept flush-mounted pressure transducers for the measurement of the dynamic blade surface pressures. Also, a boom was installed on the wing tip on the instrumented propeller side and used to support two microphones. Finally, a hot-wire anemometer was used to measure atmospheric turbulence.

The test aircraft was operated statically and under various flight conditions for a range of propeller tip speeds and powers. Blade surface pressures, wing tip microphone data, far-field flyover noise data, hot-wire anemometer data, and aircraft operating parameters were simultaneously recorded on magnetic tape for subsequent analysis.

The data analysis revealed that there were significant differences in blade surface pressures and far-field noise between static and flight conditions. The static data shows many high-intensity, tone-like peaks which extend well into the mid-frequency range. These tones are generally not present in the flight data. The turbulence ingested by the propeller operating statically was deduced from the blade surface pressures to be dominated by long, thin eddies having aspect ratios of between 25:1 and 50:1. In flight, strong levels of once-per-revolution distortion, caused by non-normal inflow due to aircraft attitude, wing upwash, etc., precluded analysis of the blade surface pressure data using available processing procedures. However, it is clear that the scale of the turbulence was greatly reduced from that observed statically.

From diagnosis of the propeller noise sources, it was concluded that statically the low frequency tones were primarily steady loading noise with some contribution from thickness noise while the mid-frequency tones and broadband noise were unsteady loading noise. In flight, the tone noise was found to be thickness and steady loading noise. The broadband noise sources in flight have not yet been identified, but may consist of propeller self noise, engine noise, airframe noise, atmospheric turbulence interaction, or wind noise from the microphones.

INTRODUCTION

Recently, it has been recognized that significant differences exist in the noise signatures of propellers operating statically and in flight. Classical propeller noise theory would show a small change in noise between static and forward flight conditions due to the changes in blade loading, but limited observations have revealed that a much greater change occurs. Very little mention is made in the literature on noted differences in the character of the noise of propellers under static and flight conditions. In fact, virtually all of the experimental research programs on far-field noise have been conducted on static test facilities until a few years ago.

Recent work in the development of theoretically based methods for predicting propeller noise has revealed that ingestion of normally occurring atmospheric turbulence can significantly influence the noise of a propeller operating statically. The inflow turbulence gives rise to so-called unsteady loading noise which results in the generation of narrow-band-random noise. This appears as tone-like components which extend well into the mid frequencies and greatly increase the perceived noise.

The analyses, however, have not been rigorously applied to the forward flight case, although semi-empirical adjustments to the unsteady loading noise components to account for forward flight show a significant reduction in this component relative to static operation. It is thus apparent that estimates of aircraft flyover noise derived from static test stand noise measurements may lead to erroneous conclusions. Also, propeller noise trend studies for minimizing propeller noise conducted statically may not result in the quietest propellers in flight. Since transport aircraft noise certification is based on the noise measured while the aircraft is in flight, it is clear that experimental noise research programs must be carefully designed to provide noise data which is valid under forward flight conditions.

A comprehensive research program, which includes full scale outdoor forward flight test, model scale outdoor test, full scale acoustic wind tunnel test, and model scale acoustic wind tunnel test is necessary for the development of propeller noise test techniques which are valid under forward flight. The long range goals of such a program are the development of optimum test techniques for propeller noise research which consider cost of testing as well as validity of the test results. Such a program requires a coordinated exploration of the influence of scale and test environment. After the mechanisms of noise generation are understood, simplified test techniques might be developed so that inexpensive model scale tests in a controlled environment could be conducted to develop quiet propulsors.

This report describes the results from a test program which has the same objectives as the first phase of the comprehensive program described above, i.e., the investigation of noise of a full-scale propeller under forward flight.

The program was funded by NASA-Langley. Hamilton Standard was responsible for implementing the special instrumentation, reducing the test data, and performing the analyses. NASA-Langley provided the modified test aircraft and was responsible for conducting the test program.

LIST OF SYMBOLS

A	A-weighted sound pressure level
c	local circumference or blade chord
C_B	blade chord
C_e	effective blade chord
d	diameter
e	2.7182818...
k	exponent for blade loading law
K	lag value for correlation function calculation
LIN	overall sound pressure level
L_n	amplitude of the n'th loading harmonic
L_o	average blade load
M	Number of propeller revolutions used in statistical analyses
n	loading harmonic order
N	circumferential sample point number or number of sample points per revolution
P	digitizing channel identifier for channel 1
Q	digitizing channel identifier for channel 2
r	local radius
R	tip radius or digitizing channel identifier for channel 3
r_T	blade tip radius
S	digitizing channel identifier for channel 4
t	blade thickness
Δ_C	increment in local circumference

LIST OF SYMBOLS (Cont)

Δ_r	local radius at which the radial cross-correlation coefficient reaches the value $1/e$
$\Delta \tau$	lag time for which the autocorrelation coefficient reaches the value $1/e$
θ	blade angle
μ	ratio of radial to circumferential turbulence length scales
π	3.1415926...
τ	coorelation function lag value

APPARATUS AND METHODS

Test Aircraft

The test airplane, shown in the photograph of figure 1, was a twin-engine, high-wing, light STOL transport with fixed, tricycle gear. Figure 2 is a dimensioned-three view of the aircraft. Gross weight of the airplane during the tests varied from a takeoff weight of approximately 44,500 N (10,000 lb.) to a landing weight of about 40,000 N (9,000 lb.). The aircraft was powered by two free turbine engines driving three-bladed controllable pitch propellers.

The instrumented propeller was installed on the left engine as shown in figure 3. Blade profile curves for the propeller are given in figure 4.

Test Site

Tests were conducted at the NASA Wallops Flight Center, Wallops Island, Virginia. Figure 5 indicates the location of the test area in relation to the overall runway layout. Typical terrain features of the Wallops Flight Center are shown in the photograph of figure 6, which is a view looking north from the end of runway 4-22. Indicated on the photograph are the flight track and the microphone positions for the tests. The static runup tests were made with the aircraft flying from south to north along the centerline of runway 4-22.

Instrumentation

Blade Surface Pressures

Pressure transducers. - The pressure transducers used in this test program were manufactured by Kulite Semiconductor Products, Inc. These transducers consist of a miniature silicon diaphragm on which a fully active four-arm Wheatstone bridge has been atomically bonded using solid state diffusion. The type used is designated LQ-59-125-4 and measures approximately 4.76 mm (3/16 in) by 3.18 mm (1/8 in) and is about 0.64 mm (0.025 in) thick. The active element is 2.16 mm (0.085 in) in diameter. The nominal sensitivity is 1.74 $\mu\text{V}/\text{Pa}$ (12 mv/psi) with an excitation of 15 volts.

These transducers were recently recognized as being sensitive to changes in ambient illumination. In this program this light sensitivity could be a serious problem since the test program had to be conducted during daylight hours with probable full sun-light illumination. Since a shadow falling on the rotating propeller would cause a change in incident illumination on the transducers, the light response of the transducers could generate spurious signals which would be indistinguishable from the pressure response signals.

As a consequence, special transducers, in which an aluminum film was deposited on the diaphragms under cleanroom conditions before final assembly, were ordered from the manufacturer. Then, for added erosion protection, a coating of black RTV rubber was also used. The response to equivalent sunlight illumination of these transducers was found to be approximately 40 dB below the anticipated pressure signal, thereby ensuring adequate dynamic range.

Transducer installation. - Seven pressure transducers were flush mounted on one of the three blades as shown in figure 7. The transducers were installed on the pressure side of the blade as close to the leading edge as possible. Also, one transducer was located toward the trailing edge at the tip to investigate tip effects. Recesses were machined in the blade to allow flush-mounting of the transducers and lead wires. A stress analysis of the propeller blade modified for the transducer installation was performed to insure that the machining operation would not weaken the blade. Subsequent to the installation of the transducers, the lead wire channels were filled with epoxy to restore the original blade section contour. The spaces between the blade and the transducers were filled with RTV rubber which restored the blade contour while providing isolation from blade strain.

Rotating amplifier. - An amplifier was used with each of the pressure transducers to boost the pressure signal levels for improved signal-to-noise ratio. This was accomplished using an eight-channel rotating amplifier which was installed on the propeller hub, as shown in figure 3. Each amplifier channel has a nominal gain of 54 dB over the frequency range 15 to 10,000 Hz. The anticipated amplified pressure signal level was ± 3.5 volts, well above the anticipated electrical noise levels.

Only seven channels of the rotating amplifier were used. Of these, one channel was used as a dummy for which a pressure transducer was synthesized with four passive resistors. This was done to simulate an inactive pressure transducer which would give an equivalent signal without any pressure response. The purpose of this was to allow continuous recording of system noise, including that from the amplifier, rotating interface, power supply, signal lines, and recording system. Thus, at any one time, six active pressure transducers and one dummy transducer were wired to the rotating amplifier for recording. The seventh pressure transducer was retained as a spare. Also, the recording system limitations allowed only six transducers to be recorded (see later discussion).

Slip ring assembly. - An aircraft instrumentation type slip ring assembly was used to transfer transducer excitation, amplifier power, and amplified pressure signals between the nacelle and the rotating propeller. The slip ring was installed instead of the de-icer ring and spinner bulkhead normally installed on the propeller and may be seen in figure 3. A baffle was used to increase the diameter of the slip ring to prevent ram

air from entering the nacelle cowl, since the spinner could not be used. A brush-block assembly was installed on the nose of the engine. Two carbon-silver brushes contacted each of the 11 coin silver rings for power and signal transfer.

An investigative test was conducted to estimate the slip ring noise prior to installation on the aircraft. For this test, the slip ring, brush block, and rotating amplifier were installed on a rig and operated at 2200 RPM for about ten minutes to allow the system to warm up. A dummy transducer was installed on one channel of the rotating amplifier and transmitted through the outermost signal ring (i.e., the one with the highest surface speed) to evaluate the system residual noise. A narrow band frequency analysis was made of the signal to establish the level and frequency distribution of the noise. The analysis showed an essentially flat spectrum at a level of about 70 dB below one volt using a 30 Hz bandwidth filter. Since the estimated pressure signal range was 20 to 60 dB below one volt, a minimum margin of 10 dB was apparent. It was thus concluded that slip ring noise would not be a problem.

The brush block/slip ring assembly included a magnetic pick-up which was designed to give a sharp pulse once per propeller revolution. This 1P pipper signal was used for propeller speed correction and phase reference during the data reduction and analysis. The relative location of the pipper and pressure transducers was such that the pipper pulse occurred when the transducers were at approximately eight o'clock when viewed from the front.

Acoustic Measurement Systems

Ground system. - Four mobile data-acquisition vans (inset of figure 6), each containing three microphones, signal conditioning equipment, and a tape recorder, were used for ground noise measurements. A schematic diagram of the noise data acquisition system is shown in figure 8. During the entire test program, the microphones were fitted with wind screens and were oriented for grazing incidence; microphone heights were generally set at 1.2m except as shown in figure 9. The microphones are commercially available, piezoelectric ceramic type having a frequency response flat to within 3 dB over the frequency range of 20 to 12,000 Hz. The signal outputs from all microphones at each of the four mobile data-acquisition stations were recorded on multi-channel, frequency modulated magnetic tape recorders at 76.2 cm/sec (30 ips) with a center frequency of 54 kHz. The frequency response of the complete recording system was flat to within 3 dB from 20 to 12,000 Hz.

Aircraft system. - The test aircraft was instrumented to measure and record propeller noise using two microphones mounted on the left wing tip as shown in figure 1. One microphone was in the plane of propeller rotation; the second microphone was below the wing and behind the plane of propeller rotation. The microphones were oriented with their axes along the flight path and fitted with nosecone windscreens. Pre-amplifiers with step-attenuators were used so that the microphone signals could be recorded at close to full scale amplitudes.

Hot Wire Anemometer

Atmospheric turbulence in the longitudinal direction was sensed by a hot wire anemometer mounted on the aircraft noseboom shown in figure 1. An adjustable bias supply was used to cancel the average velocity component leaving only the velocity fluctuations. This was done so that the fluctuating portion of the signal (which is the portion of interest) could be recorded at high gain without overloading the direct coupled amplifiers.

Other Aircraft Instrumentation

The following operating parameters were recorded onboard the test aircraft: airspeed, altitude, angles-of-attack and sideslip, roll, pitch, and yaw attitude angles, normal, lateral, and longitudinal accelerations, engine torque, and propeller speed. The noseboom contained a pitot-static system. Angles-of-attack and sideslip were measured by noseboom-mounted flow direction vanes. All operating parameters were digitized and recorded directly on magnetic tape at 76.2 cm/sec (30 ips) with a maximum frequency response of 10 Hz.

A VHF/FM downlink transmitted the once-per-revolution pipper to the ground recording station to be recorded by the ground based acoustic tape recorders along with signals from the ground based microphones. All data were time correlated by recording common time signals on each data tape.

Aircraft Data Recording System

Blade surface pressures, propeller noise, anemometer, and aircraft operating parameters were recorded simultaneously on a 14 channel instrumentation magnetic tape recorder operating at 76.2 cm/sec (30 ips). The pressure, acoustic, anemometer and 1P pipper signals were FM recorded using wideband, 54 kHz center frequency voltage controlled oscillators (VCO's) with 40 percent frequency shift for full scale voltage inputs. This system enabled data playback on an intermediate band system with 0 to 10 kHz frequency response and good dynamic range.

The record and playback tape transports use two head stacks of seven channels each. The odd numbered tracks are assigned to one head stack, while the even numbered channels are assigned to the second head stack. Since the two head stacks are physically separated, tape flutter, uneven tape motion, tape stretch, etc. could cause significant time lag errors between even and odd channels. The data analysis included cross-correlations between transducer pairs to obtain radial length scales. Therefore, the 1P pipper and the six active pressure transducers were recorded on one head stack to minimize inter-channel phase distortion. The resulting channel allocation was as follows:

Tape Channel		Type of Recording	Frequency Range
1	1P Pipper	FM	15-10K Hz
2	Voice	Direct	-
3	Blade pressure	FM	15-10K Hz
4	Wing-tip Microphone	FM	20-10K Hz
5	Blade pressure	FM	15-10K Hz
6	Wing-tip Microphone	FM	20-10K Hz
7	Blade pressure	FM	15-10K Hz
8	Aircraft parameters*	Direct	0-10 Hz
9	Blade pressure	FM	15-10K Hz
10	Dummy transducer	FM	15-10K Hz
11	Blade pressure	FM	15-10K Hz
12	Time code**	Direct	-
13	Blade pressure	FM	15-10K Hz
14	Hot wire anemometer	FM	0-5K Hz

* Pulse code modulation (PCM)

** NASA 36-bit code

Calibration

The airborne data system was calibrated for each test. Each operating parameter was given a three point calibration by substituting known voltages for transducer outputs to provide a calibration of all signal conditioning and the digitizing channel.

The 54 KHz VCO's were calibrated simultaneously at full scale with a 6.25 KHz sine wave signal.

Airborne microphones were calibrated at 1,000 Hz and 124 dB with a pistonphone calibrator. Pink noise was used to verify system frequency response.

Each blade pressure transducer was calibrated with a 1,000 Hz sine wave signal at a sound pressure level of 150 dB generated by a pistonphone calibrator. The calibrator was fitted with a rubber adapter to maintain a seal between the calibrator and the blade surface. In order to establish that transducer signals exceeded the system background noise, pressure transducer excitation was removed and records were made of system noise at each test propeller speed.

The anemometer system was calibrated in two parts. A portable wind tunnel was used to determine a sensitivity factor for each probe at the linearizer output. During each preflight, a known input was applied with the system set at a known gain.

Atmospheric Conditions

The U.S. Weather Bureau (NOAA) support facility at Wallops Flight Center recorded temperature, barometric pressure, relative humidity, wind direction, and wind velocity. The various parameters are listed in table I. Surface observations of temperature, humidity, wind velocity, and wind direction were made at a location approximately 305 meters (1000 ft) from the center of the test area as indicated in figure 5.

Atmospheric soundings were obtained from ground level up to about 610 meters (2,000 ft) mean sea level by means of a constant-rate-of-ascent balloon ascending at approximately 5.8 m/sec (19 ft/sec) and a double-optical theodolite tracking system. In order to insure valid results, noise measurements were made only when the weather was generally clear with low surface winds as recommended in reference 1.

Test Procedure

Tests were performed for various combinations of airspeed, altitude, propeller speed, and engine power as listed in table II. Flyover tests were executed first; high speed taxi tests and static runup tests were performed with propeller speeds and engine power settings that duplicated flight conditions.

Flyover Tests

With the right engine shutdown, the aircraft was flown at constant altitude and airspeed over a ground measuring station, as shown in figure 5, where aircraft noise was recorded. Aircraft position relative to the microphones was computed from radar tracking data. Aircraft altitude over the microphones was checked using a photographic technique. Aircraft operating parameters, fluctuating blade pressures, inflow conditions, and far-field noise were measured and recorded onboard the aircraft. Flight crew comments were also recorded on the airborne data tape. Barometric pressure, relative humidity, temperature, and wind speed and directions were recorded at the surface. Air temperature, humidity, and wind speed and direction were measured from the surface to 610m (2,000 ft) above ground level using radiosonde. All data were time correlated. Measurements were made at airspeeds from 80 to 150 knots, with propeller speeds from 1760 to 2145 RPM, at altitudes of 61m (200 ft) and 305m (1,000 ft).

Taxi Tests

For taxi tests, the acoustic ground station was moved to a point 61m (200 ft) west of the centerline of runway 04 and south of the intersection with runway 17-35 as shown in figure 5. The aircraft was flown at 80 knots down the runway centerline and just

above the surface. Noise, aircraft operating parameters, fluctuating blade pressures, inflow conditions, aircraft position, and airfield weather were recorded and time correlated. Propeller speeds tested during the flyovers were duplicated for the taxi runs at power required for flight at 80 knots.

Static Tests

Static runup measurements were made with ground microphones arranged in circular arcs of 15.3m (50 ft) and 61m (200 ft) radii from the test propeller as shown in figure 5. Noise, propeller speed, engine power, fluctuating blade pressures, inflow conditions, and surface weather conditions were recorded with time correlation. All flyover propeller speeds and power settings were duplicated.

DATA REDUCTION

Pressure Data

Time History Plots

A special technique has been developed to qualitatively evaluate the response of the pressure transducer signals (ref. 2). This technique allows visualization of pressure disturbances which move through the plane of rotation.

Figure 10 shows a short sample of such a time-history plot. In order to generate this plot, analog tape data were digitized using a special clock with a frequency multiplier which generated exactly 150 equally spaced pulses per propeller revolution. The digital sampling rate was thus phase-locked to the 1P pinner on the propeller so that the samples were taken at the same location during each revolution. In figure 10 the vertical axis is the number of the pressure sample starting from a reference position which, in this program, was the point at the top of rotation as indicated in the sketch. Thus, 150 samples represent 360 degrees of rotation. Succeeding revolutions were plotted with a slight horizontal displacement to allow evaluation of the blade pressures as a function of time. The amplitude variation of the blade surface pressure over a complete revolution can thus be seen. Successive revolutions show disturbances which persist for long periods of time or may show random components. Also, the size of disturbances may be estimated from these plots. The width of the pulse indicates the size in the circumferential direction while the number of revolutions indicate the axial length. Size in the radial direction may be estimated from examination of traces from adjacent transducers. Finally, it is readily apparent from these traces whether the disturbance is moving radially or circumferentially.

In the data reduction effort conducted for this program, time history plots were made for representative test conditions including aircraft take-offs, static operation, taxi conditions, low altitude flyover, and high altitude flyover. The runs for which their time history plots were made are summarized in table III.

Narrow-Band Frequency Analyses

Narrow-band frequency analysis plots were made of the pressure data summarized in table III. For this analysis, Spectral Dynamics SD301D Real-Time Narrow-Band Spectrum Analyzer and SD308 Signature Ratio Adapter were used. A Signature Ratio Adapter was used to allow the analyzer to track the signal to correct for any RPM variation by phase locking on the 1P pinner. Two analysis ranges were used. A low fre-

quency, narrow-band range was used to identify the "tones" in the data while a higher frequency range was used to allow identification of high frequency components. For the low frequency analysis, 50 orders of the propeller shaft speed were analyzed. This resulted in effective analyzer bandwidth of 4.4 Hz for the 80% RPM data extending to 5.4 Hz bandwidth for the 97.5% RPM data, with frequency analysis ranges of 0 to 1467 Hz and 0 to 1788 Hz, respectively. For the higher frequency range, 200 orders were analyzed with effective bandwidths of 17.6 Hz and 21.5 Hz and frequency ranges 0 to 5866 Hz and 0 to 7150 Hz for 80% RPM, respectively.

Statistical Properties

Quantitative evaluation of the blade surface pressure properties were made to assess the nature of the inflow turbulence. The digitized blade pressure data were processed using a special computer program to calculate rms pressure levels, transverse correlation lengths, radial correlation lengths, streamwise correlation lengths, signal-enhanced waveforms, and power-spectral-densities (PSD's) of the pressure signals and the signal-enhanced signals. A detailed description of the computations performed by the computer program is given in reference 2. The following discussion summarizes the calculations which were made in processing the blade pressure data for this program. The results are discussed in a later section.

RMS pressure levels. - The rms levels of the blade surface pressures were computed at each of the 150 points defining a complete propeller revolution and for each data channel by summing the squared value of the pressure signal for up to 1,000 propeller revolutions. The sum of the squares were then divided by the number of samples and the square root taken of the quotient. This gave the rms pressure distribution over the path of one propeller revolution.

One summation was also made of the pressure squared for as many samples as specified. The square root of the sum divided by the total number of samples is then an indication of the average signal rms level. This value was also used in the time history plots to determine the plotter amplitude scale.

Streamwise correlation. - Streamwise correlation functions were obtained by using the pressure samples measured once per revolution at a given radial and circumferential location. Normalized autocorrelation functions were thus obtained with time lags equal to the time for one propeller revolution. The data analysis program allows the user to define the circumferential position at which the correlation function is calculated. For this analysis, position 1, 38, 75, and 113 were selected. (These locations are identified in figure 10).

Transverse correlation. - Correlations across the waveform plots were also made. In this calculation, the time lags were equal to the inverse of the sampling rate, i.e., the time for one propeller revolution divided by 150. This calculation gave the correlation

function in the circumferential direction. Again, the point along the circumference for which the time lag is zero can be specified and the same four locations as for stream-wise correlation were selected.

Radial correlation. - To complete the calculation of correlation length scales, the correlation functions between pairs of pressure transducer signals were computed. This computation procedure calculated the zero lag correlation coefficient averaged over the 150 samples per revolution and the number of revolutions. A second calculation was also done in which the average correlation coefficient was computed from the data with the effects of steady inflow distortion removed.

Signal spectra and coherence. - The last data manipulation calculated the PSD of the raw input data and of the signal enhanced data. The first PSD included all components, i.e., periodic, quasi-periodic (narrow-band random), and random signals, whereas the second PSD showed only those components which are periodic.

Alternate Procedures for Statistical Properties

As will be discussed in a later section, certain characteristics noted in the blade surface pressure data, notably the intrusion of a very large 1P component in all the flight data due to non-normal inflow, prevented the calculation of many of the statistical properties, as they were dominated by the 1P component which tended to mask the desired random data. Although signal enhancing the data would normally greatly reduce the effects of a steady distortion, in actuality, the 1P component was not steady, ostensibly because of small changes in the aircraft attitude during the data sample, and was thus not entirely removed from the data. The result of the digitized data processing of the flight data was therefore strongly distorted by the 1P component. As an alternate, a Saicor model SA143A correlation and probability analyzer was used to obtain the transverse and radial correlation lengths for one representative static condition and its corresponding flight condition.

For the static condition, the analyzer was allowed to free run at a rate such that the complete sample of 400 points would take slightly longer than the time for one complete propeller revolution. In this manner, the average correlation coefficient over the complete circumference was obtained. For the flight data, high quality highpass filters were used to precondition the data. The pass-point was set to three times the 1P frequency so that the 1P and twice 1P components were completely eliminated.

Transverse correlation lengths were obtained from autocorrelograms for each pressure signal while radial correlation lengths were obtained from cross correlations of pairs of data channels at zero time lag. Good averaging was obtained by using approximately one minute of data.

Although this approach appears successful for the flight data where there does not appear to be any low frequency data of interest, it is in general, less flexible than the numerical procedures developed for the computer program. Unfortunately, the funding of this program was limited so that other conditions could not be reanalyzed in this manner. The results from the two conditions which were analyzed with the SAI43A will be discussed in a later section.

Acoustic Data

1/3 Octave Band Analyses

Ground-based microphone data. - 1/3 octave band analysis were made of selected data channels of the far field noise data recordings. In the case of the aircraft flyovers, the data from the array of three microphones under the flight path were analyzed (see figure 9). For the static runs, the 61m (200 ft) microphone data were analyzed.

In the case of the flyover, only the peak noise was analyzed. This was accomplished by capturing a 1/2 second of noise signal at the peak for the low altitude, high-flight-speed conditions and 1 second samples for the low altitude, low-flight-speed and high altitude conditions. The data was analyzed using a General Radio model 1921 Real-Time Analyzer set to 1/2 or 1 second integrating time for 1/3 octave band center frequencies from 50 to 10,000 Hz and linear and A-weighted overall levels.

Similar analysis was used for the taxi data.

Wing-tip microphone data. - All the data from the two wing tip microphones were analyzed by 1/3 octave bands using a General Radio Model 1921 real-time analyzer with 16 seconds integration time. The frequency analysis range was 22.5 to 11,200 Hz. Overall and A-weighted levels were also determined.

Data processing. - The 1/3 octave band levels were punched on paper tape then transferred to IBM punched cards. These were processed on a digital computer which tabulated the 1/3 octave band levels as presented in the data summary at the end of this report.

Narrow-Band Frequency Analyses

Selected conditions, i.e. those listed in table III, were also analyzed using narrow-band filters. The data from the two-wing tip microphones for the conditions listed in table III were analyzed using a Spectral Dynamic SD301D analyzer. A Spectral Dynamics SD308 Signature Ratio Adapter was used to provide a control signal locked to the propeller speed through the 1P pickup signal. For this analysis, 100 orders of the propeller

ler shaft speed were analyzed. This corresponds to 33 harmonics of propeller blade passing frequency. These were speed-corrected using the 1P pipper signal to avoid "smearing" of the higher harmonics. The effective analysis bandwidth was 8.8 Hz at 80% RPM and 10.7 Hz at 97.5% RPM and resulted in an analysis range of 0 to 2939 Hz and 0 to 3564 Hz for 80% RPM and 97.5% RPM, respectively.

This analysis was done primarily to separate the tones from the broadband and to establish the harmonic roll-off characteristics, particularly for comparisons between static and flight conditions.

Hot-Wire Anemometer Data

The hot wire anemometer data was processed on a Saicor SA143A Correlation and Probability Analyzer in auto-correlation mode. Only the flight and taxi data were processed since the static data is meaningless. Due to the very low frequency content of the data, A.C. coupling could not be used. Therefore, the analyzer was first used in the probability density mode and a D.C. suppression level adjusted to put the peak in the amplitude probability density function at zero. However, very low frequency variations of the order of 10 to 30 seconds per cycle, ostensibly due to the observed 0.05 to 0.07 rad variation in aircraft angle of attack during the run, precluded perfect D.C. suppression. In the auto-correlation mode, the lag values were chosen so that the asymptotic value was reached by the 400th lag. The zero lag value gives the mean squared value while the integral of the normalized auto-correlation function gives the integral time scale. Multiplying this integral time scale by the flight speed gives the integral length scale. This analysis was done on the hot-wire anemometer data for the conditions listed in table III.

Aircraft Operating Conditions

The aircraft operating conditions data was processed by NASA-Langley. The air-speed, altitude, angles-of-attack, sideslip, roll, pitch, and yaw attitude angles, normal, lateral, and longitudinal accelerations, engine torque, and propeller speed were decoded and tabulated for each tenth of a second for each condition.

DISCUSSION OF RESULTS

Transient Conditions (Take-Offs)

Blade Surface Pressure Data

Time history plots. - A particularly interesting plot of blade surface pressure time histories is shown in figure 11 for a 97% RPM take-off condition. The data represents approximately 30 seconds of data and shows the blade surface pressures for static operation prior to ground roll, during the ground roll, and during lift-off and initial climb.

At the 0th propeller revolution, the aircraft is static. A strong disturbance may be seen at approximately the 40th circumferential sample, which corresponds to about 95 degrees from the top of rotation. A second, weaker disturbance may be seen at about the 75th sample, or approximately 180 degrees of rotation from the top. It is conjectured that the first disturbance is a result of ingestion of a vortex which originates on the aircraft fuselage, while the second disturbance may be indicative of a ground vortex. These disturbances are seen in the outer 25% of the blade. The transducer at the 40% radius does not show any significant activity. As the aircraft begins to roll, the disturbances disappear quickly. The "vortex" first disappears at the 77% radius transducer at about the 350th revolution, while the other radii show the "vortex" disappearing at about the 380th revolution.

Near the end of the time history traces in figure 11, the aircraft has lifted off and is climbing. At the 1,000th propeller revolution, it can be seen that the sharp spikes have disappeared. However, a general, low frequency once-per-revolution (1P) variation in the blade surface pressure level may be seen at all locations. The 40% radius transducer shows an accentuated flow distortion near the bottom of the propeller revolution which is believed to be caused by nacelle blockage. The once-per-revolution distortion is probably due to the inflow which is non-normal to the propeller axis, thereby causing a cyclic angle-of-attack change on the propeller blades. This is a result of aircraft attitude, upwash from the wing, nacelle blockage, fuselage blockage, etc.

An interesting, and totally unanticipated aspect of the blade surface pressures in flight is the increase in high frequency activity which extends over slightly less than one-half of a revolution at the outboard blade stations. The origin of this high frequency signal is not known.

Narrow-band spectra. - Narrow-band spectra of blade surface pressure signals are compared in figures 12 to 15. The blade surface pressures during the static portion of the take-off (i.e. near the 0th propeller revolution in figure 11) are compared to those after the aircraft has lifted off (i.e. near the 1,000th propeller revolution in figure 11).

Figures 12 and 13 show 50 orders of revolution. They identify the tones for the 94% and 77% radius transducers, respectively. The static data shows many tones extending to beyond 50 times the rotational frequency, while the flight data shows only 4 or 5 tones which quickly fall to below the level of the broadband signal. The harmonic roll-off for the static data is slight, being down about 30 dB from the fundamental at the 50th harmonic in figure 12 and about 20 dB in figure 13. The flight data shows a much steeper roll-off, the 30 dB down point occurring at the fifth harmonic for both transducer locations. Figures 14 and 15 show similar results to those described in figures 12 and 13 except that this data extends to 200 orders. Again, the static data tends to decrease in level with increasing frequency significantly more slowly than does the flight data. It may be noted in figure 14 that the flight data shows an initial rapid drop in level but levels off and actually remains above the level of the static data at high frequency. This high level of high frequency noise is probably a manifestation of the high frequency noise which was noted at the top of the propeller revolution in figure 11.

Wing-Tip Microphone Data

Time history plots. - Figure 16 shows the time history plots for the two wing tip microphones for the 97% RPM take-off condition. For each propeller revolution prior to the aircraft lift-off, 9 distinct "blips" may be discerned in the in-plane microphone signal. The three strongest pulses are caused by the direct pressure pulse from each blade. The slightly weaker pulses, which remain at a fixed delay from the primary pulses are believed to be echoes from the ground. Since the travel time for the reflected signal is longer than that of the direct signal due to the greater path length, its time of arrival is slightly delayed. The third set of pulses, which are significantly weaker than the others, are not phased with the instrumented propeller, but rather appear to sweep across at the rate of about once for every 67 revolutions of the instrumented propeller. Since this condition was a two-engine take-off, it is apparent that these pulses are due to the second propeller which is running slightly slower than the other instrumented propeller.

As the aircraft begins its ground roll, the relative speed between the propellers is seen to change as evidenced by the apparent sweep rate of the secondary propeller pulses. At about the 750th propeller revolution, the aircraft lifts off. This is apparent from the increased delay between the direct signal and the reflected signal due to the increase in the path length by virtue of the ground moving away from the propeller, whereas the path length for the direct signal remains fixed.

Generally similar effects occur for the aft microphone signal, although the pulses are not as well defined.

Narrow-band spectra. - Figures 17 and 18 show spectra of the front and aft wing-tip microphones, respectively, and compare the static and flight data as was done for the blade surface pressures previously discussed. In general, the flight data shows a more

rapid roll-off in the levels of the harmonics. This is very apparent in figure 18 for the aft microphone where the levels of the harmonics decrease in a very regular fashion and blend into the broadband noise at the 12th harmonic.

Static Propeller Operating Conditions

Blade Surface Pressure Data

Time history plots. - The time history plots for the static conditions identified in table III represent all the available good quality static data. In all cases but one, the data was processed to show approximately 500 propeller revolutions, or about 15 to 20 seconds of data depending on the RPM. Run 2S was plotted for over 1,000 revolutions to show any long term effects.

Runs 2S, 4S, and 6S are the operating conditions for 97.5% RPM and 351, 256, and 224 KW, respectively. The time history plots for these conditions are shown in figures 19, 20, and 21. The plots have similarities in that much activity occurs at or near the 38th sample of the revolution, which was previously tentatively identified as the result of a fuselage vortex. Other disturbances, notably in the 77% radius location for run 6S (figure 21) are seen to appear, move around, and disappear. Of significance is a relatively strong disturbance, which may be seen at the 82% radius location in both figures 20 and 21, between 60 and 220 revolutions and again between 240 and 300 revolutions in figure 20. This appears to be a patch of turbulence which moves through the propeller and occurs near the top of the propeller revolution. Due to its high frequency content, it is expected to contribute significantly to the high frequency propeller acoustic noise. The size of this disturbance extends for about one quarter of a revolution, or about 1.7 m (5.5 ft) in the transverse direction. Since it does not appear in either adjacent channel, the radial scale is less than the space between the 77% and 89% locations and thus has an upper limit of about 15 cm (6 in). Finally, the disturbance persists for approximately 140 propeller revolutions. Assuming a through-flow velocity of 24 m/sec (80 ft/sec), this represents a streamwise length of approximately 90 m (300 ft).

Run 2S (figure 19) shows an interesting phenomenon in that there are three distinct pulses per propeller revolutions which persist for long periods of time. Of significance is the fact that these pulses are almost always exactly 120 degrees of rotation apart and that they occur at all blade stations simultaneously. It may also be seen that from the 0th revolution to the 80th revolution, the pulses move toward the top of the propeller revolution then back again. This relative motion is seen to occur at all the blade stations at the same time. Another point is that the signal from the 89% location appears to be of opposite polarity from the others in this run, although other runs from the same flight (i.e. run 5S) show it to be in phase. At the present time, it is not known if this is real pressure data or a result of propeller vibration causing the slip ring to vibrate and cause intermittent contact. Removing transducer excitation does eliminate the signals, so that it apparently is not a result of intermittent amplifier power. Also, between the 560th

and 620th revolution, relatively little activity is seen at the 89% station while the other three show several pulses, although they are no longer 120 degrees apart, there being two 120 degrees apart and one inbetween at about 30 degrees from one of the others. Although this phenomenon is extremely interesting, it is beyond the scope of the present program to thoroughly investigate it. Certainly much more study is required to establish whether it is a result of actual blade surface pressures or some other phenomenon.

Runs 16S and 17S presented as figures 22 and 23, respectively, show similar results for 90% RPM conditions. In general, the data has similar characteristics to the 97% RPM data in that some strong disturbances persist for long periods of time. Also, much activity of what appears as high frequency noise is apparent at or near the top of the propeller revolution. An example of this is the plot of the signal at the 82% station for run 17S, figure 23. A strong disturbance is seen to appear near the top starting at about the 20th revolution, peak in intensity near the 120th revolution, decrease in intensity and pick up again near the 300th revolution. A fairly sharp pulse may also be seen in this trace at about the 50th sample of revolution (i.e. 120 degrees past the top) which stays more or less fixed to the 360th revolution then moves in the direction of rotation and then fades away. Some evidence of flow distortion, due to nacelle blockage, may be seen in the 40% station of run 17S, figure 23. Finally, a plurality of spikes may be observed in the 94% aft station in figure 22. Although these do not appear in the other data channels, they look suspicious and may need to be qualified as do the data from run 2S.

The data from 80% and 75% RPM, figures 24 to 27, show generally similar results, except that the 75% RPM data does not show quite as much activity as do the higher RPM's.

In general, the static data show much activity, particularly at the top of the propeller rotation. Sharp spikes may be seen at or near the closest approach to the fuselage and again at the bottom of rotation which may be indications of ingestion of fuselage and ground vortices. Distinct patches of turbulence may be seen to move through the propeller and persist for one to two hundred revolutions of the propeller.

Narrow-band frequency analyses. - Representative narrow-band frequency analyses of the blade surface pressure data for a static condition are shown in figures 28 to 33. Figures 28, 29, and 30 show 50-order analyses for blade surface pressures at 77%, 82%, and 89% radius respectively, while figures 31, 32, and 33 show the corresponding data analyzed for 200 orders. Both sets of data are for run 16S which is a 90% RPM condition. Figures 28 to 30 show that the static data contains many harmonics of rotational frequency. Up to 40 harmonics may be readily distinguished. Figures 31 to 33 show an initial decrease in level with increasing frequency followed by a levelling off at high frequency.

Lowson and Ollerhead have formulated an equation which relates the noise harmonic levels to fluctuating blade loading harmonics (ref. 3). When fitted through the then

available test data, an equation of the form

$$L_n = L_0 n^k$$

was obtained, where L_n is the amplitude of the n 'th loading harmonic and k is the slope of a straight-line fit through the data plotted on log-log paper. This form has been used extensively for calculating non-steady blade loading noise. In fact, measured noise levels have been used to compute blade loads (refs. 4 and 5). A recent propeller noise prediction procedure (ref. 6) based, in part, on the results reported in references 4 and 5 uses a value of -1.62 for k in the loading law. Inspection of the blade surface pressure data shows that a slope of between -1.5 and -1.7 is a good fit.

The analyses for 200 orders show similar results except that the individual harmonics are not well resolved. However, a reasonable good fit to a slope of -1.6 may be obtained which is also independent of operating conditions.

Statistical properties. - The statistical analyses for the static blade surface pressure data included the calculation of transverse, radial, and streamwise correlograms and also PSD's of enhanced and unconditioned pressure signals.

Figure 34 shows transverse correlation functions for run 2S. The data used in computing these functions was roughly the same as was shown in the time history plot of figure 19. Due to possible differences in inflow distortion at different positions around the propeller circumference, the origin for the transverse correlation functions, defined as the point where the time delay (lag value) is zero, was taken at four points. This resulted in four transverse correlation functions which were used to estimate the transverse length scales at four points around the propeller circumference. The four points selected are: 1) the top of rotation, 2) 90 degrees from the top, where the blade is near its closest to the fuselage, 3) the bottom of rotation, and 4) 270 degrees from the top, where the blade is approximately furthest from the fuselage.

Although the turbulence scales are correctly computed by integration of the correlograms, an estimate may be made of the turbulence scales from the time it takes the function to reach a value of $1/e \approx 0.37$. For isentropic turbulence, the time at the $1/e$ point is equal to the value of the integral.

Some variation in length scales for the four azimuthal locations is apparent in figure 34. Also, differences may be noted among the transducer signals at each azimuthal location. The transducer at the 89% radius shows some very long time scales; which, recalling the time history plots (fig. 19), may be due to the three pulses per revolution which persist for many revolutions.

The correlation functions for transducer number 4, at the 82% radius show fairly consistent correlation lengths. The transverse lengths are seen to be about 3 samples, which corresponds to 7.2 degrees of rotation or about 13.4cm (5.3 in) for the 82% radius. The streamwise length scales shown in figure 35 are short at three azimuths, but about 9 revolutions long at the bottom, which is enough to cause 25 to 30 pulses on the blades thereby producing tone-like noise. At 2145 RPM the time for one propeller revolution is 0.028 sec. Thus, 9 propeller revolutions will take approximately 0.252 sec. Assuming a velocity of 27 m / sec (90 ft/sec) at the plane of rotation, a disturbance passing through the plane of rotation will move approximately 7m (23 ft) in 0.252 sec. Thus, the 9 revolutions which define the streamwise length scale at the bottom of rotation represent average turbulence length scales of 7m (23 ft). The ratio of streamwise to transverse lengths is then about 50 to 1, which defines long, thin turbulent eddies passing through the disc.

Figure 36 shows spectrum analyses for the four data channels. The curves labeled "PSD" represent the total signal and are comparable to the narrow-band analyses discussed in the previous section. The curves labeled "HAR" represent spectrum analysis of the signal enhanced data, i.e. with the non-periodic portions taken out. As may be seen for the 94% and 89% transducers, the fundamental is essentially fully periodic. The second harmonic is almost fully periodic, while the third and subsequent harmonics are essentially narrow-band-random data with no periodic components. The 82% and 77% transducers show similar results, but the fundamentals contain a greater portion of narrow-band-random components. It is clear from these computations that only small portions of the blade pressure signals are harmonic at frequencies of interest.

Figures 37 to 39 show similar calculations for run 6S, which is the same RPM as run 2S but at a lower power. The four transducer signals are similar at the bottom location in figure 37. The 1/e down point indicates approximately 10 samples or 1/15 of a revolution for the 82% transducer, which corresponds to a length of 44 cm (1.46 ft). The streamwise length scale is about 18 propeller revolutions, i.e. 0.51 seconds or, assuming an estimated induced velocity of 23 m/sec (75 ft/sec), a length of 11.6 m (38 ft). The aspect ratio in this case is 26:1 or about one-half of that estimated for run 2S.

Figure 39 shows that most of the signals for this run are also non-harmonic.

Figures 40 to 42 show the results from a third run. This run was selected to indicate the changes in statistical properties with changes in propeller RPM. Run 5S is an 80% RPM operating condition with a similar power to that of run 6S. Again, using the 82% radius data as representative, the transverse and streamwise length scales may be computed to be 53 cm (1.75 ft) and 12 m (38 ft) respectively. This results in a streamwise to transverse length scale ratio of about 22:1, which is close to that calculated for run 6S. The PSD's shown in figure 42 are similar to the others discussed.

It is thus apparent that similar power levels result in similar turbulence scales, probably due to the equal induced velocity which results from similar propeller thrust levels.

Acoustic Data

1/3 Octave band analyses. - Representative 1/3 octave band analyses for the propeller far-field noise are presented in figures 43 to 48. These are for the wing-tip microphones for the three propeller operating conditions discussed above. These show high levels of mid-frequency noise which hold up well into the limits of the frequency range which contributes to annoyance.

A hump in the spectrum may be seen, particularly in figures 46 and 47, at 1,000 to 2,000 Hz which will contribute heavily to A-weighted noise levels. Historically, this hump would have been identified as the broadband, or vortex, noise peak. However, this is not so, as will be evident in the narrow-band spectrum analyses.

Narrow-band frequency analyses. - Figures 49 to 54 show the narrow-band frequency analyses which were done on the same three propeller operating conditions. It is to be noted that this data is dominated by harmonics of blade passing frequency which appear to extend well past the 33 harmonics shown in figures 49 to 54. Recalling the discussion of the time history plots and the turbulence length scales presented in earlier sections, the character of the propeller noise spectrum is an apparent manifestation of the interaction of the propeller blades with the ingested turbulences. The streamwise length scale was noted to be sufficiently long to be cut by the propeller many times, thus giving rise to tone-like noise. Also, the transverse length scale was noted to be relatively small thus causing localized sharp loading pulses on the propeller blades. The sharper the pulse, the greater the high frequency energy content. The measured static noise spectrum is then consistent with the inflow turbulence model in that the many harmonics generated are a consequence of the ingestion of high-intensity turbulences having small transverse scale but large streamwise length.

The peaks in the 1/3 octave band plots are now identified as a result of the accumulation of many tones within each band and not a result of vortex noise. The broadband noise is actually seen to be 10dB or more below the levels of the tones.

The harmonic roll-off is seen to be gradual and almost linear with frequency, except for the first two or three harmonics which show an initial steep roll-off, particularly evident in figures 50, 52, 53, and 54. An approximate fit to the harmonics roll-off shows a slope of about -1dB per harmonic for runs 2S and 6S and about -0.5dB per harmonic for run 5S. Since the difference between runs 2S and 6S and run 5S is tip speed, it is conjectured that the high tip speed cases include a greater contribution from the steady loading harmonics and therefore the steady and non-steady loading components combine to give the larger slope. Run 5S, however, being a lower tip speed case, has a steeper drop-off of steady loading harmonics. Thus, it is apparent that the first three or four harmonics in figures 53 and 54 are caused by the steady blade loading while the higher harmonics are due to non-steady blade loads caused by inflow turbulence interaction.

Flight Conditions

Blade Surface Pressure Data

Time history plots - Representative time history plots are shown in figures 55, 56, and 57 for the flight conditions corresponding to the static conditions previously discussed. Note that only 65 propeller revolutions were plotted. This was sufficient to define the character of the blade pressure signals since the flight data does not include slowly varying events as does the static data.

There are three notable features in this data. The first is that the overall character of the blade surface pressures does not change appreciably from one revolution to the next or even after many revolutions. This indicates that the inflow is completely steady and the turbulence scale is either too large (i.e. larger than the propeller) or too small (i.e. less than the distance traveled in one propeller revolution) to be seen in this type of analysis.

A second feature is the presence of a high frequency signal which is particularly evident in the two outboard transducers for run 2 (figure 55). This high frequency signal is seen to extend for nearly one-half of the revolution and occurs near the top of rotation. It is usually apparent in all of the 97% and 90% RPM conditions and somewhat less evident in the 80% RPM condition (e.g. see figure 56). The origin of this signal is not known at the present time, but it is expected that these levels of high frequency fluctuating blade pressures will contribute to the high frequency far-field propeller noise.

The third significant characteristic in the time history plots is the level of 1P signal. This is seen to exceed the other signals in all cases, but especially for the 80% RPM case in figure 57. It will be seen in the next section that this high level of 1P is the dominant feature of the blade pressure signals and therefore precludes obtaining good statistical analyses of the data. An attempt was made to reduce the level of 1P by utilizing flaps to improve the aircraft attitude. The results of one of these flights is shown in figure 58. Although the level of 1P has been reduced, it is still very much in evidence. It may also be noted that the phase of the 1P distortion relative to the propeller blade position has been changed.

Figure 59 shows a time history plot for the 90% RPM taxi condition. As may be seen, the character of the pressure signal is essentially the same as for the flight conditions, despite the differences in altitude above the ground.

Narrow-band frequency analyses - Figure 60 shows representative narrow-band frequency analyses for a high and low tip speed condition. This analysis shows that the tones fall-off very rapidly in contrast to the static data. Also, the level of the low RPM data decreases to that of the electrical noise after a few harmonics. It may also be seen that the level of the 1P signal is high, which is consistent with the strong level of 1P distortion which was evident in the time history plots.

Figure 61 shows the same signals analyzed over a greater frequency range. Again, it may be seen that the low RPM high frequency signal is low in level and significantly below that of the high RPM condition. The relatively flat high frequency spectrum of the high RPM pressure signal is consistent with the high frequency content observed in all the time history plots of the high RPM conditions.

Statistical properties. - Local transverse covariance plots are shown in figure 62 for an 80% RPM flight condition. As may be seen, the dominant character is the 1P component which dominates all data channels at all azimuthal locations. A hint of the inflow turbulence scale may be seen for the 94% radius pressure data where a rapid drop may be seen on either side of the zero lag value, but this is quickly overtaken by the 1P component. The streamwise autocorrelation functions are shown in figure 63. Again, a hint of small scale turbulence may be seen in the tip transducer data. The very long scale apparent in these plots is actually the autocorrelation function of the 1P distortion. This shows that the 1P component was not actually steady, but varied slowly, perhaps completing a cycle in 100 propeller revolutions.

Figure 64 shows that the first few harmonics are phased to the propeller, but that the high frequency components are random. It is thus apparent that the 1P distortion has a few low order harmonics which are phased to the propeller rotation but that the high frequency signal, which is of relatively low amplitude, being 40 to 50 dB below the overall level, is random and probably the actual atmospheric turbulence ingested by the propeller.

A representative 97% RPM condition is shown in figures 65 to 67. Even here, the signal is mostly 1P. However, the 94% radius signal shows some very small scale turbulence as evidenced by the rapid drop in level which is not really resolved since it falls to 0.37 within one sample.

It is thus apparent that the 1P component is dominating the blade surface pressures. The 1P component is not steady, since the transverse correlation plots (figures 62 and 65) show significant 1P content even though the data has been signal enhanced to remove steady flow distortion effects. It was thus not possible to establish correlation length scales, although a few samples show very steep initial slopes in the correlograms which are not well resolved by the 150 point per revolution sampling rate.

As an alternative to the computerized statistical processing discussed above, a different procedure was used for determining the statistical properties of one of the blade pressure signals in one of the flight test runs. In this approach, high pass filters were used to eliminate the 1P components and the lag values were chosen to better resolve the turbulence length scales. The results from this limited analysis will be discussed in a later section.

Acoustic Data

1/3 Octave band analyses. - The 1/3 octave band analyses of propeller far-field noise for the flight conditions corresponding in RPM and power to the static conditions previously discussed are shown in figures 68 to 73. As may be seen, the fundamental blade passing frequency, the second harmonic, and the third harmonic are readily apparent. The higher frequency 1/3 octave band levels, however, decrease in level with increasing frequency. The 80% RPM data, in figures 72 and 73, do not show as pronounced levels of harmonics of blade passing frequency but the general decrease in level with increasing frequency is still apparent.

Figure 74 shows the variation in noise in flight with RPM. It can be seen that reducing RPM from 97.5% to 90% results in reduction in levels of both harmonics of blade passing frequency and broadband noise. Reductions in RPM from 90% to 80% results in further reductions in low and mid-frequency noise, but not much change at high frequency. It is thus apparent that other noise sources, such as the turboshaft drive engine, for example, may be contributing to the high frequency noise signature.

Narrow-band frequency analyses. - Figures 75 to 80 show the narrowband frequency analyses corresponding to the three flight conditions described above. Both 97% RPM conditions show significant harmonic content particularly for the in-plane location. However, the harmonic roll-off is seen to be relatively constant. A slope of about -2dB per harmonic is seen at 97% RPM for the in-plane location while the aft location shows a slope of approximately -4dB per harmonic.

The 80% RPM data, in figures 79 and 80, show very little harmonic content since the tones drop in level relatively quickly and disappear into the broadband noise at the fifth or sixth harmonic.

Hot Wire Anemometer Data

Auto-correlation analyses of the hot-wire anemometer data for the three illustrative flight conditions are shown in figures 81, 82, and 83. Although D.C. suppression was used to null the residual D.C. component, some evidence of a D.C. offset may be seen in the data. This was caused, in part, by low frequency variations in the D.C. component due to aircraft motion which made it impossible to null it completely. Thus, the asymptotic values have also been indicated in figures 81 to 83. The value at zero time lag represents the mean squared value, so that the square root of the zero value indicates the root-mean-square (rms) level of turbulence. For the three conditions shown, the rms values are 0.67 m/sec (2.19 ft/sec), 3.91 m/sec (12.8 ft/sec), and 1.8 m/sec (5.94 ft/sec) for high-power 97% RPM, low-power 97% RPM, and 80% RPM respectively.

Assuming an effective radius of 80% of the actual propeller tip radius, the rms values of the turbulence can be converted to equivalent rms values of angle-of-attack fluctuations. The effective radius rotational speeds are 232 m/sec (760 ft/sec) and 191 m/sec (627 ft/sec) for 97% and 80% RPM respectively. Thus, for the three cases shown in figures 81 to 83, the fluctuating angles-of-attack may be estimated as the inverse tangent of the rms fluctuations divided by the rotational speed. This results in rms angle-of-attack fluctuations of 0.0029 rad, 0.0168 rad, and 0.0095 rad respectively. Now, assuming a slope of approximately 6.28 for the lift vs. angle-of-attack variation and that the thrust is proportional to the lift, these fluctuating angles-of-attack represent rms thrust fluctuations of 1.81%, 10.6%, and 5.95% respectively. Although the spectral distribution of these fluctuating lifts are not known, the above values may be considered to represent an overall level. Also, fluctuating lifts of 0.1% of the steady lift have been shown to contribute significantly to propeller noise. Thus, it is apparent that this level of turbulence may cause significant levels of propeller noise. It appears worthwhile to further analyze the anemometer data and obtain the spectral content of the turbulence to establish the contribution to propeller noise in the frequency range of interest. However, this analysis is beyond the current scope of this program.

The auto-correlations of figures 81 to 83 were integrated to obtain the integral time scales of the turbulence. Integration of the curves and normalizing by the mean-square value (at zero time lag) give integral time scales of 0.38 sec, 5.32 sec, and 2.07 sec, respectively. It may be noted that these times correspond closely to the times at which the function reaches a value of $1/e \approx 0.37$ times the mean-square value, thus indicating that the turbulence may well be isotropic. The turbulence integral length scales may be obtained through the flight speeds and are found to be 24 m (80 ft), 219 m (718 ft), and 85 m (280 ft), respectively. The third condition, with an integral length scale of 85 m (280 ft), is consistent with estimates of integral length scale approximately equal to the altitude found in the literature (ref 7). However, the variance in turbulence scale is large and a few isolated conditions may show wide ranges. It is possible, also, that the second condition is showing slow variations due to accelerations of the aircraft.

Comparison of Flight and Static Data

Blade Surface Pressures

Narrow-band spectra. - Narrow-band spectra of blade surface pressure are shown overplotted for representative 97% RPM static and flight conditions in figure 84. The low frequency analyses show higher levels of tone noise statically than in flight, particularly at the tip location. The high frequency analyses show similar trends. However, the two tip locations show an initial rapid drop in level with increasing frequency, then an essentially flat spectrum in flight. At high frequency, the static and flight levels

are essentially the same. In figure 85, similar results are shown for a 90% RPM condition. Here the high-frequency pressure signal in flight exceeds that for the static condition. The origin of the high levels high-frequencies is not known, but it was observed in the time history plots as a high level of activity occurring at the top of the propeller revolution. It is expected that this may contribute to high-frequency broadband noise generation by the propeller.

The differences between the blade surface pressures measured statically and in-flight show that the levels of tone-like noise at lower frequencies should be lower in flight than statically, since the pressures are lower in flight. The levels of mid-frequency noise should also be reduced in flight and should not contain tone-like components. The high frequency noise will also be lower in flight, since the levels of the blade surface pressure are generally lower in flight than statically at high frequencies.

Statistical properties. - The computer program (ref 2) was not used to establish the statistical properties for the flight data in the current program due to the high levels of 1P signal. A limited discussion on comparisons between static and flight conditions will be presented in the next section based on a limited analysis of data analyzed using high-pass filters to reject the 1P signals.

Acoustic Data

1/3 Octave Band analyses. - Comparisons of far-field noise 1/3 octave band analyses for comparable static and flight conditions are shown in figure 86 for 97% propeller RPM and in figure 87 for 90% RPM. Aft wing-tip microphone data and peak 61 m (200 ft) flyover data are presented. The aft microphone was found to show higher levels than the in-plane microphone, so its data are presented as a good indication of the differences between static and flight. The most striking feature in these comparisons is the marked reduction in the level of the noise in the 500 to 10,000 Hz range from static to flight operation. At 97% RPM, figure 86 shows reductions of about 10dB in the mid to high-frequency noise. The differences in dB(A) levels between static and flight are 6 dB and 4 dB for the wing-tip and ground based microphones, respectively. At 90% RPM, the differences in the dB(A) levels are 13 dB and 10 dB for the wing-tip and ground based systems, respectively. The greater change at 90% RPM may be attributed, in part, to more consistent reductions in the entire spectrum. The reductions in low frequency noise at 97% RPM were not pronounced, probably because there is a greater contribution from steady loading and thickness noise at this high tip speed condition.

Narrow-band frequency analyses. - Representative narrow-band frequency analyses are shown in figures 88 to 90. Figure 88 shows a comparison of static and flight aft wing-tip microphone data for a 97% RPM condition. The static condition is dominated by harmonics of blade passing frequency which extend to frequencies higher than the limit of the analysis. The flight condition shows initially high levels, but these drop rapidly into the broadband noise. It is also apparent that the broadband noise, which may be seen between harmonics, also decreases in level in flight.

Similar results may be seen in figure 89, at 90% RPM, and figure 90, at 80% RPM. The decrease in level in the harmonics is more dramatic for these two tip speeds. Also, it may be seen that the broadband noise levels in flight are lower relative to those of the static conditions than may be observed for the 97% RPM conditions.

It is apparent from these analyses that the reduction in propeller noise in flight relative to that under static condition is significant. There appears a dramatic reduction in the levels of the higher harmonics and a significant reduction in the broadband noise. The broadband noise reduction may be related to the thrust lapse rate, since broadband noise prediction methods would show the broadband level to vary with the thrust (ref. 6). For example, the thrust computed for the 90% RPM condition is 6712 N (1509 lbs) statically and 3621 N (814 lbs) for the 80 kts flight. At a tip Mach number of 0.79 and a total blade area of 0.49 m² (5.3 sq. ft), the method of reference 6 shows a decrease of about 9 dB from static to flight, which is in good agreement with the data of figure 89 which shows a 10 to 12 dB reduction.

It is apparent that the noise generating mechanisms of propeller tone noise are vastly different in flight than statically. In fact, both the tone noise levels and the tone noise spectra show marked differences so that inferring propeller noise levels in flight based on static test stand measurements will result in over-predictions.

Comparison of Measurements With Theory

Background

Propeller noise radiation is caused by volume displacement of the air by the blades and by forces that the blades impose on the air. The volume displacement effect produces "thickness noise"; the force effect produces "loading noise". For analytical purposes, the blade loading may be divided into a steady (lift producing) component and an unsteady portion. The unsteady loading, in turn, is further divided into a random component (associated with incoming turbulence and self-excited effects) and a periodic component (due to angular inflow to the propeller). Propeller noise spectra and directivities for all but the self-excited effects can be calculated using several computer programs which are described below. In addition to propeller radiation, the microphones also measure noise from the engine, airframe, and self-generated wind noise whose levels have not yet been adequately assessed.

Thickness and steady loading noise have been calculated from a theory recently developed at Hamilton Standard for analysis of high speed propellers in flight (ref. 8). This analysis can be described as a linear addition of wavelets from each element of blade surface by means of a numerical integration over the blade planform area. As shown in reference 8, this theory produces excellent agreement with test data at tip relative Mach numbers from 0.75 to 1.00.

The random loading noise caused by inflow turbulence has been calculated using a theory originally developed for turbofan analysis (ref. 2); however, since the analysis assumes an open rotor, it is well suited to propeller studies. To use this computer program the unsteady blade loads are described by several statistical parameters related to the length scales and intensities of the incoming turbulence. The user chooses these parameters by forcing the theoretical blade pressure spectrum to match (as nearly as possible) the measured blade pressure spectrum. When this has been accomplished, the noise spectrum and directivity are calculated from the same blade pressures by integrating radiation effects over the blade chords and spans. Reference 2 shows this to be a very satisfactory tool for diagnosis of noise from static propulsors. It has not previously been used for in-flight studies.

Noise due to harmonic blade loads can be calculated using the rotor noise theory developed by Lawson (ref. 3) provided the load harmonic levels are known. The computer program for this theory is described in reference 4.

Propeller Noise Diagnosis

Noise diagnosis is the attempt to account for the source of each portion of a measured noise spectrum in terms of noise generating mechanisms. This is done below for the two wing tip mounted microphones at the 90% RPM, 215 kw (285 shp) static and flight conditions (runs 17S, and 17, respectively) described in previous sections.

The test noise spectrum measured statically by the in-plane wing tip microphone is shown at the top of figure 91. The heavy dots show harmonic levels predicted from steady loading and thickness effects. Since the first interference due to ground reflection is estimated to occur at about 160 Hz, predictions for the steady components were increased 6 dB at blade passing frequency and 3 dB at the high harmonics.

The other contributing mechanism is noise caused by unsteady blade loading. The lower spectrum in figure 91 shows the spectrum shape predicted from blade pressure data for this effect. The peaks and valleys of this spectrum are shown by the dashed lines superimposed on the test spectrum. Figure 92 shows the corresponding predictions for the aft boom-mounted microphone. From these two figures, it is clear that the noise at blade passing frequency and at least part of the noise at the second harmonic is caused by steady thickness and loading. The remainder of the spectrum, including the narrowband peaks and the broadband components, is caused by inflow turbulence. Further details on predictions of noise caused by random blade loads will be given at the end of this section.

The spectra of noise measured in flight by the two wing-tip mounted microphones are shown in figure 93. These are substantially reduced from the static levels shown in figure 91 and conclusions regarding dominant sources in flight are therefore different than those during static operation. Again, the heavy dots show the combined effect of the steady loading and thickness noise mechanisms. However, in flight, these steady

effects (mostly thickness) are important at much higher frequencies. The slight over-prediction of the higher harmonics for the in-plane microphone location shown at the top of figure 93 may be caused by off-design operation of the propeller as described in reference 8. When an attempt was made to calculate the noise spectra associated with measured unsteady blade pressures, it was discovered that the methodology described in reference 2 is inadequate because of an approximation, to be described later, regarding turbulence length scales. This approximation could be eliminated at the expense of some additional complexity in the analysis but this was beyond the scope of the present program. Similarly, no estimates of noise caused by harmonic loads were made because there was no calibration which would permit calculation of blade forces from the measured pressure signals. (It is possible that this could be remedied by use of aircraft attitude data to calculate blade force harmonics.) However, the strong level of the first harmonic shown for the flight data in figure 94 appears to be the dominant cause of the noise harmonic at blade passing frequency. Thus, the flight noise harmonics are reasonably well understood; however, the broadband sources have not been identified. These could be atmospheric turbulence, self-excited random effects, airframe noise, engine noise, or wind interaction with the microphone.

Calculation of Unsteady Blade Loading Noise

This section describes in more detail the derivations of the parameters which were used for the noise predictions in the lower halves of figures 91 and 92. The fit of the theoretical blade pressure spectrum to the measured spectrum shown in figure 95 is satisfactory in shape and level. In order to compute noise, the remaining parameters needed were the ratio of radial to circumferential turbulence length scales (μ in reference 2) and the ratio of effective chord to actual chord (C_e/C_B in reference 2). These were established as follows.

Transverse length scales were estimated from figures 96 and 97. The autocorrelation plots in figure 96 were generated by a 400 point correlation analyzer set with full scale on the time axis corresponding to slightly more than the time for one propeller revolution. Since the instrument sampled the pressure data as the blade rotated, the time scale can be equated to circumferential distance. For the static data at the top of figure 96, the correlation coefficient drops to $1/e (\approx 0.37)$ at $\Delta\tau/\tau$ (or $\Delta c/c$ where c is the local circumference) equal to 0.04. For figure 97, the same correlation analyzer was used to determine the cross-correlation coefficient between pairs of transducers at zero time lag as a measure of radial length scale. The curve at the top indicates that the coefficient drops to $1/e$ for $\Delta r/r_T \approx 0.1$. Thus, the required ratio μ for the static curve is given by

$$\mu = \frac{\Delta r}{\Delta c} = \frac{\Delta r/r_T}{\Delta c/r_T} = \frac{1}{2\pi} \frac{\Delta r/r_T}{\Delta c/c} = \frac{0.1}{2\pi \times 0.04} = 0.4$$

This compares well with the value $\mu = 0.5$ used for subsonic tip speed turbofan noise predictions in reference 4. When the same procedure was tried with the flight data obtained in the current test series, two difficulties arose. First, the aircraft angle of attack caused a strong once-per-revolution (1P) blade pressure signal component at 33 Hz. This component was eliminated by a high pass filter set at 99 Hz. The resulting auto-and cross-correlation plots shown in the lower halves of figures 96 and 97 suggest very small transverse length scales. However, these are due to the localized high frequency signal component described previously in the discussion of flight blade surface pressure time history plots and shown in figures 55 to 57. Thus, it is concluded that in flight, the blade pressure signal is dominated by two effects unrelated to inflow turbulence: a low frequency, harmonic component caused by skewed inflow and a high frequency random component apparently generated on the airfoil itself. Since the noise prediction methodology of reference 2 is not appropriate for either of these effects, it was not possible to predict noise associated with these unsteady blade pressures.

In reference 2, the effective chord ratio C_e/C_B was determined by measuring sound pressure and blade pressure simultaneously with a wake-generating cylinder in the duct just upstream of the fan rotor. For safety reasons, it was not considered practical to perform an equivalent test with the propeller. However, the objective of such a test is to insure that the cause-and-effect relationship between blade pressures and sound pressures is not obscured by other noise sources. As there was no such problem with the static data, since both the blade surface pressures and the propeller noise levels were clearly above any other sources, the cylinder "calibration" scheme was really unnecessary. Thus, the value $C_e/C_B = 0.7$, which is the average value used for the calculations reported in reference 2, was also used in the calculations shown in figures 91 and 92.

CONCLUSIONS

On the basis of the analysis of the data acquired in this test program, the following conclusions were reached.

1. The noise generating mechanisms under static condition are different than those under forward flight.
2. During static operation, the first few harmonics of blade passing frequency are controlled by steady loading and thickness effects. The higher harmonics and broadband noise components are caused by interaction with inflow turbulence.
3. Under flight conditions, the peaks at harmonics of blade passage frequency and the high frequency broadband noise are substantially reduced. This appears due to the change in inflow turbulence interacting with the blades.
4. In flight, the steady loading and thickness effects control the harmonic levels up to about the 10th.
5. The origin of the broadband noise in flight has not yet been identified, but may be due to engine noise, airframe noise, atmospheric turbulence interaction noise, propeller self-noise, and/or microphone wind noise.
6. High frequency blade surface pressures, which are apparent at the blade tips for the higher tip speeds in flight, may contribute to the high frequency propeller noise. The source of this high frequency noise has not yet been determined.

TABLE I
ATMOSPHERIC TEST CONDITIONS

<u>Run</u>	<u>Ambient Pressure (Pa x 10⁵)</u>	<u>Ambient Temperature (Deg K)</u>	<u>Relative Humidity (%)</u>	<u>Wind Speed (kts)</u>
1	1.0230	296	47	10
2	1.0201	305	56	4
3	1.0232	296	47	10
4	1.0232	296	47	10
5	1.0232	296	47	10
6	1.0231	296	47	10
7	1.0231	296	47	10
8	1.0231	296	47	10
9	1.0231	296	47	10
10	1.0231	296	47	10
11	1.0231	296	47	10
12	1.0231	296	47	10
13	1.0231	296	47	10
14	1.0231	296	47	10
15	1.0231	296	47	10
16	1.0199	305	56	4
17	1.0195	306	54	7
18	1.0191	306	53	10
19	1.0190	306	54	10
20	1.0190	306	54	10
2S	1.0245	301	74	14
16S	1.0245	301	74	14
3S	1.0245	301	74	14
5S	1.0245	301	74	14
21	1.0222	302	72	12
22	1.0222	302	72	12
23	1.0220	302	72	13
24	1.0220	302	72	13
25	1.0140	301	77	13
26	1.0140	301	77	13
21S	1.0175	301	53	4
22S	1.0175	301	53	4
4S	1.0147	300	89	16
6S	1.0147	300	89	16
17S	1.0147	300	89	16

TABLE II
PROPELLER NOISE TEST CONDITIONS

<u>Run</u>	<u>%rpm</u>	<u>Power (KW)</u>	<u>V (kts)</u>	<u>ALT (m)</u>	
1	97.5	450	150	61	2 Engines
2	97.5	363	121	61	1 Engine
3	80	249	97	61	1 Engine
4	97.5	205	97	61	1 Engine
5	80	210	78	61	1 Engine
6	97.5	229	78	61	1 Engine
7	97.5	430	150	305	2 Engines
8	97.5	392	124	305	1 Engine
9	80	262	97	305	1 Engine
10	97.5	262	97	305	1 Engine
11	80	210	78	305	1 Engine
12	97.5	215	78	305	1 Engine
13	90	-	75	Low	Run Void
14	90	119	80	Low	2 Engines
15	90	-	120	61	Not Flown
16	90	262	97	61	1 Engine
17	90	204	78	61	1 Engine
18	80	163	80	Low	1 Engine
19	90	172	85	Low	1 Engine
20	97.5	232	89	Low	1 Engine
2S	97.5	351	0	0	Static
16S	90	265	0	0	Static
3S	80	253	0	0	Static
5S	80	210	0	0	Static
21	80	293	88	61	Flaps Down
22	90	293	85	61	Flaps Down
23	97.5	345	93	61	Flaps Down
24	80	310	98	61	Flaps Down
25	90	305	100	305	Flaps Down
26	97.5	296	100	305	Flaps Down
21S	75	102	0	0	Static
22S	72.5	85	0	0	Static
4S	97.5	256	0	0	Static
6S	97.4	224	0	0	Static
17S	90.5	213	0	0	Static

TABLE III
OPERATING CONDITIONS FOR WHICH
DATA WAS FULLY ANALYZED

<u>Run</u>	<u>% RPM</u>	<u>Power (KW)</u>	<u>V (kts)</u>	<u>Alt (m)</u>
6S	97.4	224	0	0
4S	97.5	256	0	0
2S	97.5	351	0	0
17S	90.5	213	0	0
16S	90	265	0	0
5S	80	210	0	0
3S	80	253	0	0
21S	75	102	0	0
22S	72.5	85	0	0
20A	97.5	232	89	0 (Taxi)
19A	90	172	85	0 (Taxi)
18	80	163	80	0 (Taxi)
6	97.5	229	78	61
4	97.5	205	97	61
2	97.5	363	121	61
17	90	204	78	61
16	90	262	97	61
5	80	210	78	61
3A	80	249	97	61
8	97.5	392	124	305
10	97.5	262	97	305
12	97.5	215	78	305
9	80	262	97	305
11	80	210	78	305
C	80	210	83	305 (20° Flaps)

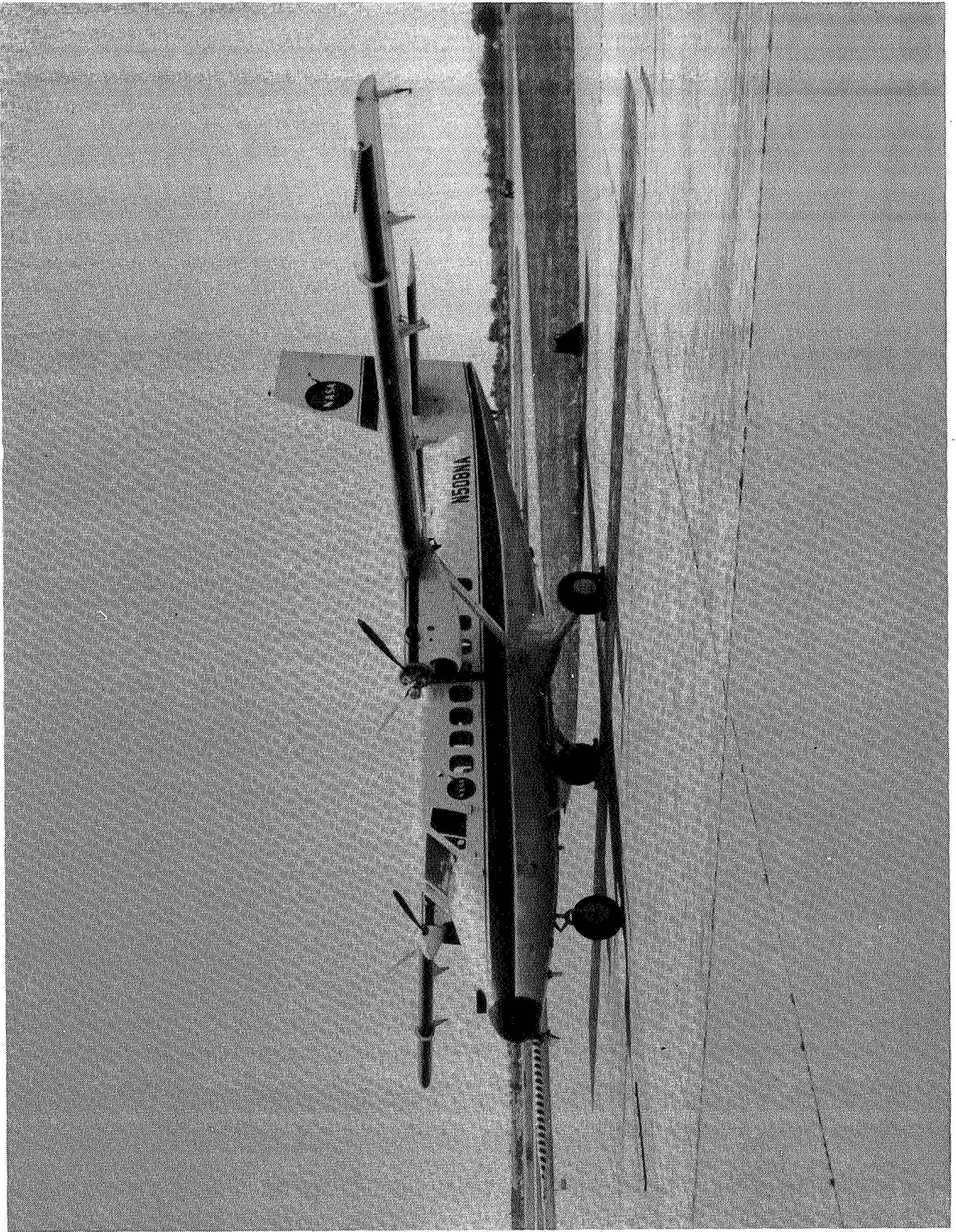
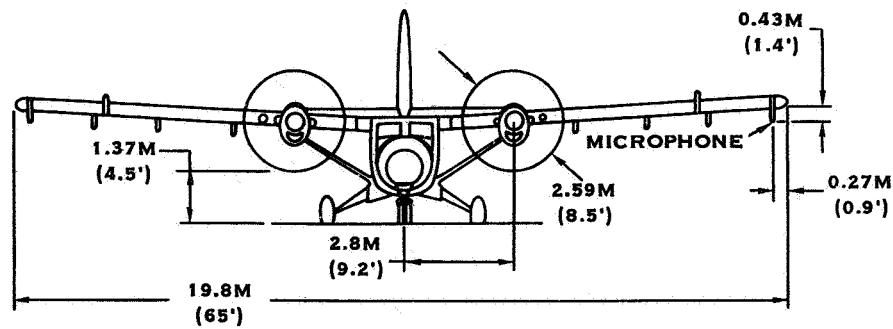
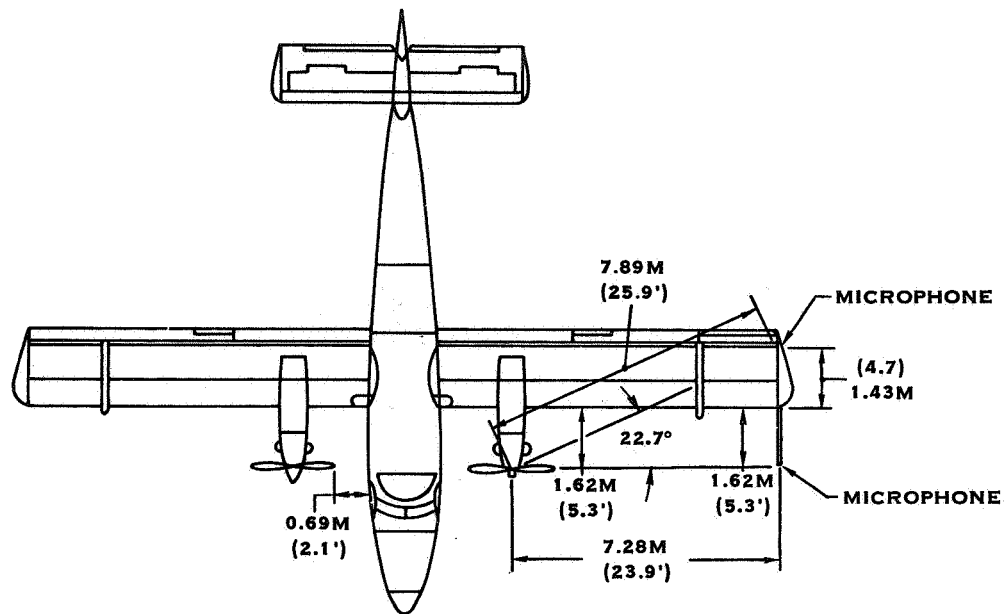


FIGURE 1. FORWARD FLIGHT PROPELLER NOISE RESEARCH AIRCRAFT



**NOISE BOOM FOR PITCH, YAW,
AND ATMOSPHERIC TURBULENCE
MEASUREMENT**

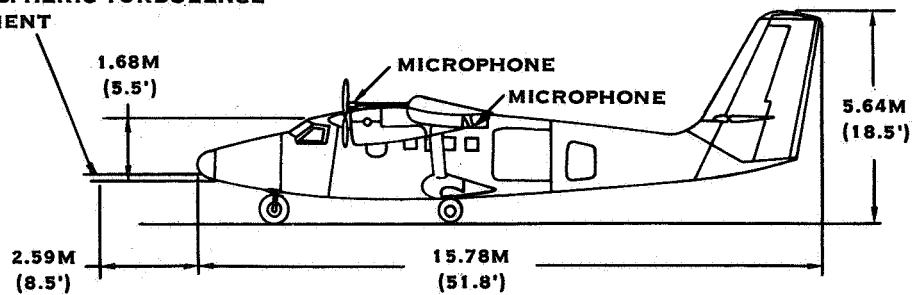


FIGURE 2. THREE-VIEW OF FORWARD FLIGHT PROPELLER NOISE RESEARCH AIRCRAFT

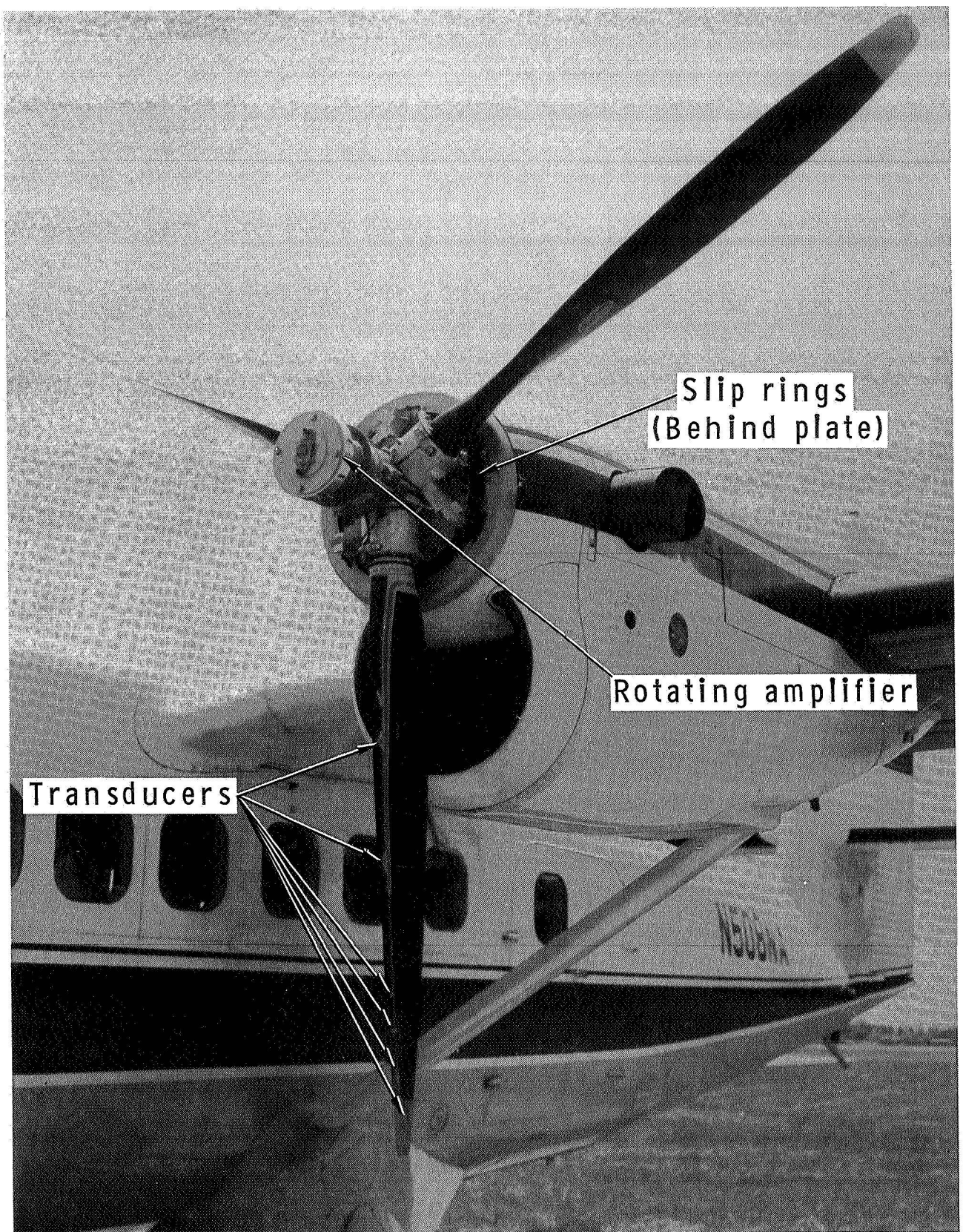


FIGURE 3. PRESSURE TRANSDUCER INSTALLATION

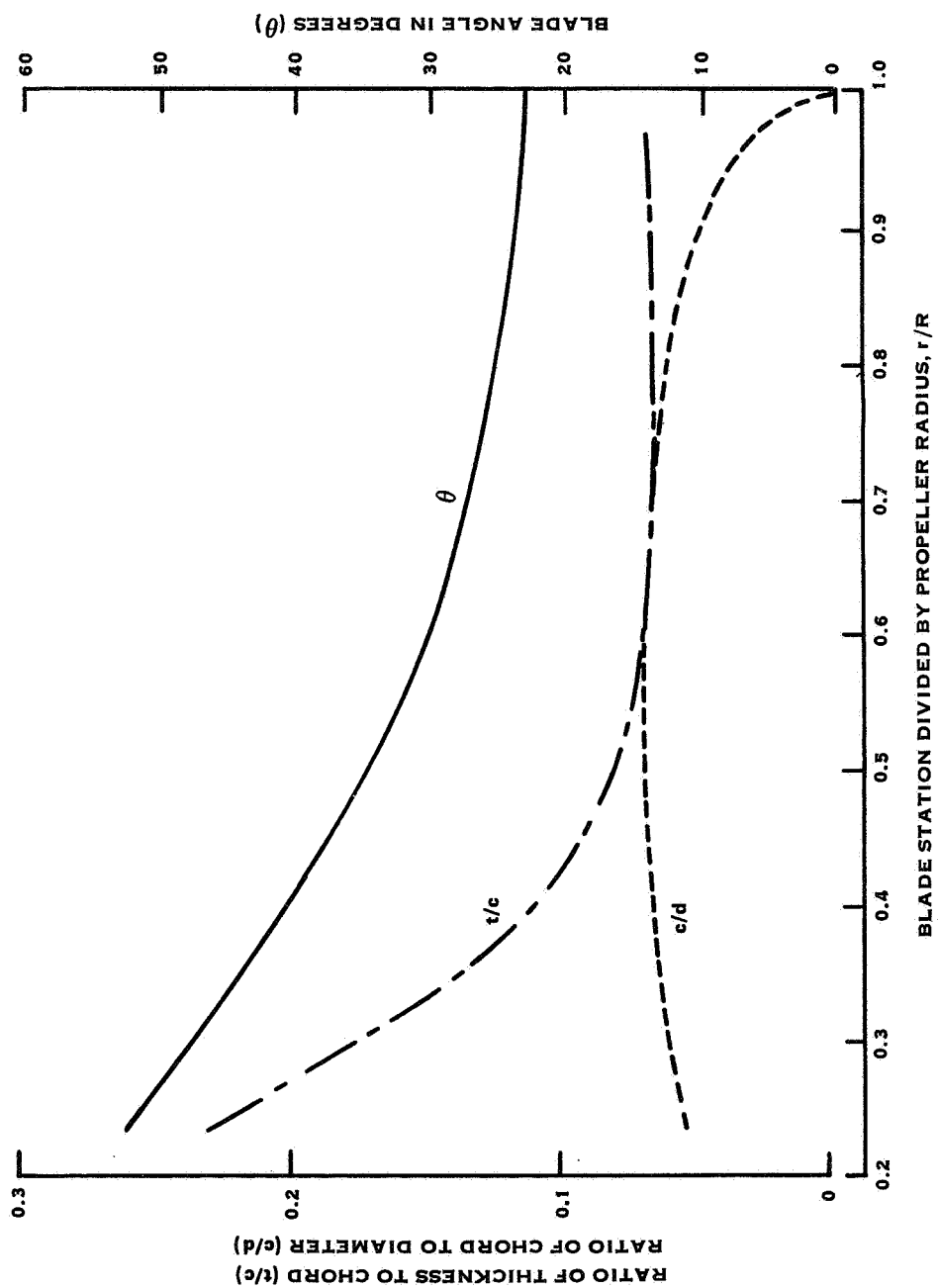


FIGURE 4. BLADE FORM CURVES FOR TEST PROPELLER

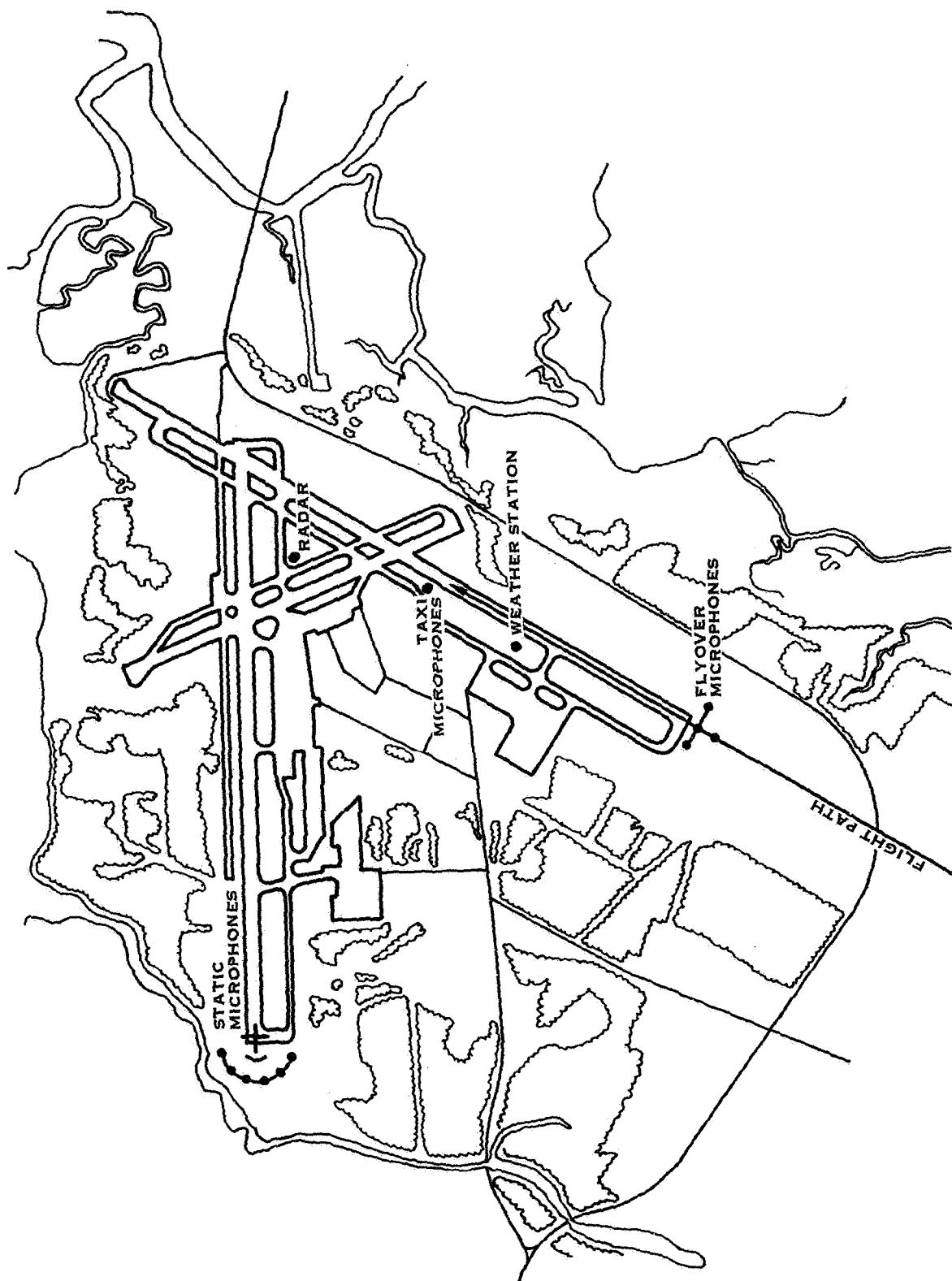


FIGURE 5. WALLOPS STATION TEST SITE

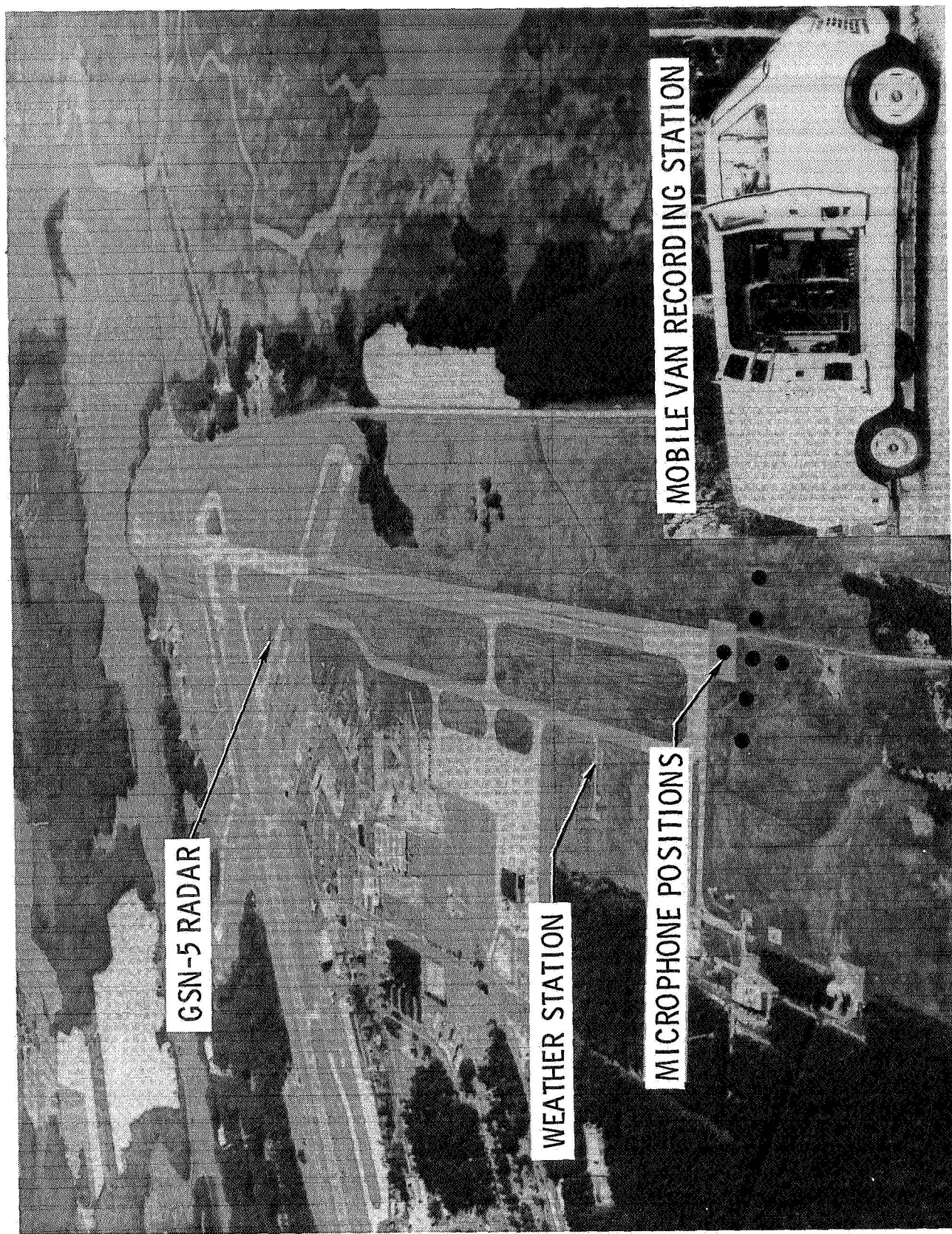


FIGURE 6. WALLOPS STATION TEST RANGE

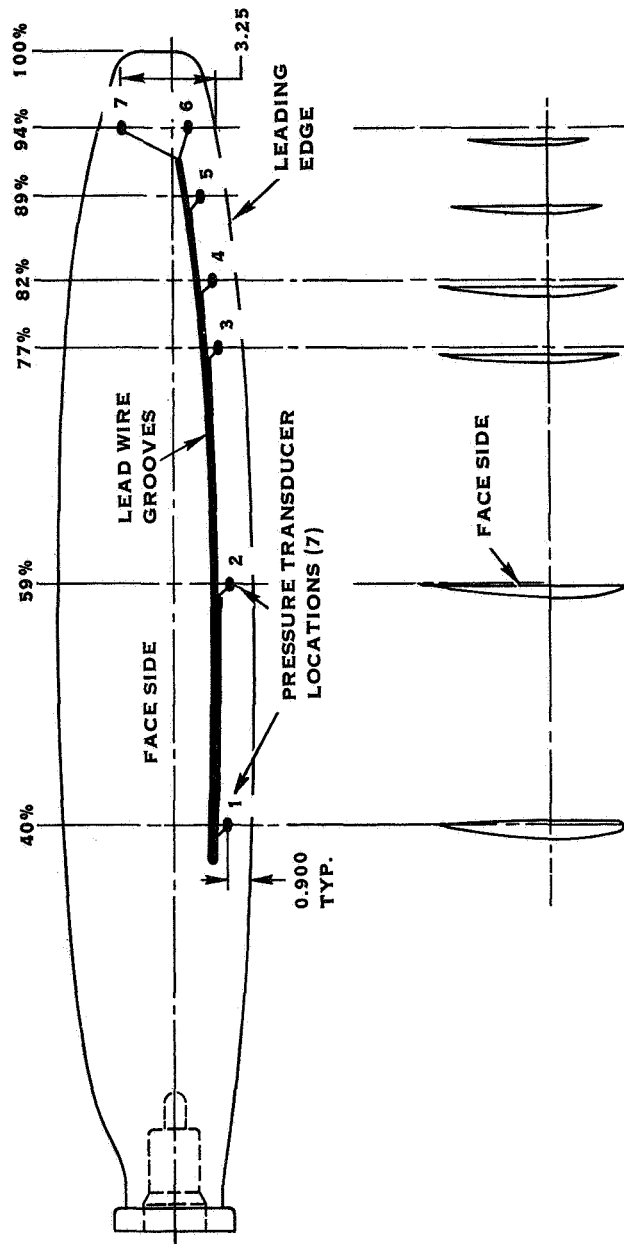


FIGURE 7. PRESSURE TRANSDUCER LOCATIONS ON INSTRUMENTED BLADE

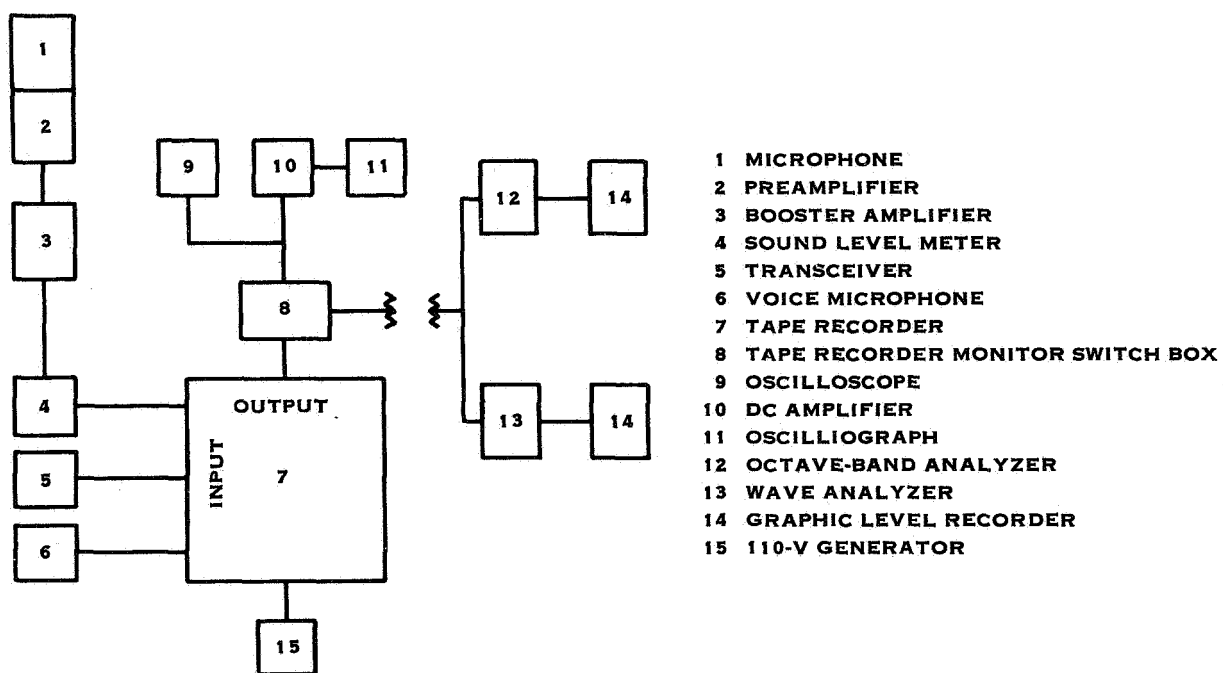


FIGURE 8. BLOCK DIAGRAM OF DATA ACQUISITION SYSTEM

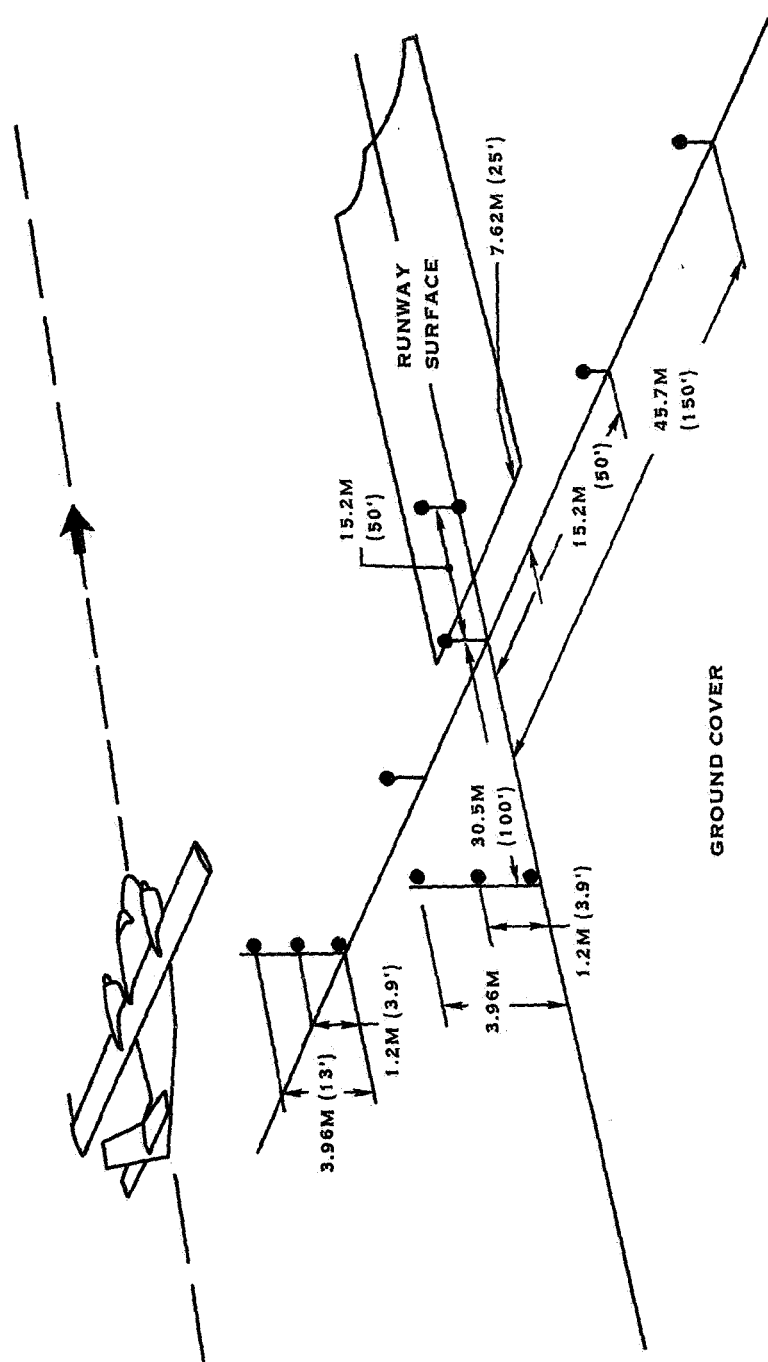


FIGURE 9. MICROPHONE LOCATIONS FOR THE FLY-OVER NOISE MEASUREMENTS

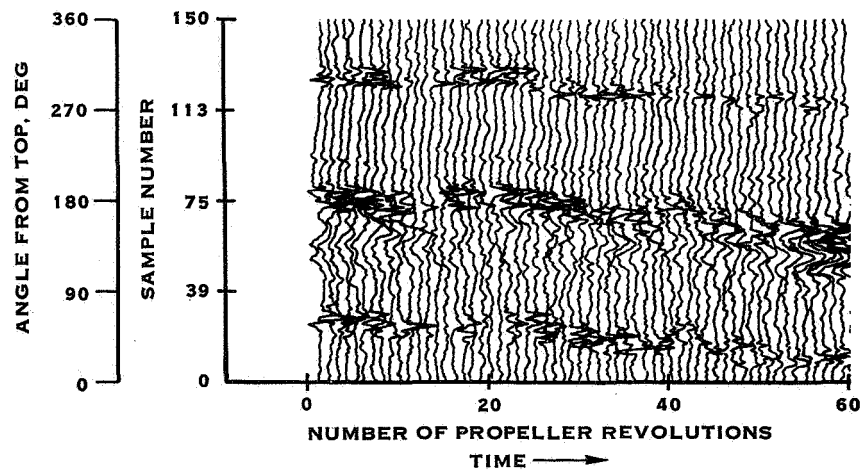
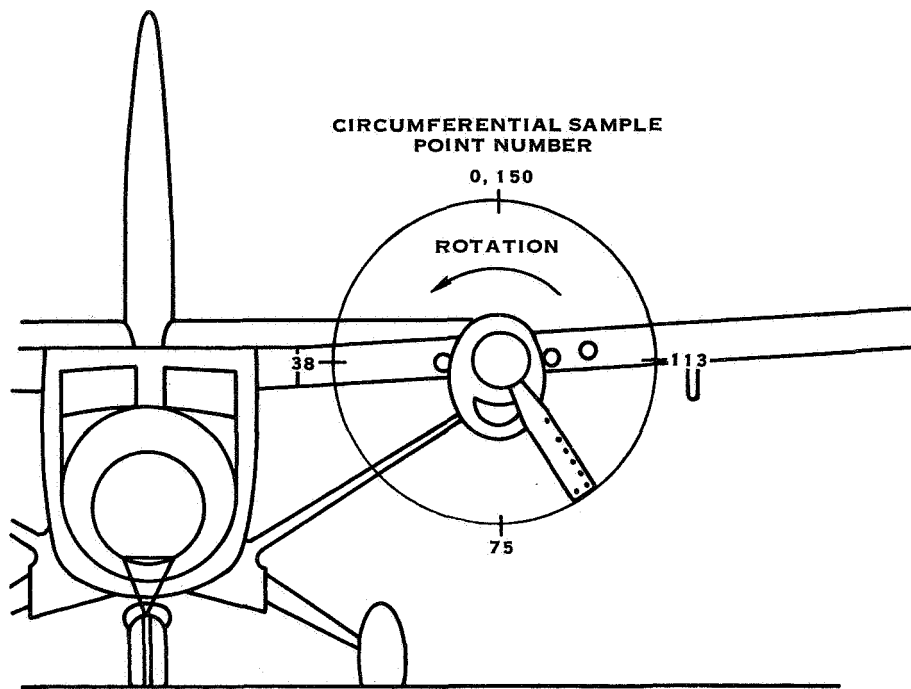


FIGURE 10. RELATIONSHIP OF BLADE POSITION AND TIME - HISTORY PLOTS

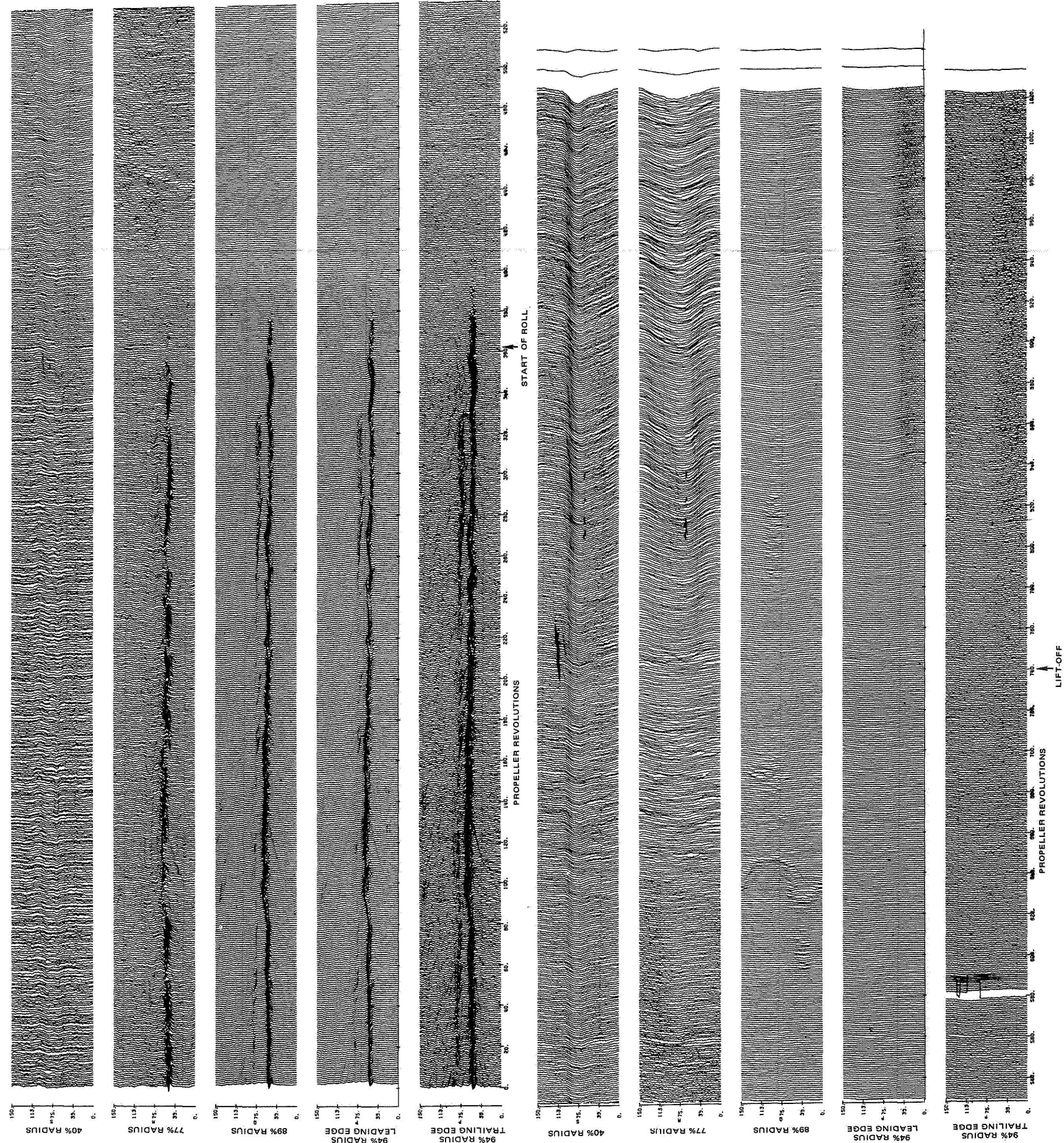


FIGURE 11. TAKE-OFF BLADE PRESSURE TIME HISTORY PLOT
97.5% RPM (RUN 1)

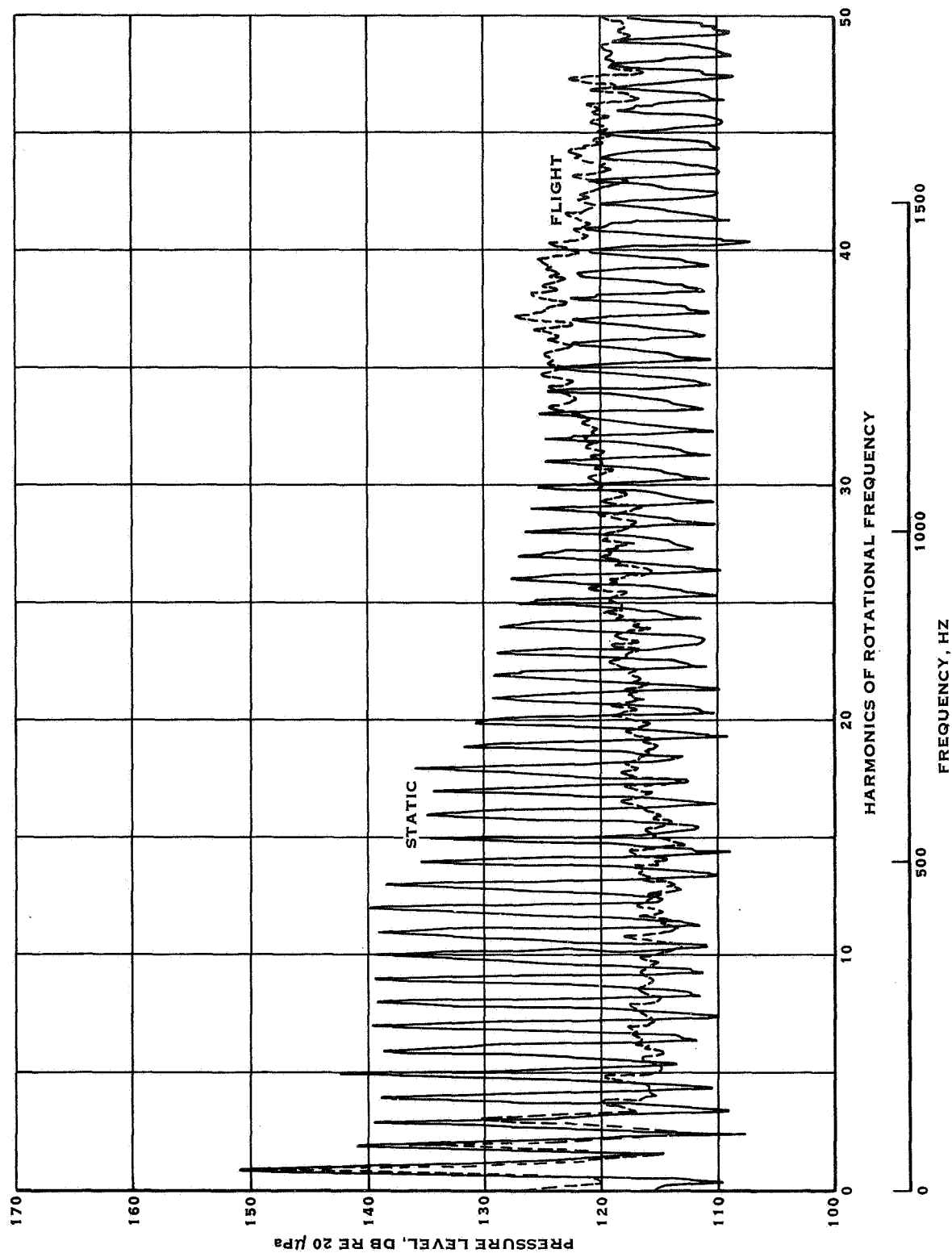


FIGURE 12. BLADE SURFACE PRESSURE SPECTRA AT THE 94% RADIUS DURING A 97.5% RPM TAKE-OFF, (RUN 1). 50 ORDERS ANALYSIS

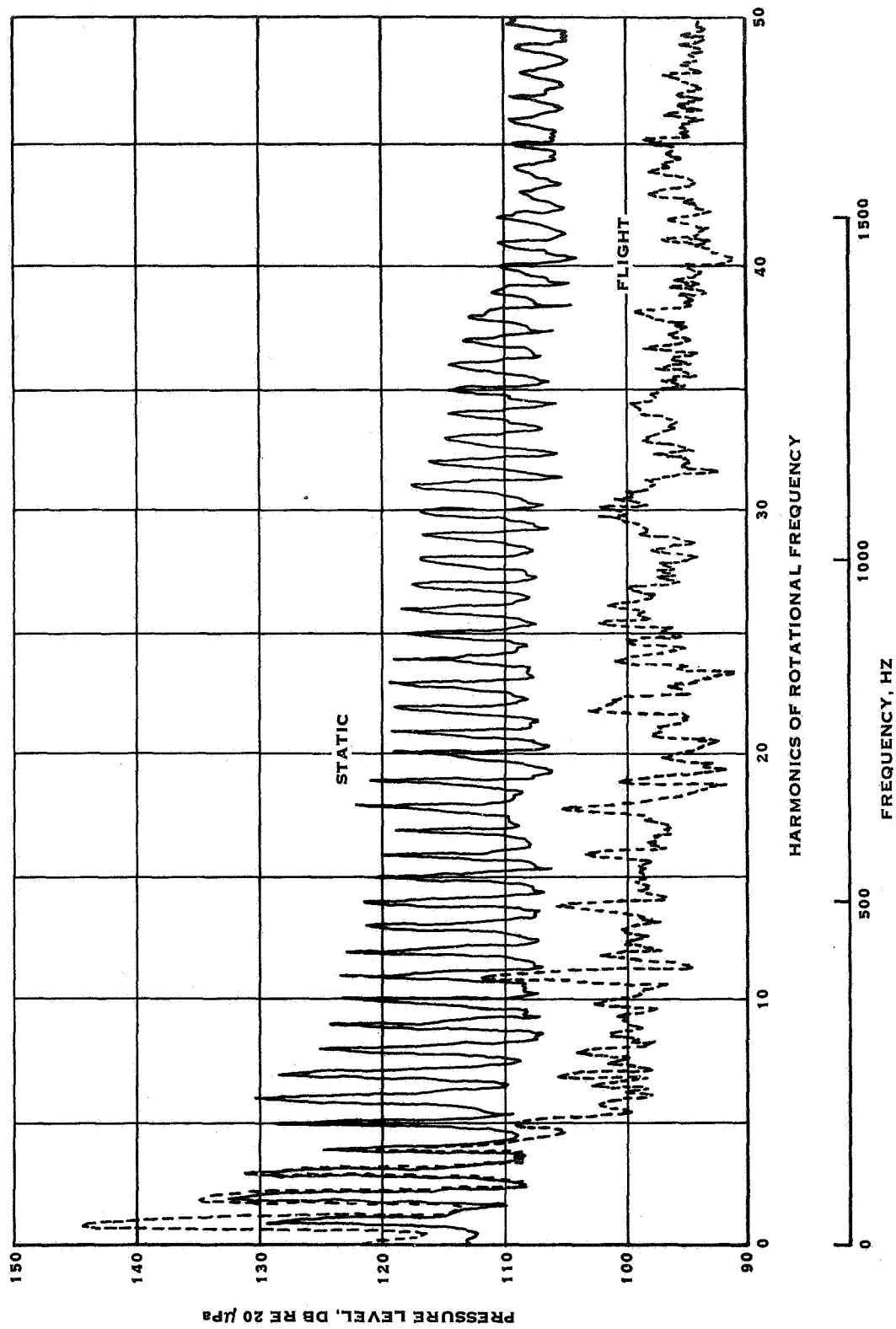


FIGURE 13. BLADE SURFACE PRESSURE SPECTRA AT THE 77% RADIUS DURING A 97.5% RPM TAKE-OFF (RUN 1). 50 ORDERS ANALYSIS

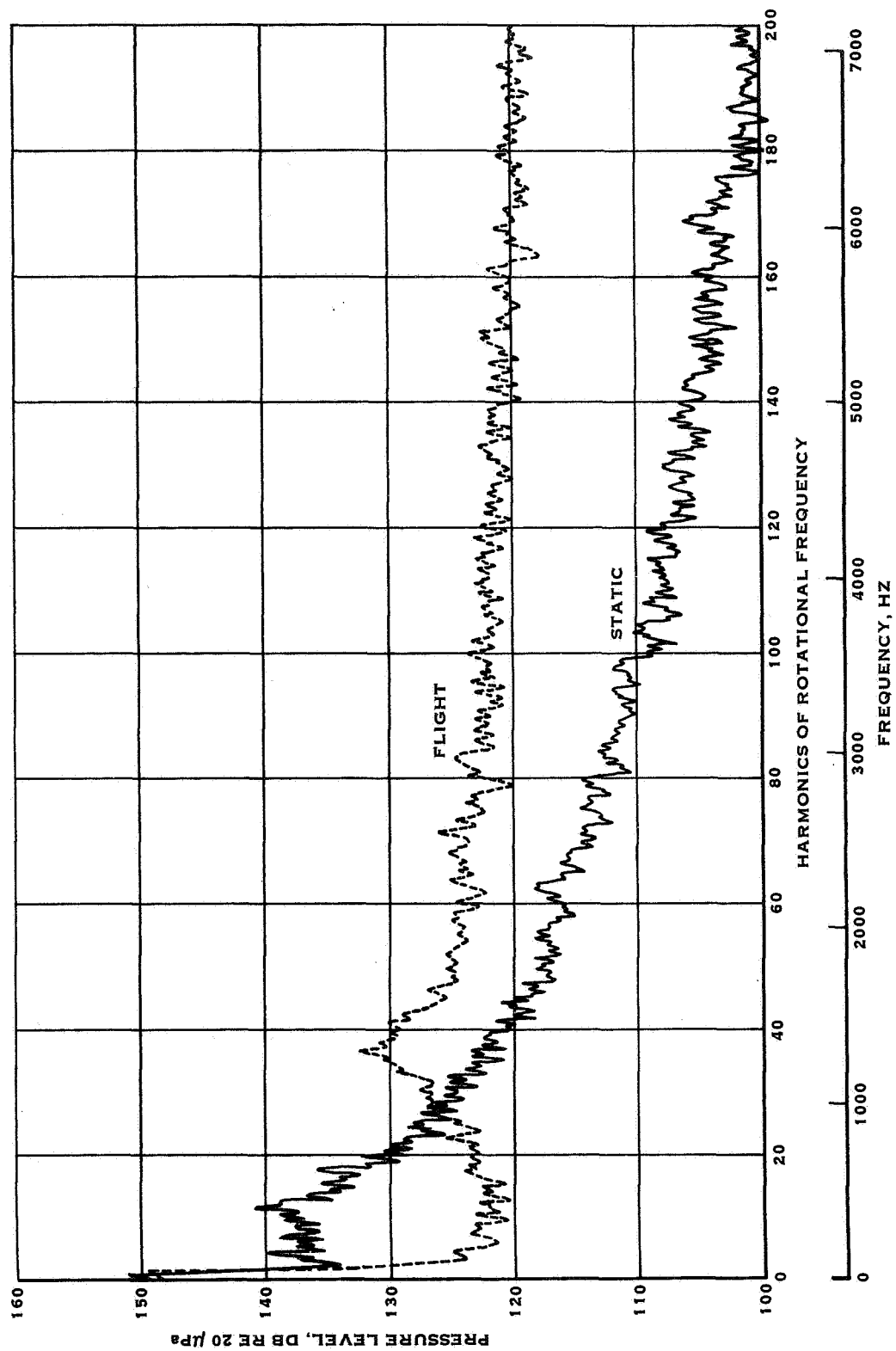


FIGURE 14. BLADE SURFACE PRESSURE SPECTRA AT THE 94% RADIUS DURING A 97.5% RPM
TAKE-OFF (RUN 1) 200 ORDERS ANALYSIS

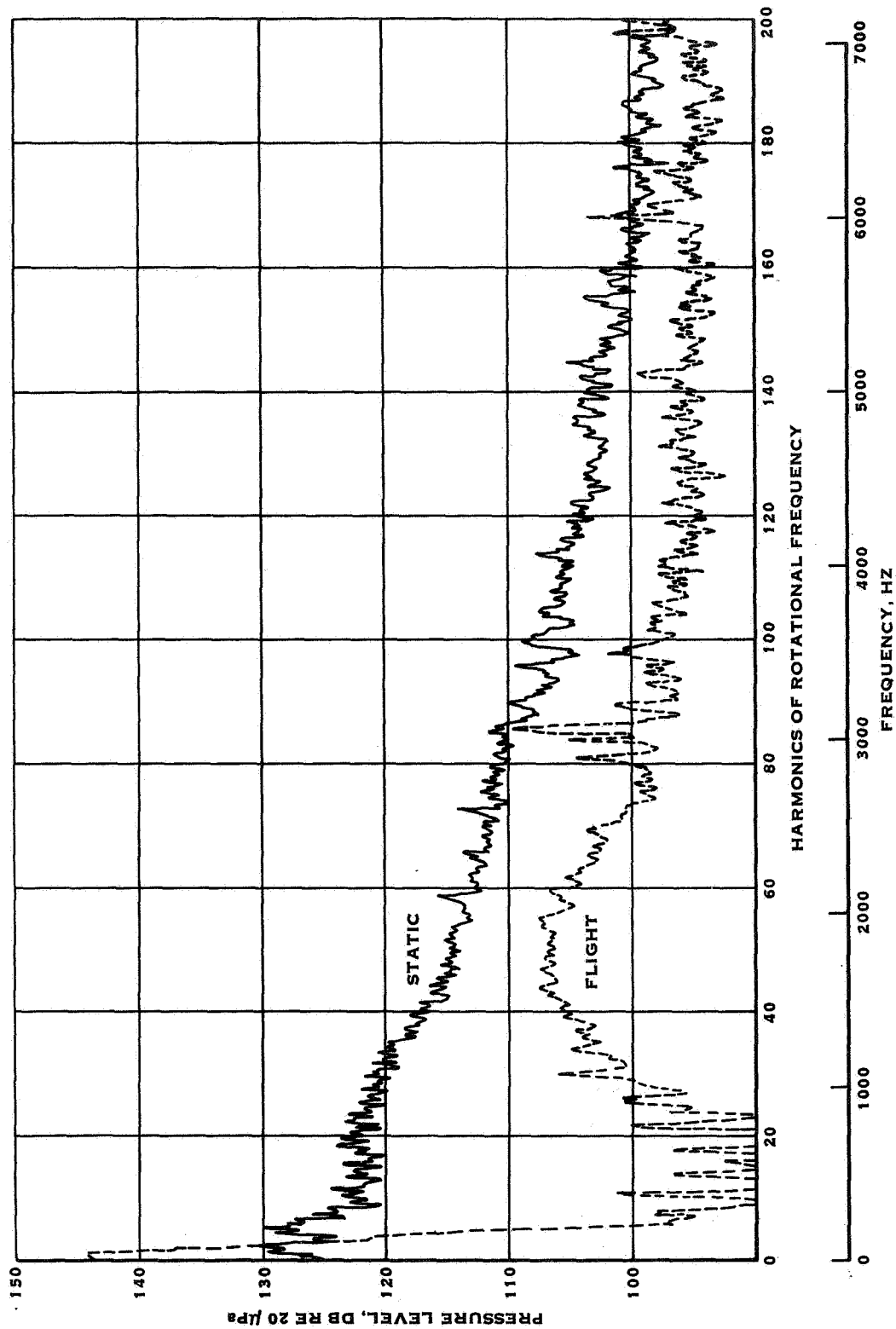


FIGURE 15. BLADE SURFACE PRESSURE SPECTRA AT THE 77% RADIUS DURING A 97.5% RPM TAKE-OFF (RUN 1). 200 ORDERS ANALYSIS

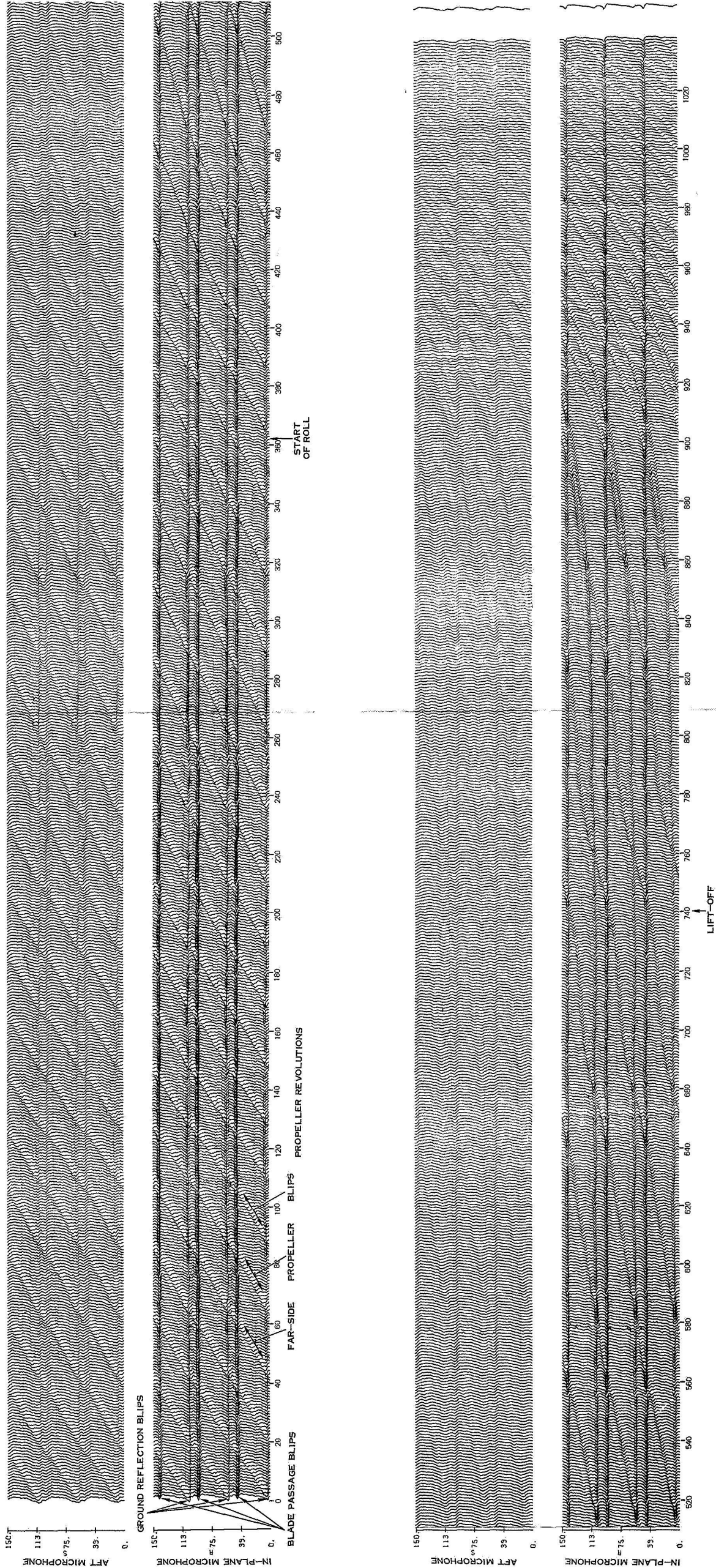


FIGURE 16. WING-TIP MICROPHONE TIME HISTORY PLOT
FOR A 97.5% RPM TAKE-OFF (RUN1)

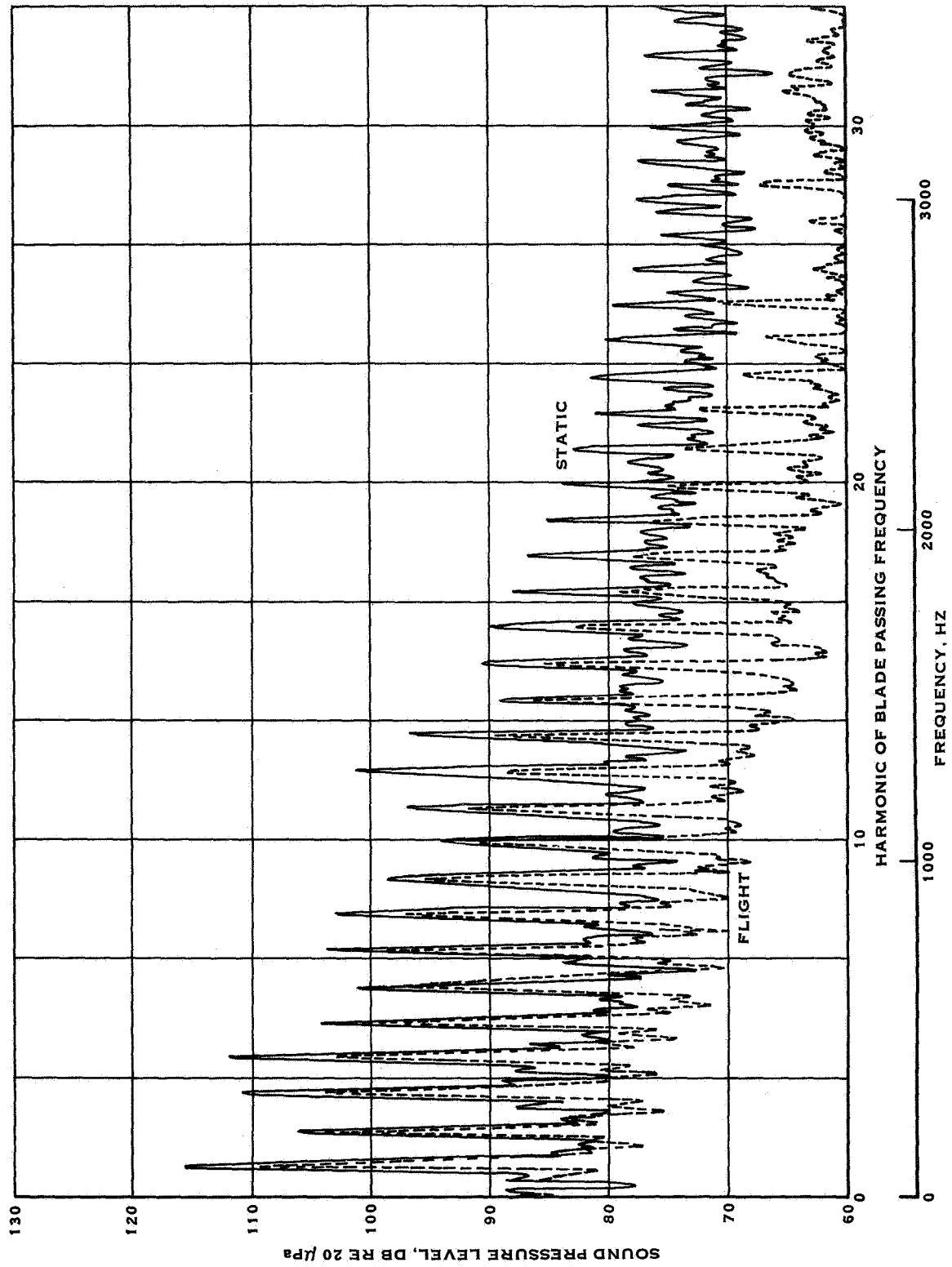


FIGURE 17. IN-PLANE MICROPHONE SPECTRA FOR A 97.5% RPM TAKE-OFF (RUN 1)

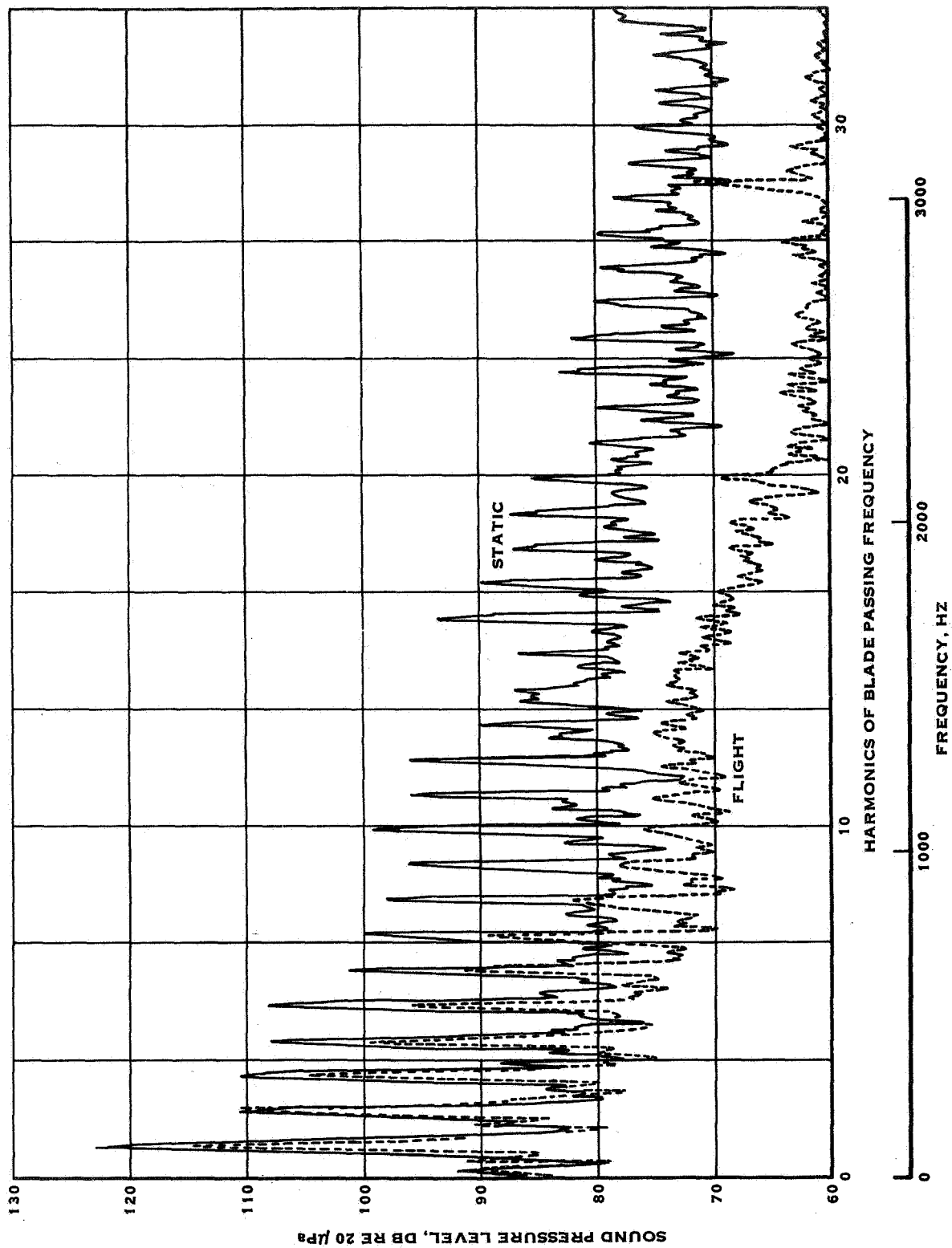


FIGURE 18. AFT MICROPHONE SPECTRA FOR A 97.5% RPM TAKE-OFF. (RUN 1)

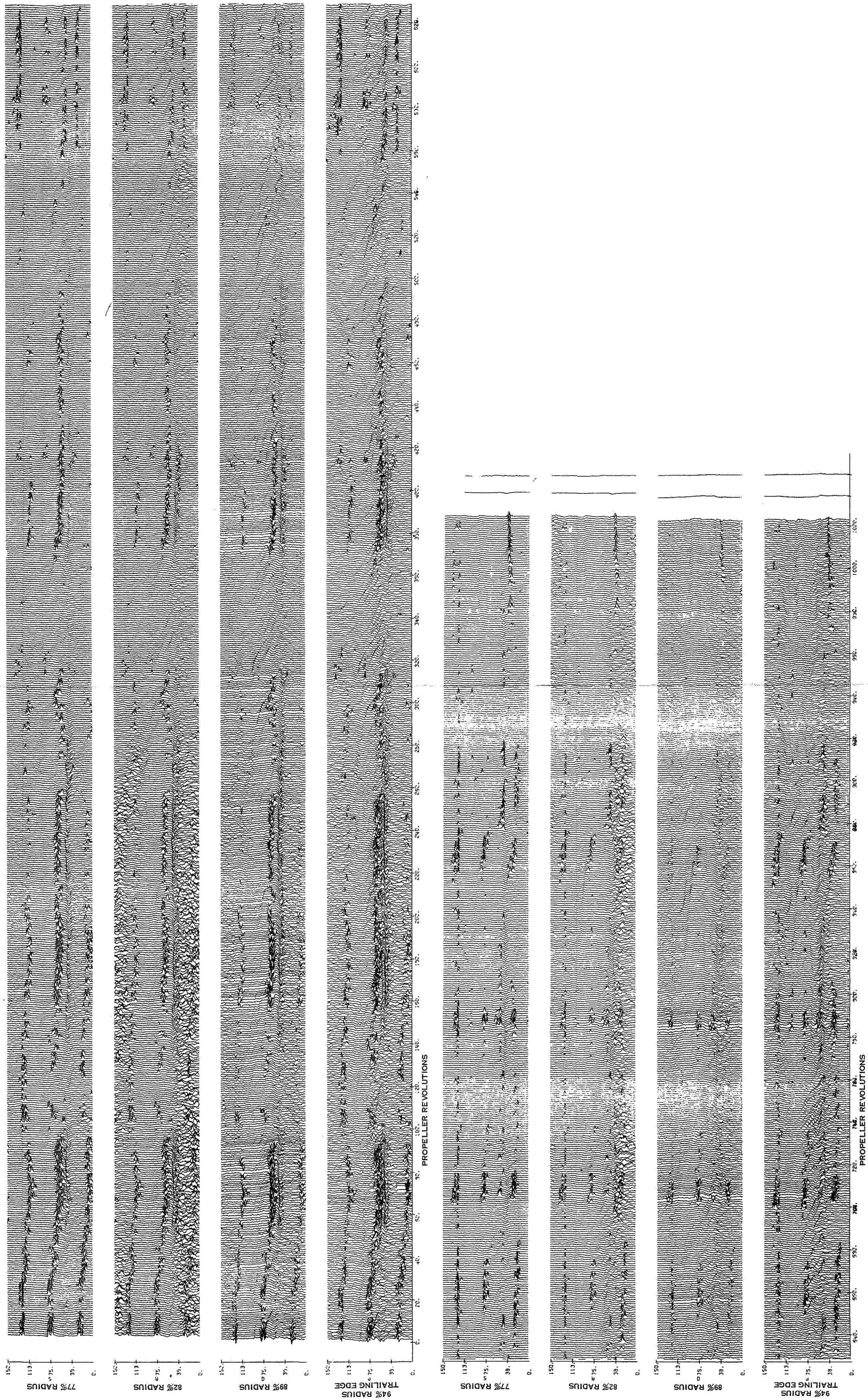


FIGURE 19. BLADE SURFACE PRESSURE TIME HISTORY PLOT

97.5% RPM AND 351 KW, STATIC CONDITION. (RUN 2S)

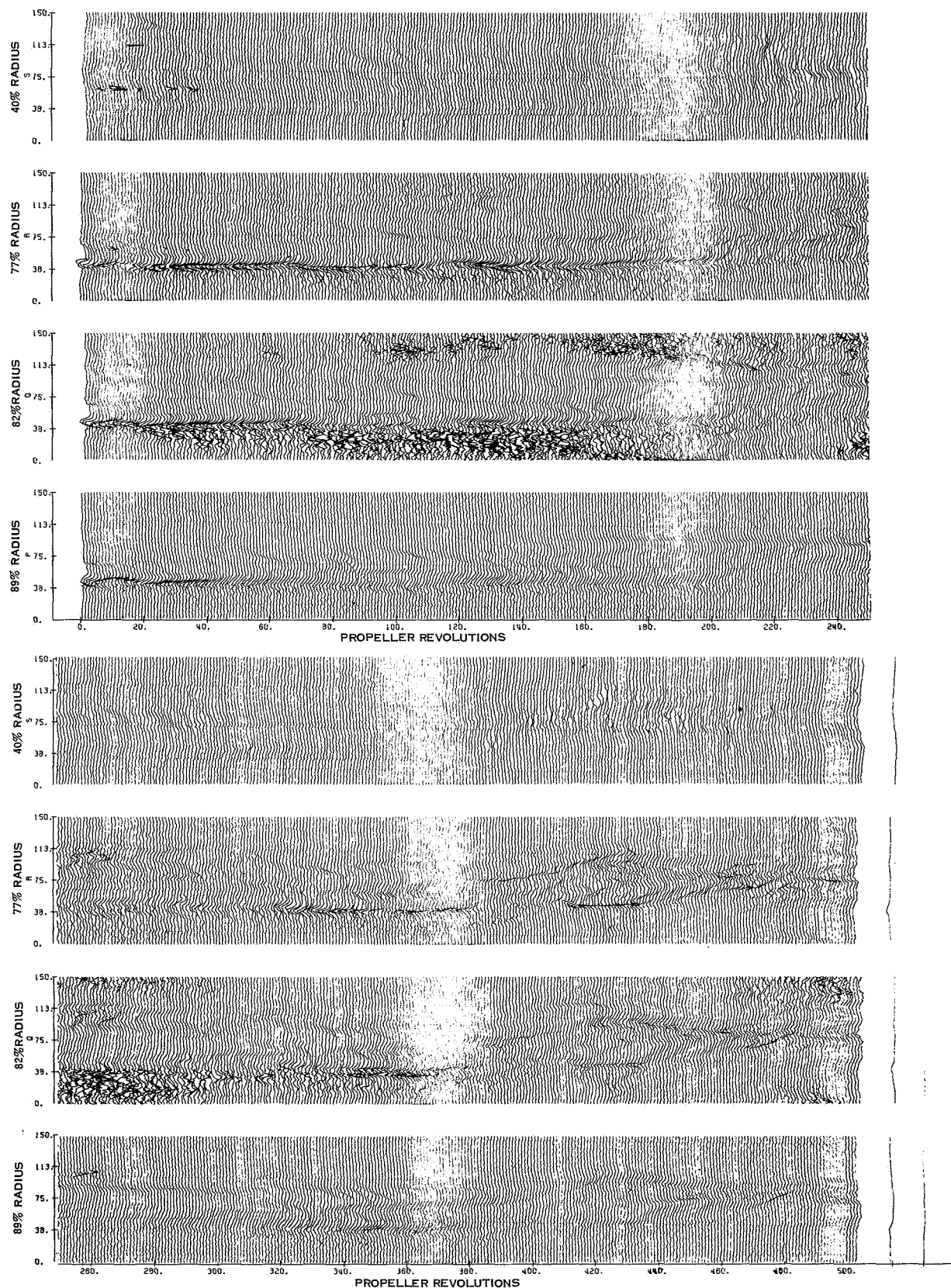


FIGURE 20. BLADE SURFACE PRESSURE TIME HISTORY PLOT
97.5 RPM, 256KW, STATIC CONDITION (RUN 4S)

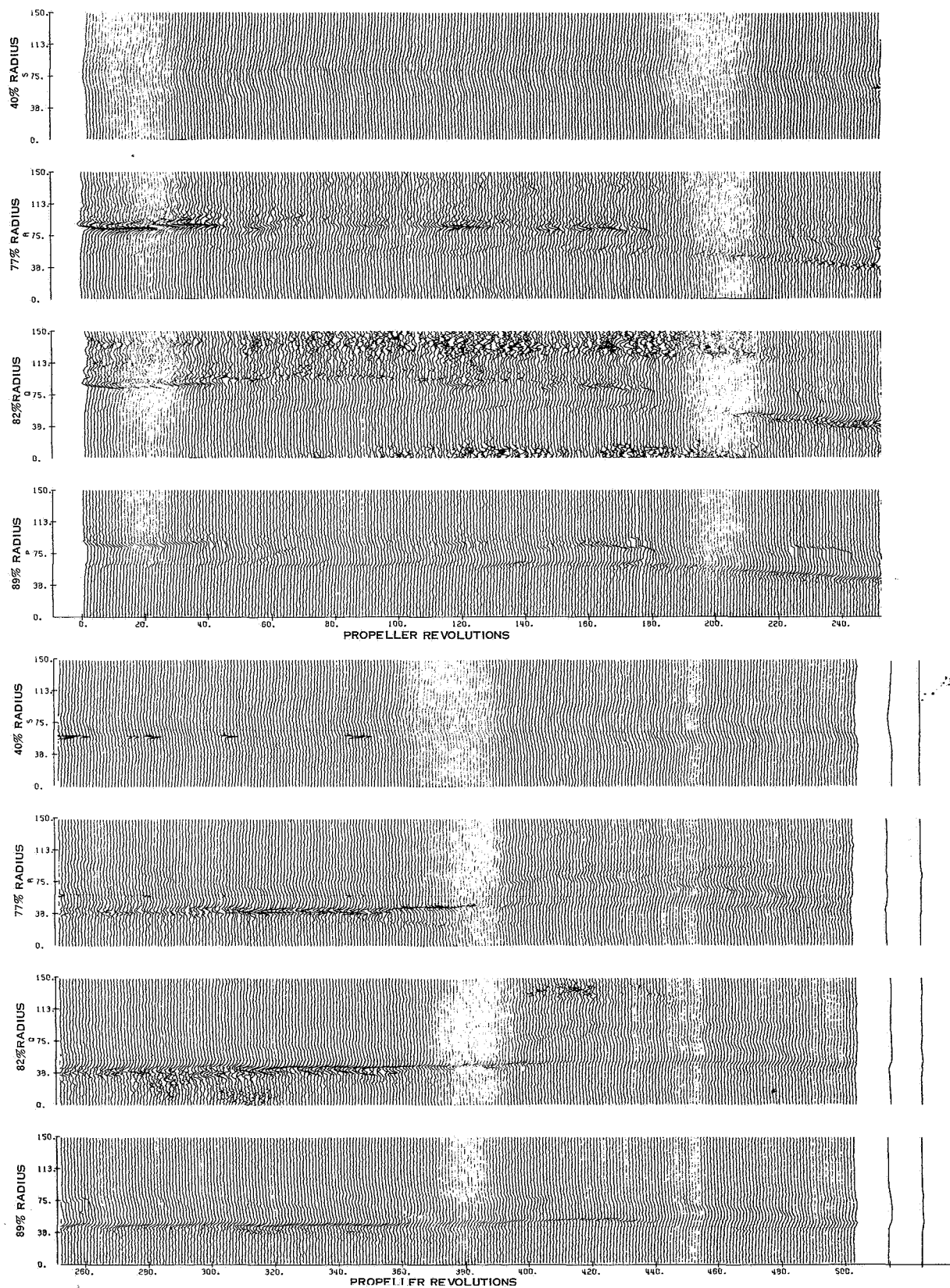
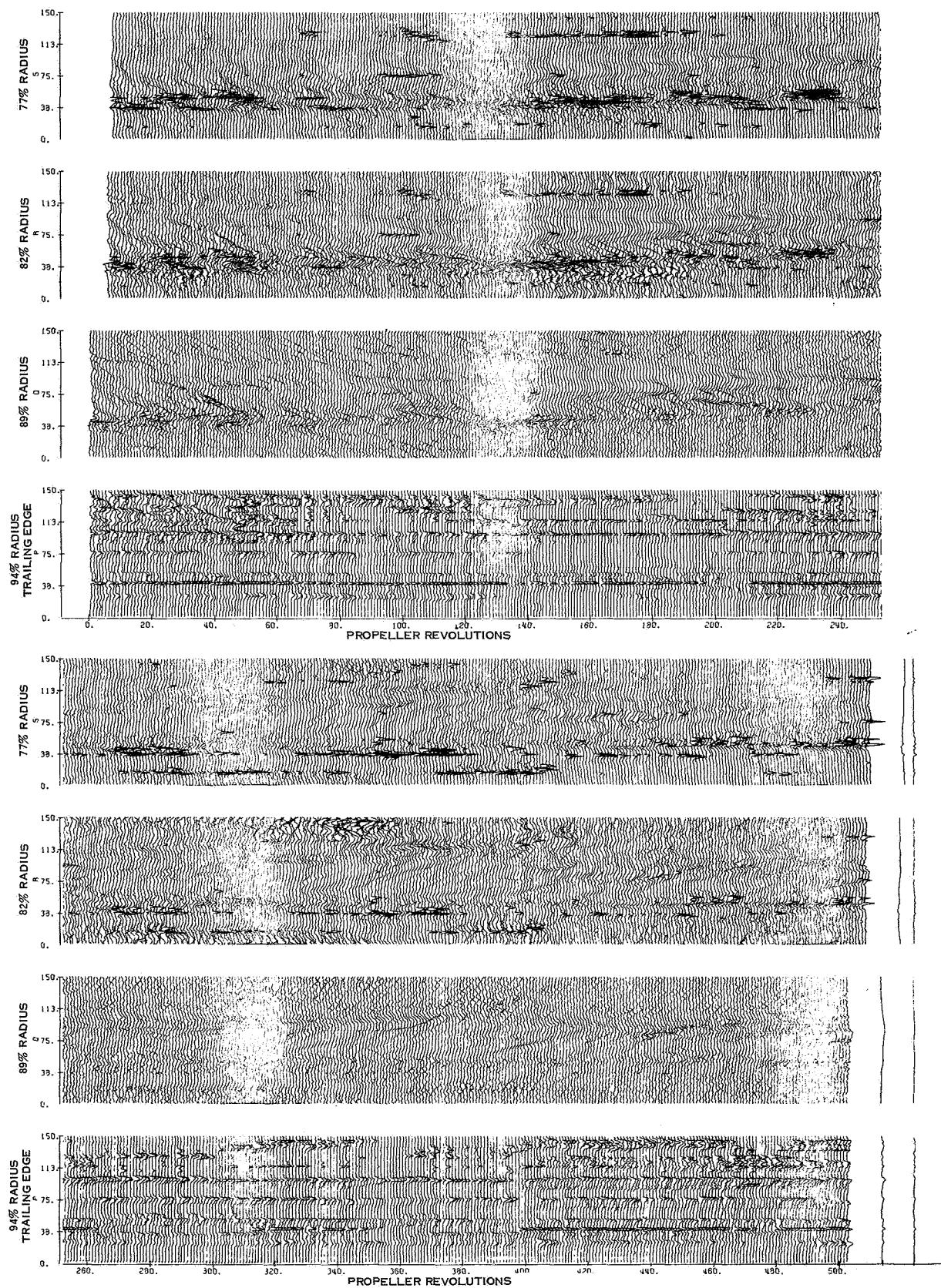


FIGURE 21. BLADE SURFACE PRESSURE TIME HISTORY PLOT
97.5% RPM, 227 KW, STATIC CONDITION (RUN 6S)



**FIGURE 22. BLADE SURFACE PRESSURE TIME HISTORY PLOT
90% RPM, 265 KW, STATIC CONDITION (RUN 16S)**

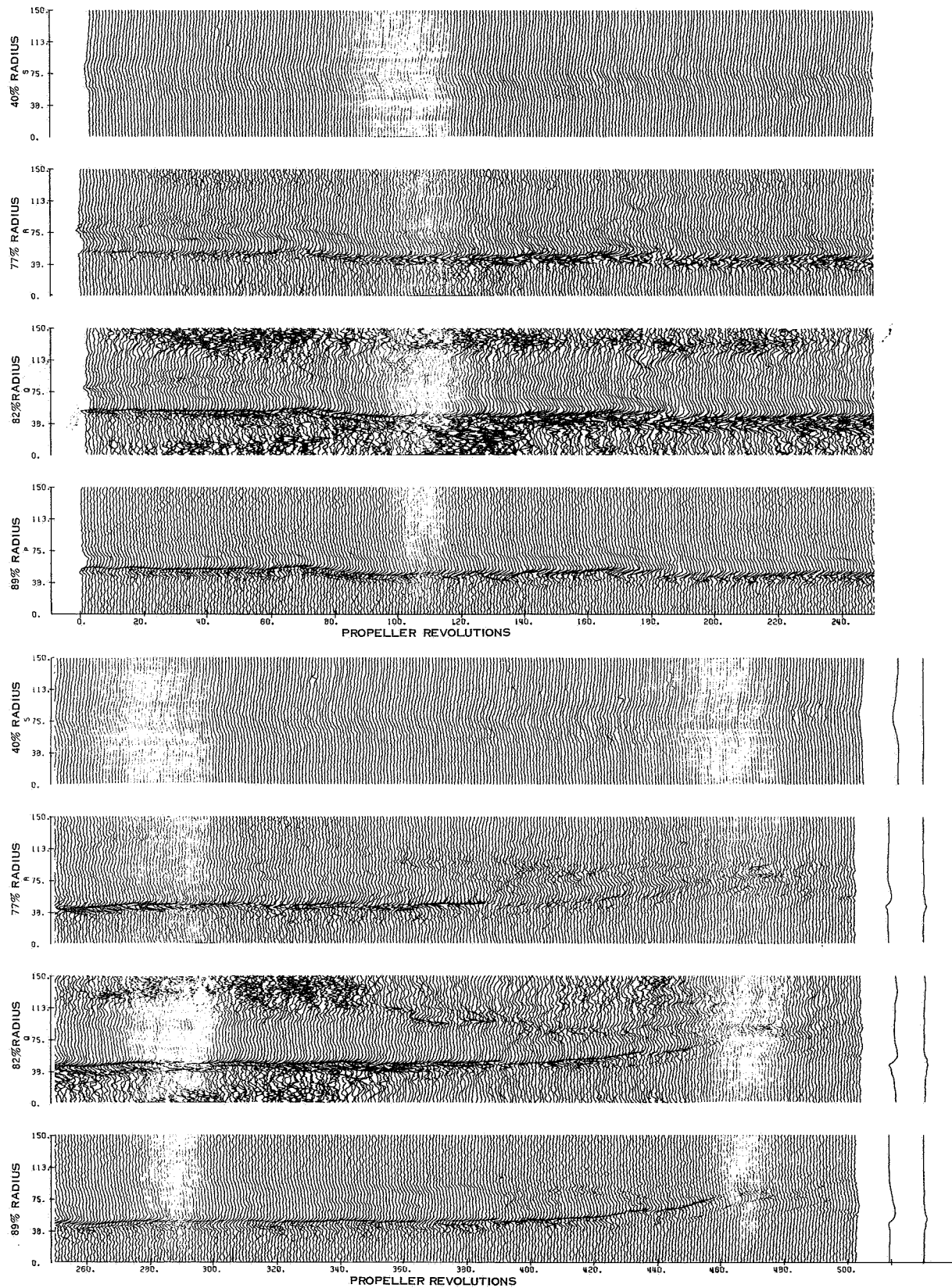


FIGURE 23. BLADE SURFACE PRESSURE TIME HISTORY PLOT,
90.5% RPM, 213 KW, STATIC CONDITION (RUN 17S)

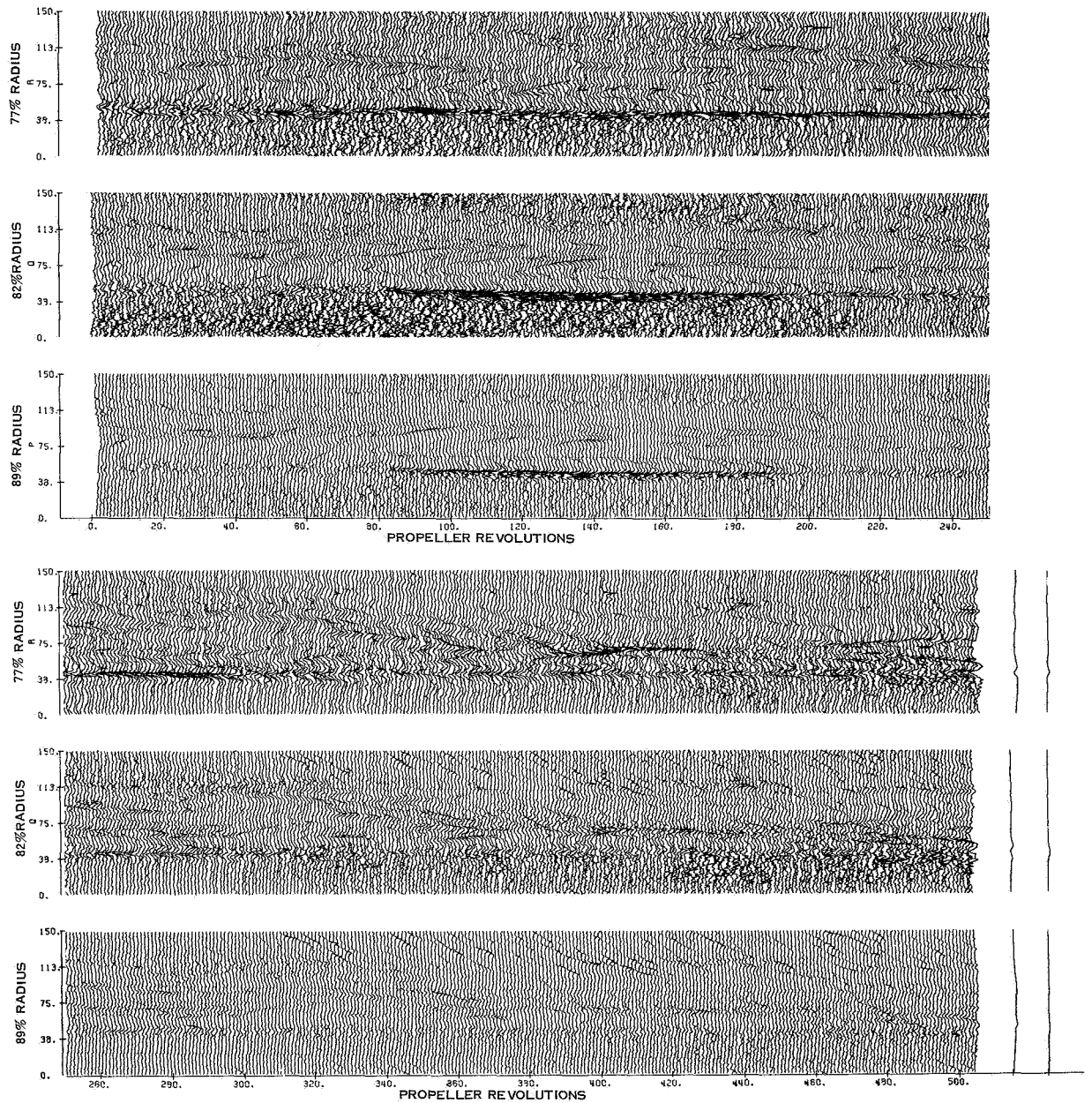


FIGURE 24. BLADE SURFACE PRESSURE TIME HISTORY PLOT,
80% RPM AND 253 KW, STATIC CONDITION (RUN 3S)

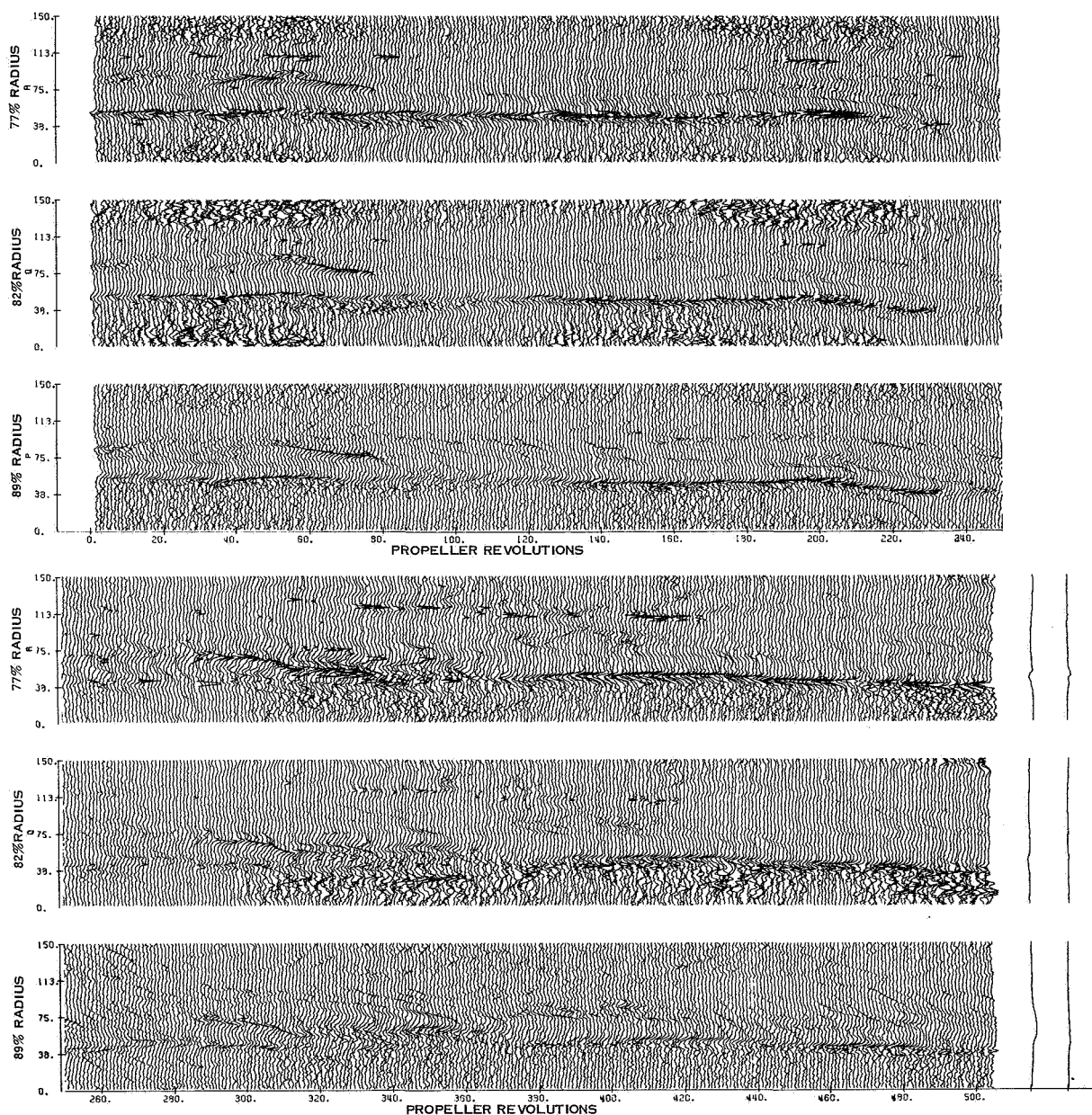


FIGURE 25. BLADE SURFACE PRESSURE TIME HISTORY PLOT,
80% RPM AND 210 KW. STATIC CONDITION. (RUN 5S)

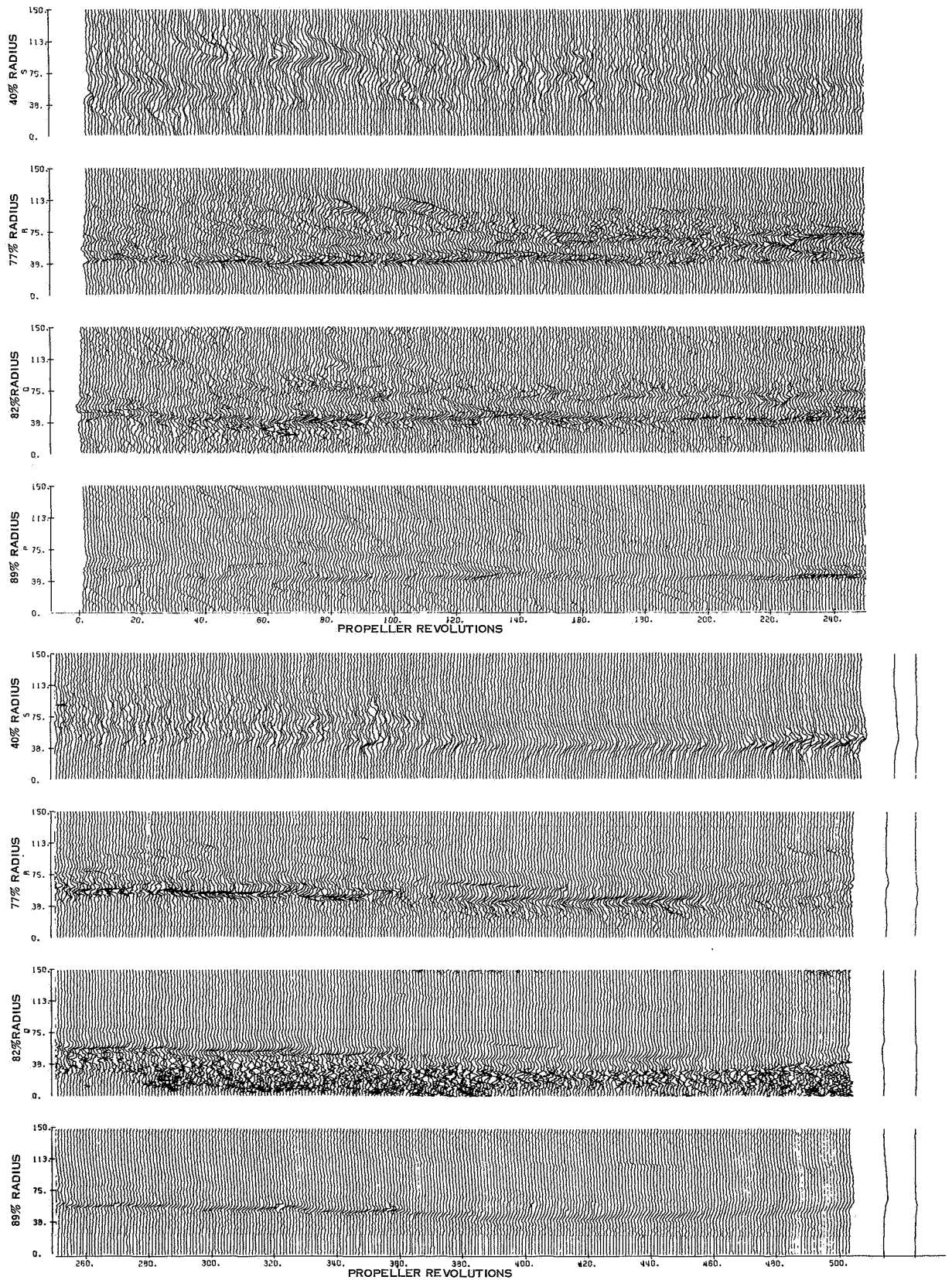


FIGURE 26. BLADE SURFACE PRESSURE TIME HISTORY PLOT
75% RPM AND 93 KW. STATIC CONDITION. (RUN 21S)

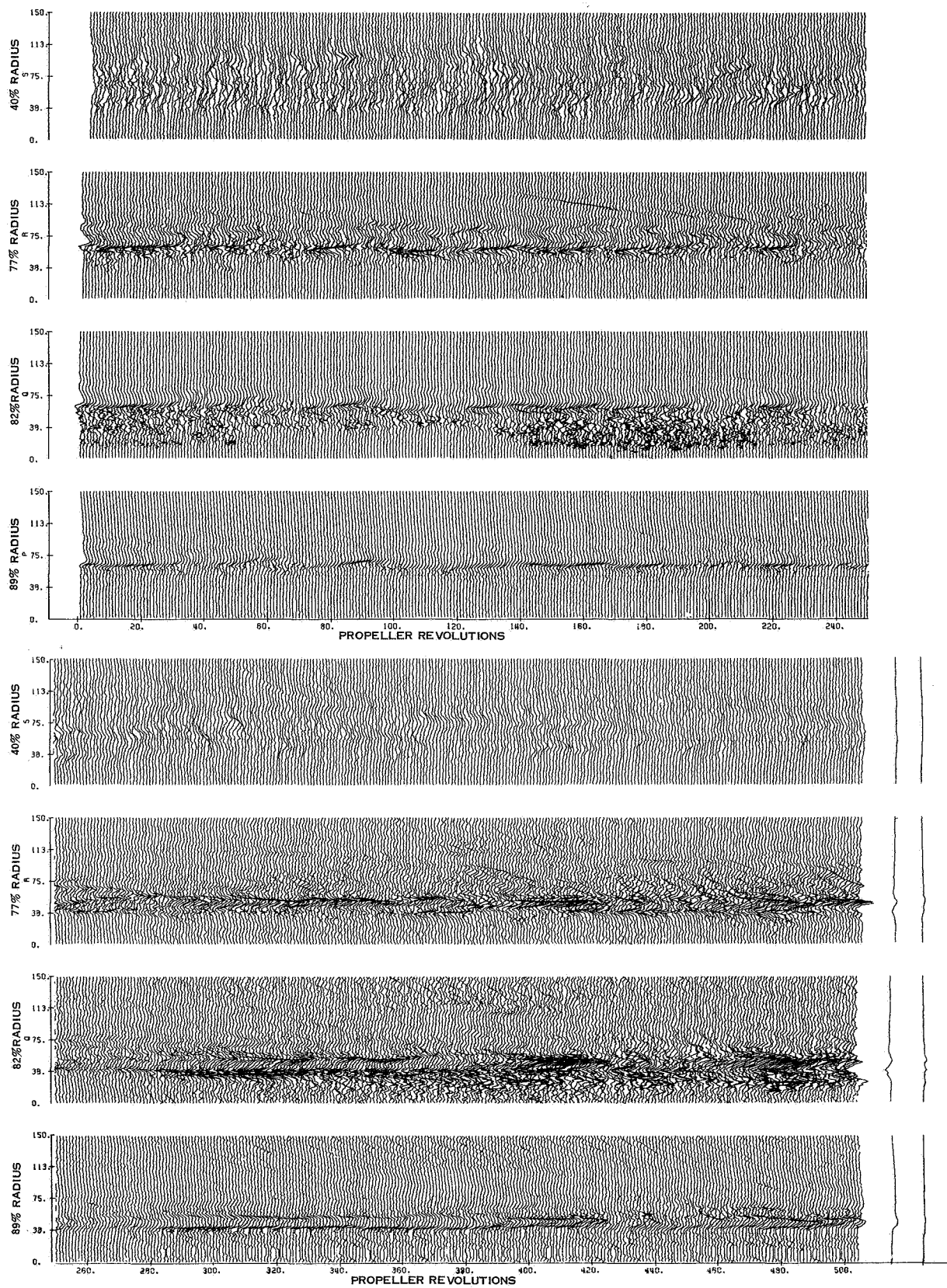


FIGURE 27. BLADE SURFACE PRESSURE TIME HISTORY PLOT
72.5% RPM AND 75 KW, STATIC CONDITION. (RUN 22S)

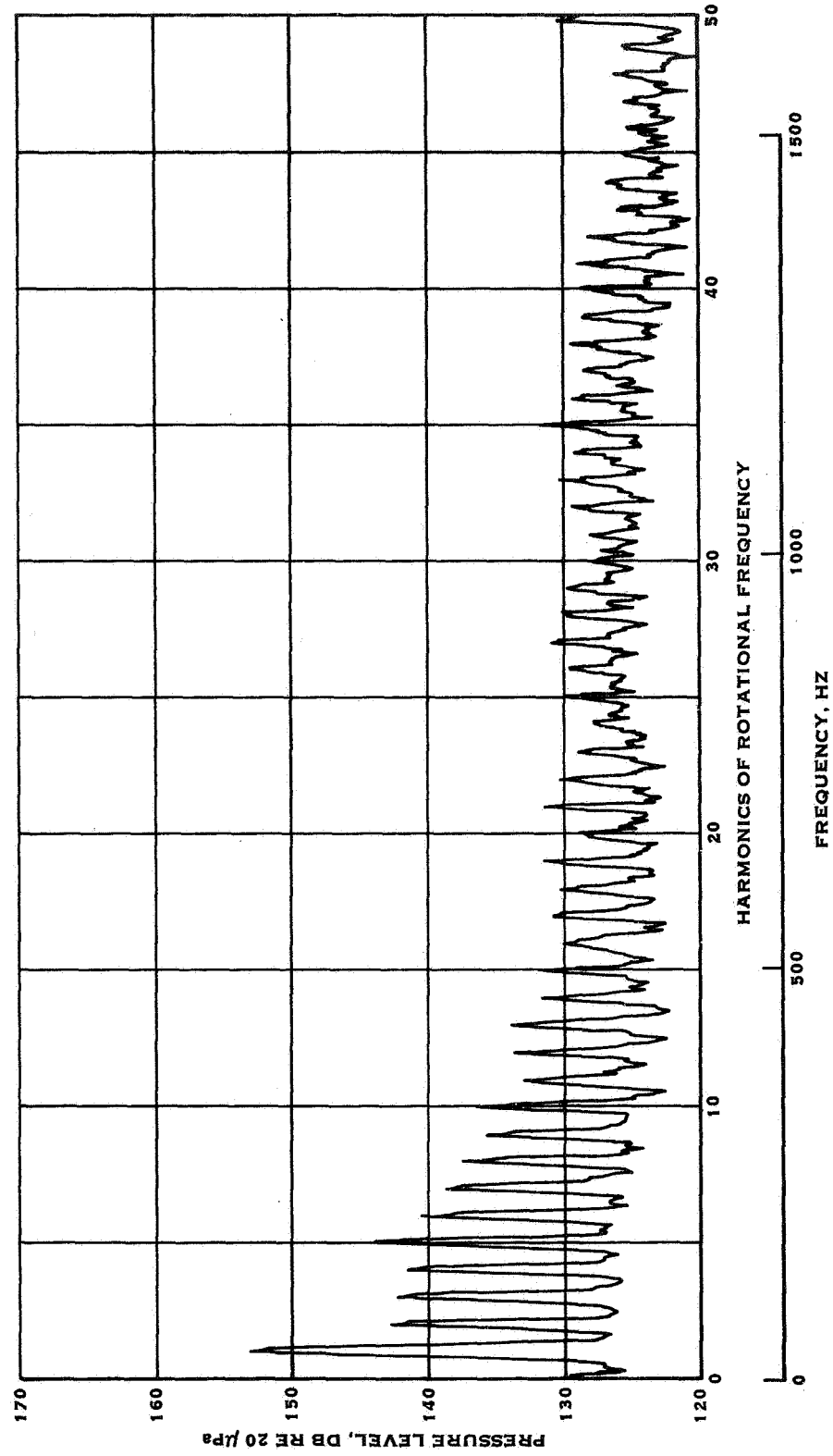


FIGURE 28. 50-ORDER ANALYSIS OF BLADE SURFACE PRESSURES FOR 90% RPM AND 265 KW, STATIC CONDITION (RUN 16S) - 77% RADIUS

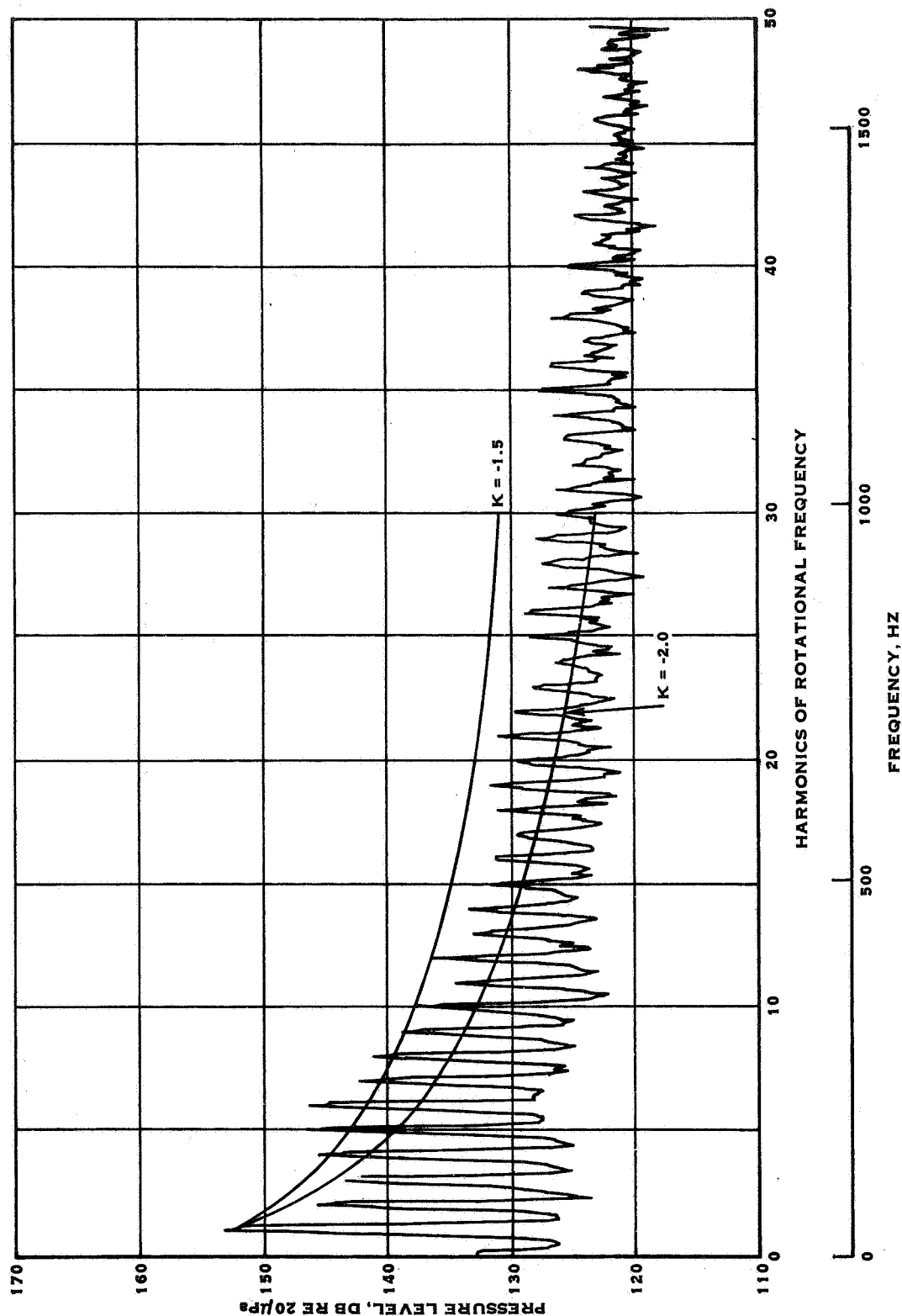


FIGURE 29. 50-ORDER ANALYSIS OF BLADE SURFACE PRESSURES FOR 90% RPM AND 265 KW, STATIC CONDITION (RUN 16S) - 82% RADIUS

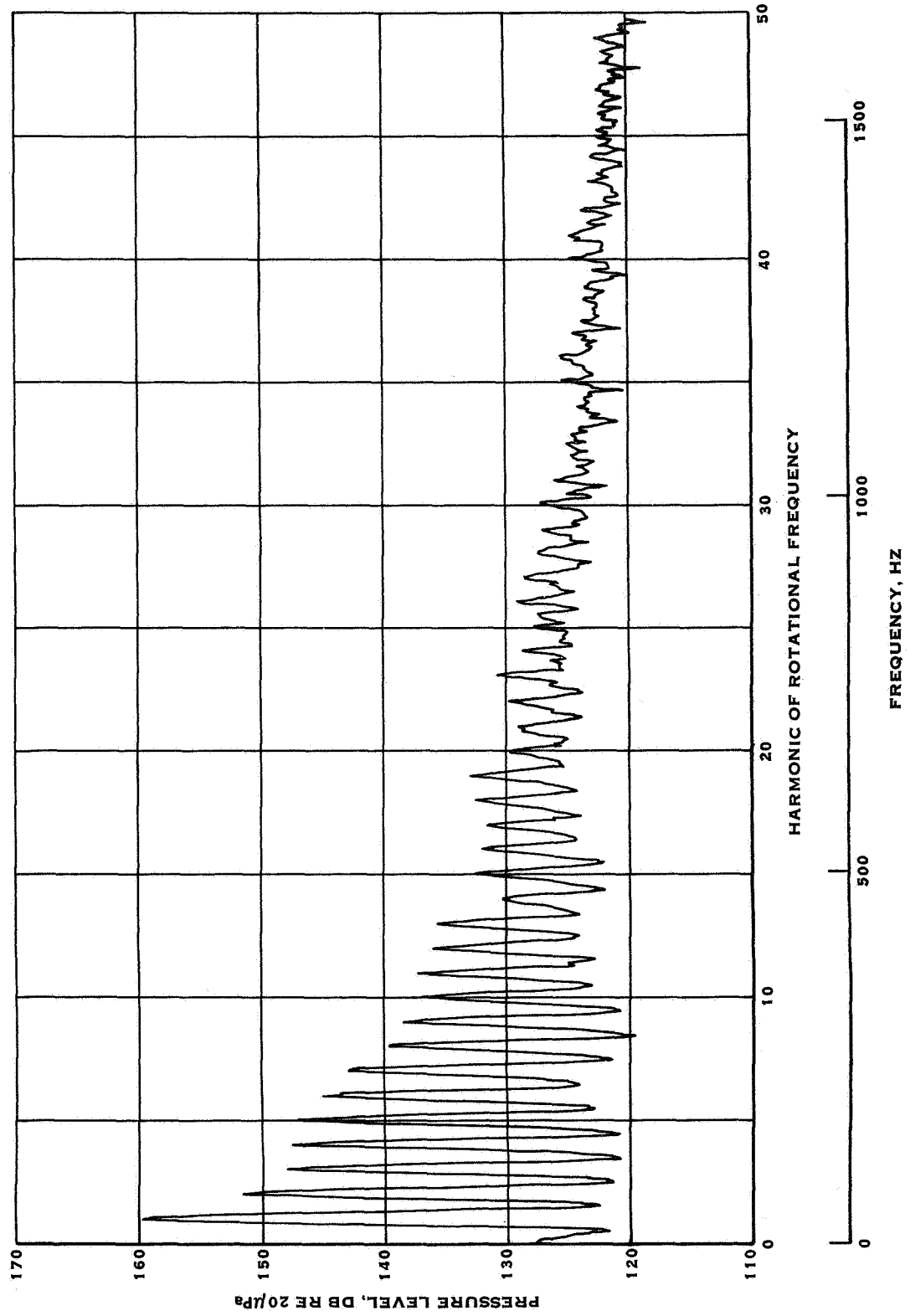


FIGURE 30. 50 ORDER ANALYSIS OF BLADE SURFACE PRESSURES FOR 90% RPM AND 265 KW,
STATIC CONDITION (RUN 16S) - 89% RADIUS

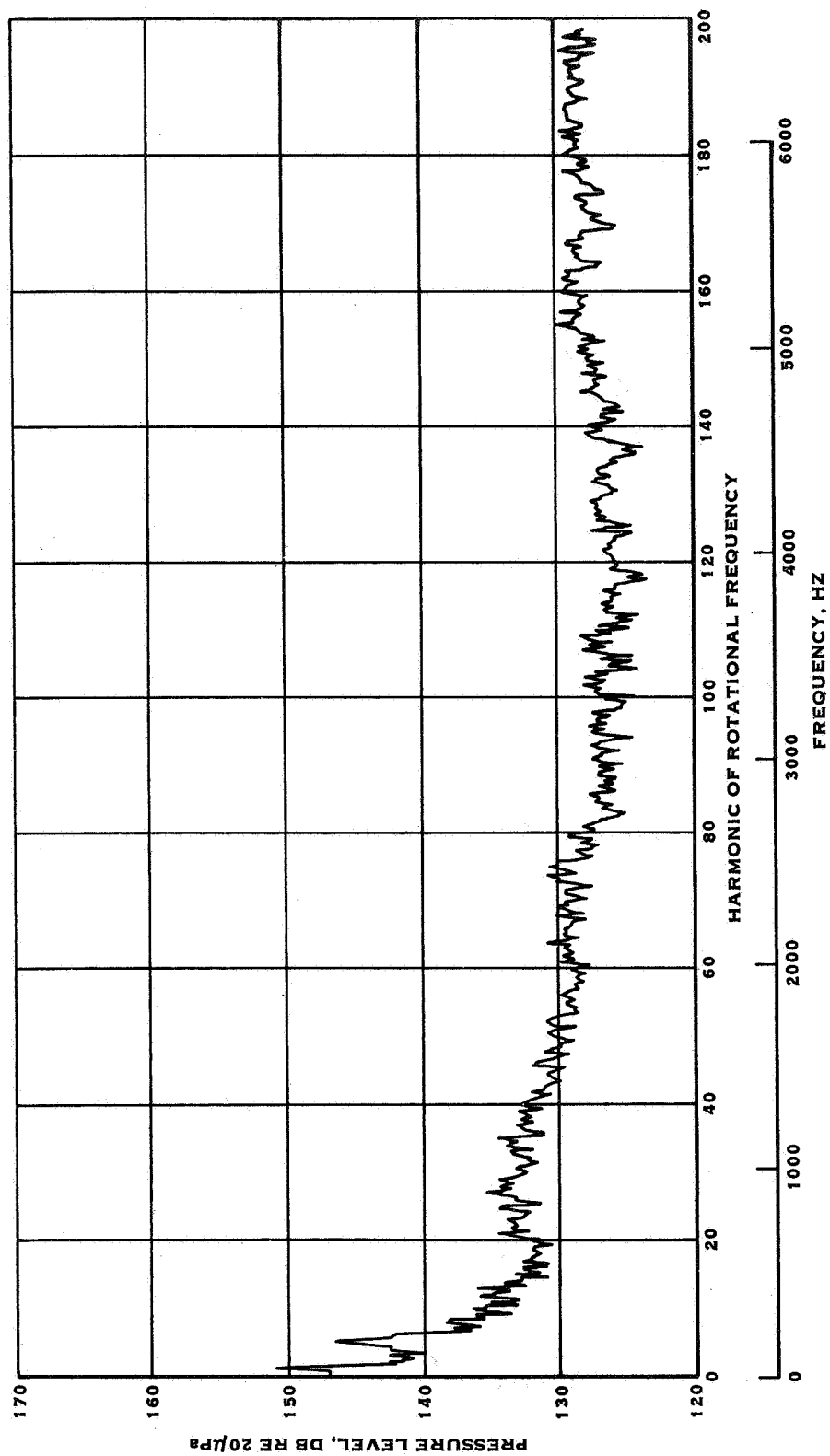


FIGURE 31. 200-ORDER ANALYSIS OF BLADE SURFACE PRESSURE FOR 90% RPM AND 265 KW,
STATIC CONDITION (RUN 16S) - 77% RADIUS

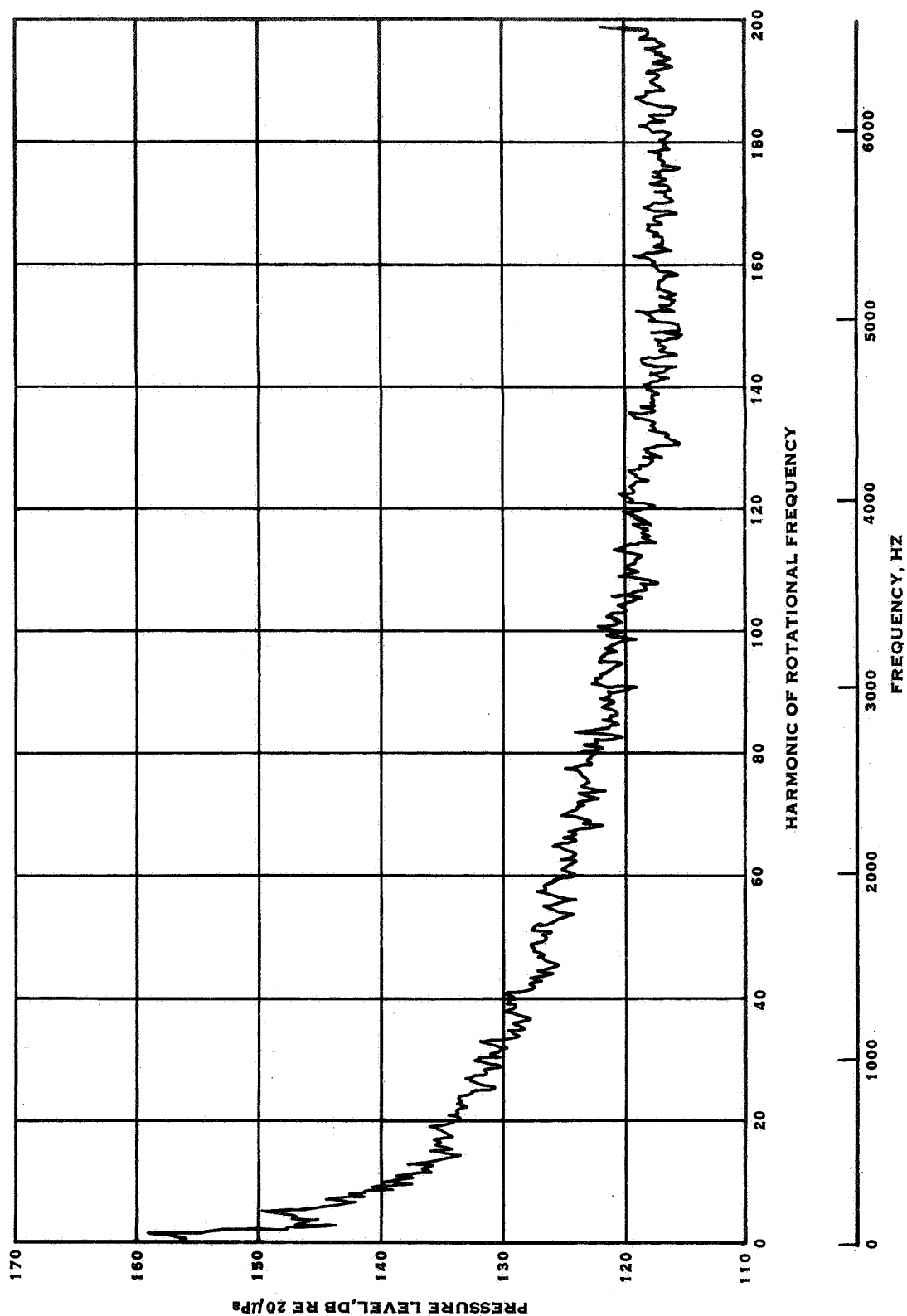


FIGURE 33. 200-ORDER ANALYSIS OF BLADE SURFACE PRESSURE FOR 90% RPM AND 265 KW, STATIC CONDITION (RUN 16S) - 89% RADIUS

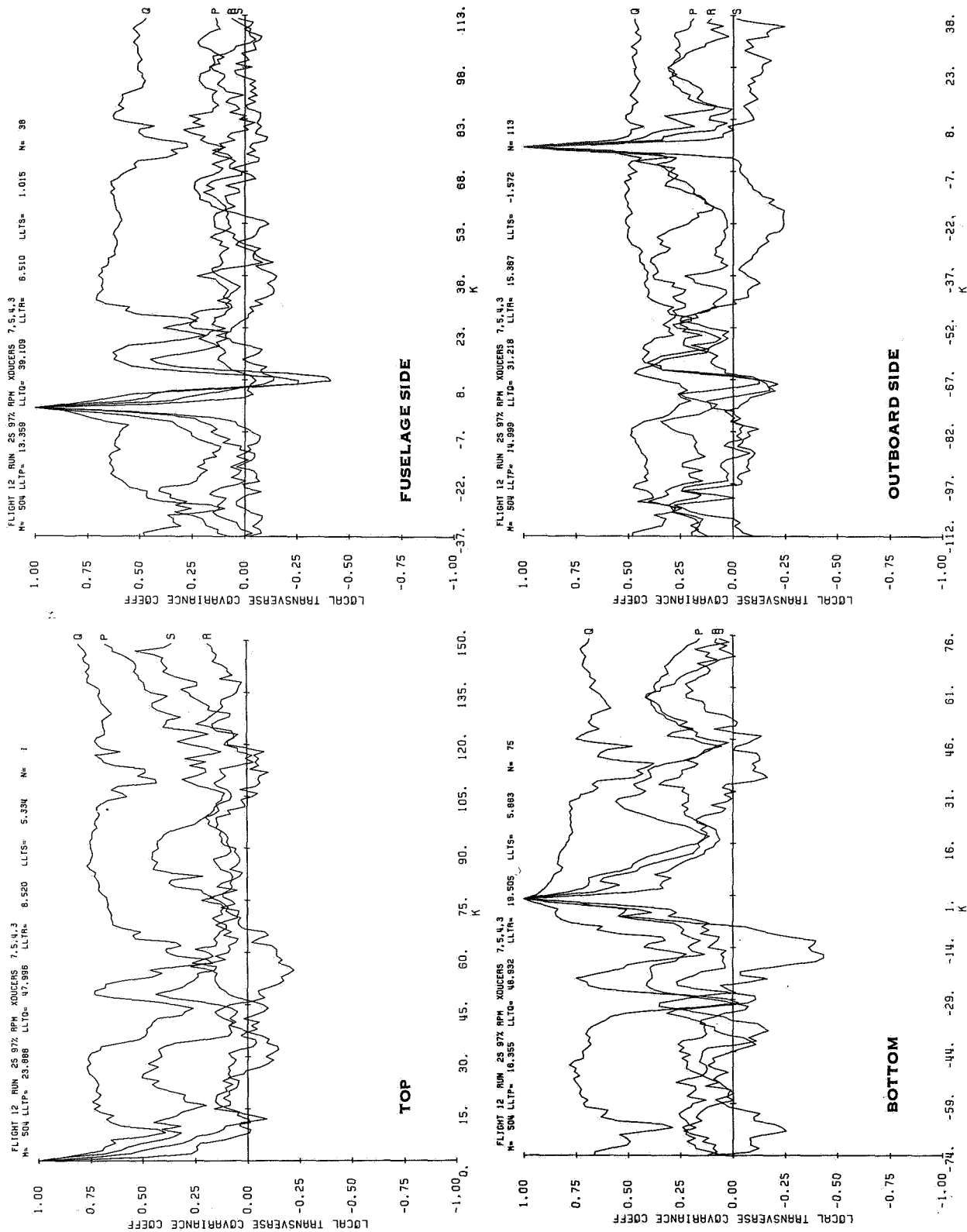


FIGURE 34. TRANSVERSE CORRELATION FUNCTIONS FOR RUN 25

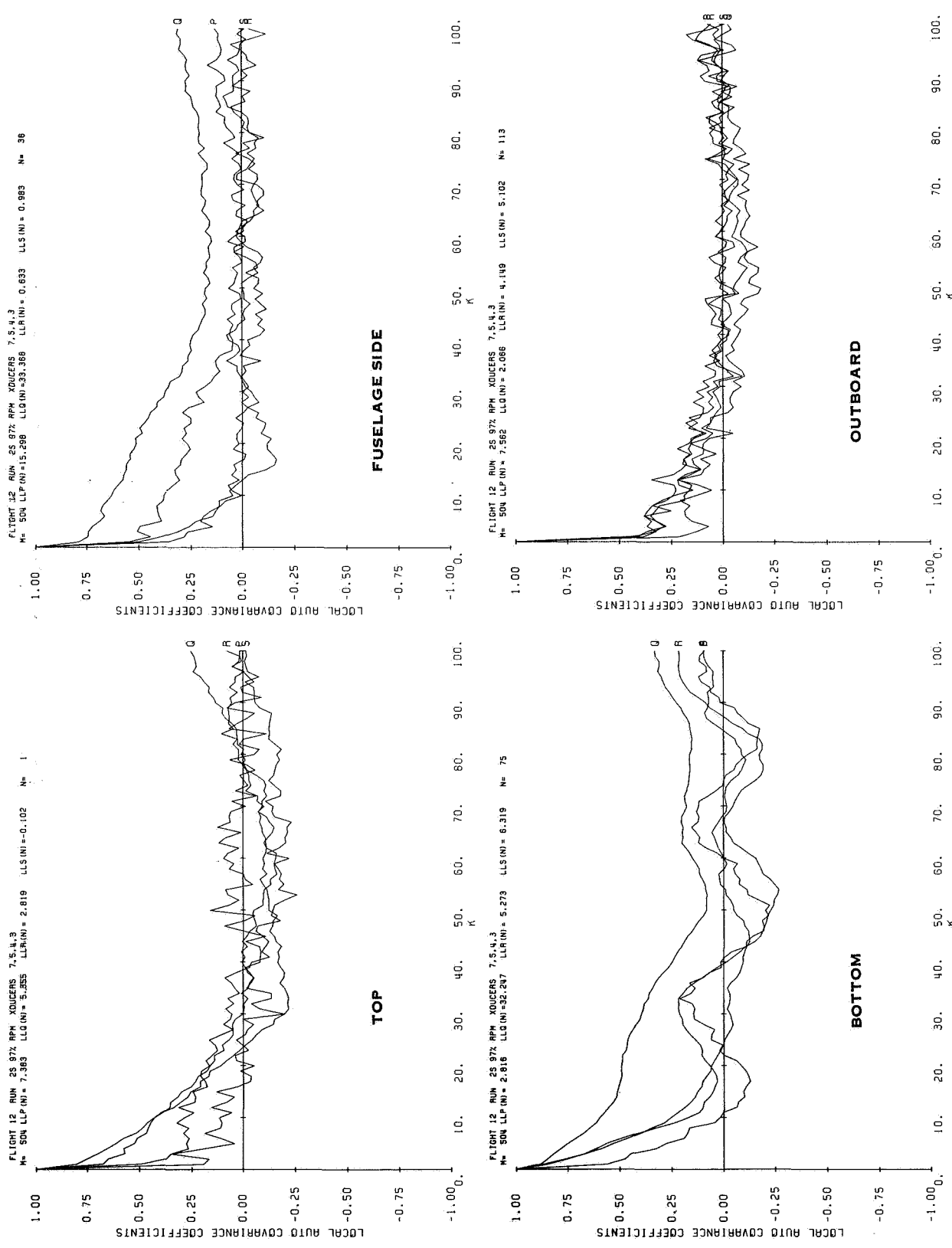


FIGURE 35. STREAMWISE CORRELATION FUNCTIONS FOR RUN 2S

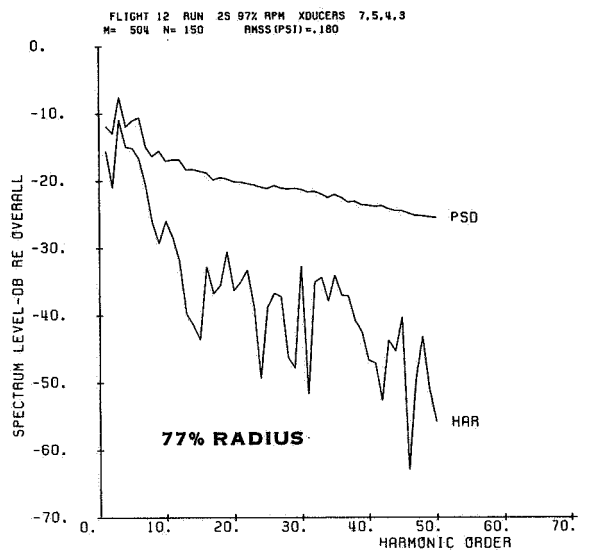
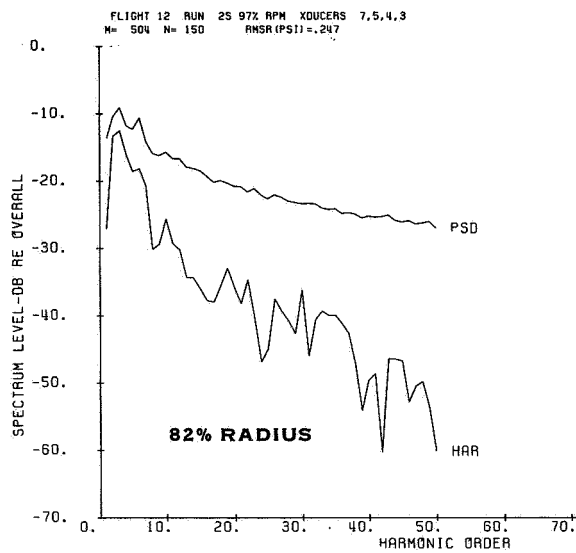
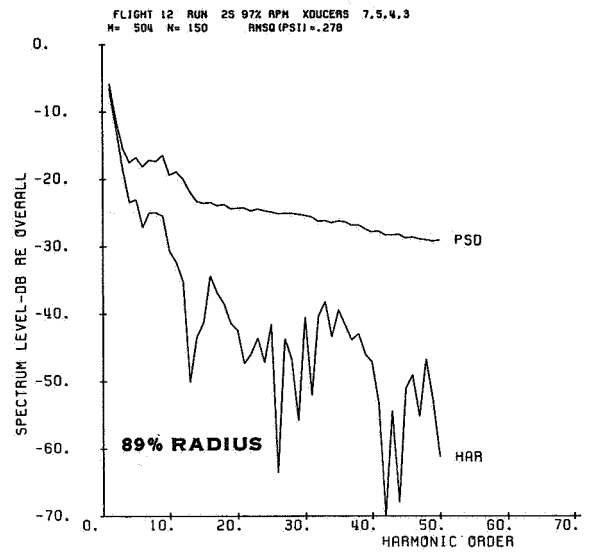
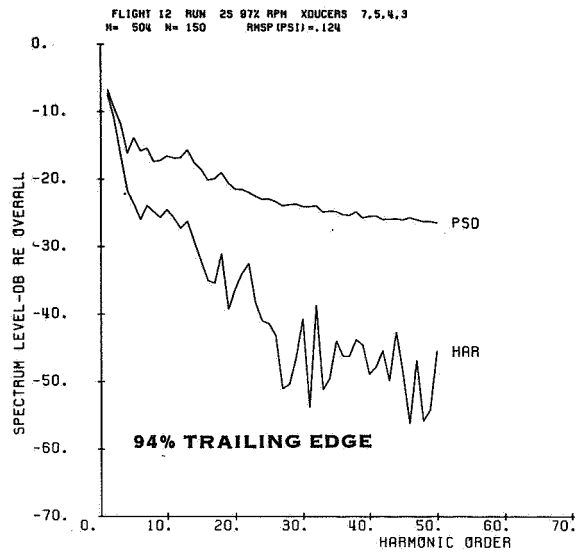


FIGURE 36. POWER SPECTRAL DENSITIES FOR RUN 25

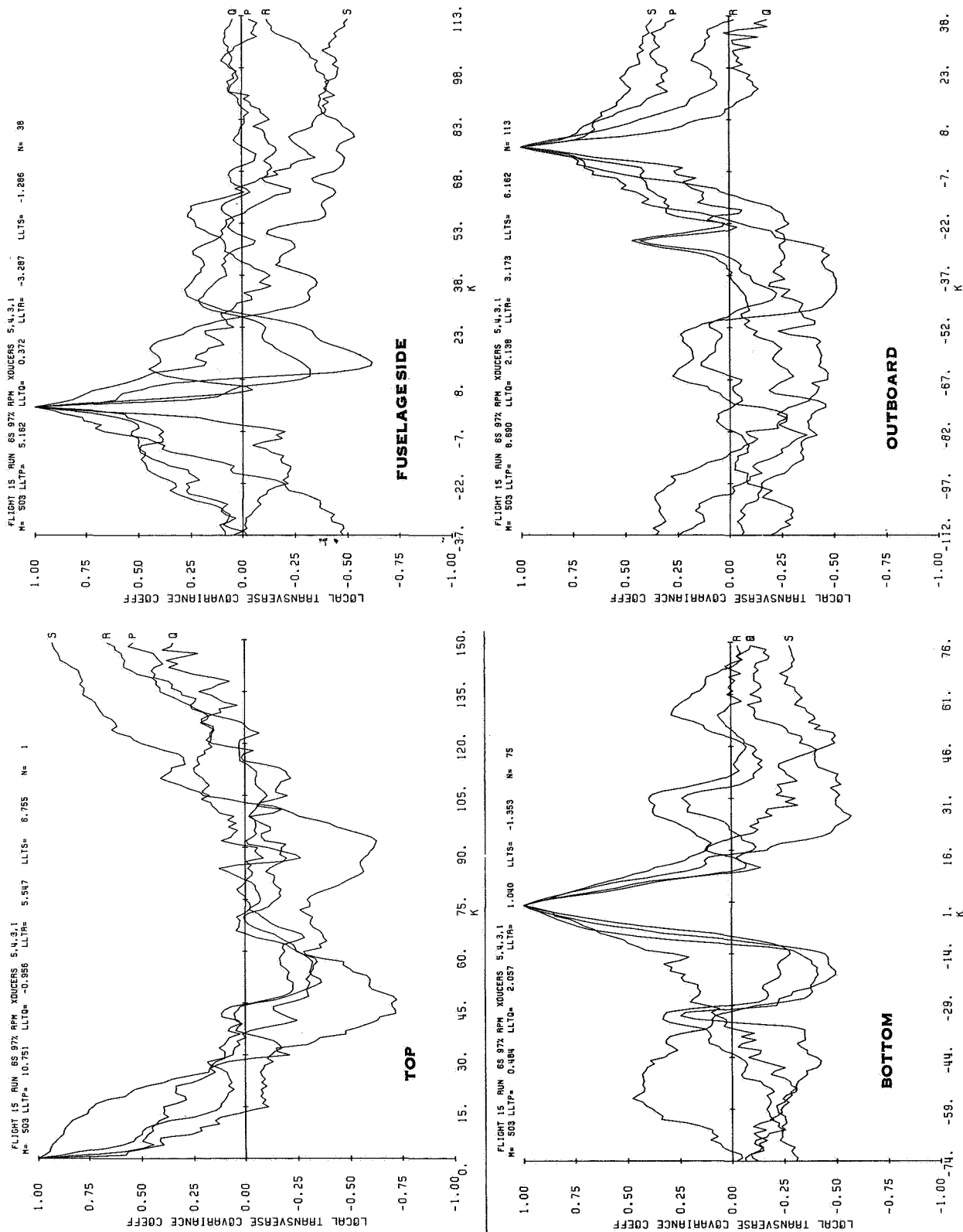


FIGURE 37. TRANSVERSE CORRELATION FUNCTIONS FOR RUN 6S

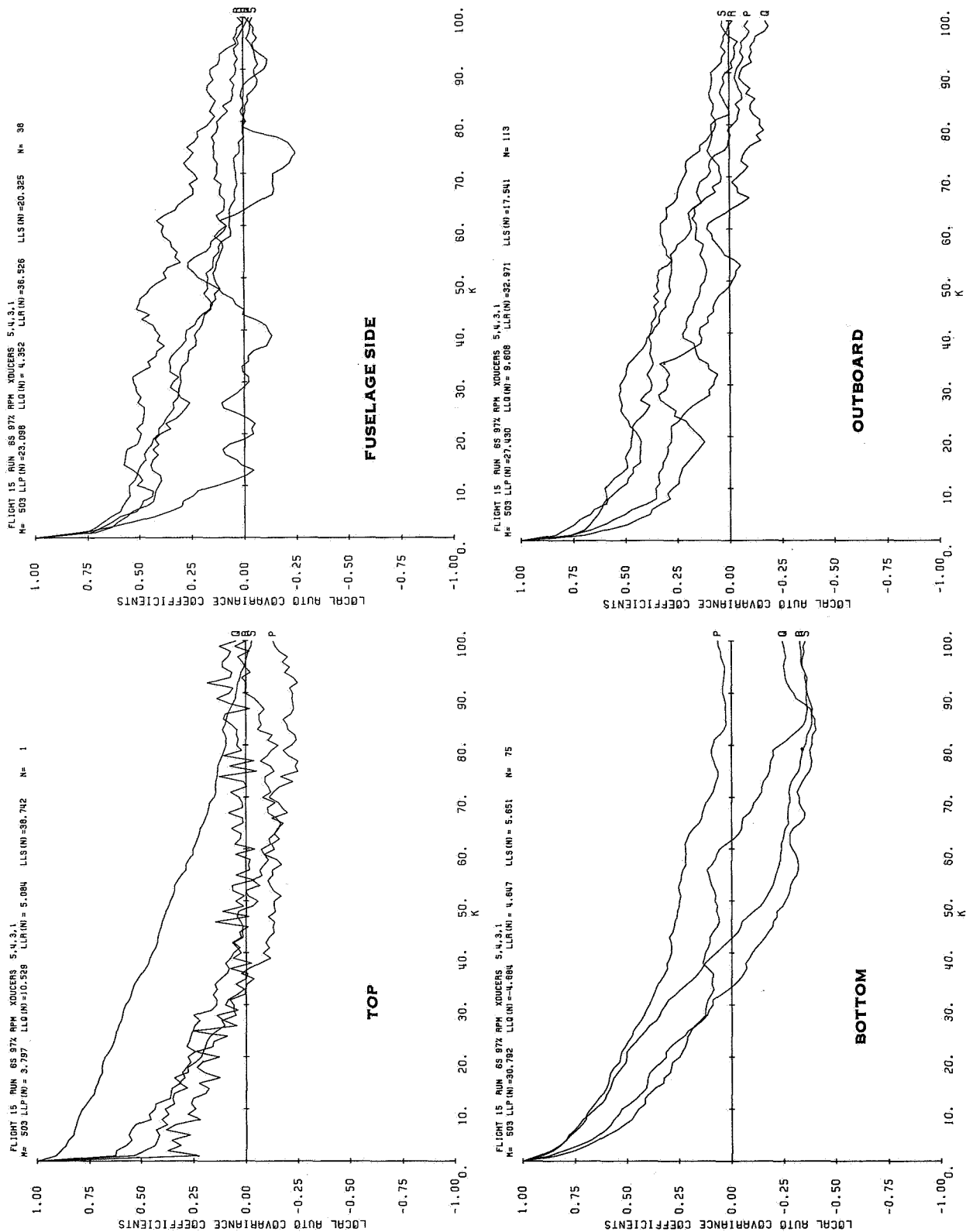


FIGURE 38. STREAMWISE CORRELATION FUNCTIONS FOR RUN 6S

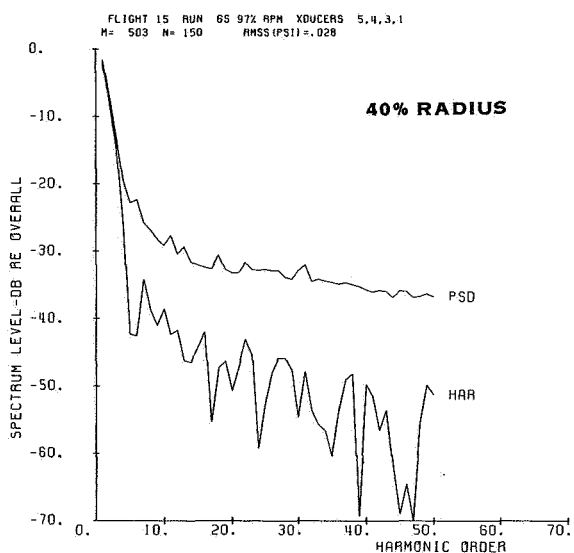
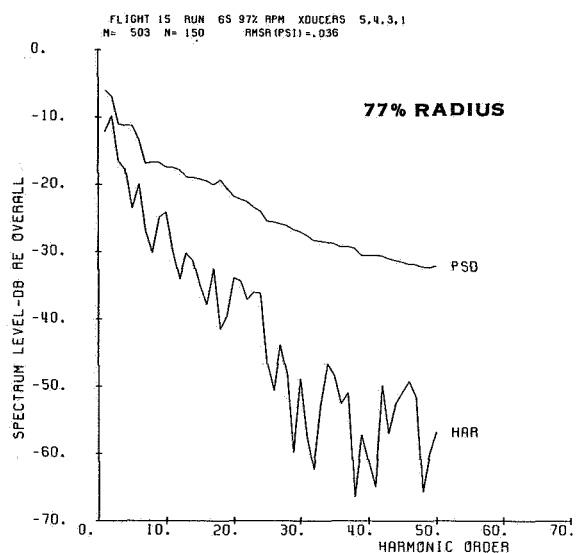
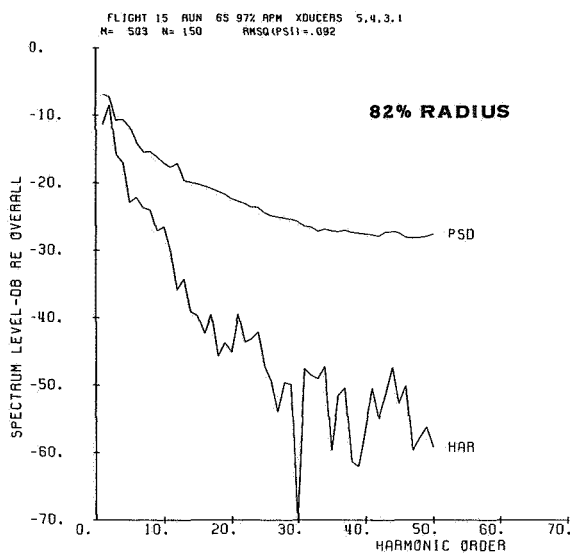
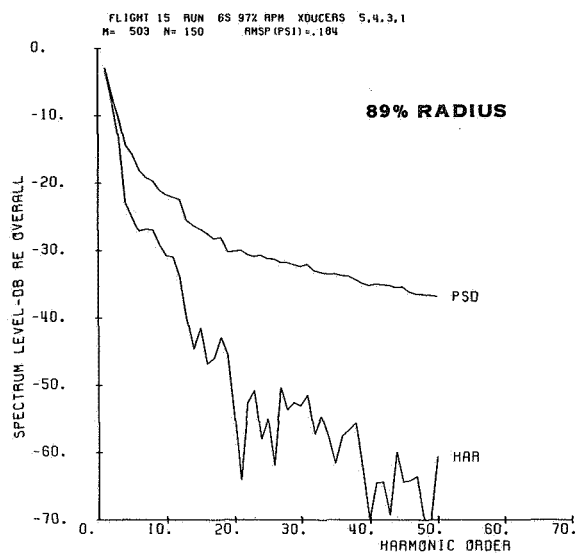


FIGURE 39. POWER SPECTRAL DENSITIES FOR RUN 65

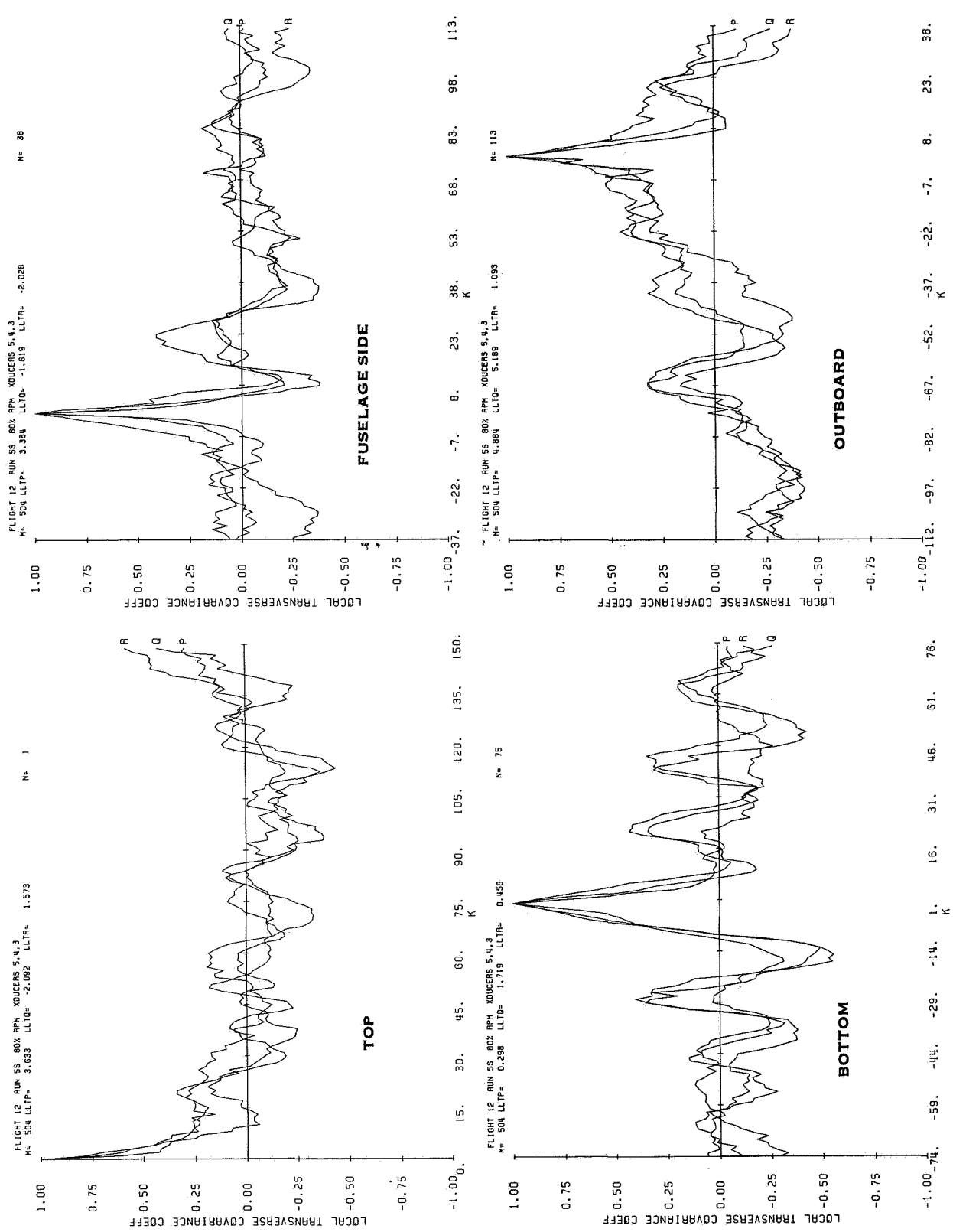


FIGURE 40. TRANSVERSE CORRELATION FUNCTIONS FOR RUN 55

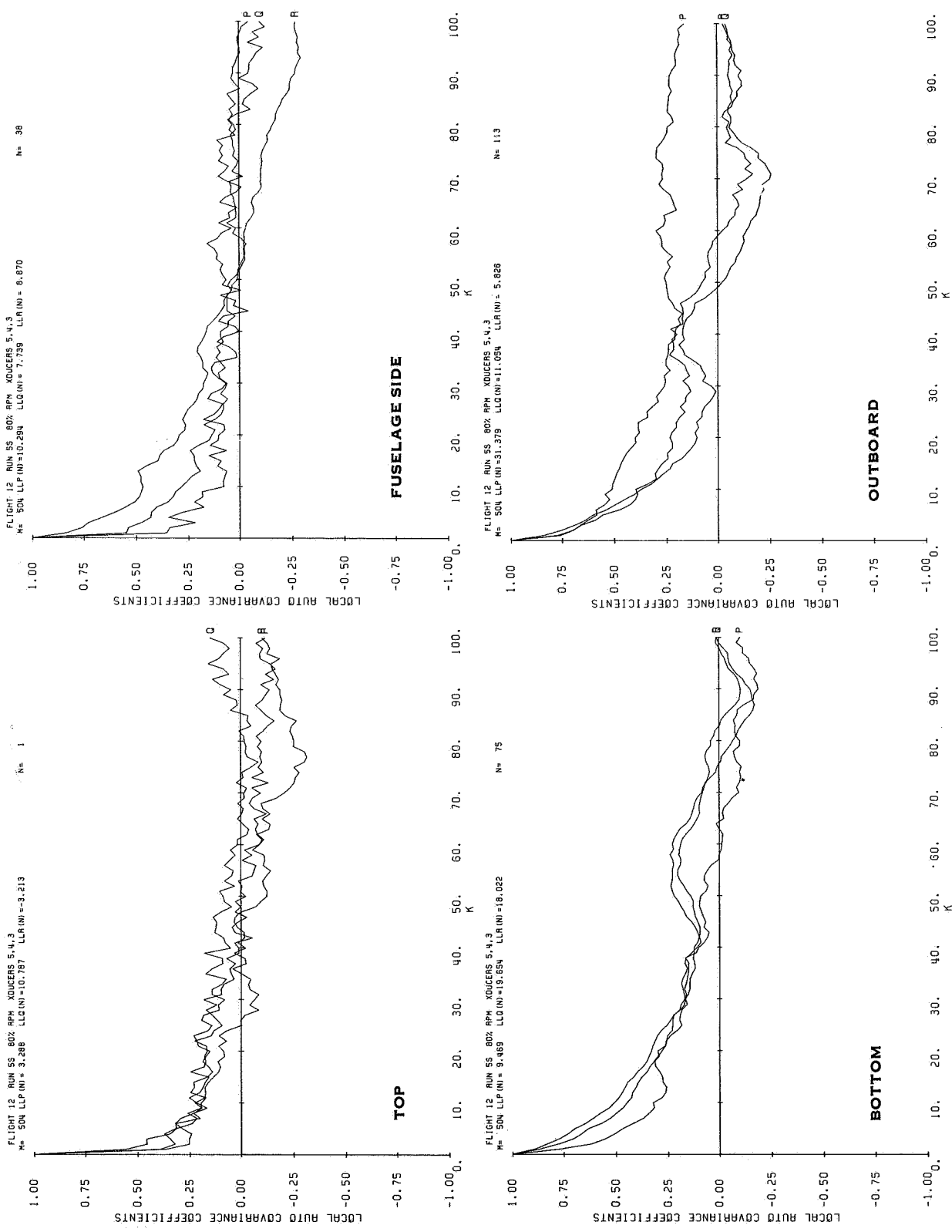


FIGURE 41. STREAMWISE CORRELATION FUNCTIONS FOR RUN 5S

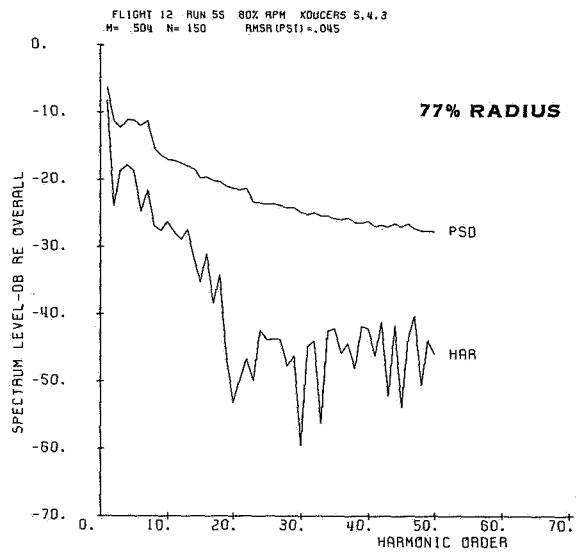
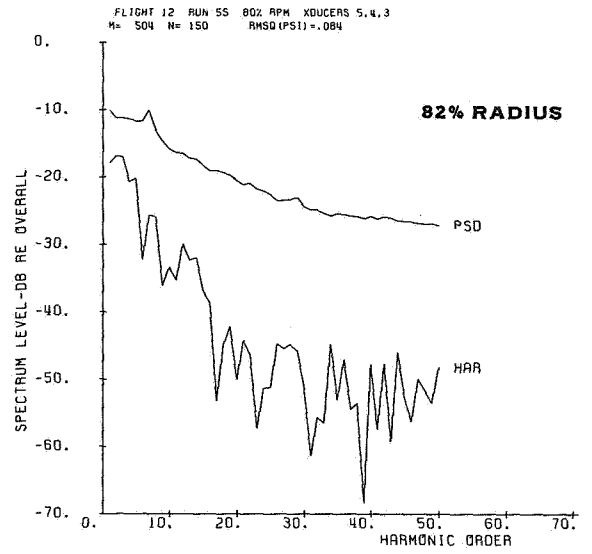
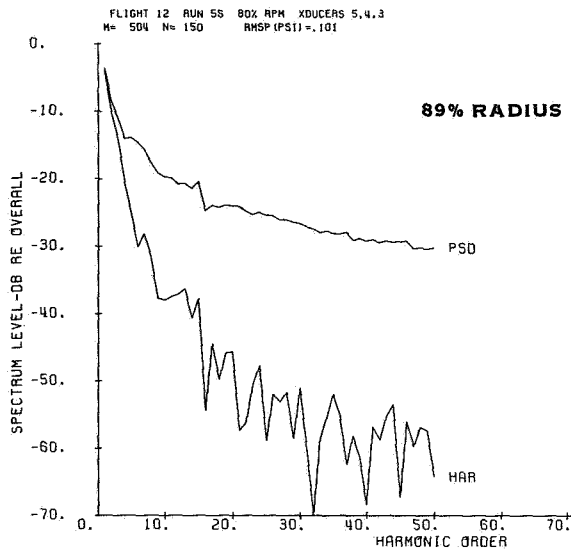
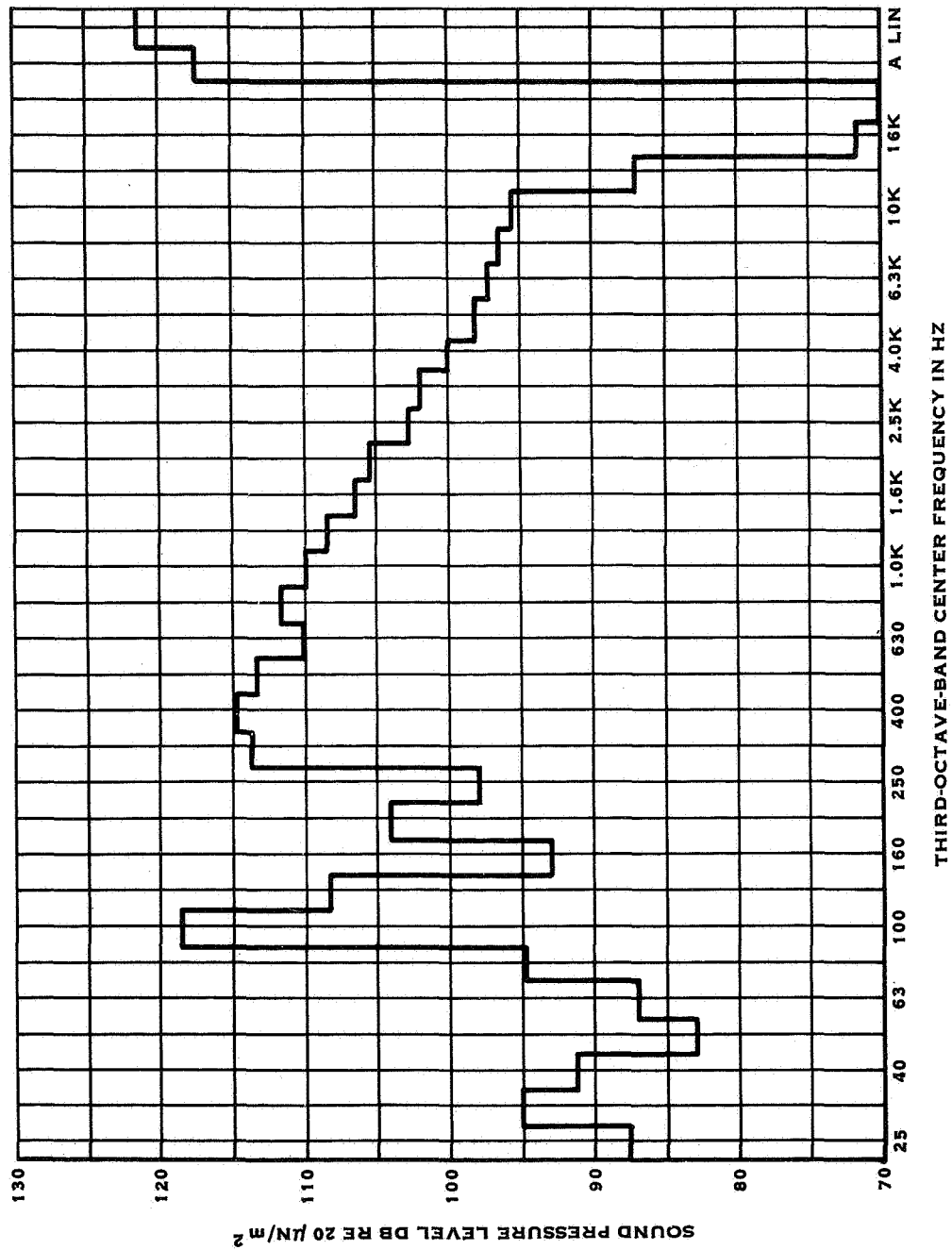


FIGURE 42. POWER SPECTRAL DENSITIES FOR RUN 55



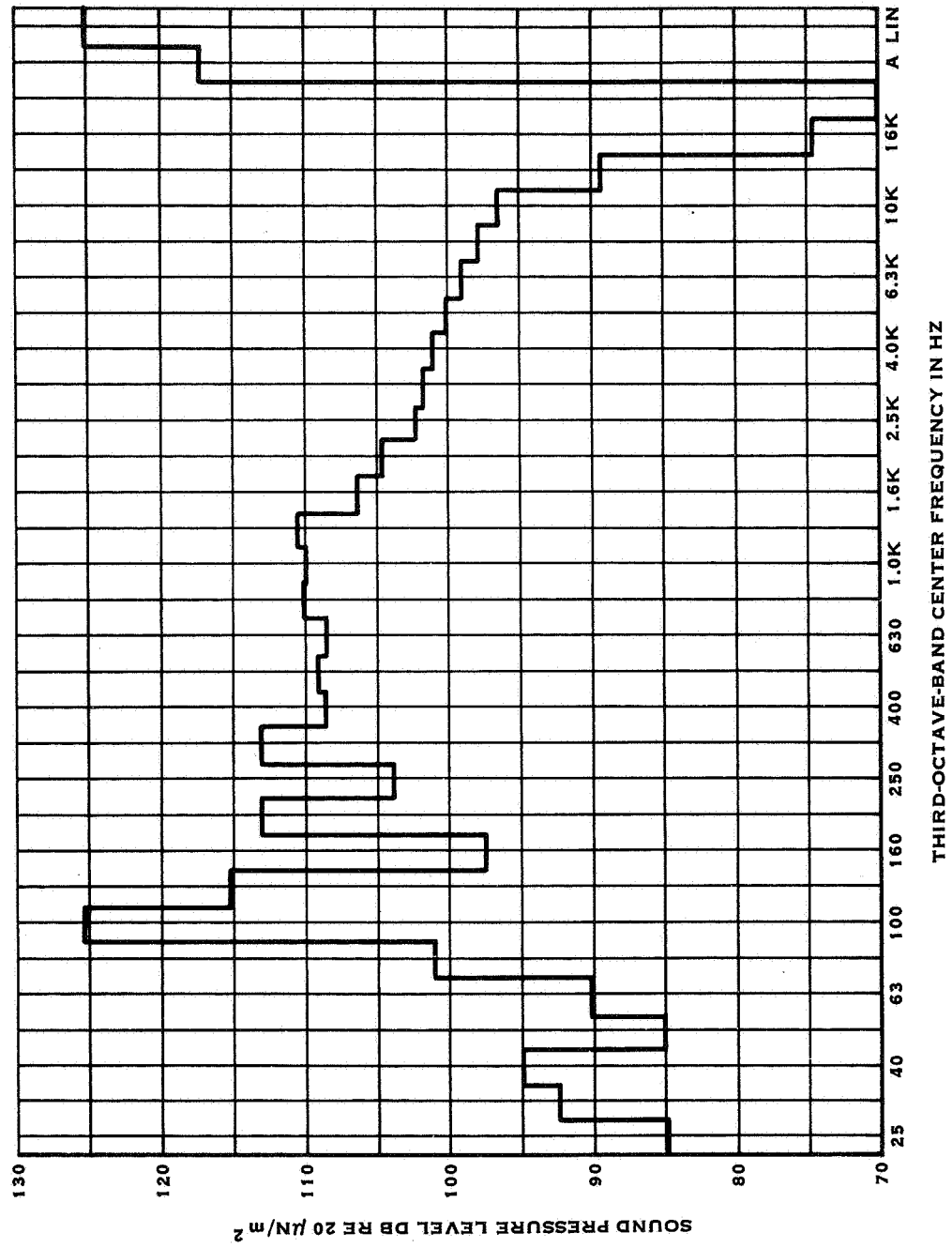


FIGURE 44. AFT MICROPHONE 1/3 OCTAVE BAND ANALYSIS FOR RUN 2S

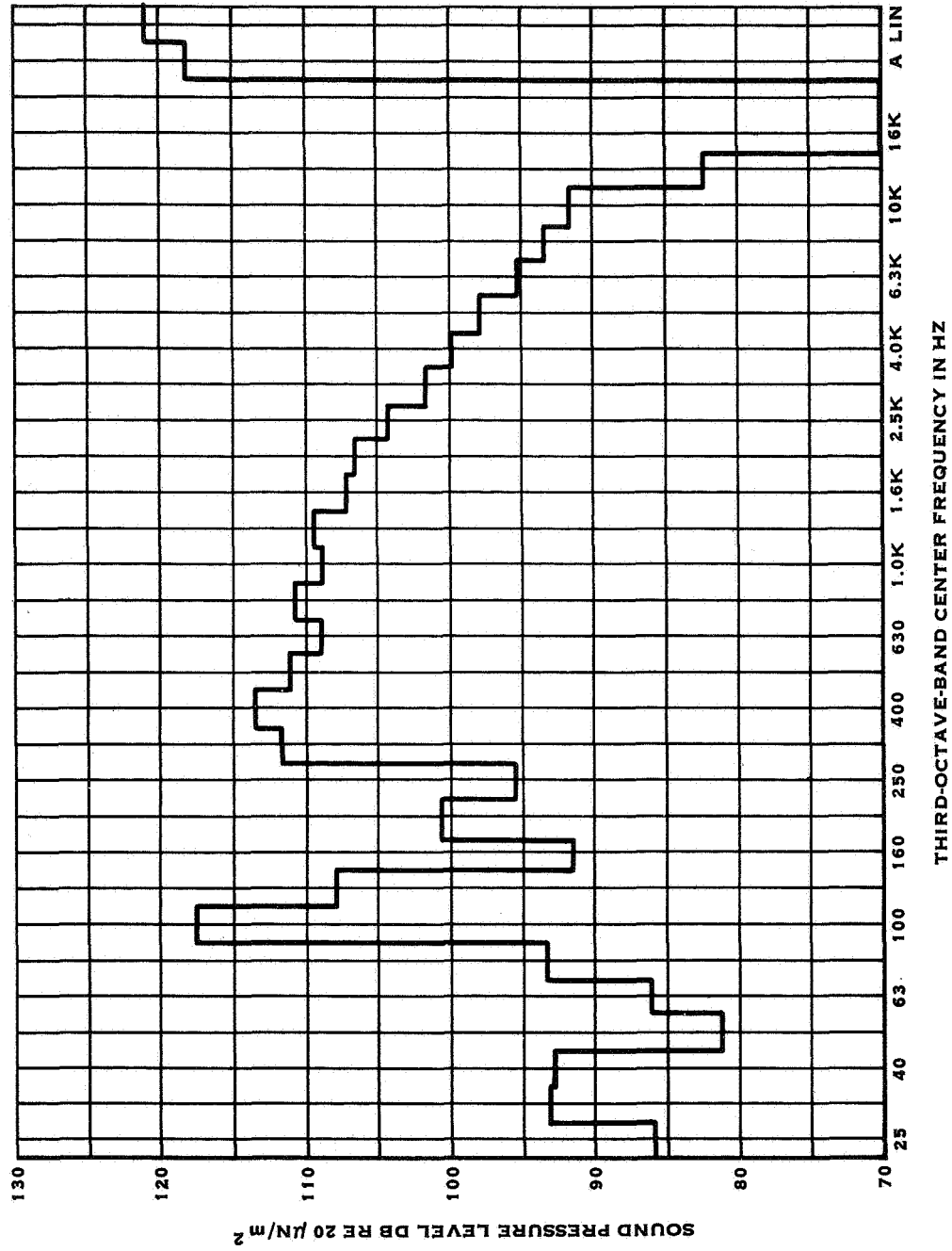


FIGURE 45. IN-PLANE MICROPHONE 1/3 OCTAVE BAND ANALYSIS FOR RUN 6S

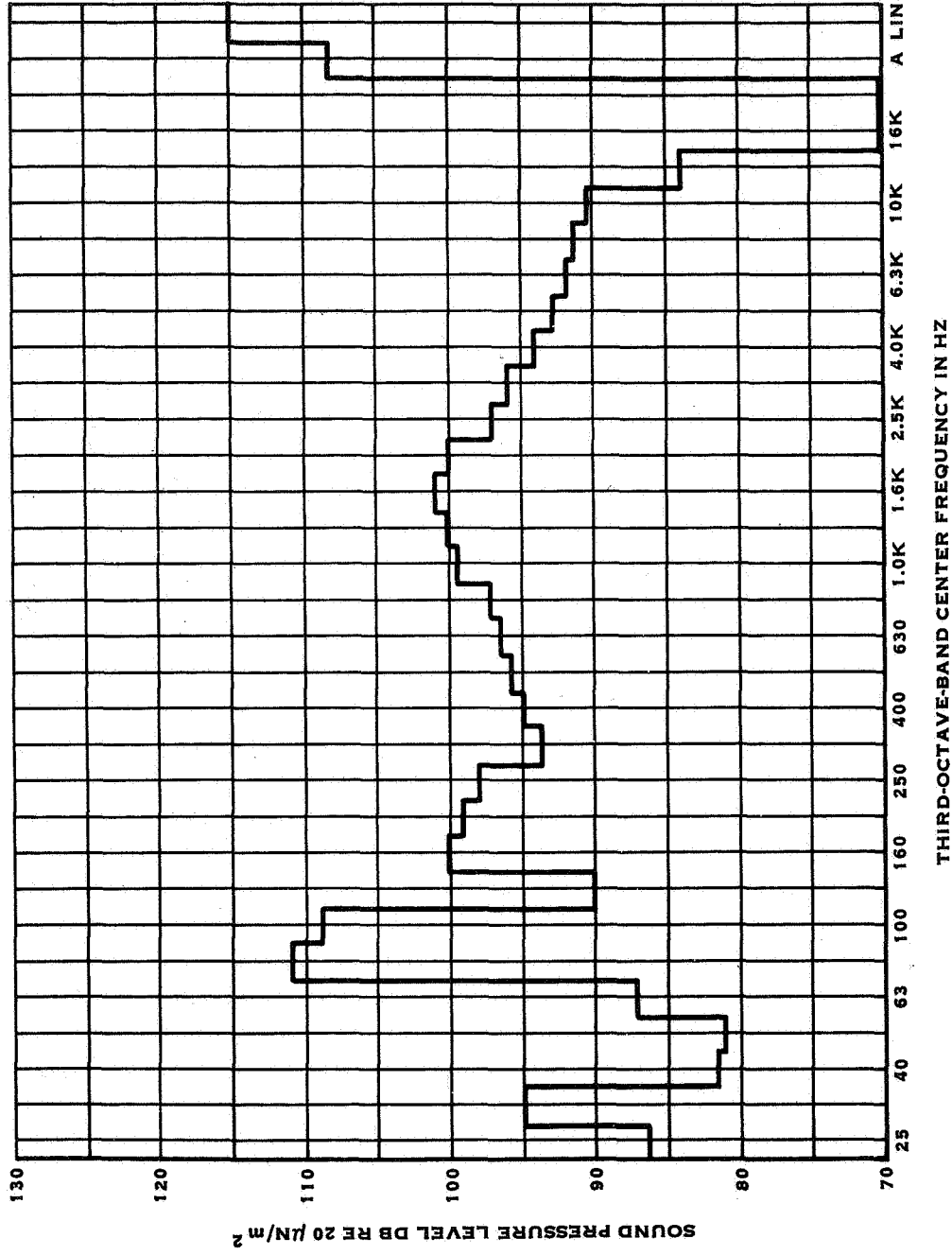
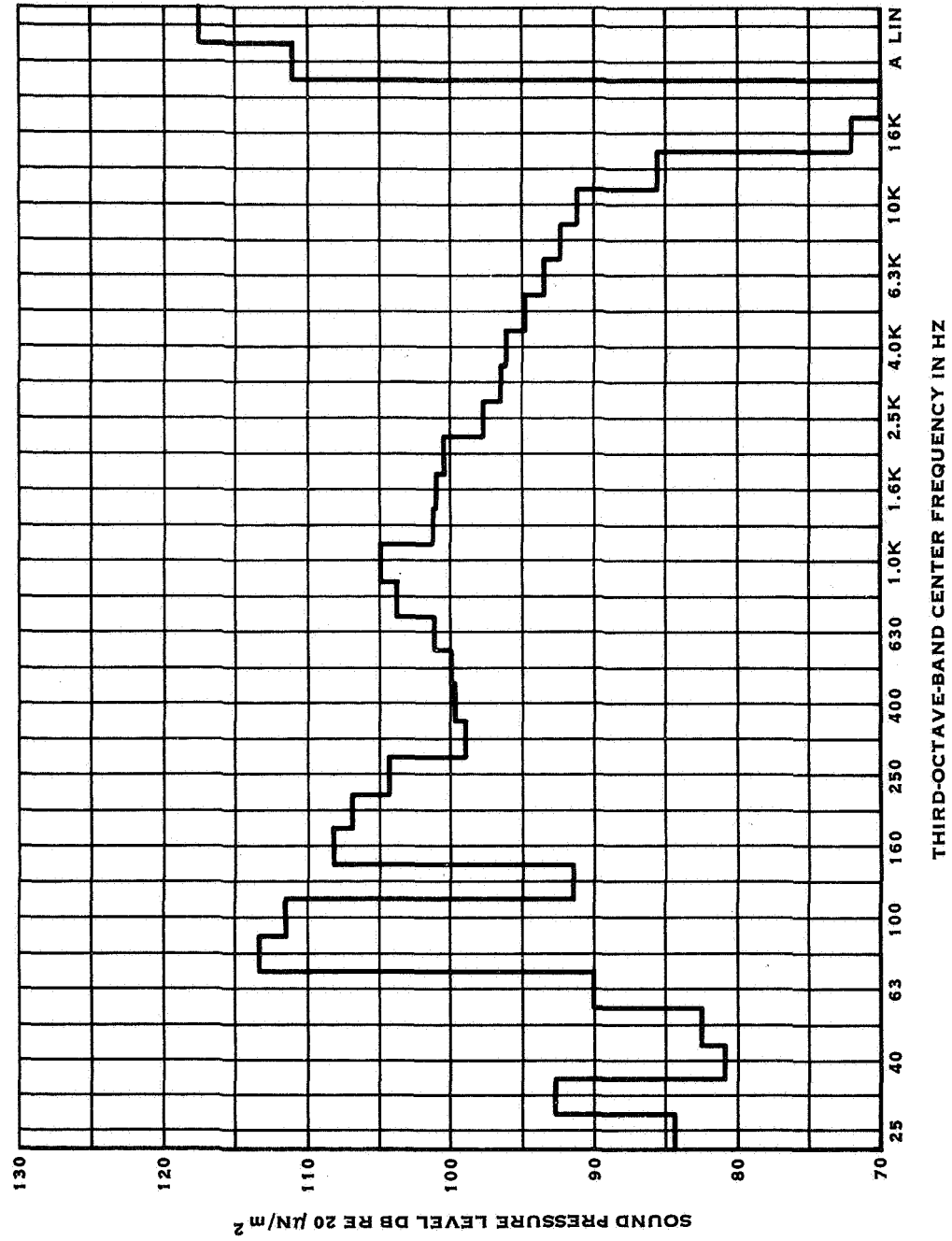


FIGURE 47. IN-PLANE MICROPHONE 1/3 OCTAVE BAND ANALYSIS FOR RUN 55



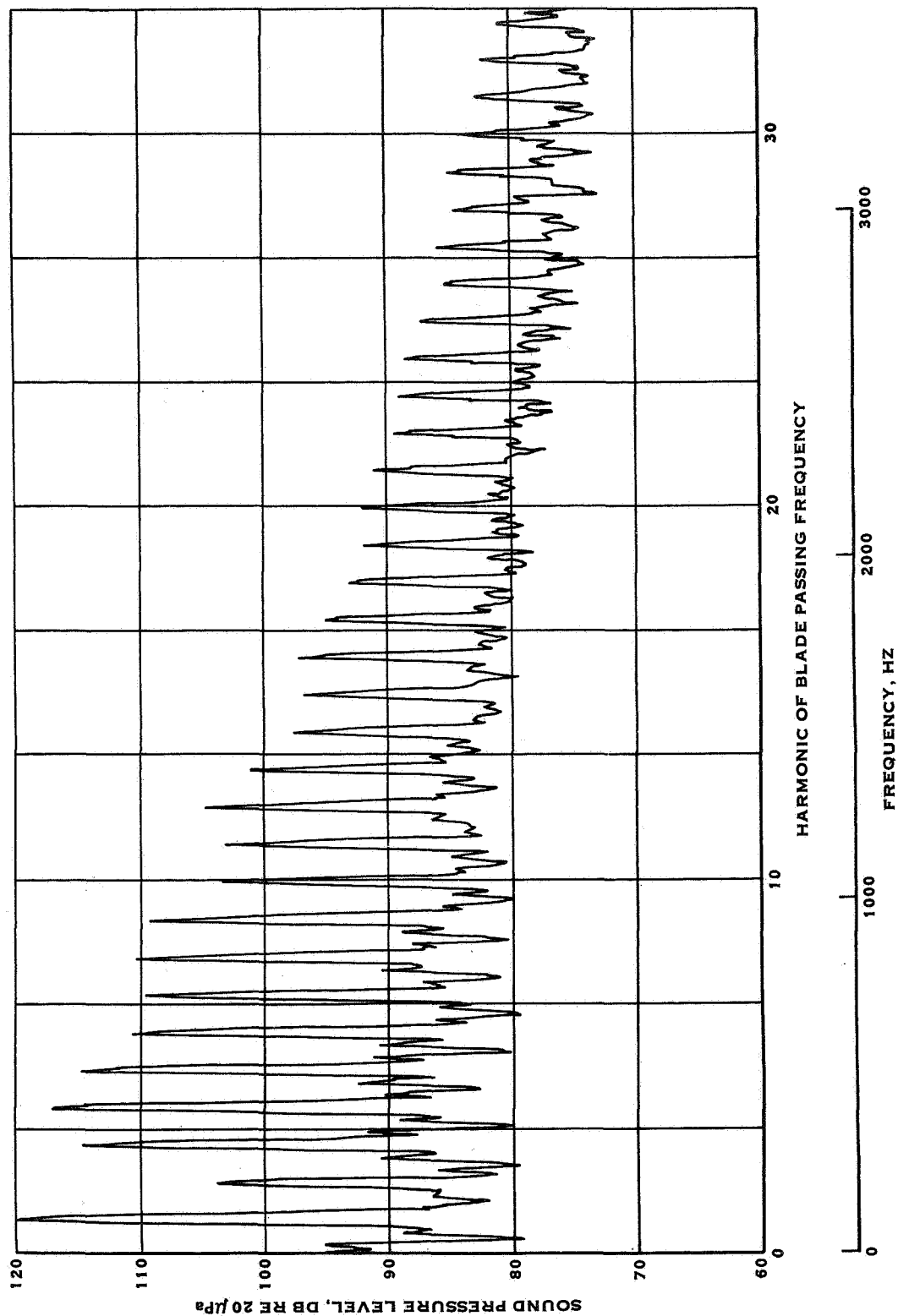


FIGURE 49. NARROW BAND FREQUENCY ANALYSIS OF THE IN-PLANE MICROPHONE
DATA FOR RUN 2S

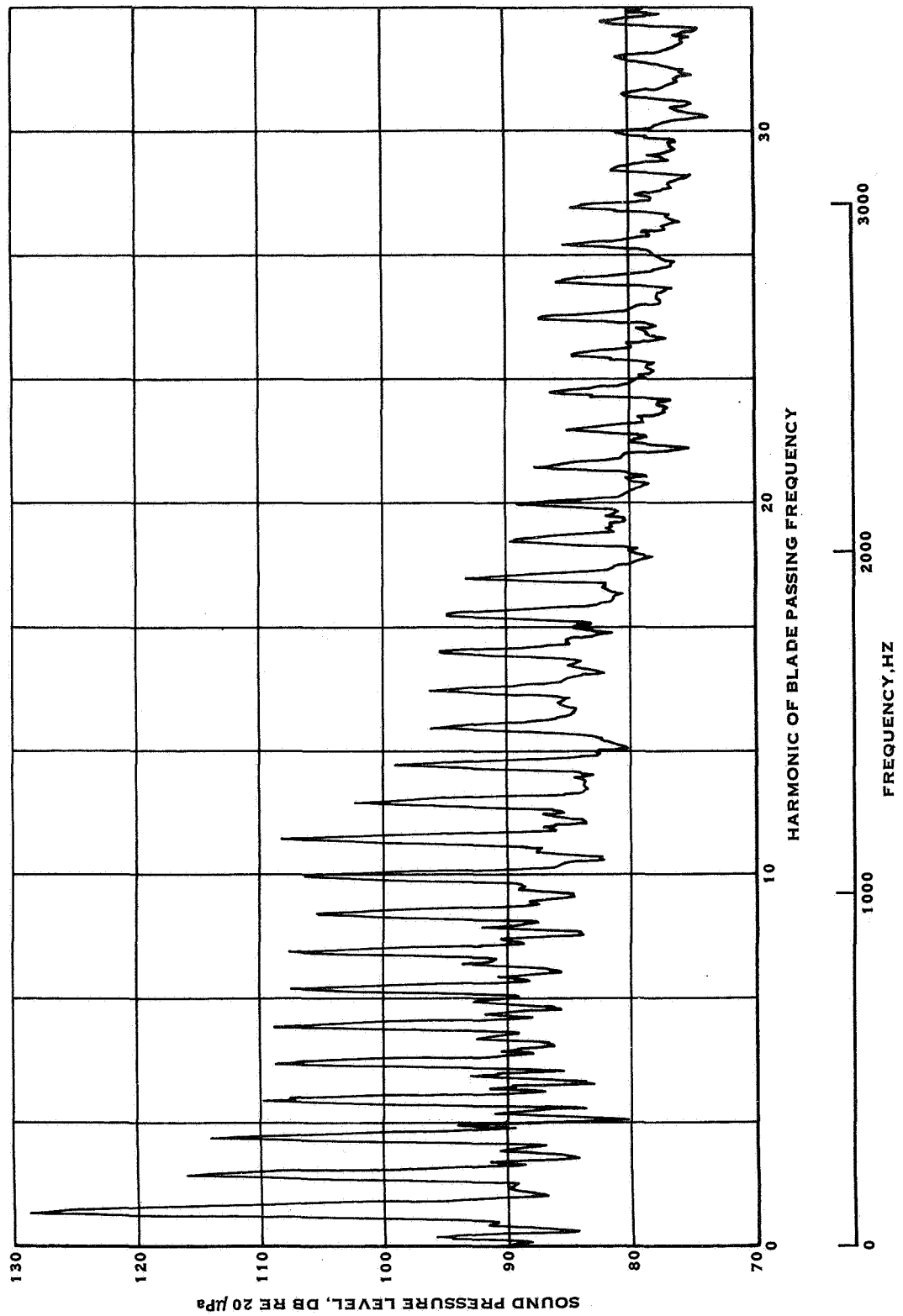


FIGURE 50. NARROW BAND FREQUENCY ANALYSIS OF THE AFT MICROPHONE DATA FOR RUN 25

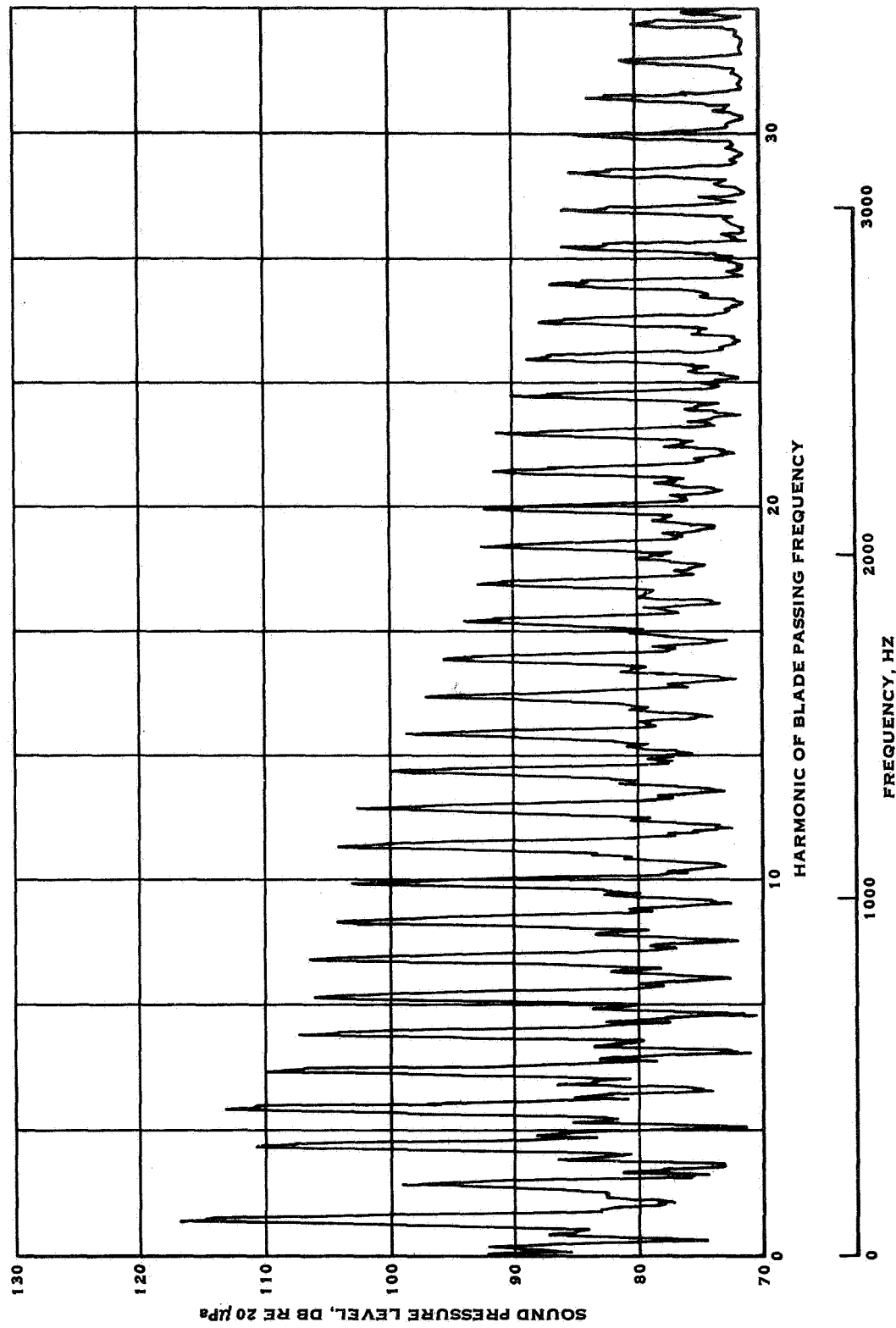


FIGURE 51. NARROW BAND FREQUENCY ANALYSIS OF THE IN-PLANE MICROPHONE
DATA FOR RUN 6S

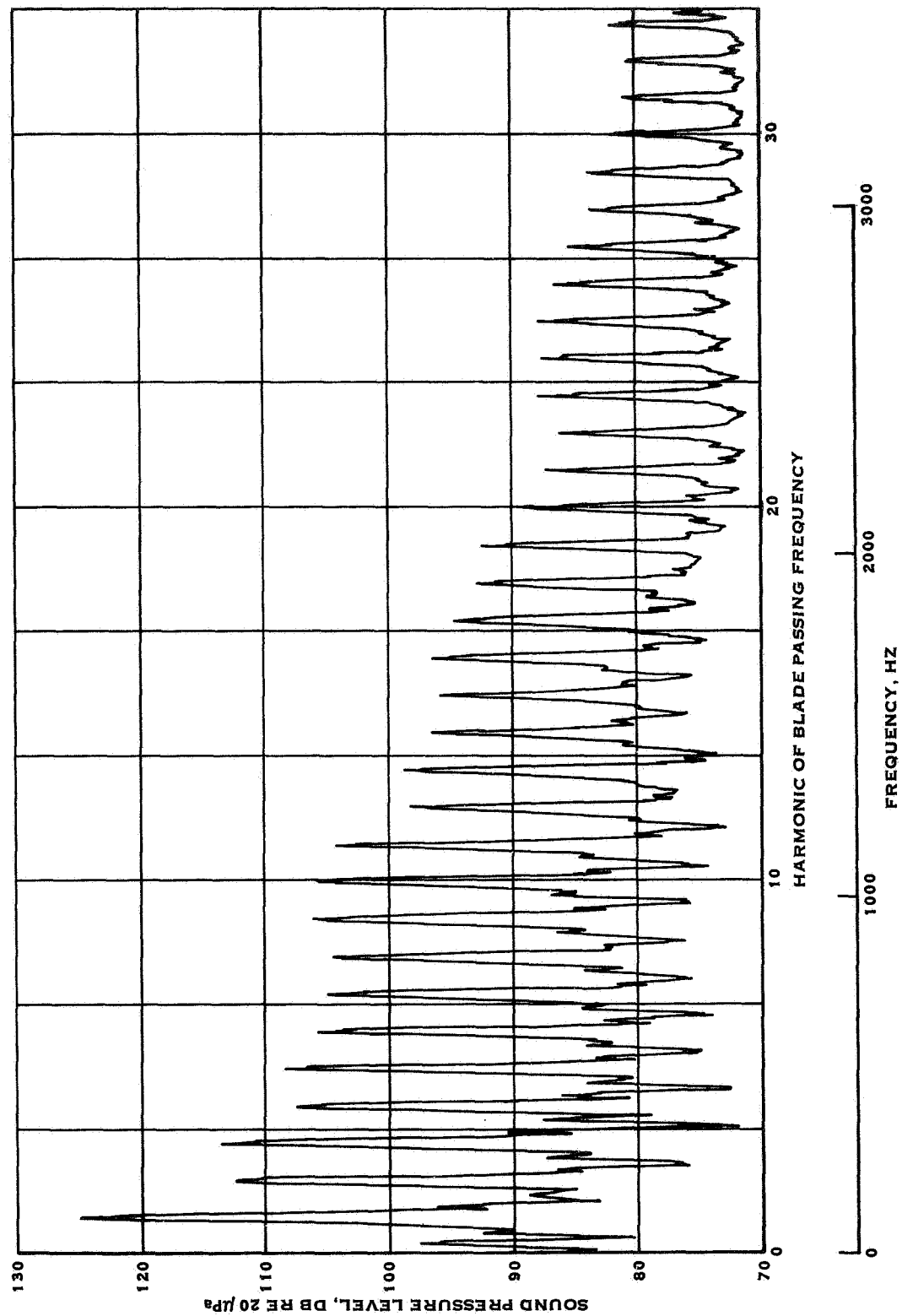


FIGURE 52. NARROW BAND FREQUENCY ANALYSIS OF THE AFT MICROPHONE DATA FOR RUN 6S

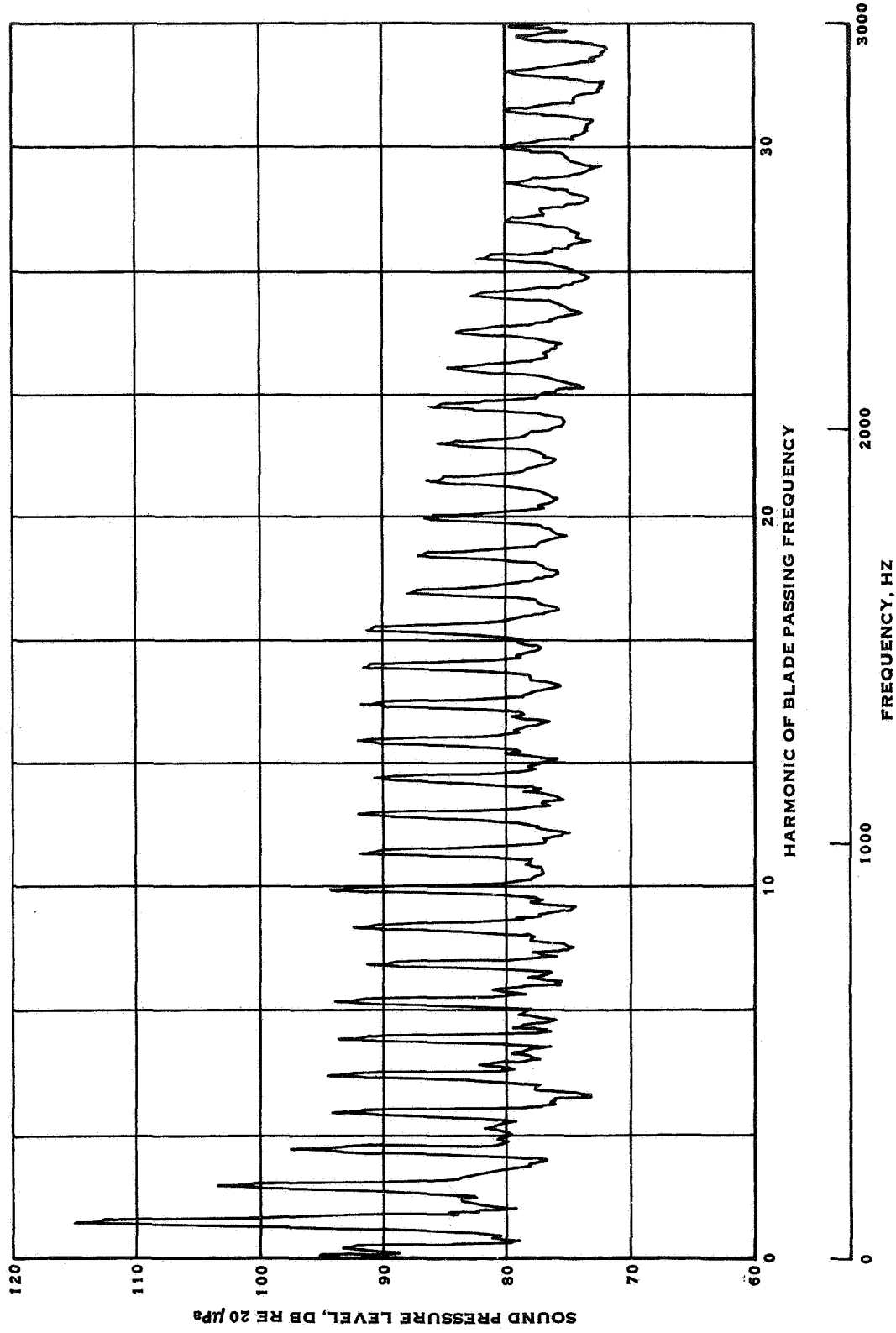


FIGURE 53. NARROW BAND FREQUENCY ANALYSIS OF THE IN-PLANE MICROPHONE
DATA FOR RUN 5S

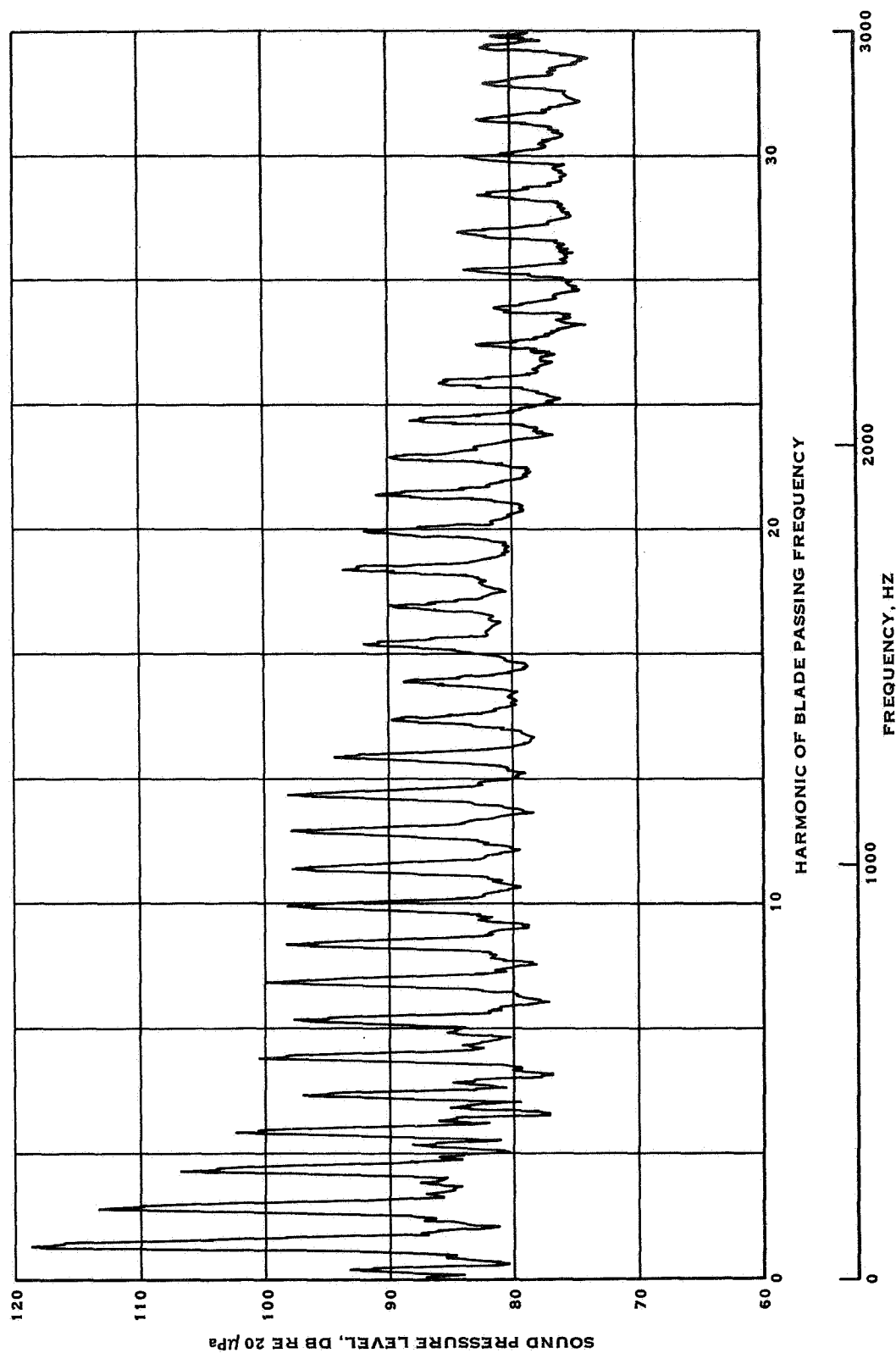


FIGURE 54. NARROW BAND FREQUENCY ANALYSIS OF THE AFT MICROPHONE DATA
FOR RUN 55

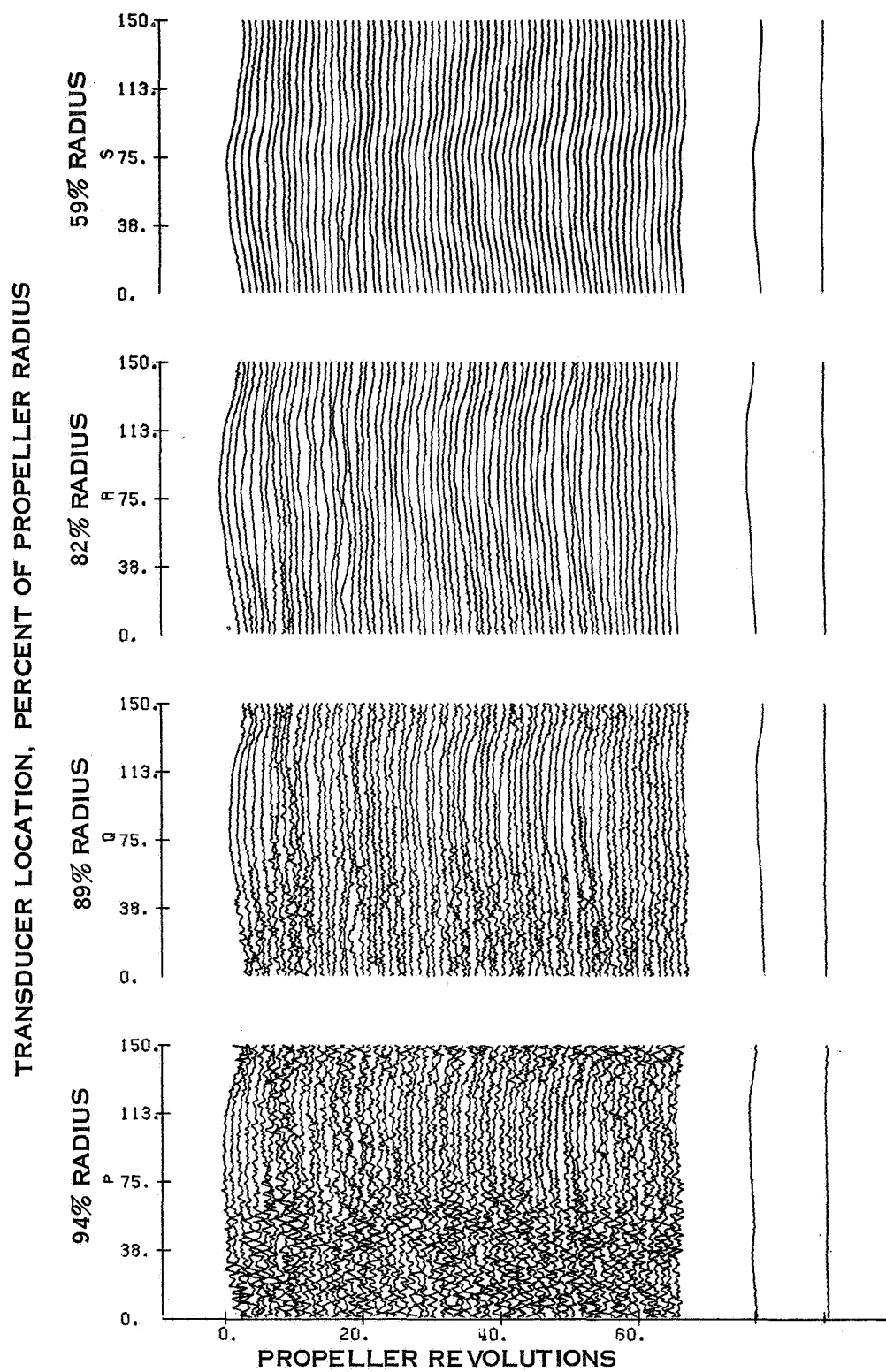


FIGURE 55. BLADE SURFACE PRESSURE TIME HISTORY PLOT FOR RUN 2-97, 5% RPM FLIGHT CONDITION

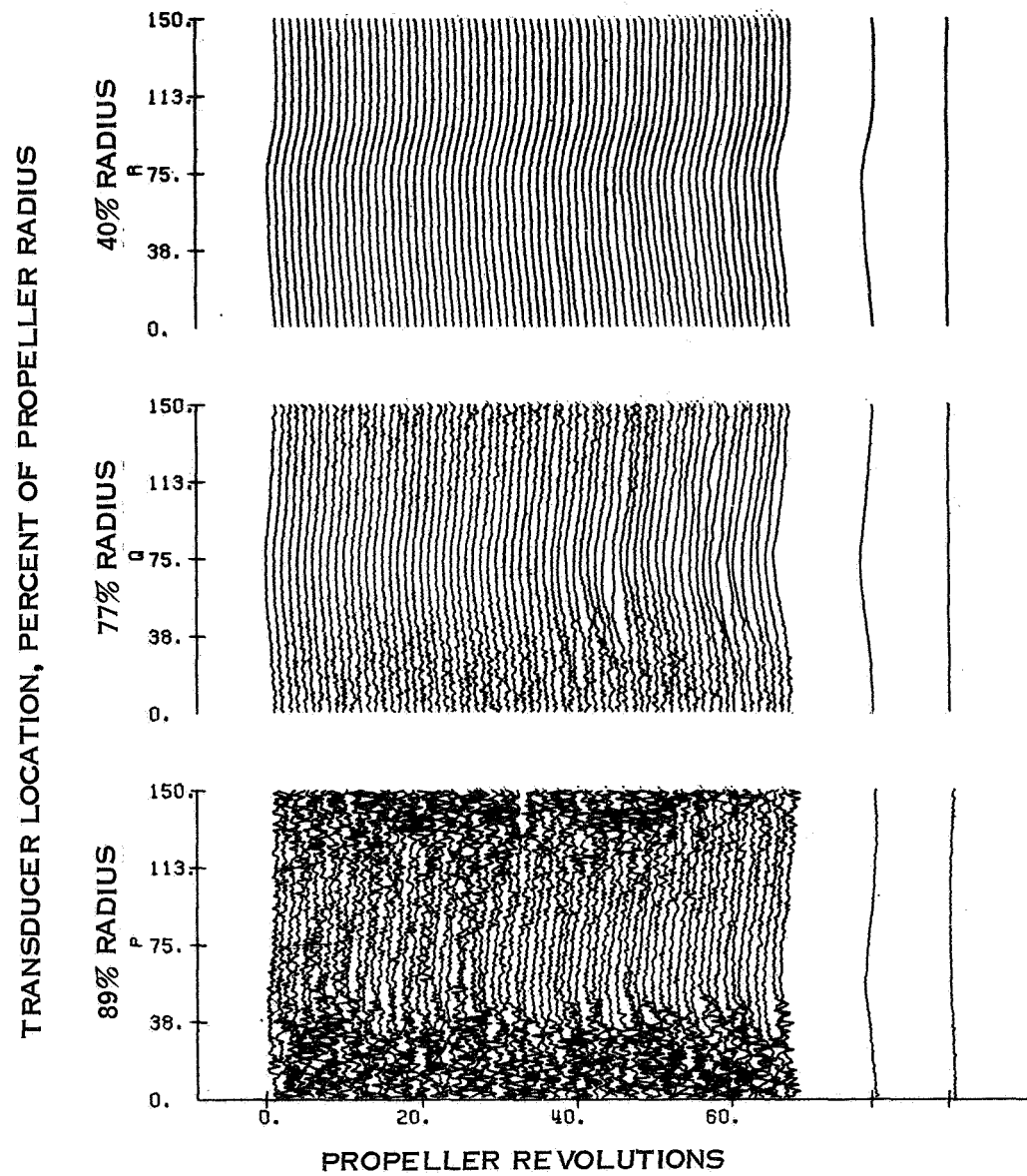
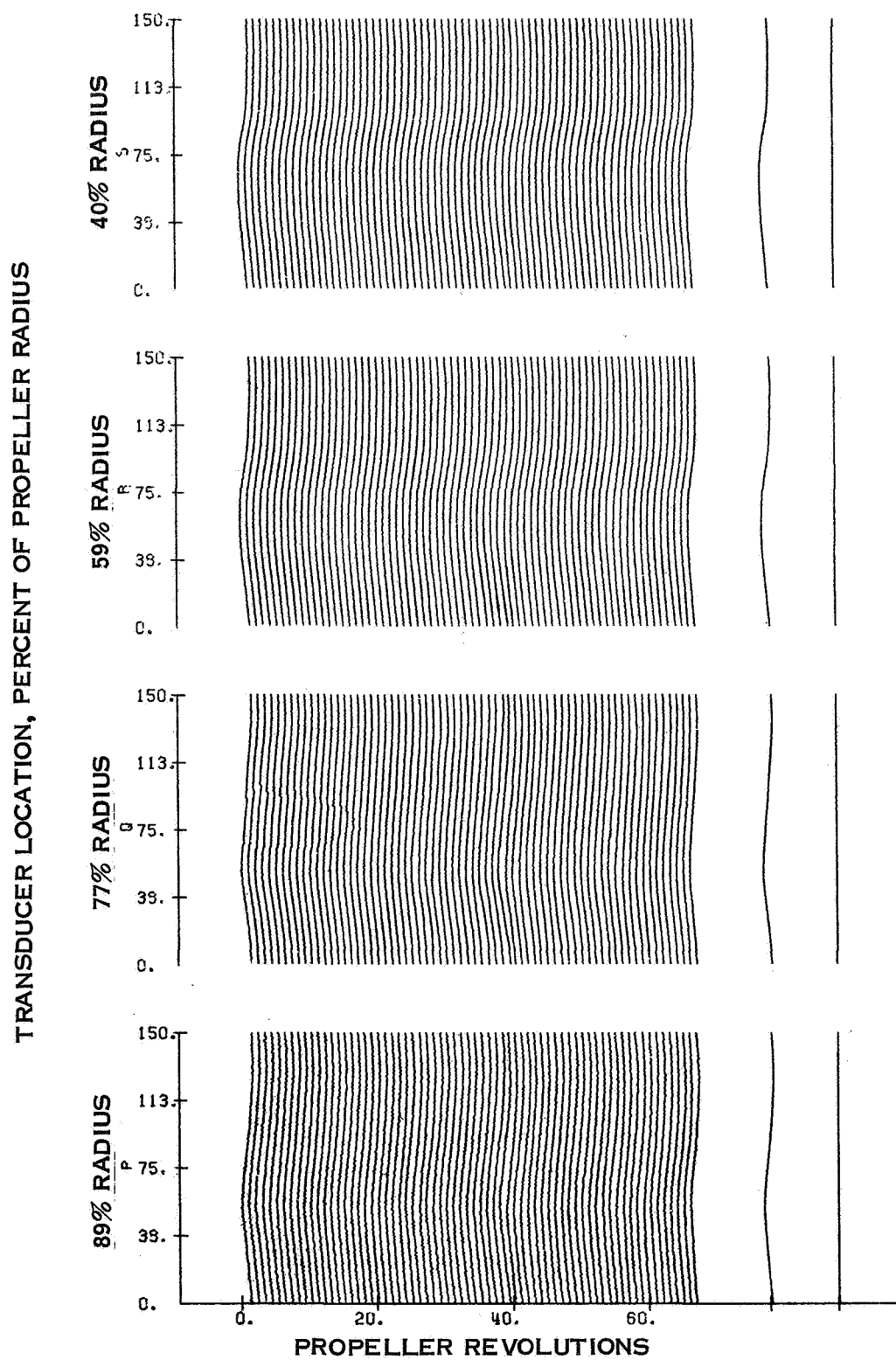


FIGURE 56. BLADE SURFACE PRESSURE TIME HISTROY PLOT
FOR RUN 6-97.5% RPM FLIGHT CONDITION



**FIGURE 57. BLADE SURFACE PRESSURE TIME HISTORY PLOT
FOR RUN 5—80% RPM FLIGHT CONDITION**

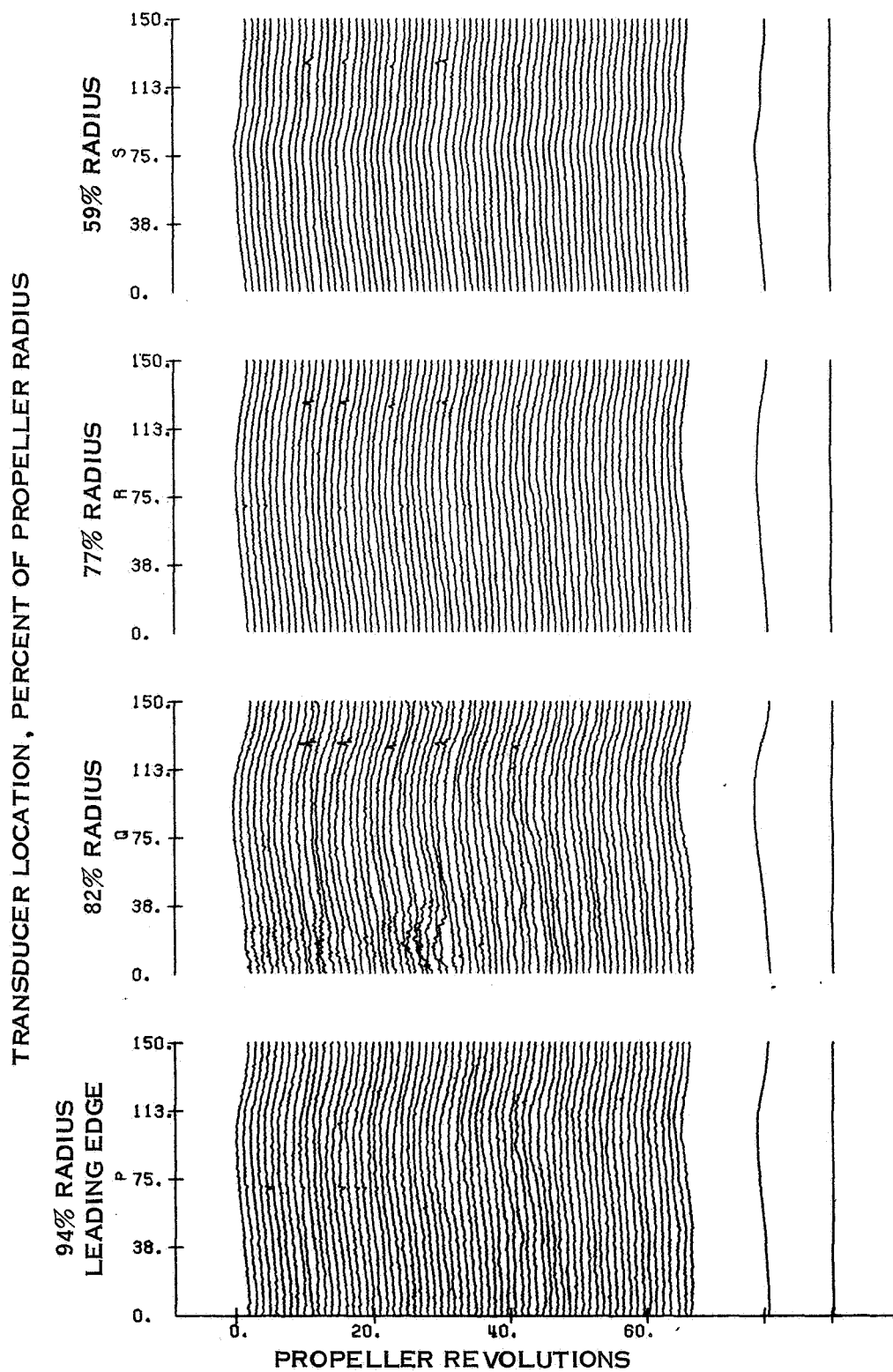
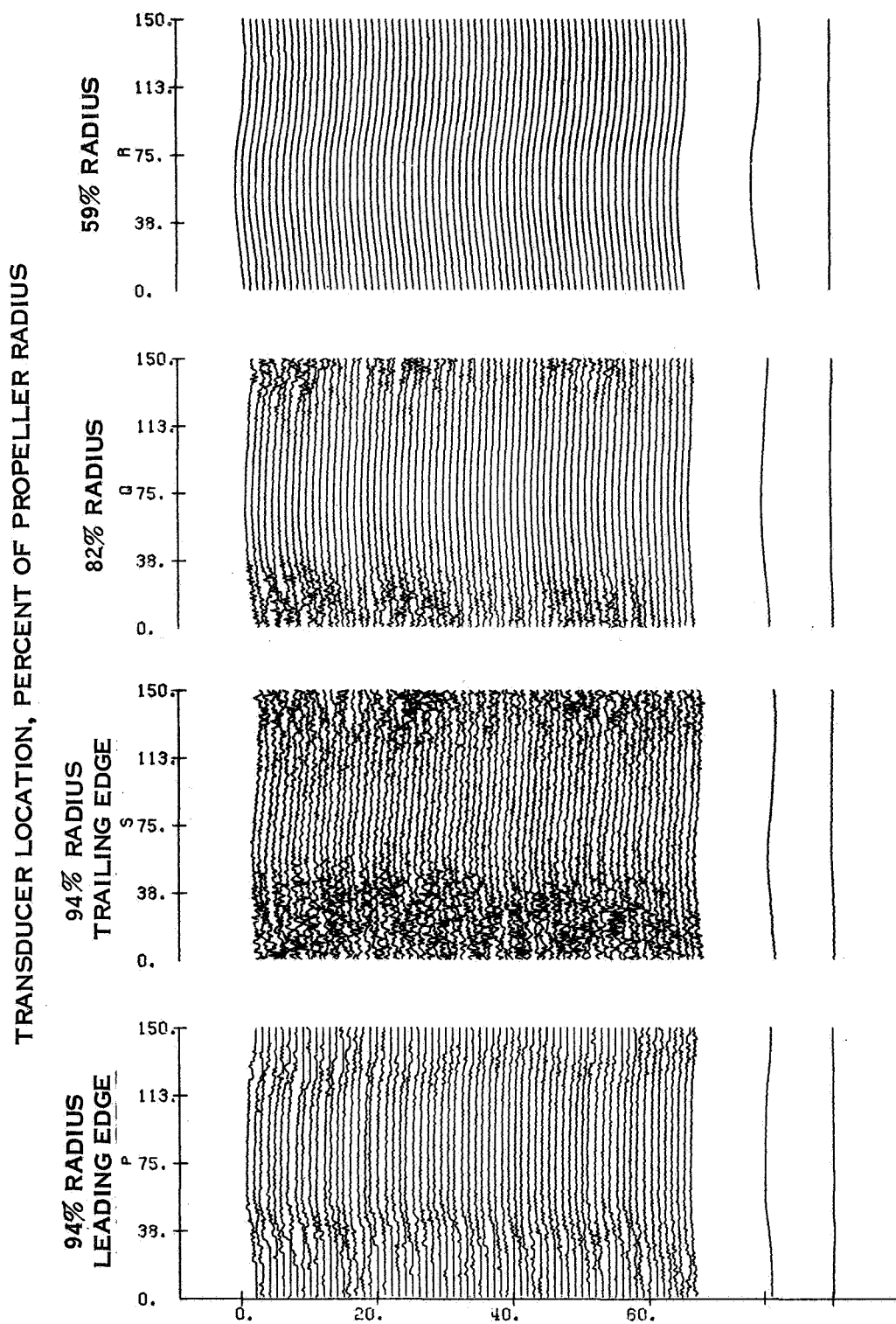


FIGURE 58. BLADE SURFACE PRESSURE TIME HISTORY PLOT FOR RUN C-80% RPM, 20 DEGREE FLAP EFFECT



**FIGURE 59. BLADE SURFACE PRESSURE TIME HISTORY PLOT
FOR RUN 19A—90% RPM TAXI CONDITION**

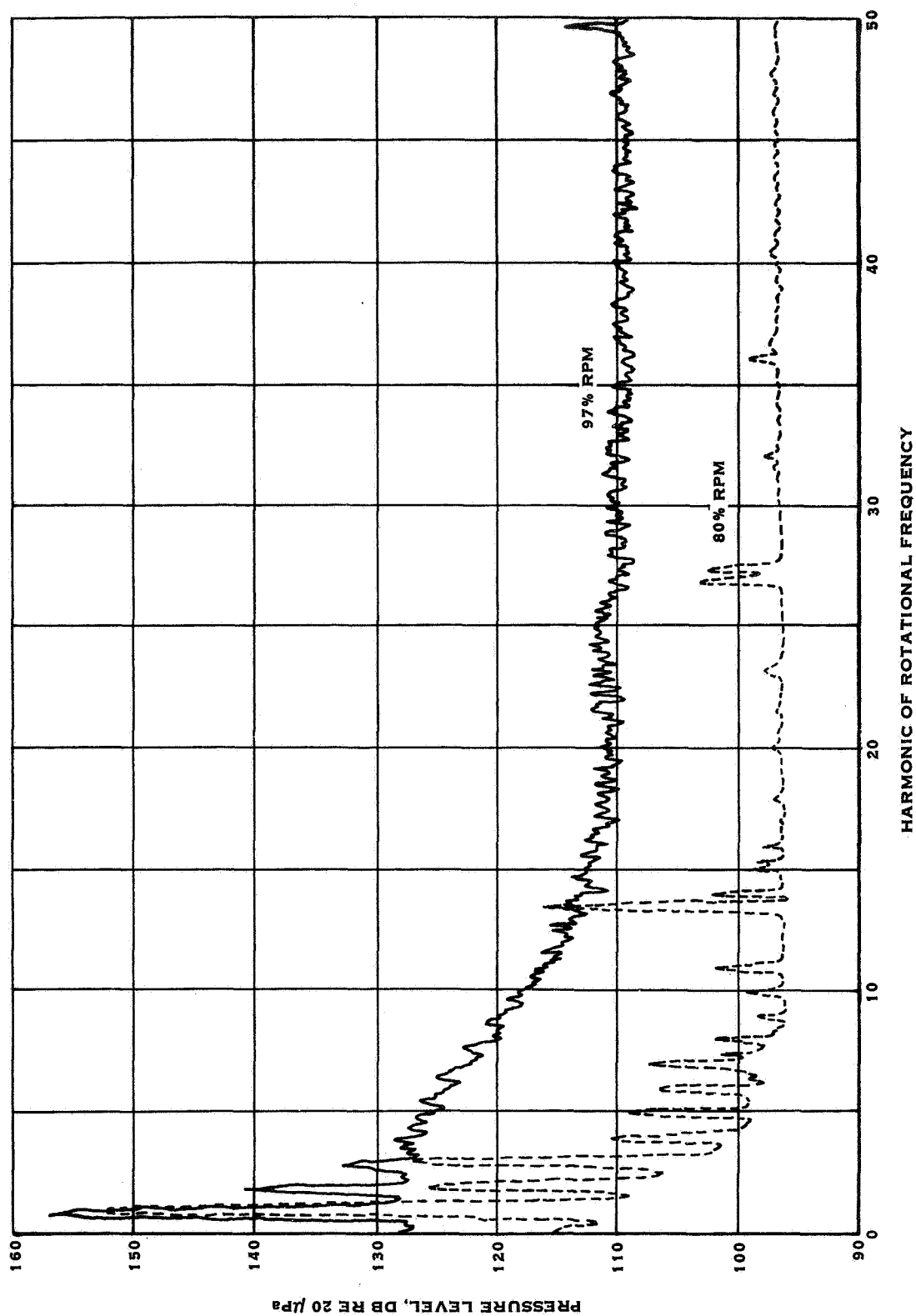


FIGURE 60. COMPARISON OF BLADE SURFACE PRESSURES FOR TWO TIP SPEED CONDITIONS -
50 ORDER ANALYSIS

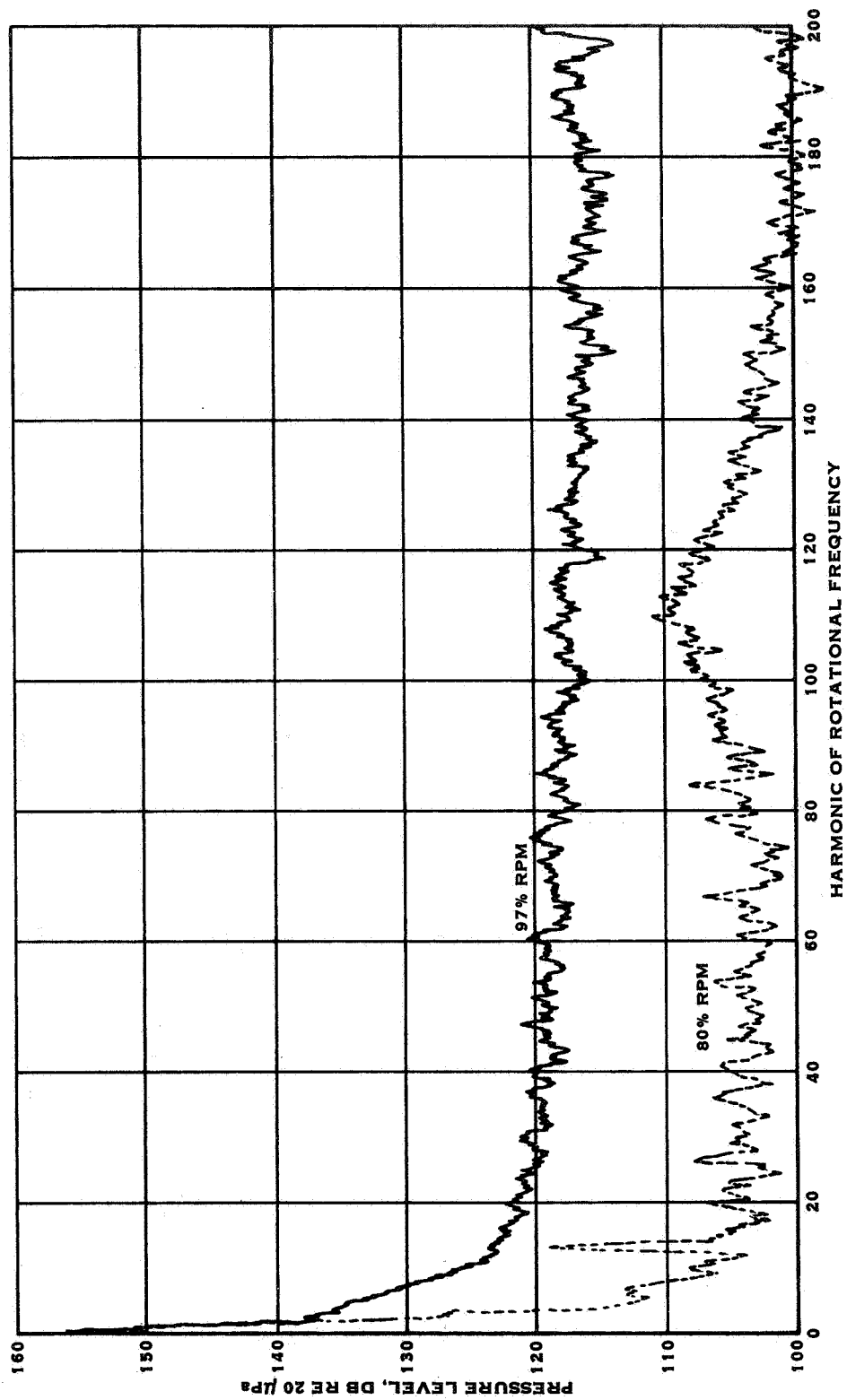


FIGURE 61. COMPARISON OF BLADE SURFACE PRESSURES FOR TWO TIP SPEED CONDITIONS -
200 ORDER ANALYSIS

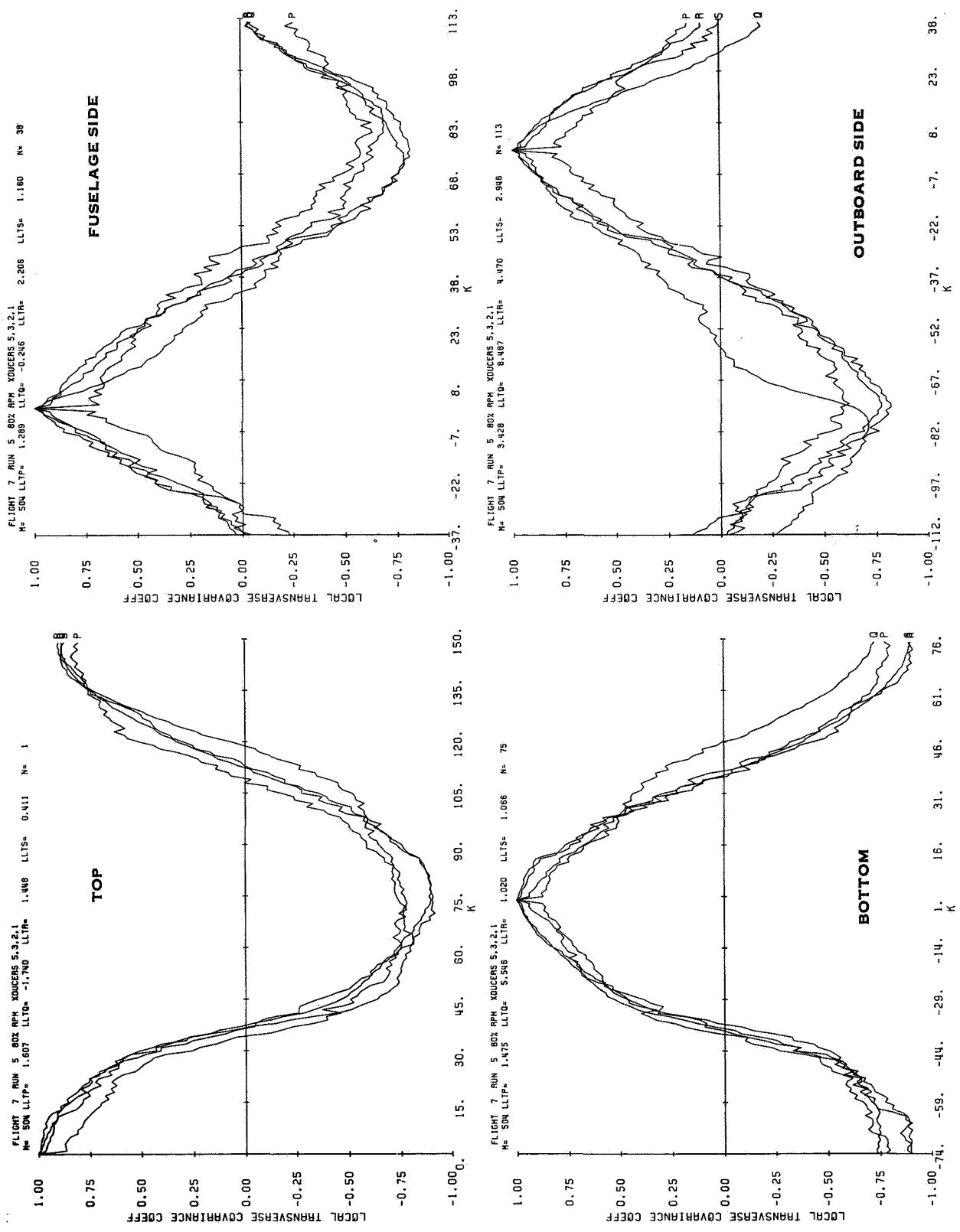


FIGURE 62. TRANSVERSE CORRELATION FUNCTIONS FOR RUN 5

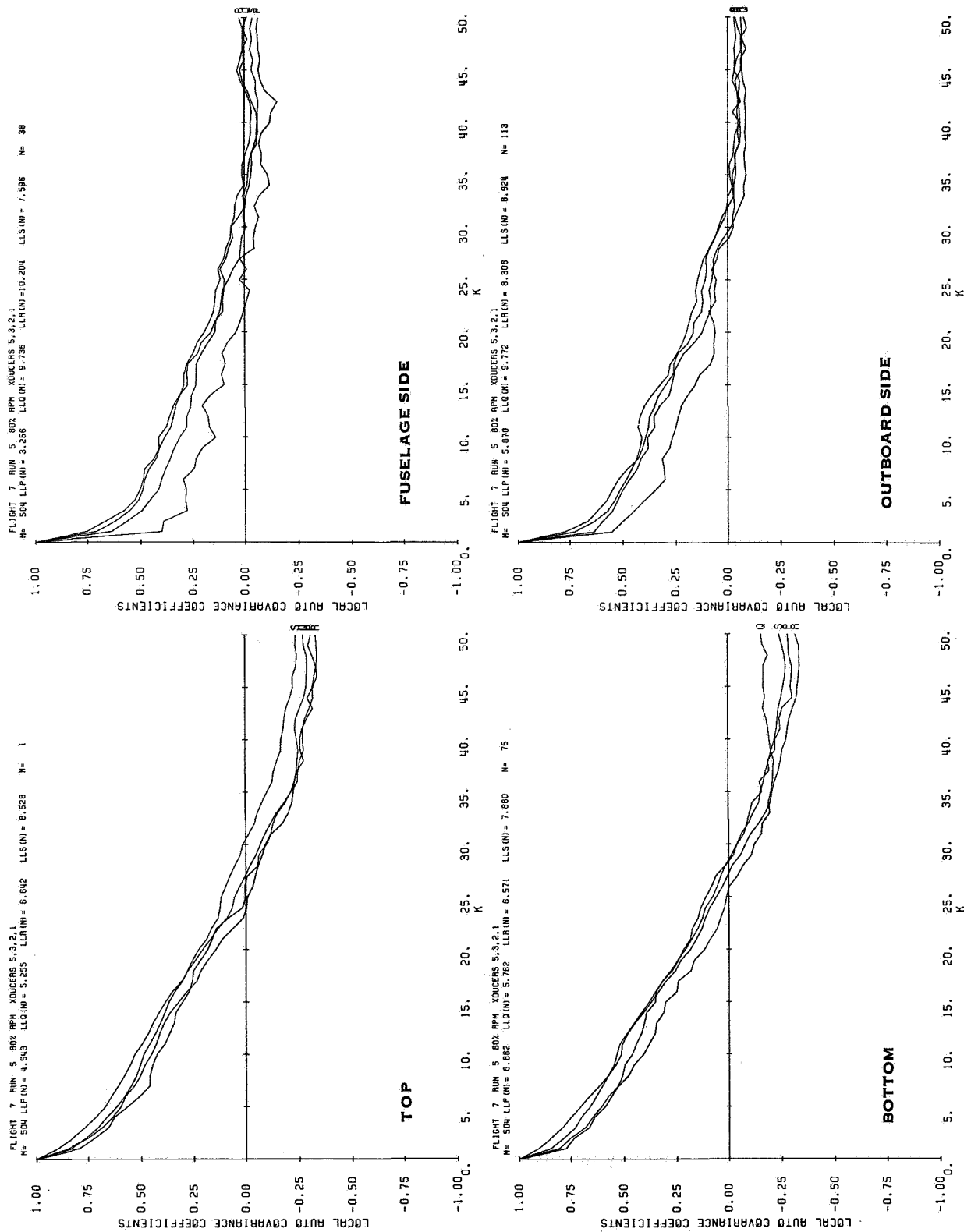


FIGURE 63. STREAMWISE CORRELATION FUNCTIONS FOR RUN 5

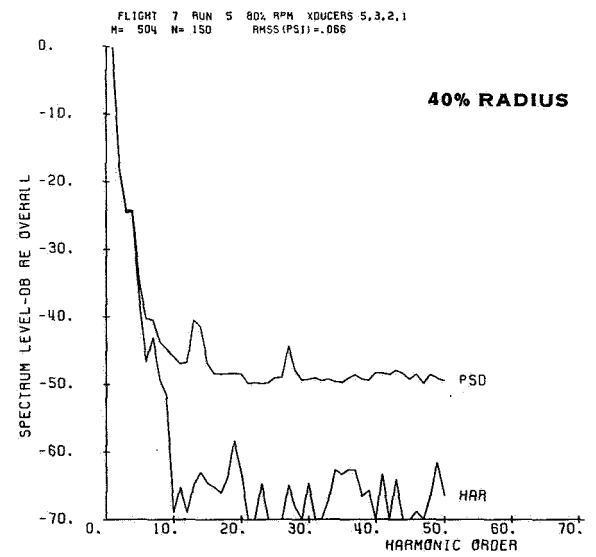
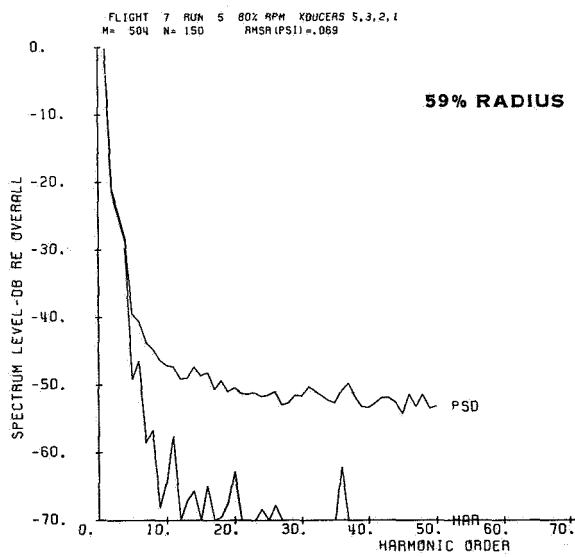
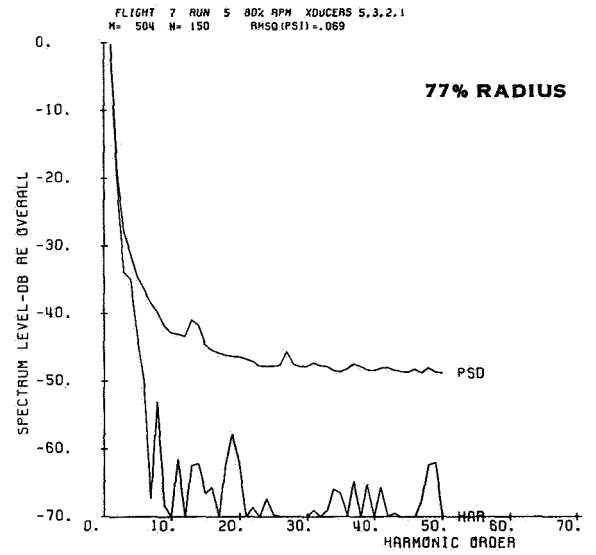
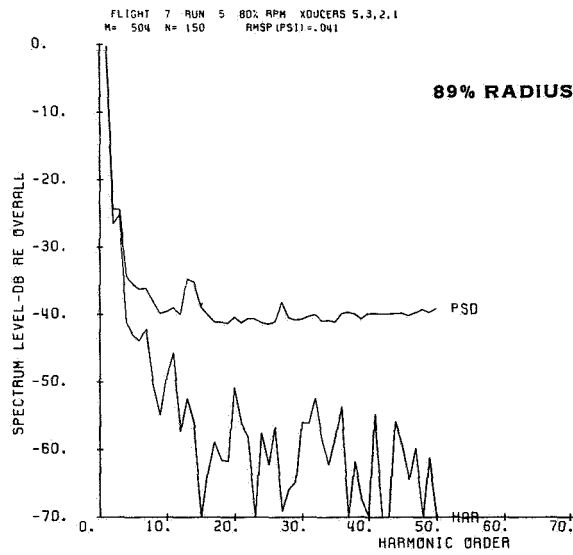


FIGURE 64. POWER SPECTRAL DENSITIES FOR RUN 5

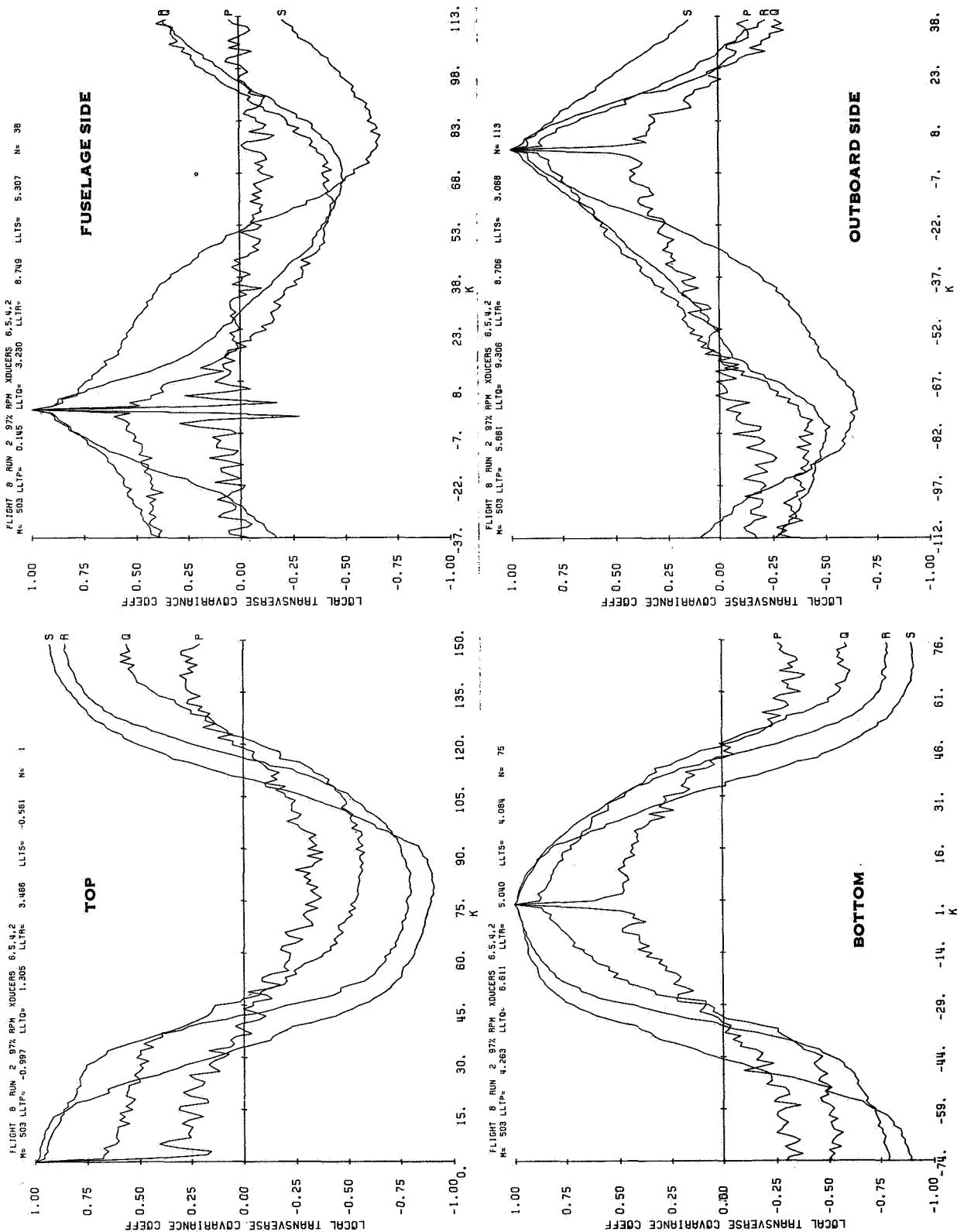


FIGURE 65. TRANSVERSE CORRELATION FUNCTIONS FOR RUN 2

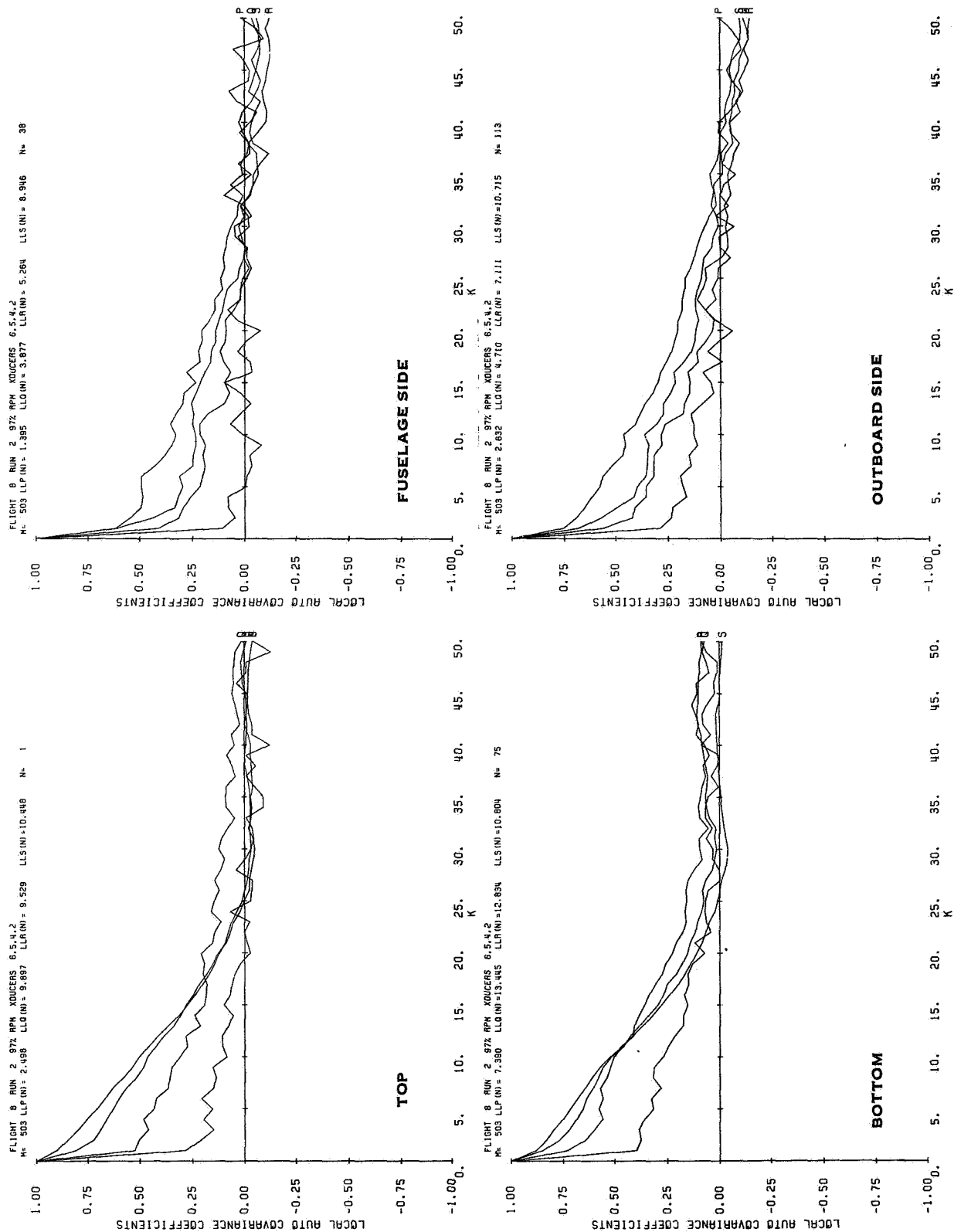


FIGURE 66. STREAMWISE CORRELATION FUNCTIONS FOR RUN 2

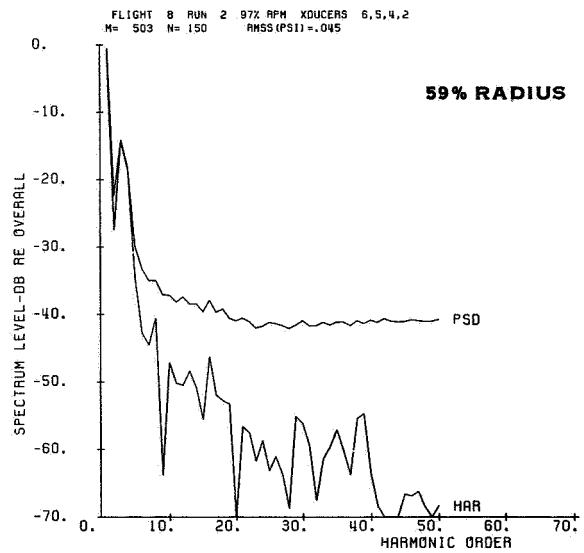
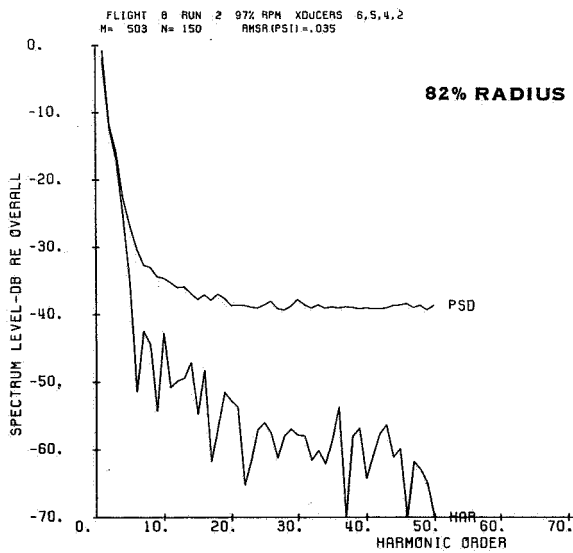
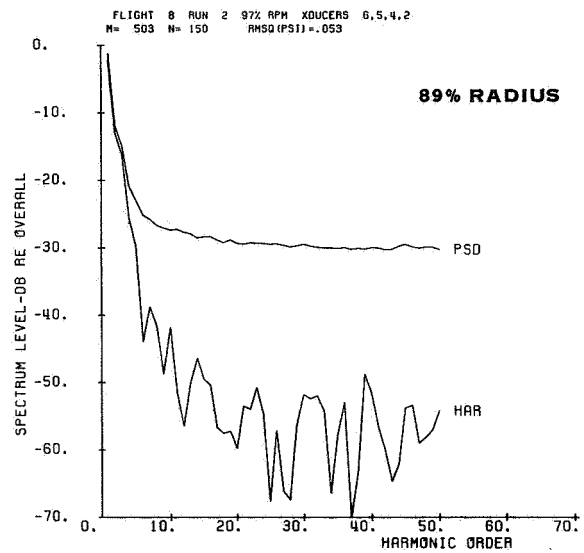
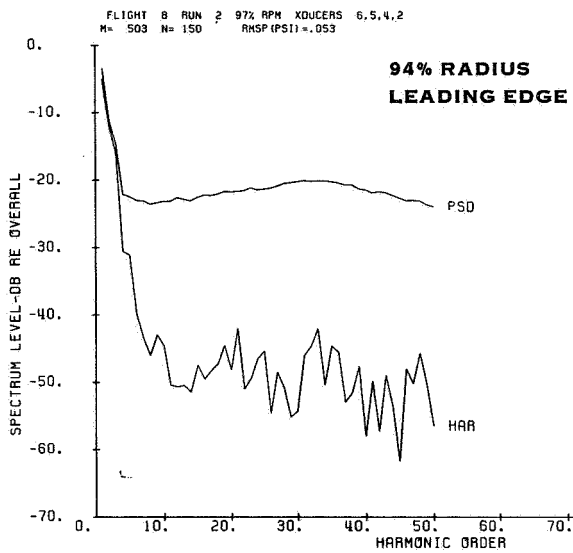


FIGURE 67. POWER SPECTRAL DENSITIES FOR RUN 2

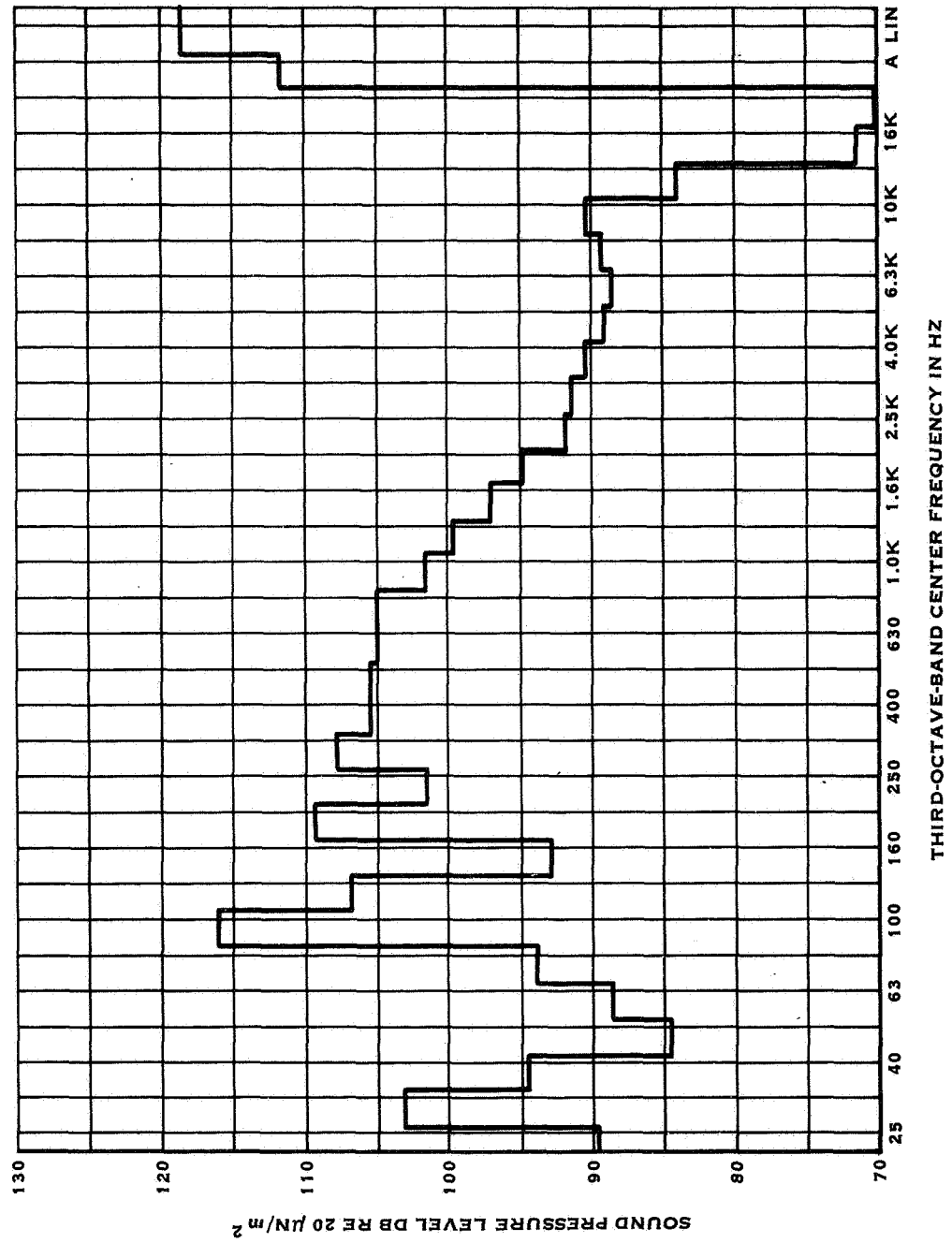


FIGURE 68. IN-PLANE MICROPHONE 1/3 OCTAVE BAND ANALYSIS FOR RUN 2

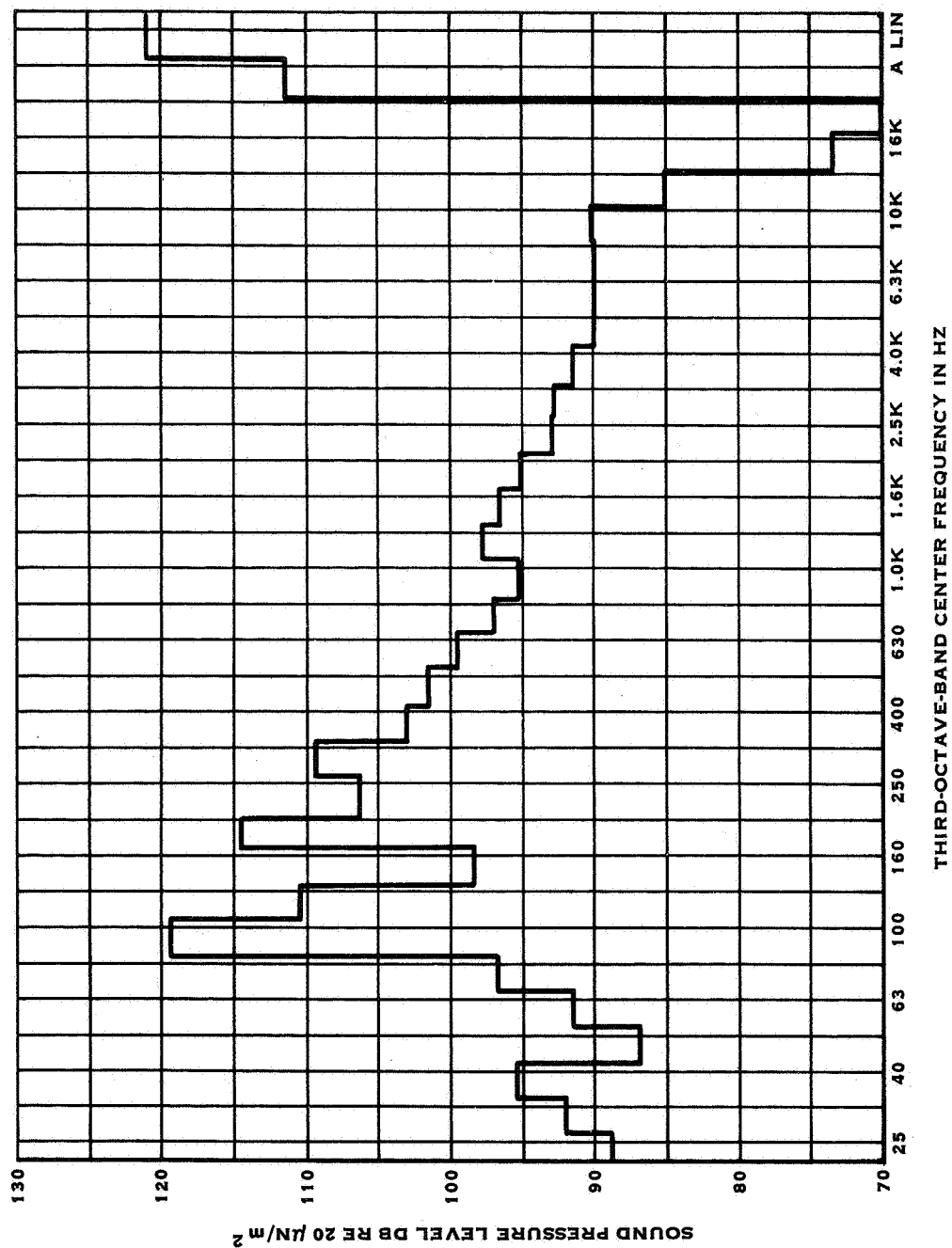


FIGURE 69. AFT MICROPHONE 1/3 OCTAVE BAND ANALYSIS FOR RUN 2

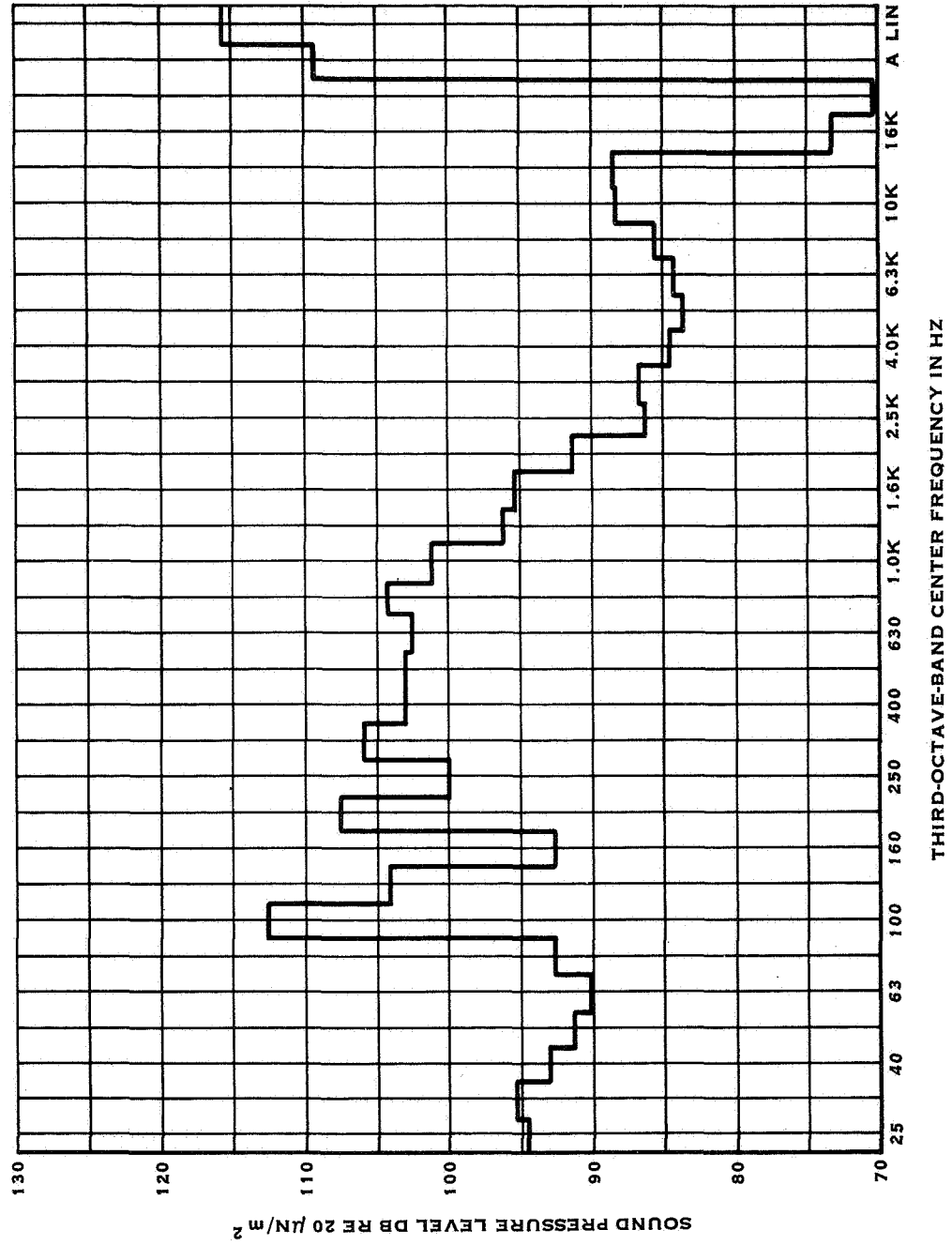


FIGURE 70. IN-PLANE MICROPHONE 1/3 OCTAVE BAND ANALYSIS FOR RUN 6

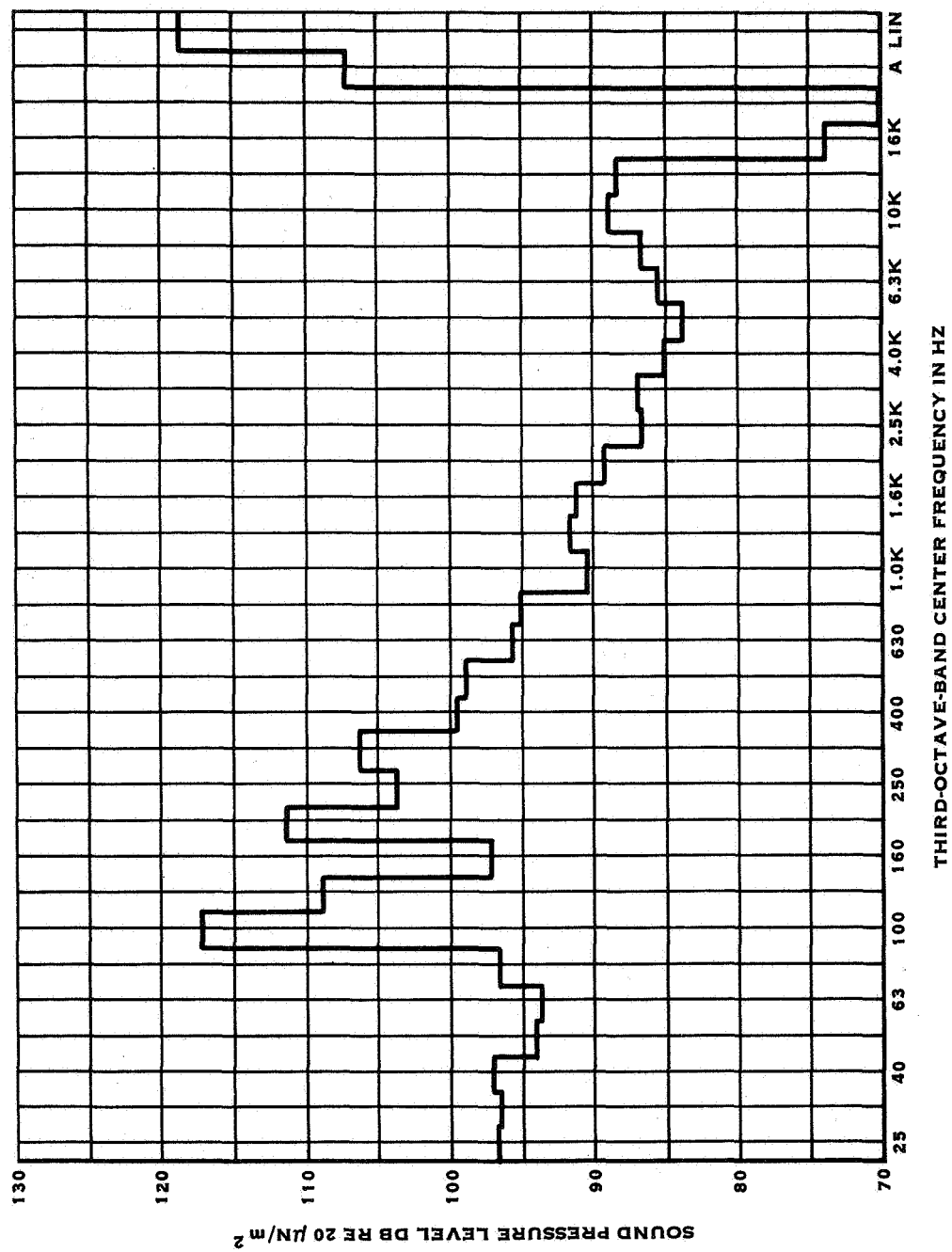


FIGURE 71. AFT MICROPHONE 1/3 OCTAVE BAND ANALYSIS FOR RUN 6

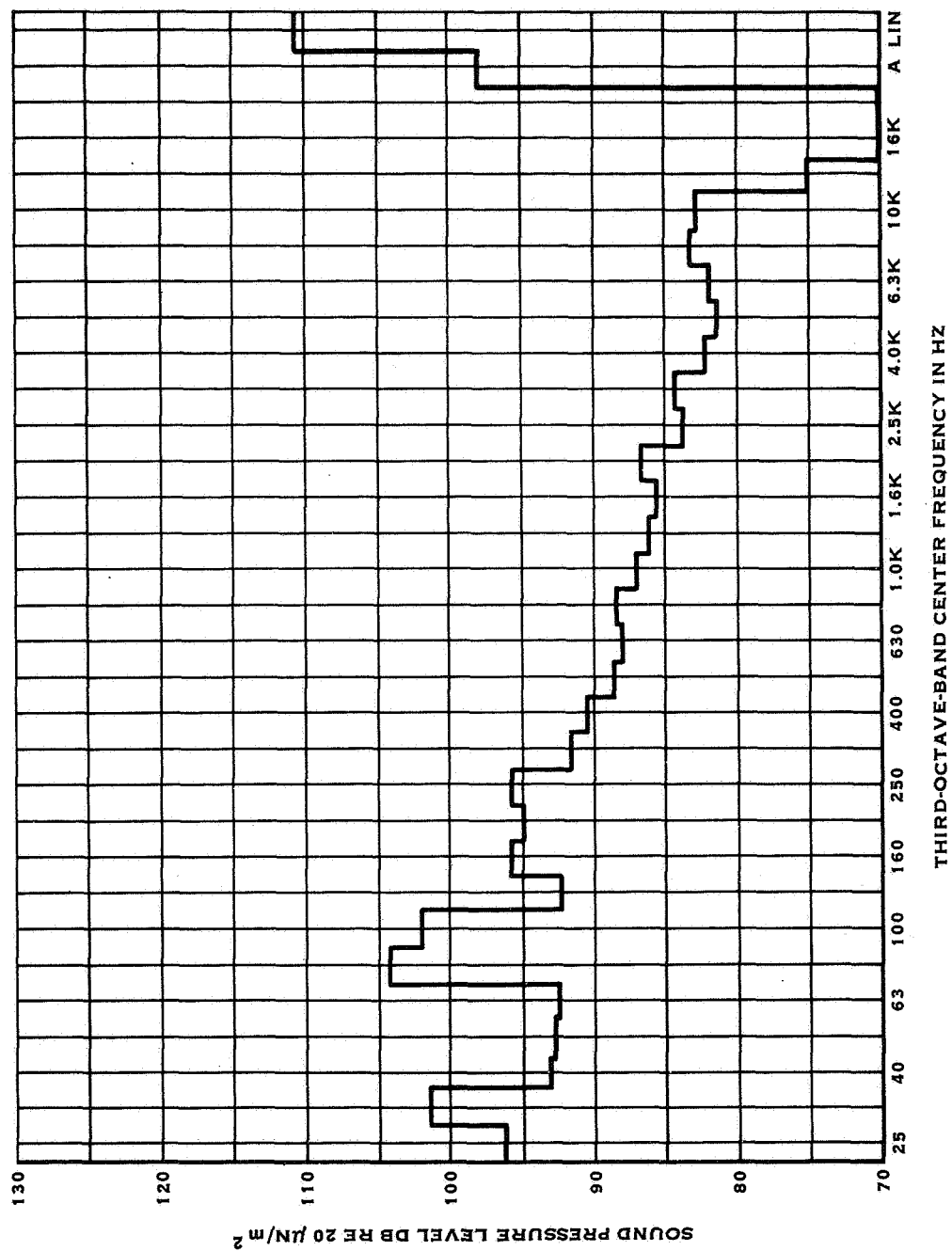


FIGURE 72. IN-PLANE MICROPHONE 1/3 OCTAVE BAND ANALYSIS FOR RUN 5

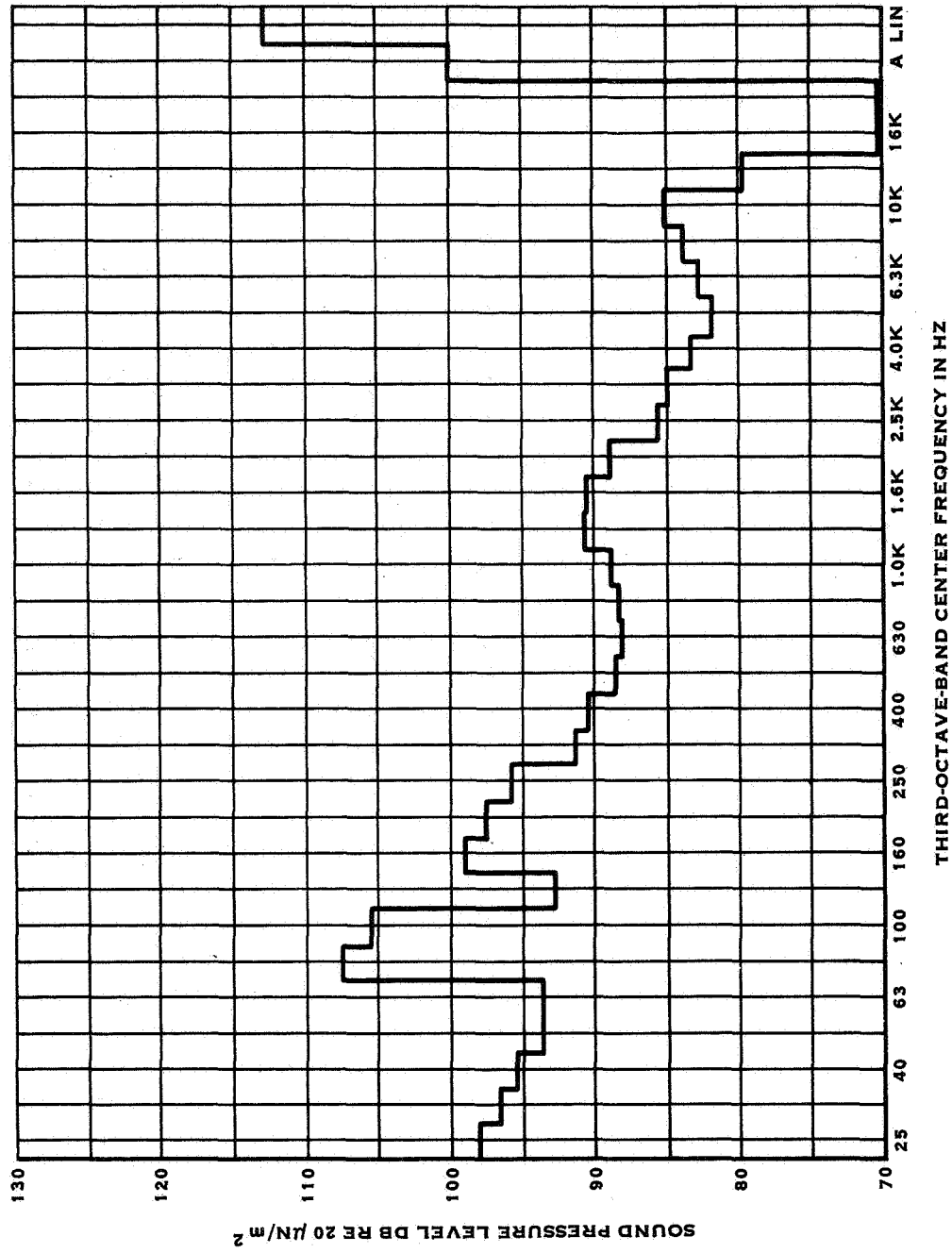


FIGURE 73. AFT MICROPHONE 1/3 OCTAVE BAND ANALYSIS FOR RUN 5

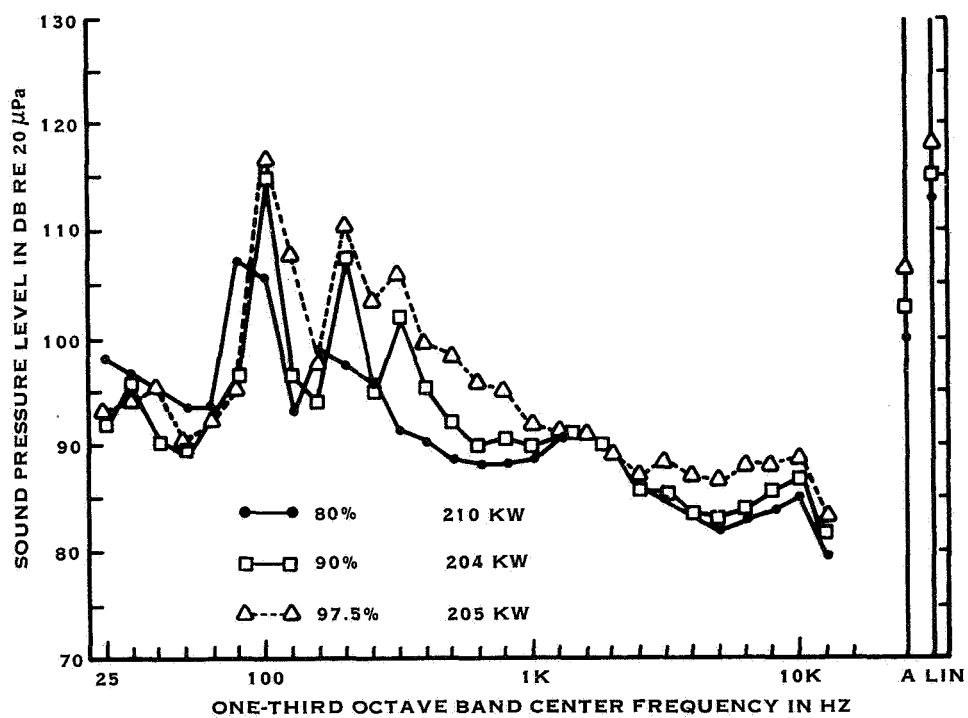


FIGURE 74. INFLUENCE OF TIP SPEED ON NOISE AT AFT WING TIP MICROPHONE IN FLIGHT

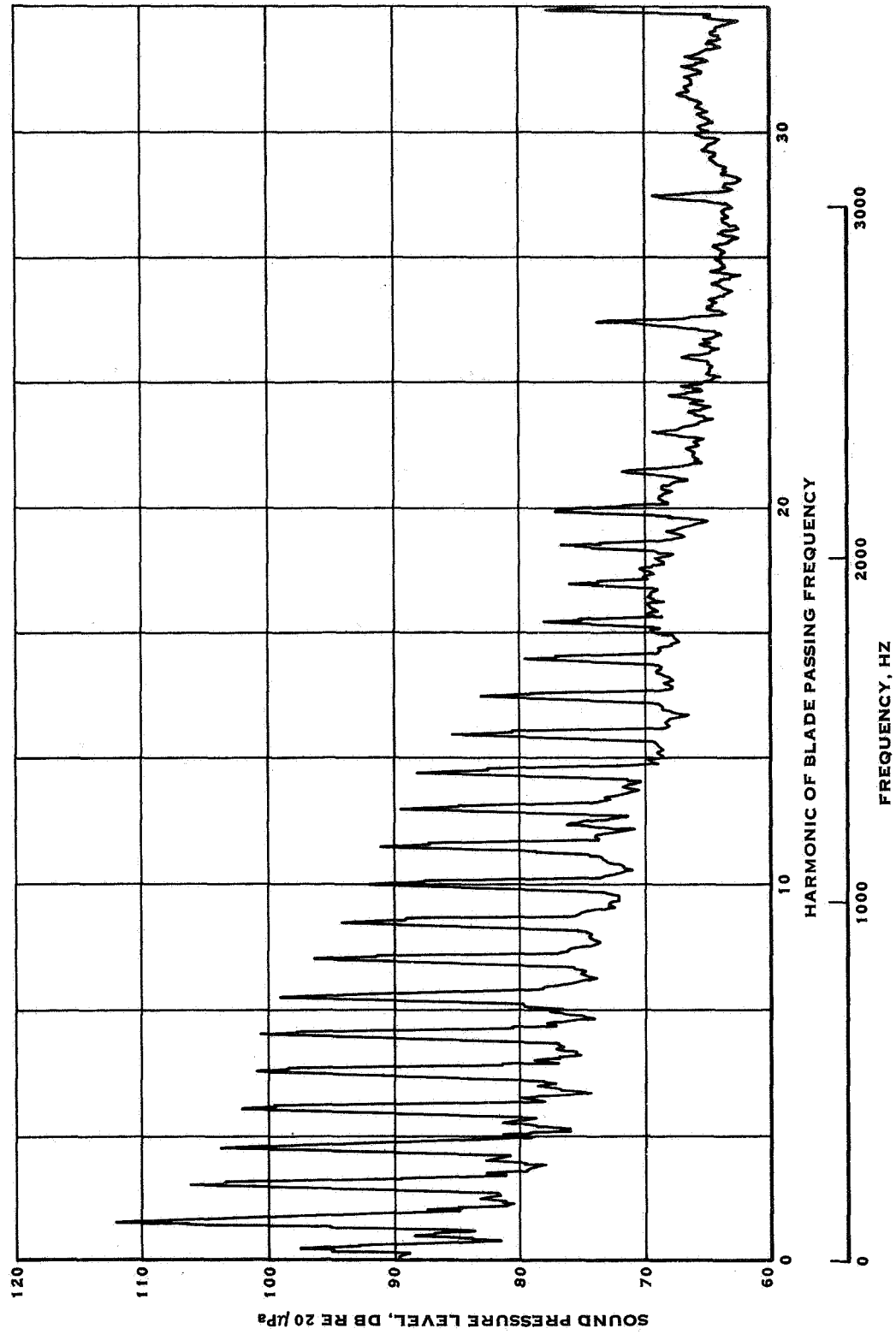


FIGURE 75. NARROW BAND FREQUENCY ANALYSIS OF THE IN-PLANE MICROPHONE DATA FOR RUN 2

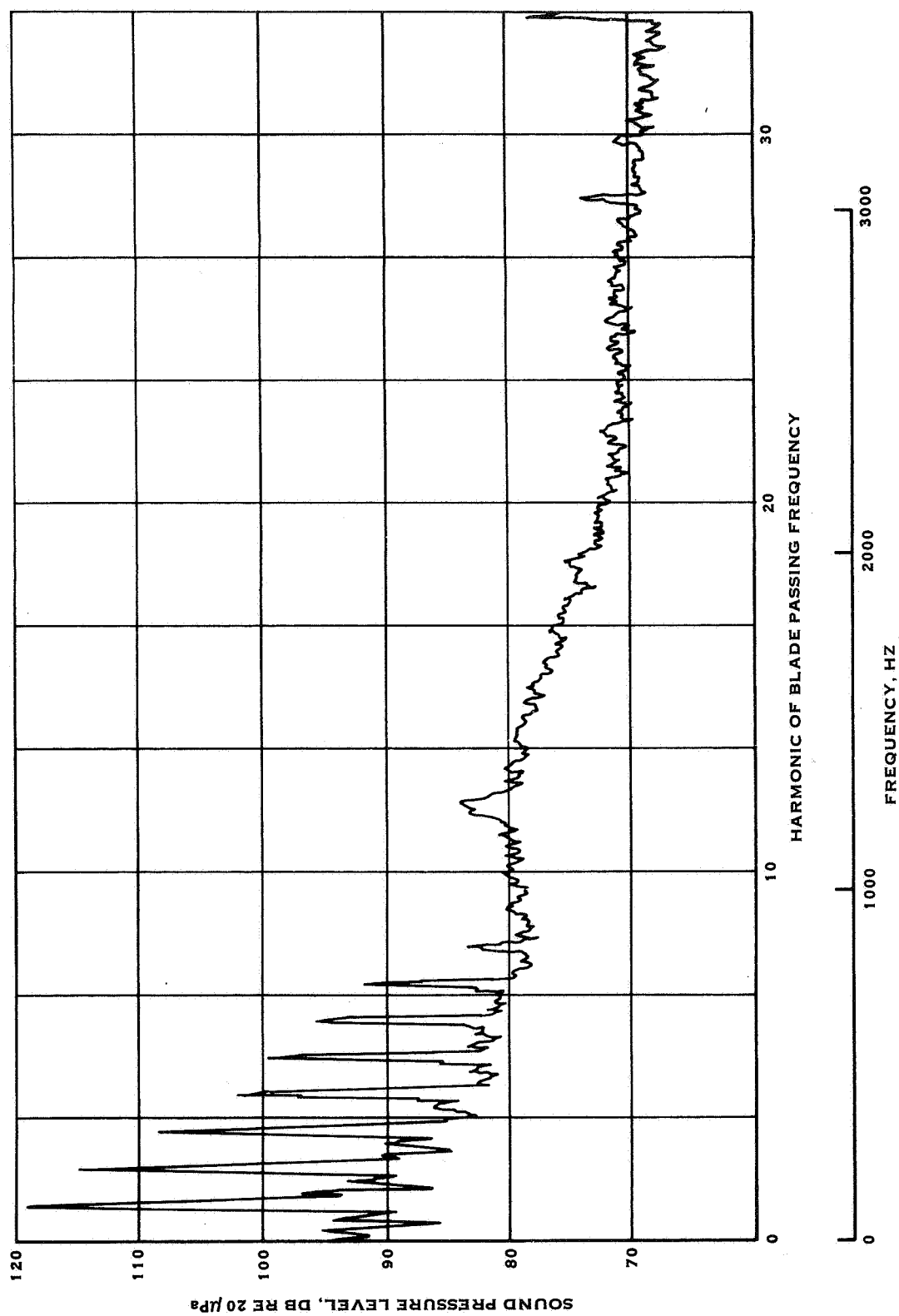


FIGURE 76. NARROW BAND FREQUENCY ANALYSIS OF THE AFT
MICROPHONE DATA FOR RUN 2

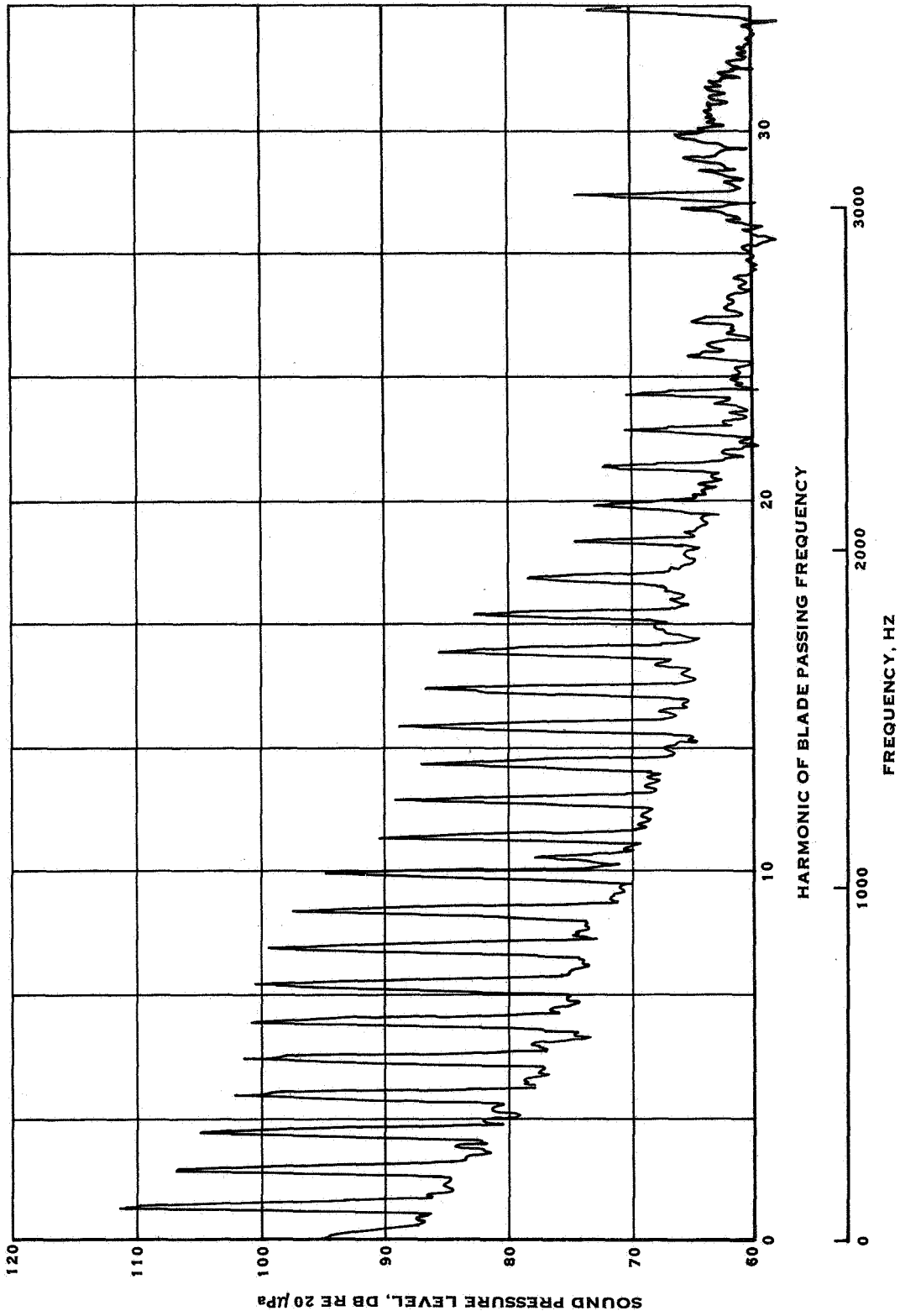


FIGURE 77. NARROW BAND FREQUENCY ANALYSIS OF THE IN-PLANE MICROPHONE DATA FOR RUN 6

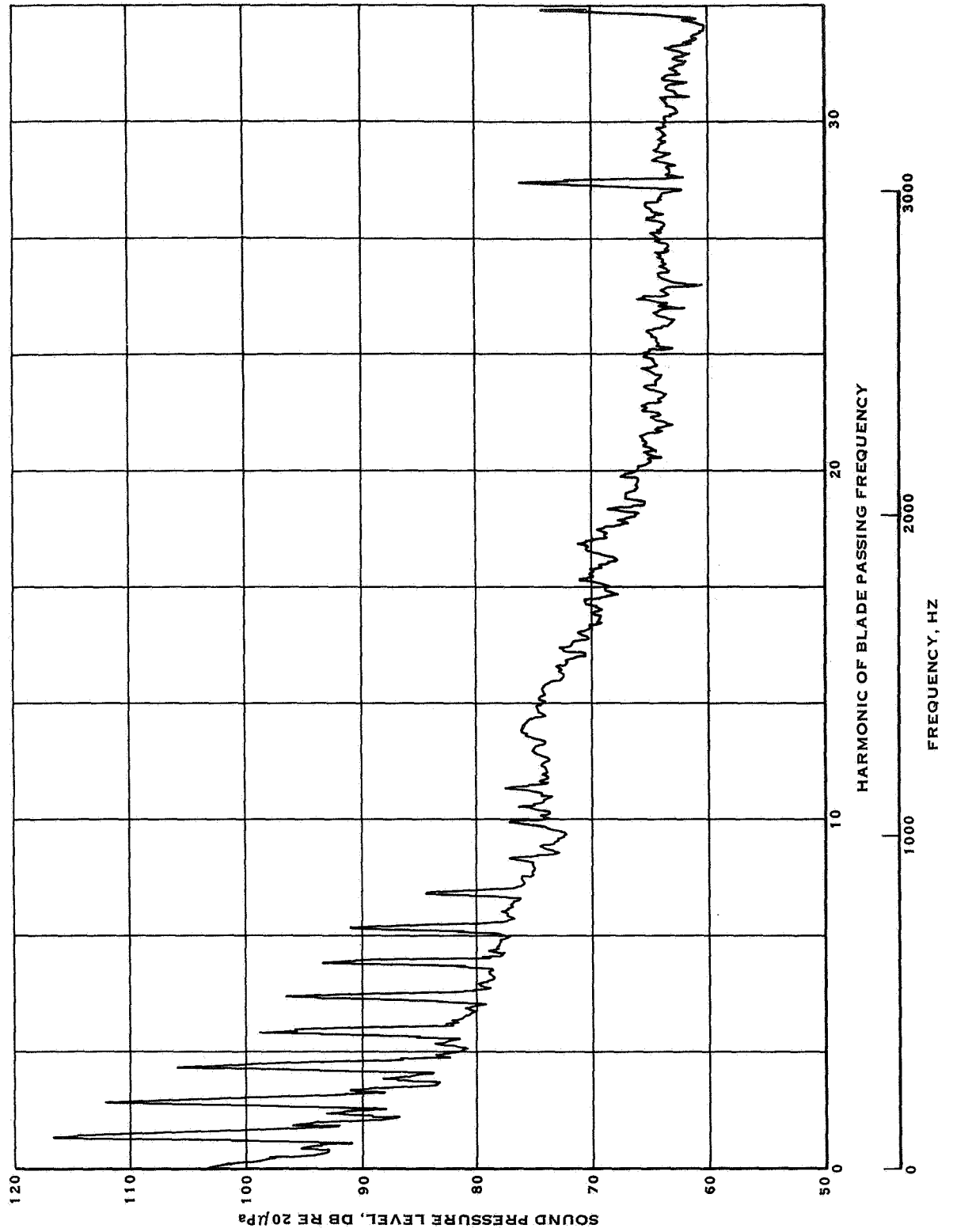


FIGURE 78. NARROW BAND FREQUENCY ANALYSIS OF THE AFT MICROPHONE DATA FOR RUN 6

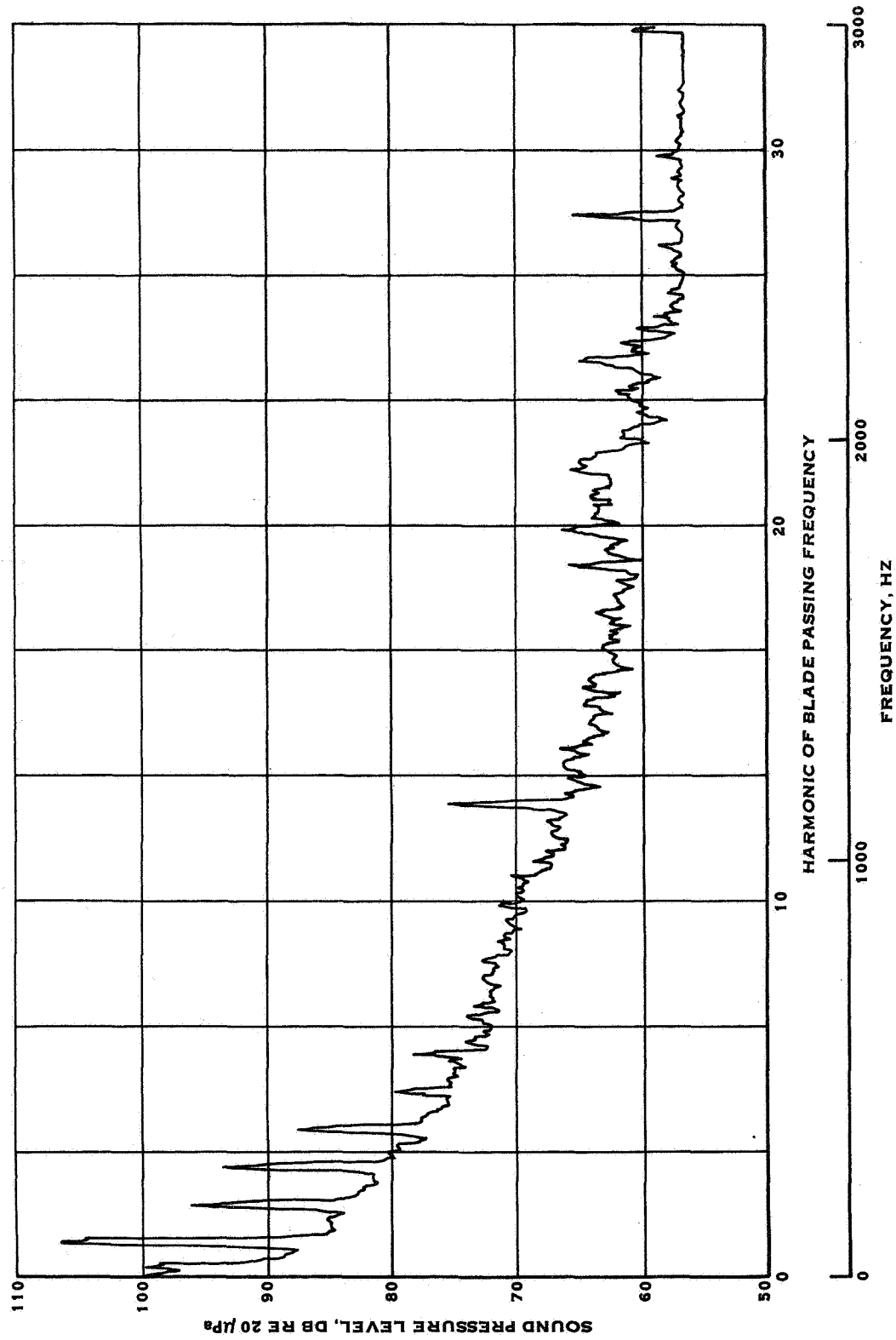


FIGURE 79. NARROW BAND FREQUENCY ANALYSIS OF THE IN-PLANE MICROPHONE DATA FOR RUN 5

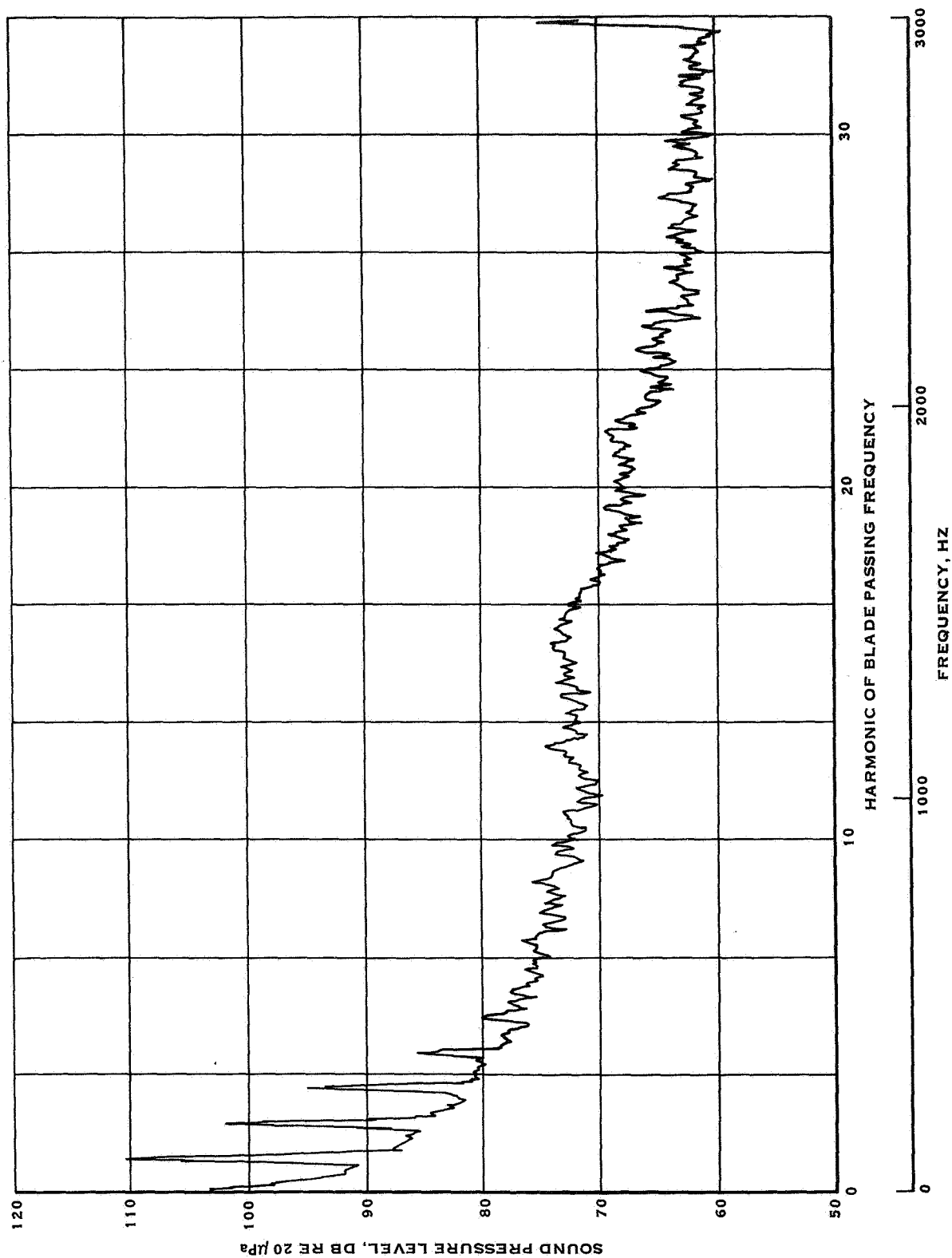


FIGURE 80. NARROW BAND FREQUENCY ANALYSIS OF THE AFT MICROPHONE DATA FOR RUN 5

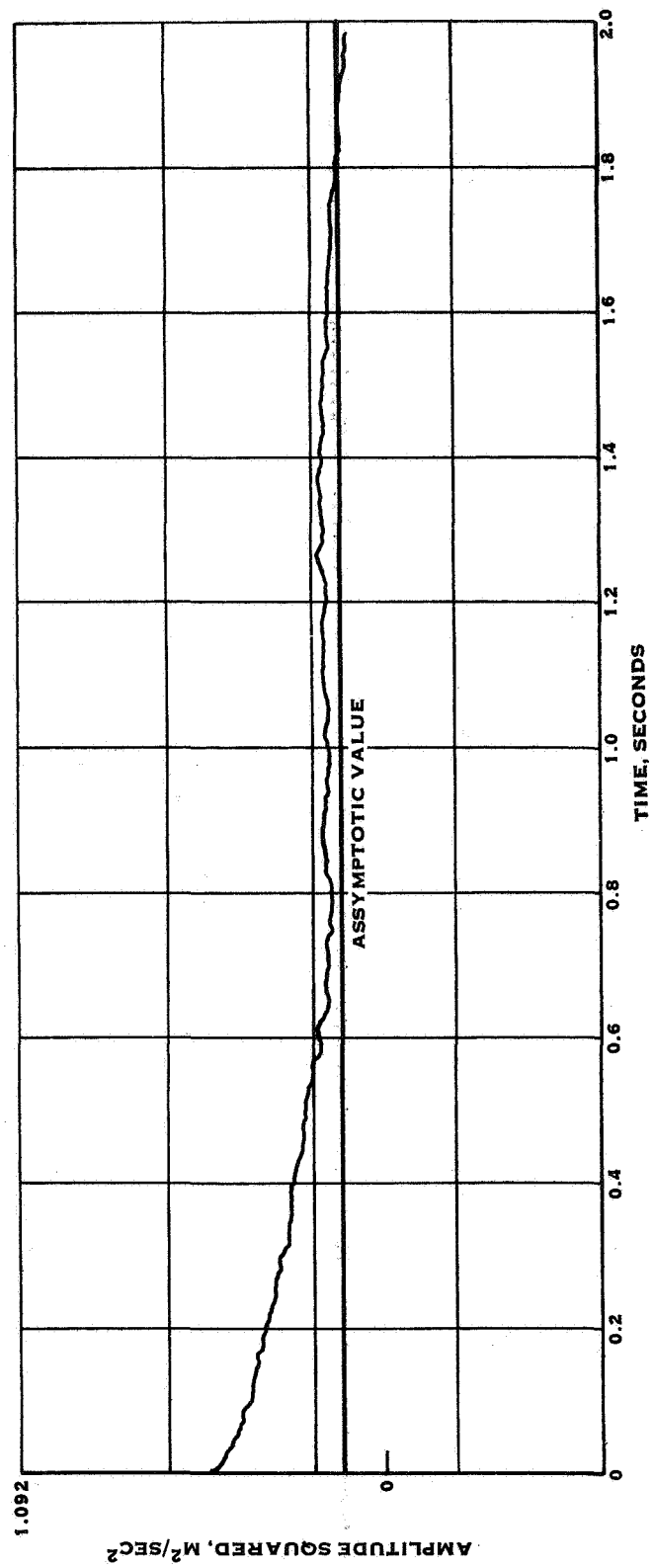


FIGURE 81. AUTOCORRELATION OF THE ANEMOMETER DATA FOR RUN 2

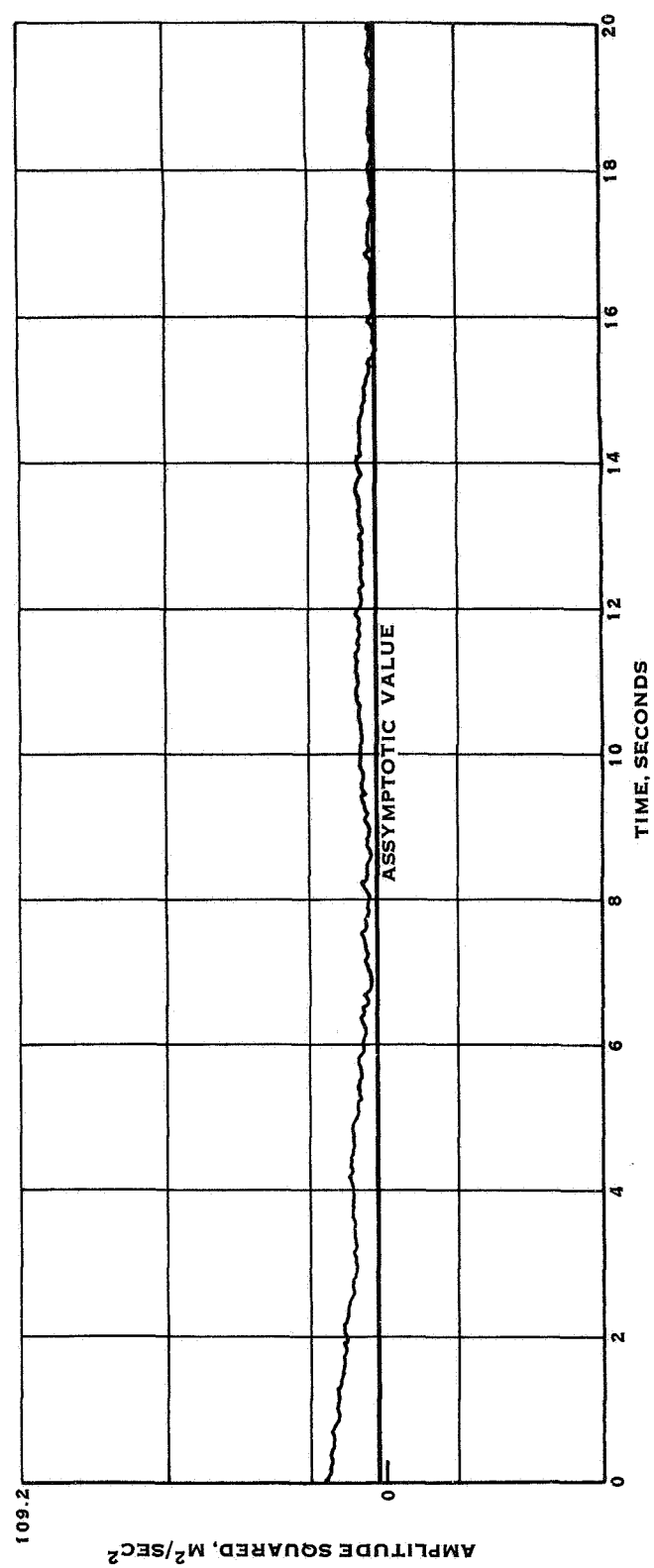


FIGURE 82. AUTOCORRELATION OF THE ANEMOMETER DATA FOR RUN 6

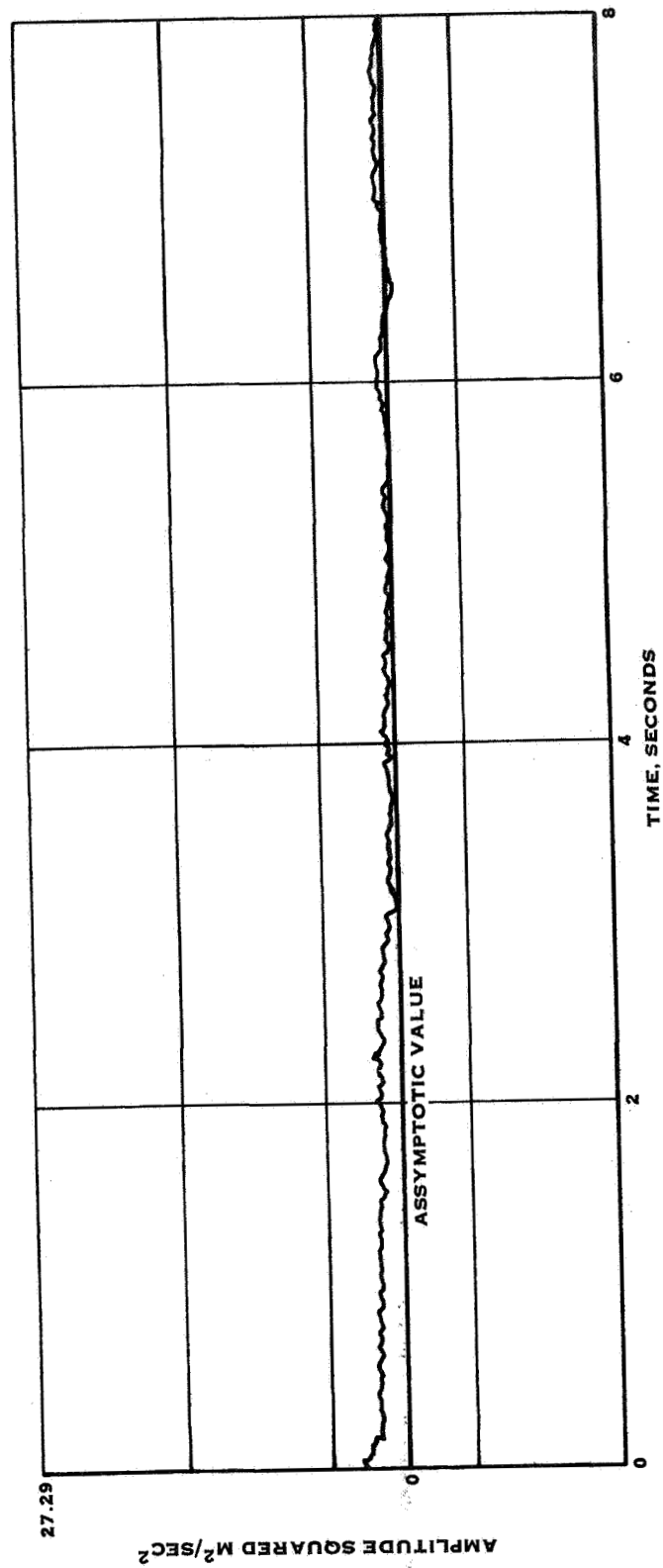


FIGURE 83. AUTOCORRELATION OF THE ANEMOMETER DATA FOR RUN 6

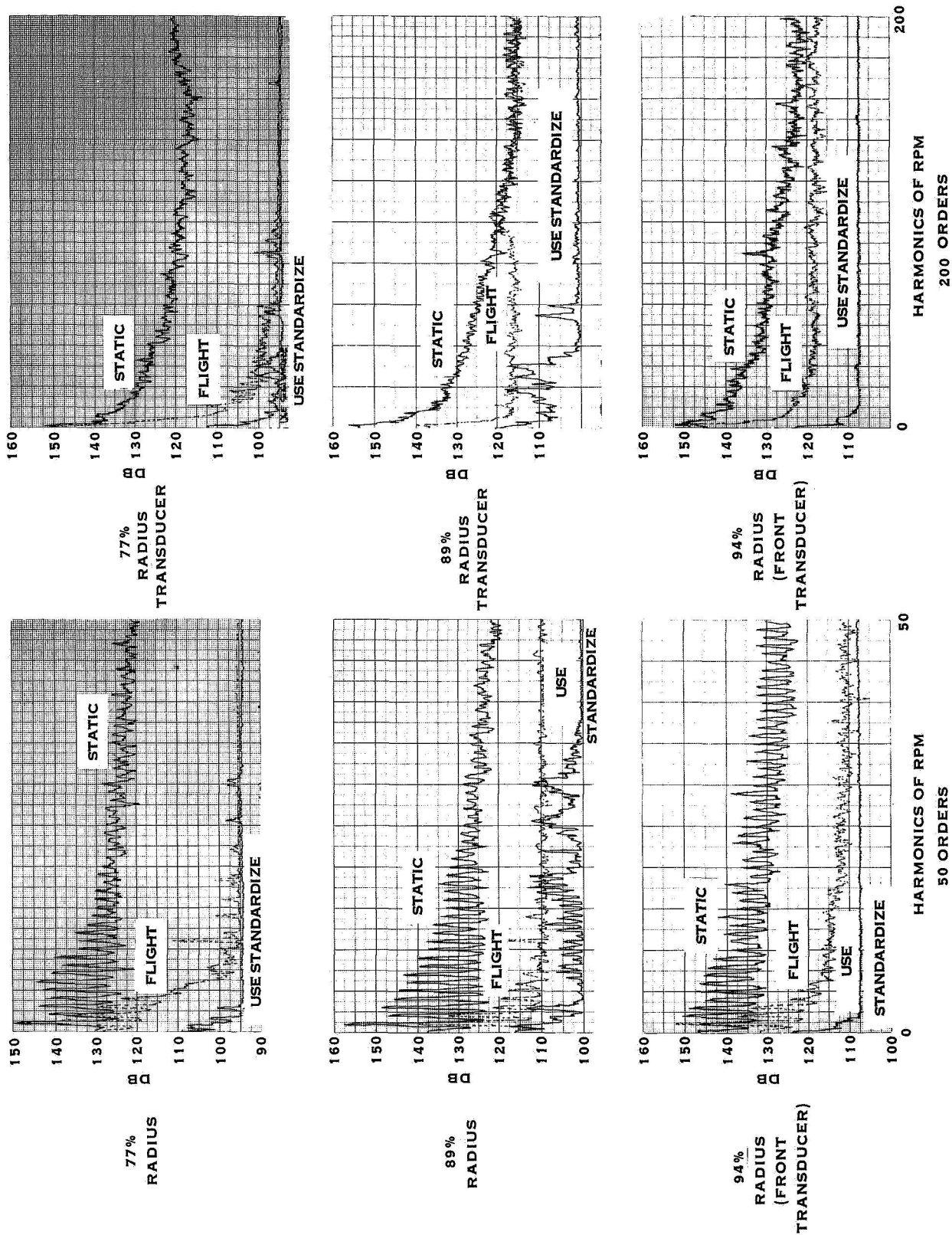


FIGURE 84. COMPARISON OF STATIC AND FLIGHT BLADE SURFACE PRESSURES AT 97.5% RPM
(RUNS 6S AND 6, RESPECTIVELY)

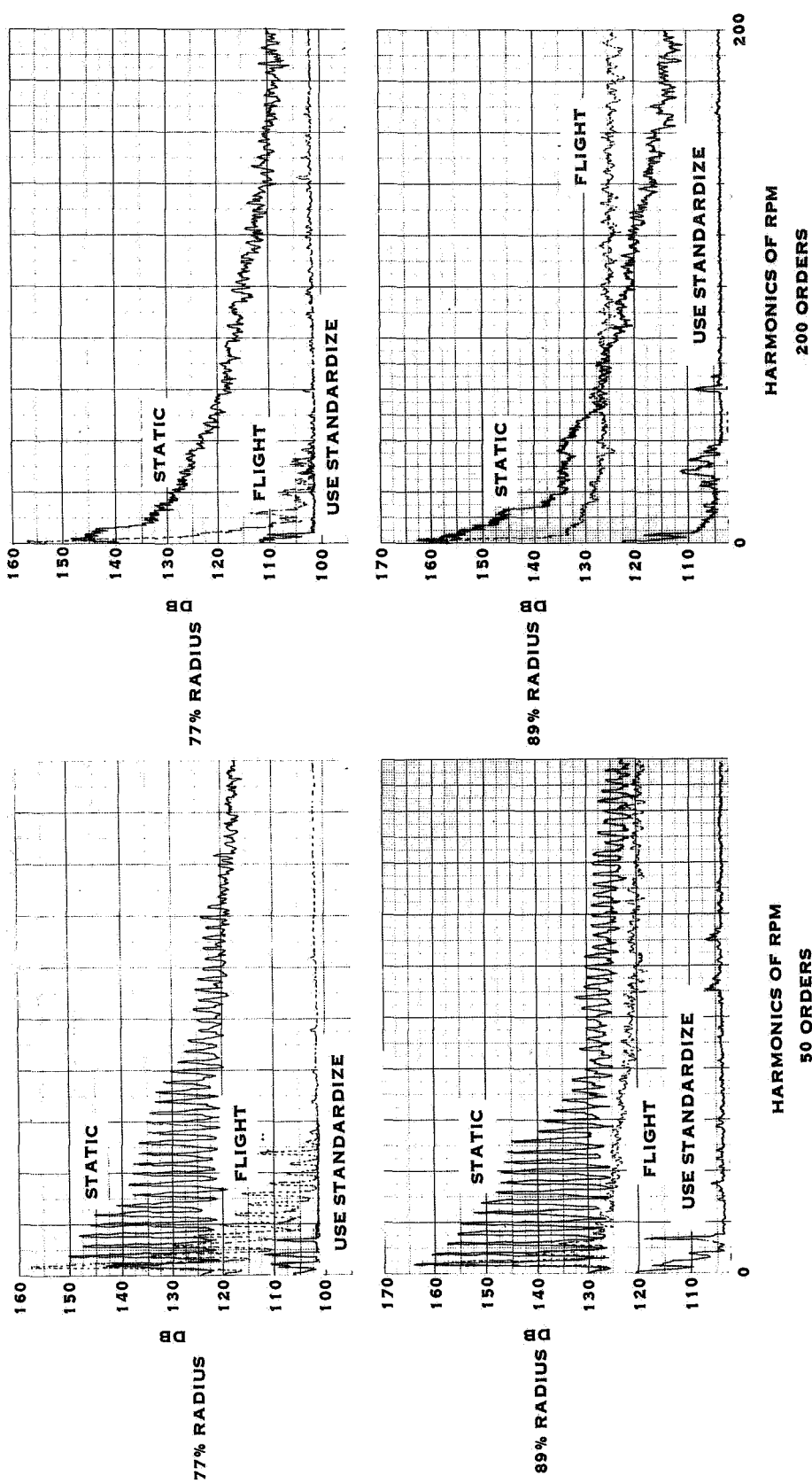


FIGURE 85. COMPARISON OF STATIC AND FLIGHT BLADE SURFACE PRESSURES AT 90% RPM
(RUNS 17S AND 17, RESPECTIVELY)

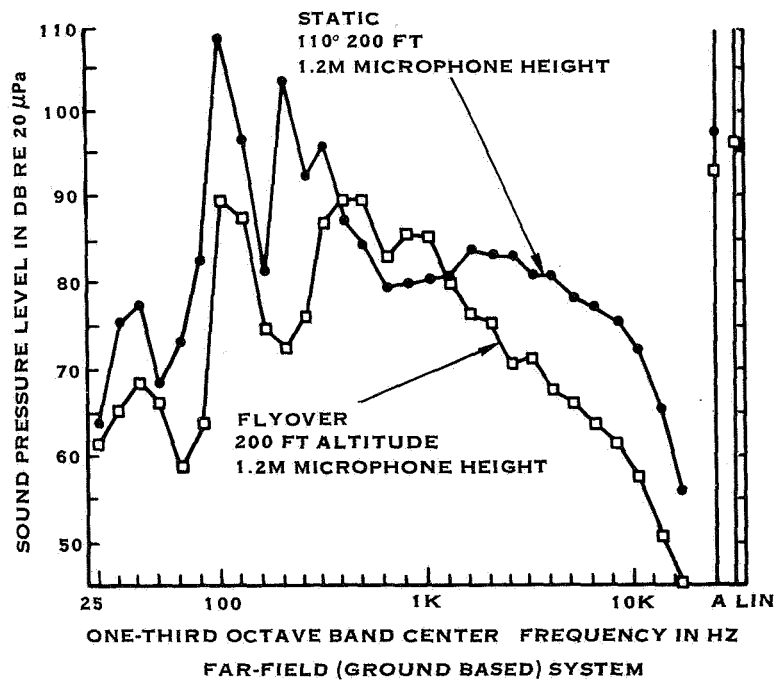
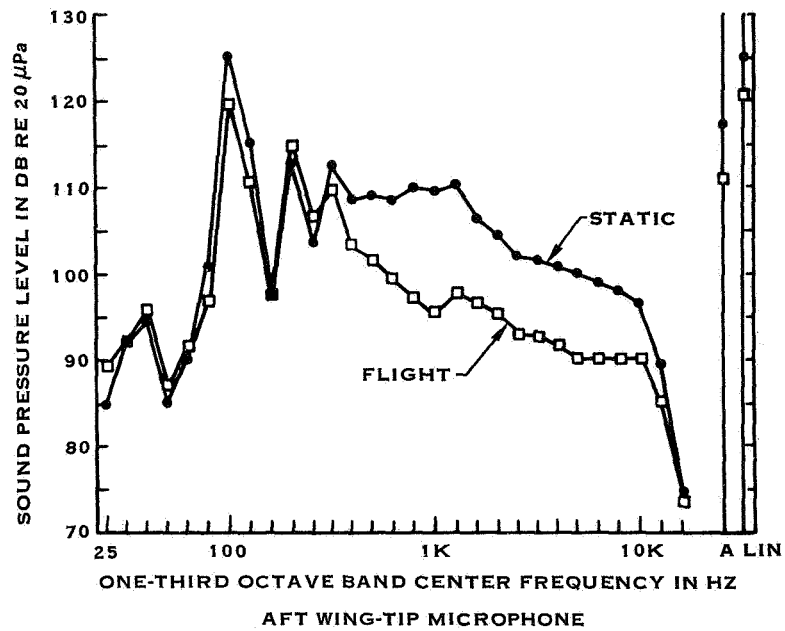


FIGURE 86. COMPARISON OF STATIC AND FLIGHT 1/3 OCTAVE BAND SPECTRA AT 97.5% RPM (RUNS 6S AND 6, RESPECTIVELY)

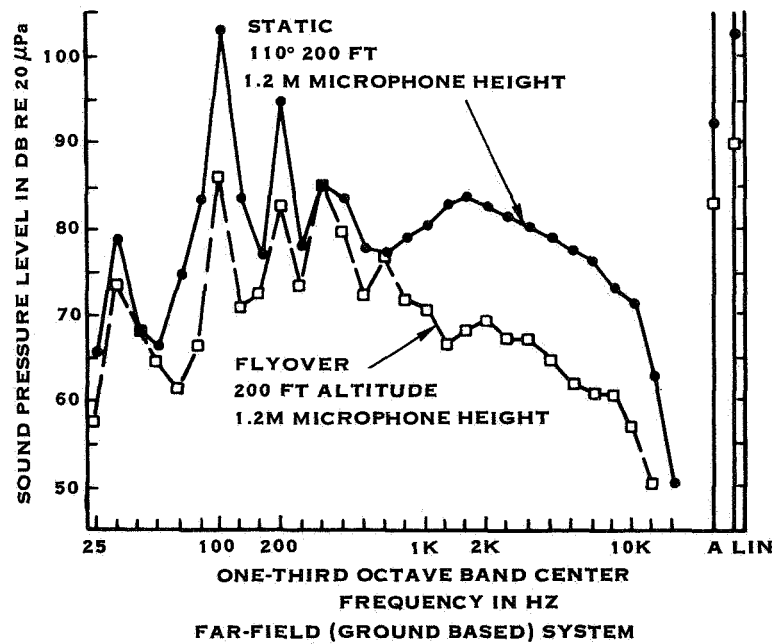
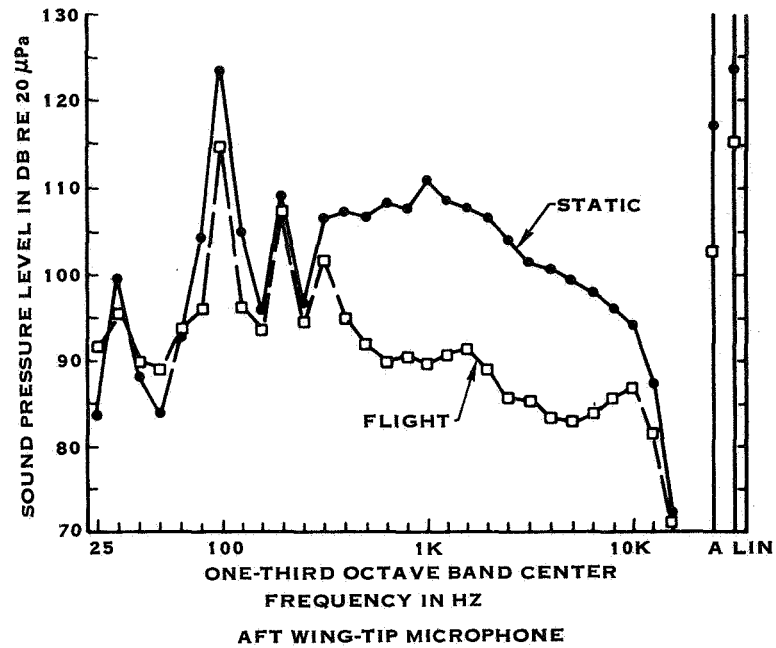


FIGURE 87. COMPARISON OF STATIC AND FLIGHT 1/3 OCTAVE BAND SPECTRA AT 90% RPM
(RUNS 17S AND 17, RESPECTIVELY)

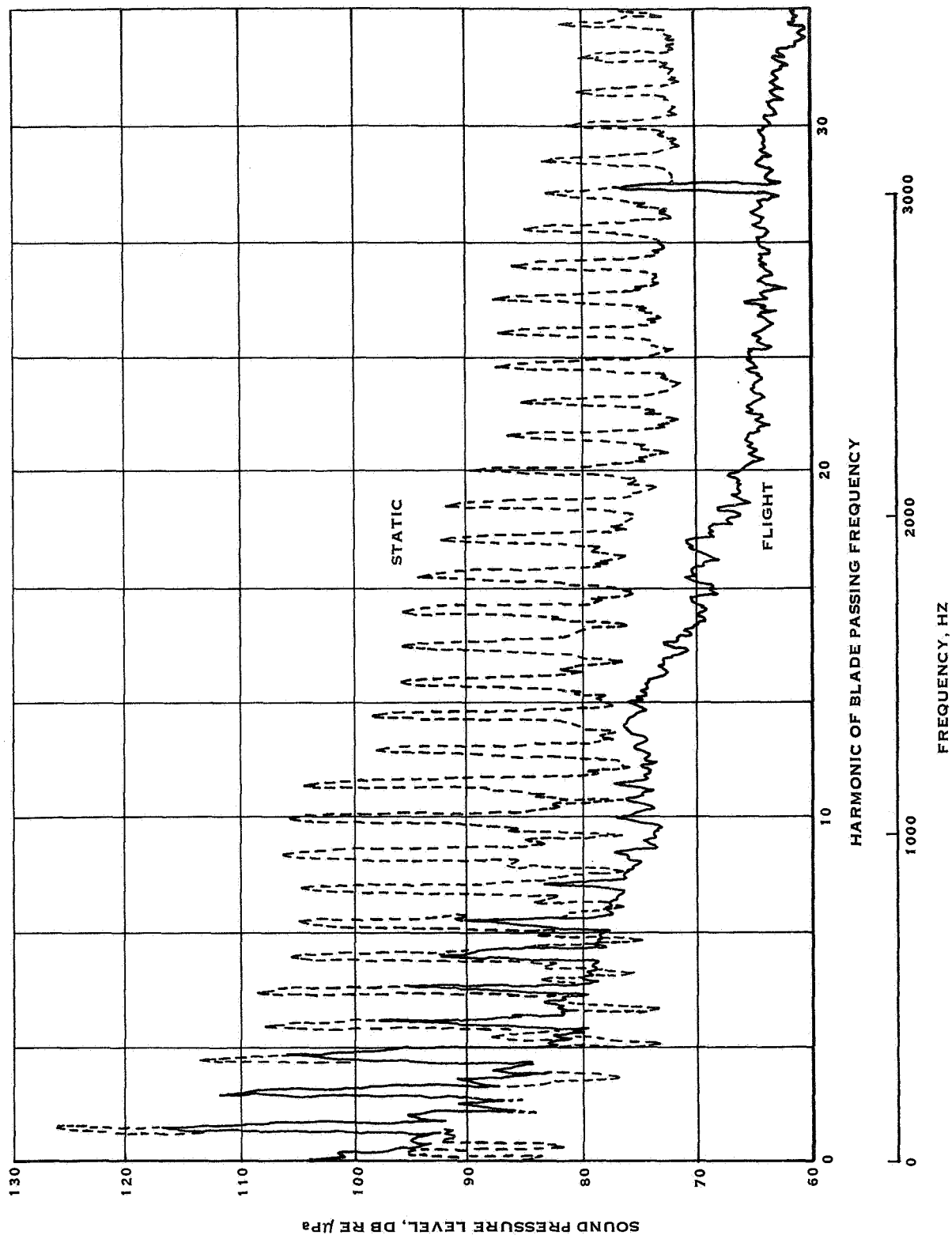


FIGURE 88. COMPARISON OF STATIC AND FLIGHT NARROW BAND SPECTRA AT 97.5% RPM
(RUNS 6S AND 6, RESPECTIVELY)

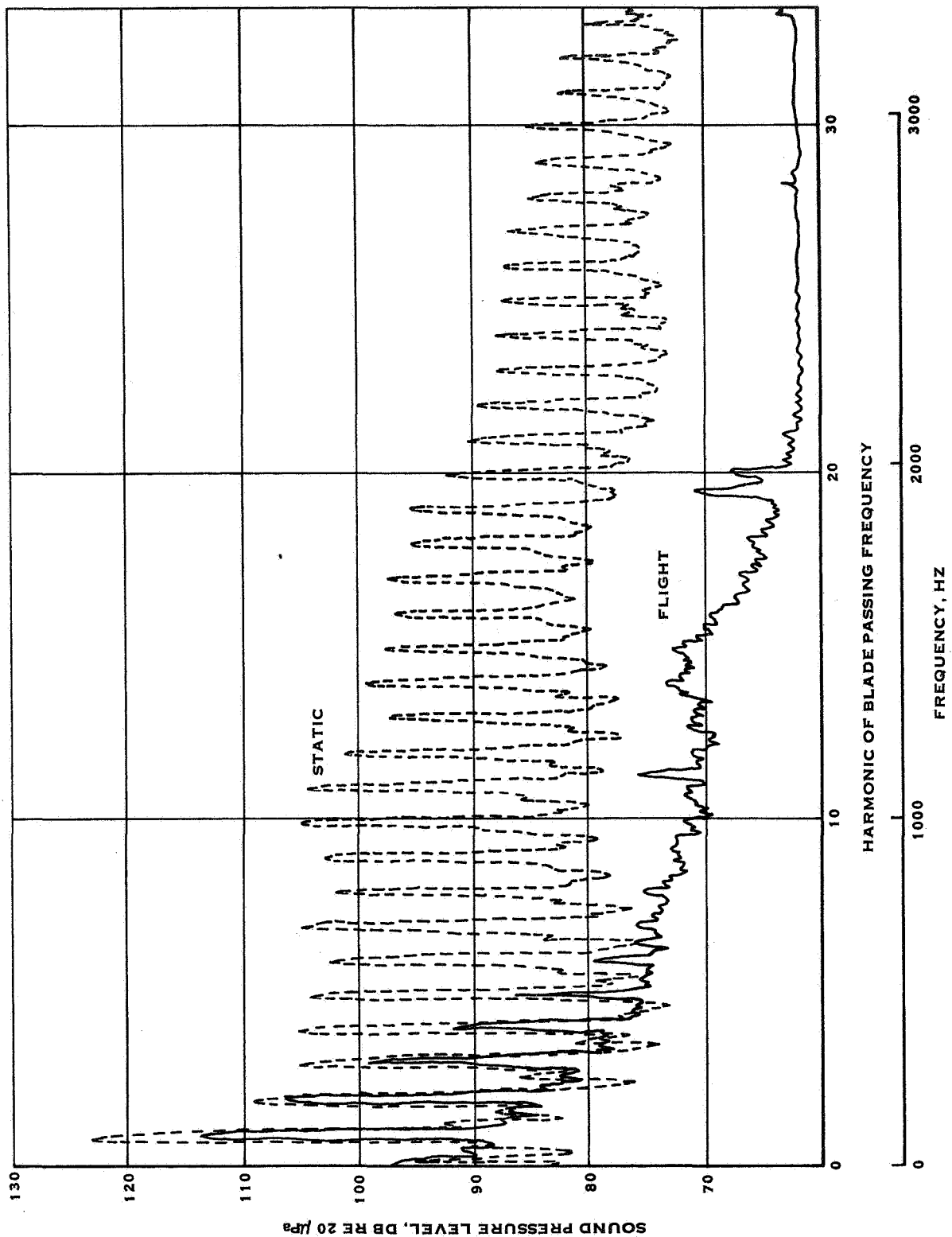


FIGURE 89. COMPARISON OF STATIC AND FLIGHT NARROW BAND SPECTRA AT 90% RPM
(RUNS 17S AND 17, RESPECTIVELY)

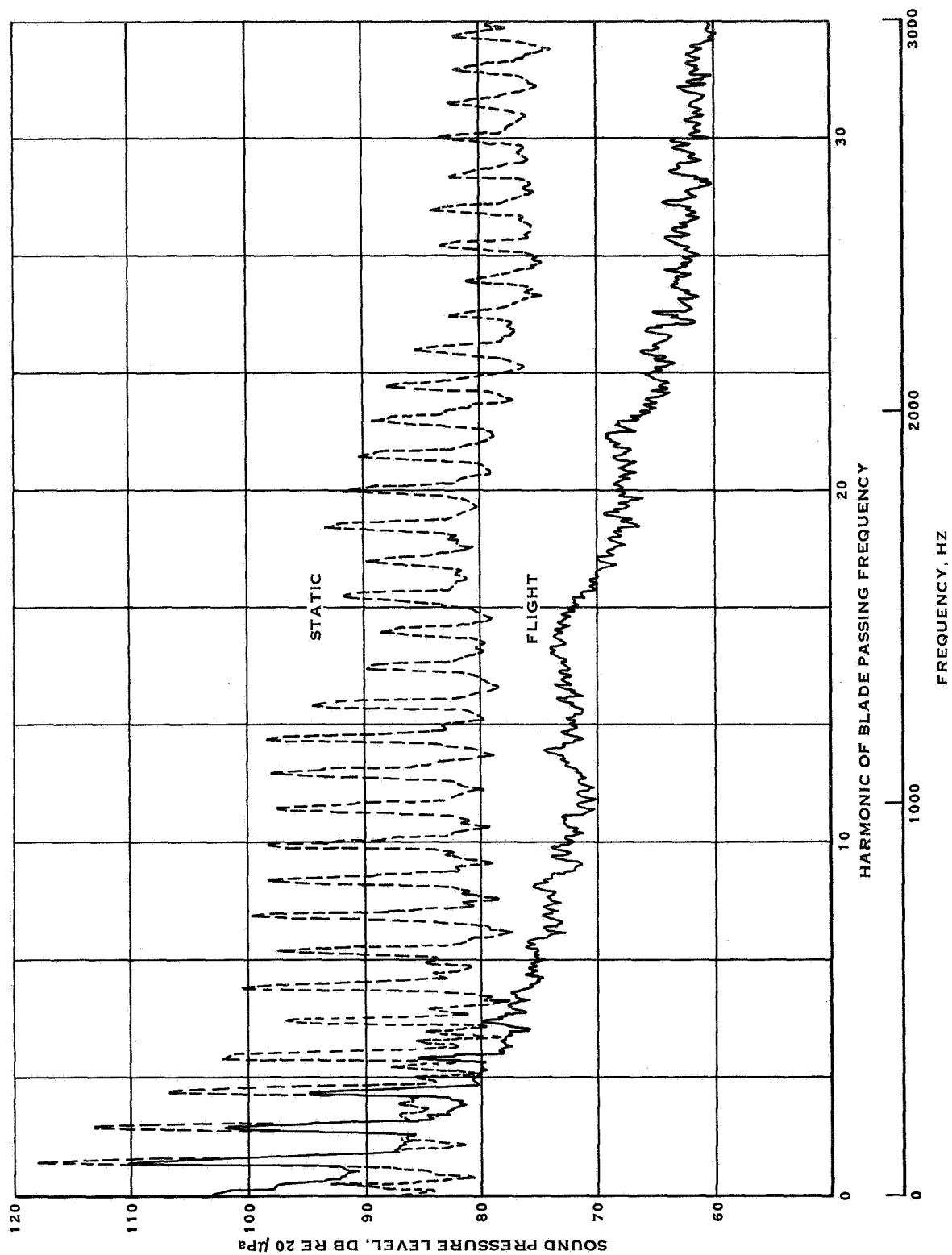


FIGURE 90. COMPARISON OF STATIC AND FLIGHT NARROW BAND SPECTRA AT 80% RPM
(RUNS 5S AND 5, RESPECTIVELY)

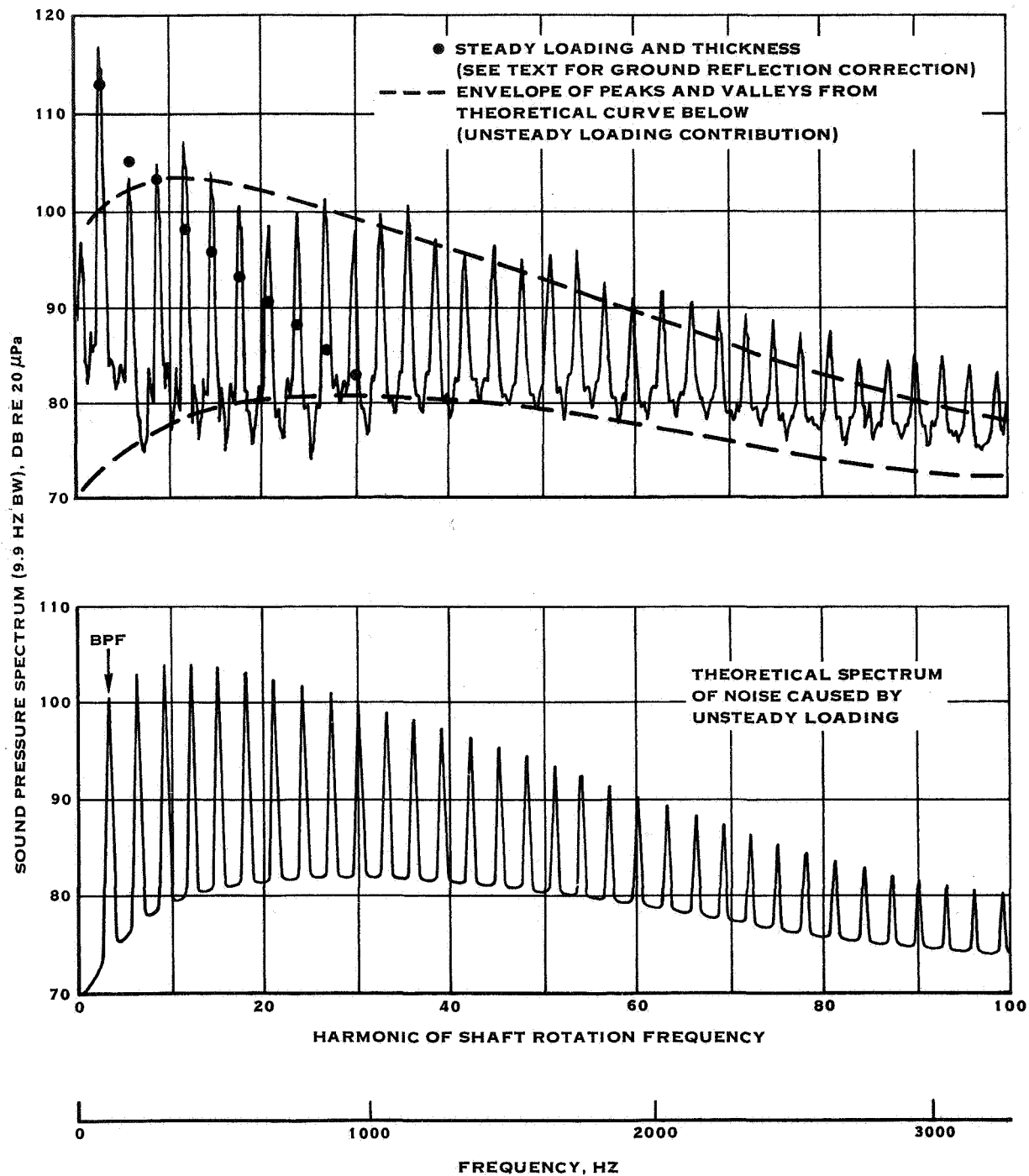


FIGURE 91. ACCOUNT OF NOISE SOURCES DURING STATIC OPERATION AT 90% RPM AND 213 KW (RUN 17S). IN-PLANE WING TIP MICROPHONE

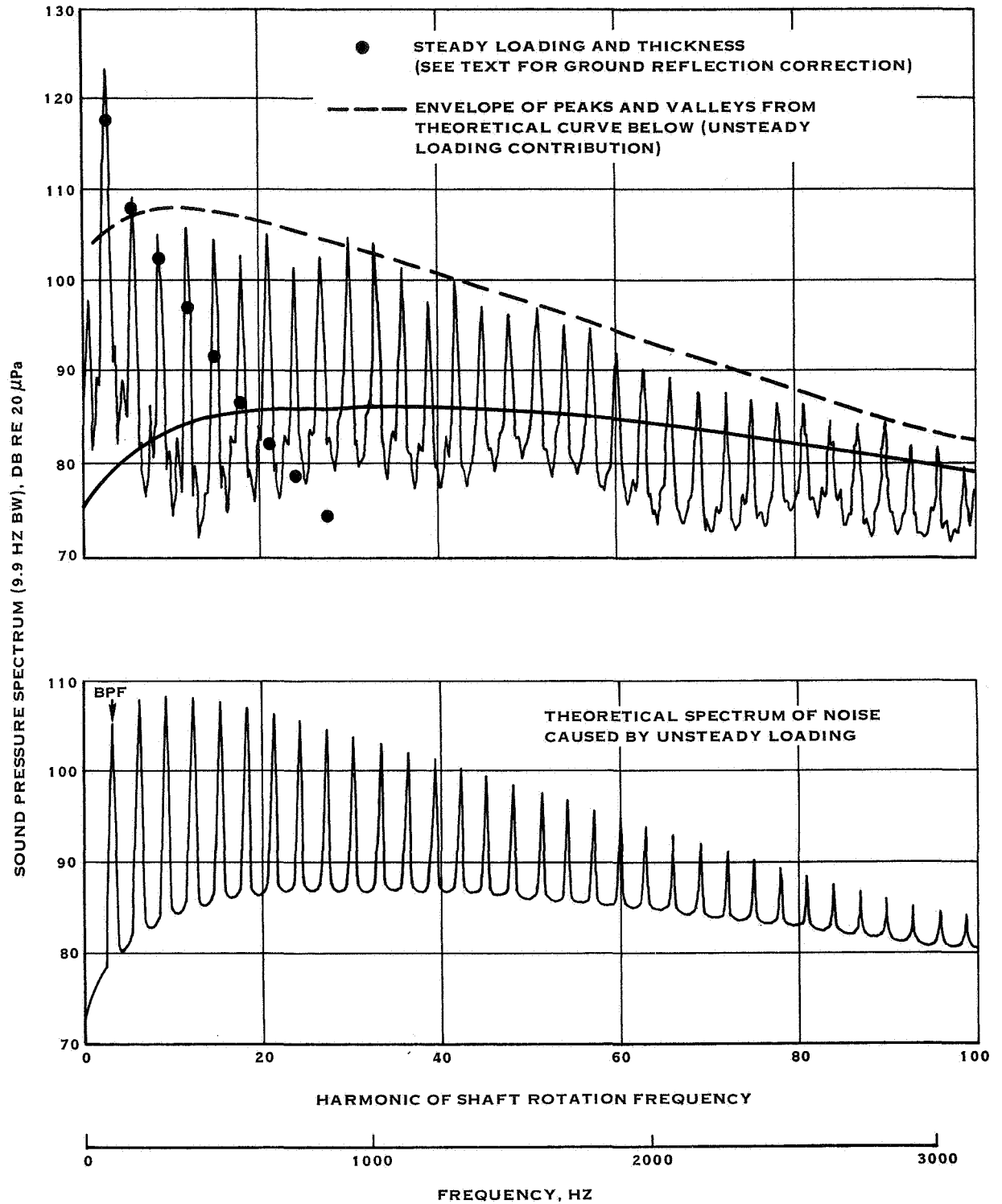


FIGURE 92. ACCOUNT OF NOISE SOURCES DURING STATIC OPERATION AT 90% RPM AND 213 KW (RUN 17S). AFT WING TIP MICROPHONE

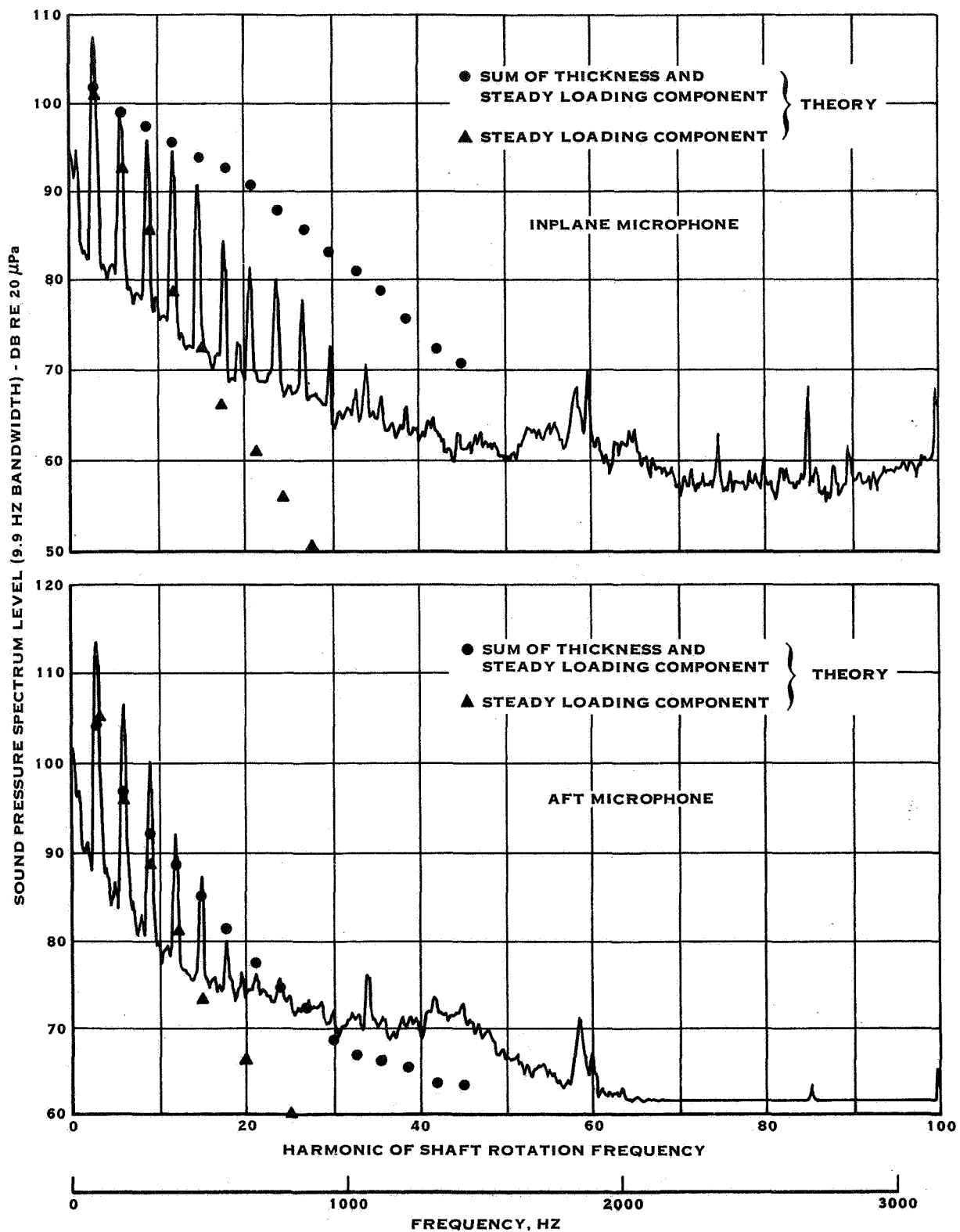


FIGURE 93. ACCOUNT OF PROPELLER NOISE SOURCES IN FLIGHT AT 90% RPM AND 204 KW (RUN 17) WING TIP MOUNTED MICROPHONES

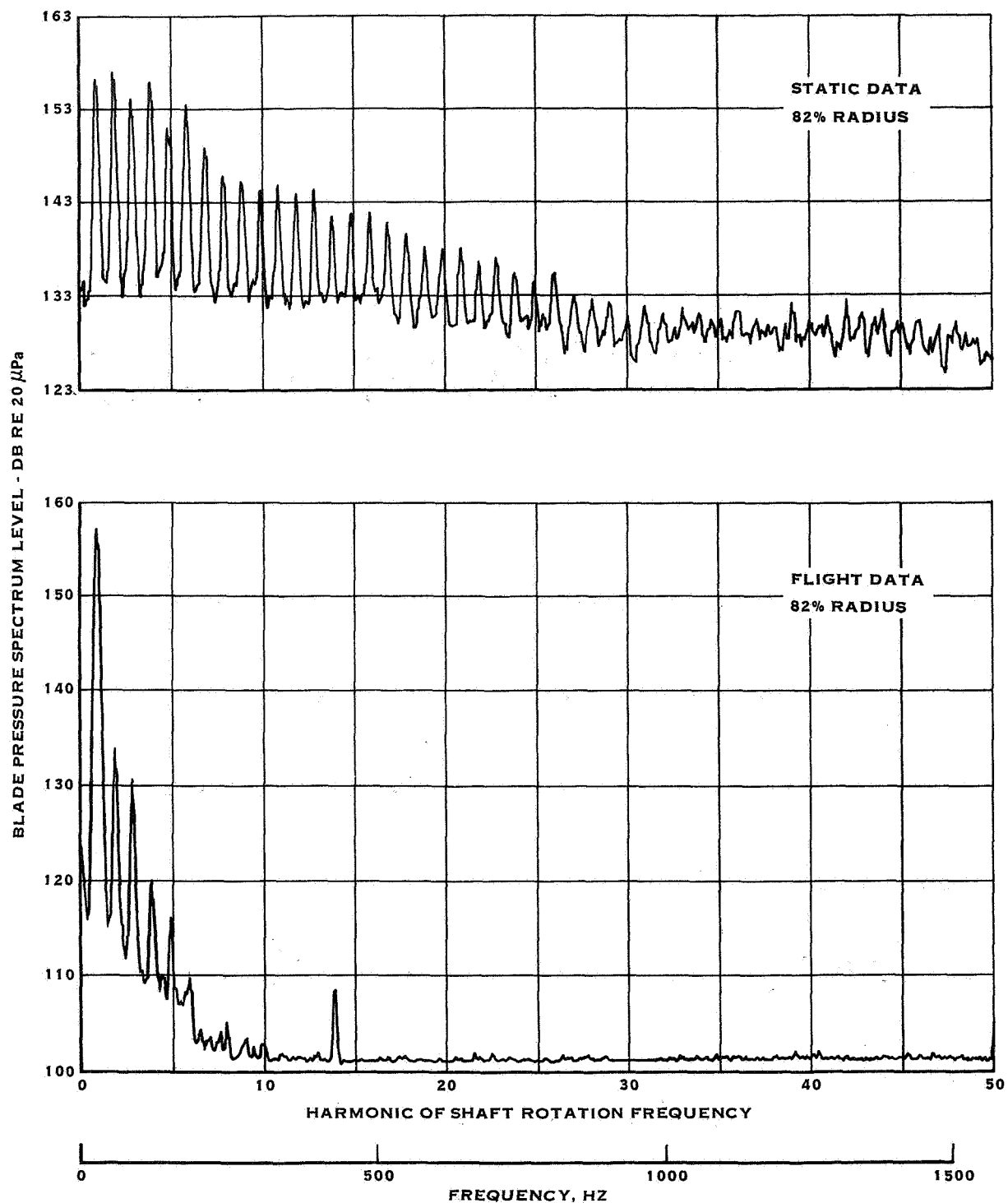


FIGURE 94. REDUCTION IN BLADE SURFACE PRESSURE SPECTRUM FROM THE STATIC TO FLIGHT CONDITION AT 90% RPM AND 204-213 KW (RUNS 17S AND 17, RESPECTIVELY)

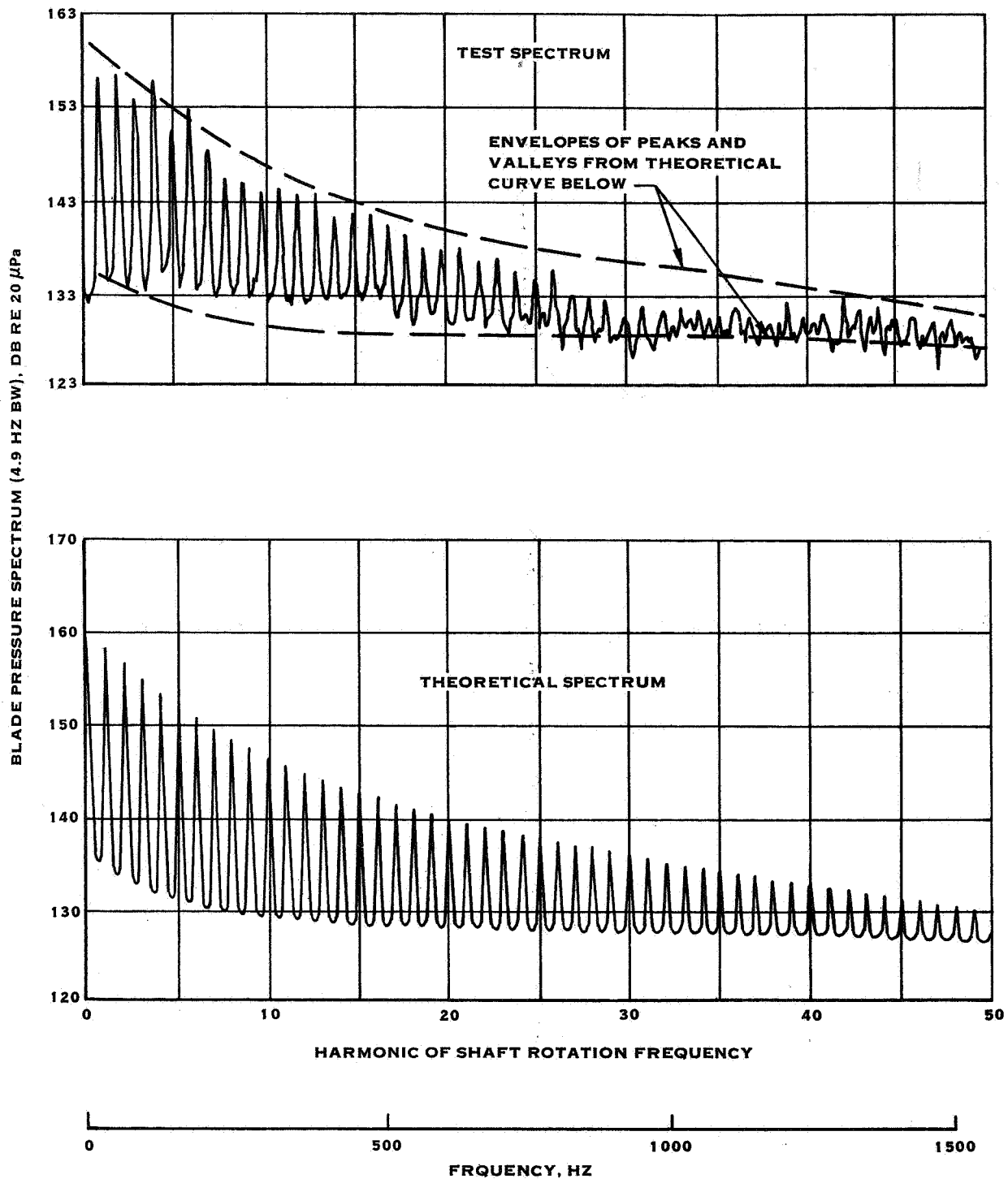


FIGURE 95. FIT OF THEORETICAL BLADE PRESSURE SPECTRUM TO CORRESPONDING TEST SPECTRUM (82% RADIUS TRANSDUCER)

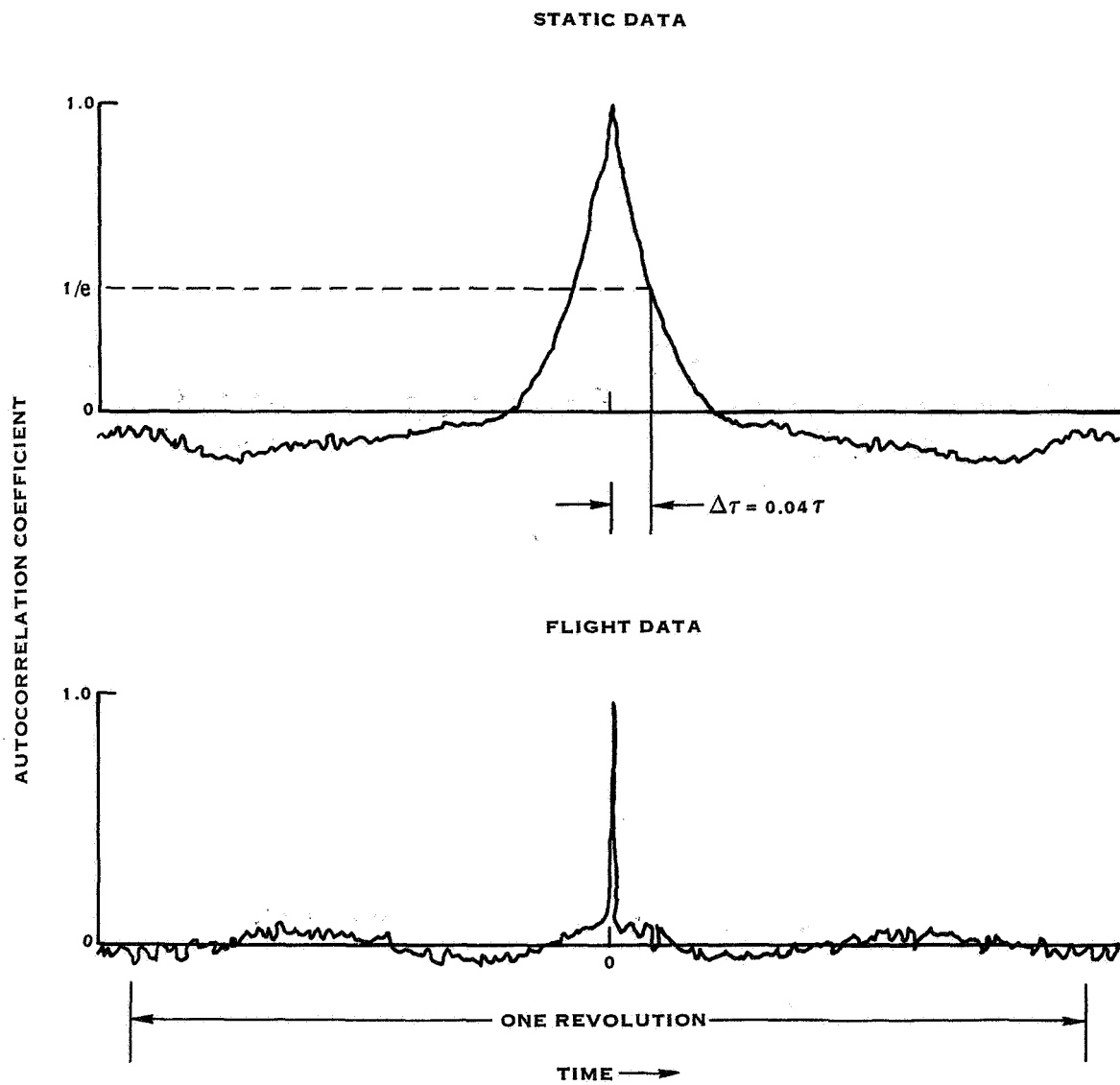


FIGURE 96. AUTOCORRELATION COEFFICIENT FOR THE 82% RADIUS PRESSURE TRANSDUCER INDICATING CIRCUMFERENTIAL LENGTH SCALE OF TURBULENCE.

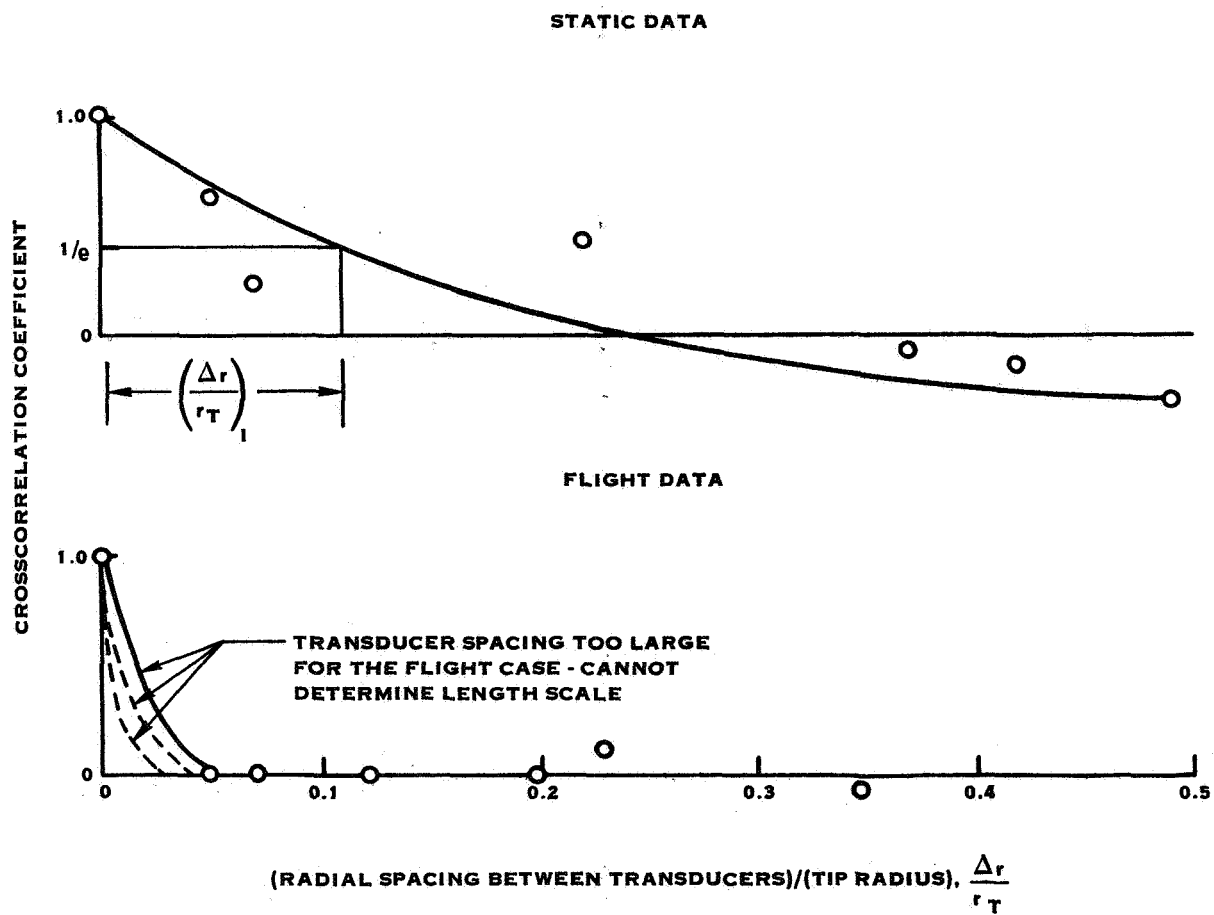
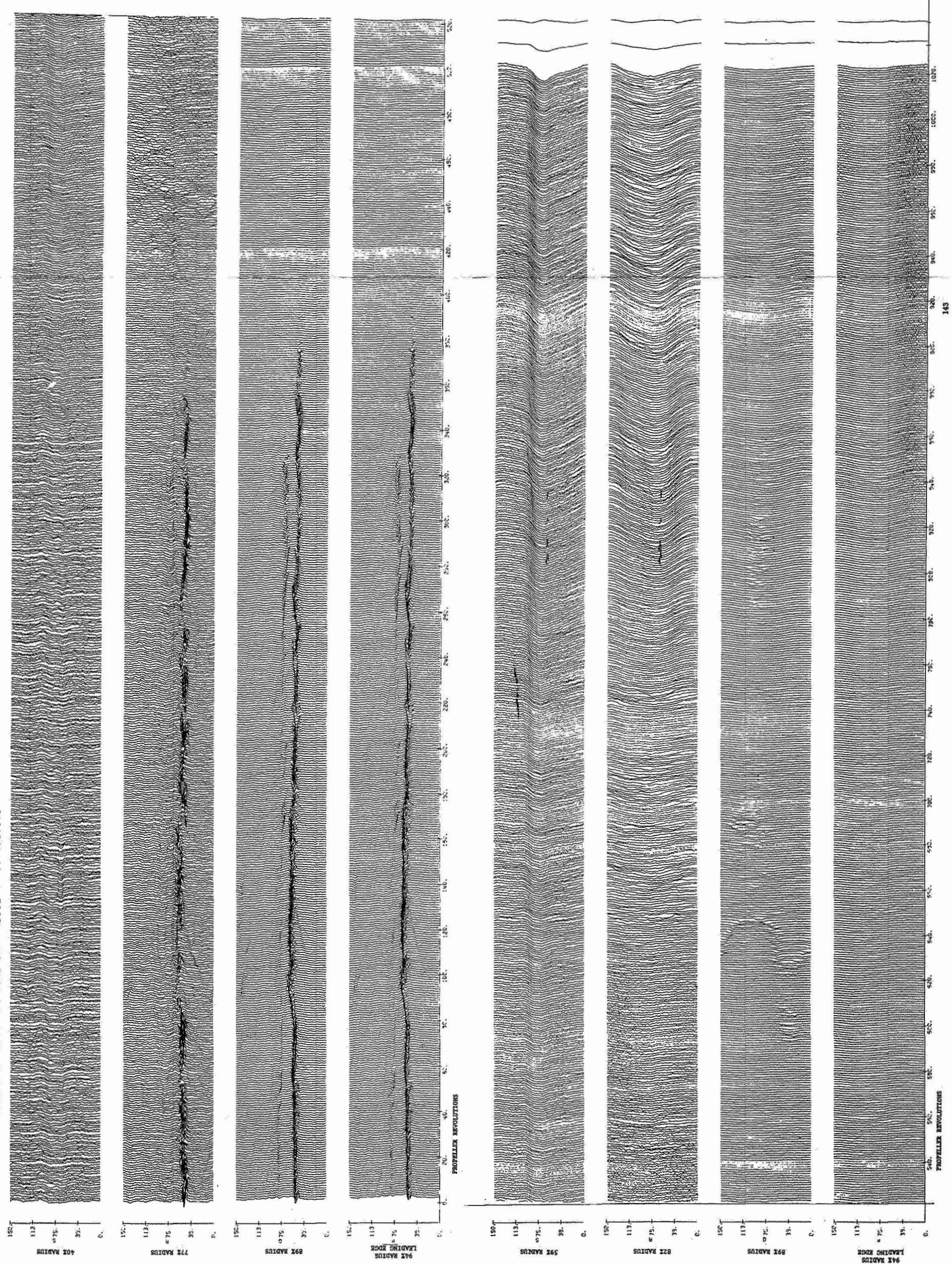


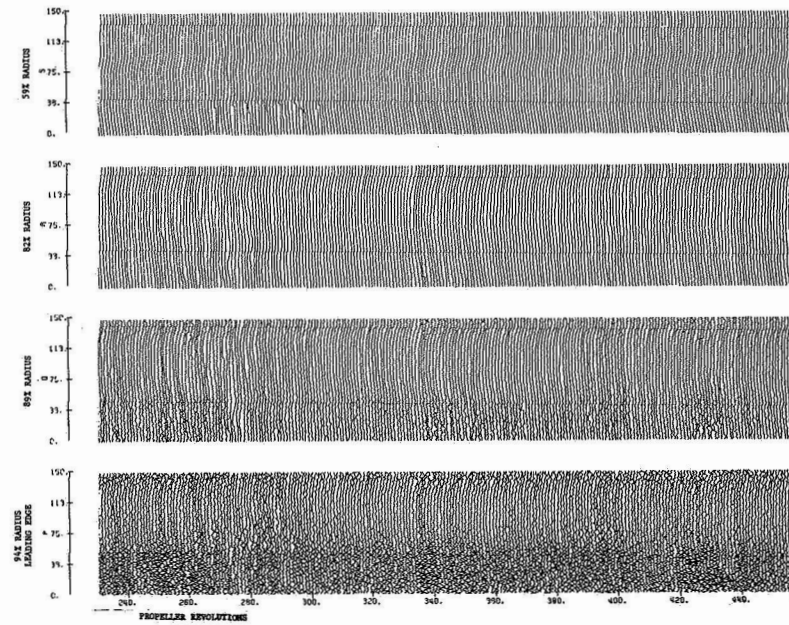
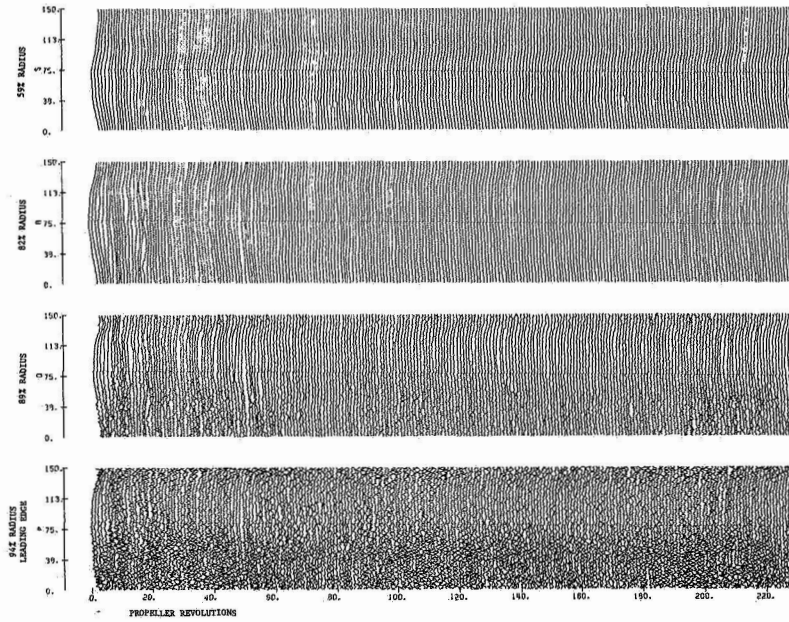
FIGURE 97. CROSSCORRELATION COEFFICIENT OF PAIRS OF BLADE PRESSURE SIGNALS AT ZERO TIME LAG INDICATING RADIAL TURBULENCE LENGTH SCALE

APPENDIX A - BLADE SURFACE PRESSURE
TIME HISTORY PLOTS

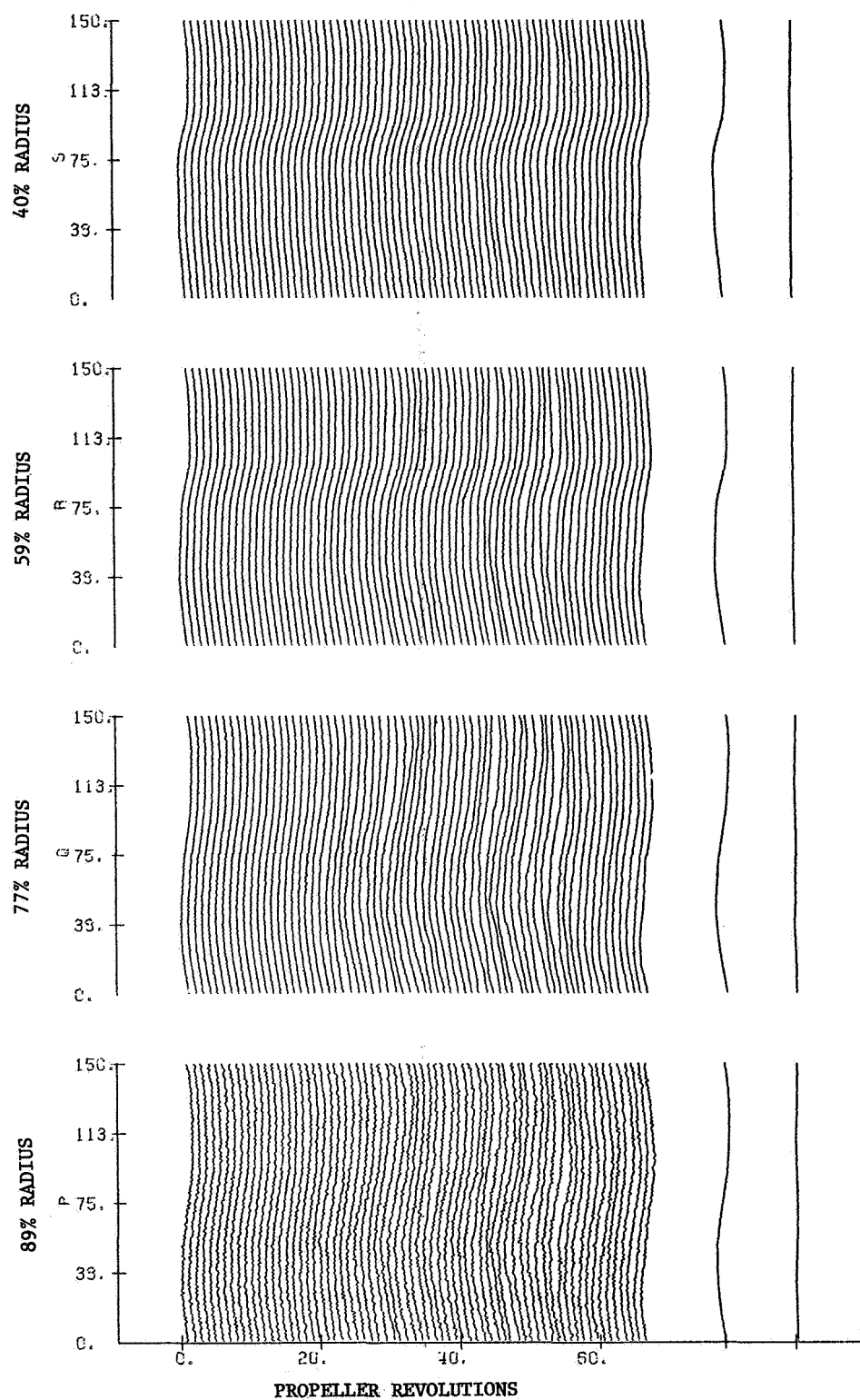
FLIGHT 5 97.5 PCT TAKE OFF XDCERS NO. 6.5.3.1



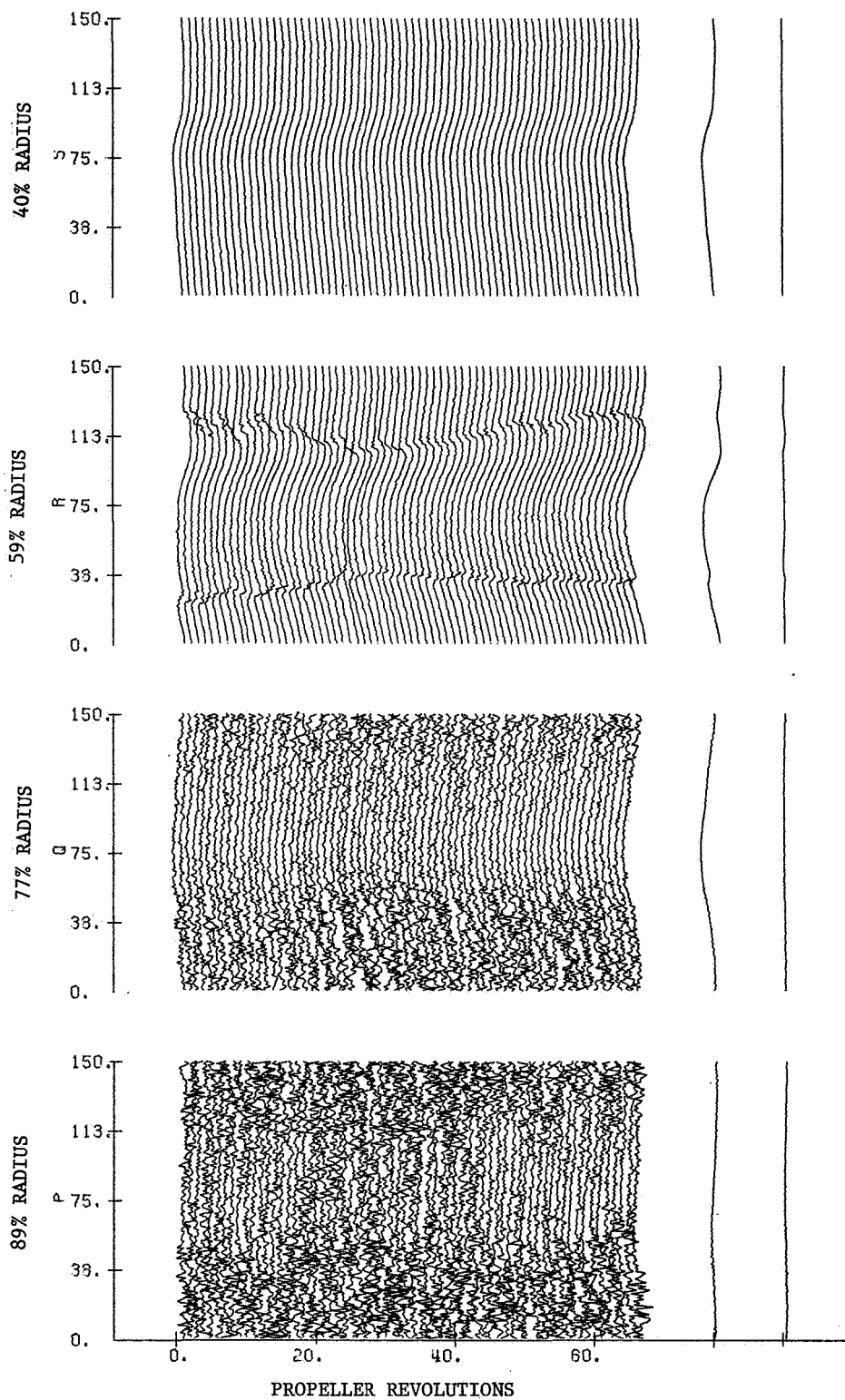
FLIGHT 8 RUN 2 97% RPM XDUCERS 6,5,4,2



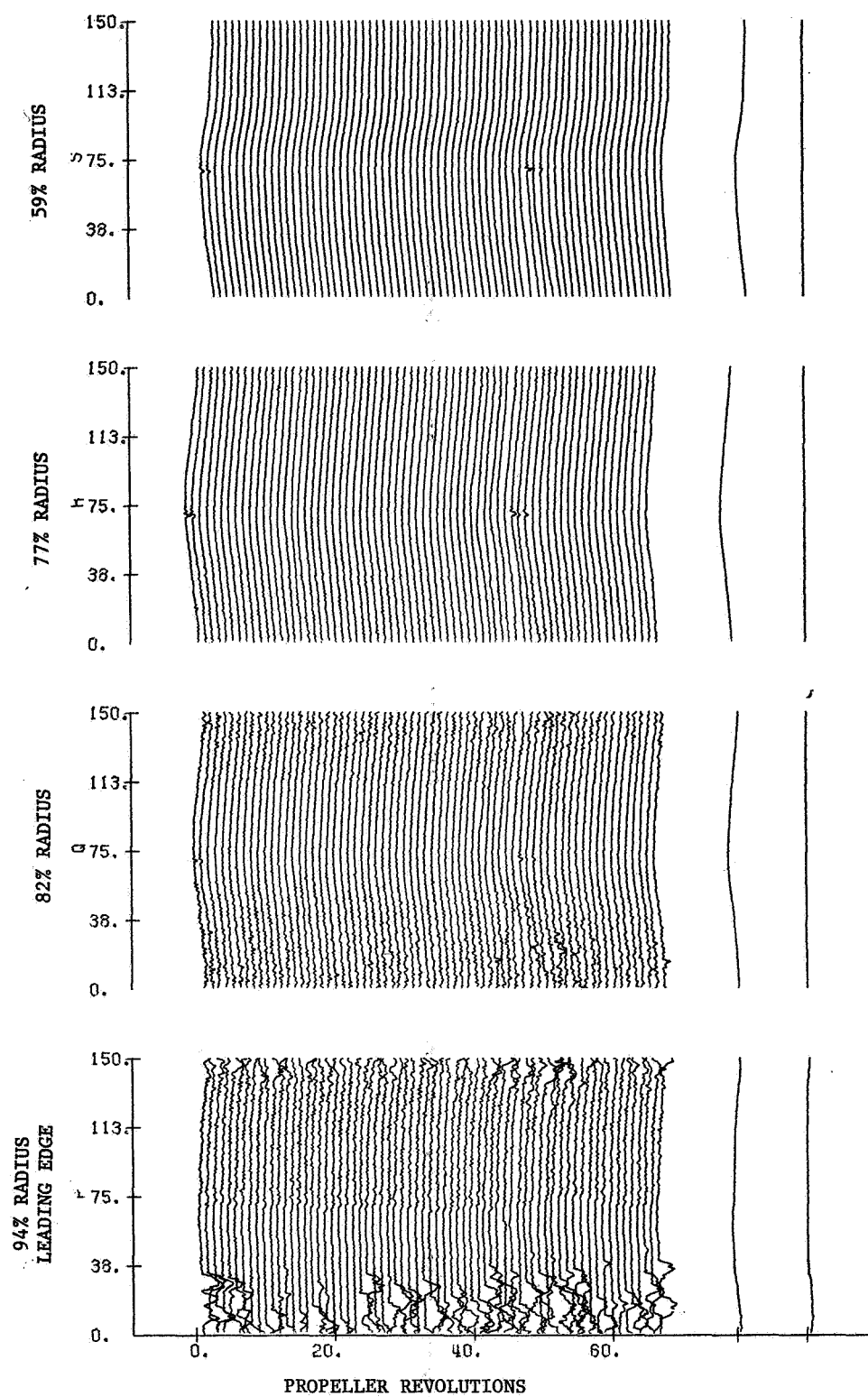
FLIGHT 7 RUN 3A 80% RPM XDUCERS 5,3,2,1.



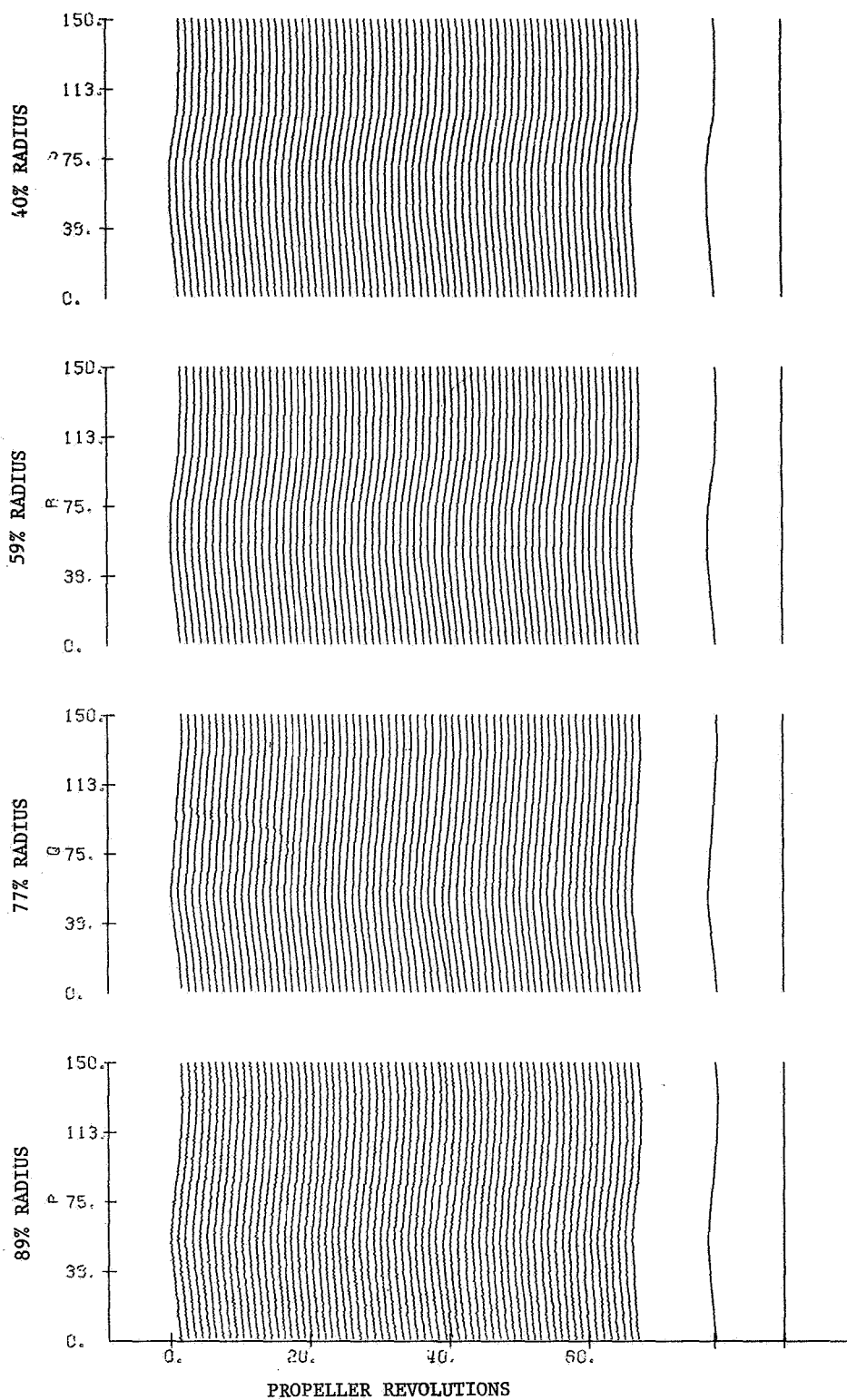
FLIGHT 7 RUN 4 97% RPM XDUCERS 5,3,2,1



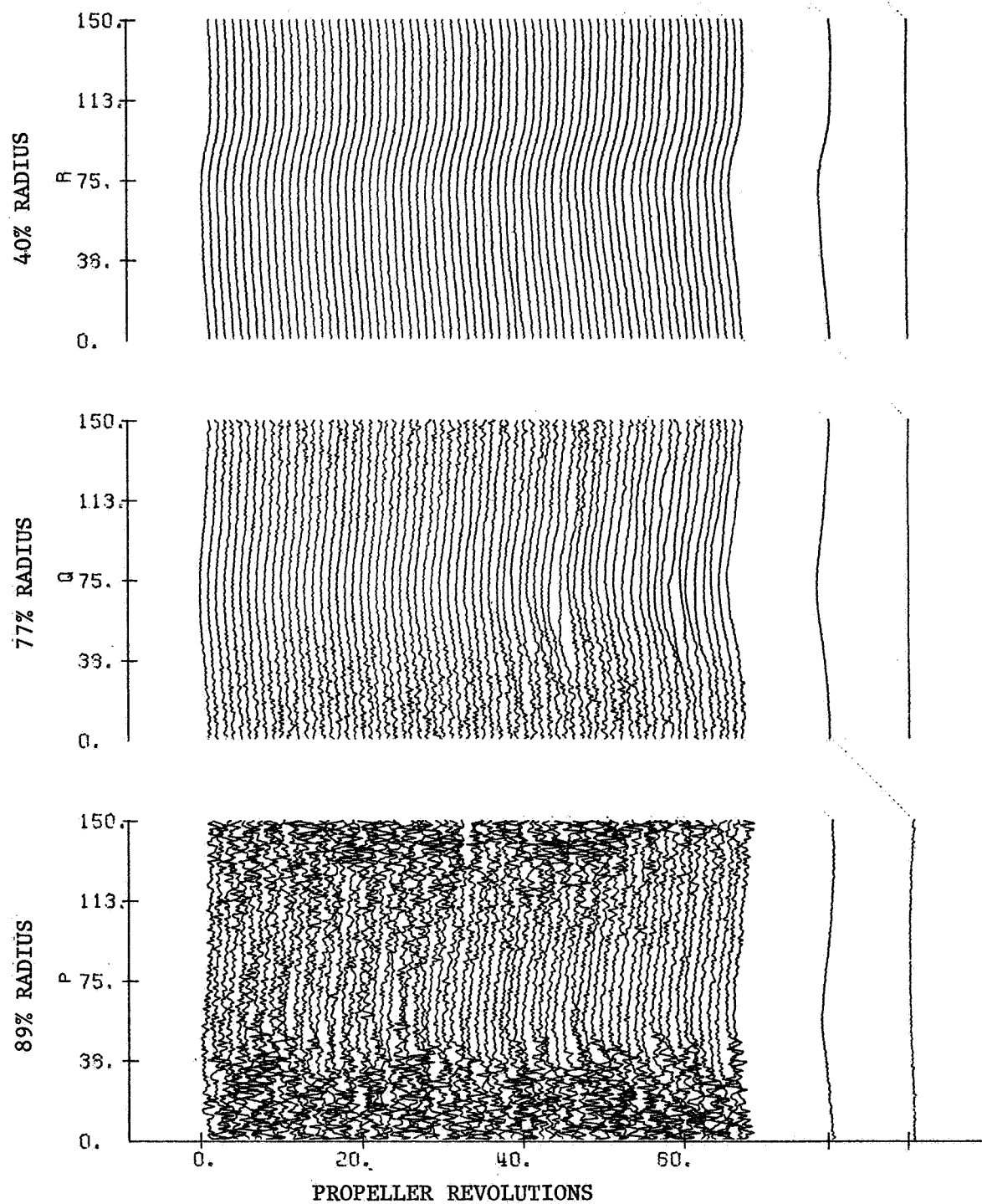
FLIGHT 11 RUN 4 97% RPM XDUCERS 6,4,3,2



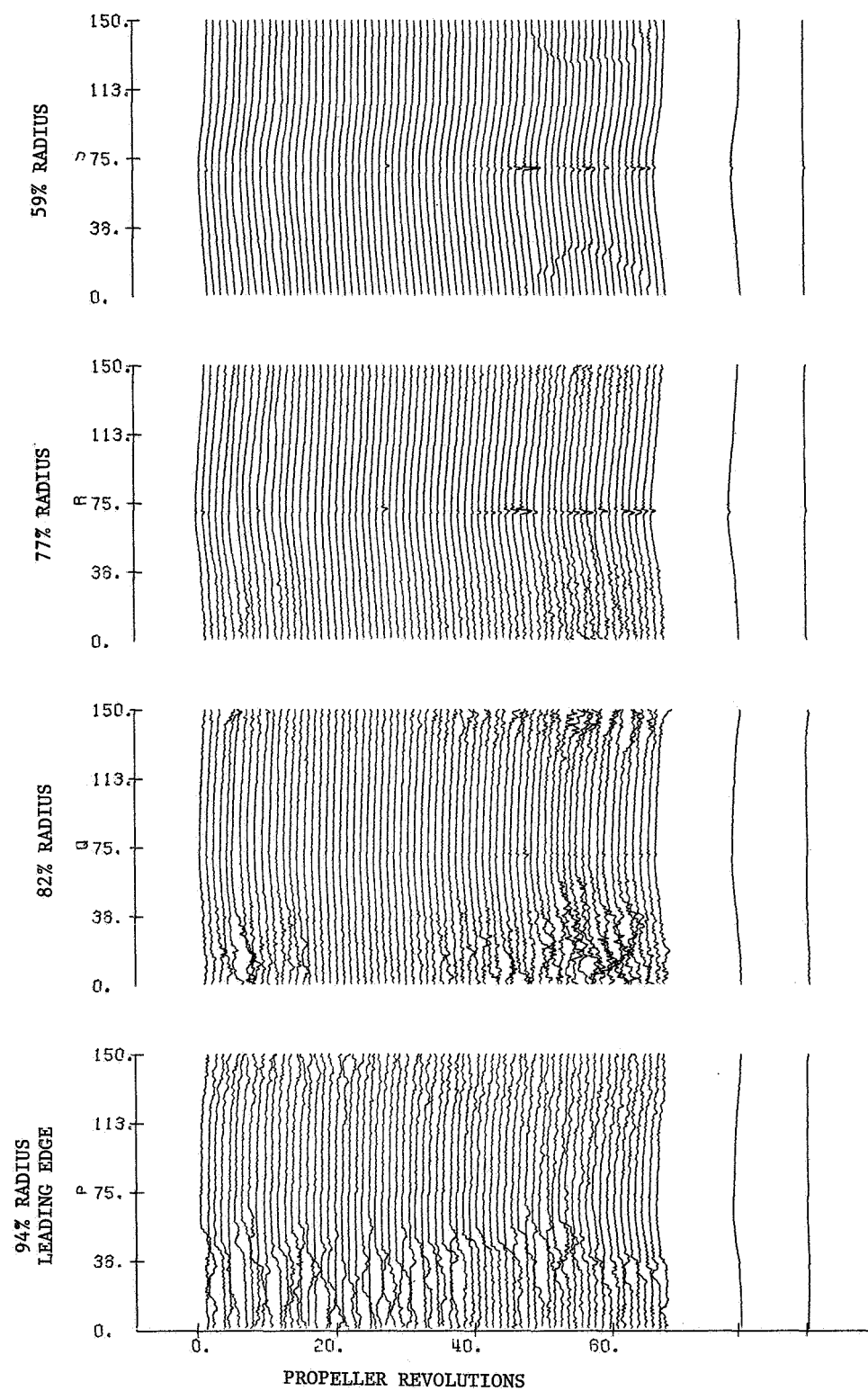
FLIGHT 7 RUN 5 80% RPM XDUCERS 5,3,2,1



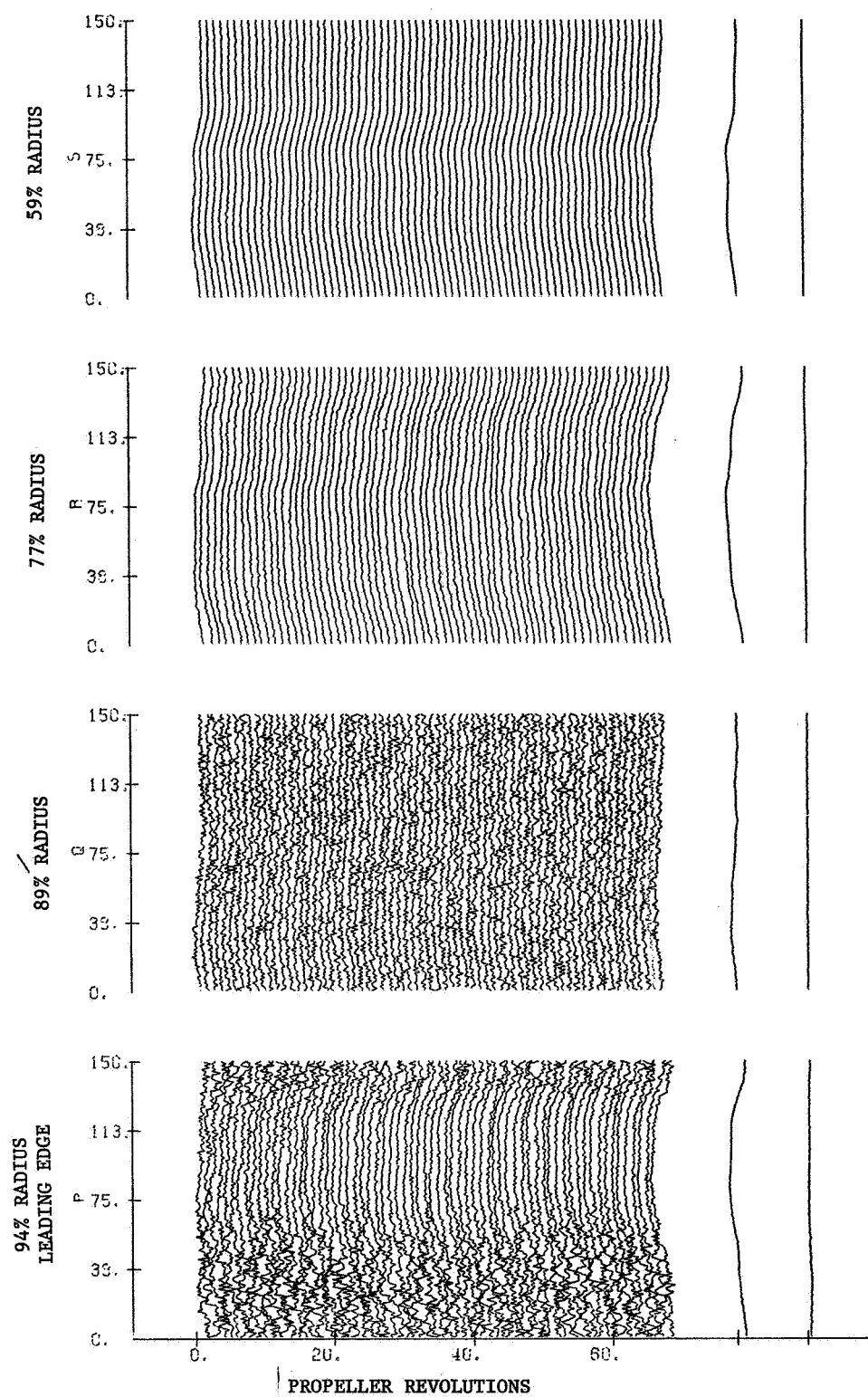
FLIGHT 7 RUN 6 97% RPM XDUCERS 5,3,1



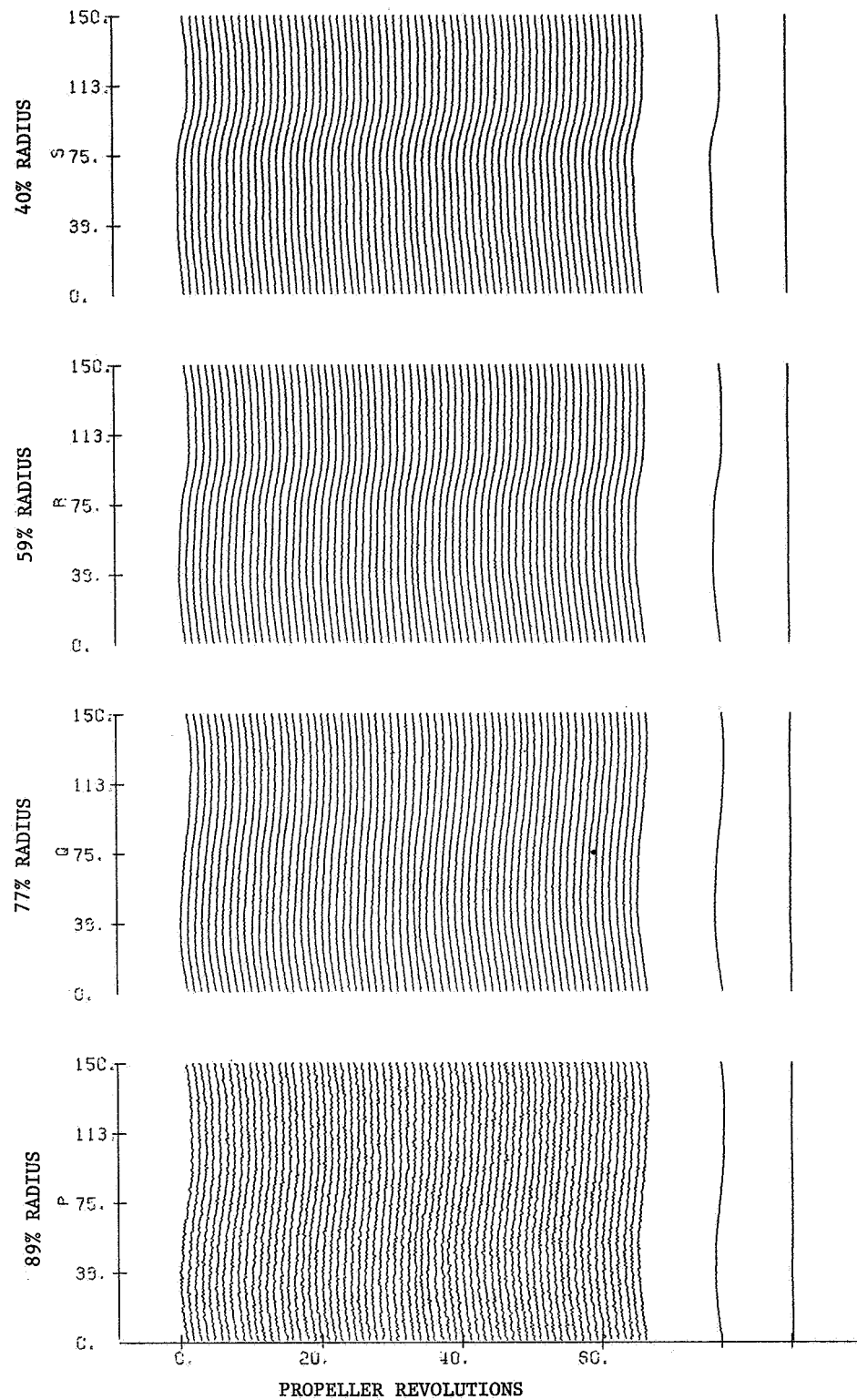
FLIGHT 11 RUN 6 97% RPM XDUCERS 6,4,3,2



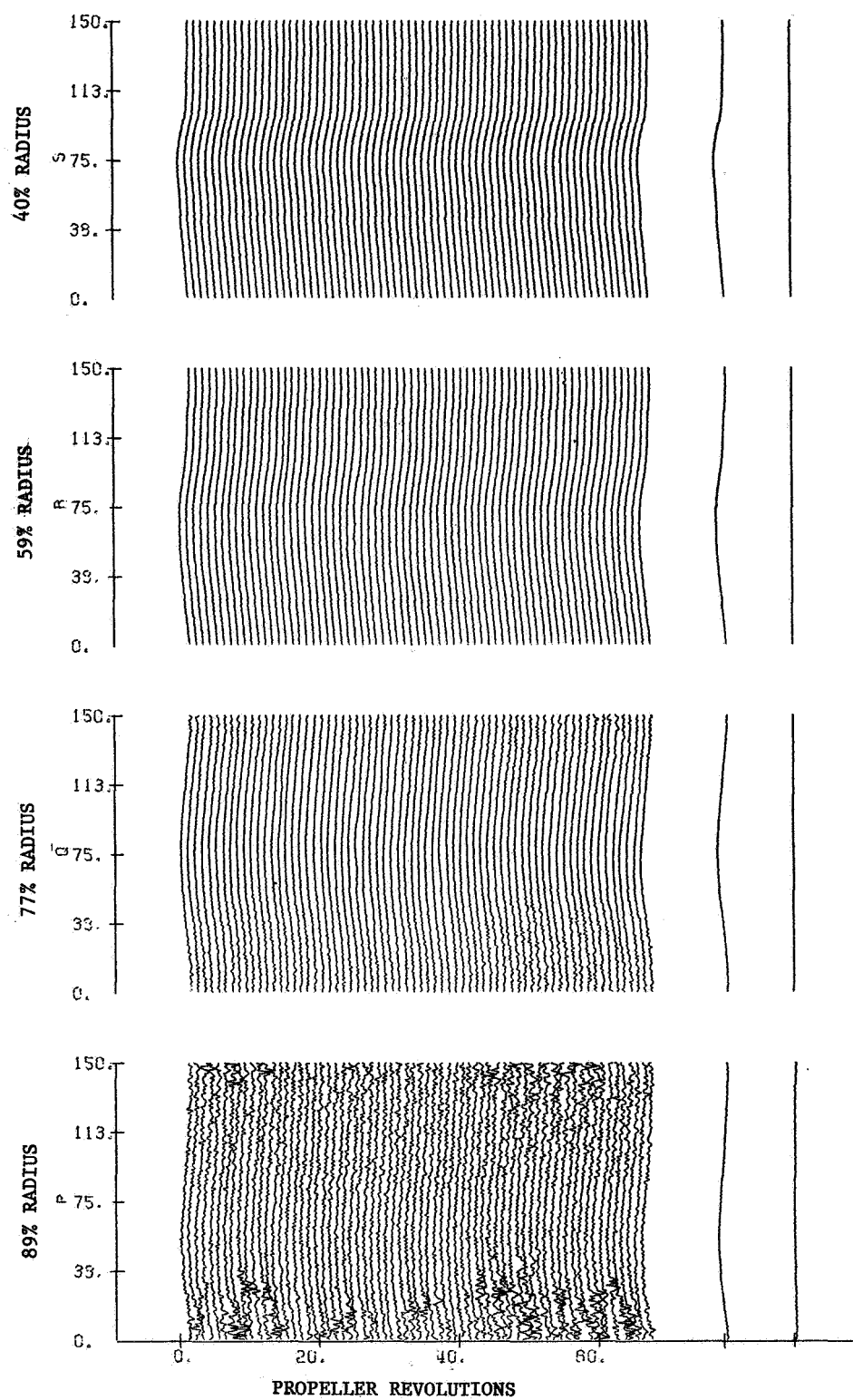
FLIGHT 7 RUN 8 97% RPM XDUCERS 6,5,3,2



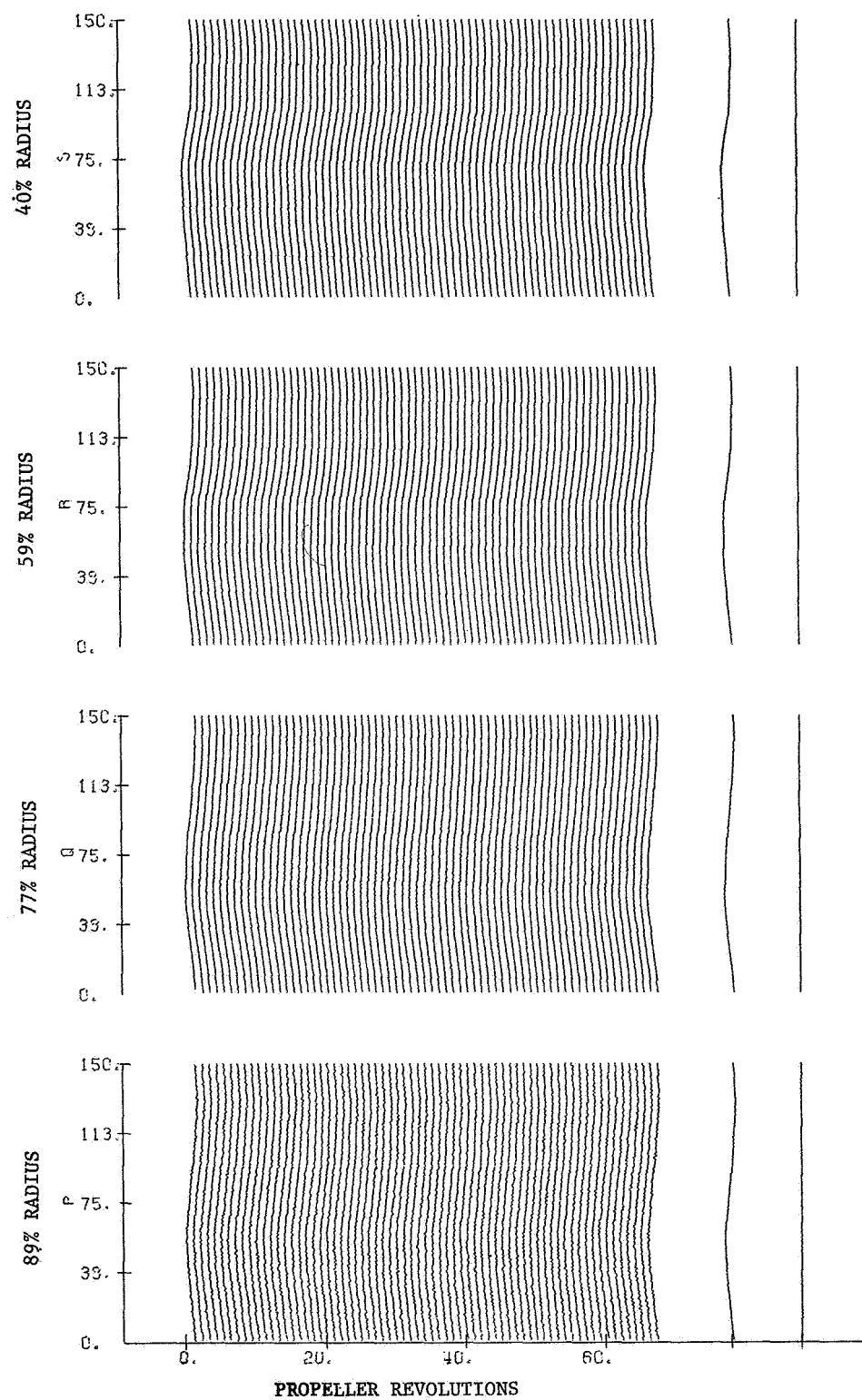
FLIGHT 7 RUN 9 80% RPM XDUCERS 5,3,2,1



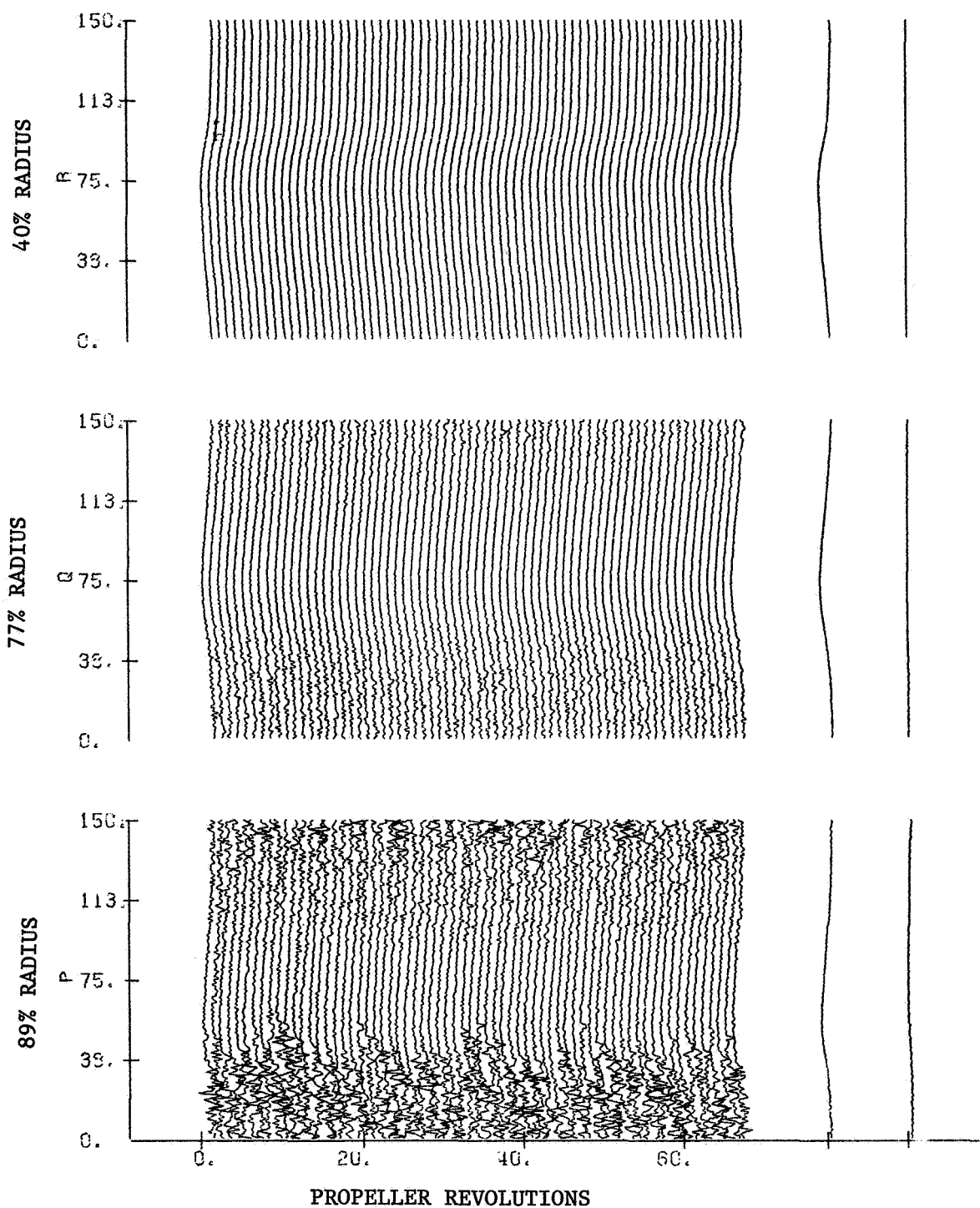
FLIGHT 7 RUN 10 97% RPM XDUCERS 5,3,2,1



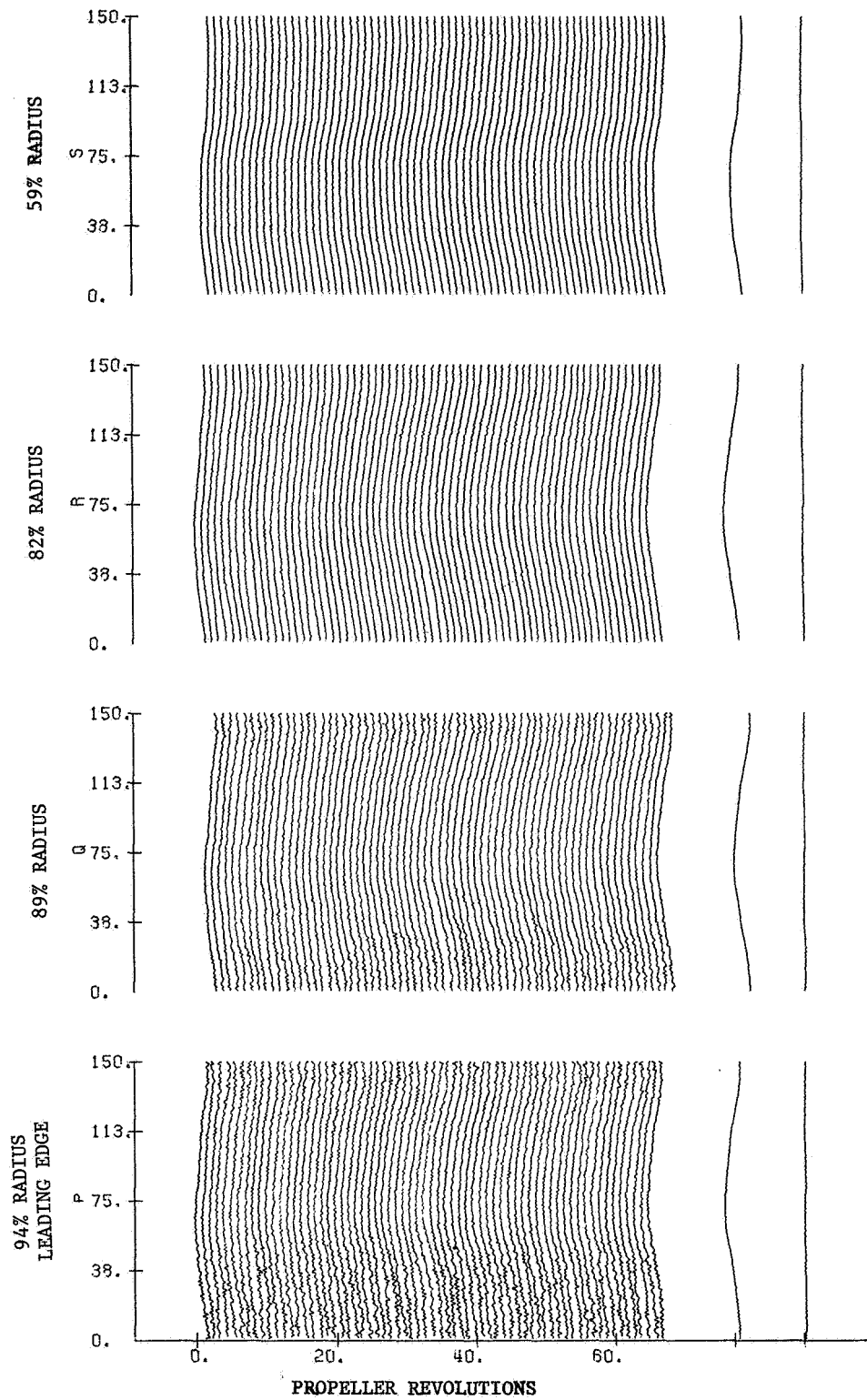
FLIGHT 7 RUN 11 80% RPM XDUCERS 5,3,2,1



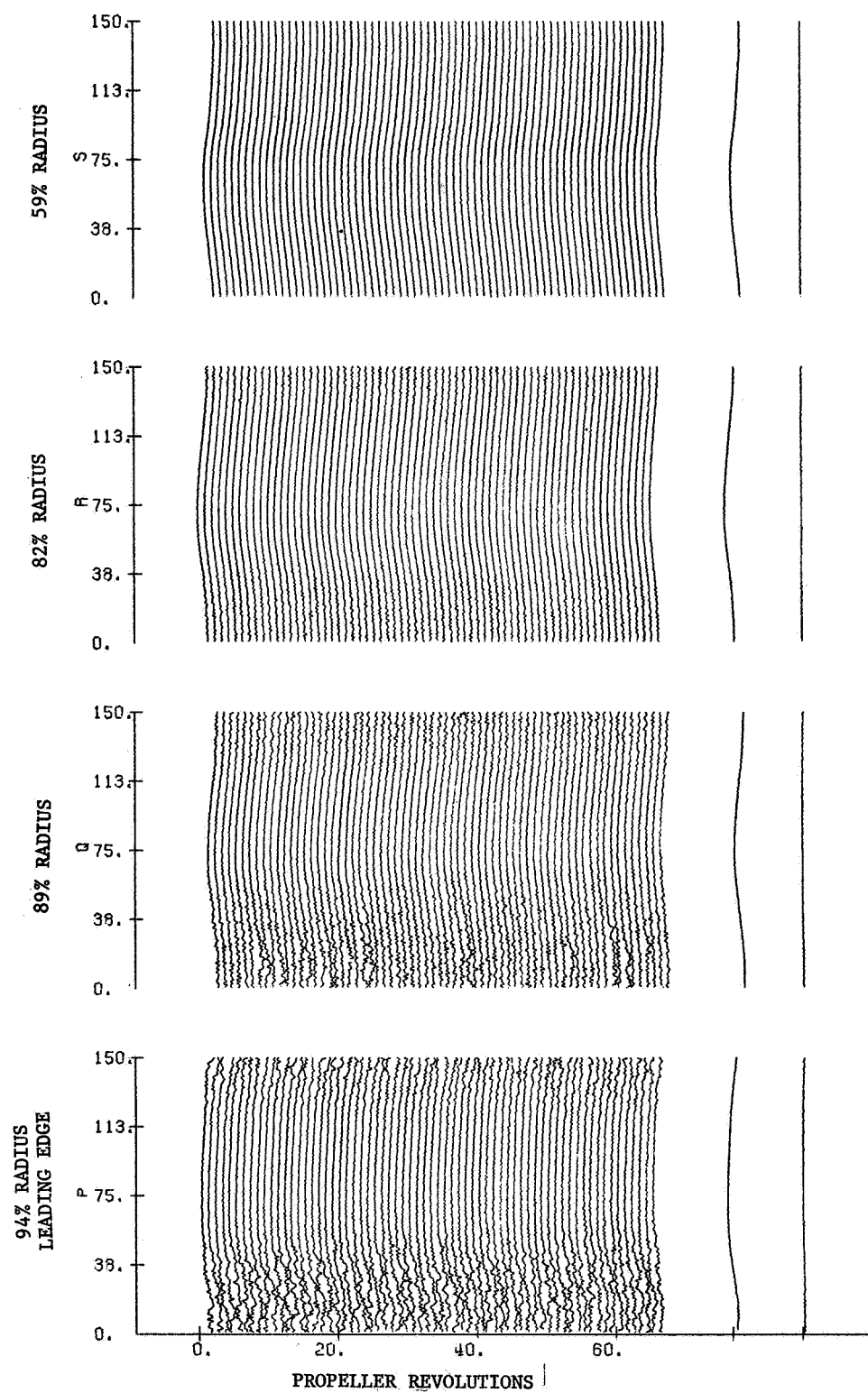
FLIGHT 7 RUN 12 97% RPM XDUCERS 5,3,1



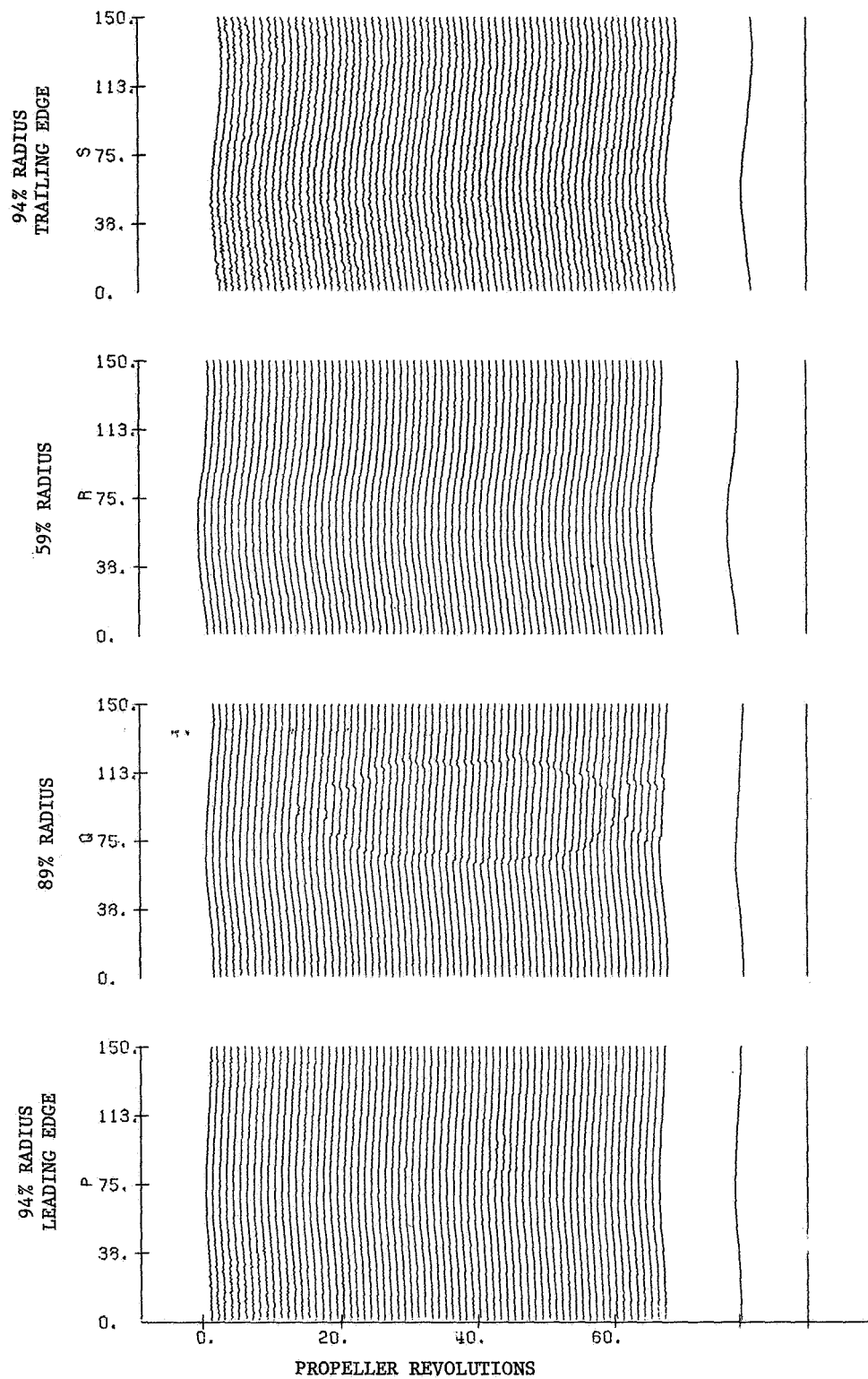
FLIGHT 8 RUN 16 90% RPM XDUCERS 6,5,4,2



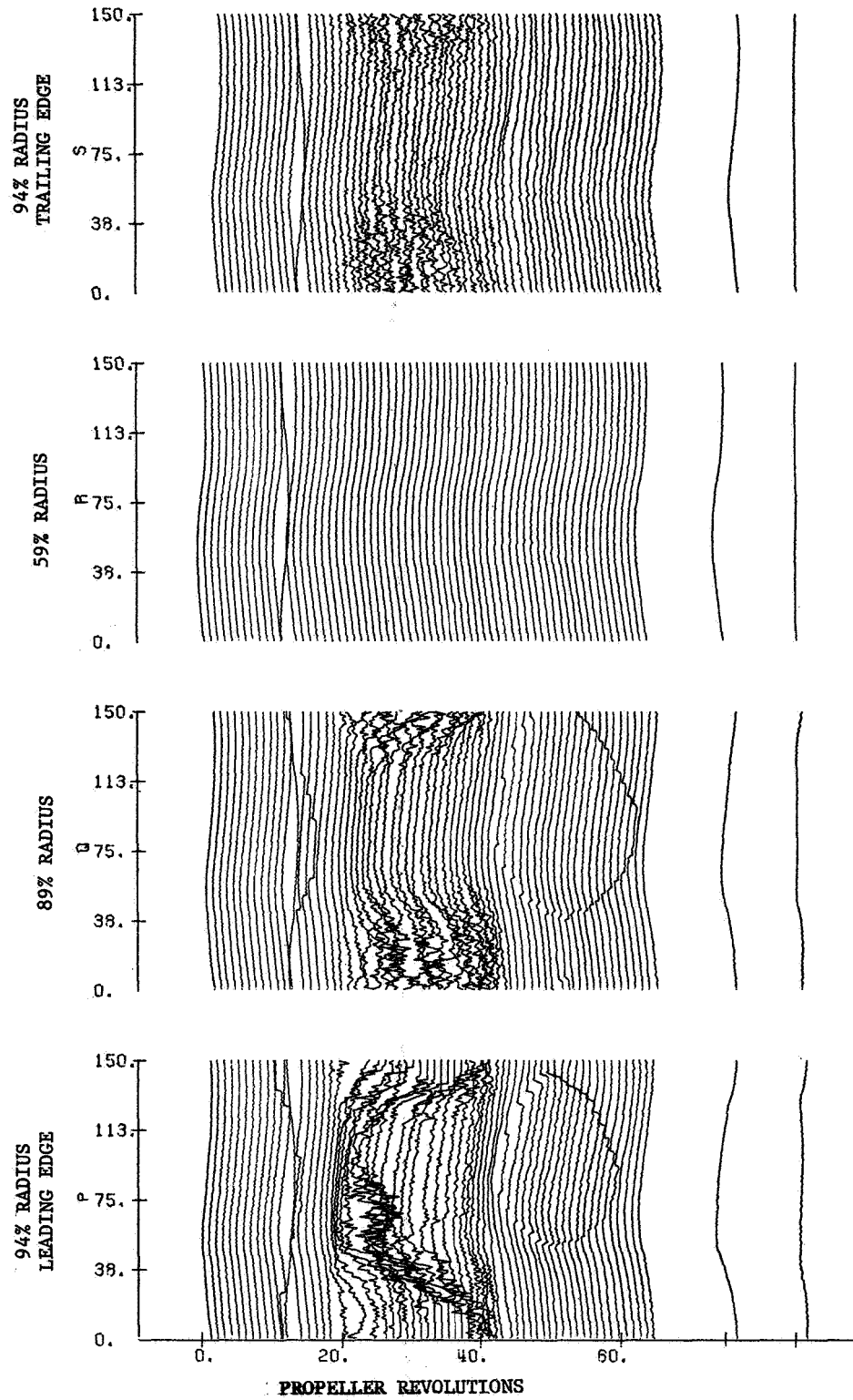
FLIGHT 8 RUN 17 90% RPM XDUCERS 6,5,4,2



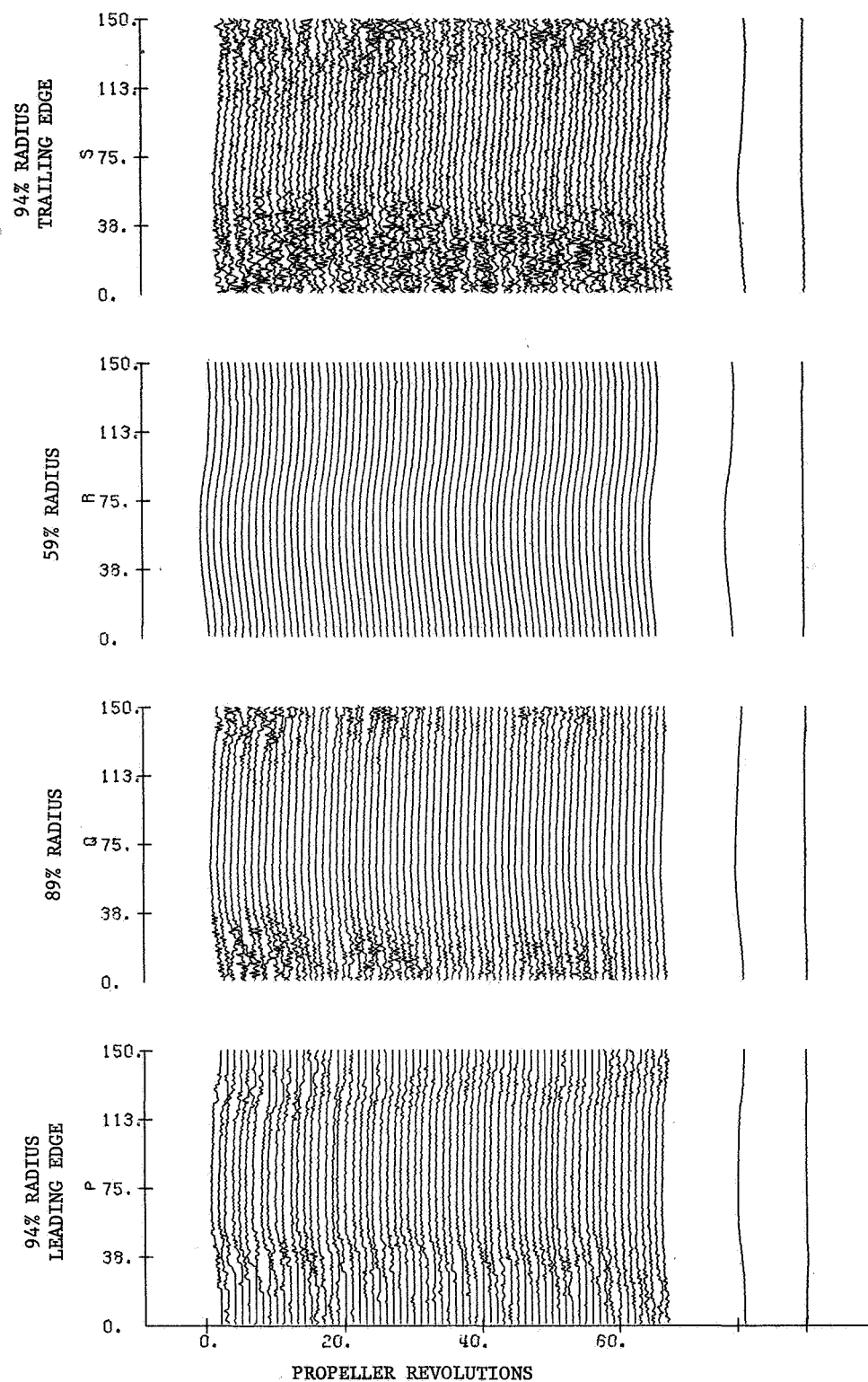
FLIGHT 8 RUN 18 80% RPM TAXI XDUCERS 6,5,2,7



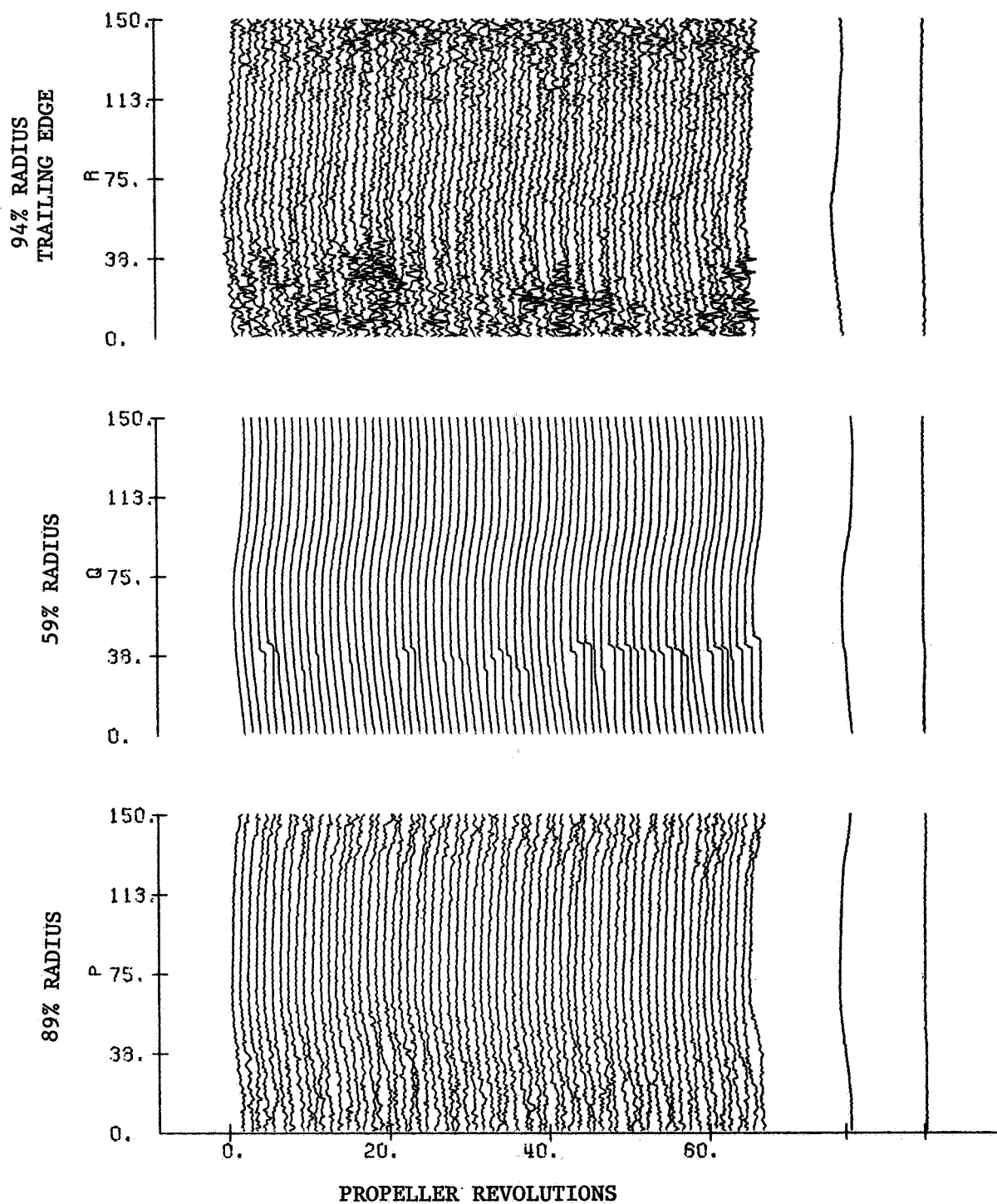
FLIGHT 8 RUN 18 80% RPM TAXI XDUCERS 6,5,2,7



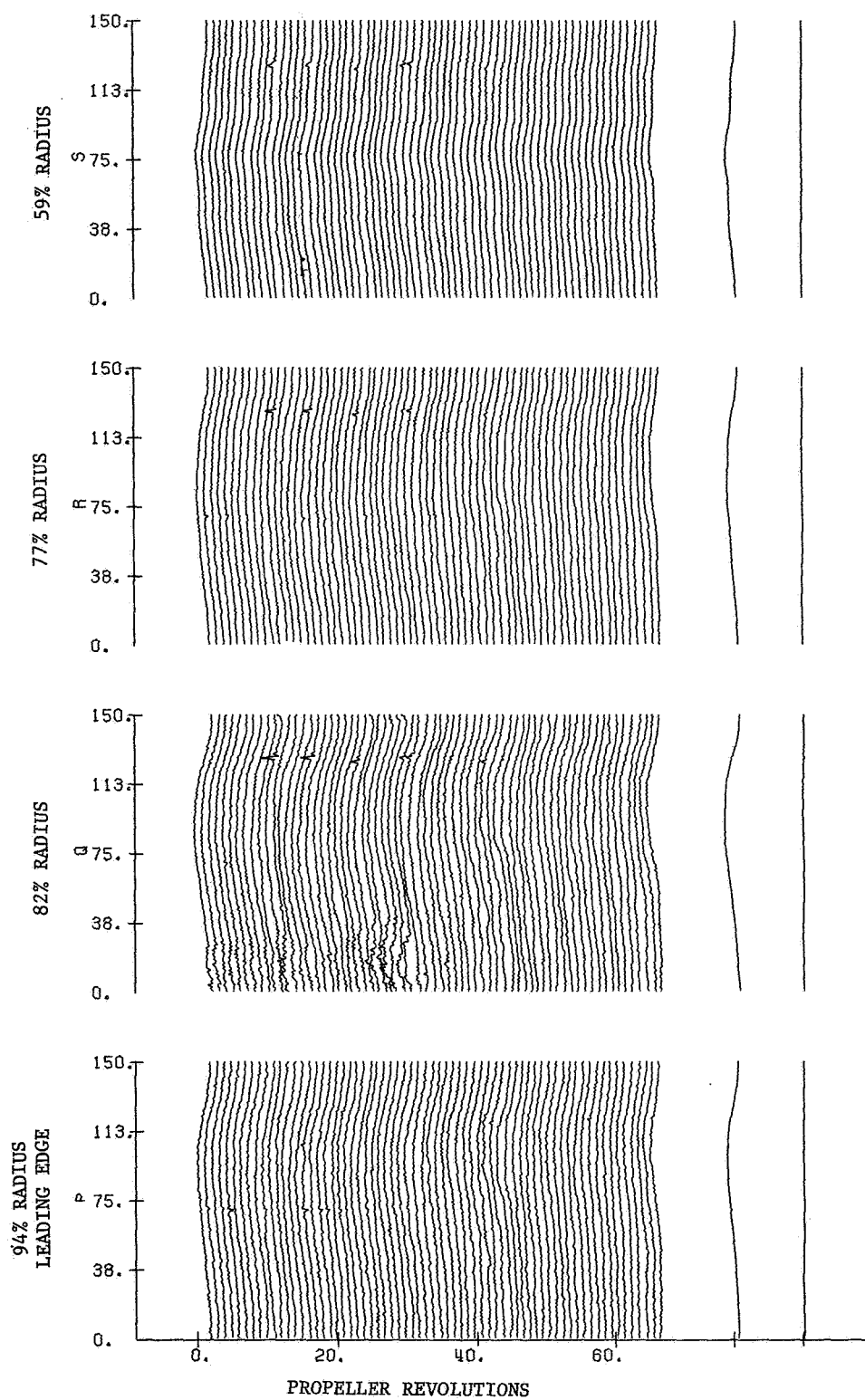
FLIGHT 8 RUN 19A 90% RPM TAXI XDUCERS 6,5,2,7



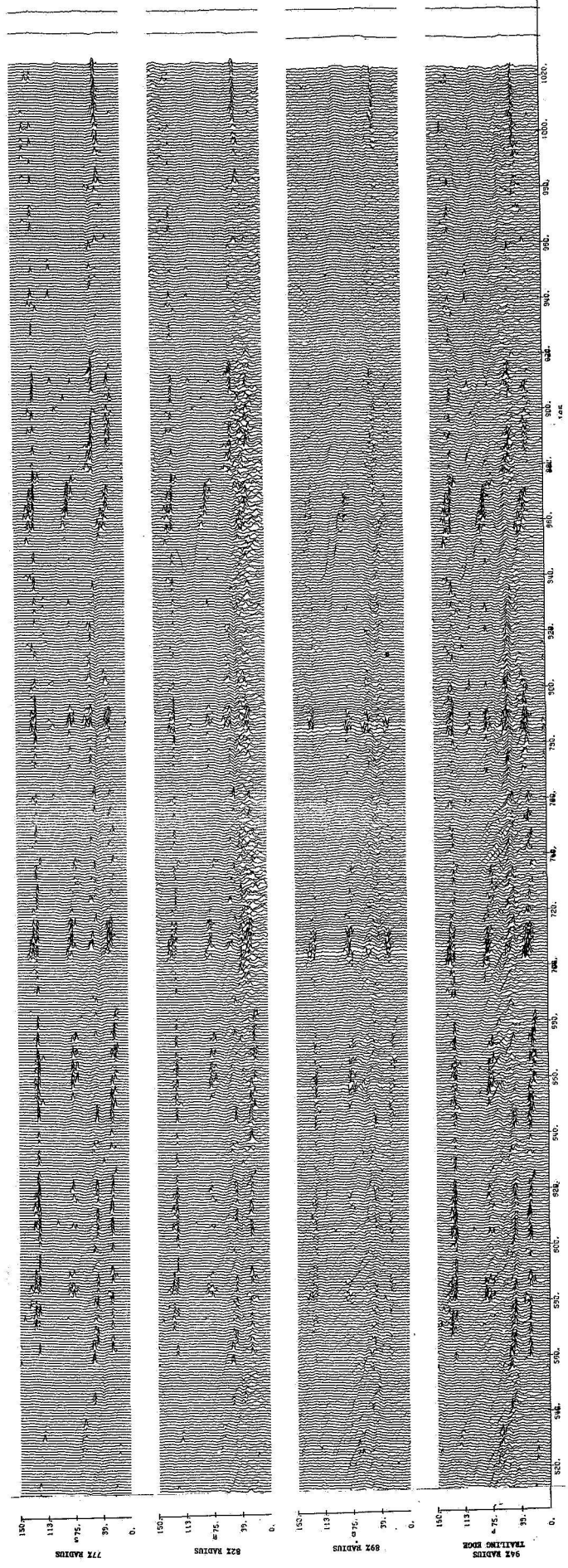
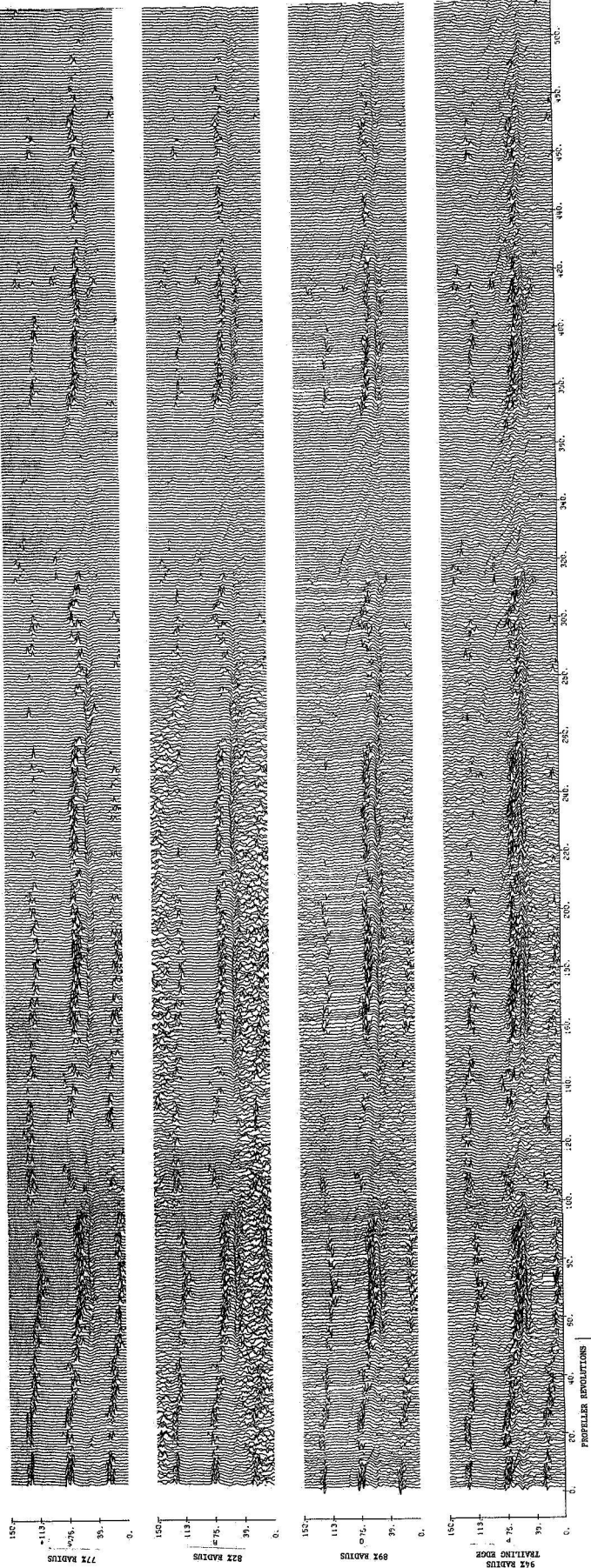
FLIGHT 8 RUN 20A 97% RPM TAXI XDUCERS 5,2,7



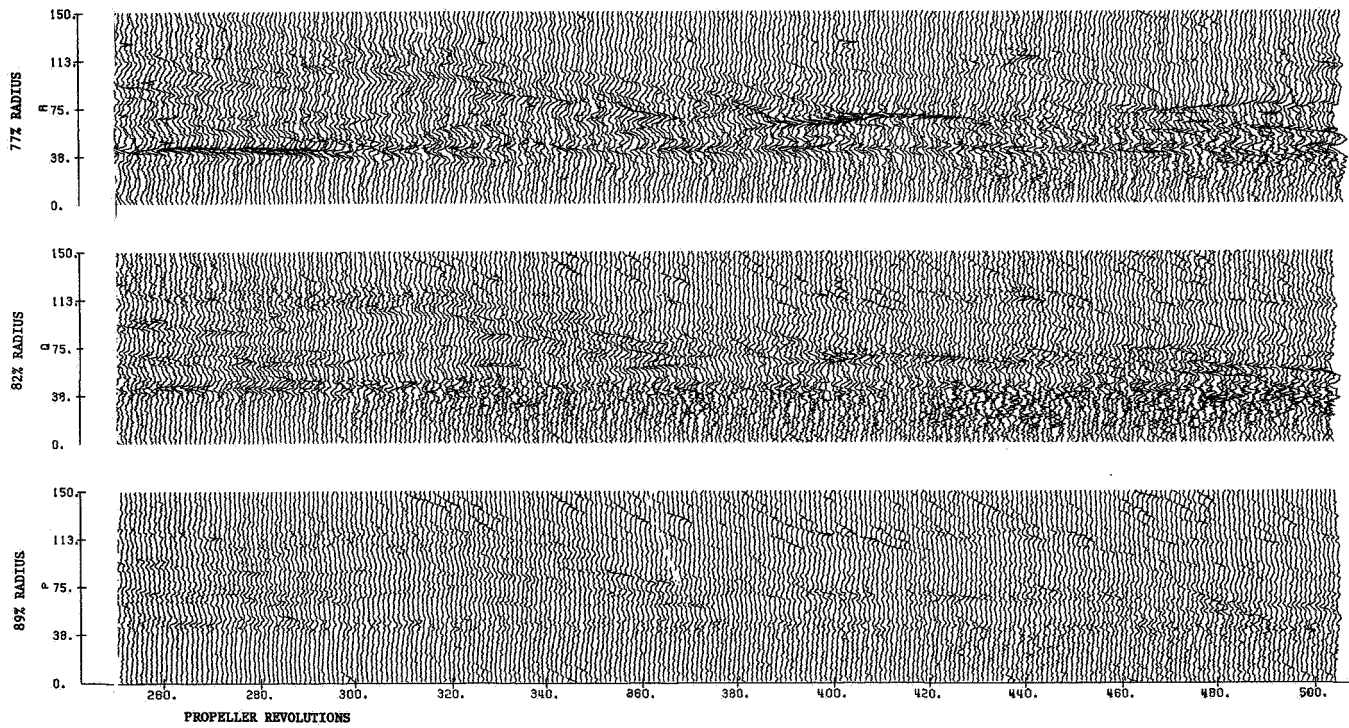
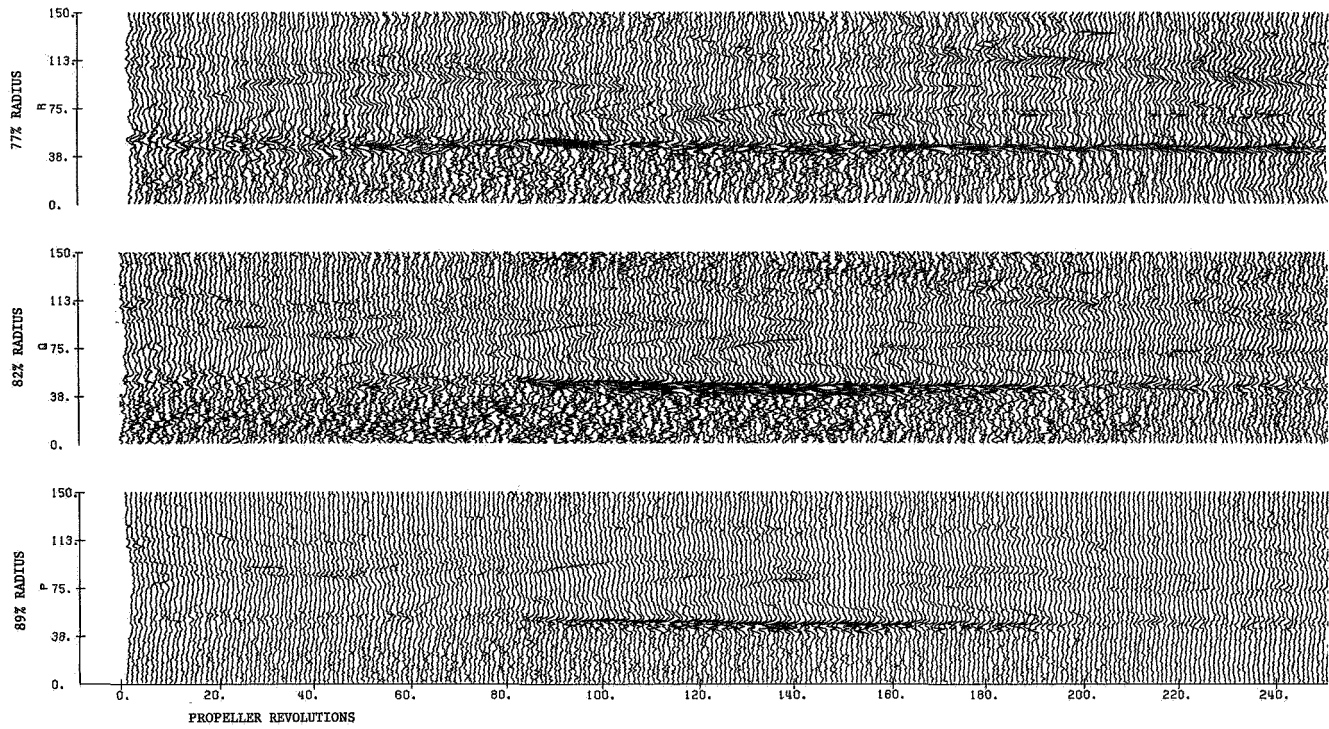
FLIGHT 10 RUN C 80% RPM XDUCERS 6,4,3,2



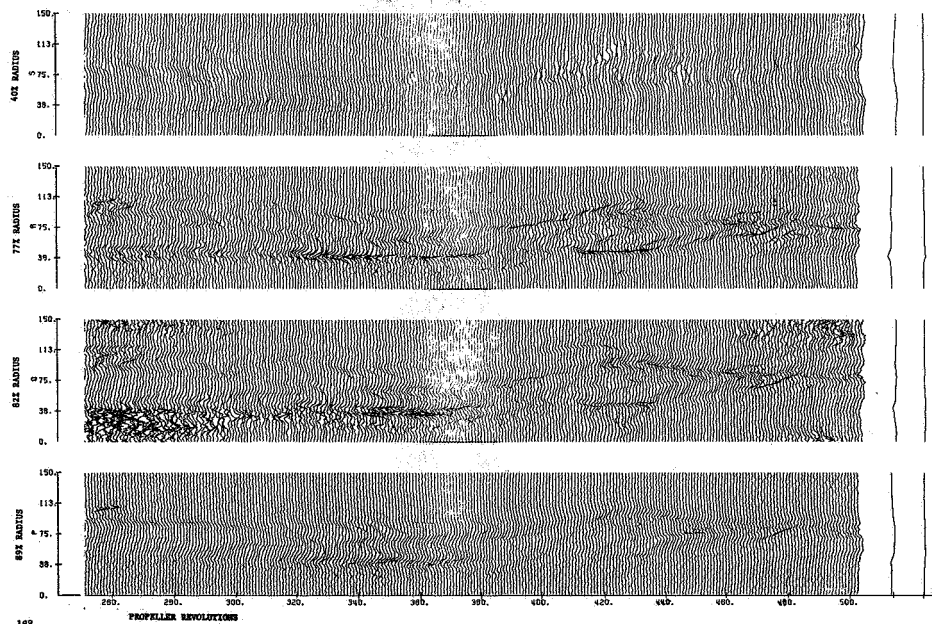
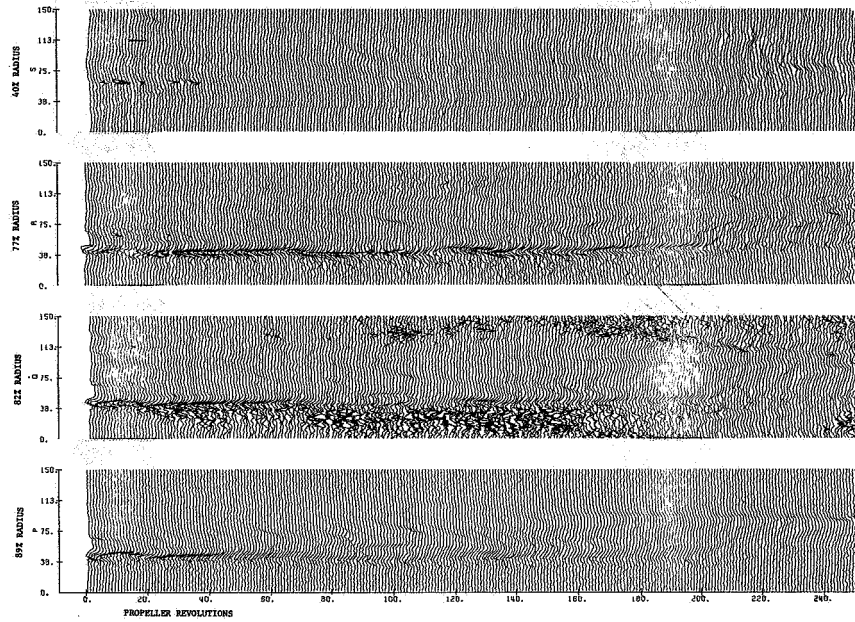
FLIGHT 12 RUN 25 97 PCT RPM XDCERS NO. 7.5.4.3



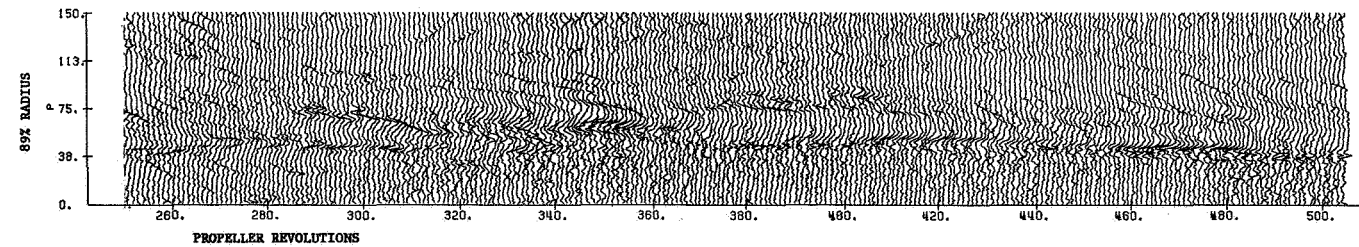
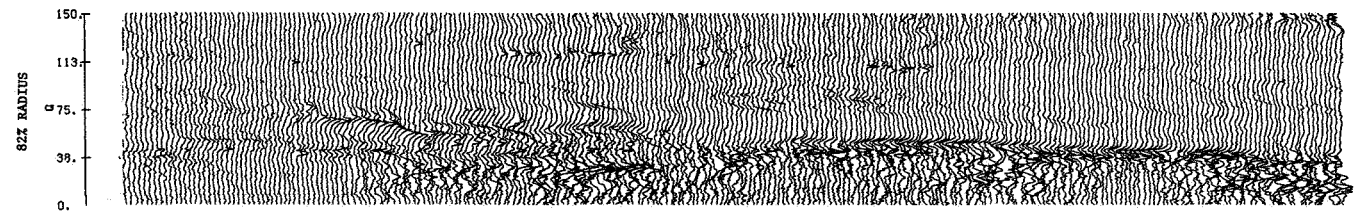
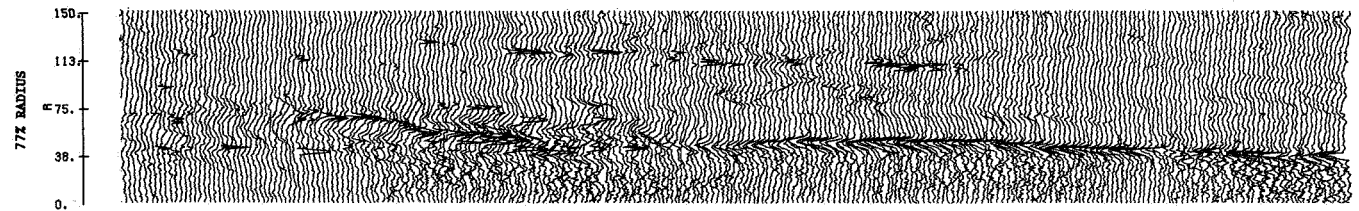
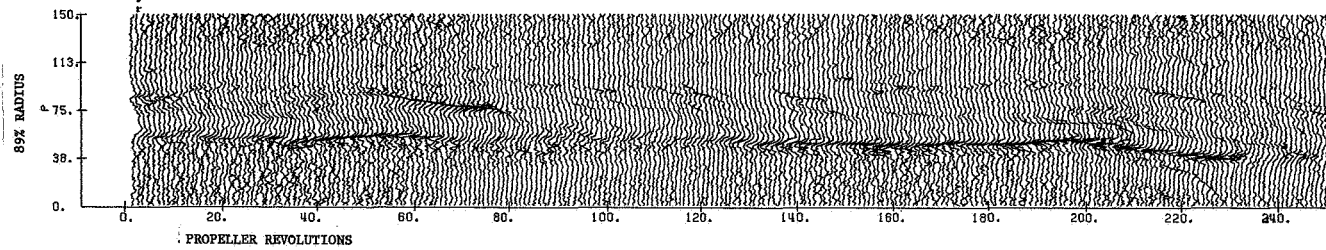
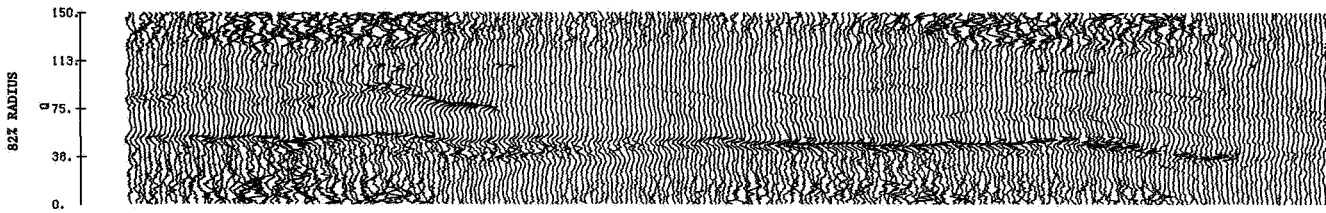
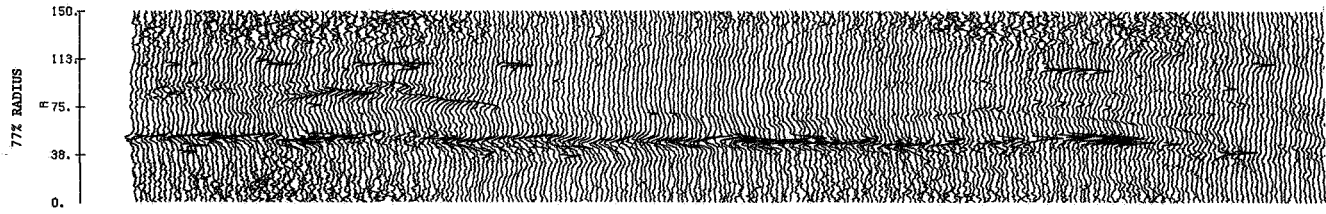
FLIGHT 12 RUN 3S 80% RPM XDUCERS NO. 5,4,3



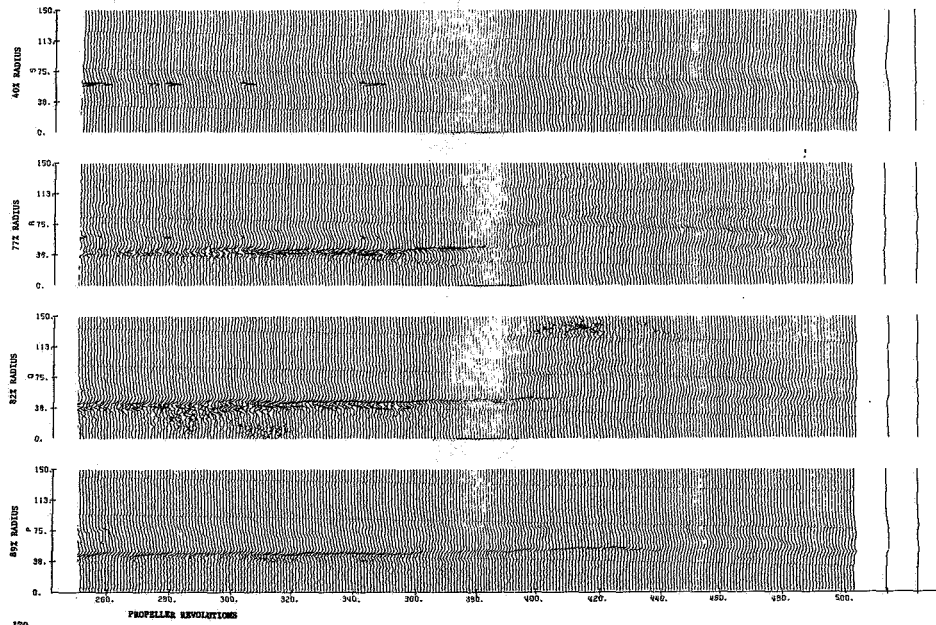
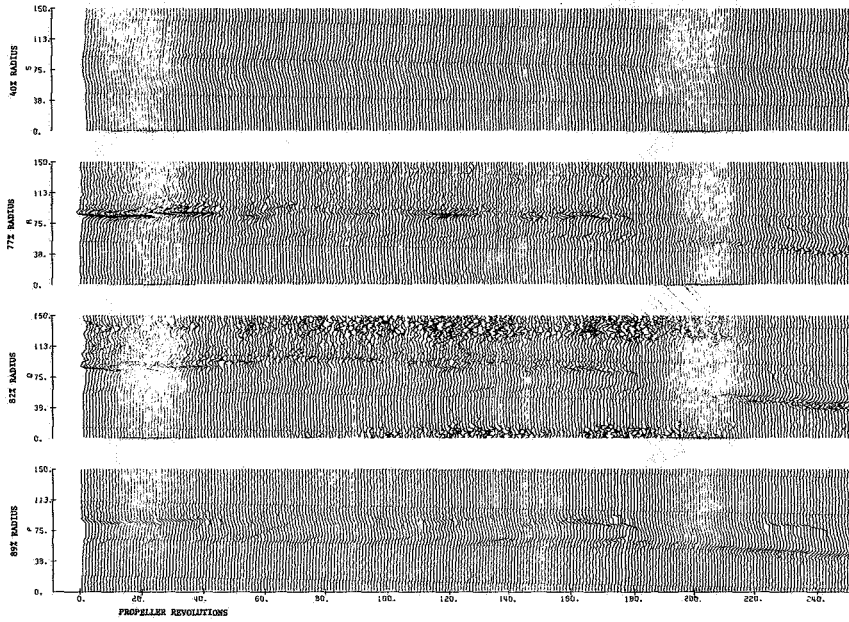
FLIGHT 15 RUN 4S 97% RPM XDUCERS NO. 5,4,3,1



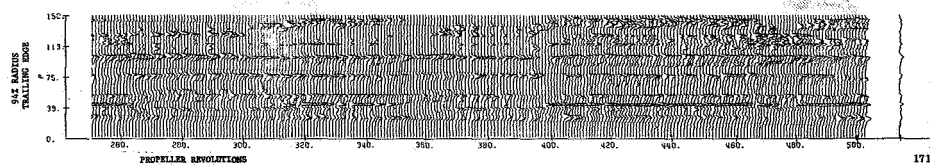
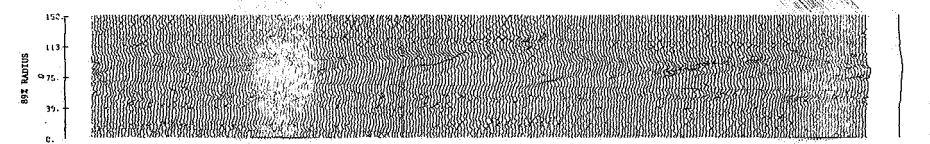
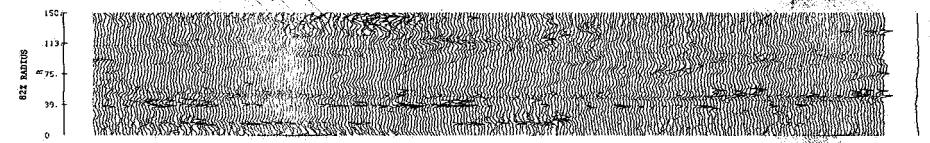
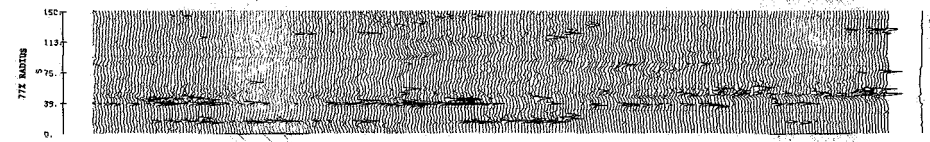
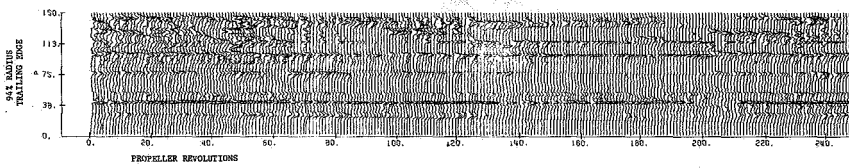
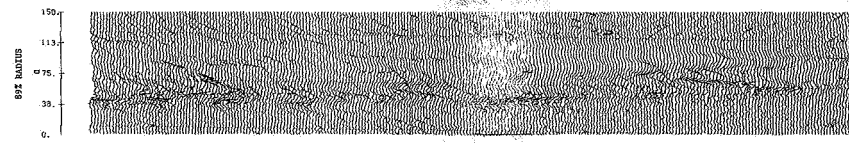
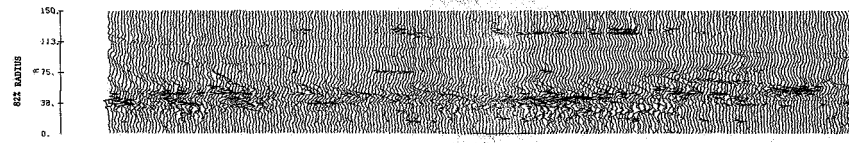
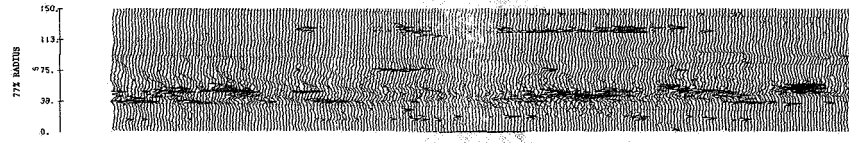
FLIGHT 12 RUN 5S 80% RPM XDUCERS NO. 5,4,3



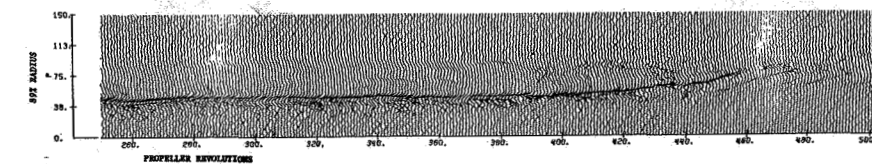
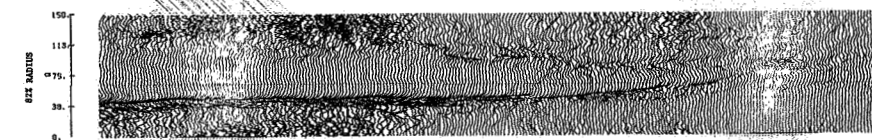
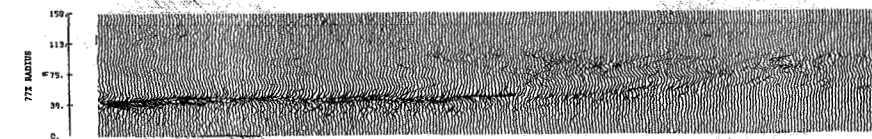
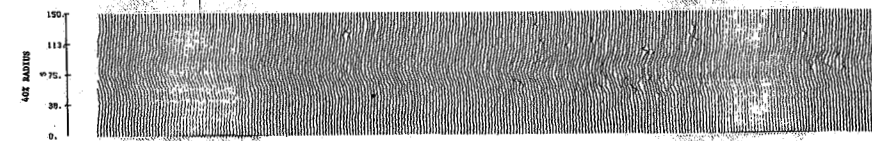
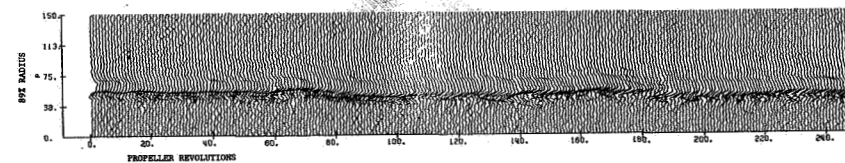
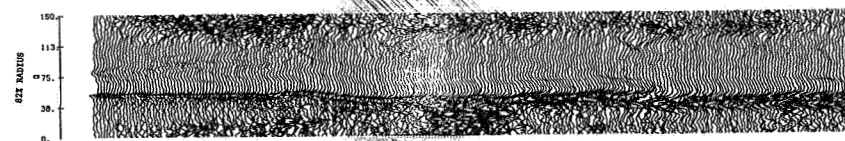
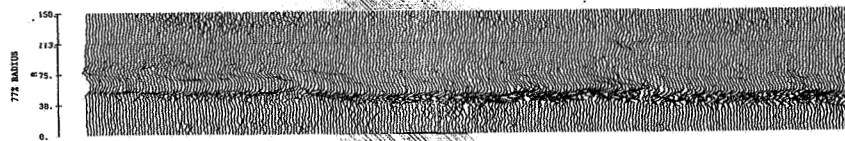
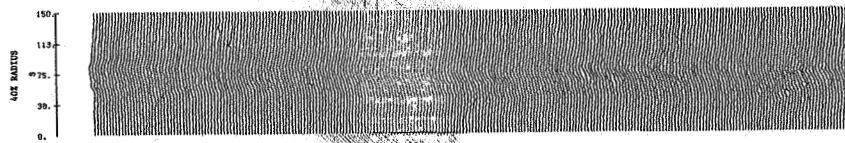
FLIGHT 15 RUN 65 97% RPM XDUCERS NO. 5,4,3,1



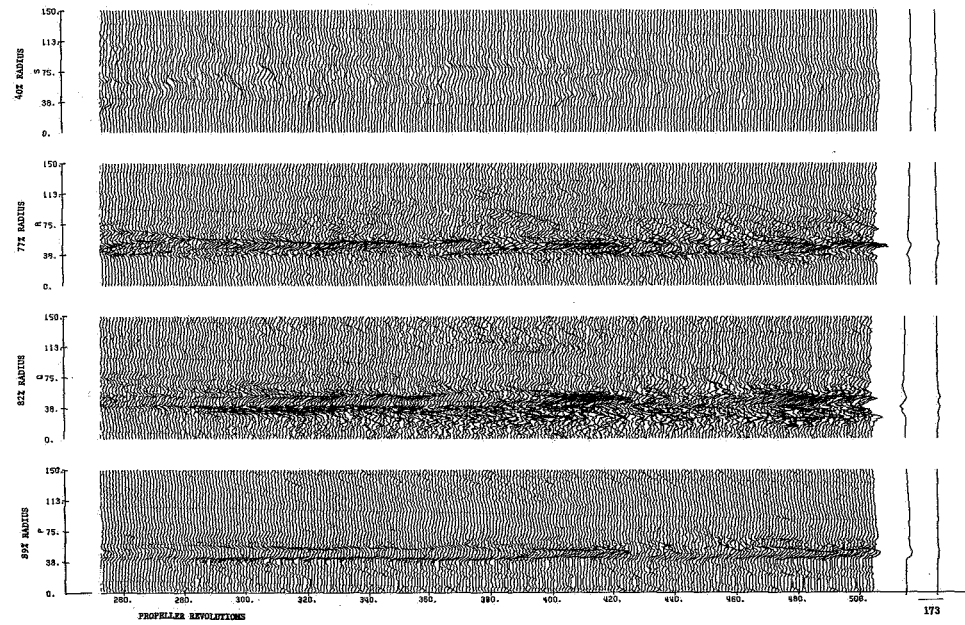
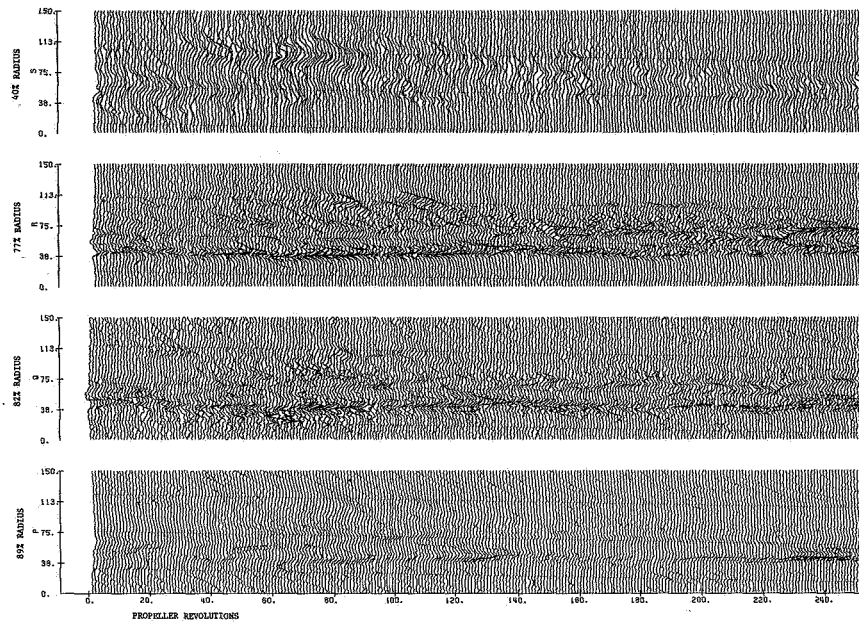
FLIGHT 12 RUN 165 90% RPM XDUCCERS NO. 7.5.4.3



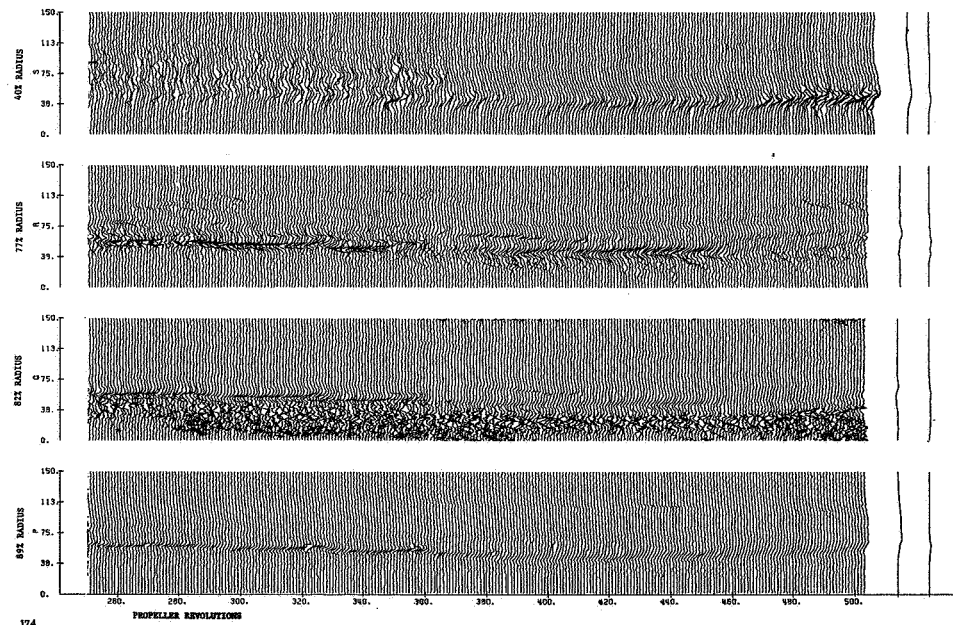
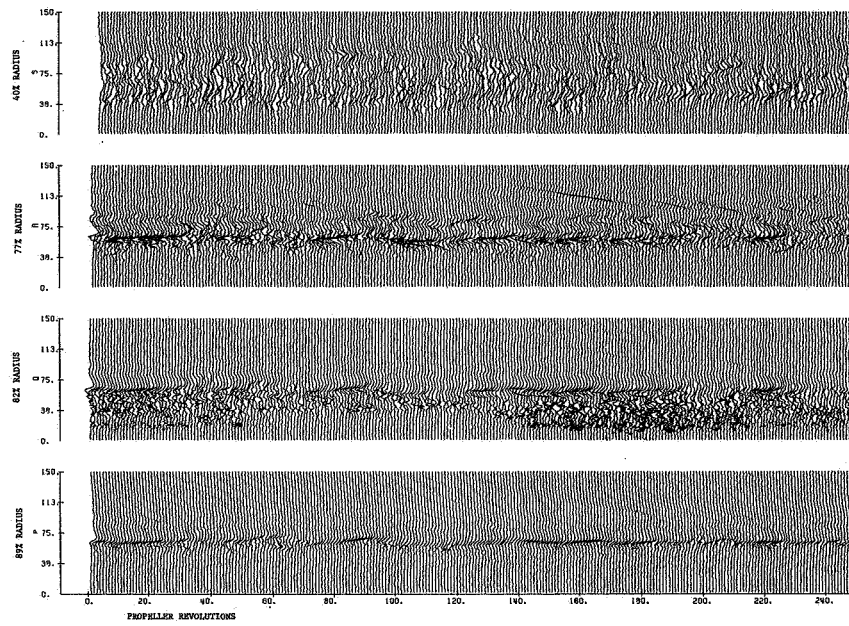
FLIGHT 15 RUN 175 90% RPM XDUCERS NO. 5,4,3,1



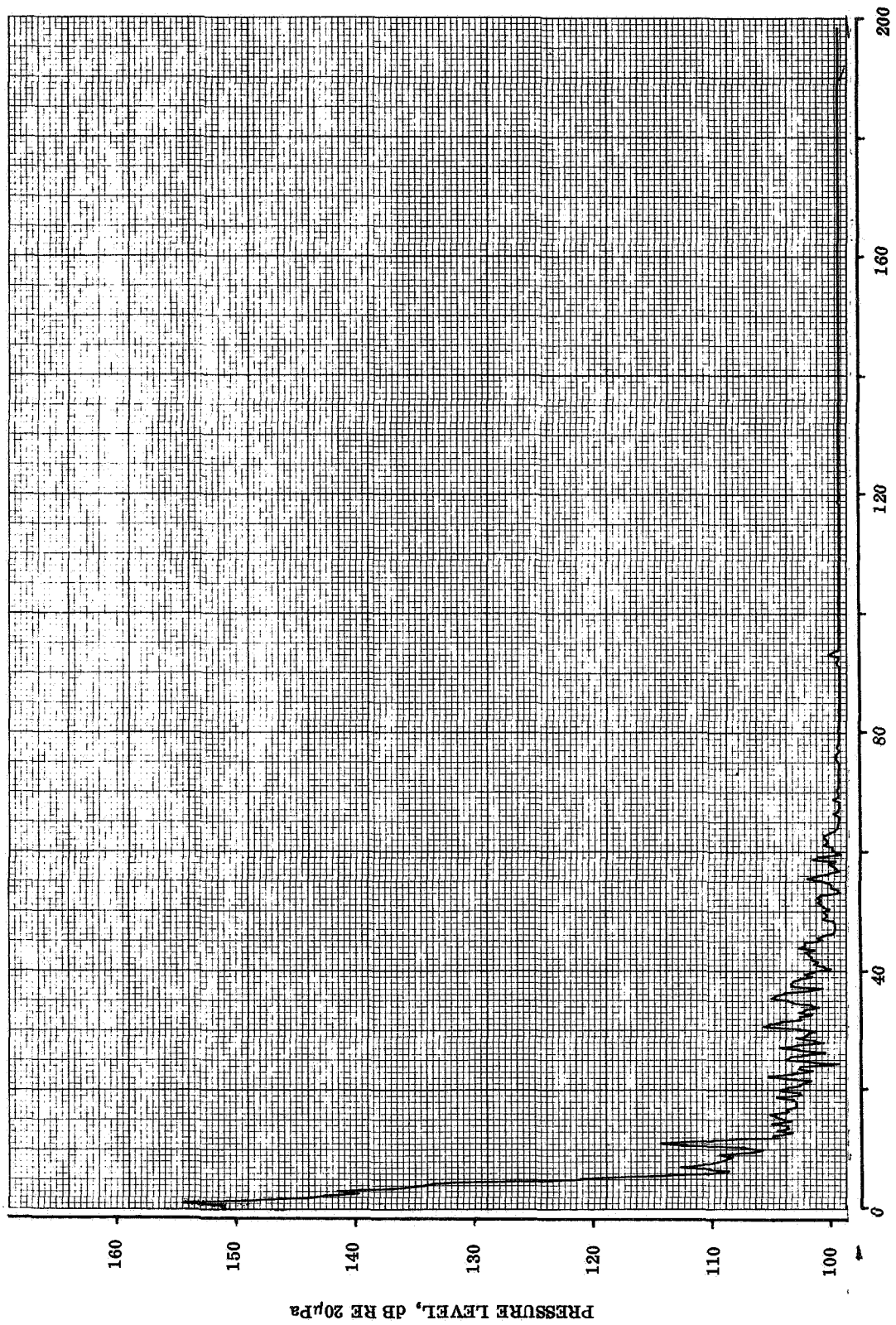
FLIGHT 14 RUN 21S 75% RPM XDUCERS NO. 5.4,3.1



FLIGHT 14 RUN 225 72% RPM XDUCERS NO. 5,4,3,1



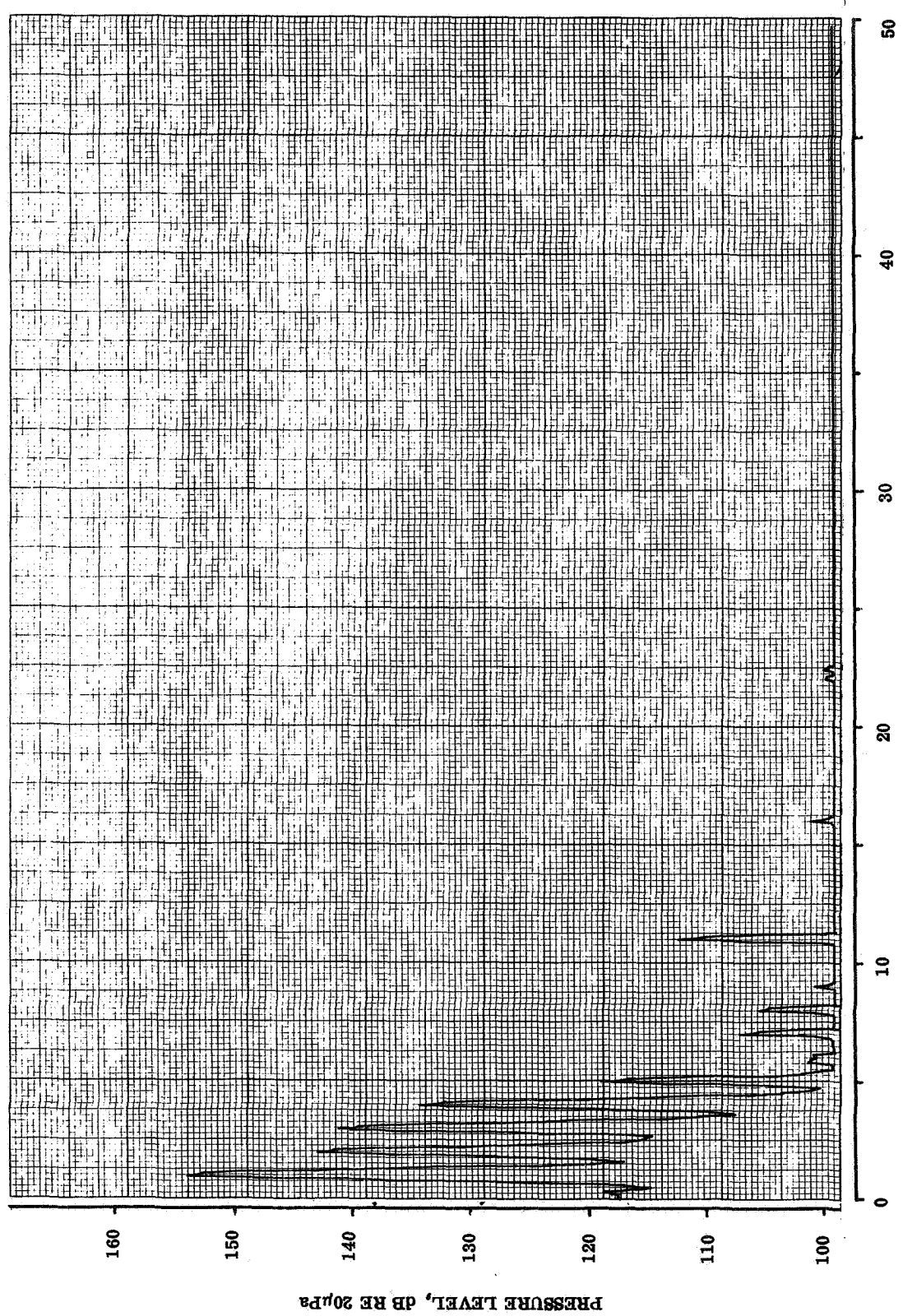
APPENDIX B - BLADE SURFACE PRESSURE
NARROW-BAND SPECTRUM PLOTS

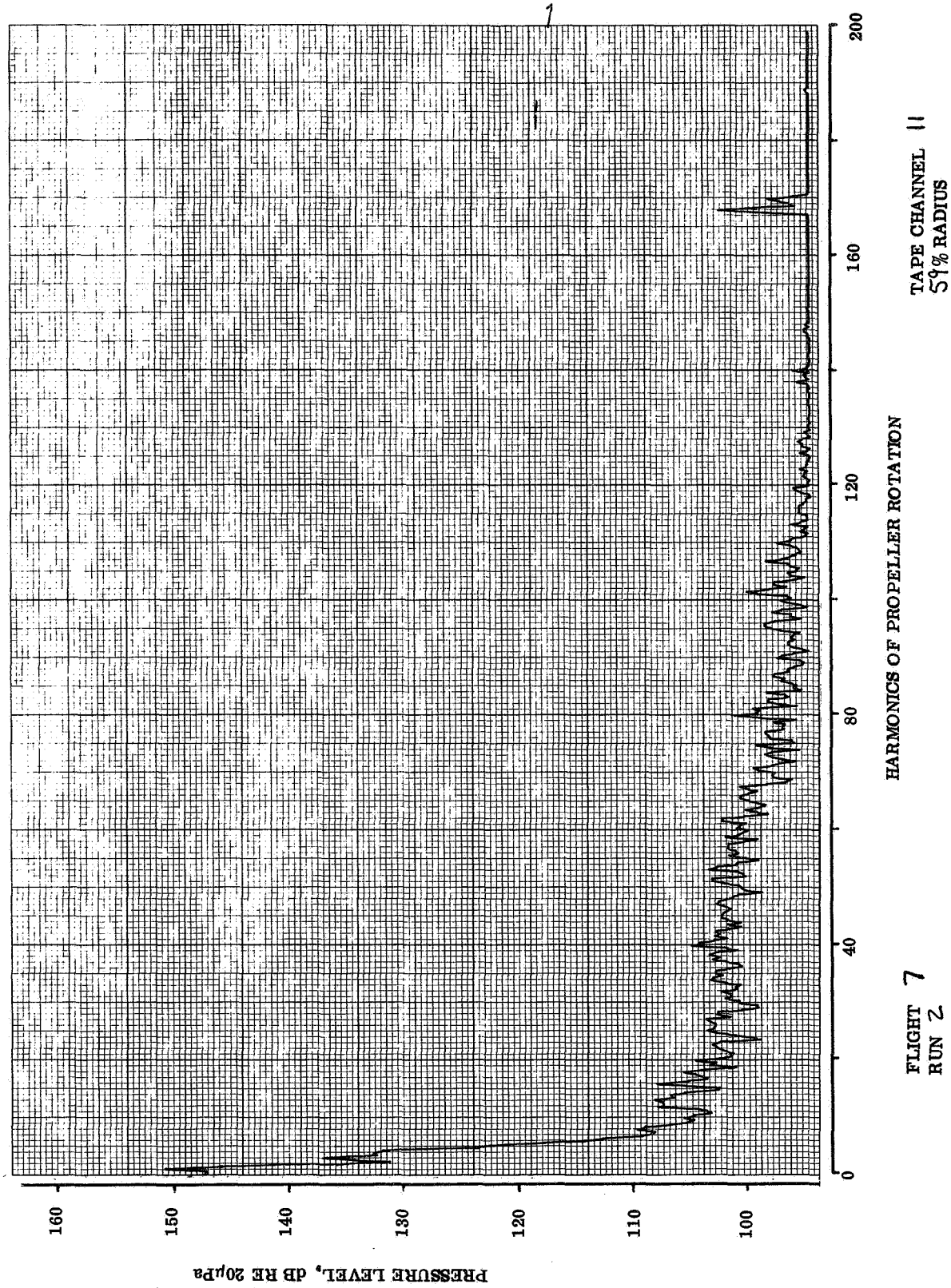


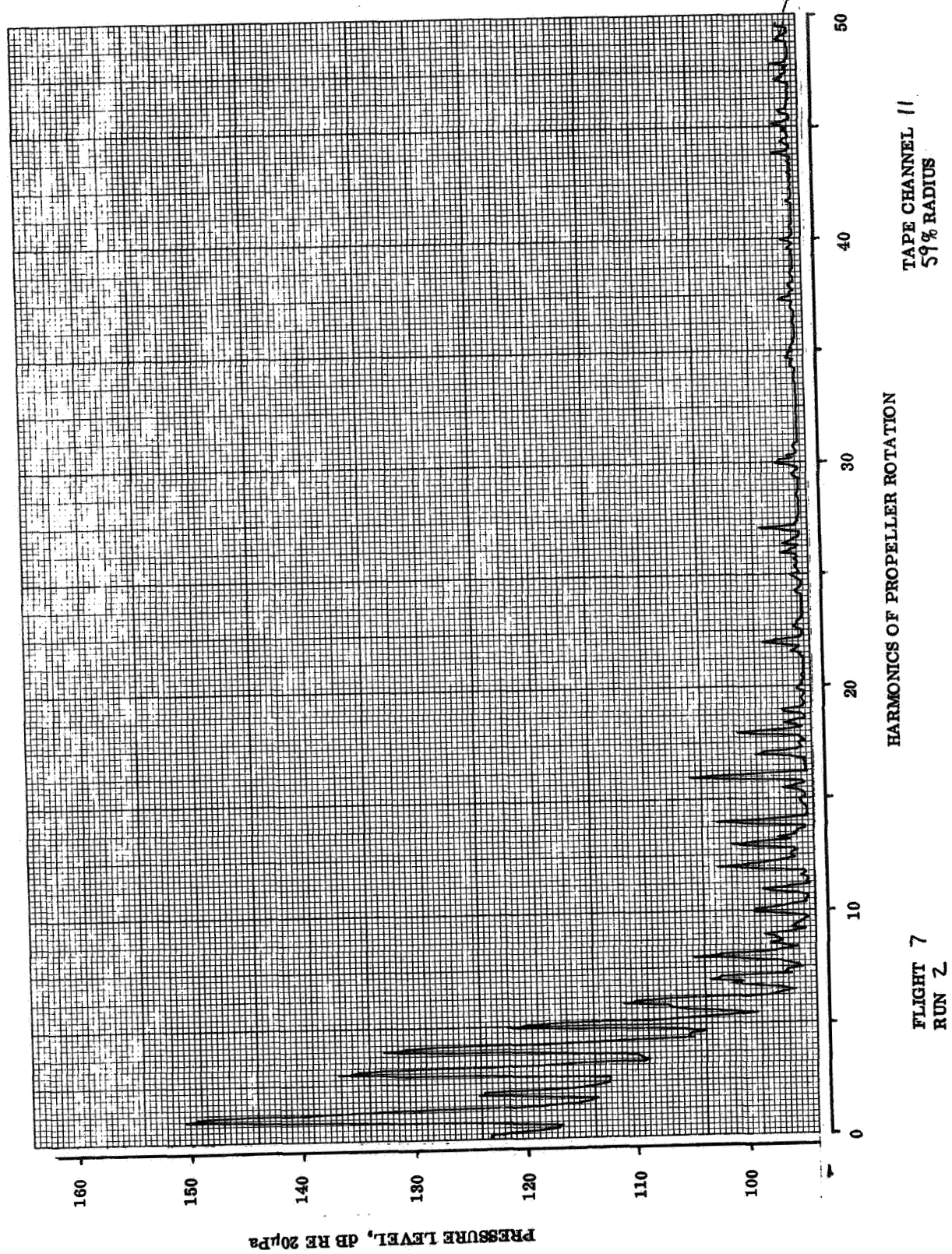
TAPE CHANNEL 3
40 % RADIUS

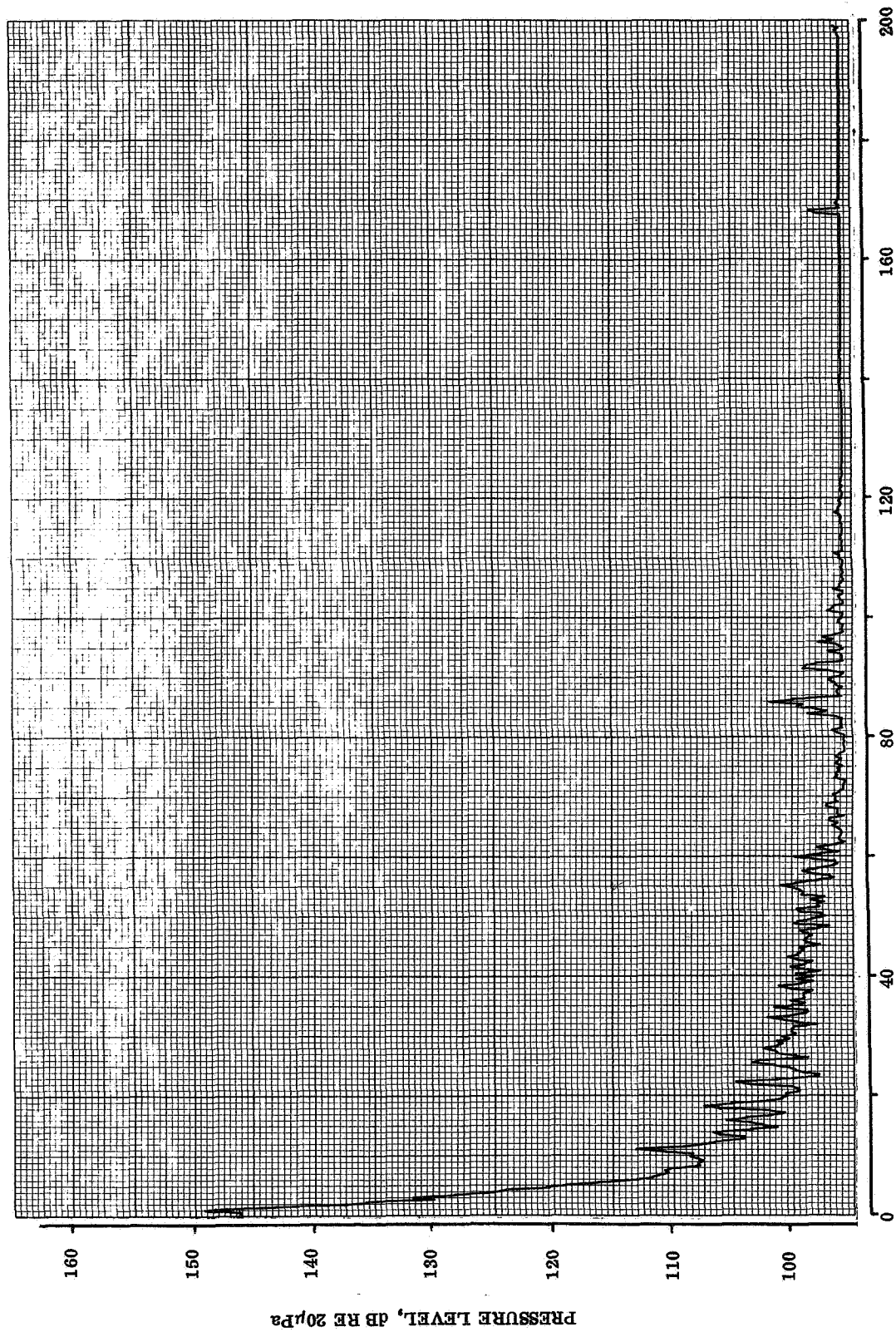
HARMONICS OF PROPELLER ROTATION

FLIGHT 7
RUN 2





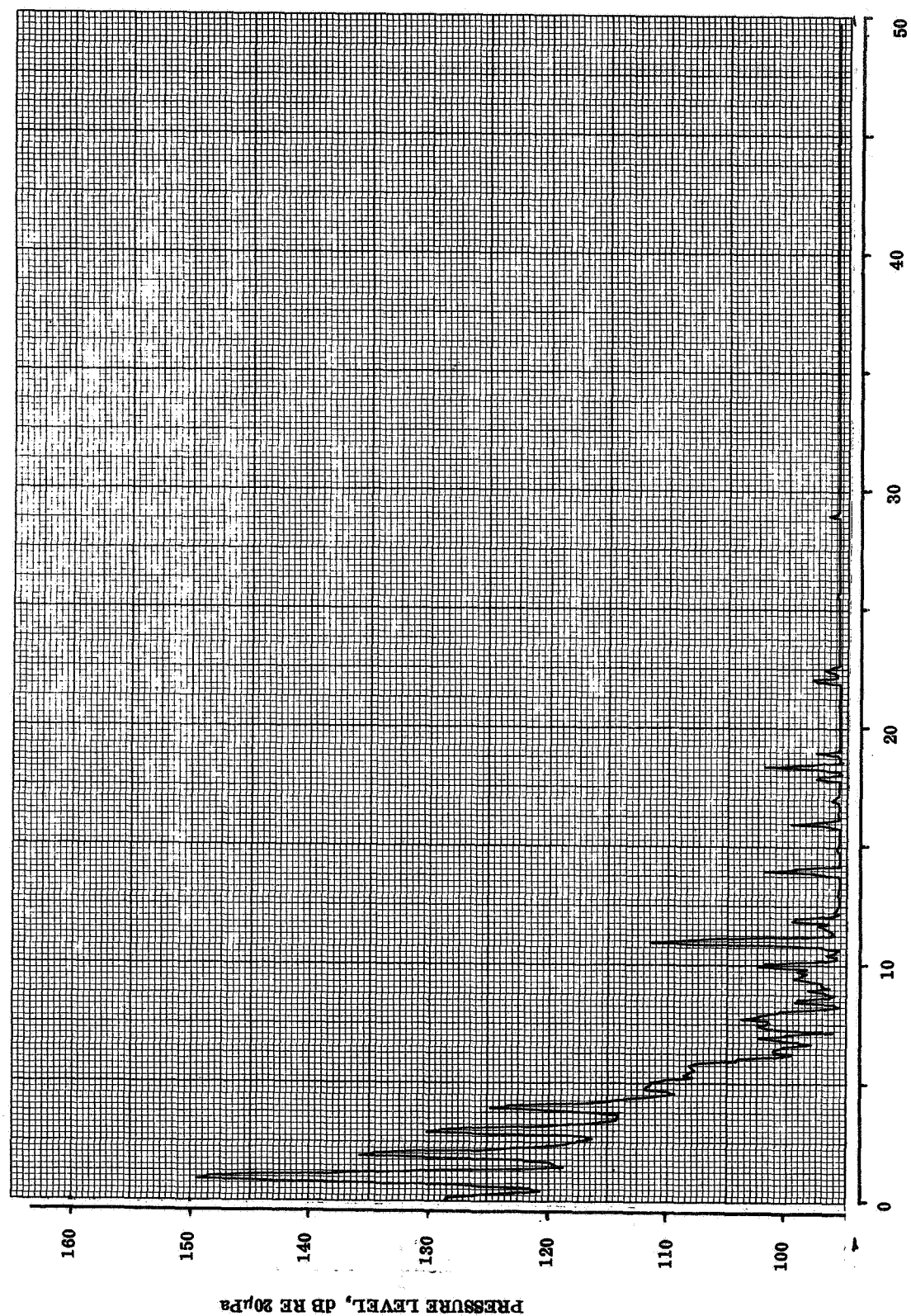


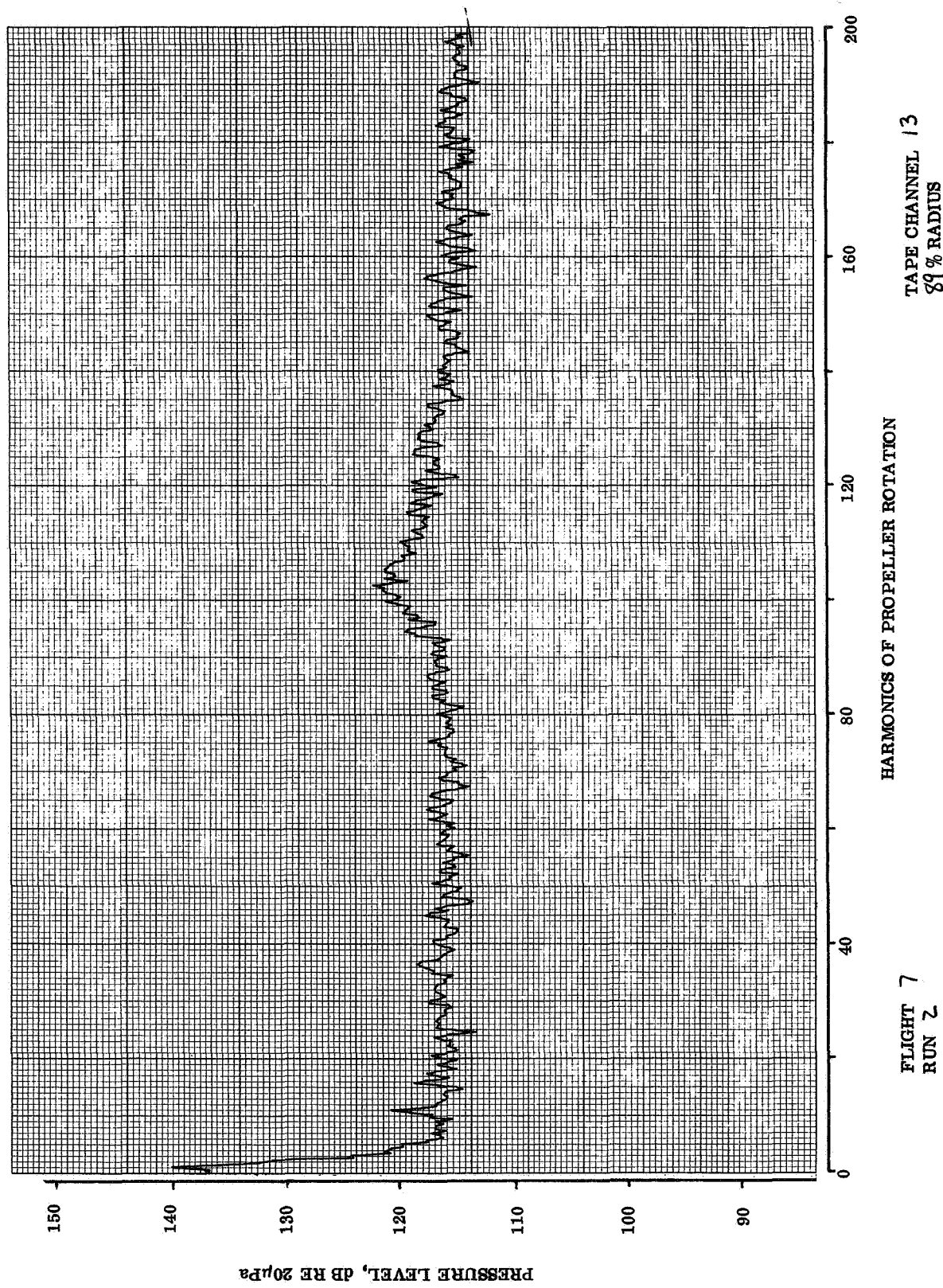


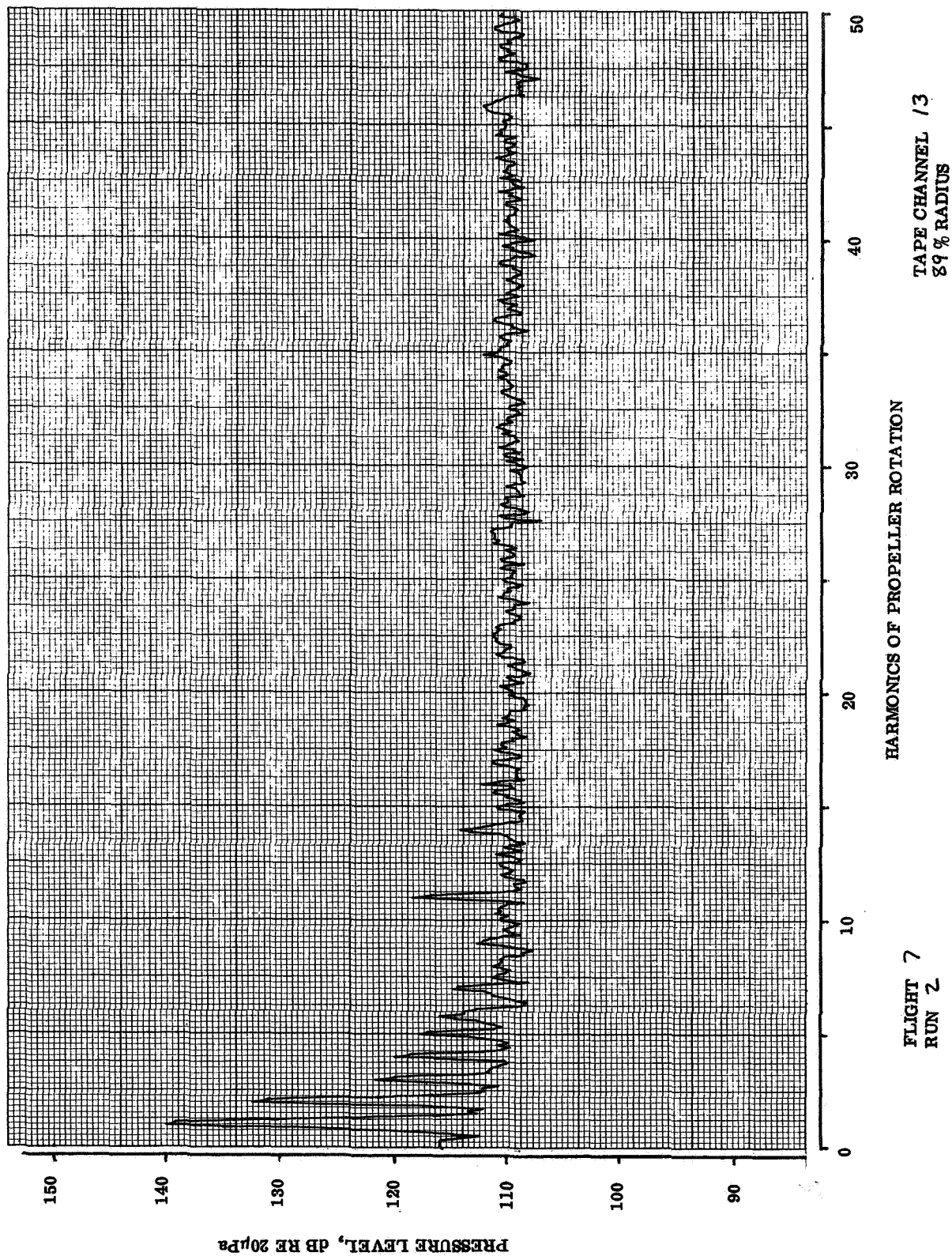
TAPE CHANNEL 5
77% RADIUS

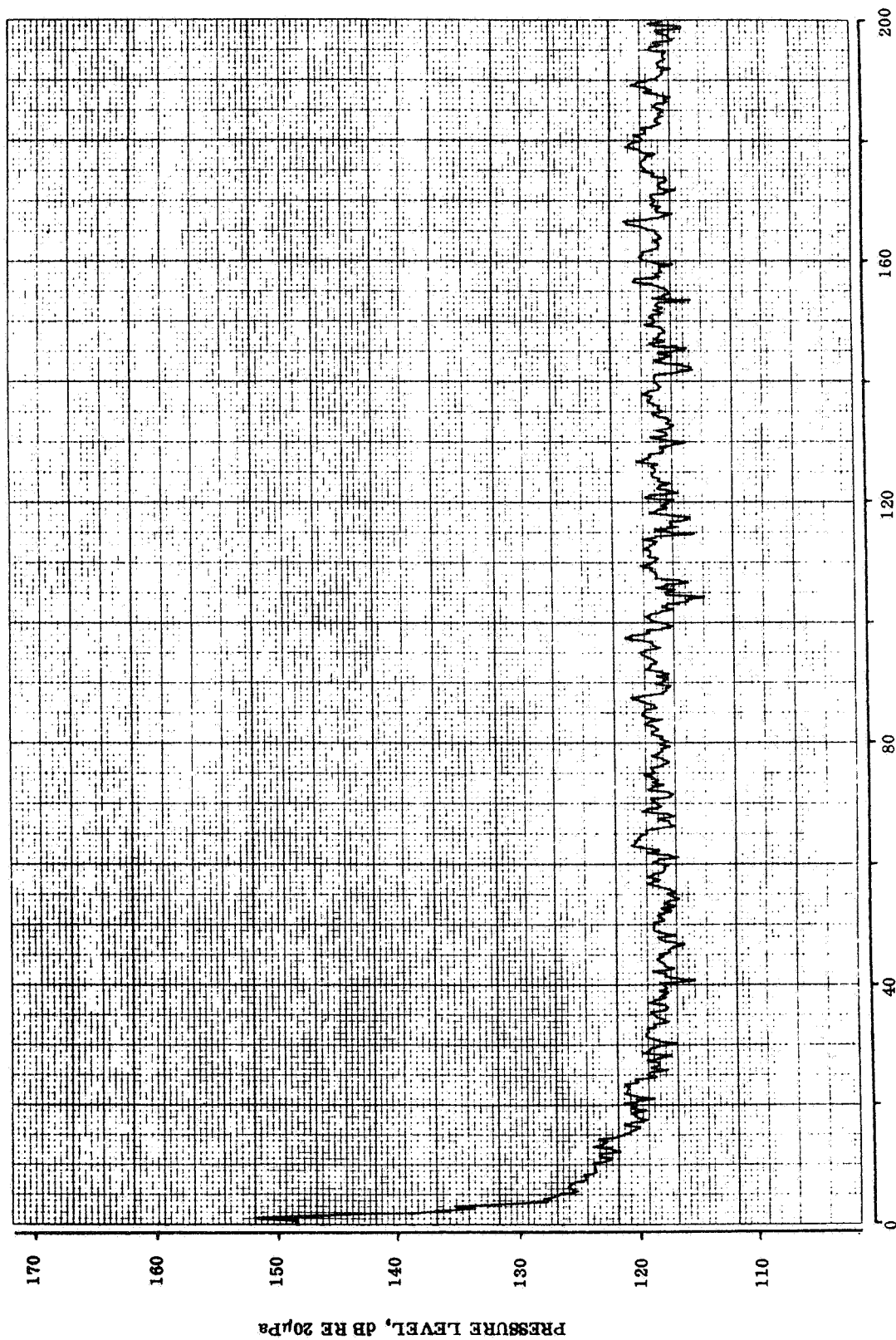
HARMONICS OF PROPELLER ROTATION

FLIGHT 7
RUN 2





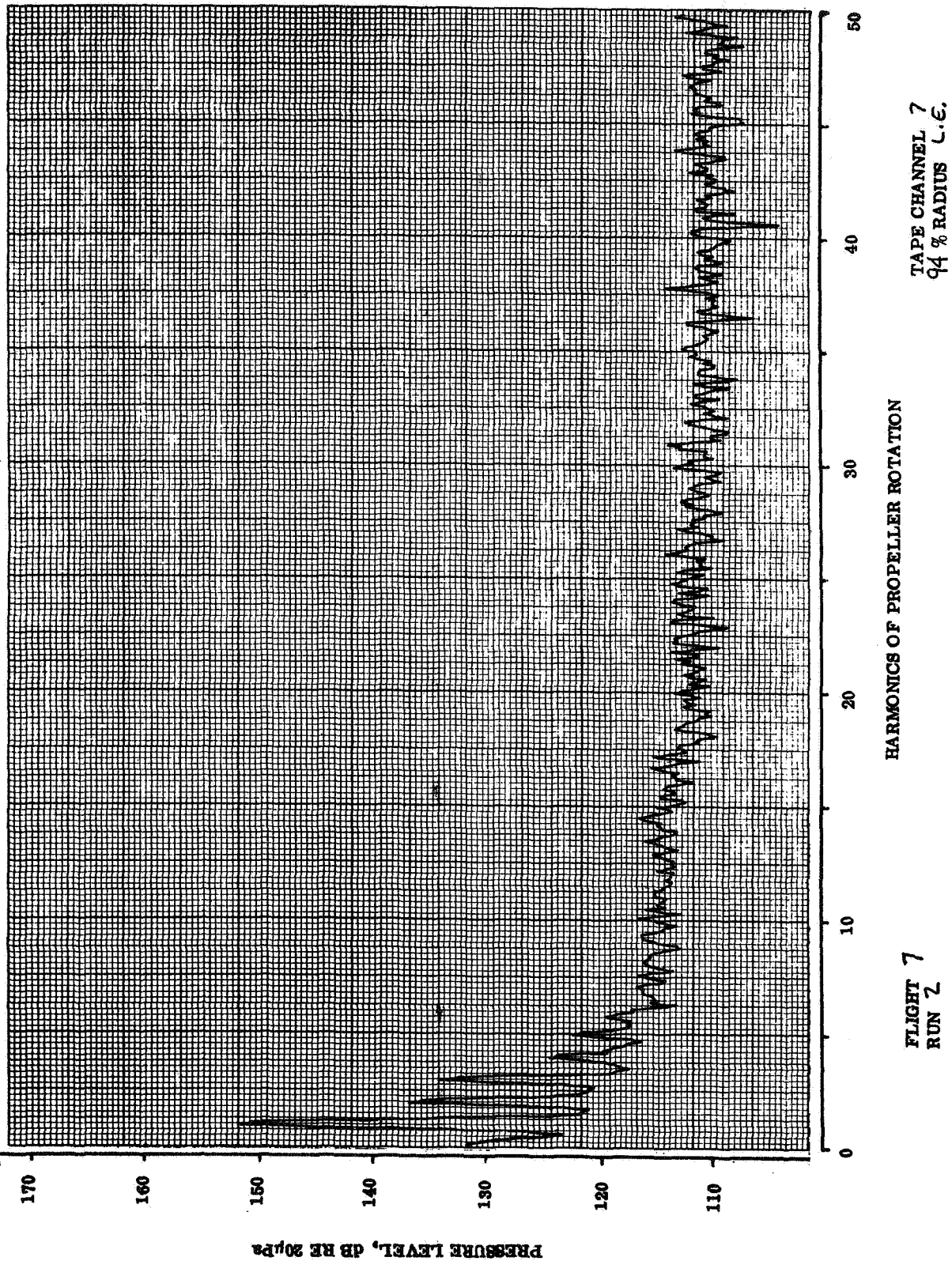


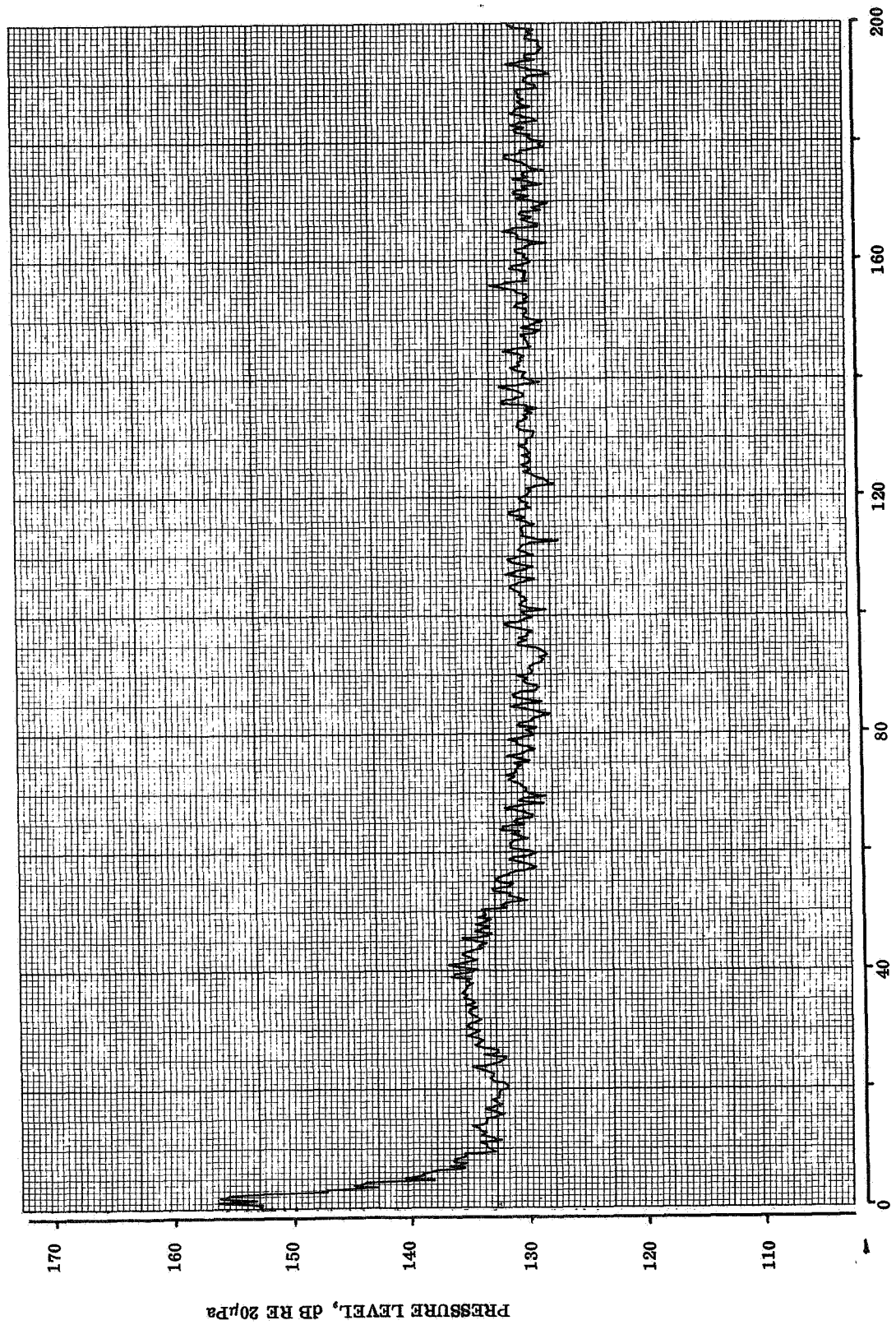


TAPE CHANNEL 7
Q4 % RADIUS L.E.

HARMONICS OF PROPELLER ROTATION

FLIGHT 7
RUN 2

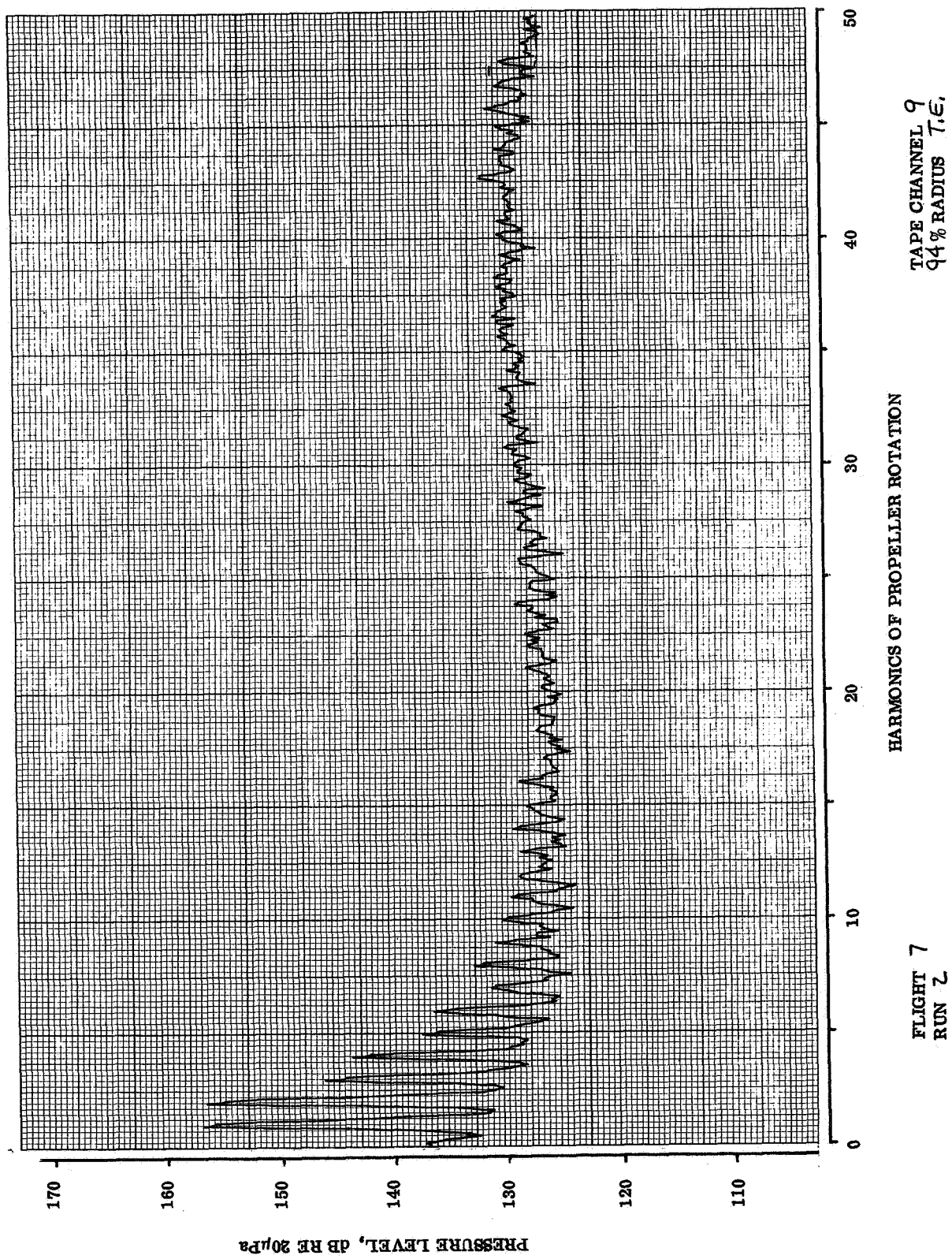


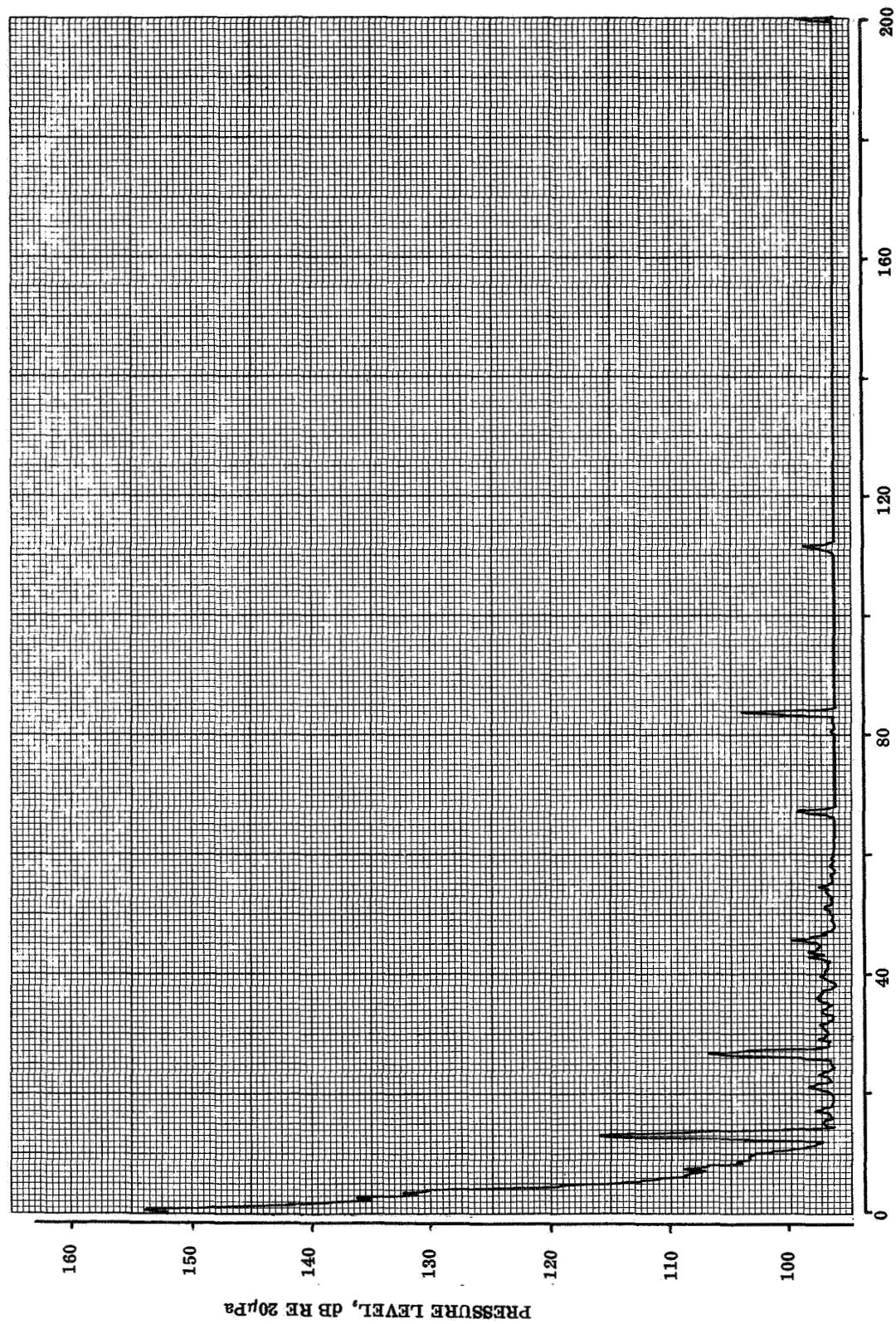


TAPE CHANNEL 9
94 % RADIUS T.C.

HARMONICS OF PROPELLER ROTATION

FLIGHT 7
RUN 2

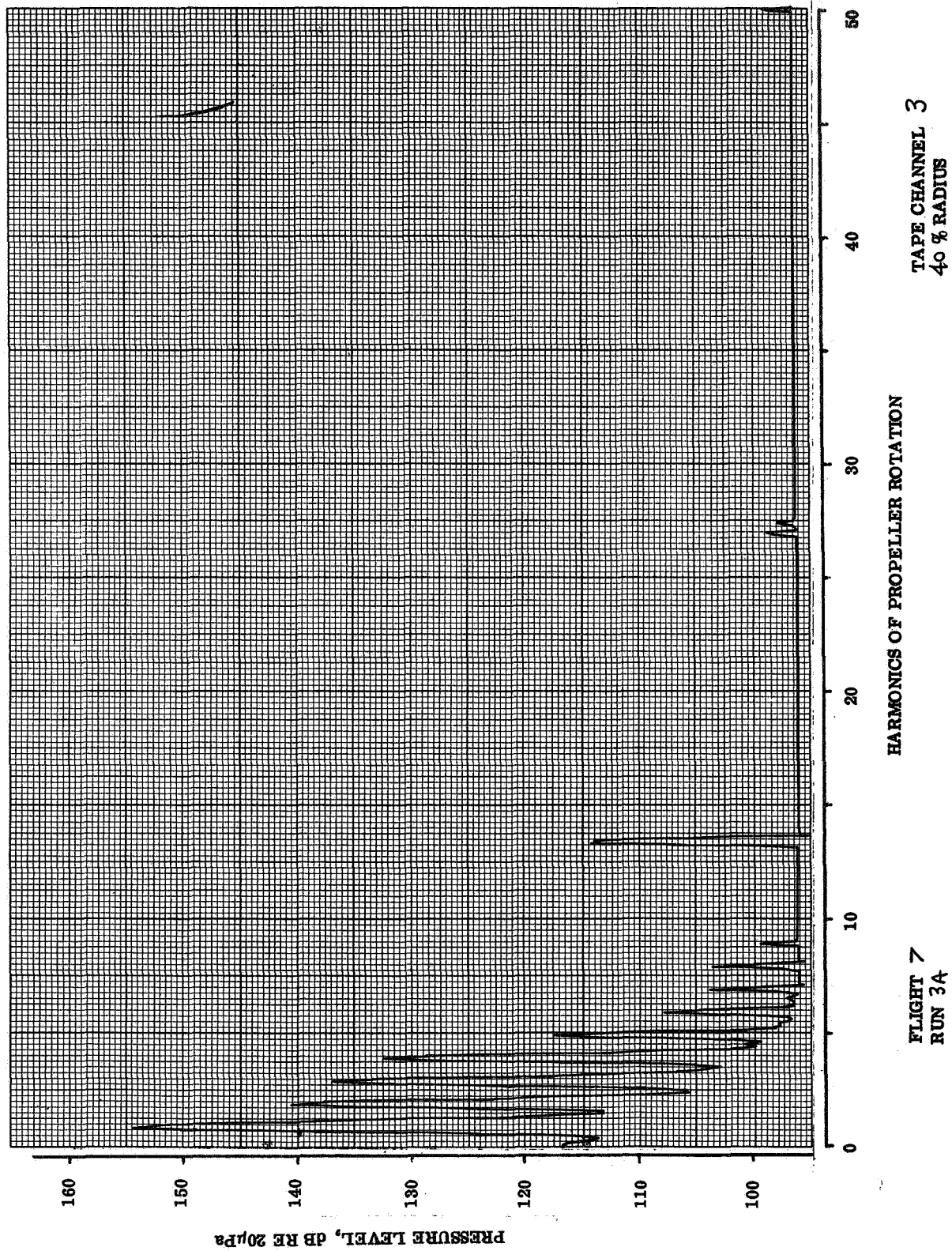


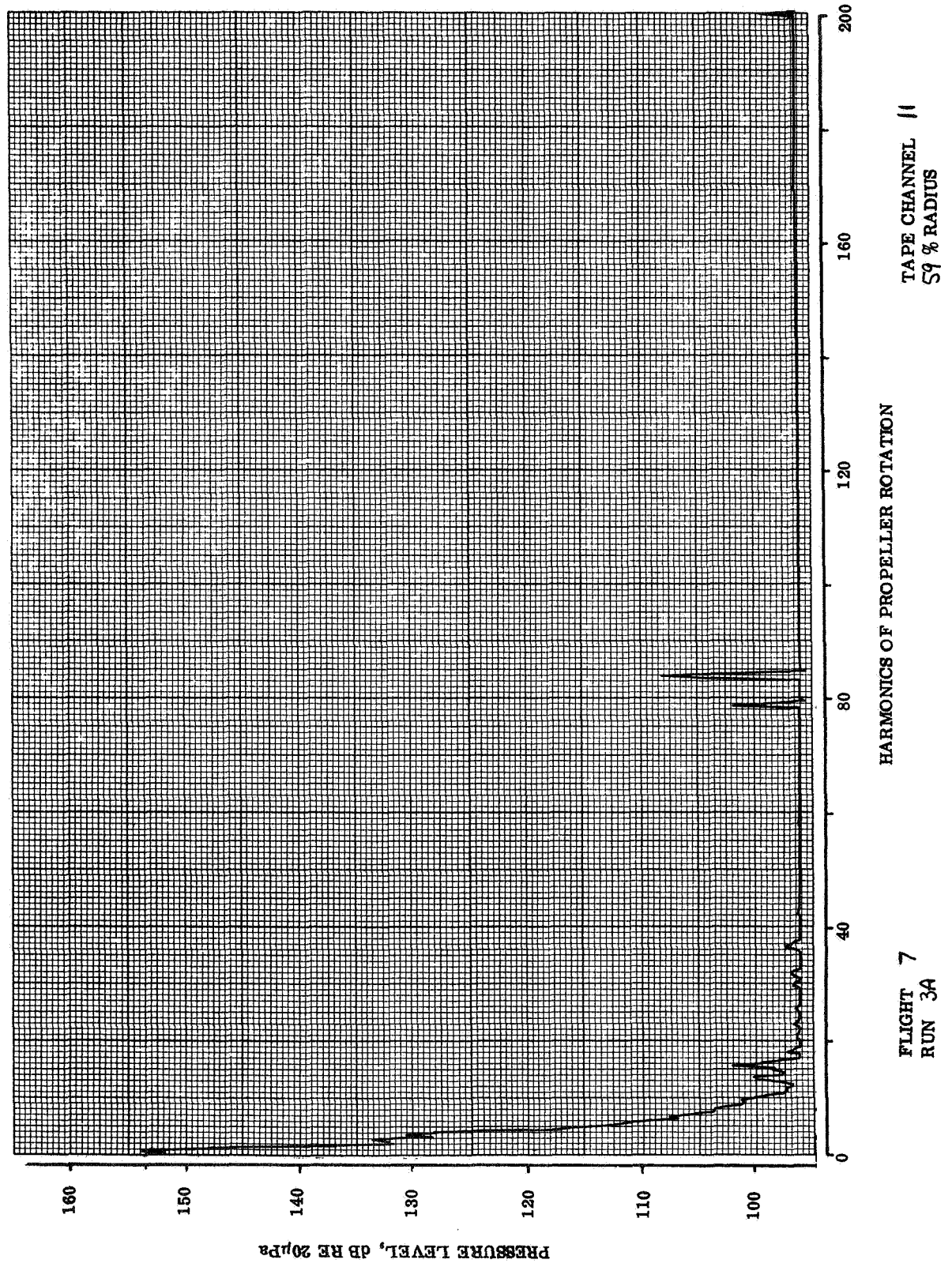


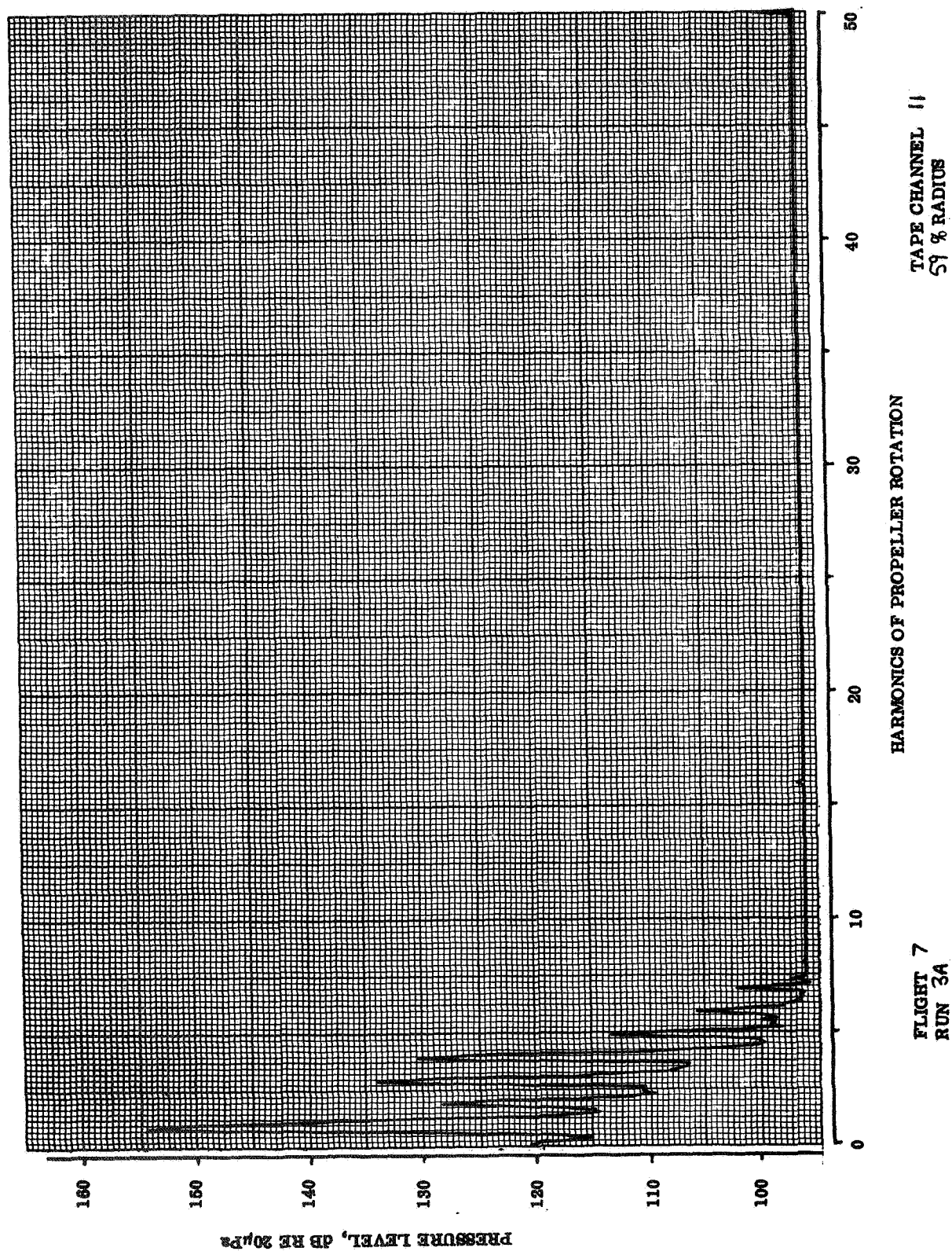
TAPE CHANNEL 3
40 % RADIUS

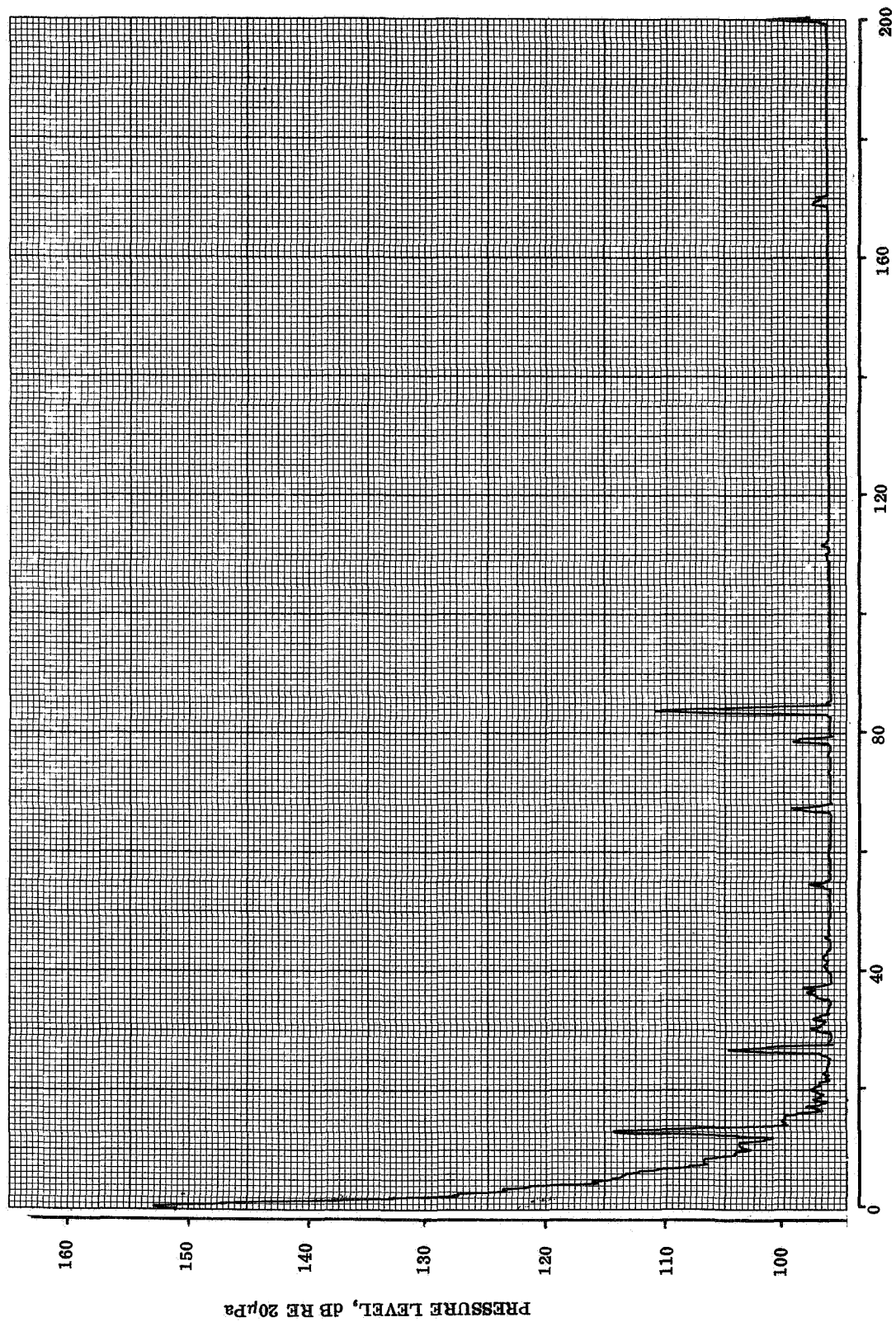
HARMONICS OF PROPELLER ROTATION

FLIGHT 7
RUN 3A



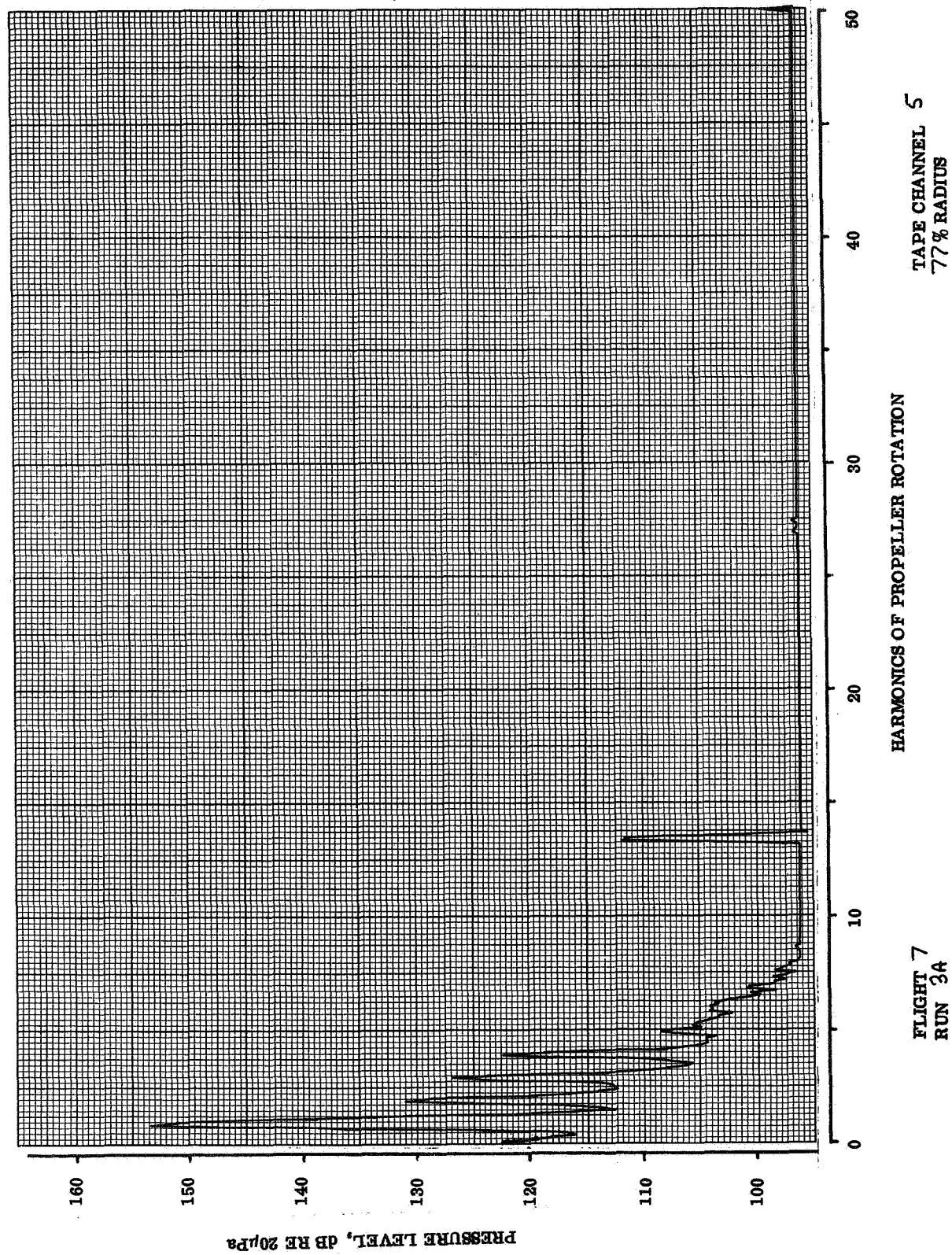


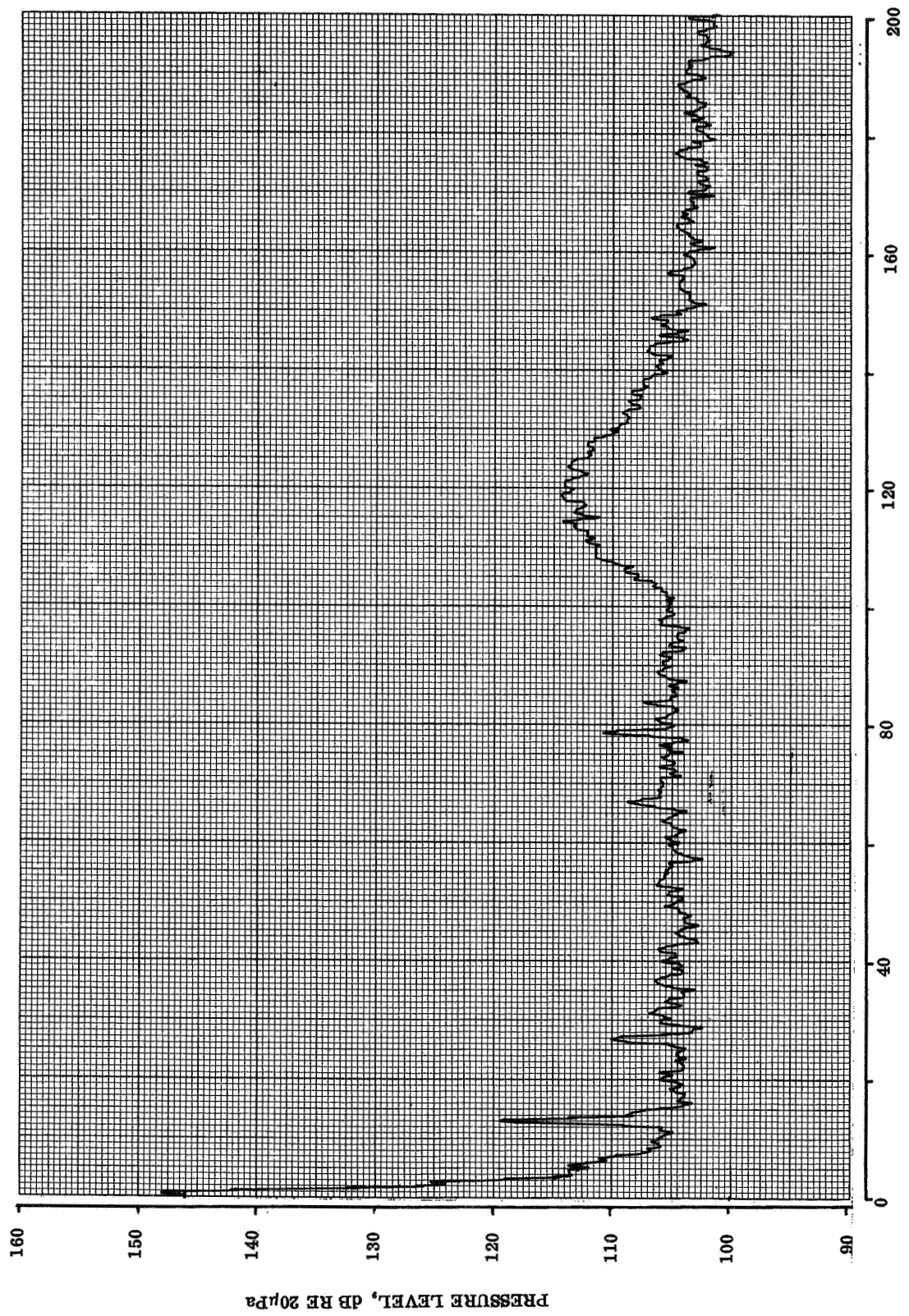




TAPE CHANNEL 5
77% RADIUS

FLIGHT 7
RUN 3A

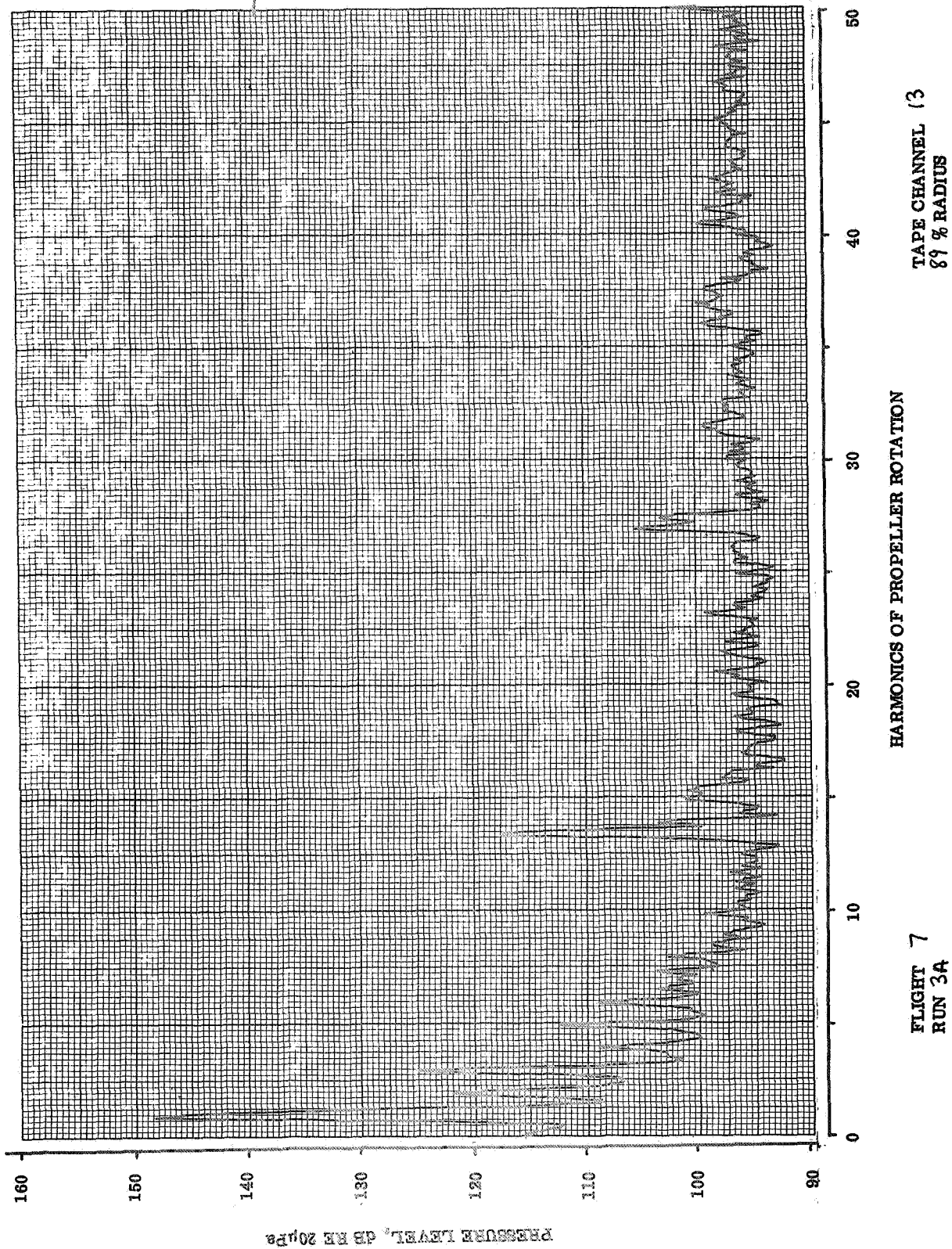


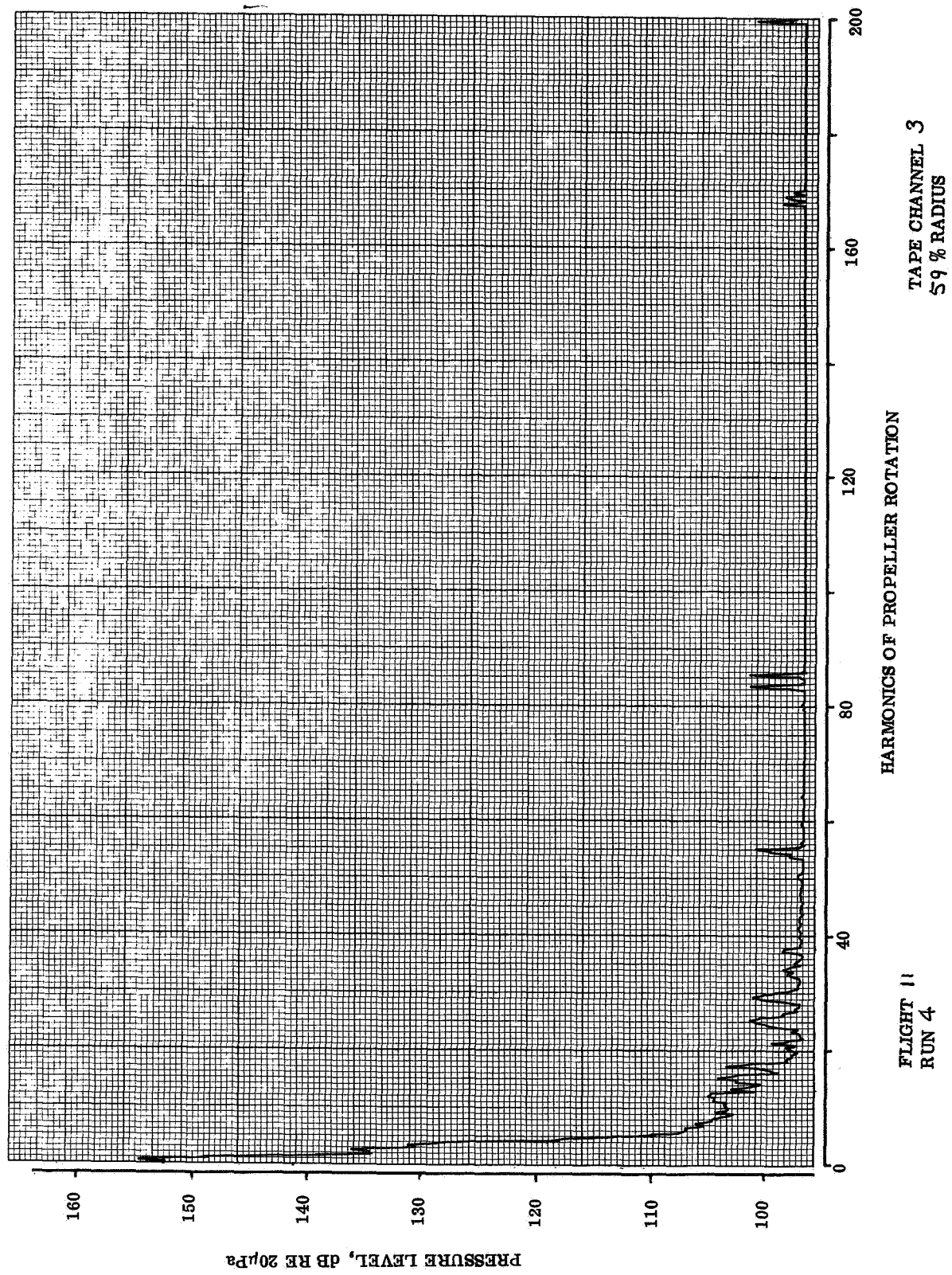


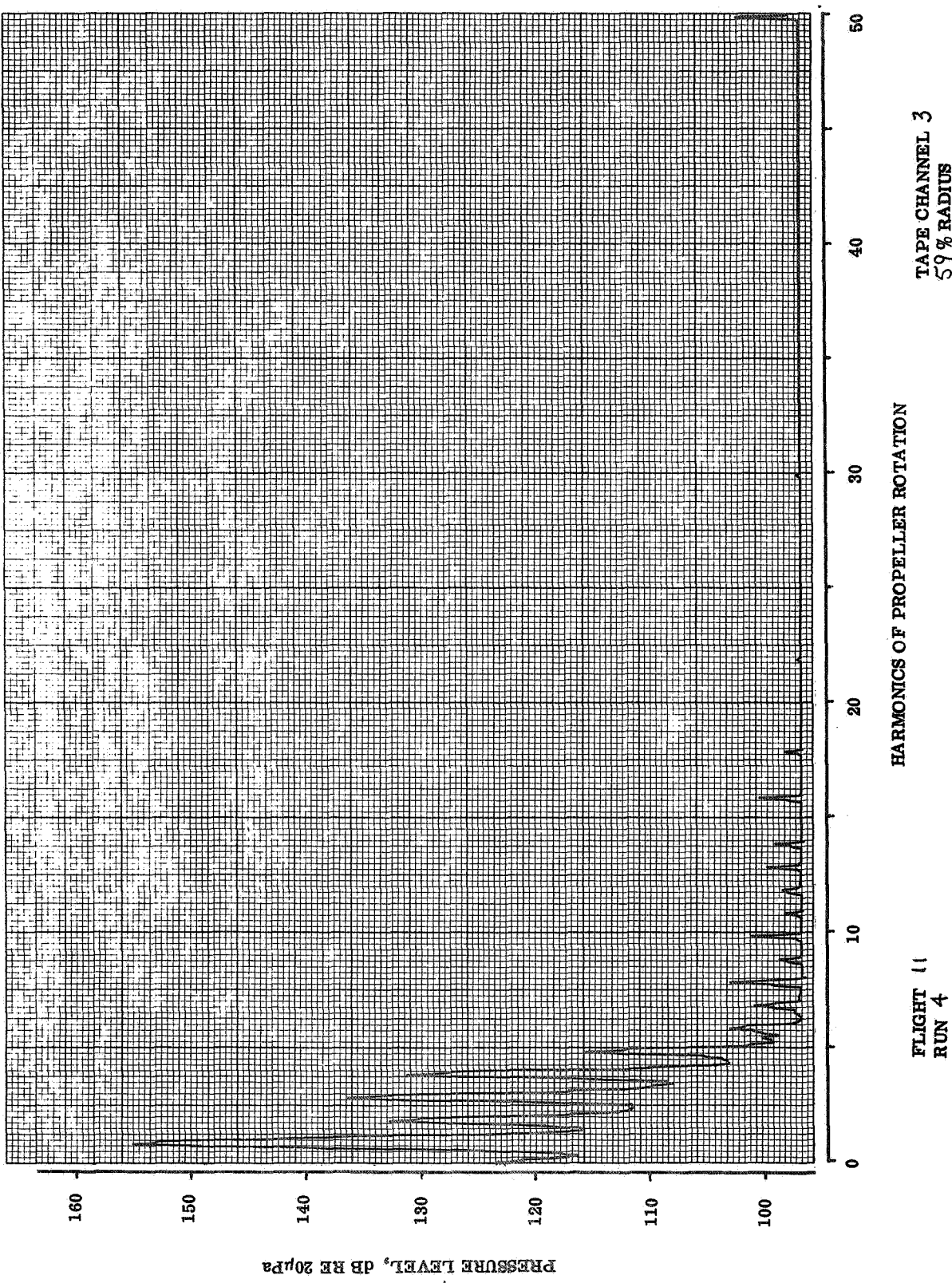
FLIGHT 7
RUN 3A

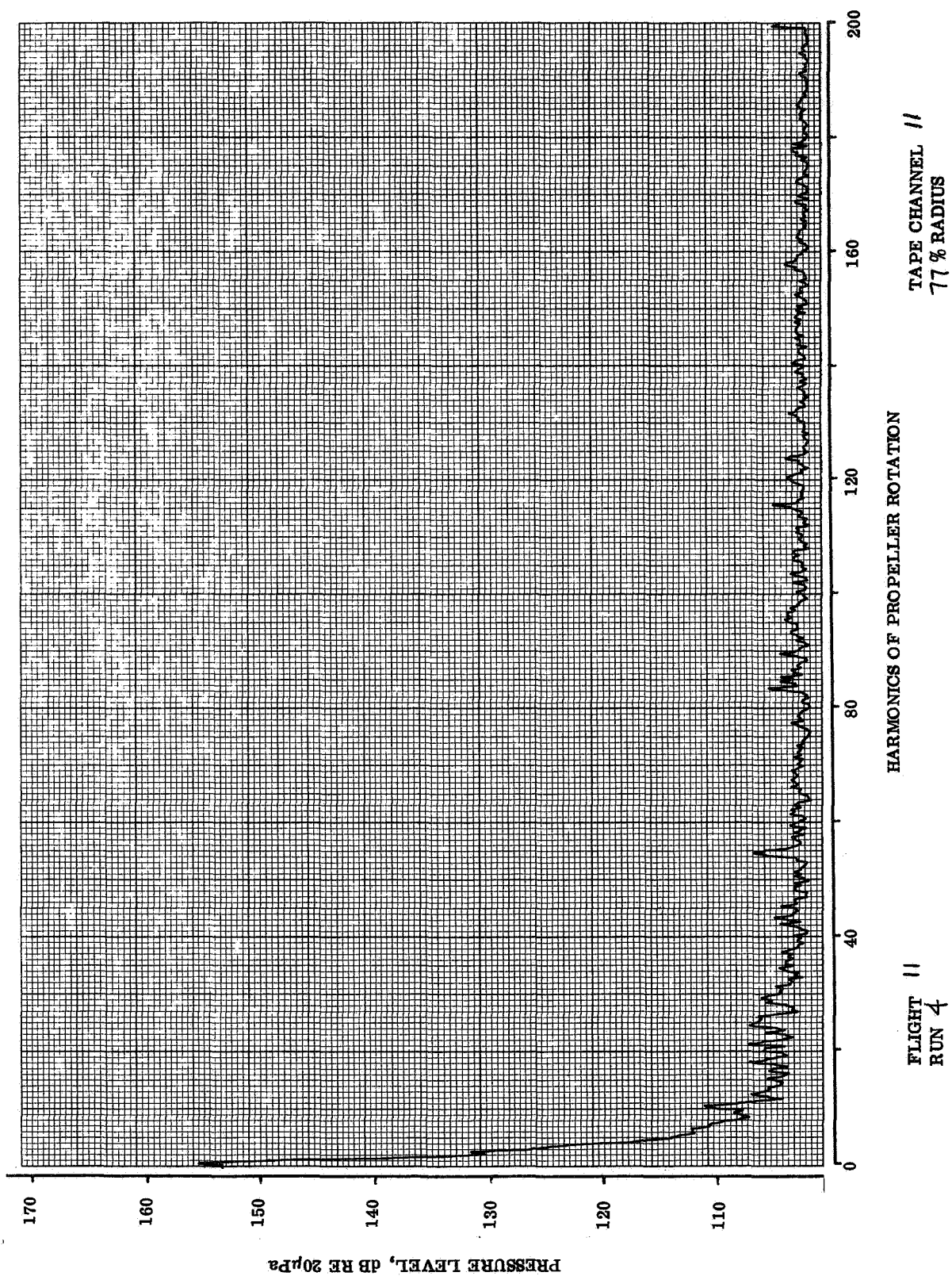
HARMONICS OF PROPELLER ROTATION

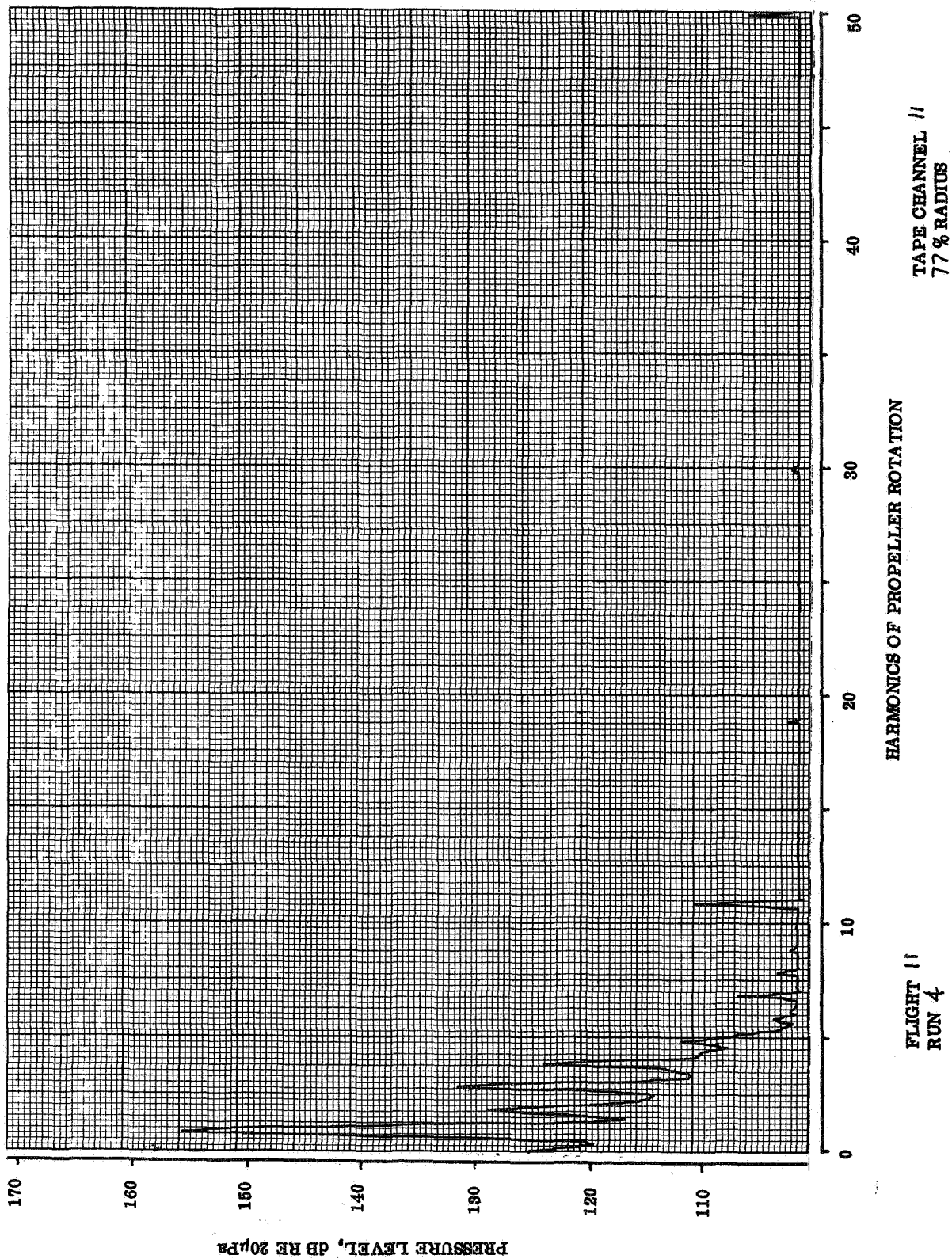
TAPE CHANNEL 13
89 % RADIUS

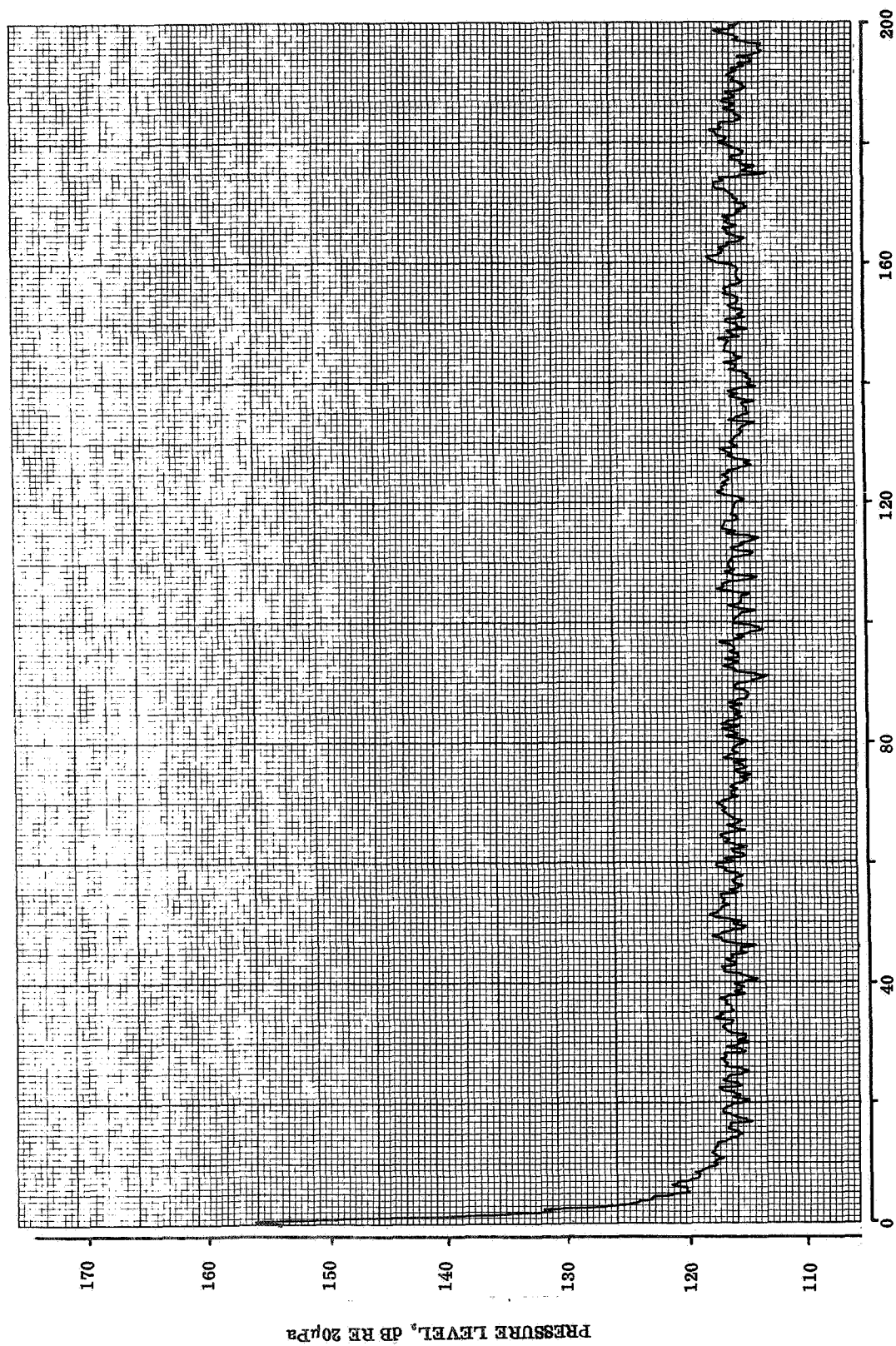








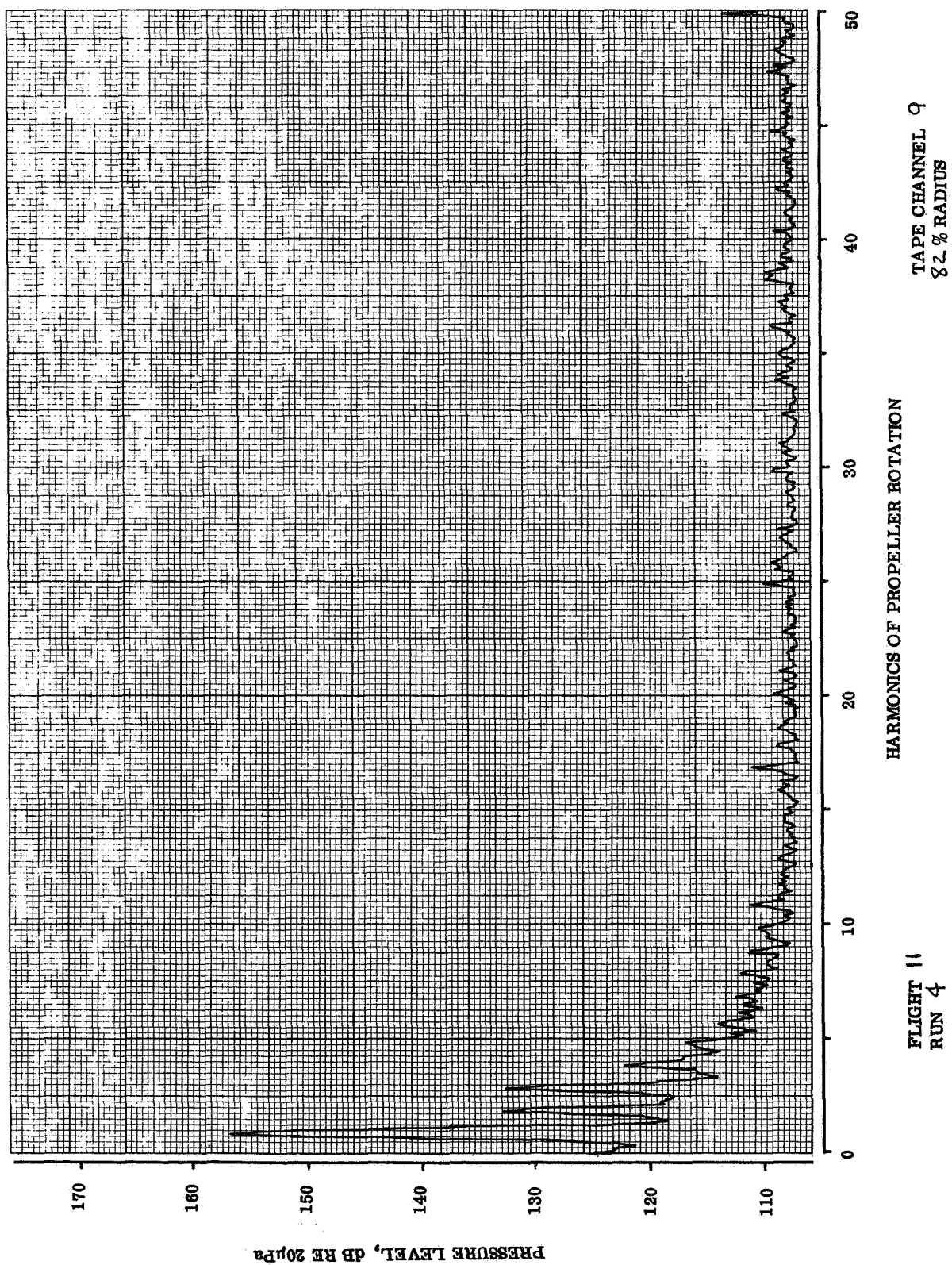


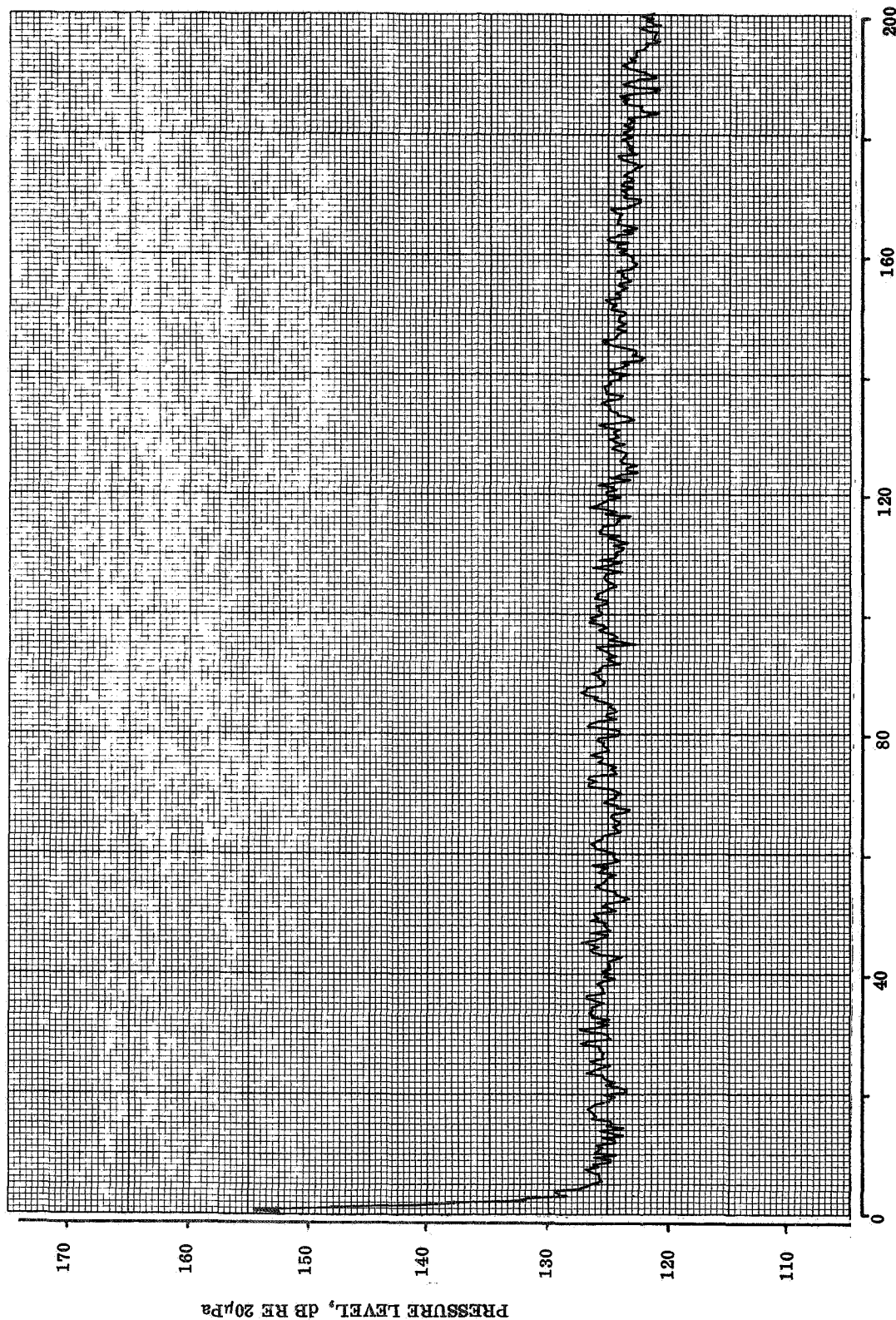


TAPE CHANNEL 9
82 % RADIUS

HARMONICS OF PROPELLER ROTATION

FLIGHT 11
RUN 4

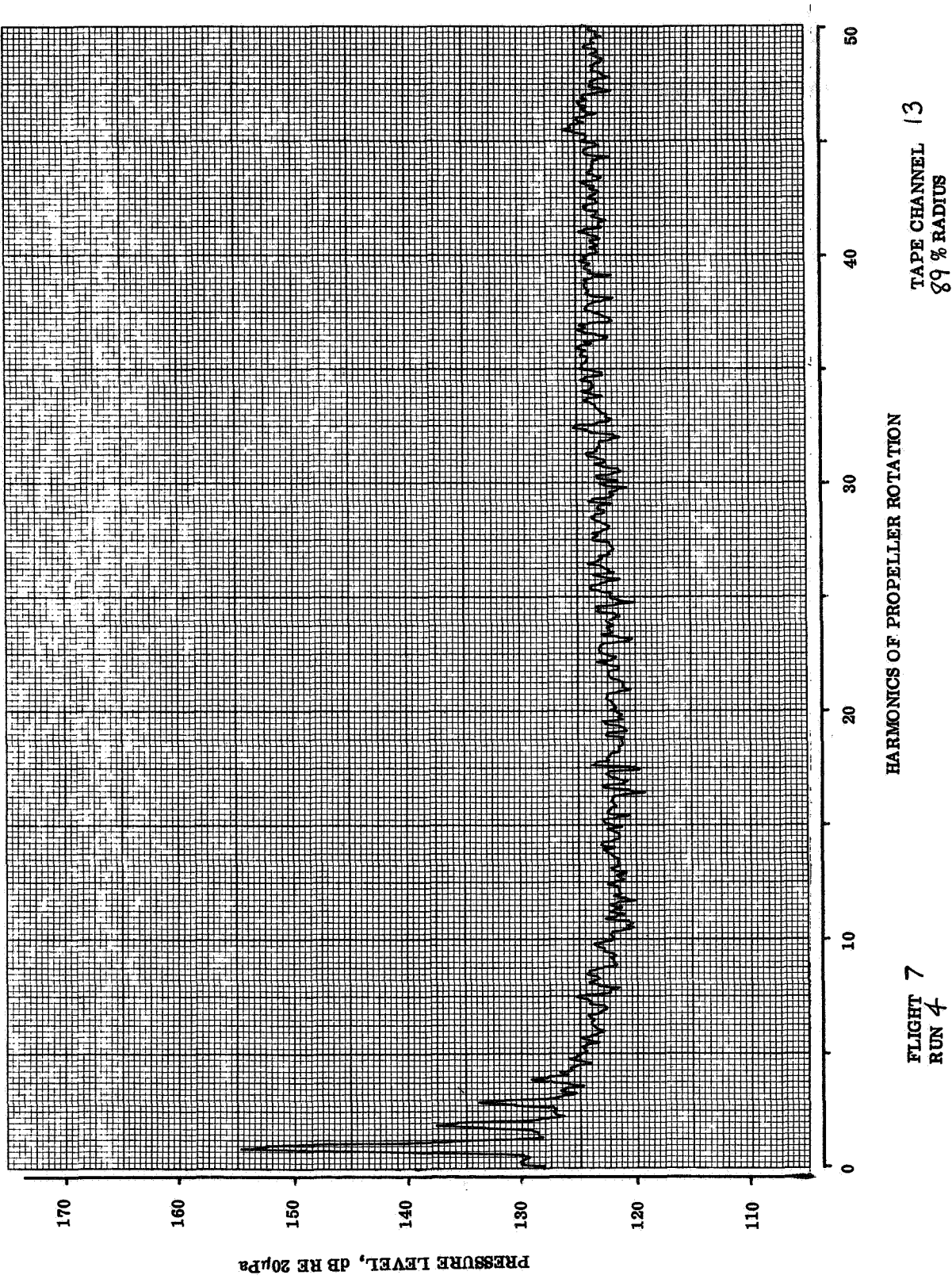


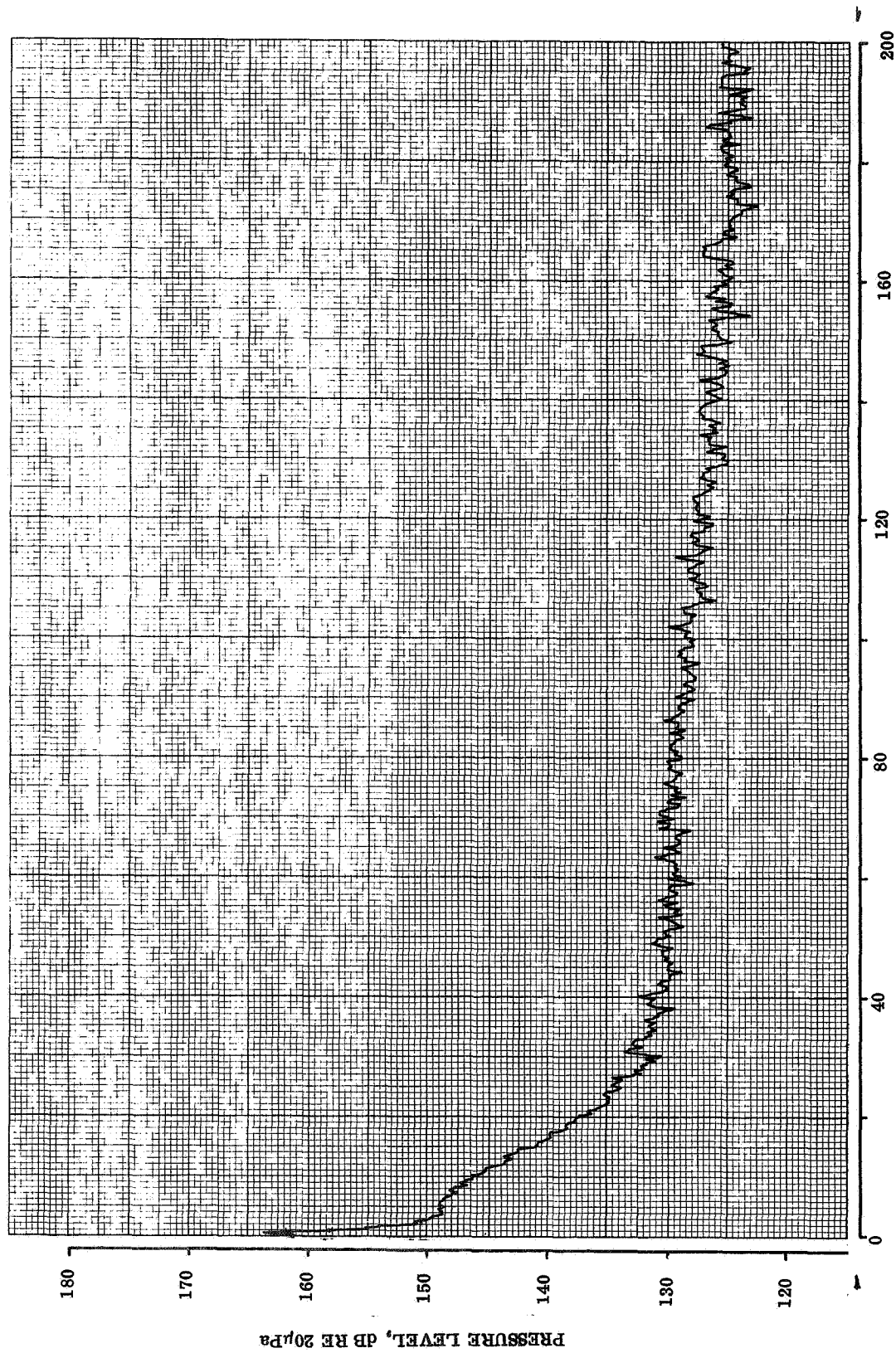


TAPE CHANNEL 13
89 % RADIUS

HARMONICS OF PROPELLER ROTATION

FLIGHT 7
RUN 4

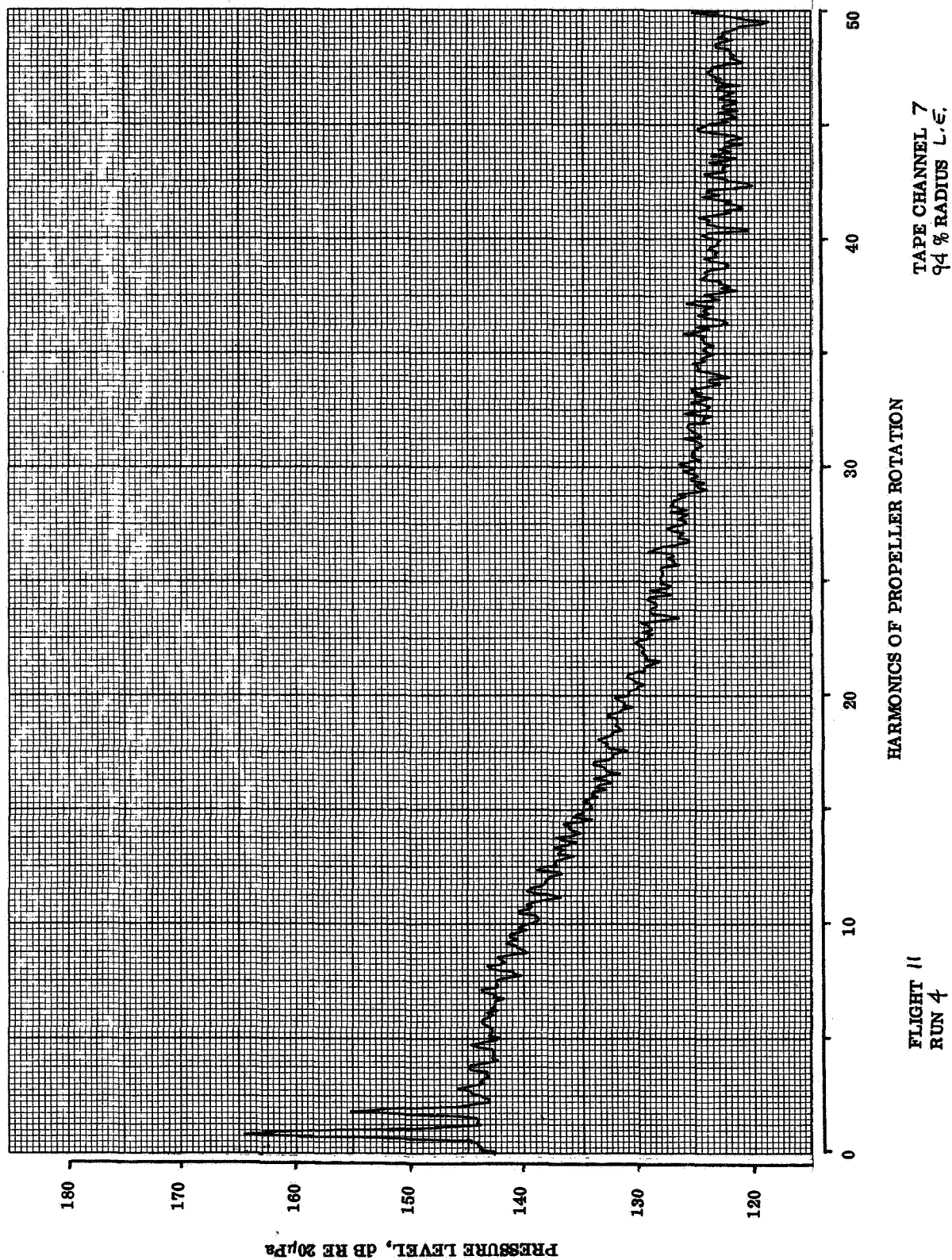


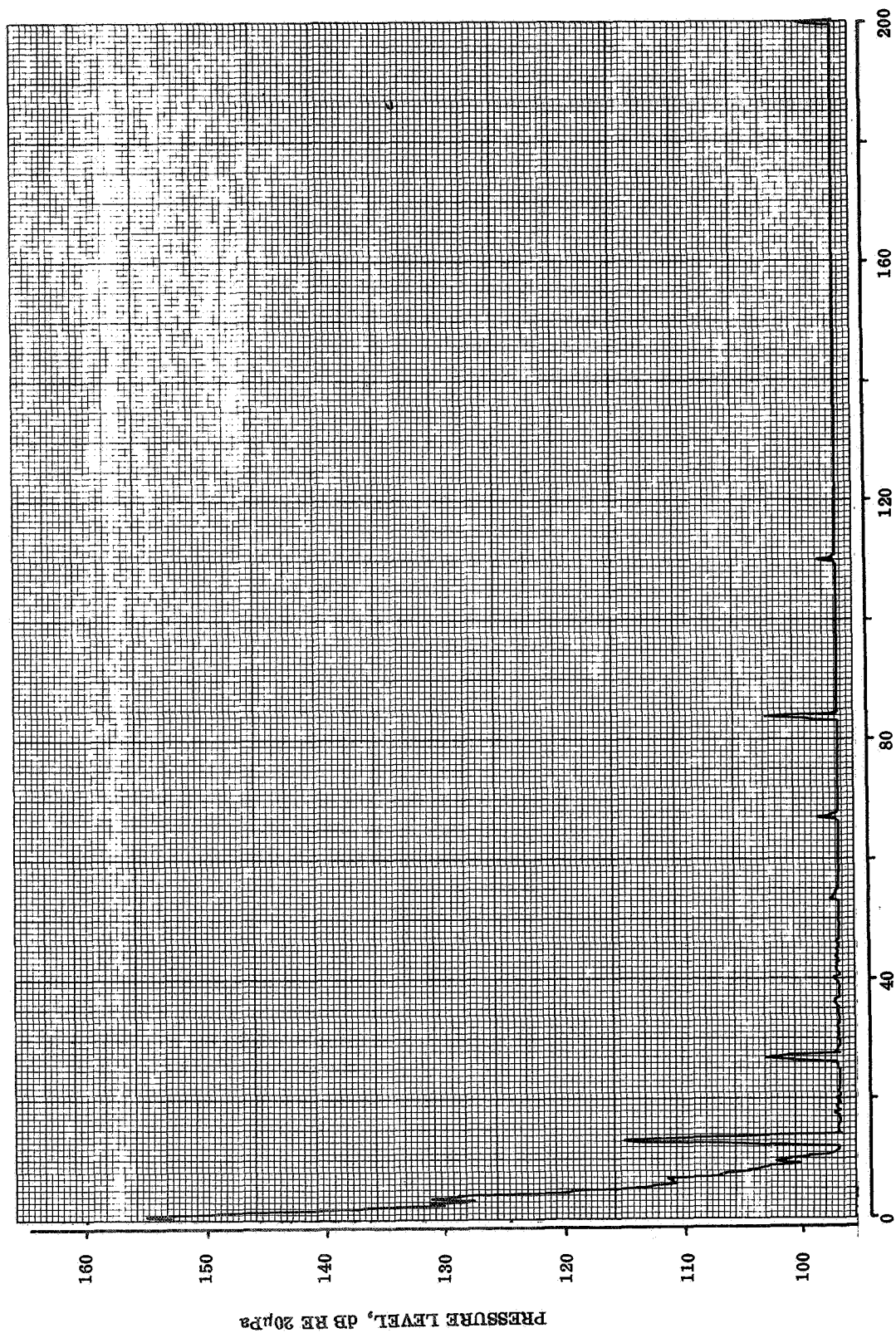


TAPE CHANNEL 7
Q4 % RADIUS L.E.

HARMONICS OF PROPELLER ROTATION

FLIGHT 11
RUN 4

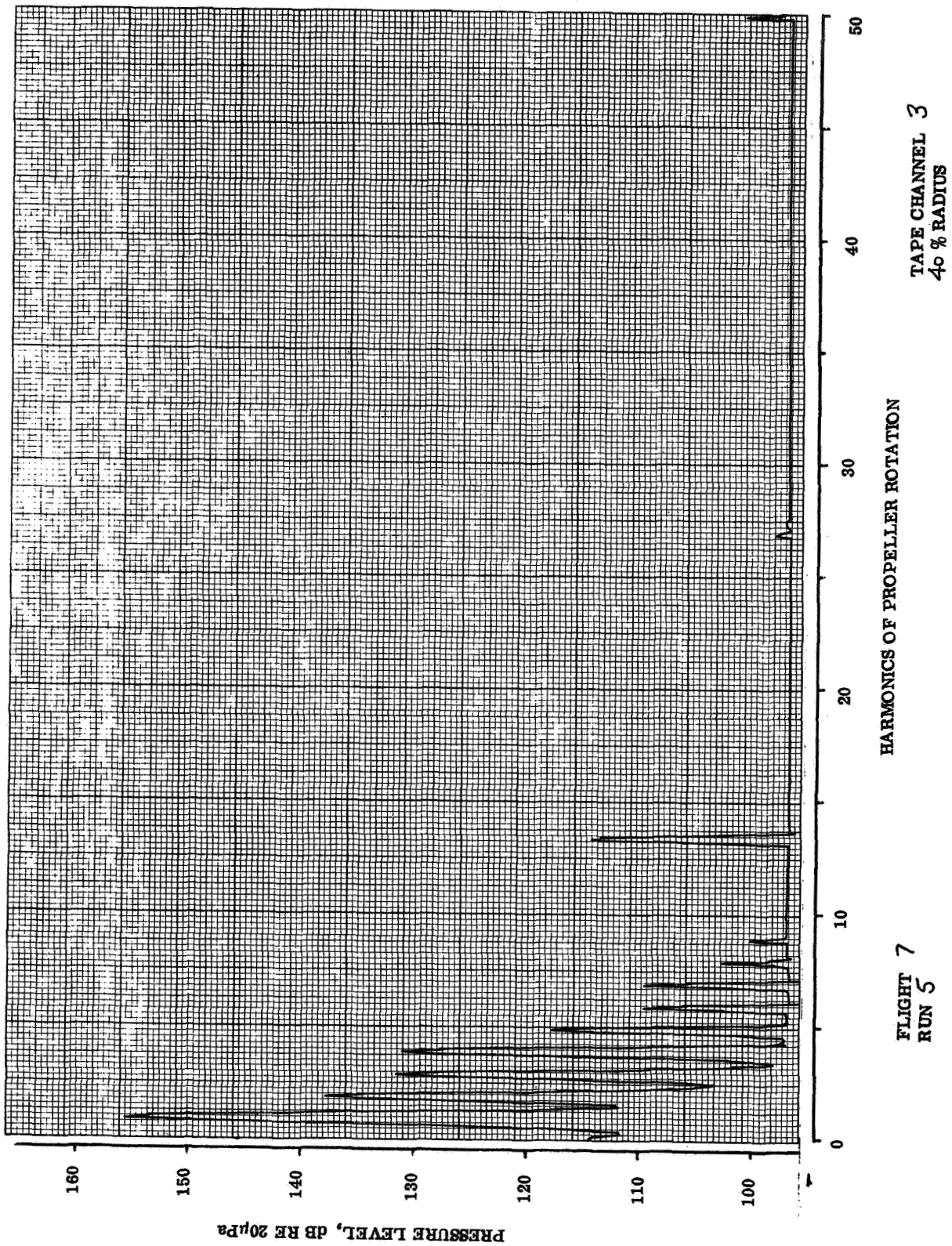


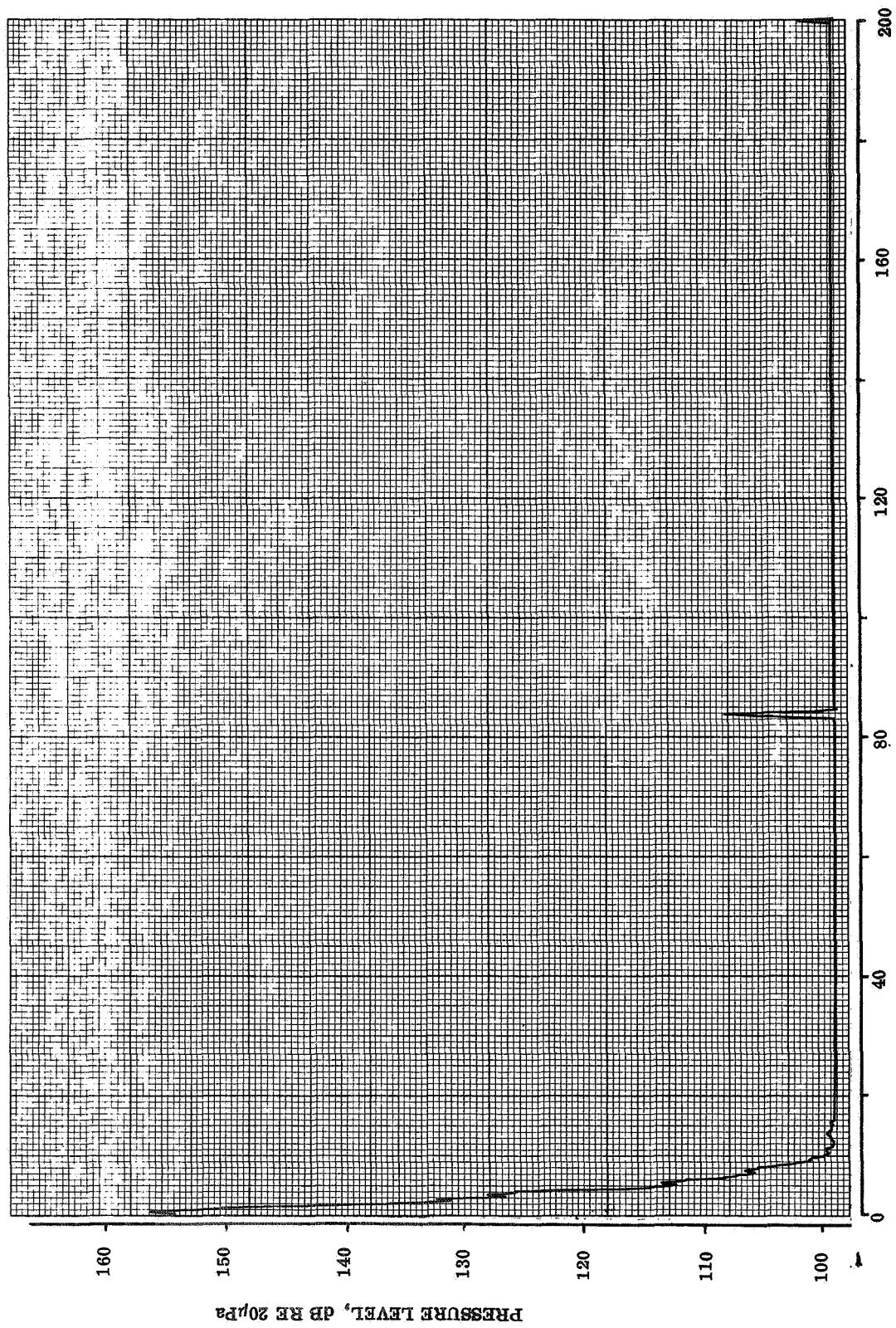


TAPE CHANNEL 3
40 % RADIUS

HARMONICS OF PROPELLER ROTATION

FLIGHT 7
RUN 5

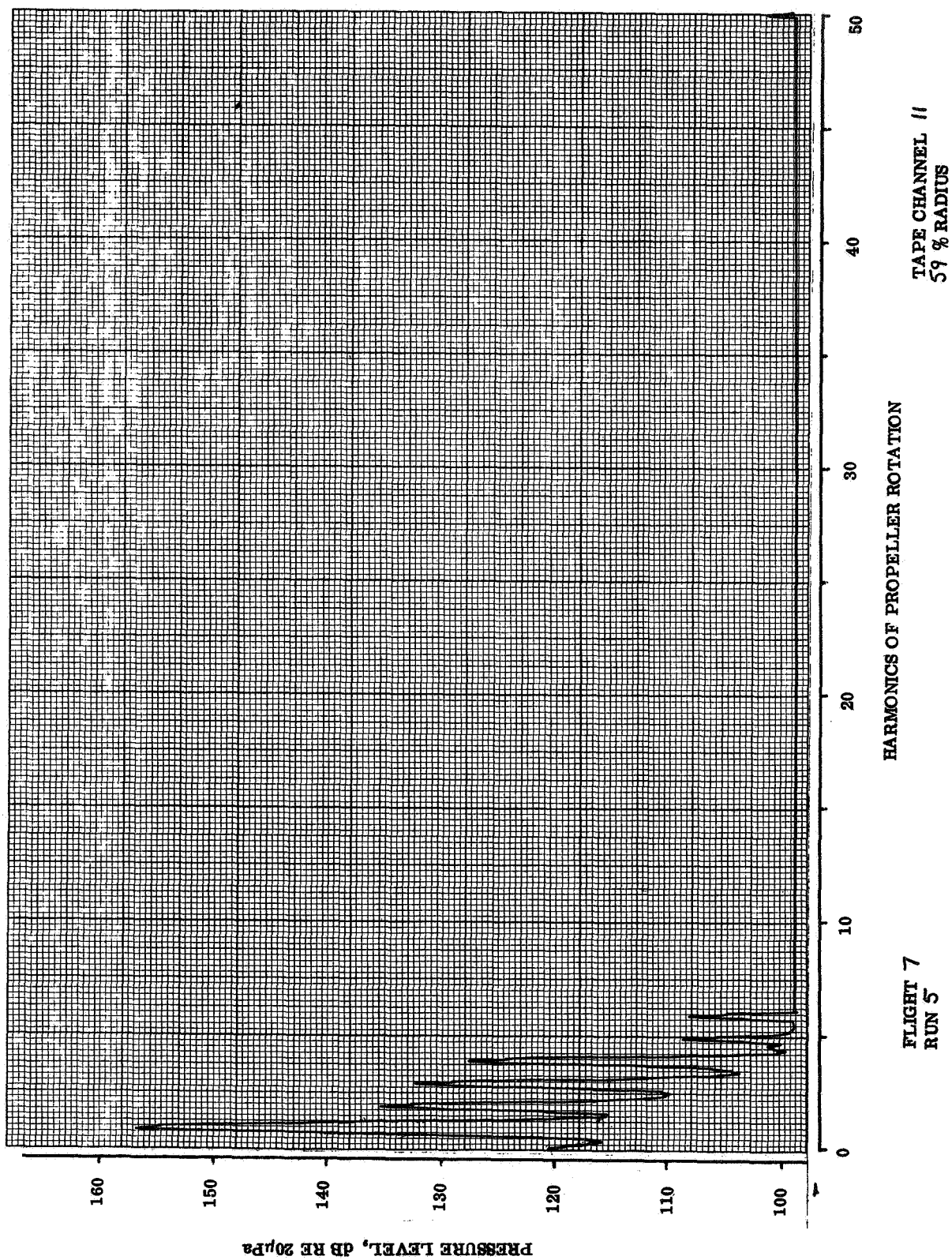


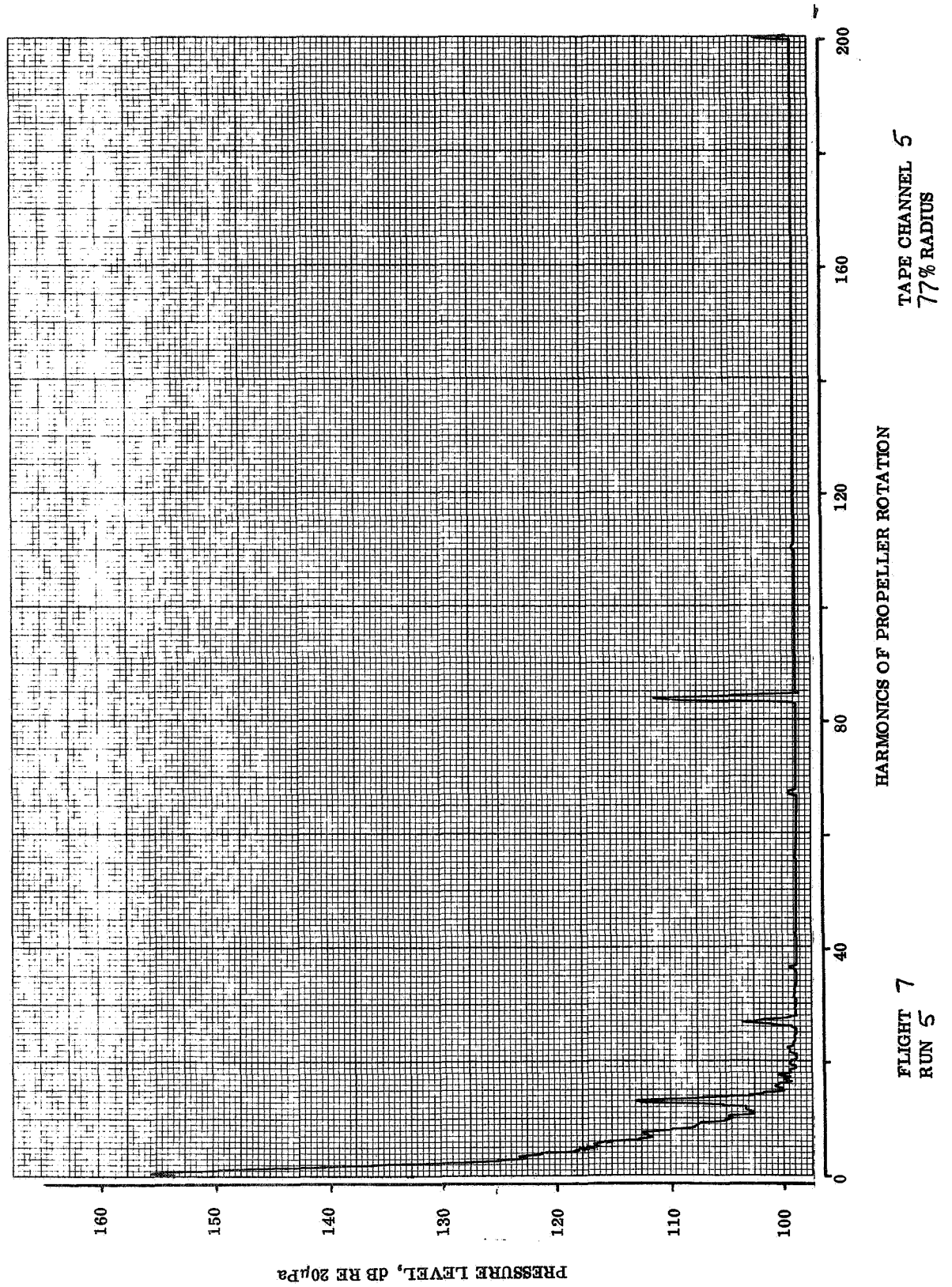


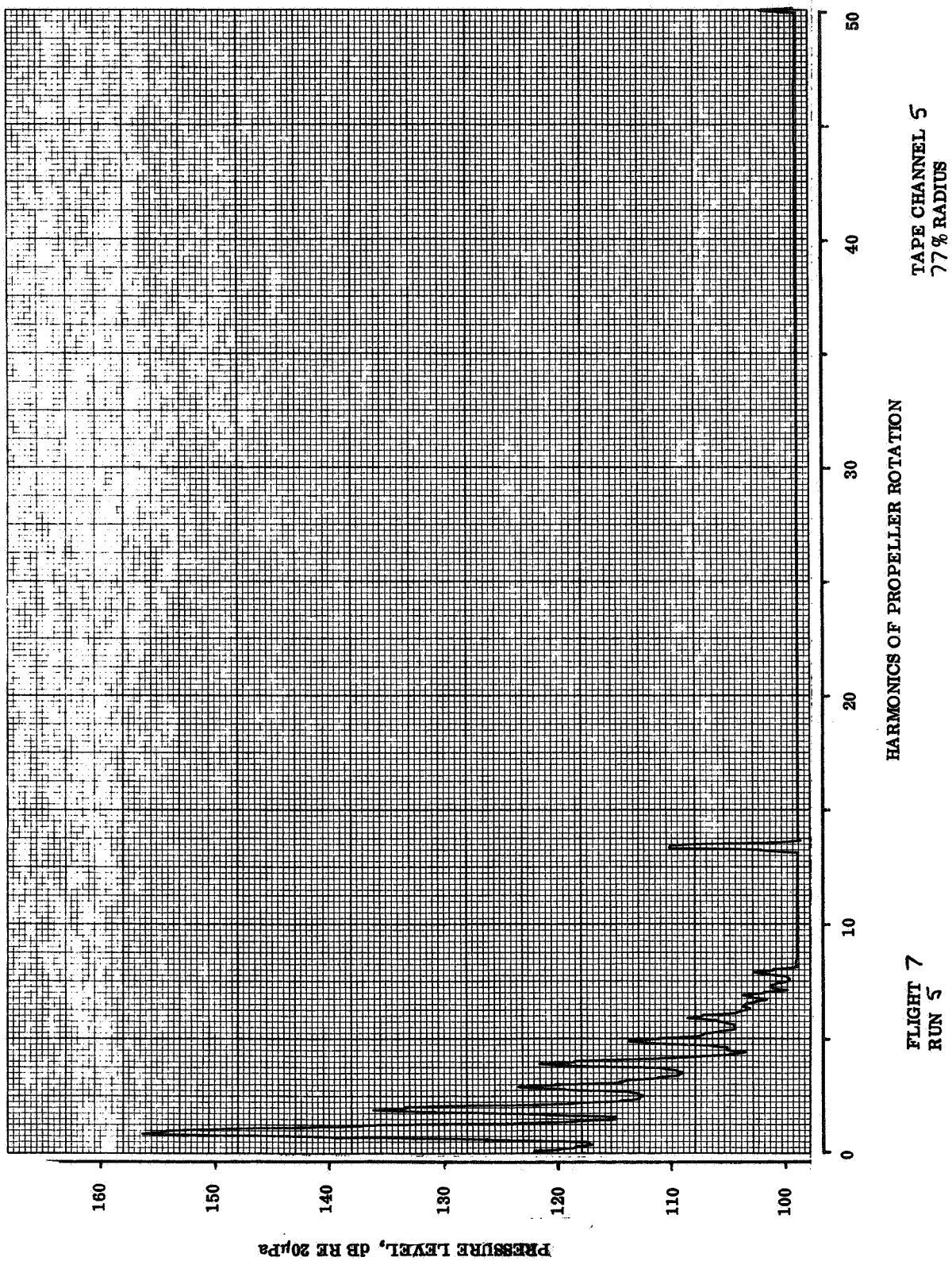
TAPE CHANNEL 11
59 % RADIUS

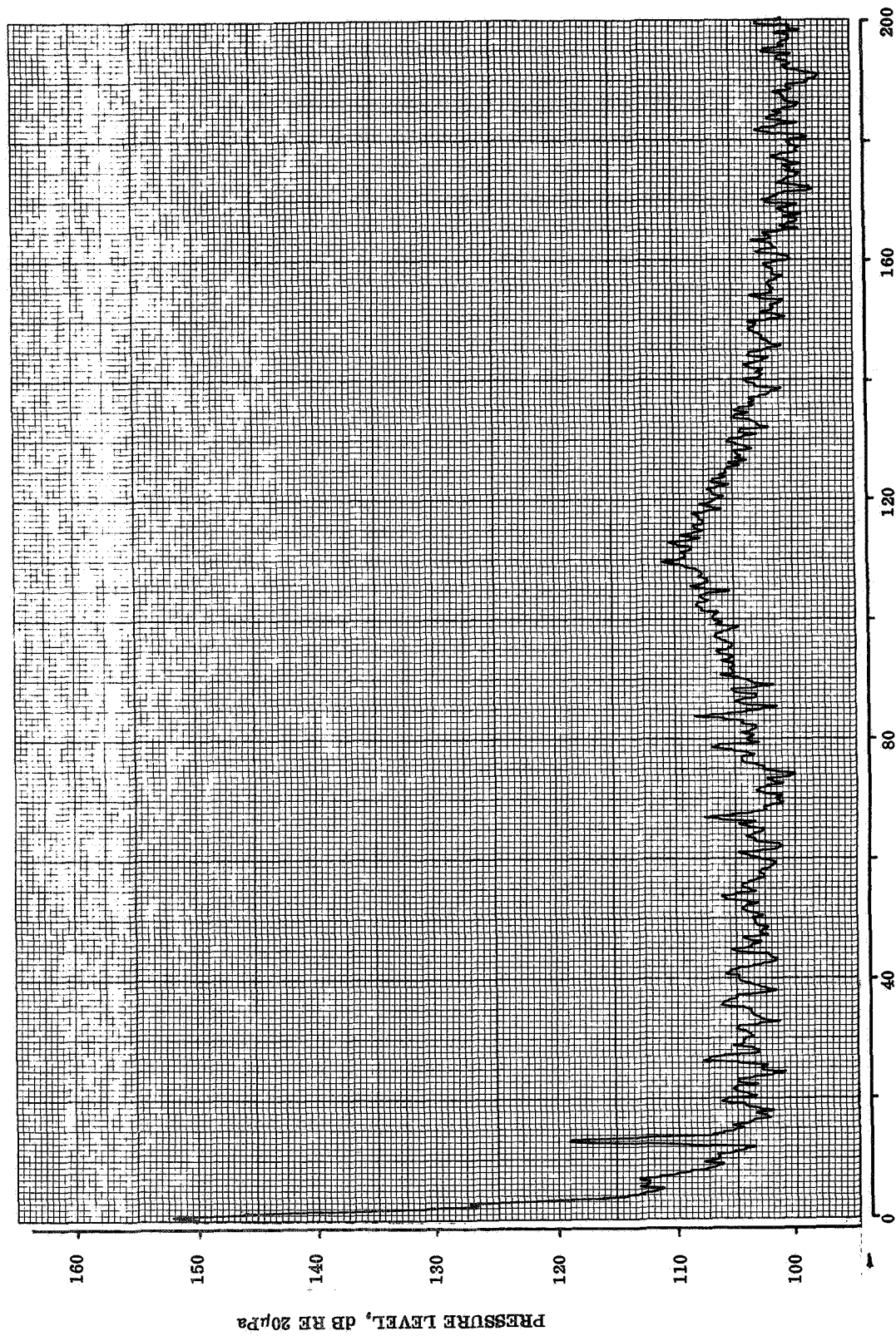
HARMONICS OF PROPELLER ROTATION

FLIGHT 7
RUN 5



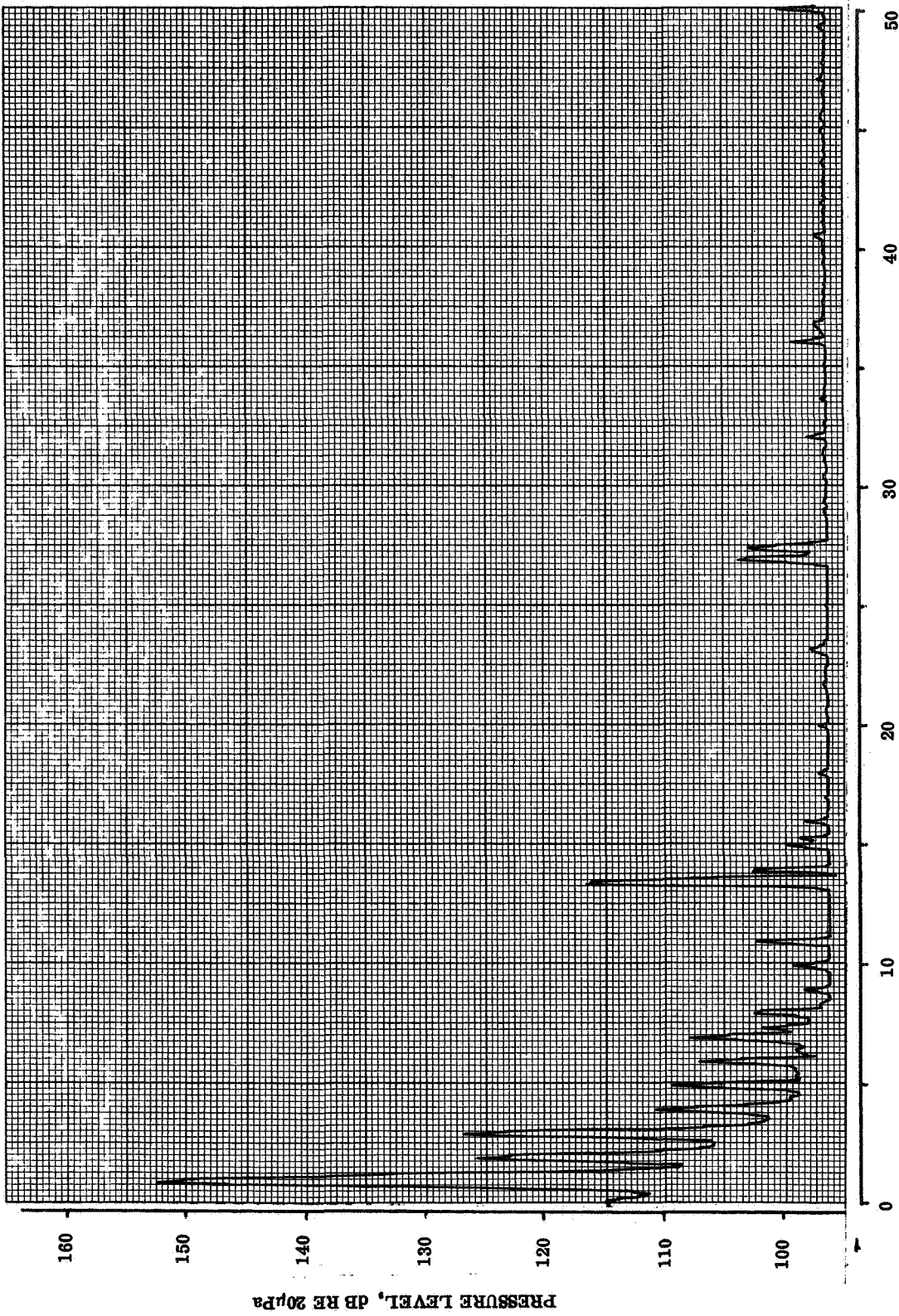






TAPE CHANNEL 13
89 % RADIUS

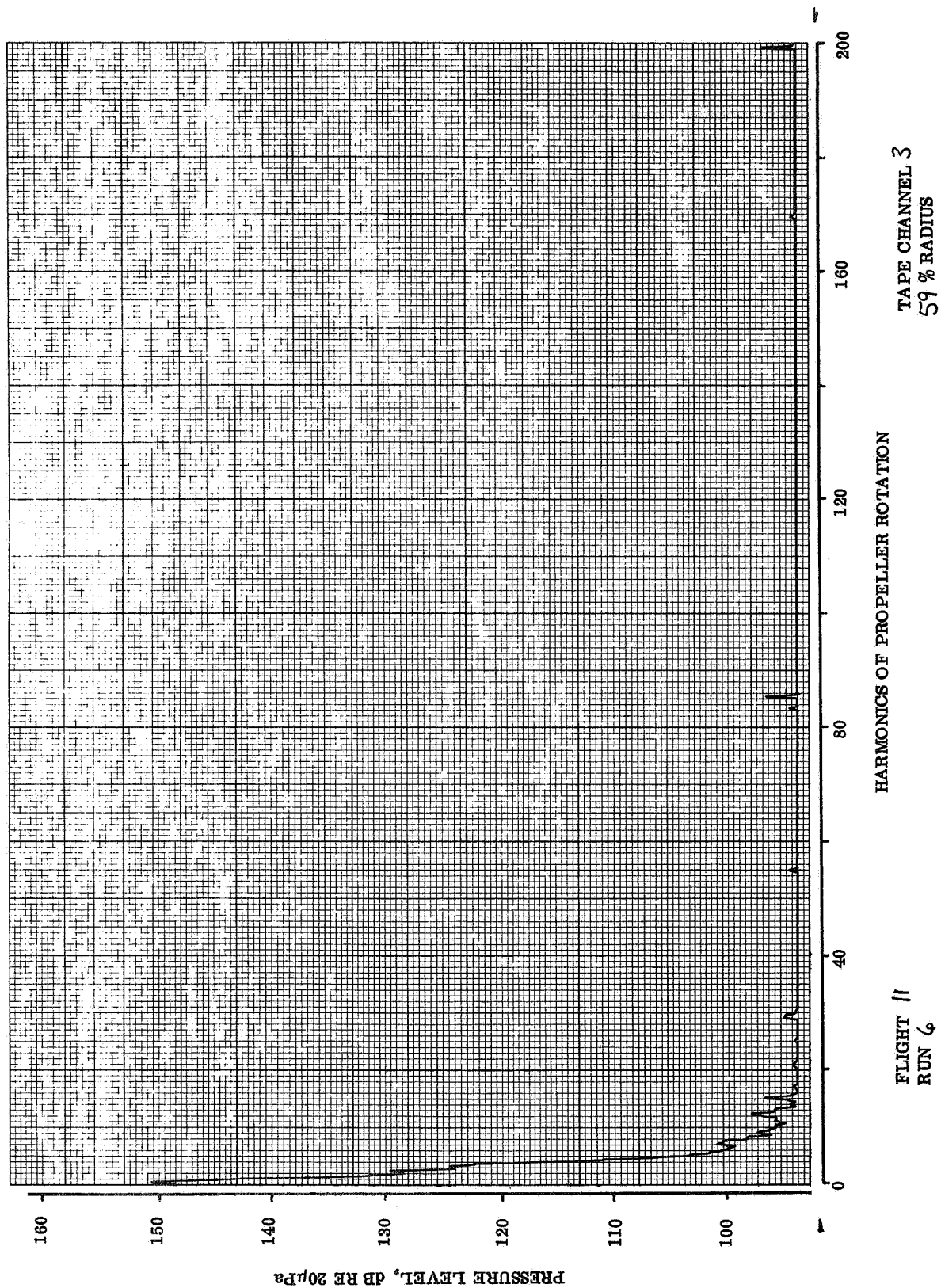
FLIGHT 7
RUN 5

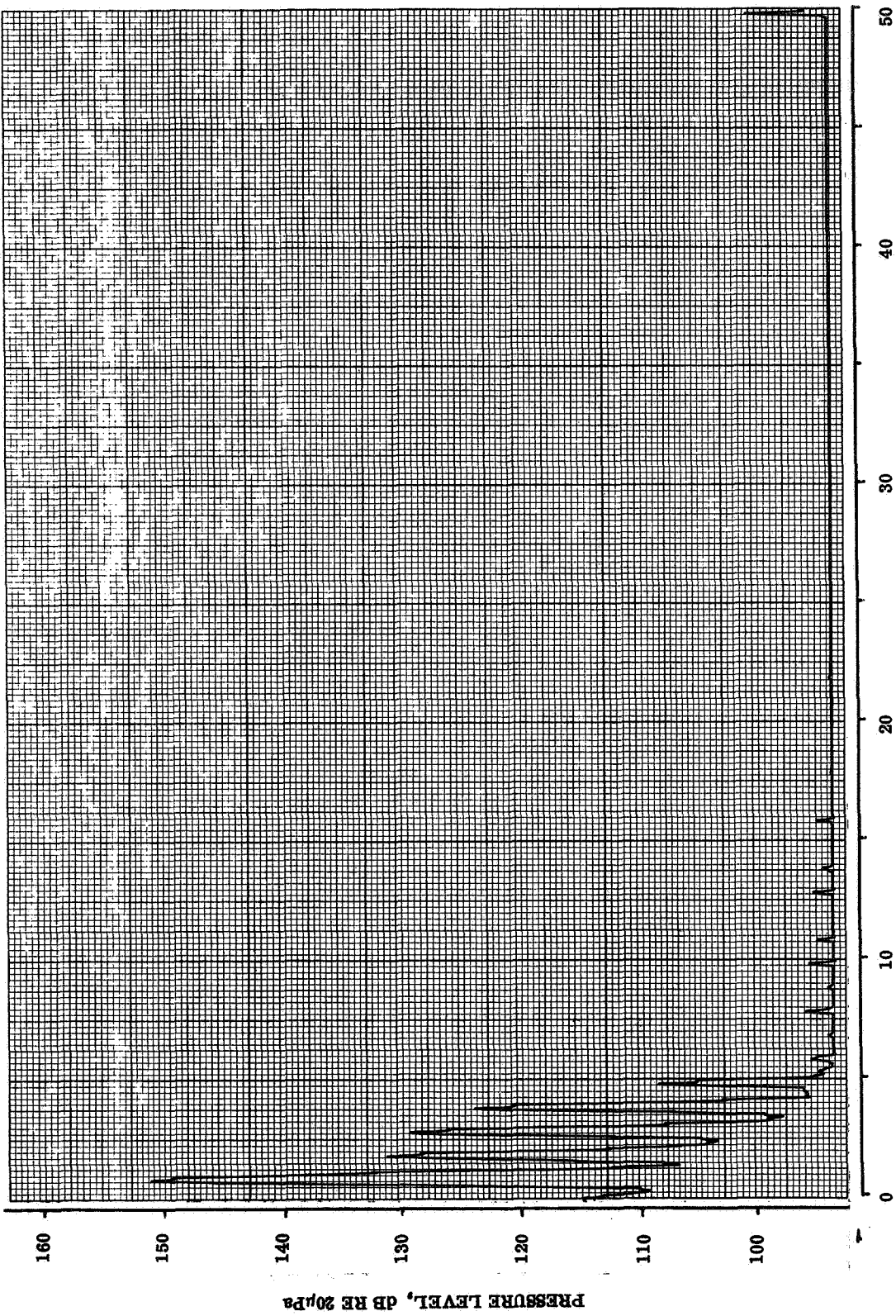


TAPE CHANNEL 13
89 % RADIUS

HARMONICS OF PROPELLER ROTATION

FLIGHT 7
RUN 5

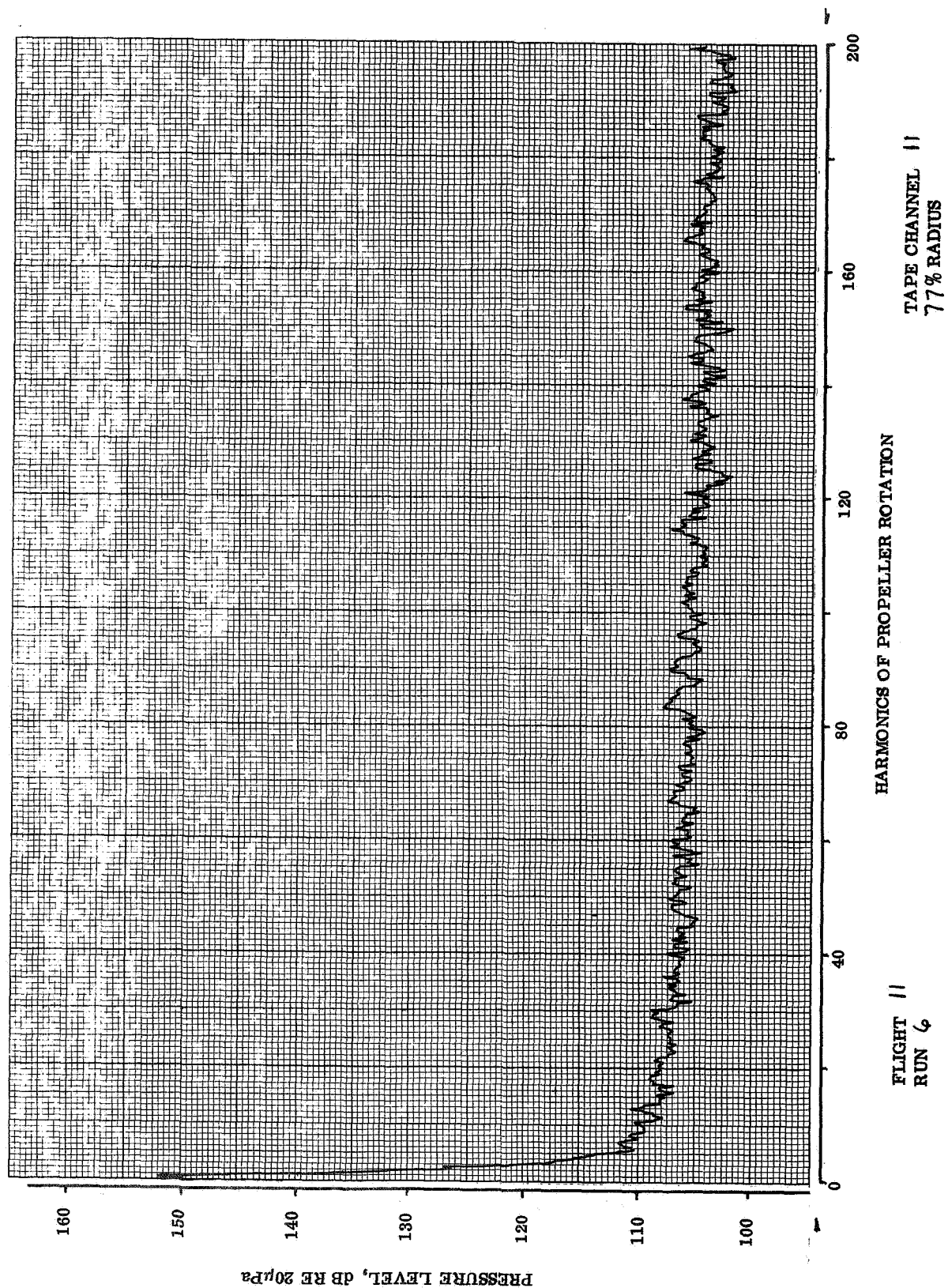


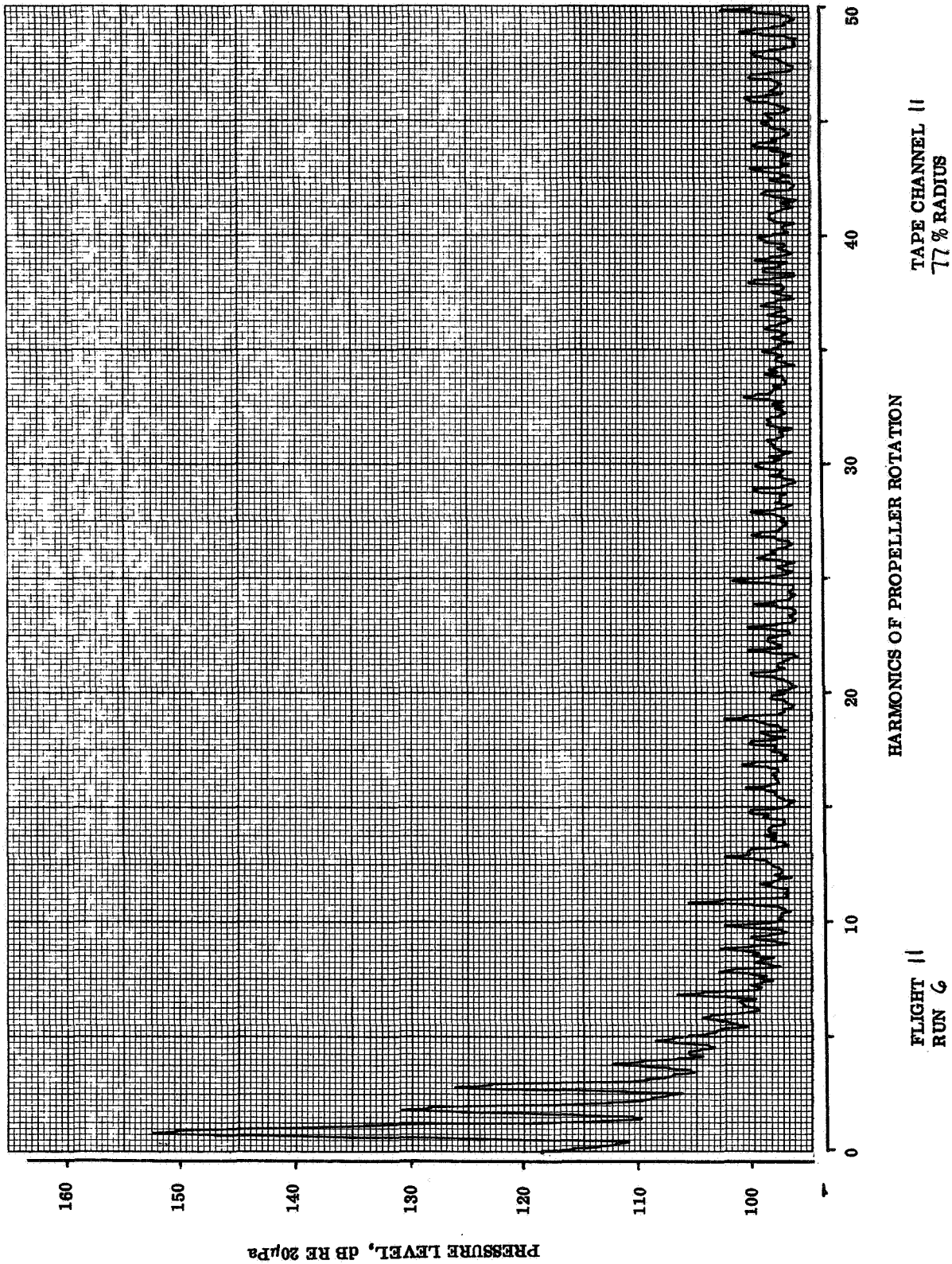


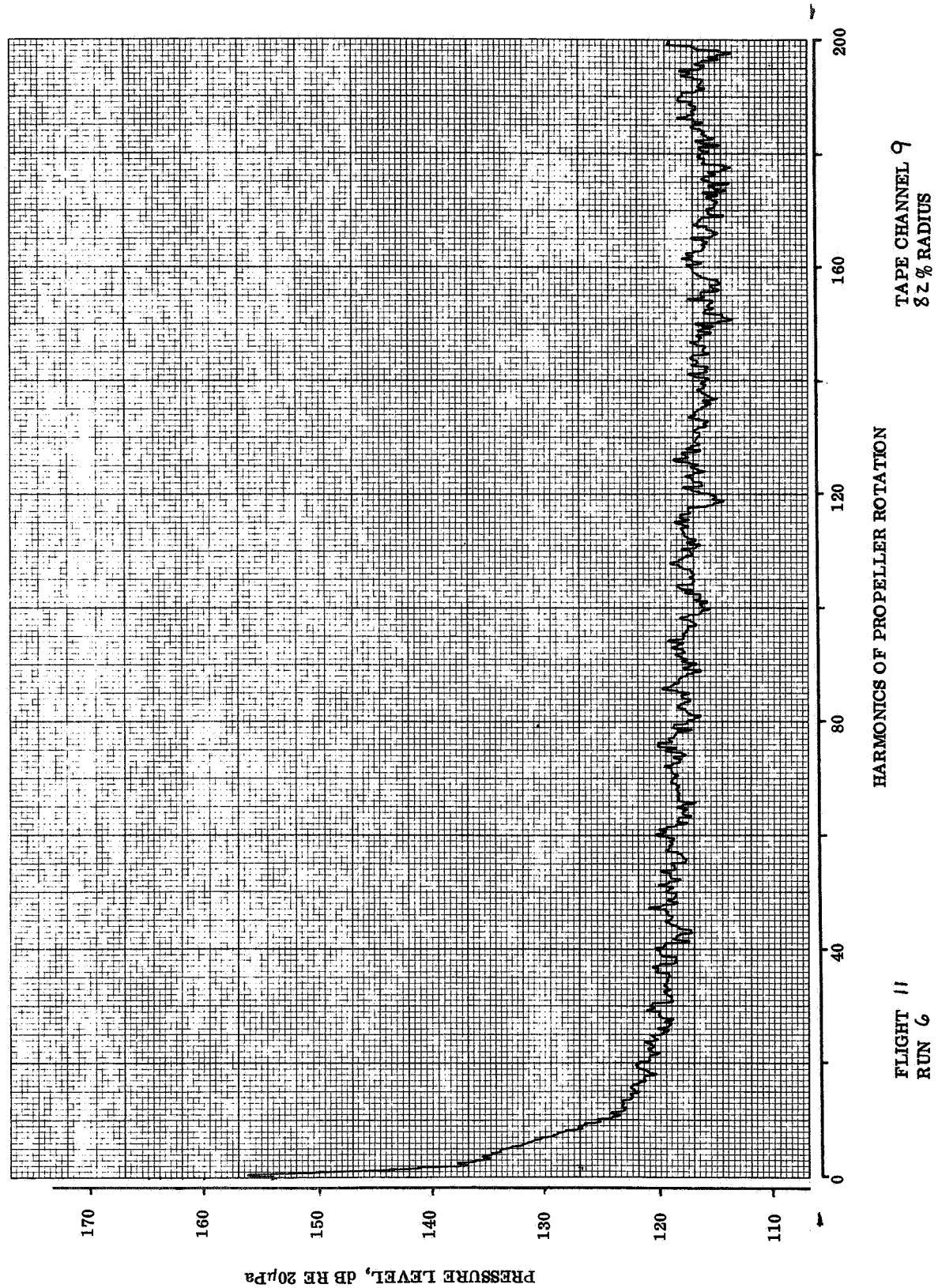
TAPE CHANNEL 3
59% RADIUS

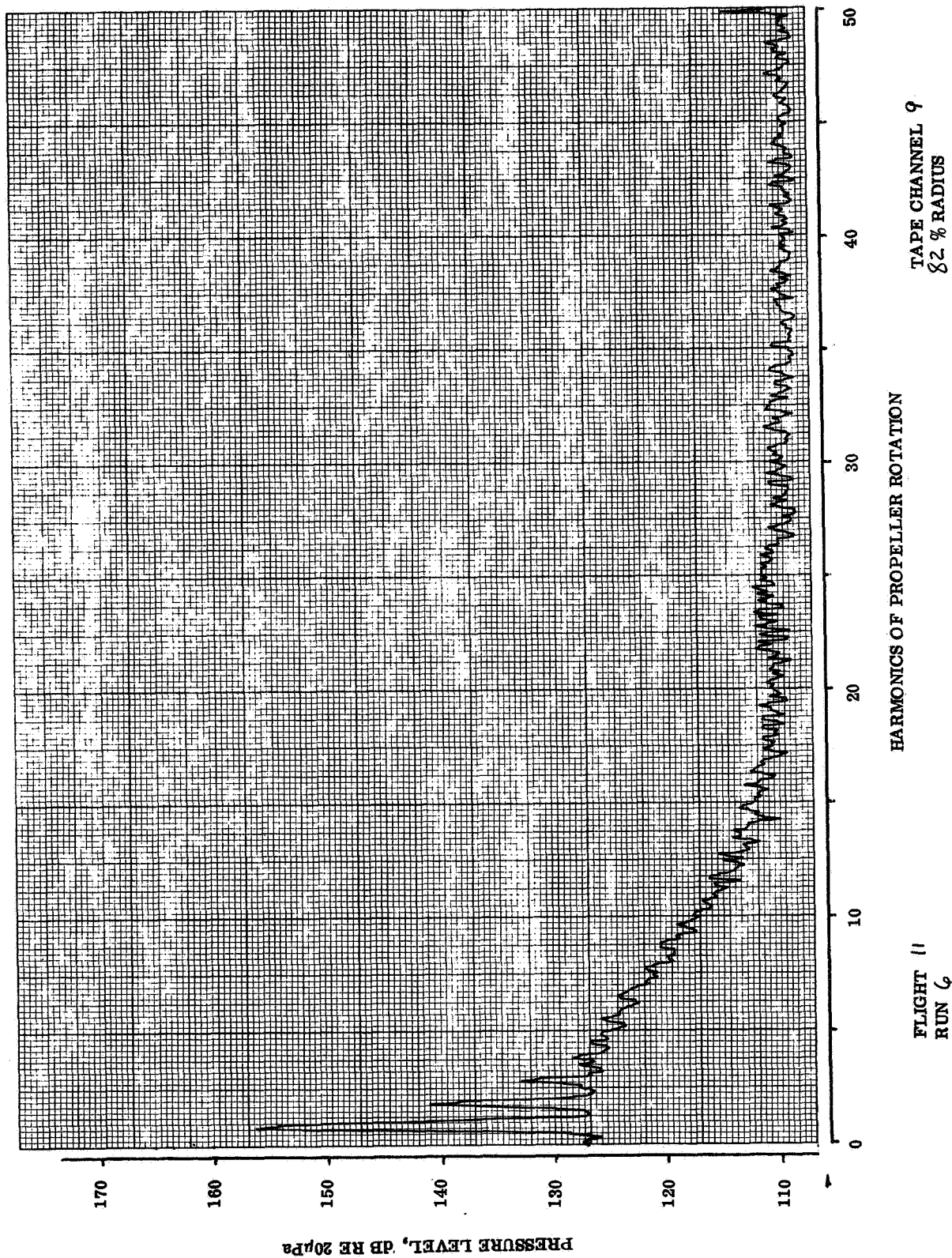
HARMONICS OF PROPELLER ROTATION

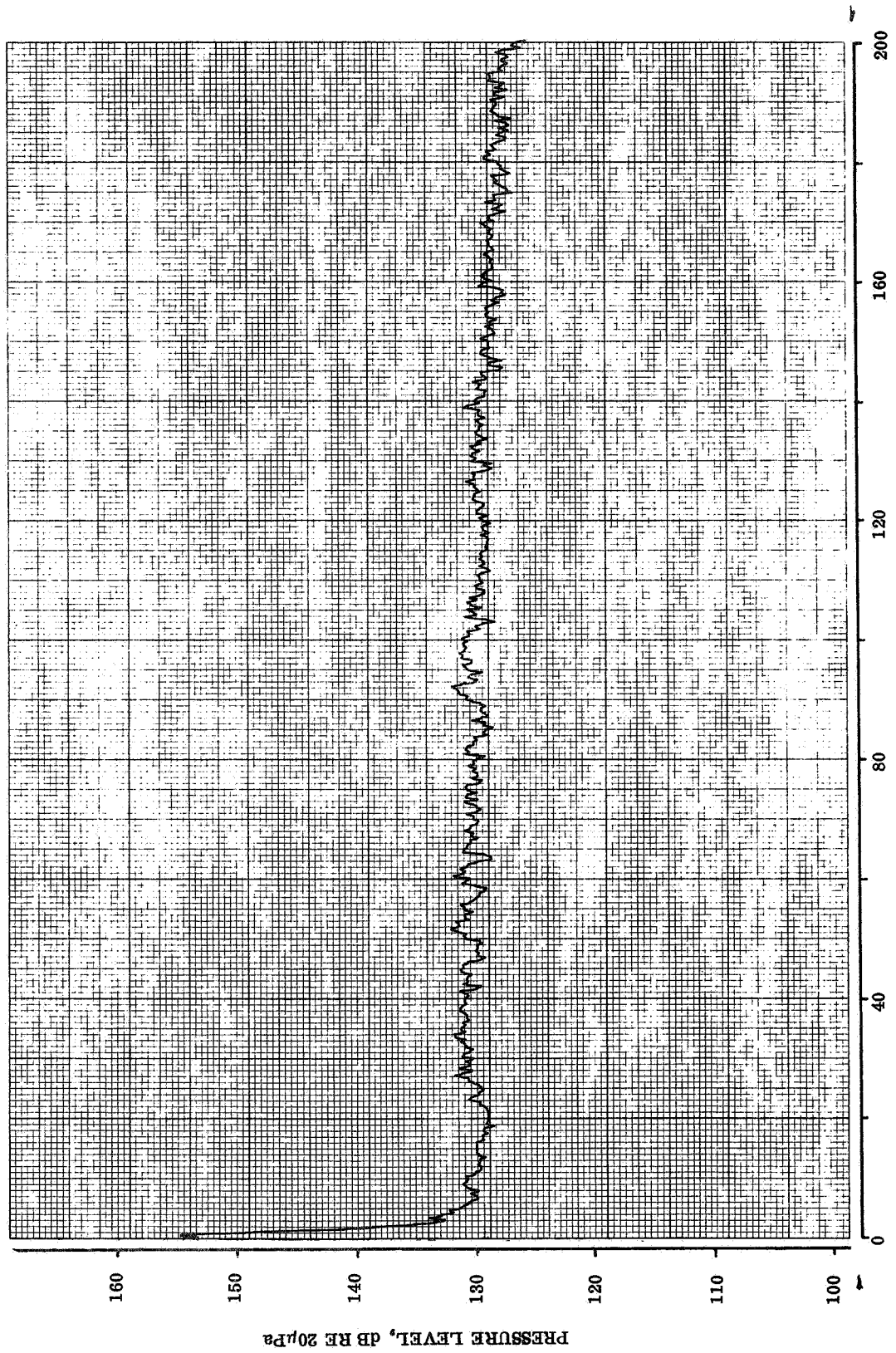
FLIGHT II
RUN 6







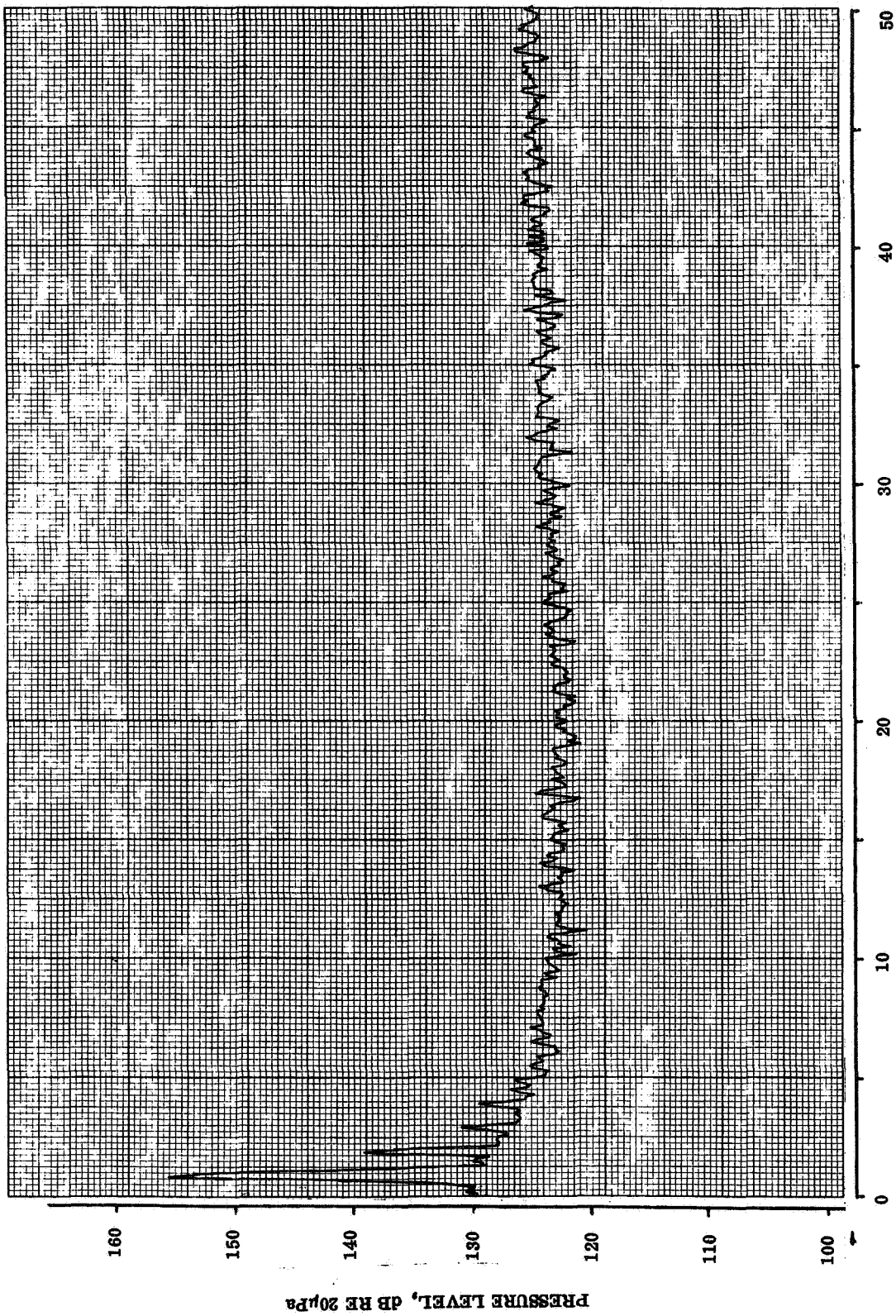




TAPE CHANNEL 13
89 % RADIUS

HARMONICS OF PROPELLER ROTATION

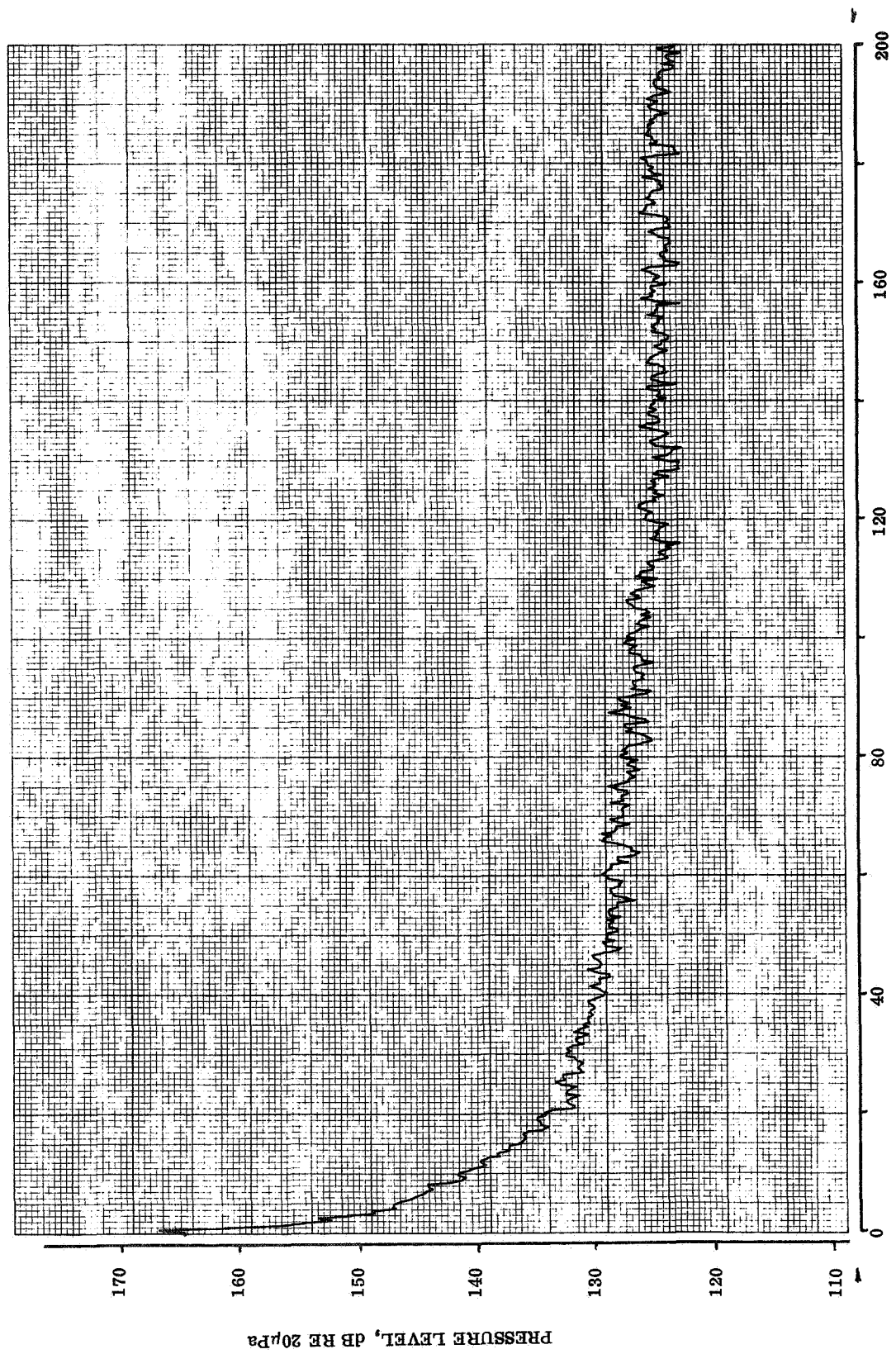
FLIGHT 7
RUN 6

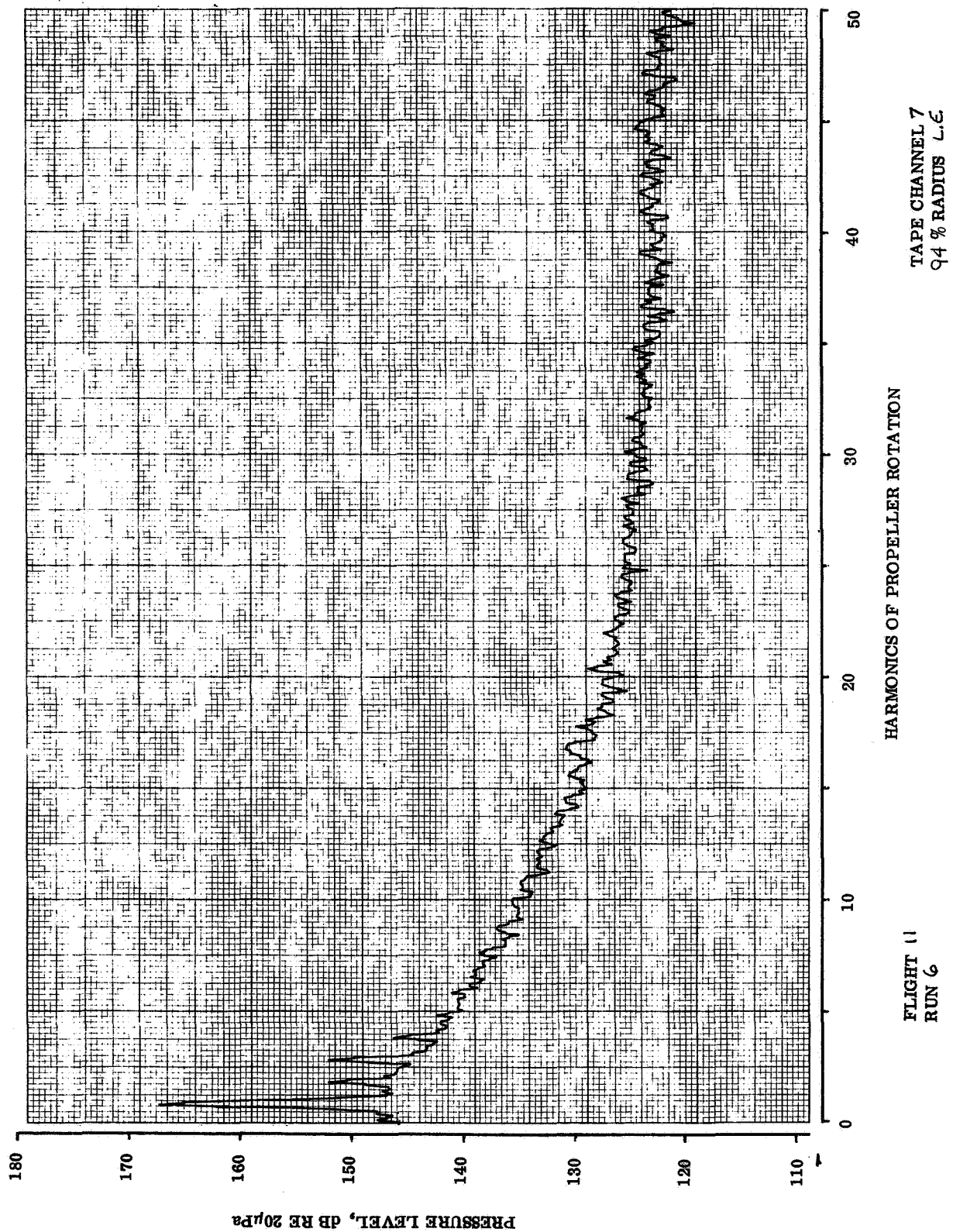


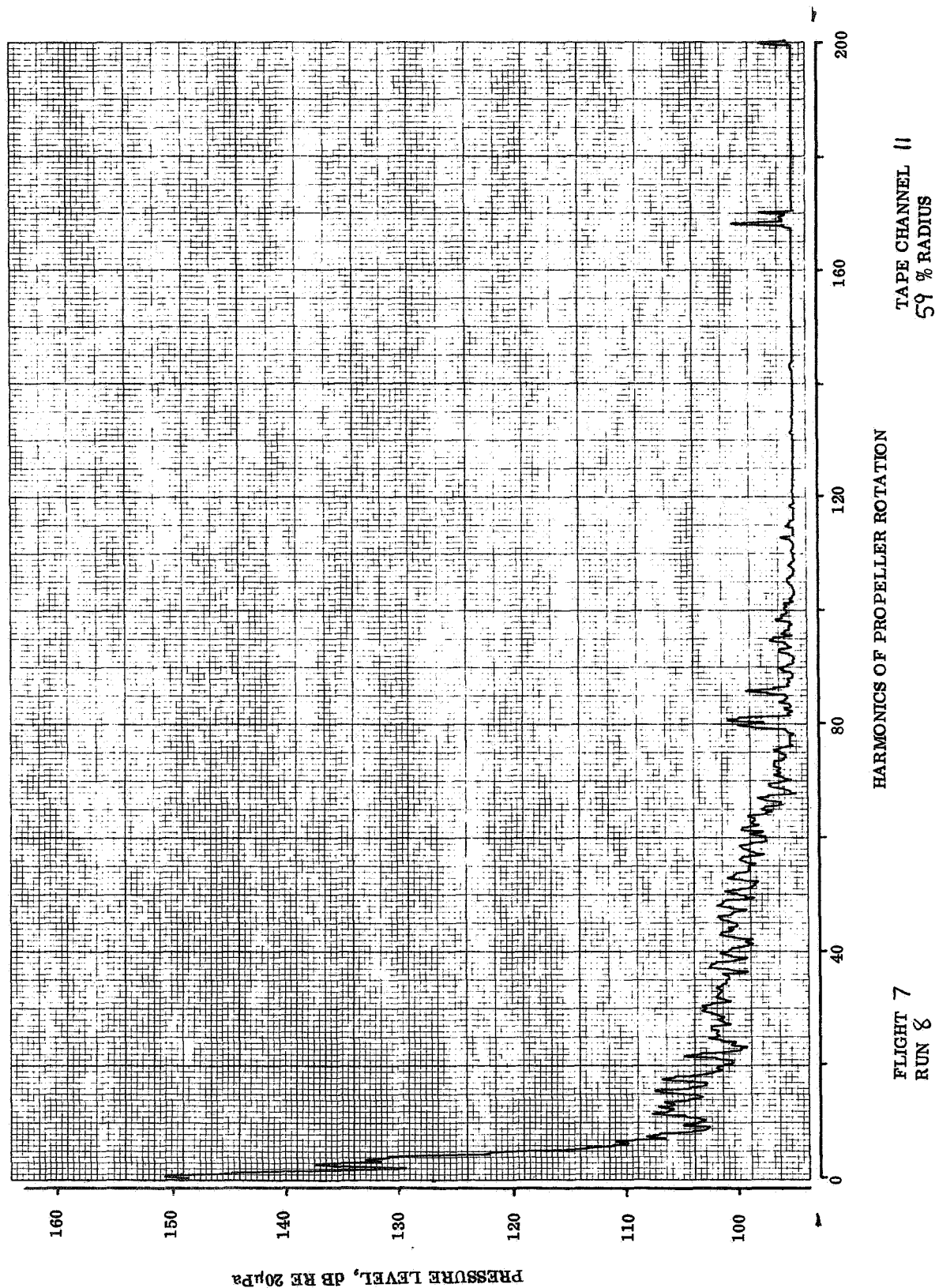
FLIGHT 7
 RUN 6

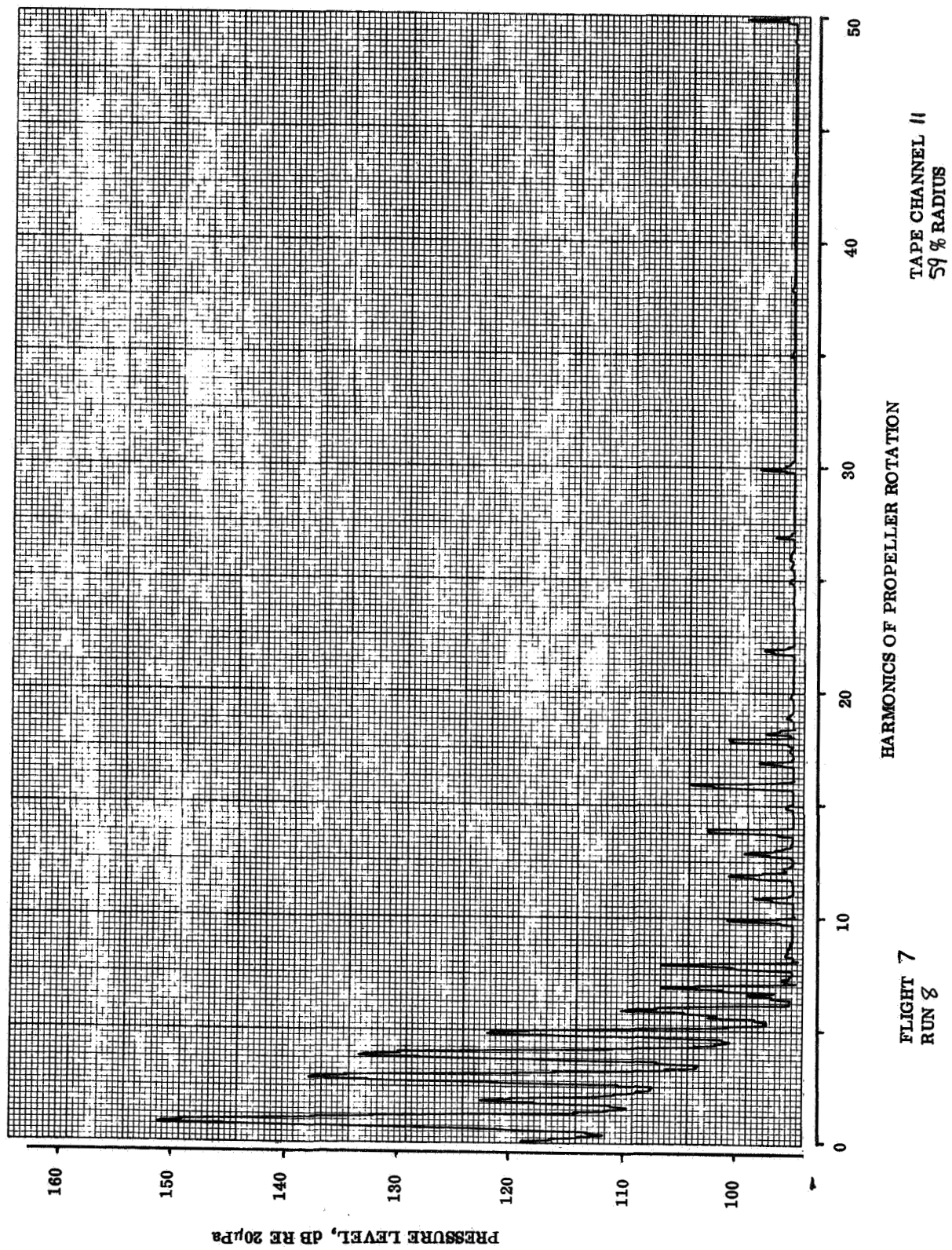
HARMONICS OF PROPELLER ROTATION

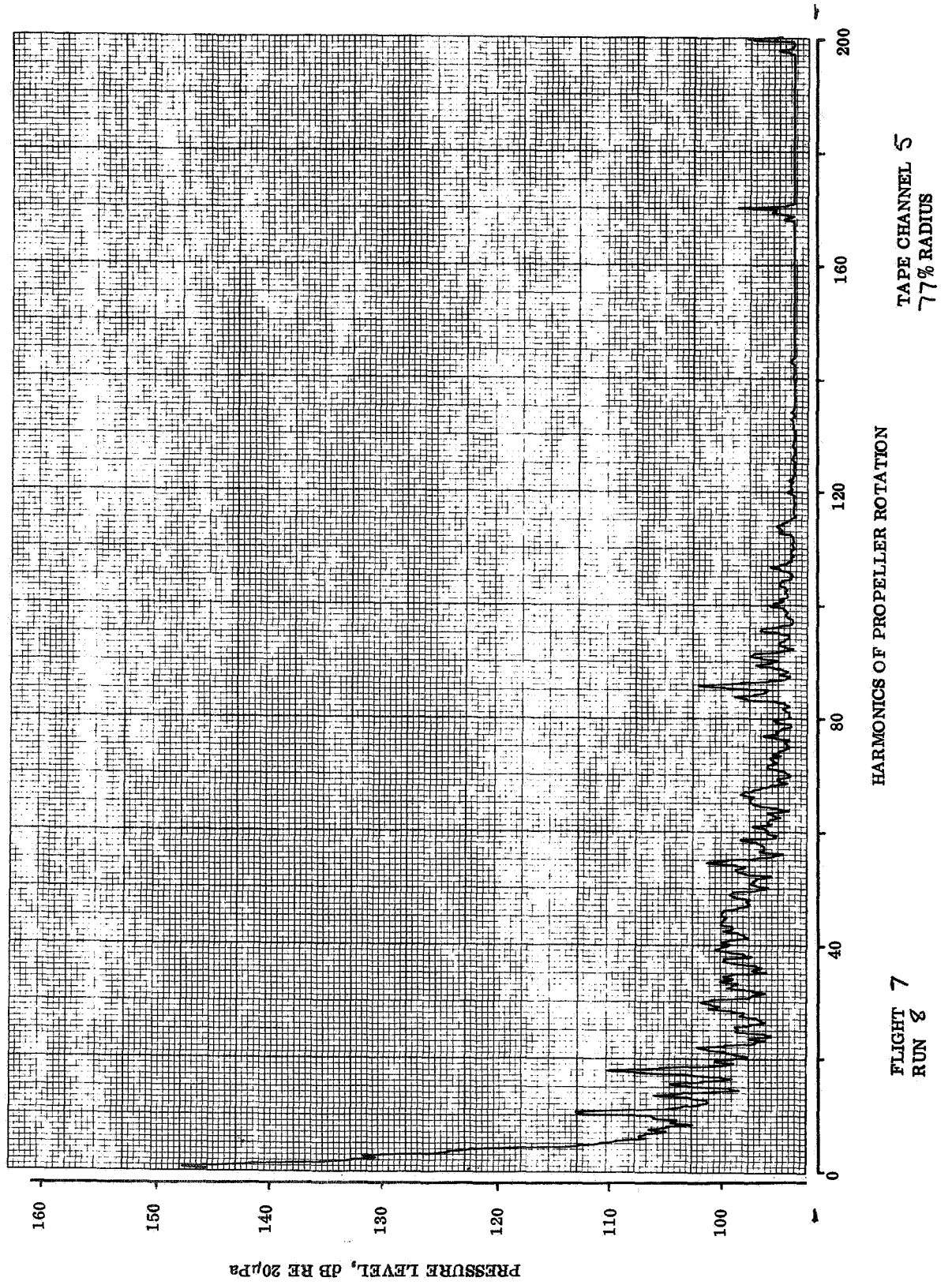
TAPE CHANNEL 13
 89 % RADIUS

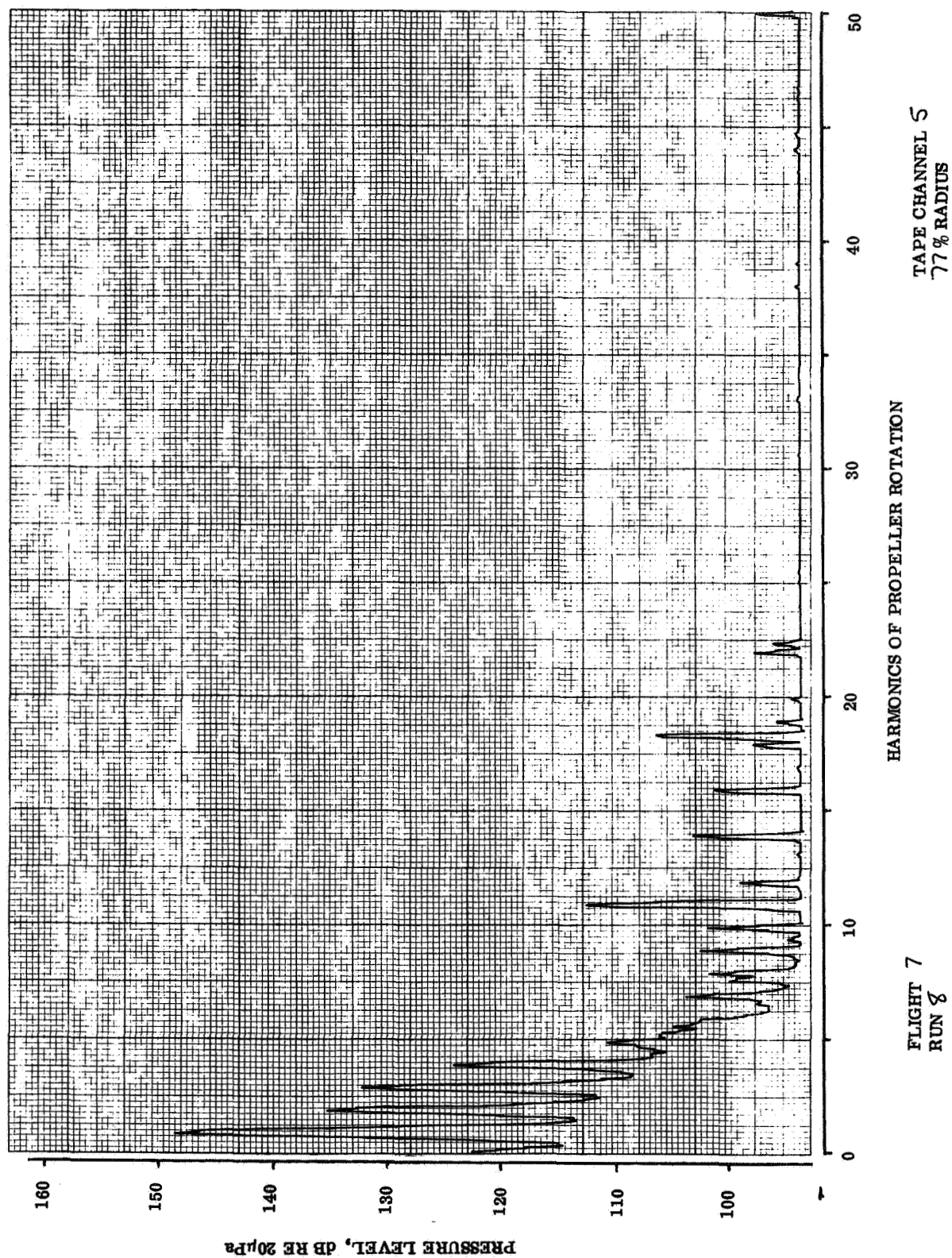


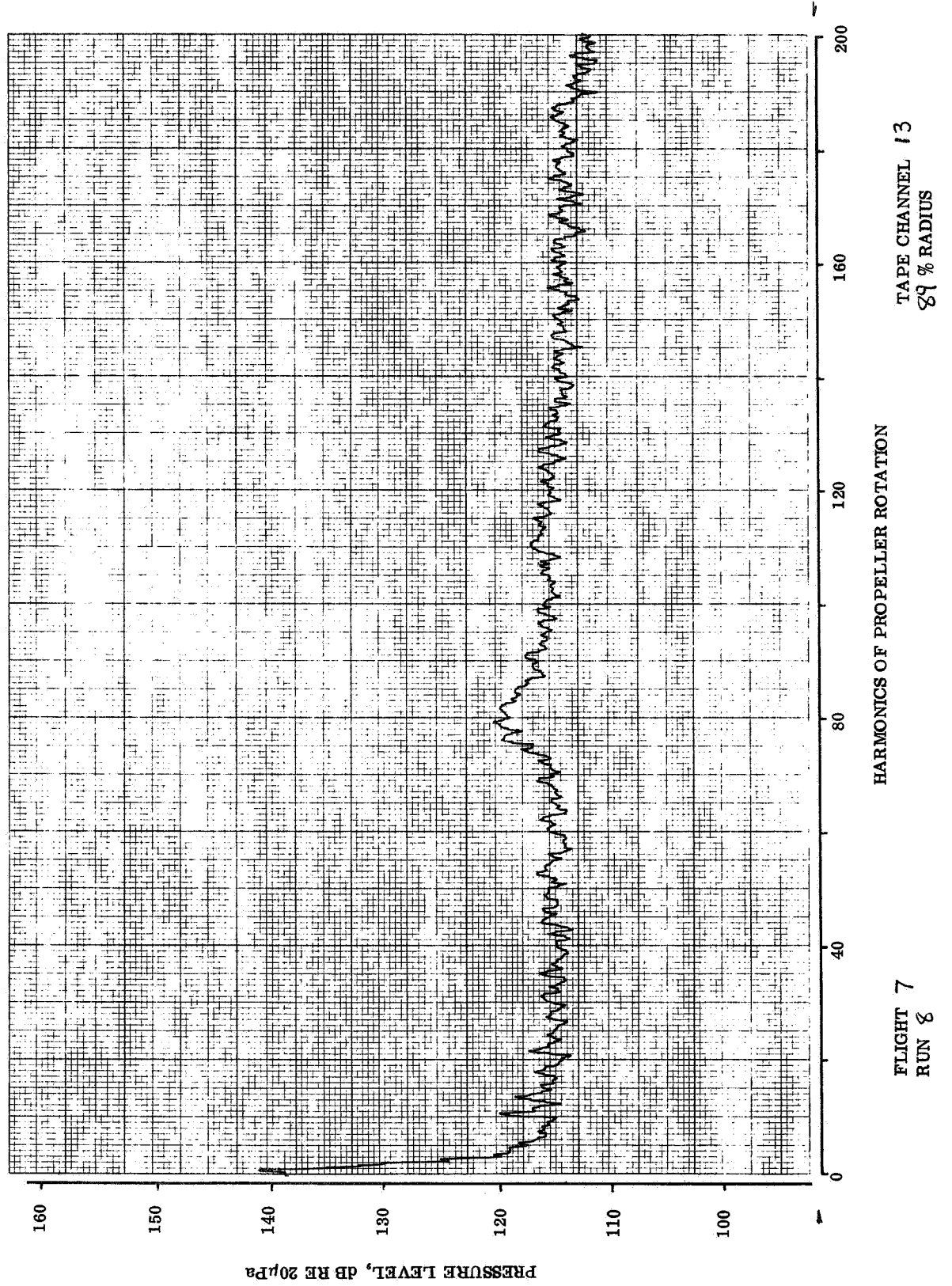


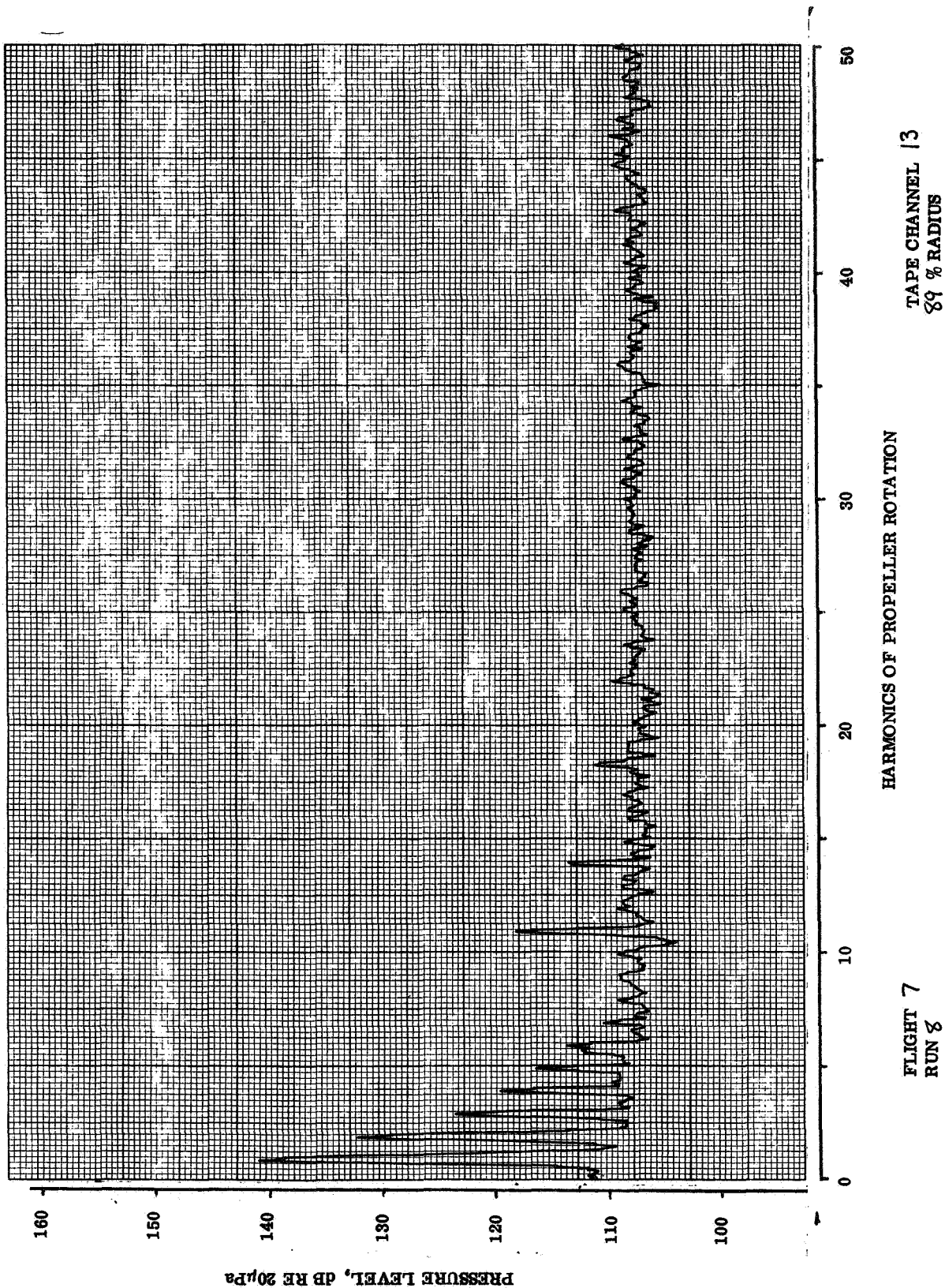


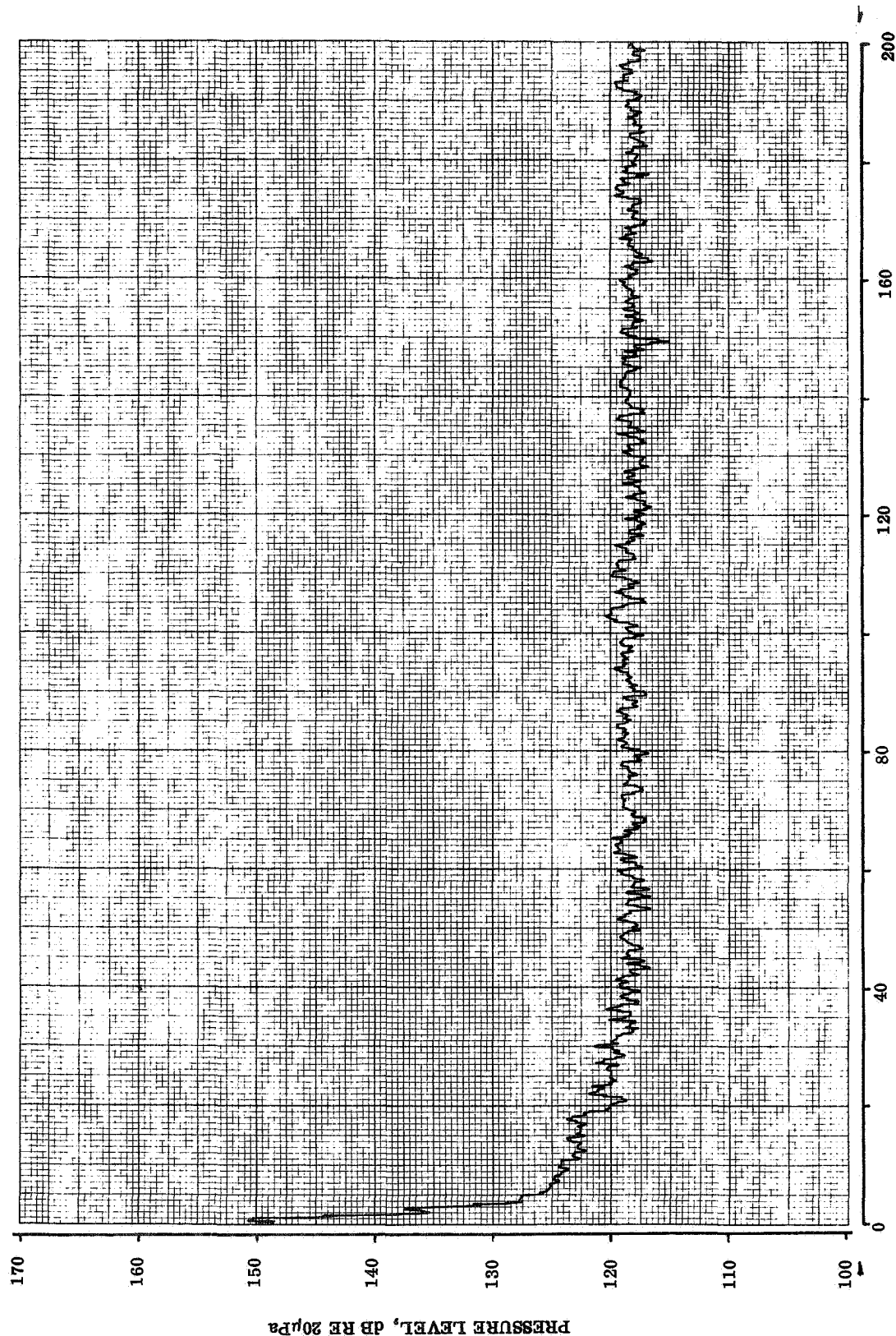








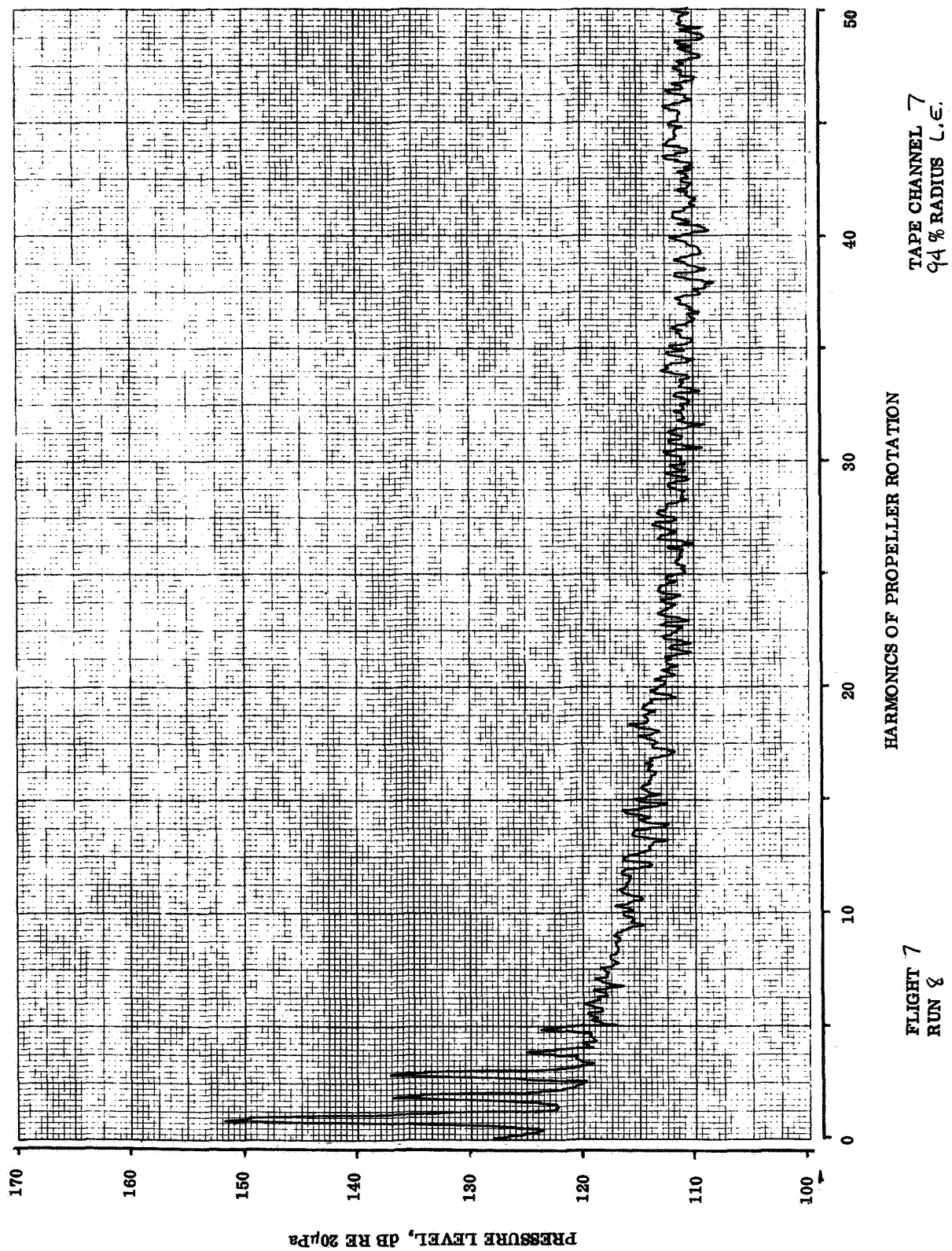


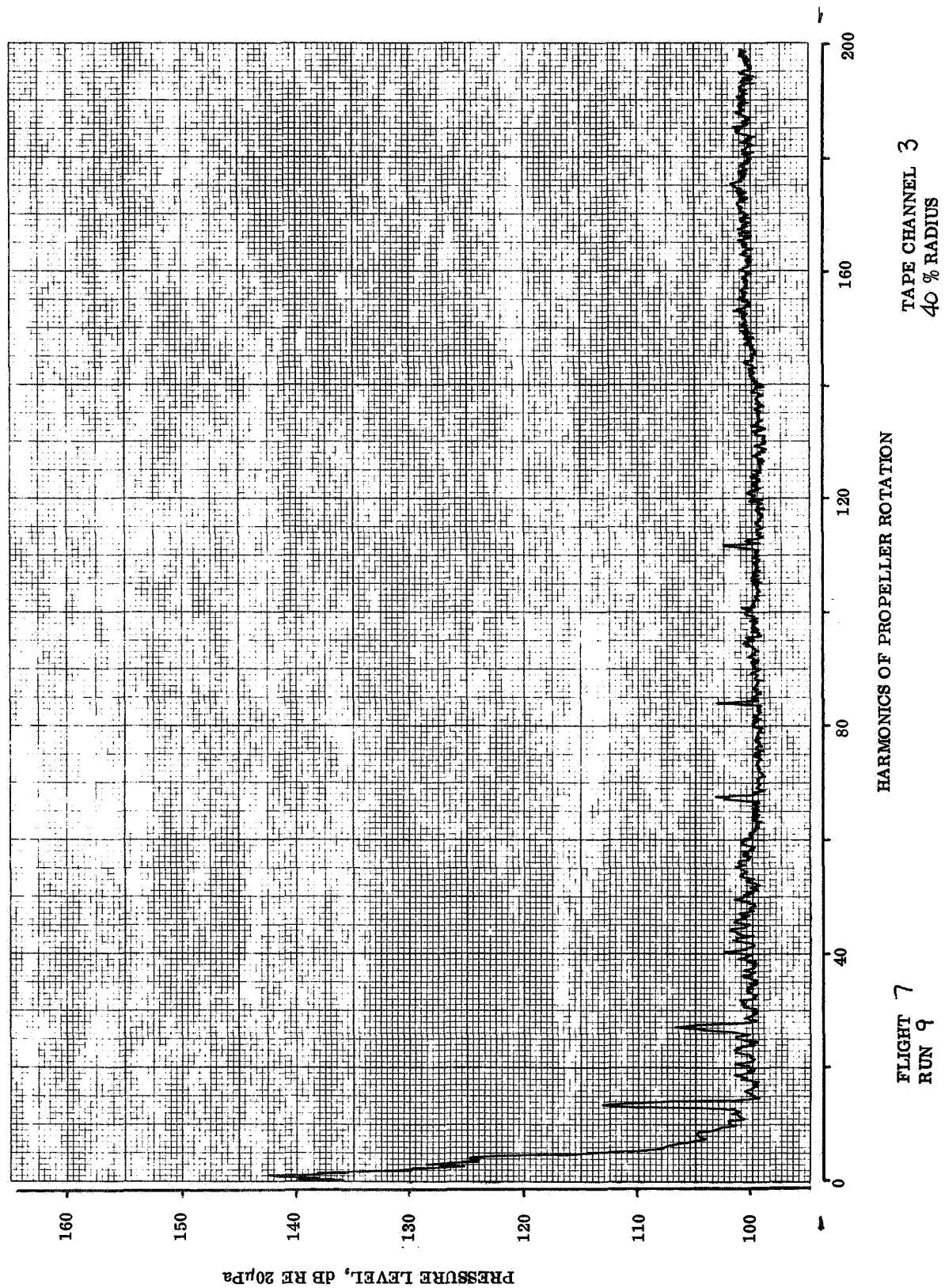


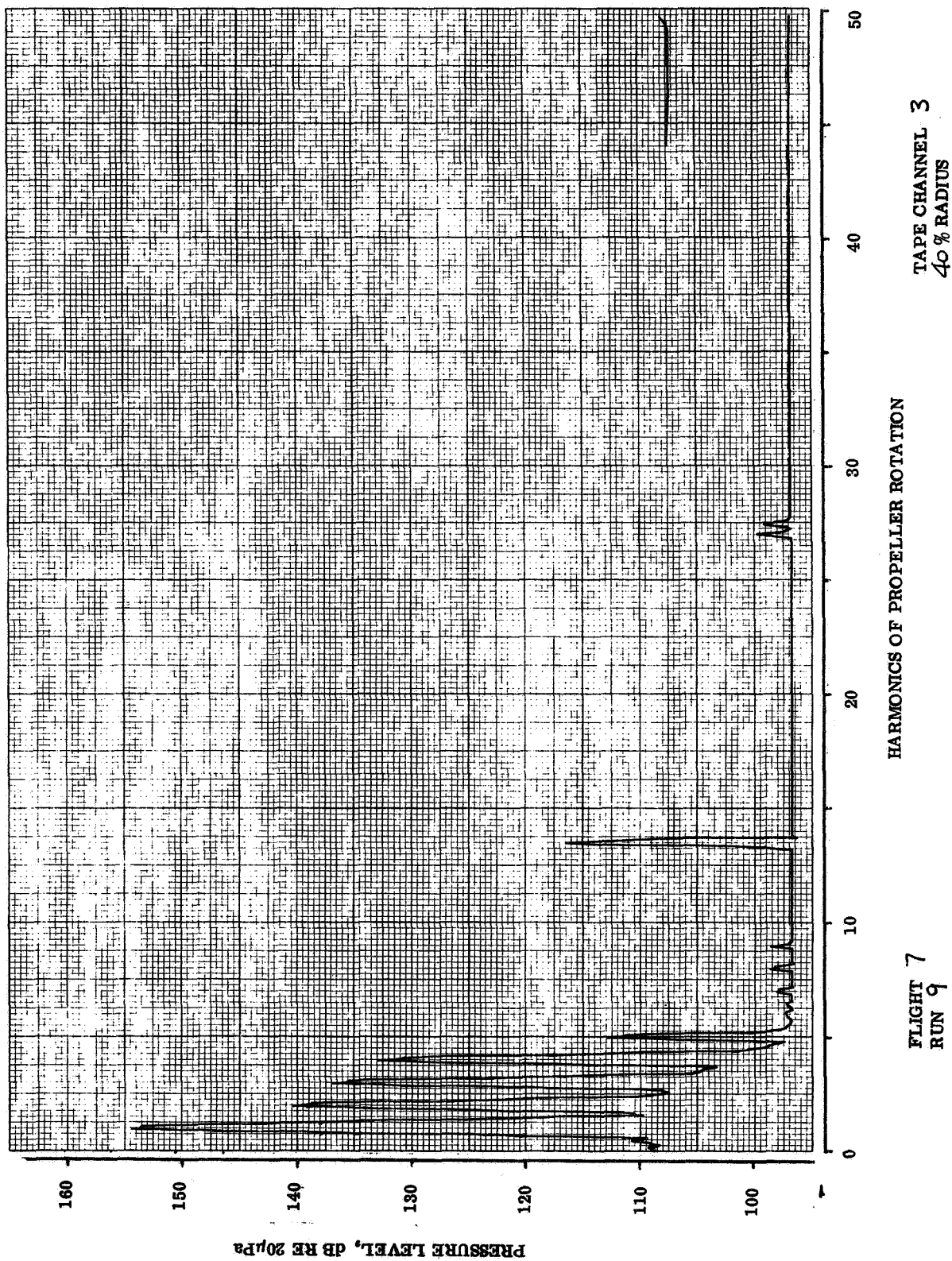
TAPE CHANNEL 7
94 % RADIUS L.E.

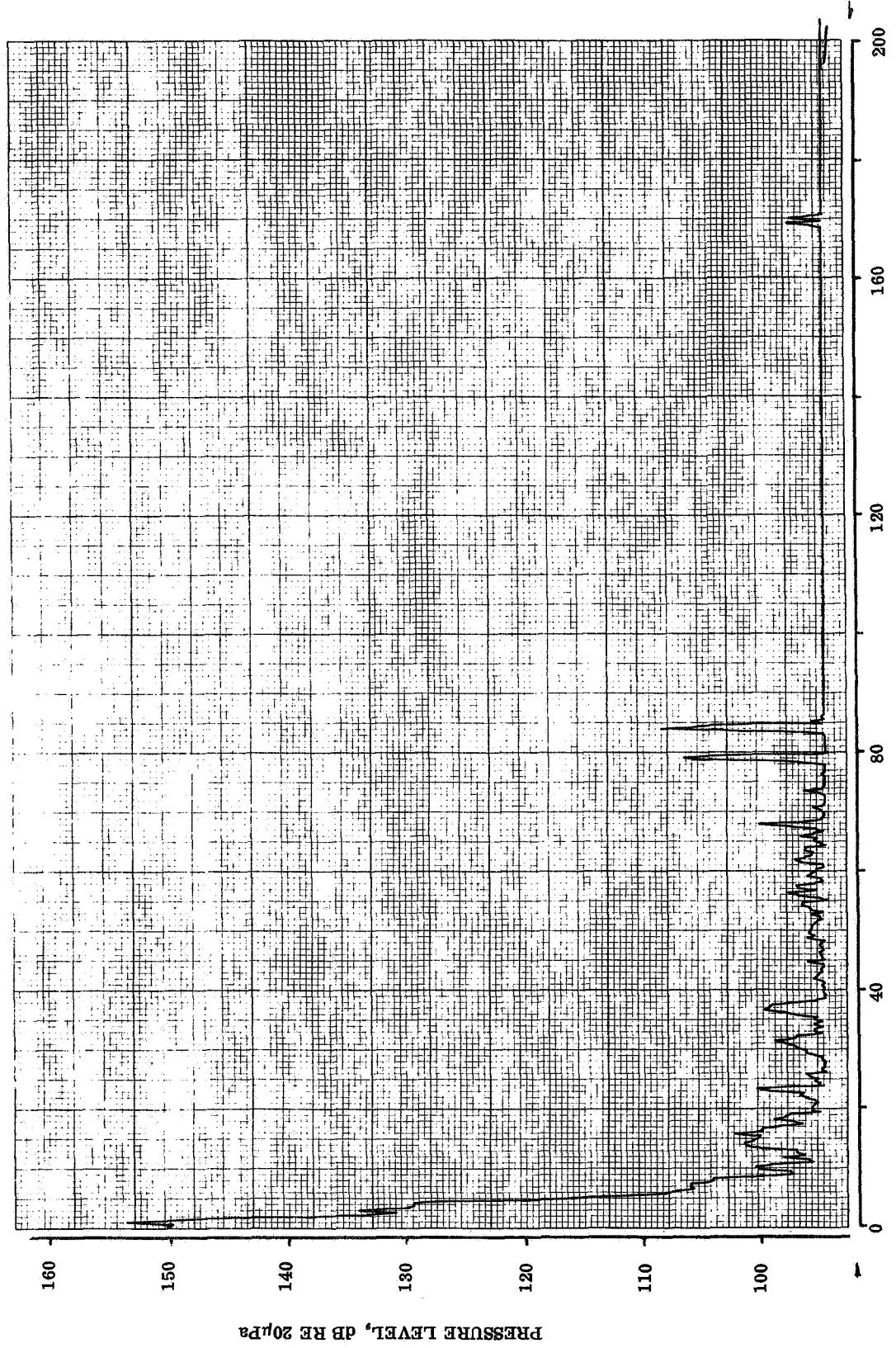
HARMONICS OF PROPELLER ROTATION

FLIGHT 7
RUN 8





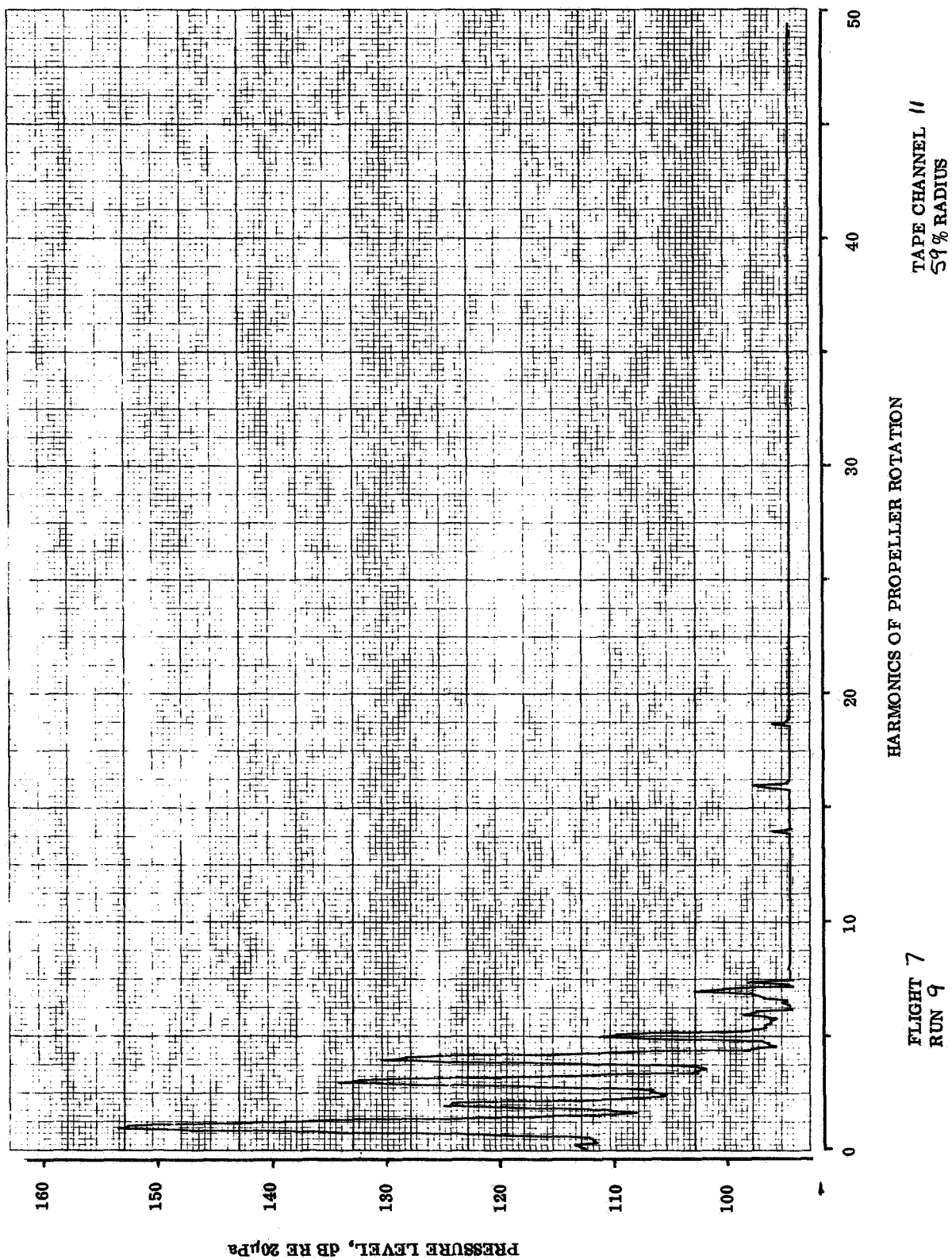


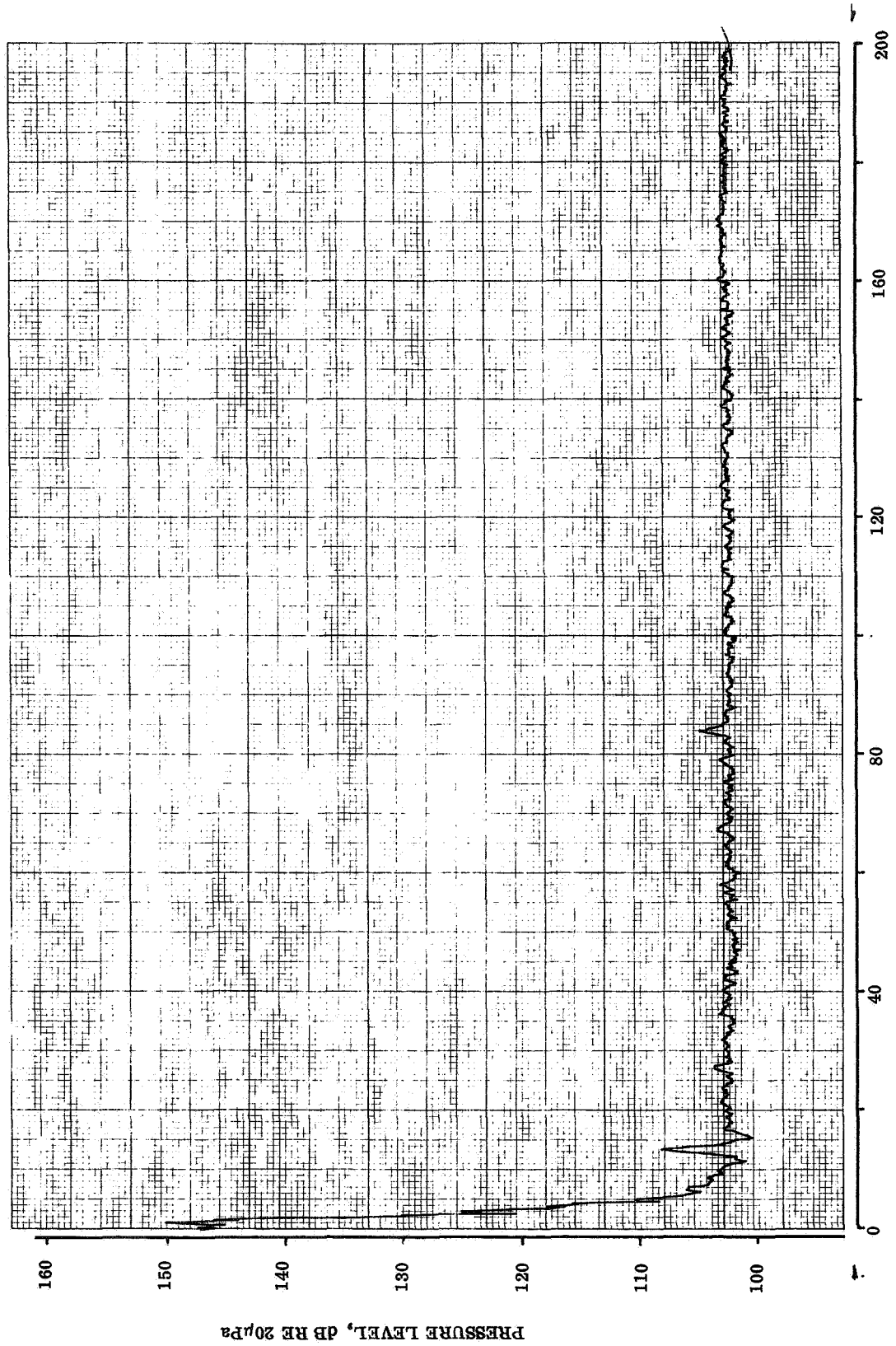


TAPE CHANNEL 11
59% RADIUS

HARMONICS OF PROPELLER ROTATION

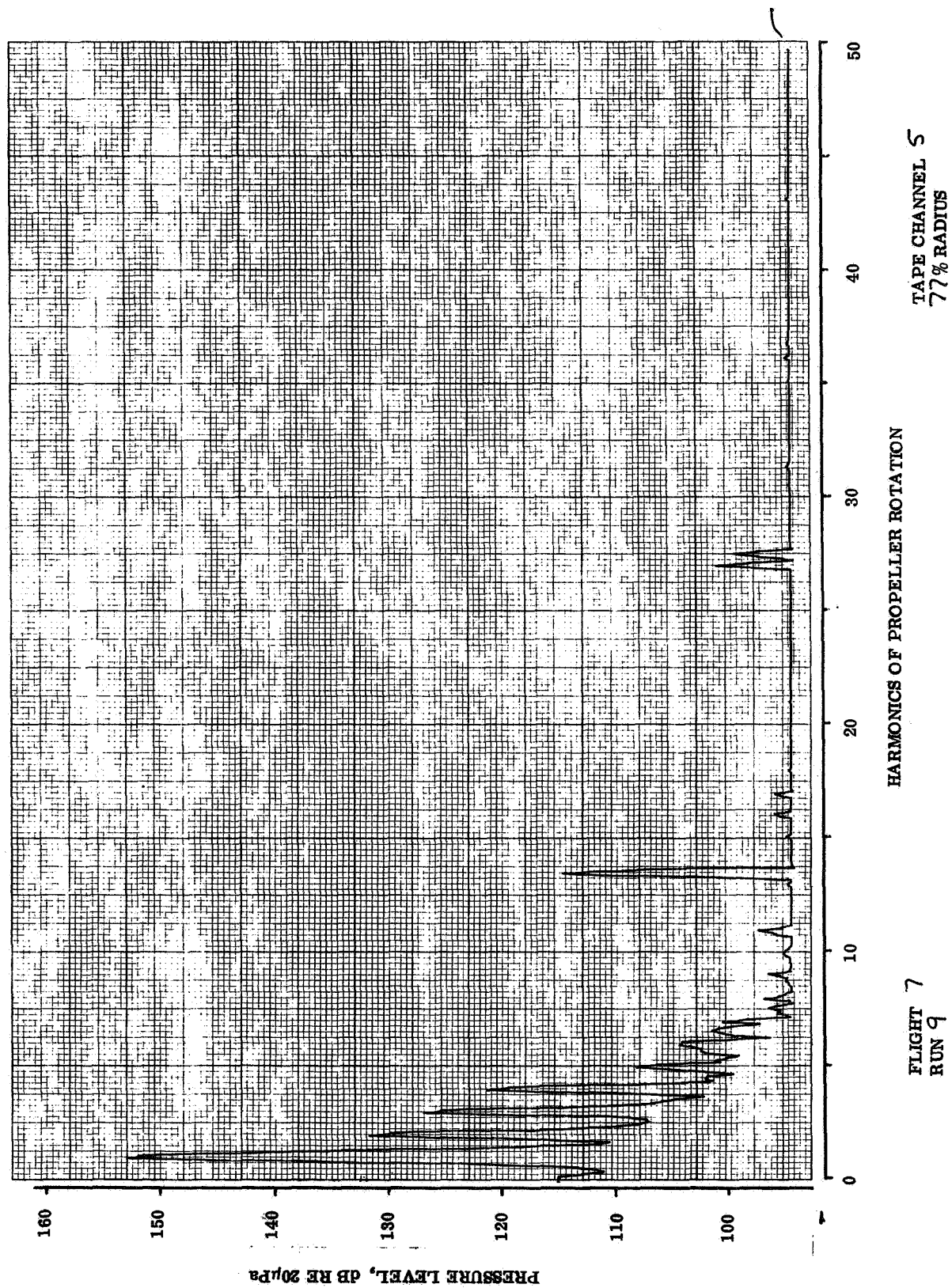
FLIGHT 7
RUN 9

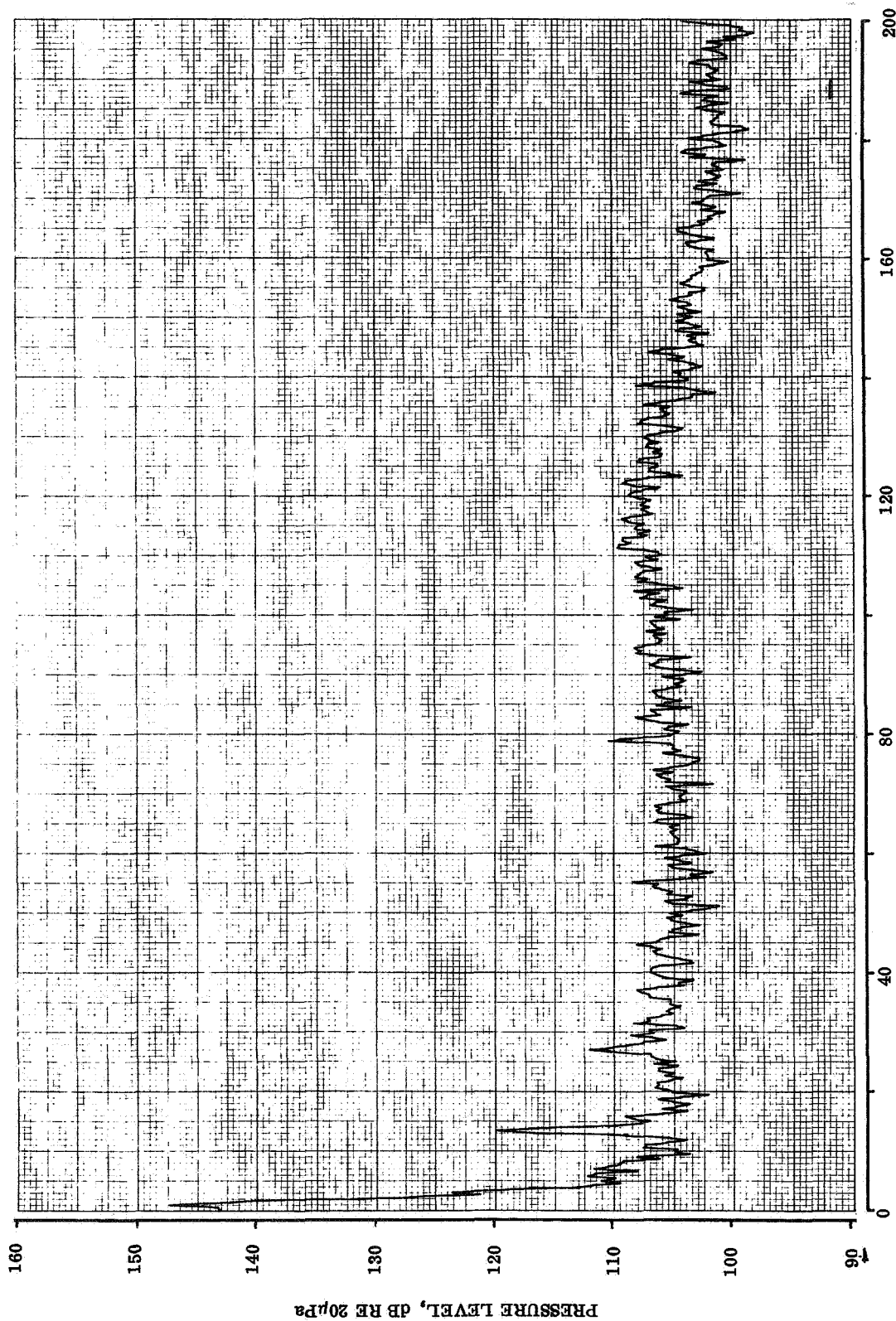




TAPE CHANNEL 5
77% RADIUS

FLIGHT 7
RUN 9

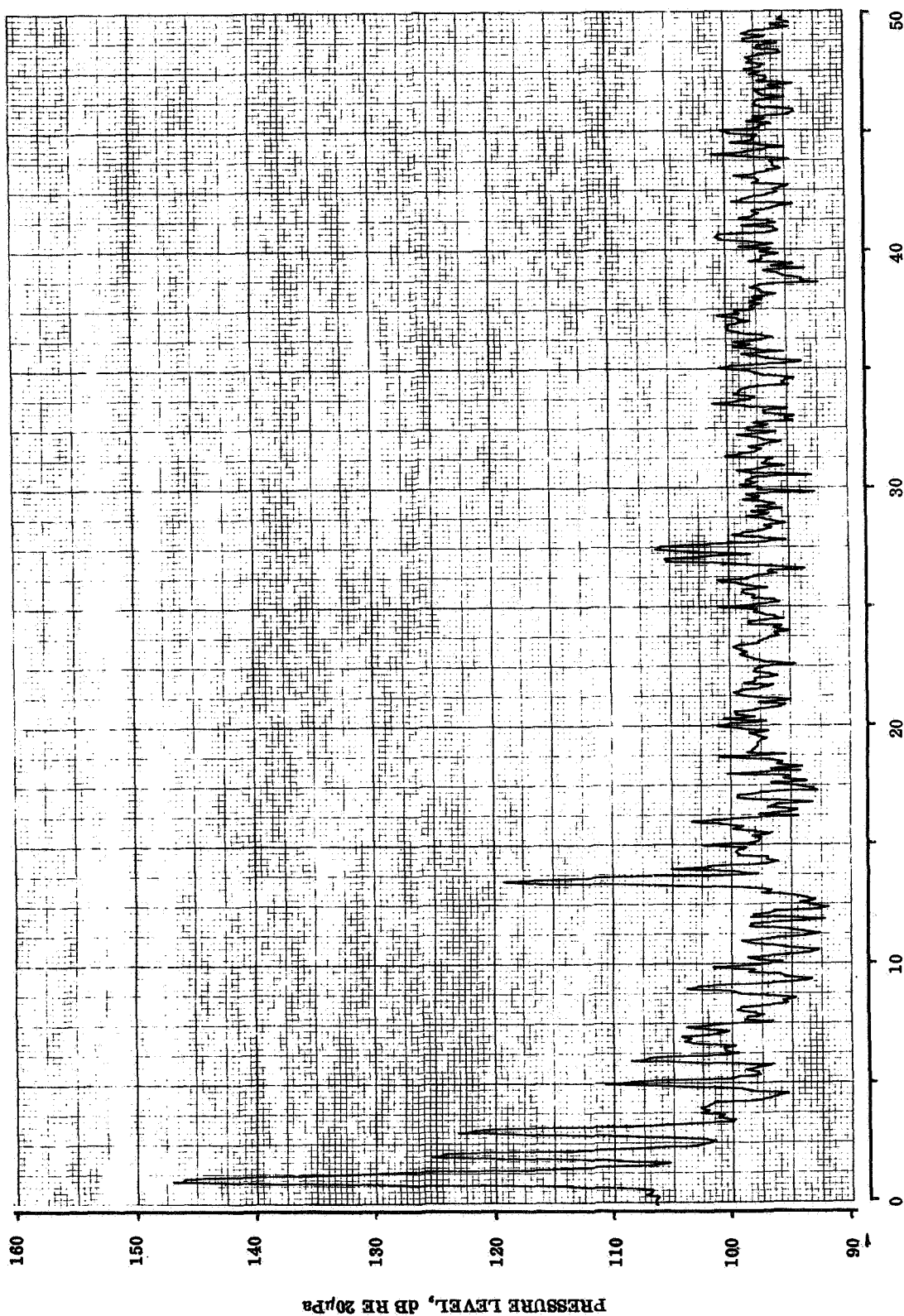




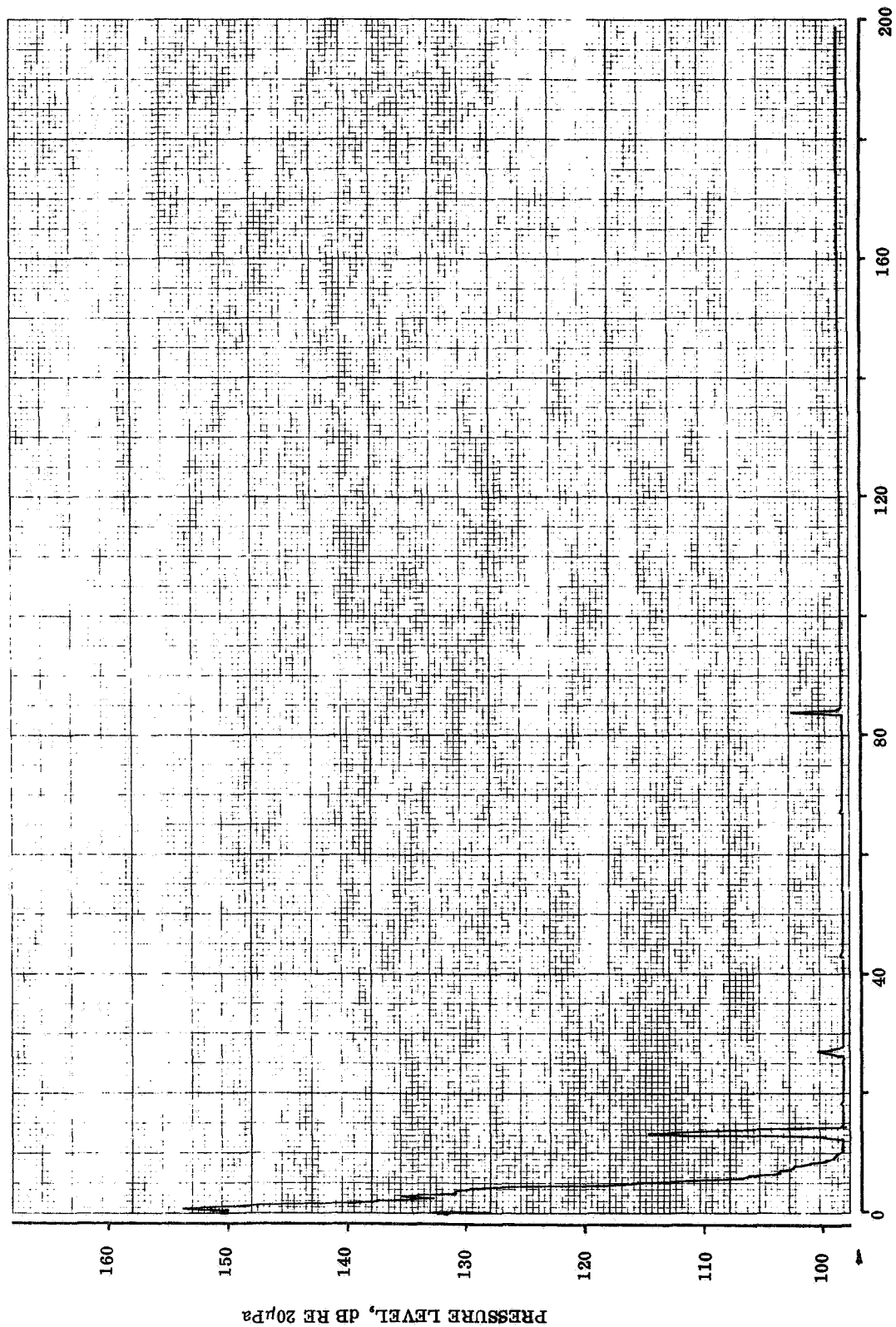
TAPE CHANNEL 13
89 % RADIUS

HARMONICS OF PROPELLER ROTATION

FLIGHT 7
RUN 9



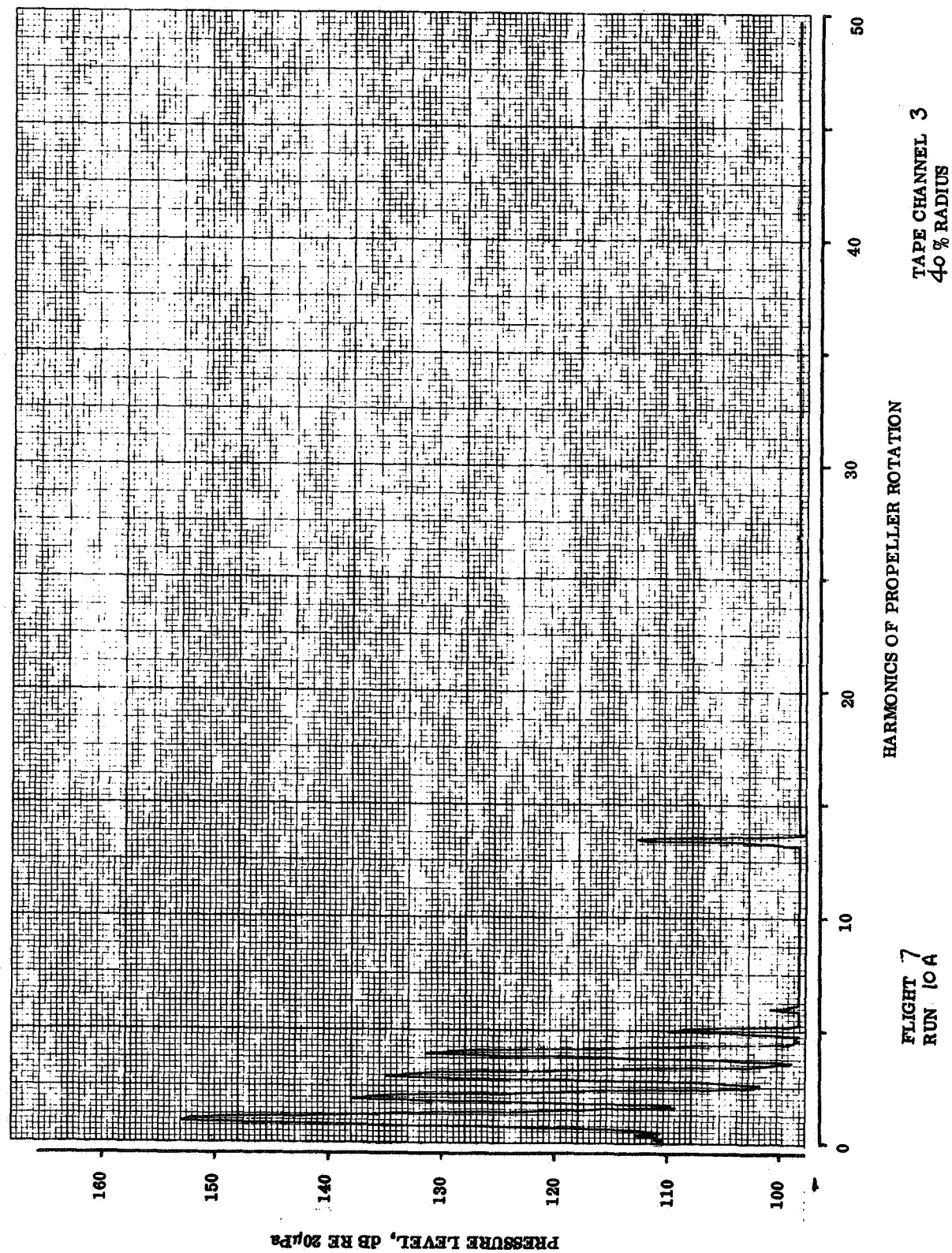
FLIGHT 7
RUN 9

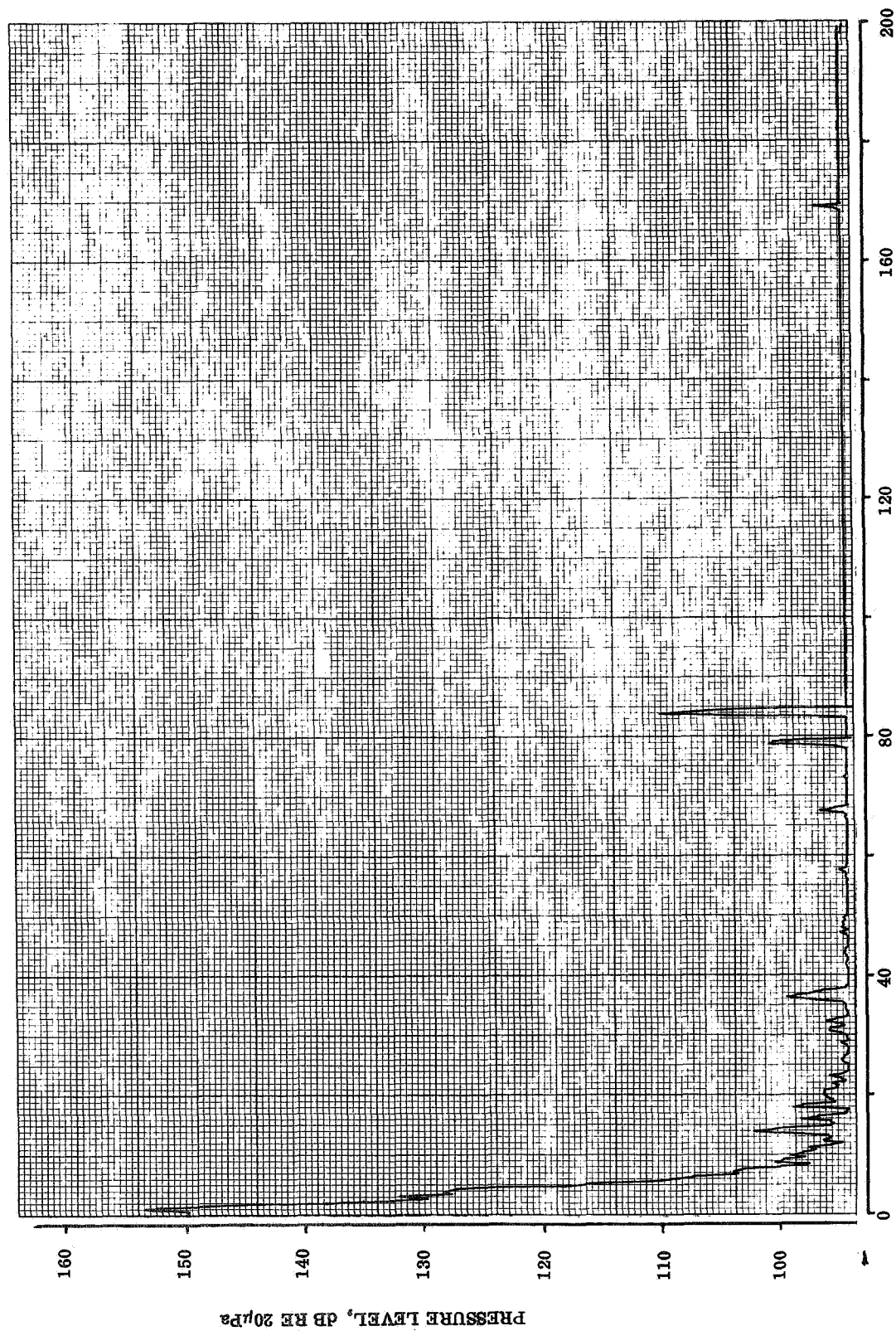


TAPE CHANNEL 3
40% RADIUS

HARMONICS OF PROPELLER ROTATION

FLIGHT 7
RUN 10A

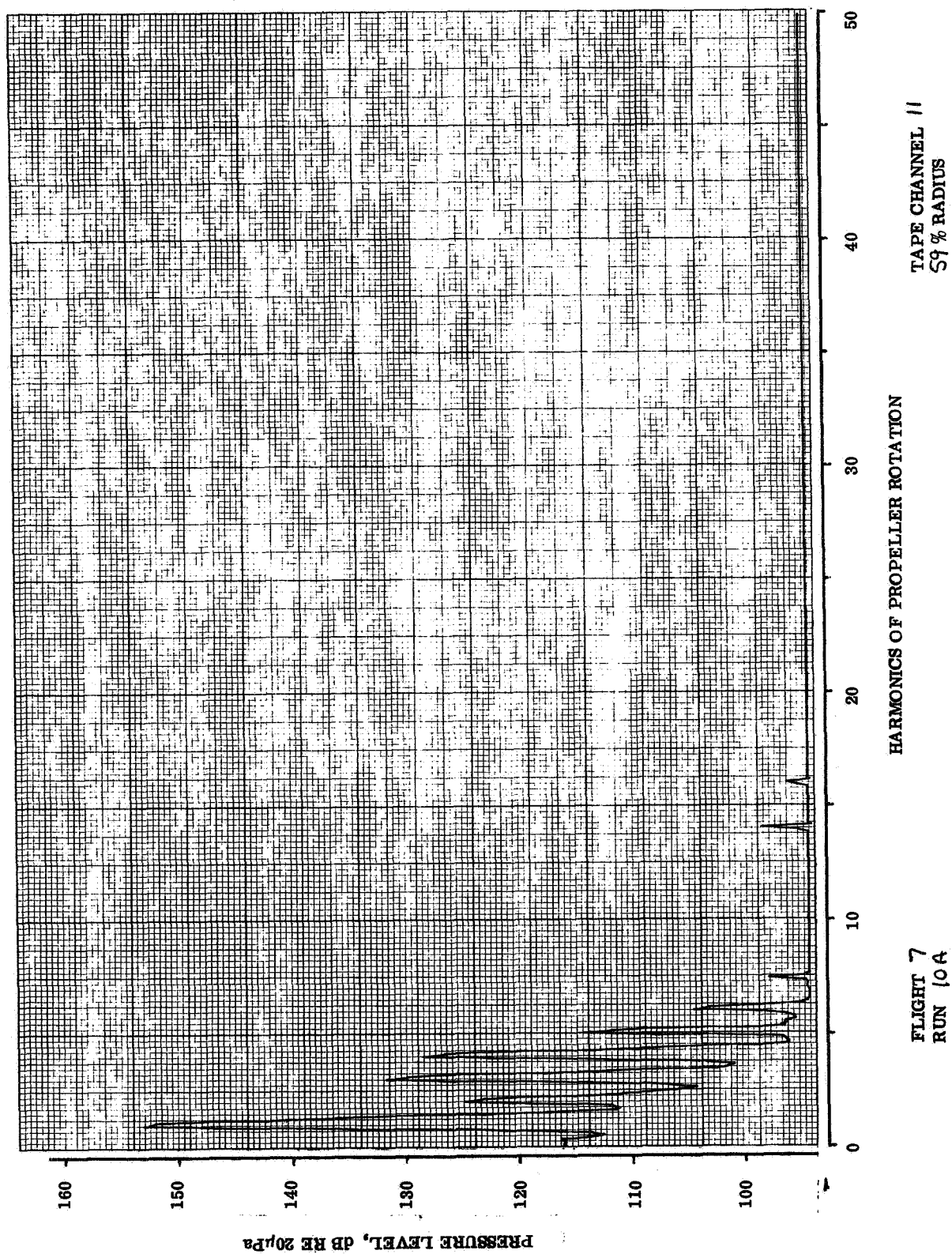


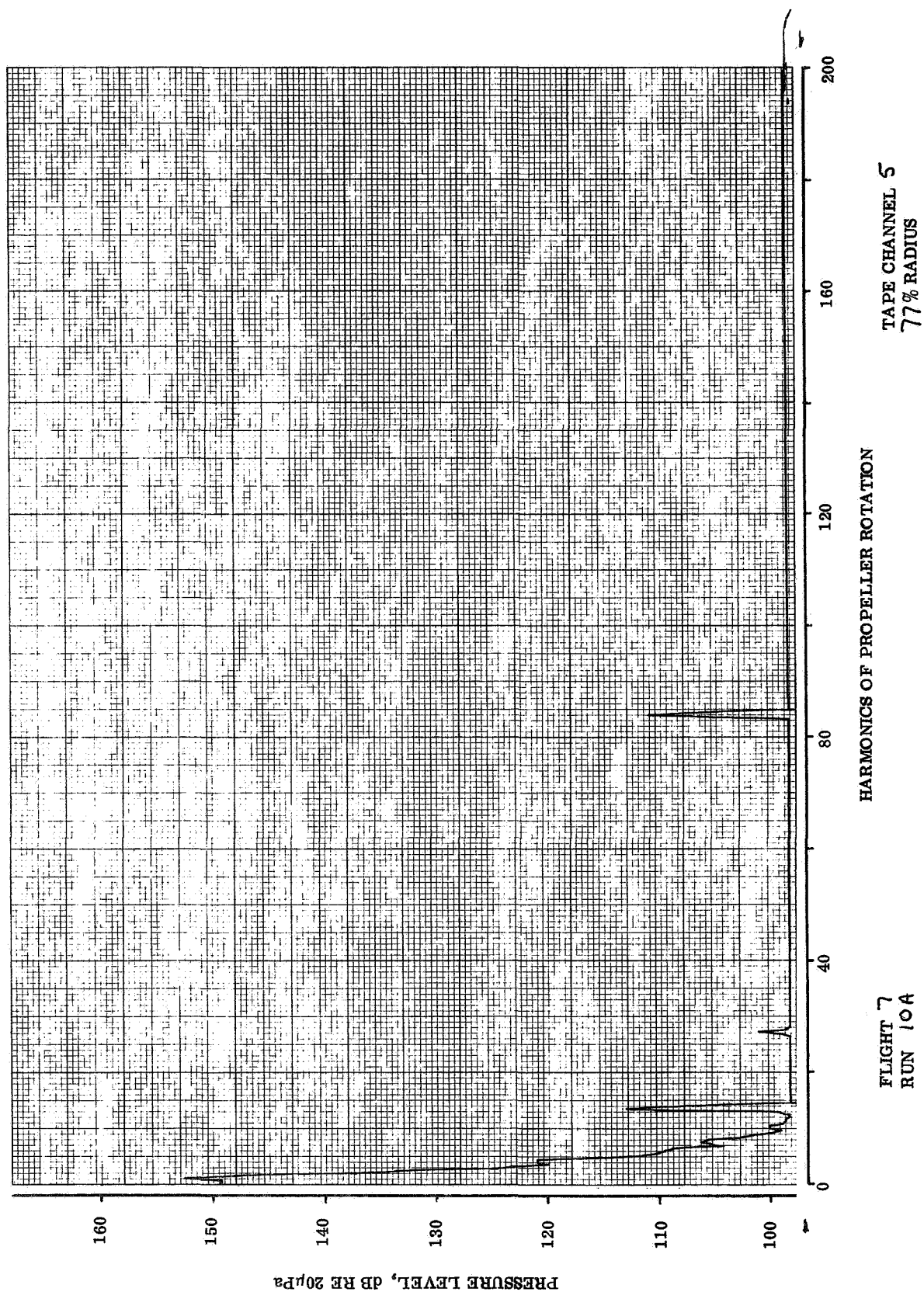


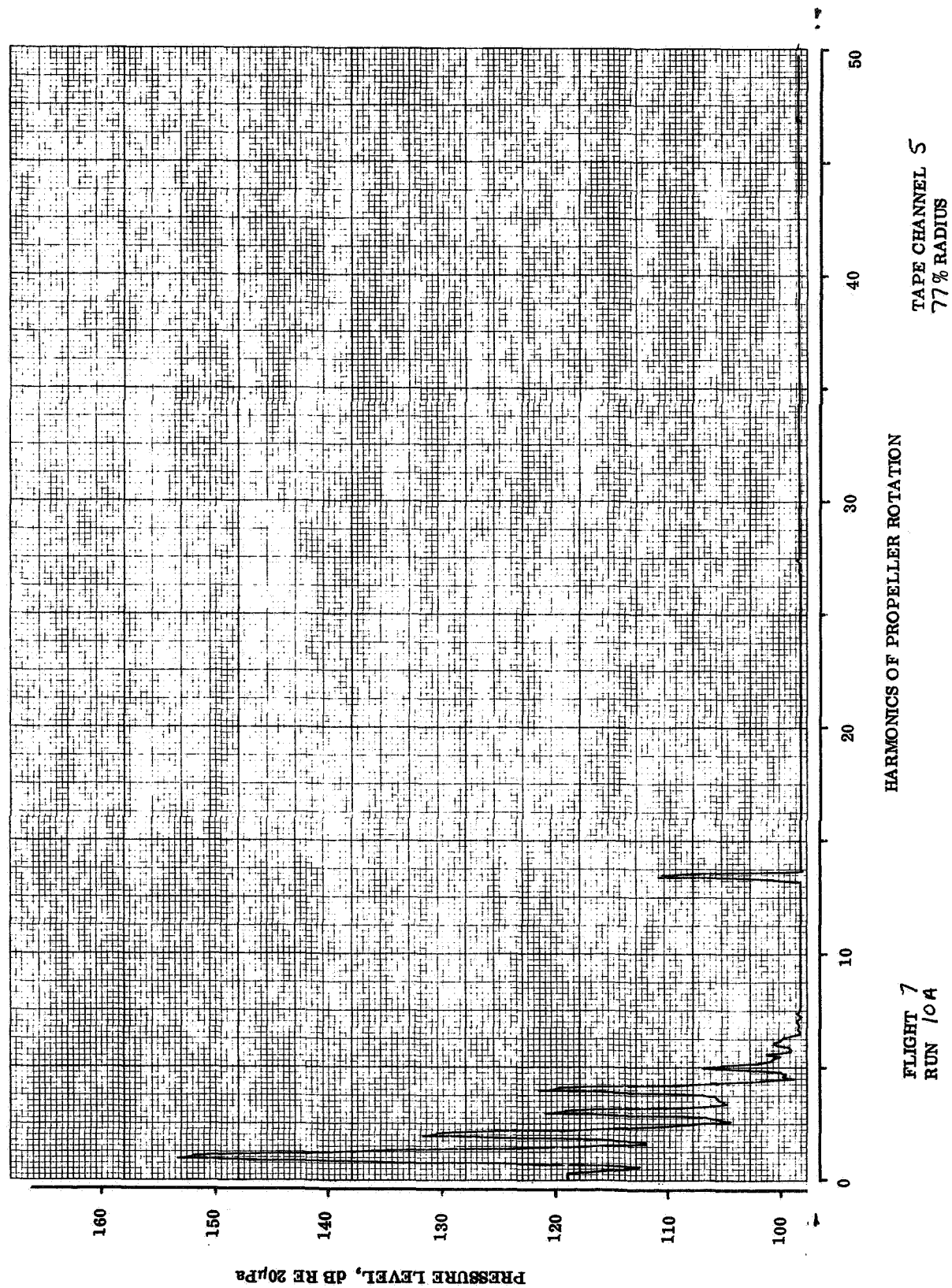
TAPE CHANNEL 11
59 % RADIUS

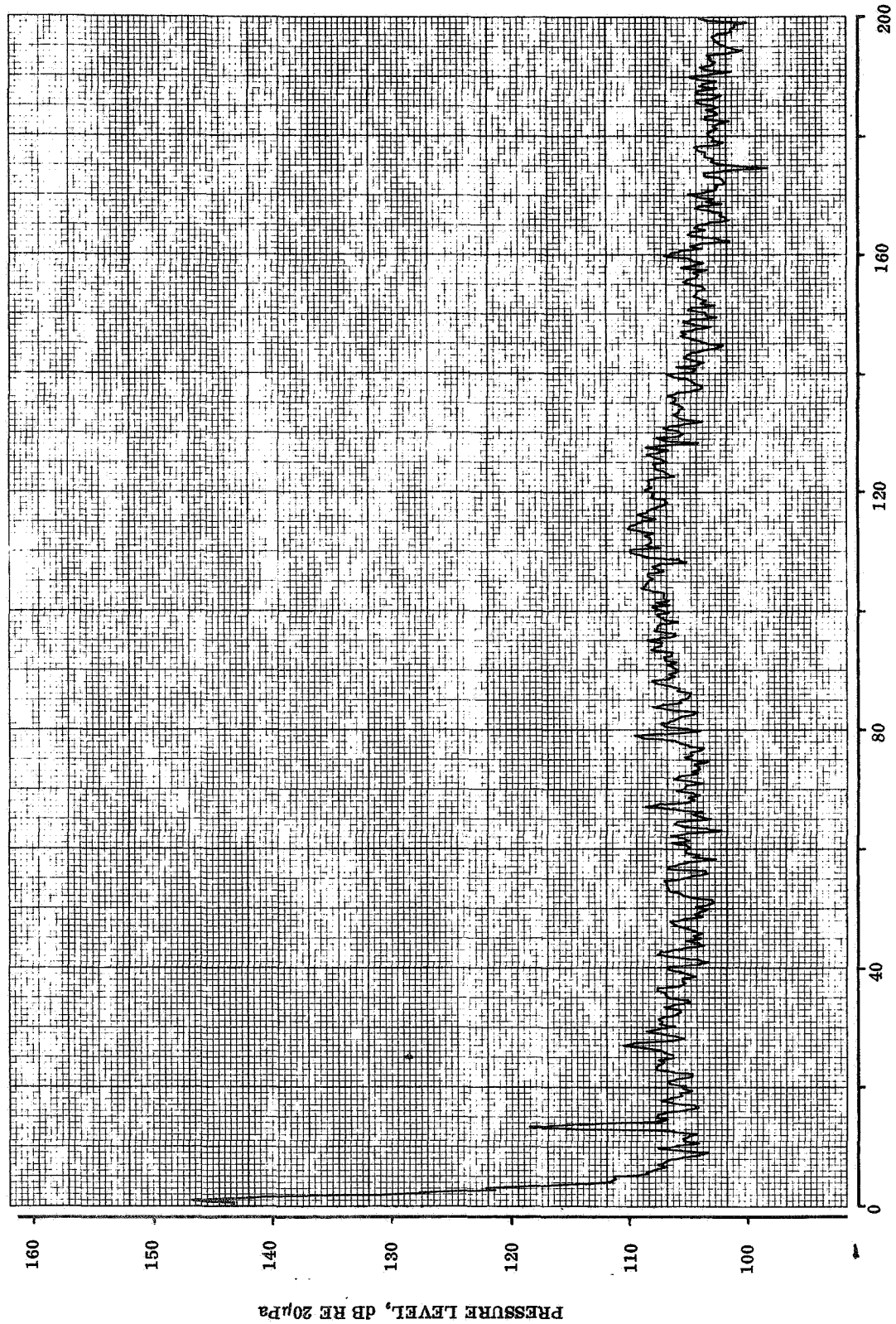
HARMONICS OF PROPELLER ROTATION

FLIGHT 7
RUN 10A





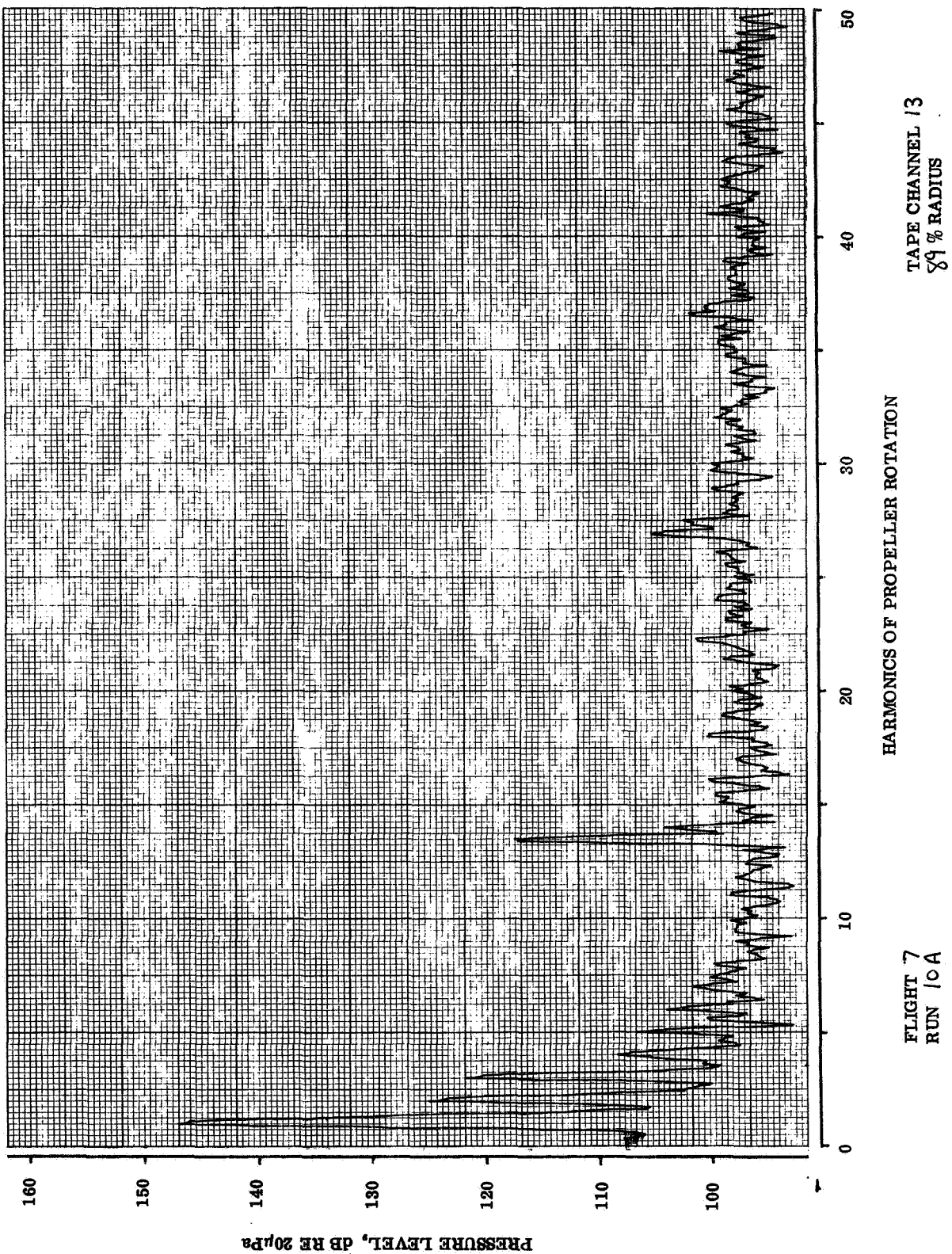


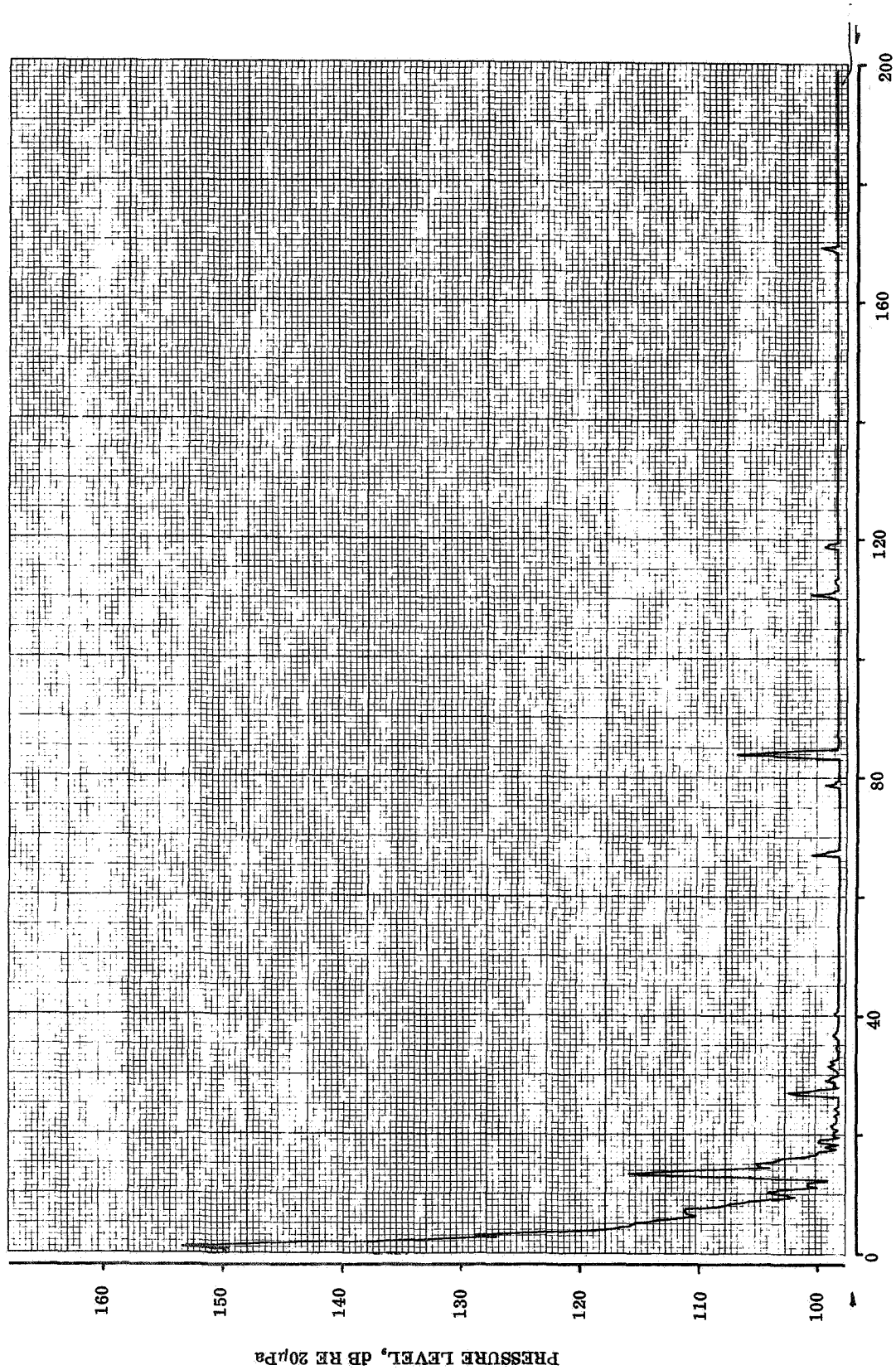


TAPE CHANNEL 13
89 % RADIUS

HARMONICS OF PROPELLER ROTATION

FLIGHT 7
RUN 10A

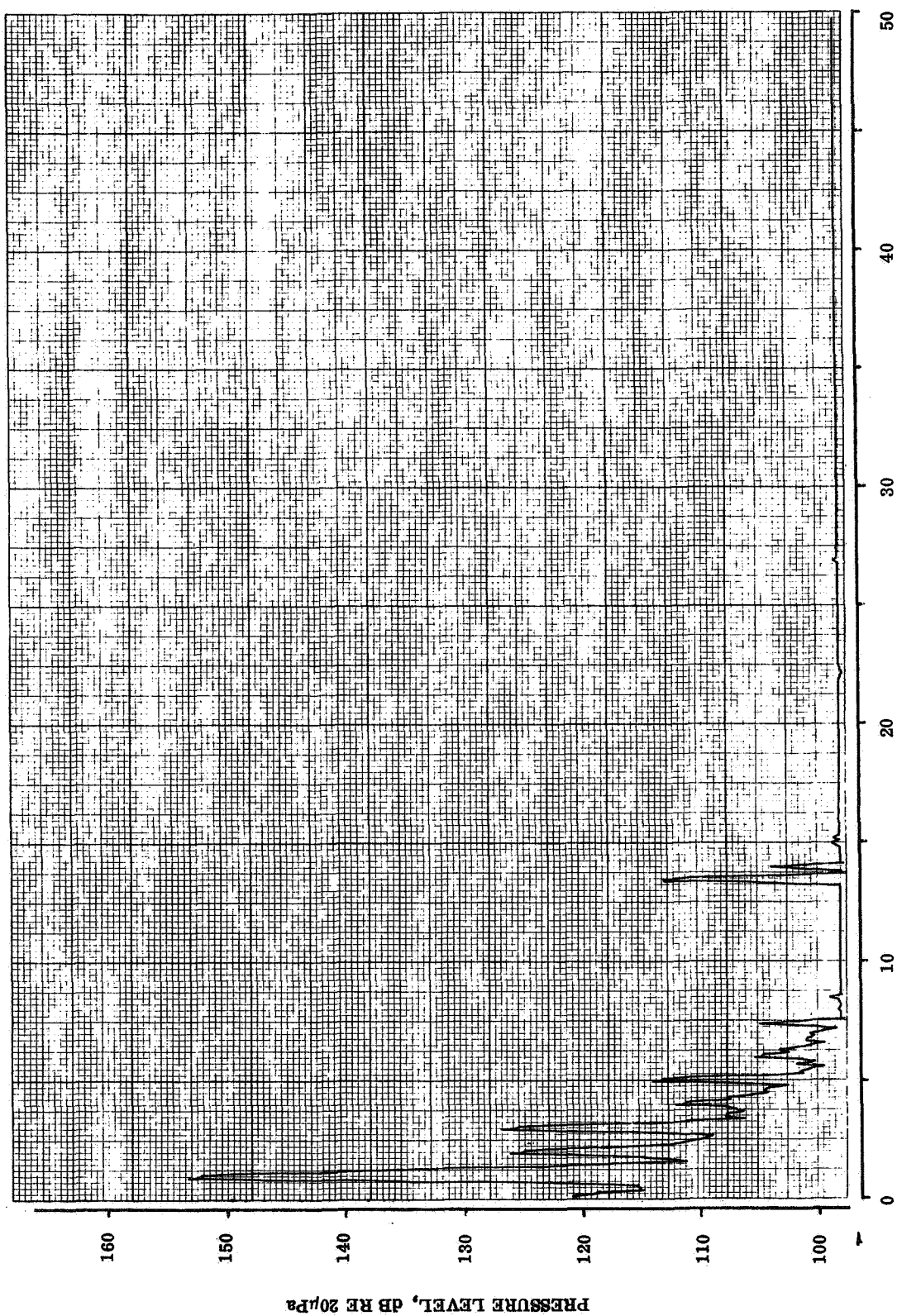




TAPE CHANNEL 9
Q4 % RADIUS T.E.

HARMONICS OF PROPELLER ROTATION

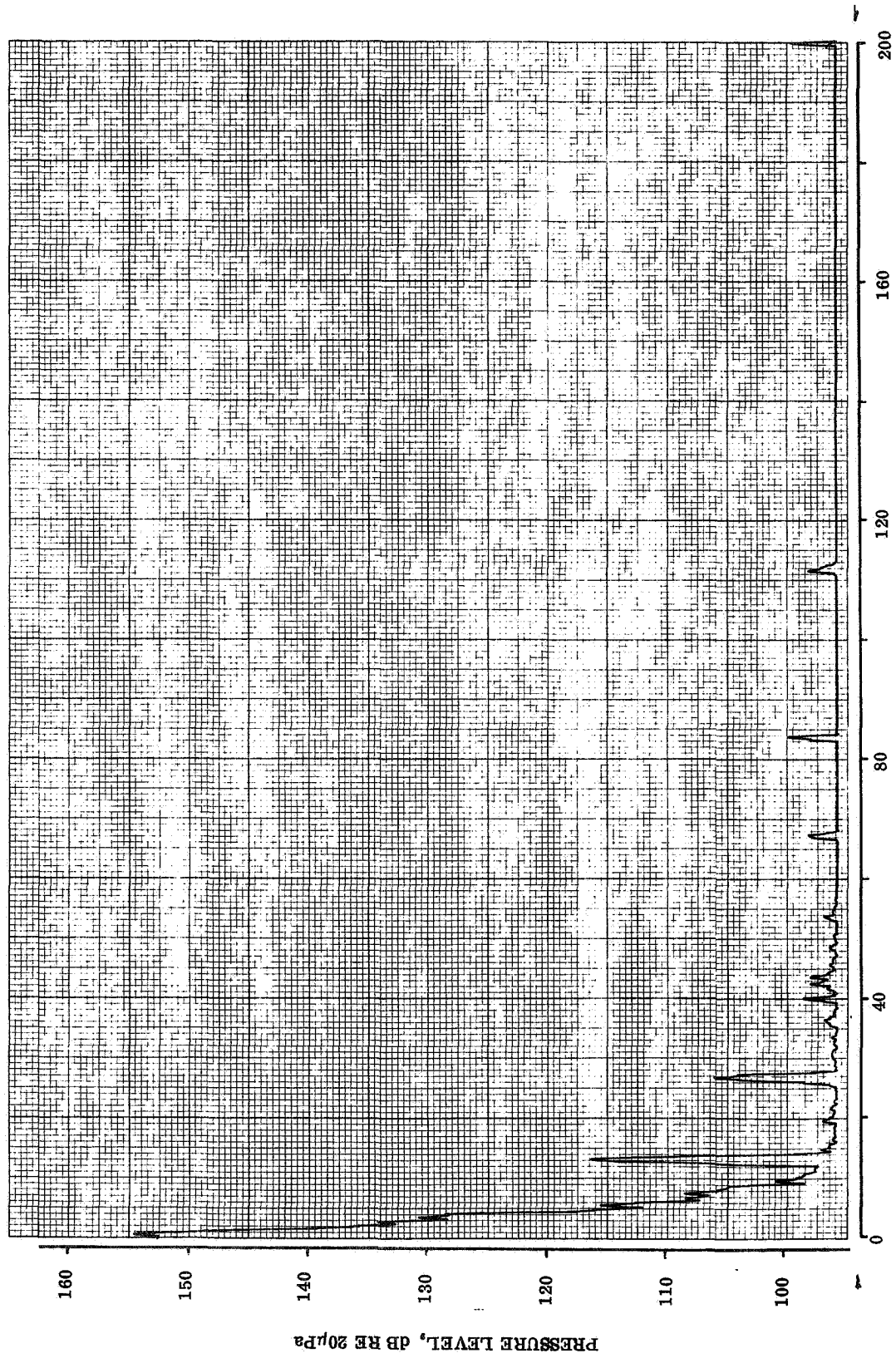
FLIGHT 7
RUN 10A



HARMONICS OF PROPELLER ROTATION

TAPE CHANNEL 9
Q4% RADIUS T.E.

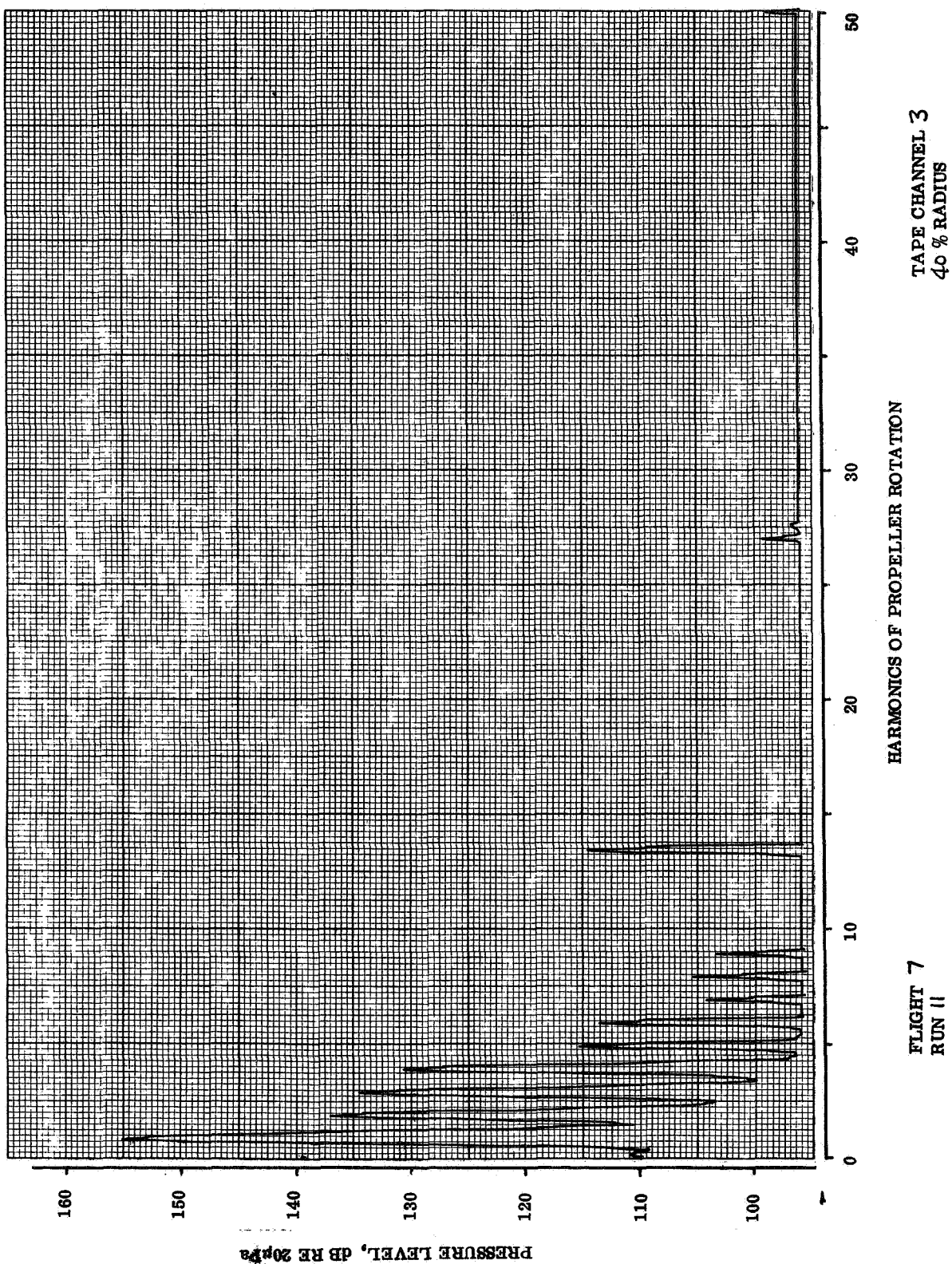
FLIGHT 7
RUN 10A

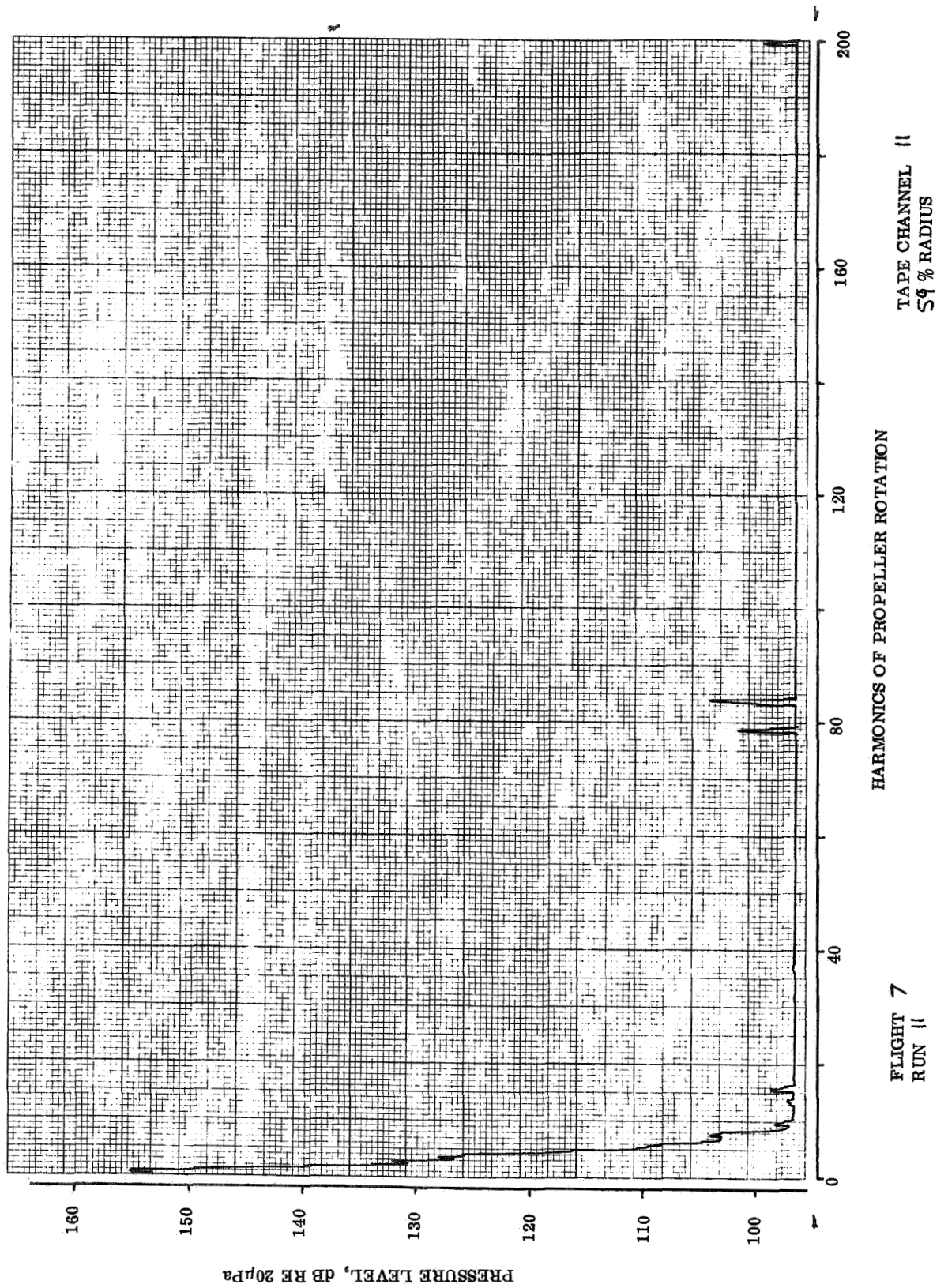


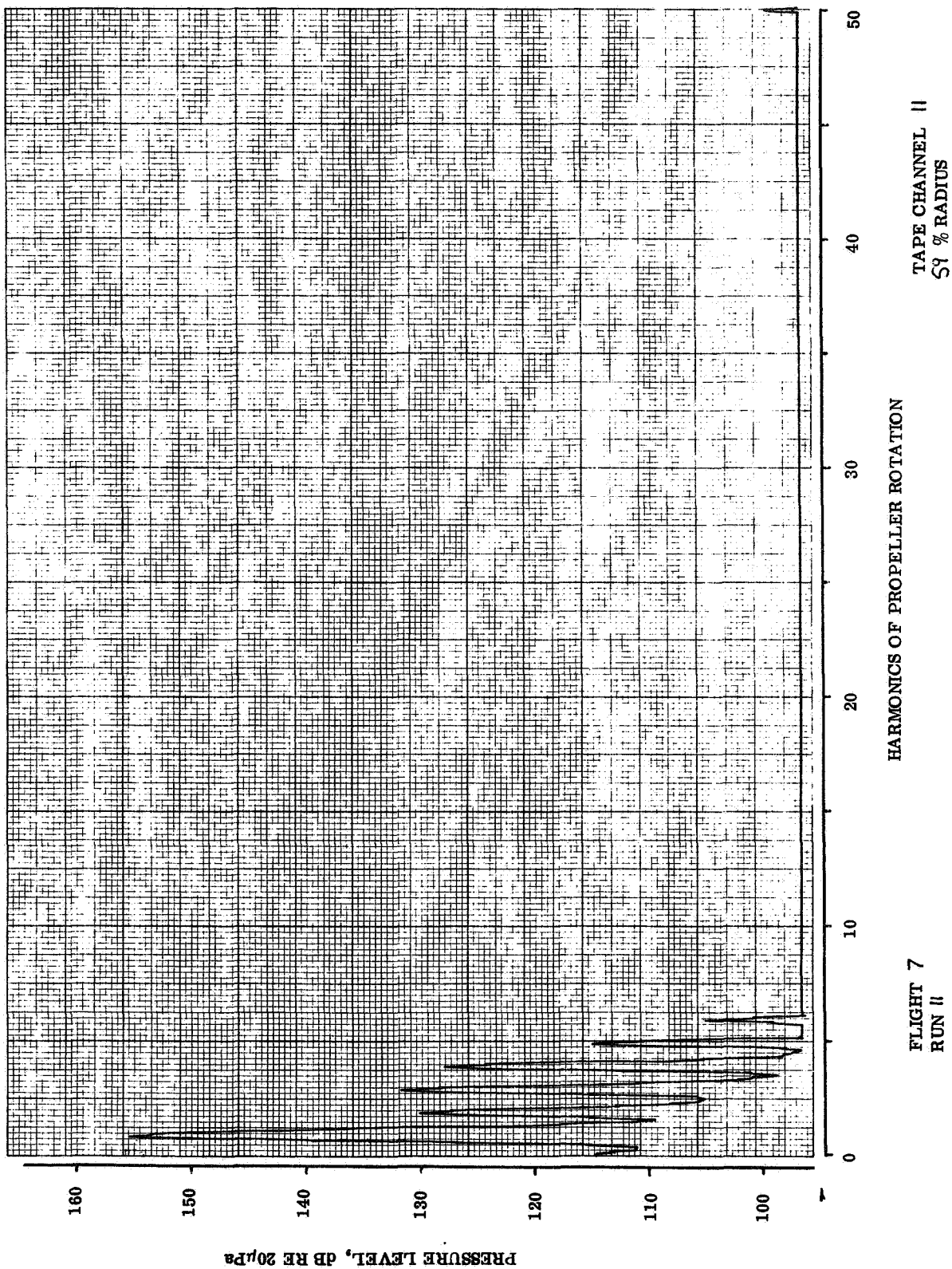
TAPE CHANNEL 3
40% RADIUS

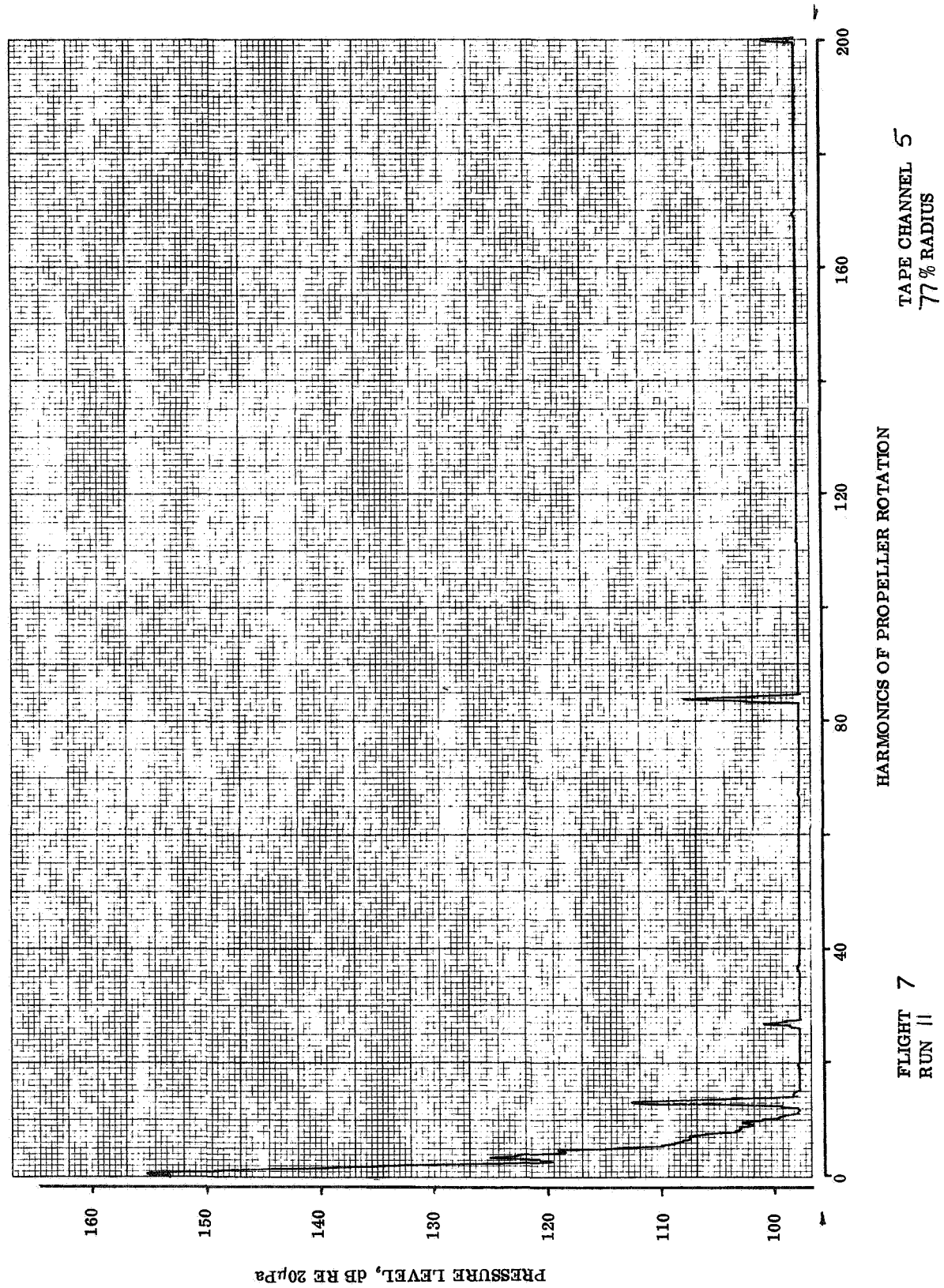
HARMONICS OF PROPELLER ROTATION

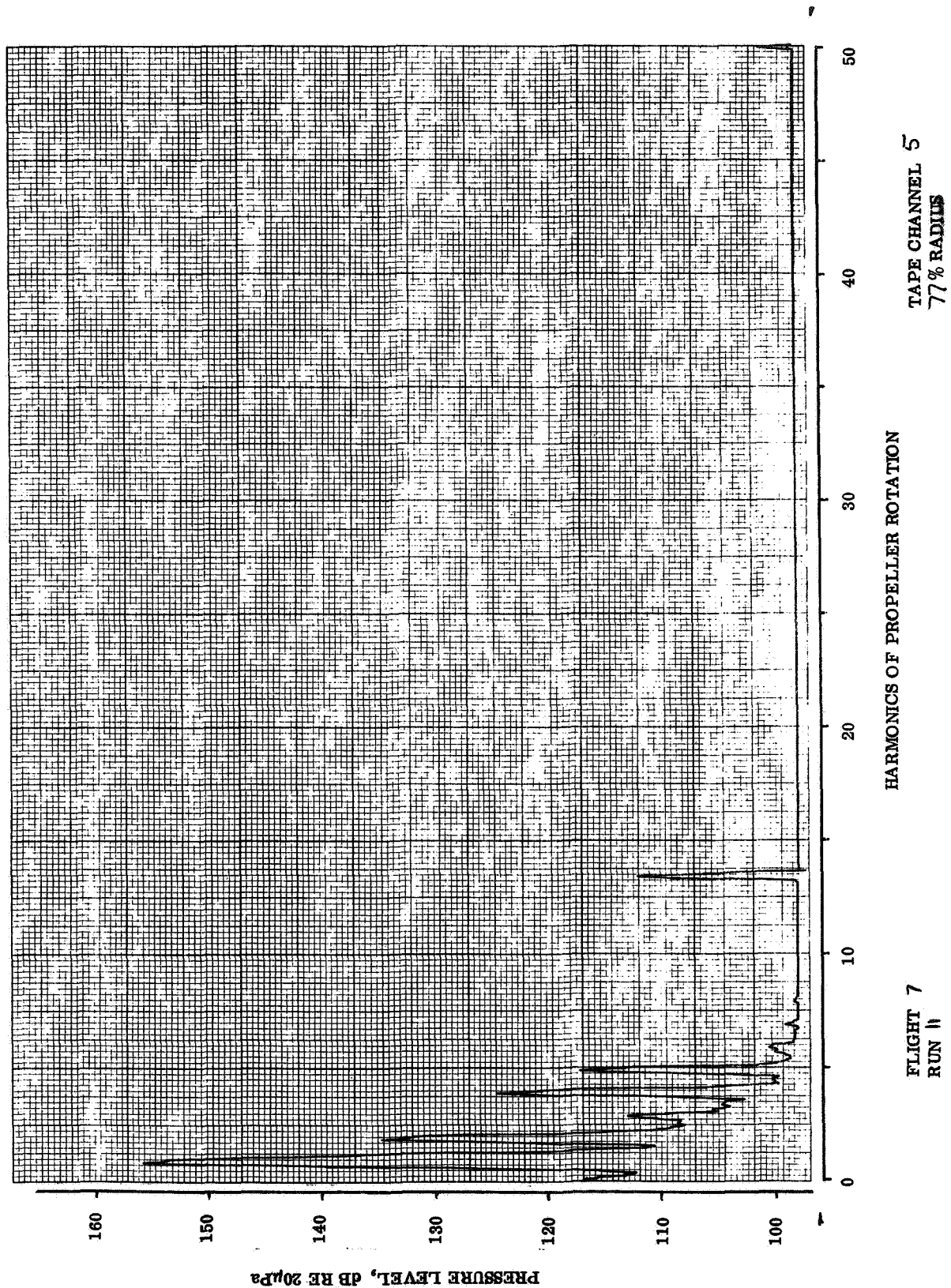
FLIGHT 7
RUN 11

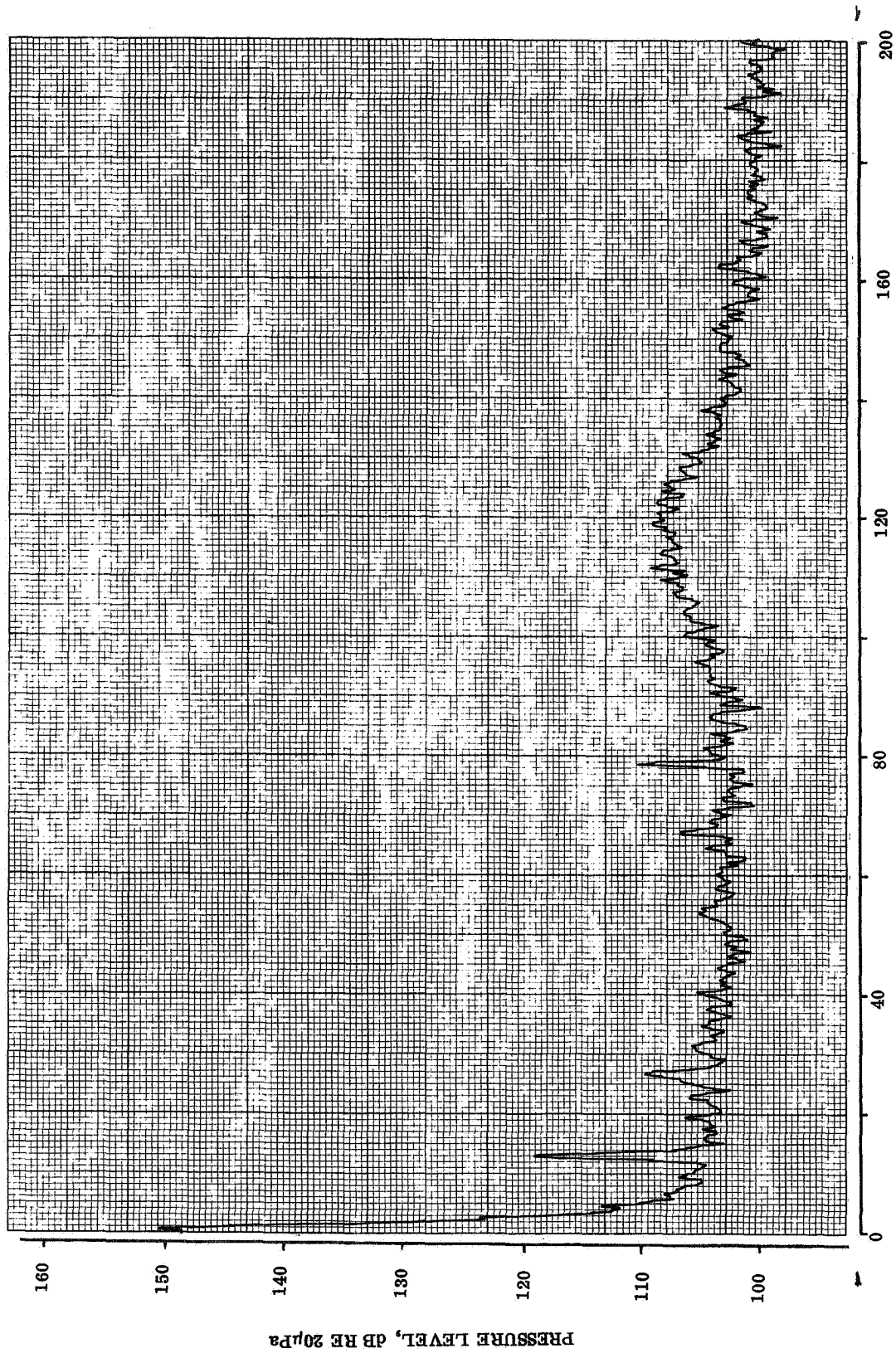








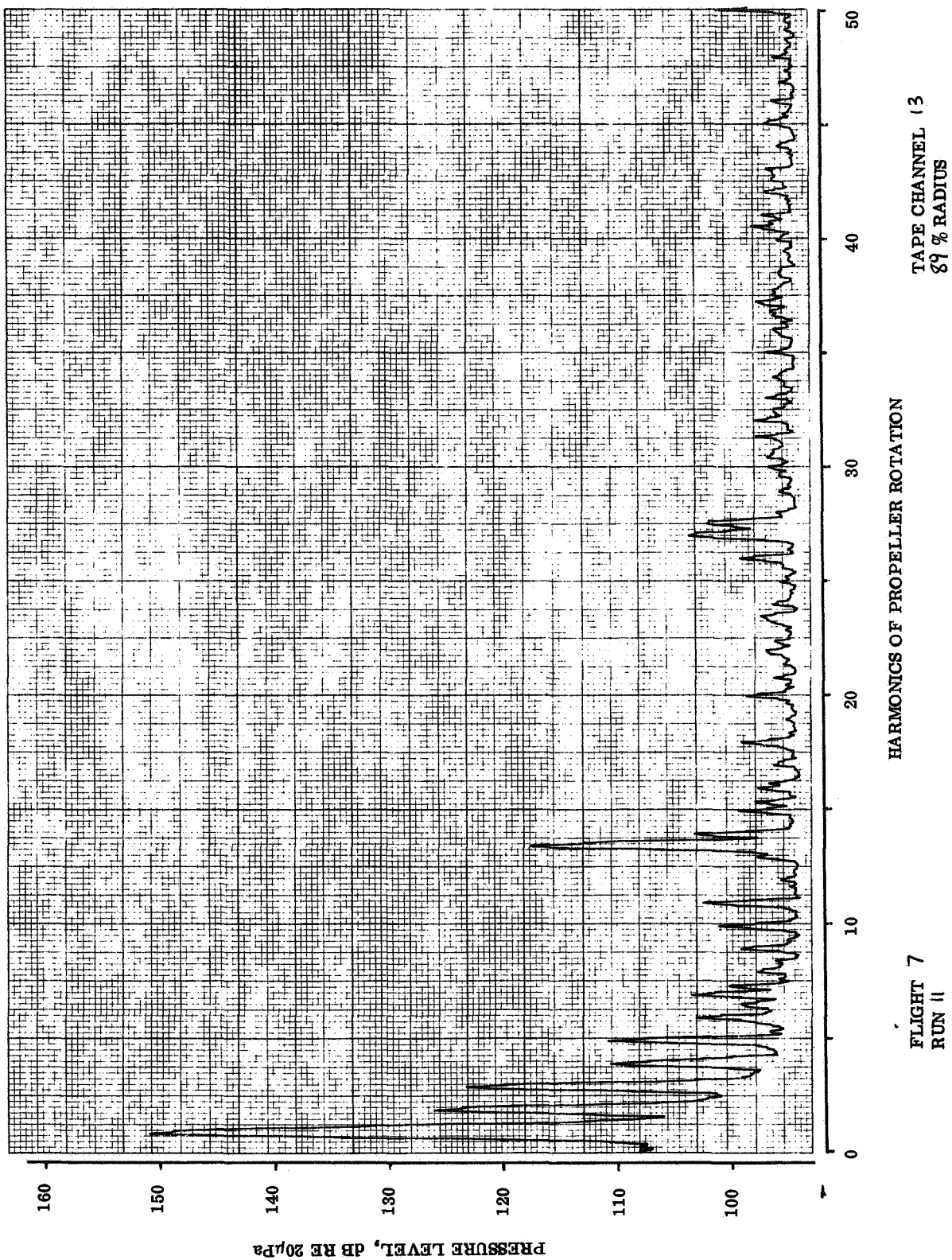


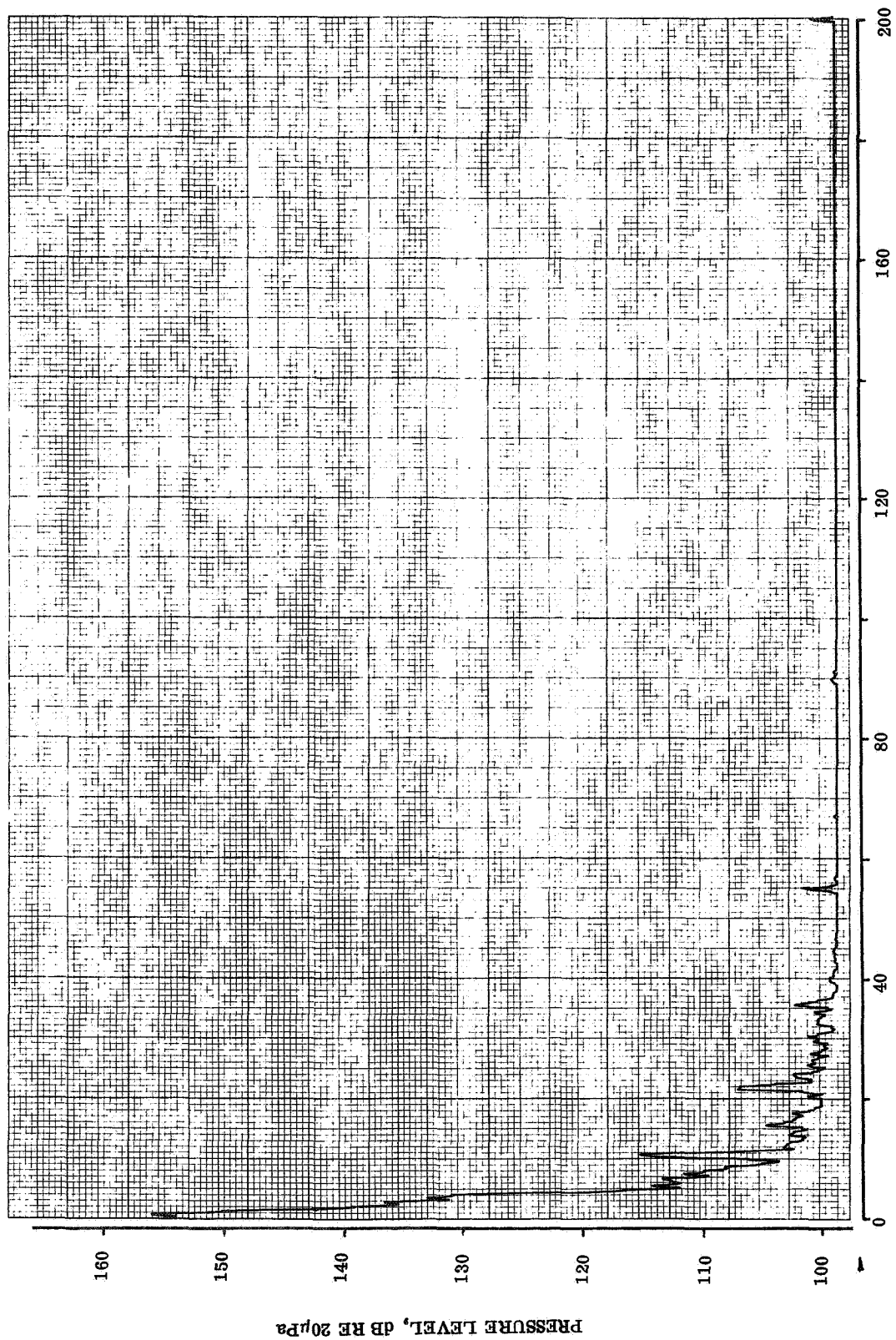


TAPE CHANNEL 13
89 % RADIUS

HARMONICS OF PROPELLER ROTATION

FLIGHT 7
RUN 11

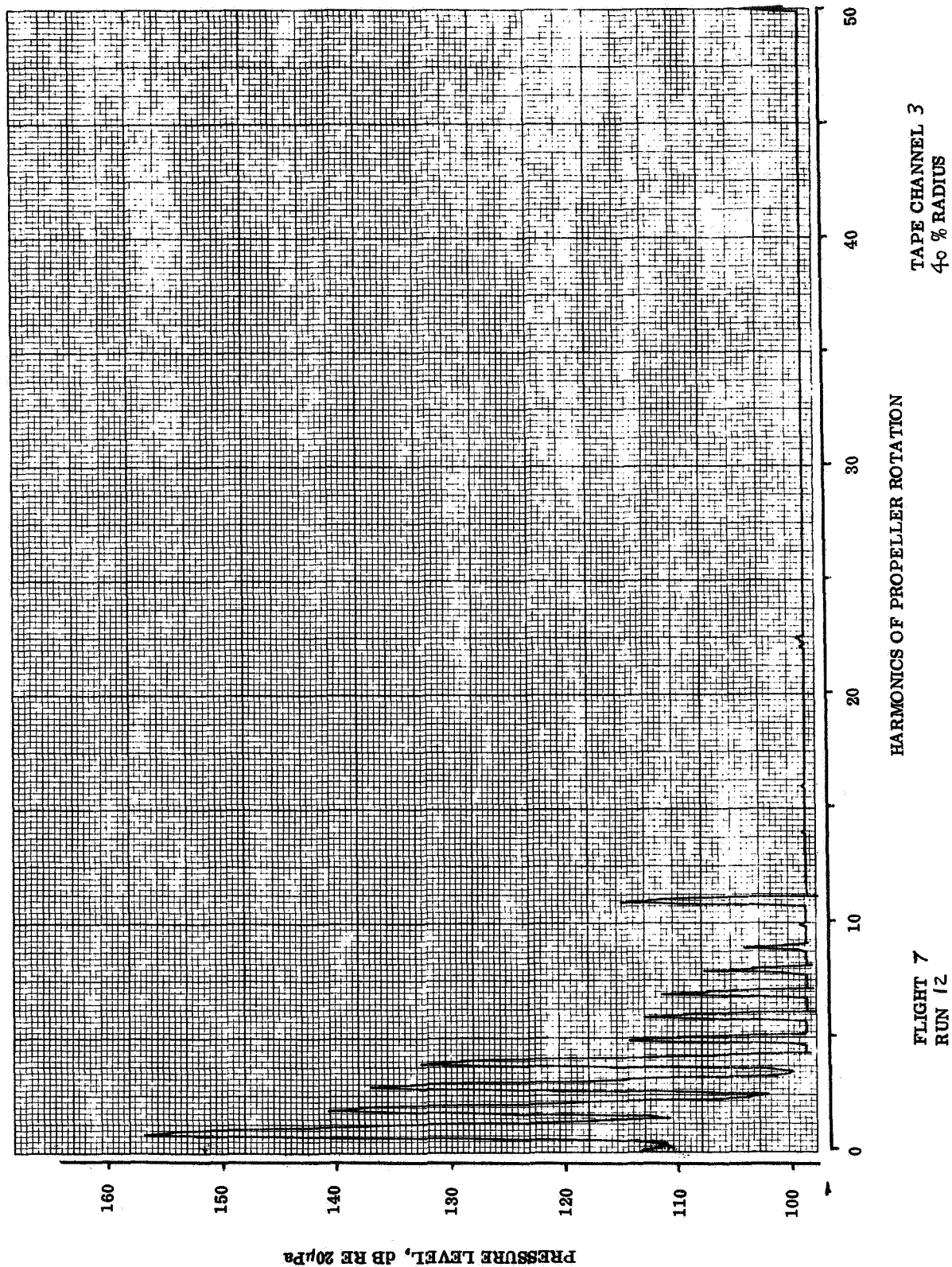


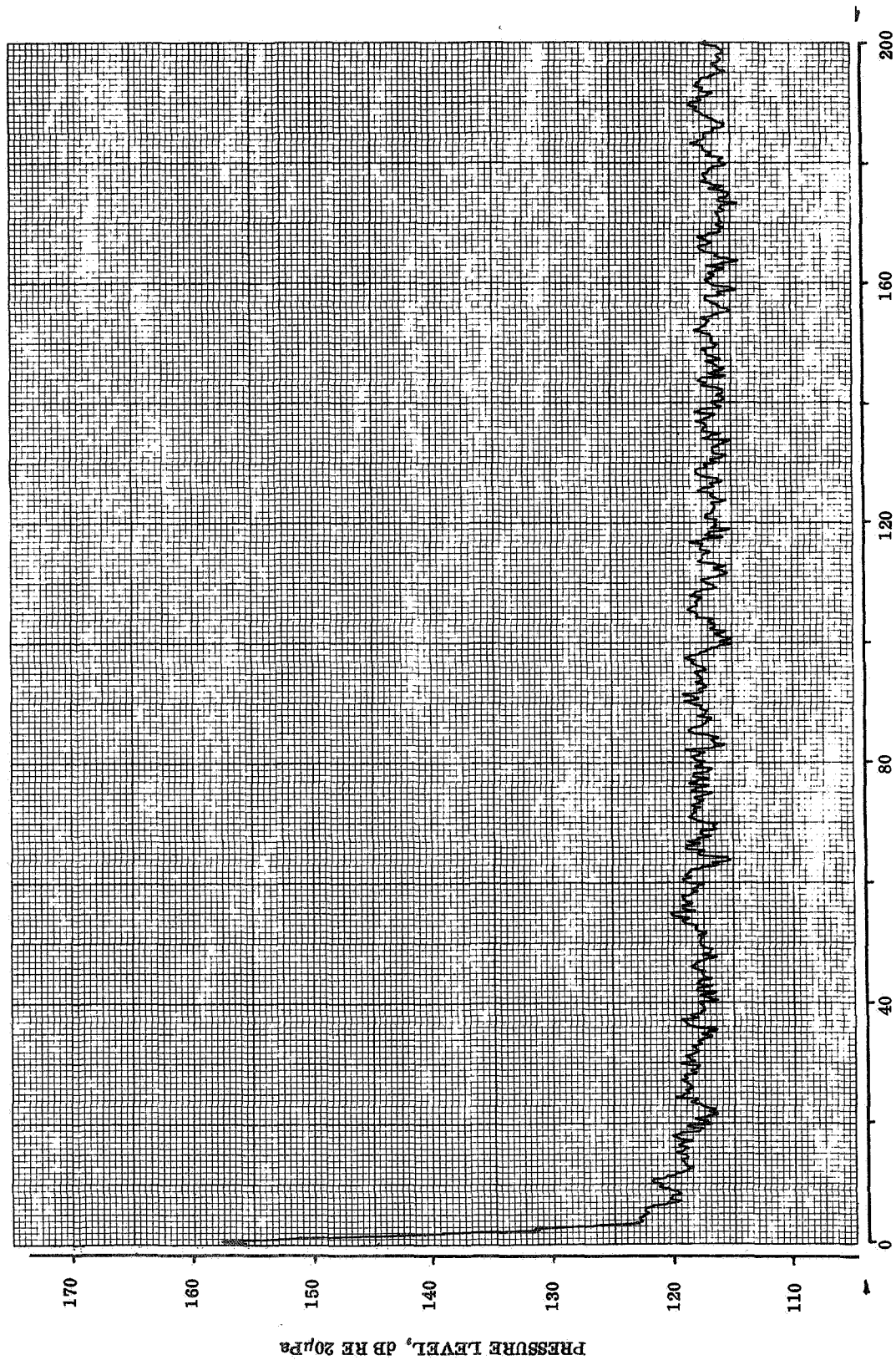


TAPE CHANNEL 3
40 % RADIUS

HARMONICS OF PROPELLER ROTATION

FLIGHT 7
RUN 12

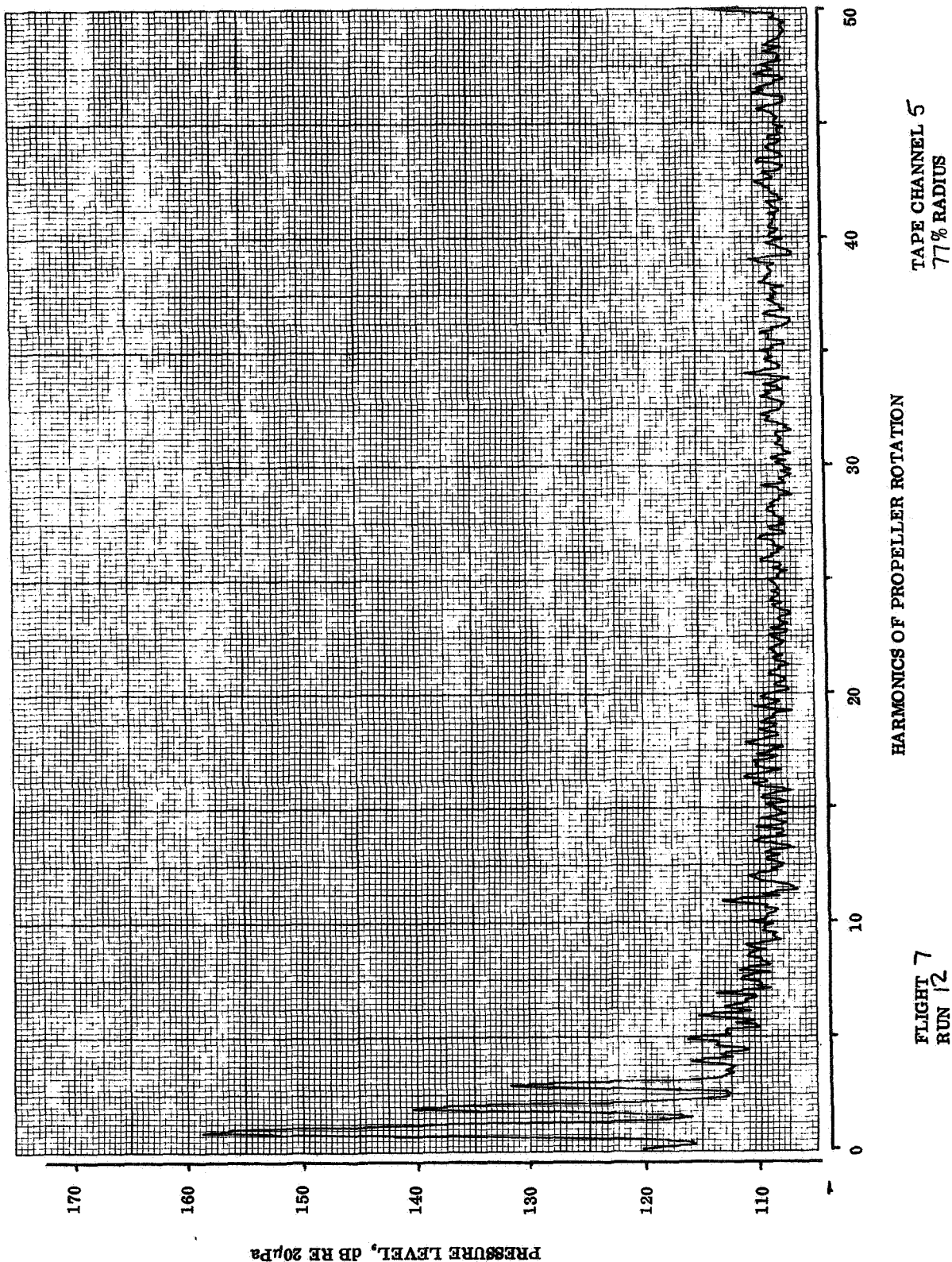


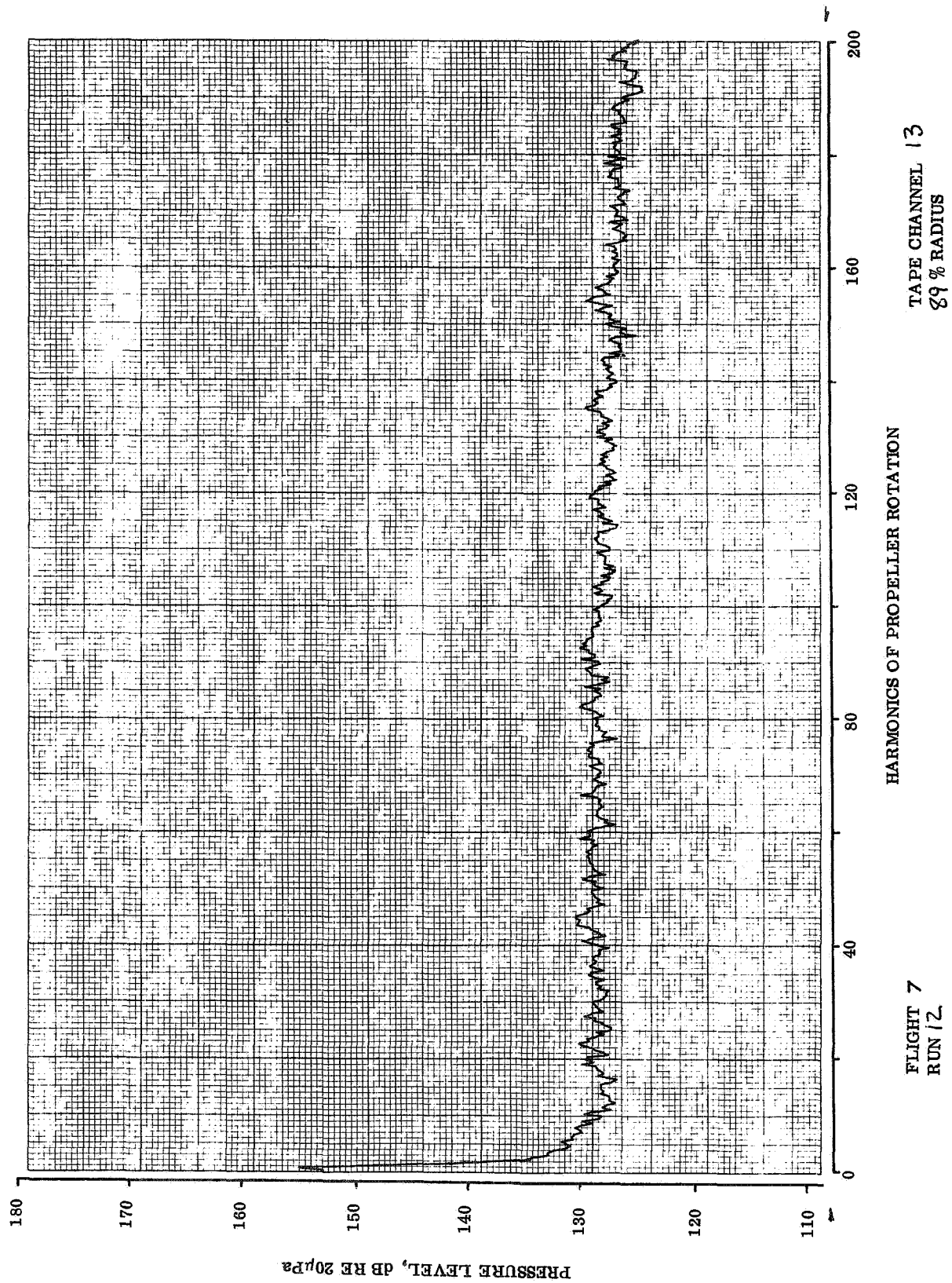


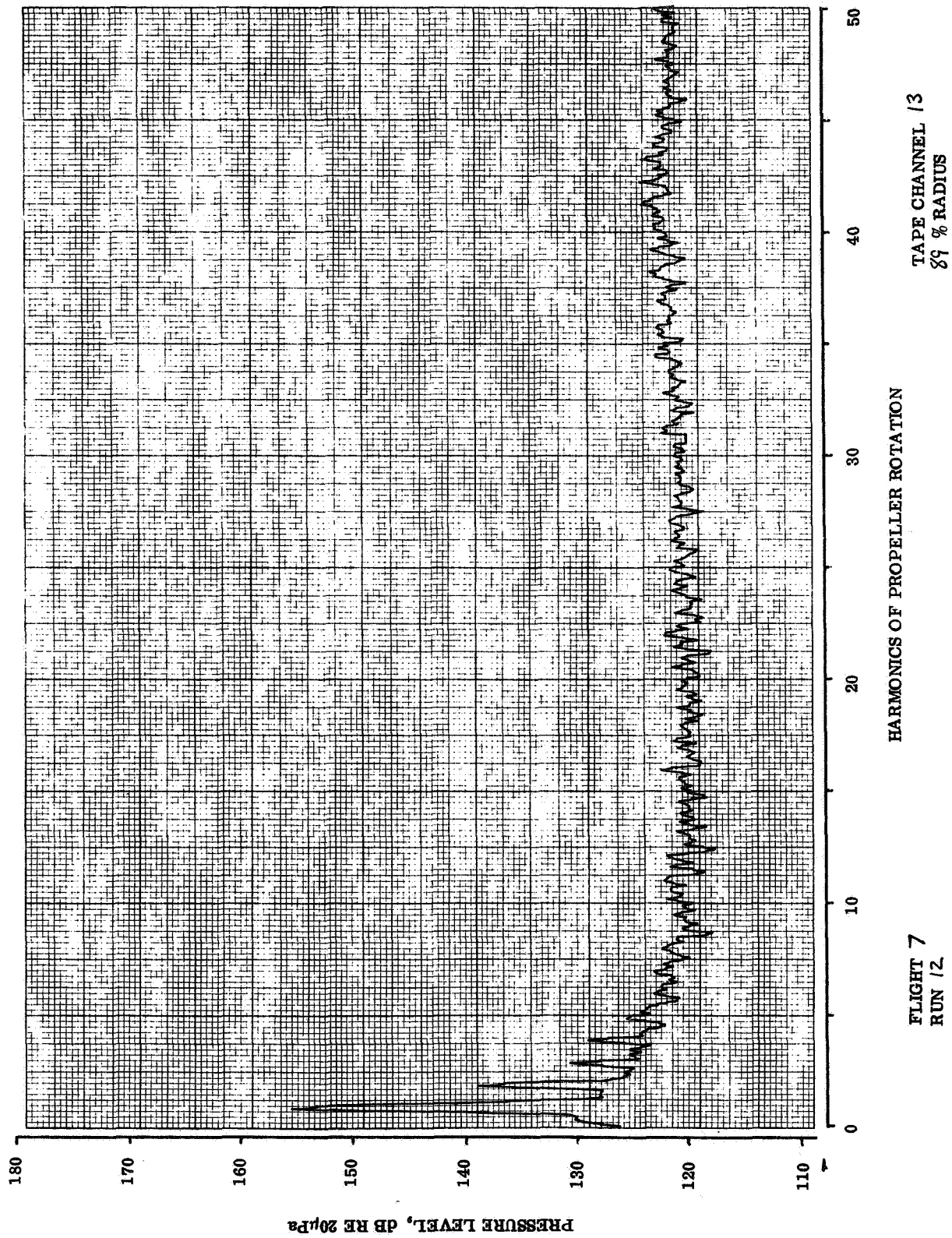
TAPE CHANNEL 5
77% RADIUS

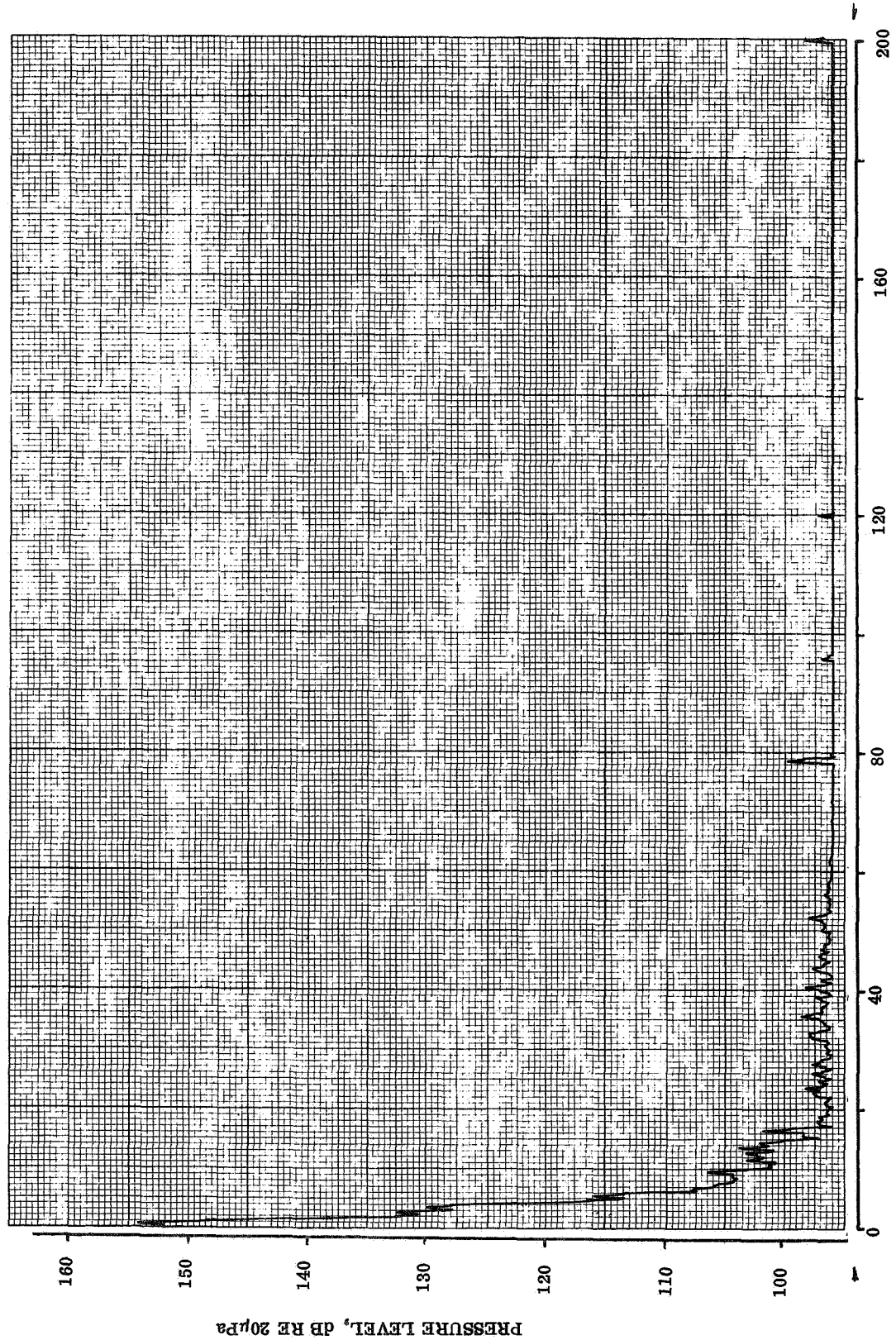
HARMONICS OF PROPELLER ROTATION

FLIGHT 7
RUN 12





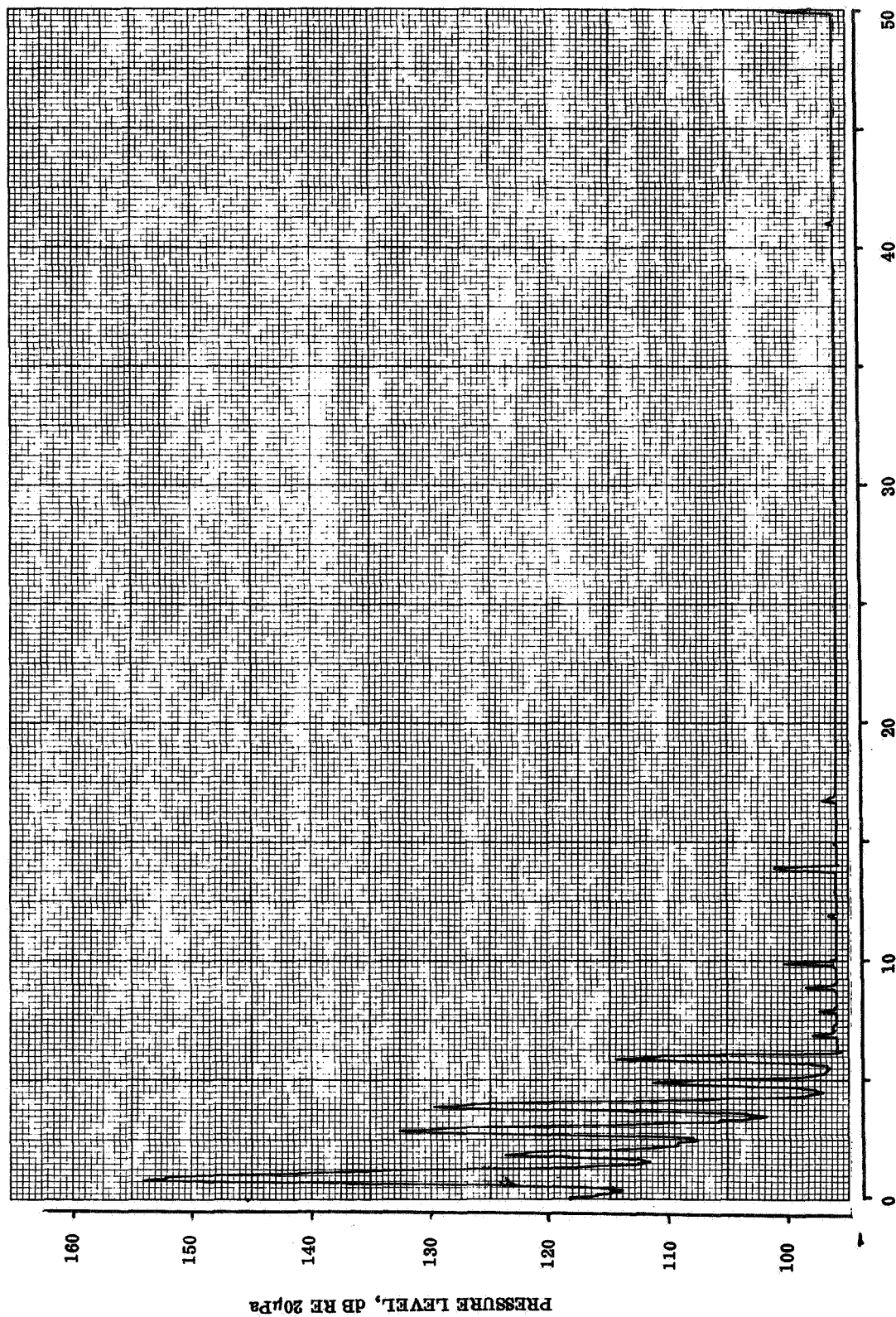




TAPE CHANNEL 3
59% RADIUS

HARMONICS OF PROPELLER ROTATION

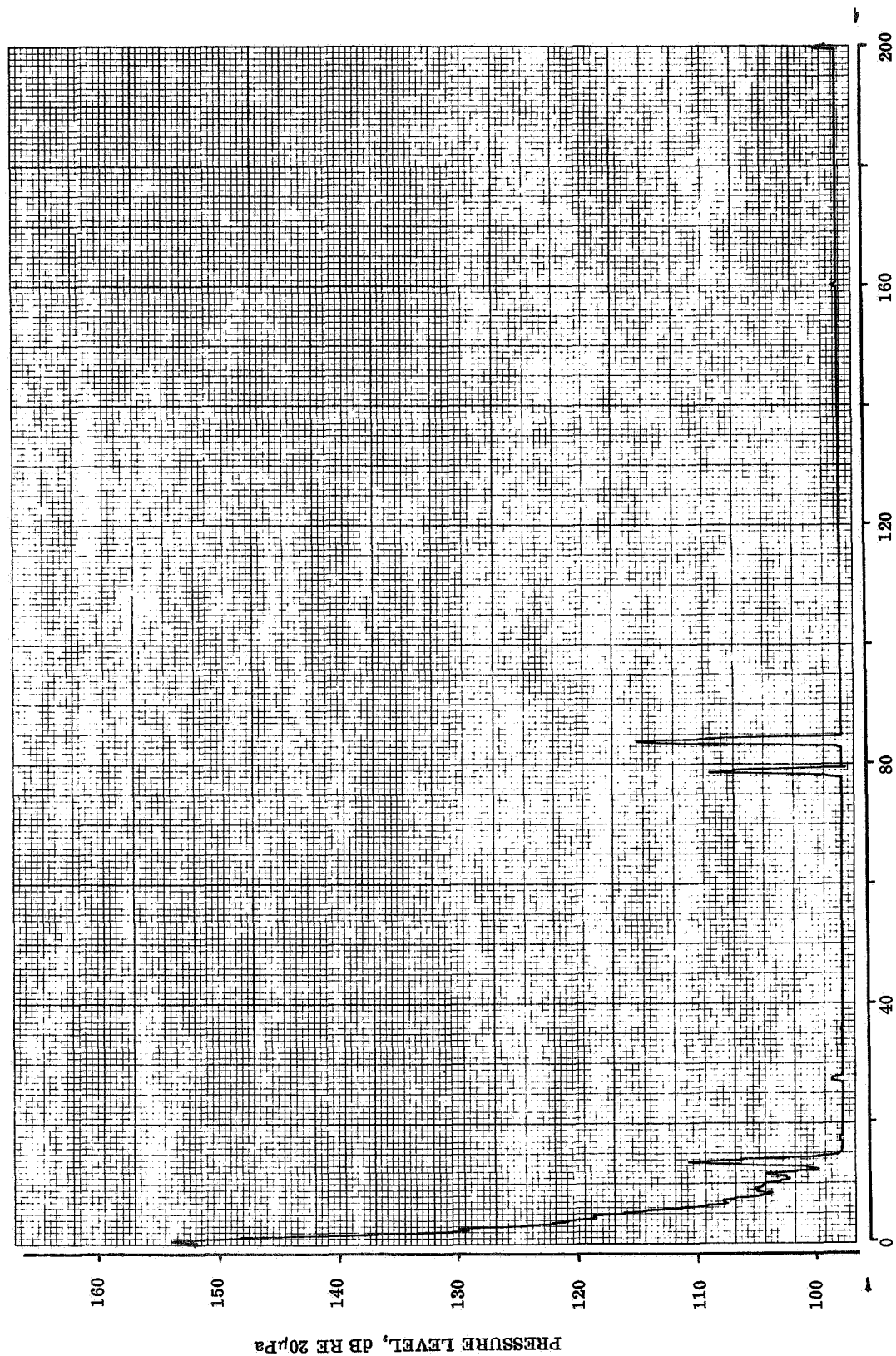
FLIGHT 8
RUN 16



HARMONICS OF PROPELLER ROTATION

TAPE CHANNEL 3
59 % RADIUS

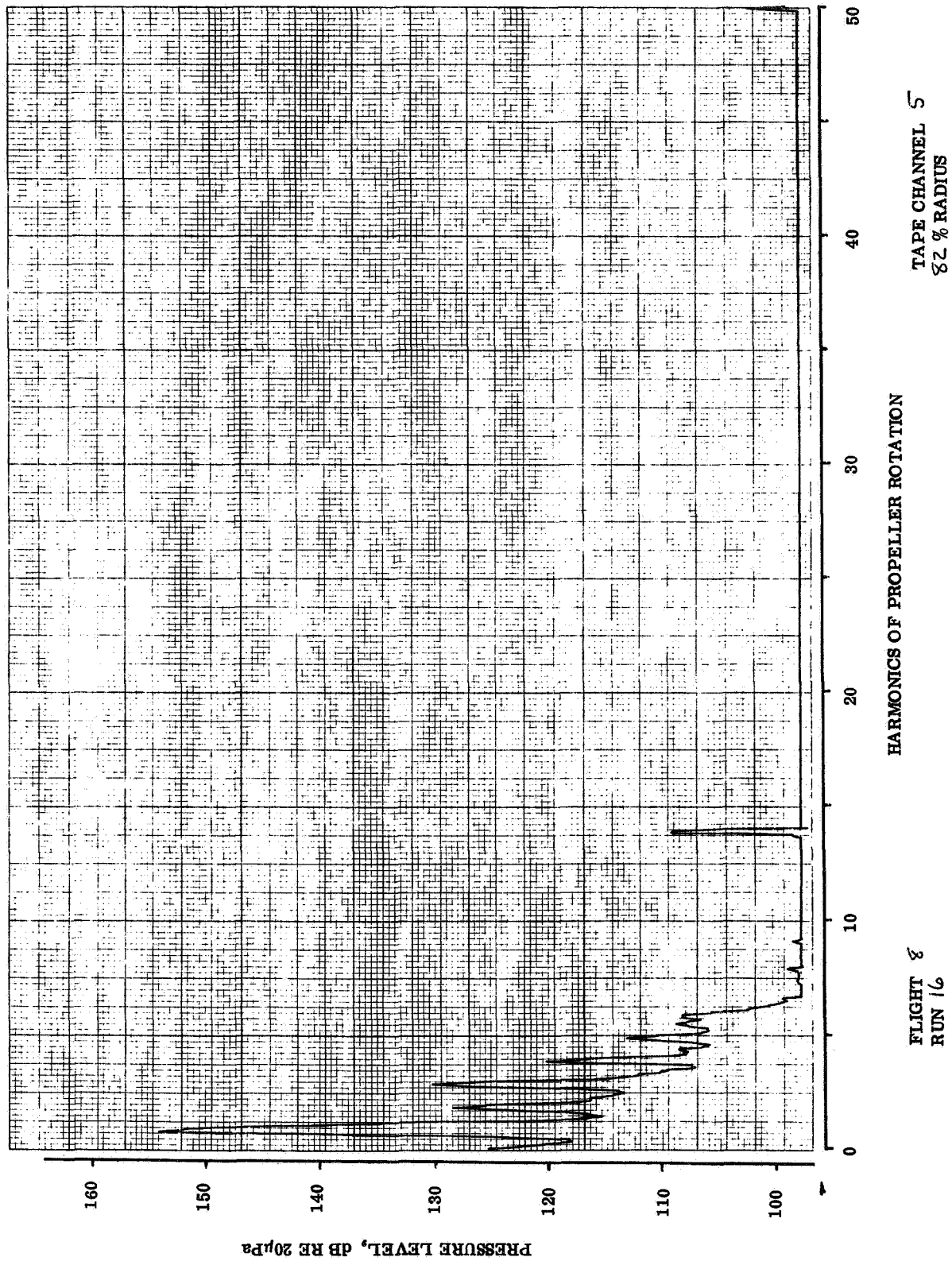
FLIGHT 8
RUN 16

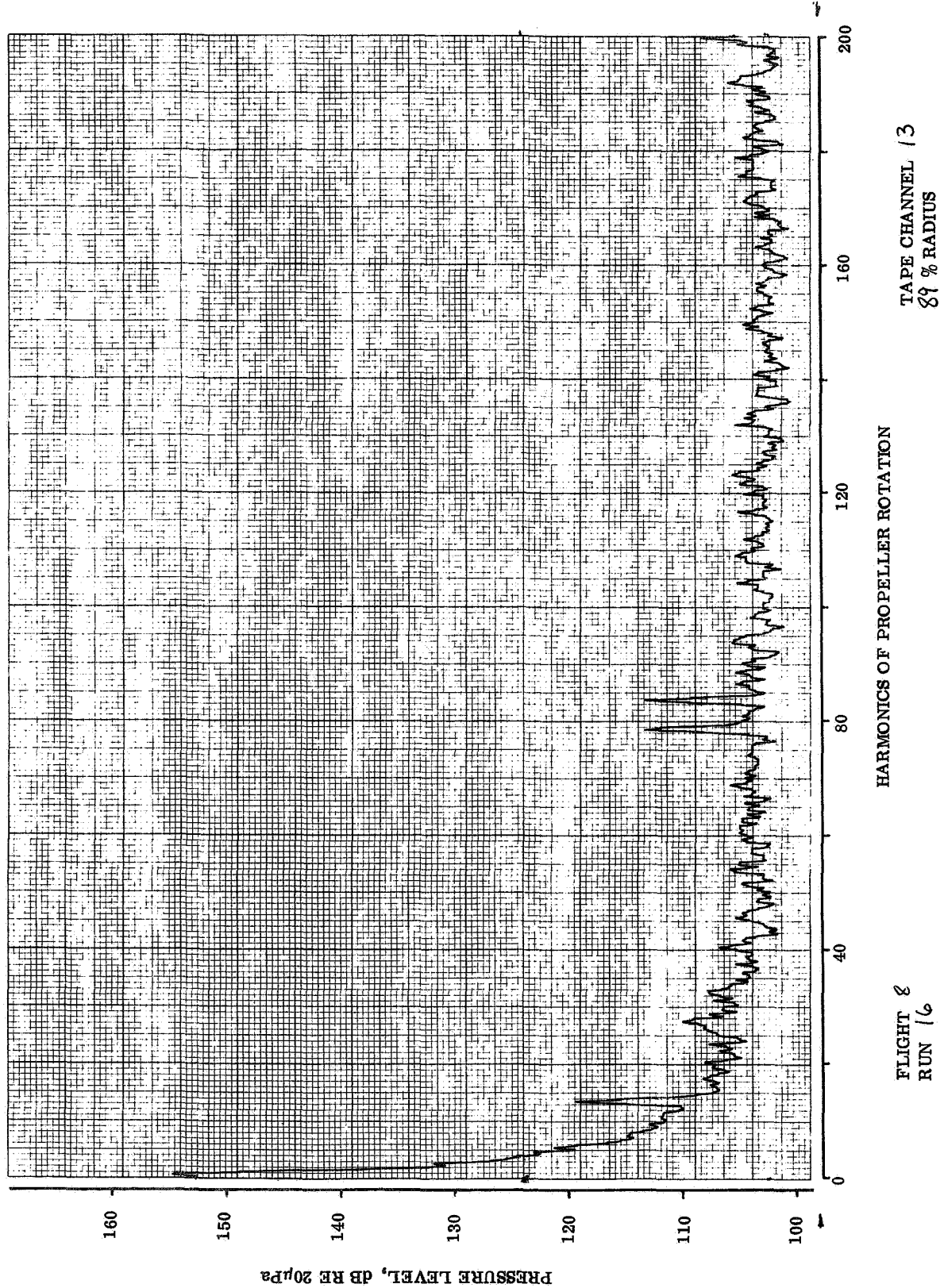


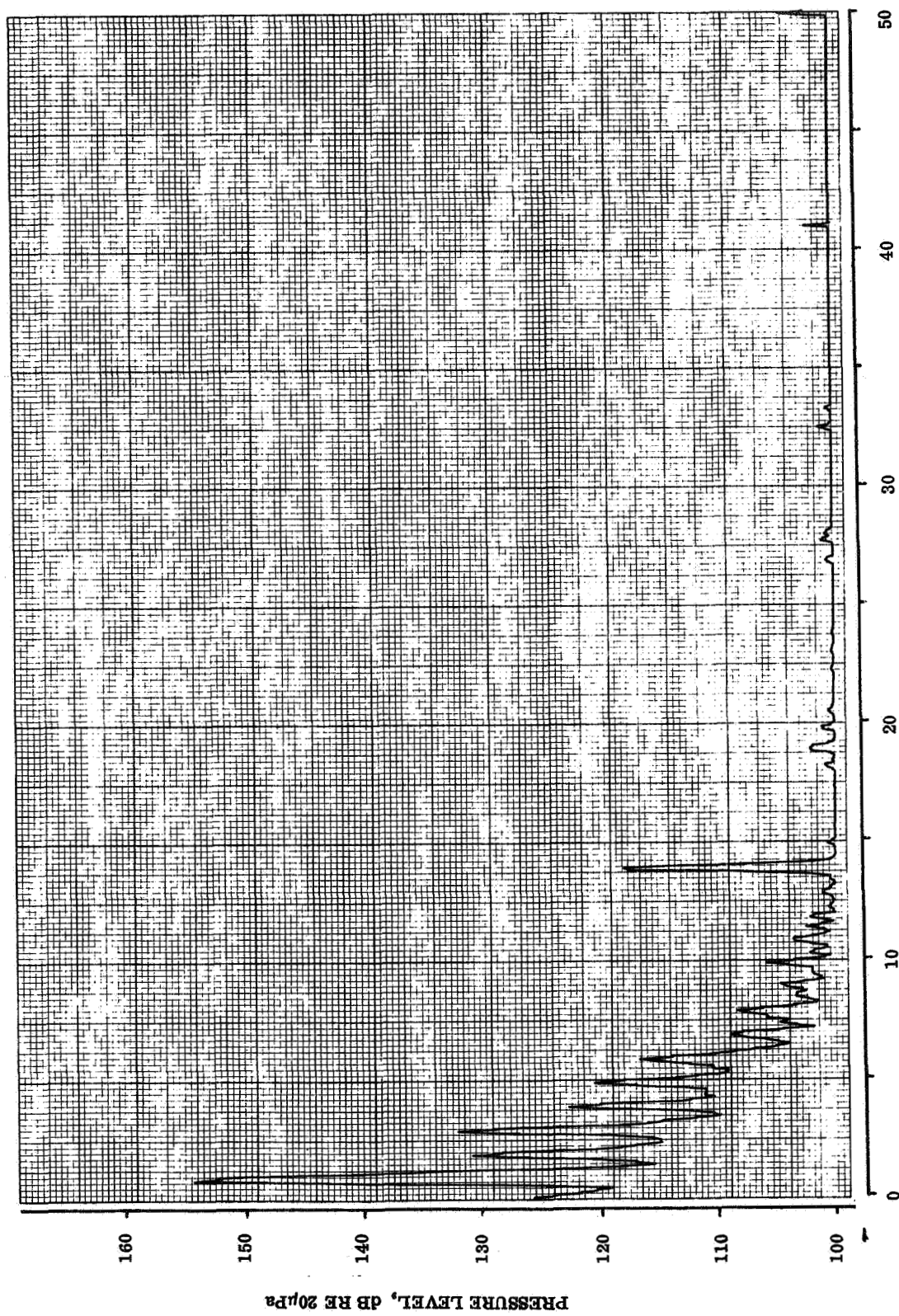
TAPE CHANNEL 5
82 % RADIUS

HARMONICS OF PROPELLER ROTATION

FLIGHT 8
RUN 16



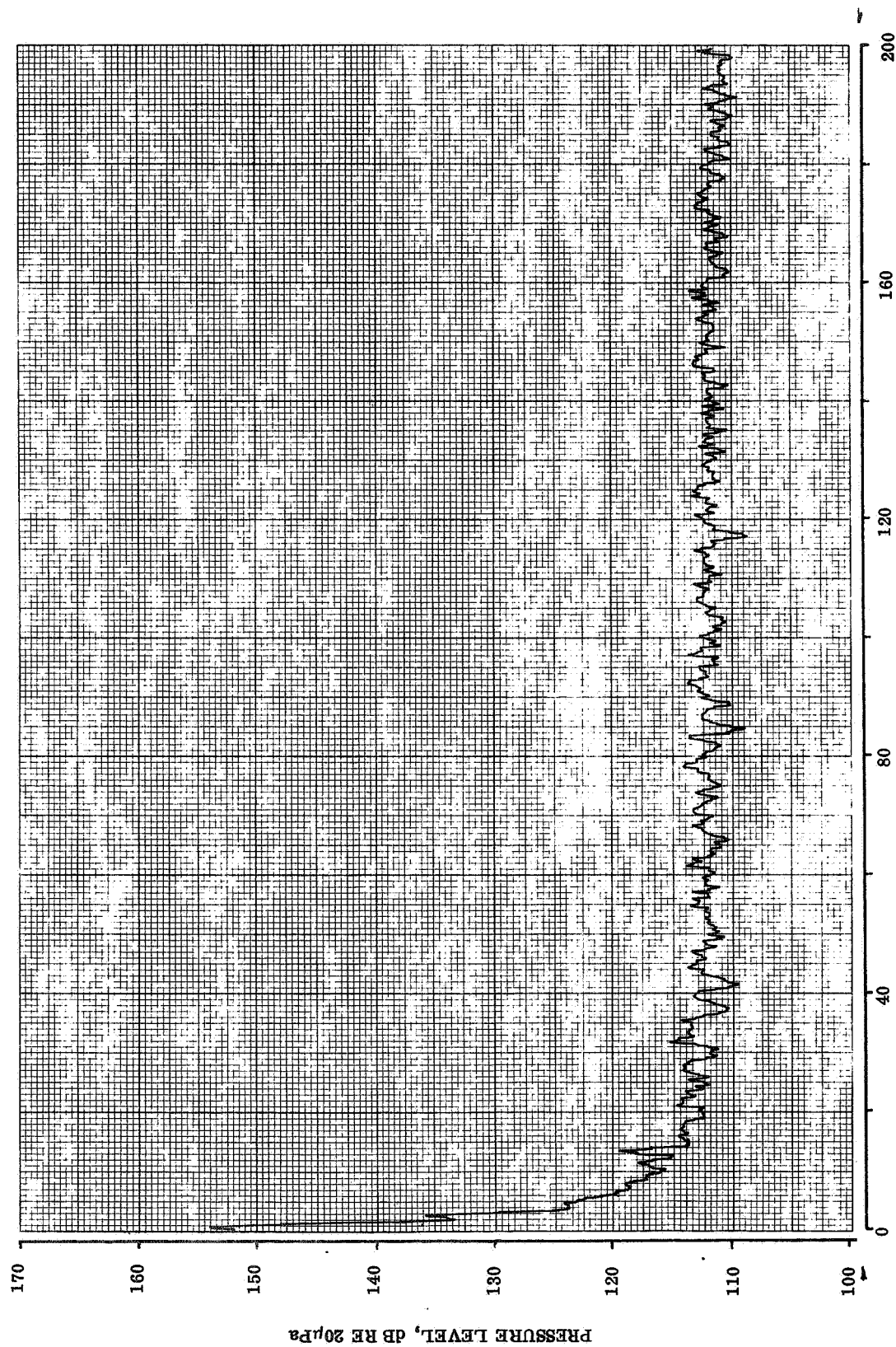




TAPE CHANNEL 13
89 % RADIUS

HARMONICS OF PROPELLER ROTATION

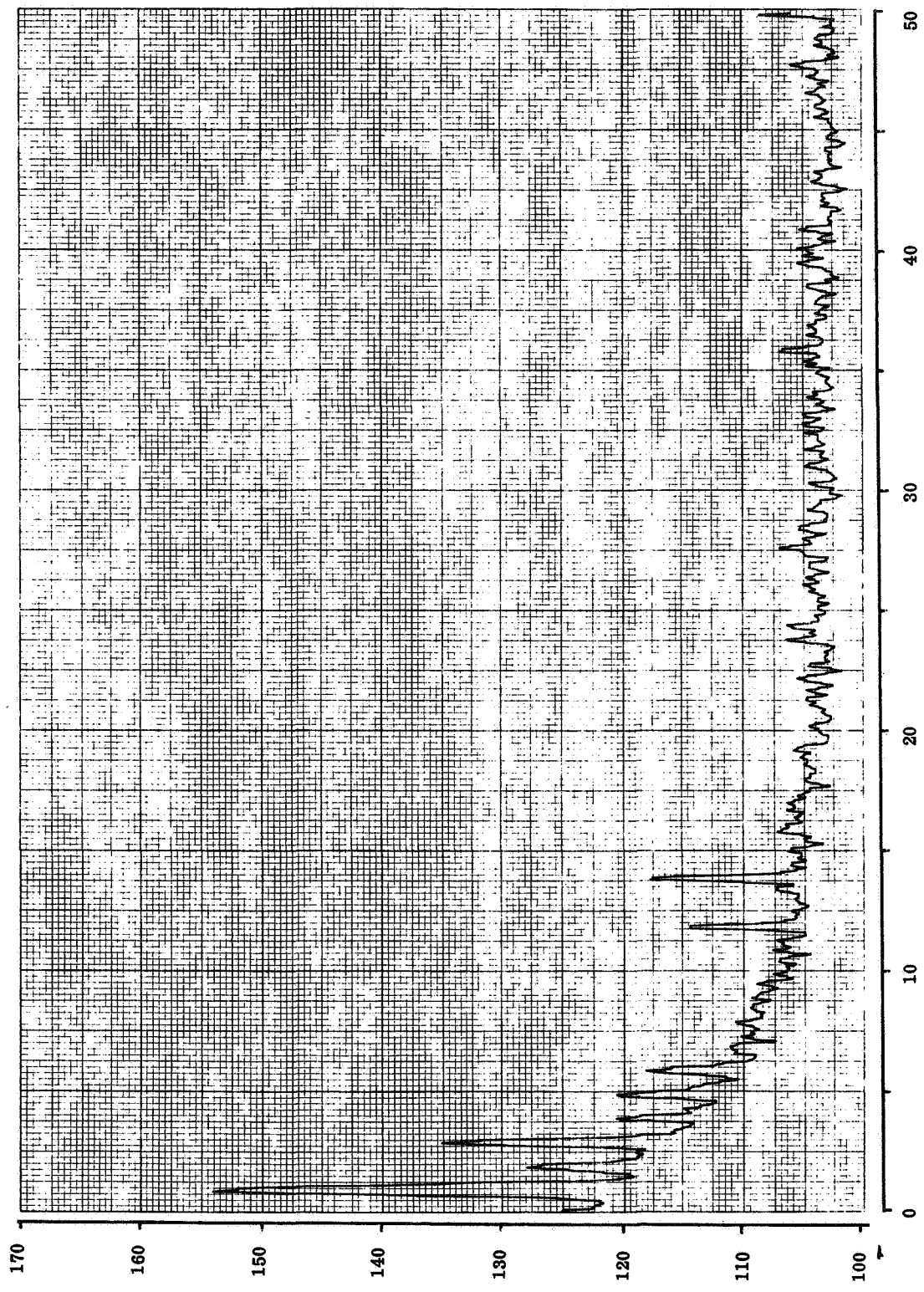
FLIGHT 8
RUN 16



TAPE CHANNEL 7
94 % RADIUS L.E.

HARMONICS OF PROPELLER ROTATION

FLIGHT 8
RUN 16

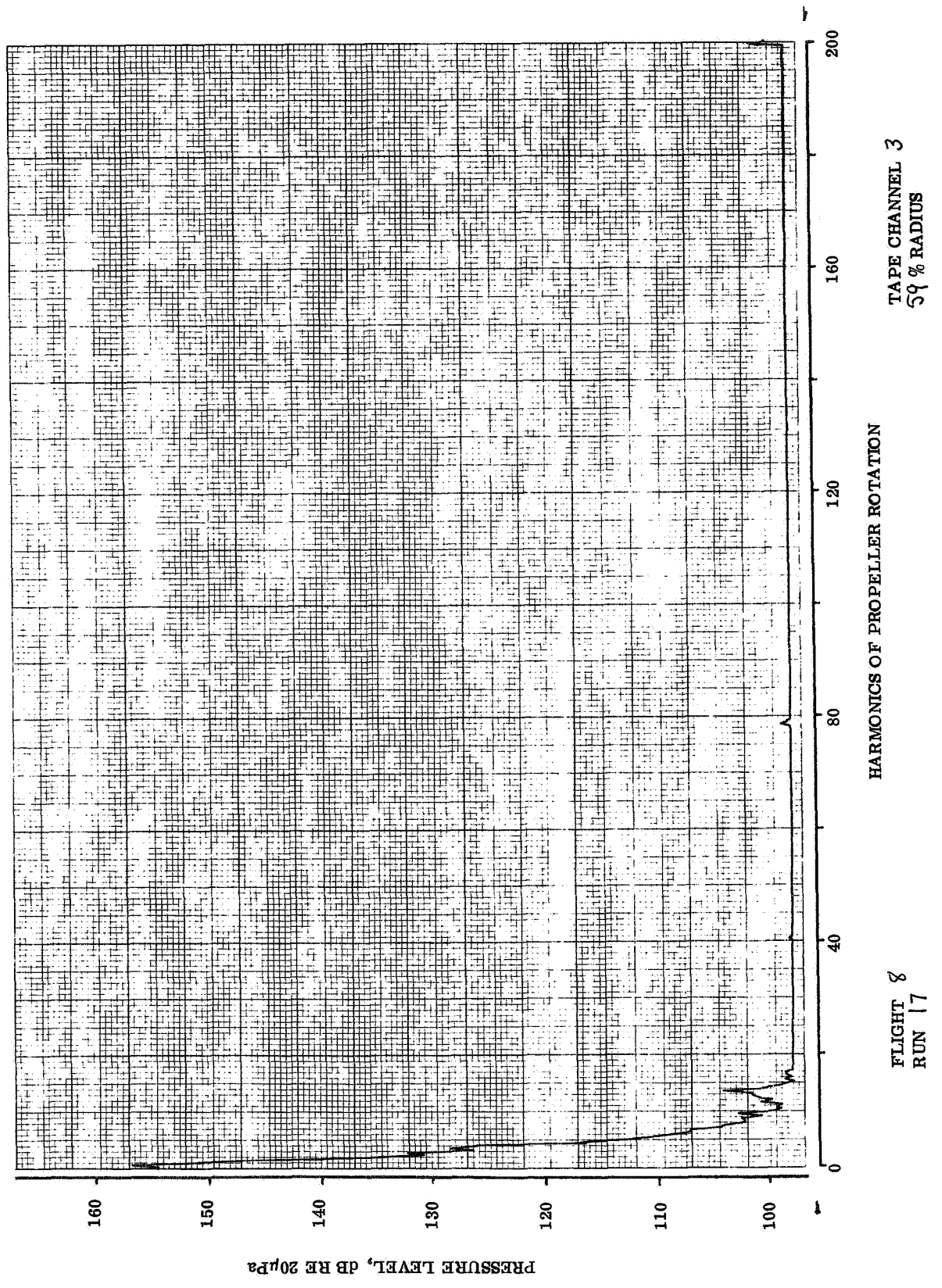


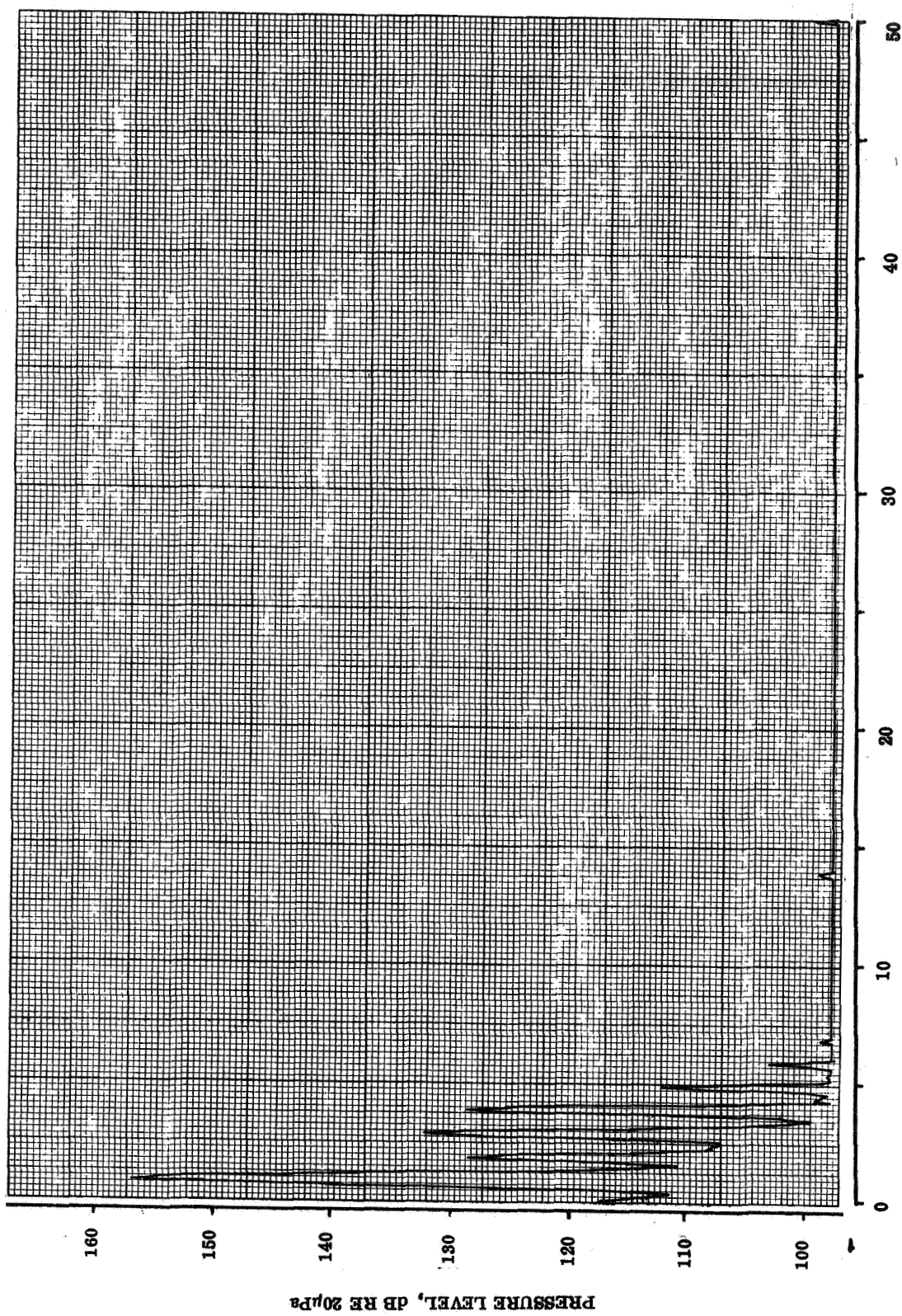
HARMONICS OF PROPELLER ROTATION

TAPE CHANNEL 7
94 % RADIUS L.E.

FLIGHT 8
RUN 16

PRESSURE LEVEL, DB RE 20 μ Pa

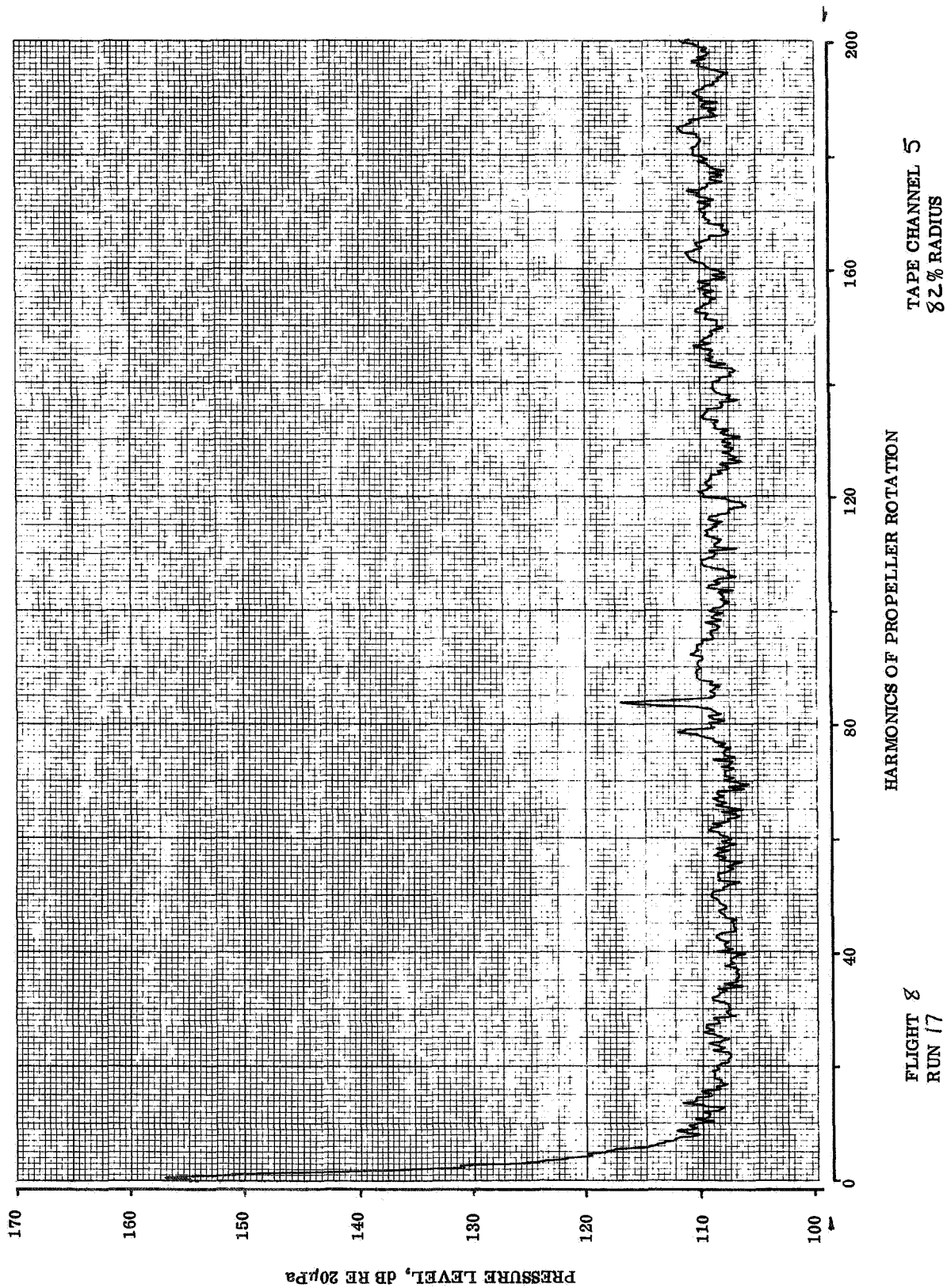


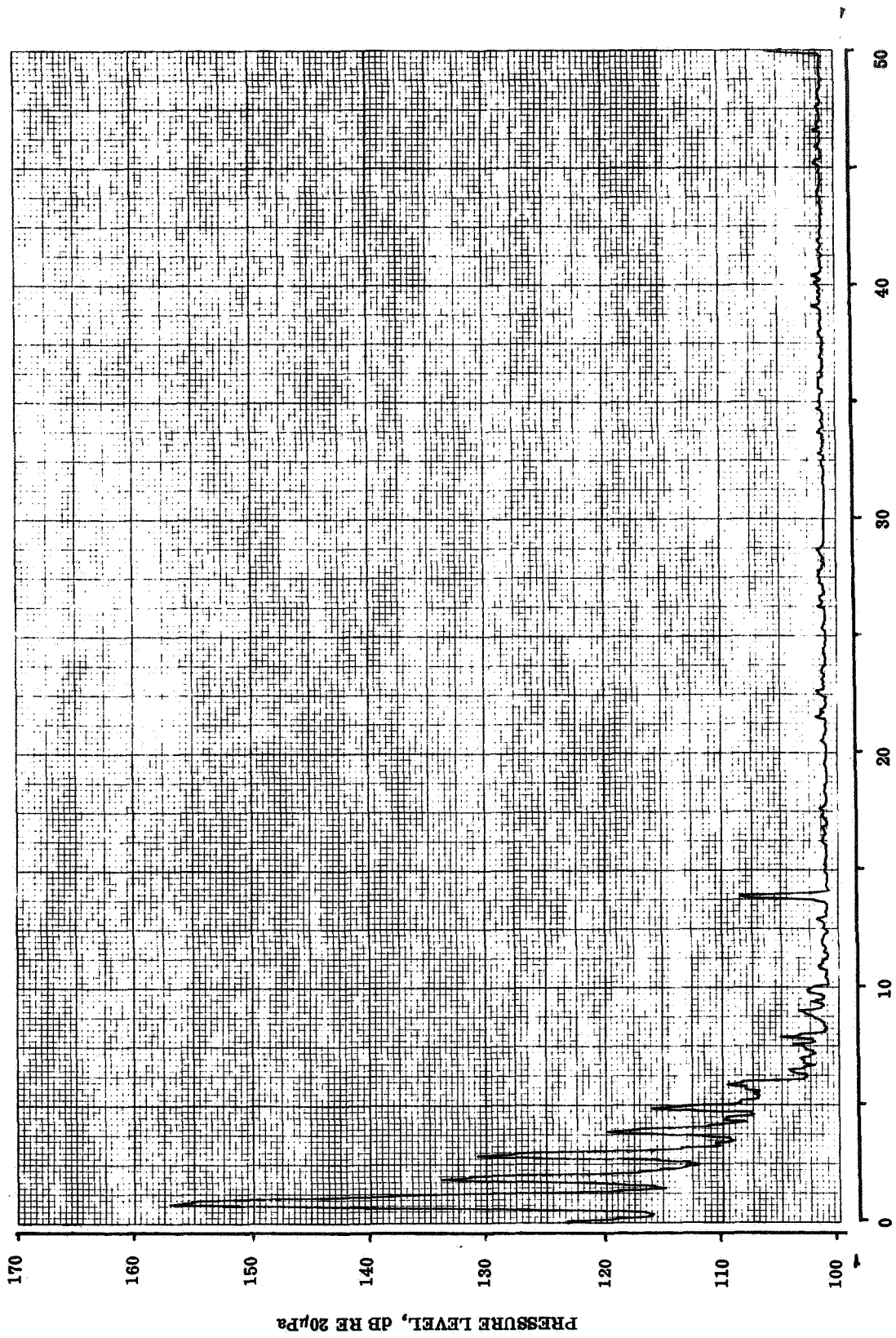


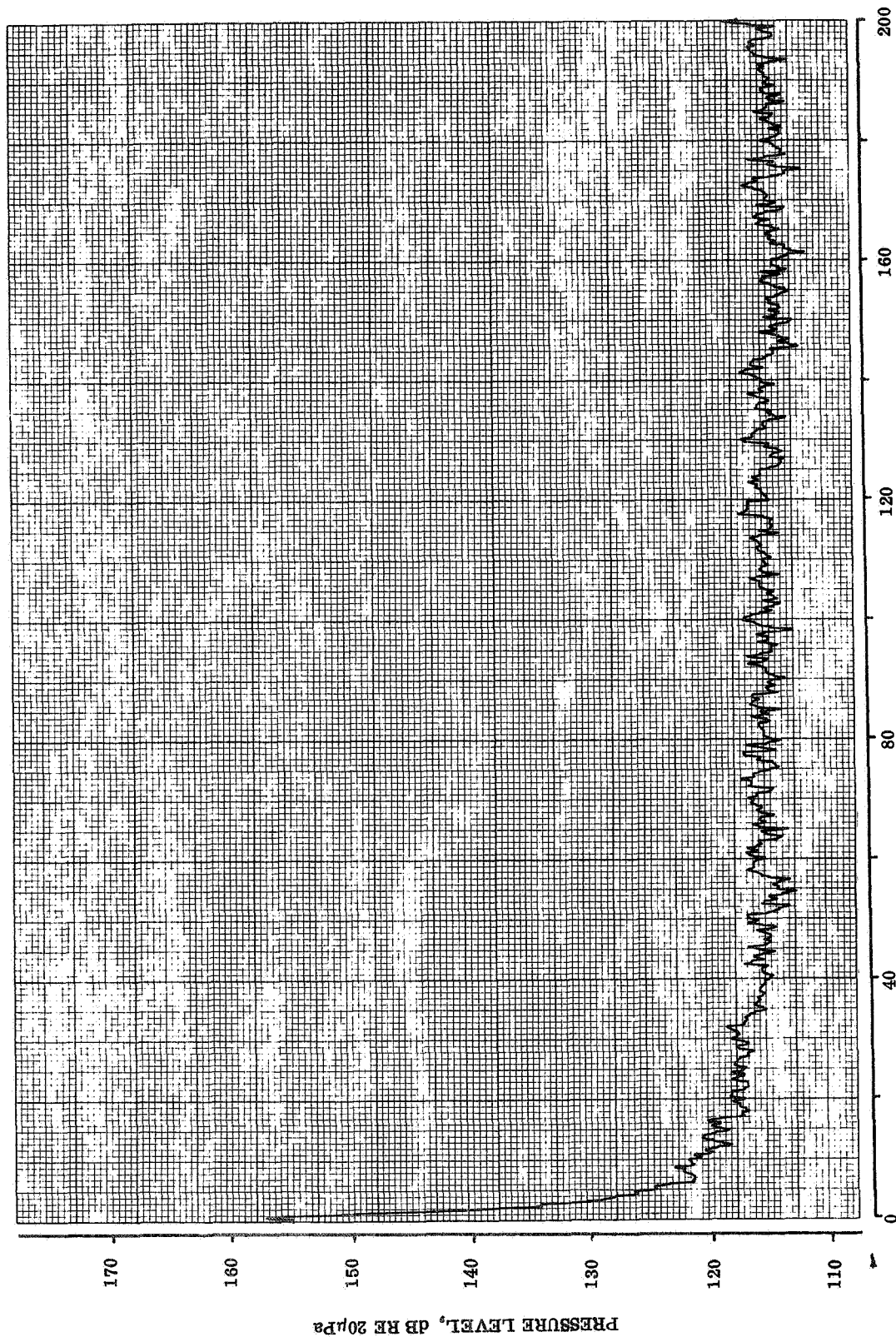
FLIGHT 8
 RUN 17

HARMONICS OF PROPELLER ROTATION

TAPE CHANNEL 3
 59 % RADIUS





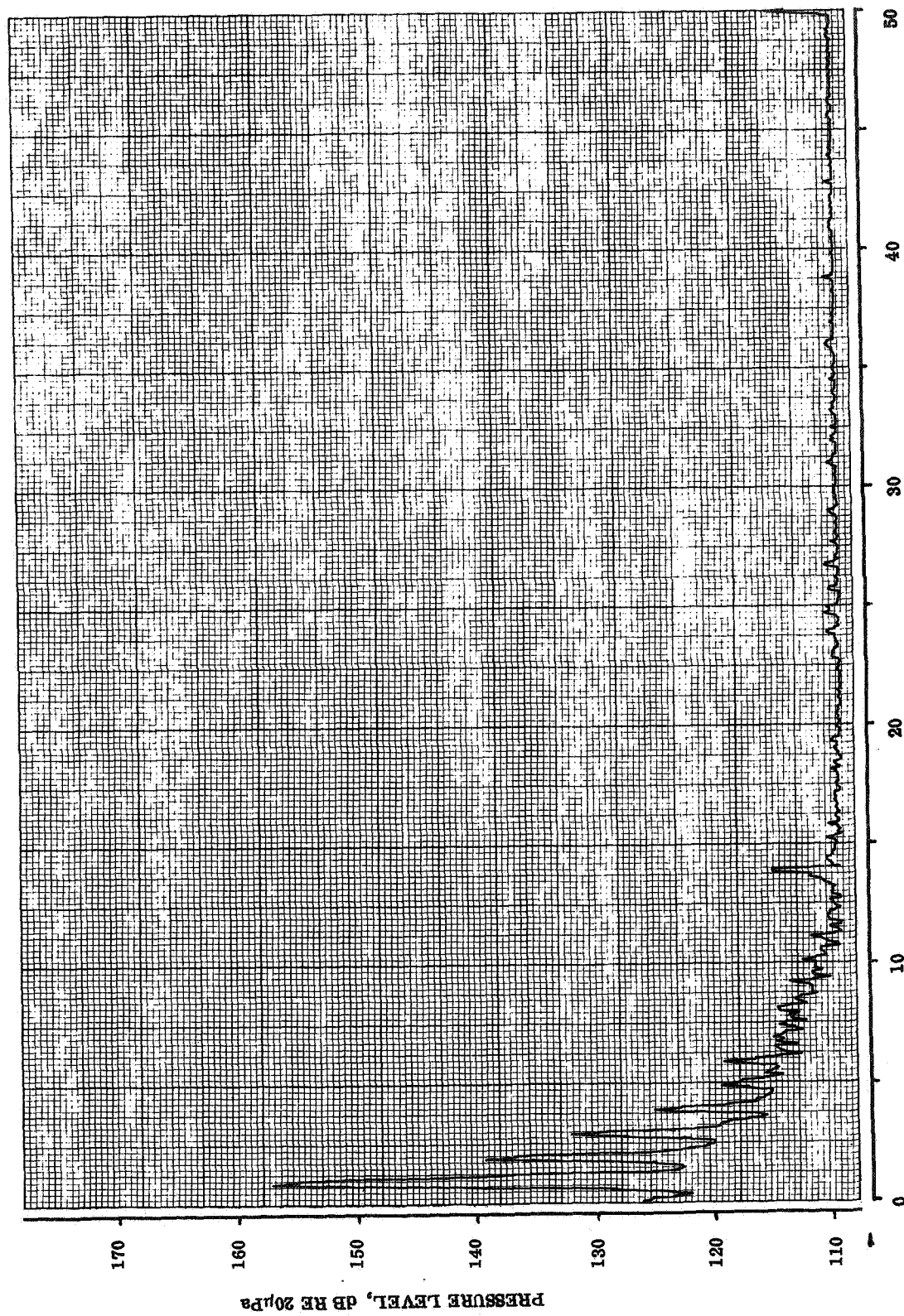


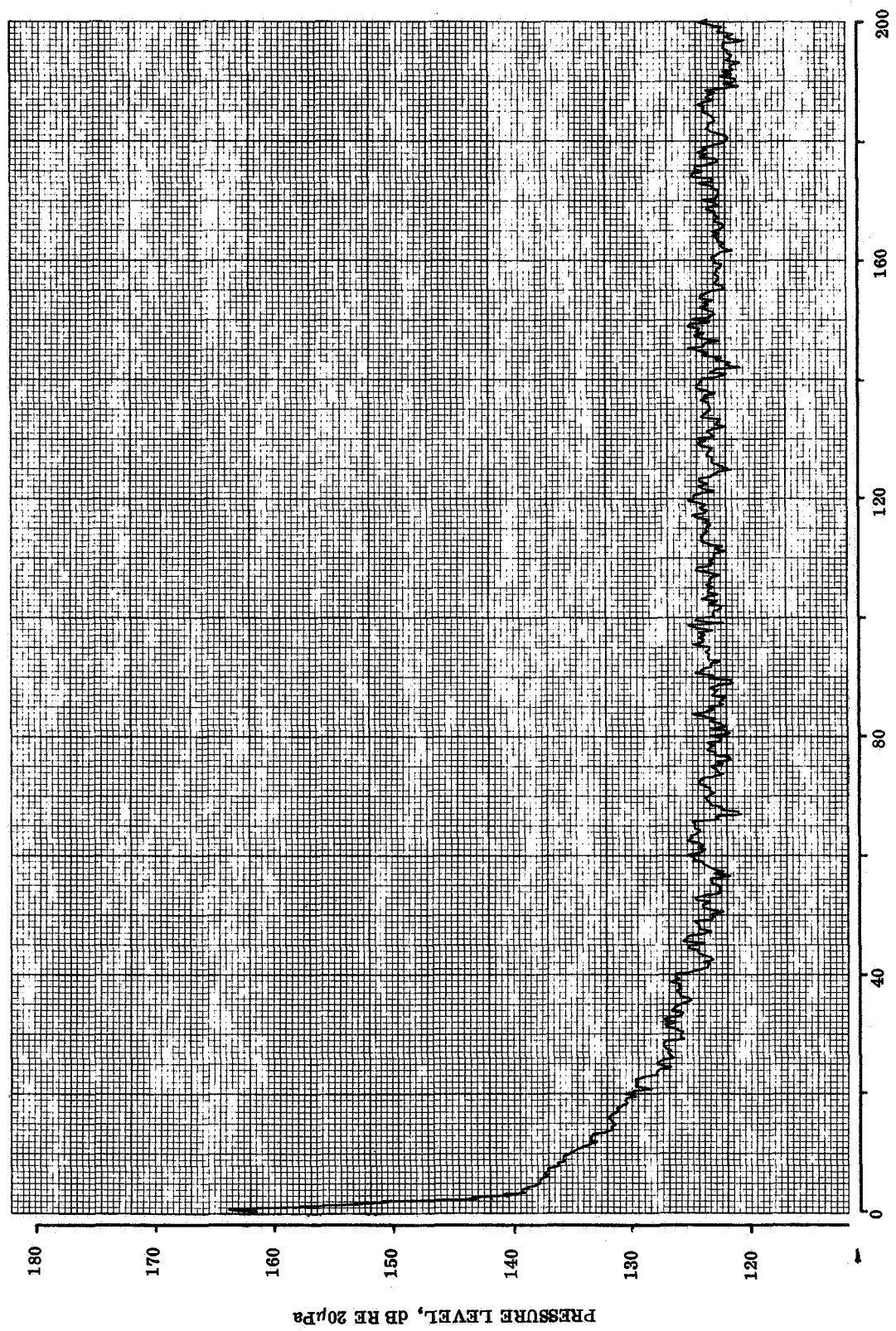
HARMONICS OF PROPELLER ROTATION

TAPE CHANNEL 13
89% RADIUS

FLIGHT 8
RUN 17

PRESSURE LEVEL, DB RE 20μPa

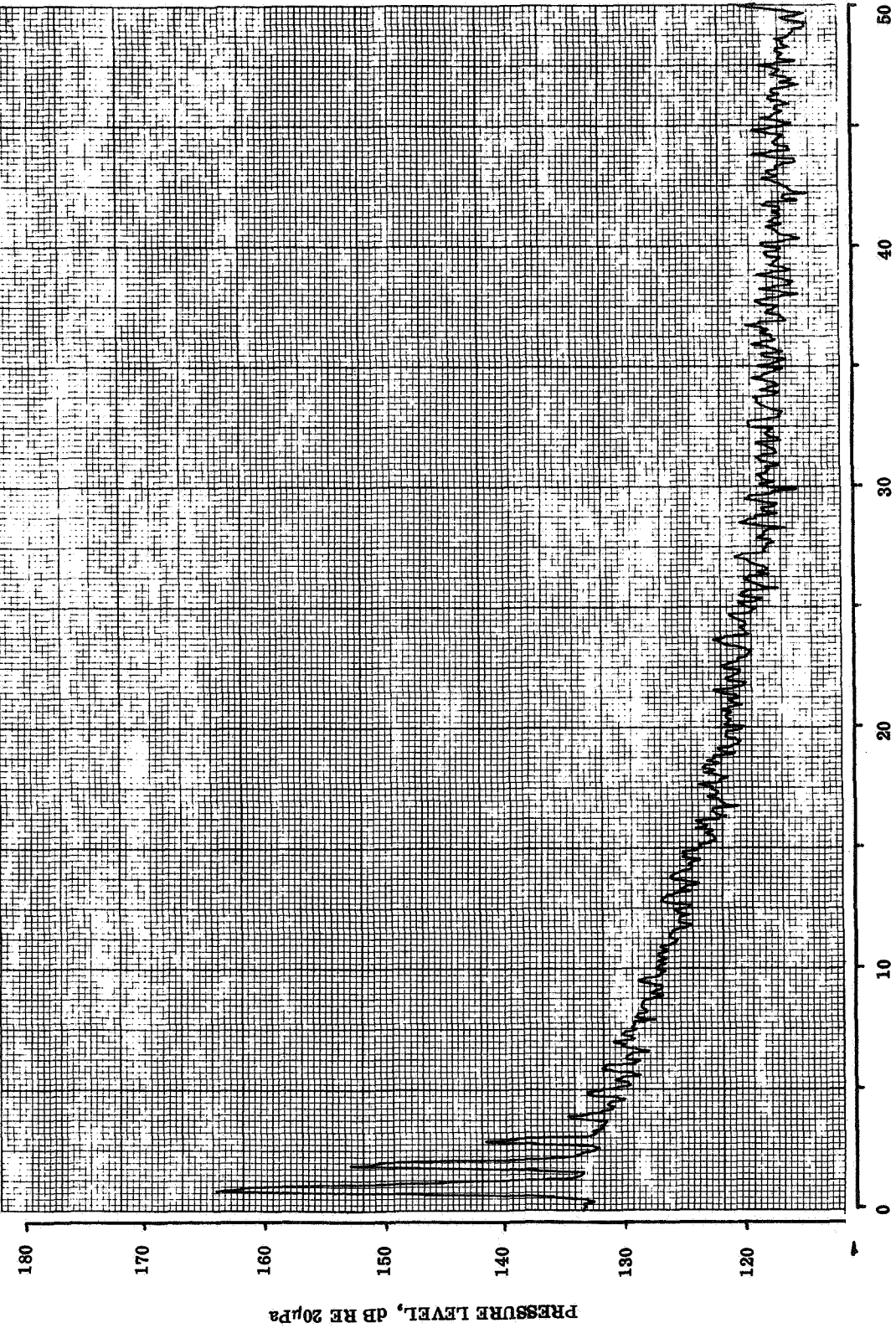




TAPE CHANNEL 7
94 % RADIUS L-ε.

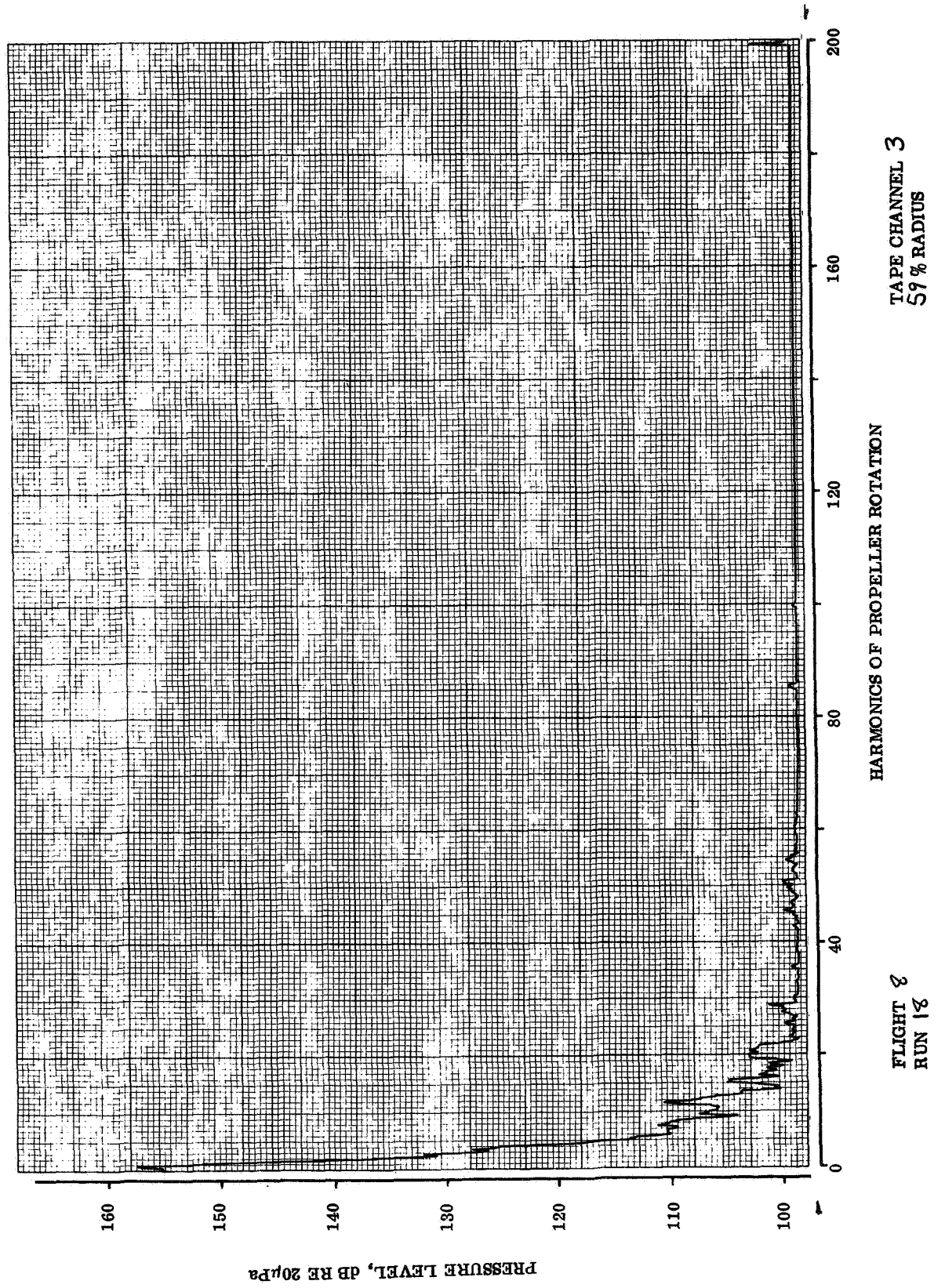
HARMONICS OF PROPELLER ROTATION

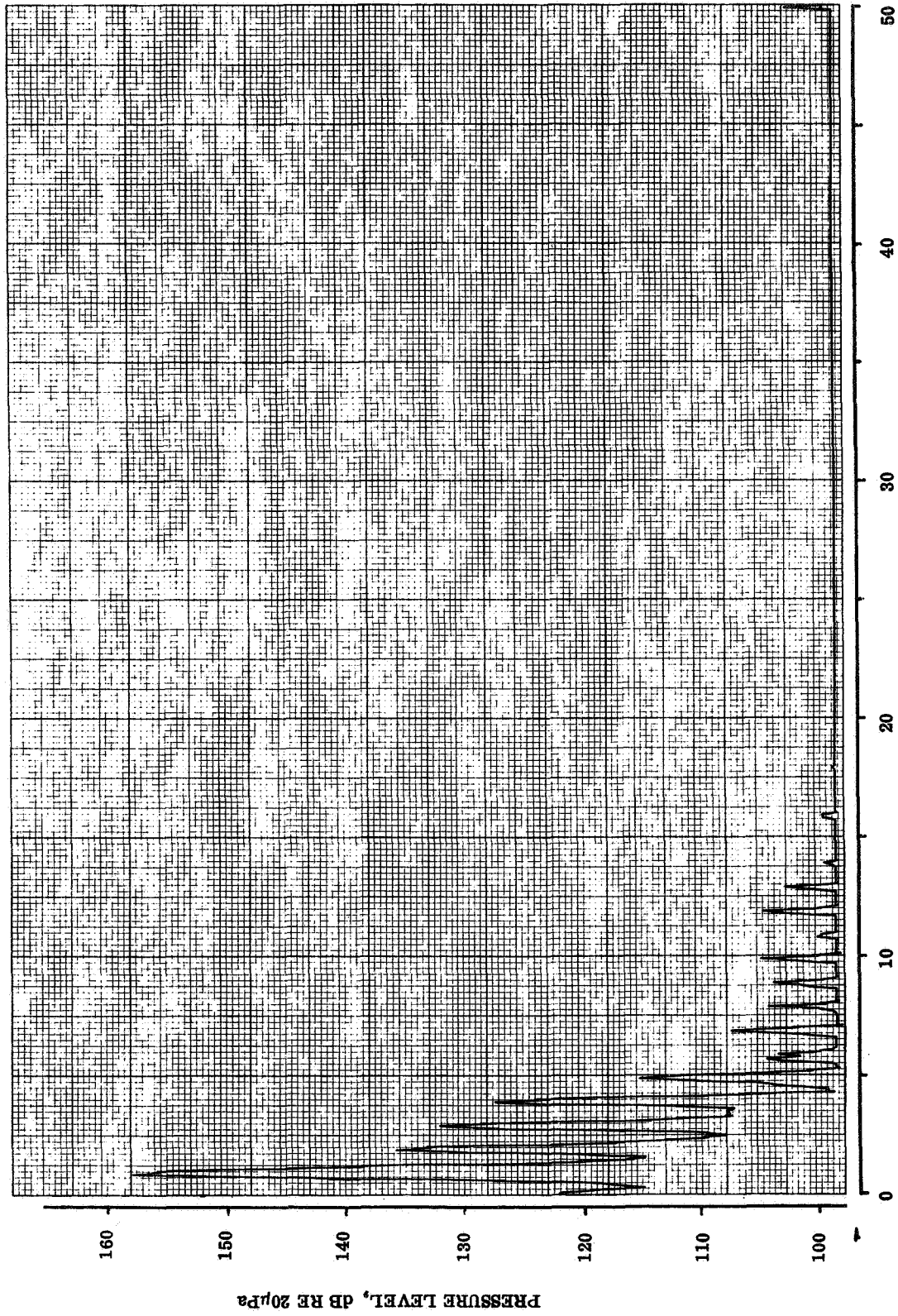
FLIGHT 8
RUN 17



FLIGHT 8
RUN 17

TAPE CHANNEL 7
94 % RADIUS L.E.

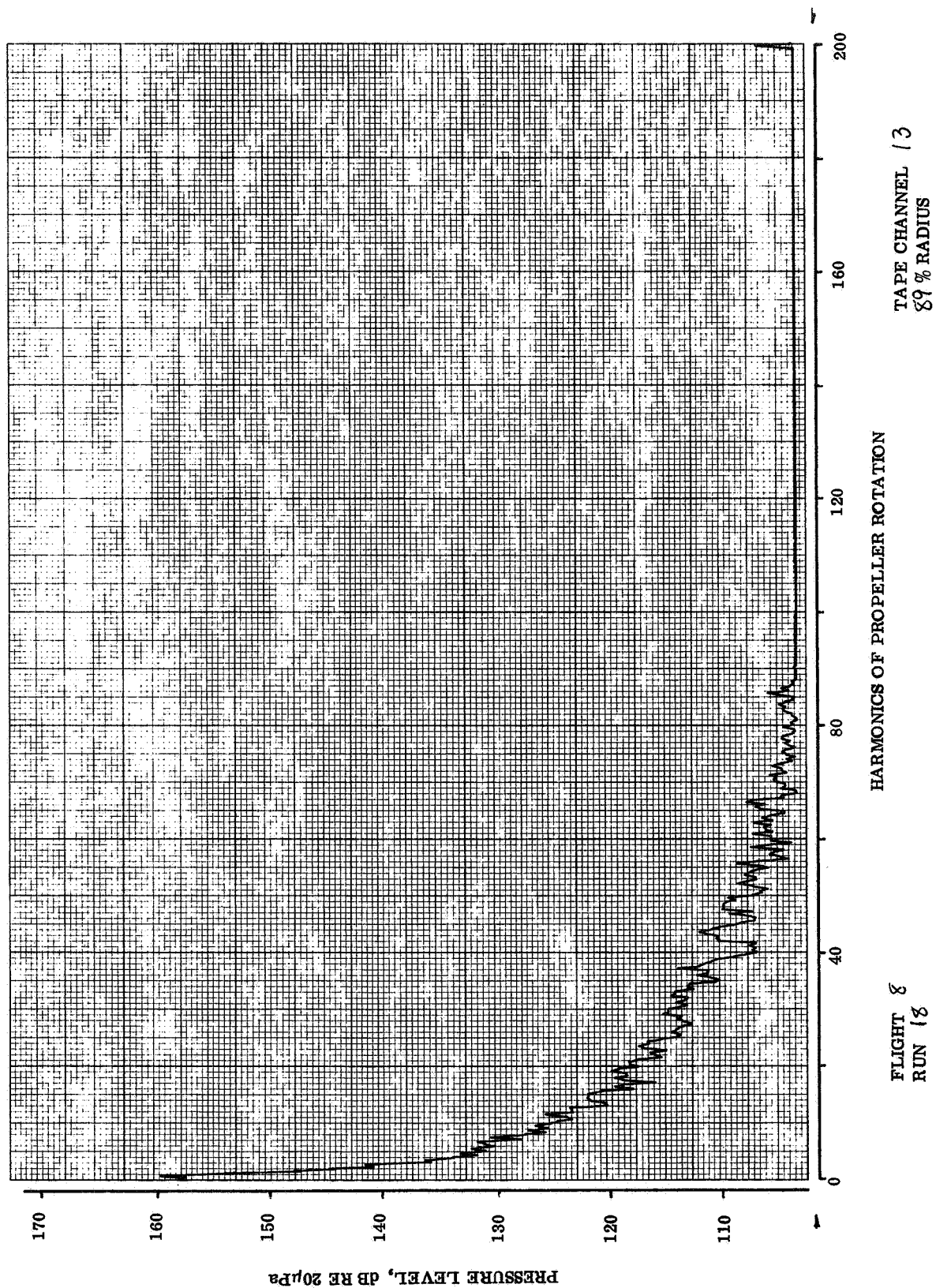


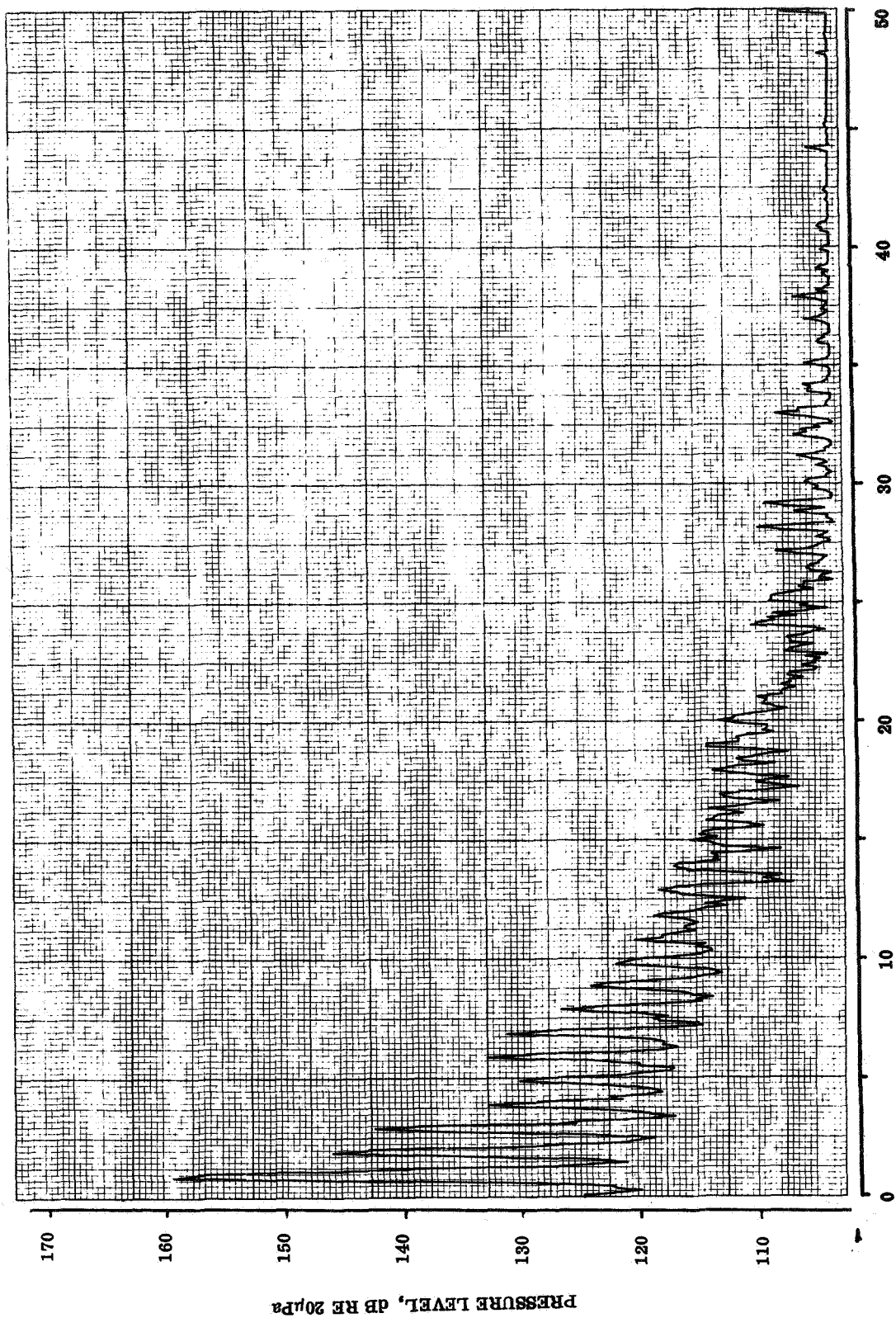


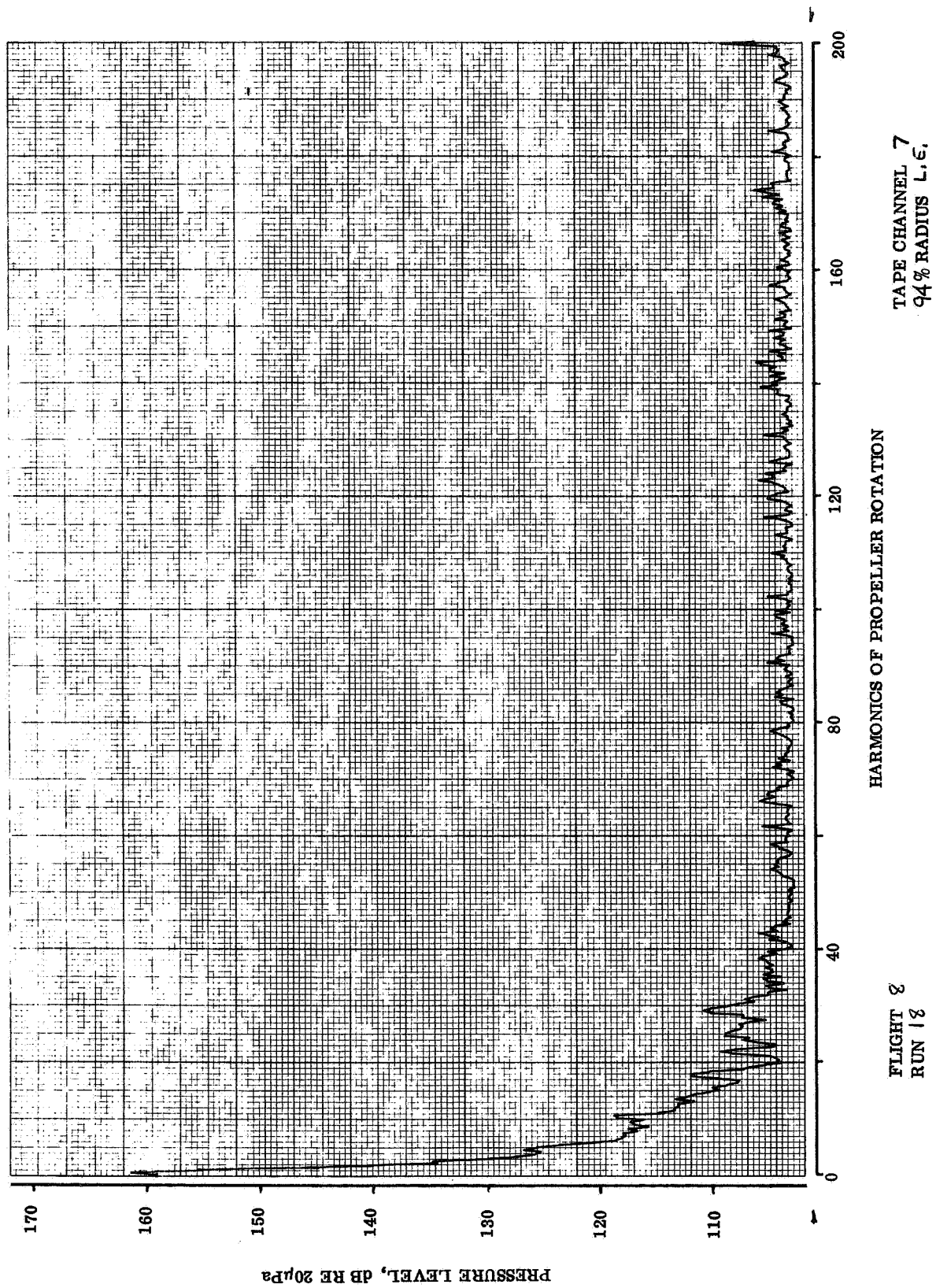
TAPE CHANNEL 3
59% RADIUS

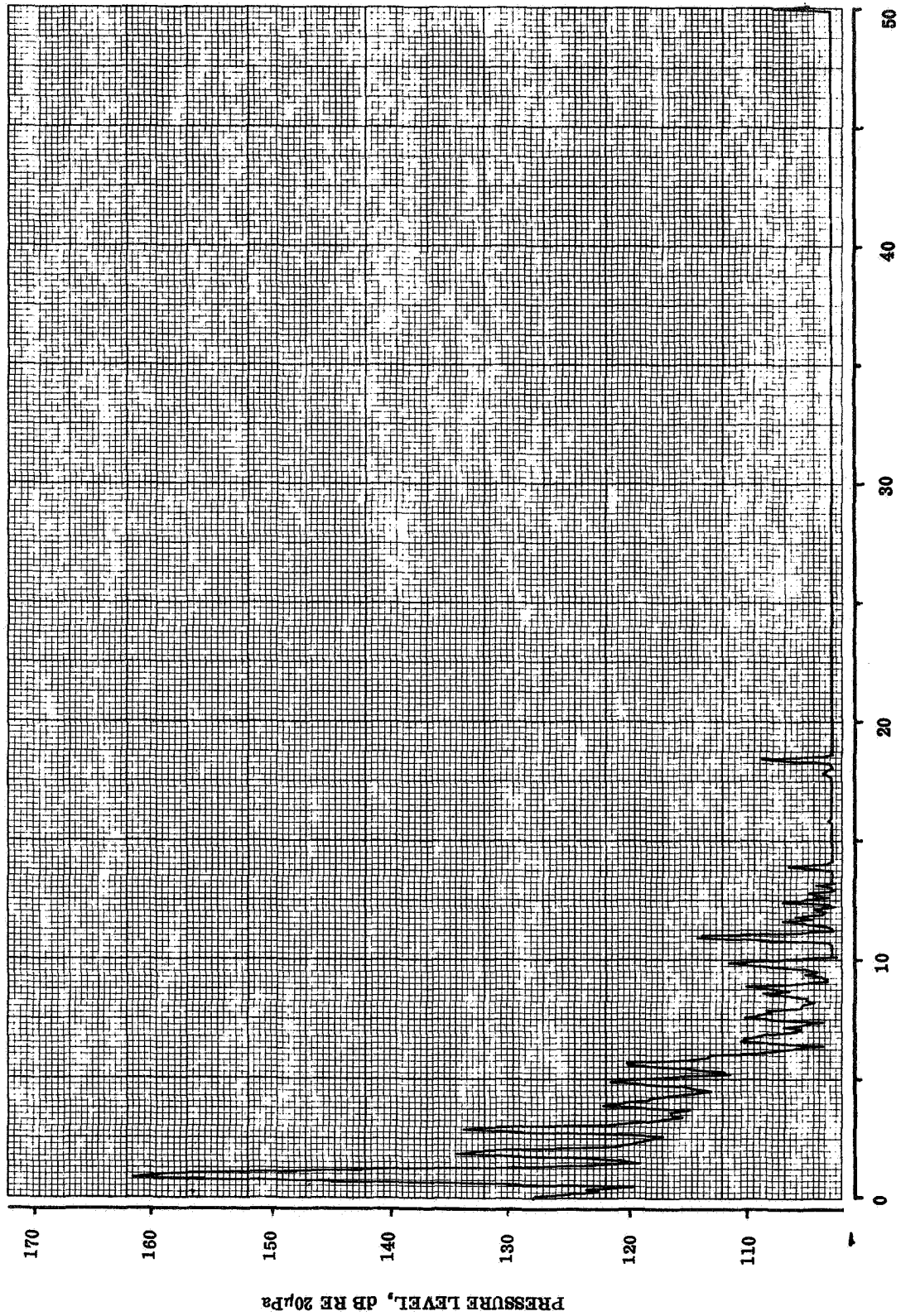
HARMONICS OF PROPELLER ROTATION

FLIGHT 8
RUN 18









FLIGHT 8
 RUN 18

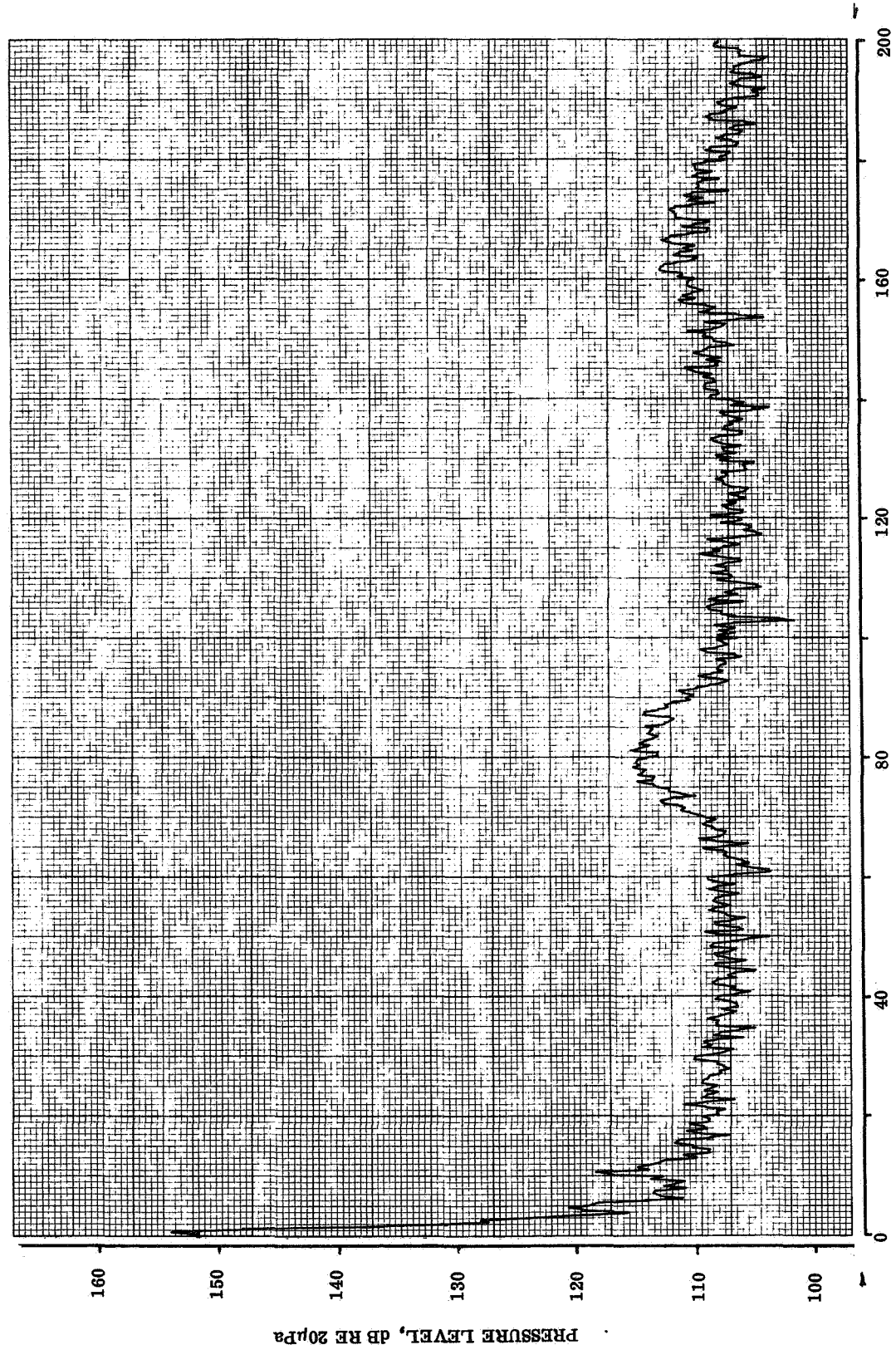
HARMONICS OF PROPELLER ROTATION

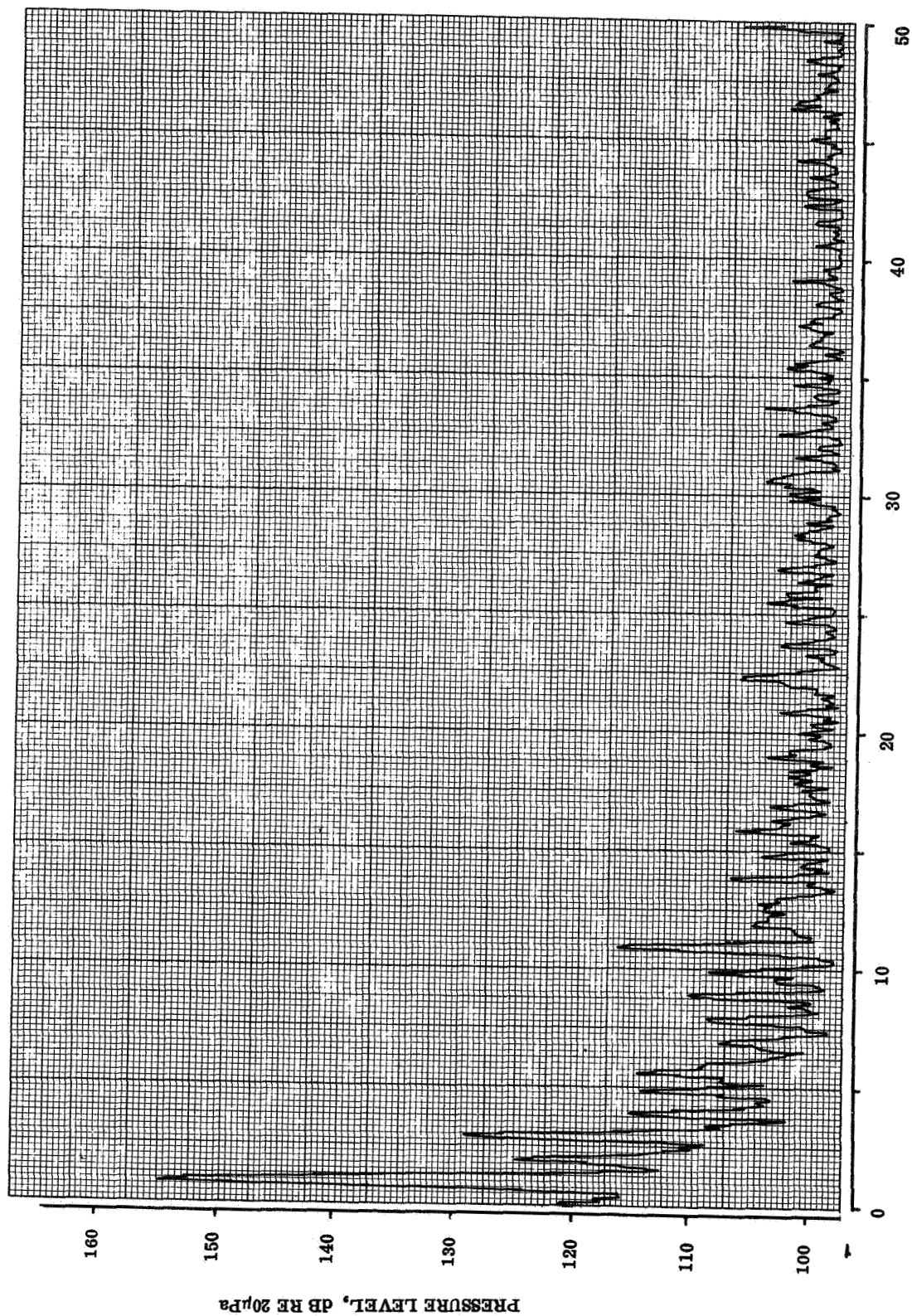
TAPE CHANNEL 7
 94 % RADIUS L.E.

TAPE CHANNEL 9
94% RADIUS T.E.

HARMONICS OF PROPELLER ROTATION

FLIGHT 8
RUN 18

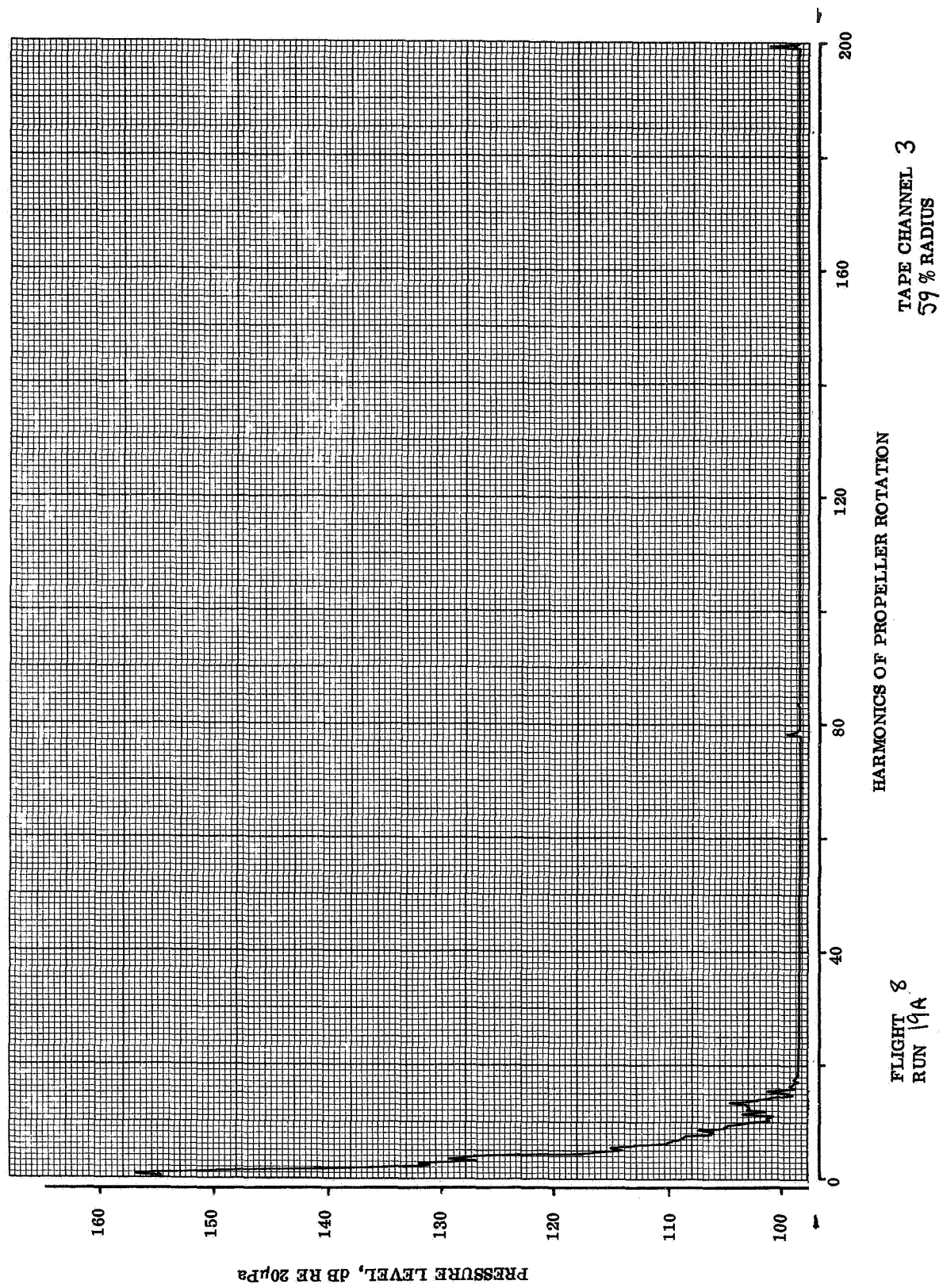


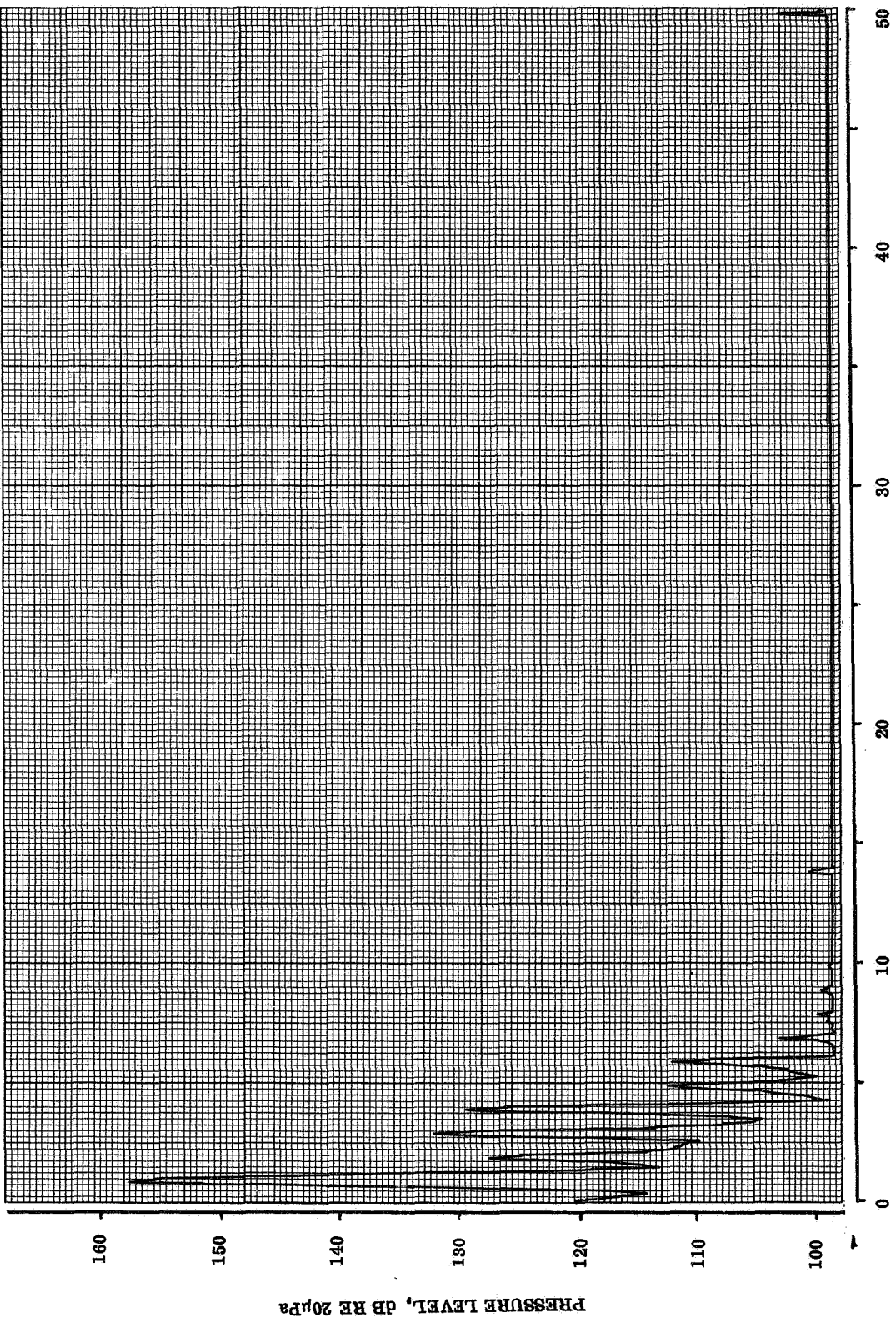


FLIGHT 8
 RUN 18

HARMONICS OF PROPELLER ROTATION

TAPE CHANNEL 9
 94 % RADIUS T.C.

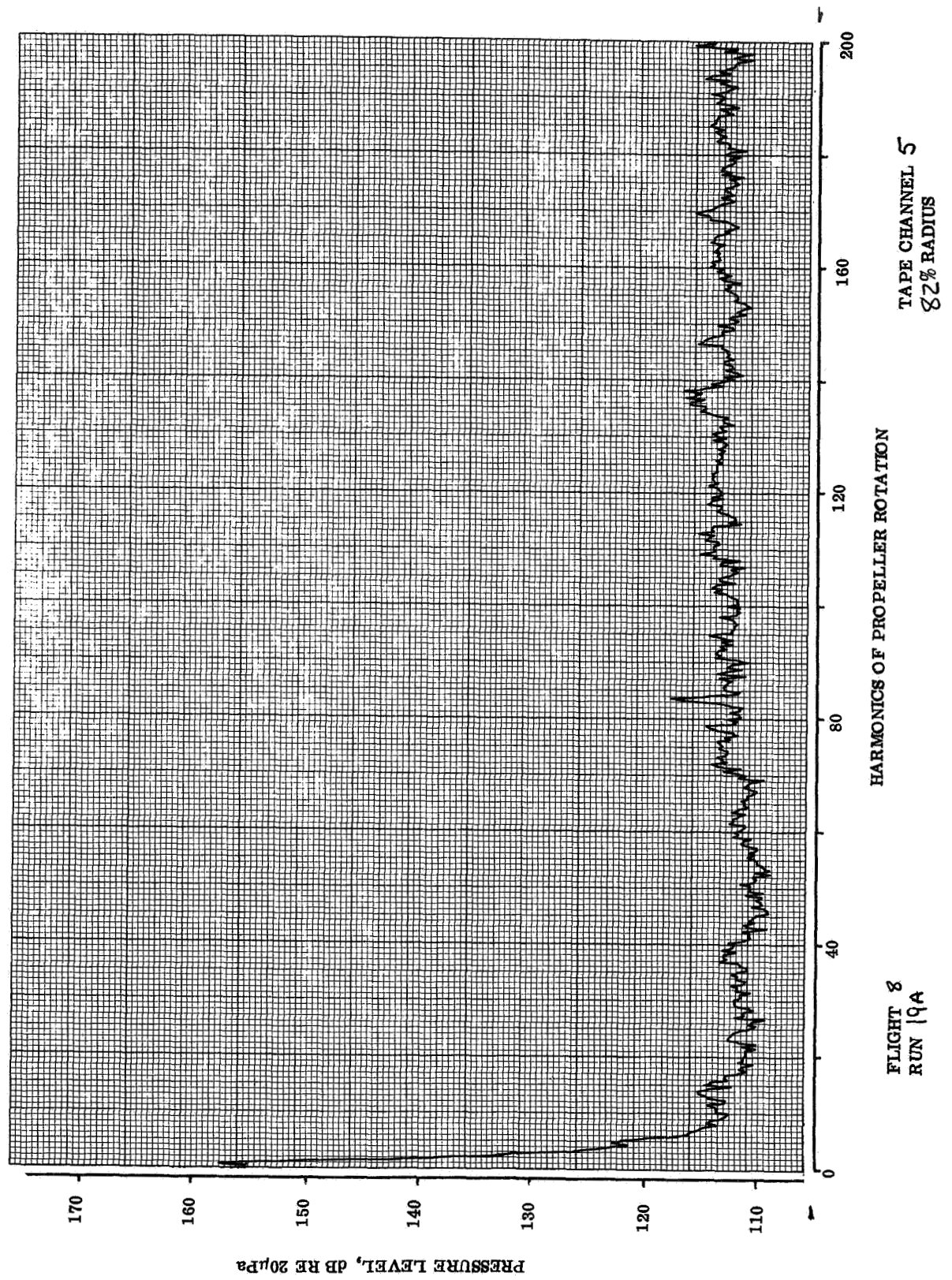


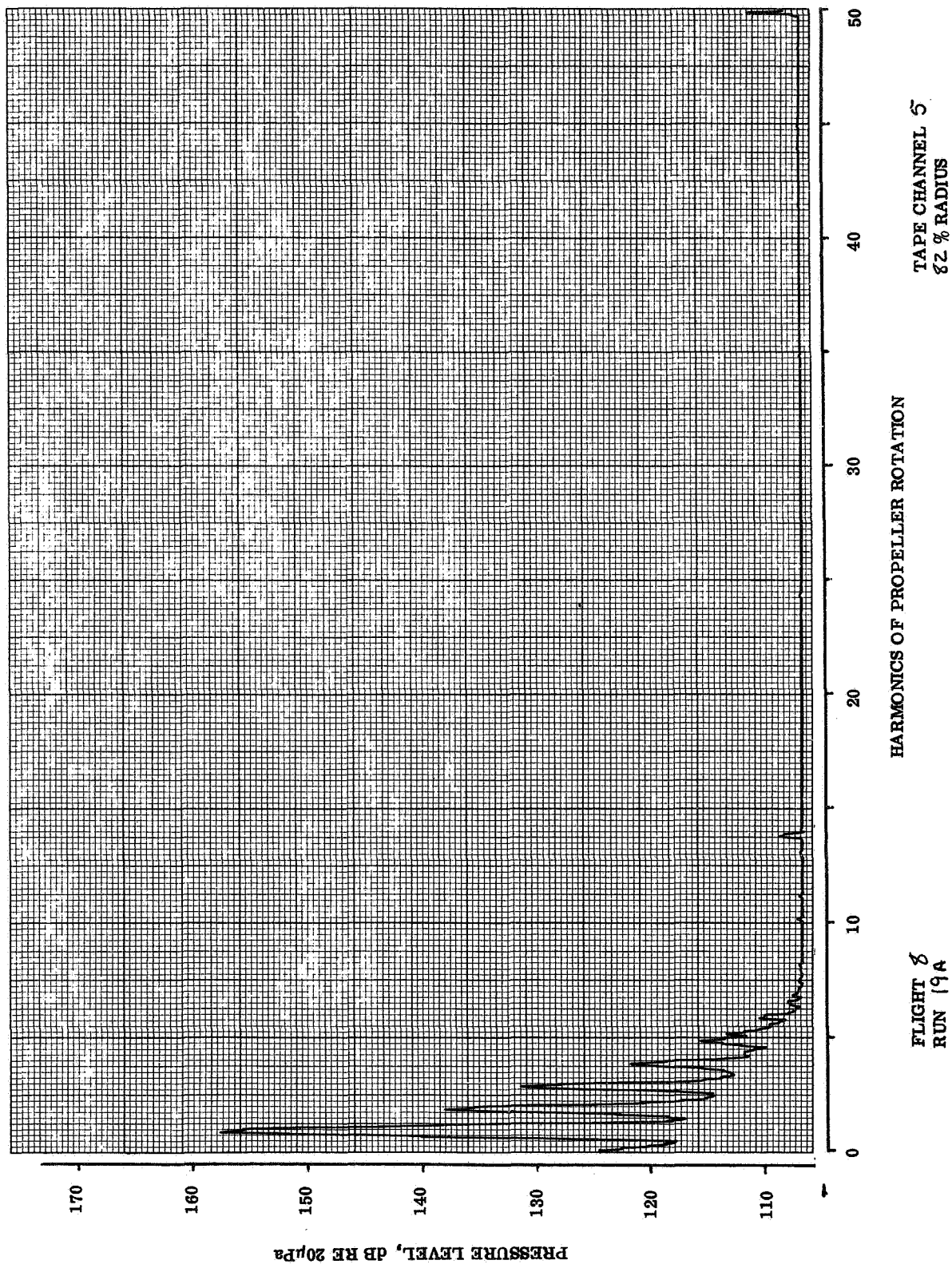


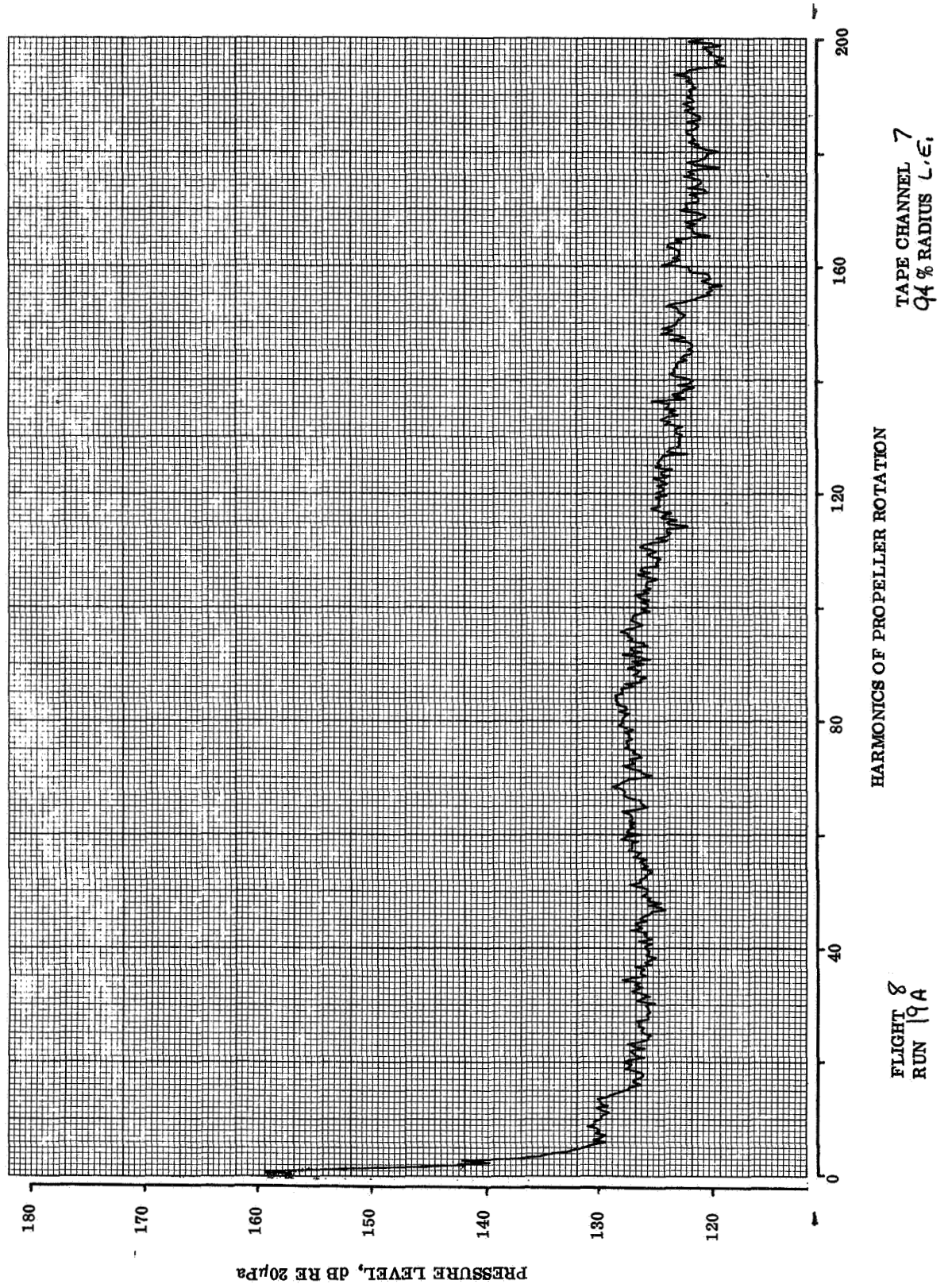
TAPE CHANNEL 3
59% RADIUS

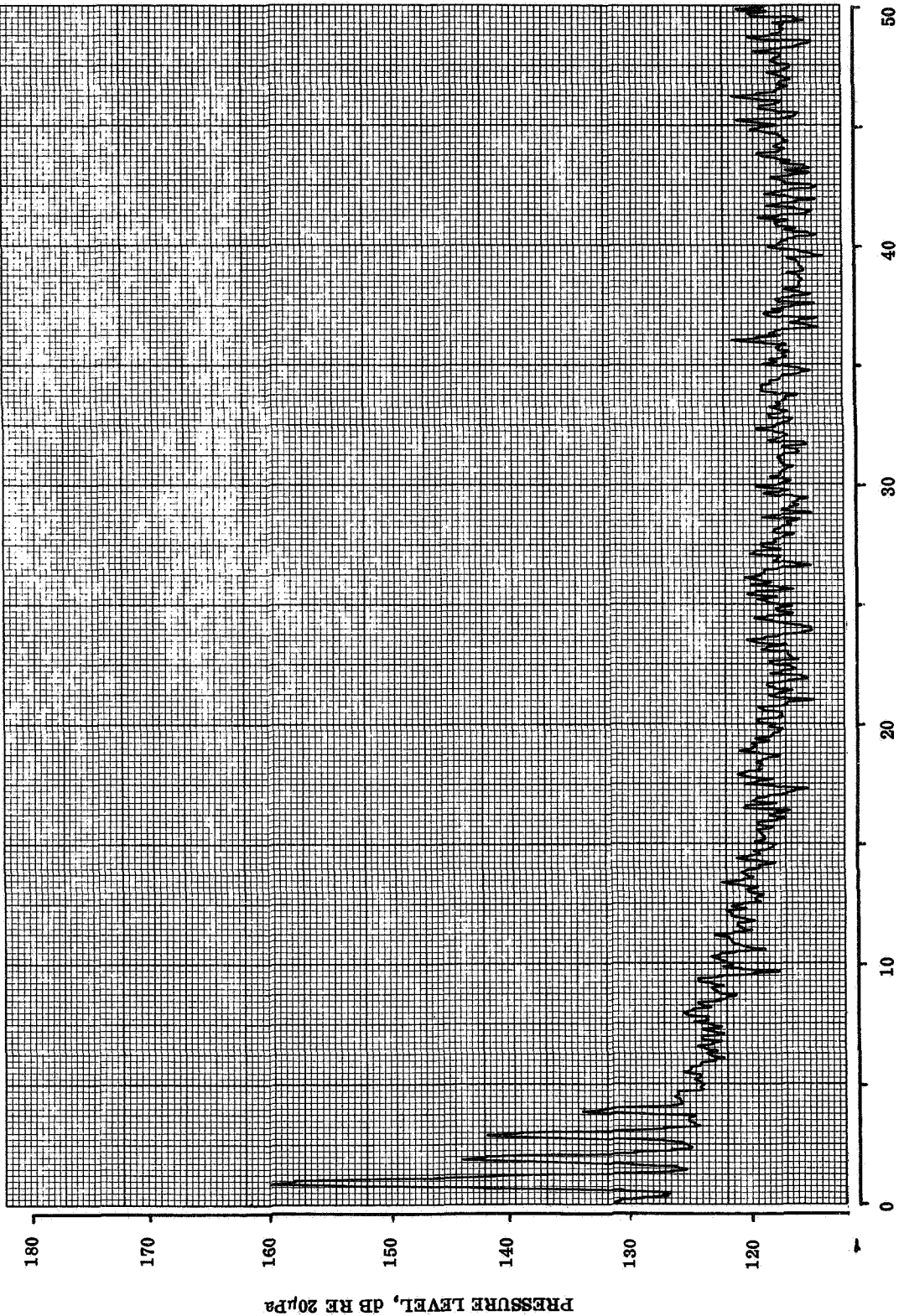
HARMONICS OF PROPELLER ROTATION

FLIGHT 8
RUN 19A





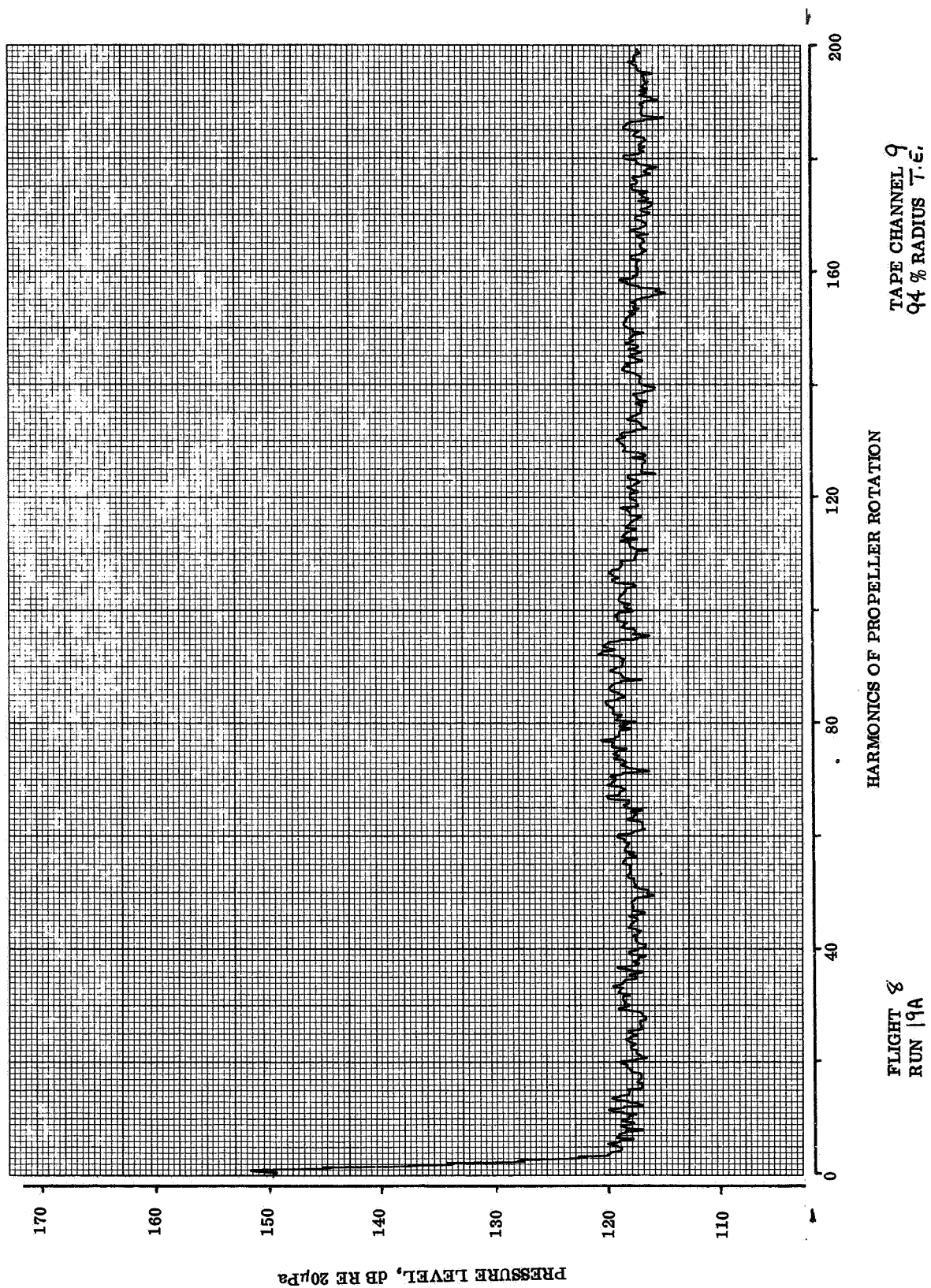


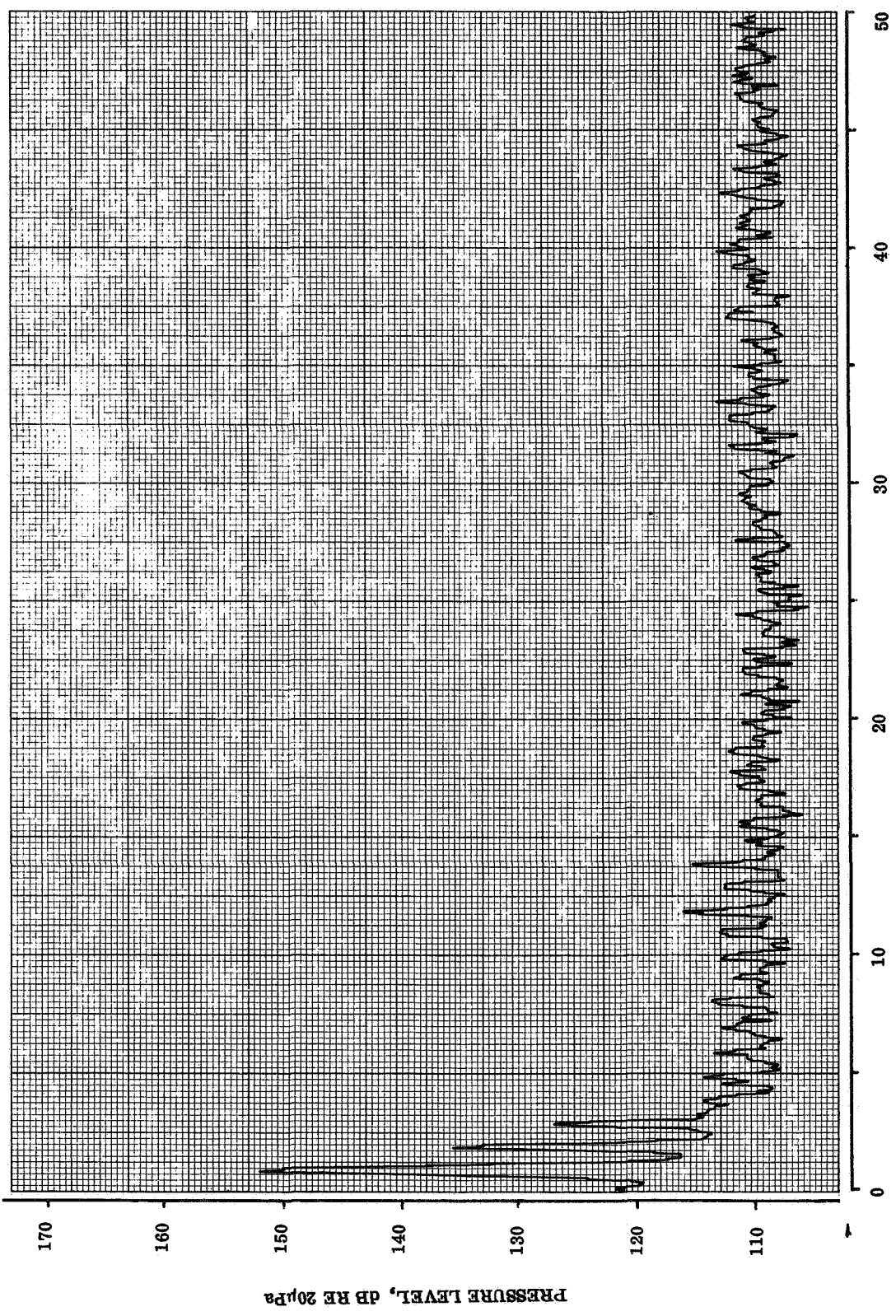


FLIGHT 8
RUN 19A

HARMONICS OF PROPELLER ROTATION

TAPE CHANNEL 7
94 % RADIUS L.E.

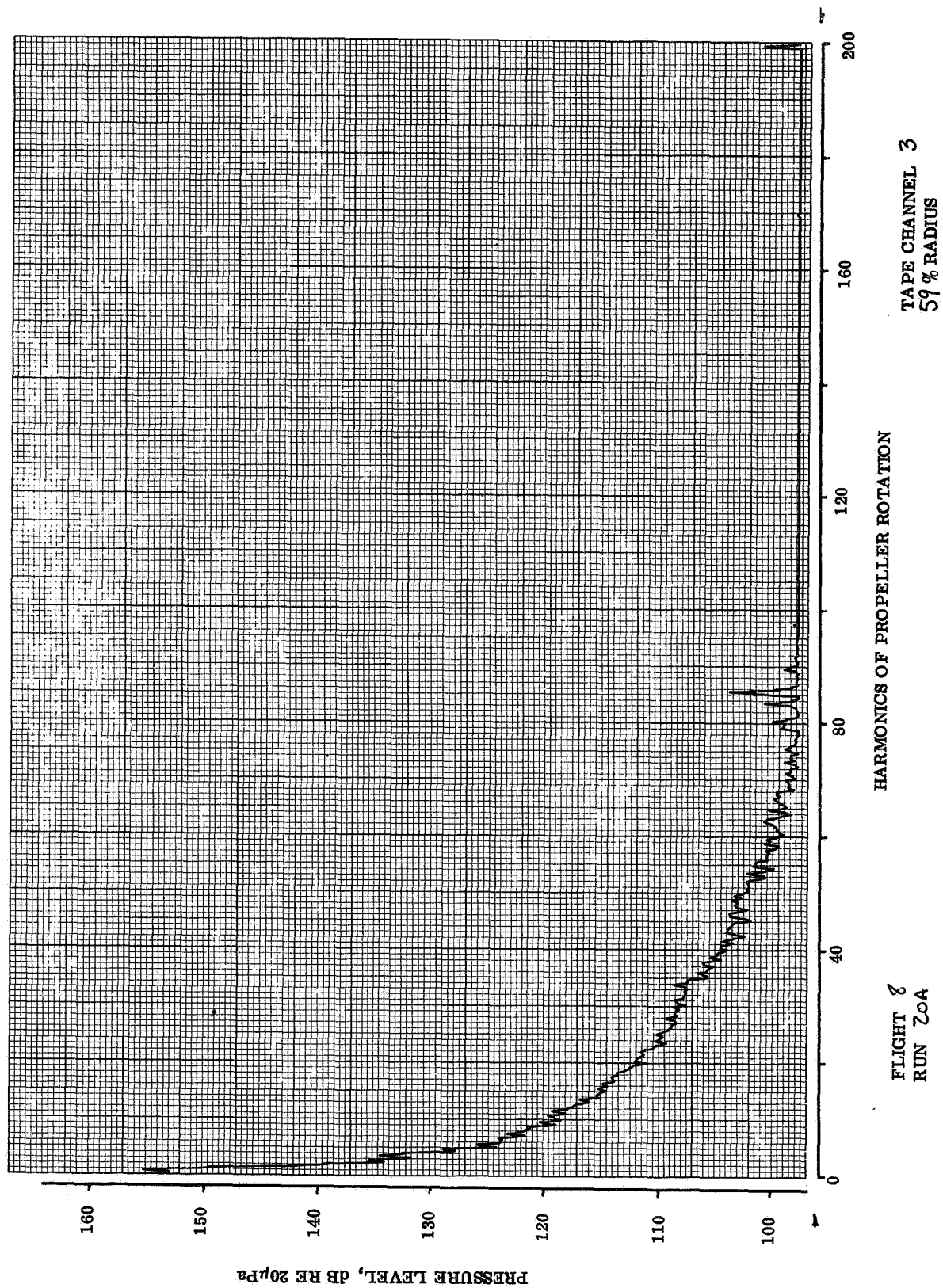


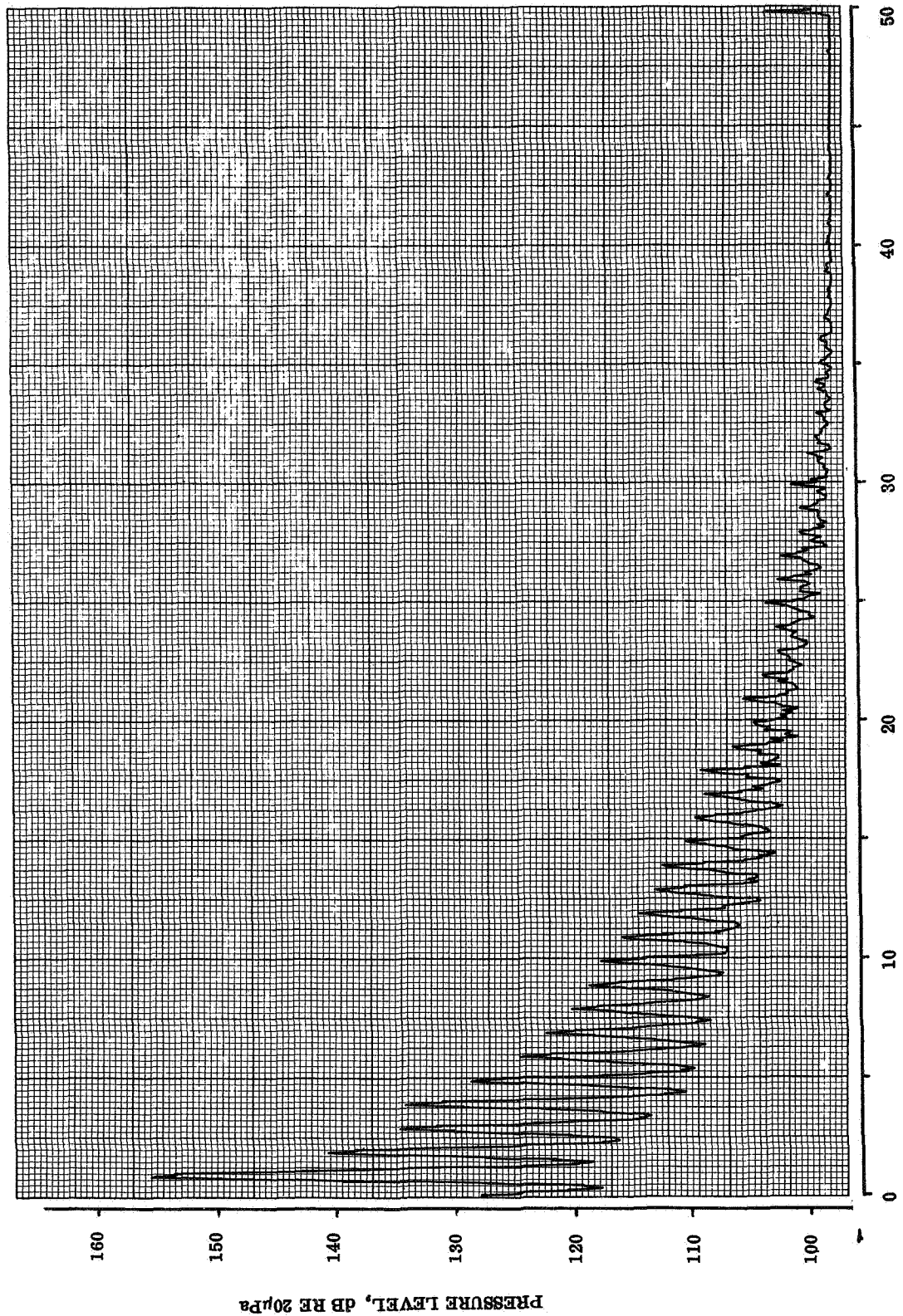


FLIGHT 8
 RUN 19A

HARMONICS OF PROPELLER ROTATION

TAPE CHANNEL 9
 Q4 % RADIUS T.E.

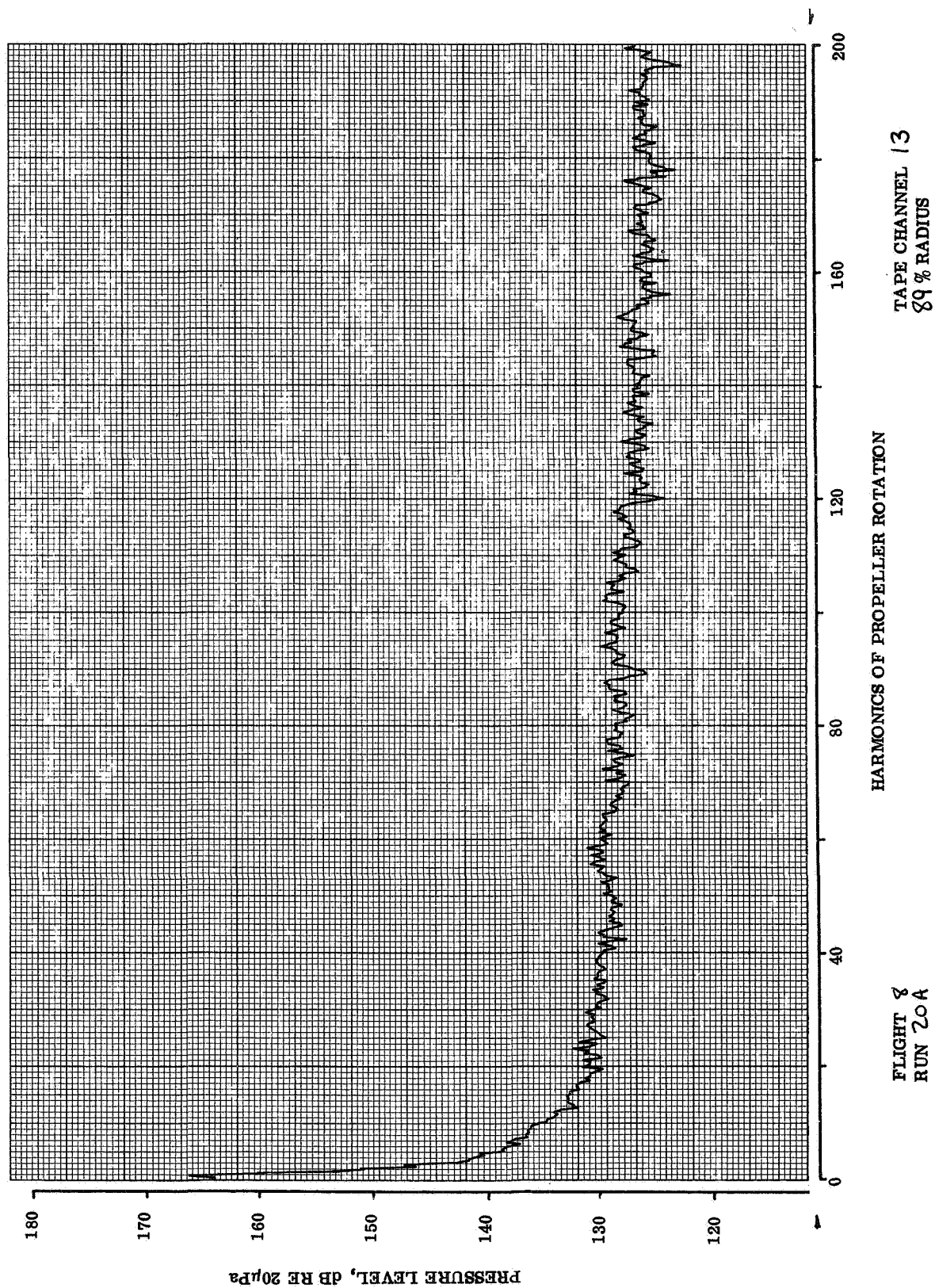


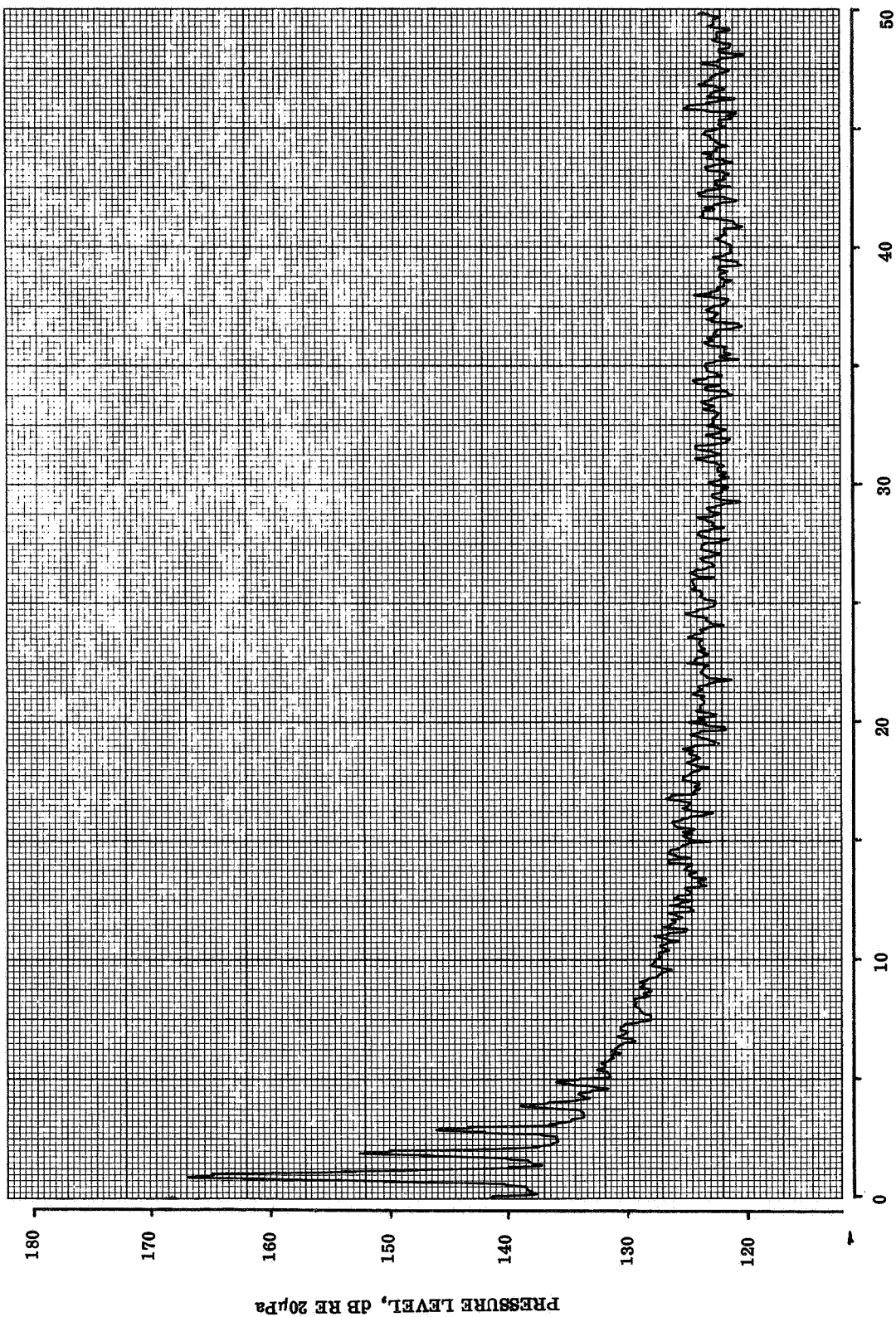


FLIGHT 8
RUN 20A

HARMONICS OF PROPELLER ROTATION

TAPE CHANNEL 3
59 % RADIUS

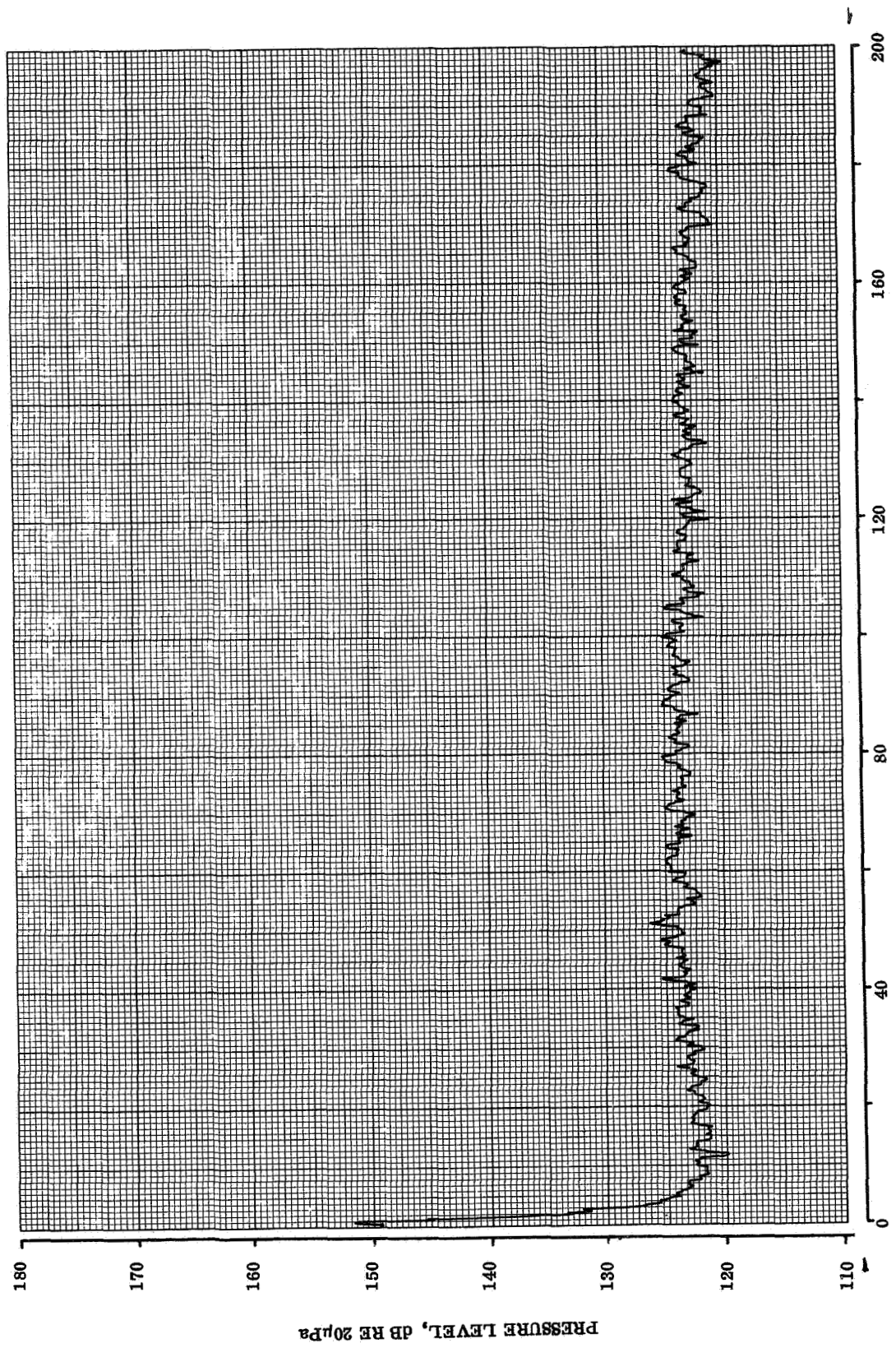




FLIGHT 8
 RUN 20A

HARMONICS OF PROPELLER ROTATION

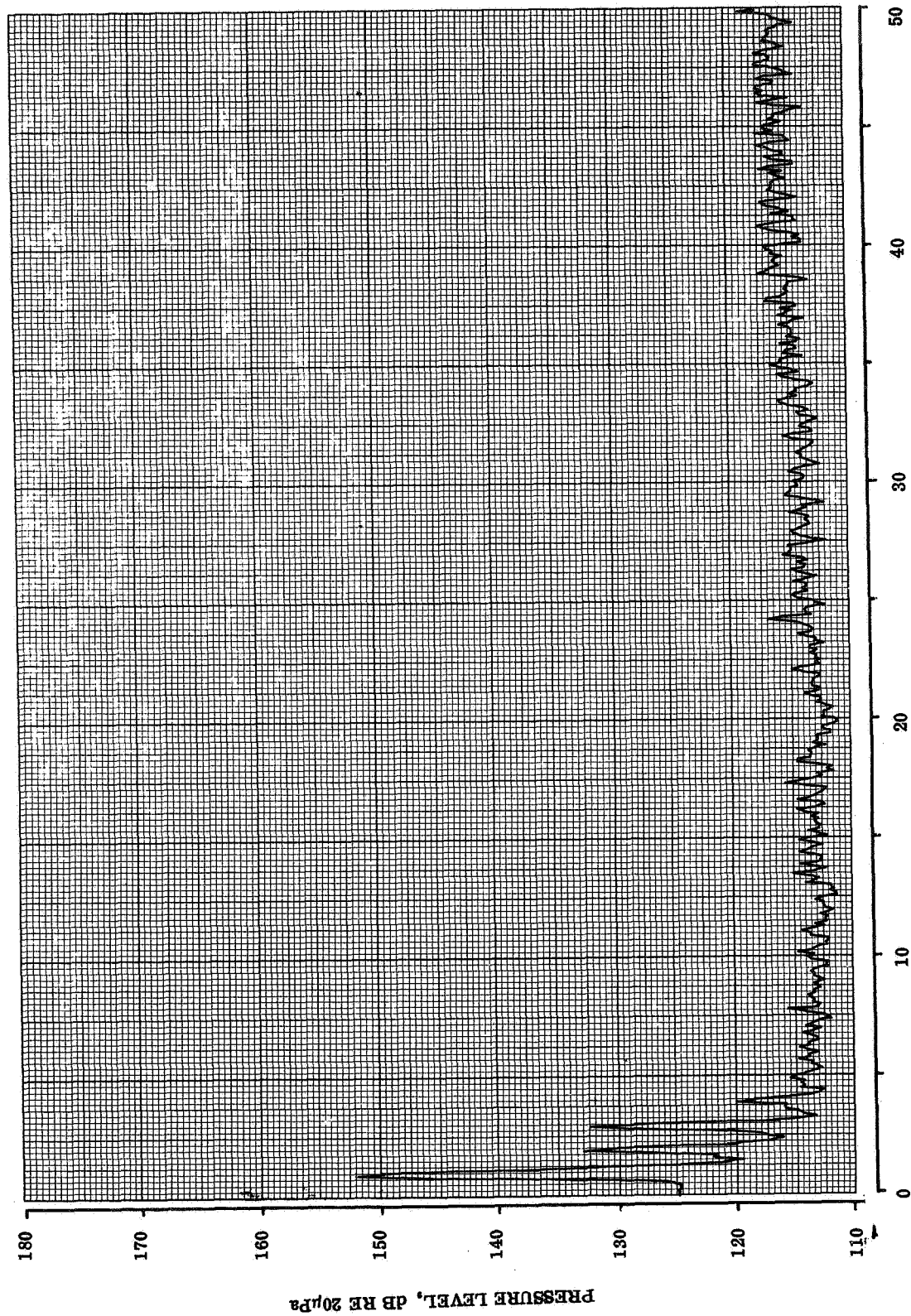
TAPE CHANNEL 13
 89 % RADIUS



TAPE CHANNEL 9
Q4 % RADIUS T.E.

HARMONICS OF PROPELLER ROTATION

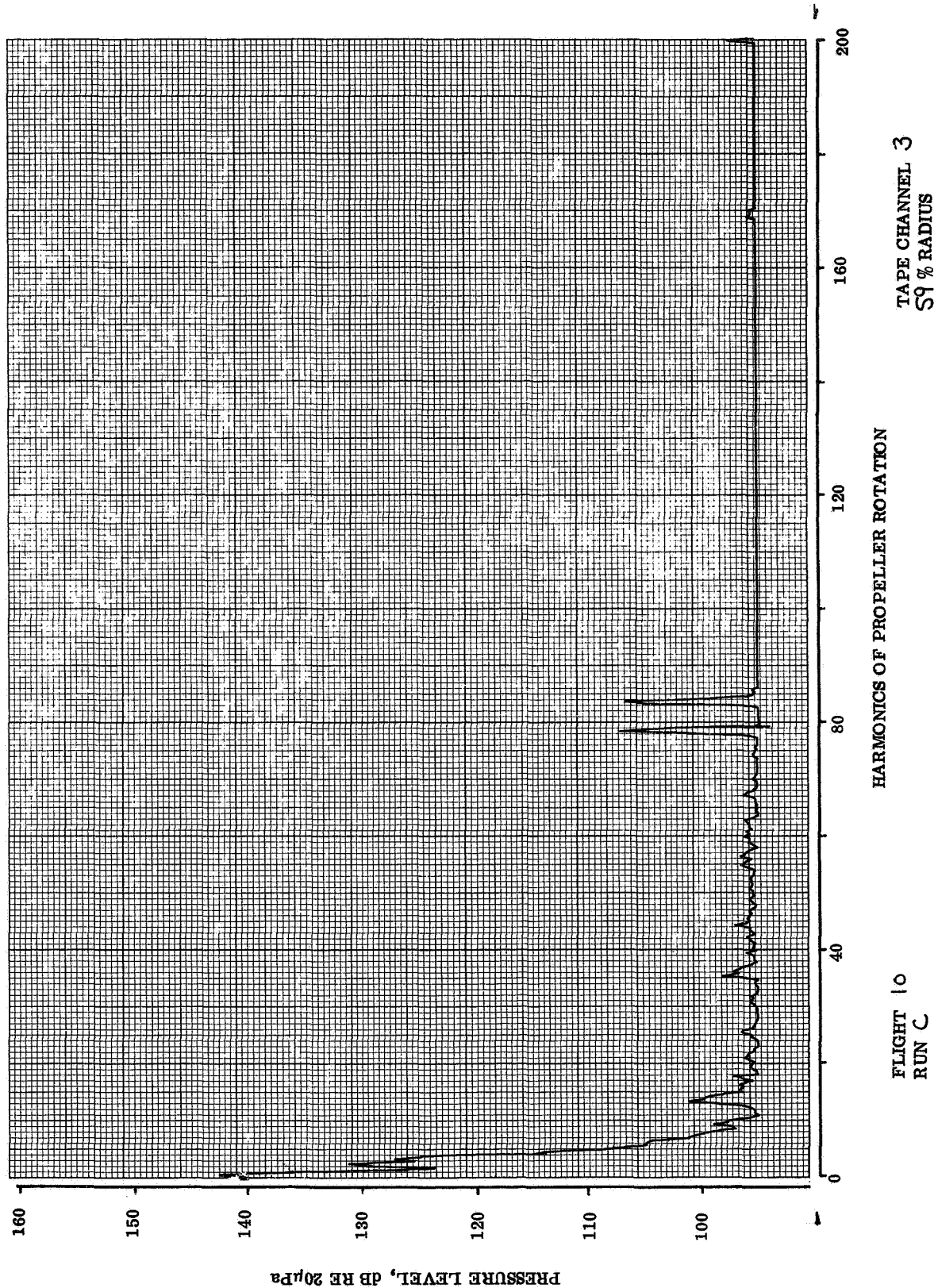
FLIGHT 8
RUN 20A

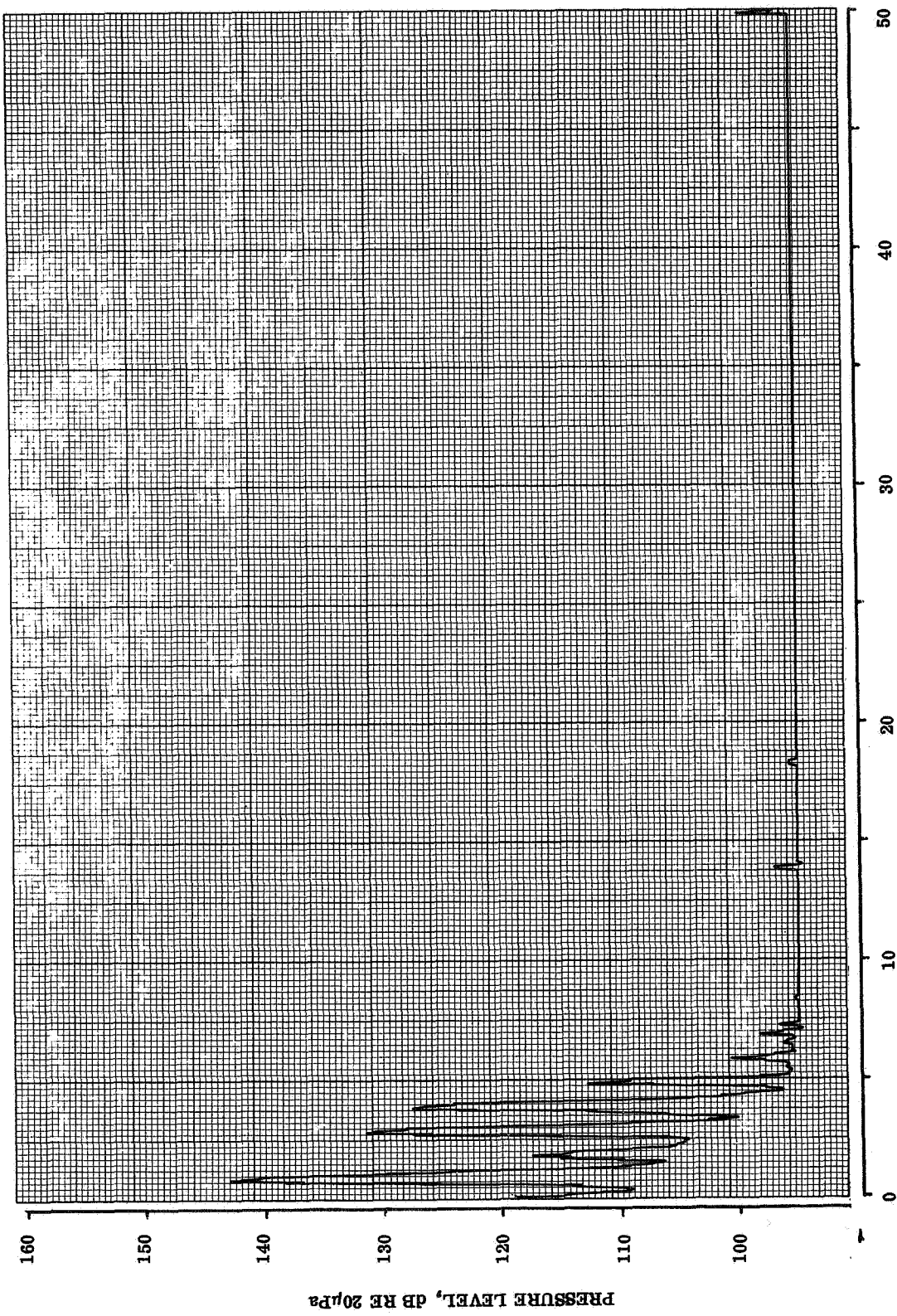


TAPE CHANNEL Q
Q4 % RADIUS T.E.

HARMONICS OF PROPELLER ROTATION

FLIGHT 8
RUN 20A

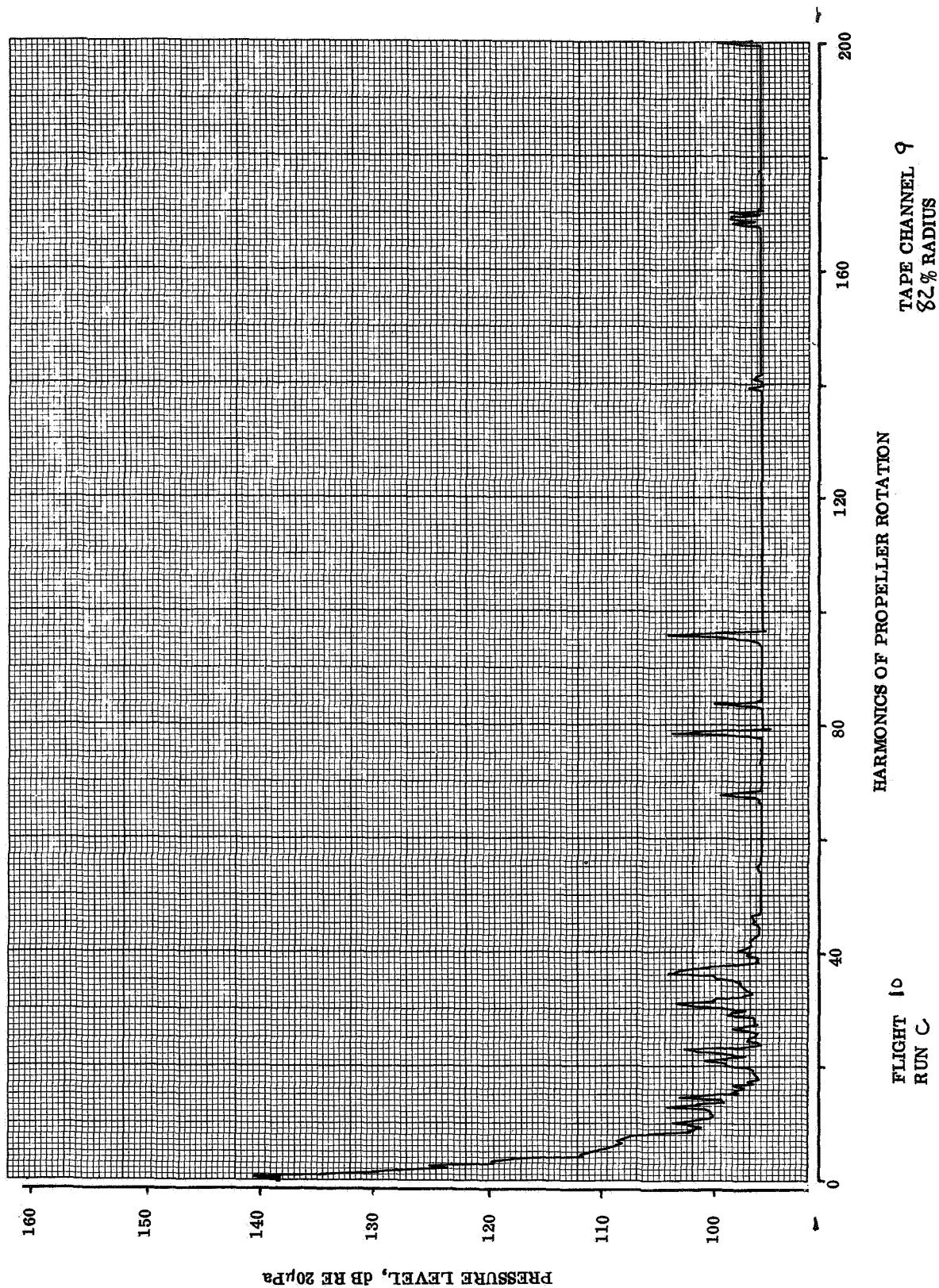


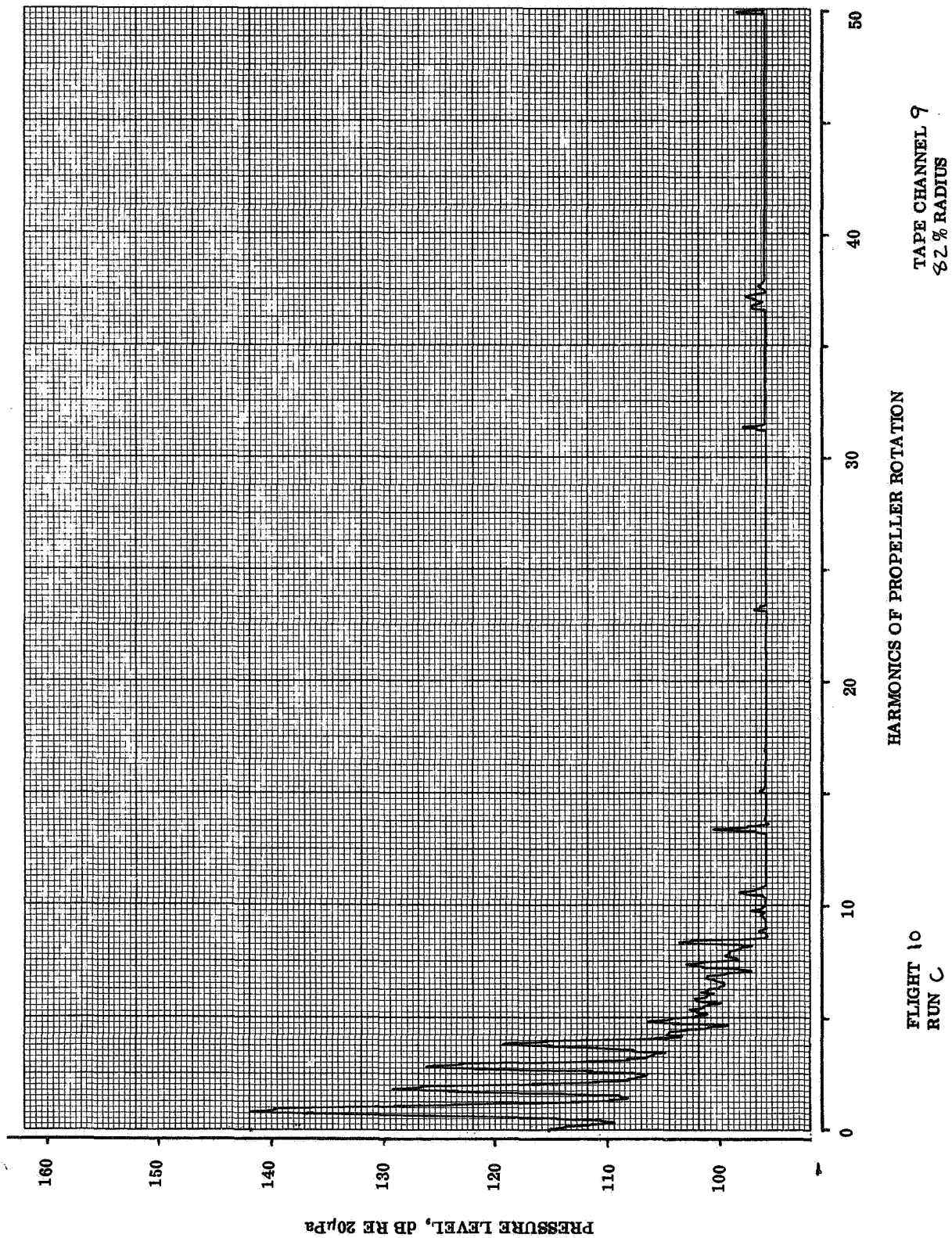


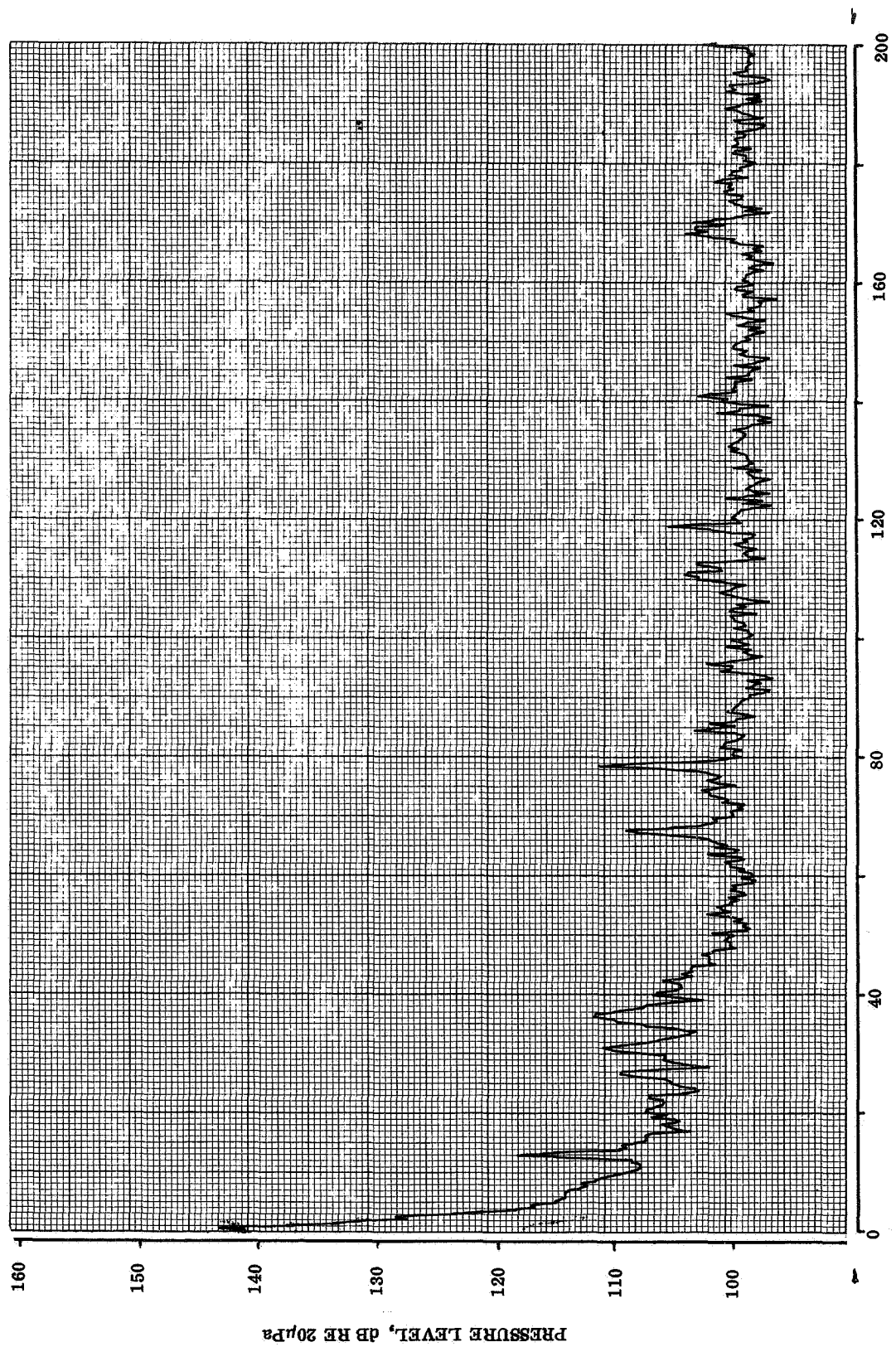
TAPE CHANNEL 3
59% RADIUS

HARMONICS OF PROPELLER ROTATION

FLIGHT 10
RUN C



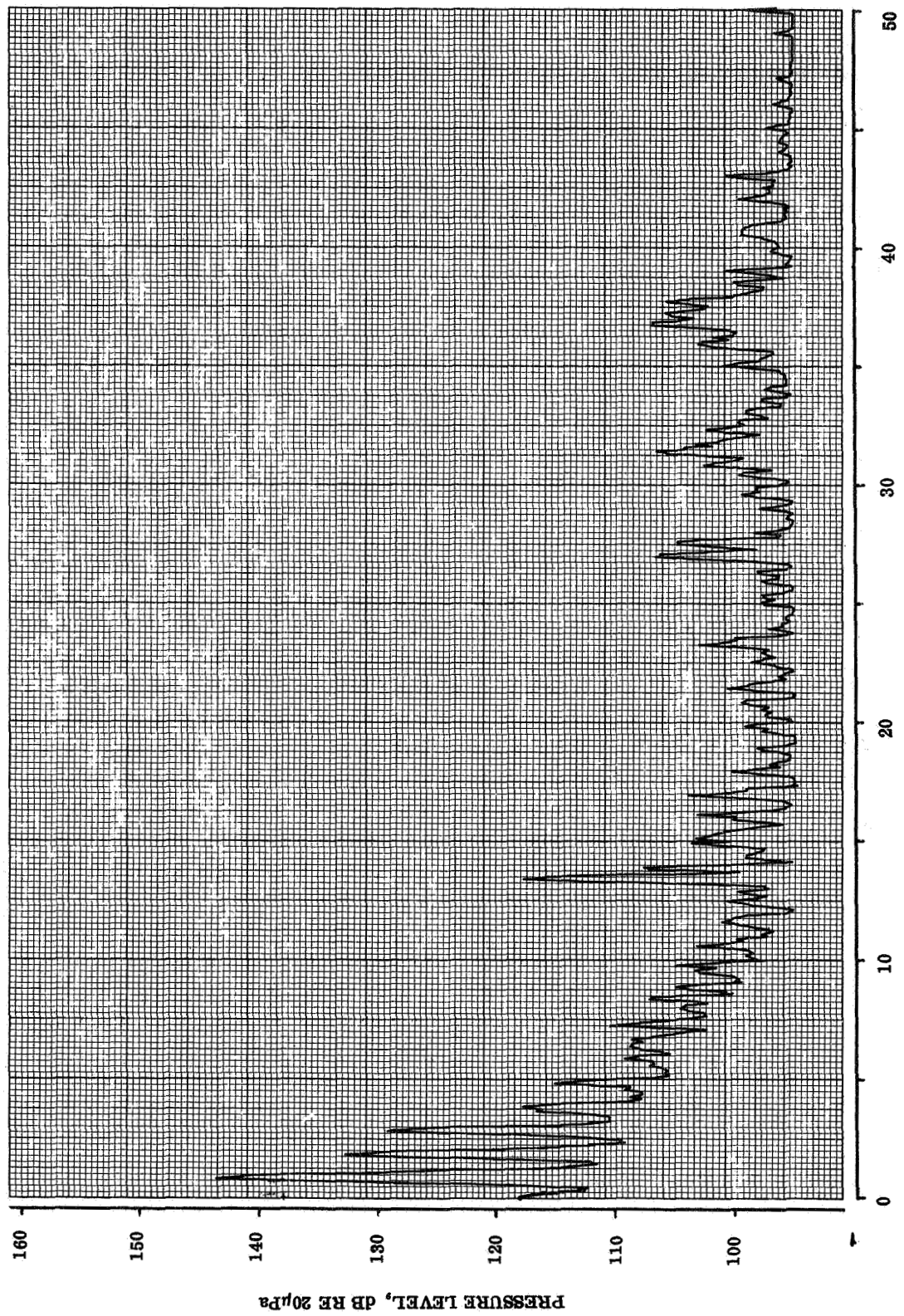




TAPE CHANNEL 7
94 % RADIUS L.S.

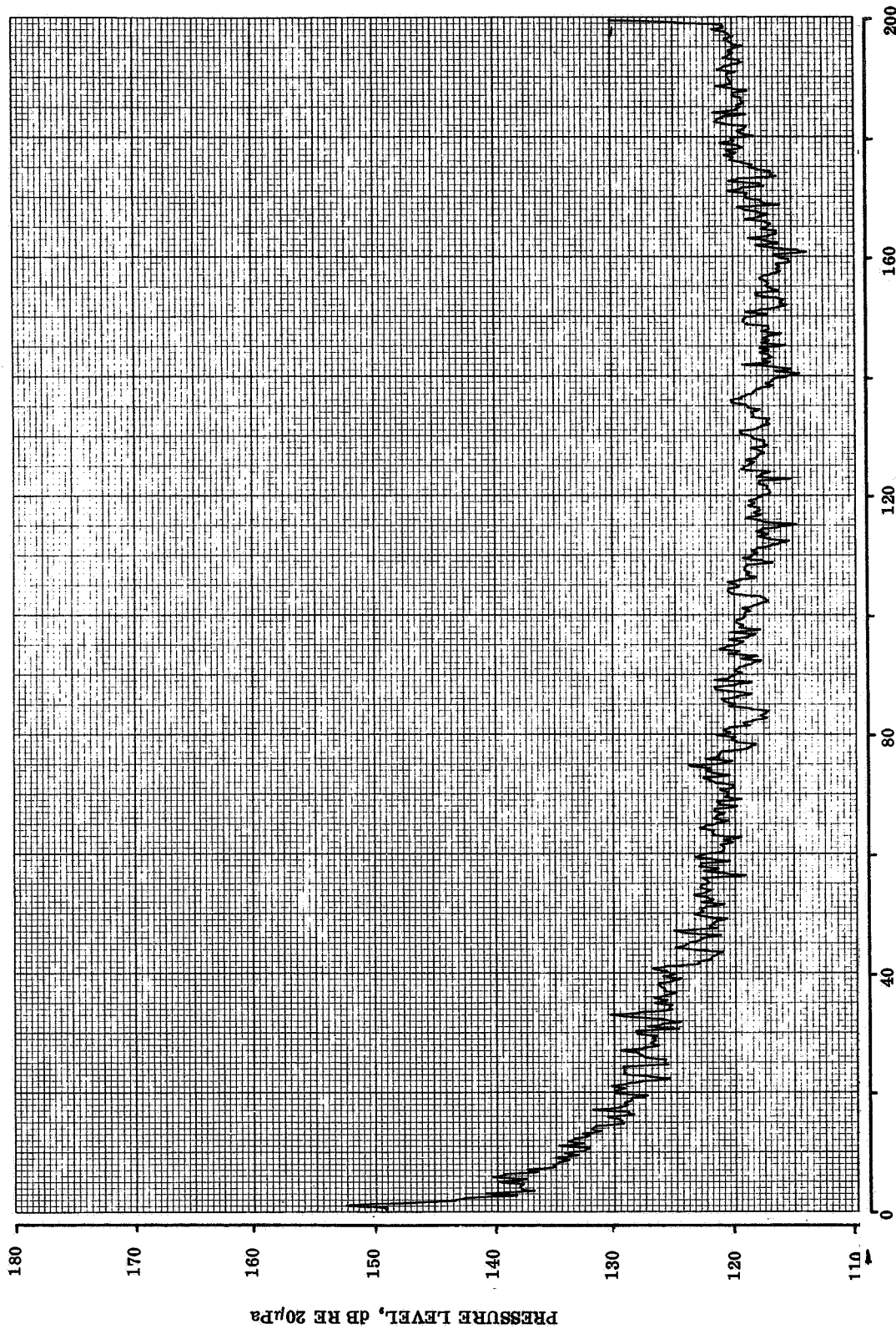
HARMONICS OF PROPELLER ROTATION

FLIGHT 10
RUN C



TAPE CHANNEL 7
94 % RADIUS L.E.

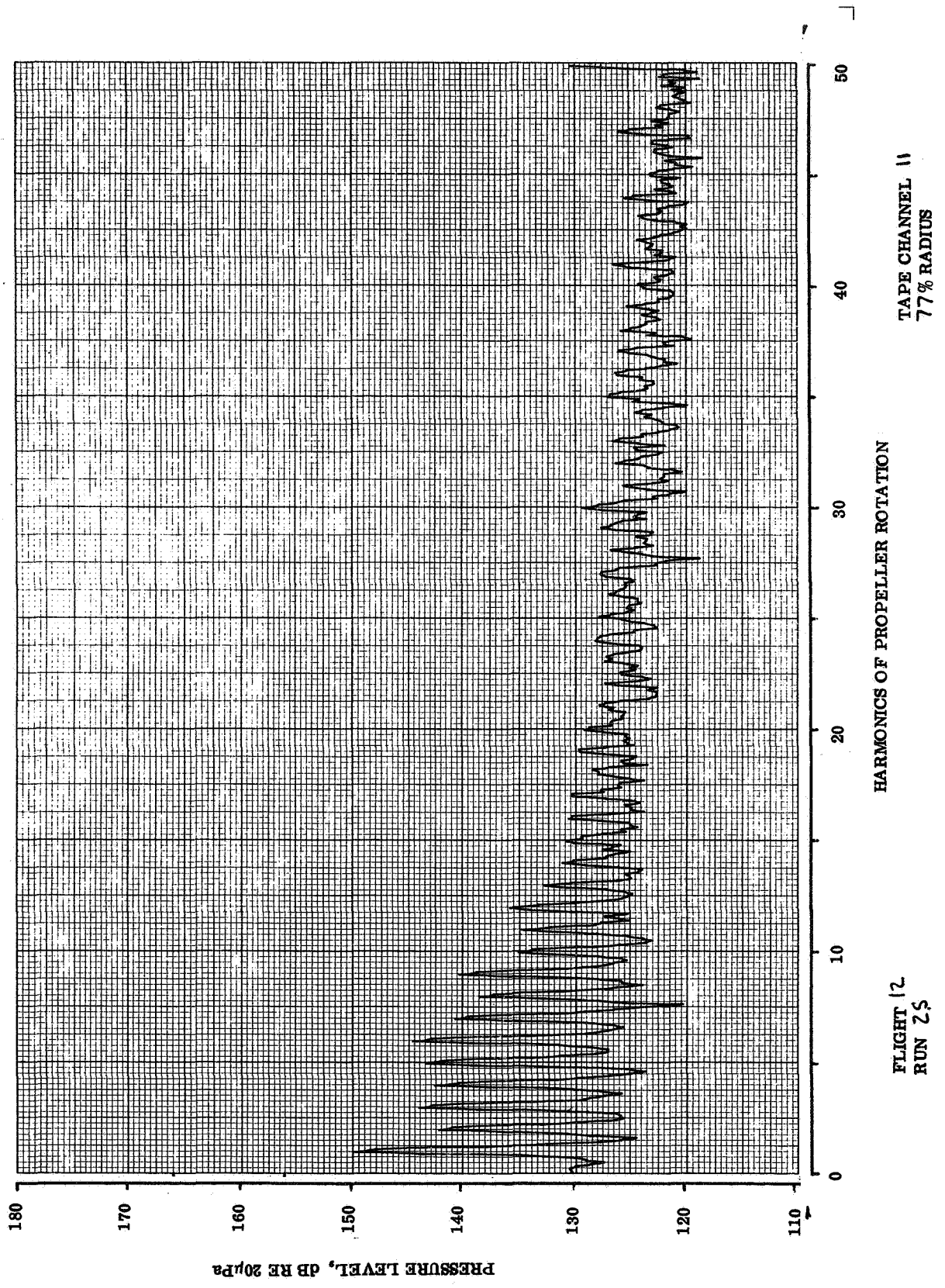
FLIGHT 10
RUN C

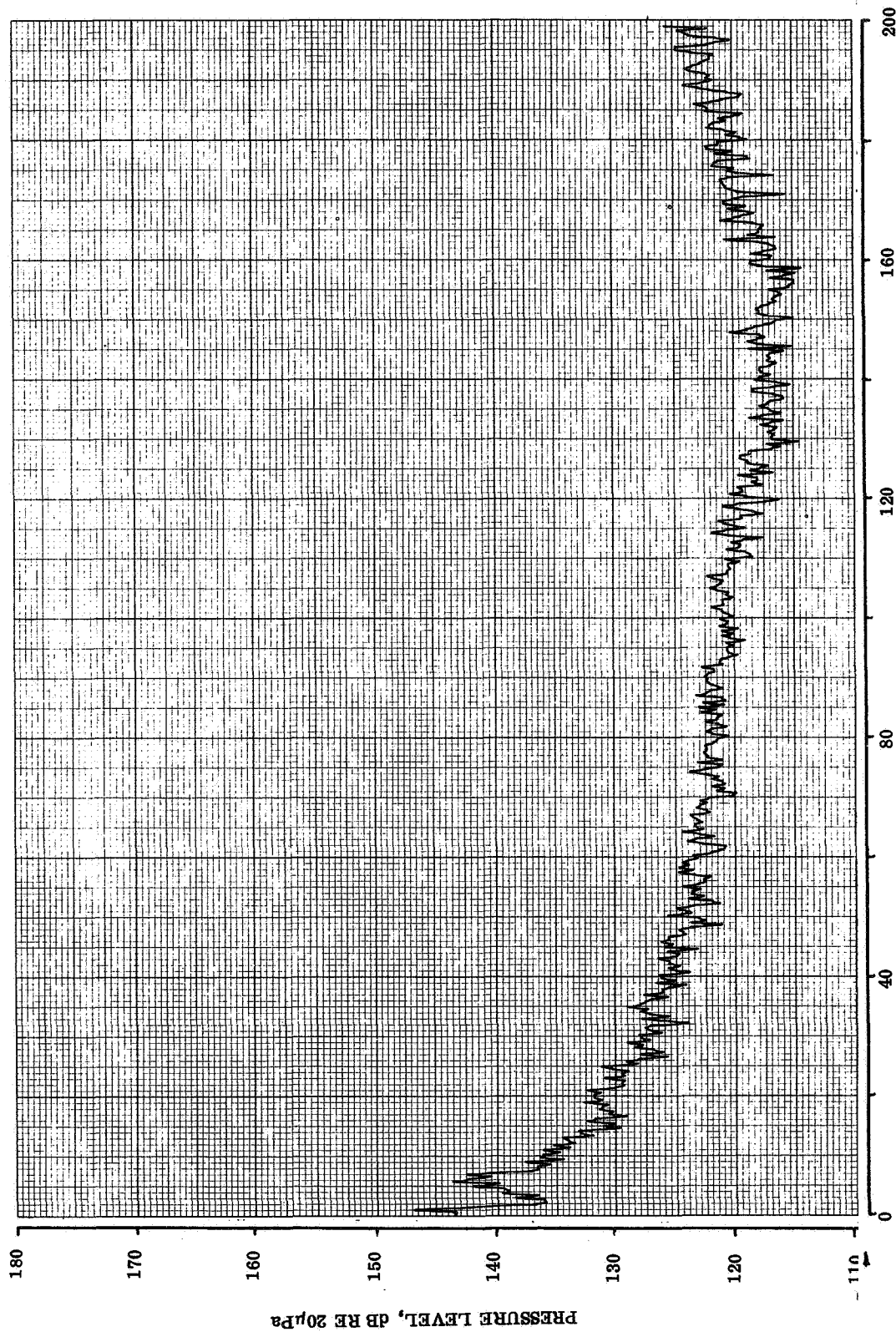


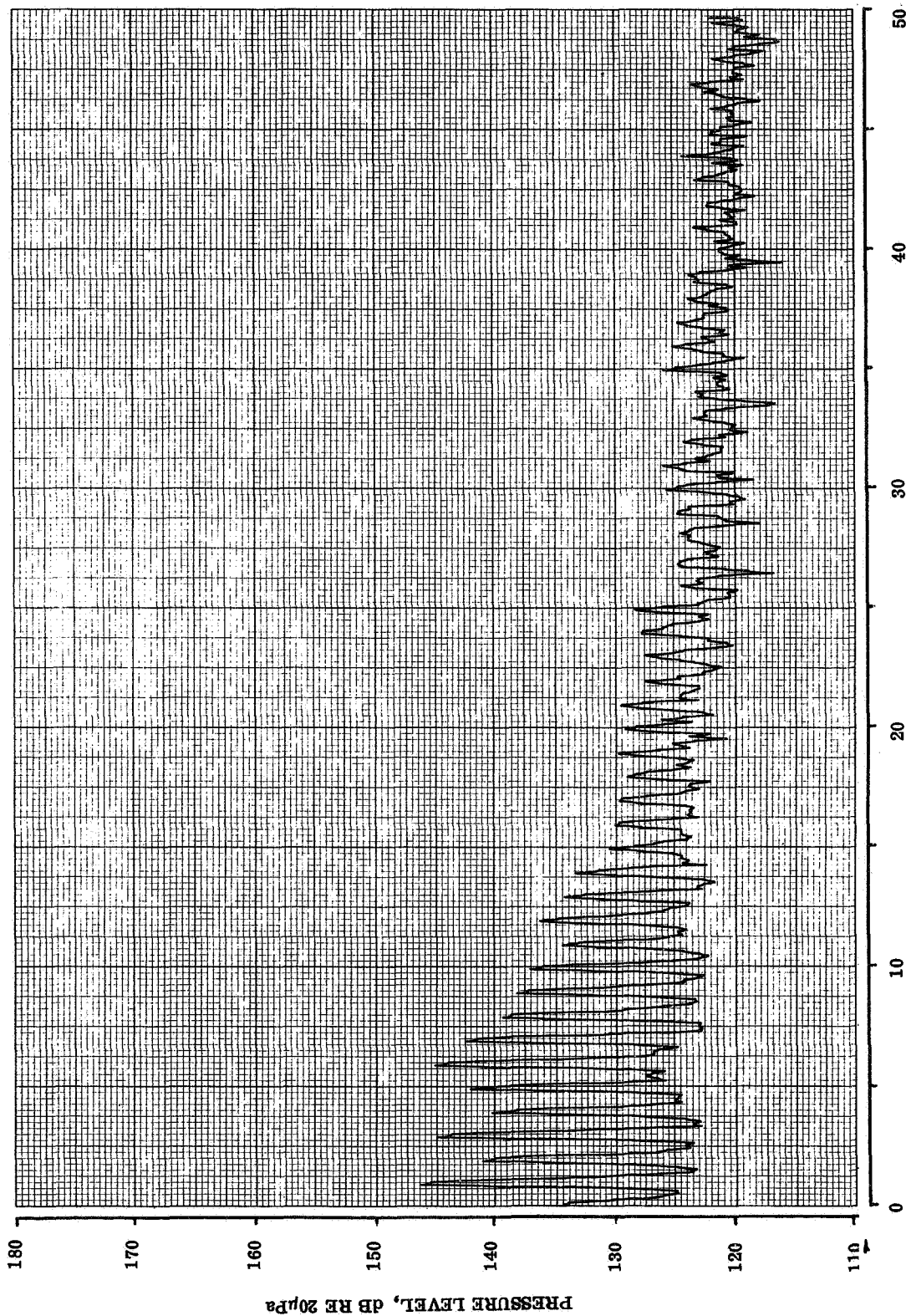
TAPE CHANNEL II
77% RADIUS

HARMONICS OF PROPELLER ROTATION

FLIGHT 12
RUN 25



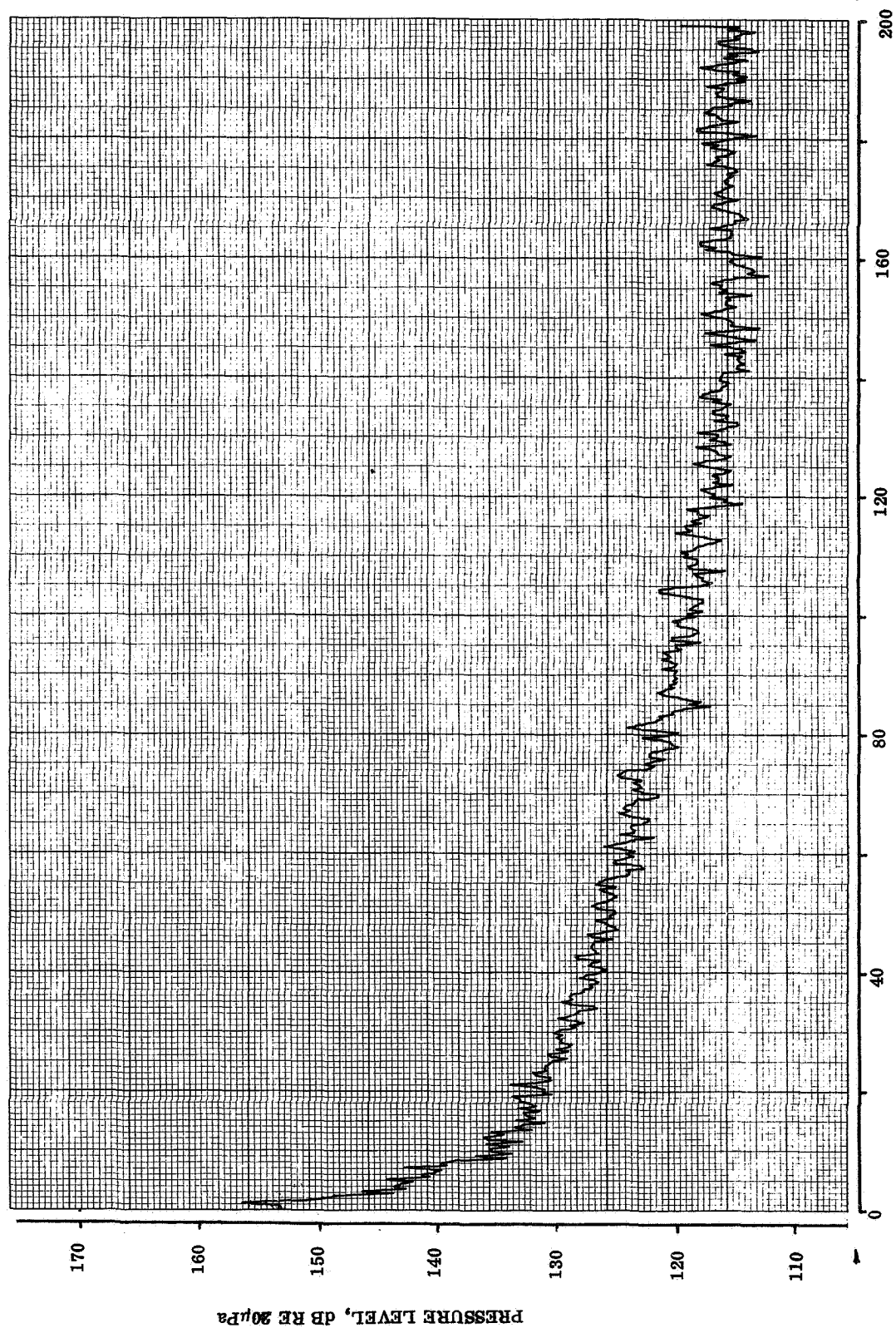




TAPE CHANNEL 9
82 % RADIUS

HARMONICS OF PROPELLER ROTATION

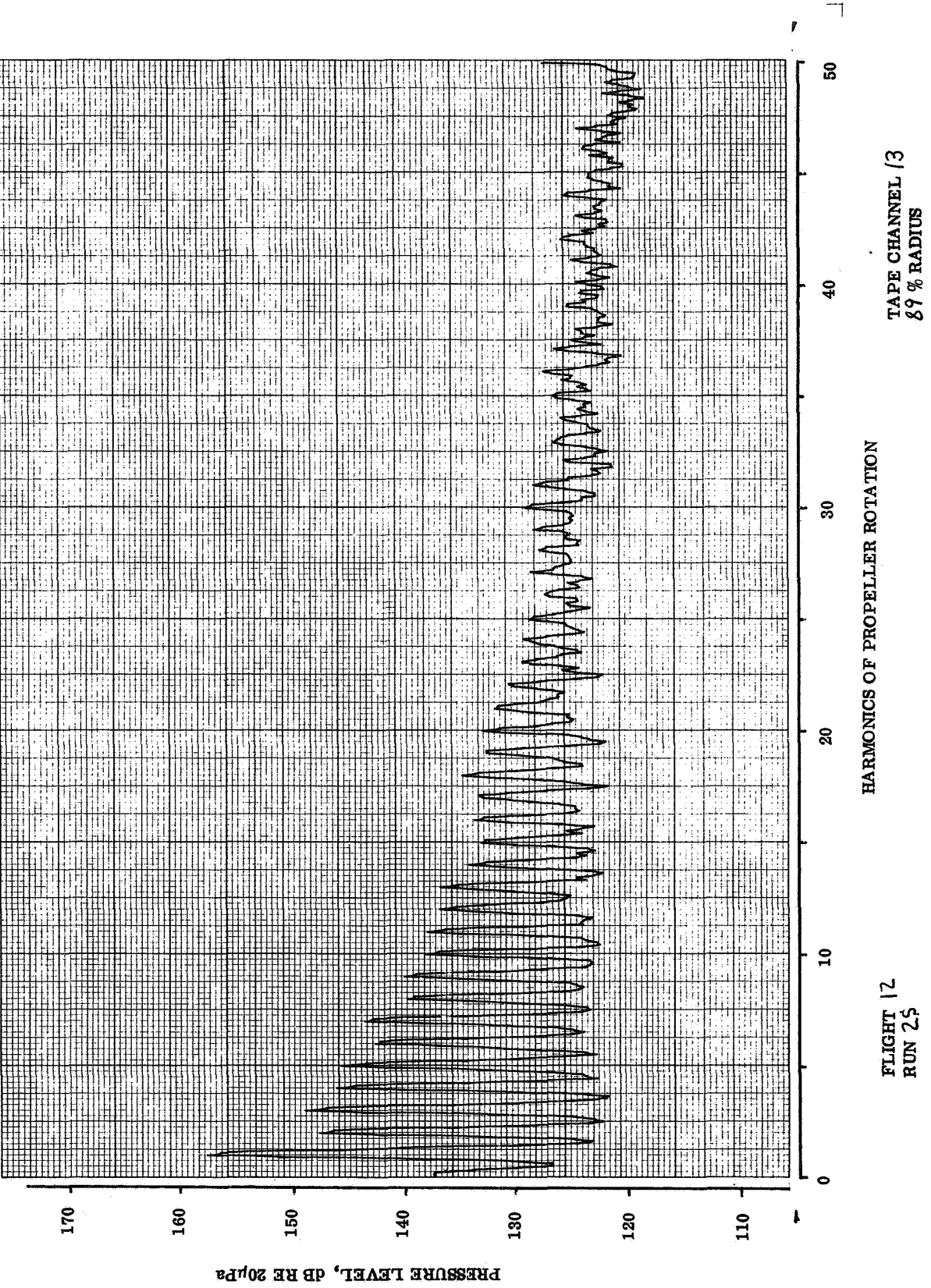
FLIGHT 12
RUN 25

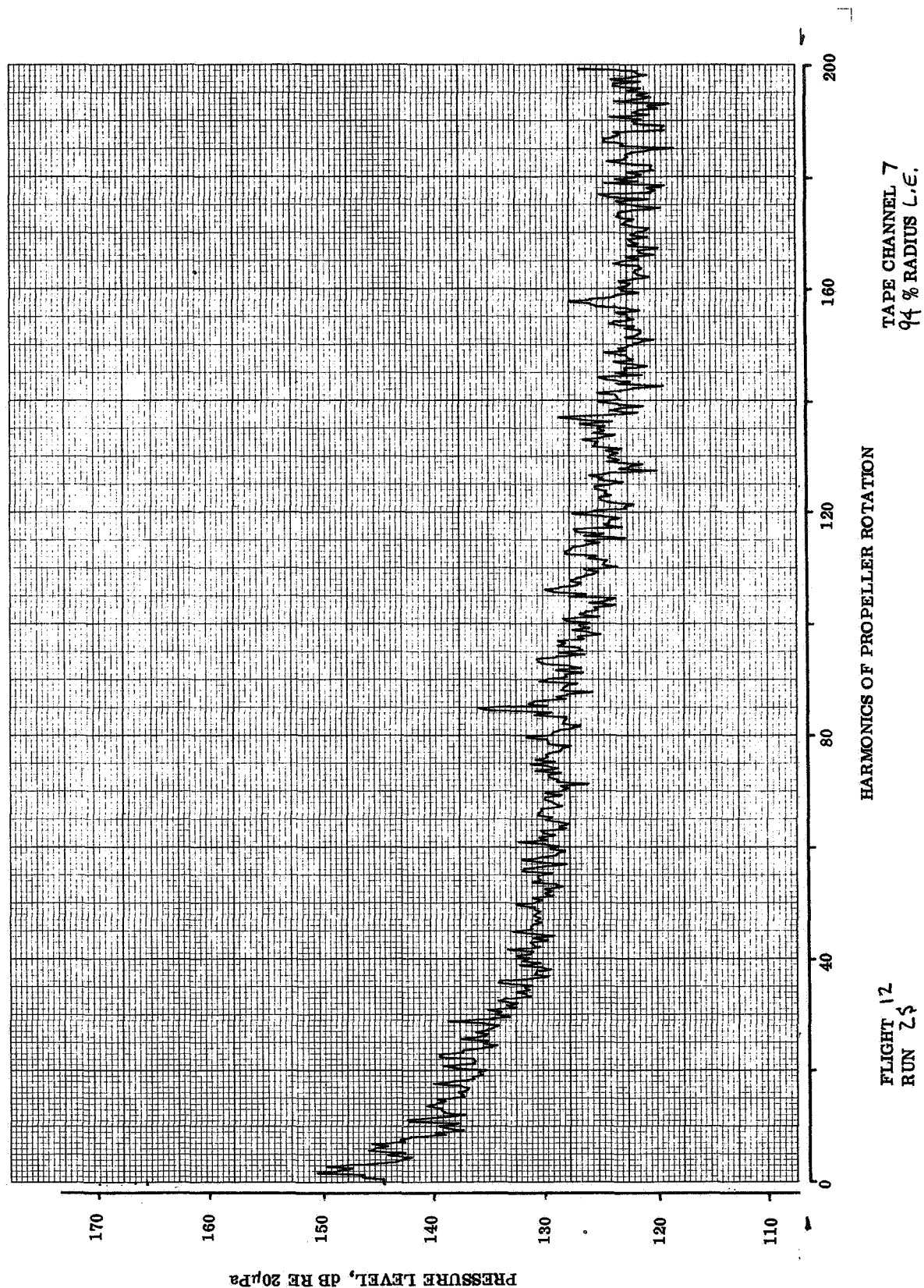


TAPE CHANNEL 13
89 % RADIUS

HARMONICS OF PROPELLER ROTATION

FLIGHT 12
RUN 24

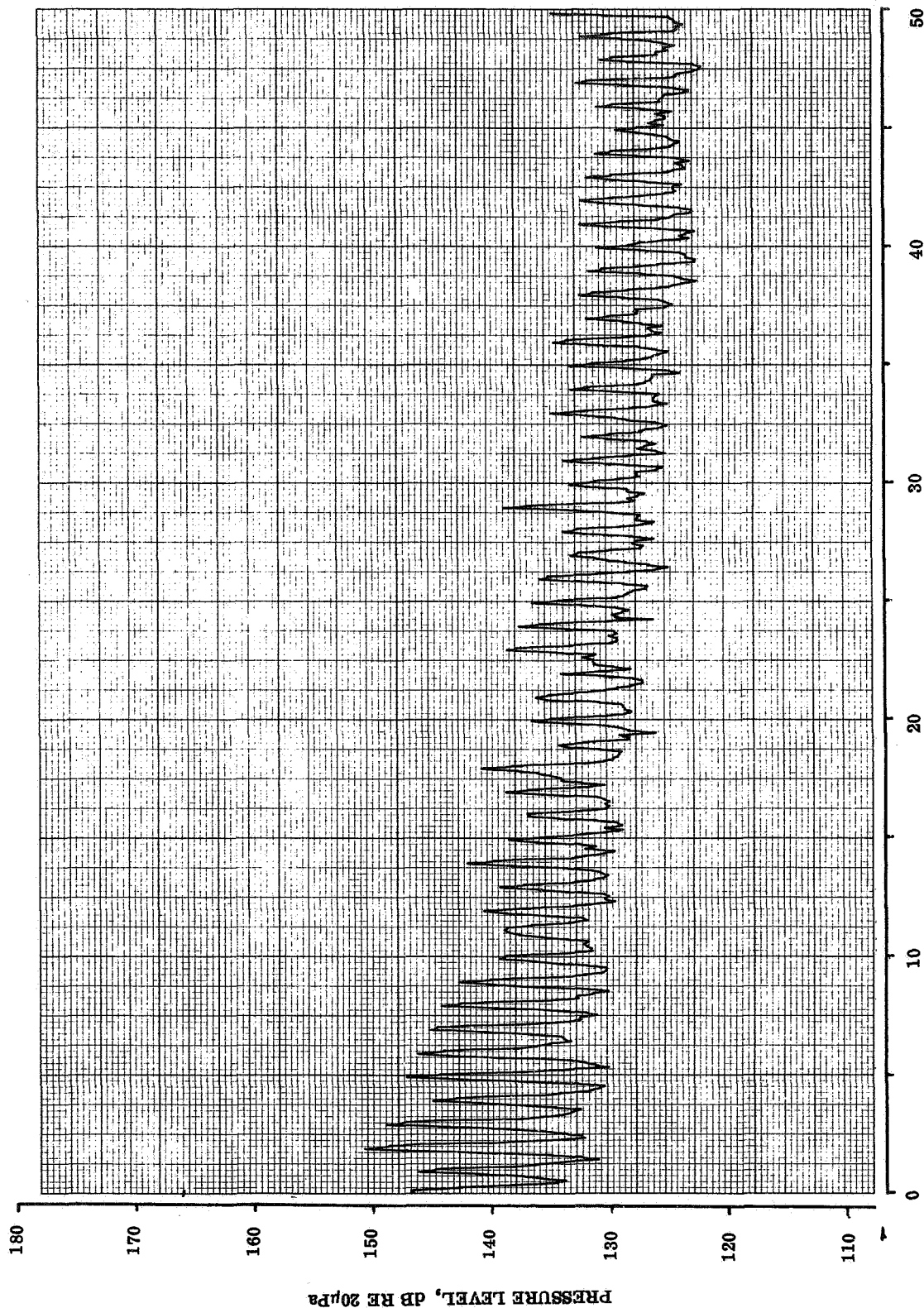




EUGENE DIETZGEN CO.
MADE IN U. S. A.

NO. 340-20 DIETZGEN GRAPH PAPER
20 X 20 PER INCH

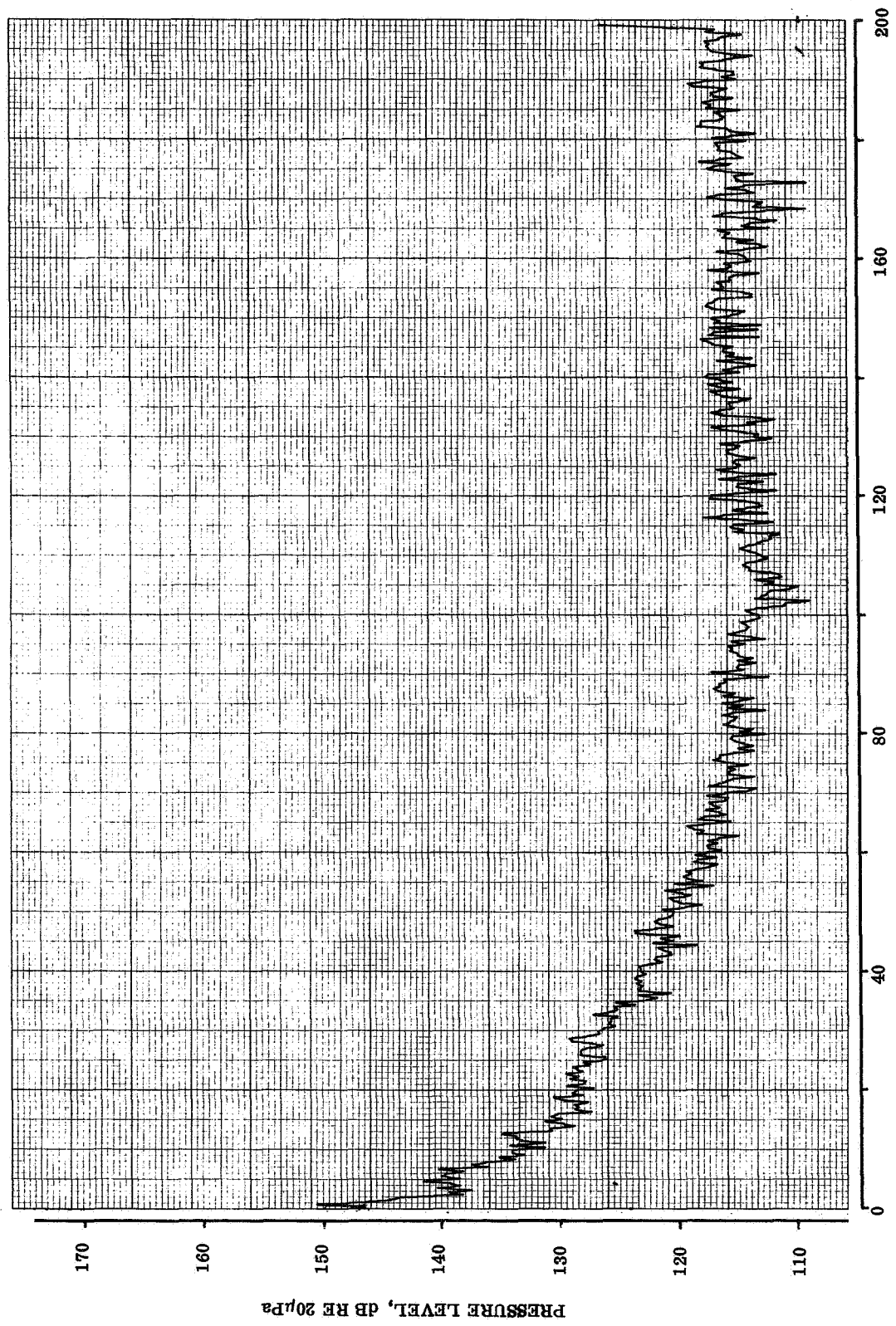
2A



HARMONICS OF PROPELLER ROTATION

TAPE CHANNEL 7
94 % RADIUS L.E.

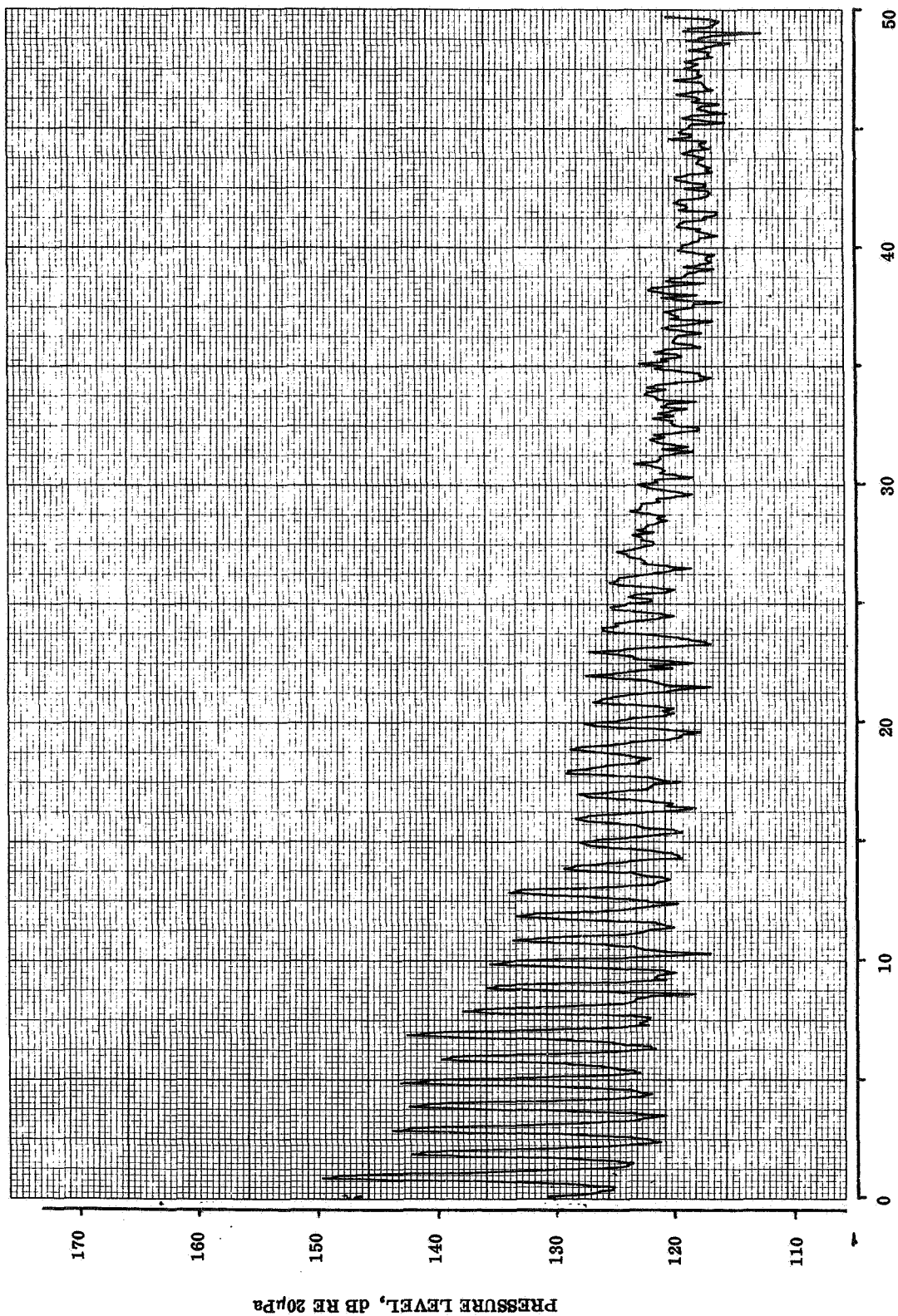
FLIGHT 12
RUN 25

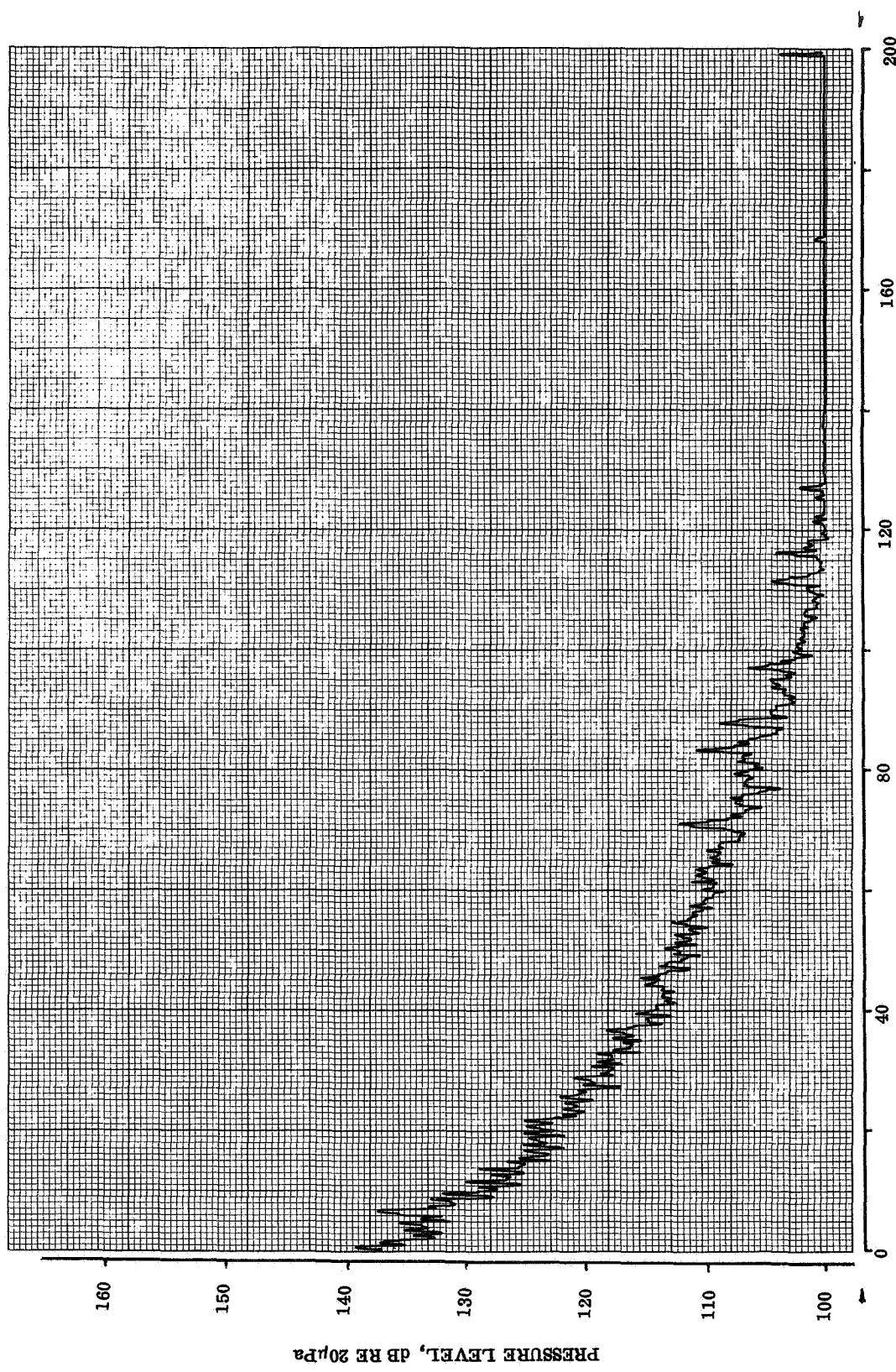


TAPE CHANNEL 5
94 % RADIUS T.E.

HARMONICS OF PROPELLER ROTATION

FLIGHT 12
RUN 28



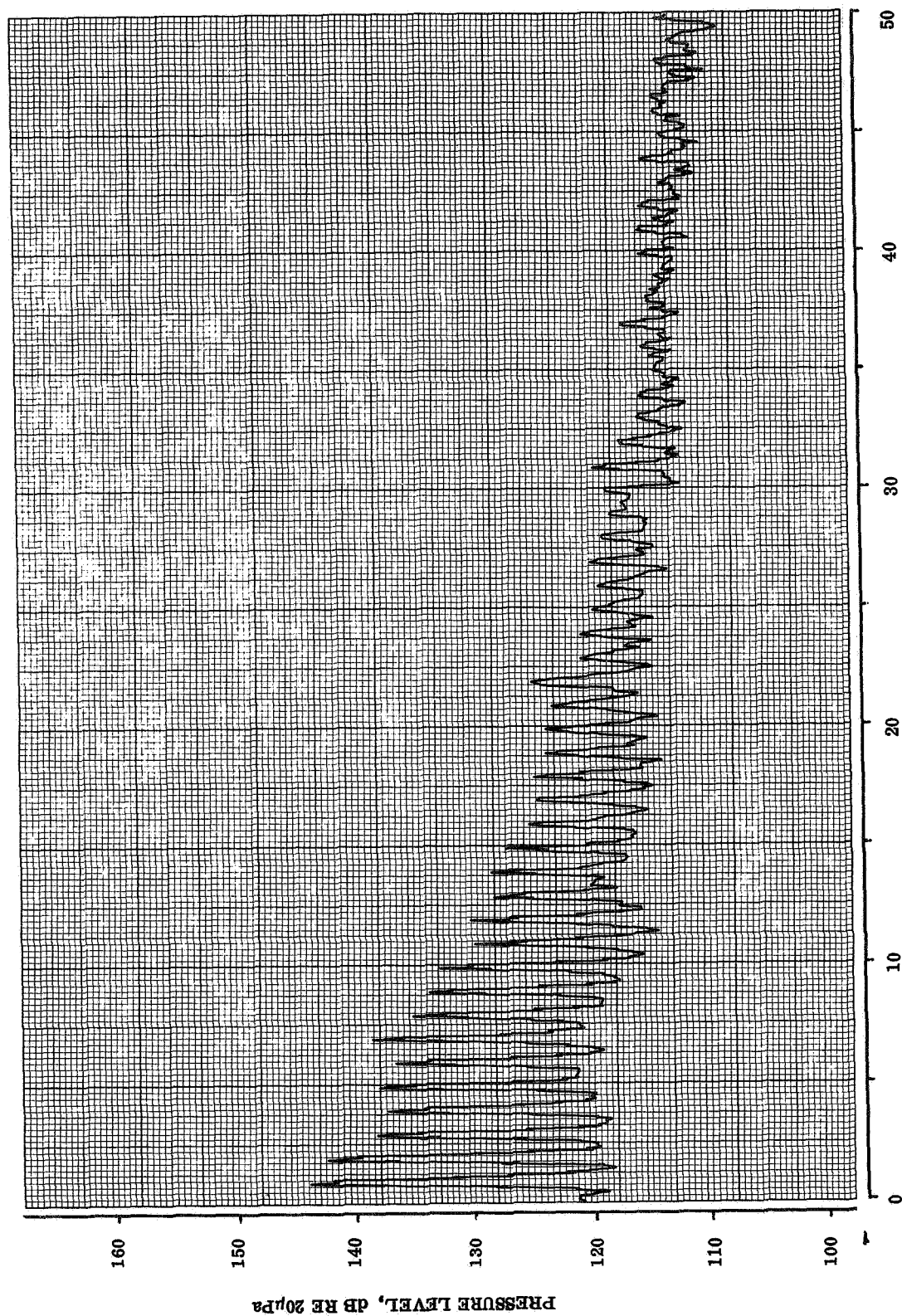


TAPE CHANNEL II
77% RADIUS

HARMONICS OF PROPELLER ROTATION

FLIGHT 12
RUN 35

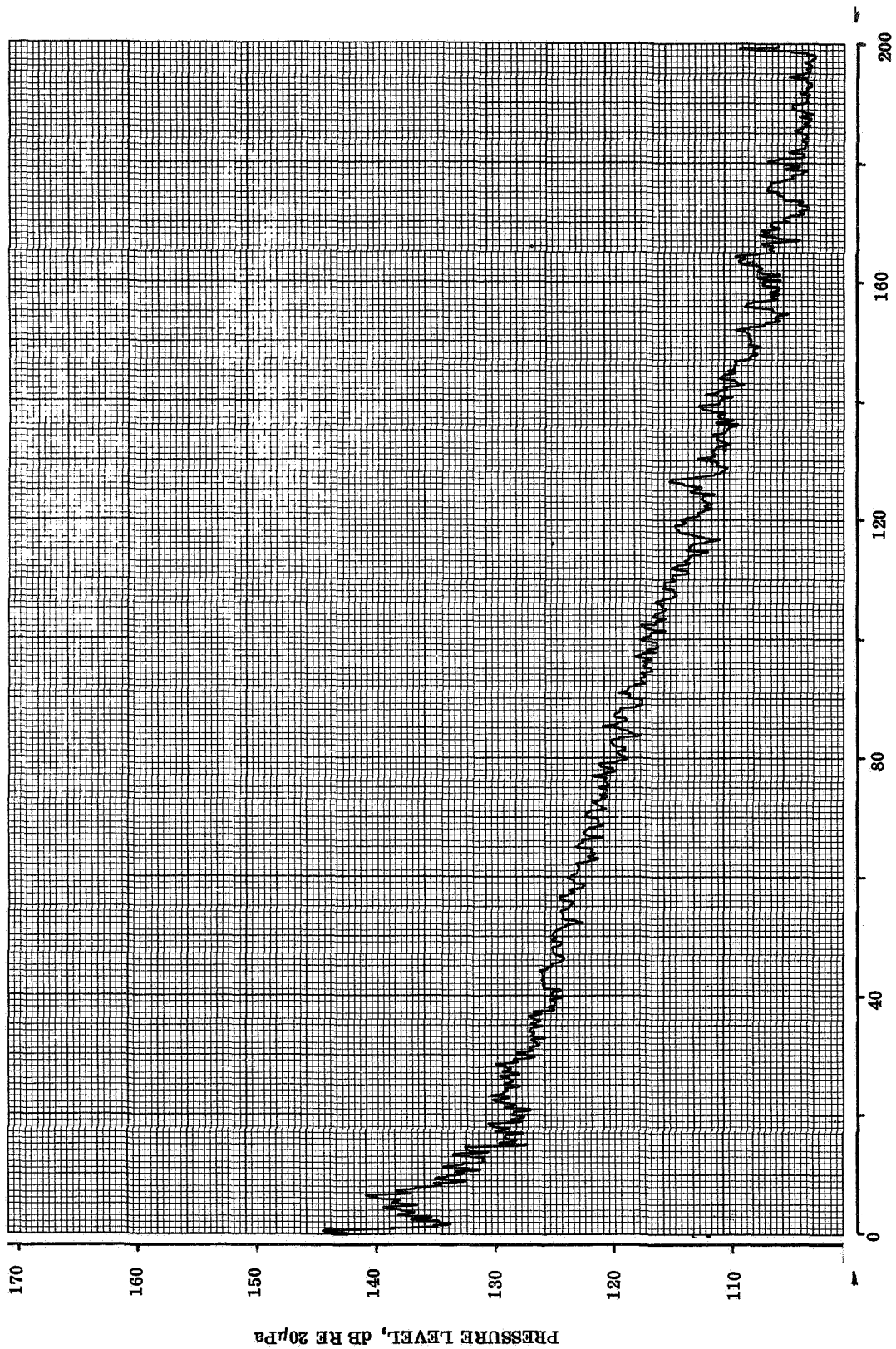
PRESSURE LEVEL, dB RE 20 μPa



TAPE CHANNEL //

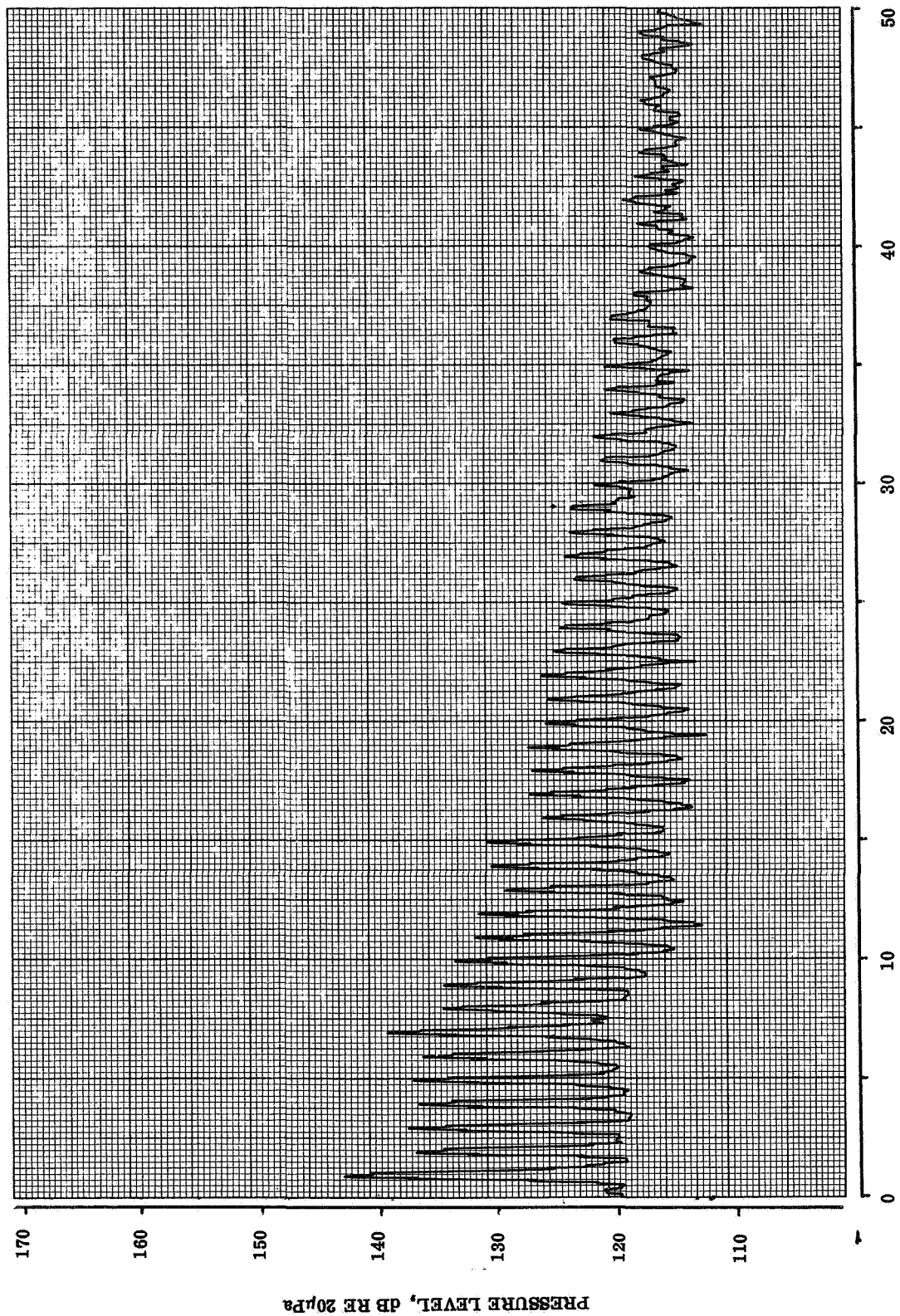
77% RADIUS

FLIGHT 12
RUN 35

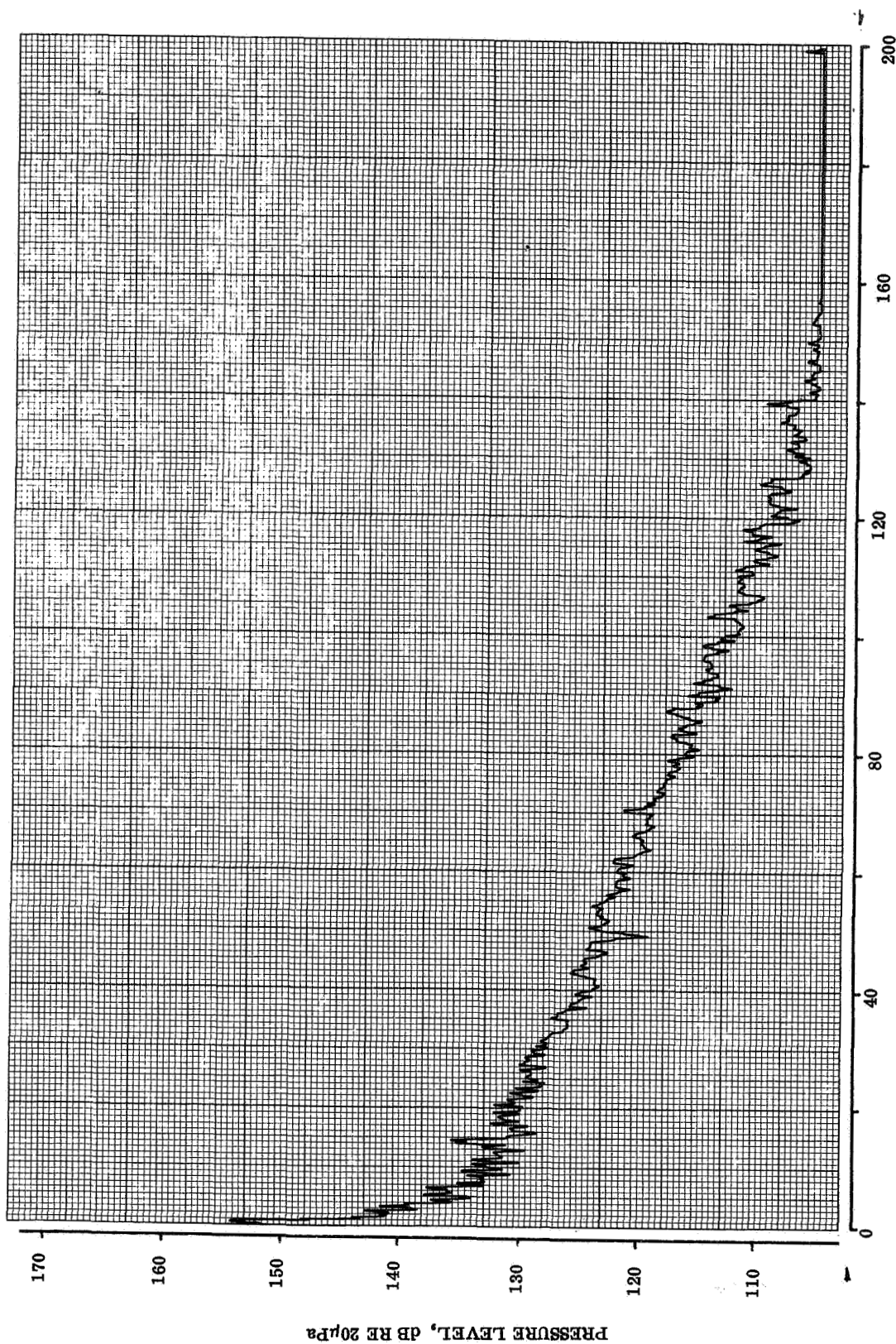


TAPE CHANNEL 9
82% RADIUS

FLIGHT 12
RUN 35



FLIGHT 12
RUN 35

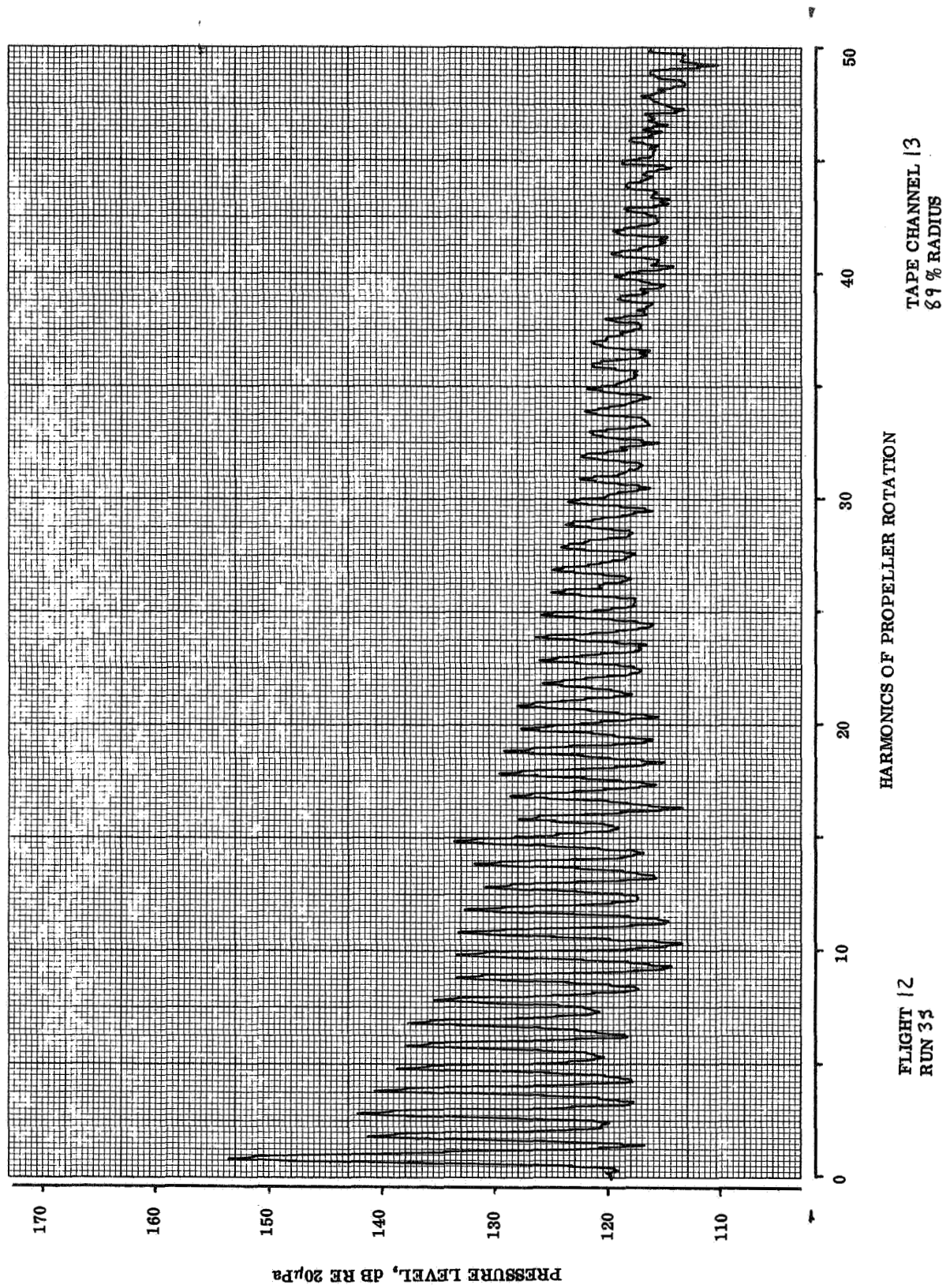


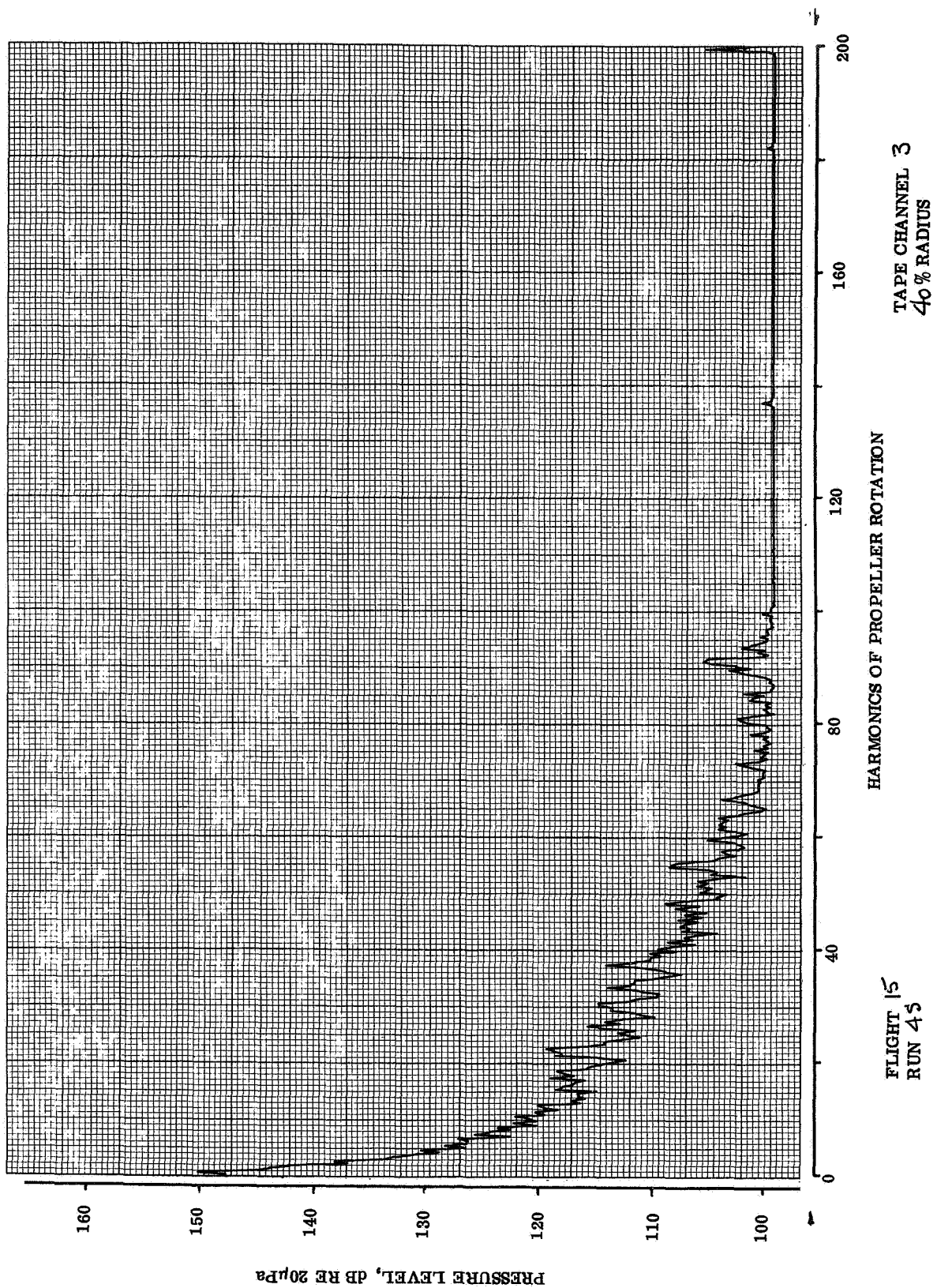
TAPE CHANNEL 13
89 % RADIUS

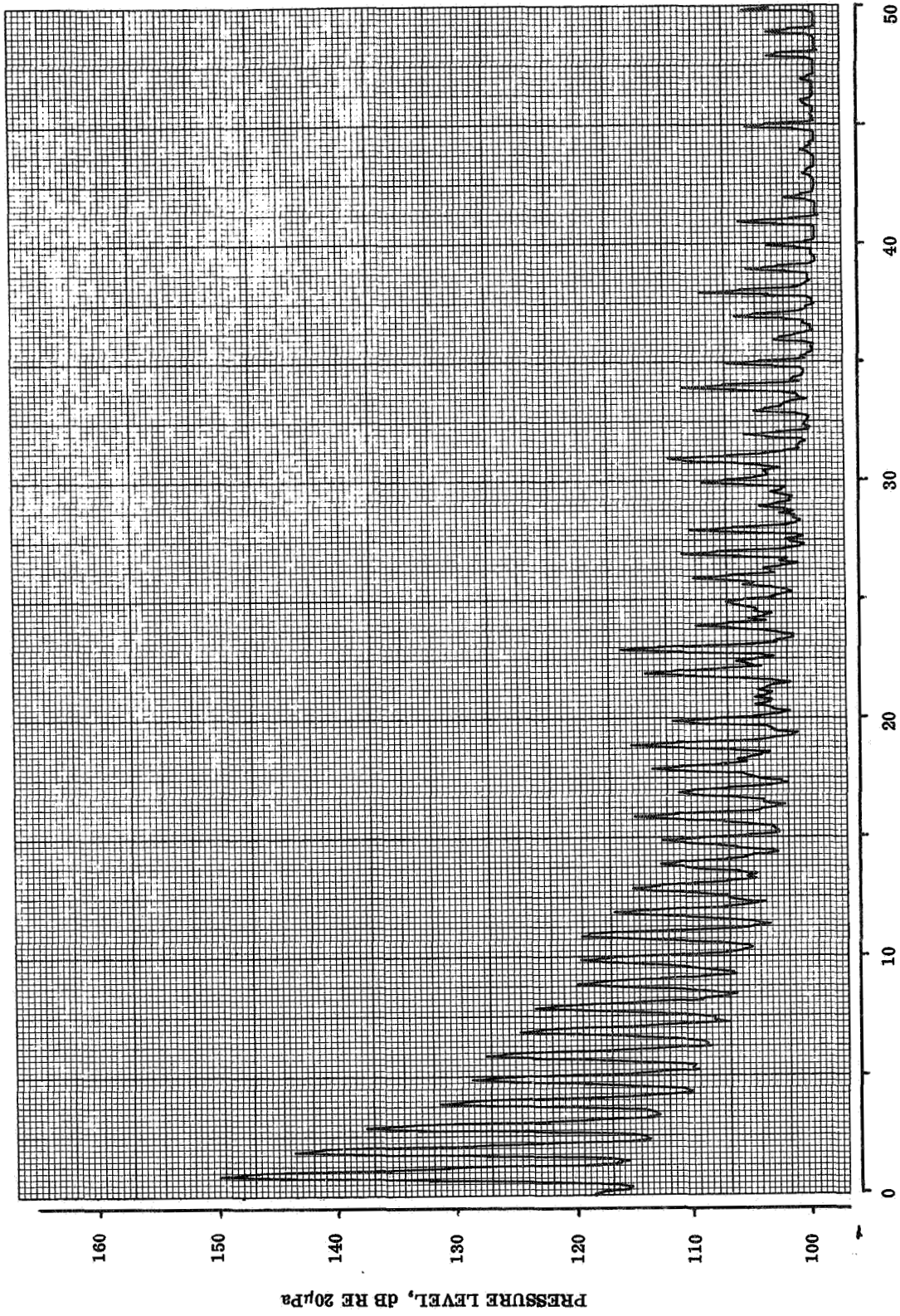
HARMONICS OF PROPELLER ROTATION

FLIGHT 12
RUN 35

PRESSURE LEVEL, DB RE 20μPa



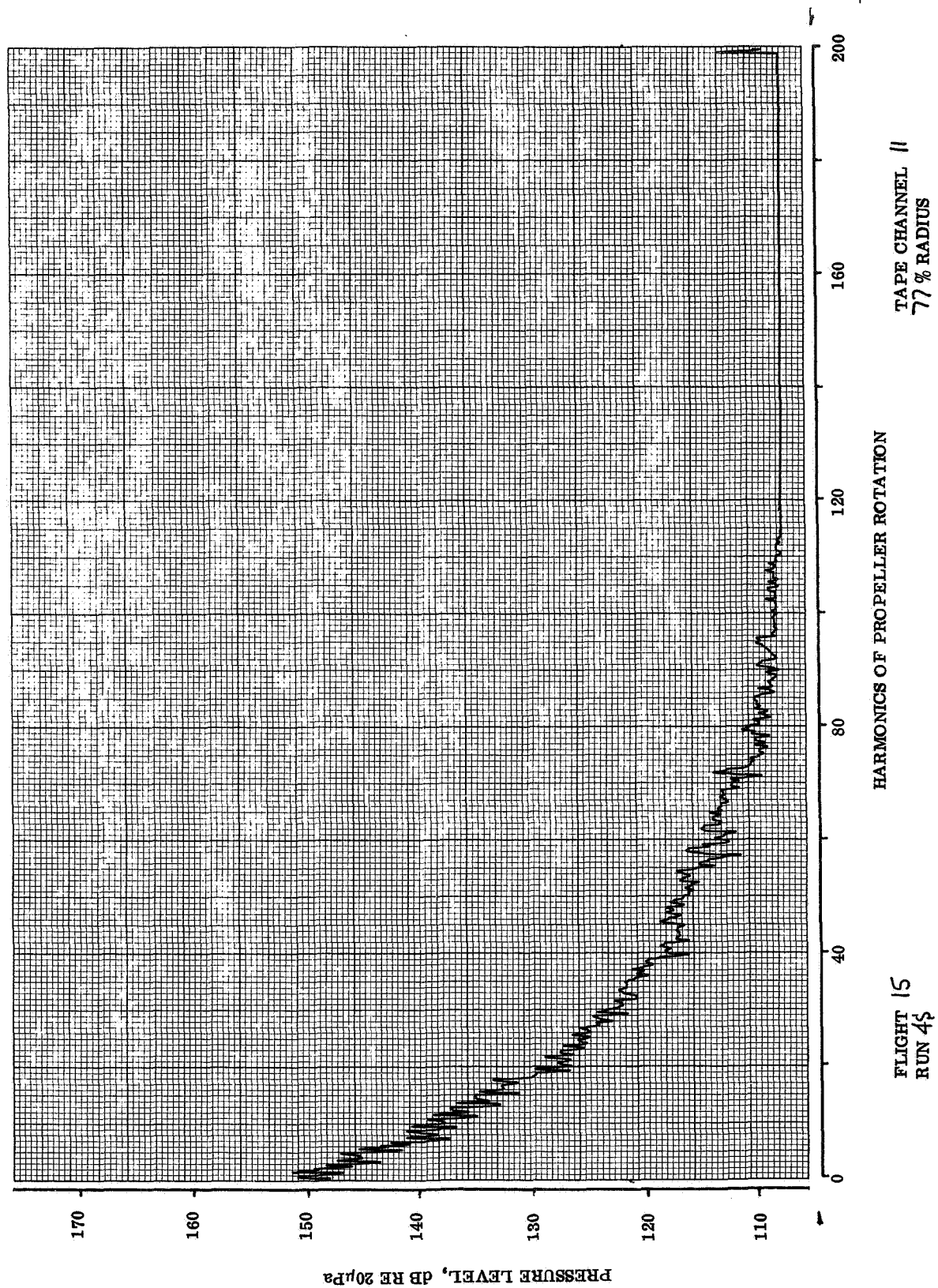


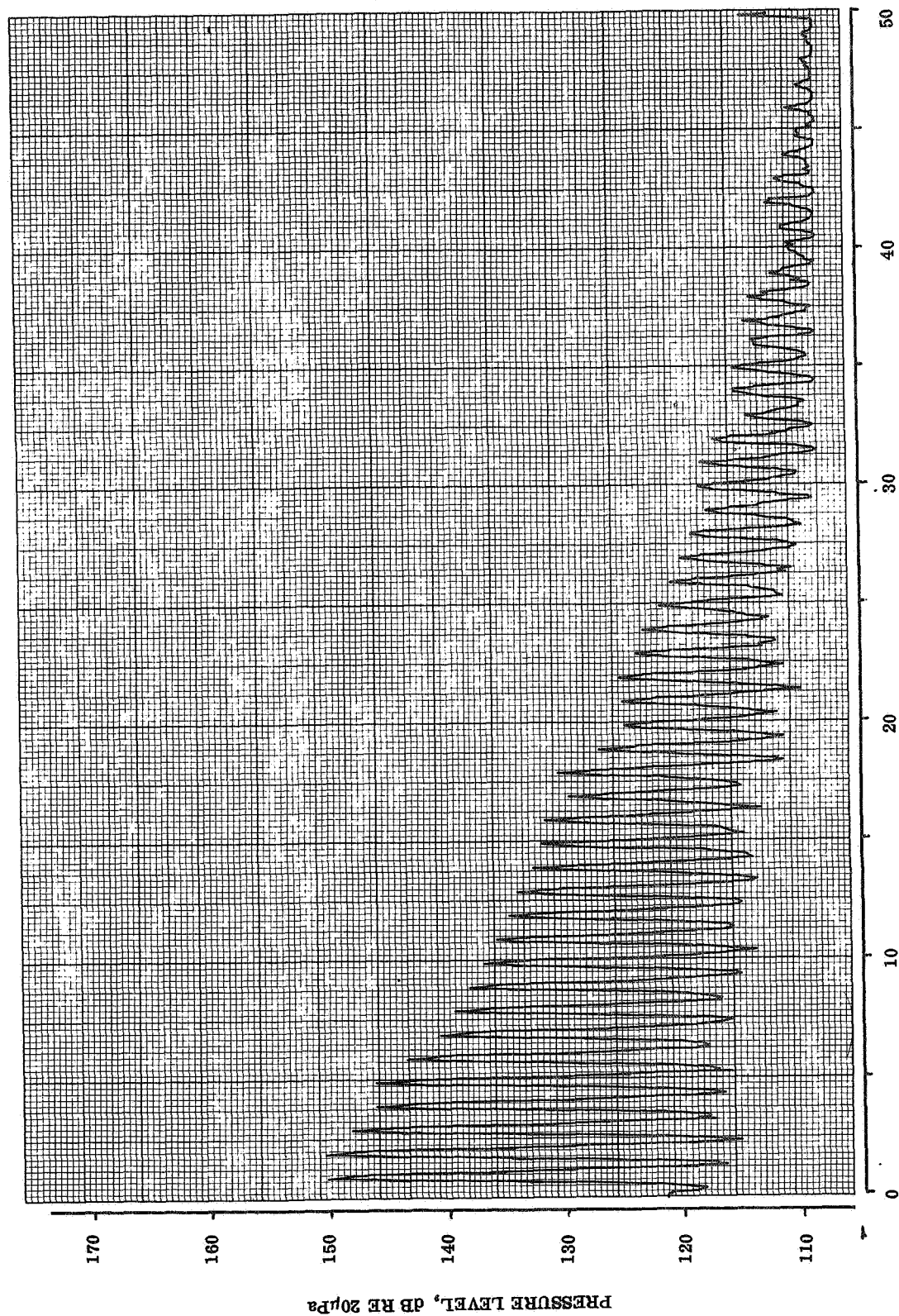


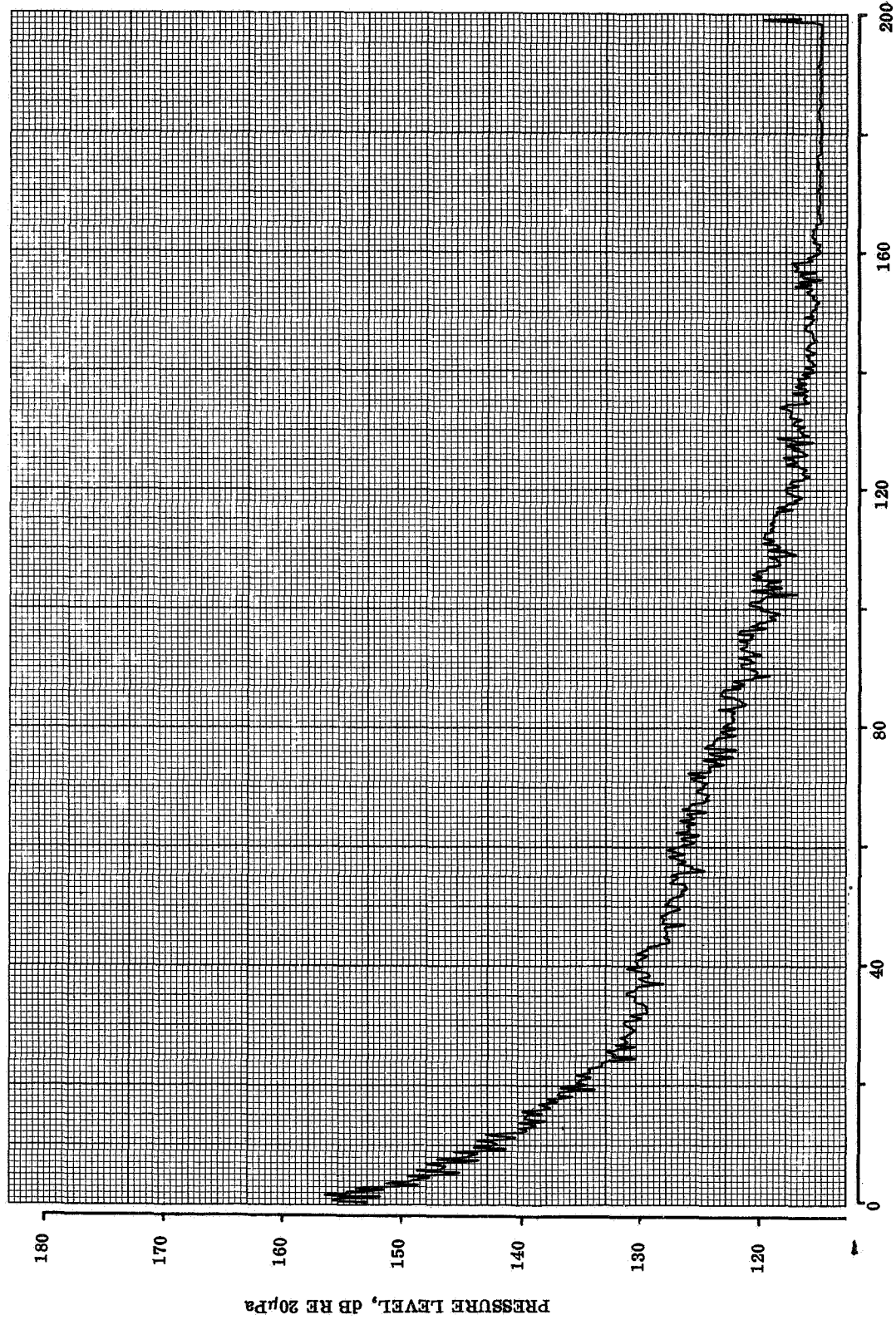
FLIGHT 15
 RUN 45

HARMONICS OF PROPELLER ROTATION

TAPE CHANNEL 3
 40 % RADIUS



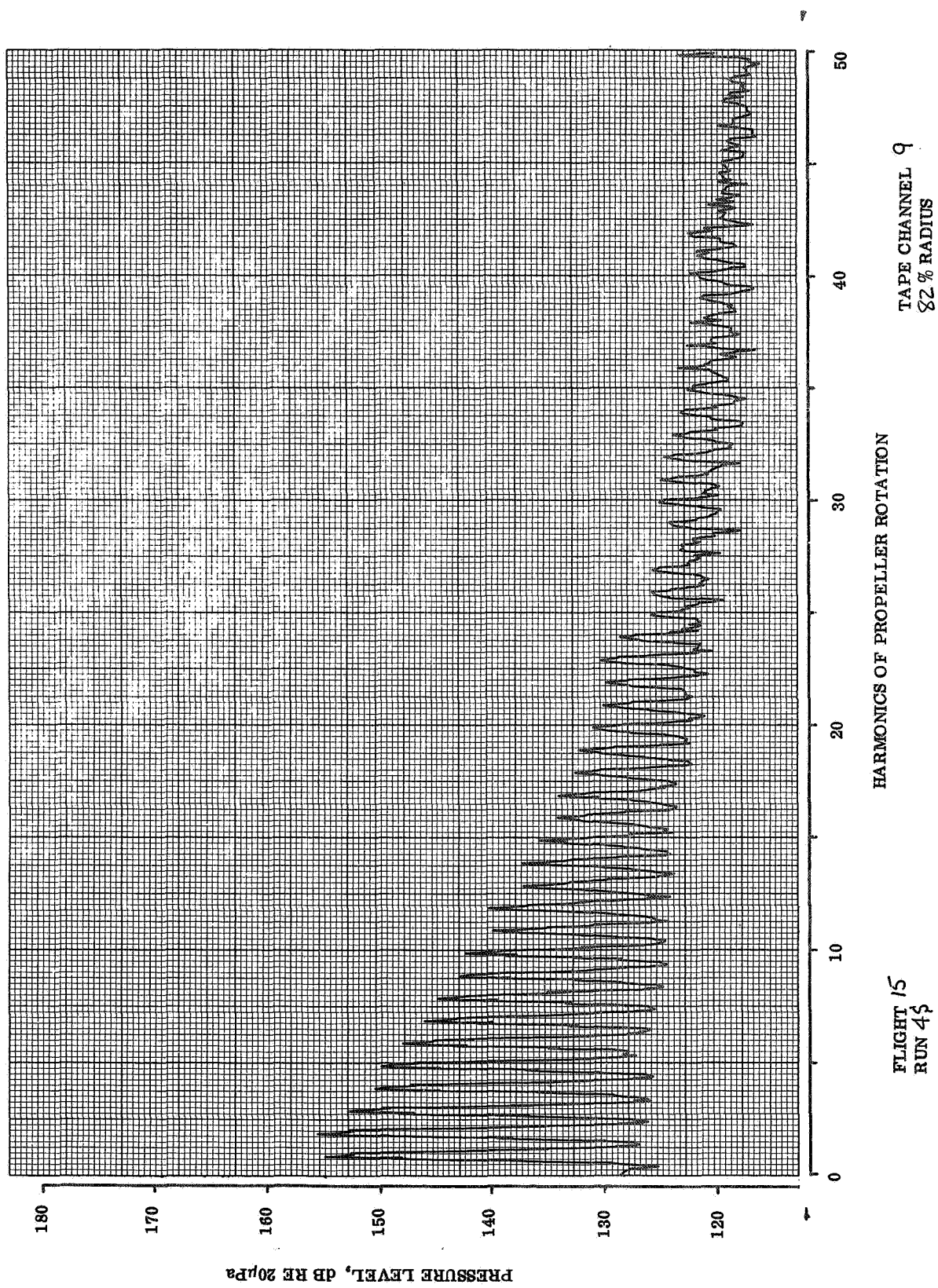


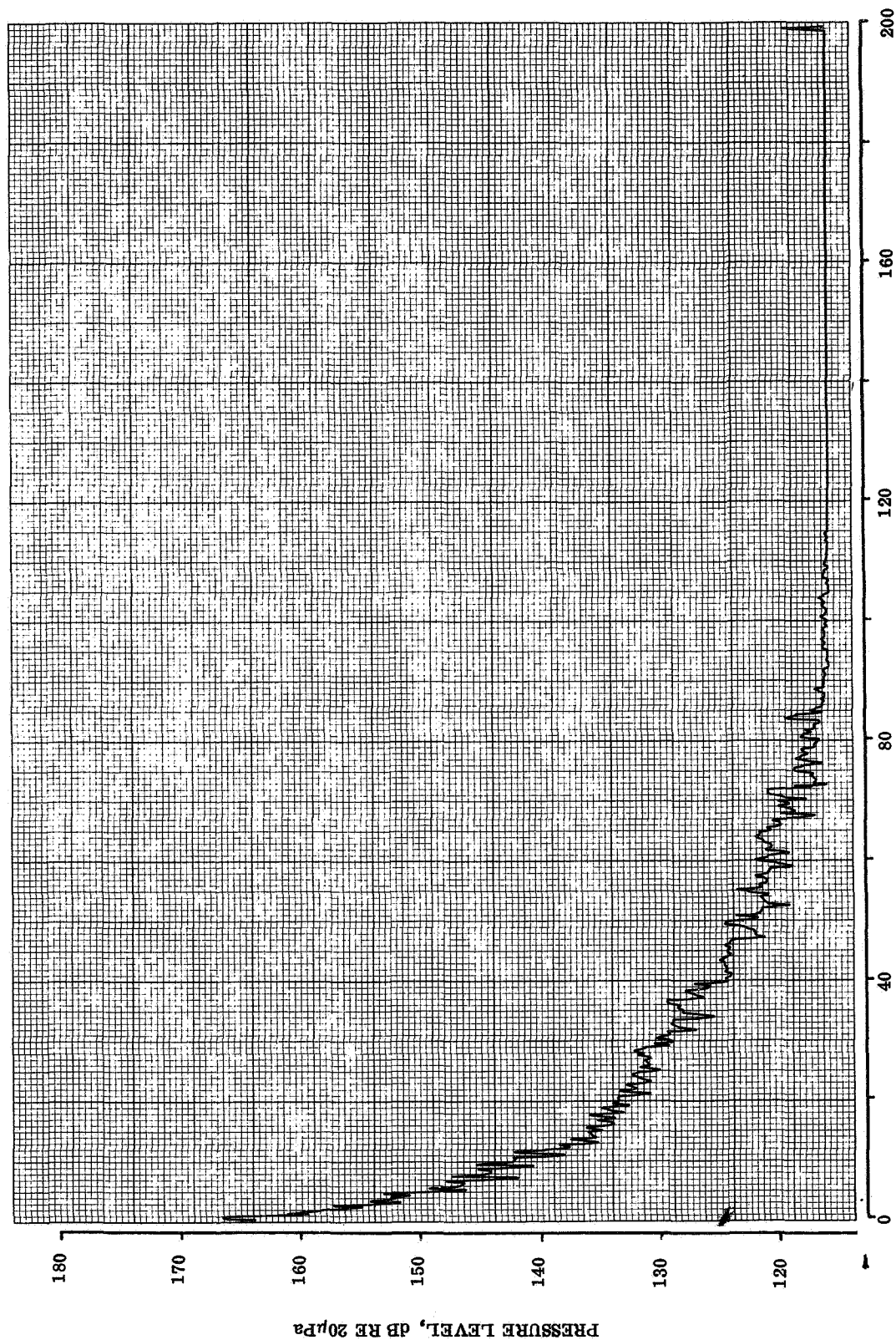


TAPE CHANNEL 9
82 % RADIUS

HARMONICS OF PROPELLER ROTATION

FLIGHT 15
RUN 45

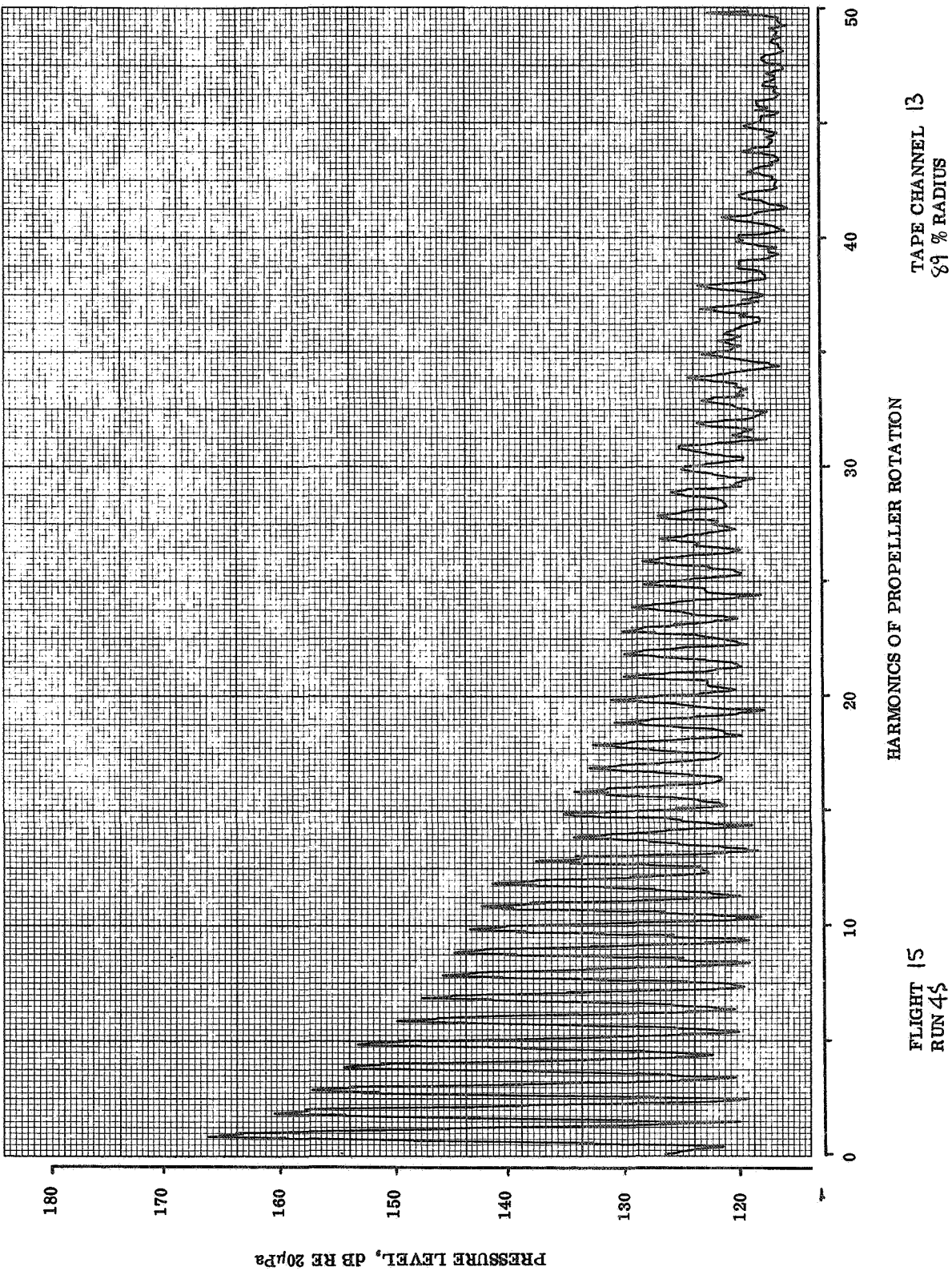


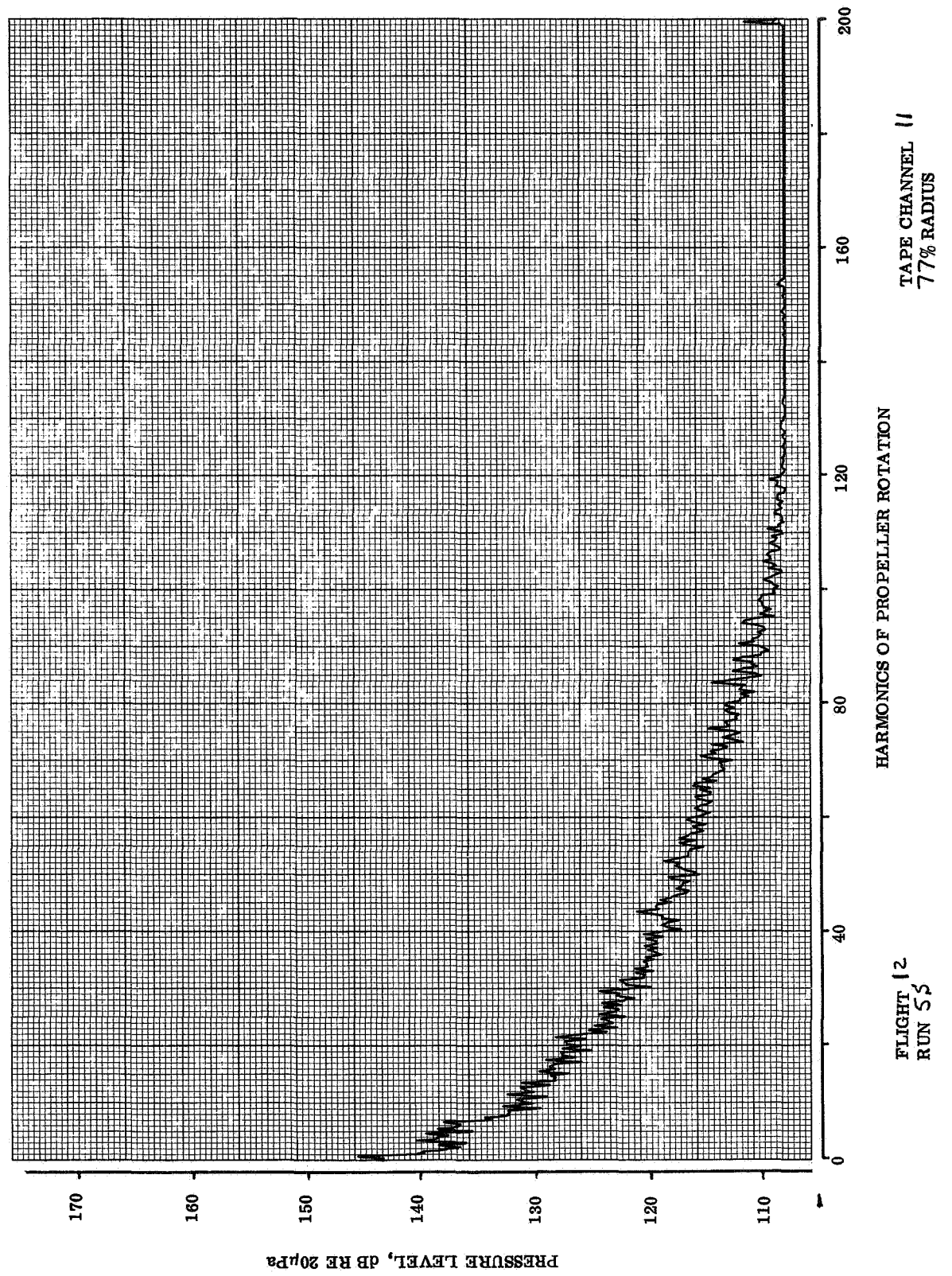


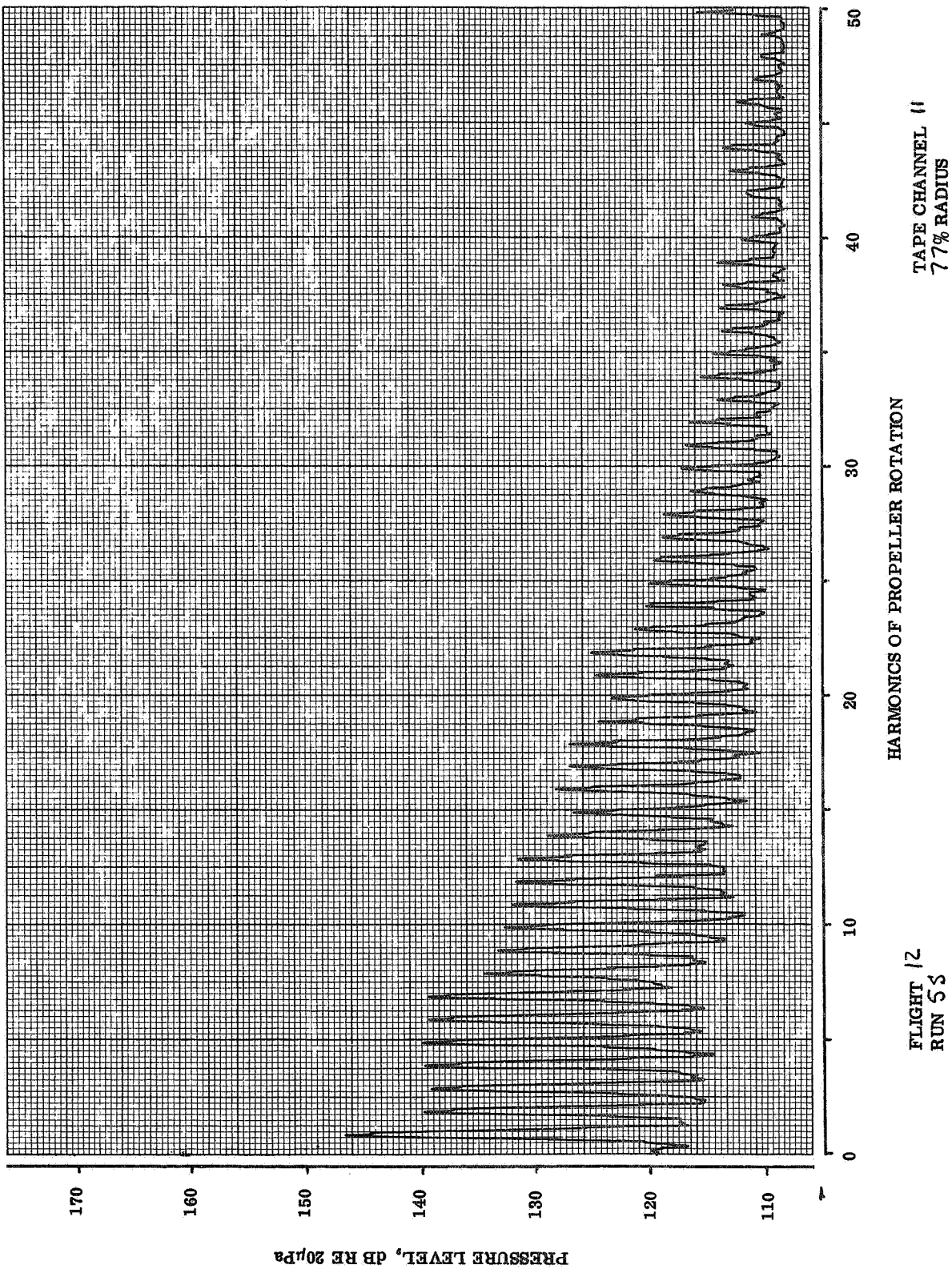
TAPE CHANNEL 13
89 % RADIUS

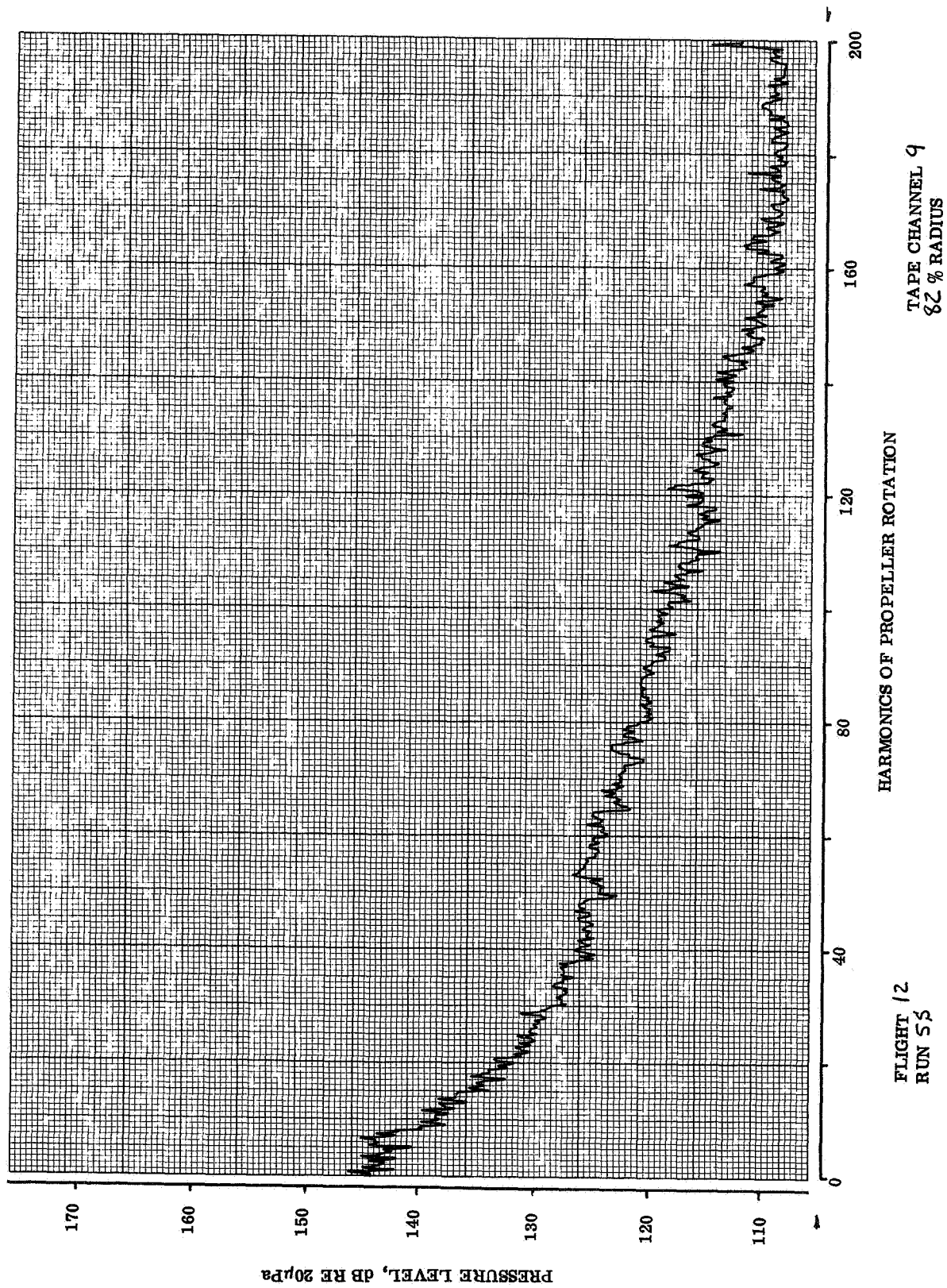
HARMONICS OF PROPELLER ROTATION

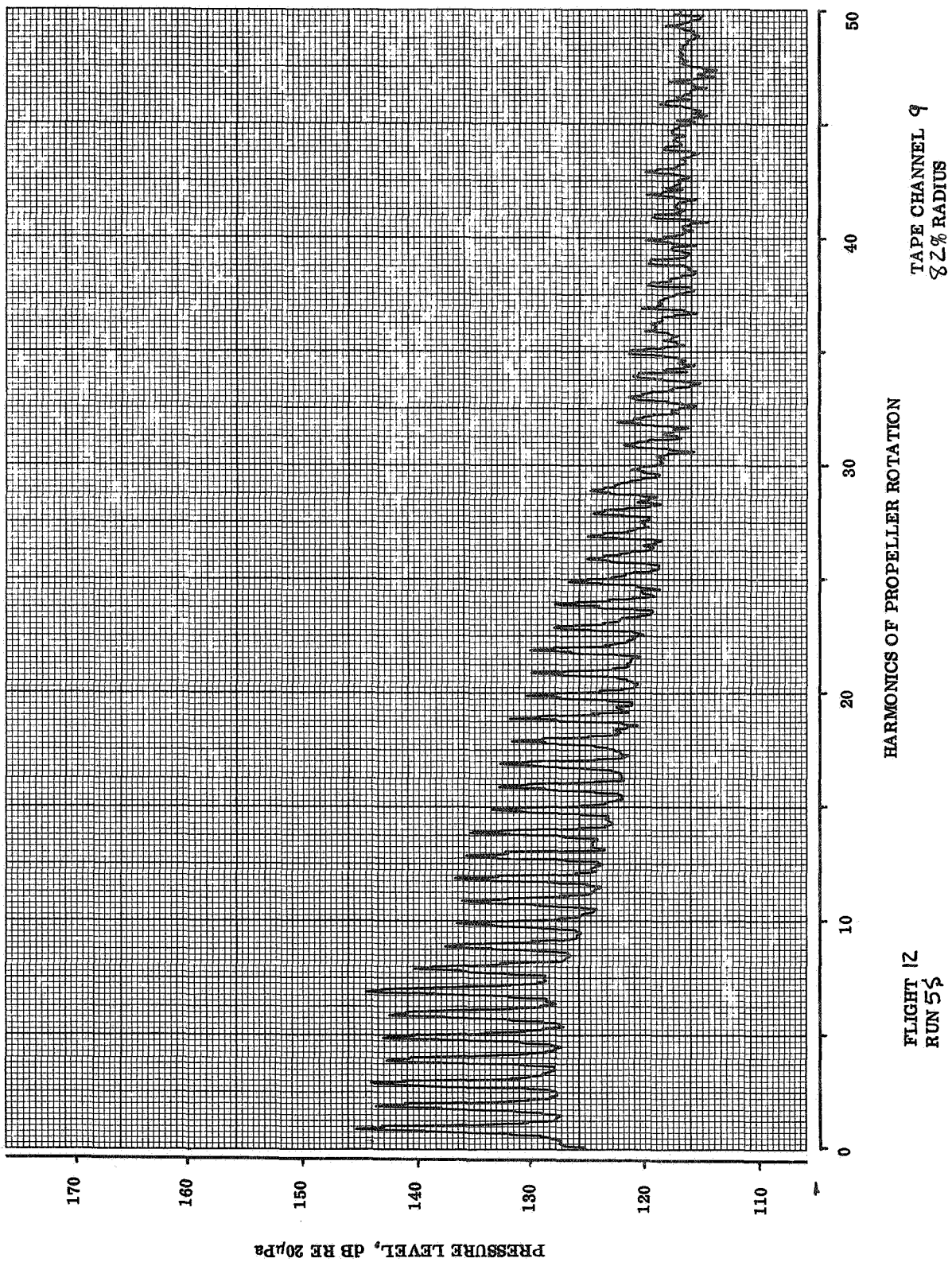
FLIGHT 15
RUN 48

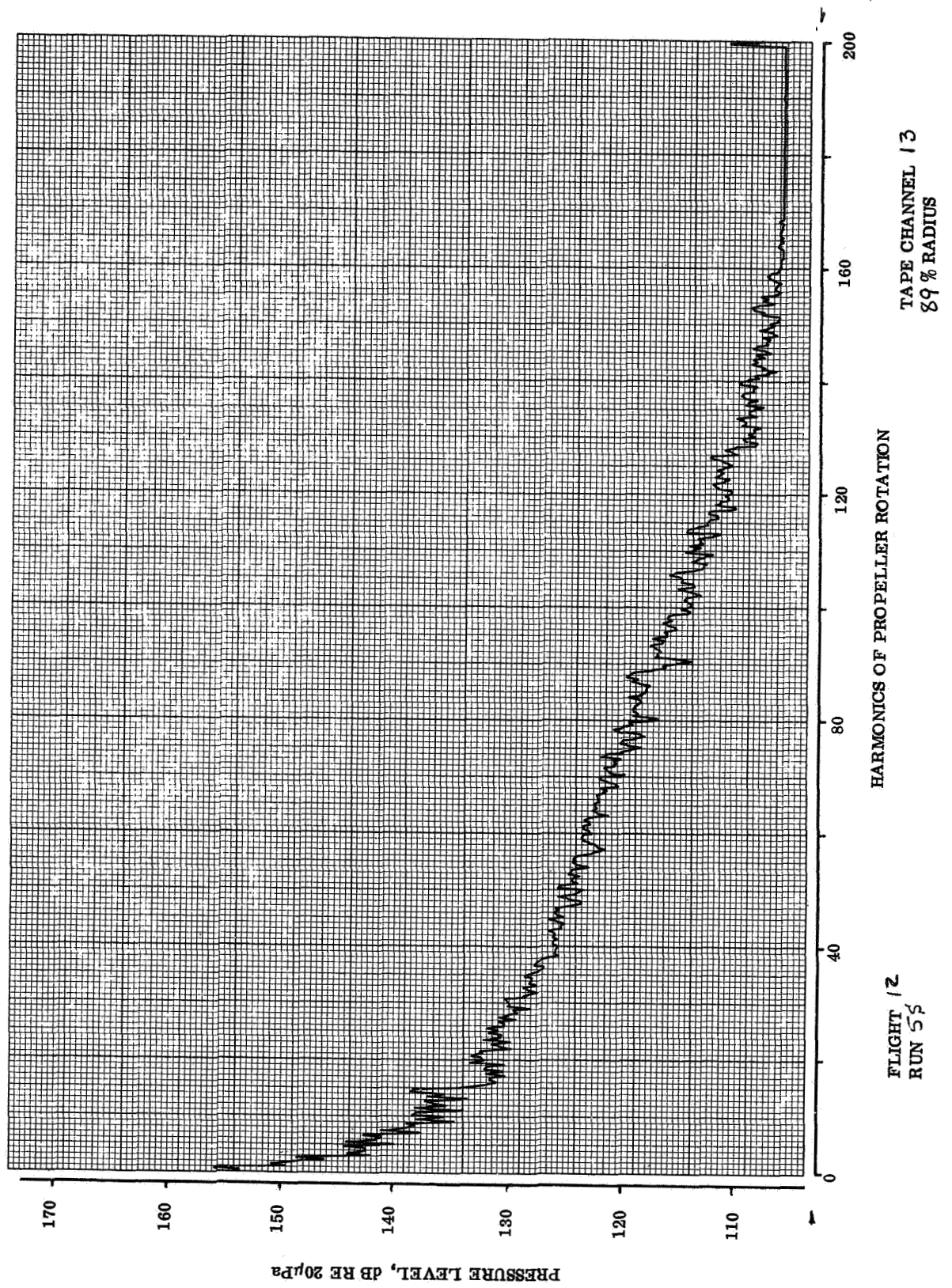


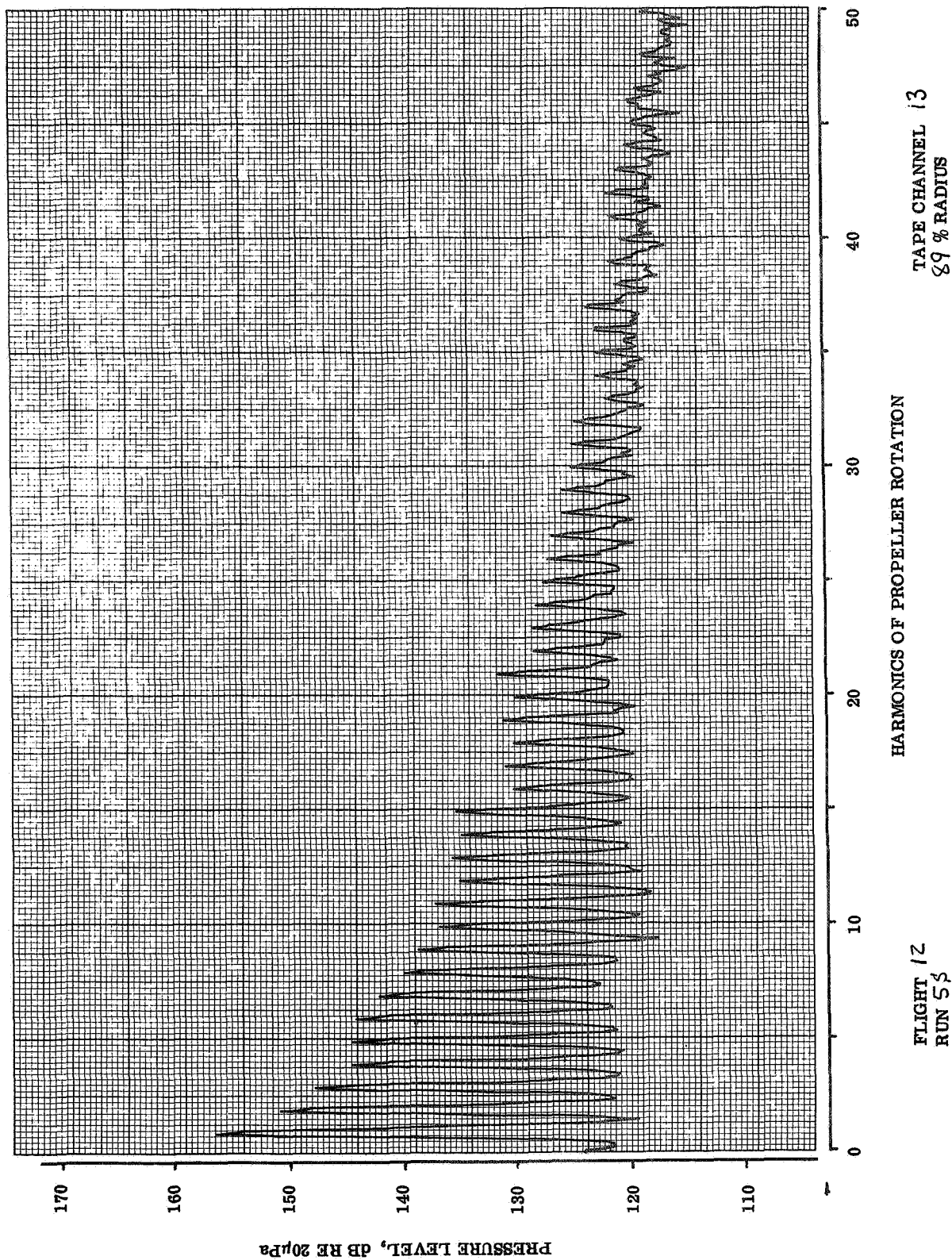


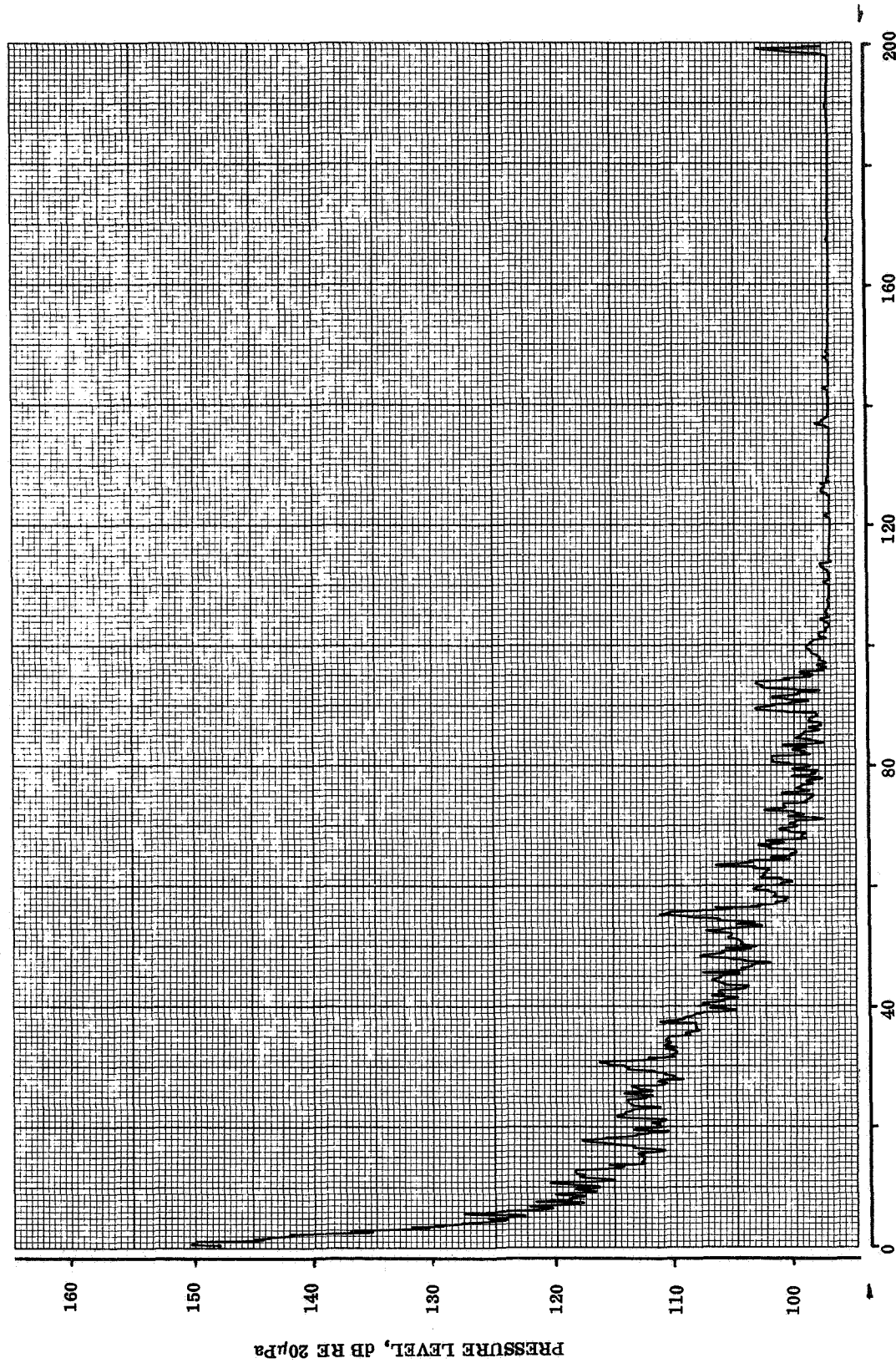








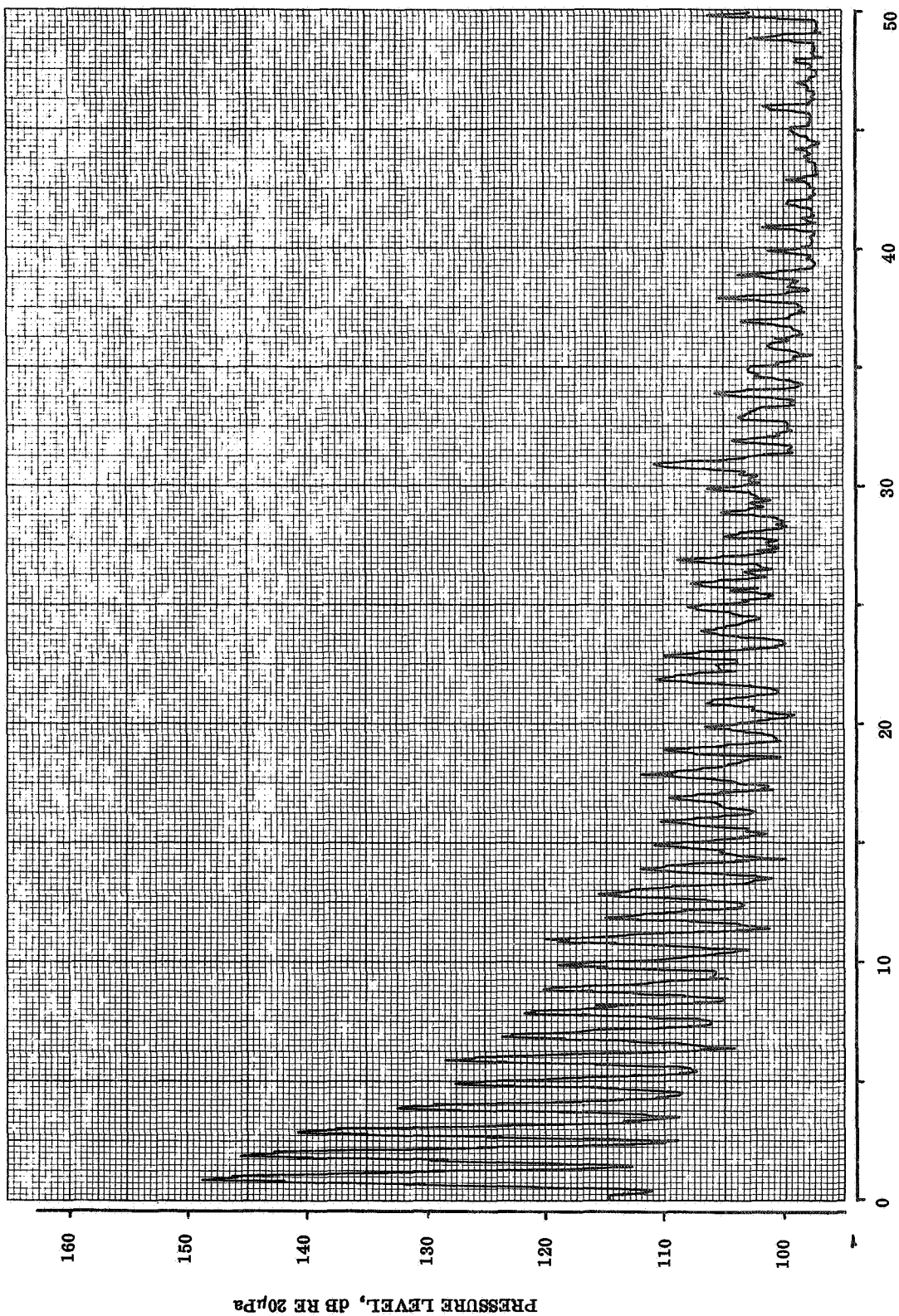




TAPE CHANNEL 3
40 % RADIUS

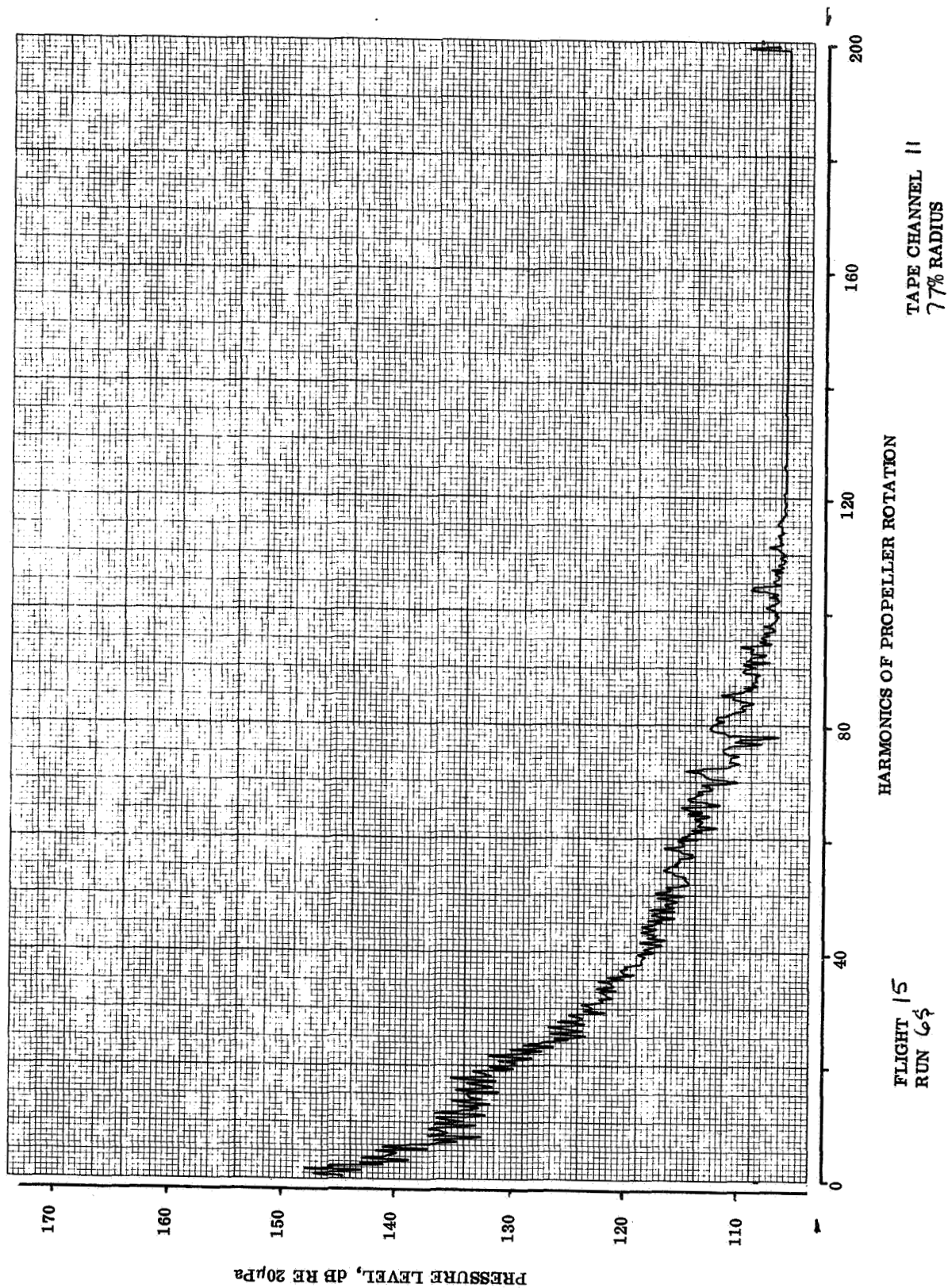
HARMONICS OF PROPELLER ROTATION

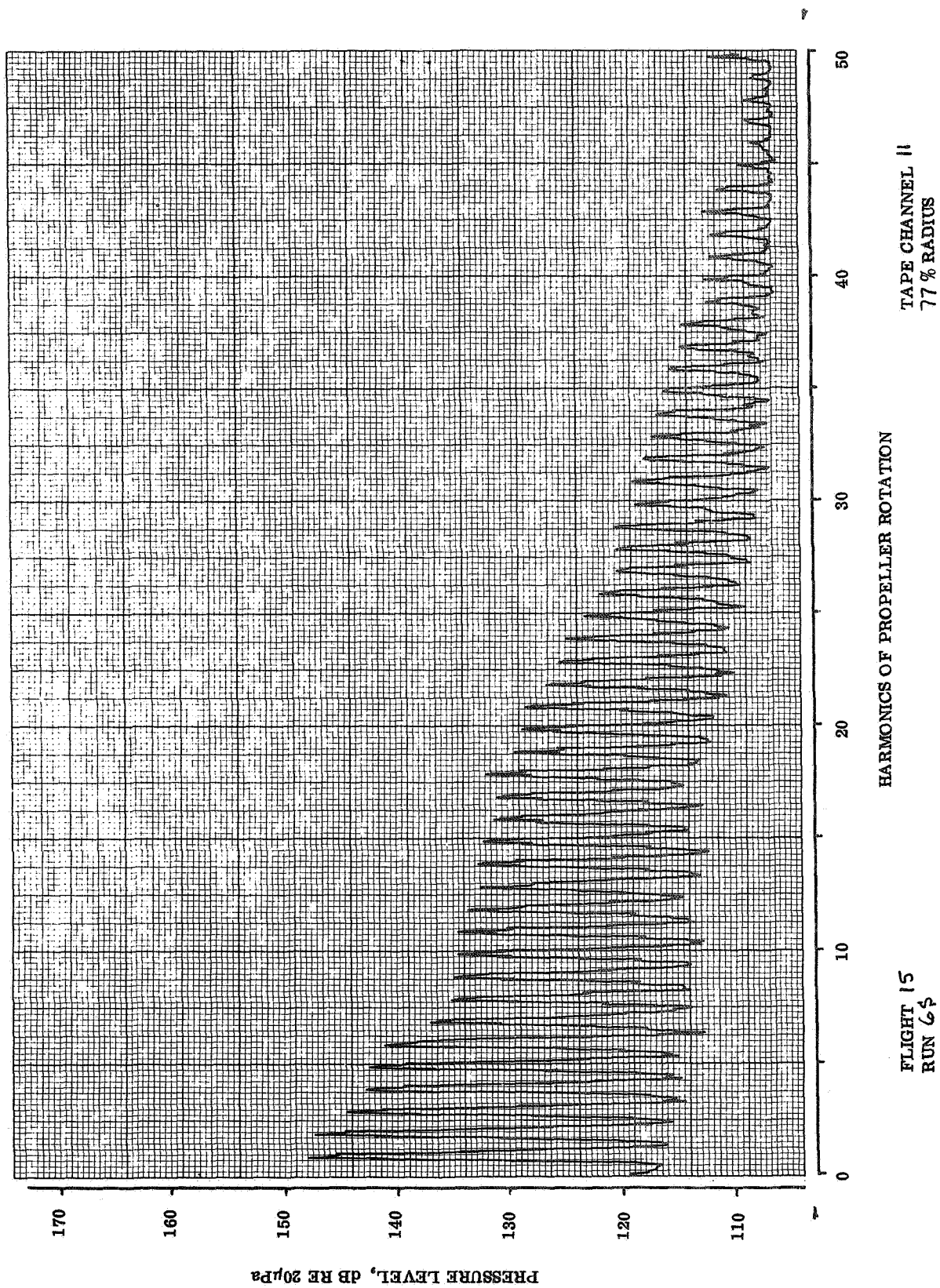
FLIGHT 15
RUN 65

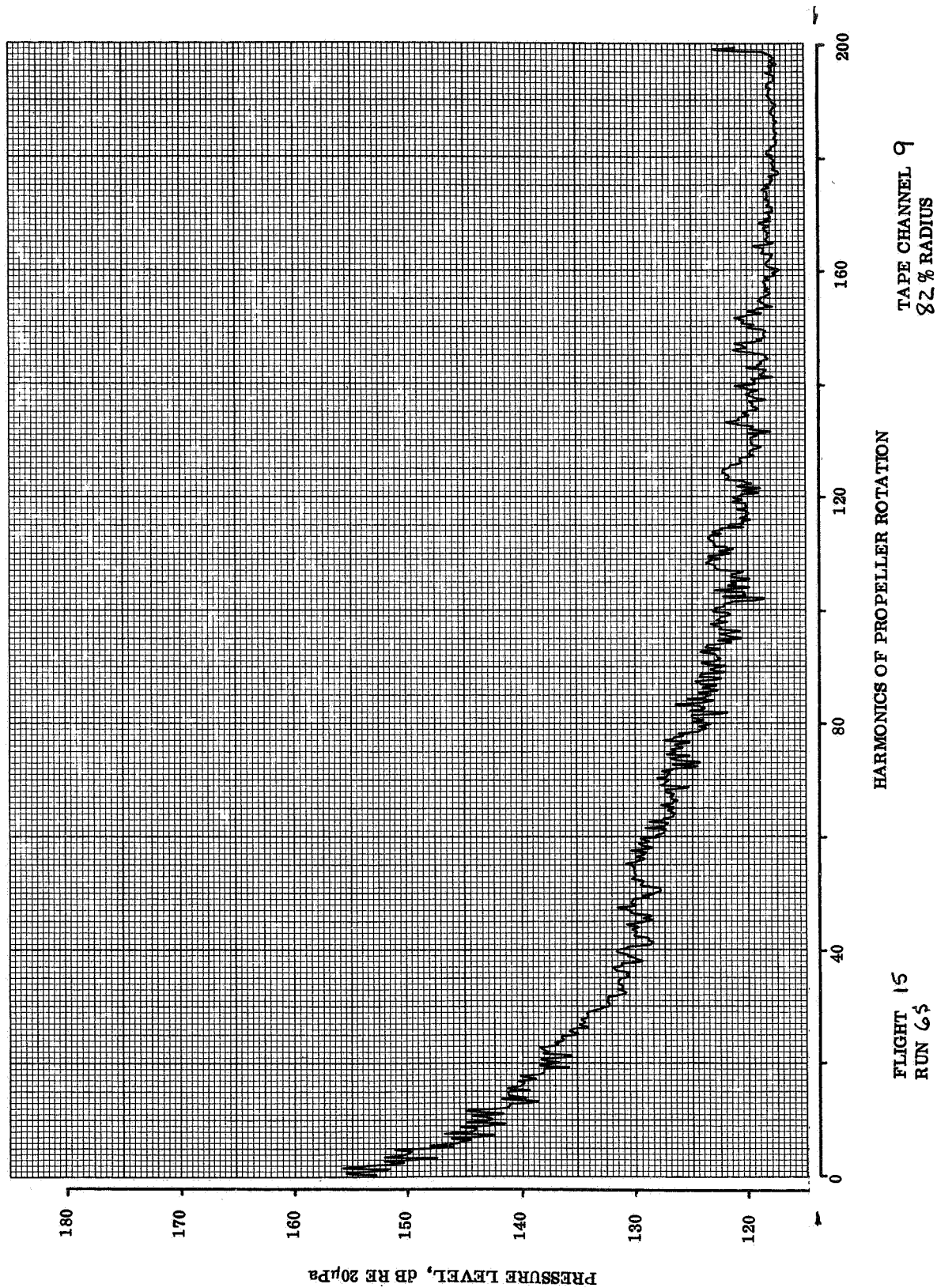


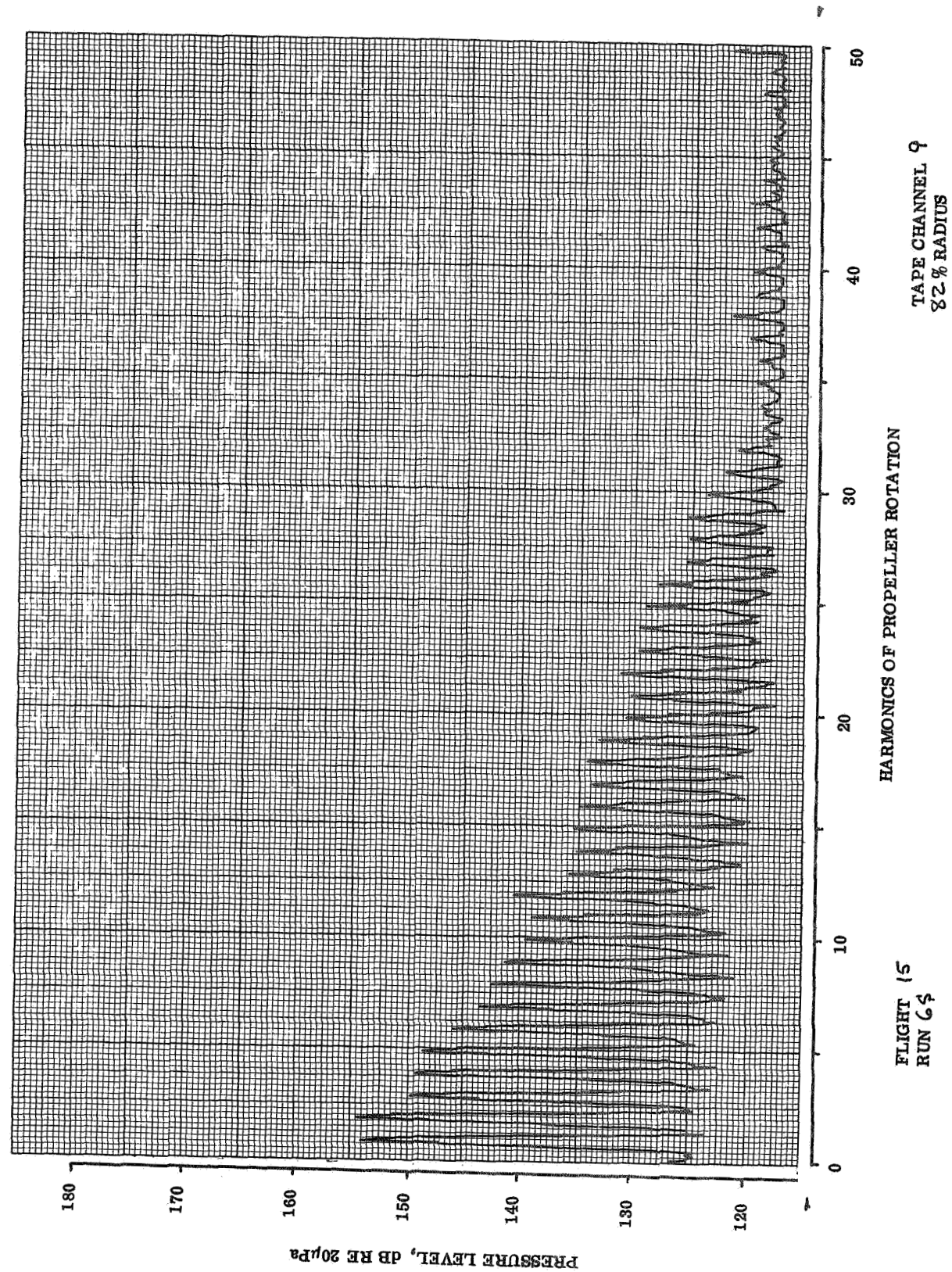
FLIGHT 15
RUN 65

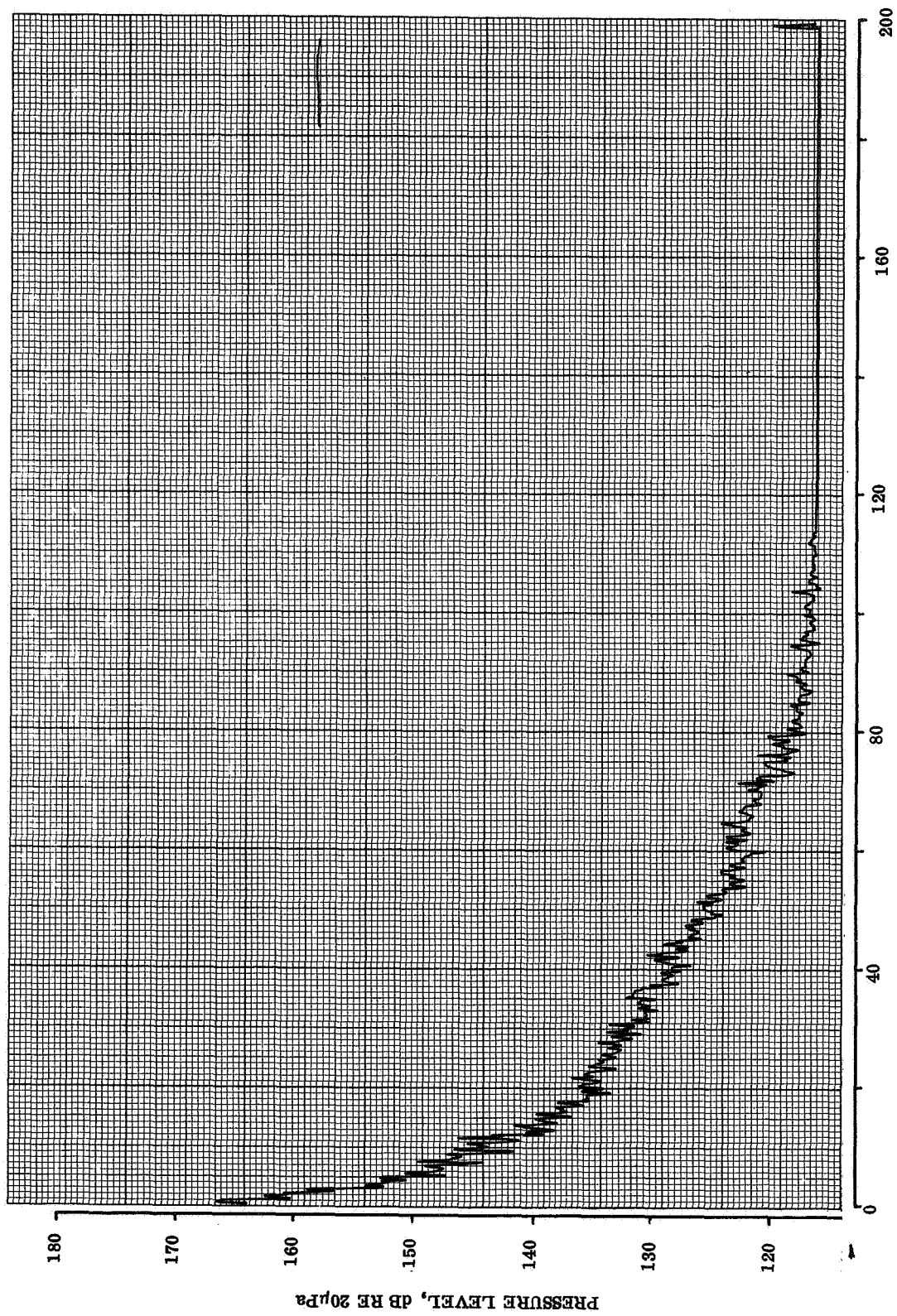
TAPE CHANNEL 3
40% RADIUS







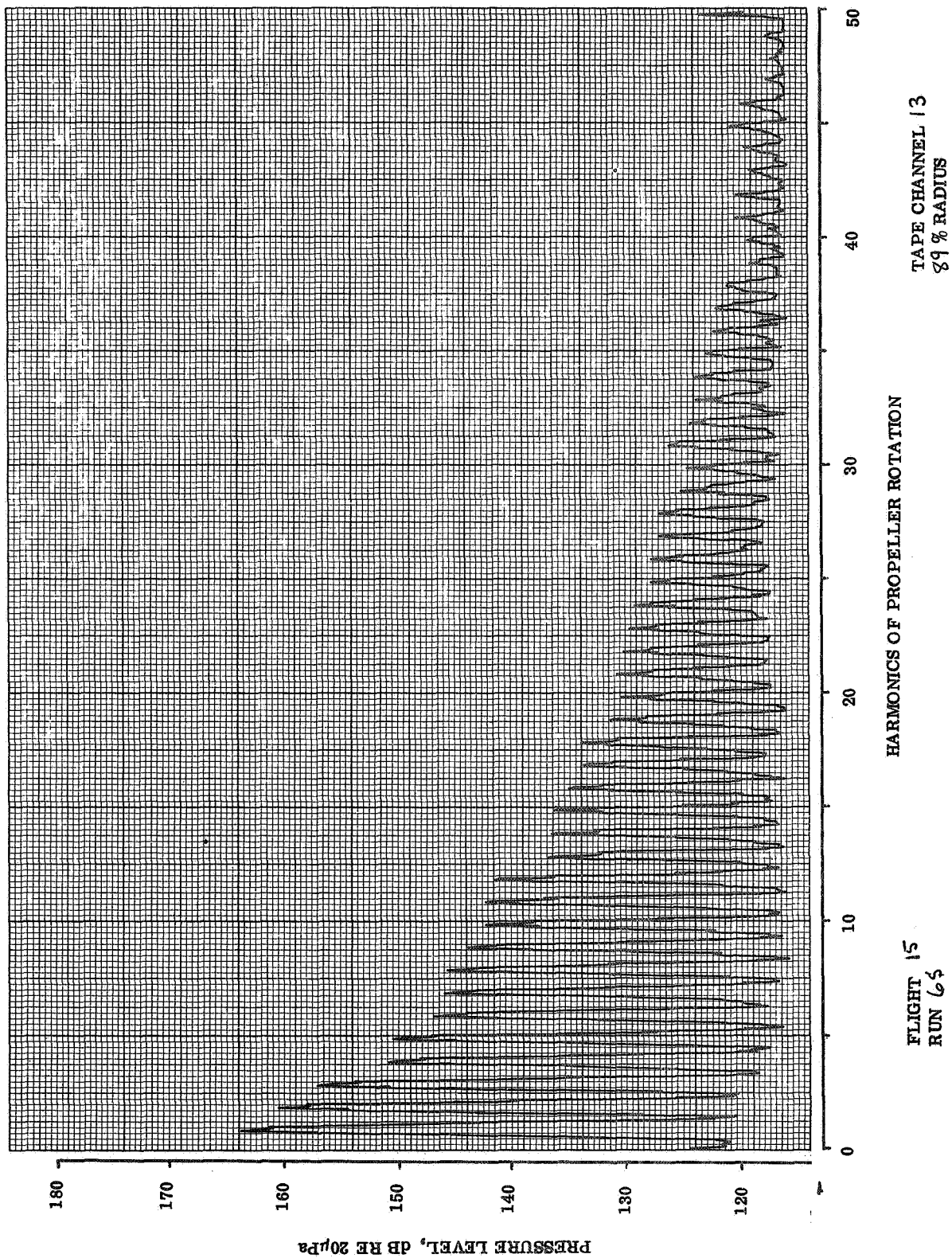


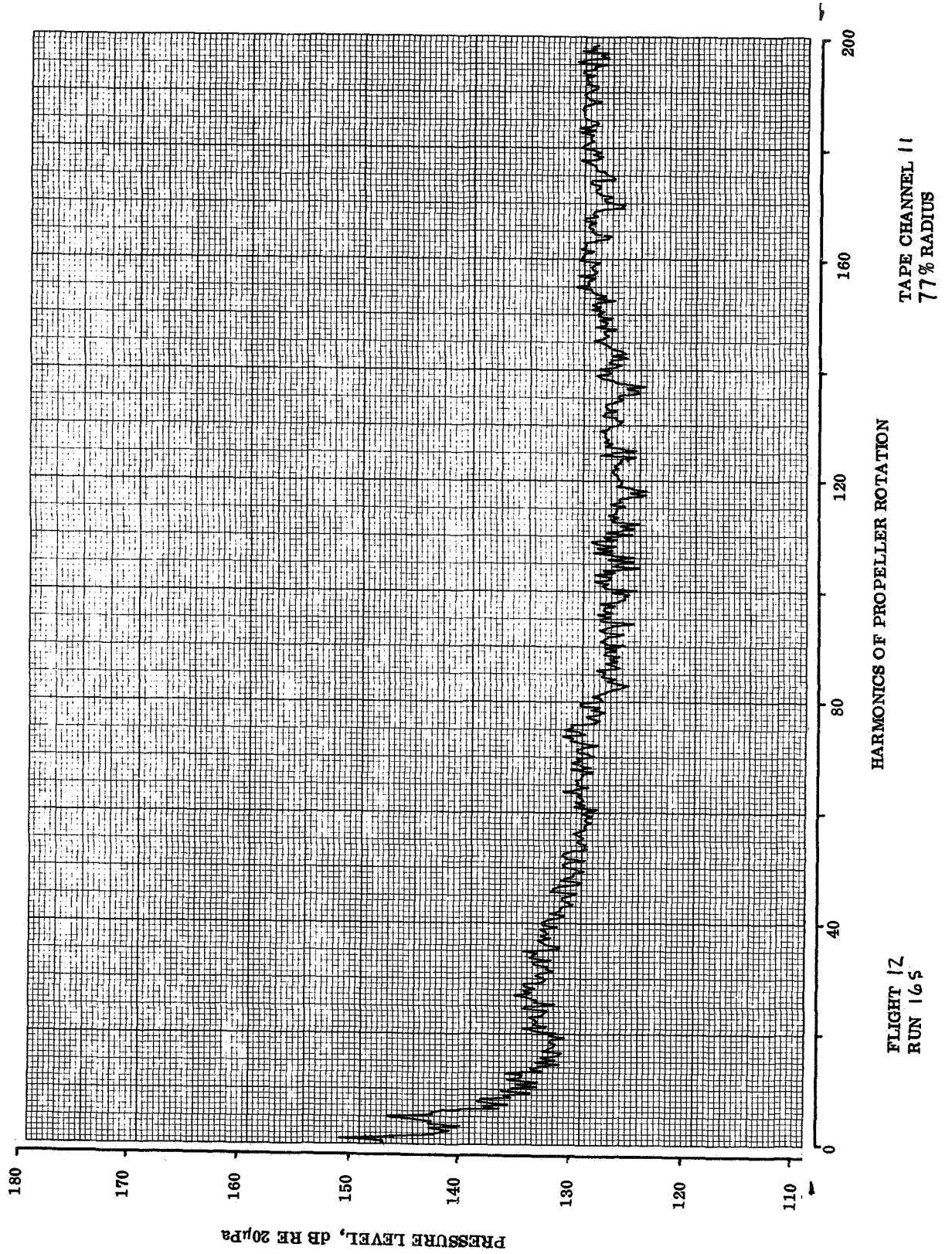


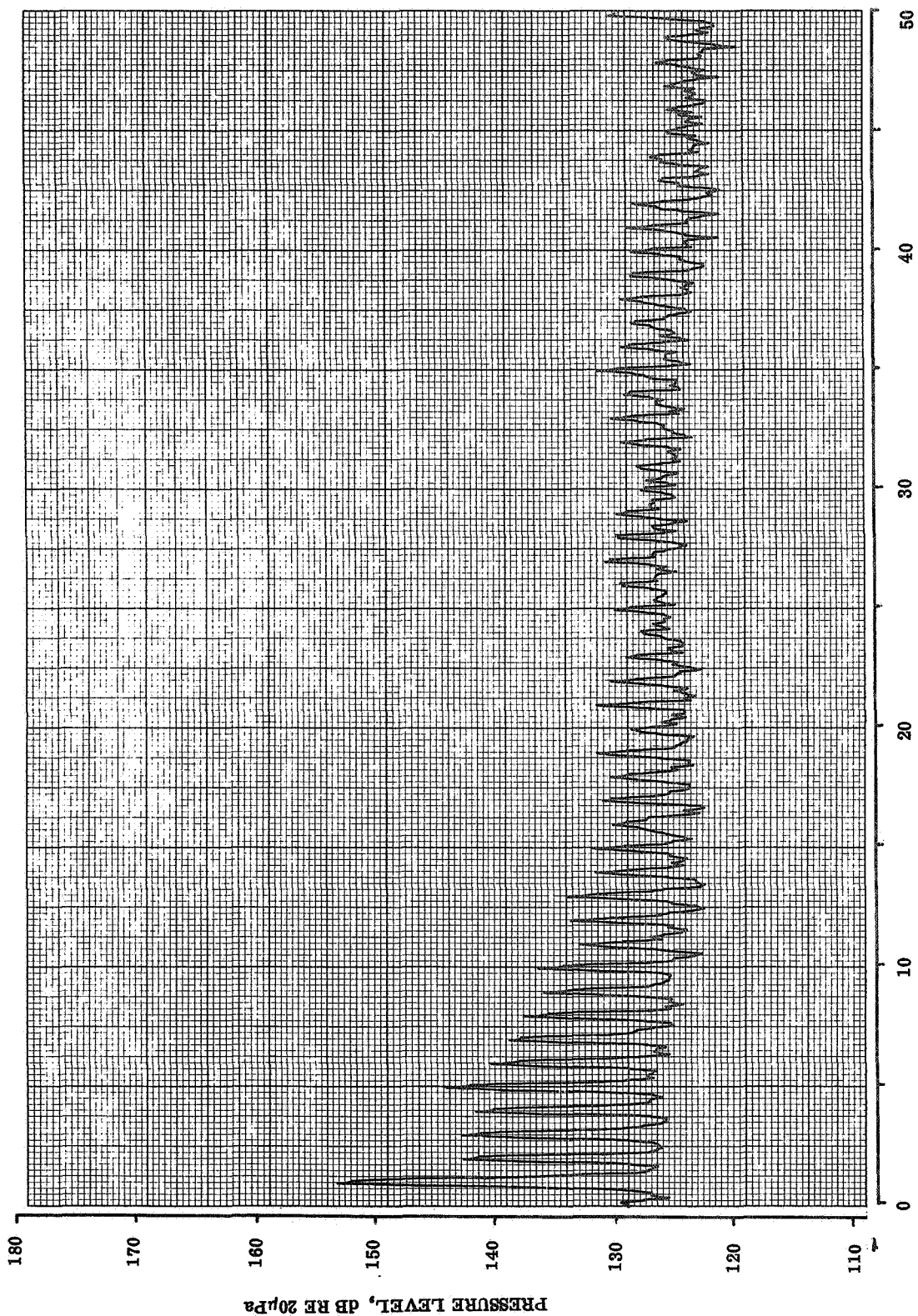
TAPE CHANNEL 13
89% RADIUS

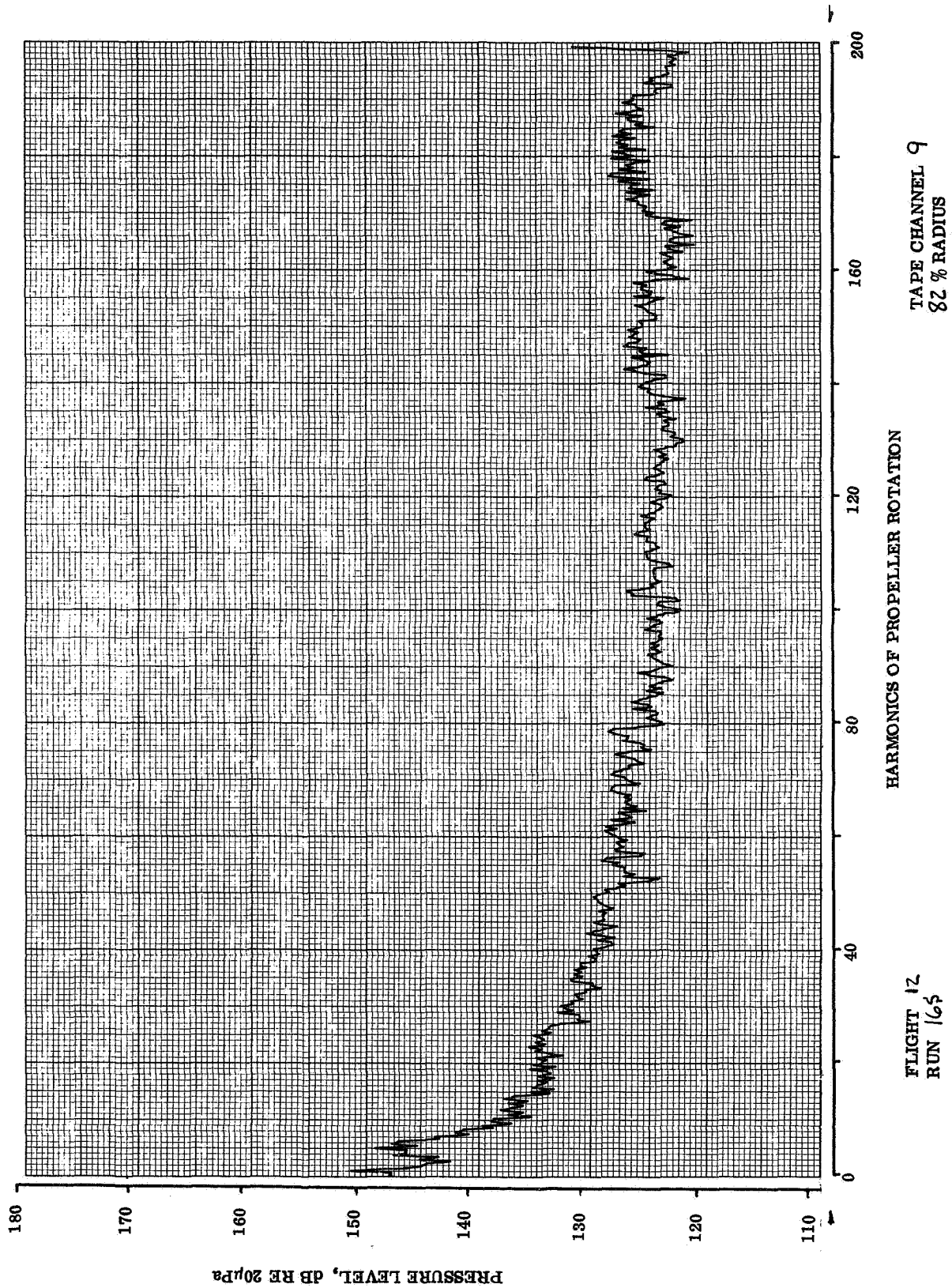
HARMONICS OF PROPELLER ROTATION

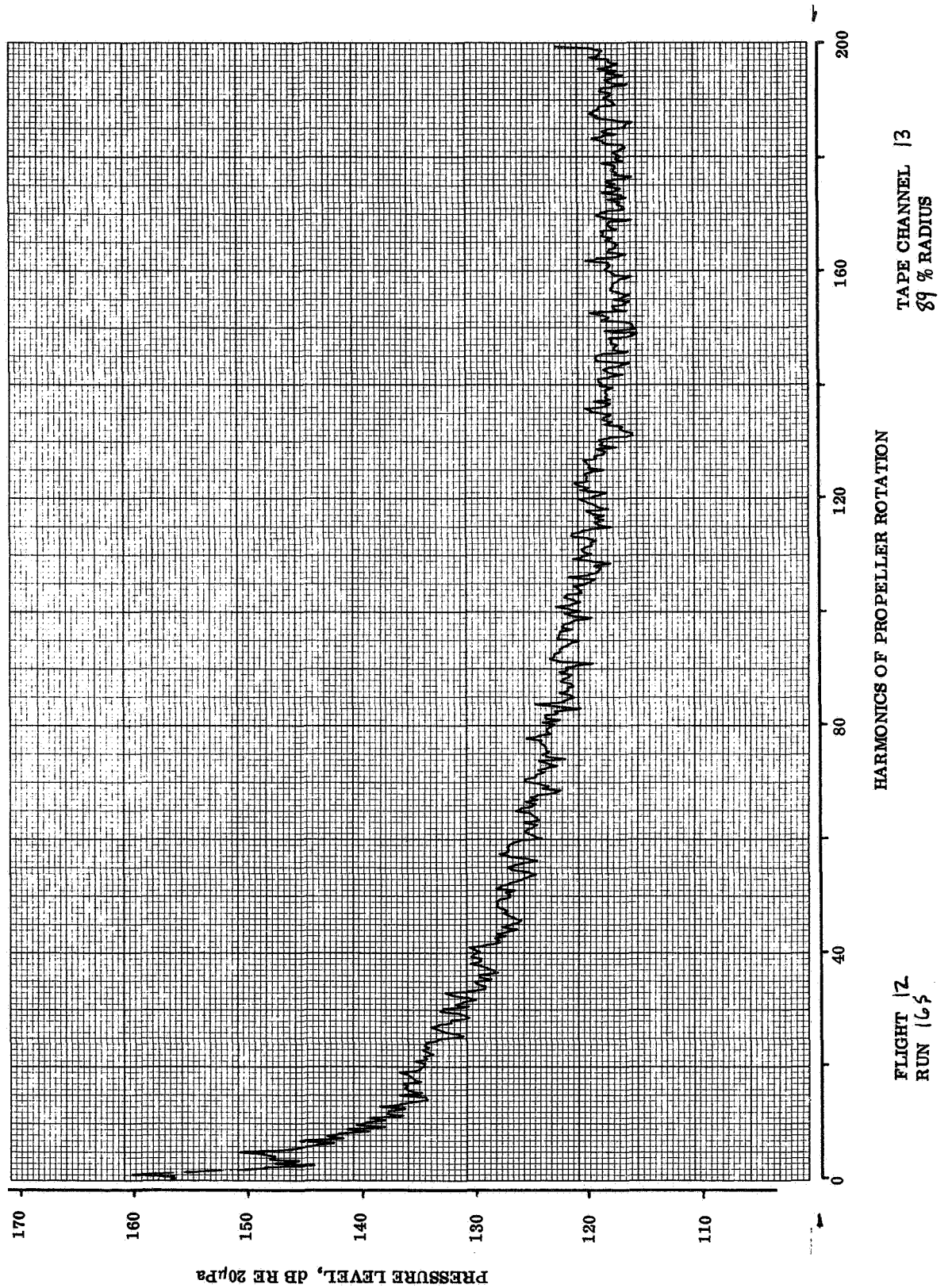
FLIGHT 15
RUN 65

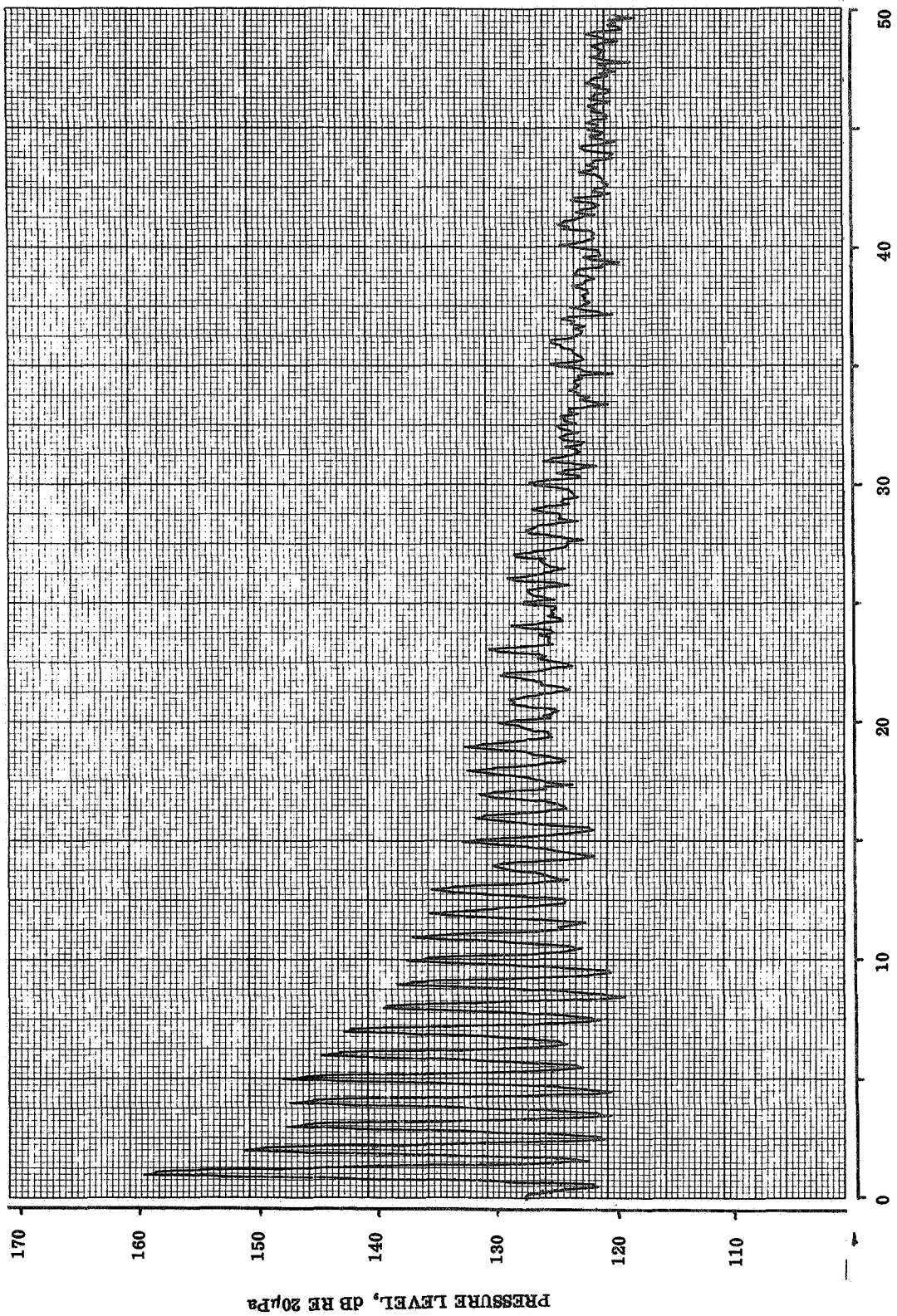








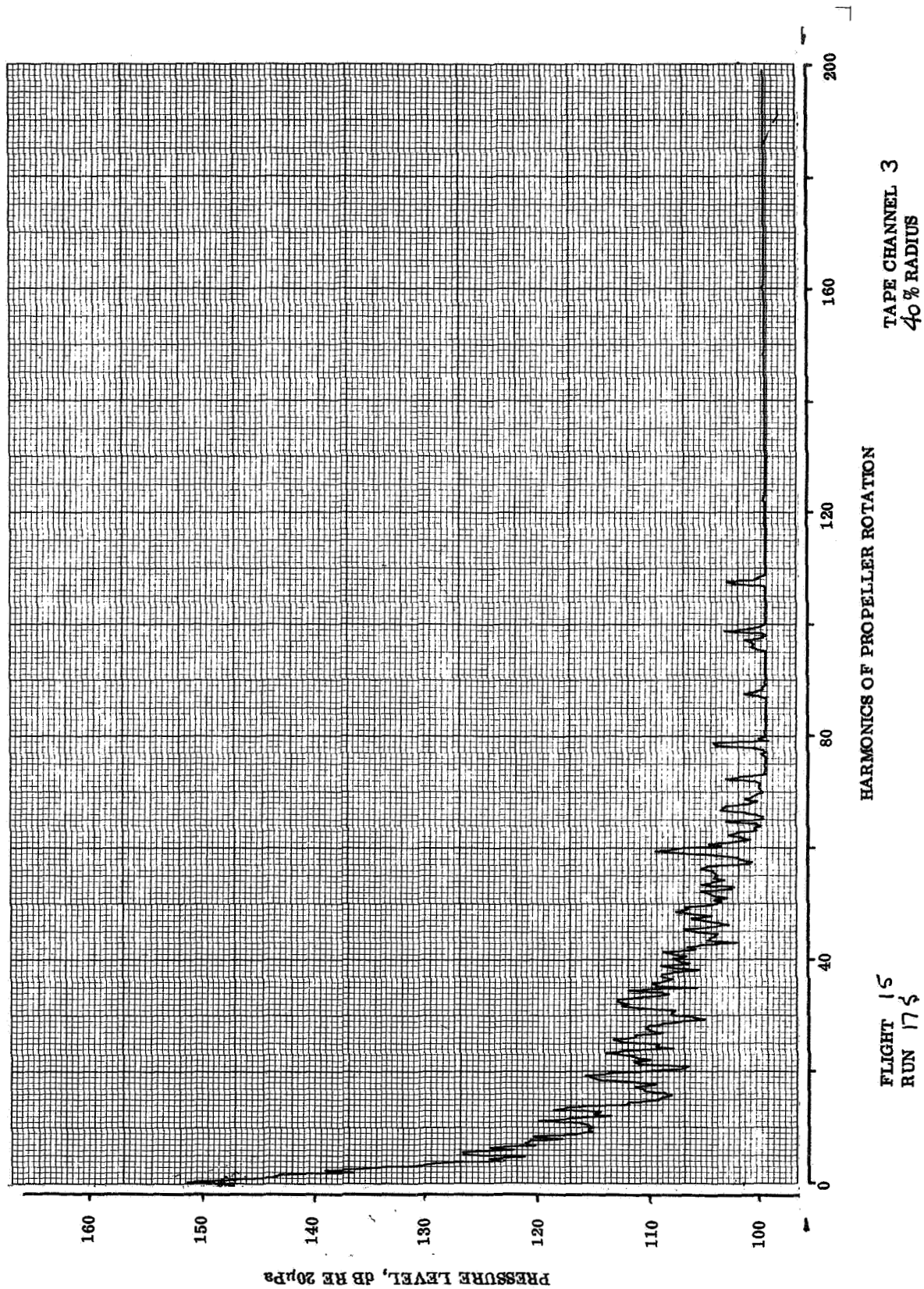


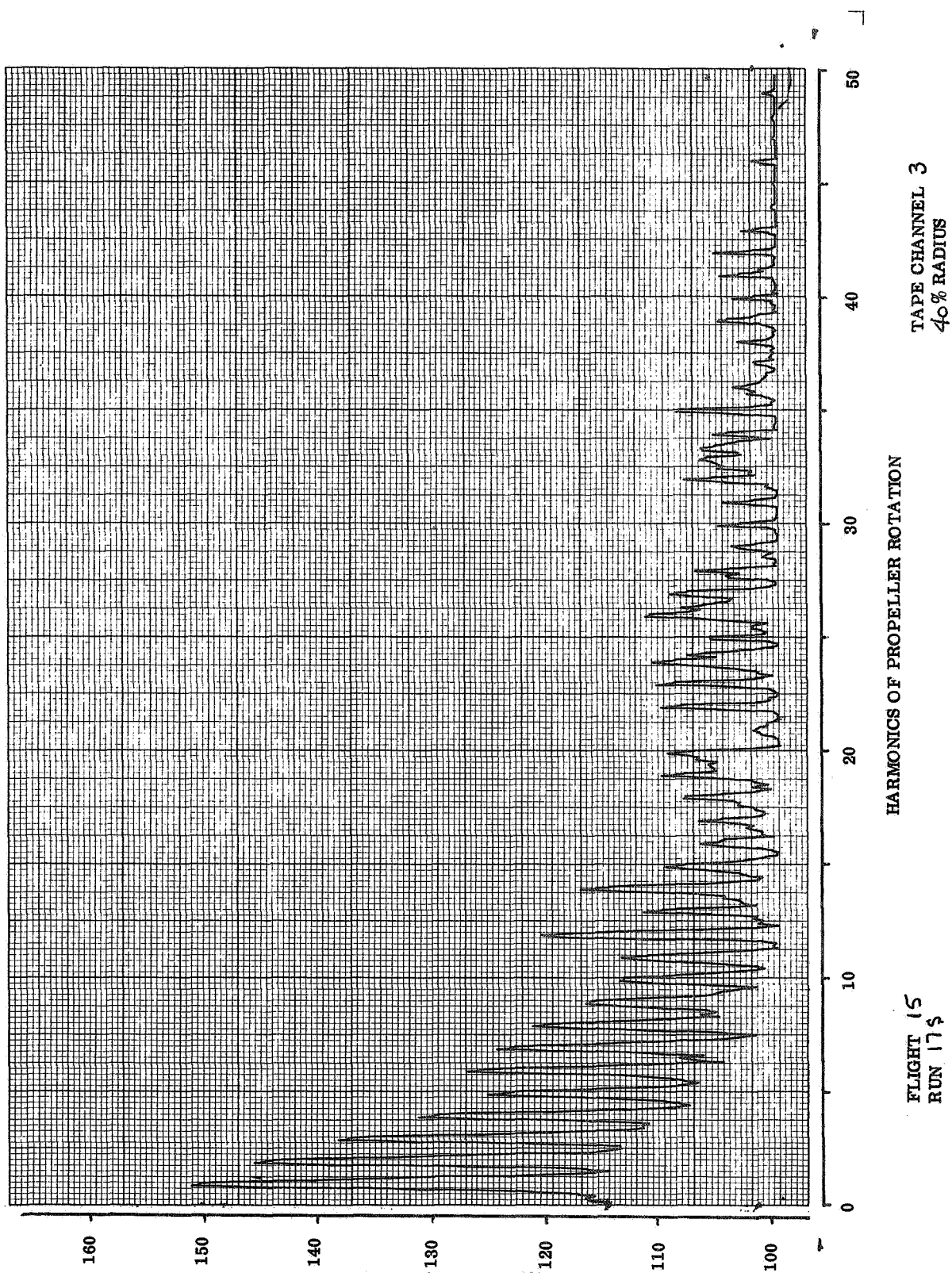


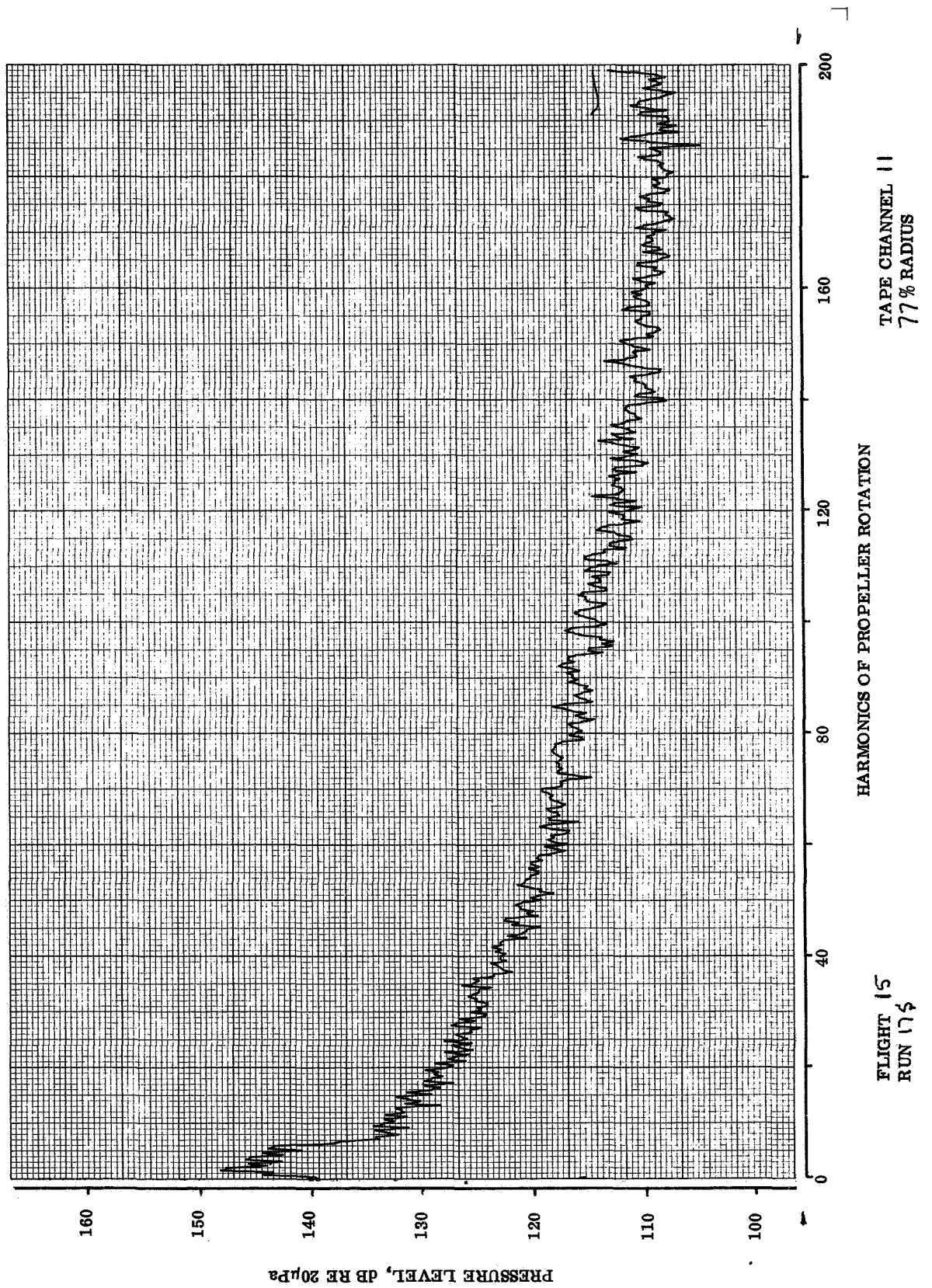
FLIGHT 12
RUN 164

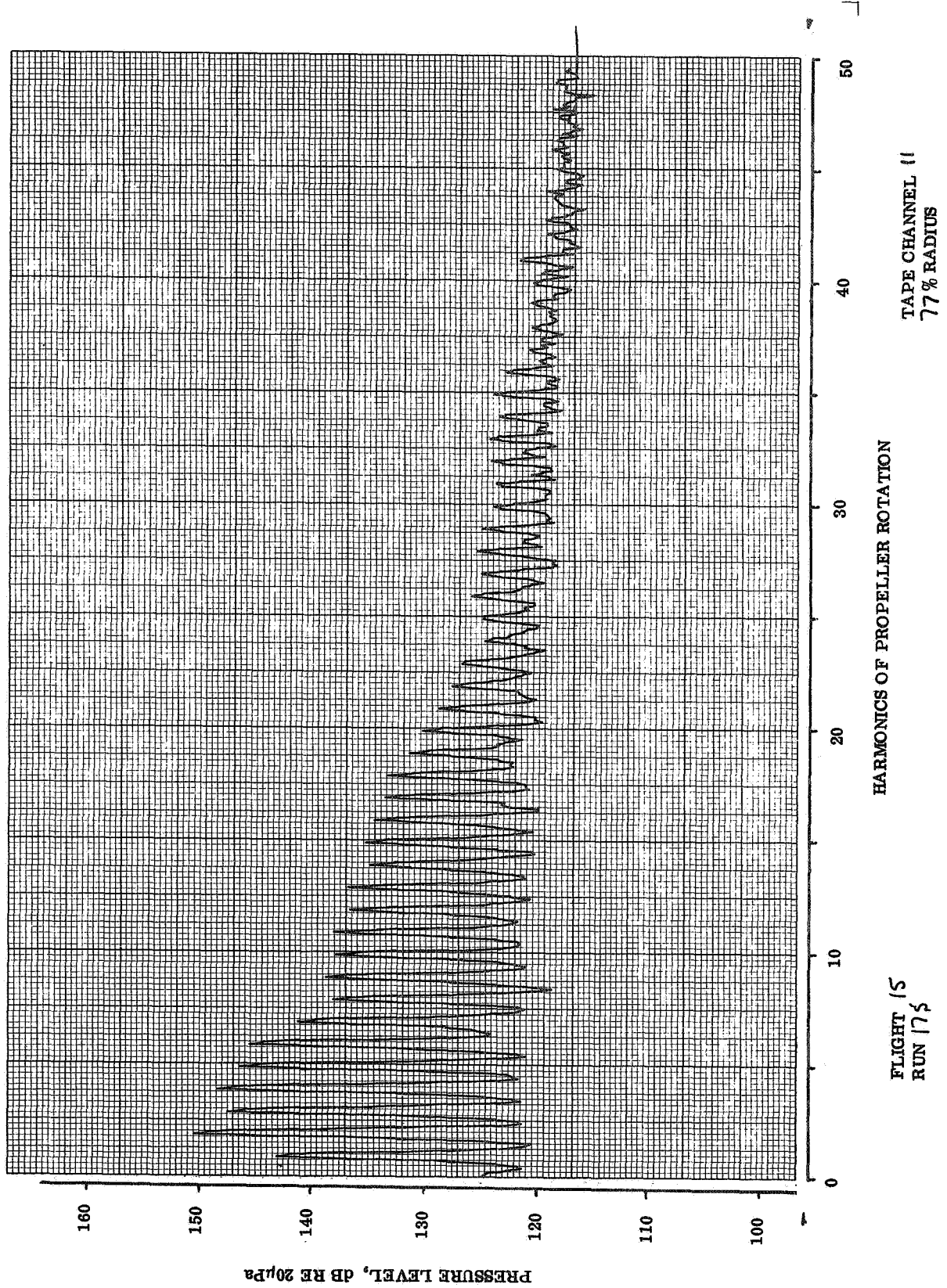
HARMONICS OF PROPELLER ROTATION

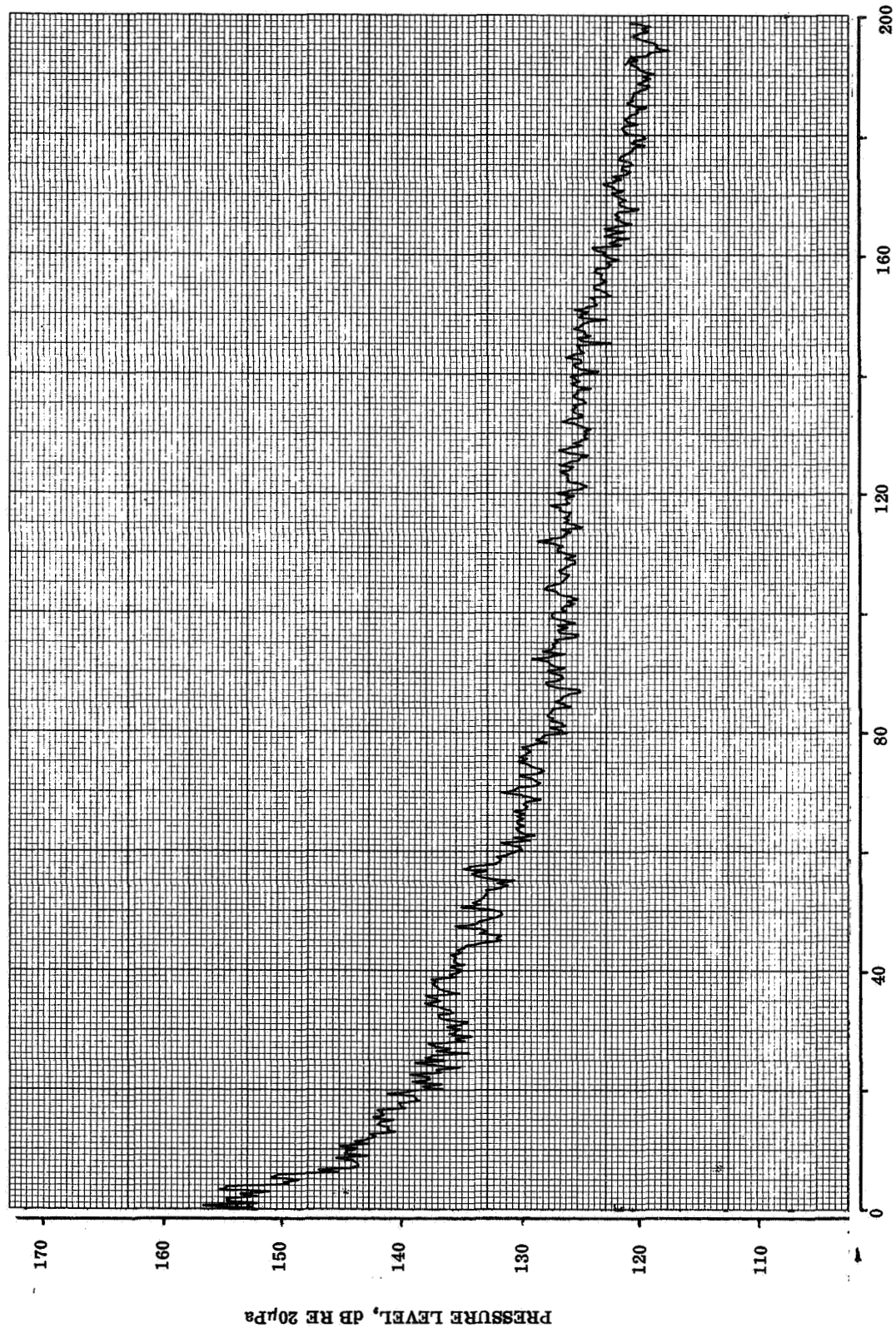
TAPE CHANNEL 13
89 % RADIUS

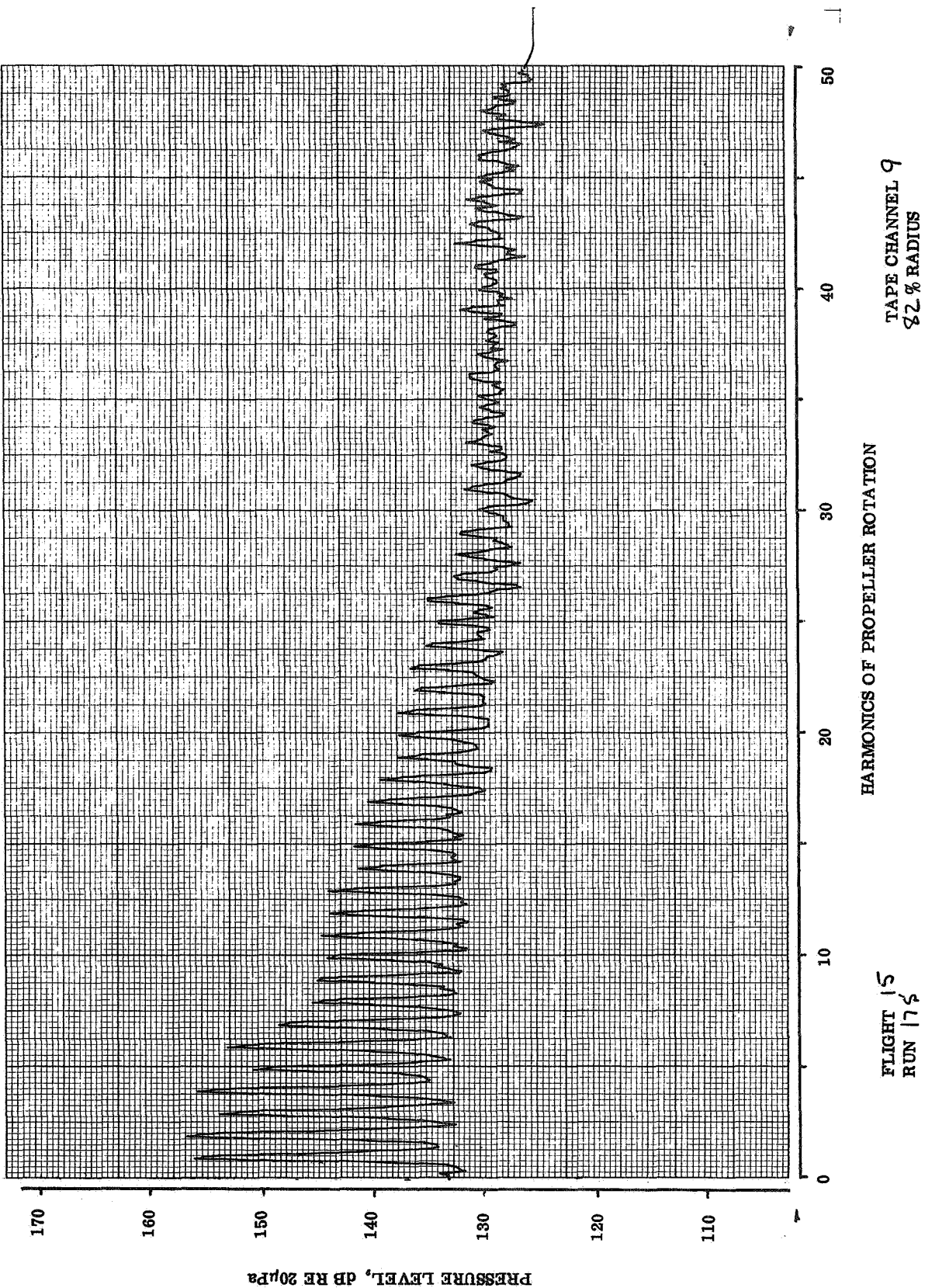


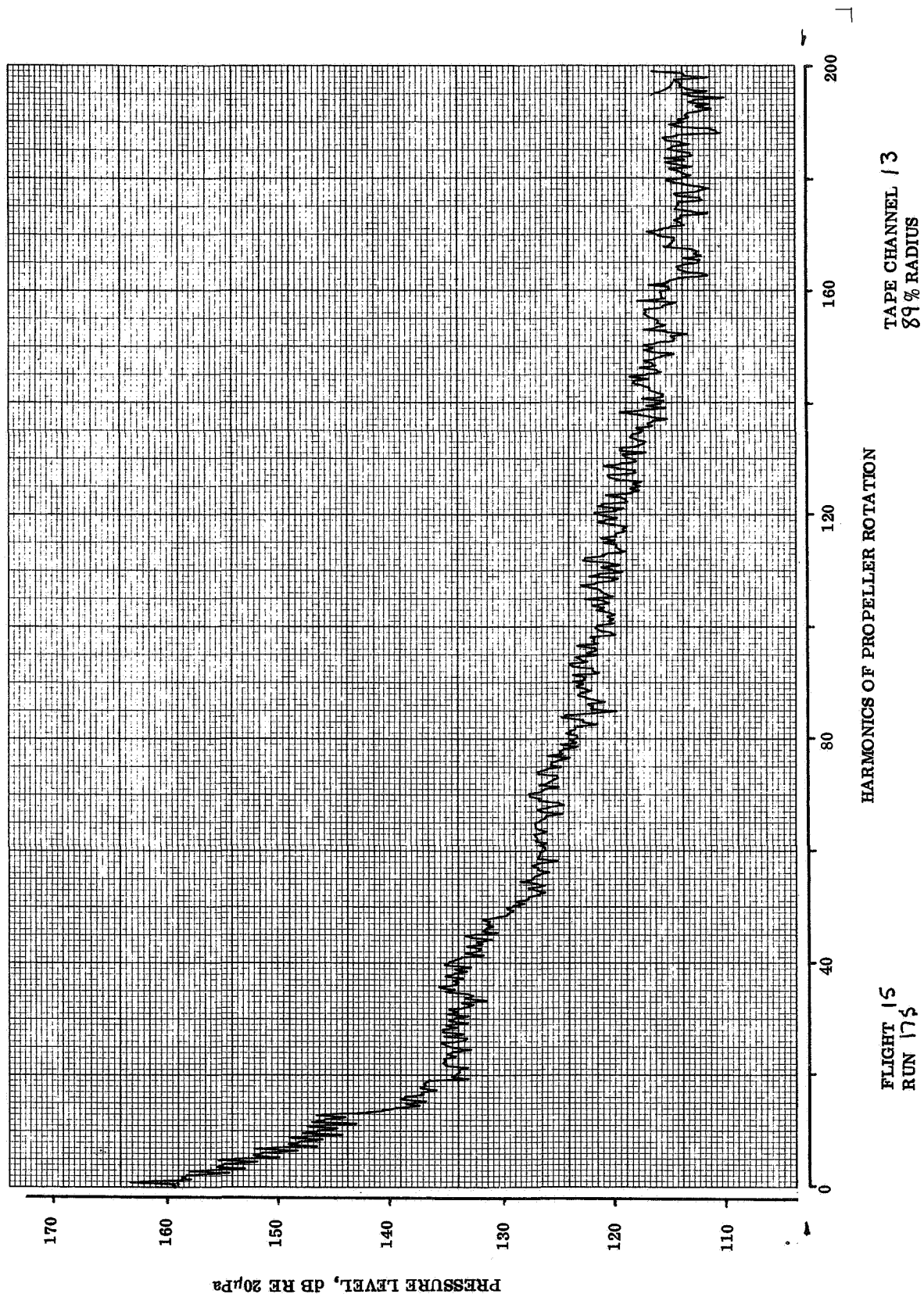


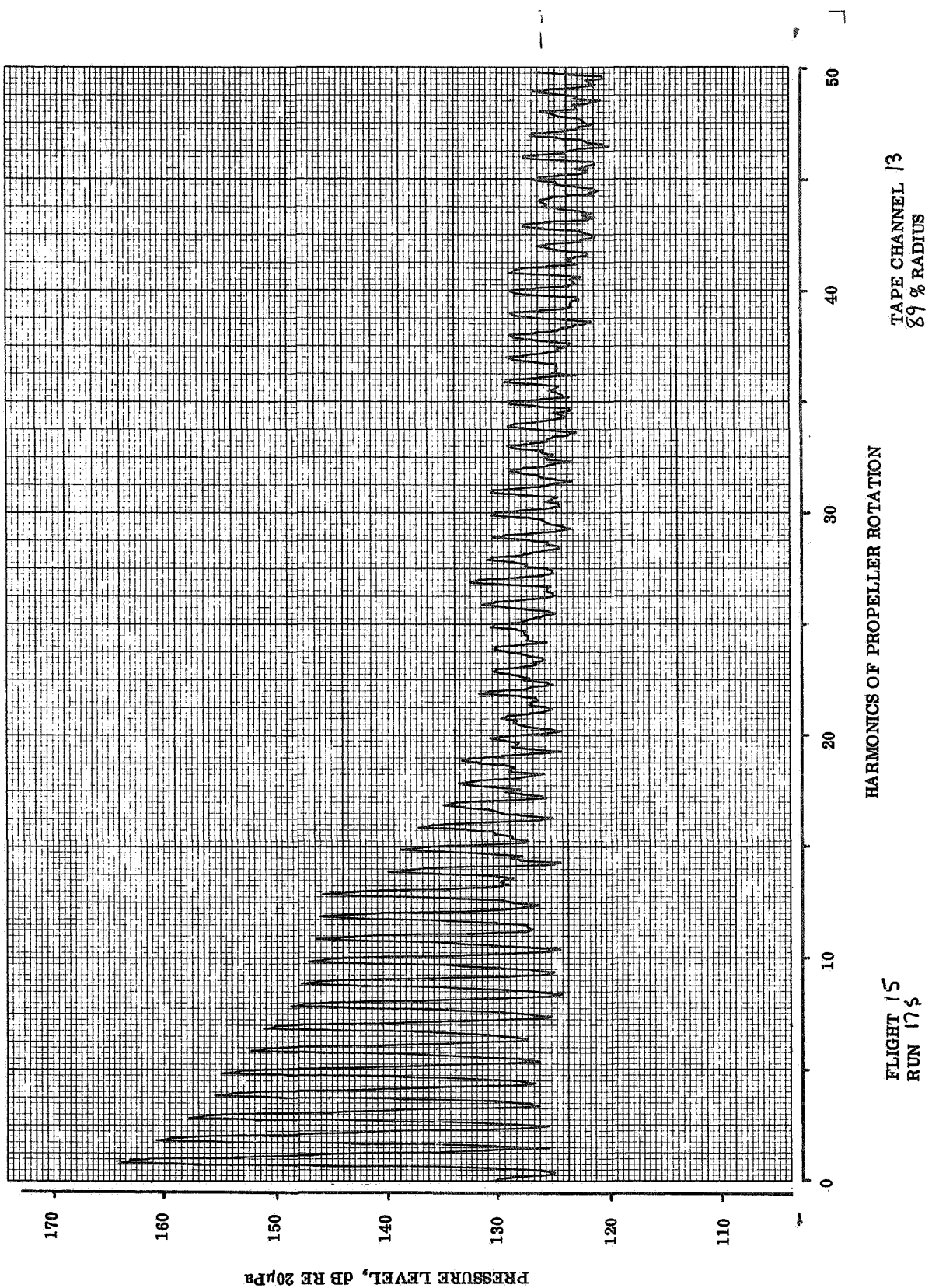


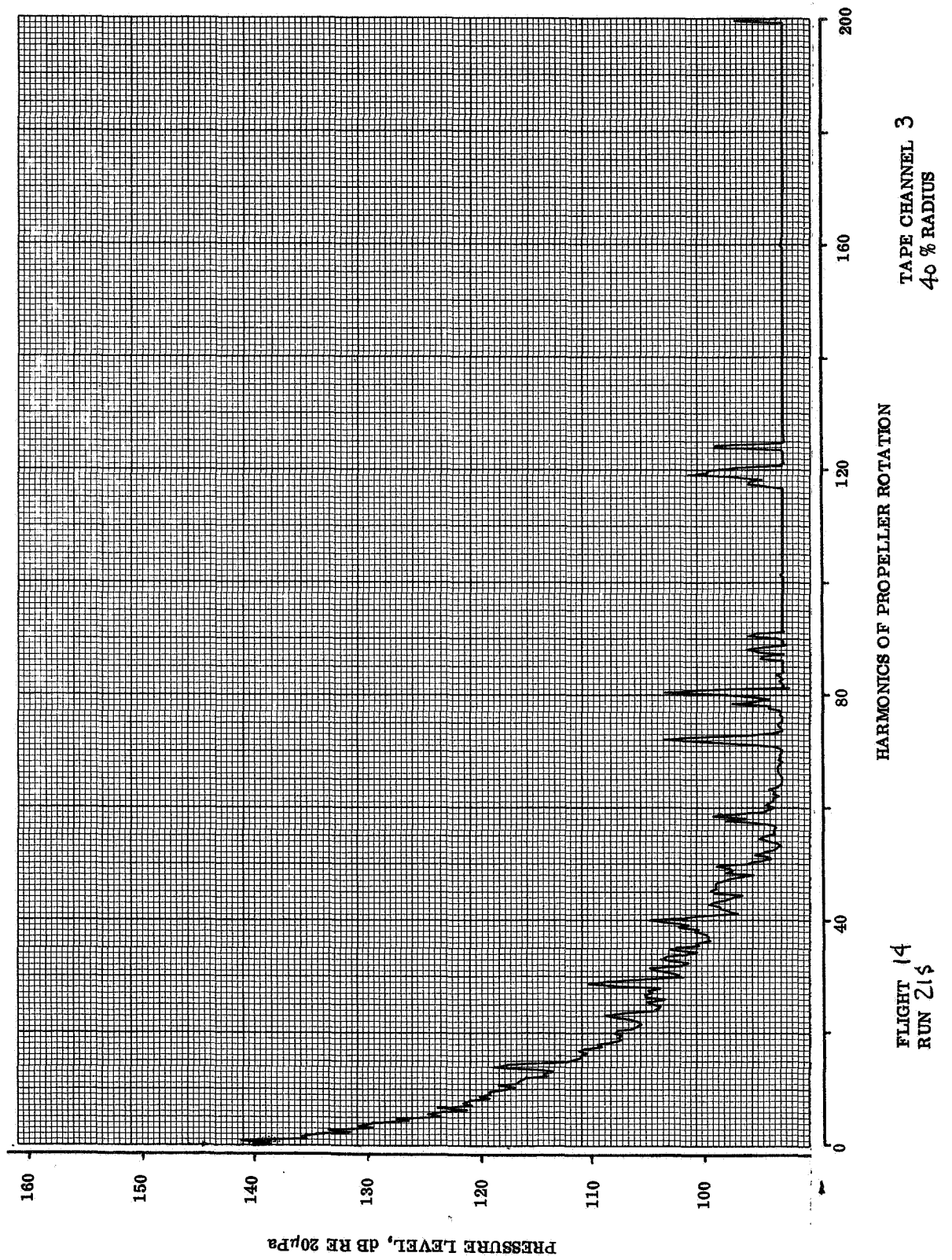


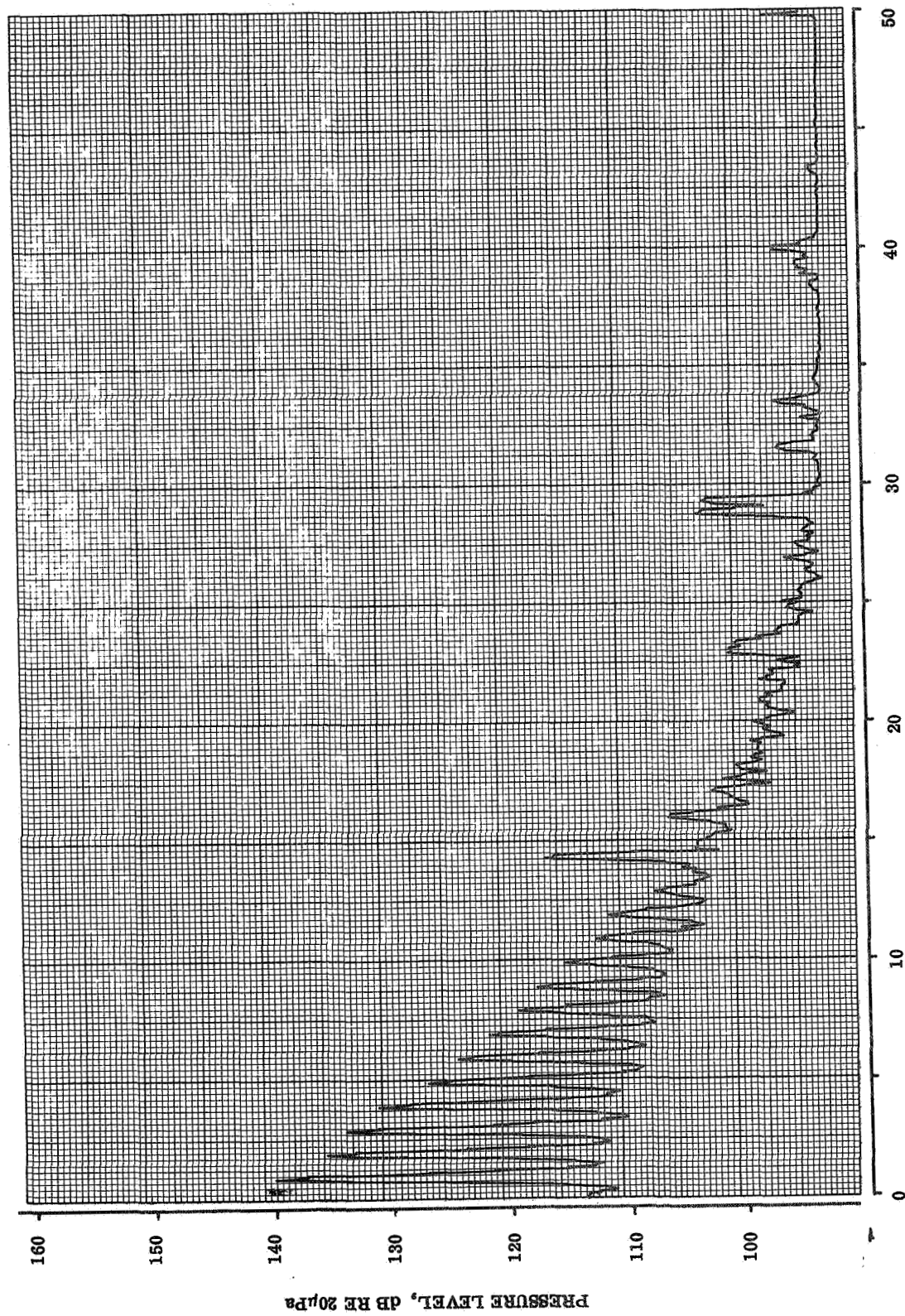








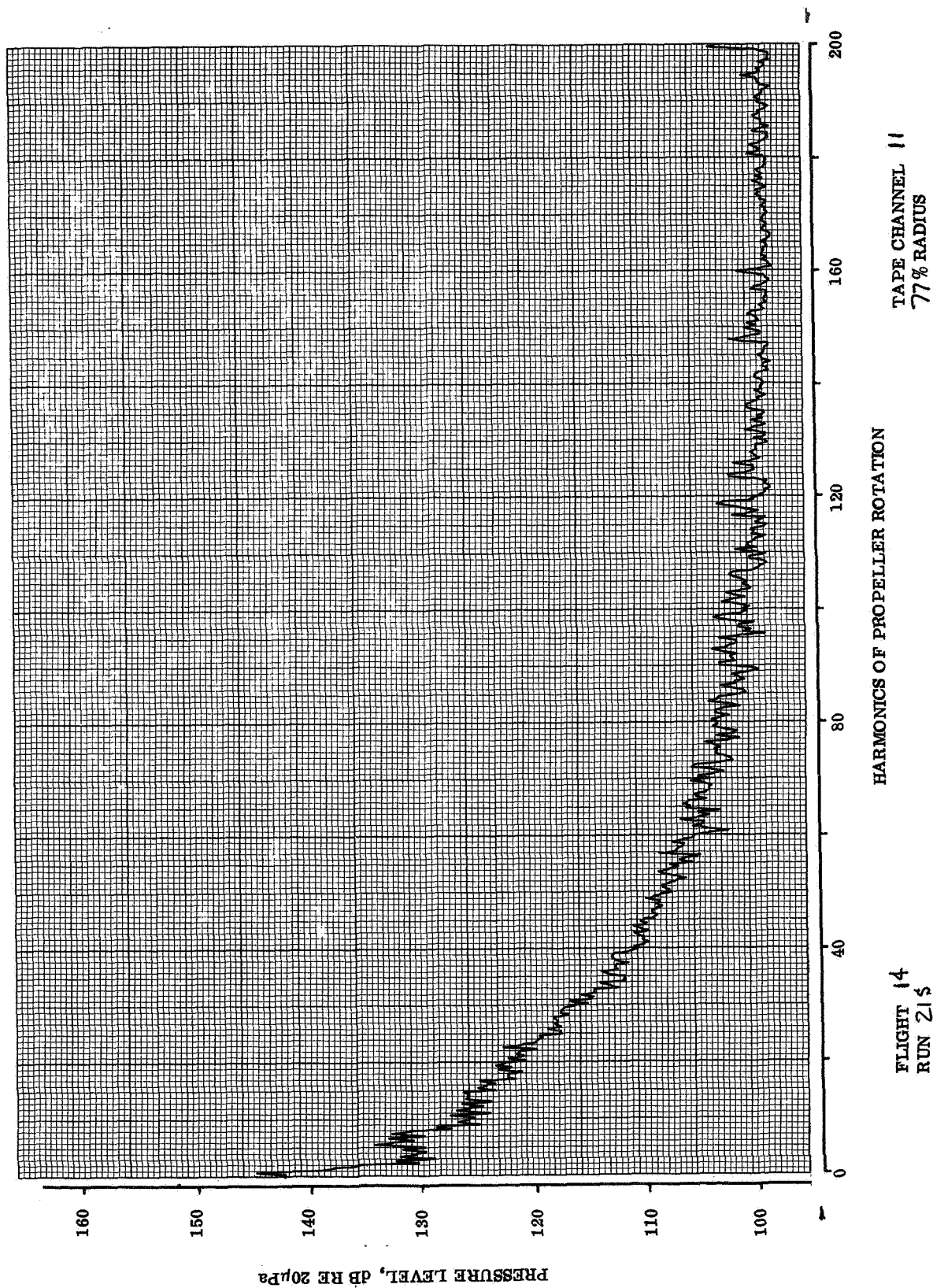


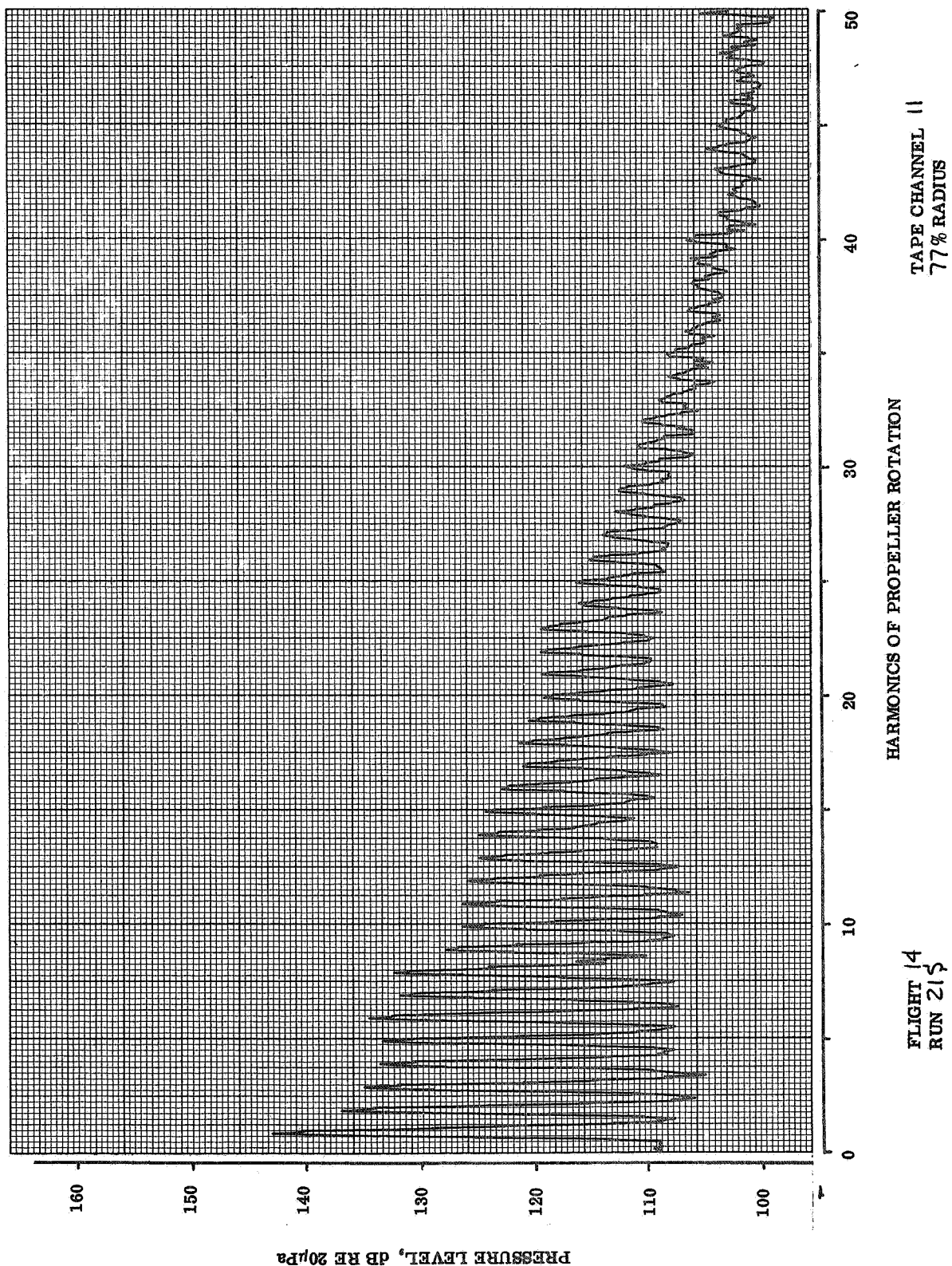


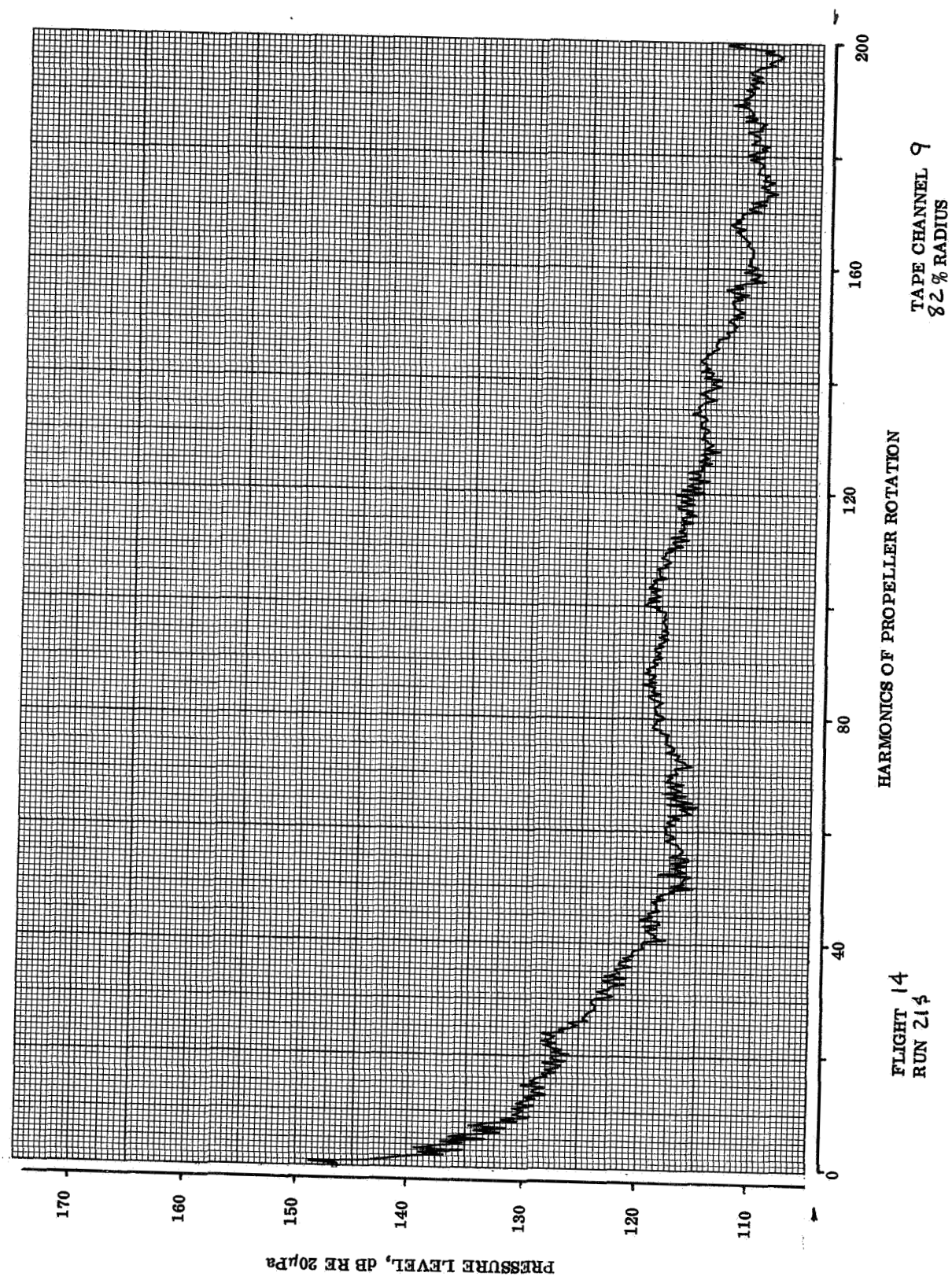
FLIGHT 14
RUN 215

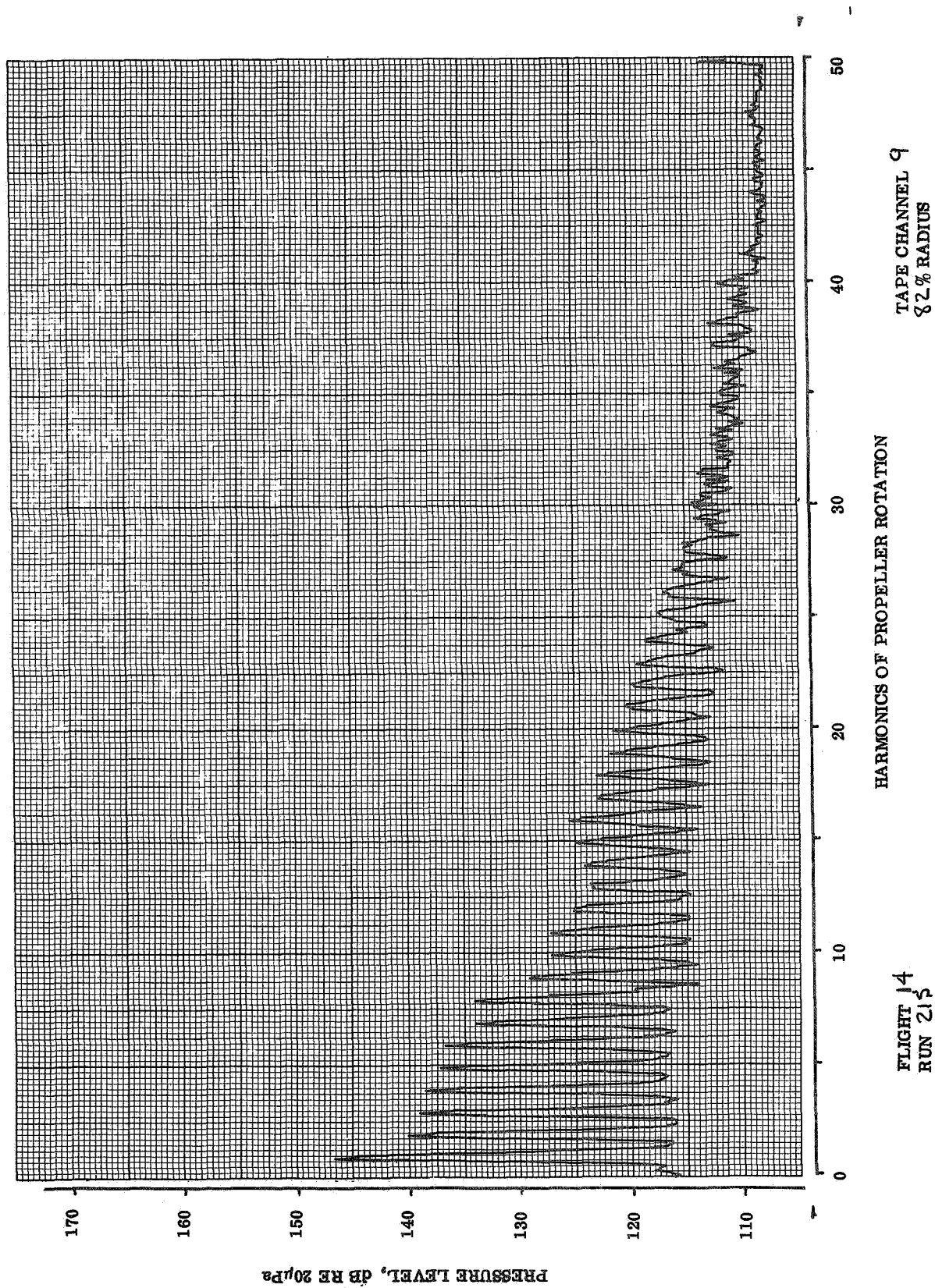
HARMONICS OF PROPELLER ROTATION

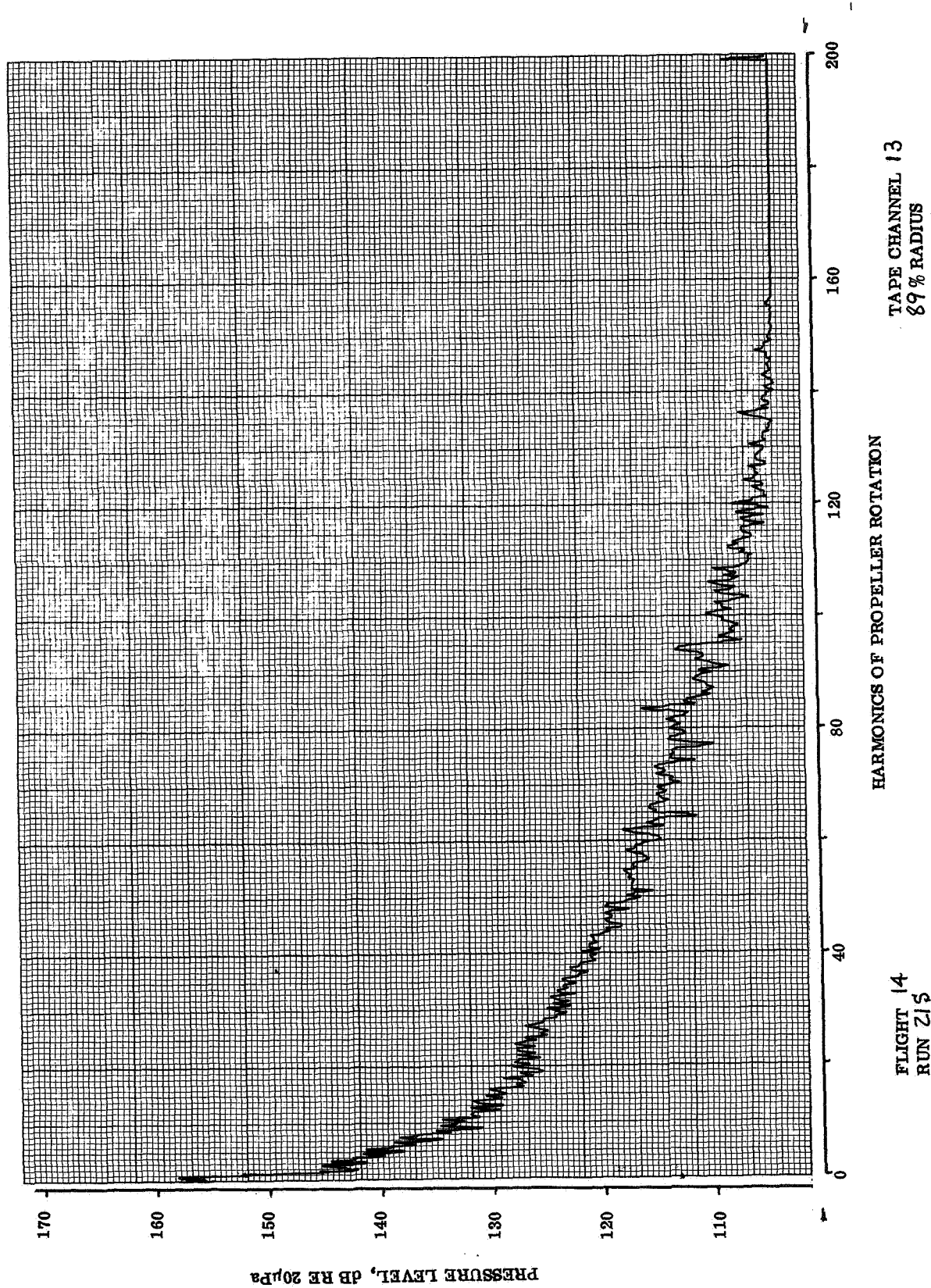
TAPE CHANNEL 3
40 % RADIUS

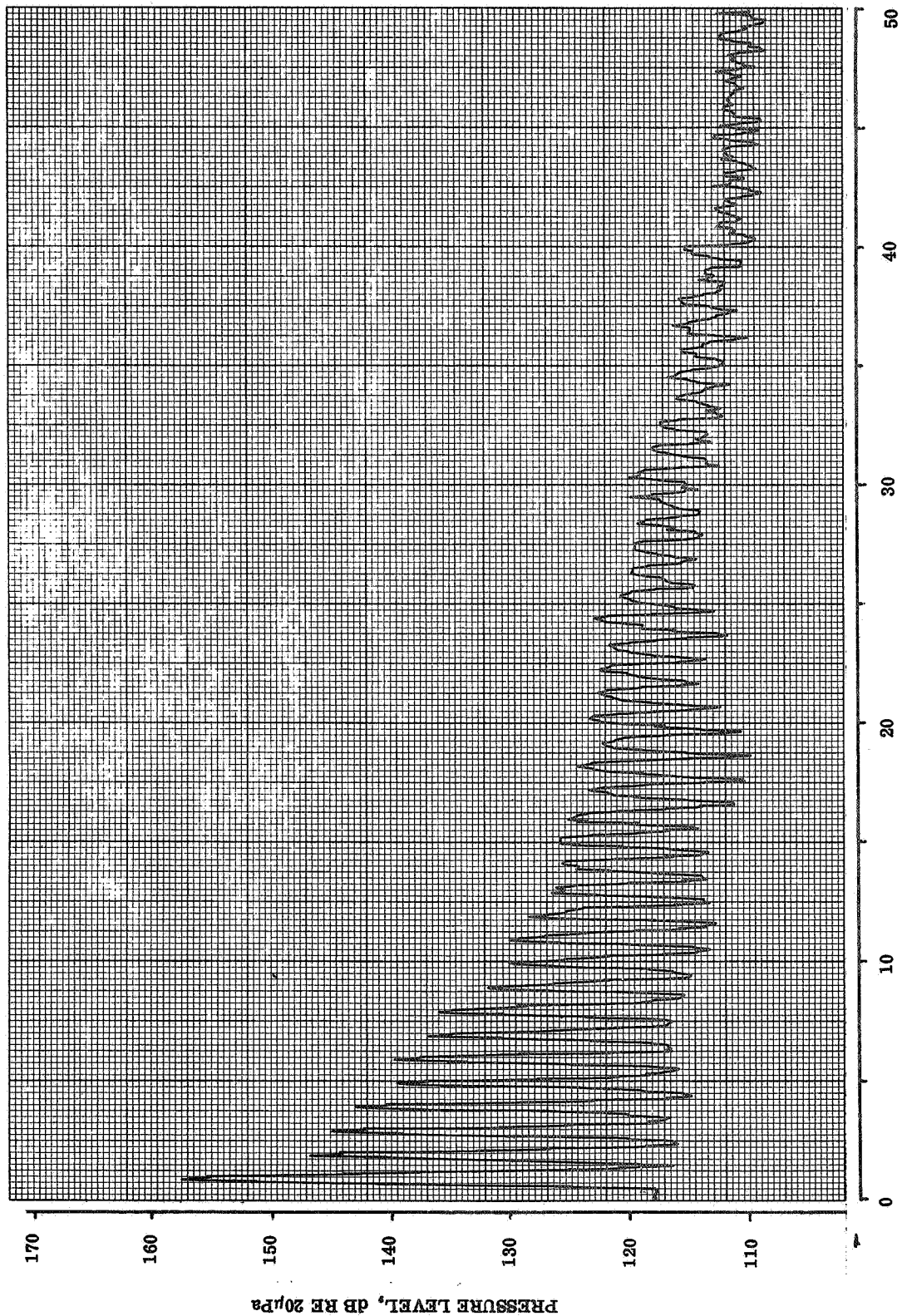


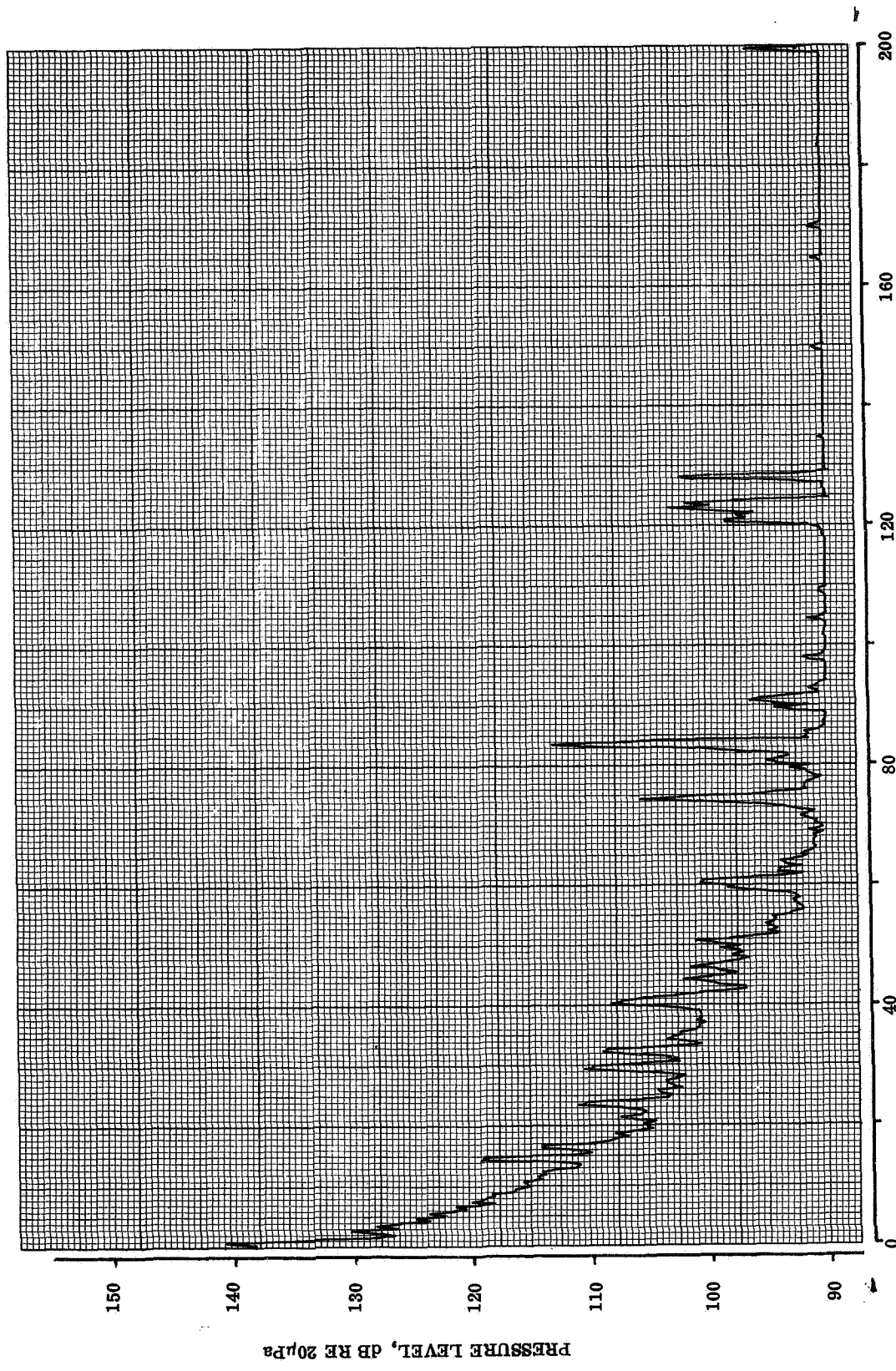








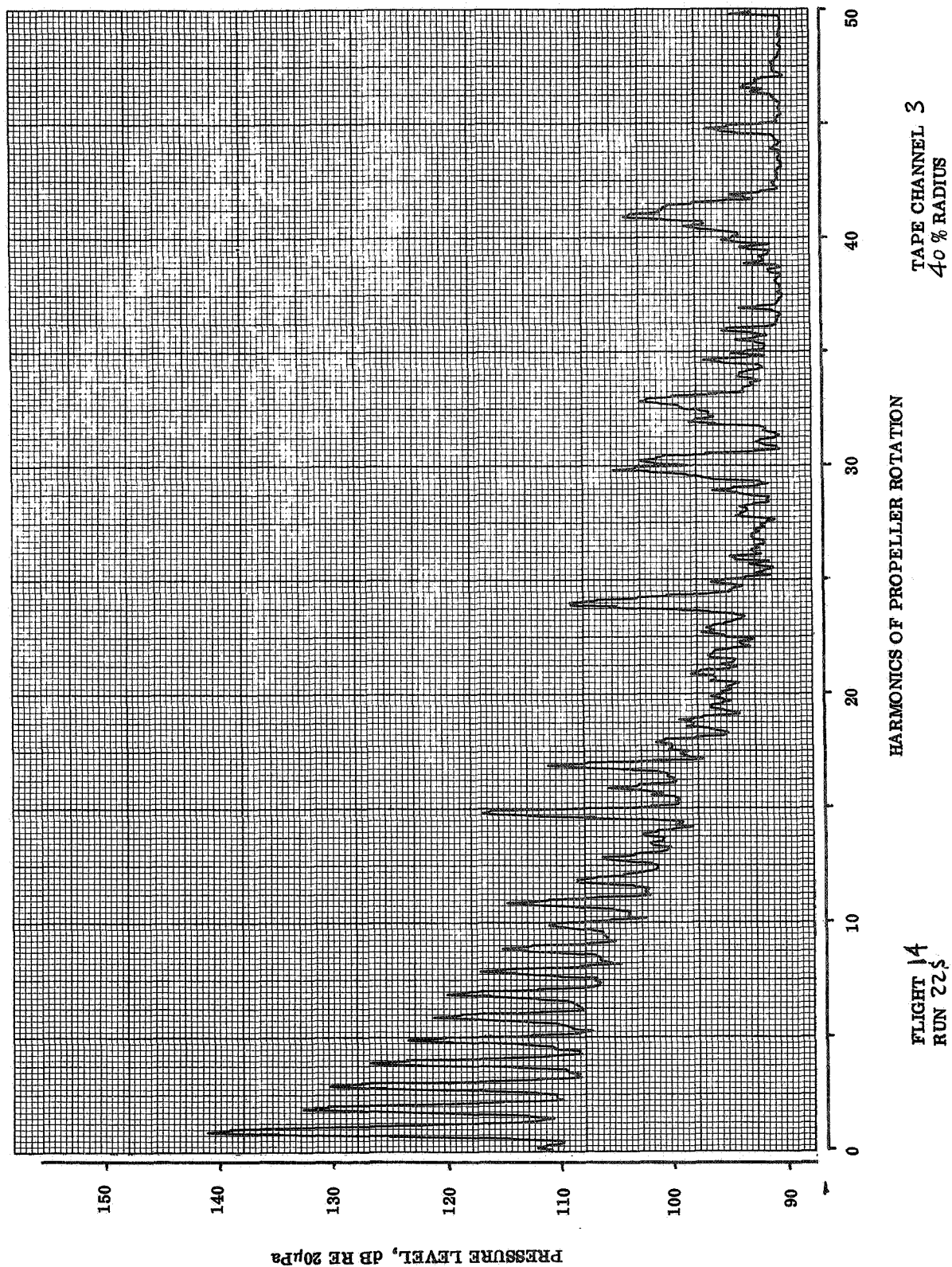


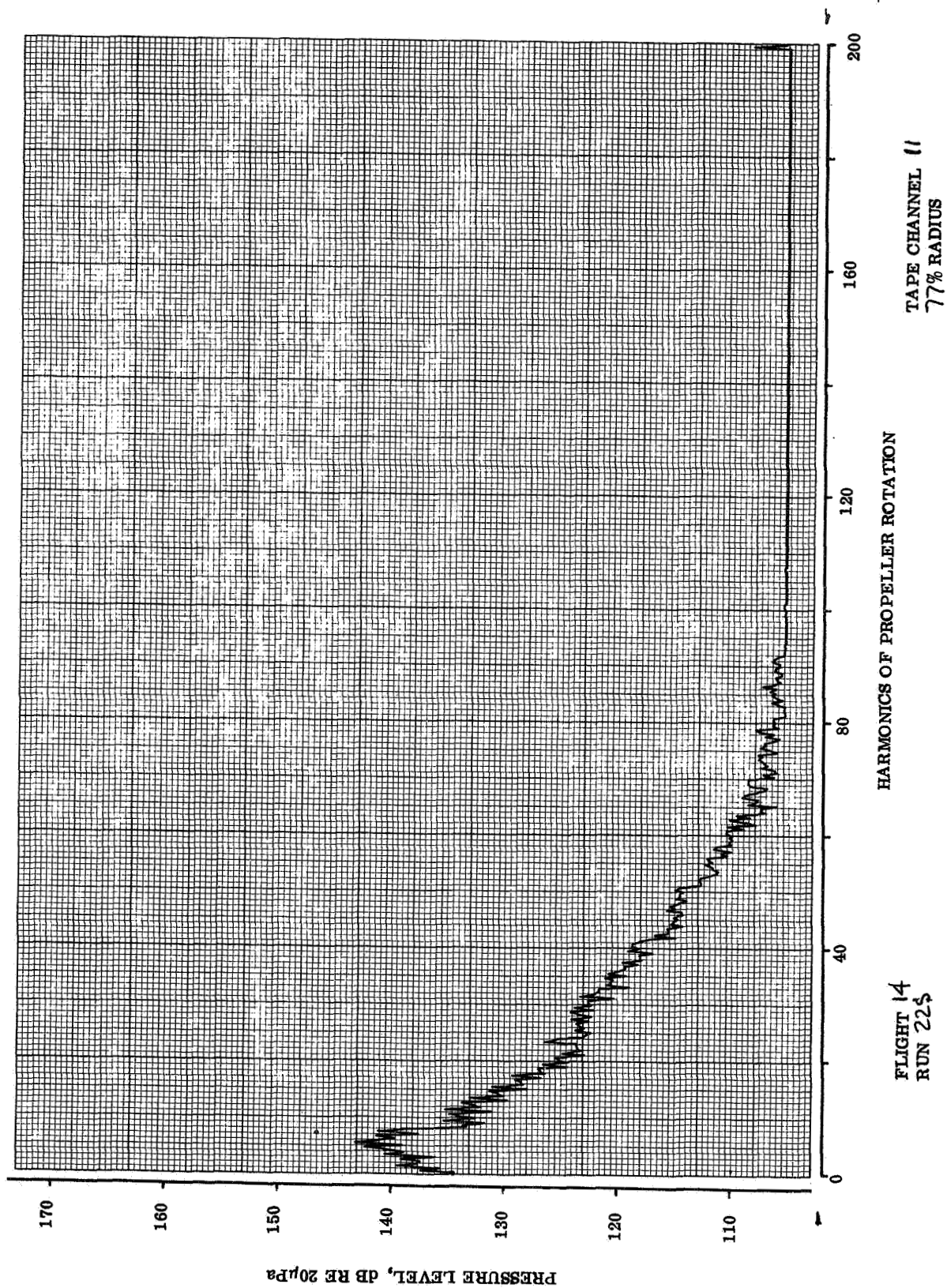


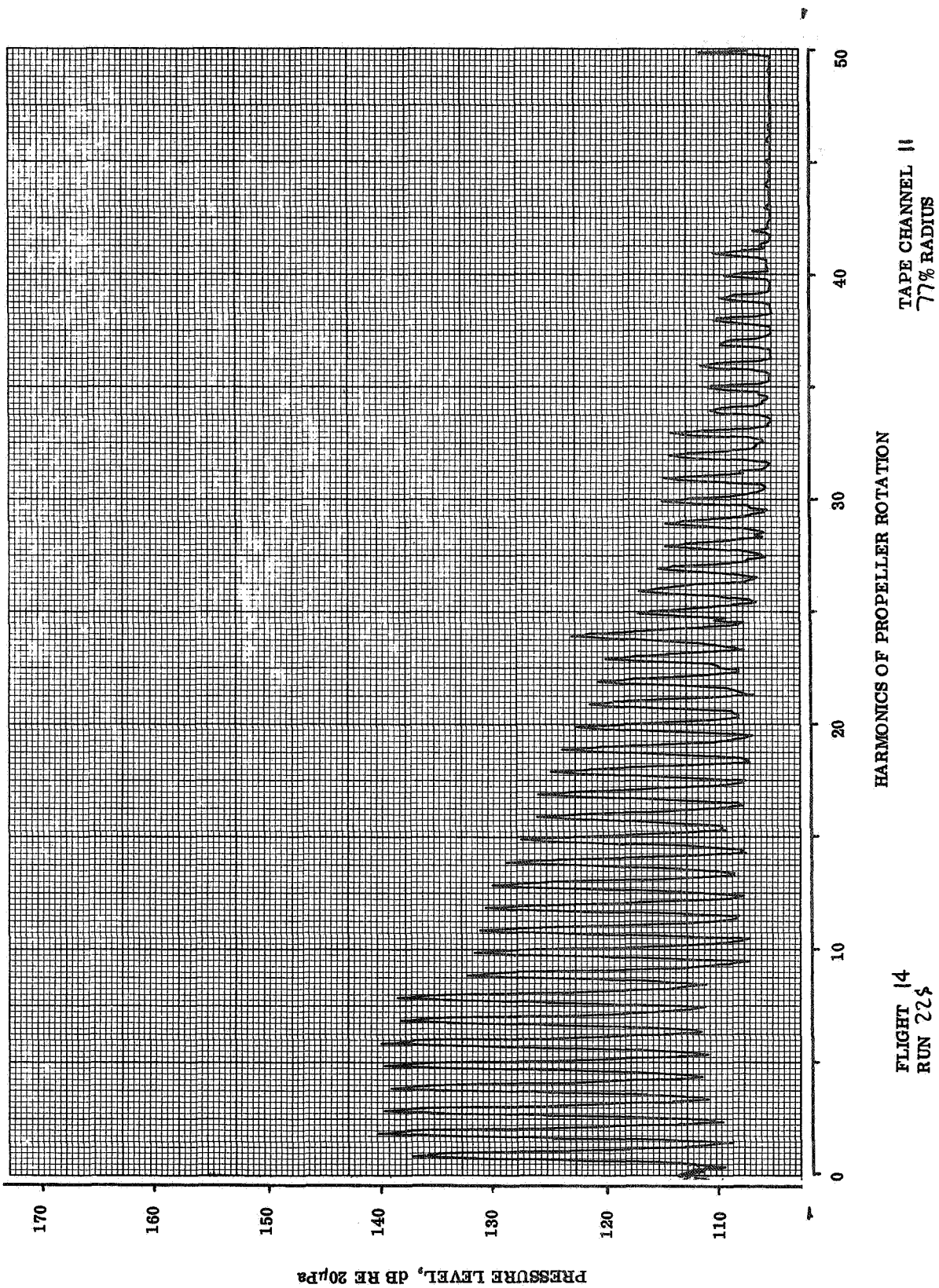
TAPE CHANNEL 3
40 % RADIUS

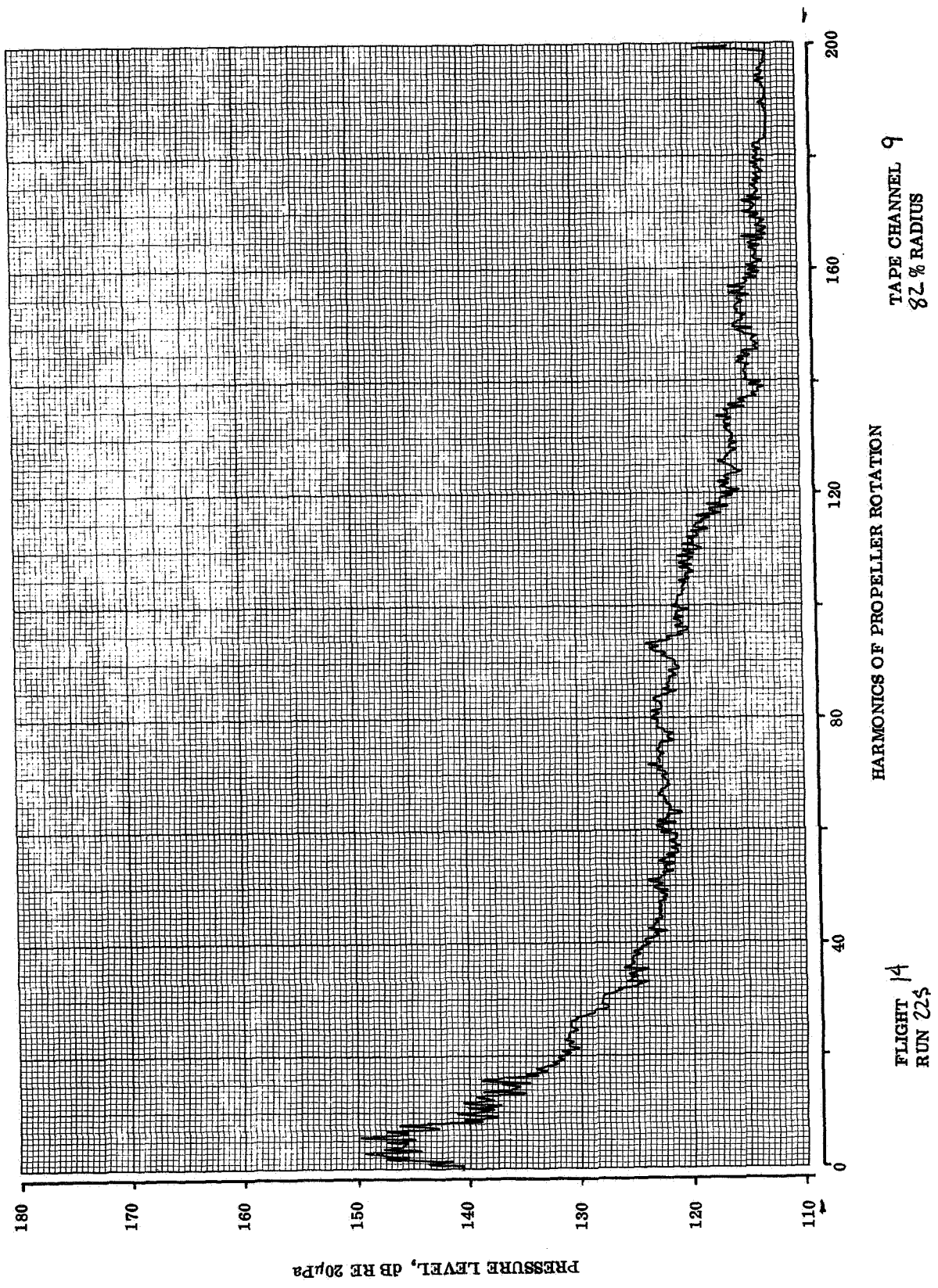
HARMONICS OF PROPELLER ROTATION

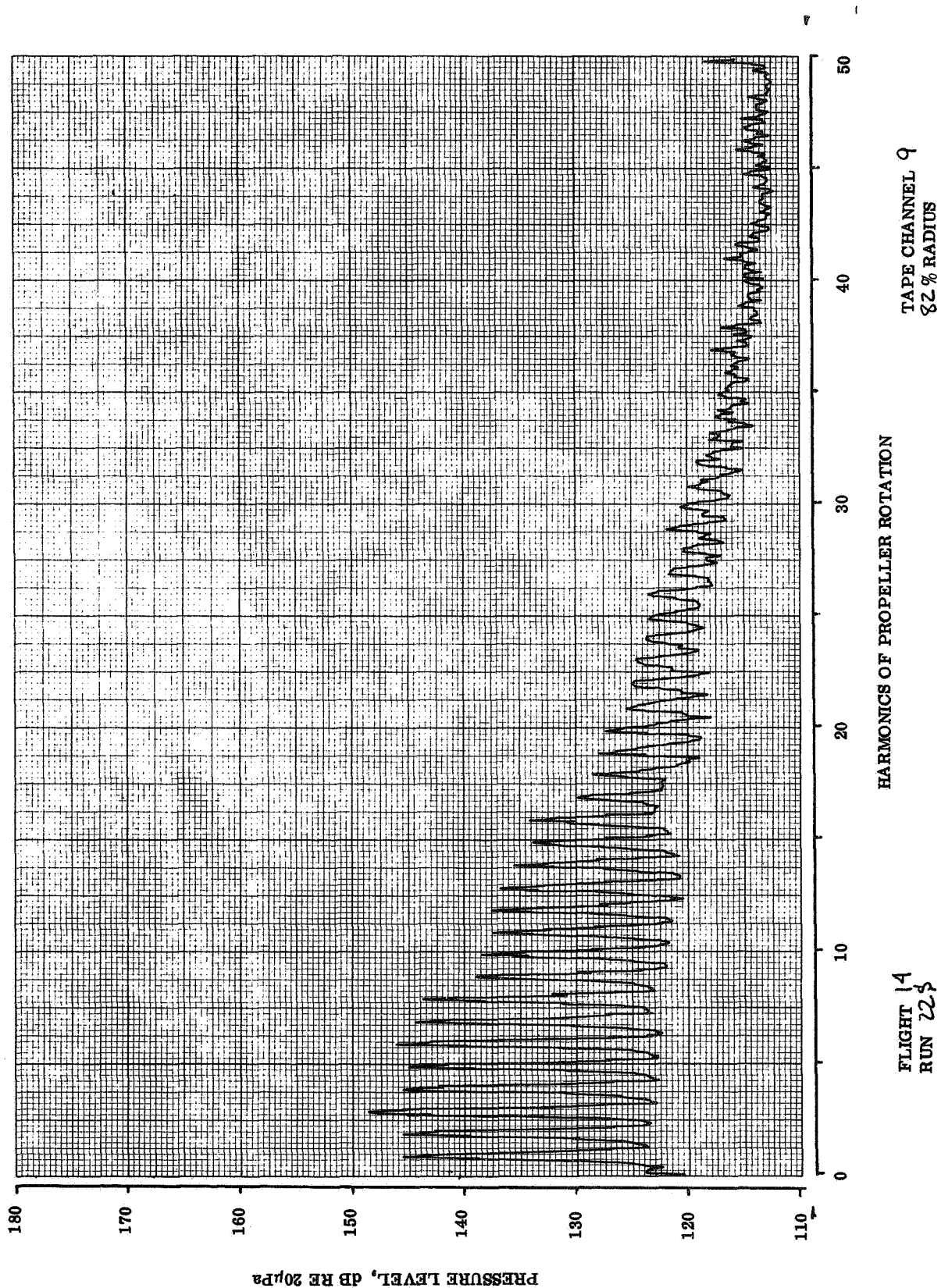
FLIGHT 14
RUN 225

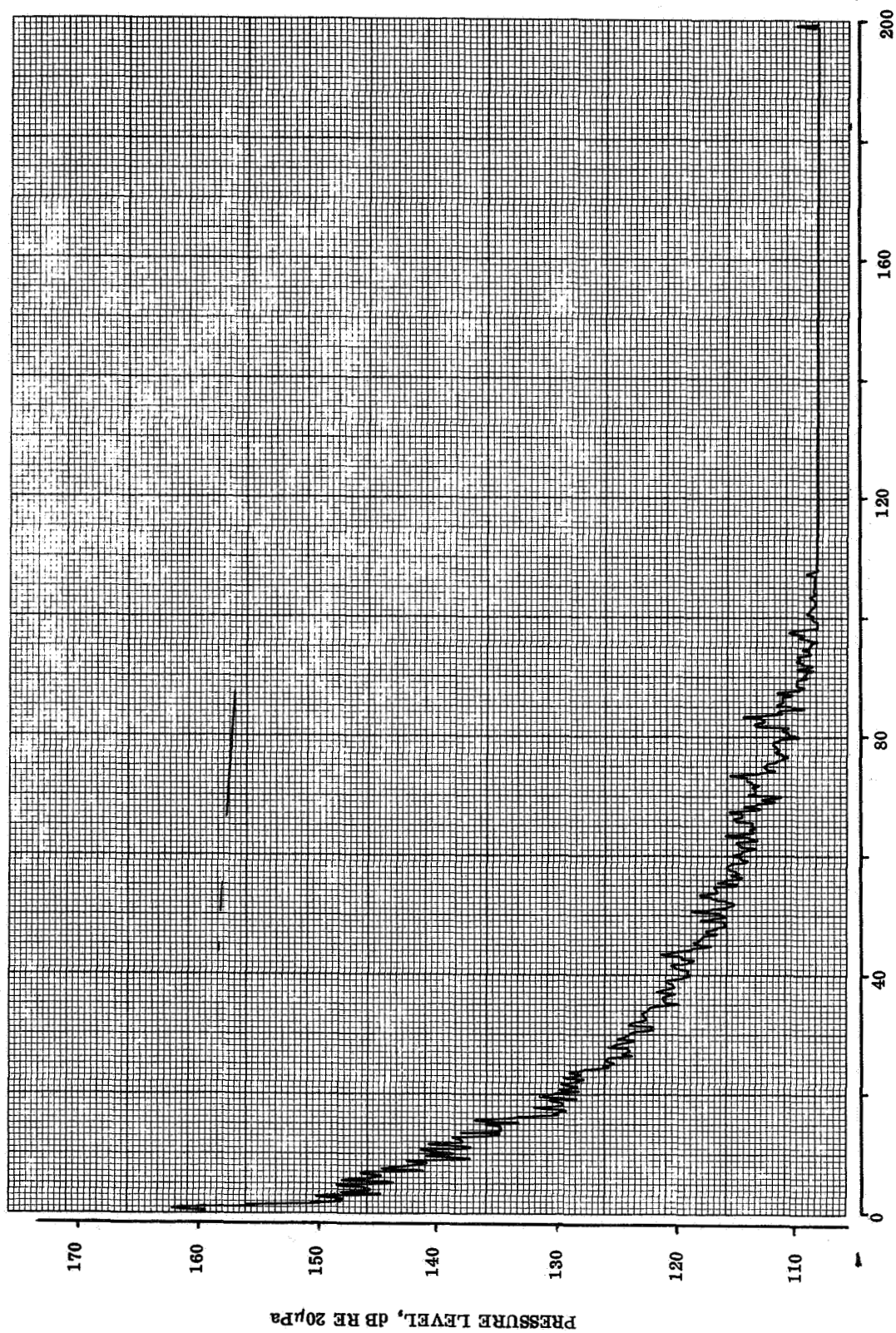








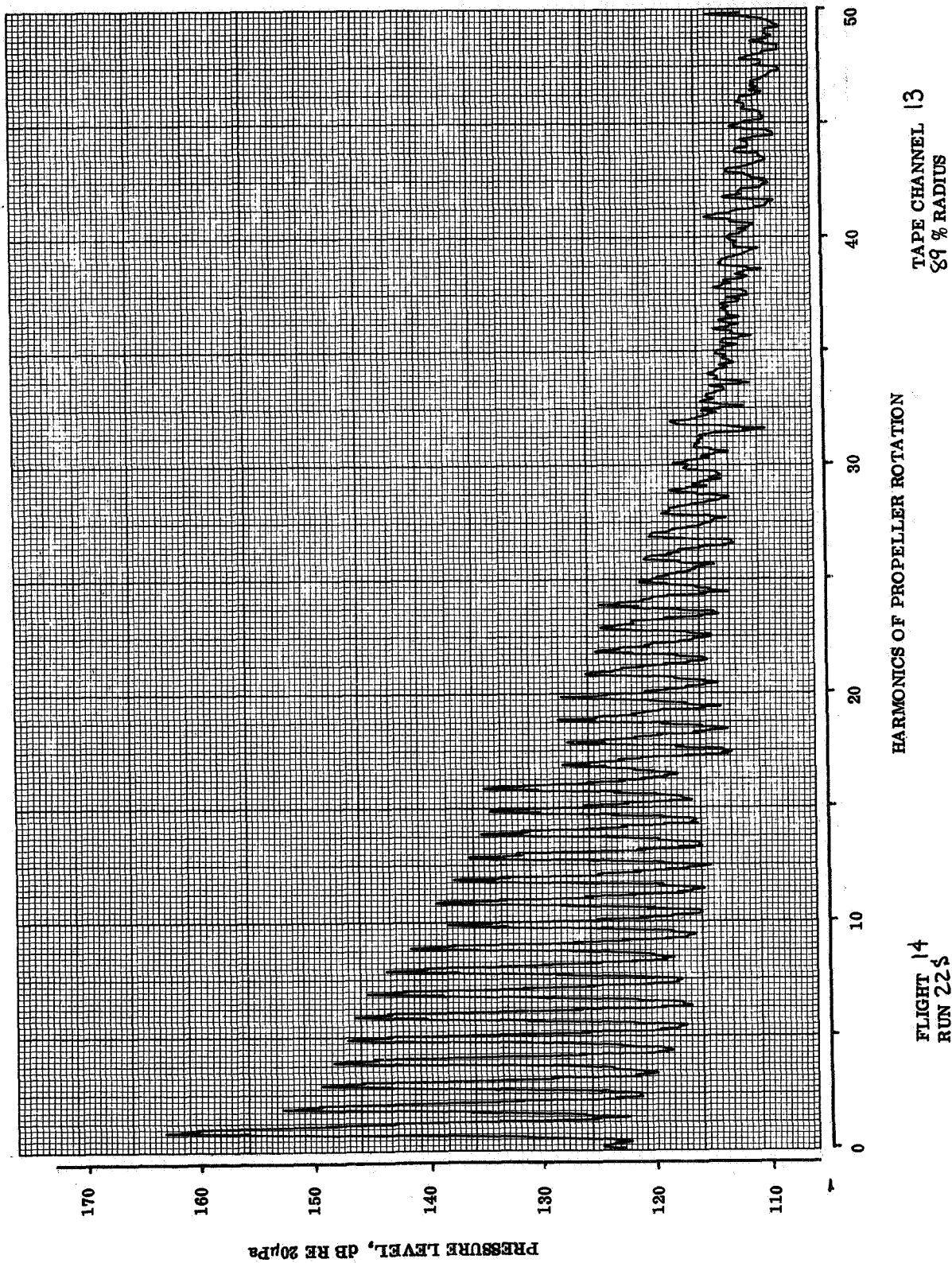




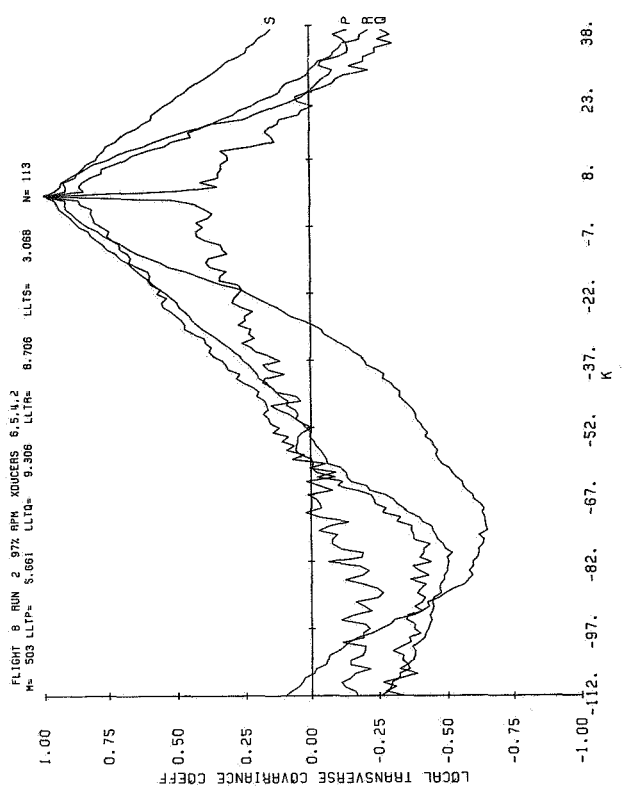
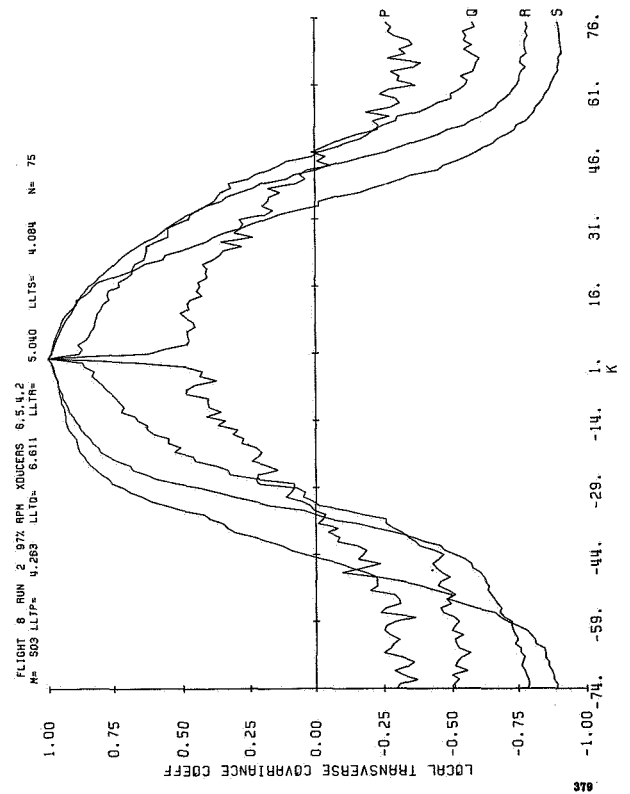
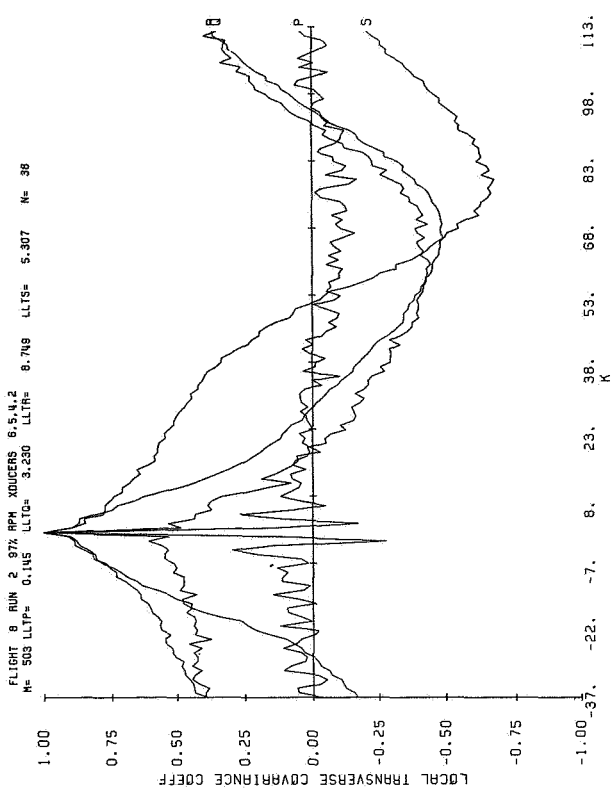
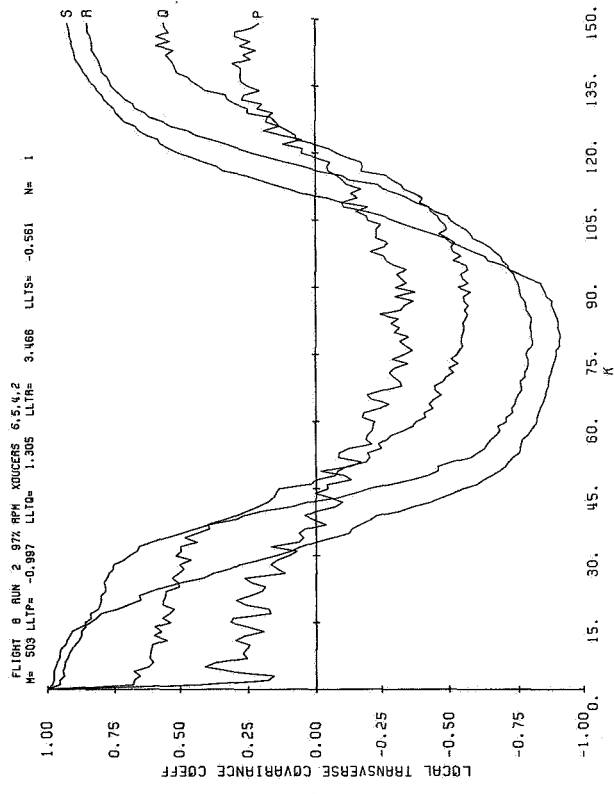
TAPE CHANNEL 13
89% RADIUS

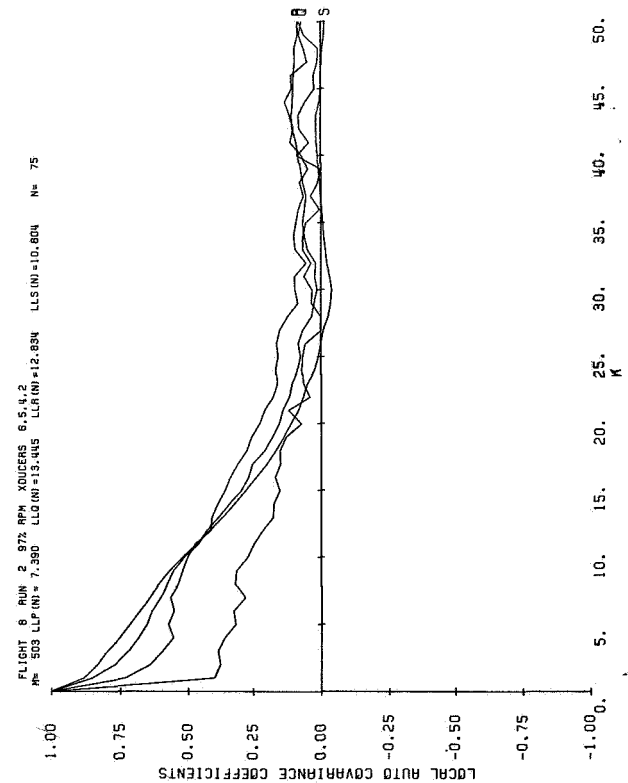
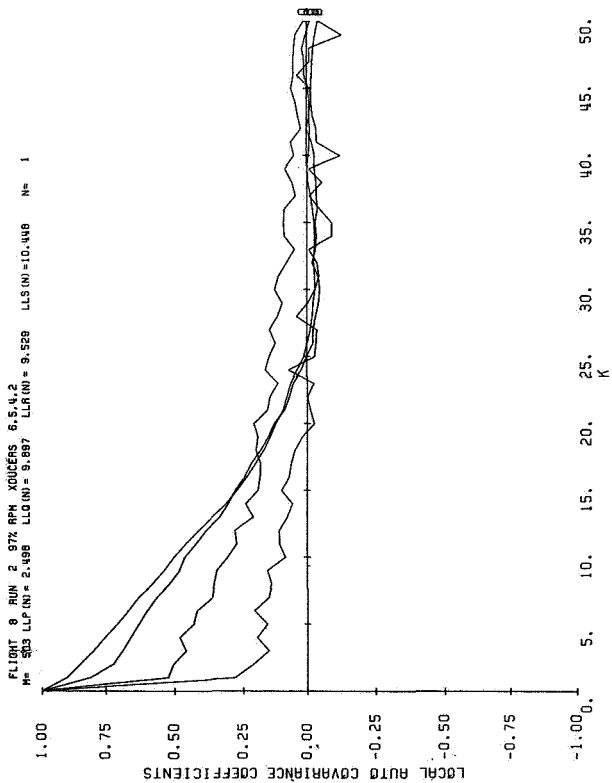
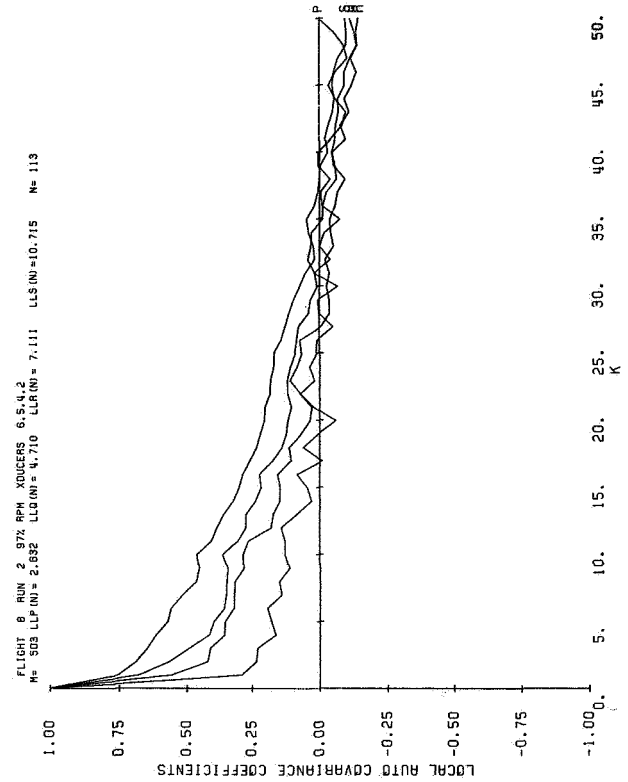
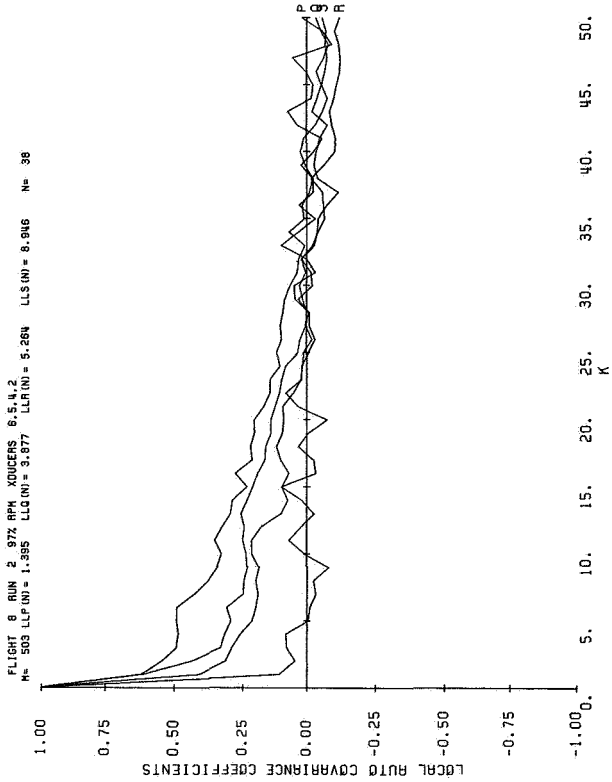
HARMONICS OF PROPELLER ROTATION

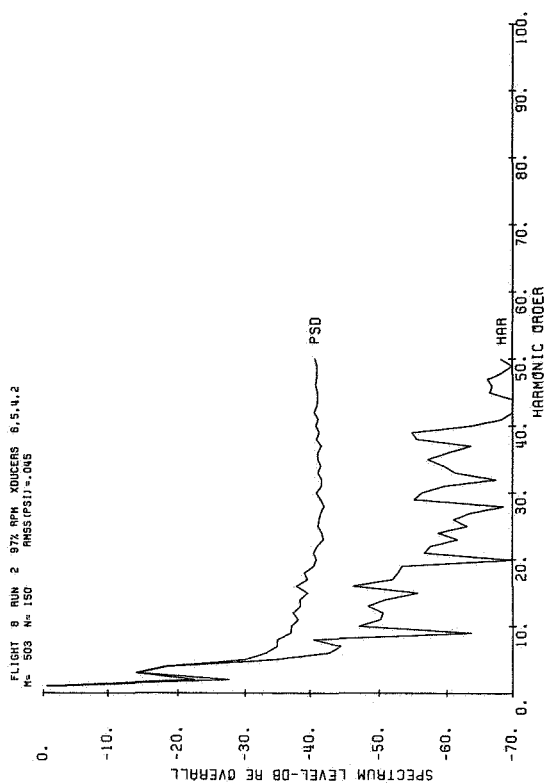
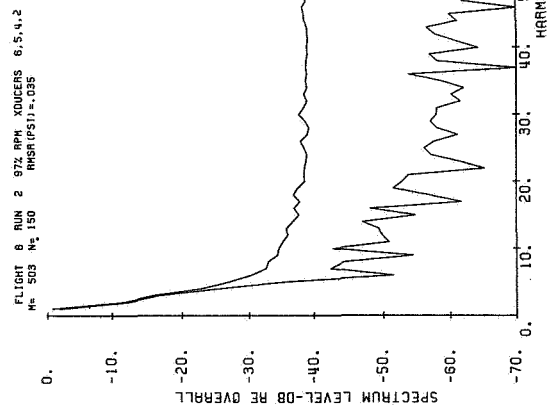
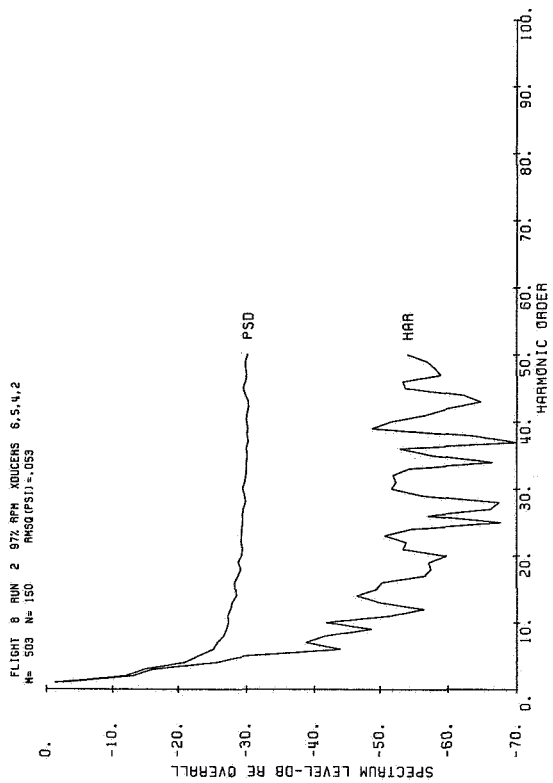
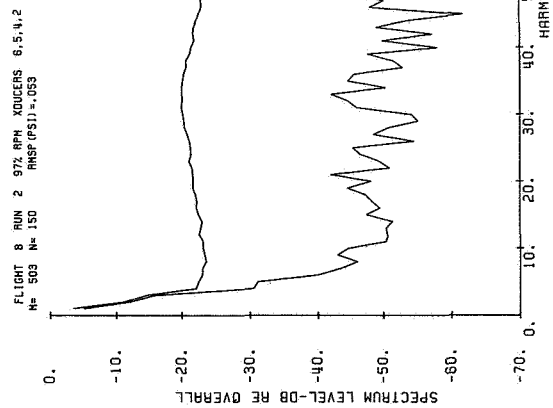
FLIGHT 14
RUN 225

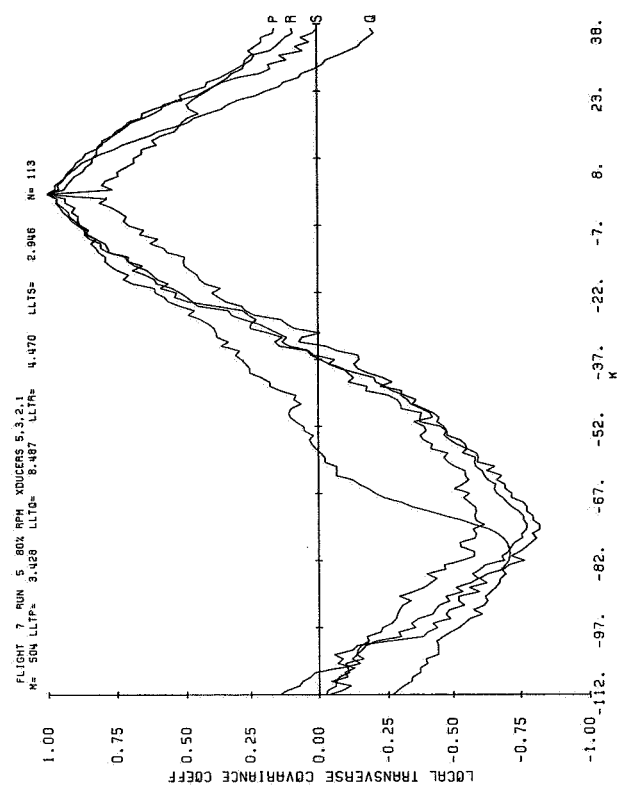
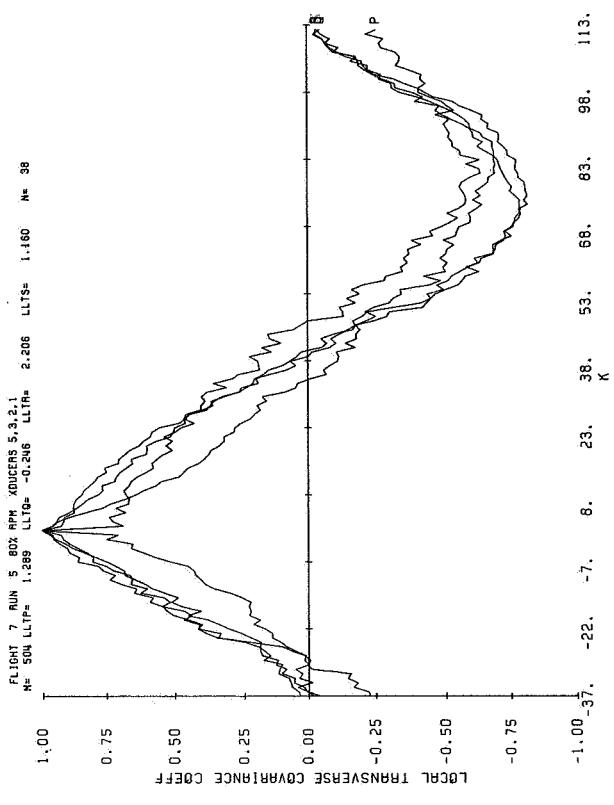
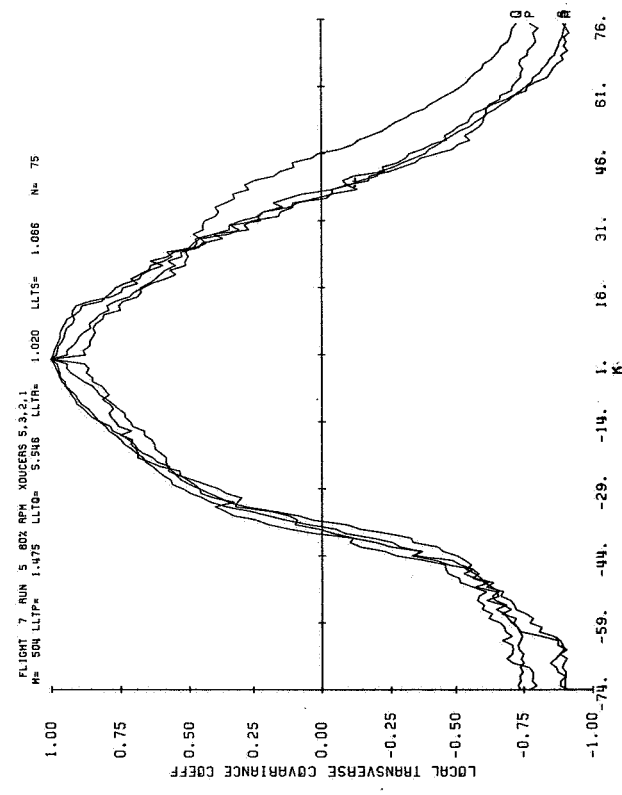
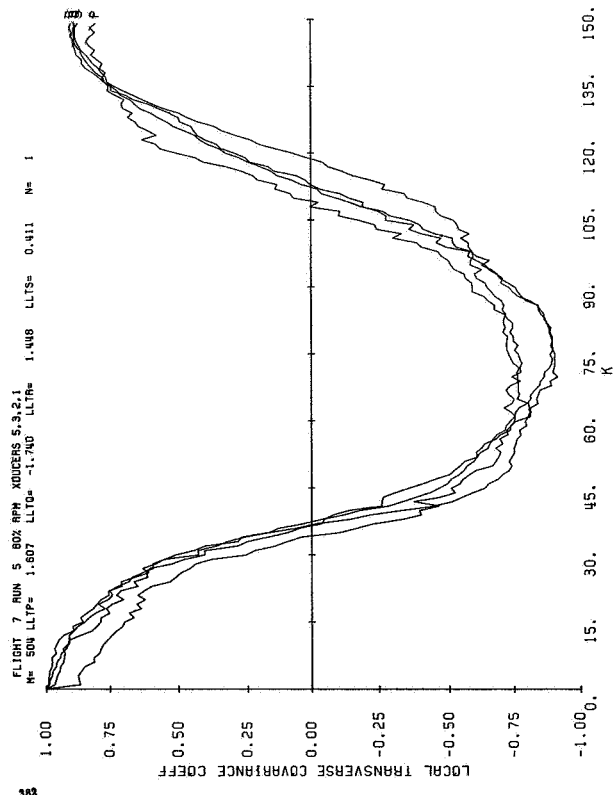


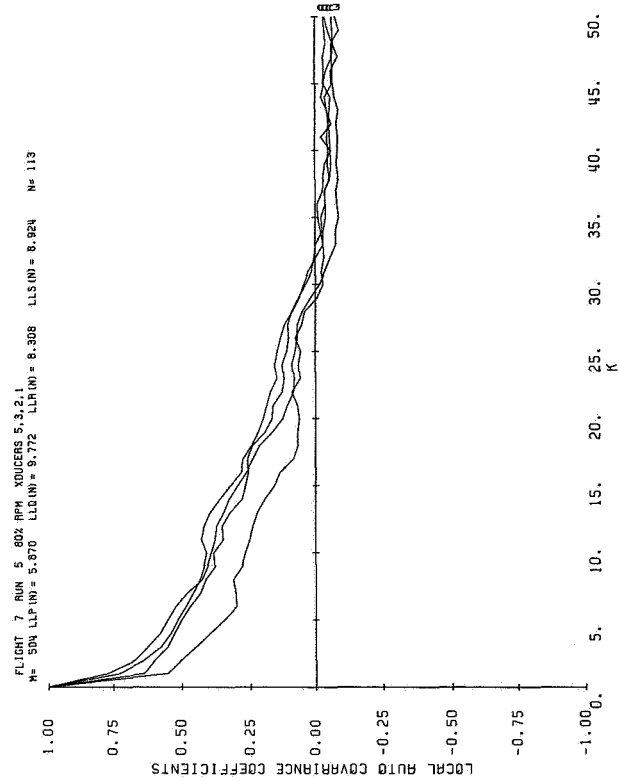
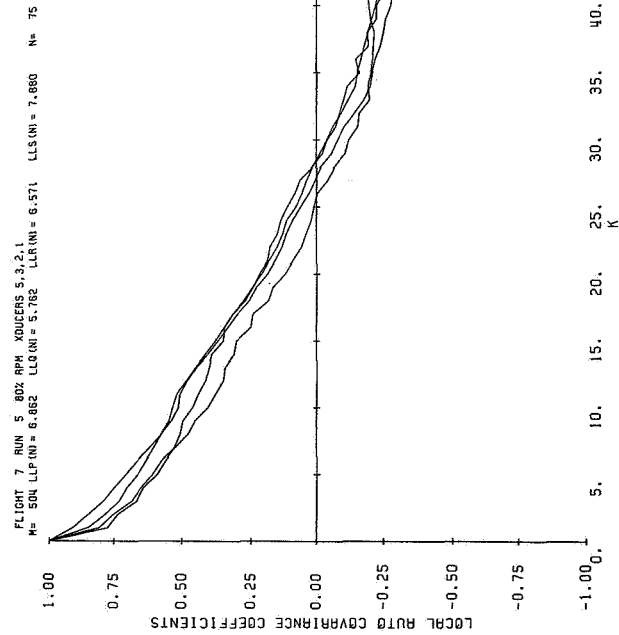
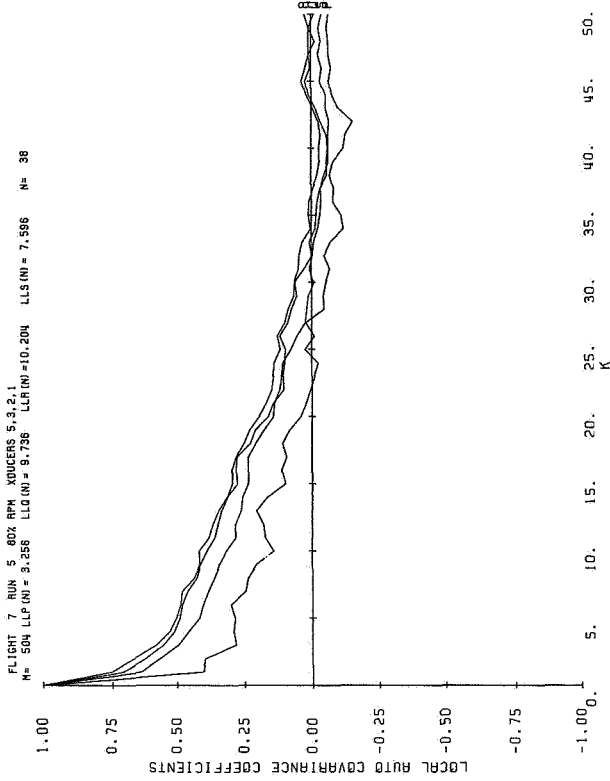
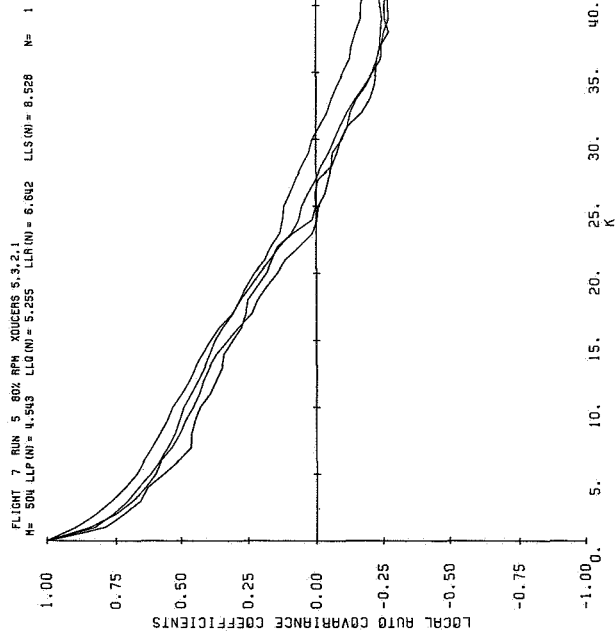
**APPENDIX C - BLADE SURFACE PRESSURE
STATISTICAL PROPERTIES**

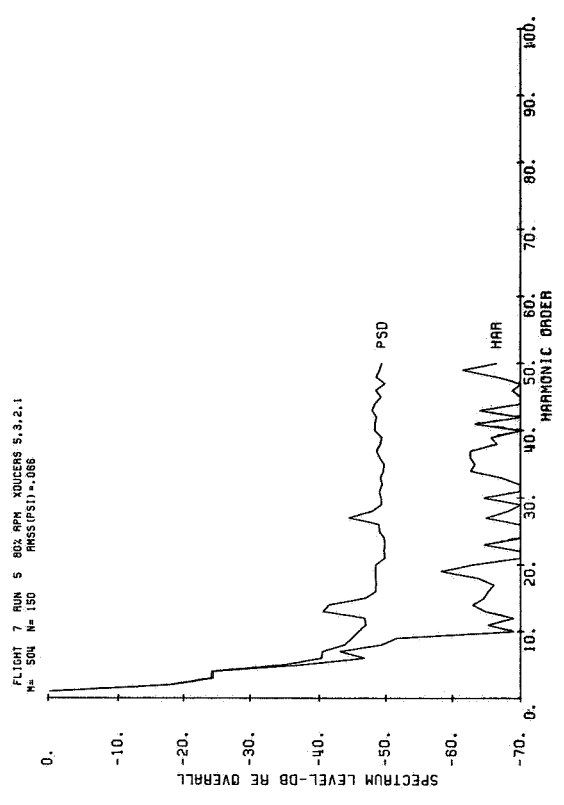
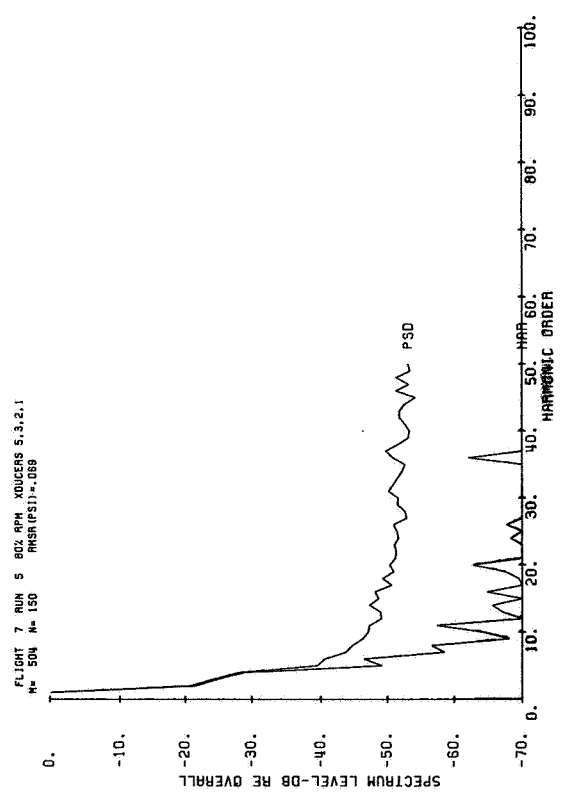
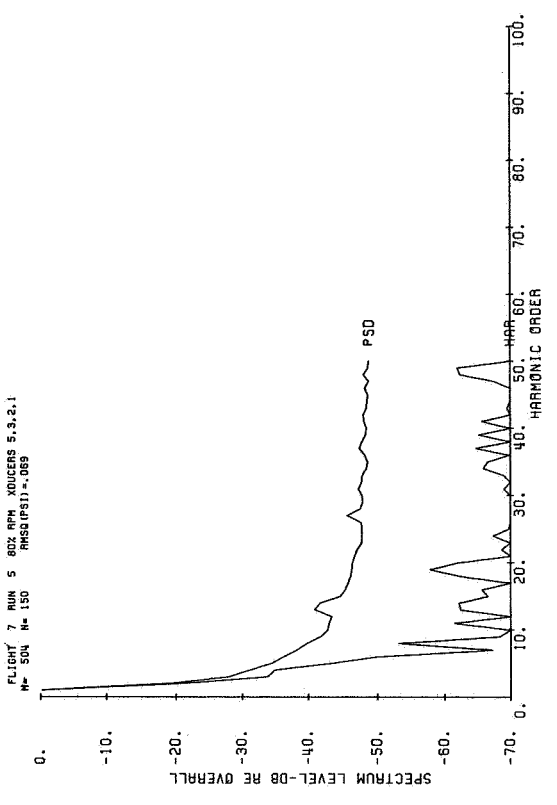
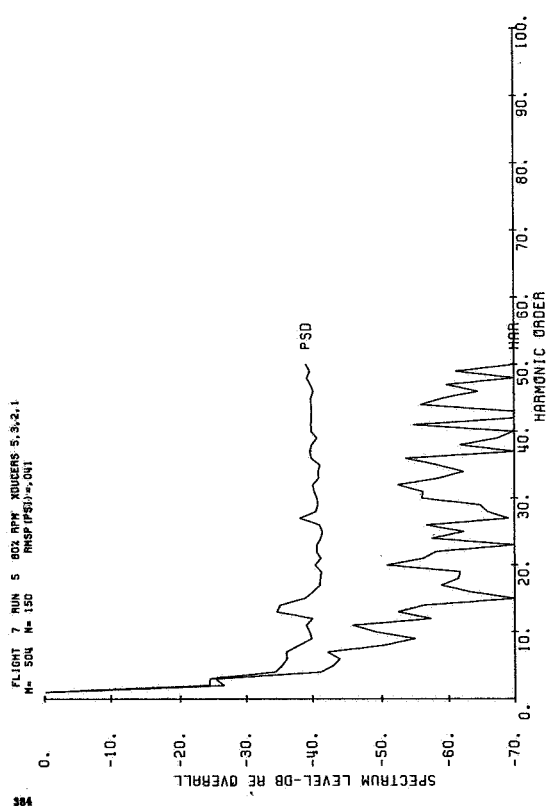


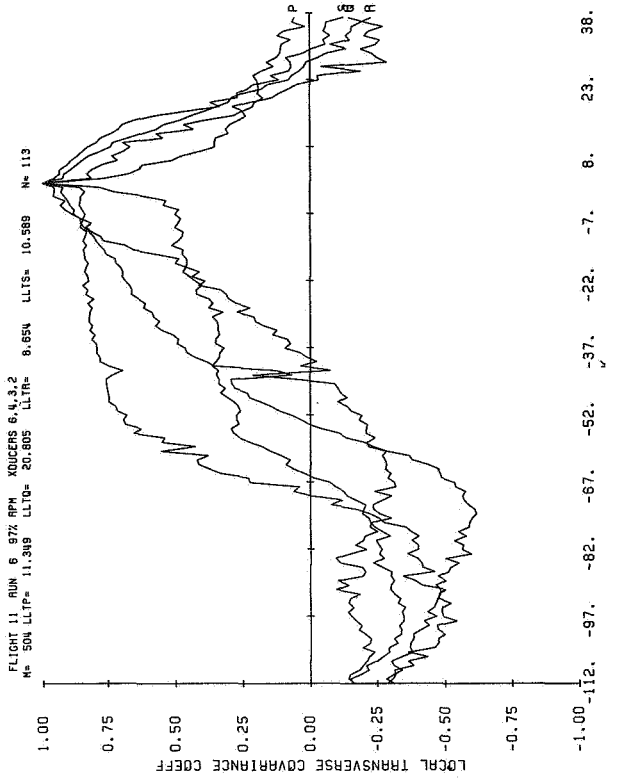
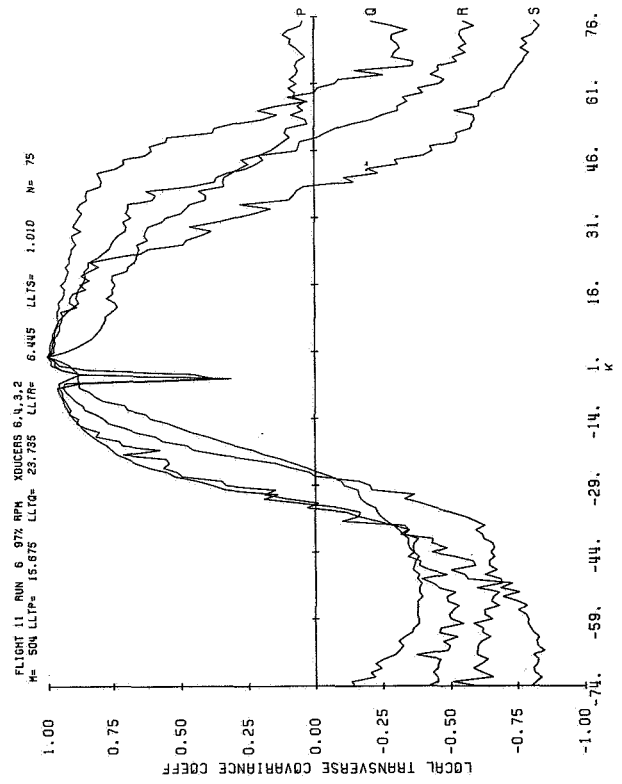
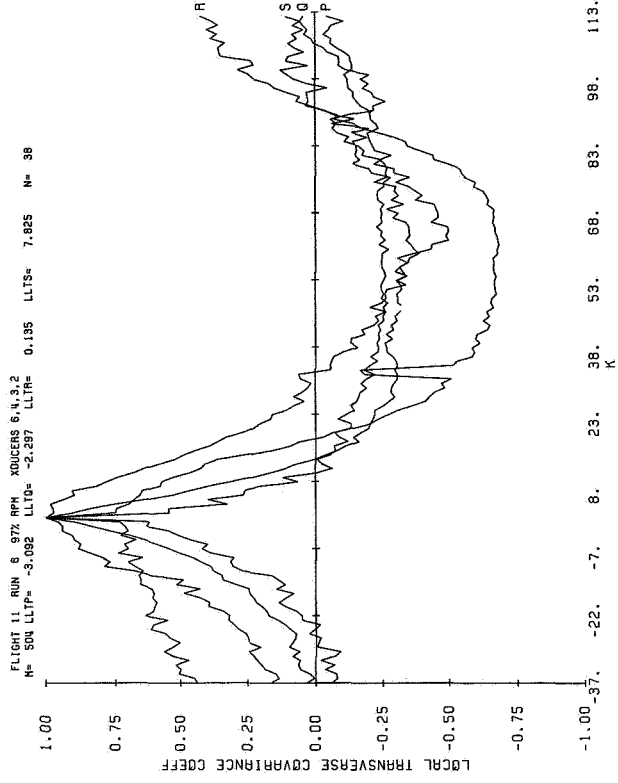
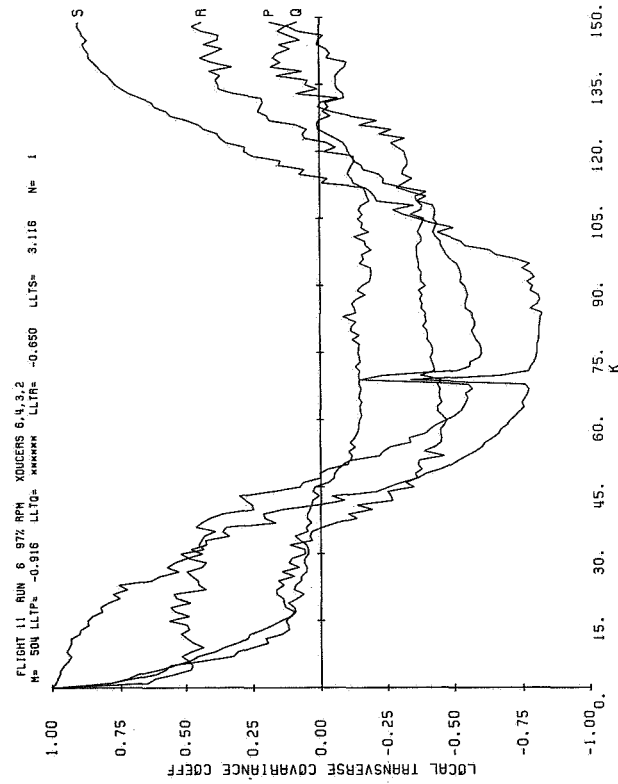


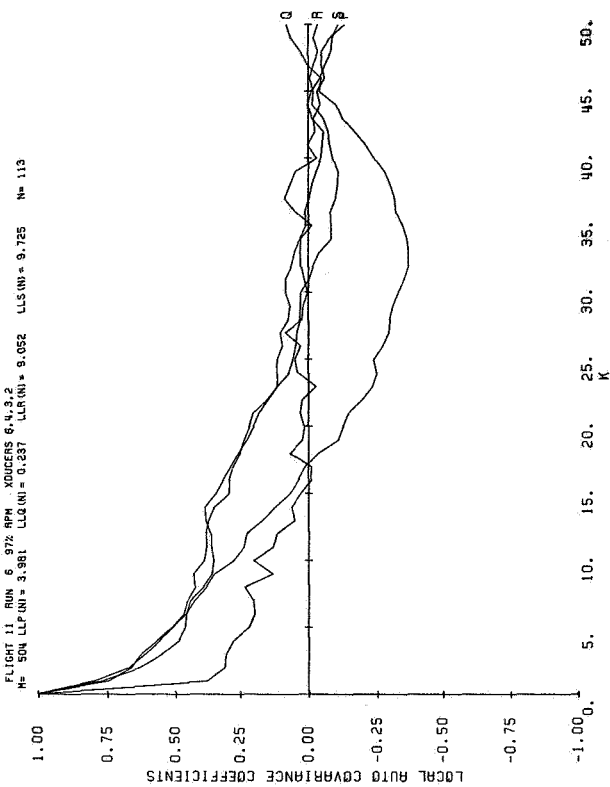
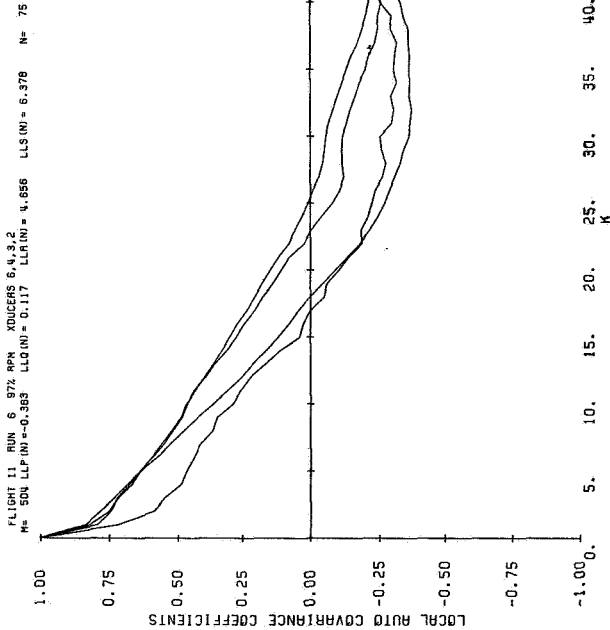
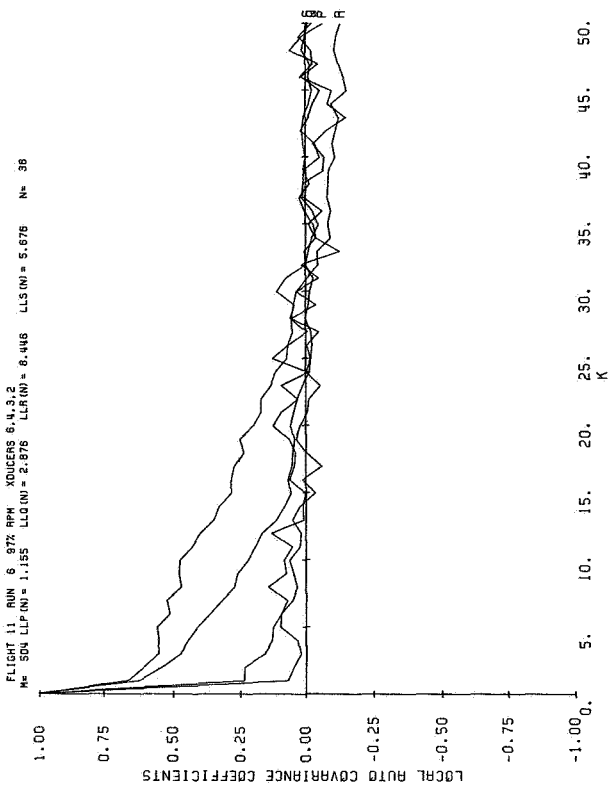
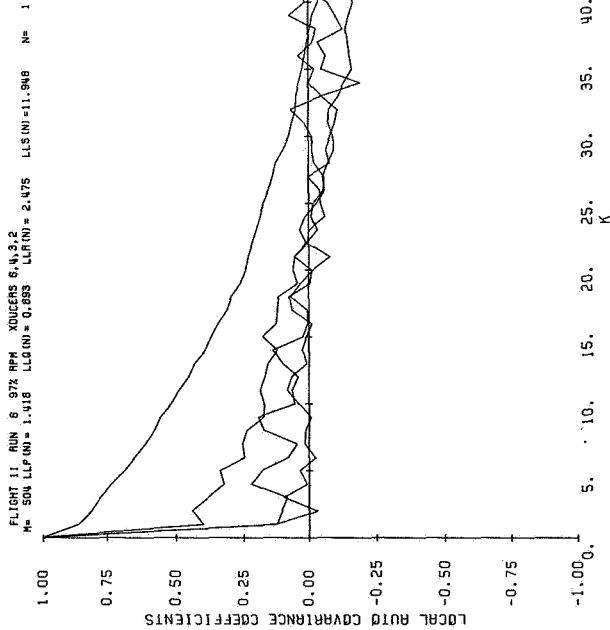


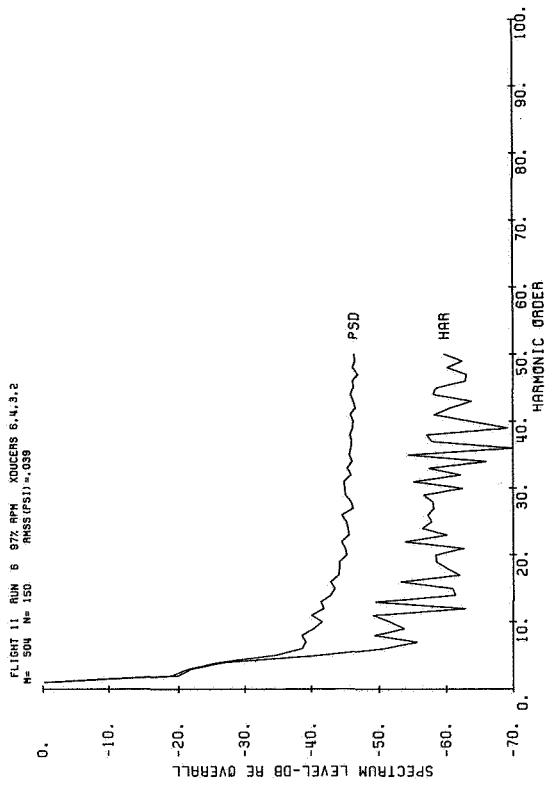
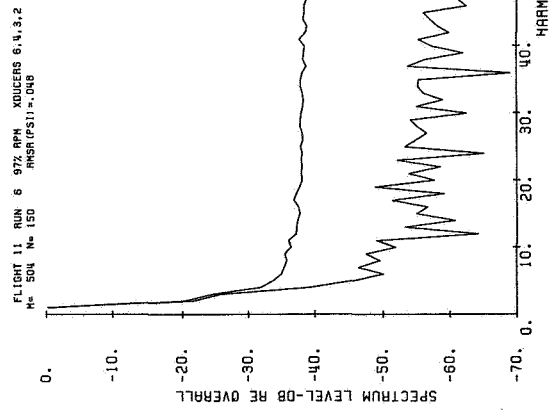
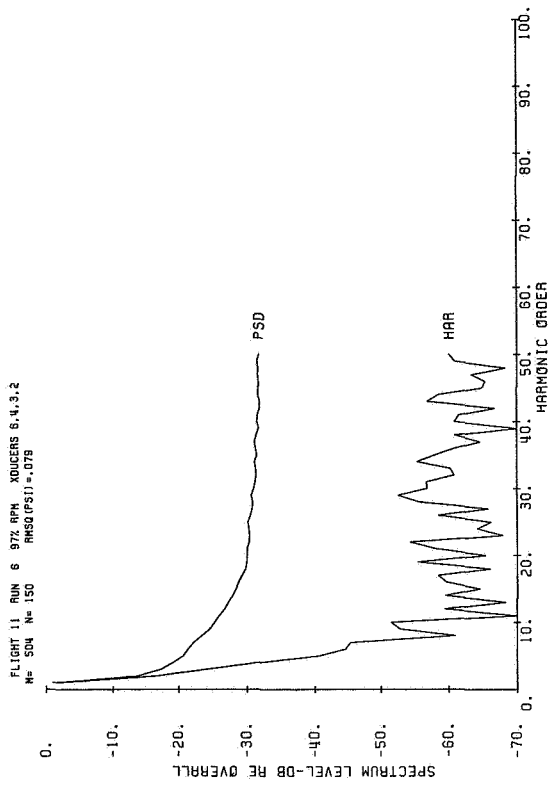
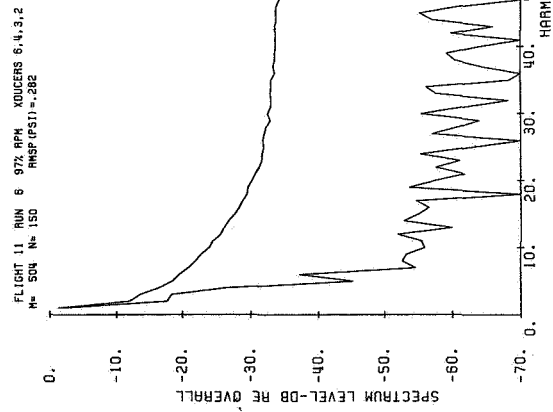


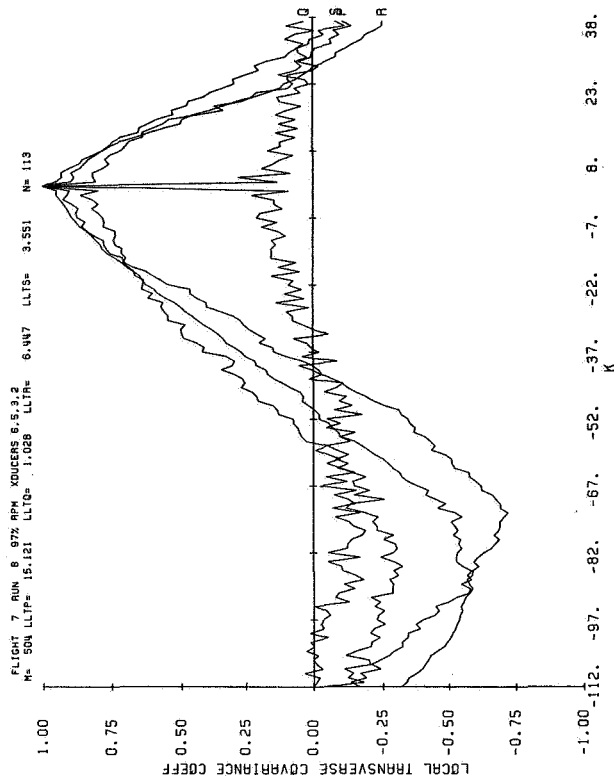
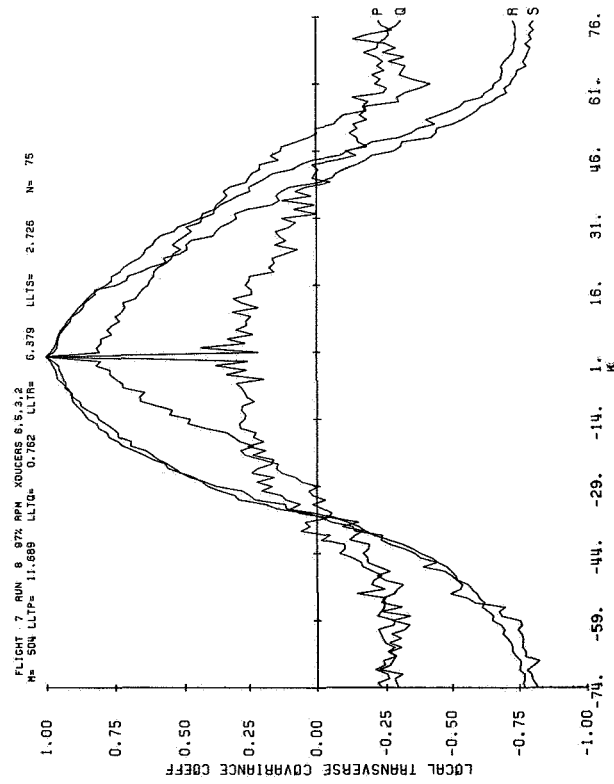
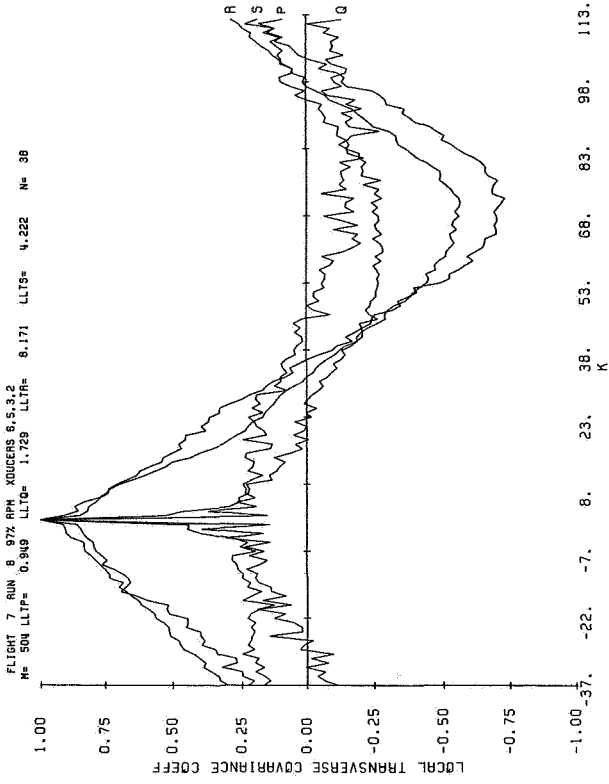
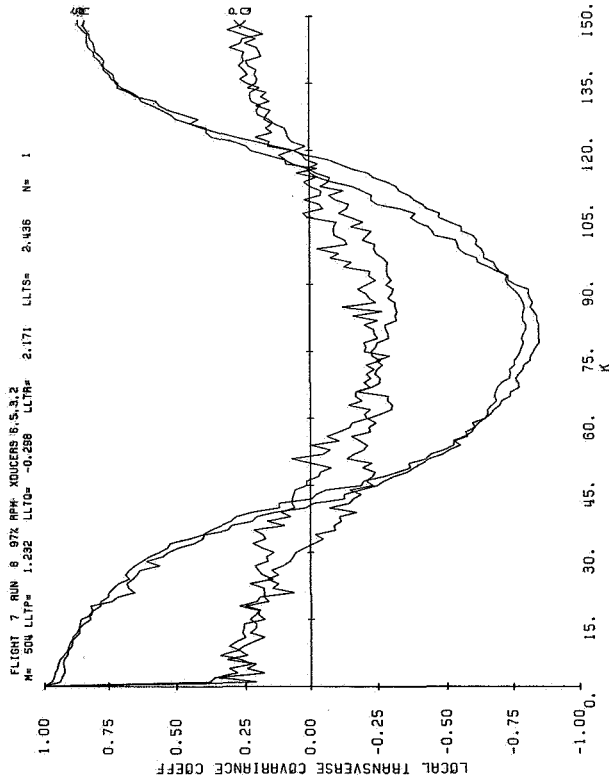






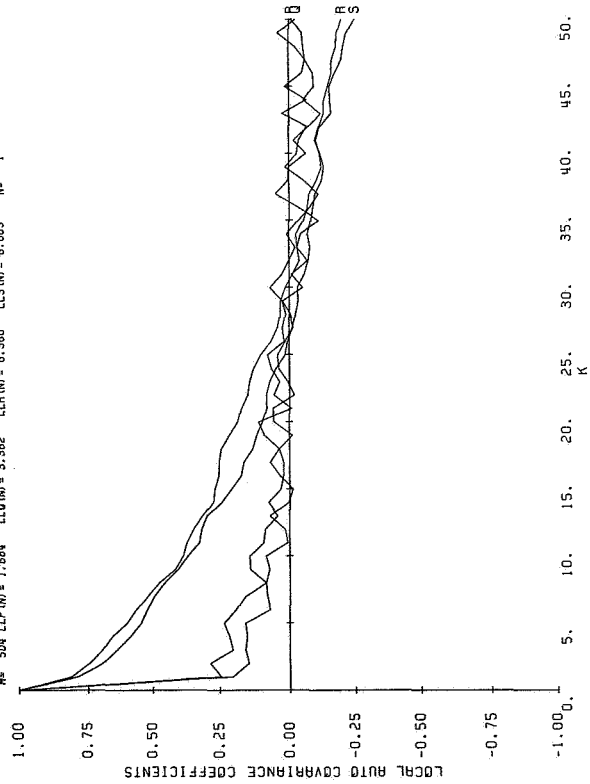






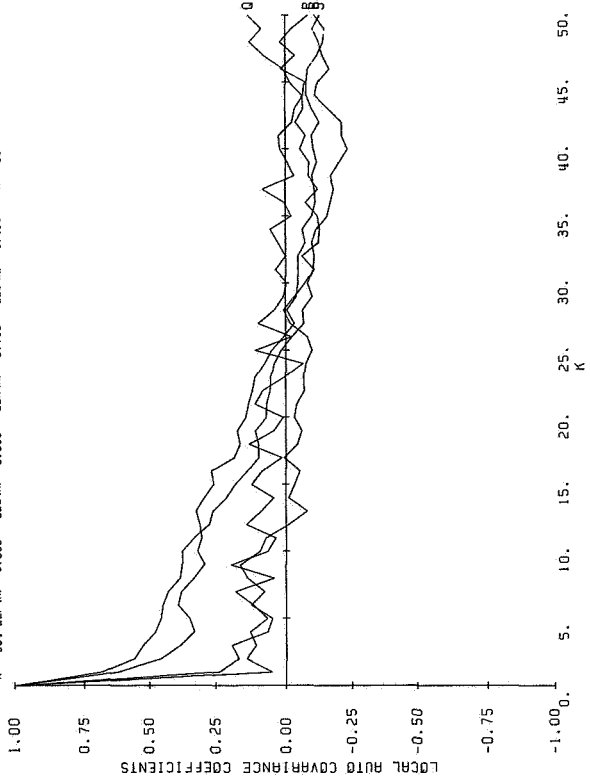
FLIGHT 7 RUN 8 97% RPM XDUCERS 6.5.3.2

M= 50% LLP (N) = 1.684 LLO (N) = 3.382 LLS (N) = 6.360 LLR (N) = 1 N= 1



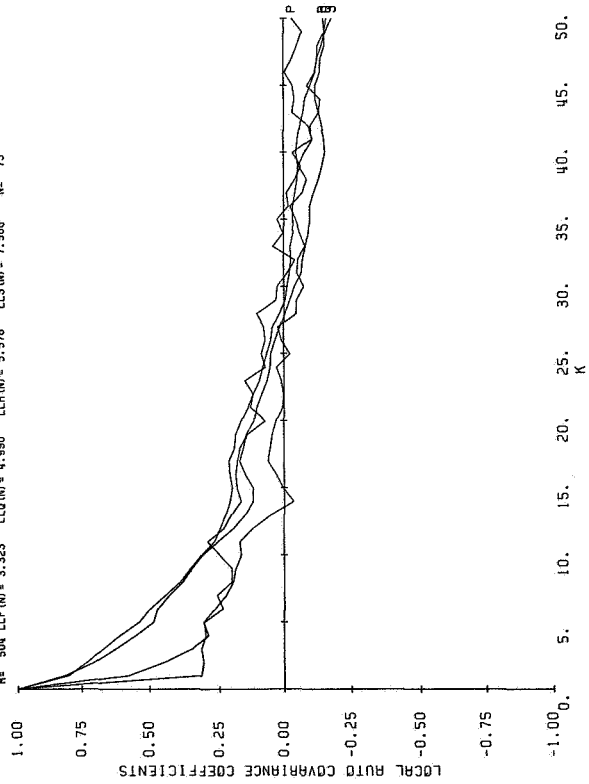
FLIGHT 7 RUN 8 97% RPM XDUCERS 6.5.3.2

M= 50% LLP (N) = 3.090 LLO (N) = 0.800 LLS (N) = 5.719 LLR (N) = 1 N= 38



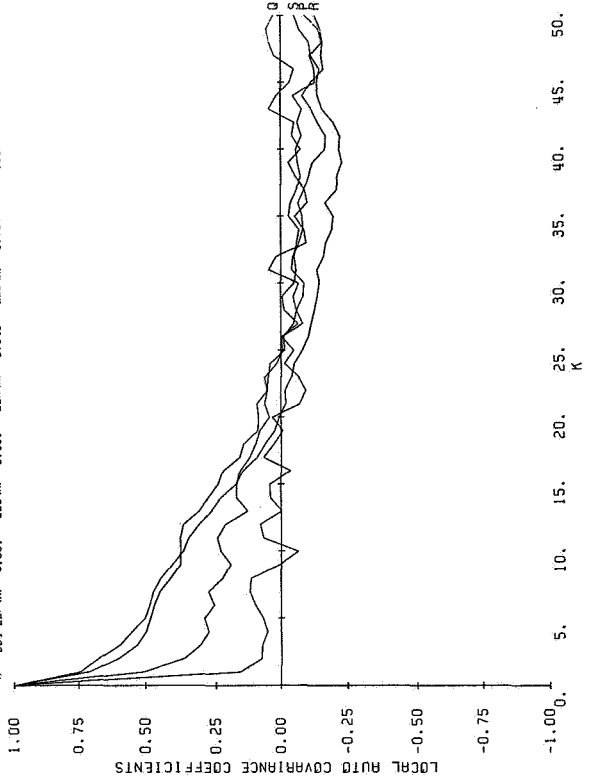
FLIGHT 7 RUN 8 97% RPM XDUCERS 6.5.3.2

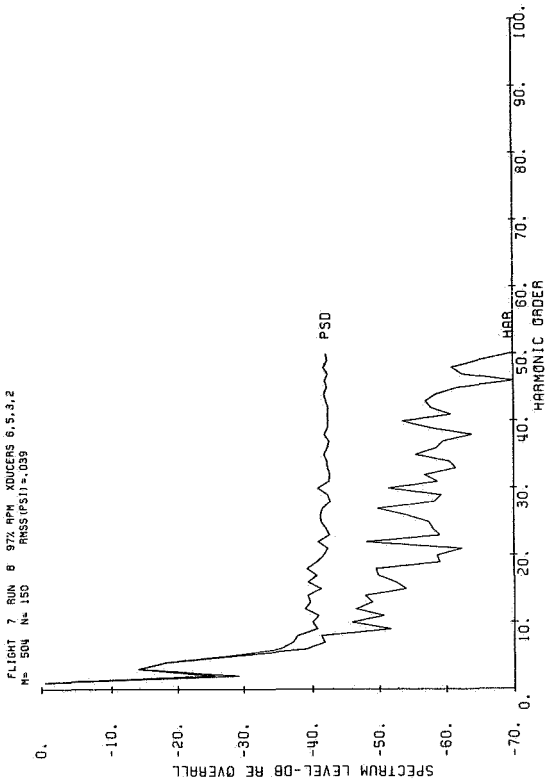
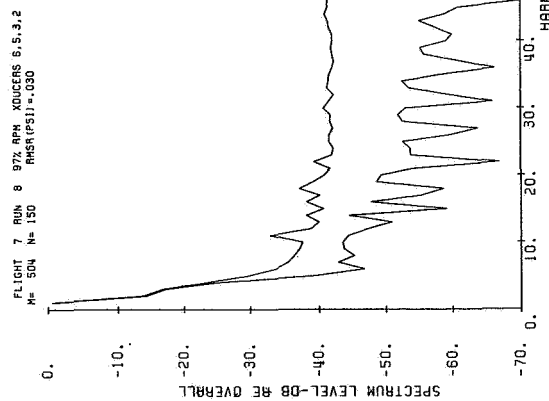
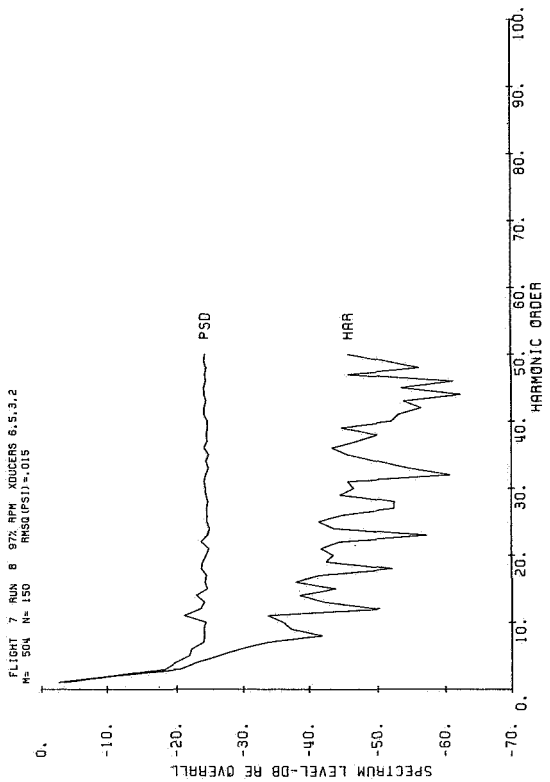
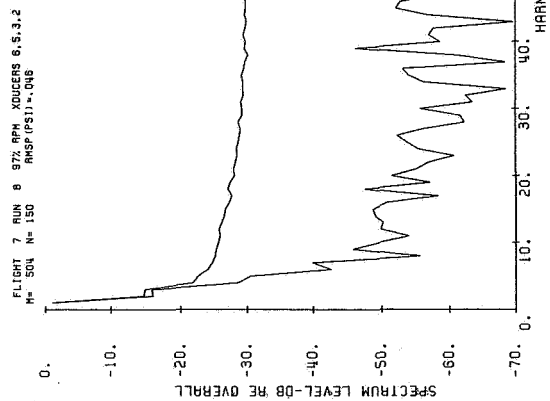
M= 50% LLP (N) = 3.323 LLO (N) = 4.990 LLS (N) = 5.576 LLR (N) = 7 N= 75

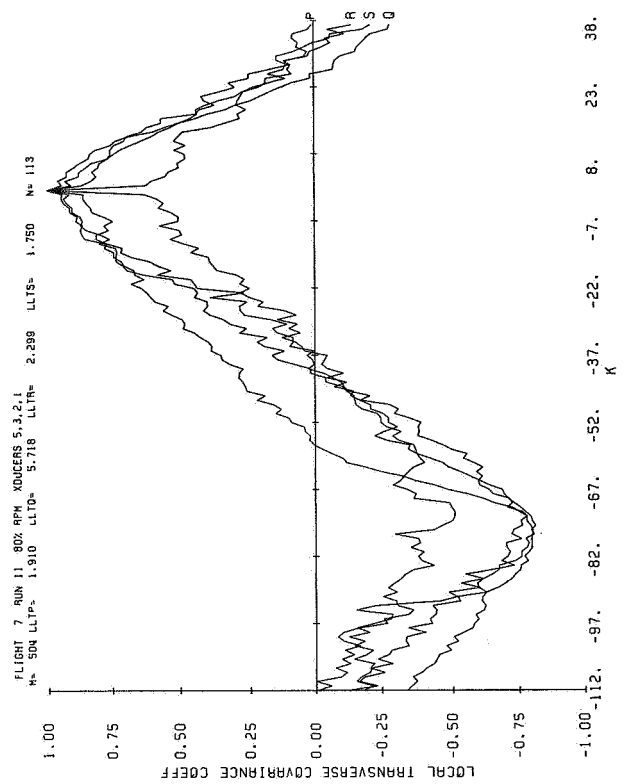
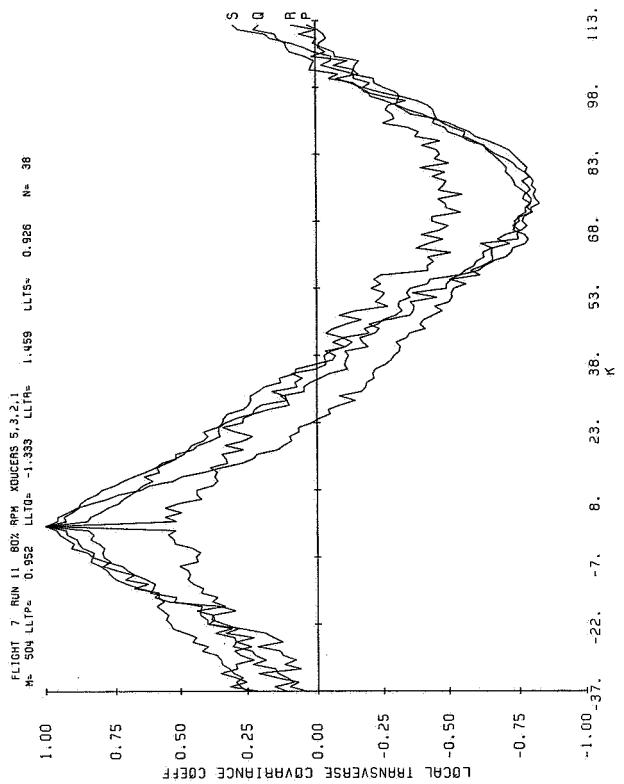
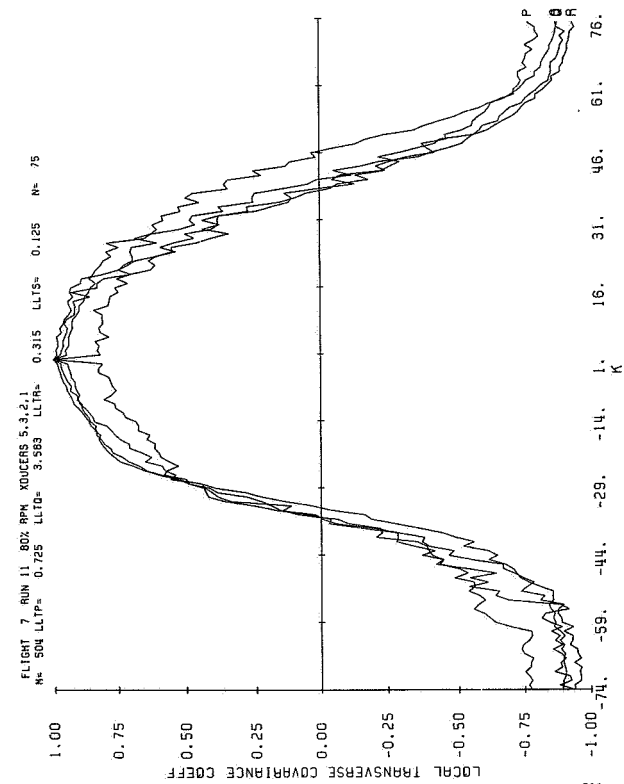
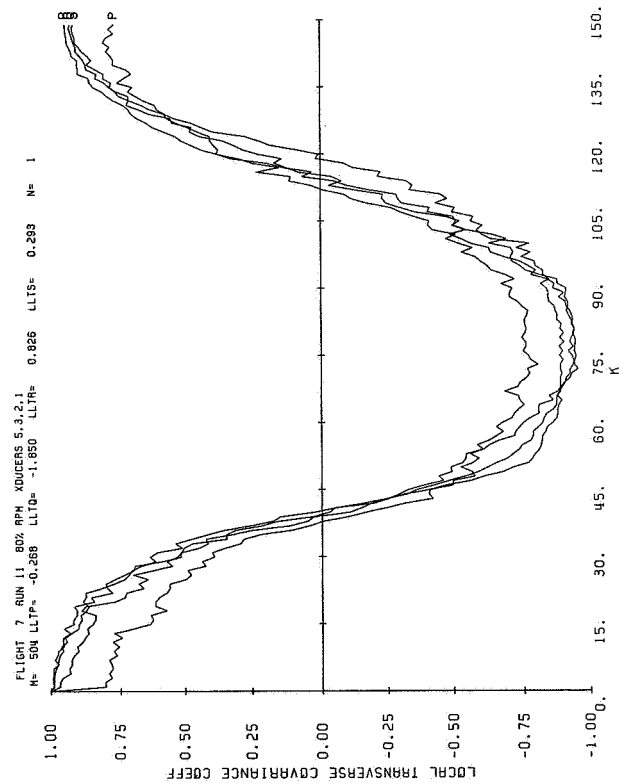


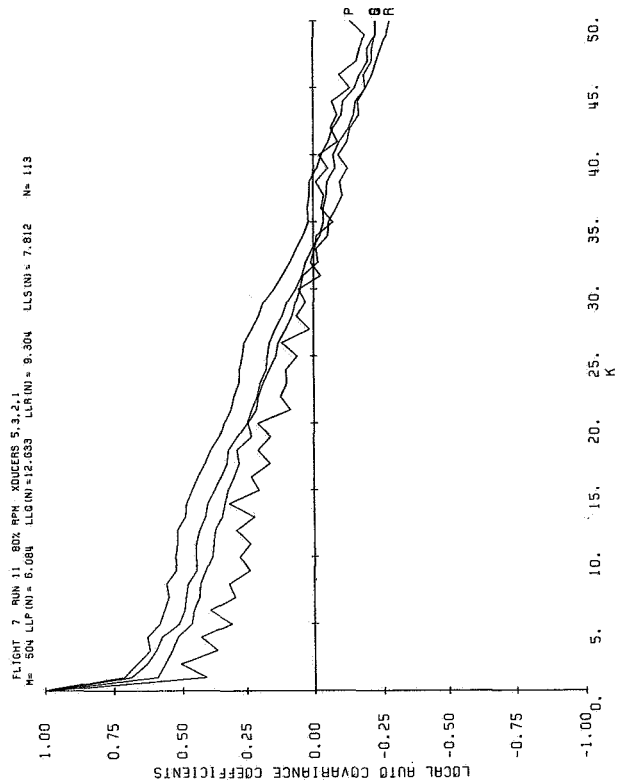
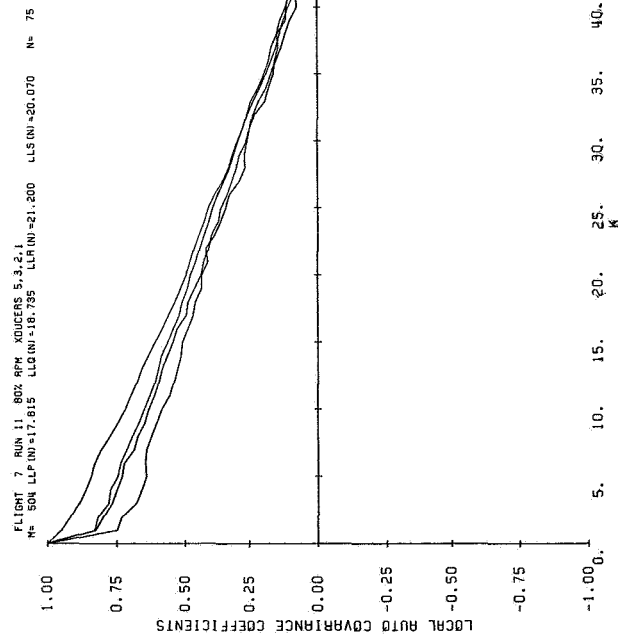
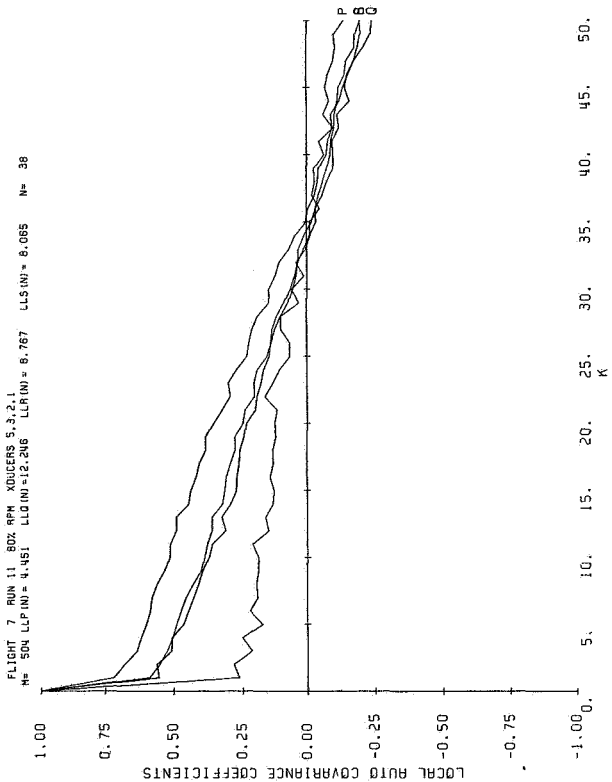
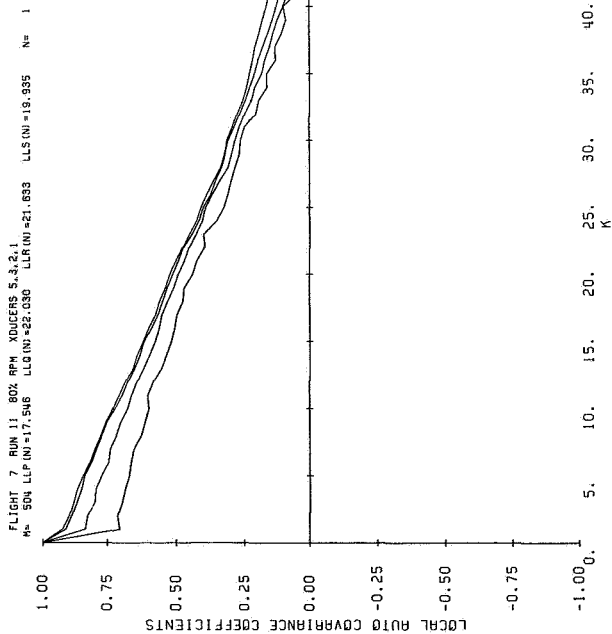
FLIGHT 7 RUN 8 97% RPM XDUCERS 6.5.3.2

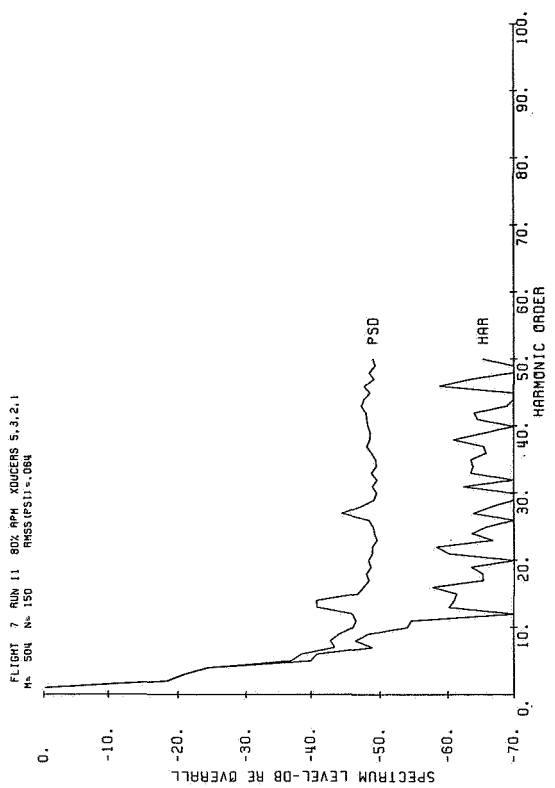
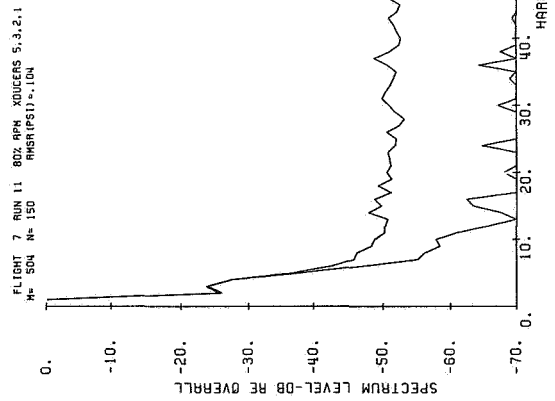
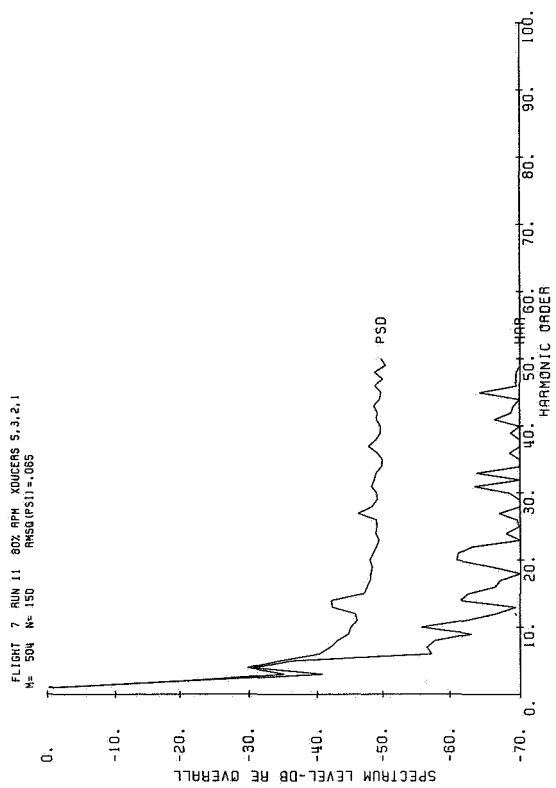
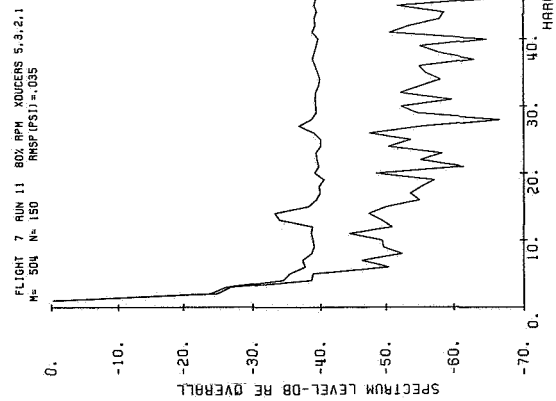
M= 50% LLP (N) = 3.631 LLO (N) = 0.991 LLS (N) = 5.843 LLR (N) = 3 N= 113

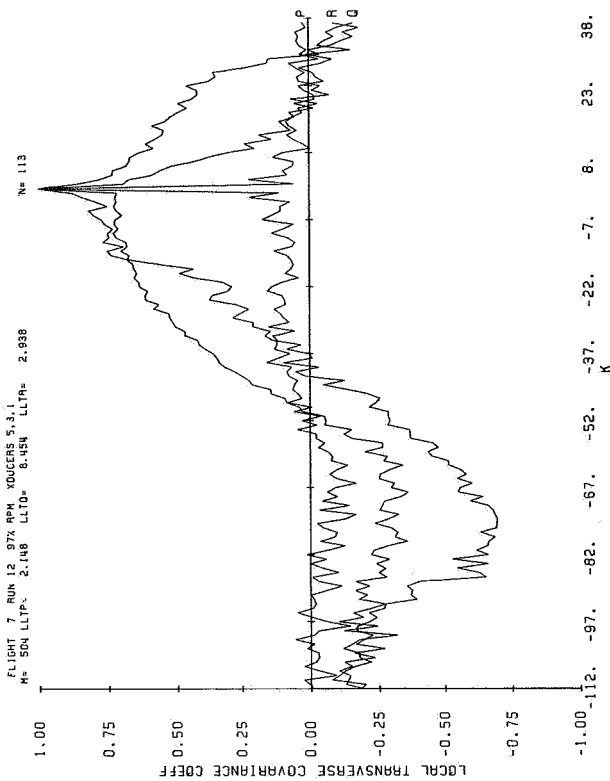
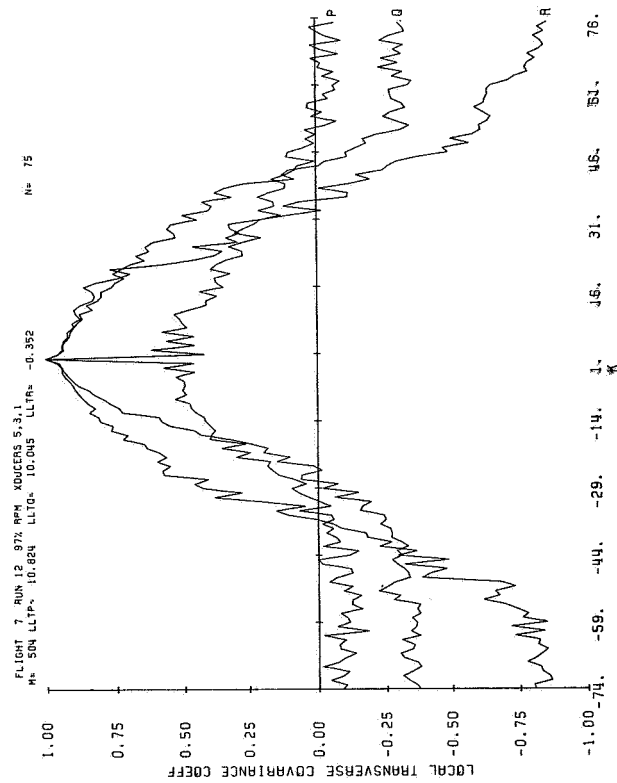
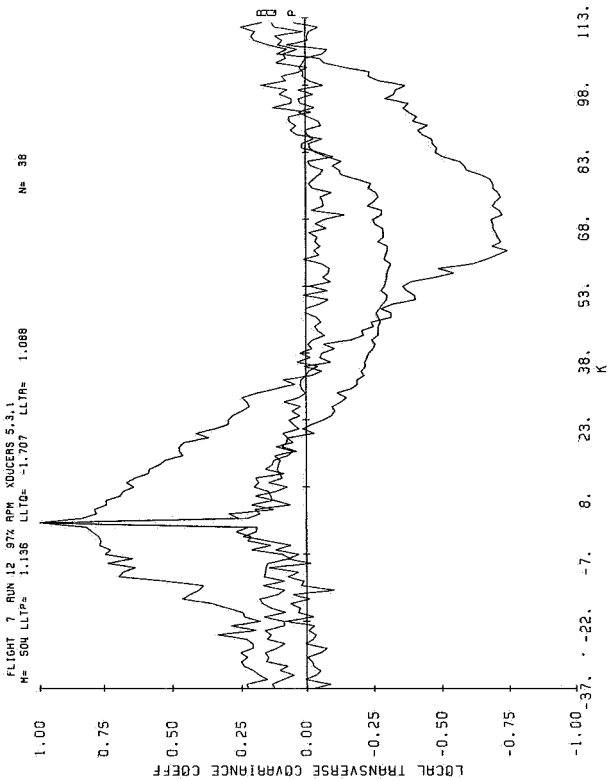
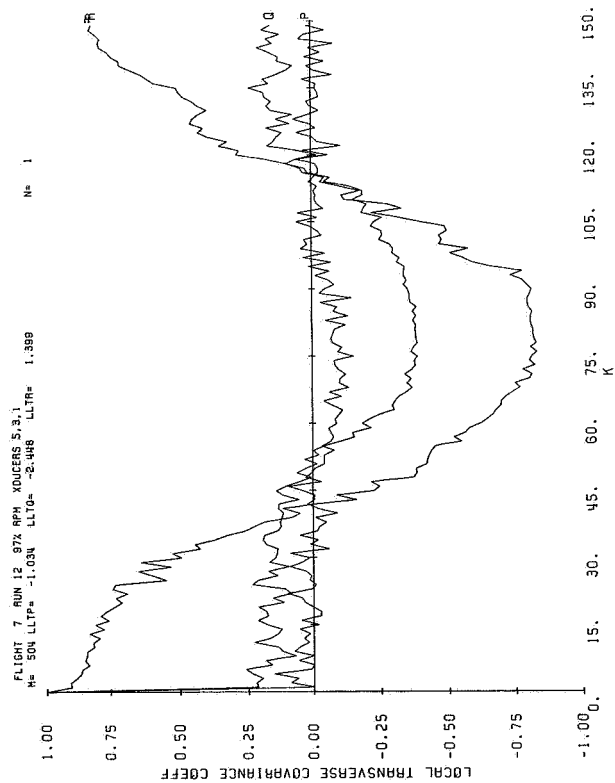






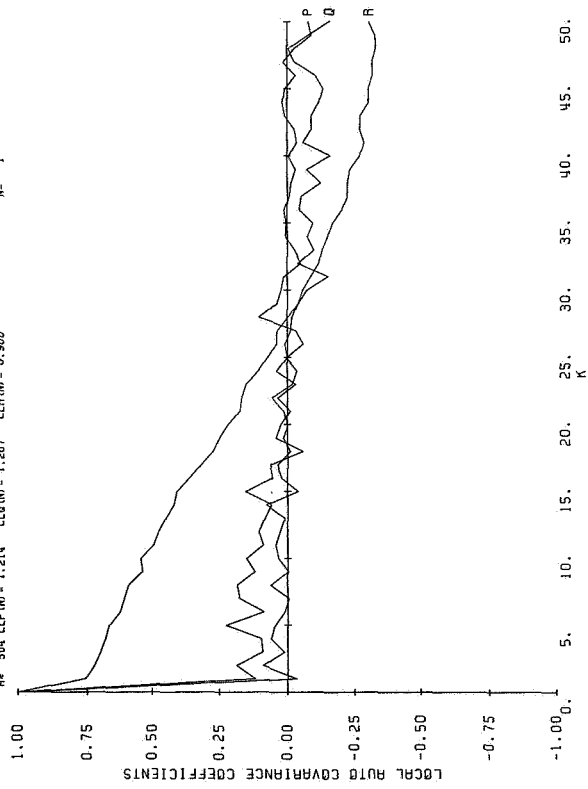






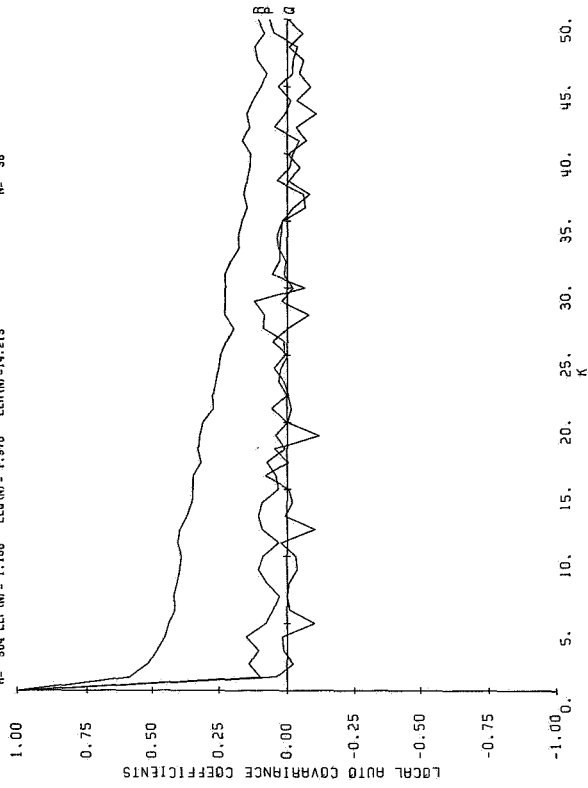
FLIGHT 7 RUN 12 97% RPM XDCERS 5.3.1
M= 504 LCP(M)= 1.214 LCO(M)= 1.207 CLR(M)= 6.900

N= 1



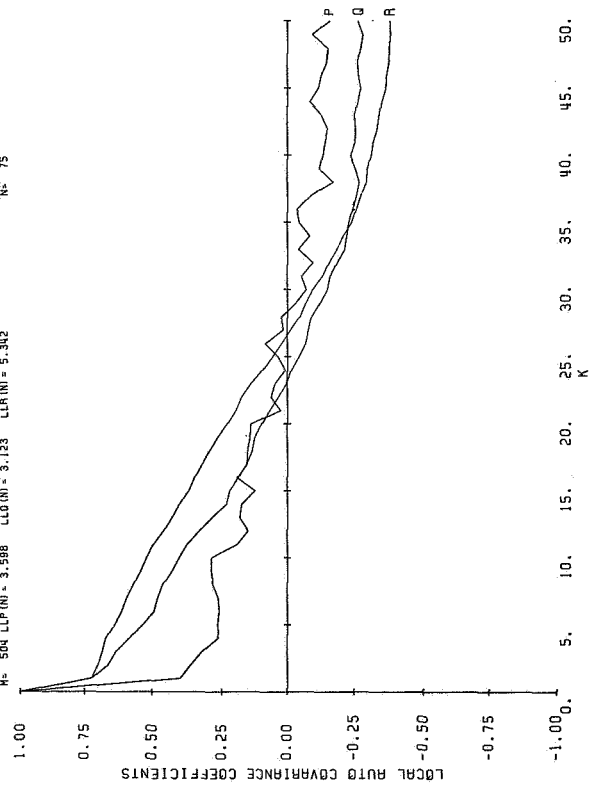
FLIGHT 7 RUN 12 97% RPM XDCERS 5.3.1
M= 504 LCP(M)= 1.180 LCO(M)= 1.970 CLR(M)= 4.215

N= 38



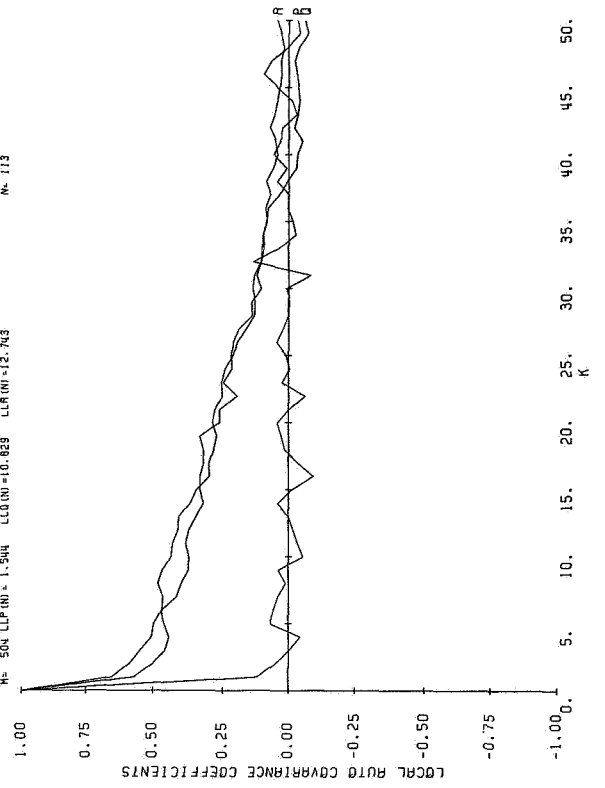
FLIGHT 7 RUN 12 97% RPM XDCERS 5.3.1
M= 504 LCP(M)= 3.586 LCO(M)= 3.123 CLR(M)= 5.342

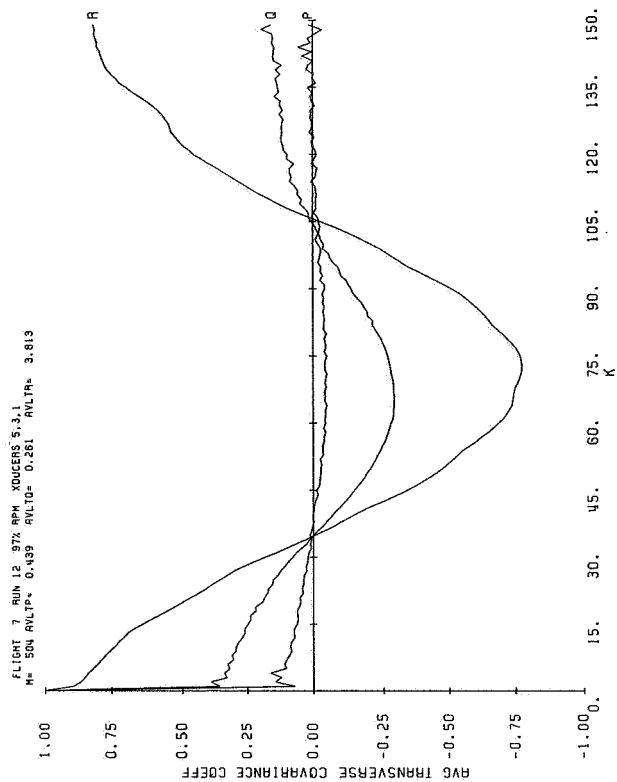
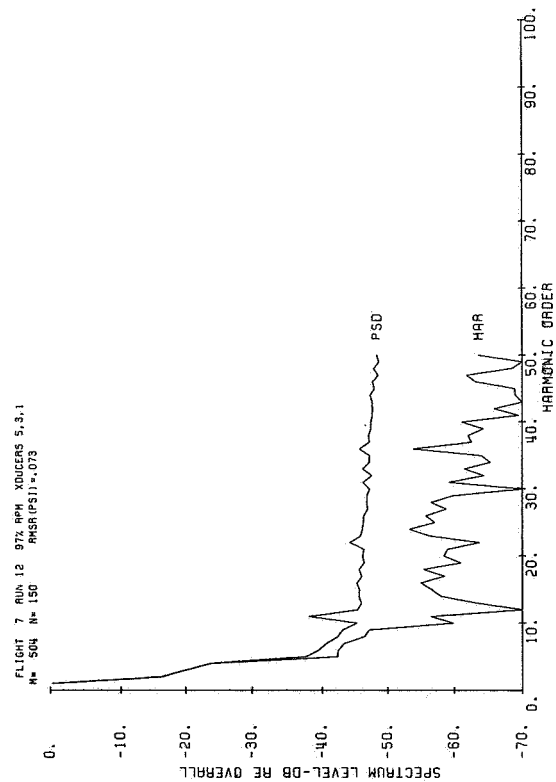
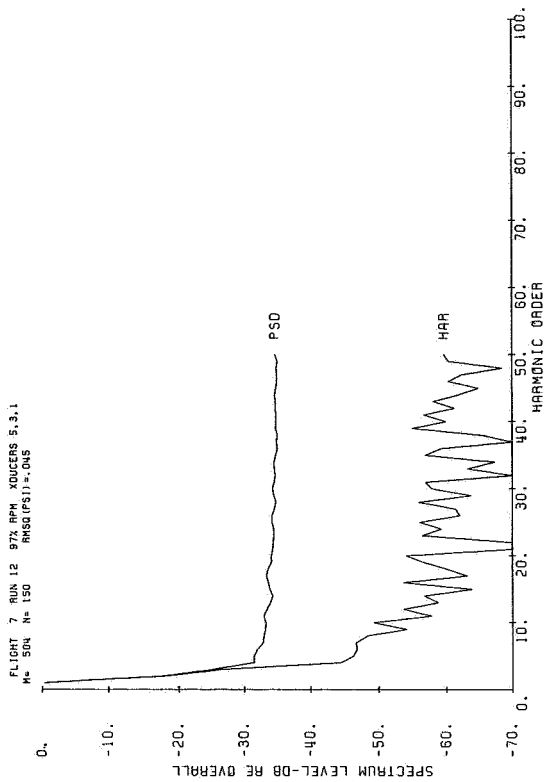
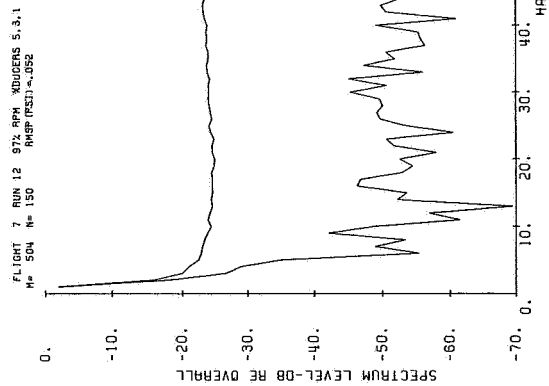
N= 75

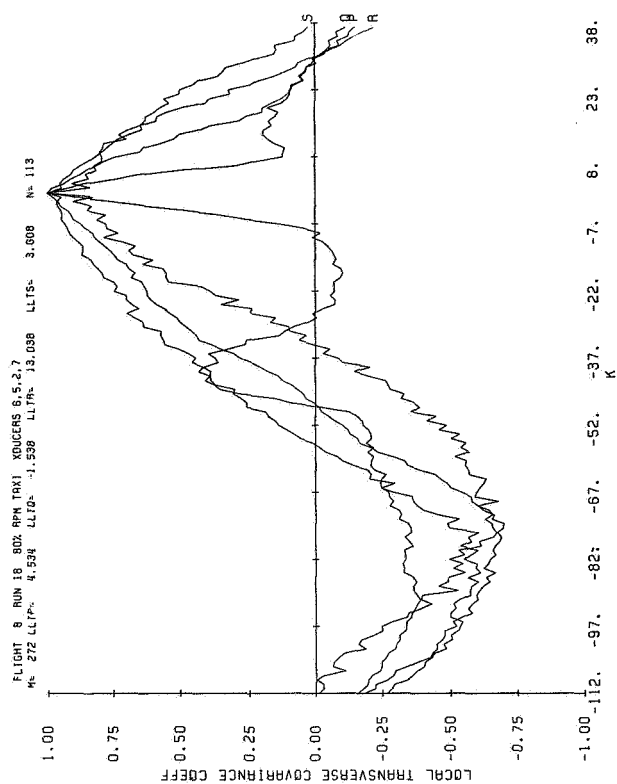
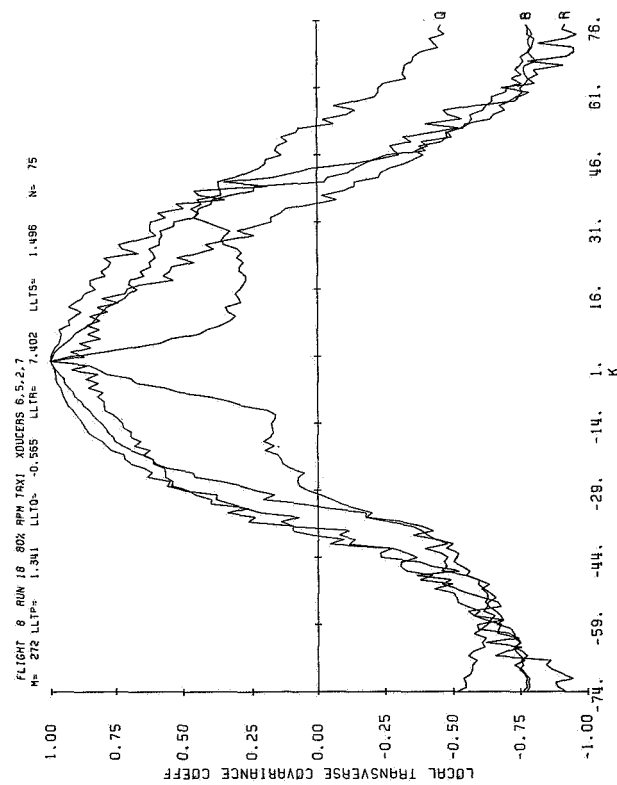
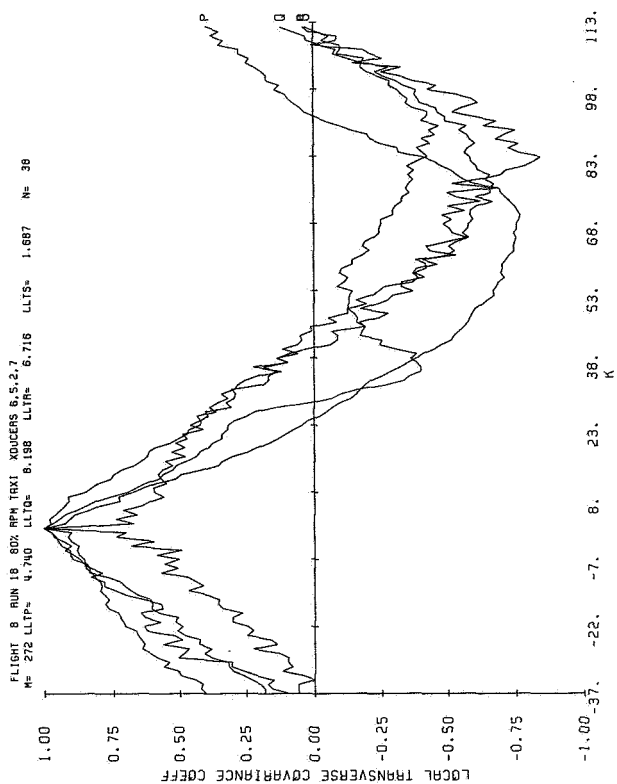
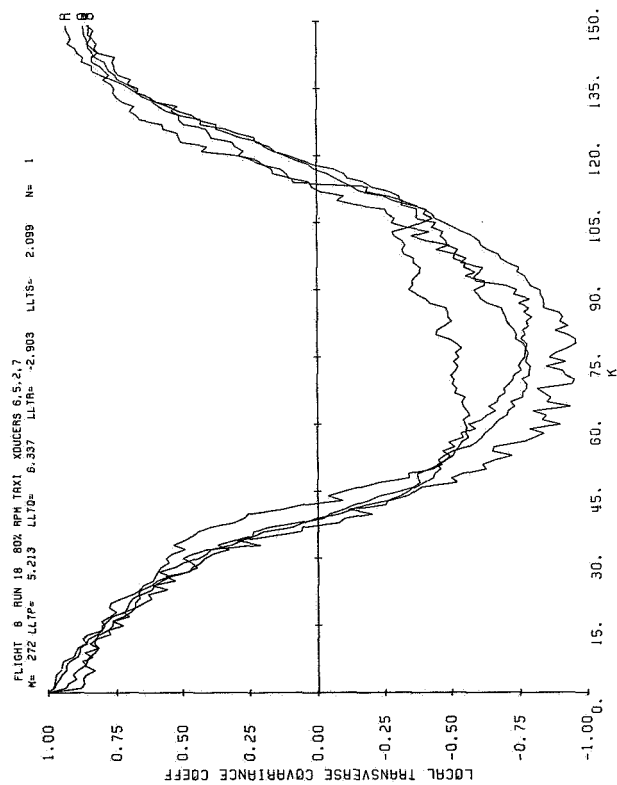


FLIGHT 7 RUN 12 97% RPM XDCERS 5.3.1
M= 504 LCP(M)= 1.544 LCO(M)= 10.829 CLR(M)= 12.743

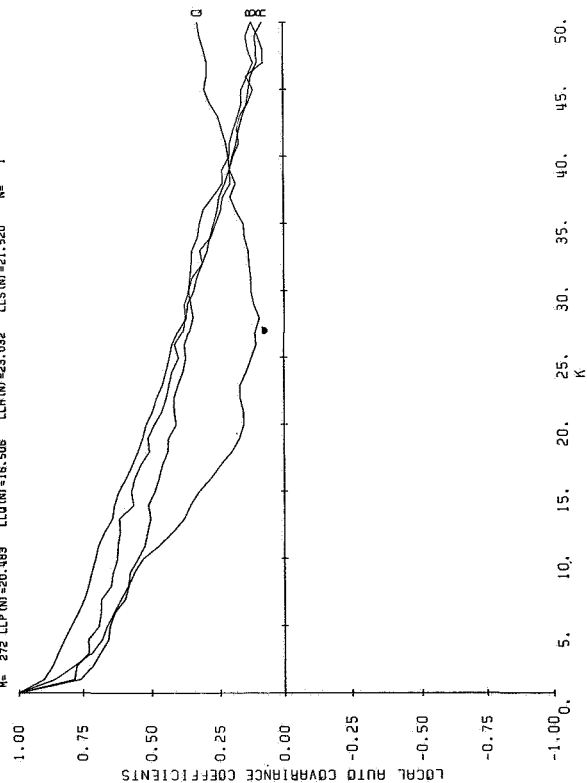
N= 113



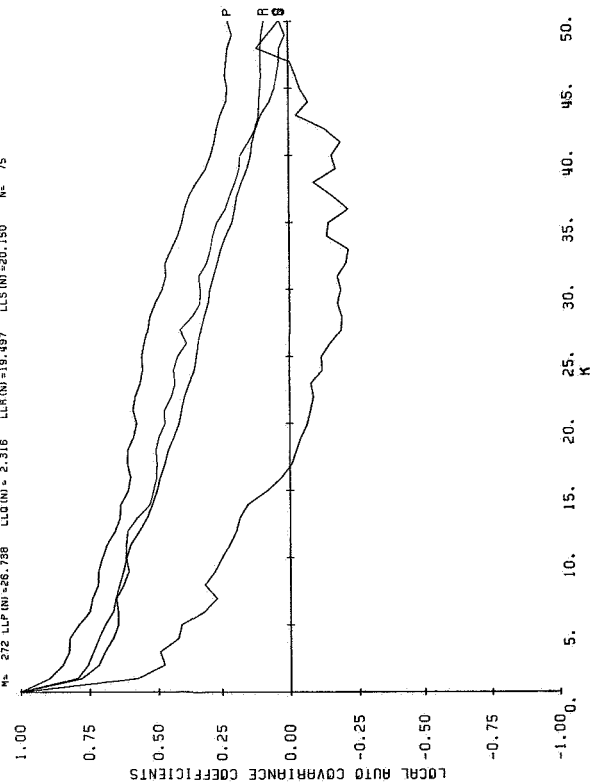




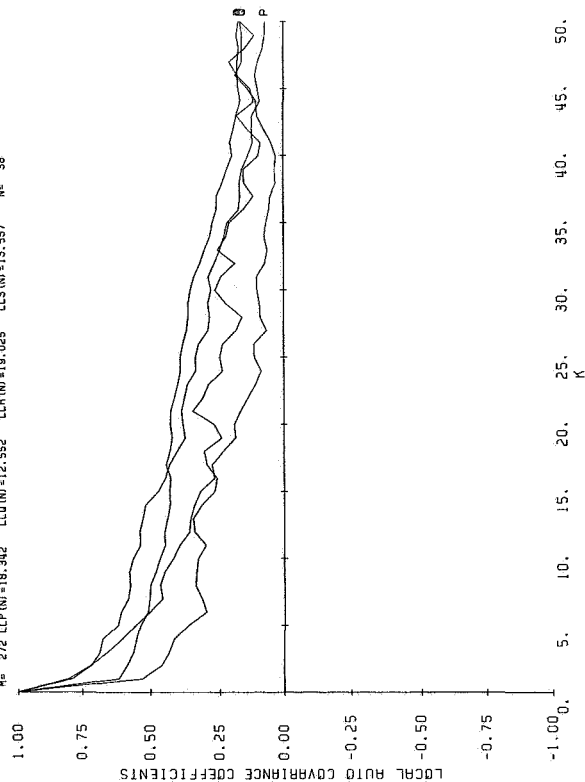
FLIGHT 8 RUN 18 802 RPM TAXI XDCERS 6.5.2.7
 No. 272 LLP IN=20.489 LLQ IN=18.506 LLH IN=23.032 LLS IN=21.520 N= 1



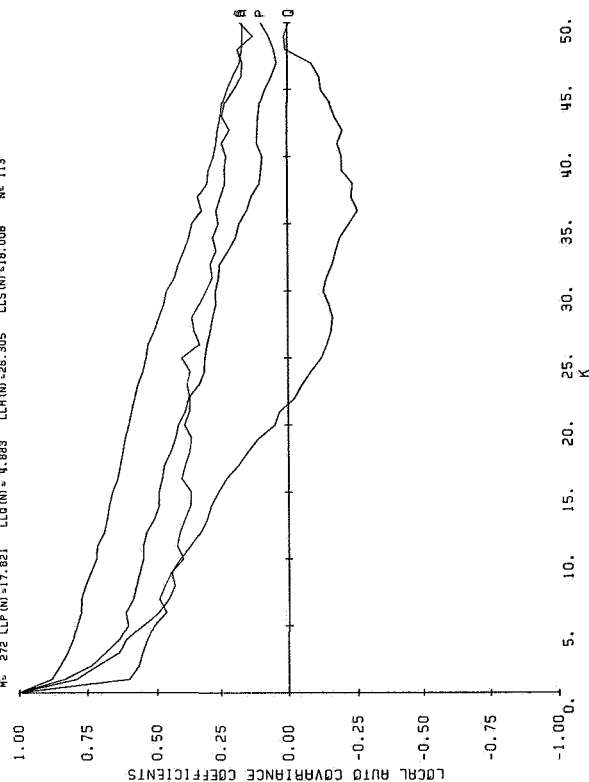
FLIGHT 8 RUN 18 802 RPM TAXI XDCERS 6.5.2.7
 No. 272 LLP IN=26.738 LLQ IN= 2.316 LLH IN=19.487 LLS IN=20.150 N= 75



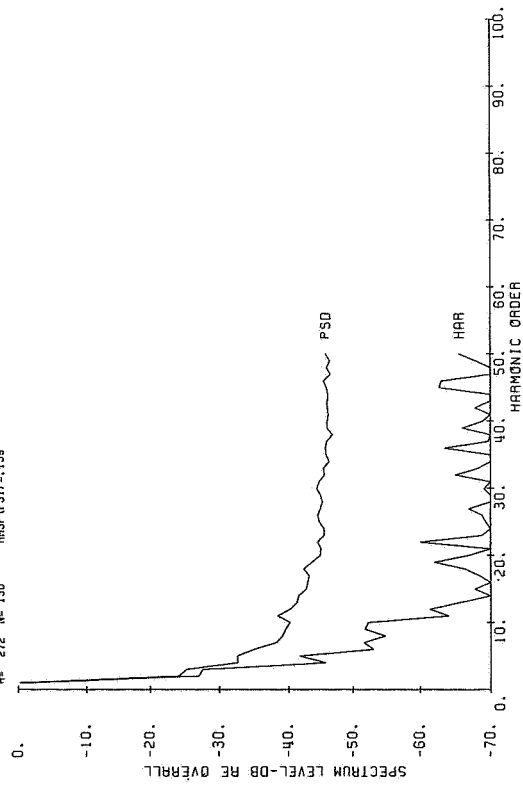
FLIGHT 8 RUN 18 802 RPM TAXI XDCERS 6.5.2.7
 No. 272 LLP IN=18.342 LLQ IN=12.552 LLH IN=19.025 LLS IN=13.557 N= 39



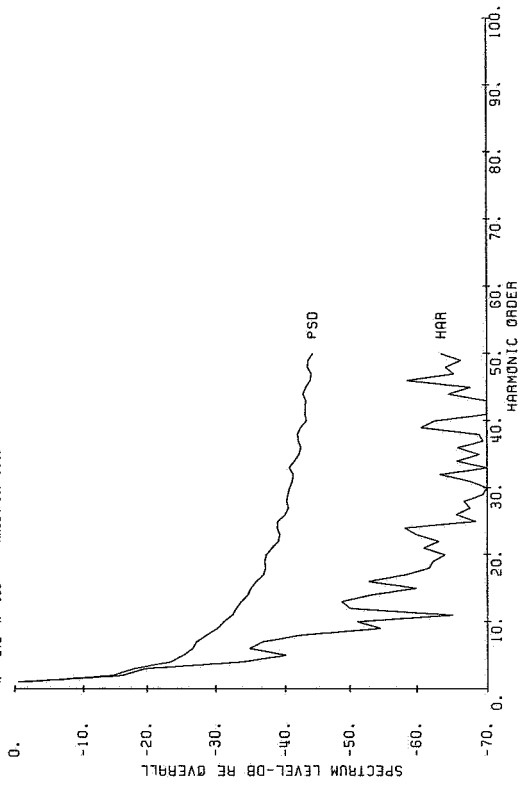
FLIGHT 8 RUN 18 802 RPM TAXI XDCERS 6.5.2.7
 No. 272 LLP IN=17.821 LLQ IN= 4.883 LLH IN=26.305 LLS IN=18.008 N= 113



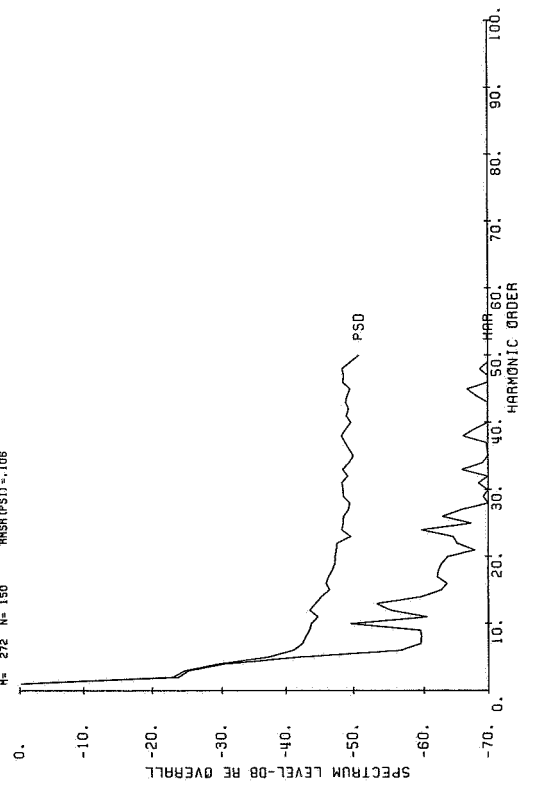
FLIGHT 8 RUN 18 802 RPM TAXI XDCERS 6.5.2.7
M= 272 N= 150 RMSD (PS1) = .139



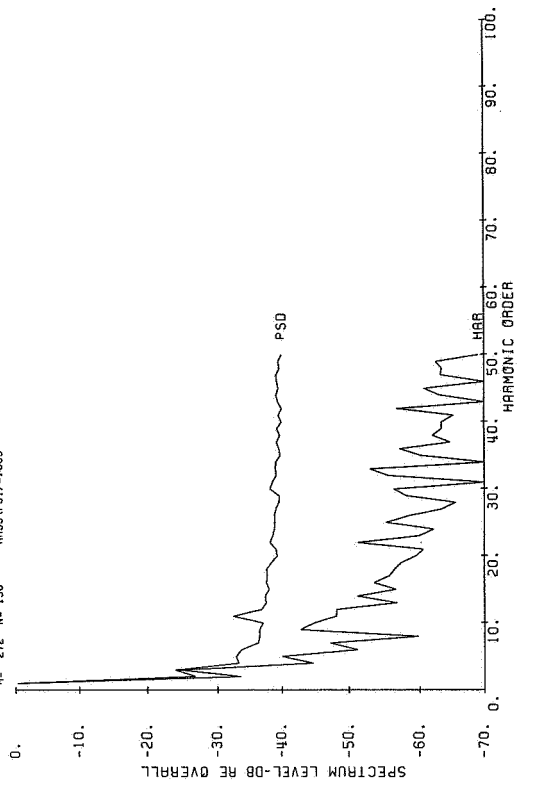
FLIGHT 8 RUN 18 802 RPM TAXI XDCERS 6.5.2.7
M= 272 N= 150 RMSD (PS1) = .149



FLIGHT 8 RUN 18 802 RPM TAXI XDCERS 6.5.2.7
M= 272 N= 150 RMSD (PS1) = .106

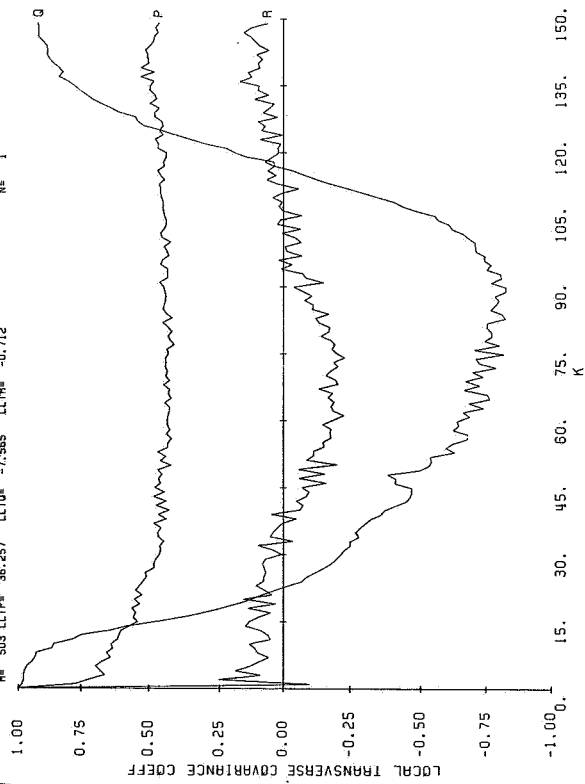


FLIGHT 8 RUN 18 802 RPM TAXI XDCERS 6.5.2.7
M= 272 N= 150 RMSD (PS1) = .069



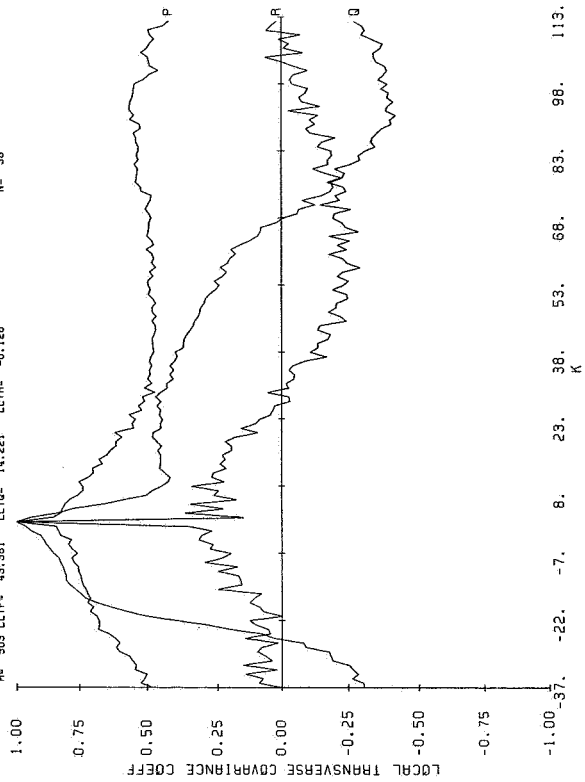
FLIGHT 8 RUN 20R 97Z RPM TAXI XDUCEERS 5.2.7
M= 503 LLTP= 36.257 LLT0= -7.585 LLTR= -0.712

N= 1



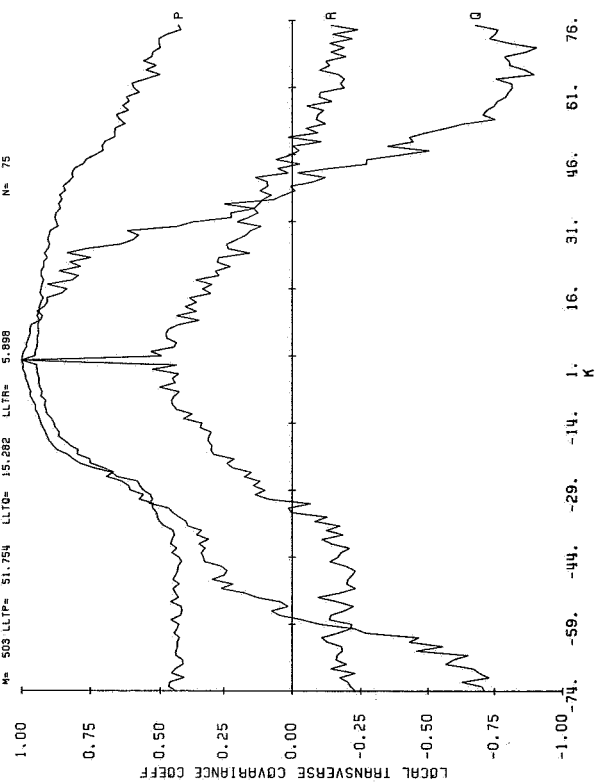
FLIGHT 8 RUN 20R 97Z RPM TAXI XDUCEERS 5.2.7
M= 503 LLTP= 43.381 LLT0= 14.221 LLTR= -0.128

N= 38



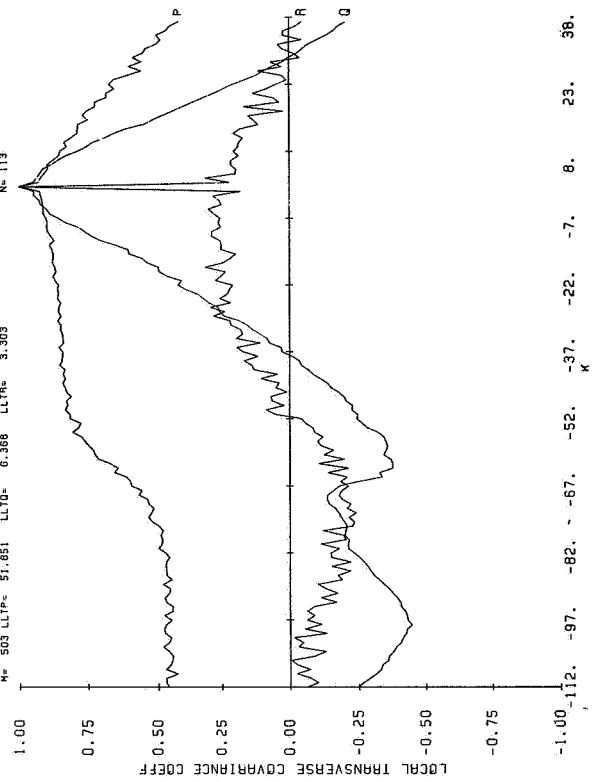
FLIGHT 8 RUN 20R 97Z RPM TAXI XDUCEERS 5.2.7
M= 503 LLTP= 51.755 LLT0= 15.282 LLTR= 5.888

N= 75



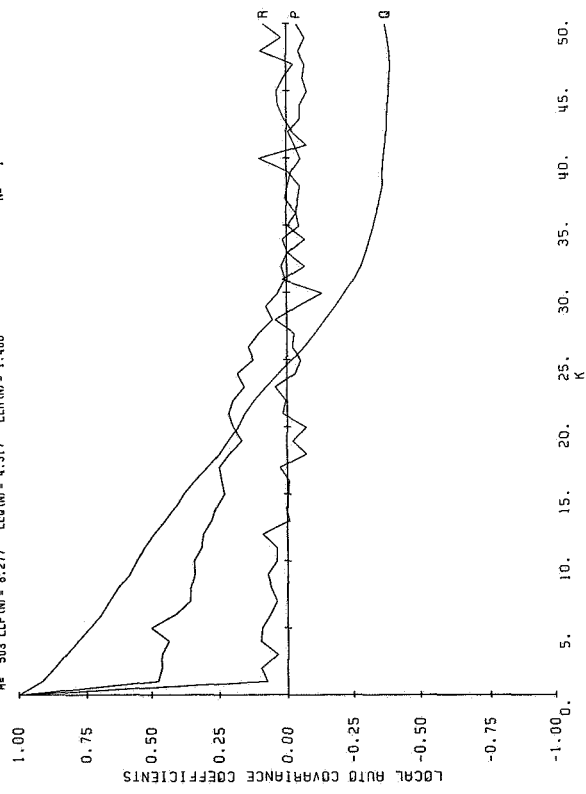
FLIGHT 8 RUN 20R 97Z RPM TAXI XDUCEERS 5.2.7
M= 503 LLTP= 51.851 LLT0= 6.368 LLTR= 3.303

N= 113



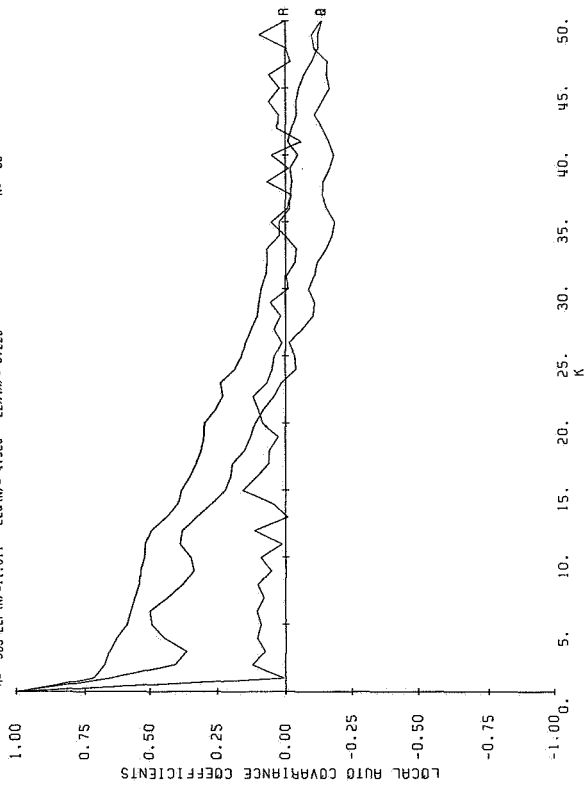
FLIGHT 8 RUN 20R 97% RPM TAXI XDCUSERS 5.2.7
M= 503 LLP (N)= 8.277 LLQ (N)= 4.317 LLR (N)= 1.480

N= 1



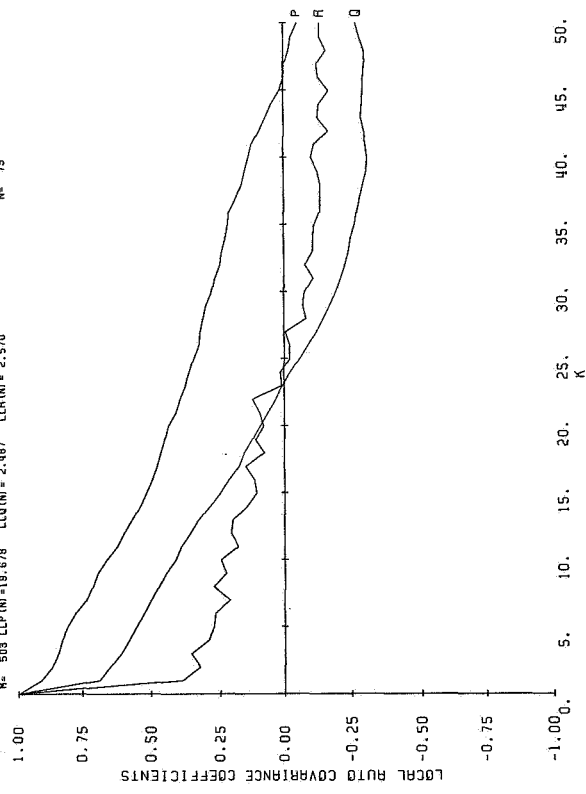
FLIGHT 8 RUN 20R 97% RPM TAXI XDCUSERS 5.2.7
M= 503 LLP (N)= 11.011 LLQ (N)= 4.528 LLR (N)= 3.228

N= 39



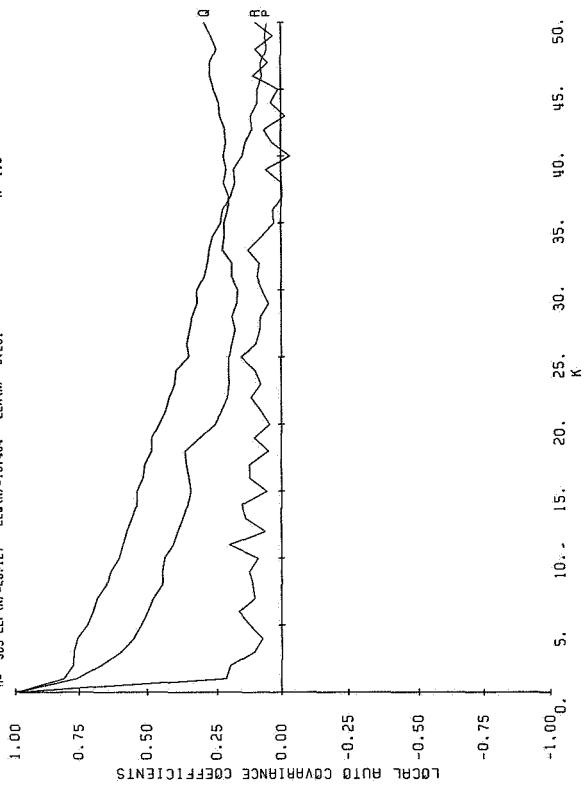
FLIGHT 8 RUN 20R 97% RPM TAXI XDCUSERS 5.2.7
M= 503 LLP (N)= 18.678 LLQ (N)= 2.487 LLR (N)= 2.570

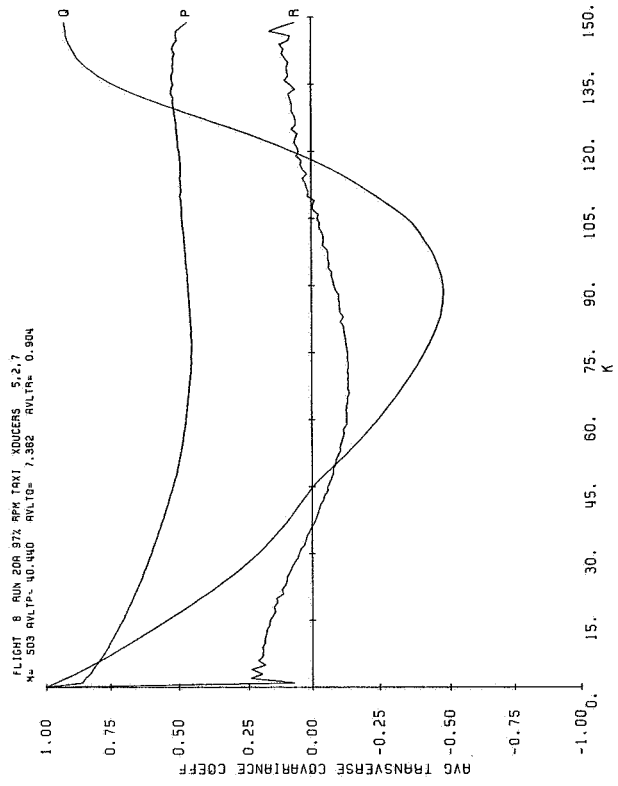
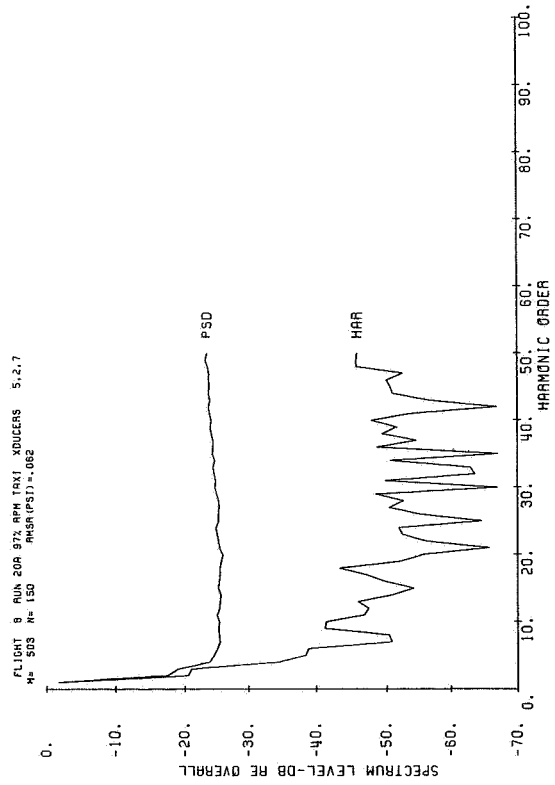
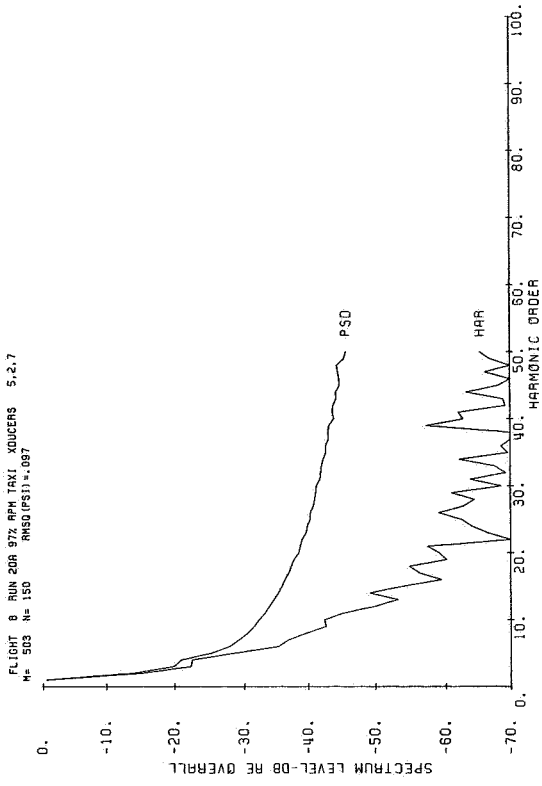
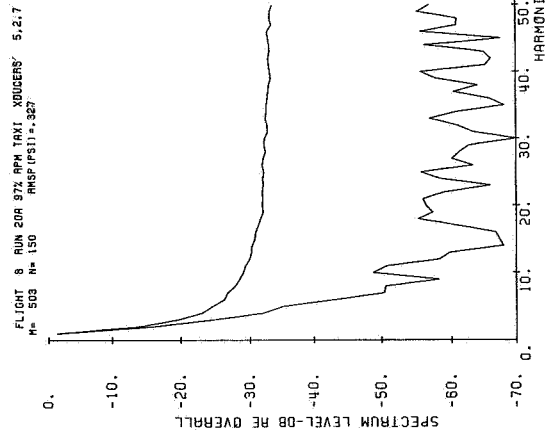
N= 75

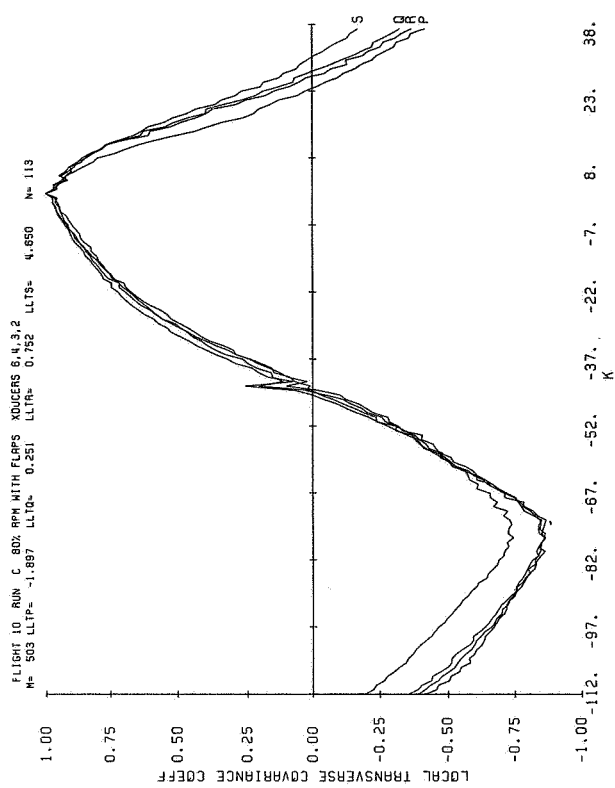
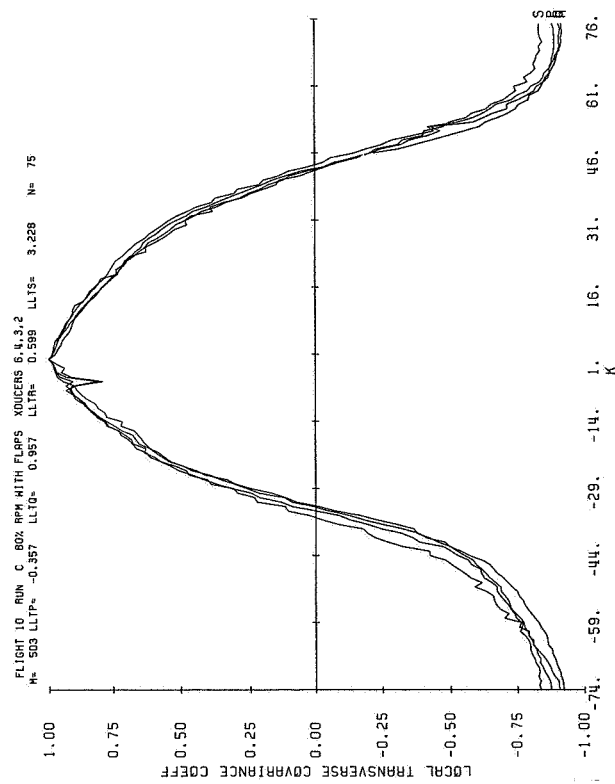
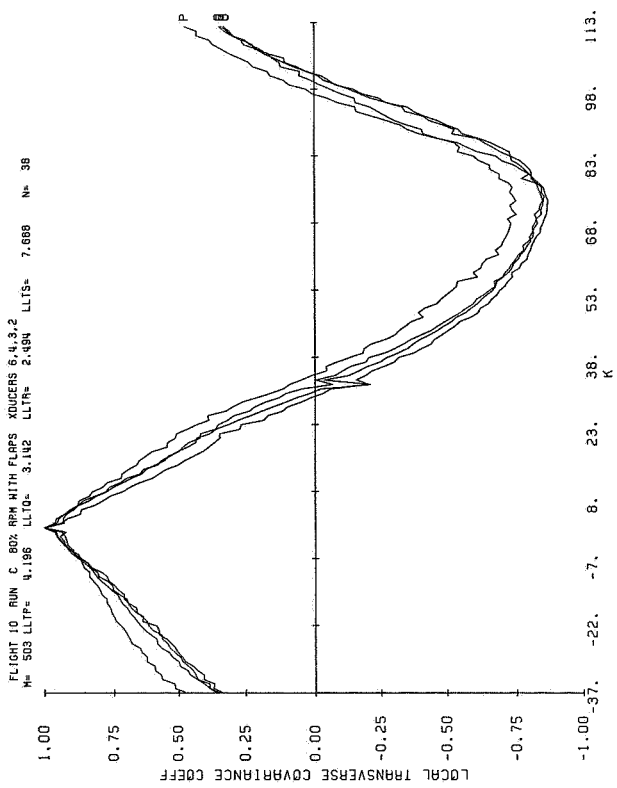
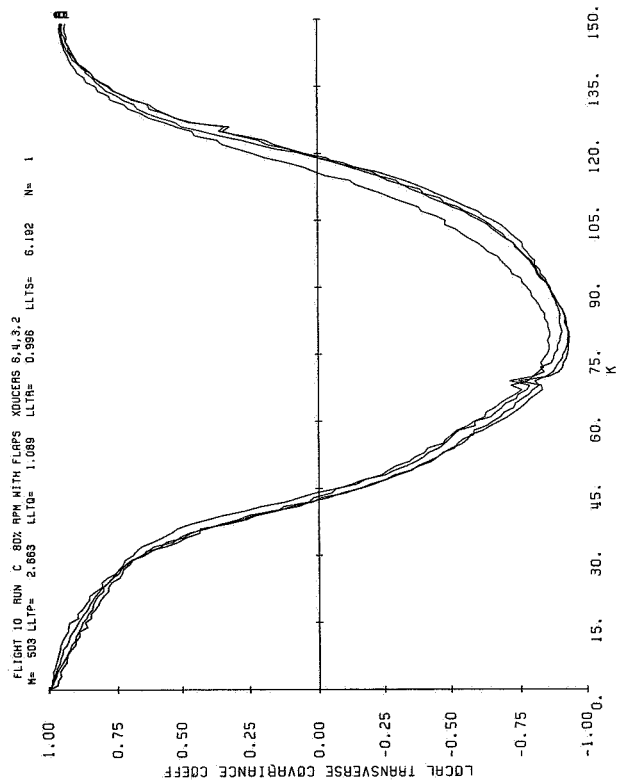


FLIGHT 8 RUN 20R 97% RPM TAXI XDCUSERS 5.2.7
M= 503 LLP (N)= 20.127 LLQ (N)= 18.484 LLR (N)= 5.281

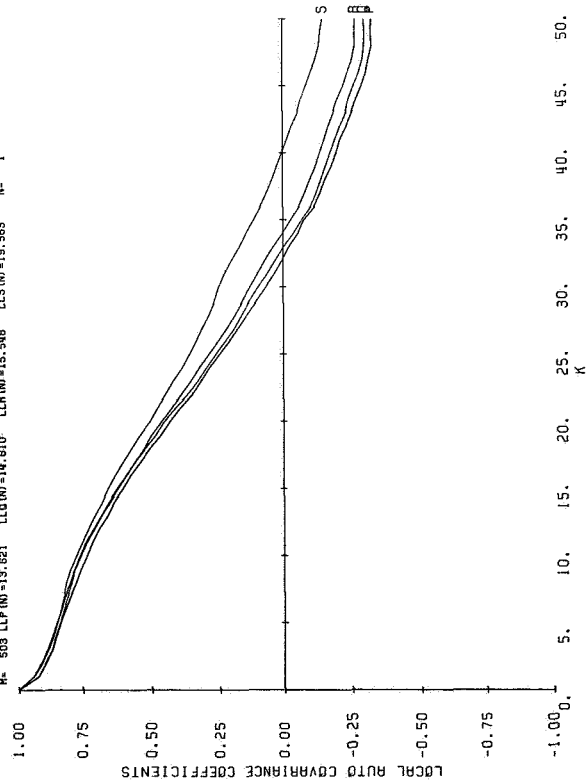
N= 113



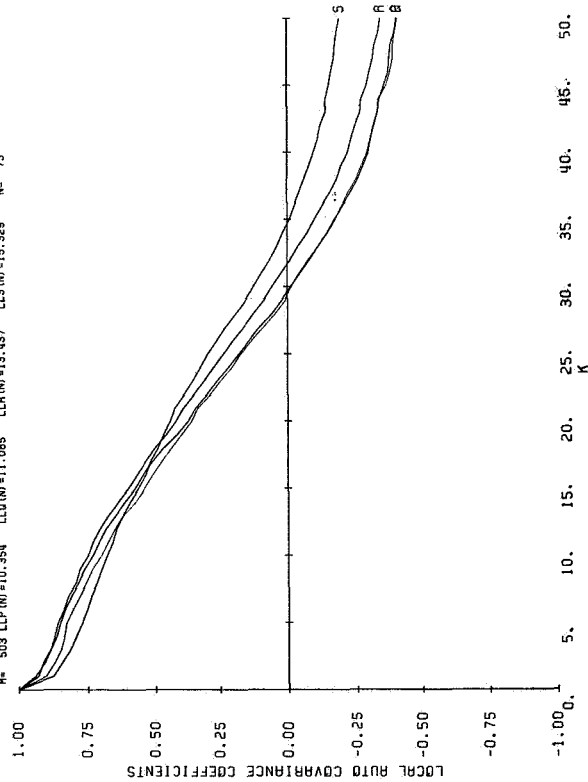




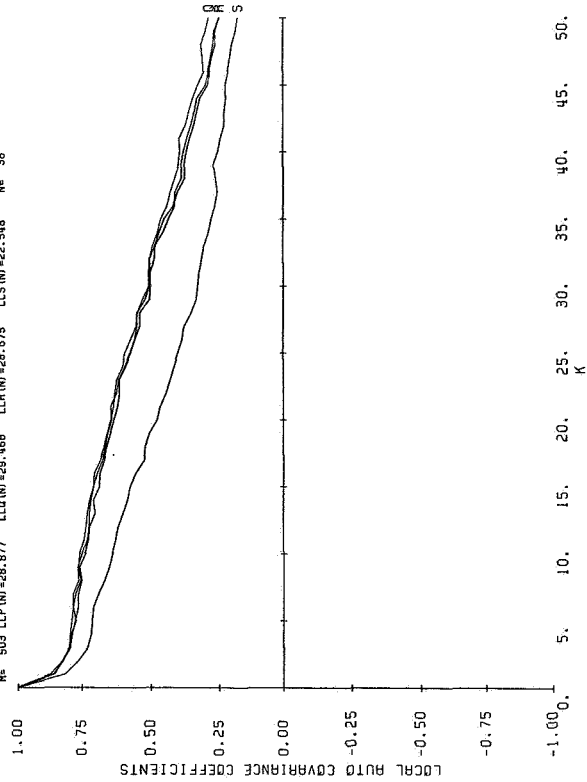
FLIGHT 10 RUN C 80% RPM WITH FLAPS XDCERS 6.4,3,2
M= 503 LLP (N)=15.621 LLQ (N)=14.610 LLS (N)=15.563 N= 1



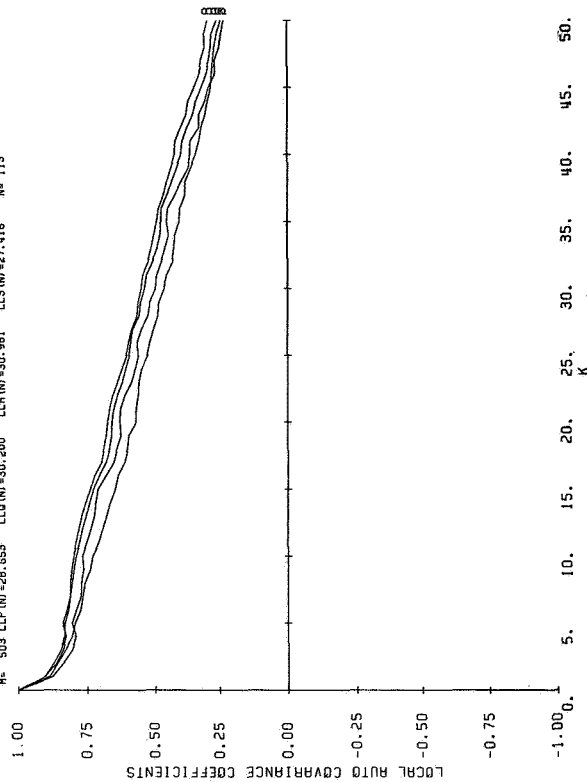
FLIGHT 10 RUN C 80% RPM WITH FLAPS XDCERS 6.4,3,2
M= 503 LLP (N)=10.354 LLS (N)=11.065 LLS (N)=15.323 N= 75

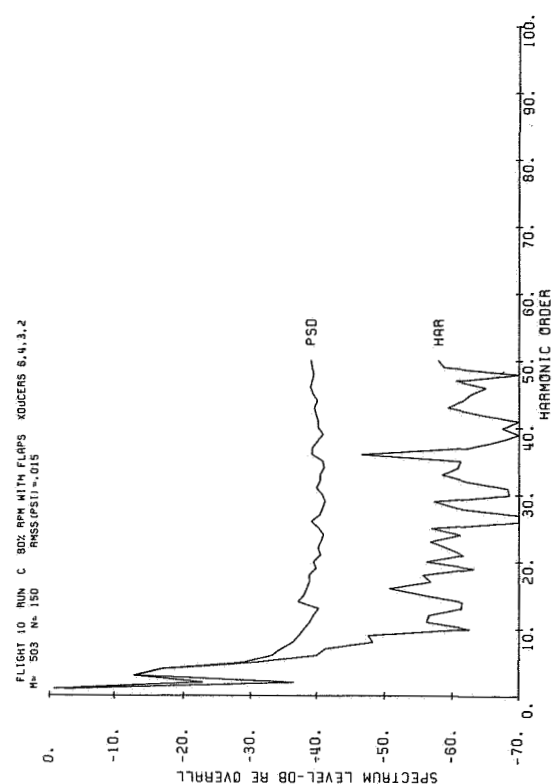
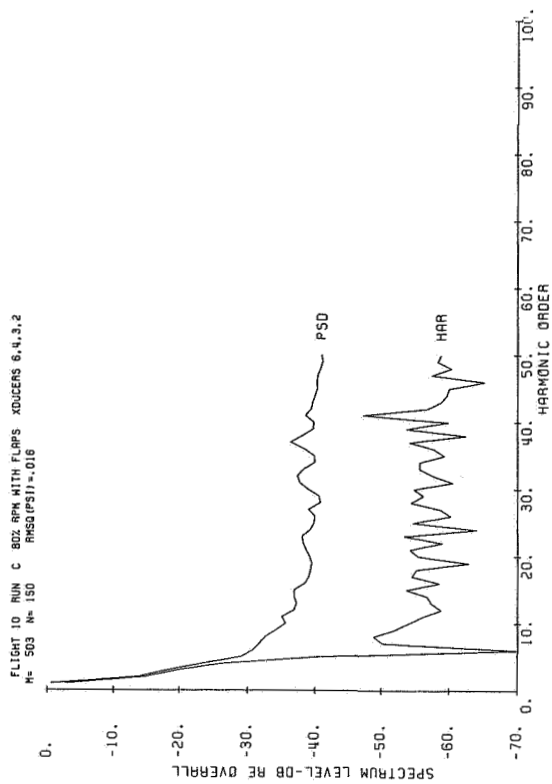
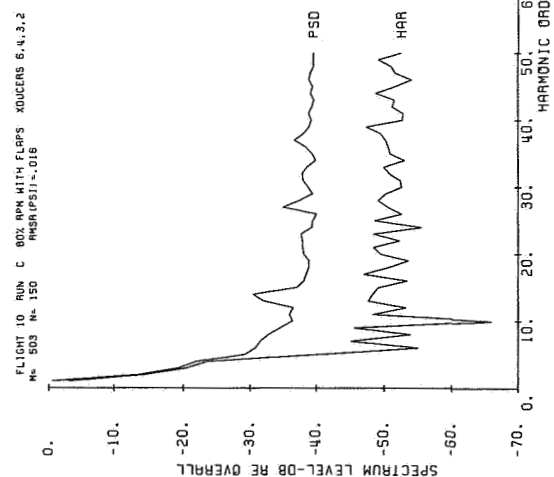
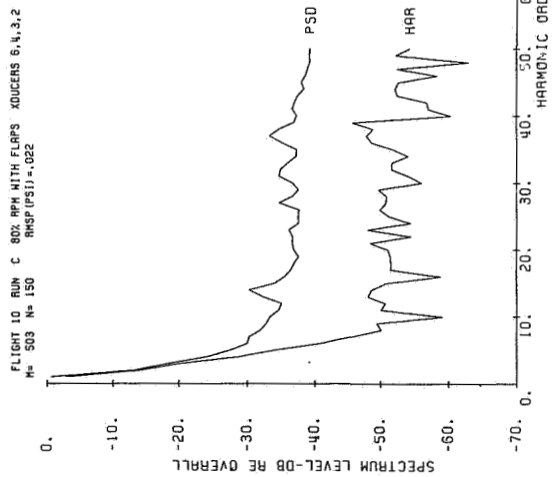


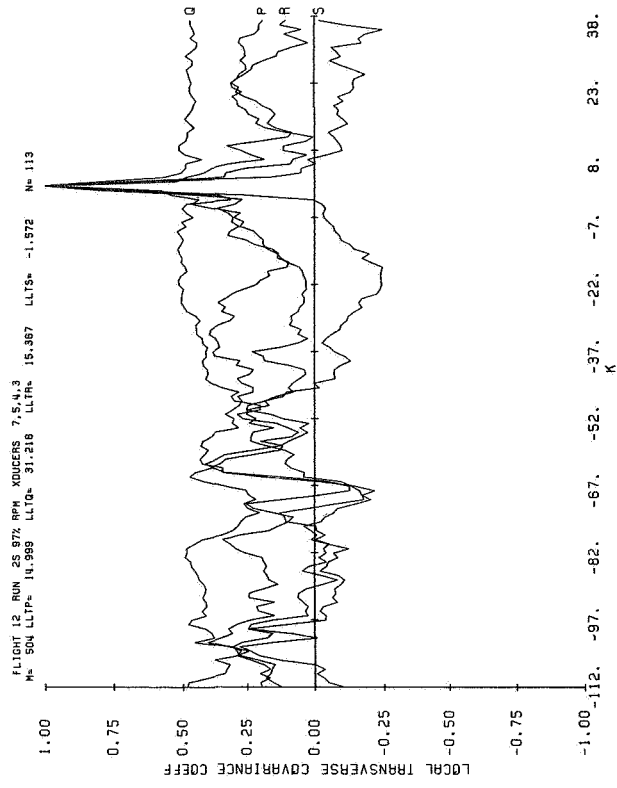
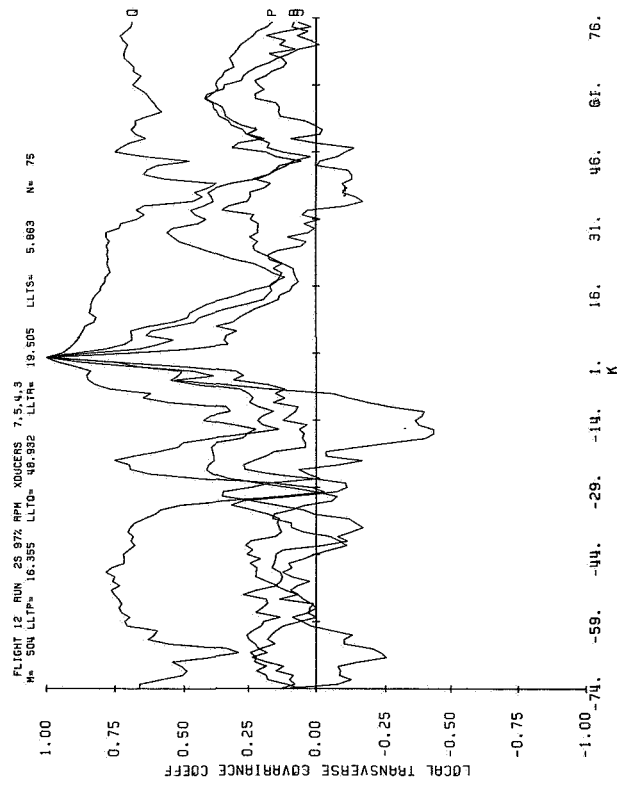
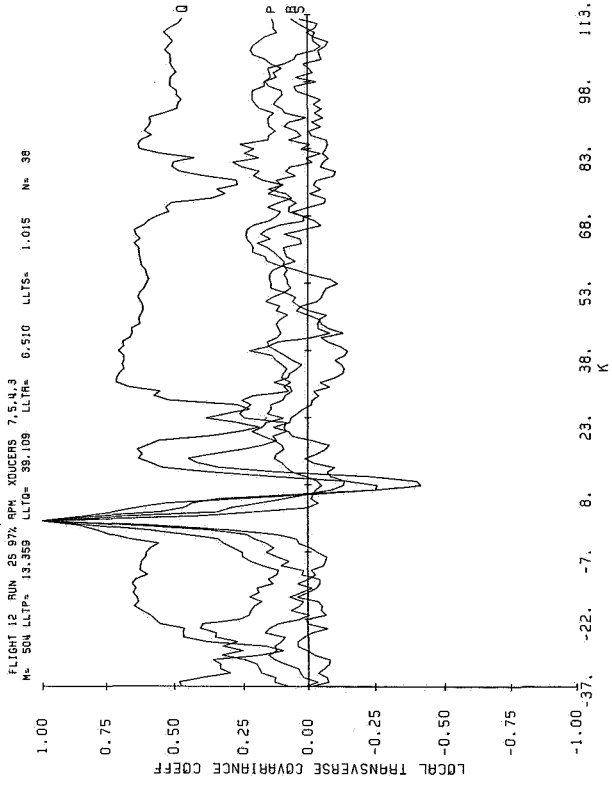
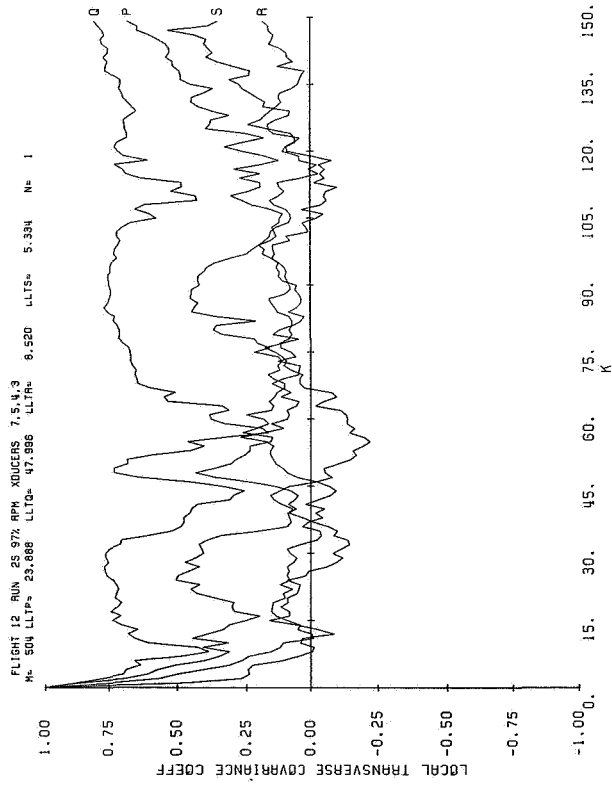
FLIGHT 10 RUN C 80% RPM WITH FLAPS XDCERS 6.4,3,2
M= 503 LLP (N)=26.877 LLQ (N)=23.468 LLS (N)=25.675 N= 38

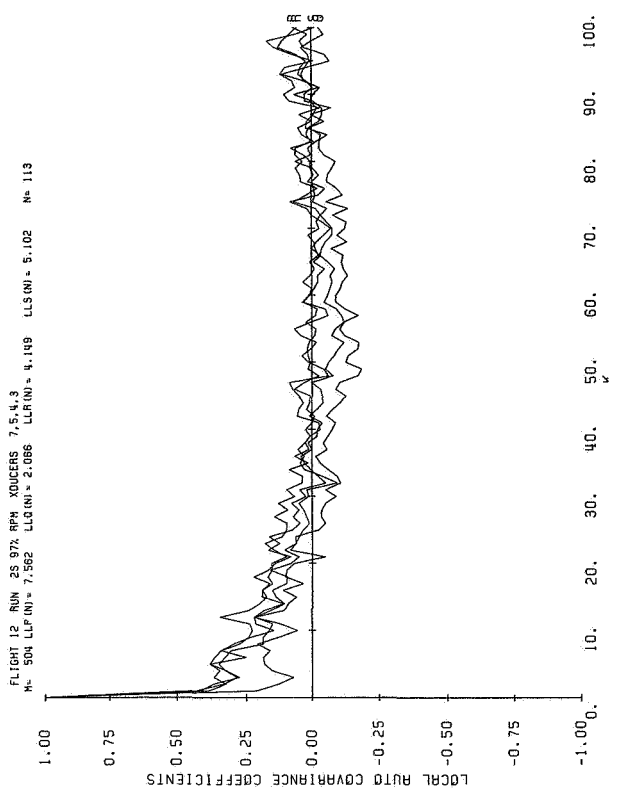
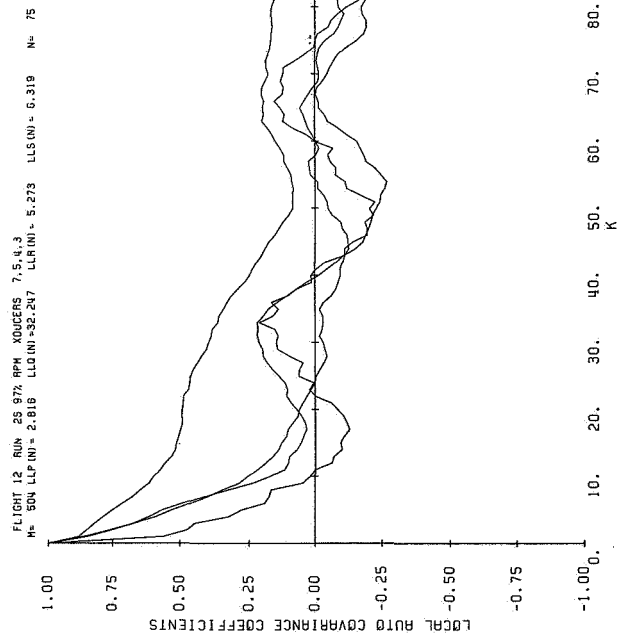
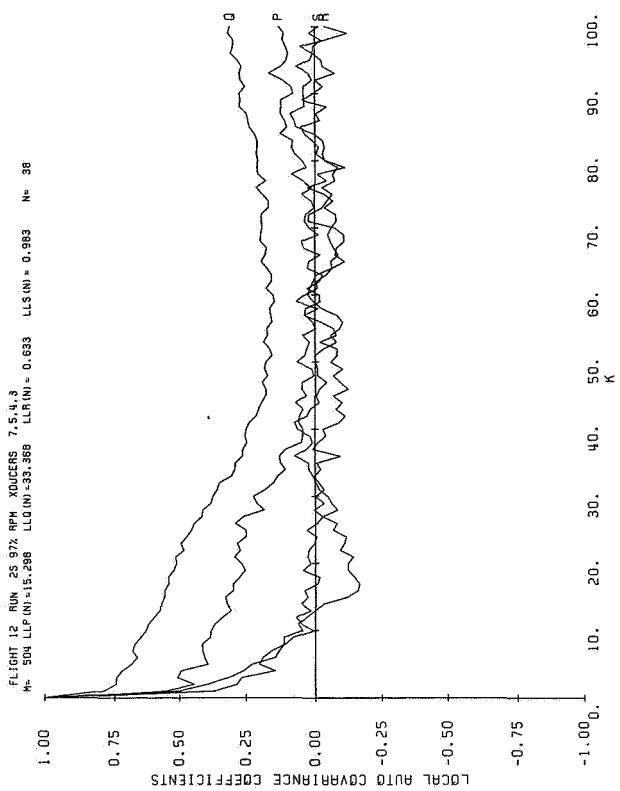
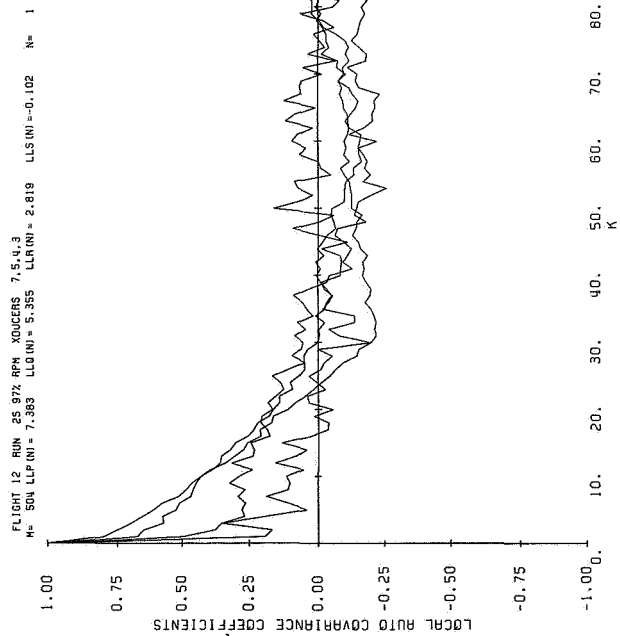


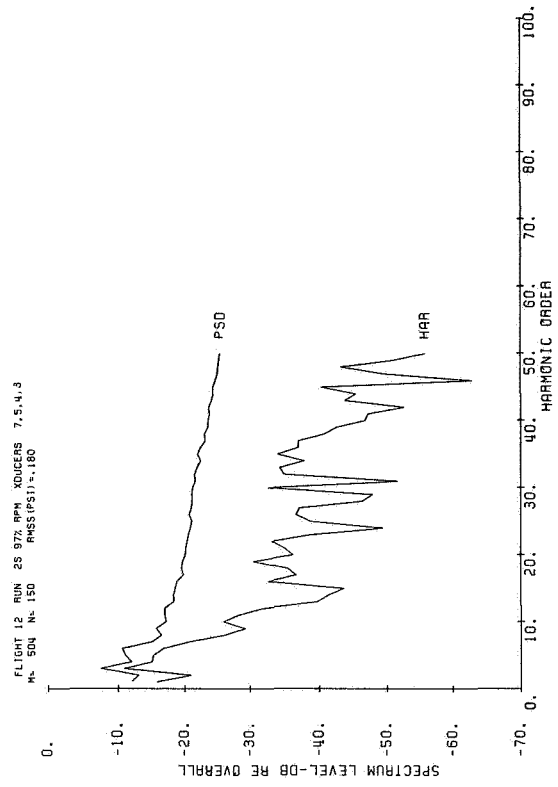
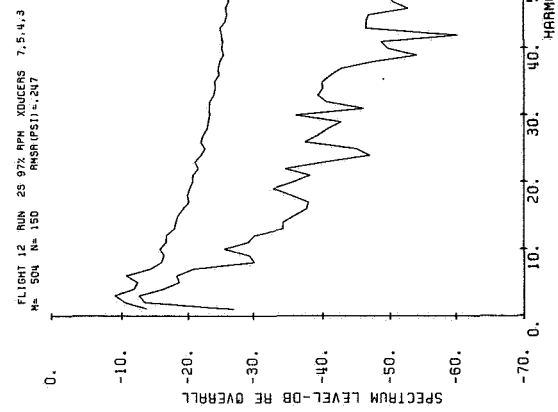
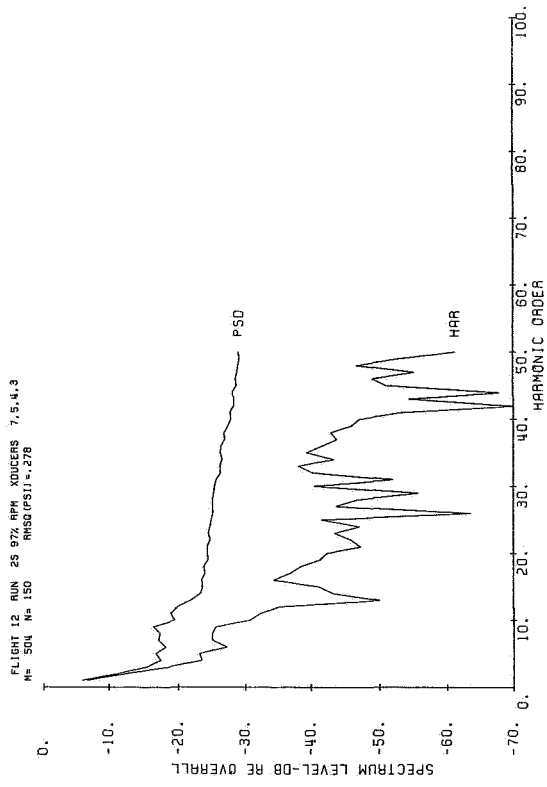
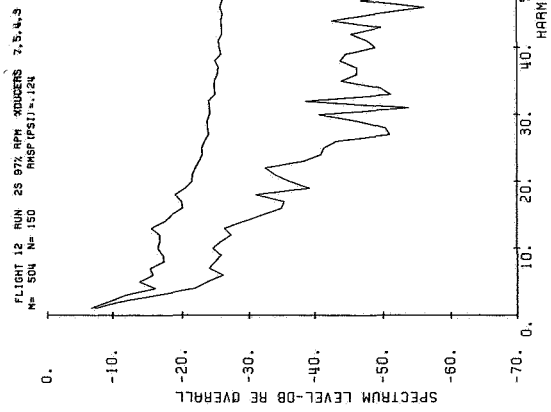
FLIGHT 10 RUN C 80% RPM WITH FLAPS XDCERS 6.4,3,2
M= 503 LLP (N)=28.653 LLQ (N)=30.200 LLS (N)=27.416 N= 113





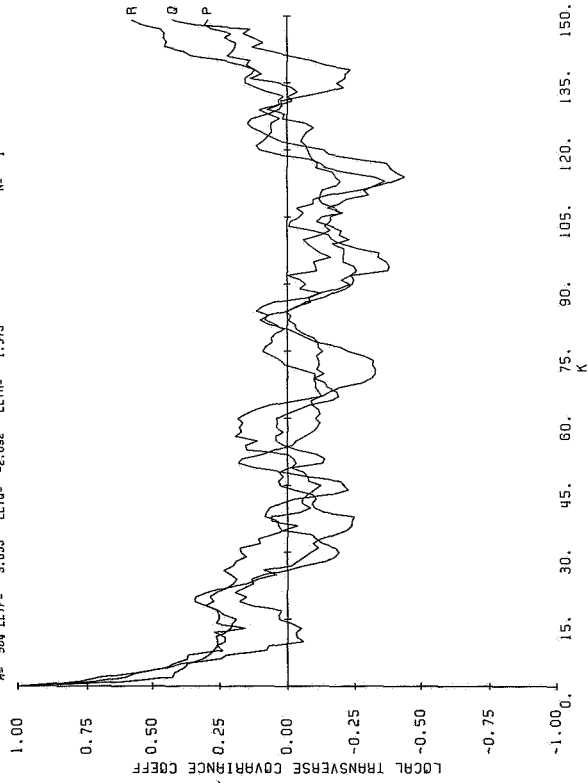






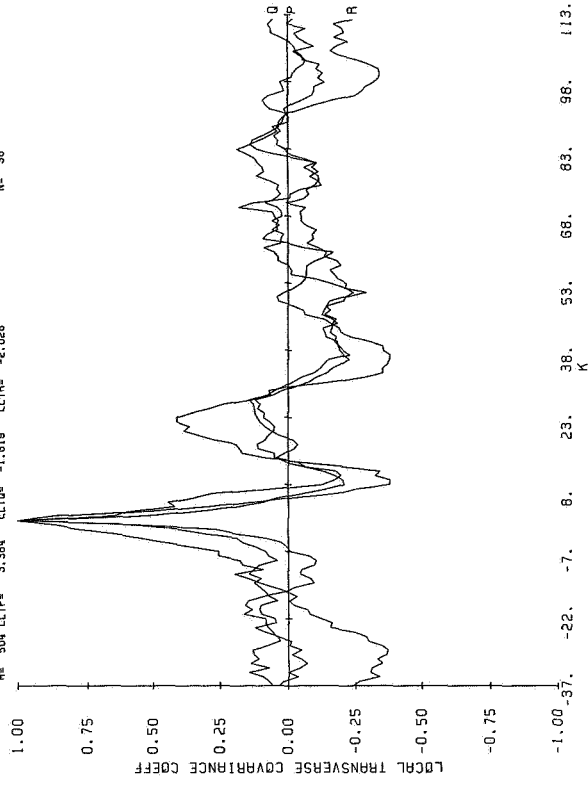
FLIGHT 12 RUN 55 80Z RPN XDUCCERS 5,4,3
M= 504 LLTP= 3.033 LLTD= -2.092 LLTR= 1.573

N= 1



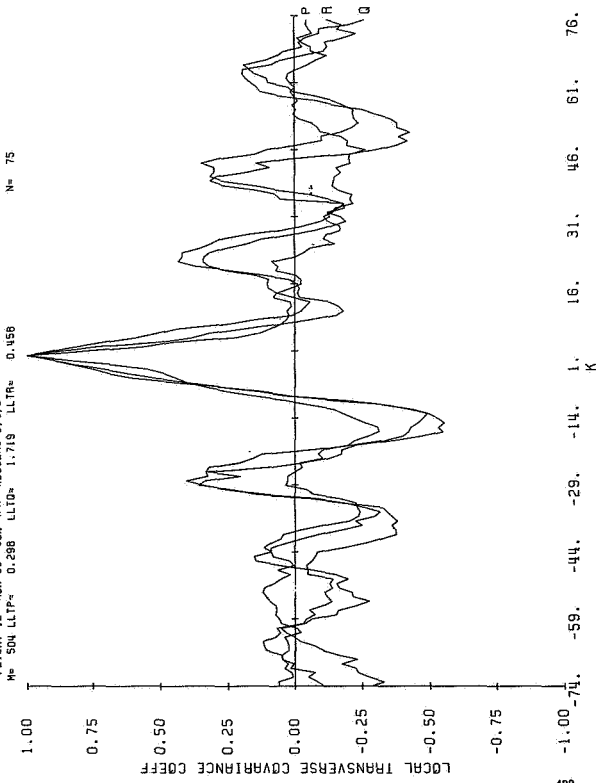
FLIGHT 12 RUN 55 80Z RPN XDUCCERS 5,4,3
M= 504 LLTP= 3.384 LLTD= -1.610 LLTR= -2.028

N= 38



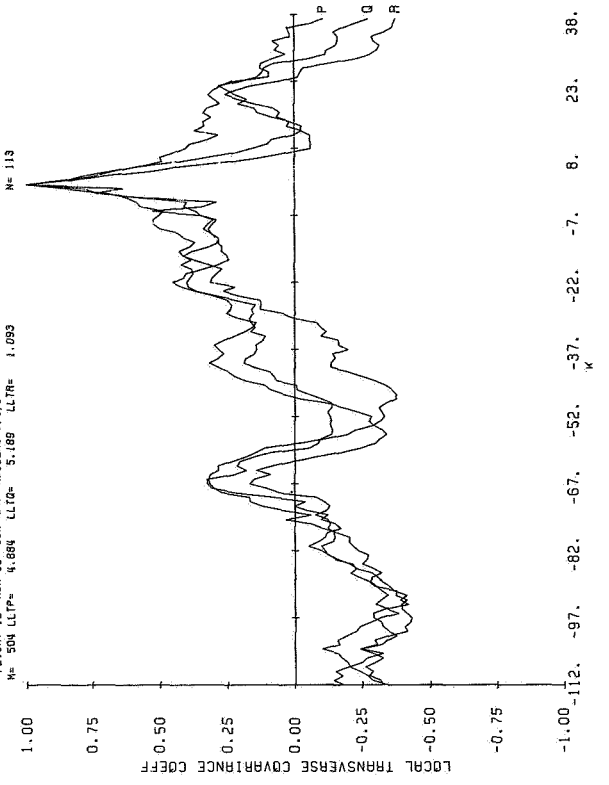
FLIGHT 12 RUN 55 80Z RPN XDUCCERS 5,4,3
M= 504 LLTP= 0.288 LLTD= 1.713 LLTR= 0.458

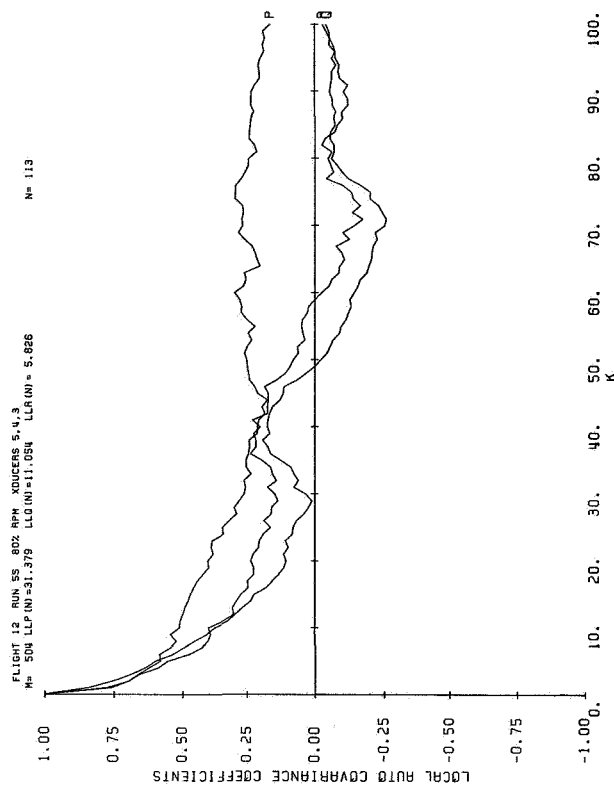
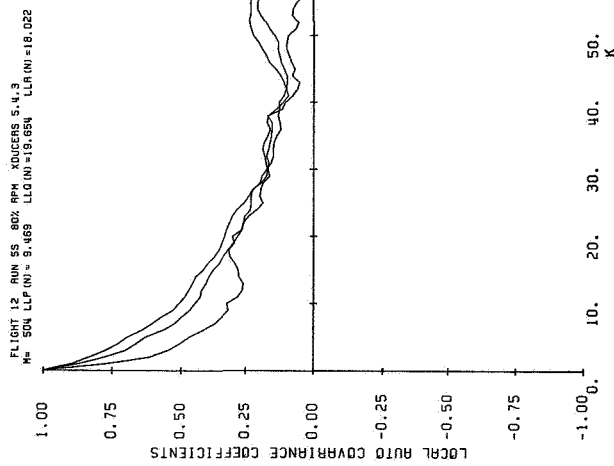
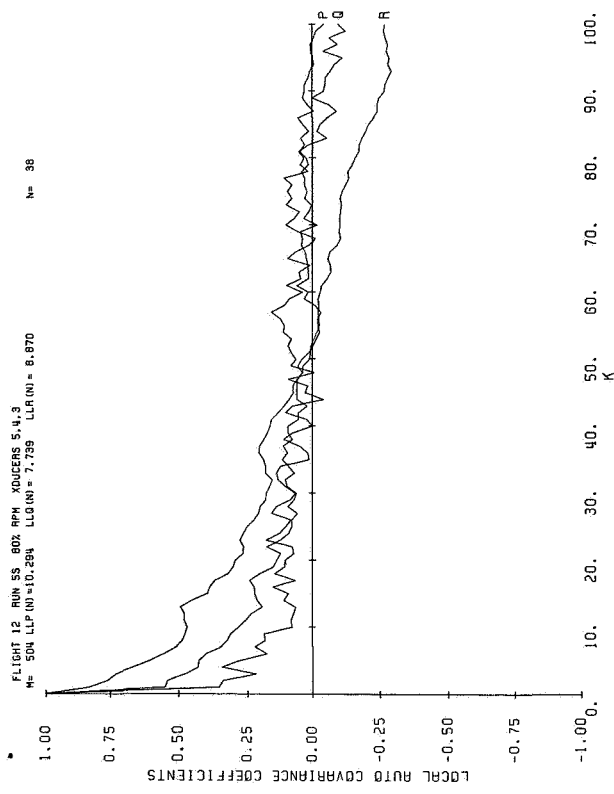
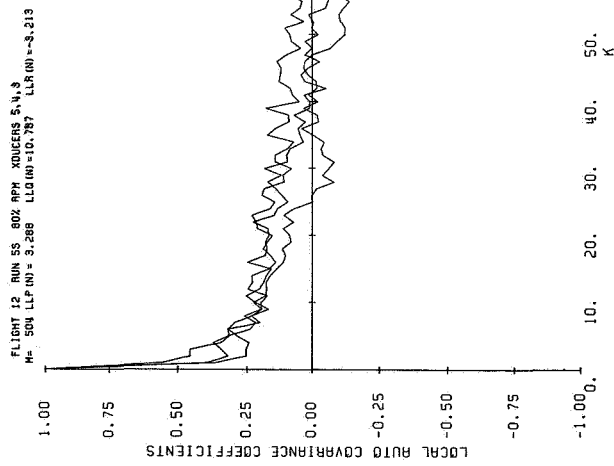
N= 75

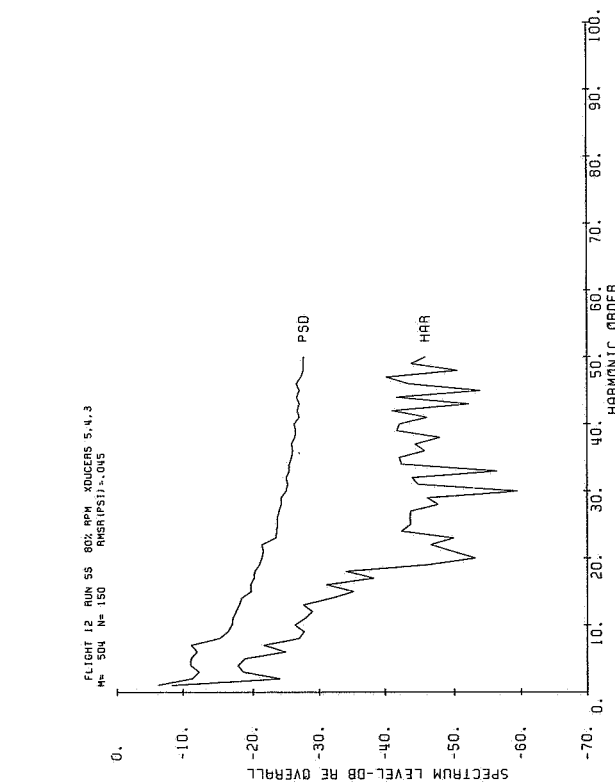
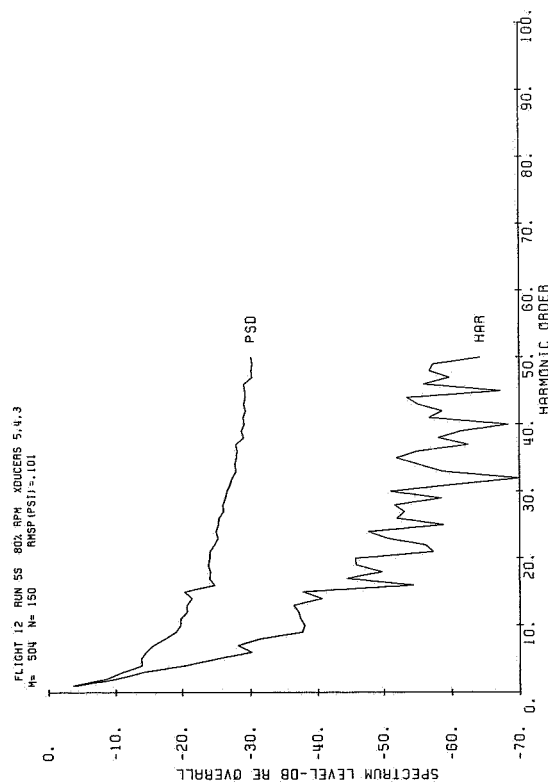
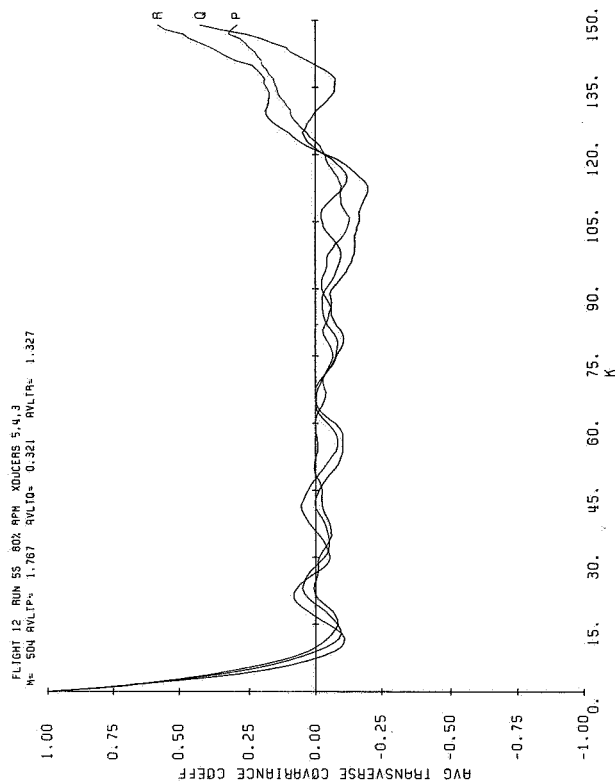
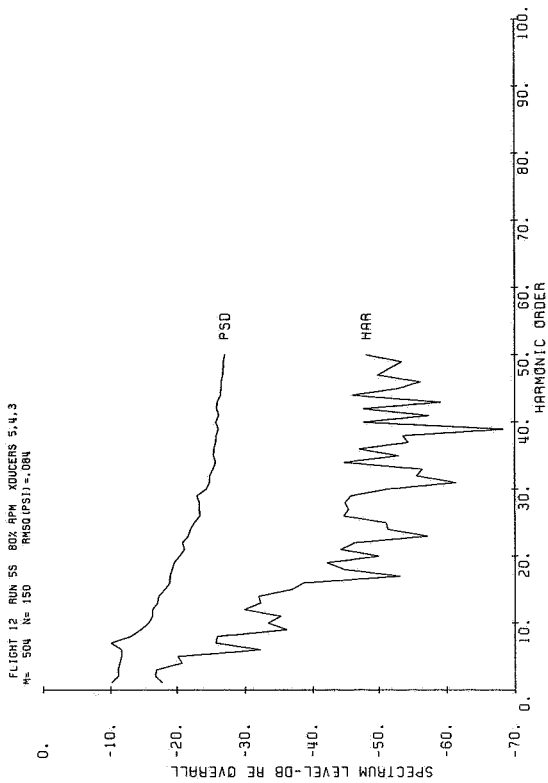


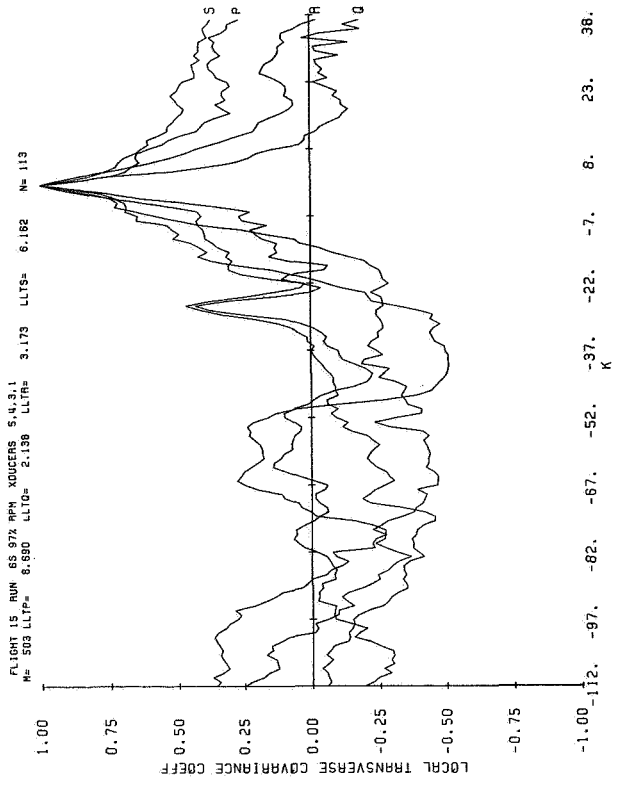
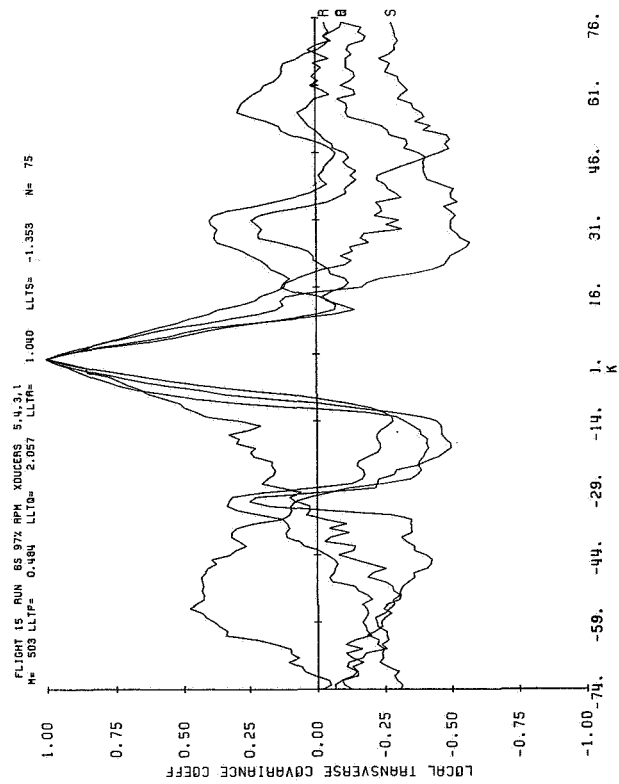
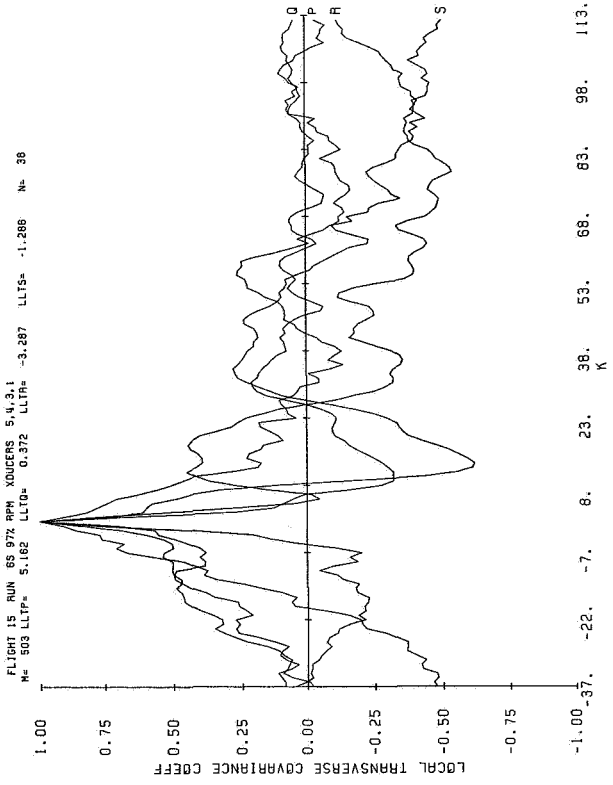
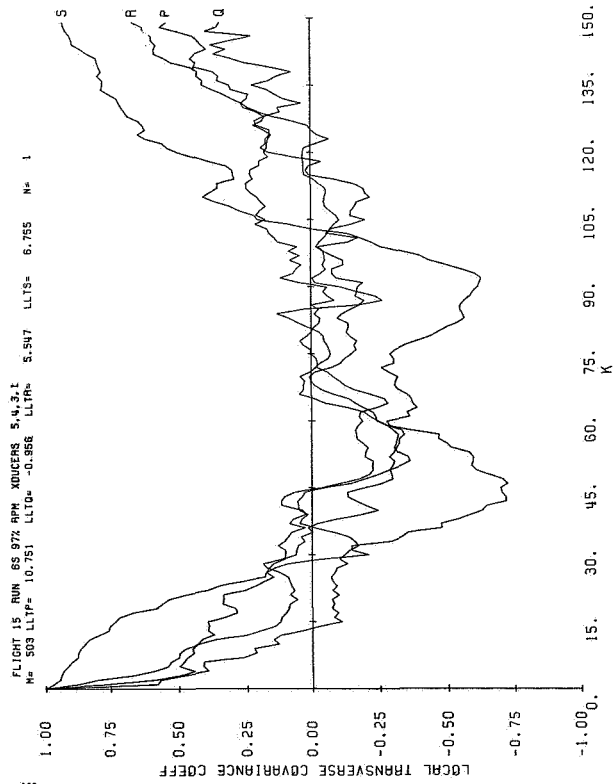
FLIGHT 12 RUN 55 80Z RPN XDUCCERS 5,4,3
M= 504 LLTP= 4.084 LLTD= 3.189 LLTR= 1.093

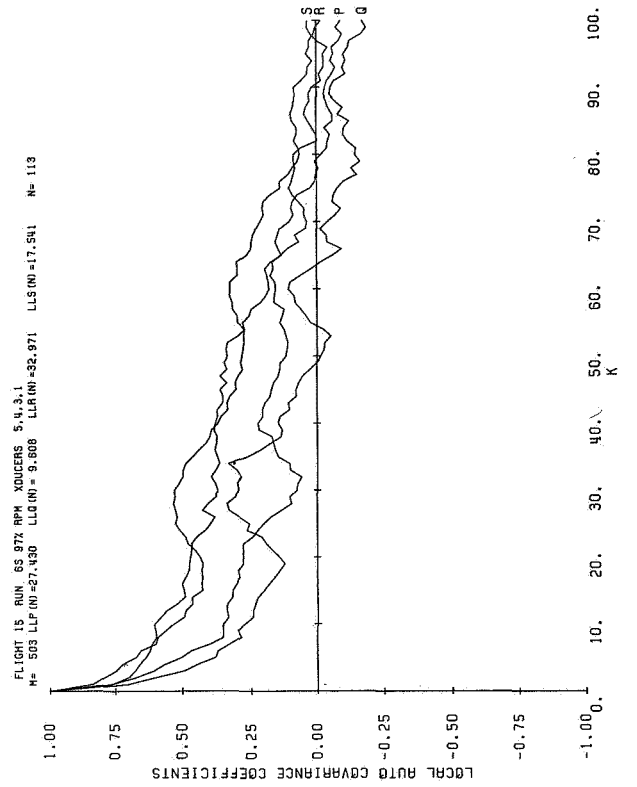
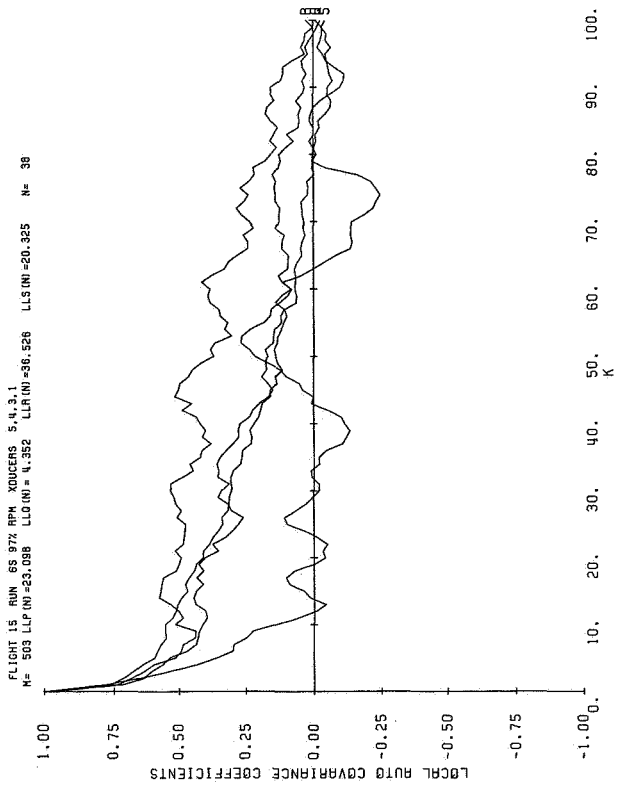
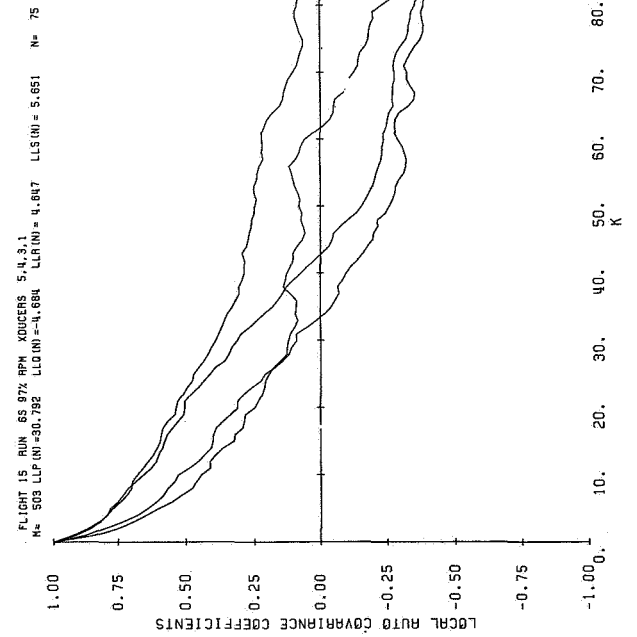
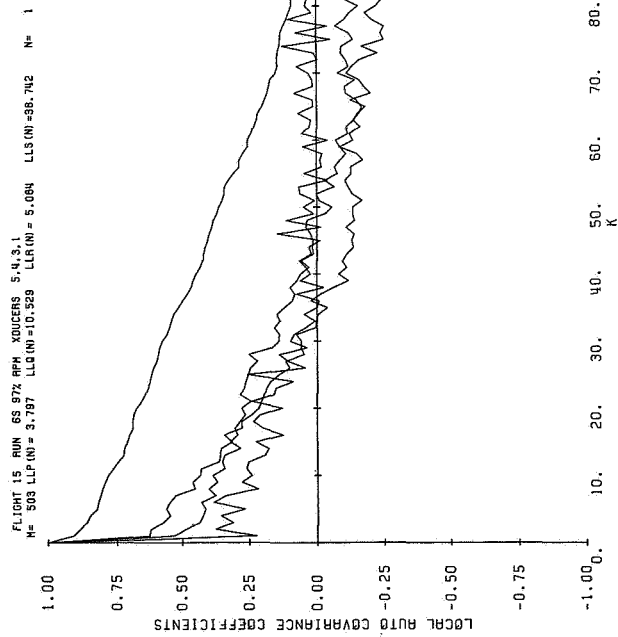
N= 113

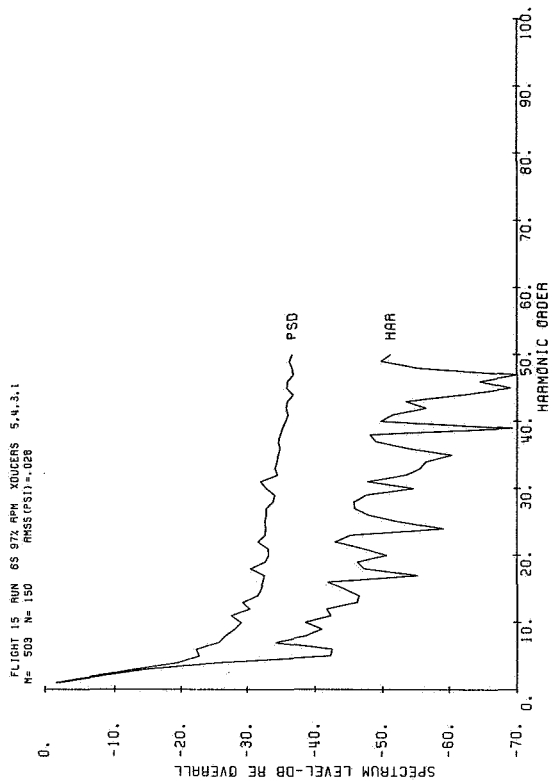
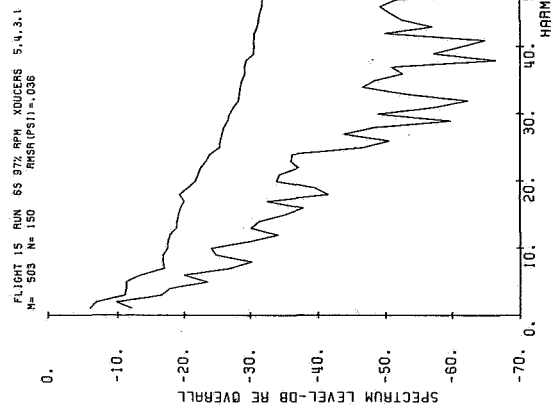
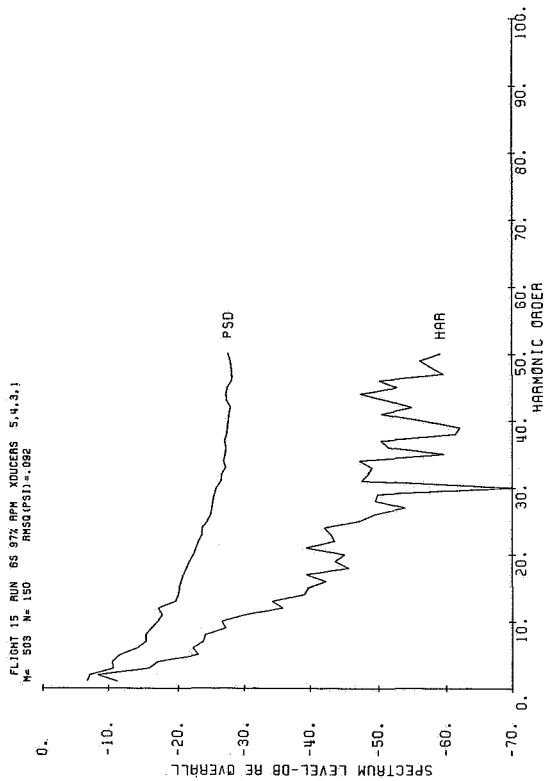
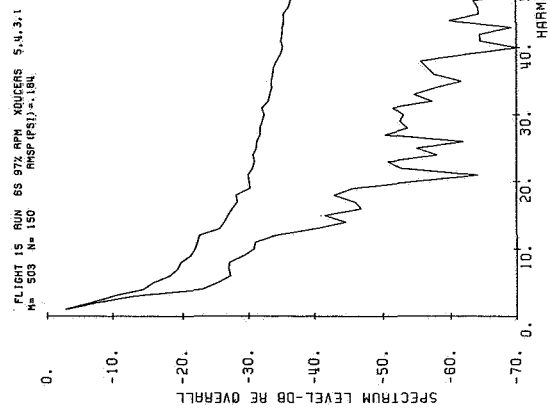












**APPENDIX D - FAR-FIELD NOISE 1/3 OCTAVE
BAND DATA TABULATIONS**

TWIN OTTER ACOUSTIC DATA - 1/3 O.B. ANALYSIS

	FLIGHT DATA			AIRCRAFT WING-TIP SYSTEM			FRONT MICROPHONE LOCATION			
1/3 O.B. FREQ. HZ	FLT 7 RN 1	FLT 7 RN 2	FLT 7 RN 3	FLT 7 RN 4	FLT 7 RN 5	FLT 7 RN 6	FLT 7 RN 7	FLT 7 RN 8	FLT 7 RN 9	FLT 7 RN 10
50	87.0	84.2	89.0	86.7	92.0	90.2	84.5	83.5	83.0	94.2
63	90.7	88.5	89.0	86.2	91.7	89.2	89.0	87.7	86.5	93.5
80	94.2	93.5	103.5	89.2	103.2	91.5	92.7	93.5	104.0	103.7
100	115.0	115.2	101.2	111.5	101.2	111.5	114.5	115.0	102.0	107.2
125	107.0	106.5	89.7	103.0	91.7	103.0	106.2	107.0	87.7	99.7
160	94.0	93.2	95.7	90.7	95.0	91.7	92.7	93.0	95.5	97.0
200	110.5	109.5	95.0	106.2	94.2	106.2	109.5	109.2	94.7	102.7
250	104.5	102.5	95.7	99.2	95.0	99.0	102.5	102.5	95.7	98.2
315	110.2	109.2	92.0	105.5	91.0	104.7	109.0	109.2	91.5	101.0
400	107.7	106.7	91.7	102.2	89.7	102.0	106.0	106.2	90.7	97.7
500	107.2	106.0	90.5	102.5	88.0	102.0	106.0	105.7	89.5	98.5
630	107.5	106.0	90.2	102.5	87.2	101.5	106.0	105.5	90.0	99.5
800	108.7	107.2	89.7	103.5	87.7	103.0	107.5	106.7	89.7	98.2
1000	108.0	105.5	88.2	101.0	86.2	100.2	106.2	105.2	88.7	97.5
1250	104.7	102.2	87.2	96.2	85.2	95.2	102.7	101.7	87.5	96.5
1600	103.2	100.5	86.2	95.5	84.7	94.2	100.7	99.0	86.7	94.5
2000	100.5	97.2	87.5	91.0	86.0	90.5	98.2	96.7	88.2	94.5
2500	94.5	92.0	84.5	85.7	83.0	85.2	92.2	91.5	85.2	93.7
3150	91.2	90.5	84.7	86.0	83.5	85.5	89.5	90.2	85.7	97.0
4000	90.2	89.0	83.0	84.7	81.5	83.5	88.2	88.5	84.7	95.0
5000	89.0	88.2	83.0	84.0	80.7	82.5	87.7	87.5	83.7	97.2
6300	89.5	87.7	83.0	84.5	81.2	83.2	88.5	87.5	84.0	101.0
8000	91.7	88.0	84.2	85.7	82.5	84.5	90.0	87.5	86.2	96.2
10000	96.0	87.7	87.2	84.7	82.0	87.2	95.0	87.7	91.7	102.0
DB(A)	115.0	112.7	98.2	108.5	96.7	107.7	112.5	112.2	99.5	112.5
DB(L)	119.7	118.2	109.0	114.5	109.2	114.2	117.2	118.2	108.2	115.5

TWIN OTTER ACOUSTIC DATA - 1/3 O.B. ANALYSIS

	FLIGHT DATA		AIRCRAFT WING-TIP SYSTEM				FRONT MICROPHONE LOCATION			
1/3 O.B. FREQ. HZ	FLT 7 RN 11	FLT 7 RN 12	FLT 8 RN 16	FLT 8 RN 17	FLT 10 RN 18	FLT 10 RN 19	FLT 10 RN 20	FLT 16 RN 21	FLT 16 RN 22	FLT 16 RN 23
50	85.0	86.0	84.2	87.5	91.5	92.5	90.0	83.2	81.5	81.5
63	87.0	86.5	88.7	88.2	91.0	93.2	90.5	87.0	85.0	83.0
80	103.2	89.5	93.2	92.7	105.5	96.7	92.7	103.2	92.2	87.2
100	100.5	111.5	112.2	110.7	105.5	114.7	116.0	101.5	111.2	111.5
125	87.7	103.0	93.7	93.5	92.0	97.0	107.0	86.7	92.5	101.7
160	95.7	90.5	90.0	91.0	97.7	94.2	95.0	95.7	89.2	88.0
200	94.2	106.2	103.7	102.7	98.2	106.5	108.7	94.7	104.0	105.2
250	95.5	98.7	92.2	92.0	99.0	95.2	101.7	95.2	92.0	97.0
315	91.5	105.2	100.5	99.0	94.2	101.7	109.0	89.5	100.7	103.2
400	90.2	102.2	98.5	97.5	92.7	99.0	102.0	88.7	99.0	102.0
500	88.7	101.7	95.7	95.0	90.5	98.0	104.7	86.2	96.0	102.2
630	87.2	101.5	92.5	90.7	89.7	94.5	105.5	85.5	92.2	101.5
800	86.5	103.2	91.2	89.0	89.0	92.0	106.0	86.7	90.7	101.2
1000	85.5	101.0	89.0	86.7	88.2	90.2	103.7	86.0	88.0	97.0
1250	84.7	95.7	87.5	84.5	88.5	89.0	97.5	86.0	86.2	94.7
1600	84.5	94.7	86.5	84.0	87.5	88.5	97.7	85.0	85.5	91.5
2000	85.5	91.7	89.2	86.5	89.7	90.0	94.0	86.7	88.0	88.7
2500	82.5	85.0	86.5	83.2	87.7	87.5	90.2	84.0	84.7	83.5
3150	83.7	85.7	87.0	84.5	88.7	89.2	90.2	84.5	85.2	84.0
4000	82.2	83.2	85.2	82.7	87.0	86.5	87.7	83.7	83.5	82.5
5000	82.0	83.2	84.5	81.5	85.2	84.7	86.7	82.7	82.5	82.5
6300	83.7	84.5	84.2	82.7	84.7	85.2	86.7	82.7	82.7	82.7
8000	89.2	90.7	86.0	84.2	87.7	88.2	88.5	84.2	83.5	84.2
10000	96.0	94.2	87.7	85.0	86.0	85.2	87.2	83.5	83.7	84.2
DB(A)	98.5	108.7	101.5	100.2	100.5	103.2	111.7	97.2	101.0	107.0
DB(L)	108.5	114.5	112.5	111.5	111.2	115.2	118.0	108.0	111.5	113.5

TWIN OTTER ACOUSTIC DATA - 1/3 O.B. ANALYSIS

	FLIGHT DATA		AIRCRAFT WING-TIP SYSTEM	FRONT MICROPHONE LOCATION
1/3 O.B. FREQ. HZ	FLT 16 RN 24	FLT 16 RN 25	FLT 16 RN 26	
50	84.0	82.5	79.7	
63	87.0	89.5	83.5	
80	102.2	92.5	88.0	
100	99.7	111.2	112.2	
125	88.5	93.0	103.0	
160	95.2	90.0	89.0	
200	94.0	104.0	106.5	
250	95.0	92.7	98.5	
315	89.2	101.5	104.2	
400	88.5	99.5	102.5	
500	87.5	96.7	103.2	
630	88.0	93.0	102.7	
800	88.7	92.5	102.7	
1000	87.7	90.0	99.0	
1250	87.5	88.5	96.7	
1600	87.0	87.7	93.7	
2000	88.5	89.2	91.2	
2500	85.5	87.0	86.0	
3150	85.7	86.7	86.2	
4000	84.5	85.2	84.2	
5000	84.0	84.7	83.7	
6300	83.7	84.7	83.5	
8000	86.0	87.0	86.0	
10000	92.0	90.0	87.2	
DB(A)	98.2	102.5	108.0	
DB(L)	107.2	112.0	114.5	

TWIN OTTER ACOUSTIC DATA - 1/3 O.B. ANALYSIS

1/3 O.B. FREQ. HZ	FLIGHT DATA		AIRCRAFT WING-TIP SYSTEM				AFT MICROPHONE LOCATION			
	FLT 7 RN 1	FLT 7 RN 2	FLT 7 RN 3	FLT 7 RN 4	FLT 7 RN 5	FLT 7 RN 6	FLT 7 RN 7	FLT 7 RN 8	FLT 7 RN 9	FLT 7 RN 10
50	88.0	88.0	93.2	89.5	92.7	93.2	87.7	87.7	88.0	92.0
63	95.2	91.7	93.0	91.0	92.7	92.7	93.0	91.2	89.7	93.7
80	99.0	96.7	106.5	94.2	106.2	95.7	96.7	97.2	107.5	107.0
100	117.7	119.5	104.5	115.7	104.5	116.5	117.5	119.2	105.7	110.5
125	110.5	110.7	92.0	106.7	92.0	108.0	109.2	111.0	90.0	102.2
160	100.2	99.0	99.2	96.5	98.0	96.5	99.2	99.0	100.0	103.7
200	113.5	115.5	98.5	109.5	96.7	110.5	113.5	115.2	98.7	105.2
250	107.5	107.7	96.2	102.2	95.0	102.7	106.2	108.5	96.0	100.2
315	107.5	109.7	92.5	105.0	90.5	105.2	107.7	109.0	91.7	100.5
400	103.0	104.0	91.7	98.5	89.5	98.7	103.0	103.5	91.2	97.0
500	101.7	103.0	92.0	97.5	87.7	98.0	101.2	102.2	91.0	97.7
630	100.7	100.7	92.5	95.0	87.2	95.0	99.7	100.7	91.7	96.2
800	99.0	98.7	91.2	94.2	87.5	94.2	99.0	98.7	90.2	98.0
1000	96.2	95.7	91.7	91.0	88.0	89.7	95.7	95.5	91.5	96.2
1250	96.2	97.0	92.0	90.2	89.7	90.7	95.5	96.0	92.5	93.7
1600	99.0	95.7	91.0	90.2	89.5	90.2	96.5	95.5	92.0	94.7
2000	95.7	94.0	89.5	88.2	88.0	88.5	94.5	93.5	89.7	97.2
2500	94.0	92.5	87.0	86.2	84.7	85.7	92.7	91.5	87.5	99.0
3150	95.7	92.0	85.7	87.7	84.0	86.2	94.5	91.0	86.2	93.0
4000	94.0	90.5	85.7	86.2	82.5	84.2	92.0	89.7	85.5	95.7
5000	92.7	90.0	84.2	85.7	81.0	83.0	91.2	89.0	85.0	96.7
6300	93.5	89.2	84.5	87.5	82.0	84.7	91.0	89.0	85.0	104.0
8000	93.0	89.0	84.2	87.5	83.0	85.7	91.2	88.2	86.0	101.2
10000	96.2	89.0	85.0	88.0	84.2	88.0	95.0	88.5	91.0	99.2
DB(A)	110.5	110.5	100.5	105.5	98.7	105.7	109.5	111.0	101.2	108.5
DB(L)	120.2	121.0	111.7	117.0	111.5	117.7	118.7	121.0	111.5	116.5

TWIN OTTER ACOUSTIC DATA - 1/3 O.B. ANALYSIS

	FLIGHT DATA		AIRCRAFT WING-TIP SYSTEM				AFT MICROPHONE LOCATION			
1/3 O.B. FREQ. HZ	FLT 7 RN 11	FLT 7 RN 12	FLT 8 RN 16	FLT 8 RN 17	FLT 10 RN 18	FLT 10 RN 19	FLT 10 RN 20	FLT 16 RN 21	FLT 16 RN 22	FLT 16 RN 23
50	88.0	88.7	89.0	88.2	95.0	96.5	95.0	83.7	81.5	87.2
63	89.7	90.7	92.7	92.7	95.5	97.0	94.5	87.7	91.2	89.2
80	107.5	94.5	95.7	95.5	108.7	98.5	96.7	107.5	95.0	94.5
100	105.0	116.2	114.5	113.7	109.0	114.5	117.7	105.5	114.2	115.0
125	90.2	107.5	96.2	95.5	96.0	100.2	109.5	88.5	96.7	105.0
160	99.7	96.0	93.2	92.7	103.7	99.2	101.2	99.5	92.0	96.2
200	98.0	110.0	107.0	106.5	104.0	111.5	115.0	98.5	107.5	110.2
250	95.7	102.7	94.0	93.7	100.5	98.0	107.0	96.2	94.2	101.5
315	90.7	105.2	101.5	100.7	94.2	105.5	107.0	89.0	101.7	104.2
400	90.2	98.7	95.5	94.2	93.2	97.0	102.0	91.0	96.2	105.0
500	89.5	97.0	92.5	91.2	94.0	100.0	103.2	95.5	94.5	97.7
630	89.0	94.5	91.7	89.0	92.7	97.2	101.0	90.0	90.2	95.7
800	89.5	93.0	90.7	89.5	91.0	92.5	98.0	89.2	88.7	95.2
1000	89.5	88.7	91.5	88.7	91.5	92.0	95.0	88.2	87.7	92.0
1250	89.5	89.5	92.5	90.0	93.2	94.0	96.7	90.5	90.7	90.2
1600	89.5	89.7	93.0	90.5	94.0	95.0	96.5	91.5	92.2	91.5
2000	87.7	87.7	90.7	88.2	93.2	92.5	94.0	88.5	88.5	88.0
2500	85.0	85.2	87.5	84.7	91.2	91.2	92.5	85.2	85.0	84.7
3150	84.0	85.7	87.5	84.5	91.7	91.2	92.5	84.7	84.7	85.7
4000	83.0	84.5	85.7	82.7	90.7	90.0	91.2	84.2	84.0	84.5
5000	82.2	83.2	85.0	82.2	89.0	88.5	90.7	83.0	83.0	83.5
6300	83.5	86.0	84.7	83.0	88.0	88.5	92.0	83.7	83.5	85.2
8000	87.7	90.5	85.2	84.7	88.7	89.2	91.7	84.0	84.2	86.5
10000	94.7	92.7	86.5	85.7	88.0	88.0	91.5	85.0	84.7	87.2
DB(A)	99.7	105.5	103.0	101.5	103.5	106.0	109.7	99.7	102.5	106.2
DB(L)	111.2	117.0	115.0	114.0	115.0	117.0	120.2	111.2	114.2	116.5

TWIN OTTER ACOUSTIC DATA - 1/3 O.B. ANALYSIS

	FLIGHT DATA		AIRCRAFT WING-TIP SYSTEM	AFT MICROPHONE LOCATION
1/3 O.B. FREQ. HZ	FLT 16 RN 24	FLT 16 RN 25	FLT 16 RN 26	
50	89.7	84.2	80.5	
63	89.5	92.5	87.5	
80	106.5	96.0	92.7	
100	104.0	115.0	115.7	
125	91.0	96.7	106.2	
160	100.2	94.7	96.2	
200	101.0	108.5	110.2	
250	96.7	95.7	102.5	
315	92.2	102.2	104.7	
400	102.2	102.7	100.0	
500	100.7	99.7	102.0	
630	100.0	98.7	99.5	
800	95.7	95.0	95.2	
1000	94.2	93.5	93.2	
1250	94.2	94.2	93.5	
1600	94.2	95.0	94.0	
2000	91.2	91.2	91.0	
2500	88.2	87.7	87.0	
3150	87.7	87.2	87.2	
4000	86.7	86.7	86.2	
5000	85.5	85.5	85.2	
6300	86.0	86.0	86.5	
8000	85.7	86.0	86.2	
10000	86.0	86.5	87.0	
DB(A)	105.5	105.5	107.0	
DB(L)	111.7	115.5	117.0	

TWIN OTTER ACOUSTIC DATA - 1/3 O.B. ANALYSIS

	FLYOVER DATA		GROUND-BASED SYSTEM				MICROPHONE AT GROUND LEVEL				
1/3 O.B. FREQ. HZ	FLT 7 RN 1	FLT 7 RN 2	FLT 7 RN 3	FLT 7 RN 4	FLT 7 RN 5	FLT 7 RN 7	FLT 7 RN 8	FLT 7 RN 9	FLT 7 RN 10	FLT 7 RN 11	
50	80.5	70.2	70.0	67.0	74.2	64.0	69.0	60.5	71.0	61.0	
63	83.7	77.7	73.2	76.0	75.5	68.7	66.0	62.2	69.2	59.7	
80	84.5	79.2	80.7	78.0	95.5	69.2	68.2	76.5	67.5	75.2	
100	100.0	94.5	87.5	96.0	90.5	77.5	83.5	72.0	79.7	74.0	
125	91.0	93.0	71.2	85.7	71.7	83.0	76.2	57.0	79.0	57.0	
160	81.0	78.7	76.7	76.7	84.7	66.0	65.7	68.2	62.7	70.2	
200	91.0	96.7	83.2	94.5	84.5	81.5	85.7	65.0	82.0	70.0	
250	92.0	96.2	81.7	88.0	85.5	86.7	79.5	69.0	82.0	72.0	
315	102.2	99.7	80.2	97.5	80.0	86.7	85.7	65.5	87.7	66.5	
400	99.0	97.0	77.0	93.0	77.2	83.2	85.2	62.7	83.7	66.0	
500	94.0	96.5	73.5	90.0	73.5	84.5	81.0	56.7	84.0	58.5	
630	95.0	95.5	73.7	91.0	73.0	84.5	81.2	57.2	83.2	55.2	
800	97.2	96.0	74.7	93.2	73.5	84.5	83.2	60.0	84.0	59.2	
1000	93.5	95.2	72.5	89.5	73.0	85.0	79.5	57.7	82.7	55.7	
1250	90.0	92.5	74.2	86.0	76.0	80.7	76.5	57.7	78.0	55.7	
1600	88.5	88.5	77.2	82.5	76.2	77.5	74.0	59.2	74.5	57.5	
2000	84.7	85.2	77.7	78.5	77.5	73.7	72.2	61.5	69.2	60.5	
2500	82.2	80.0	75.5	76.0	74.7	68.7	67.5	58.7	65.0	55.7	
3150	80.7	79.2	74.5	76.7	74.5	65.7	64.2	57.7	63.2	54.5	
4000	80.7	78.2	72.7	76.7	74.2	62.2	61.0	55.7	60.7	53.2	
5000	80.0	76.2	71.2	77.0	72.5	58.2	57.5	51.7	55.7	50.0	
6300	77.7	72.2	68.2	75.2	71.7	54.7	50.7	48.5	50.5	49.2	
8000	76.0	69.0	68.7	73.0	69.7	55.2	50.7	50.0	50.5	50.7	
10000	75.7	66.7	64.7	73.0	67.2	56.2	51.5	51.2	51.5	51.7	
DB(A)	102.2	102.0	85.7	98.0	86.5	90.7	88.2	70.0	90.0	70.0	
DB(L)	107.0	106.7	92.0	102.0	97.5	94.0	92.5	81.2	93.7	81.0	

TWIN OTTER ACOUSTIC DATA - 1/3 O.B. ANALYSIS

	FLYOVER DATA			GROUND-BASED SYSTEM			MICROPHONE AT GROUND LEVEL			
1/3 O.B. FREQ. HZ	FLT 7 RN 12	FLT 8 RN 16	FLT 8 RN 17	FLT 10 RN 18T	FLT 10 RN 19T	FLT 10 RN 20T	FLT 16 RN 21	FLT 16 RN 22	FLT 16 RN 23	FLT 7 RN AMB
50	62.7	70.0	68.7	66.5	64.7	61.7	73.0	69.5	69.5	66.7
63	62.5	74.2	72.2	73.5	75.7	77.2	75.7	77.0	77.0	65.5
80	66.2	80.2	73.0	98.5	83.5	79.5	93.5	84.0	78.0	63.5
100	79.5	93.0	91.0	90.7	97.5	101.0	82.2	95.7	96.0	63.0
125	75.7	73.2	73.7	71.5	75.5	84.0	70.0	75.2	84.2	58.5
160	61.2	75.7	73.7	82.0	74.7	73.0	81.5	79.0	76.7	60.5
200	82.2	89.7	90.0	75.5	87.2	89.2	75.7	92.5	95.5	59.7
250	80.0	81.7	78.7	72.0	69.7	73.5	80.2	84.0	86.7	55.0
315	84.7	89.5	89.0	62.7	72.5	72.0	79.7	90.2	95.0	55.0
400	83.2	84.0	86.5	58.2	65.2	65.5	75.5	86.5	93.7	55.0
500	82.2	79.0	81.0	56.5	58.0	60.5	74.5	82.5	89.2	55.0
630	81.5	74.5	78.5	56.0	56.2	56.2	74.7	77.5	87.5	55.0
800	82.2	75.2	77.5	56.2	54.7	57.0	74.5	77.5	89.2	55.0
1000	81.2	72.7	75.2	58.2	56.5	58.0	75.0	75.5	86.2	55.5
1250	78.5	71.2	71.5	61.7	61.0	62.7	76.0	76.2	82.7	55.0
1600	76.0	73.5	72.7	65.0	63.5	64.5	78.2	78.5	81.2	55.0
2000	71.5	75.2	74.2	63.5	61.7	61.5	79.5	80.0	81.5	55.0
2500	65.2	73.7	71.7	61.7	58.5	59.2	78.7	78.7	79.5	55.0
3150	61.7	73.2	72.7	62.2	59.5	60.0	78.5	78.7	80.5	55.0
4000	57.0	73.2	71.0	62.5	59.0	59.7	79.0	78.2	80.0	55.0
5000	54.5	72.0	69.2	61.7	57.0	58.2	77.5	77.2	79.0	55.0
6300	50.7	70.0	68.0	61.5	60.0	58.2	76.0	75.7	76.5	56.0
8000	51.0	66.7	65.2	63.2	63.5	60.0	73.0	73.0	73.5	62.0
10000	51.5	62.5	62.7	60.5	59.0	57.2	69.7	69.2	70.2	61.2
DB(A)	88.5	87.5	88.0	79.2	79.7	82.7	88.2	90.7	96.2	65.0
DB(L)	92.2	95.7	95.2	98.5	97.0	99.7	94.5	98.5	101.5	80.5

TWIN OTTER ACOUSTIC DATA - 1/3 O.B. ANALYSIS

	FLYOVER DATA		GROUND-BASED SYSTEM				1.2M (4FT) MICROPHONE HEIGHT			
1/3 O.B. FREQ. HZ	FLT 7 RN 1	FLT 7 RN 2	FLT 7 RN 3	FLT 7 RN 4	FLT 7 RN 5	FLT 7 RN 7	FLT 7 RN 8	FLT 7 RN 9	FLT 7 RN 10	FLT 7 RN 11
50	73.2	65.0	65.5	61.2	65.5	56.5	55.5	56.5	61.2	51.7
63	70.5	64.2	63.2	60.5	63.0	53.5	55.7	53.0	59.0	51.0
80	75.5	69.0	80.5	66.5	83.5	58.5	58.0	64.0	60.5	67.2
100	98.5	94.2	78.7	92.0	77.7	79.7	82.2	71.0	78.2	65.2
125	93.0	89.2	71.7	87.0	69.5	81.0	75.5	58.7	76.5	57.7
160	82.0	78.7	83.5	76.0	83.2	65.5	64.2	62.7	61.7	69.7
200	81.7	81.5	81.2	79.0	78.2	70.0	68.7	68.2	68.2	68.0
250	83.5	80.7	80.7	75.7	77.5	72.7	67.7	65.0	67.5	69.2
315	92.7	90.2	76.2	90.7	69.7	76.5	76.2	64.7	77.2	59.7
400	96.5	93.0	69.0	91.7	65.7	80.0	81.0	55.0	80.7	56.5
500	93.5	92.7	69.2	93.7	66.7	83.5	80.2	57.0	83.5	55.2
630	93.2	89.5	69.7	89.5	66.5	81.7	78.0	56.2	80.2	51.7
800	90.7	87.0	68.2	89.7	67.0	75.7	74.5	56.0	75.2	52.2
1000	92.7	89.0	67.2	91.5	66.7	80.0	76.0	56.0	79.2	49.5
1250	88.2	83.5	68.7	85.5	69.5	75.7	70.5	54.2	72.5	50.7
1600	86.0	82.0	70.0	83.2	71.2	72.7	70.2	56.7	70.0	52.5
2000	83.5	78.0	71.7	79.2	70.7	69.0	66.5	57.2	65.0	55.0
2500	79.5	74.7	70.5	74.5	69.7	63.7	61.2	54.0	60.0	51.7
3150	77.2	74.0	69.5	73.2	68.7	60.2	57.7	52.0	59.5	50.2
4000	75.7	71.5	67.7	71.5	67.0	55.7	54.7	48.7	55.0	49.0
5000	75.2	70.5	65.7	71.2	65.0	52.5	51.2	46.7	50.0	45.7
6300	73.0	68.0	63.7	70.0	64.7	48.5	46.0	44.2	46.5	44.7
8000	71.5	64.0	62.0	69.2	61.5	49.0	46.0	45.7	46.5	45.7
10000	68.2	61.2	58.7	66.7	58.0	49.5	47.2	47.5	47.5	46.2
DB(A)	98.7	95.7	81.2	97.0	79.7	86.2	83.5	66.7	85.5	65.7
DB(L)	102.7	99.7	88.7	99.2	88.0	89.2	88.0	79.0	88.7	77.0

TWIN OTTER ACOUSTIC DATA - 1/3 O.B. ANALYSIS

	FLYOVER DATA		GROUND-BASED SYSTEM			1.2M (4FT) MICROPHONE HEIGHT				
1/3 O.B. FREQ. HZ	FLT 7 RN 12	FLT 8 RN 16	FLT 8 RN 17	FLT 10 RN 18T	FLT 10 RN 19T	FLT 10 RN 20T	FLT 16 RN 21	FLT 16 RN 22	FLT 16 RN 23	FLT 7 RN AMB
50	54.0	64.5	65.0	65.5	63.0	61.0	65.7	62.0	64.0	61.7
63	49.7	61.5	61.7	73.0	74.0	76.2	63.0	62.0	64.2	56.5
80	52.5	71.0	66.7	98.0	83.5	78.2	80.0	72.7	69.0	57.7
100	76.2	86.5	85.7	91.2	96.0	99.5	72.5	89.0	93.0	56.0
125	74.0	72.7	71.5	71.2	73.7	83.0	69.5	73.2	82.2	52.7
160	58.0	74.0	72.5	80.5	70.7	71.2	81.2	76.5	76.5	55.7
200	61.2	84.7	82.7	74.7	82.0	85.7	73.7	86.2	86.7	55.0
250	62.0	77.2	74.0	69.2	65.0	70.0	76.5	80.0	78.5	52.5
315	77.0	85.7	85.2	59.7	67.7	67.2	75.2	88.0	90.0	51.5
400	80.0	78.2	80.2	59.7	63.2	66.5	69.0	83.5	90.5	51.0
500	81.2	71.2	72.5	59.7	61.0	66.5	69.0	74.2	87.0	51.5
630	76.5	74.5	77.0	60.2	58.2	62.7	70.5	76.0	82.2	51.7
800	77.0	71.0	72.2	63.5	58.5	64.0	70.7	74.0	82.7	52.0
1000	80.0	69.5	71.0	66.5	62.0	65.2	71.0	71.2	82.0	51.2
1250	74.2	68.2	67.0	71.2	70.7	70.0	73.2	72.5	77.7	51.7
1600	72.0	69.2	68.5	73.7	73.5	71.0	75.5	74.5	78.0	51.5
2000	68.0	71.7	70.0	68.7	70.0	65.0	76.0	76.0	77.5	51.2
2500	63.2	70.0	67.7	66.0	65.7	63.5	75.2	74.7	76.5	50.7
3150	57.7	68.7	67.5	65.7	63.7	62.7	75.0	74.5	76.2	50.7
4000	53.0	67.2	65.0	64.7	63.0	60.7	74.5	72.7	75.2	51.2
5000	49.0	64.5	62.0	62.5	60.0	57.2	72.7	70.7	73.7	51.5
6300	46.0	63.0	61.0	60.7	60.0	57.7	70.2	69.0	70.7	52.7
8000	45.5	60.5	60.5	60.7	59.7	58.2	67.2	67.0	68.5	55.0
10000	46.7	56.5	57.2	58.2	56.2	56.2	64.5	63.5	65.7	55.5
DB(A)	84.5	83.2	83.0	81.0	80.0	82.0	84.2	87.0	91.5	59.7
DB(L)	87.2	90.7	89.7	98.2	95.5	98.5	87.5	93.2	96.7	76.5

TWIN OTTER ACOUSTIC DATA - 1/3 O.B. ANALYSIS

	FLYOVER DATA		GROUND-BASED SYSTEM		4M (12FT) MICROPHONE HEIGHT					
1/3 O.B. FREQ. HZ	FLT 7 RN 1	FLT 7 RN 2	FLT 7 RN 3	FLT 7 RN 4	FLT 7 RN 5	FLT 7 RN 7	FLT 7 RN 8	FLT 7 RN 9	FLT 7 RN 10	FLT 7 RN 11
50	77.5	71.2	70.5	66.0	73.2	60.7	67.7	65.0	59.7	59.7
63	75.5	71.5	70.5	69.2	71.5	60.0	68.7	65.0	57.0	54.5
80	83.0	78.0	91.2	74.0	95.0	67.7	66.7	71.2	60.5	71.7
100	91.0	90.2	87.7	87.5	89.0	77.2	77.5	74.7	74.2	73.7
125	90.7	87.0	72.0	82.5	71.5	80.5	70.7	60.2	74.0	57.2
160	79.7	77.7	84.5	74.5	83.5	62.2	62.5	62.0	58.0	66.5
200	86.5	96.2	83.0	93.2	81.2	74.7	83.0	65.0	76.5	68.2
250	88.2	89.7	77.5	91.5	77.0	77.2	74.5	59.0	78.0	57.7
315	99.0	94.5	76.0	94.0	70.7	83.7	79.7	63.0	84.0	58.2
400	94.2	88.7	71.0	86.2	67.7	79.0	75.2	58.7	76.2	58.7
500	90.2	91.2	70.5	92.7	69.5	80.7	78.0	58.0	77.5	59.0
630	94.0	90.0	71.0	92.2	68.7	80.2	79.5	56.7	81.0	54.7
800	93.2	88.2	70.5	91.0	68.7	79.0	75.5	54.2	76.0	54.7
1000	93.2	88.7	69.0	90.0	69.2	78.7	75.2	53.5	78.0	51.7
1250	90.2	84.7	70.7	86.7	72.5	75.2	71.2	53.2	73.5	52.2
1600	88.5	82.5	73.0	84.0	73.2	71.7	68.5	55.2	69.5	54.7
2000	87.0	80.5	75.0	80.0	73.7	69.5	67.5	57.0	66.0	56.7
2500	82.0	77.5	73.2	76.0	73.0	64.5	63.2	54.5	61.5	53.5
3150	79.7	76.7	72.2	75.5	71.0	61.7	60.7	53.0	59.7	51.7
4000	76.7	75.5	70.5	73.2	69.7	57.5	56.2	49.7	55.5	48.2
5000	74.5	72.2	67.0	71.7	67.0	53.2	52.7	47.7	50.2	46.5
6300	73.5	69.2	66.0	71.7	66.7	51.5	48.2	46.5	48.0	46.5
8000	72.0	66.5	64.7	70.5	64.7	52.7	49.0	48.2	49.2	48.0
10000	69.7	63.5	61.0	67.7	60.0	52.5	49.7	49.2	49.5	48.5
DB(A)	100.0	96.0	83.0	97.5	82.5	85.5	83.5	66.0	84.7	65.7
DB(L)	103.5	101.2	94.0	101.0	96.2	89.2	88.7	84.7	89.0	81.5

TWIN OTTER ACOUSTIC DATA - 1/3 O.B. ANALYSIS

	FLYOVER DATA		GROUND-BASED SYSTEM			4M (12FT) MICROPHONE HEIGHT				
1/3 O.B. FREQ. HZ	FLT 7 RN 12	FLT 8 RN 16	FLT 8 RN 17	FLT 10 RN 18T	FLT 10 RN 19T	FLT 10 RN 20T	FLT 16 RN 21	FLT 16 RN 22	FLT 16 RN 23	FLT 7 RN AMB
50	57.7	68.7	66.2	64.5	62.2	60.7	71.0	70.2	69.2	67.7
63	53.5	64.2	65.0	71.5	74.2	73.5	74.5	73.5	73.5	65.0
80	61.7	78.5	64.7	95.7	80.2	75.5	90.5	82.5	74.5	61.7
100	73.5	90.0	85.5	88.7	95.2	98.0	84.5	93.2	90.7	58.2
125	69.7	72.5	73.0	68.7	74.0	84.7	69.7	73.0	76.7	55.0
160	58.5	73.5	69.7	80.2	71.7	70.5	82.2	76.7	75.0	56.5
200	79.0	86.5	84.7	74.2	85.2	88.7	76.7	87.0	95.0	56.0
250	77.2	76.2	72.7	73.7	71.5	76.5	77.2	79.0	85.5	52.0
315	81.2	85.2	84.0	66.7	78.0	82.5	74.5	84.2	86.7	51.2
400	70.7	75.2	77.5	66.5	74.7	80.5	70.5	80.2	89.2	50.7
500	77.0	78.0	78.2	64.7	70.7	77.5	70.0	75.5	84.5	50.7
630	79.5	72.7	75.5	63.0	70.2	73.0	72.2	74.7	86.2	50.7
800	77.5	71.5	73.7	64.7	70.7	70.2	71.5	72.2	84.5	51.2
1000	77.5	68.2	70.0	63.2	67.0	68.5	70.7	70.7	81.5	51.7
1250	75.0	68.0	67.5	65.2	66.5	68.2	72.5	72.5	78.7	50.5
1600	72.0	70.0	69.0	66.2	69.2	68.7	74.0	73.7	77.5	51.7
2000	67.5	72.5	70.2	64.2	68.2	66.2	75.0	75.2	77.7	51.7
2500	63.2	71.5	68.0	62.7	65.5	64.0	74.5	74.2	76.2	50.7
3150	58.5	70.0	68.0	63.5	64.5	63.7	74.2	73.7	76.5	51.2
4000	52.0	68.7	64.5	62.5	62.0	62.5	73.5	72.7	75.5	52.0
5000	48.5	66.0	61.7	59.7	59.7	60.0	71.7	71.0	73.7	53.2
6300	47.5	65.0	60.7	58.7	60.2	60.2	69.5	69.2	71.0	55.7
8000	48.5	62.0	60.2	60.2	61.7	61.2	67.7	68.2	70.0	57.7
10000	49.0	58.2	56.0	56.7	57.5	58.5	65.7	65.7	67.5	57.5
DB(A)	84.5	83.5	83.0	78.2	80.7	84.5	84.0	85.7	92.5	61.7
DB(L)	87.5	92.5	90.0	96.2	95.0	97.7	92.5	95.0	98.0	85.0

TWIN OTTER ACOUSTIC DATA - 1/3 O.B. ANALYSIS

	STATIC DATA		AIRCRAFT WING-TIP SYSTEM			FRONT MICROPHONE LOCATION			
1/3 O.B. FREQ. HZ	FLT 12 RN 2S	FLT 12 RN 16S	FLT 12 RN 3S	FLT 12 RN 5S	FLT 14 RN 21S	FLT 14 RN 22S	FLT 15 RN 4S	FLT 15 RN 6S	FLT 15 RN 17S
50	83.0	82.2	81.5	80.7	77.2	77.5	81.0	80.5	80.7
63	87.0	88.2	87.7	87.0	84.0	84.5	85.0	85.0	88.2
80	95.0	98.7	112.5	111.5	107.5	105.5	92.5	92.2	97.0
100	120.2	118.0	110.0	109.5	93.0	87.2	116.7	116.7	116.5
125	109.2	98.2	90.7	90.2	82.5	81.2	108.0	107.0	97.7
160	93.2	91.5	102.5	100.5	96.7	95.5	90.7	90.7	90.7
200	104.5	104.2	101.0	99.5	87.0	84.7	100.5	99.7	103.2
250	98.5	93.2	99.2	98.2	89.7	87.7	95.5	94.7	94.2
315	114.7	101.5	94.0	94.0	86.7	88.5	111.7	110.7	105.0
400	116.0	107.0	94.0	95.0	83.2	88.0	112.7	112.7	107.0
500	114.5	106.2	95.0	96.0	86.0	90.2	111.2	110.2	105.2
630	111.2	105.2	96.2	96.7	85.7	89.5	108.7	108.0	102.2
800	112.7	101.0	97.7	97.5	86.5	89.7	108.2	109.7	103.7
1000	111.0	103.0	99.0	99.7	87.5	90.0	108.5	108.0	105.0
1250	109.2	102.7	99.7	100.5	87.2	89.5	107.7	108.5	105.2
1600	107.2	102.5	101.0	101.2	87.7	90.0	106.2	106.2	105.7
2000	106.0	102.2	101.0	100.2	86.7	89.7	104.7	105.5	105.2
2500	103.2	98.5	98.7	97.2	85.5	88.2	102.2	103.2	102.2
3150	102.2	97.2	96.5	96.0	84.7	87.0	100.2	100.7	100.0
4000	100.5	96.0	94.5	94.2	83.5	85.2	98.5	99.0	98.0
5000	98.5	94.2	92.7	92.7	82.5	83.7	96.7	97.0	96.0
6300	97.5	93.0	92.2	91.7	85.5	84.2	95.0	94.5	94.5
8000	96.7	91.7	92.0	91.2	82.7	82.7	93.2	92.5	92.5
10000	95.7	90.0	90.7	90.2	82.0	82.2	91.0	90.7	91.0
DB(A)	118.7	112.2	108.2	108.2	96.5	98.5	116.5	117.2	114.0
DB(L)	123.2	118.5	116.0	115.5	108.0	106.2	120.5	120.5	118.2

TWIN OTTER ACOUSTIC DATA - 1/3 O.B. ANALYSIS

	STATIC DATA		AIRCRAFT WING-TIP SYSTEM			AFT MICROPHONE LOCATION			
1/3 O.B. FREQ. HZ	FLT 12 RN 2S	FLT 12 RN 16S	FLT 12 RN 3S	FLT 12 RN 5S	FLT 14 RN 21S	FLT 14 RN 22S	FLT 15 RN 4S	FLT 15 RN 6S	FLT 15 RN 17S
50	85.0	85.5	83.0	82.2	83.5	87.2	83.7	82.5	83.0
63	90.2	91.7	90.2	90.0	85.5	87.0	88.7	88.7	92.0
80	101.5	105.0	115.7	114.2	107.0	104.2	98.7	98.5	103.2
100	127.7	124.2	113.0	112.5	92.7	89.2	125.0	124.5	123.0
125	116.5	104.5	93.0	91.7	87.7	86.5	116.0	115.0	104.0
160	98.0	96.2	110.0	108.7	104.2	99.2	98.2	98.5	95.2
200	114.0	110.7	108.5	107.5	91.7	89.5	113.2	113.7	108.0
250	104.5	97.5	105.7	104.7	98.2	96.2	105.5	105.5	96.2
315	114.0	106.5	99.0	99.2	93.5	102.2	113.0	114.2	105.7
400	109.5	105.7	98.5	100.0	88.2	95.7	109.0	108.0	106.5
500	110.0	104.7	99.2	100.2	89.5	93.7	112.5	109.5	106.0
630	109.2	104.7	99.7	101.5	93.0	96.7	111.0	109.2	107.5
800	111.0	104.2	102.2	104.0	93.2	99.0	111.5	110.5	106.7
1000	110.7	106.2	103.7	105.2	93.0	98.7	111.2	111.5	110.0
1250	111.5	103.5	101.5	101.7	91.7	94.5	110.0	109.7	108.0
1600	107.0	103.5	100.2	101.2	92.7	94.5	106.0	107.2	107.0
2000	105.2	102.7	99.7	100.7	91.5	92.7	105.0	105.7	105.7
2500	102.7	99.2	95.7	98.0	89.0	90.7	102.2	102.5	103.0
3150	102.0	98.0	95.0	96.7	89.0	89.2	101.0	102.5	100.7
4000	101.5	97.5	95.5	96.2	88.0	89.2	100.2	101.5	99.7
5000	100.5	95.7	94.0	95.0	87.0	87.5	98.5	99.7	98.5
6300	99.2	94.5	93.0	93.5	87.7	87.7	97.2	97.7	97.0
8000	98.0	93.2	92.2	92.5	86.5	86.0	96.0	96.0	95.2
10000	96.7	91.5	91.7	91.2	85.7	85.2	93.7	93.7	93.2
DB(A)	118.5	113.7	110.5	111.5	102.0	104.7	118.0	118.7	116.0
DB(L)	127.5	123.5	119.5	118.7	109.2	109.0	125.2	125.2	123.2

TWIN OTTER ACOUSTIC DATA - 1/3 O.B. ANALYSIS

STATIC DATA GROUND-BASED SYSTEM 61M (200 FT) RADIUS 0 DEG AZIMUTH										
1/3 O.B. FREQ. HZ	FLT 12 RN 2S	FLT 12 RN 16S	FLT 12 RN 3S	FLT 12 RN 5S	FLT 14 RN 21S	FLT 14 RN 22S	FLT 15 RN 4S	FLT 15 RN 6S	FLT 15 RN 17S	FLT 12 RN AMB
50	65.5	64.5	65.7	65.0	60.0	57.5	62.5	62.0	63.2	58.5
63	67.2	68.5	69.7	67.0	61.5	63.7	66.2	67.0	68.7	56.0
80	72.2	73.5	82.2	85.0	81.7	83.2	72.7	73.0	76.5	57.2
100	96.0	92.2	80.5	83.5	68.5	67.0	97.2	97.7	95.7	56.5
125	85.5	75.0	75.0	72.0	66.7	69.5	88.5	88.2	77.5	54.2
160	79.0	77.7	87.5	85.0	86.7	89.2	75.0	76.2	78.0	54.0
200	94.0	91.7	87.2	85.0	75.5	78.0	91.0	93.0	94.7	52.5
250	85.0	78.0	85.2	82.2	78.5	83.2	83.5	84.5	79.7	50.0
315	87.5	84.5	79.0	77.0	76.0	81.7	84.5	88.5	88.0	49.0
400	78.5	78.0	78.7	77.0	73.5	77.7	76.0	80.2	76.7	48.5
500	73.0	68.2	74.2	70.2	70.5	74.2	72.0	73.7	75.0	49.2
630	75.5	74.7	71.7	73.5	69.0	69.2	76.0	76.5	82.0	50.0
800	82.2	81.0	78.7	80.2	71.5	69.2	81.7	84.0	86.0	51.7
1000	83.7	84.5	82.5	81.7	73.7	71.7	84.0	87.0	87.7	52.2
1250	87.5	86.7	84.7	83.7	77.0	75.2	86.0	89.2	89.2	48.2
1600	88.2	87.7	86.0	84.5	78.7	77.5	86.7	90.2	90.0	49.5
2000	86.2	86.2	84.5	83.0	78.7	78.2	85.0	86.2	86.2	49.5
2500	82.5	82.0	80.0	78.2	76.2	76.5	82.0	82.5	83.0	47.7
3150	81.5	79.7	79.0	77.5	73.5	74.5	80.5	81.7	81.0	47.2
4000	79.2	77.2	76.7	74.5	72.0	71.7	77.7	78.0	77.7	47.2
5000	77.5	75.7	74.2	72.7	69.2	68.2	75.2	75.7	76.2	47.5
6300	74.5	72.7	73.2	70.0	68.0	67.2	73.0	73.0	73.2	48.7
8000	72.0	69.5	71.2	68.0	63.0	63.0	70.0	68.7	70.2	53.7
10000	68.2	65.2	67.2	63.7	59.0	58.5	66.0	64.7	65.2	50.2
DB(A)	94.5	93.2	92.0	91.0	86.0	86.0	93.0	95.5	96.2	58.0
DB(L)	99.0	96.5	94.7	94.0	89.7	91.7	99.5	99.5	99.7	73.5

TWIN OTTER ACOUSTIC DATA - 1/3 O.B. ANALYSIS

	STATIC DATA		GROUND-BASED SYSTEM		61M (200 FT) RADIUS		10 DEG AZIMUTH			
1/3 O.B. FREQ. HZ	FLT 12 RN 2S	FLT 12 RN 16S	FLT 12 RN 3S	FLT 12 RN 5S	FLT 14 RN 21S	FLT 14 RN 22S	FLT 15 RN 4S	FLT 15 RN 6S	FLT 15 RN 17S	FLT 12 RN AMB
50	66.0	63.7	65.0	62.0	60.0	56.7	62.5	62.0	62.5	55.5
63	68.0	68.2	70.2	67.2	61.5	65.2	66.0	65.7	68.0	55.7
80	73.2	75.2	84.0	85.2	81.0	85.0	72.0	72.2	78.0	56.2
100	96.5	93.7	81.7	83.7	68.5	67.5	97.5	98.0	97.5	55.5
125	86.5	76.0	75.7	72.2	66.0	69.0	88.5	89.0	78.5	54.7
160	79.7	78.0	87.0	85.2	86.0	88.7	75.5	76.5	77.0	51.5
200	92.5	91.7	86.2	85.0	74.0	78.0	91.2	92.5	93.5	51.5
250	84.0	78.0	84.7	82.2	78.2	85.5	84.0	84.2	78.0	48.7
315	86.5	84.0	79.2	76.5	75.5	81.7	86.2	87.0	87.0	47.2
400	77.5	79.2	79.7	77.0	71.5	79.2	77.7	79.0	76.7	47.0
500	77.5	73.2	74.5	71.2	70.2	76.2	73.2	72.7	71.7	48.0
630	81.0	77.0	72.7	74.0	69.0	69.5	75.5	76.2	80.2	49.5
800	85.2	81.5	78.2	79.0	70.5	69.5	82.5	81.2	83.0	49.2
1000	88.5	83.7	81.5	82.5	73.2	72.2	84.2	84.5	86.5	48.5
1250	89.0	86.7	85.2	85.0	76.5	75.2	86.7	87.5	88.2	47.2
1600	90.2	88.5	86.7	86.0	78.0	77.5	87.0	88.0	88.5	46.7
2000	86.5	87.0	84.7	83.5	77.7	77.0	84.2	86.2	85.2	47.0
2500	84.7	83.7	80.7	80.5	75.5	75.7	82.0	81.7	82.2	46.2
3150	83.2	80.5	79.5	78.7	73.0	74.2	79.7	79.0	81.0	46.2
4000	81.5	79.7	78.7	77.2	71.0	70.7	78.2	78.5	78.7	46.0
5000	80.2	78.0	77.7	75.5	69.2	68.5	76.7	76.2	76.7	46.0
6300	79.2	76.0	76.5	74.5	69.2	68.2	73.5	74.2	74.2	47.2
8000	77.5	73.5	75.0	72.5	65.0	65.0	70.7	71.0	72.0	52.5
10000	75.5	71.0	73.2	71.2	61.5	61.5	67.5	68.5	68.2	50.0
DB(A)	96.7	94.2	92.5	92.0	84.7	86.2	93.5	94.2	95.0	56.5
DB(L)	100.0	97.5	95.0	94.5	89.2	91.7	99.0	100.2	99.5	75.2

TWIN OTTER ACOUSTIC DATA - 1/3 O.B. ANALYSIS

	STATIC DATA		GROUND-BASED SYSTEM 61M (200 FT) RADIUS 20 DEG AZIMUTH							
1/3 O.B. FREQ. HZ	FLT 12 RN 2S	FLT 12 RN 16S	FLT 12 RN 3S	FLT 12 RN 5S	FLT 14 RN 21S	FLT 14 RN 22S	FLT 15 RN 4S	FLT 15 RN 6S	FLT 15 RN 17S	FLT 12 RN AMB
50	66.0	64.5	65.7	62.7	59.2	56.5	63.0	62.2	62.7	55.5
63	69.5	69.2	70.2	68.0	60.2	65.5	66.0	65.0	67.5	59.0
80	73.5	75.7	83.5	85.0	78.7	86.0	72.0	72.2	78.7	56.7
100	96.0	94.5	81.2	83.5	67.2	68.5	97.7	98.5	98.7	55.5
125	86.2	76.5	75.7	73.0	64.5	68.0	88.7	89.5	79.7	53.0
160	80.5	77.7	86.0	82.5	84.0	87.5	76.5	77.2	76.5	51.7
200	89.0	91.5	85.2	82.0	71.7	77.0	92.0	91.2	92.0	51.0
250	82.7	77.7	85.5	81.7	77.2	86.2	83.7	83.2	77.5	48.2
315	86.2	83.0	79.2	77.5	73.2	82.5	84.2	86.0	85.5	47.7
400	78.0	81.7	79.5	78.2	71.2	80.7	77.5	79.2	80.7	48.2
500	75.7	69.0	73.7	72.7	64.7	74.5	73.2	74.7	75.7	49.7
630	79.2	76.5	73.2	71.5	64.0	66.2	77.7	77.0	79.2	52.0
800	86.0	82.0	79.0	76.7	68.7	68.5	82.7	84.0	84.2	52.5
1000	88.0	85.2	83.0	80.5	70.7	71.2	85.0	86.7	86.7	52.0
1250	89.7	87.5	85.7	83.2	74.7	74.7	87.0	88.5	88.5	48.7
1600	88.5	88.0	87.0	85.0	77.0	77.5	87.7	88.7	88.5	49.0
2000	86.2	86.5	84.2	83.0	75.5	77.0	84.2	85.7	84.0	49.2
2500	85.0	83.5	81.0	80.0	74.5	76.0	82.2	83.2	83.0	47.0
3150	83.0	80.7	79.7	77.5	71.0	73.5	81.0	80.5	81.0	47.0
4000	81.5	79.0	78.5	76.0	68.5	71.2	78.2	78.2	78.2	46.5
5000	79.7	77.0	76.7	73.7	66.5	67.2	76.7	76.5	76.0	47.2
6300	77.7	75.2	75.0	72.2	66.7	67.2	74.7	74.5	73.7	49.5
8000	76.0	72.7	73.2	71.0	61.7	63.7	73.2	72.5	70.7	55.5
10000	73.0	70.2	71.0	68.2	59.2	60.2	69.5	68.7	67.5	51.7
DB(A)	95.7	94.5	92.2	90.5	83.2	86.0	94.2	95.0	94.7	59.2
DB(L)	99.2	97.5	94.5	93.2	88.2	92.0	99.5	100.2	100.0	70.0

TWIN OTTER ACOUSTIC DATA - 1/3 O.B. ANALYSIS

STATIC DATA GROUND-BASED SYSTEM 61M (200 FT) RADIUS 30 DEG AZIMUTH

1/3 O.B. FREQ. HZ	FLT 12 RN 2S	FLT 12 RN 16S	FLT 12 RN 3S	FLT 12 RN 5S	FLT 14 RN 21S	FLT 14 RN 22S	FLT 15 RN 4S	FLT 15 RN 6S	FLT 15 RN 17S	FLT 12 RN AMB
50	65.7	64.7	66.0	62.5	59.7	58.7	63.5	61.7	62.7	54.7
63	69.7	70.7	70.0	68.5	61.0	64.2	67.5	66.7	68.5	53.7
80	73.5	74.7	81.0	84.7	81.5	84.5	73.0	72.7	78.2	58.0
100	92.5	93.0	78.5	83.5	68.0	67.5	96.0	96.7	97.7	56.7
125	83.0	76.7	75.5	73.5	65.0	66.5	86.7	87.0	79.0	52.5
160	80.5	77.2	86.2	82.0	81.0	85.5	76.7	77.2	76.2	51.5
200	92.0	91.7	85.2	81.5	71.0	76.2	94.5	94.0	91.5	49.7
250	83.5	77.7	87.5	84.0	79.0	87.0	86.0	85.7	79.5	47.7
315	86.5	84.0	81.0	78.0	74.5	83.2	86.7	88.0	88.7	46.5
400	78.0	80.0	79.2	77.5	71.0	79.0	80.2	82.7	79.7	46.7
500	75.5	70.7	75.0	72.2	67.0	76.2	74.7	76.7	74.7	47.5
630	81.0	76.2	71.2	71.0	65.0	68.7	76.7	77.2	81.0	48.2
800	85.5	79.7	77.7	76.2	69.5	68.0	82.0	82.2	82.5	48.5
1000	87.0	84.0	81.5	79.5	72.2	71.7	84.0	84.0	85.5	48.5
1250	89.5	86.2	85.0	83.0	75.2	75.0	87.0	87.2	88.0	46.7
1600	89.0	87.0	85.7	84.0	77.0	76.5	87.7	88.7	88.5	46.2
2000	86.2	85.7	84.0	82.2	76.2	76.5	85.0	86.5	85.0	46.5
2500	84.0	82.7	81.7	79.5	74.2	75.2	82.7	83.7	83.0	46.0
3150	83.2	80.7	79.0	77.7	72.2	73.7	80.2	80.7	81.0	45.5
4000	81.0	78.2	77.7	75.2	69.7	70.2	78.2	79.0	79.0	45.5
5000	79.0	76.5	76.2	73.7	67.5	65.7	75.5	76.2	76.5	45.7
6300	77.5	74.2	75.0	71.7	68.0	67.0	73.2	73.7	73.5	47.5
8000	75.7	72.2	74.0	71.0	63.7	63.0	70.5	71.0	70.7	52.0
10000	73.5	69.5	71.5	67.5	59.5	57.5	68.0	68.5	68.5	49.0
DB(A)	95.7	93.5	92.0	90.0	83.5	85.7	94.2	94.7	94.5	55.7
DB(L)	98.2	97.0	94.2	93.0	86.7	91.0	99.7	99.5	99.2	64.7

TWIN OTTER ACOUSTIC DATA - 1/3 O.B. ANALYSIS

	STATIC DATA		GROUND-BASED SYSTEM 61M (200 FT) RADIUS 40 DEG AZIMUTH							
1/3 O.B. FREQ. HZ	FLT 12 RN 2S	FLT 12 RN 16S	FLT 12 RN 3S	FLT 12 RN 5S	FLT 14 RN 21S	FLT 14 RN 22S	FLT 15 RN 4S	FLT 15 RN 6S	FLT 15 RN 17S	FLT 12 RN AMB
50	66.5	64.7	66.2	65.0	60.7	61.2	64.5	65.0	63.7	59.7
63	70.7	72.2	70.5	69.2	63.2	62.2	69.2	68.2	69.2	59.7
80	74.2	74.0	83.2	87.2	85.5	81.0	74.0	72.5	77.2	59.0
100	93.5	91.7	81.0	85.0	70.5	65.7	93.0	91.7	96.5	57.7
125	83.2	75.5	75.0	73.5	64.5	66.2	84.0	82.0	78.0	62.2
160	80.0	76.2	87.5	82.2	79.2	84.7	76.5	75.2	75.5	57.0
200	90.5	91.2	85.2	81.0	70.5	76.2	93.5	92.2	91.5	60.7
250	81.7	78.2	85.2	82.7	78.5	87.5	85.0	83.2	81.0	55.7
315	87.2	86.5	79.0	76.2	71.5	84.2	89.2	88.0	91.5	53.7
400	77.2	79.5	78.0	75.5	69.0	76.5	77.7	77.2	76.5	51.5
500	75.0	71.5	72.5	71.5	67.0	73.2	73.2	73.5	72.7	51.7
630	78.0	74.5	72.2	70.0	65.0	68.0	75.7	73.2	77.2	52.2
800	83.0	79.0	77.2	75.2	65.2	68.5	81.2	79.0	81.5	52.2
1000	85.5	82.7	80.5	78.7	68.7	72.5	83.0	81.7	83.2	52.2
1250	89.0	85.2	83.7	82.0	72.5	75.5	86.2	85.5	86.7	52.0
1600	89.7	86.5	86.0	84.0	75.5	77.5	87.7	87.0	88.0	52.7
2000	86.7	84.5	85.0	82.7	75.5	76.7	86.2	86.0	85.7	52.2
2500	83.7	82.2	81.7	81.0	74.0	75.7	83.2	84.2	83.0	51.2
3150	83.5	80.7	78.5	78.0	72.0	75.0	82.2	81.7	81.7	51.7
4000	81.0	78.5	77.2	75.5	69.2	69.0	77.7	78.7	78.5	51.5
5000	79.5	76.5	76.7	74.7	67.2	68.7	76.7	75.5	76.0	51.5
6300	78.2	74.2	75.7	73.5	67.7	68.2	74.7	75.7	75.2	52.7
8000	77.0	73.2	74.2	72.7	63.7	64.2	73.5	73.5	72.7	57.5
10000	74.5	70.2	72.5	70.5	59.7	61.2	70.0	69.7	69.5	56.7
DB(A)	95.5	92.7	91.7	90.2	82.7	85.7	93.7	93.7	94.2	61.2
DB(L)	98.5	96.5	94.2	93.5	88.0	91.0	98.0	97.2	99.0	70.5

TWIN OTTER ACOUSTIC DATA - 1/3 O.B. ANALYSIS

	STATIC DATA		GROUND-BASED SYSTEM		61M (200 FT) RADIUS		50 DEG AZIMUTH			
1/3 O.B. FREQ. HZ	FLT 12 RN 2S	FLT 12 RN 16S	FLT 12 RN 3S	FLT 12 RN 5S	FLT 14 RN 21S	FLT 14 RN 22S	FLT 15 RN 4S	FLT 15 RN 6S	FLT 15 RN 17S	FLT 12 RN AMB
50	66.7	66.0	67.0	66.2	62.0	63.0	65.0	64.7	64.0	60.7
63	70.2	73.0	71.0	69.7	65.0	61.0	69.7	69.0	69.7	62.2
80	75.2	74.5	86.5	88.5	87.5	74.2	74.2	74.0	76.2	59.2
100	97.7	92.5	83.7	85.7	72.5	63.5	94.5	95.5	95.2	58.0
125	87.0	75.5	74.2	72.5	64.7	66.2	85.5	85.2	77.5	63.5
160	79.0	75.5	84.7	81.5	78.0	84.0	76.5	75.7	76.0	57.0
200	94.7	90.2	83.0	79.7	69.0	74.5	95.2	94.5	94.0	59.7
250	85.2	78.5	85.5	82.7	79.5	84.5	86.2	85.2	78.5	55.7
315	87.0	87.2	79.2	75.7	70.5	82.2	87.5	87.0	87.5	53.2
400	81.5	78.5	78.0	75.0	67.5	77.5	80.2	80.7	78.5	52.2
500	74.7	72.2	71.7	70.5	64.0	72.7	74.5	75.0	74.0	52.5
630	77.0	72.5	70.0	69.0	63.0	67.5	77.2	73.2	76.0	52.7
800	82.5	77.2	76.2	75.5	66.5	71.2	82.5	78.5	80.5	52.5
1000	86.0	81.7	80.5	78.5	68.2	75.0	84.0	80.0	84.0	53.0
1250	88.5	84.0	83.7	81.2	72.2	76.7	86.2	84.0	86.0	52.7
1600	89.2	85.0	85.2	83.5	75.5	78.5	87.0	85.5	86.5	52.5
2000	86.7	84.5	83.7	82.2	74.7	77.5	85.2	85.2	84.5	51.7
2500	83.2	81.5	80.0	79.2	72.7	75.0	82.5	83.0	81.5	51.5
3150	83.0	79.5	78.5	77.7	69.7	73.0	80.7	79.7	79.7	51.7
4000	81.0	78.0	77.5	76.0	67.0	69.0	77.5	77.5	77.2	51.7
5000	78.0	75.0	73.7	73.0	66.2	68.5	76.0	76.5	75.7	52.0
6300	78.7	73.7	74.5	73.2	66.7	68.5	74.7	74.7	74.5	52.5
8000	75.7	71.0	72.0	72.0	62.2	63.7	73.5	73.2	71.7	56.2
10000	73.7	68.2	70.0	69.5	58.2	59.7	70.5	69.2	68.5	56.0
DB(A)	95.7	92.0	91.0	89.5	82.2	85.7	93.7	93.0	93.0	60.0
DB(L)	100.2	96.2	94.2	94.2	88.2	89.5	99.0	98.7	98.0	69.7

TWIN OTTER ACOUSTIC DATA - 1/3 O.B. ANALYSIS

STATIC DATA GROUND-BASED SYSTEM 61M (200 FT) RADIUS 60 DEG AZIMUTH										
1/3 O.B. FREQ. HZ	FLT 12 RN 2S	FLT 12 RN 16S	FLT 12 RN 3S	FLT 12 RN 5S	FLT 14 RN 21S	FLT 14 RN 22S	FLT 15 RN 4S	FLT 15 RN 6S	FLT 15 RN 17S	FLT 12 RN AMB
50	66.5	66.5	66.7	65.7	61.7	62.5	65.0	67.7	72.7	59.2
63	70.0	72.0	70.7	69.0	64.7	62.2	68.7	69.0	70.5	62.0
80	75.5	75.5	87.2	87.7	86.5	75.5	73.7	74.2	75.5	58.2
100	99.5	94.2	84.0	85.0	72.0	64.0	97.0	98.2	94.2	57.0
125	88.2	75.7	74.2	72.0	64.2	66.7	87.2	88.2	76.5	62.2
160	78.5	75.7	84.0	80.7	77.0	85.2	75.7	75.2	75.2	56.5
200	97.2	90.0	82.2	79.0	68.0	72.2	94.5	94.2	92.5	59.5
250	87.0	78.0	83.7	80.7	79.0	81.5	85.5	85.0	76.2	54.5
315	88.2	87.0	78.2	75.2	70.7	80.5	88.7	87.5	85.5	52.5
400	83.5	79.2	77.2	74.7	66.2	76.2	79.0	81.0	79.2	51.0
500	77.5	75.7	72.7	70.2	64.2	69.2	74.5	77.2	72.2	51.2
630	74.5	71.7	70.2	68.0	60.7	65.5	74.0	73.7	74.0	52.0
800	79.5	75.2	76.2	72.5	65.0	70.2	80.5	78.0	78.2	51.5
1000	83.0	78.5	79.7	76.2	67.7	73.2	82.7	80.2	82.5	51.7
1250	86.7	82.0	83.5	81.0	72.0	76.5	84.5	81.2	84.2	51.5
1600	87.0	84.0	84.0	81.5	74.0	78.5	85.5	83.7	85.7	52.2
2000	85.2	83.0	83.0	81.2	73.0	77.0	85.2	85.2	85.0	51.5
2500	83.2	82.0	81.2	79.5	71.0	74.7	82.7	83.7	83.0	51.0
3150	82.0	78.5	79.7	77.5	68.0	70.5	81.2	81.7	81.2	51.2
4000	80.5	78.0	78.0	75.2	66.0	67.0	77.7	77.0	77.7	51.5
5000	78.7	75.5	76.5	73.5	65.7	68.0	74.7	73.7	73.2	52.0
6300	77.0	74.5	76.0	72.0	65.5	67.7	74.0	74.5	74.5	54.0
8000	75.0	72.0	74.2	71.0	62.0	63.0	74.2	74.2	74.0	58.2
10000	73.5	69.5	72.2	69.5	59.2	60.0	69.7	68.5	68.0	57.0
DB(A)	95.5	91.5	91.0	88.5	81.0	84.5	93.2	92.2	92.5	61.2
DB(L)	101.2	96.5	94.0	93.0	87.5	88.7	99.0	99.5	97.7	70.2

TWIN OTTER ACOUSTIC DATA - 1/3 O.B. ANALYSIS

STATIC DATA GROUND-BASED SYSTEM 61M (200 FT) RADIUS 70 DEG AZIMUTH										
1/3 O.B. FREQ. HZ	FLT 12 RN 2S	FLT 12 RN 16S	FLT 12 RN 3S	FLT 12 RN 5S	FLT 14 RN 21S	FLT 14 RN 22S	FLT 15 RN 4S	FLT 15 RN 6S	FLT 15 RN 17S	FLT 12 RN AMB
50	67.2	66.7	66.7	66.2	60.5	60.2	65.5	64.7	66.0	58.7
63	70.2	70.5	69.7	68.0	62.7	62.0	67.7	66.7	68.2	59.7
80	74.5	74.0	83.5	82.5	83.0	75.2	72.2	72.5	74.0	57.5
100	97.5	91.2	80.5	80.2	68.7	63.5	96.0	96.5	92.2	56.0
125	86.5	74.2	73.7	71.7	64.5	66.2	86.0	86.5	74.5	62.7
160	77.5	75.5	81.5	81.0	74.5	83.5	73.7	73.5	74.5	56.7
200	94.5	88.0	79.7	80.2	67.0	70.7	93.2	92.5	91.5	59.5
250	84.5	76.2	82.2	78.7	75.5	80.0	85.0	83.0	75.2	55.5
315	88.7	84.7	76.7	74.7	67.2	76.7	88.0	86.7	83.0	52.7
400	85.0	80.0	77.0	75.0	63.5	73.7	81.0	81.2	81.0	51.5
500	82.0	77.2	72.7	70.5	60.5	68.5	78.0	77.2	74.0	51.5
630	75.0	70.0	68.0	67.0	58.5	65.0	75.0	72.2	71.7	52.0
800	78.5	72.2	72.2	69.5	61.7	66.5	78.2	75.0	76.0	51.5
1000	81.5	77.2	76.0	73.0	65.5	69.2	80.2	77.5	79.2	51.7
1250	84.7	82.0	80.7	77.5	68.5	71.7	84.5	81.0	83.2	51.2
1600	87.2	84.0	83.5	80.0	70.0	74.5	86.5	83.0	84.5	52.0
2000	86.0	83.5	83.7	80.7	71.2	75.5	85.7	84.7	84.7	52.0
2500	84.2	82.2	82.7	79.7	70.5	73.5	83.0	82.5	82.5	51.7
3150	81.7	80.5	78.7	78.5	67.2	68.7	80.7	81.2	80.7	52.7
4000	80.5	78.2	77.0	75.7	65.0	65.7	77.2	77.5	77.7	52.0
5000	80.0	75.7	76.5	74.0	64.7	66.5	76.0	77.0	76.2	51.5
6300	77.7	75.0	75.0	73.0	64.7	64.7	74.5	75.7	74.2	52.2
8000	75.7	73.0	74.0	72.5	61.2	62.0	72.0	74.2	72.0	55.5
10000	73.5	69.7	71.5	70.2	58.5	59.5	69.2	71.5	68.5	54.7
DB(A)	94.2	91.2	90.2	87.7	78.5	82.0	92.5	92.2	91.2	61.2
DB(L)	99.7	94.7	92.0	91.2	84.5	86.5	98.5	98.0	96.2	70.0

TWIN OTTER ACOUSTIC DATA.- 1/3 O.B. ANALYSIS

STATIC DATA GROUND-BASED SYSTEM 61M (200 FT) RADIUS 80 DEG AZIMUTH										
1/3 O.B. FREQ. HZ	FLT 12 RN 2S	FLT 12 RN 16S	FLT 12 RN 3S	FLT 12 RN 5S	FLT 14 RN 21S	FLT 14 RN 22S	FLT 15 RN 4S	FLT 15 RN 6S	FLT 15 RN 17S	FLT 12 RN AMB
50	67.7	67.0	66.2	65.2	59.7	58.7	66.2	64.7	66.5	54.0
63	70.5	69.7	68.7	68.0	61.7	62.2	67.7	66.7	70.0	52.5
80	75.5	74.7	85.0	84.0	78.2	79.0	73.0	72.2	75.0	54.0
100	99.0	92.2	82.0	82.0	66.0	63.5	96.0	96.0	93.2	53.5
125	88.0	74.7	73.2	72.0	65.7	66.0	87.0	85.7	75.0	50.5
160	77.5	75.5	81.7	82.0	74.5	80.7	73.2	73.0	74.0	53.0
200	95.2	90.0	79.2	80.5	67.2	67.5	91.5	92.0	90.7	51.5
250	85.0	77.0	82.5	80.2	74.5	75.2	83.0	82.7	75.0	46.0
315	92.5	85.2	75.5	73.2	64.5	72.0	89.0	88.0	84.0	45.2
400	90.0	78.5	75.0	72.5	62.0	67.5	83.2	83.7	79.2	45.2
500	85.2	75.7	71.7	69.0	57.7	63.7	77.5	78.2	72.5	45.7
630	80.5	72.0	67.5	67.0	56.0	58.0	74.0	75.5	71.5	47.5
800	78.5	72.0	71.7	70.0	58.7	62.2	77.5	77.0	75.0	46.5
1000	80.7	76.0	75.5	73.2	63.0	66.2	80.2	78.5	78.0	46.0
1250	85.2	81.0	80.2	78.0	67.2	71.0	84.5	82.2	81.7	46.0
1600	86.2	83.5	83.5	80.5	70.5	73.2	86.5	83.2	83.7	47.0
2000	87.0	84.2	85.2	81.2	70.2	74.7	85.2	83.2	84.0	47.0
2500	85.0	81.7	83.5	80.2	69.5	72.5	84.7	83.0	83.2	45.2
3150	83.2	79.7	80.0	79.0	66.7	67.5	81.7	80.7	79.5	45.2
4000	79.5	77.5	77.5	75.5	65.0	68.7	79.2	79.0	78.5	45.2
5000	78.5	76.0	76.0	73.7	65.0	68.5	77.2	77.0	76.2	45.2
6300	77.7	74.2	75.0	73.7	63.5	65.5	74.0	75.2	74.5	47.0
8000	75.0	72.0	73.2	71.7	60.7	60.7	71.5	72.7	72.0	50.5
10000	73.5	69.5	71.5	70.0	57.7	58.0	69.0	70.7	69.2	49.7
DB(A)	95.0	91.5	90.2	88.7	77.0	81.2	93.7	91.7	91.5	55.7
DB(L)	101.0	95.7	92.5	91.5	82.2	84.5	98.0	98.0	95.7	64.7

TWIN OTTER ACOUSTIC DATA - 1/3 O.B. ANALYSIS

	STATIC DATA		GROUND-BASED SYSTEM		61M (200 FT) RADIUS		90 DEG AZIMUTH			
1/3 O.B. FREQ. HZ	FLT 12 RN 2S	FLT 12 RN 16S	FLT 12 RN 3S	FLT 12 RN 5S	FLT 14 RN 21S	FLT 14 RN 22S	FLT 15 RN 4S	FLT 15 RN 6S	FLT 15 RN 17S	FLT 12 RN AMB
50	67.2	65.7	65.5	65.0	61.7	61.5	66.5	65.5	64.7	54.2
63	71.2	70.5	69.2	69.0	64.5	65.5	69.0	68.5	71.2	55.5
80	78.7	78.7	91.5	90.5	85.7	84.5	75.5	74.7	78.0	53.0
100	103.5	97.7	88.0	88.2	71.2	67.0	99.2	98.7	97.0	52.0
125	92.0	78.7	72.7	71.7	66.5	65.7	89.7	88.7	78.2	49.0
160	79.7	76.2	83.2	83.5	78.0	78.2	75.5	75.2	75.0	52.0
200	101.2	92.2	80.7	81.7	68.2	67.2	96.0	95.2	91.7	51.7
250	91.2	77.7	82.2	80.0	73.7	72.7	87.2	85.5	76.0	46.5
315	96.0	87.0	74.7	72.7	65.2	66.0	89.2	89.0	85.0	46.0
400	91.2	80.2	74.0	72.5	60.5	64.5	83.0	83.7	77.7	46.0
500	85.7	77.5	70.7	69.7	60.2	64.7	77.5	79.0	75.0	47.5
630	83.0	73.0	67.7	68.0	59.0	61.7	75.2	77.2	71.7	50.2
800	80.7	73.5	70.0	71.0	59.7	64.0	78.0	78.0	75.7	48.0
1000	81.0	75.0	73.5	72.7	63.0	67.5	80.5	79.0	76.0	46.0
1250	84.0	79.2	78.2	76.5	68.2	71.2	84.0	81.5	80.7	48.0
1600	84.2	81.0	81.5	77.7	71.7	73.7	84.0	83.0	81.5	46.5
2000	83.7	81.0	81.7	78.0	69.7	73.5	83.5	82.2	81.7	47.0
2500	83.7	79.5	80.7	76.7	68.2	72.0	84.0	81.5	81.2	45.5
3150	82.7	78.2	77.0	75.2	66.0	67.0	80.0	79.2	78.5	45.7
4000	79.7	75.7	75.2	72.5	65.2	66.5	79.2	78.7	78.0	45.0
5000	78.5	73.7	73.7	71.5	62.7	64.2	75.7	76.2	75.5	45.0
6300	77.2	73.5	73.5	71.0	62.5	62.7	73.2	75.7	73.5	46.0
8000	75.7	70.5	71.2	69.7	59.7	58.7	71.5	72.5	70.5	49.2
10000	72.7	67.0	69.5	68.0	55.5	56.2	68.0	68.2	67.2	49.7
DB(A)	97.2	90.0	88.5	85.5	78.0	80.0	93.5	92.2	90.2	56.2
DB(L)	105.7	98.2	95.0	94.5	86.2	85.7	100.7	100.2	98.0	65.2

TWIN OTTER ACOUSTIC DATA - 1/3 O.B. ANALYSIS

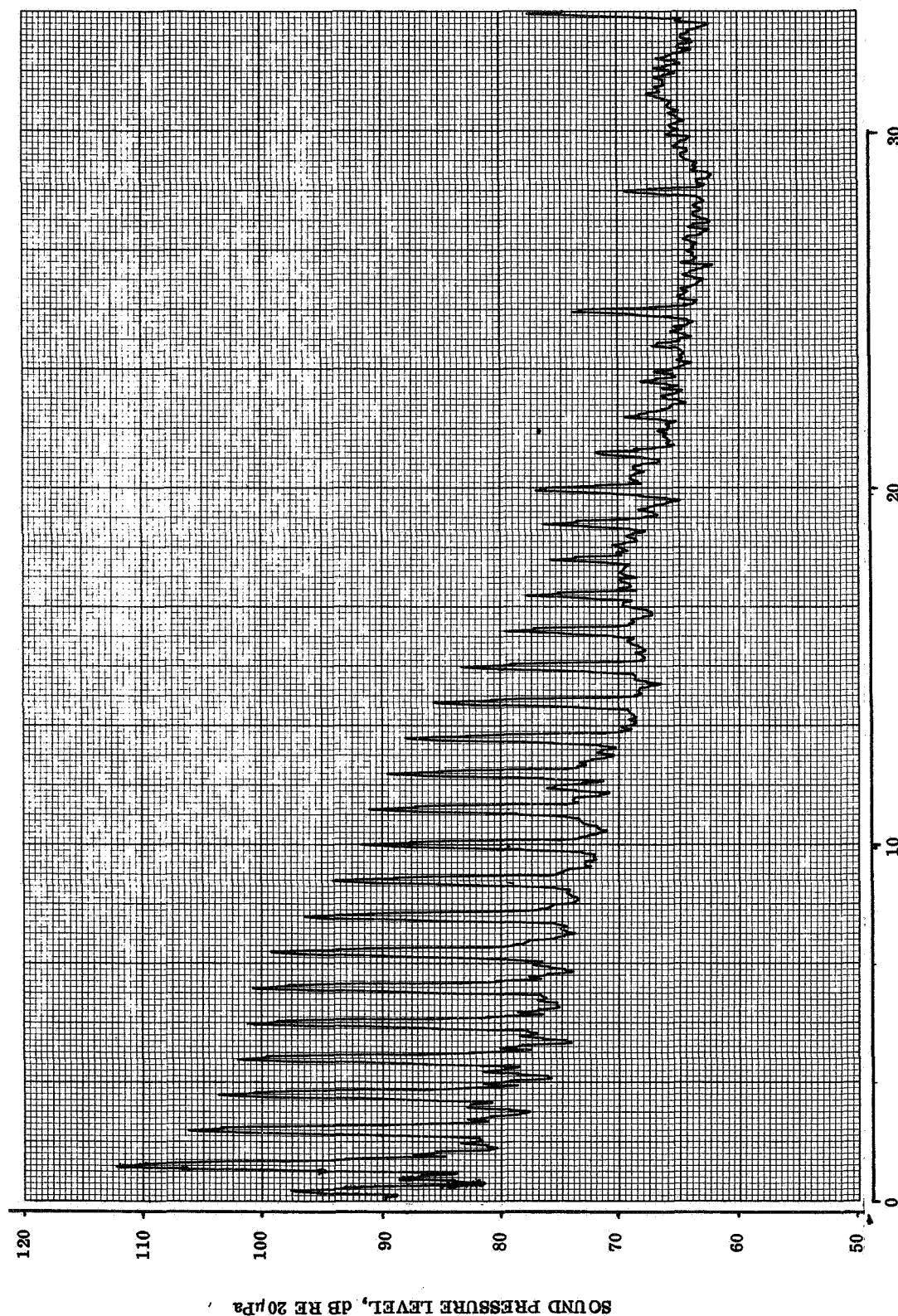
STATIC DATA GROUND-BASED SYSTEM 61M (200 FT) RADIUS 100 DEG AZIMUTH										
1/3 O.B. FREQ. HZ	FLT 12 RN 2S	FLT 12 RN 16S	FLT 12 RN 3S	FLT 12 RN 5S	FLT 14 RN 21S	FLT 14 RN 22S	FLT 15 RN 4S	FLT 15 RN 6S	FLT 15 RN 17S	FLT 12 RN AMB
50	68.7	68.2	67.2	67.0	62.7	64.0	67.7	66.5	66.0	58.2
63	73.5	73.2	72.0	71.7	66.2	67.2	72.7	72.7	74.2	58.0
80	81.5	83.7	95.7	95.5	88.7	87.2	79.2	79.0	82.0	55.2
100	107.0	102.7	92.5	93.0	74.0	68.5	103.0	103.0	101.5	54.0
125	95.5	83.2	75.0	73.7	66.7	66.2	93.2	93.0	82.7	54.7
160	81.7	79.5	82.2	84.7	79.5	77.5	78.7	78.5	78.0	56.7
200	102.7	96.7	80.0	83.0	69.0	67.2	98.0	97.2	95.2	54.7
250	92.5	80.2	85.0	85.2	71.0	73.2	89.5	88.0	78.2	51.0
315	99.5	87.5	78.5	76.7	69.0	77.0	93.7	92.7	84.7	50.7
400	93.2	81.2	77.5	74.5	67.7	71.0	87.5	87.0	79.2	50.2
500	89.0	81.2	74.7	73.0	59.0	65.2	83.2	83.0	76.2	50.7
630	85.7	77.0	69.0	70.7	57.5	60.7	80.0	80.7	76.7	51.7
800	84.0	74.5	70.5	75.0	59.7	63.0	79.7	79.5	77.7	50.7
1000	81.5	76.7	74.0	77.2	62.7	66.7	80.0	80.5	77.5	51.0
1250	83.0	80.7	78.7	79.0	68.5	71.0	81.7	82.5	82.5	50.7
1600	84.0	82.5	81.0	81.0	71.5	73.5	83.5	83.0	83.2	51.7
2000	84.0	81.7	80.7	79.5	68.7	72.2	83.0	82.7	83.2	52.0
2500	83.2	80.5	80.0	77.0	68.0	69.5	82.5	80.0	81.2	50.2
3150	82.2	78.7	77.0	75.5	66.7	67.2	79.7	78.7	79.2	51.0
4000	80.0	77.2	75.0	73.7	65.0	65.0	79.5	78.0	78.2	51.2
5000	79.0	76.0	73.5	72.7	63.0	64.0	76.0	76.0	77.2	53.2
6300	77.7	74.0	73.2	72.0	62.2	62.0	73.2	74.2	76.0	55.0
8000	75.0	72.0	70.7	71.2	60.0	58.7	71.2	73.2	73.0	57.0
10000	73.0	69.5	68.5	68.7	56.5	55.7	68.7	70.5	70.2	56.0
DB(A)	98.2	91.5	88.2	87.7	78.5	80.0	94.0	94.0	92.2	62.2
DB(L)	108.2	103.0	98.5	98.5	88.7	87.7	104.0	104.0	101.5	68.7

TWIN OTTER ACOUSTIC DATA - 1/3 O.B. ANALYSIS

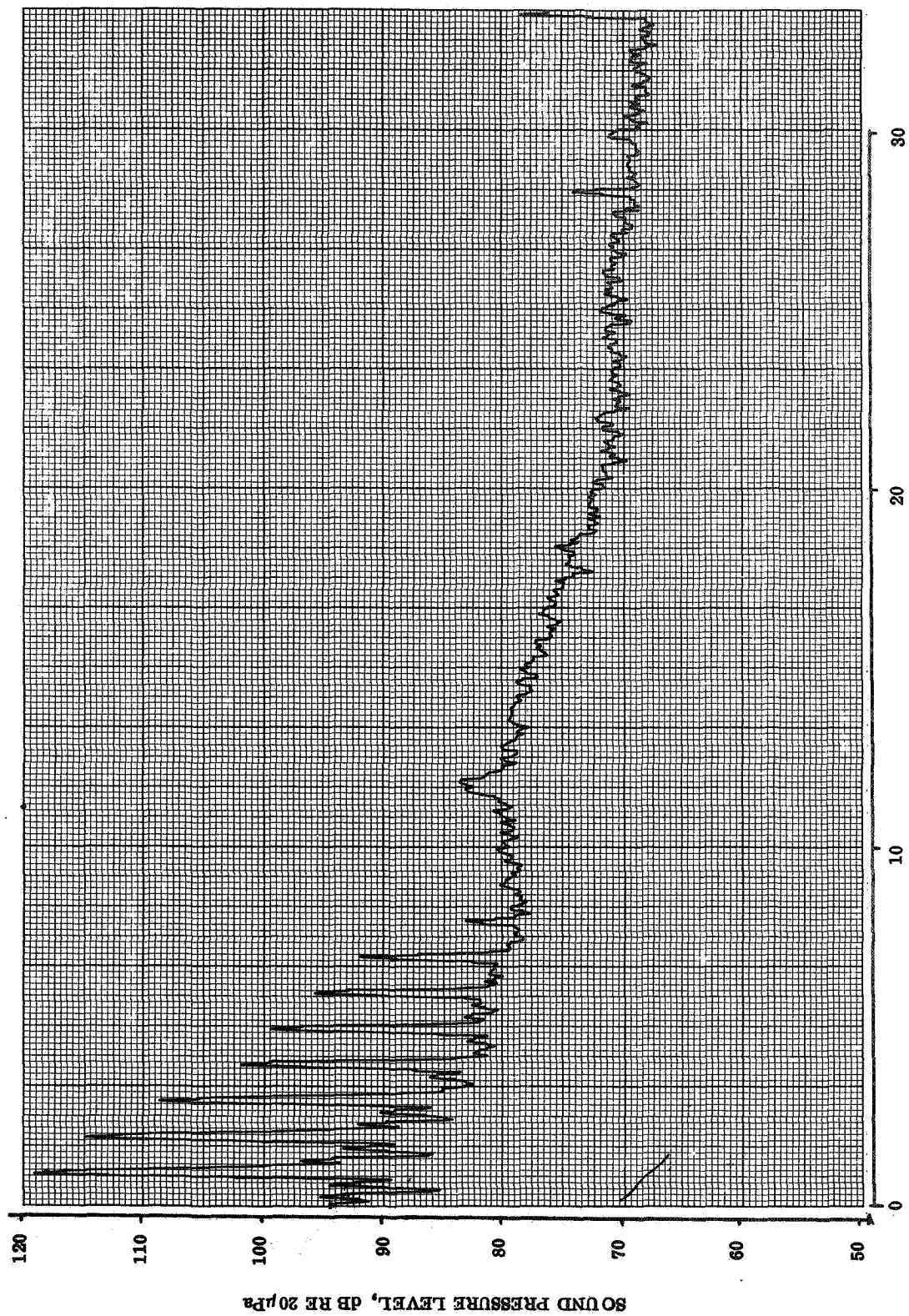
STATIC DATA GROUND-BASED SYSTEM 61M (200 FT) RADIUS 110 DEG AZIMUTH

1/3 O.B. FREQ. HZ	FLT 12 RN 2S	FLT 12 RN 16S	FLT 12 RN 3S	FLT 12 RN 5S	FLT 14 RN 21S	FLT 14 RN 22S	FLT 15 RN 4S	FLT 15 RN 6S	FLT 15 RN 17S	FLT 12 RN AMB
50	68.5	67.7	67.7	67.2	64.0	66.0	68.7	67.0	66.2	54.5
63	73.2	73.7	73.0	72.5	66.7	65.7	73.0	73.0	74.7	58.0
80	82.7	85.2	97.0	96.5	89.5	85.0	80.2	80.0	83.2	53.0
100	108.2	104.0	93.7	94.0	75.0	67.2	104.2	104.5	102.5	52.0
125	96.7	84.5	75.2	74.0	66.0	65.7	94.7	94.7	83.7	50.5
160	82.0	79.2	83.5	87.5	80.5	78.7	79.5	80.0	77.5	54.7
200	103.0	96.2	81.7	85.5	69.7	69.0	98.2	97.7	94.5	55.5
250	92.2	80.0	84.7	85.0	73.0	77.0	89.7	88.5	78.5	50.0
315	95.5	88.0	80.2	78.0	72.0	79.5	92.7	90.2	85.0	50.0
400	87.2	86.5	80.2	77.5	65.0	74.5	85.0	83.0	83.7	50.0
500	84.5	78.7	74.7	74.5	61.0	66.0	80.7	82.7	78.0	50.0
630	79.5	76.0	69.2	73.2	59.7	63.7	76.5	79.7	77.5	51.5
800	80.0	75.0	72.2	76.2	60.0	65.2	78.2	81.7	79.2	50.0
1000	80.5	76.2	75.0	77.5	63.5	68.0	78.2	80.0	80.7	50.0
1250	80.7	78.2	78.5	79.7	68.0	71.5	81.0	81.7	83.0	50.0
1600	83.5	81.5	82.0	81.2	70.5	74.0	84.0	85.0	83.7	50.0
2000	83.0	82.0	82.2	79.7	69.5	72.7	83.0	83.5	82.7	50.0
2500	82.7	80.2	79.0	77.0	67.2	70.5	84.0	81.2	81.7	50.0
3150	80.7	79.2	77.0	74.7	66.2	68.5	81.0	79.7	80.5	50.0
4000	80.5	77.5	75.2	74.7	64.2	65.7	78.0	78.5	79.0	50.0
5000	78.0	74.7	72.2	72.0	62.2	63.0	75.5	76.7	77.7	50.0
6300	77.0	73.7	72.0	72.0	61.2	61.7	75.0	75.0	76.5	50.0
8000	75.2	71.0	70.5	70.5	59.5	59.2	73.5	73.0	73.2	52.2
10000	72.0	67.7	67.5	67.7	55.7	55.5	70.5	69.7	71.2	52.7
DB(A)	96.7	92.2	88.7	89.0	78.2	81.0	94.0	94.0	92.2	59.0
DB(L)	108.2	104.0	99.2	99.7	89.5	87.5	104.5	105.0	102.5	69.0

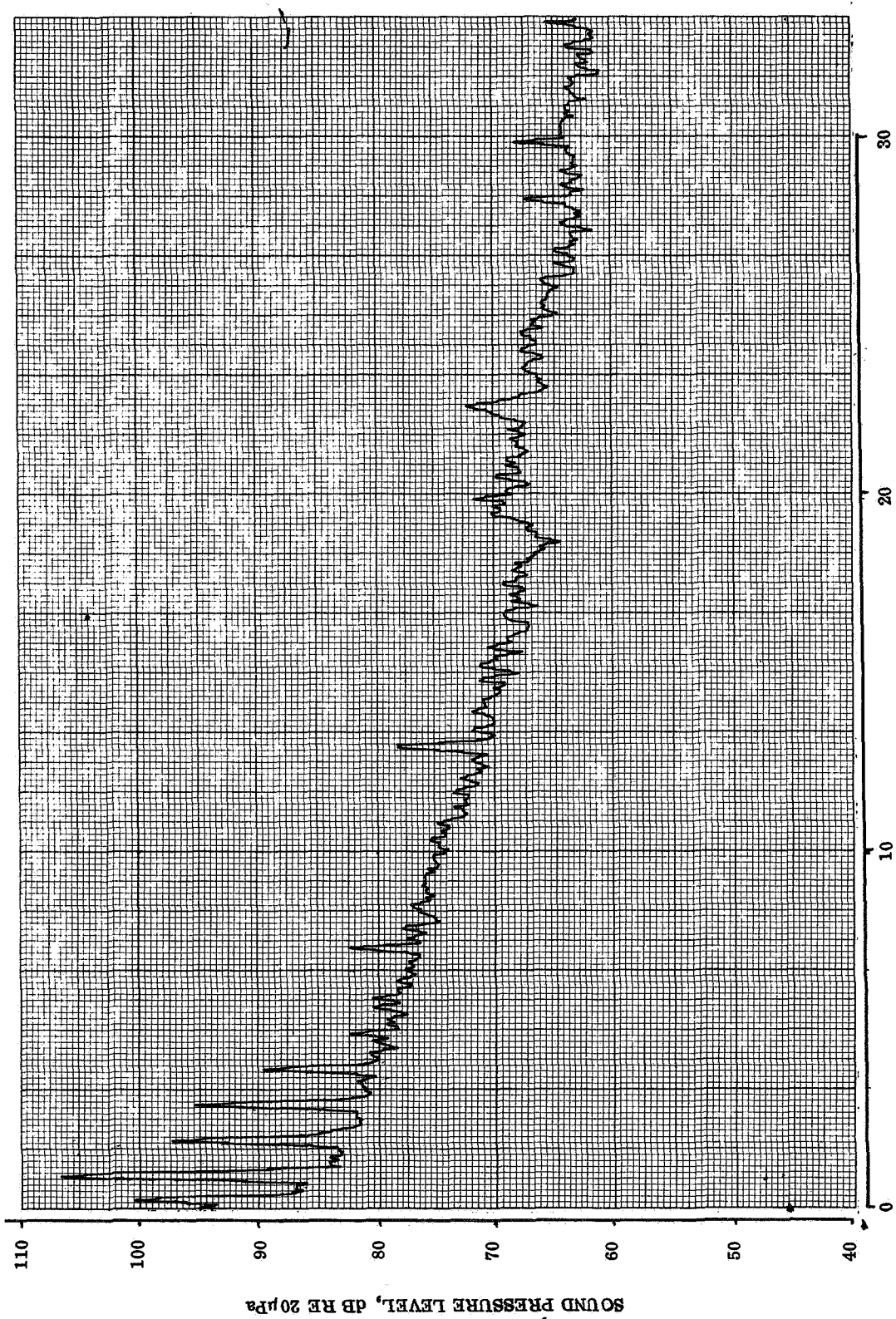
**APPENDIX E - WING-TIP MICROPHONE DATA
NARROW-BAND SPECTRUM PLOTS**



FLIGHT 8
HARMONICS OF BLADE PASSING FREQUENCY
RUN 2
IN-PLANE MICROPHONE



+



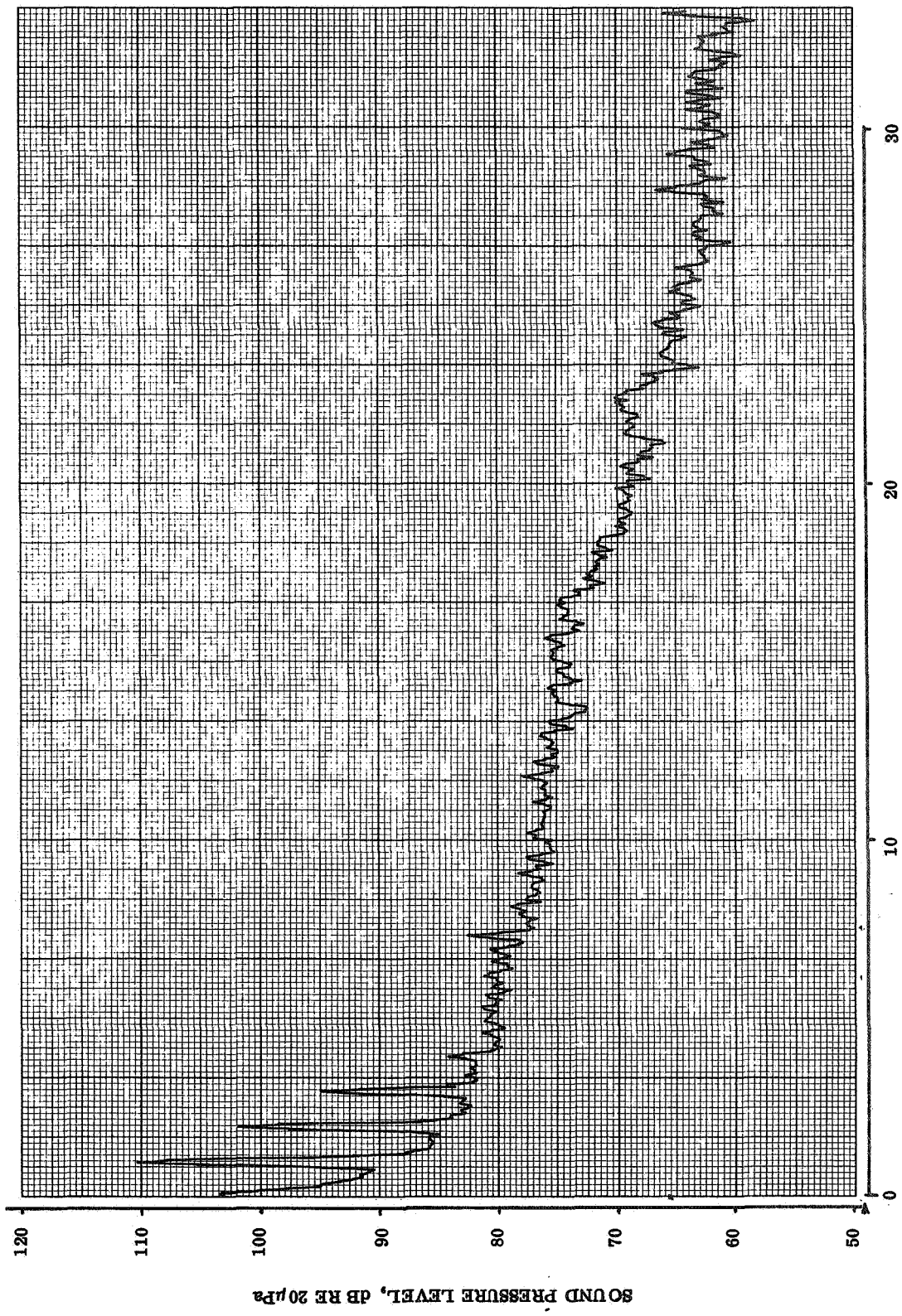
SOUND PRESSURE LEVEL, DB RE 20 μ Pa

HARMONICS OF BLADE PASSING FREQUENCY

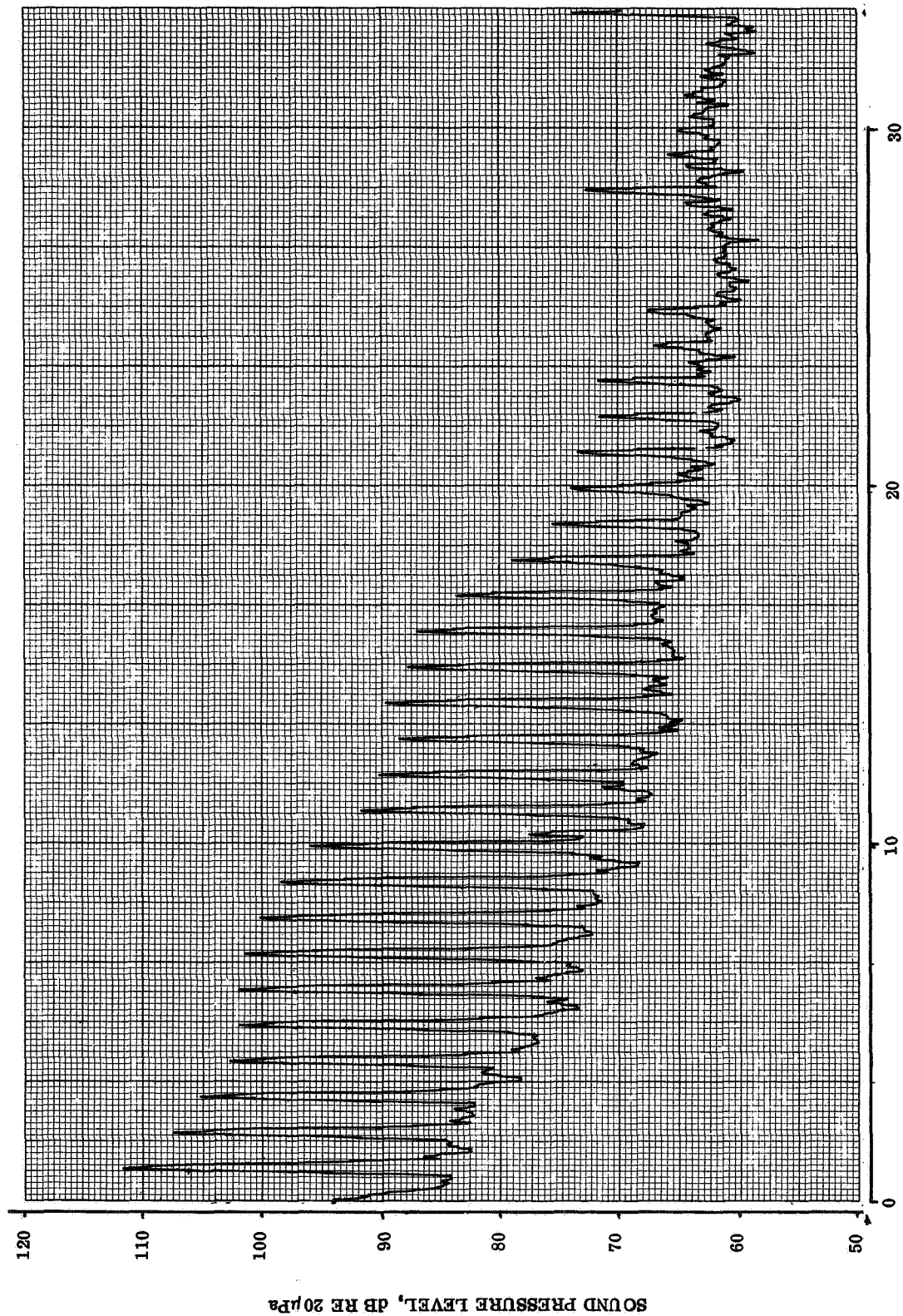
FLIGHT 7

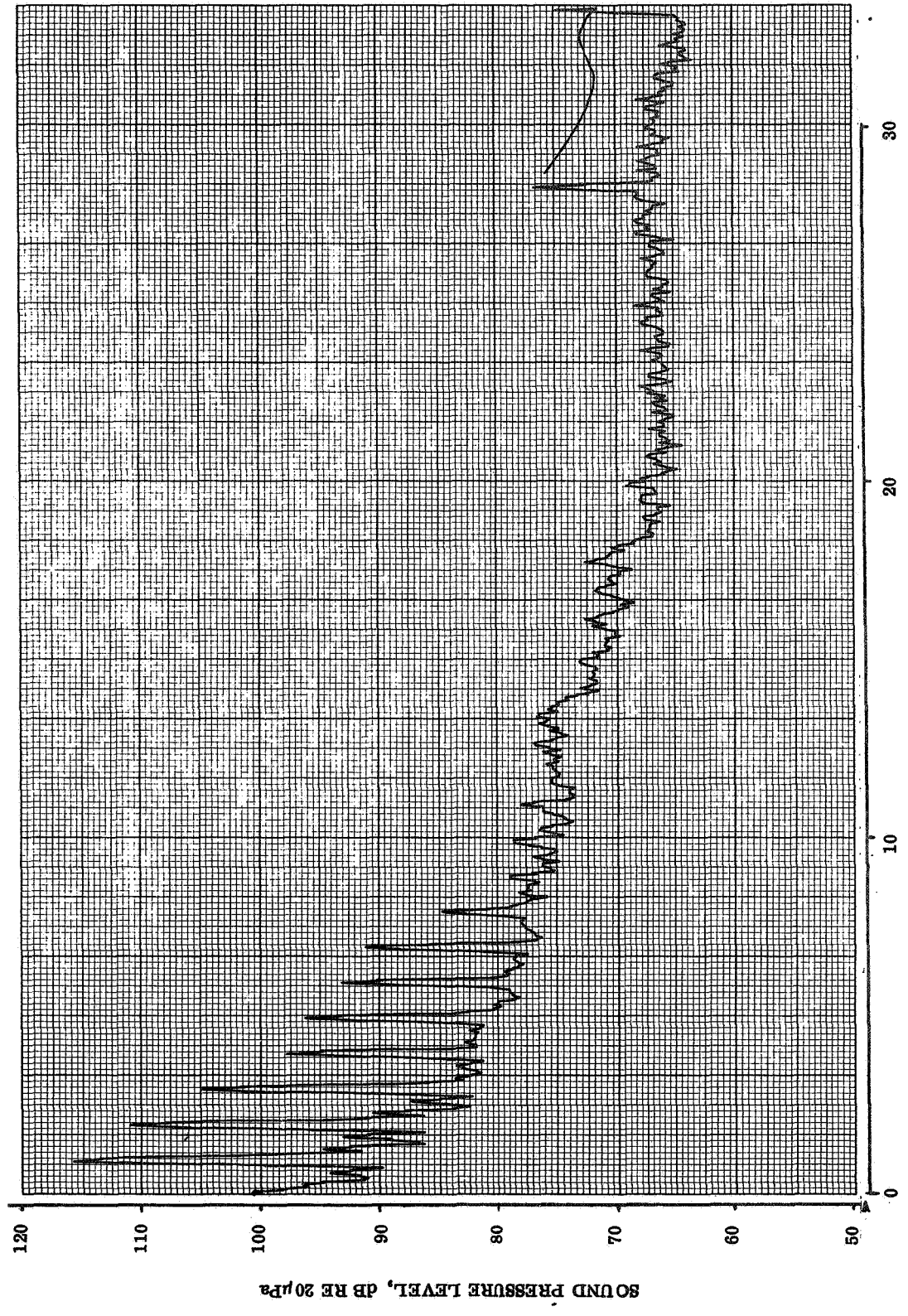
RUN 3A

IN-PLANE MICROPHONE



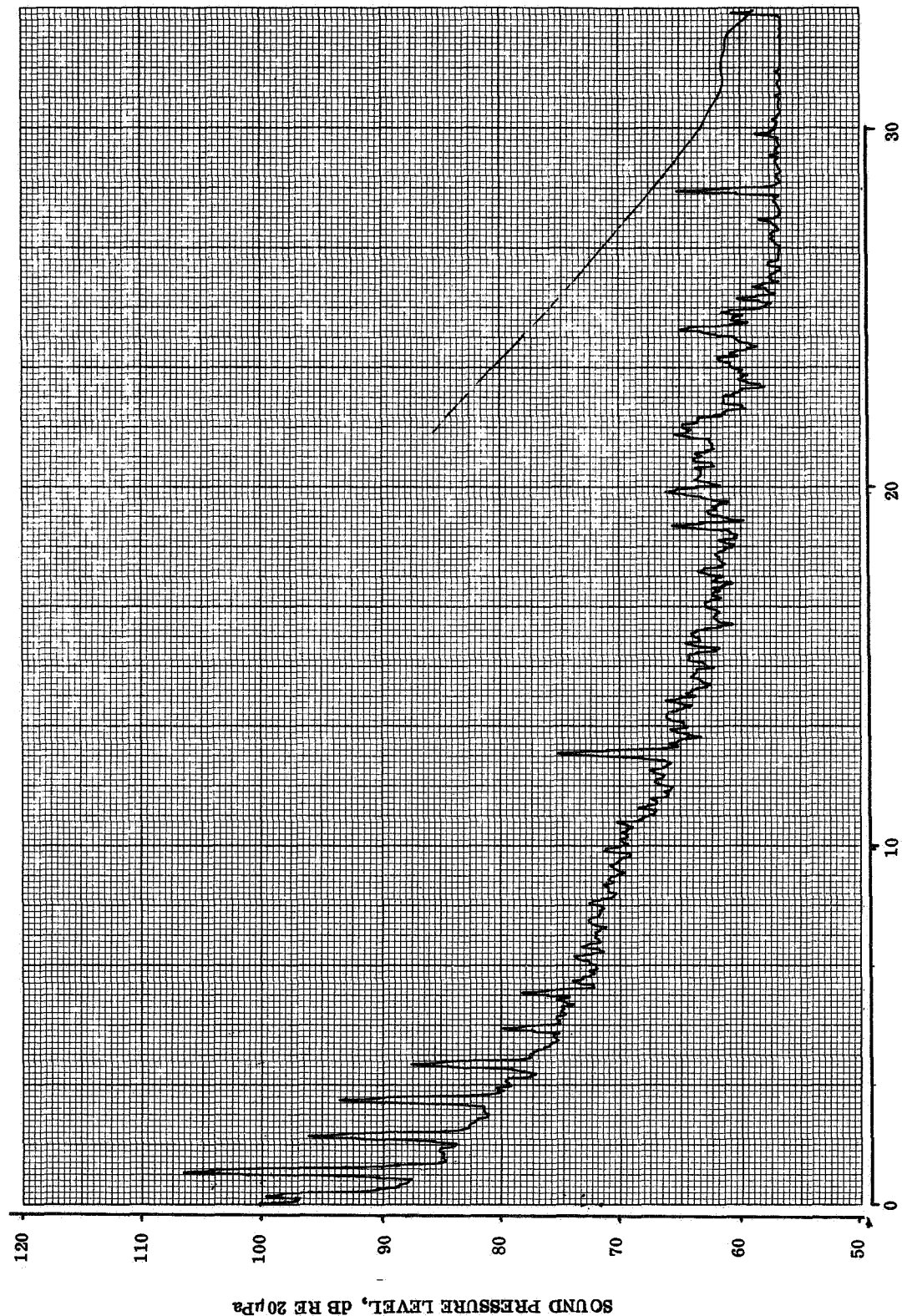
FLIGHT 10 RUN 3A AFT MICROPHONE





FLIGHT 7
HARMONICS OF BLADE PASSING FREQUENCY
RUN 4
AFT MICROPHONE

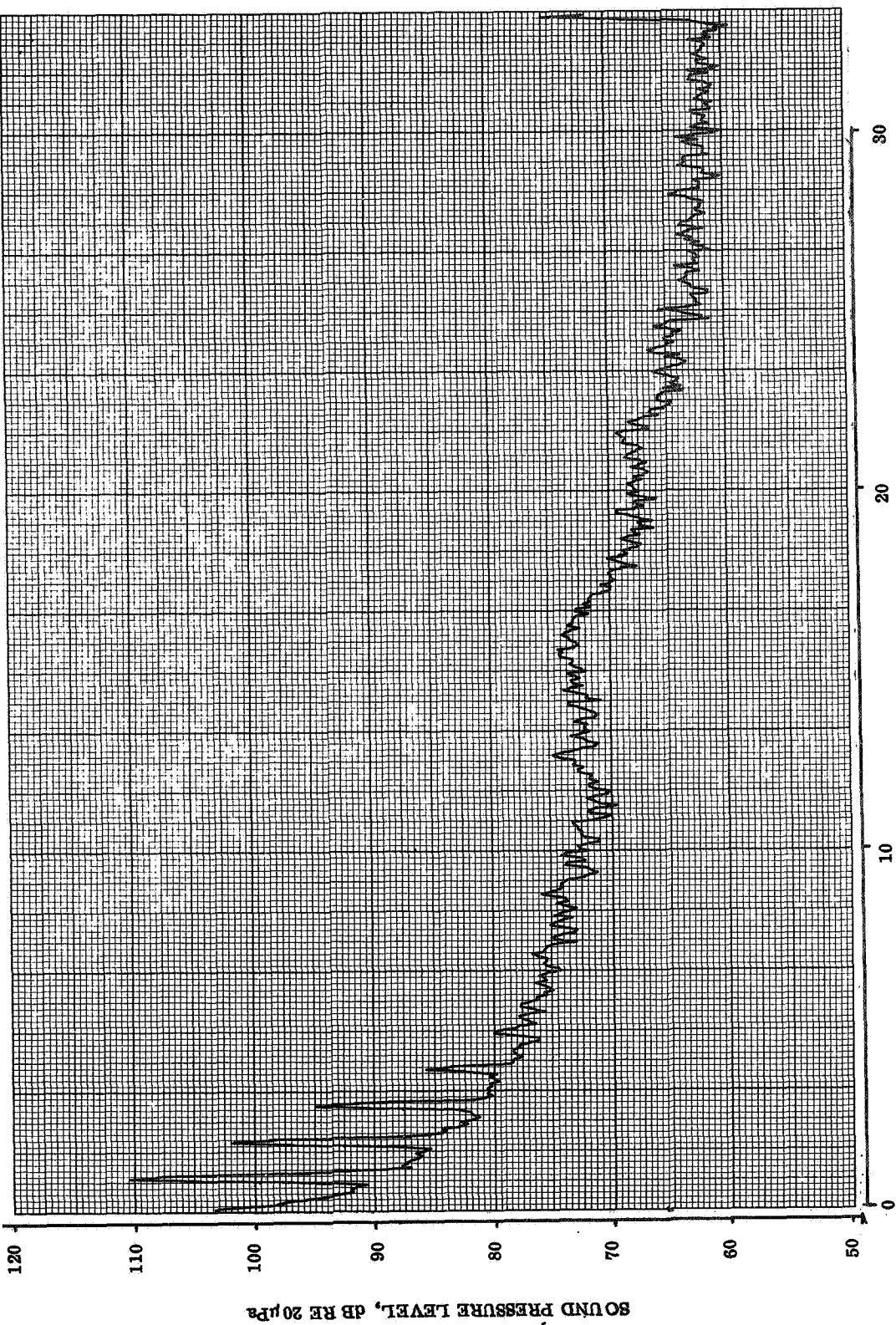
T



SOUND PRESSURE LEVEL, DB RE 20 μ Pa

HARMONICS OF BLADE PASSING FREQUENCY

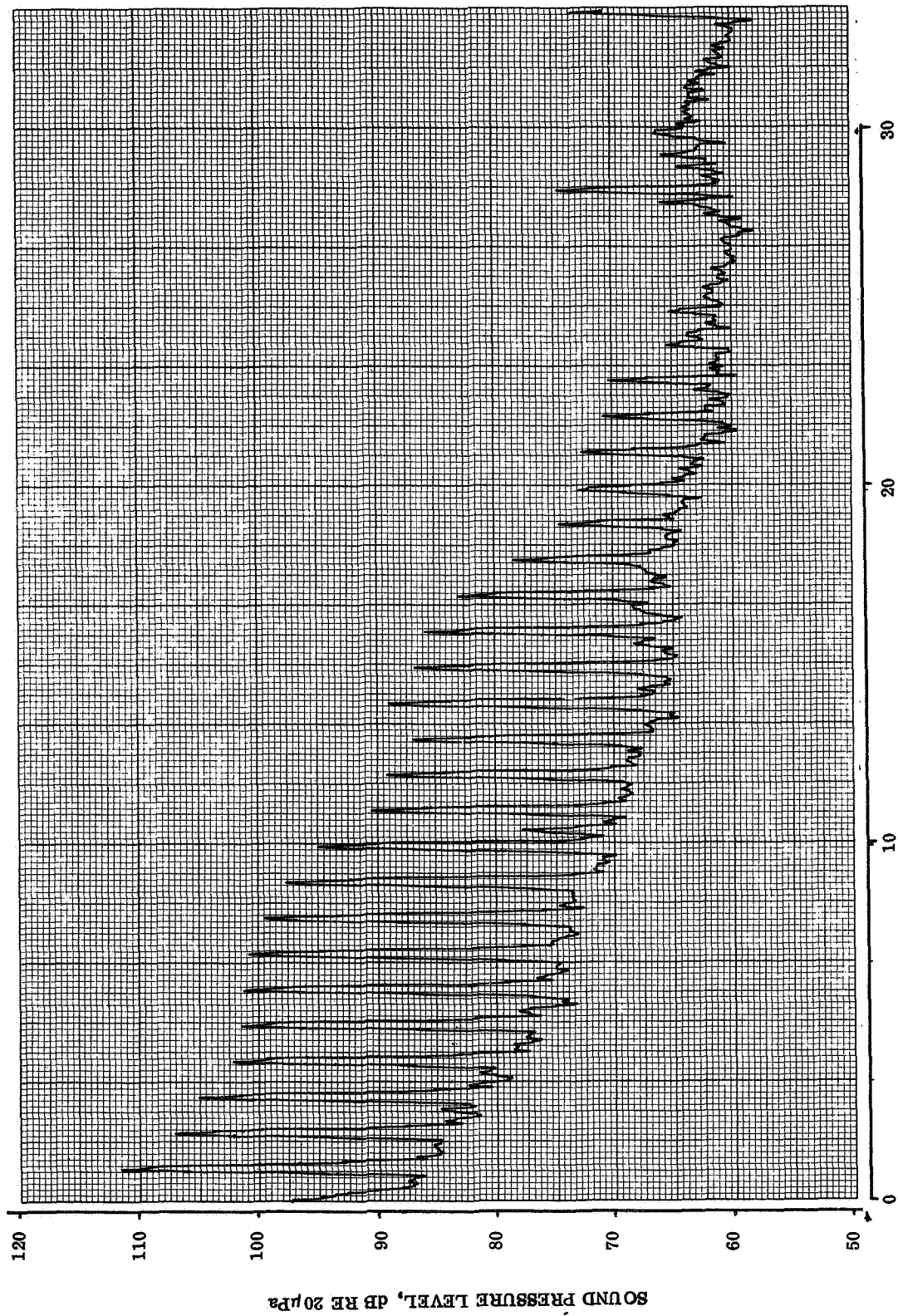
FLIGHT 7 RUN 5 IN-PLANE MICROPHONE



AFT MICROPHONE

RUN 5

FLIGHT 7

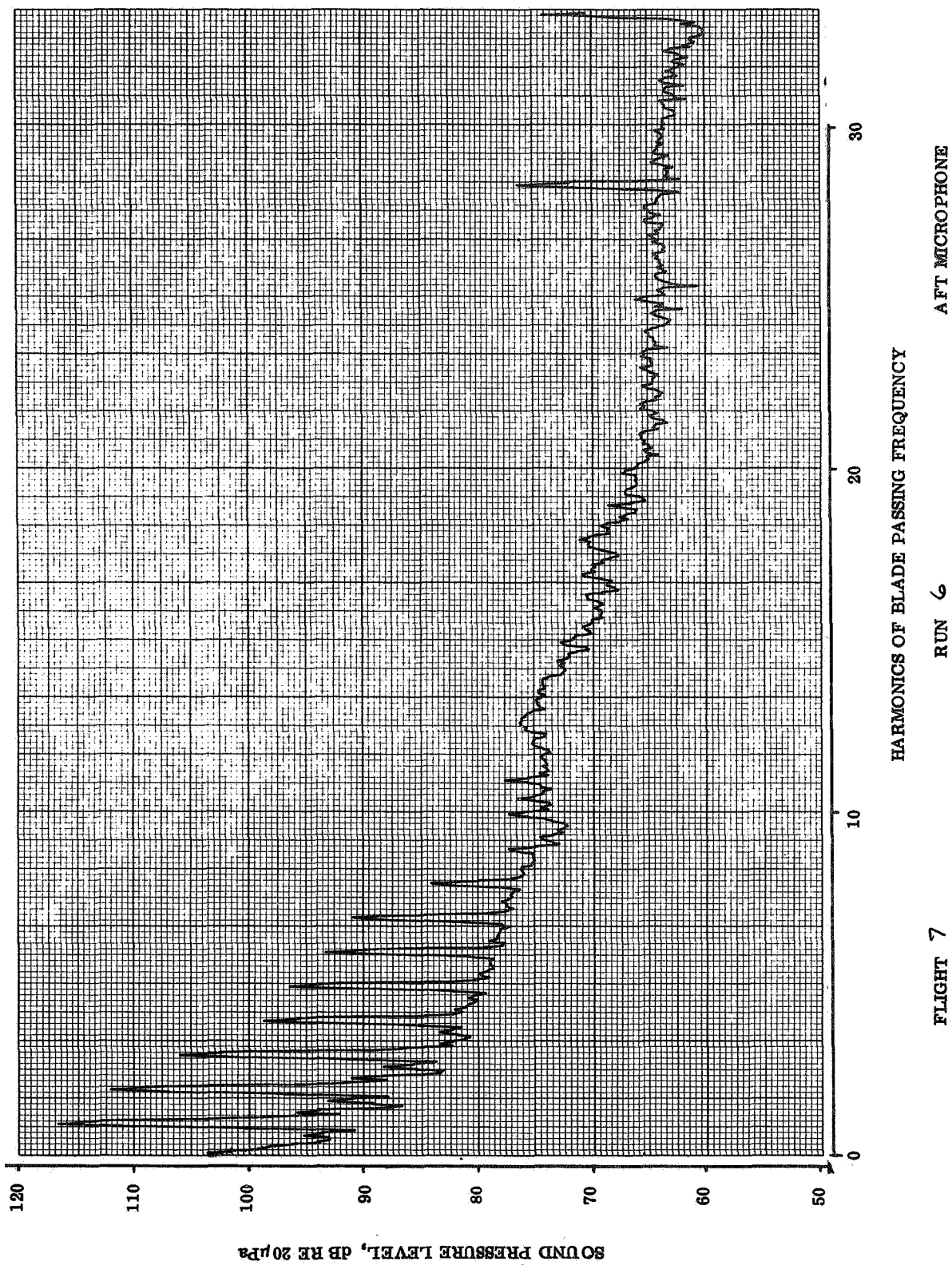


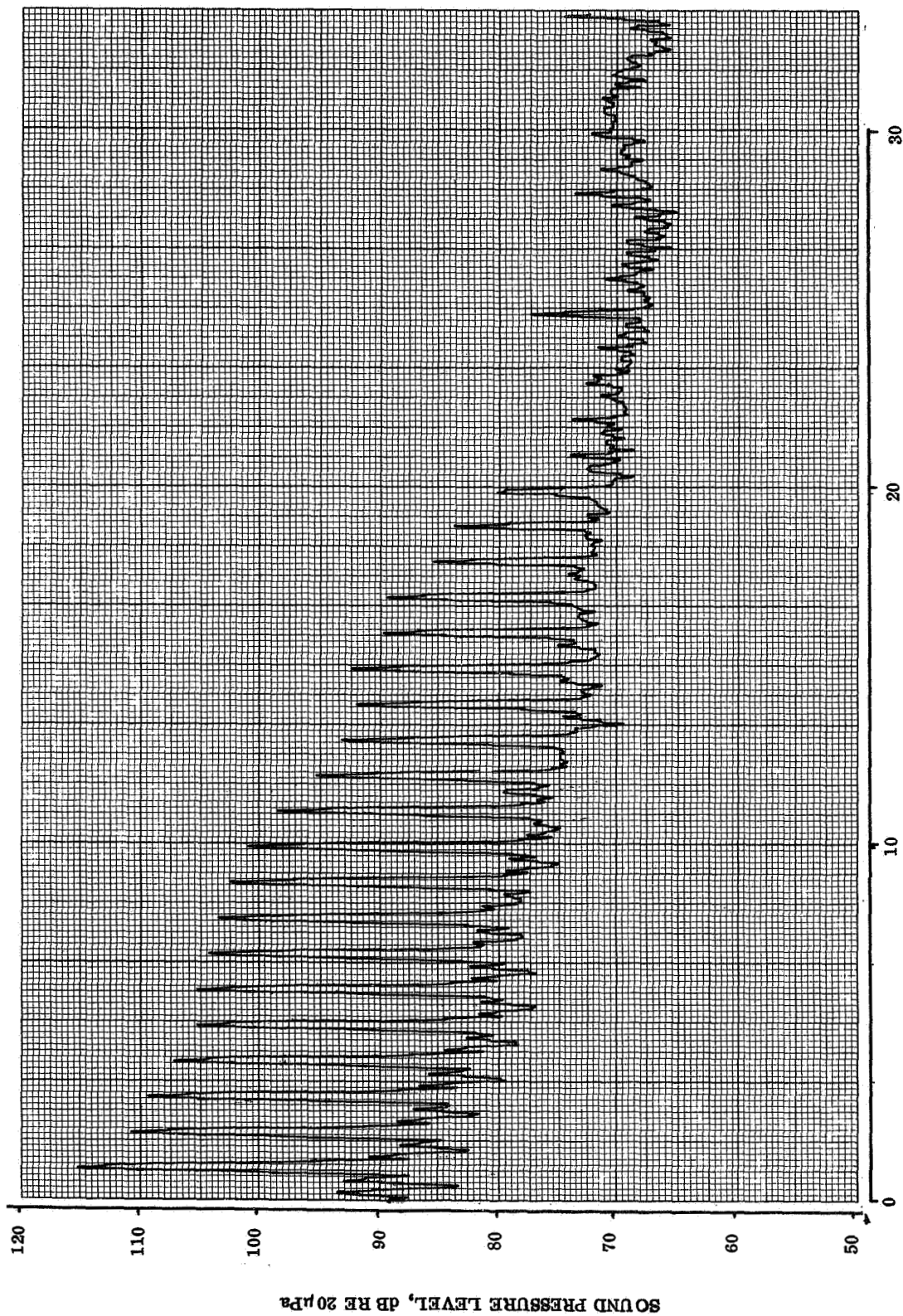
HARMONICS OF BLADE PASSING FREQUENCY

IN-PLANE MICROPHONE

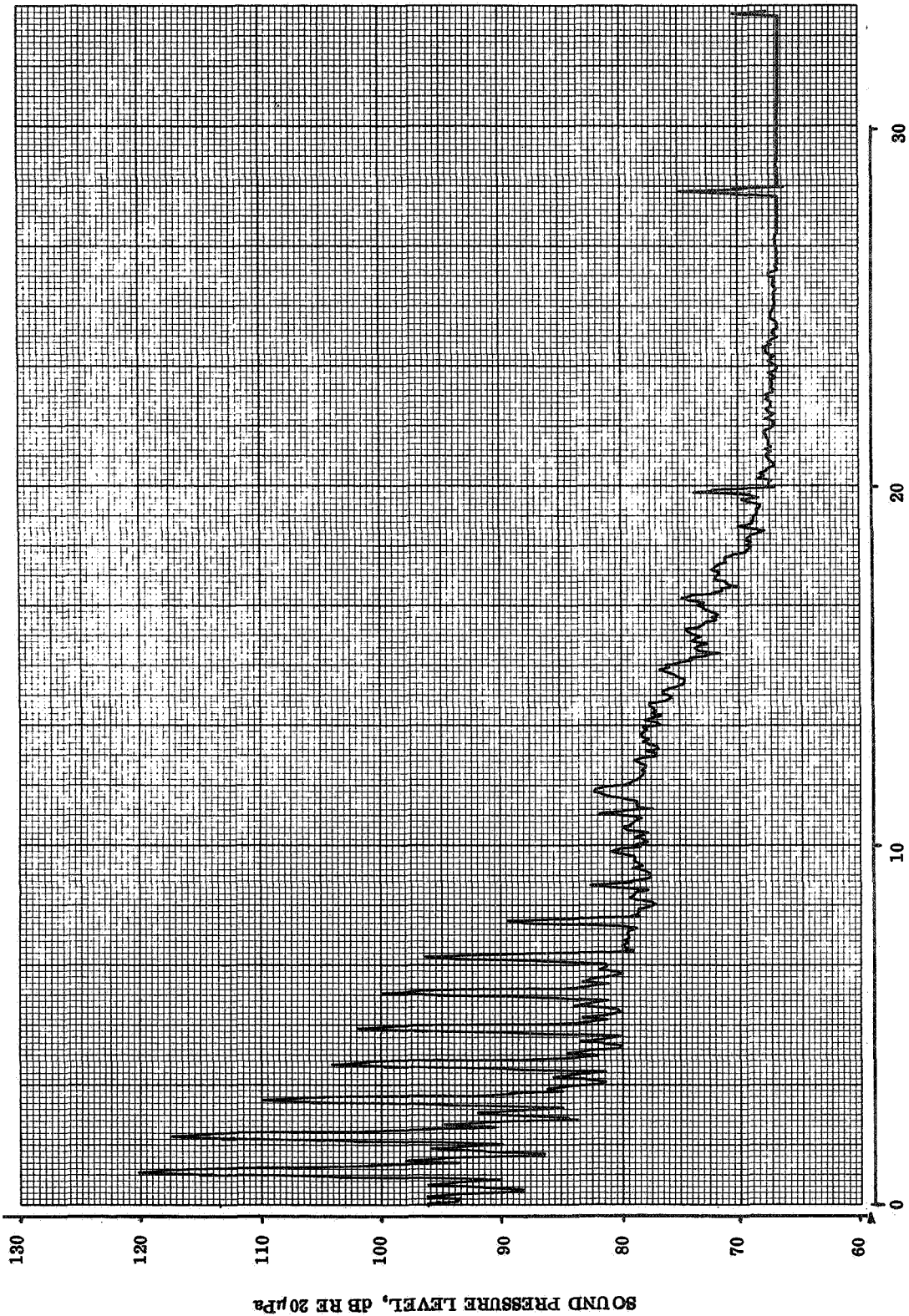
RUN 6

FLIGHT 7





FLIGHT 7
HARMONICS OF BLADE PASSING FREQUENCY
RUN 8
IN-PLANE MICROPHONE

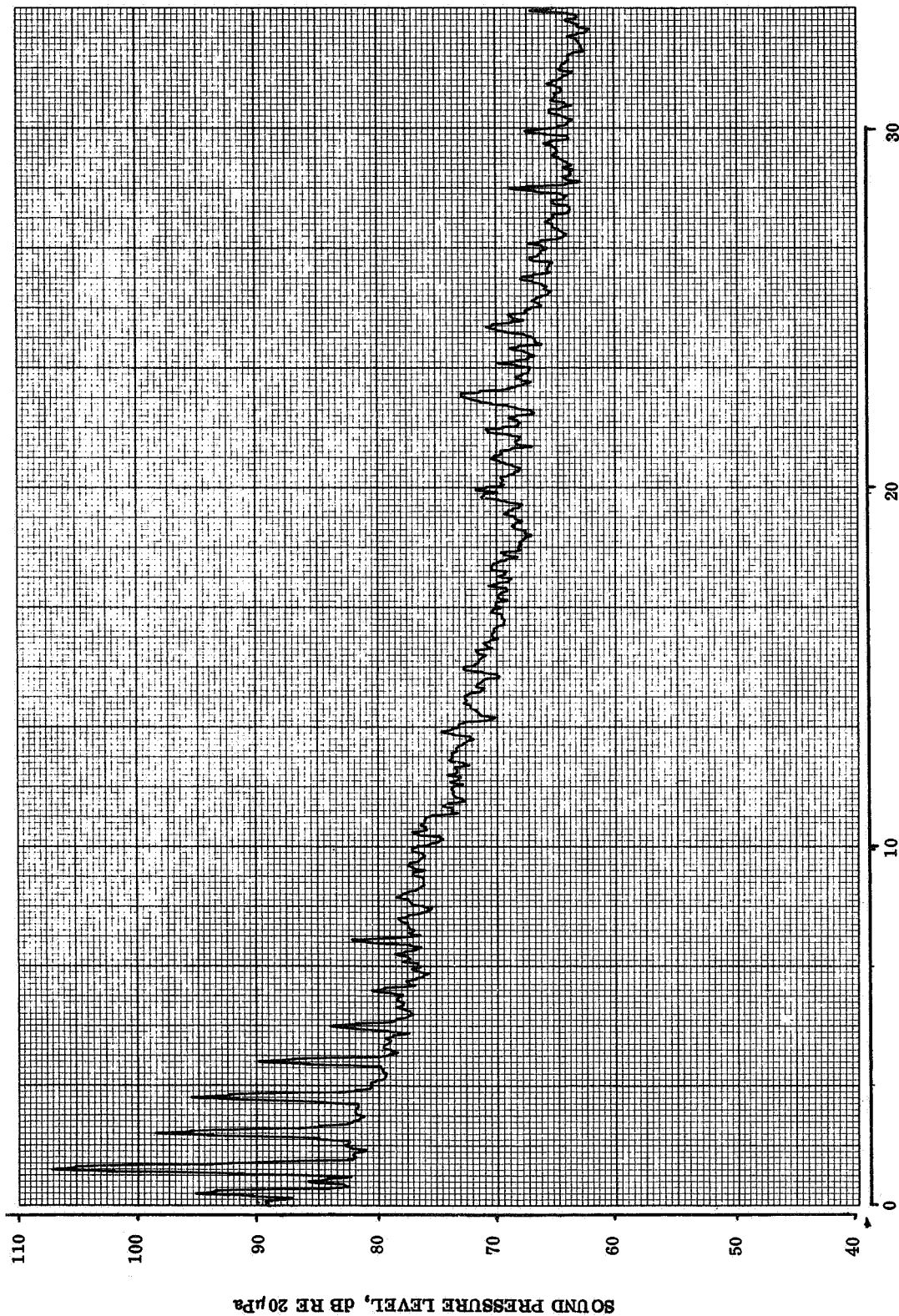


HARMONICS OF BLADE PASSING FREQUENCY

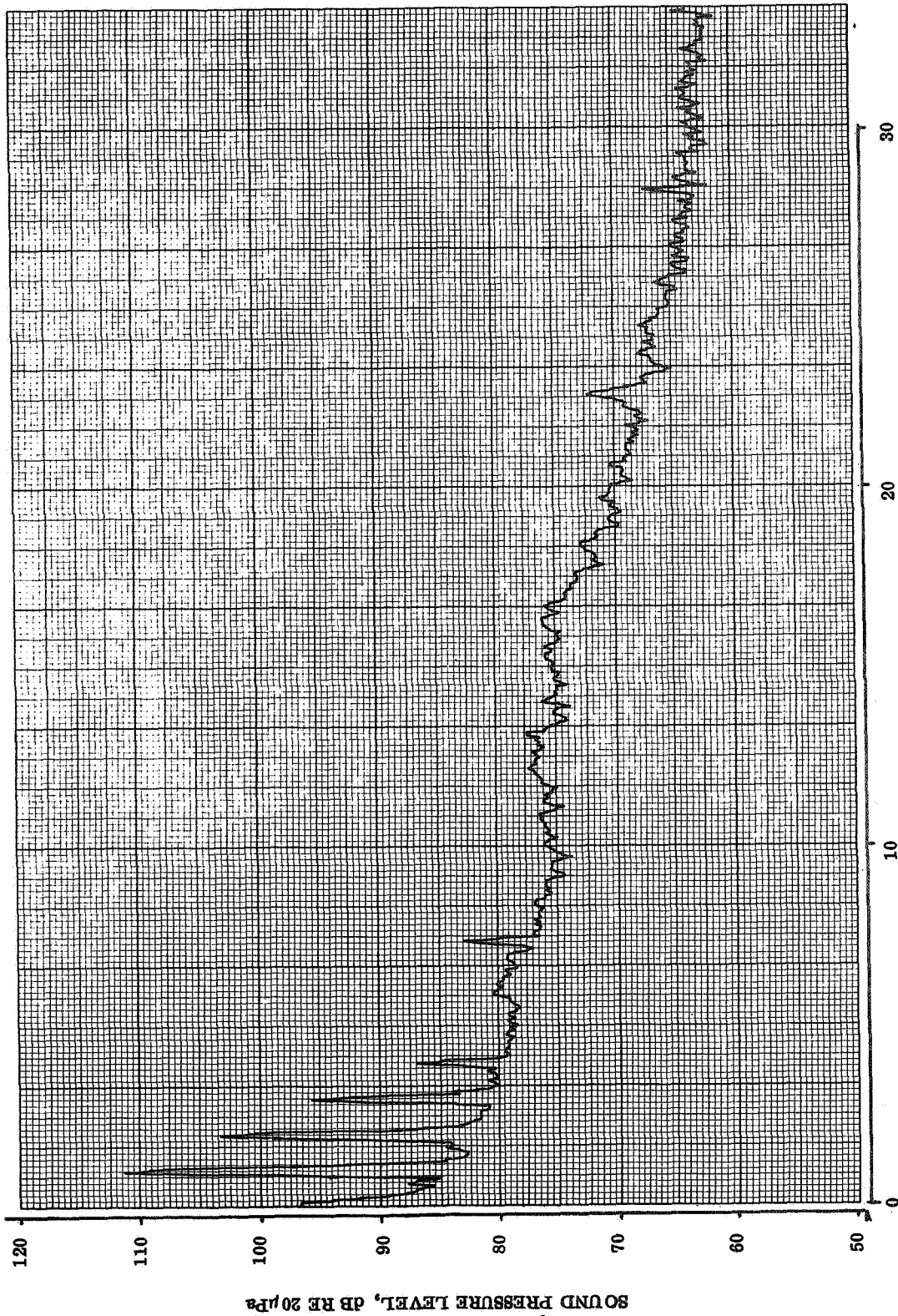
AFT MICROPHONE

RUN 8

FLIGHT 7



FLIGHT 7
HARMONICS OF BLADE PASSING FREQUENCY
RUN 9
IN-PLANE MICROPHONE

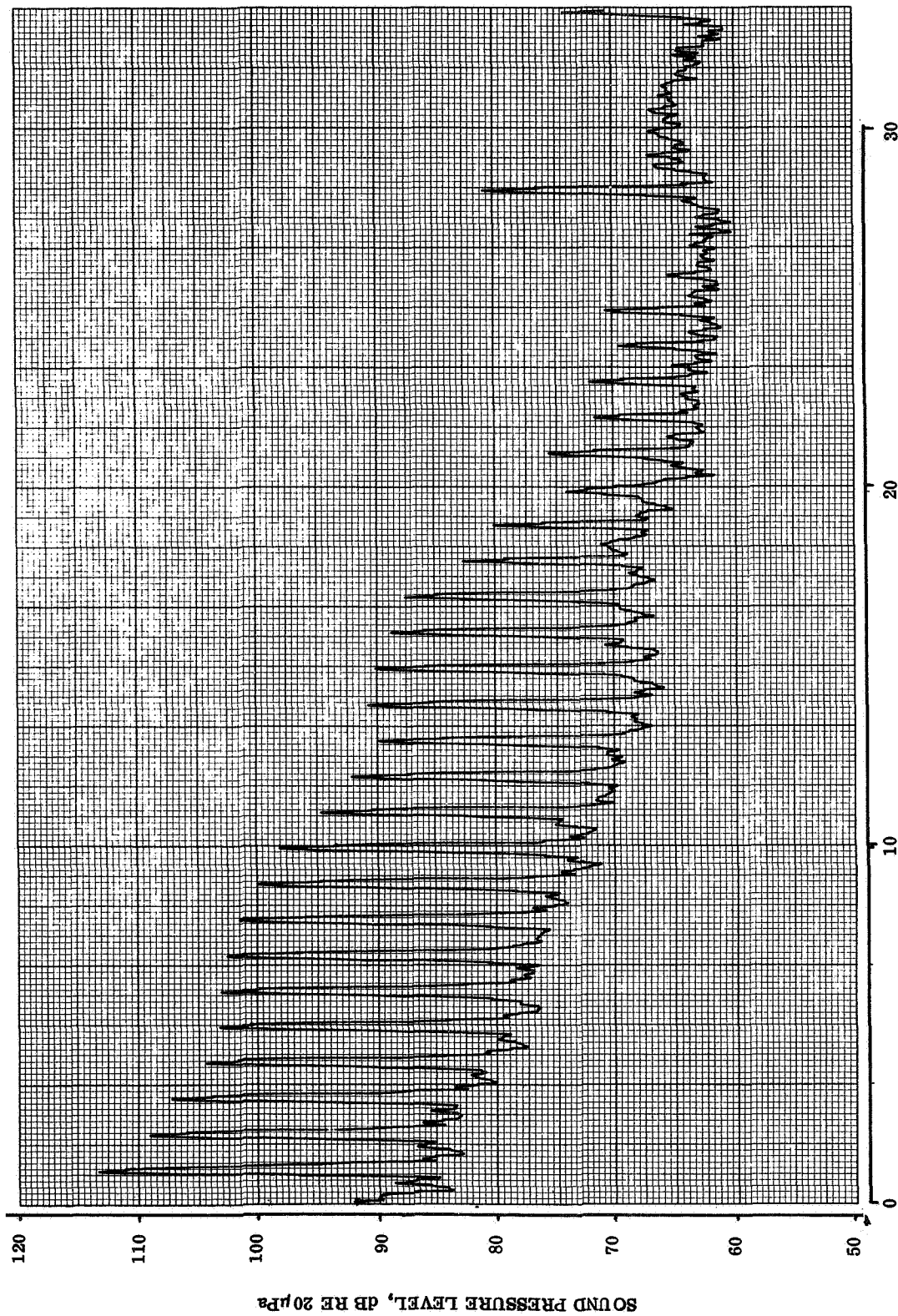


HARMONICS OF BLADE PASSING FREQUENCY

AFT MICROPHONE

RUN 9

FLIGHT 7

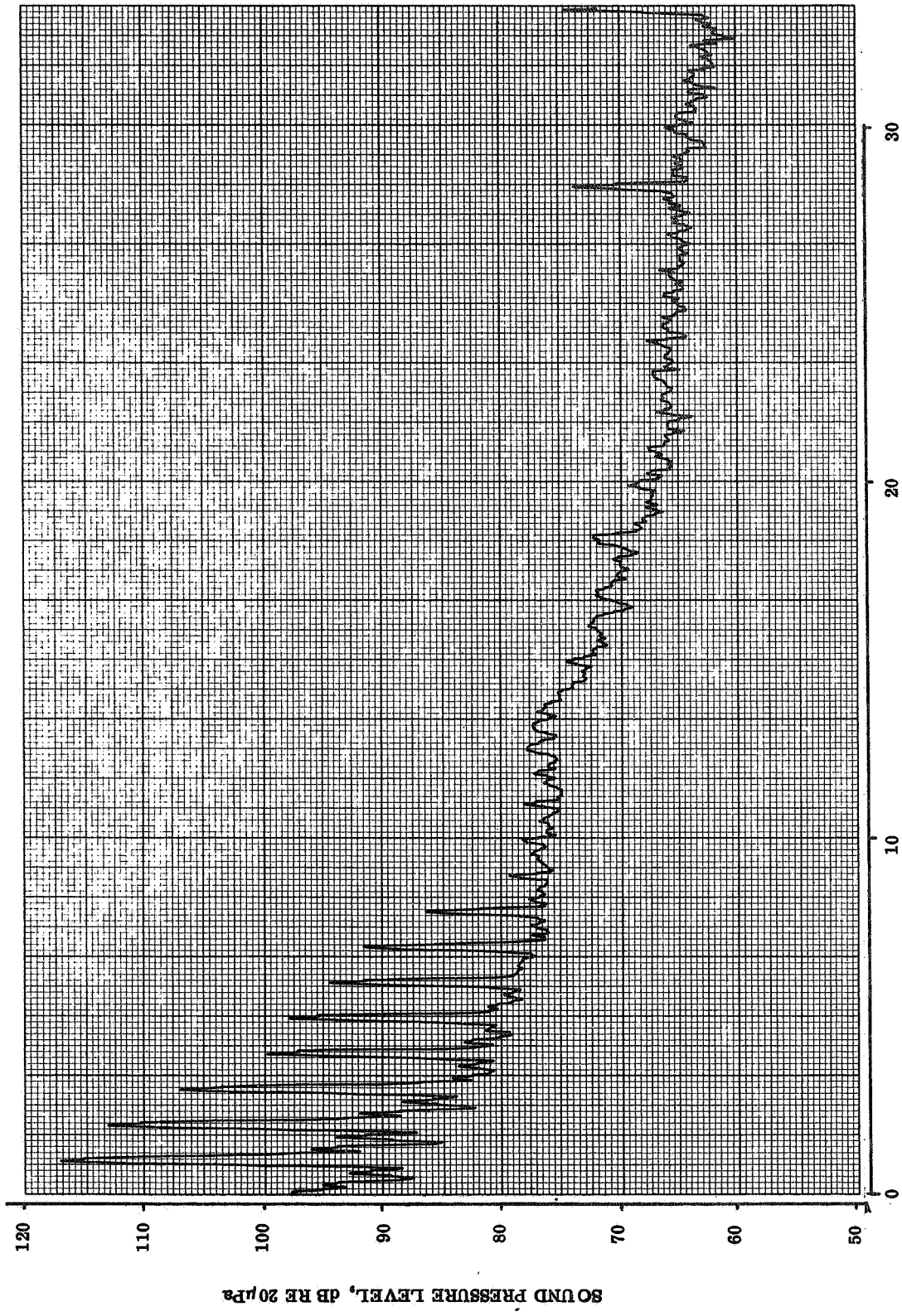


HARMONICS OF BLADE PASSING FREQUENCY

IN-PLANE MICROPHONE

RUN 10

FLIGHT 7

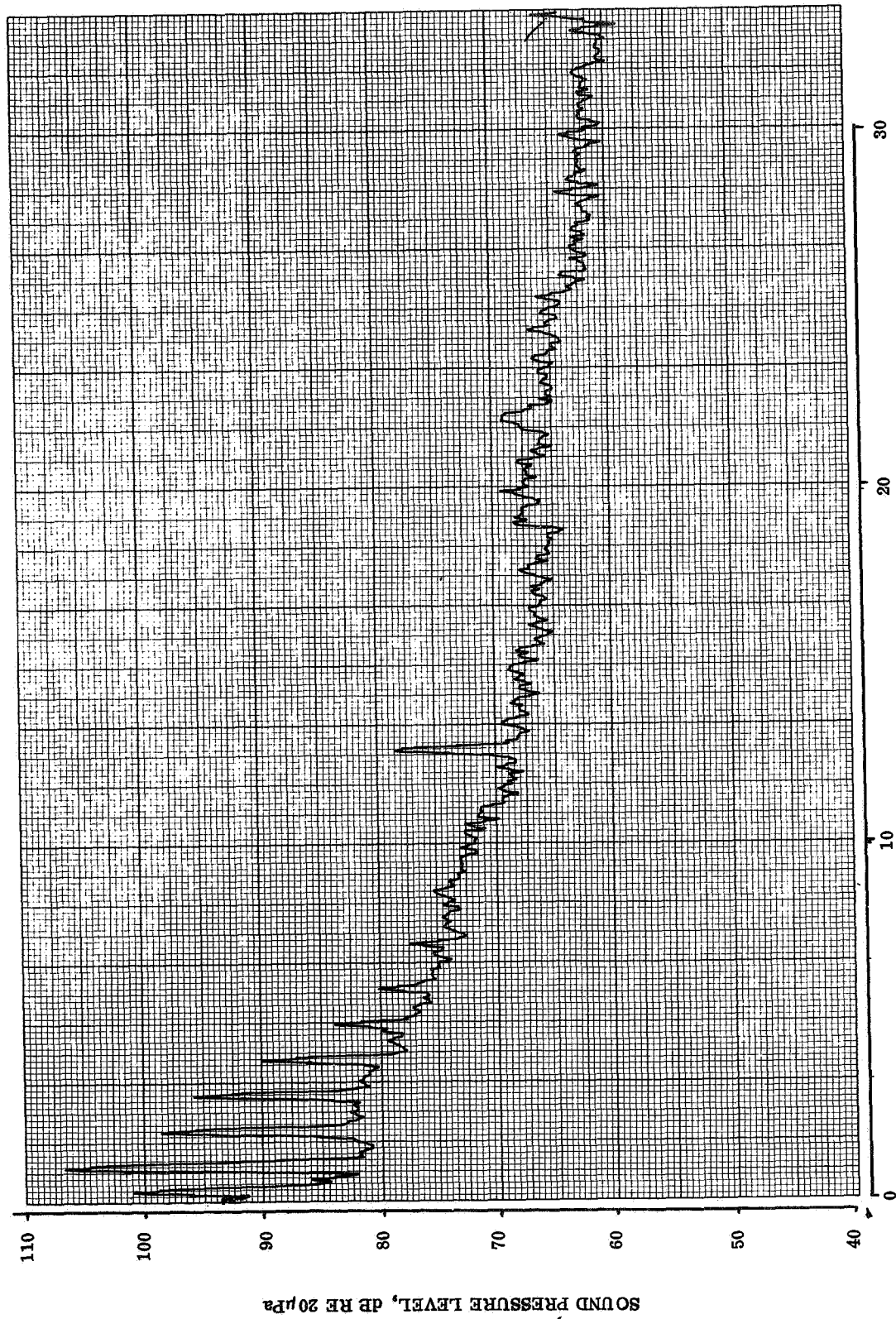


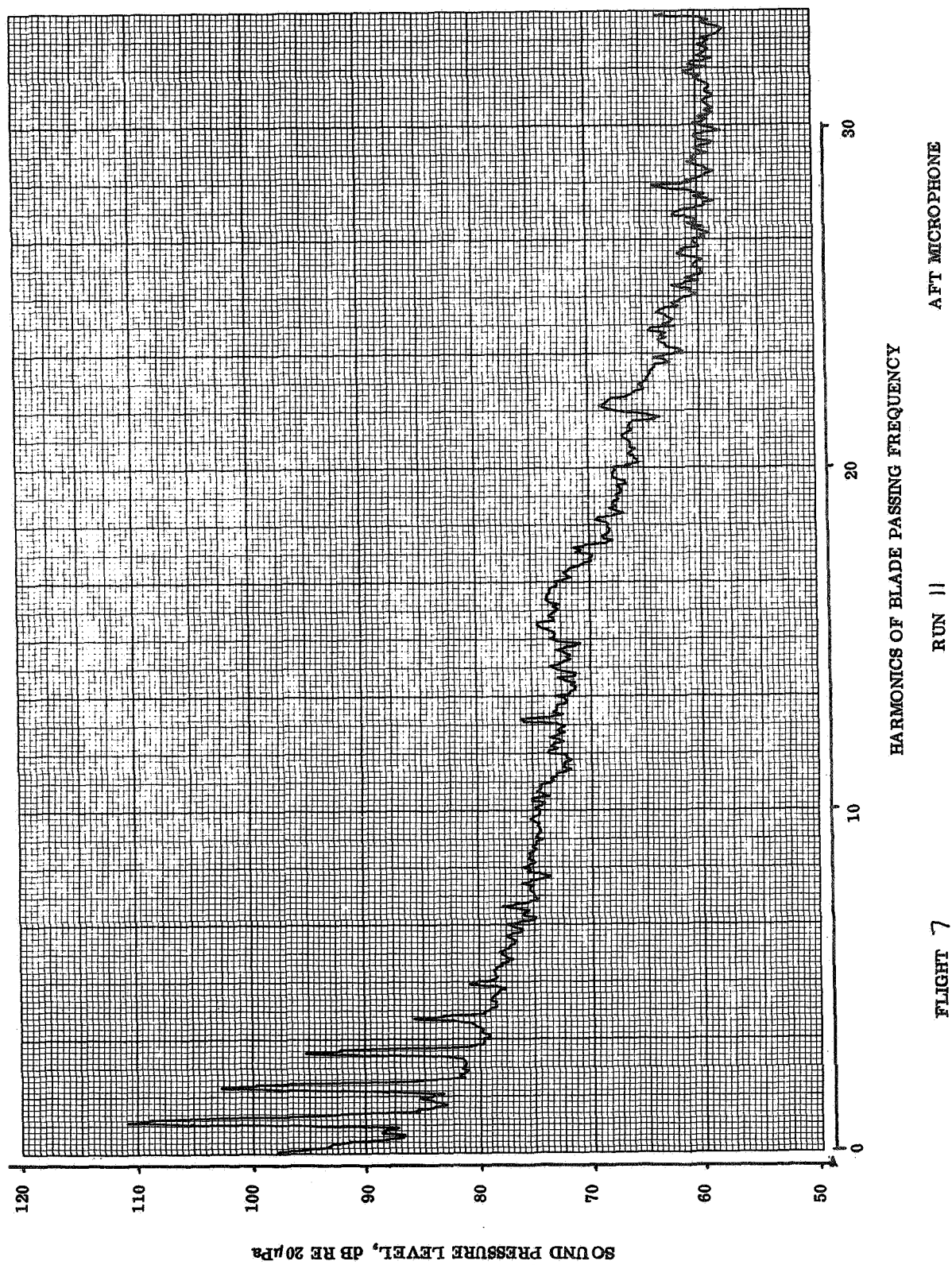
HARMONICS OF BLADE PASSING FREQUENCY

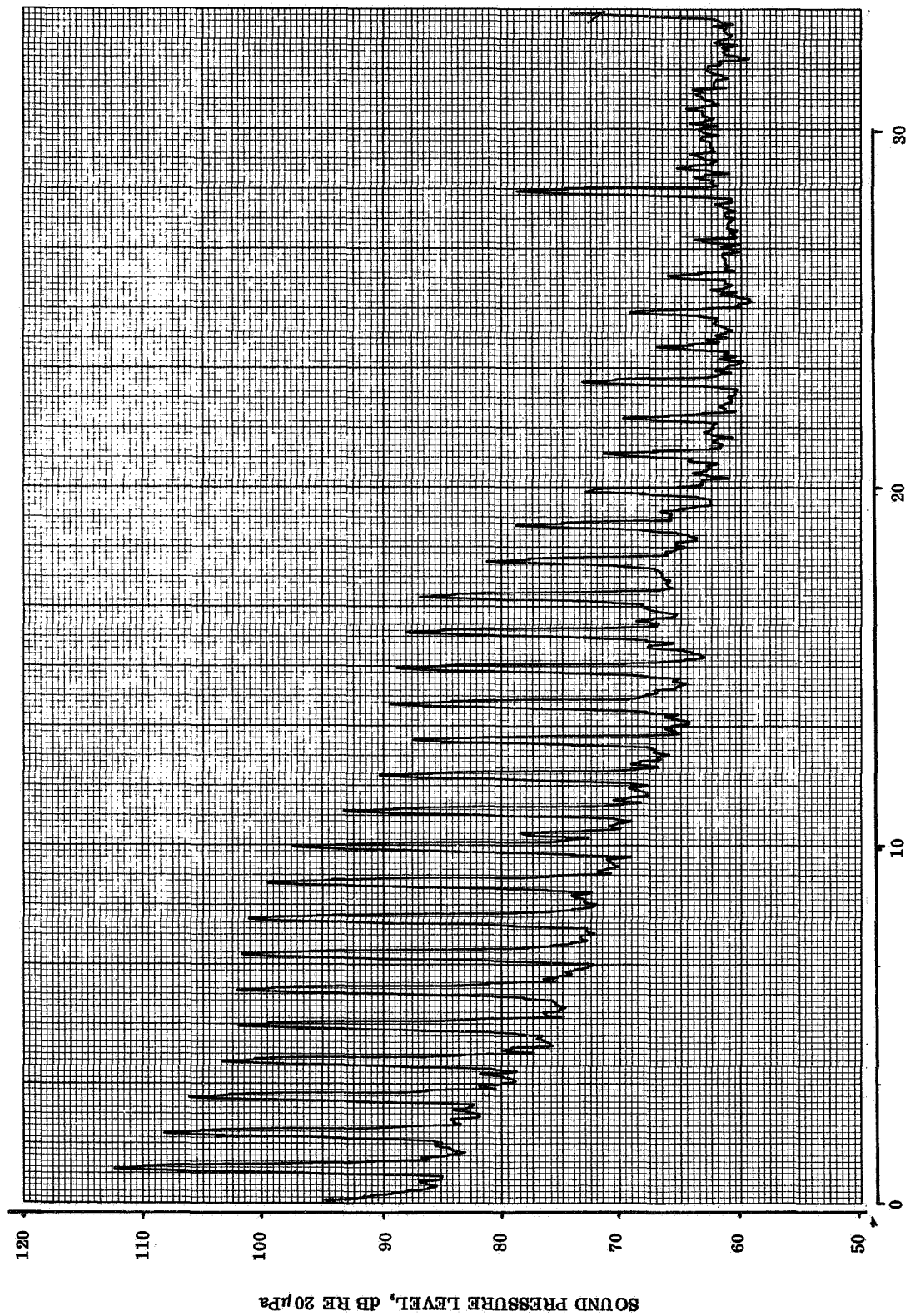
AFT MICROPHONE

RUN / 0

FLIGHT 7





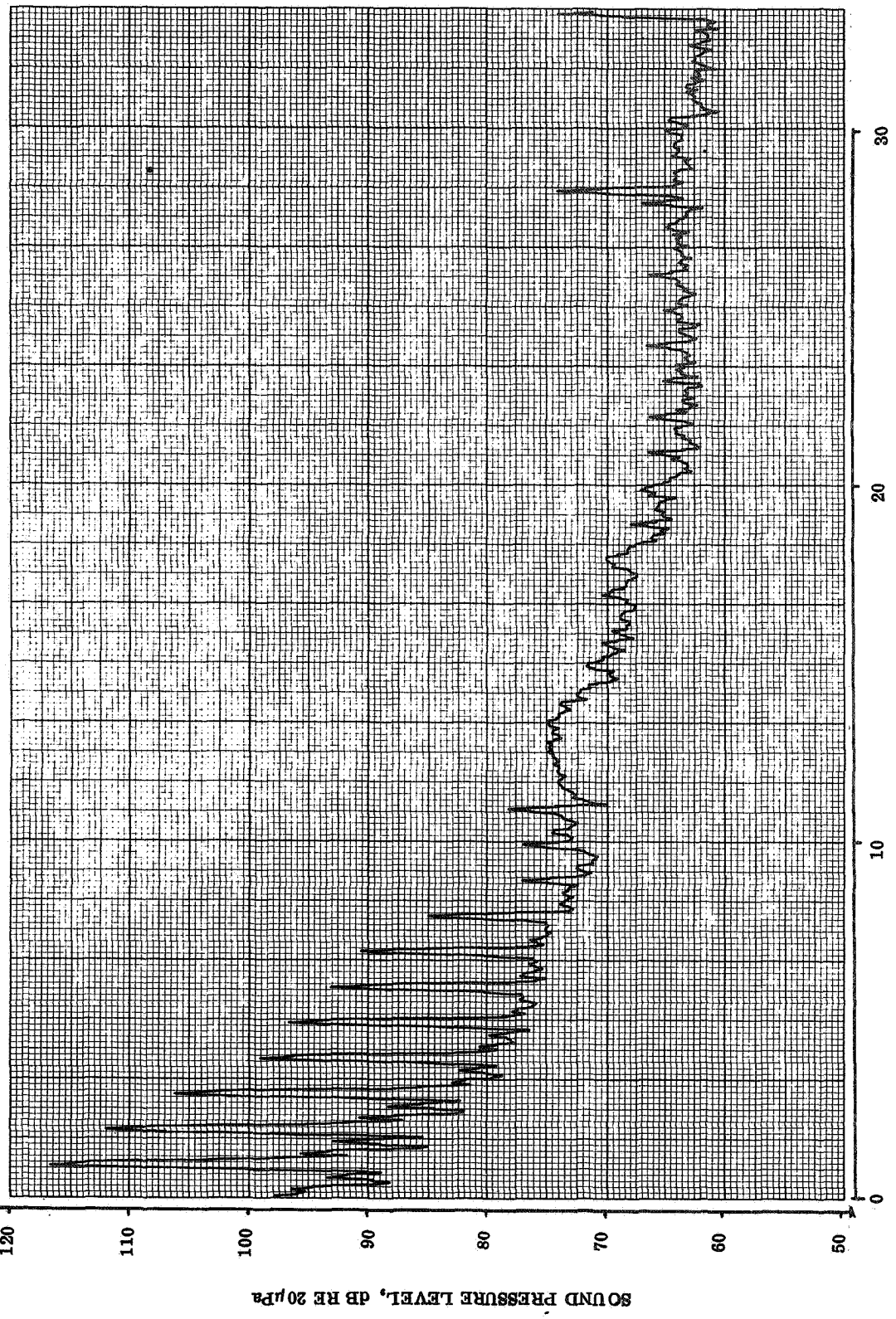


HARMONICS OF BLADE PASSING FREQUENCY

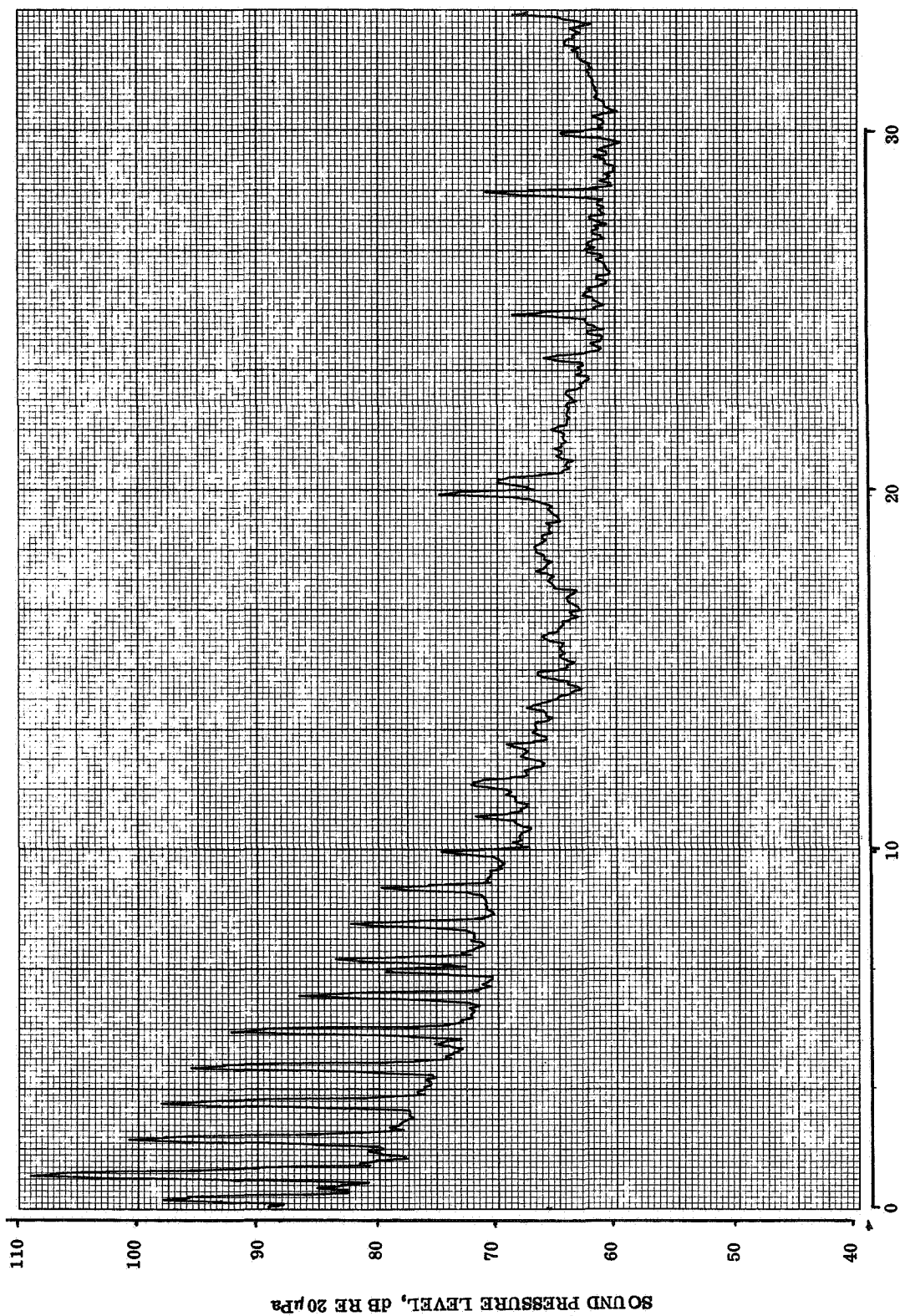
FLIGHT 7

RUN 12

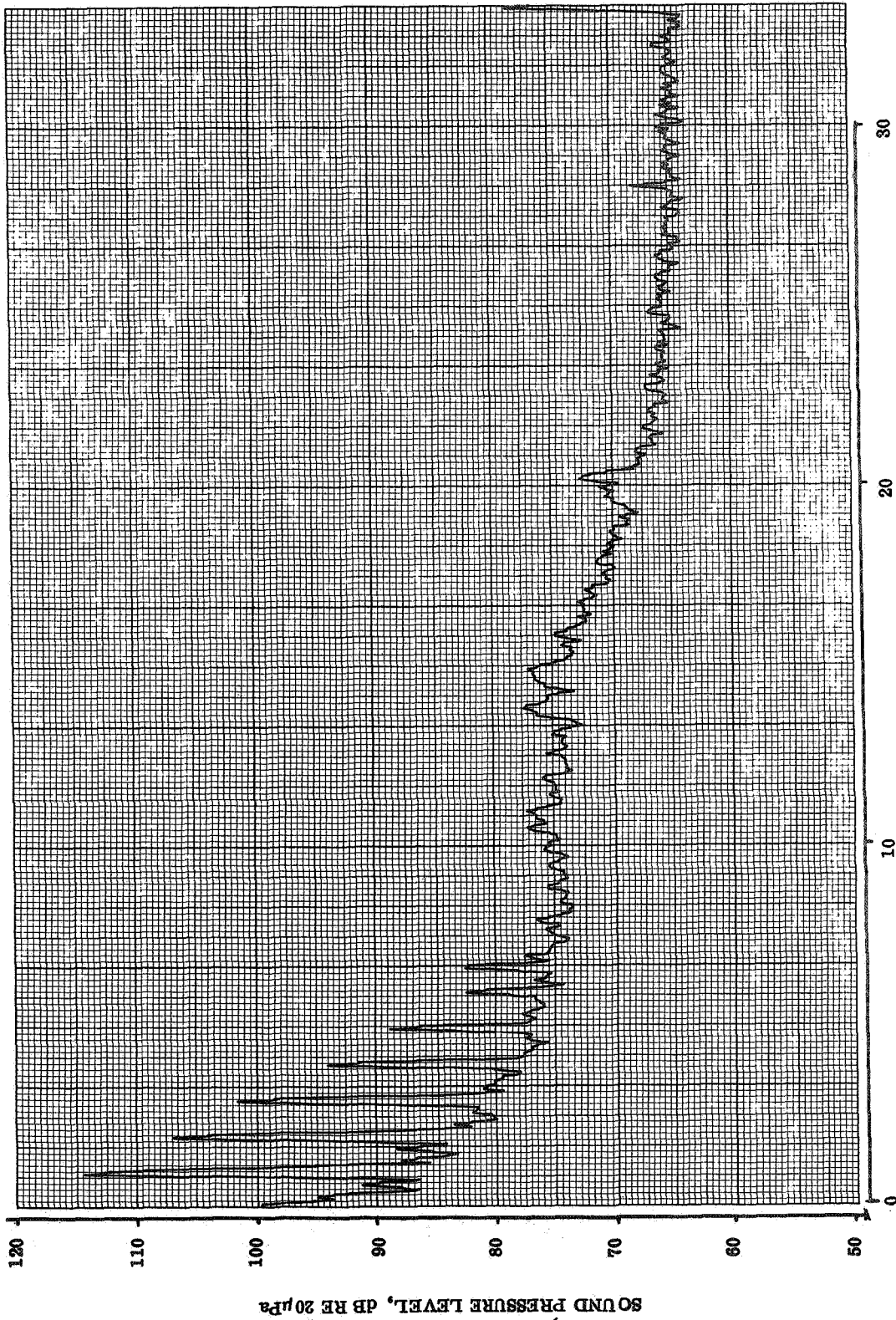
IN-PLANE MICROPHONE



FLIGHT 7
RUN 12
AFT MICROPHONE



FLIGHT 8
HARMONICS OF BLADE PASSING FREQUENCY
RUN 16
IN-PLANE MICROPHONE

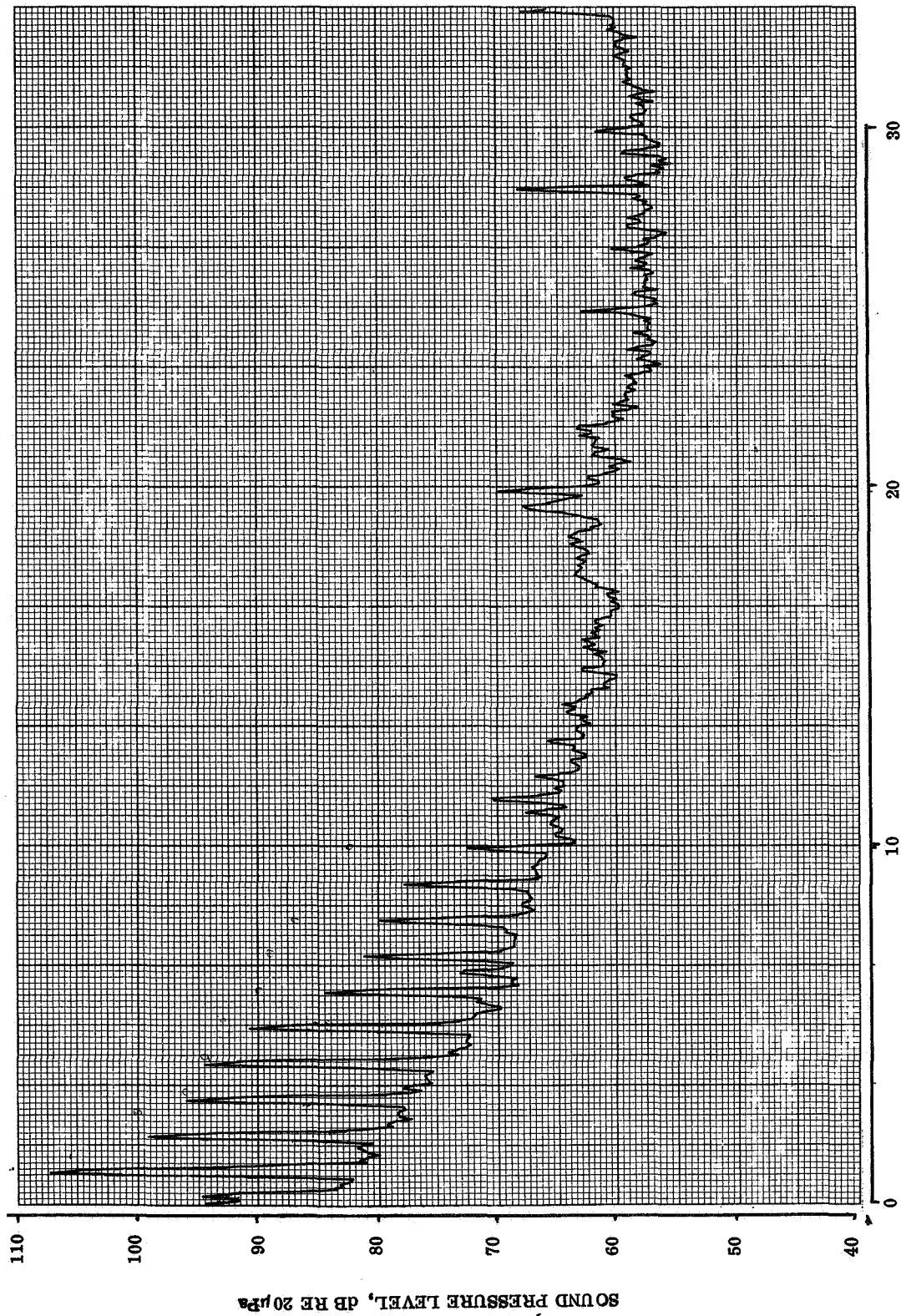


HARMONICS OF BLADE PASSING FREQUENCY

AFT MICROPHONE

RUN 16

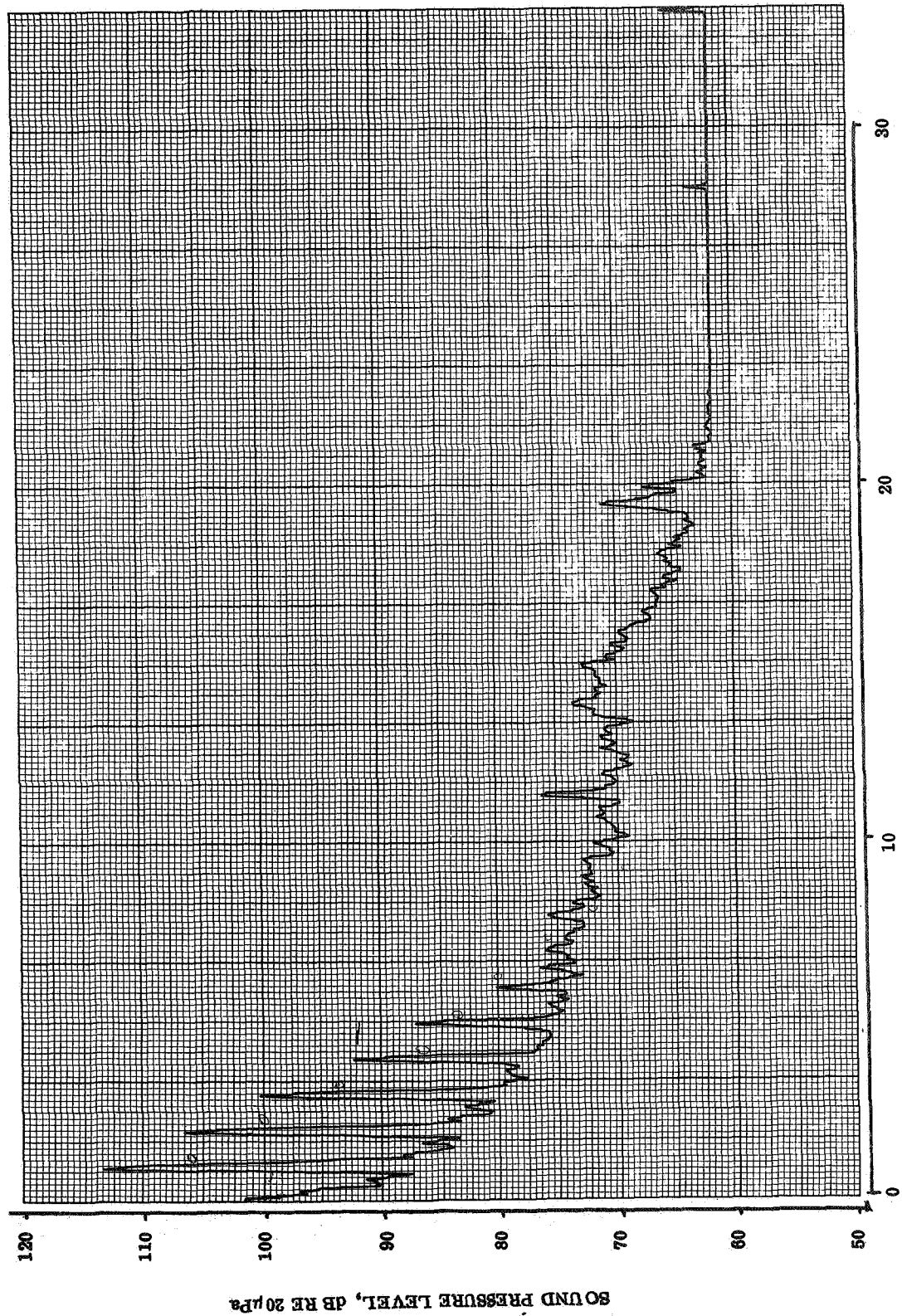
FLIGHT 2



IN-PLANE MICROPHONE

RUN 17

FLIGHT 8

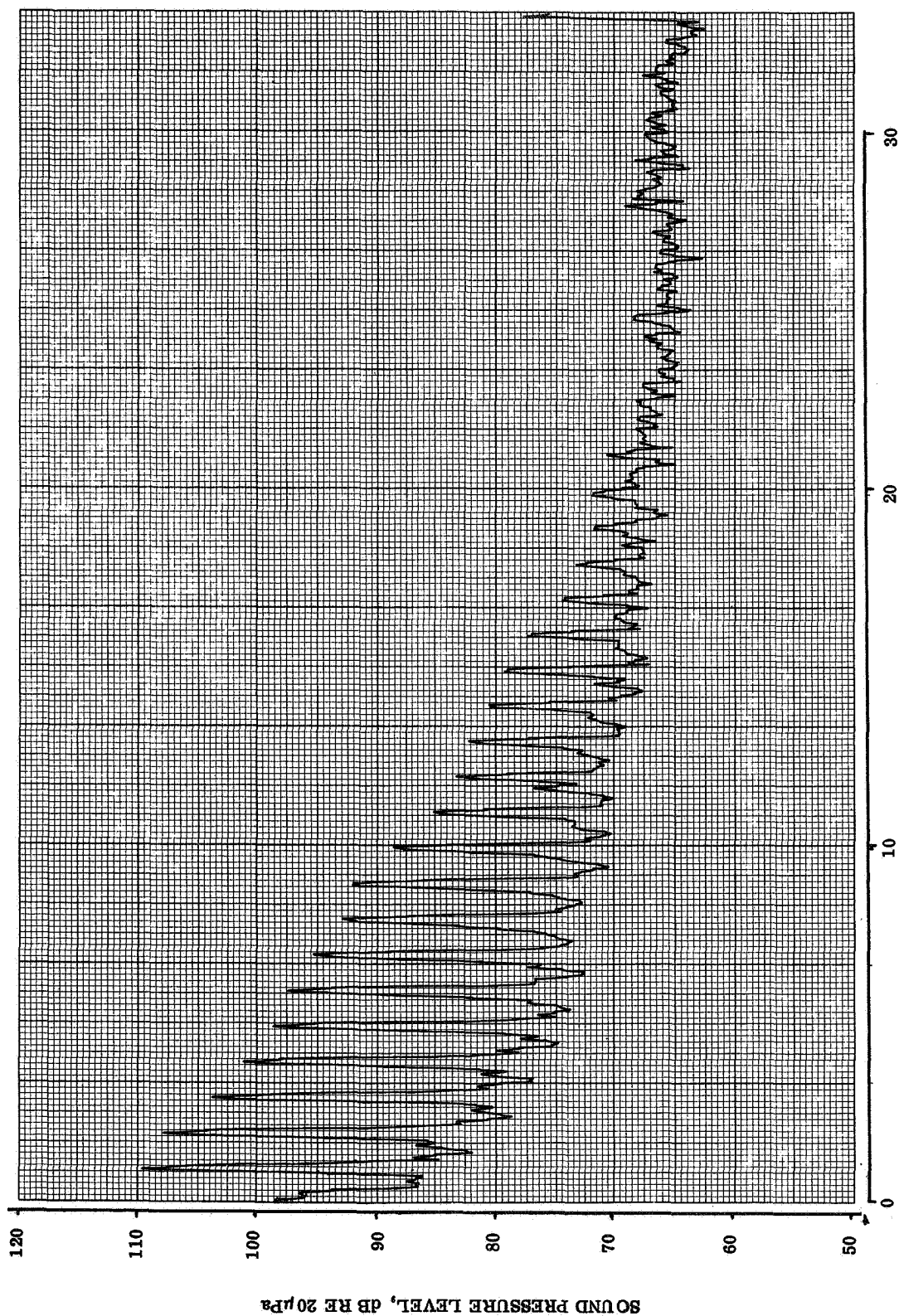


HARMONICS OF BLADE PASSING FREQUENCY

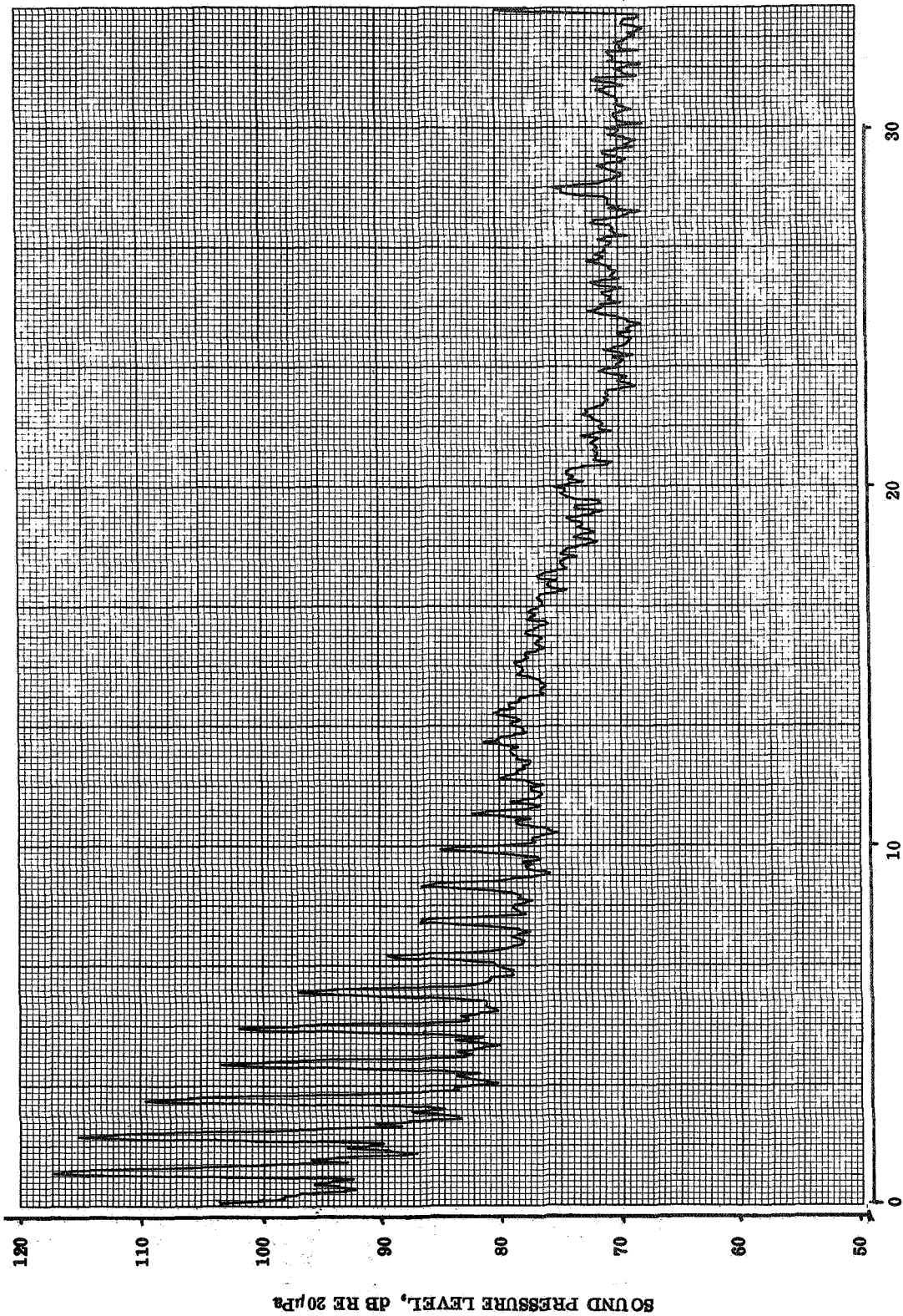
AFT MICROPHONE

RUN 17

FLIGHT 8



FLIGHT 8
HARMONICS OF BLADE PASSING FREQUENCY
RUN 18
IN-PLANE MICROPHONE

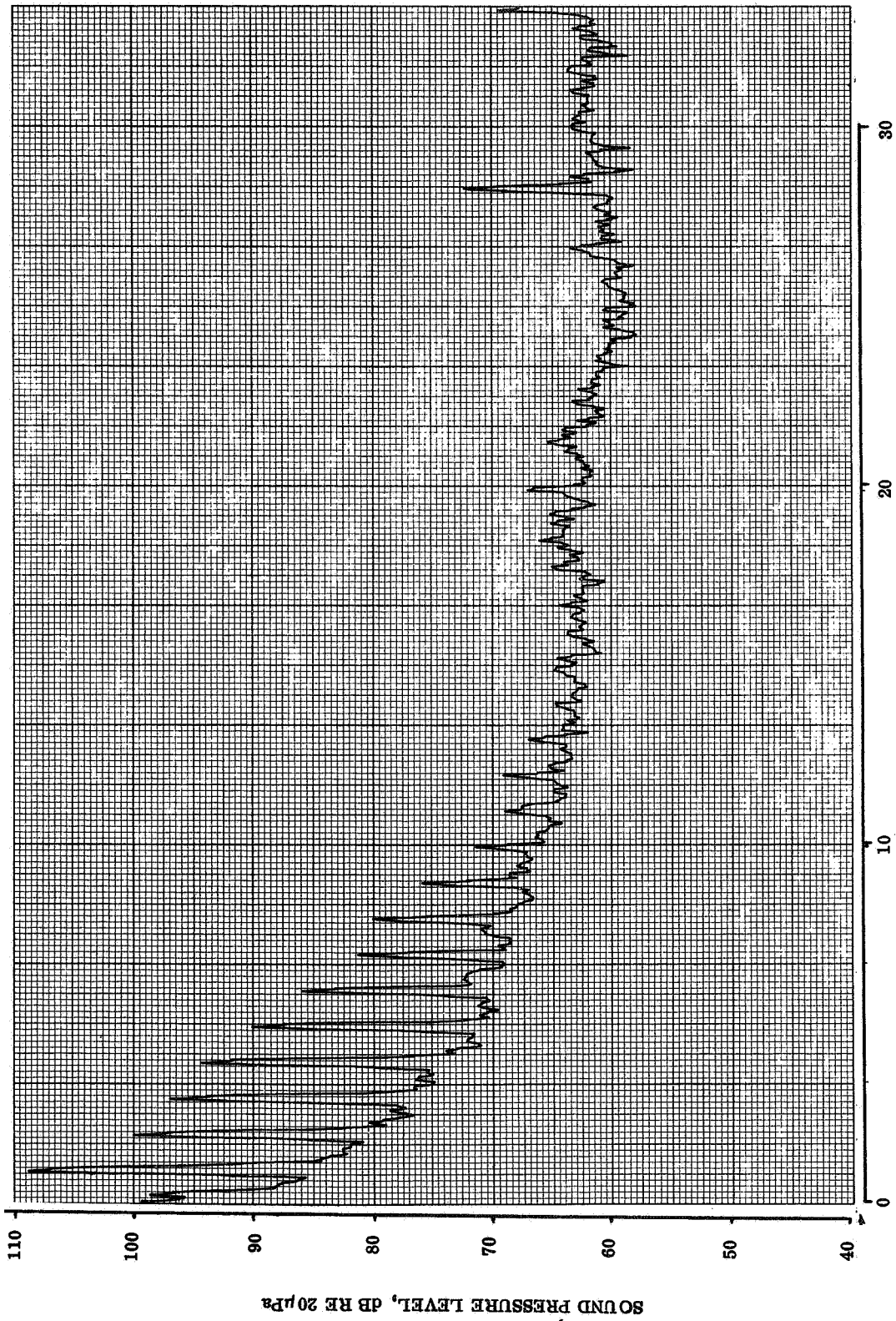


HARMONICS OF BLADE PASSING FREQUENCY

AFT MICROPHONE

RUN 13

FLIGHT 8

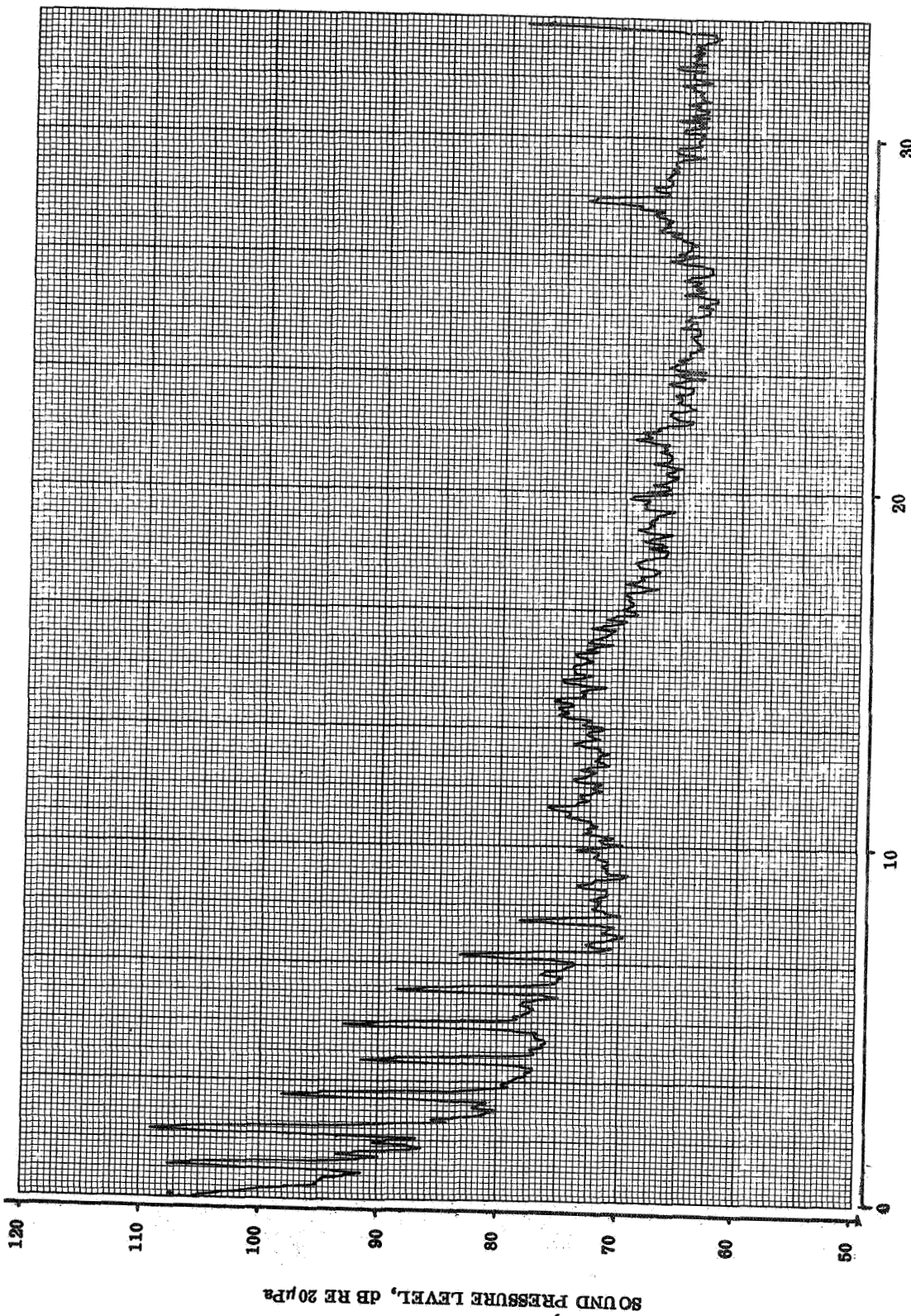


HARMONICS OF BLADE PASSING FREQUENCY

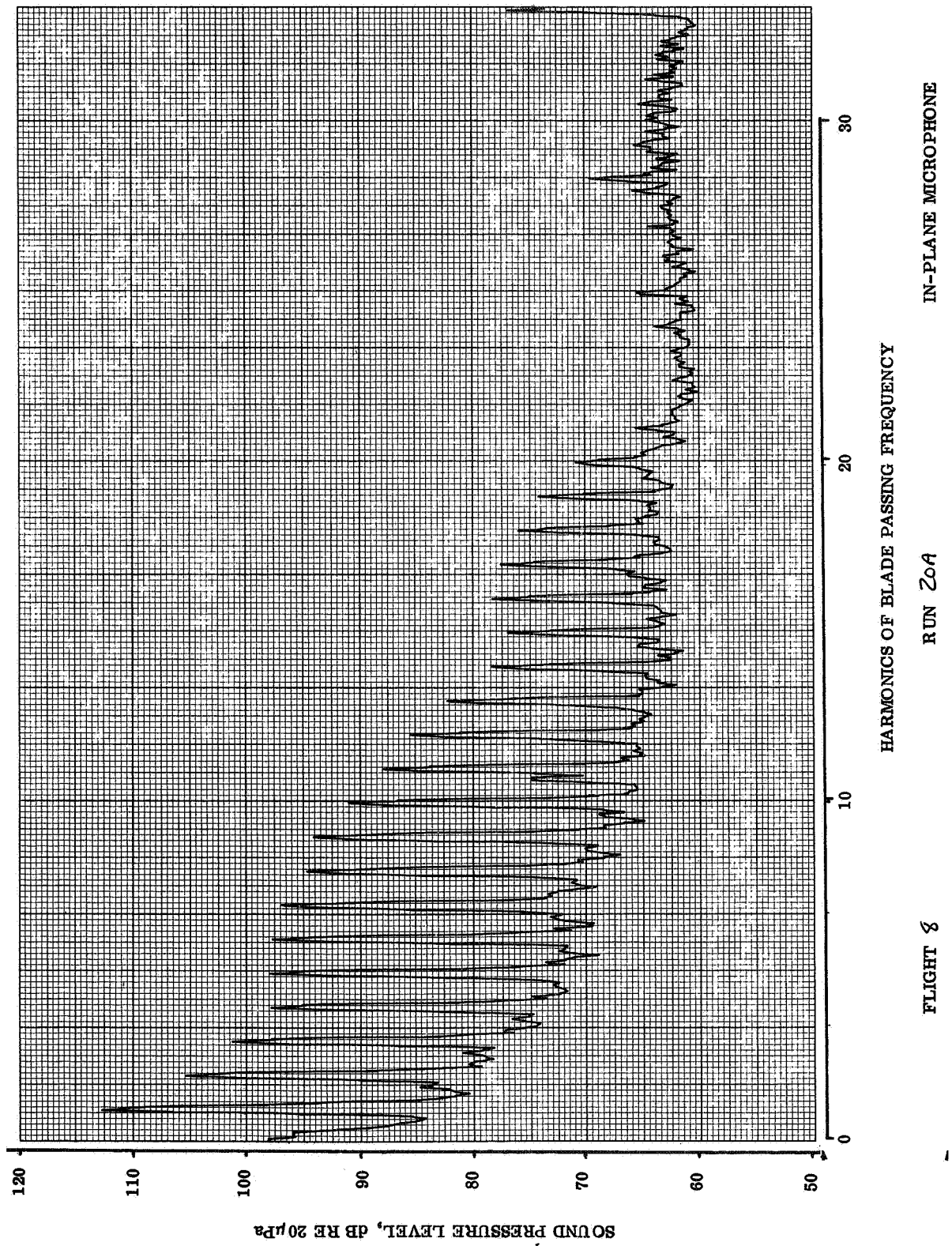
IN-PLANE MICROPHONE

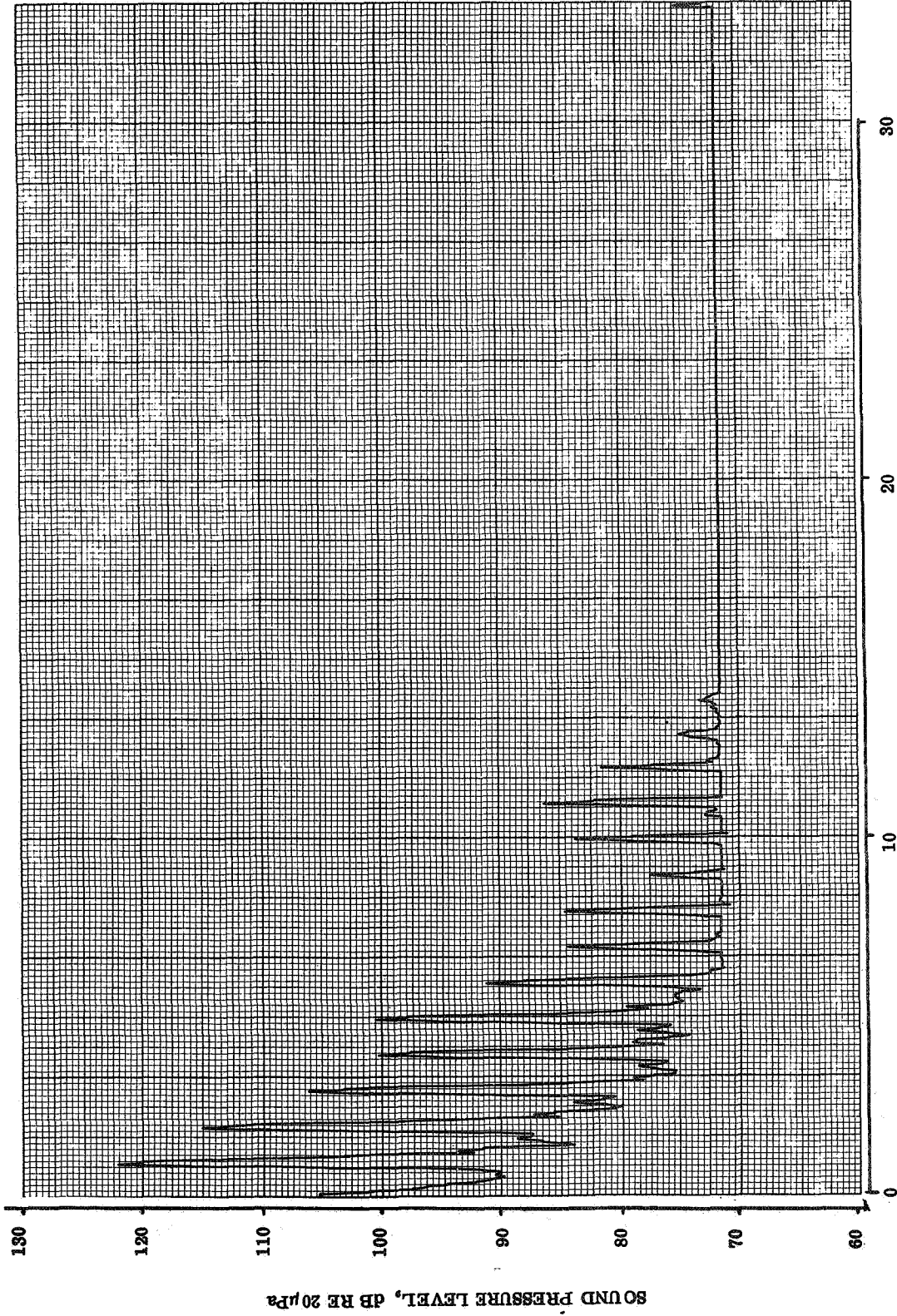
RUN 19A

FLIGHT 8



FLIGHT 8
HARMONICS OF BLADE PASSING FREQUENCY
RUN 19A
AFT MICROPHONE



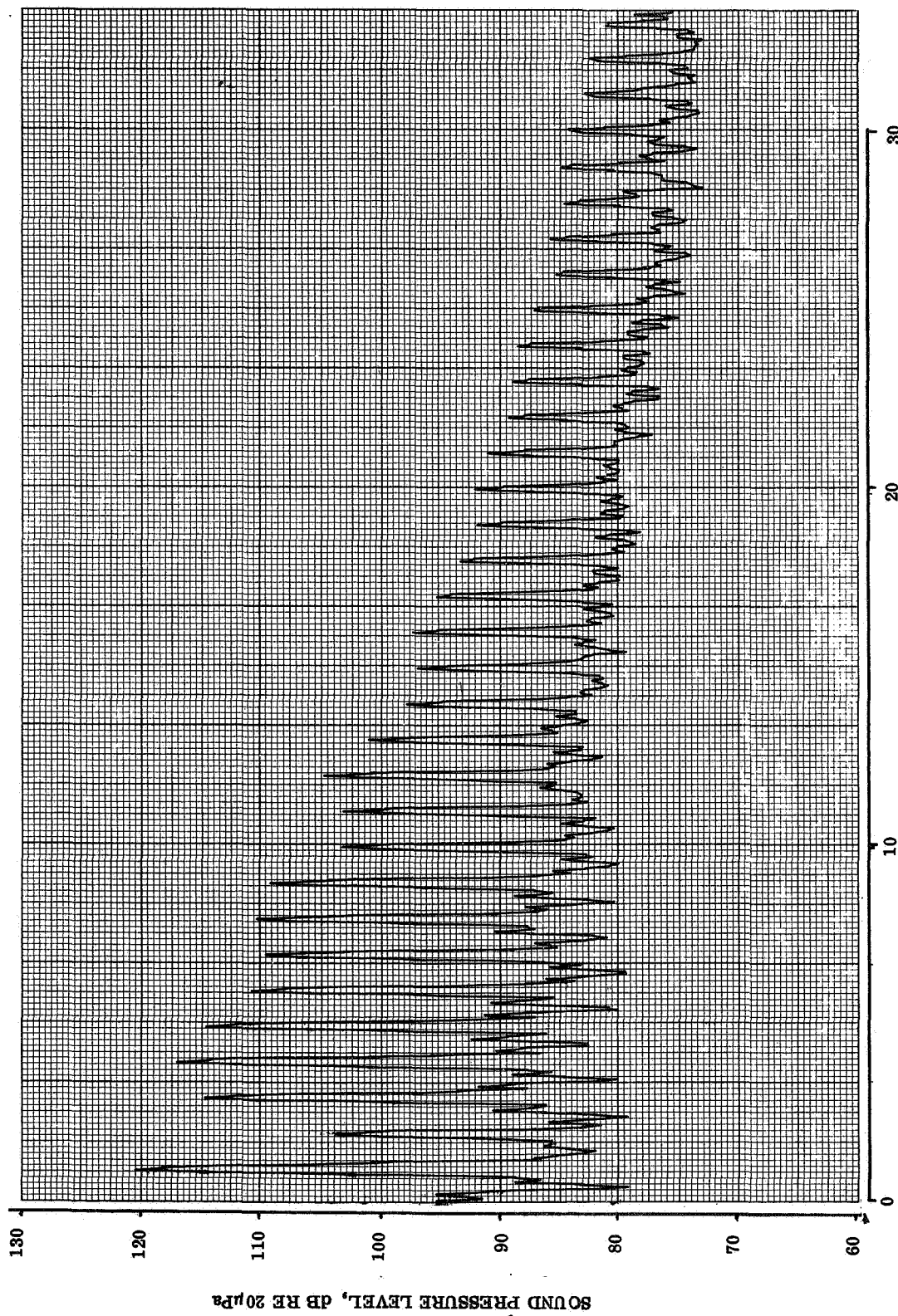


HARMONICS OF BLADE PASSING FREQUENCY

AFT MICROPHONE

RUN 20A

FLIGHT 8



HARMONICS OF BLADE PASSING FREQUENCY

FLIGHT / 2

RUN 25

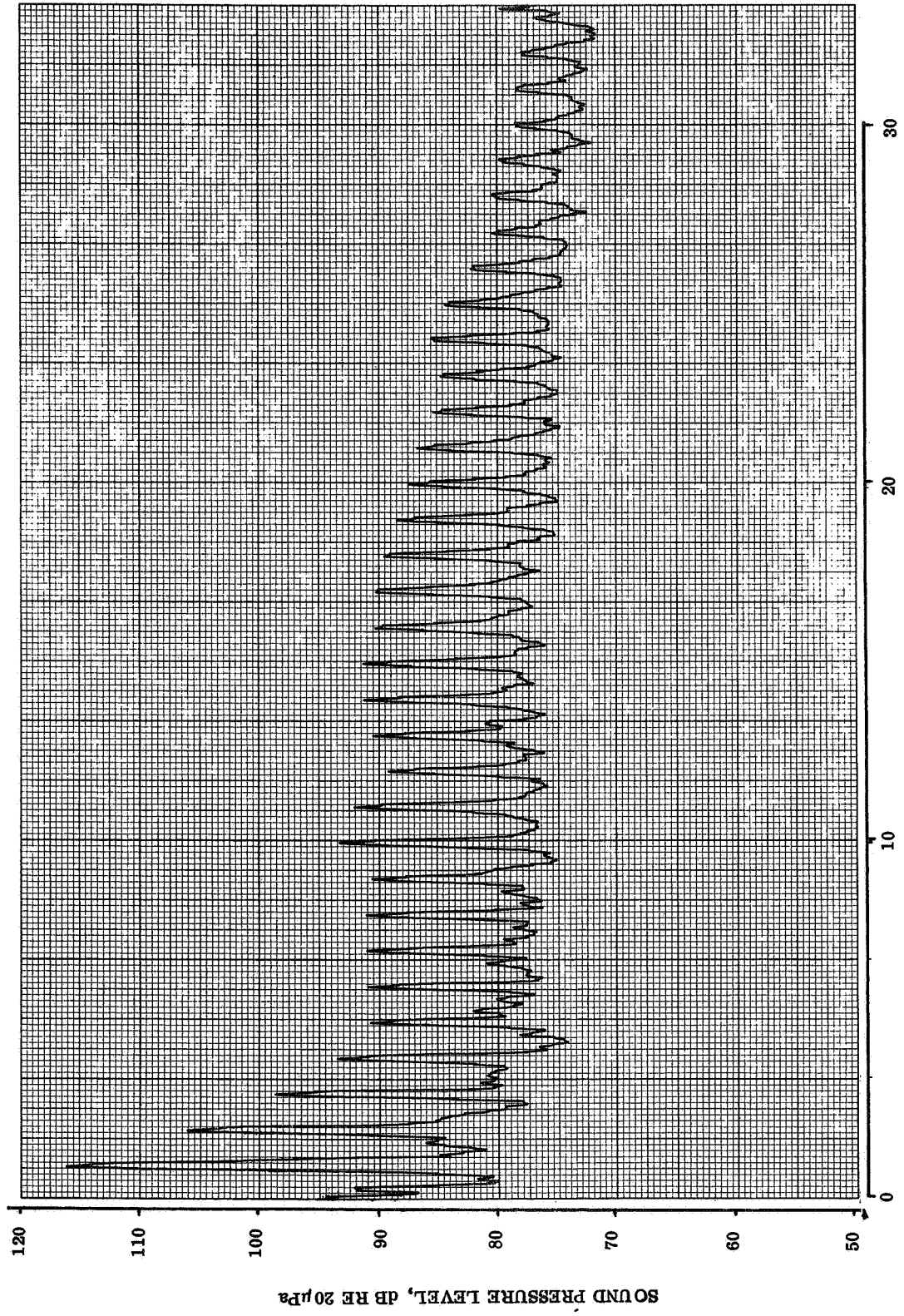
IN-PLANE MICROPHONE

HARMONICS OF BLADE PASSING FREQUENCY

AFT MICROPHONE

RUN 25

FLIGHT 12

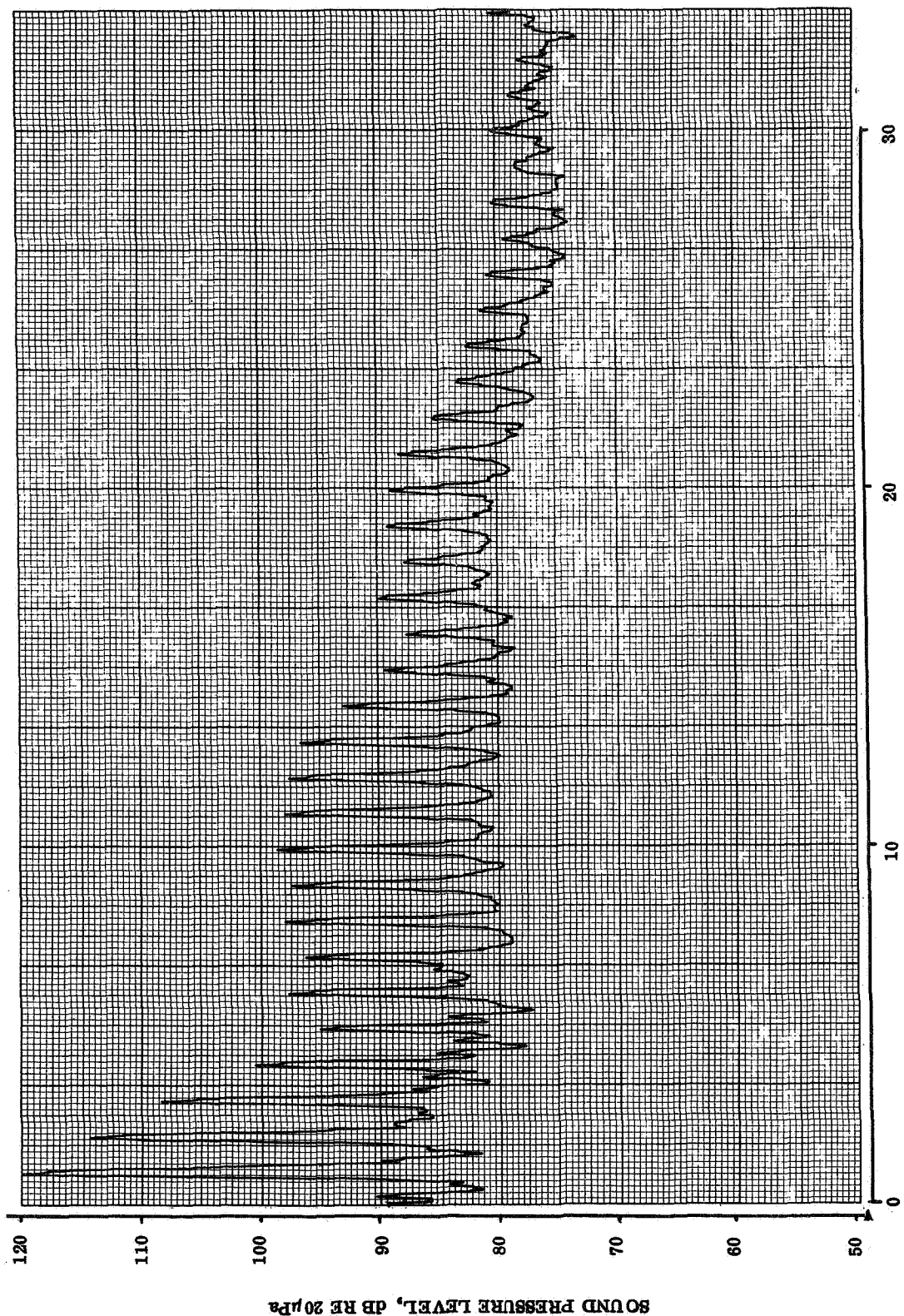


HARMONICS OF BLADE PASSING FREQUENCY

IN-PLANE MICROPHONE

RUN 35

FLIGHT 12

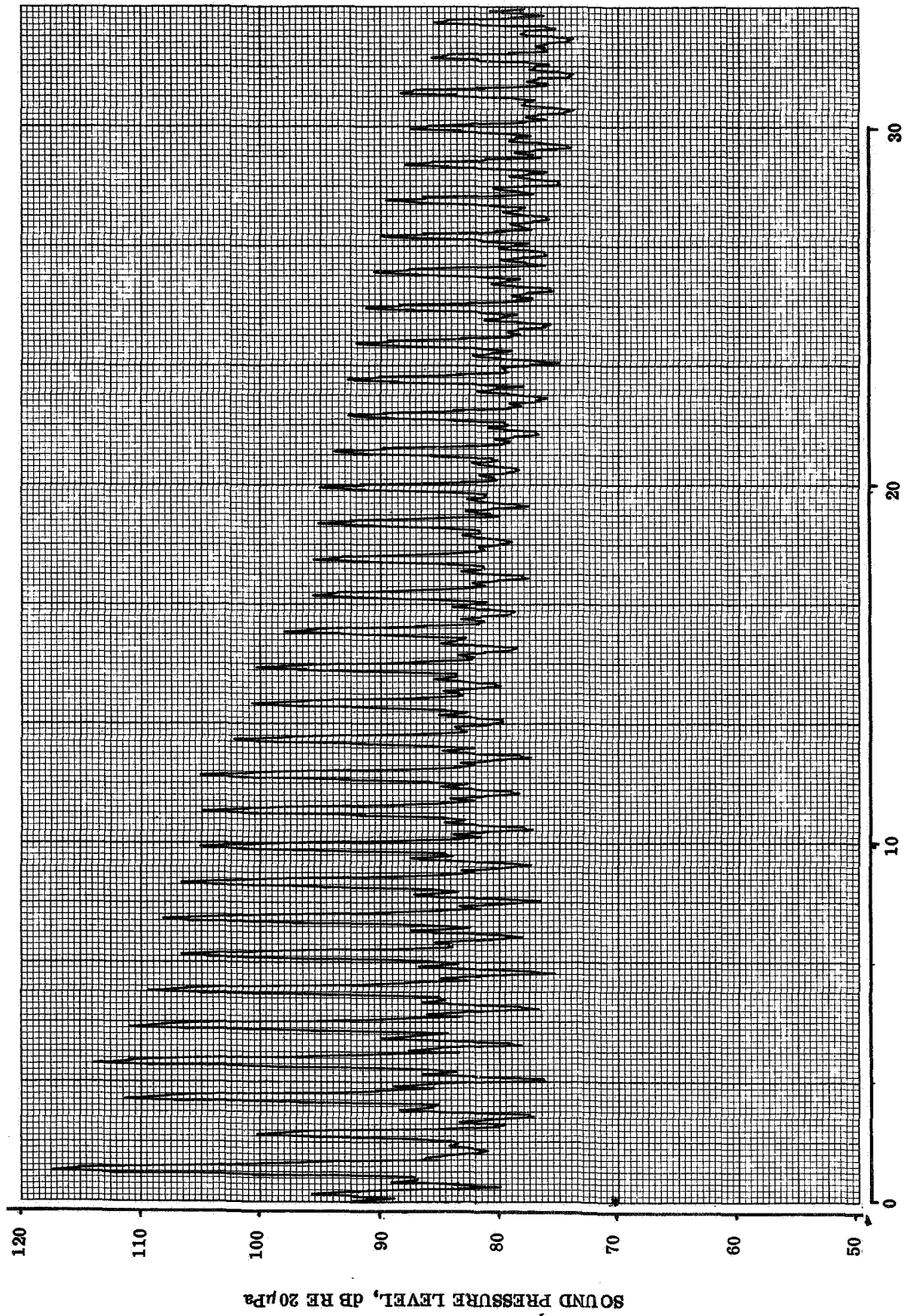


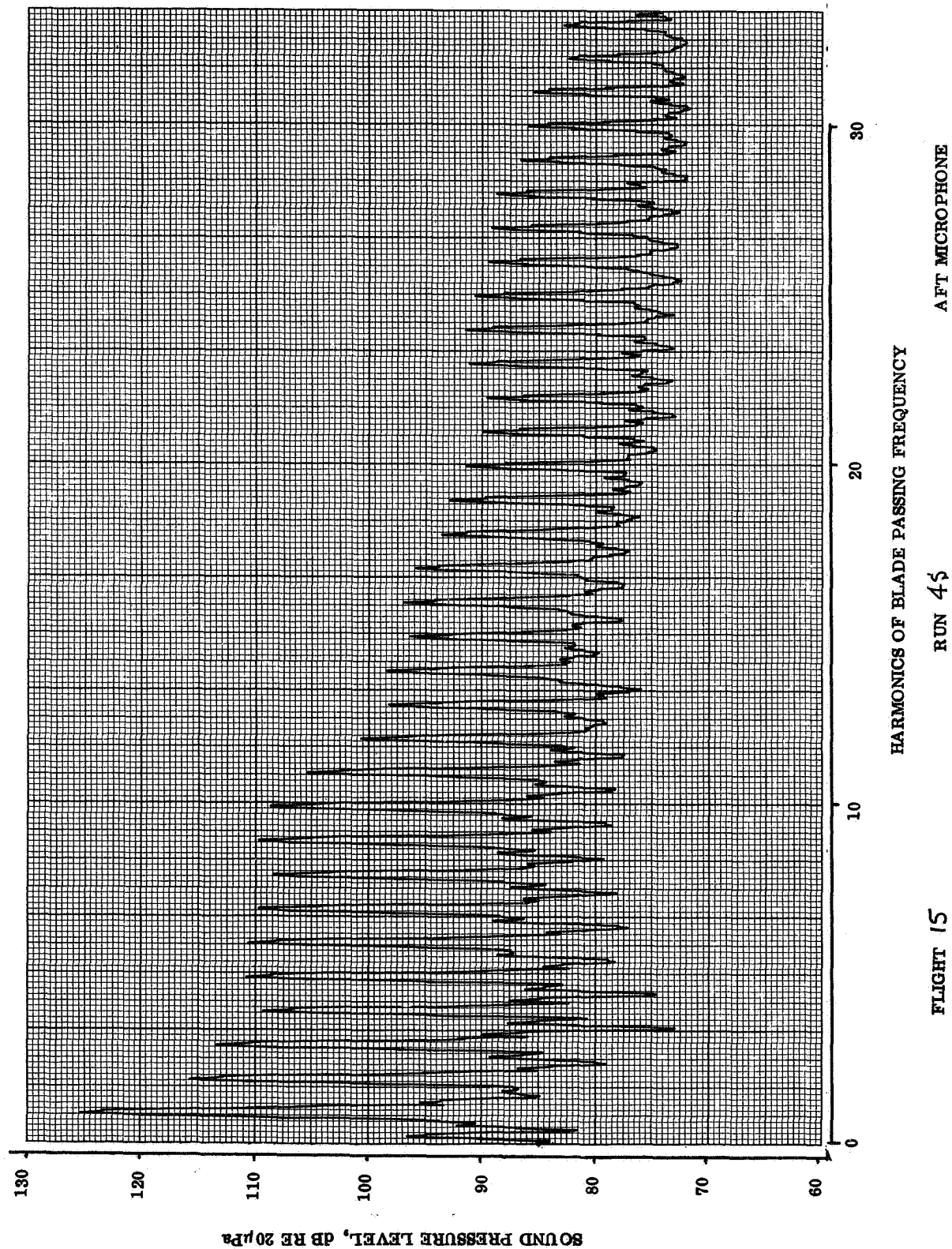
HARMONICS OF BLADE PASSING FREQUENCY

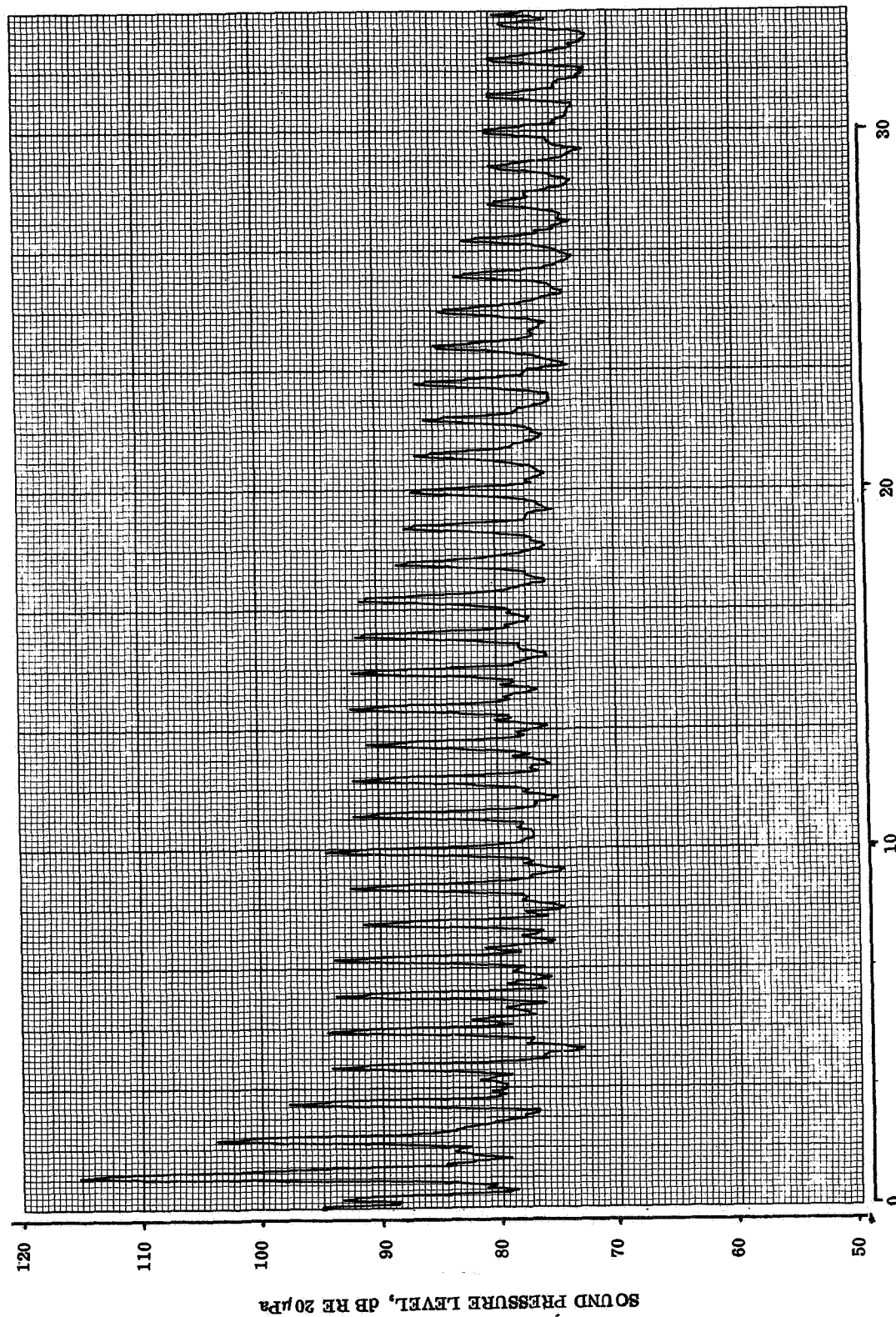
AFT MICROPHONE

RUN 35

FLIGHT 12





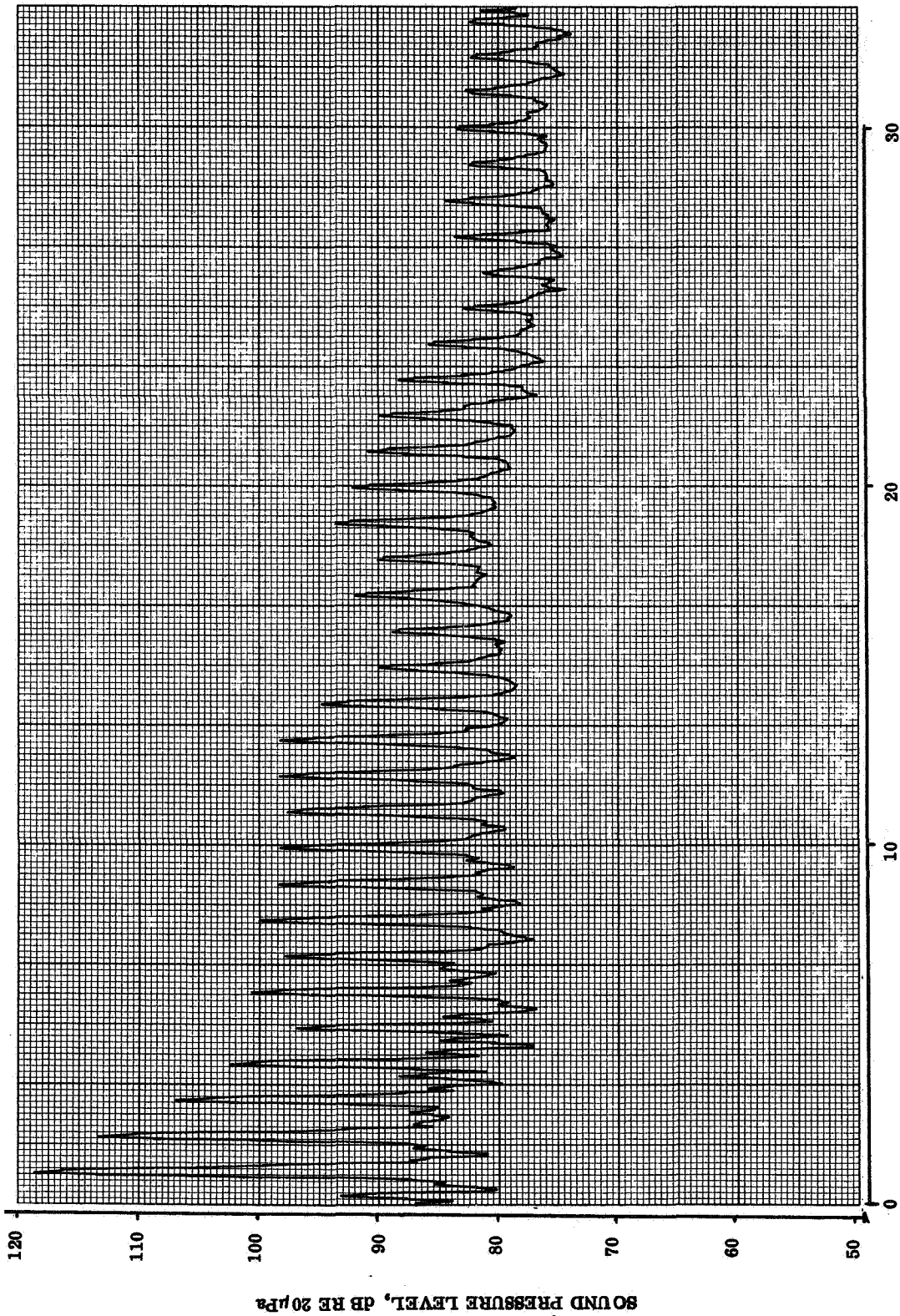


HARMONICS OF BLADE PASSING FREQUENCY

IN-PLANE MICROPHONE

RUN 53

FLIGHT 12

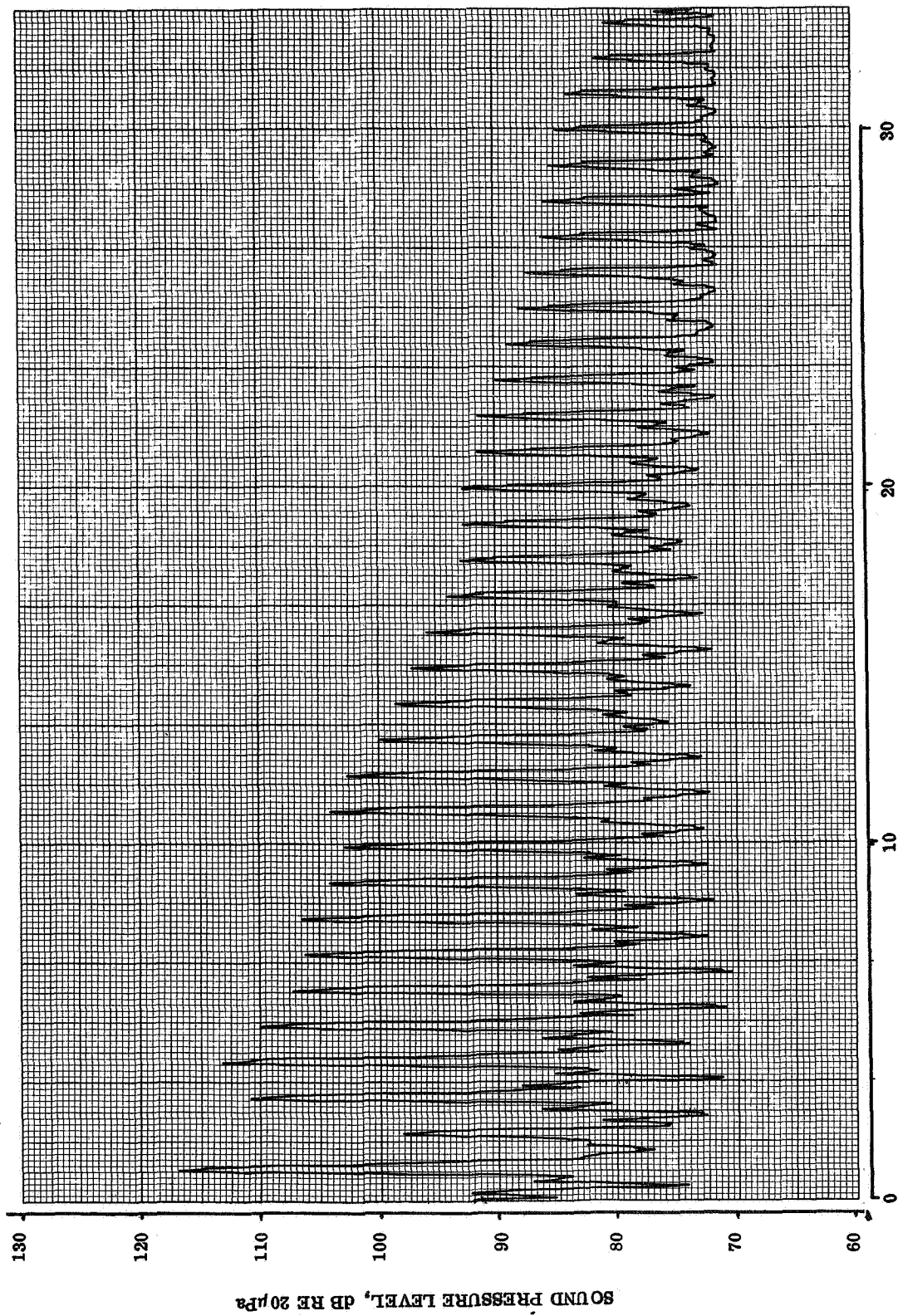


HARMONICS OF BLADE PASSING FREQUENCY

AFT MICROPHONE

RUN 55

FLIGHT 12

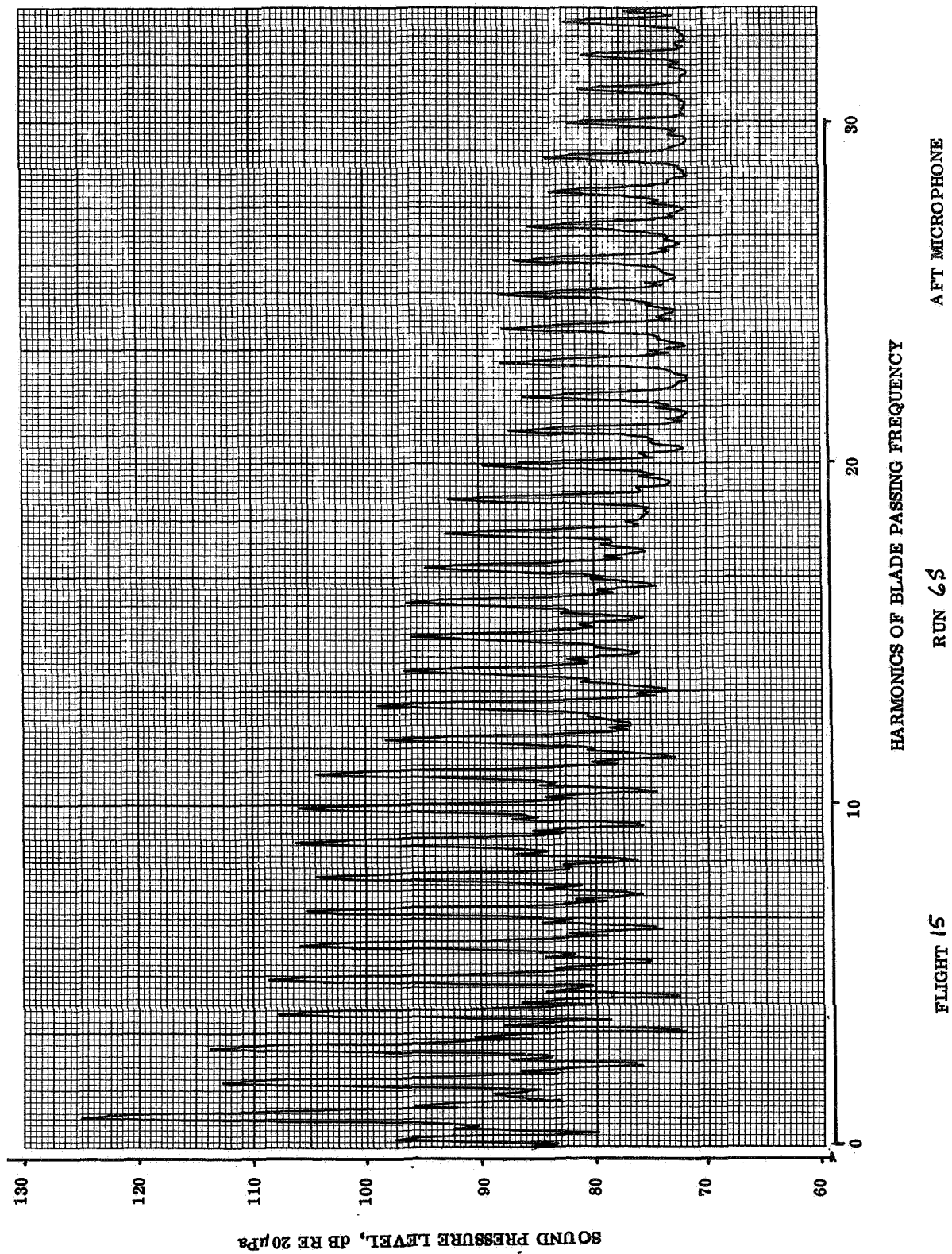


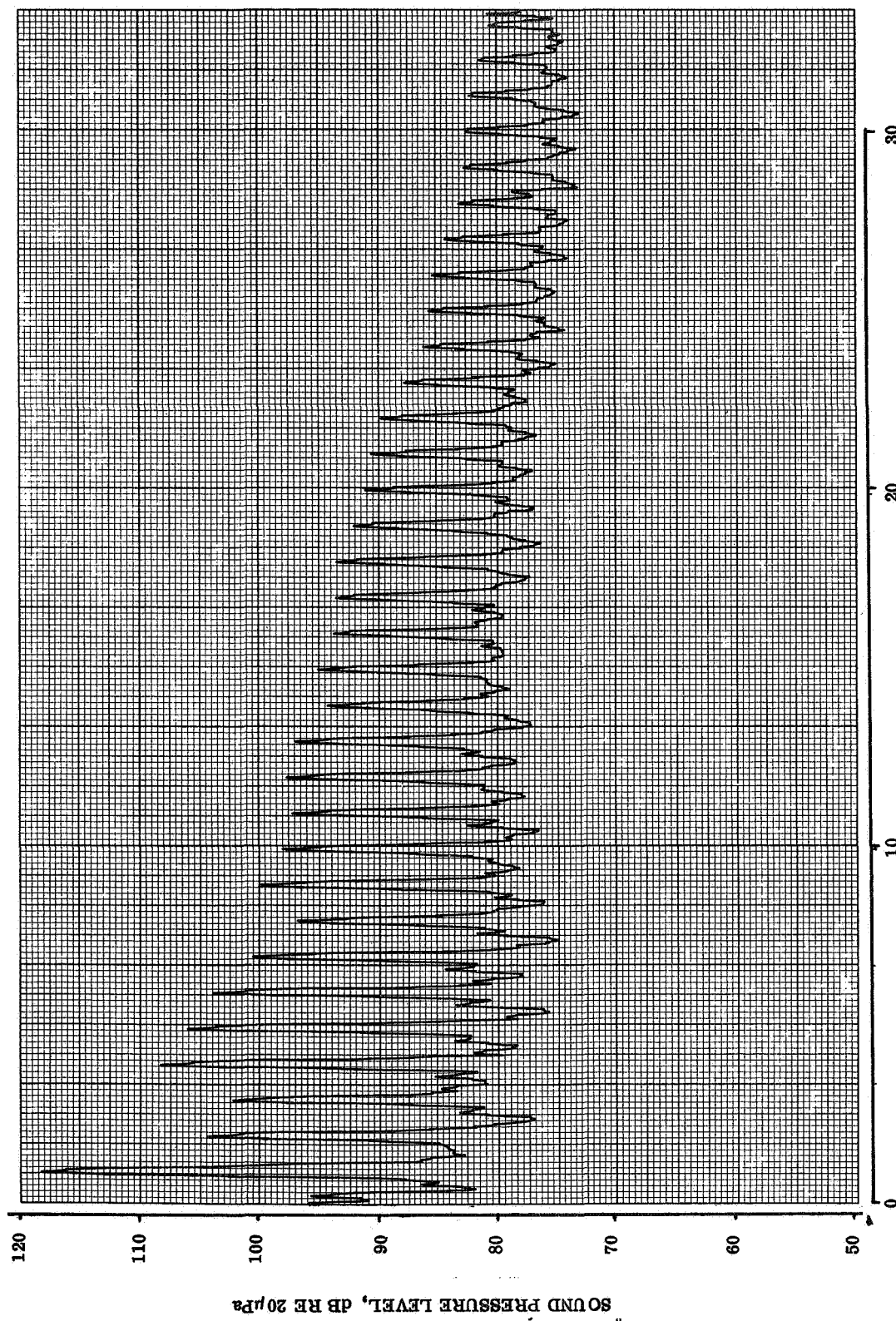
HARMONICS OF BLADE PASSING FREQUENCY

IN-PLANE MICROPHONE

RUN 65

FLIGHT 15

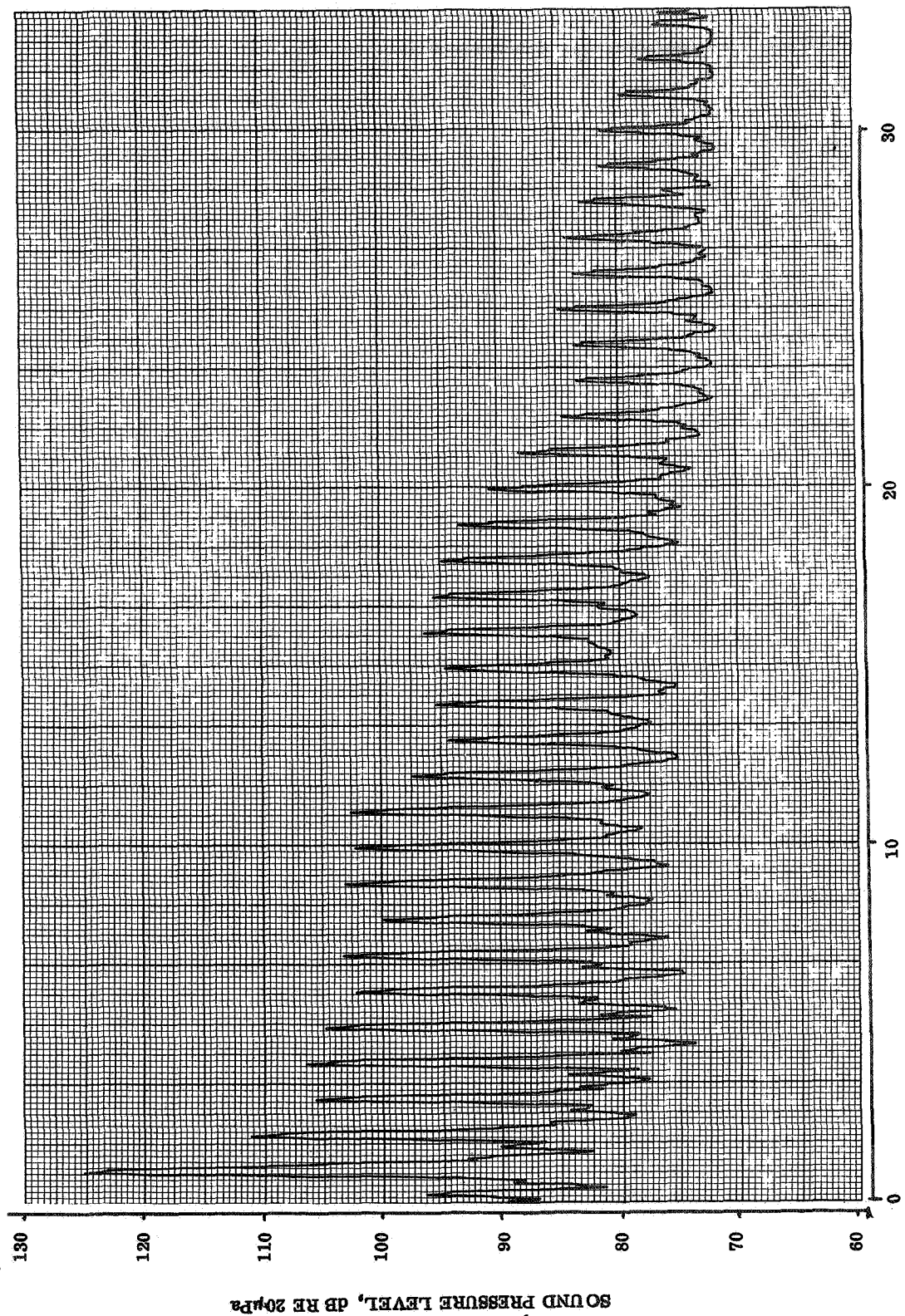




IN-PLANE MICROPHONE

RUN 165

FLIGHT 12

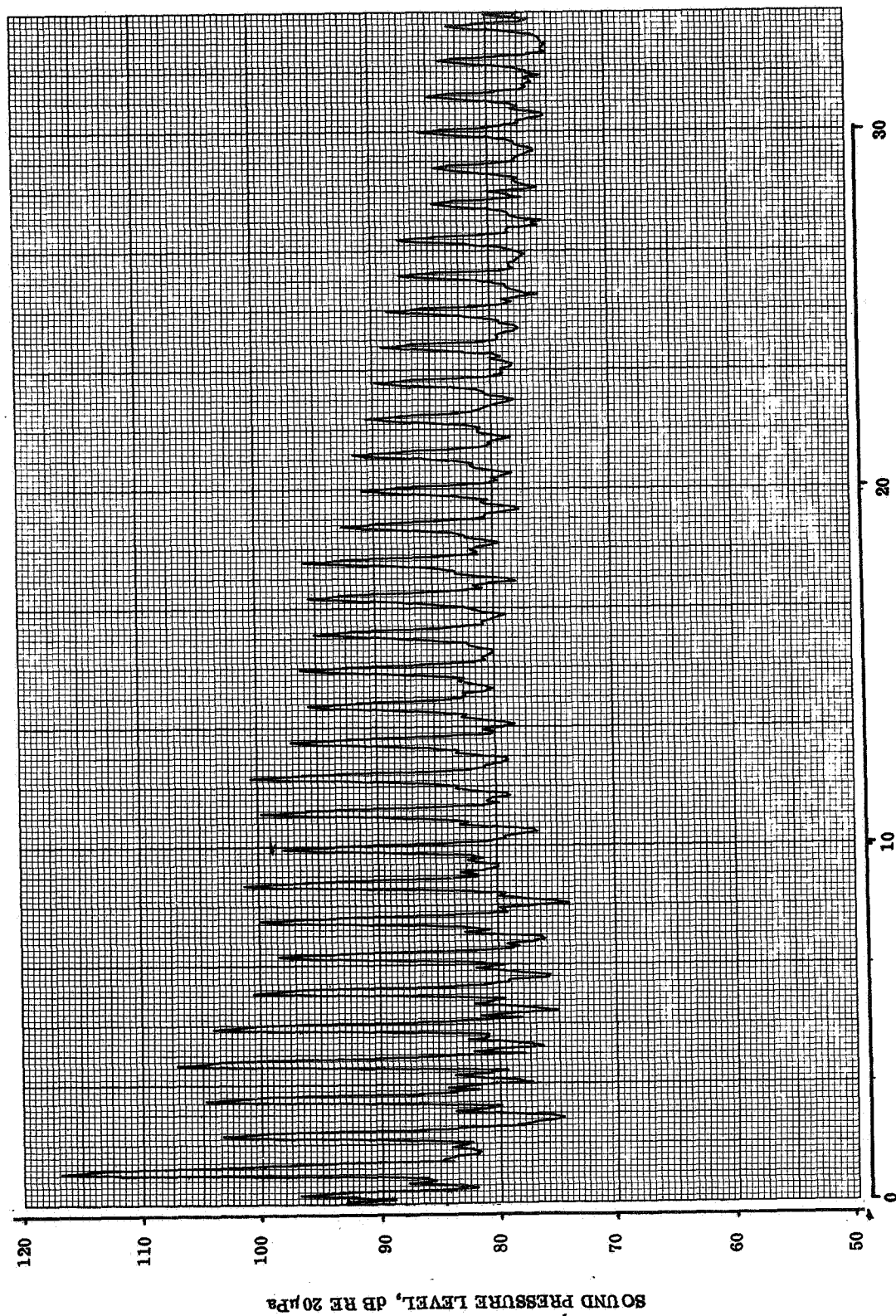


HARMONICS OF BLADE PASSING FREQUENCY

AFT MICROPHONE

RUN 165

FLIGHT 12

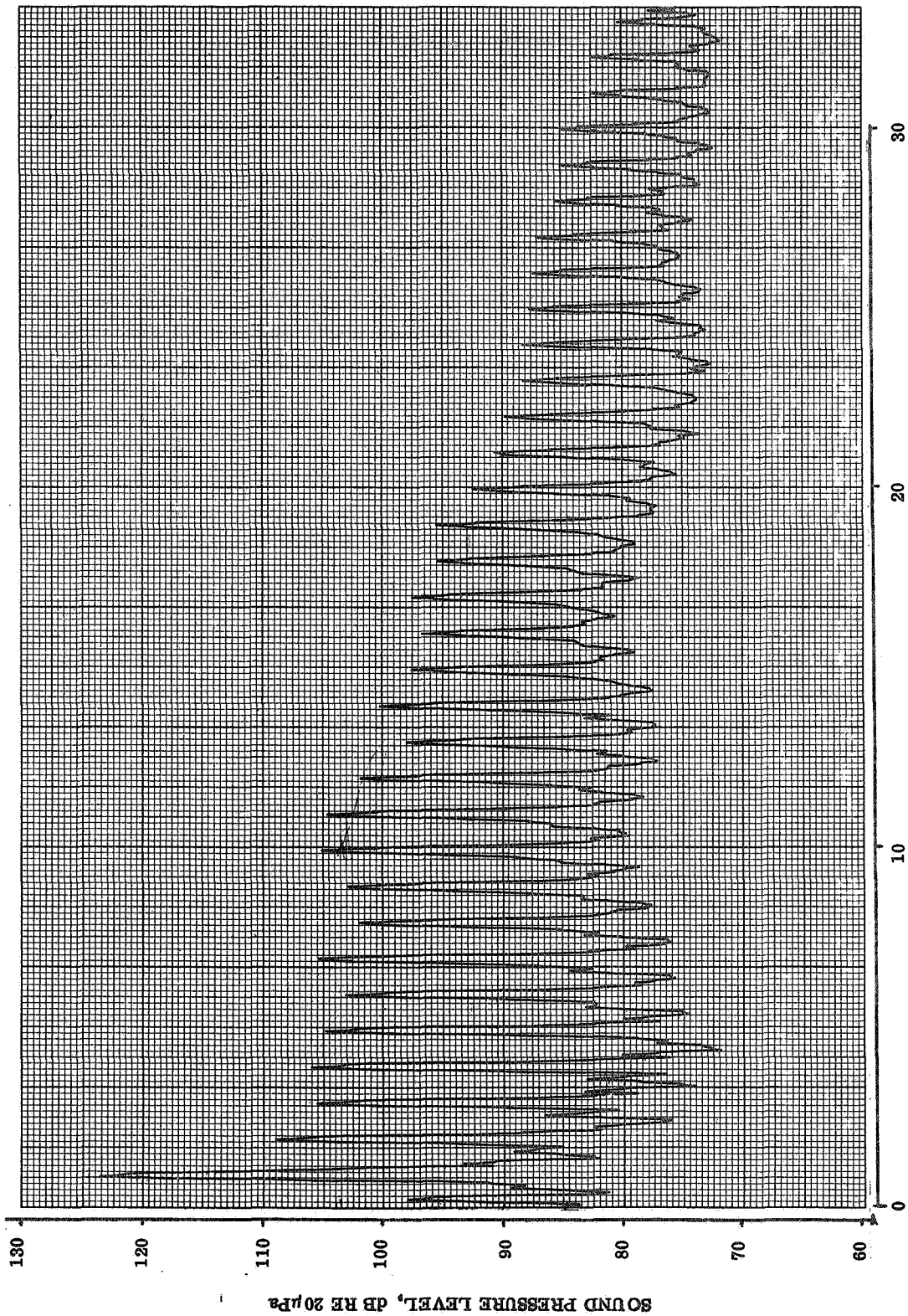


HARMONICS OF BLADE PASSING FREQUENCY

IN-PLANE MICROPHONE

RUN 17 S

FLIGHT 15

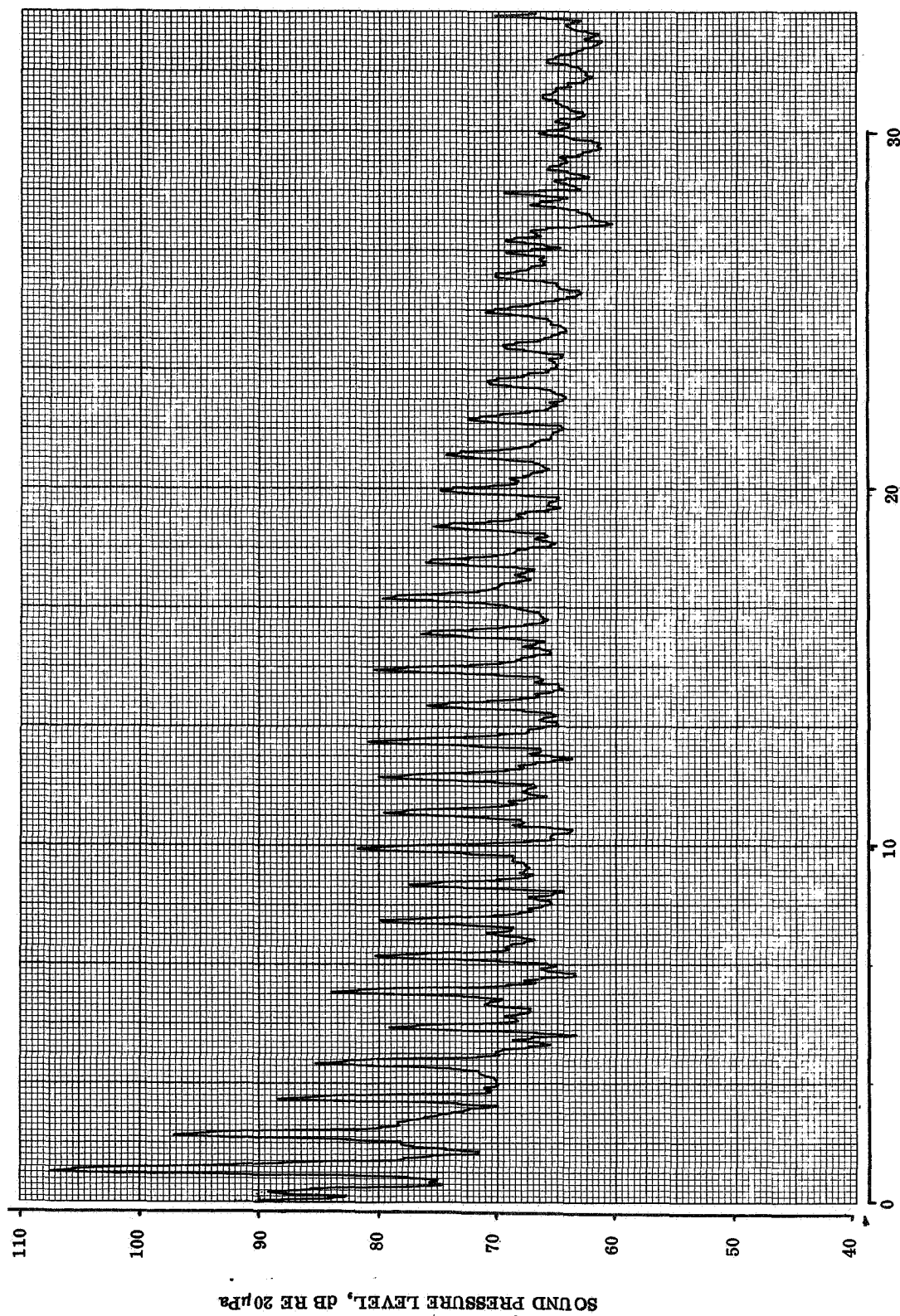


HARMONICS OF BLADE PASSING FREQUENCY

AFT MICROPHONE

RUN 175

FLIGHT 15

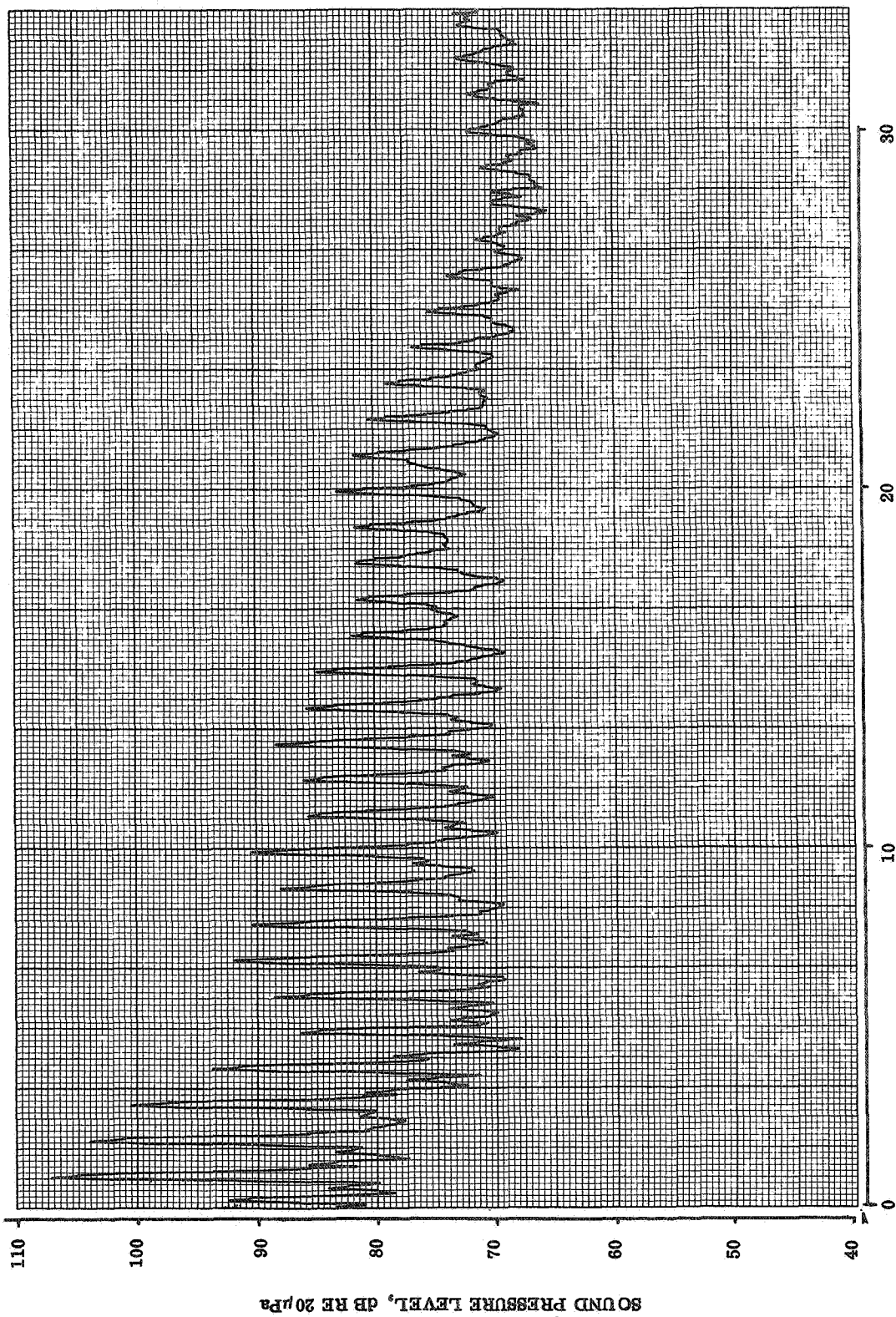


HARMONICS OF BLADE PASSING FREQUENCY

FLIGHT 14

RUN 2/5

IN-PLANE MICROPHONE

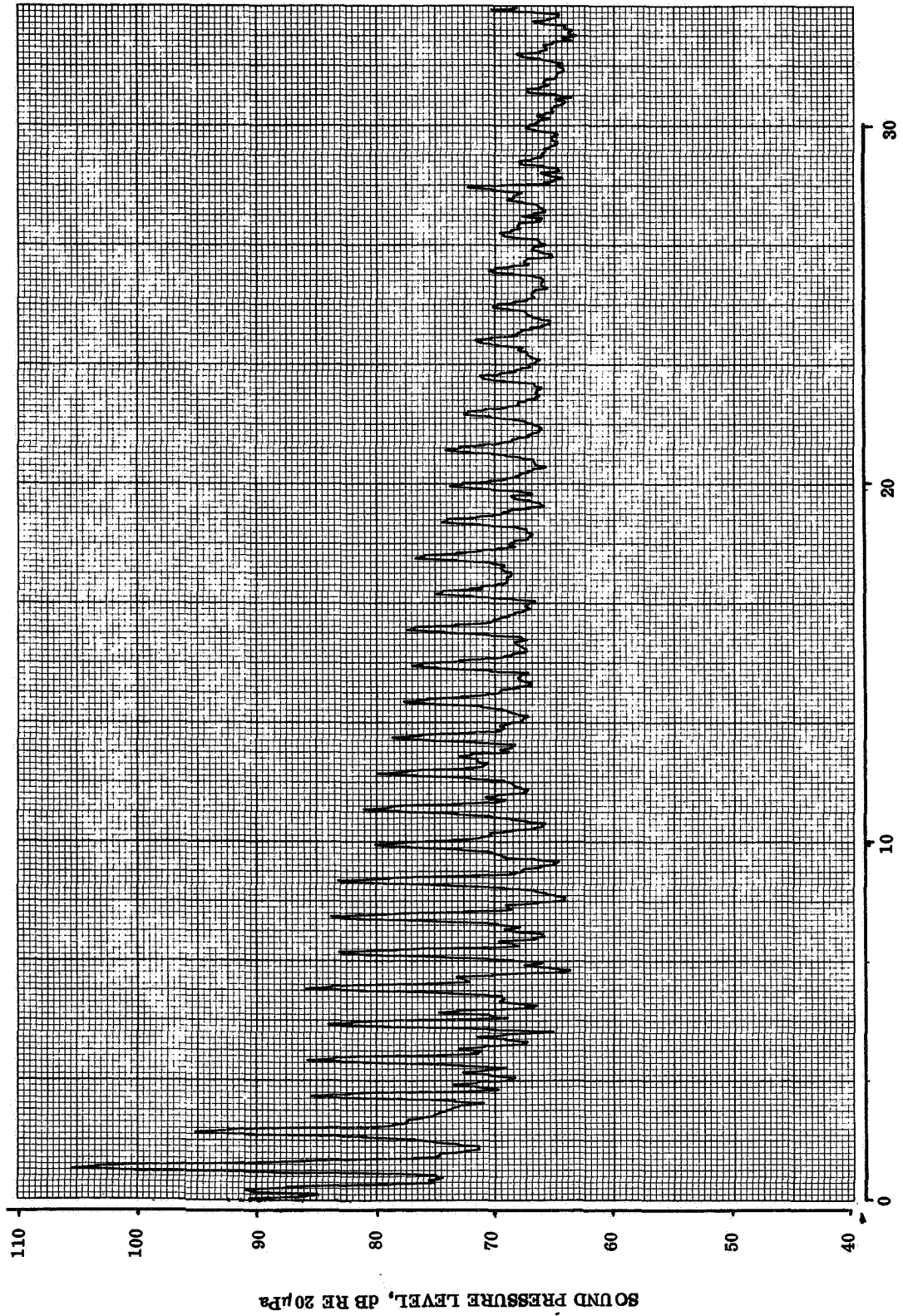


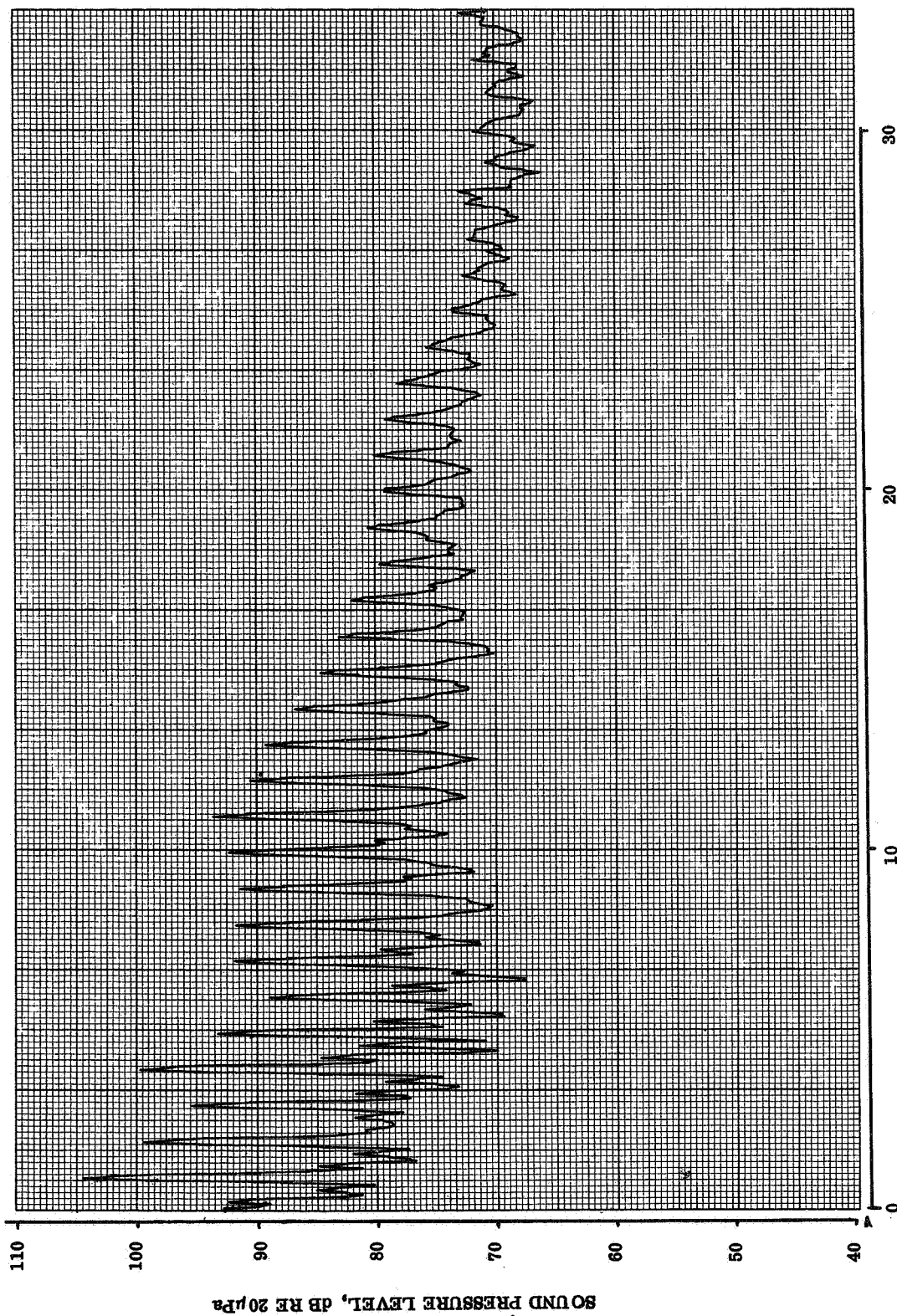
HARMONICS OF BLADE PASSING FREQUENCY

AFT MICROPHONE

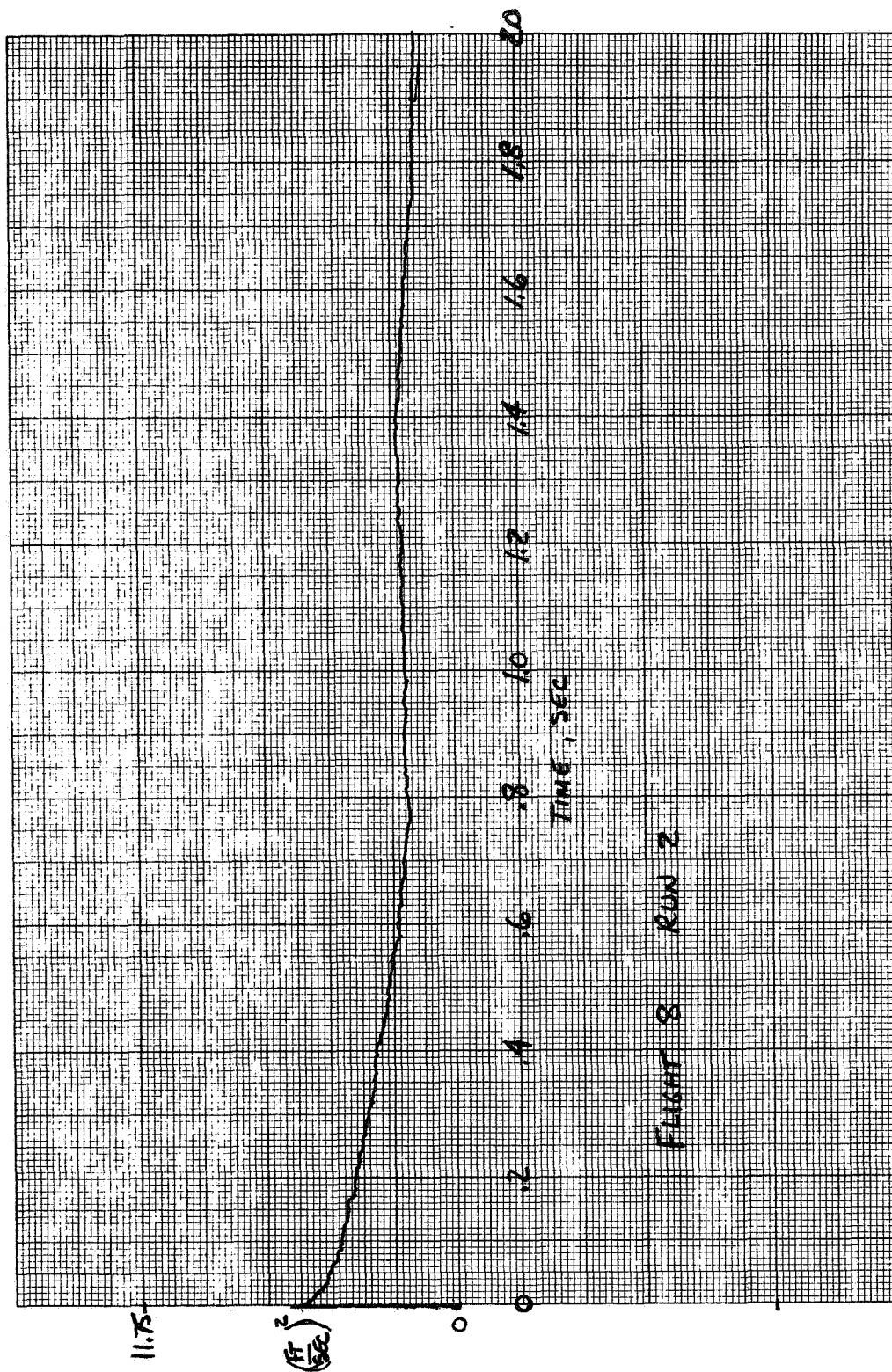
RUN 215

FLIGHT 14

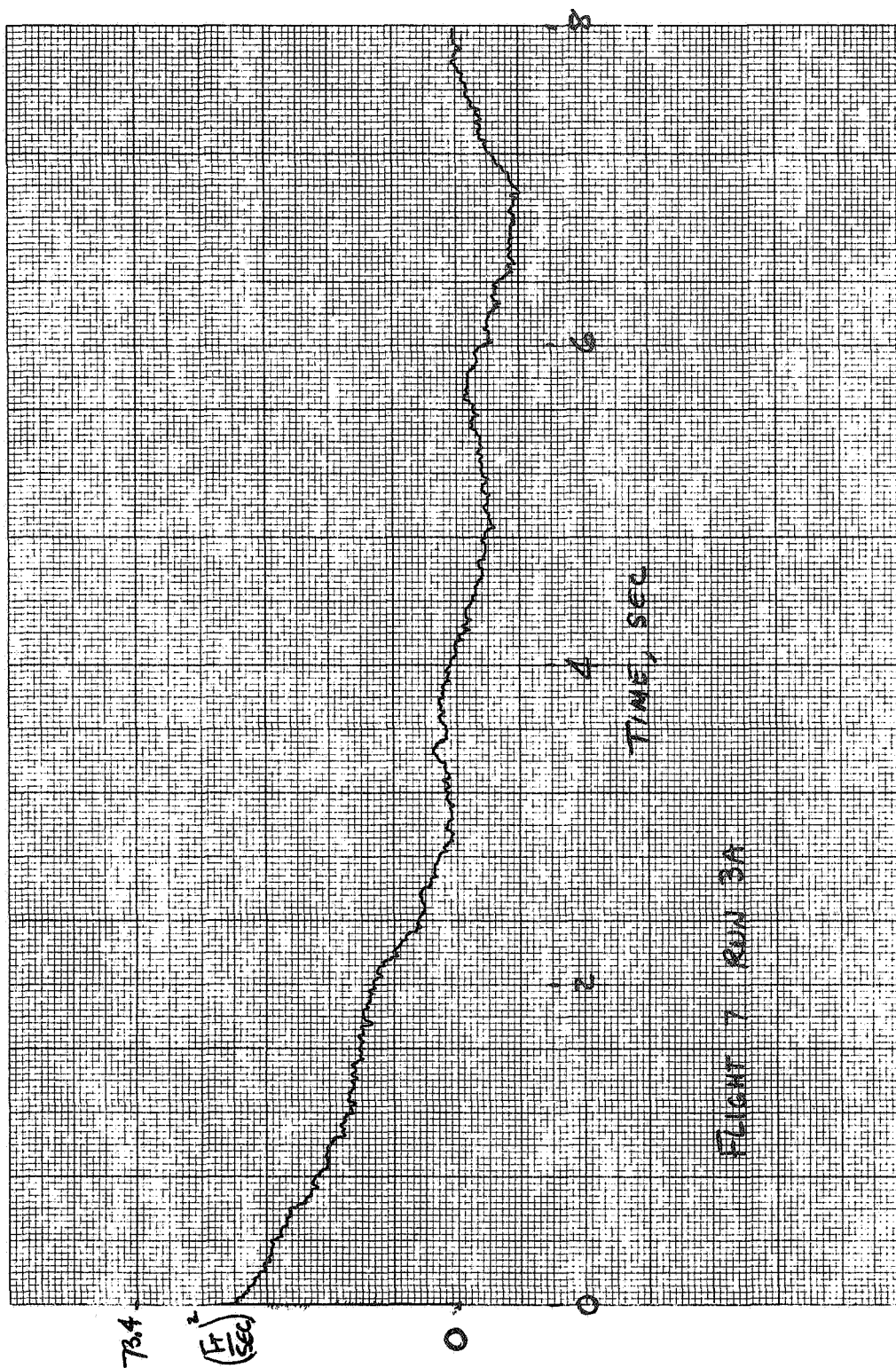


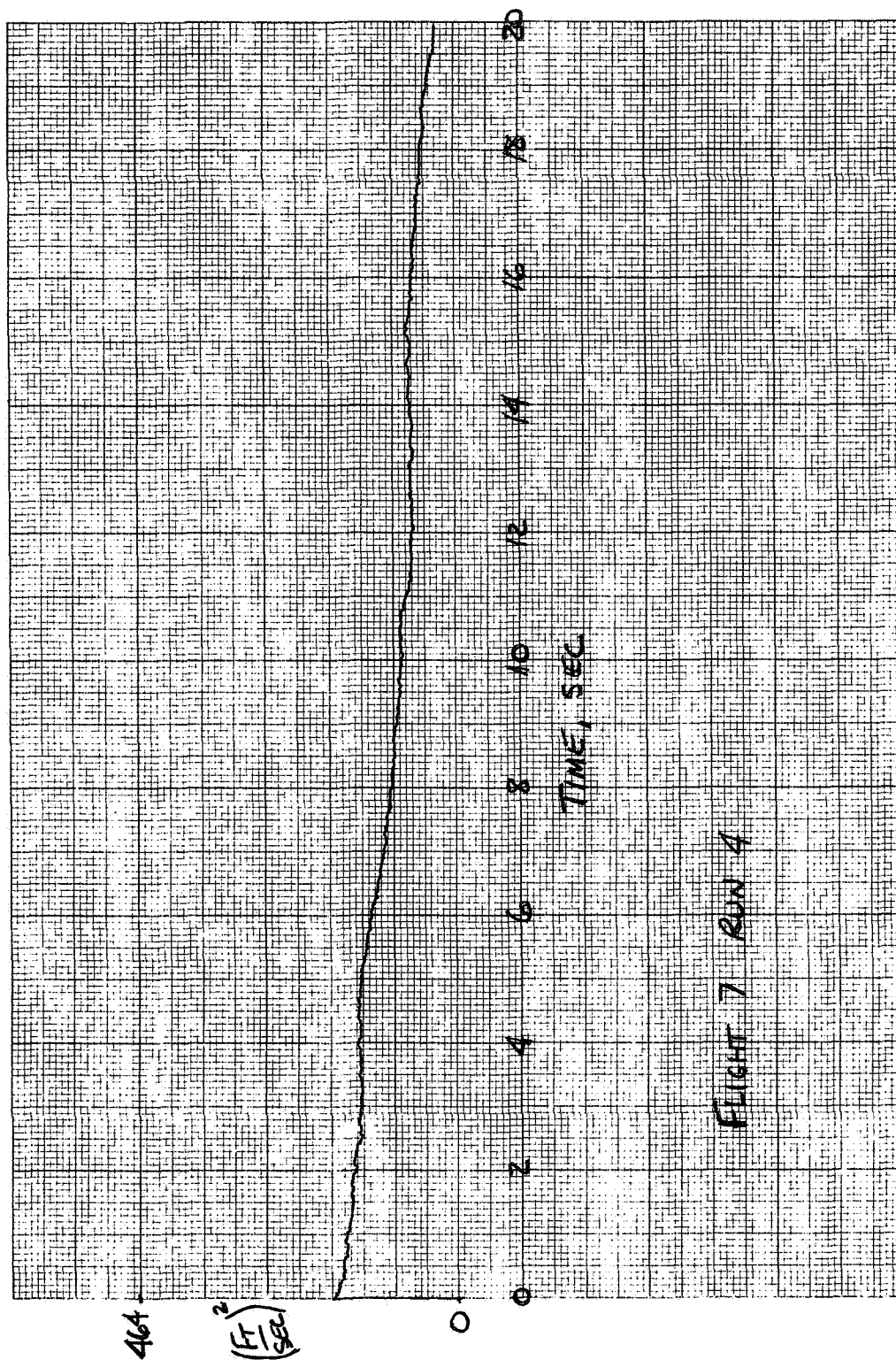


**APPENDIX F - HOT-WIRE ANEMOMETER STATISTICAL
PROPERTIES**

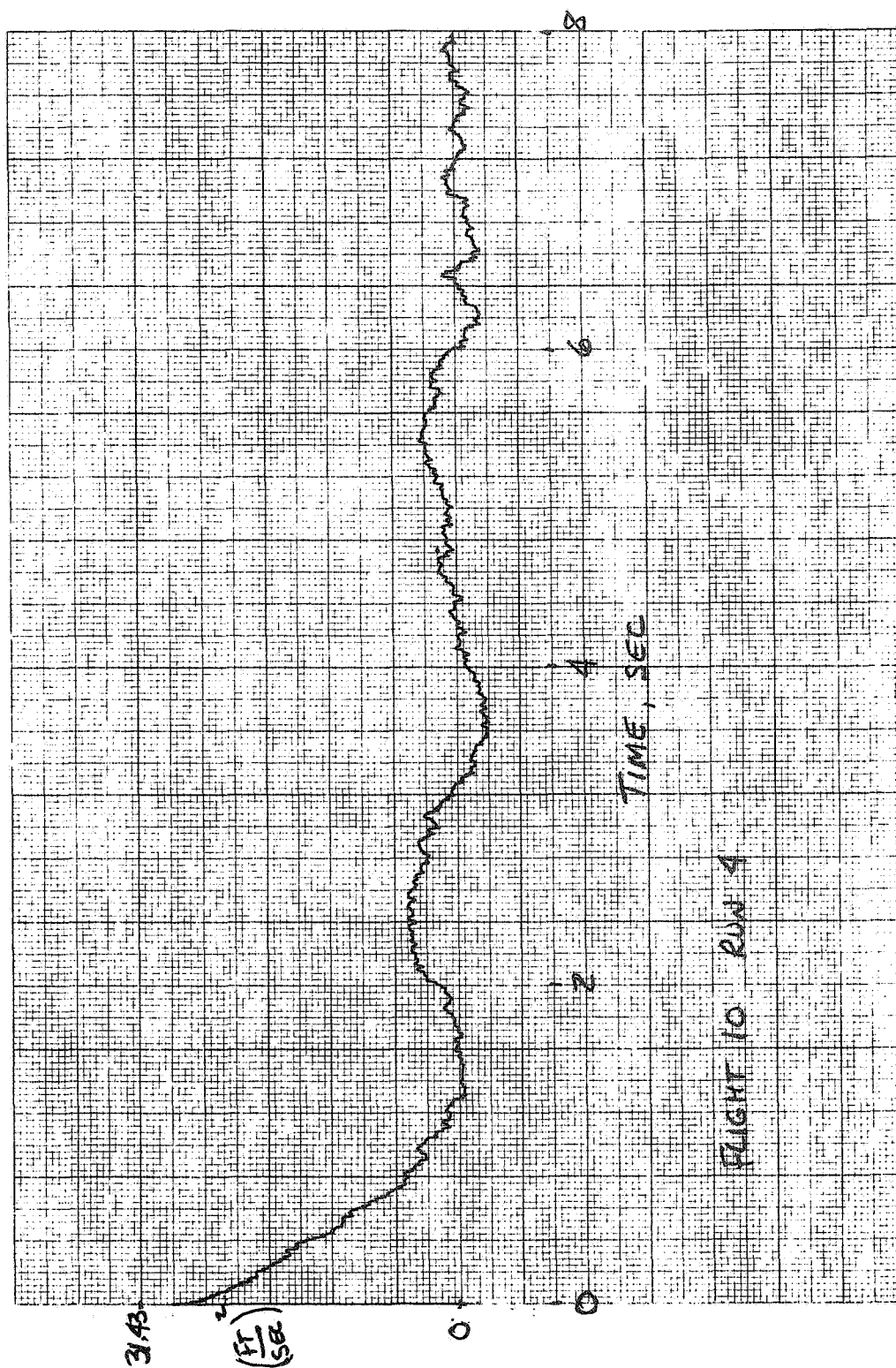


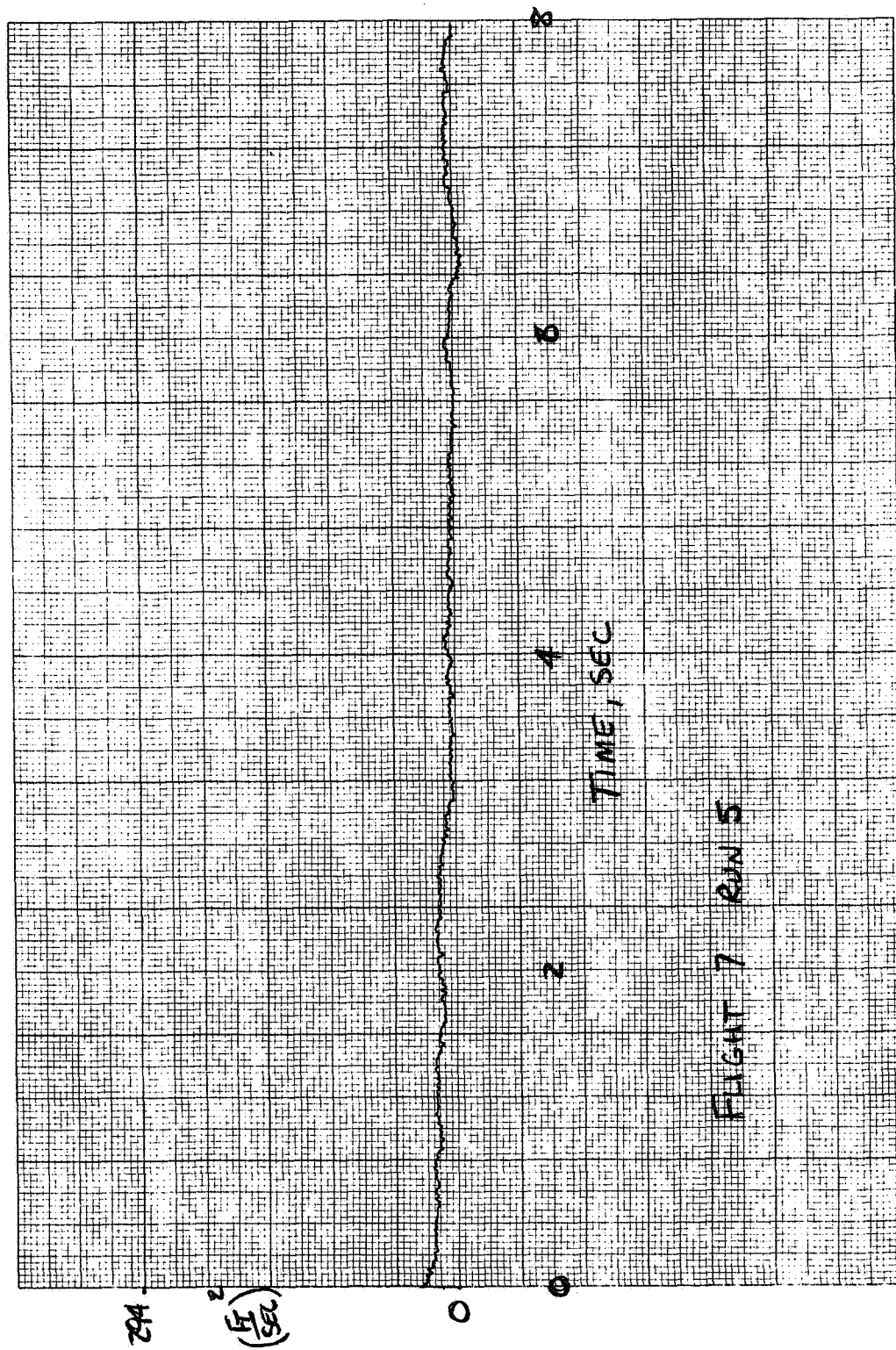
FLIGHT 8 RUN 2

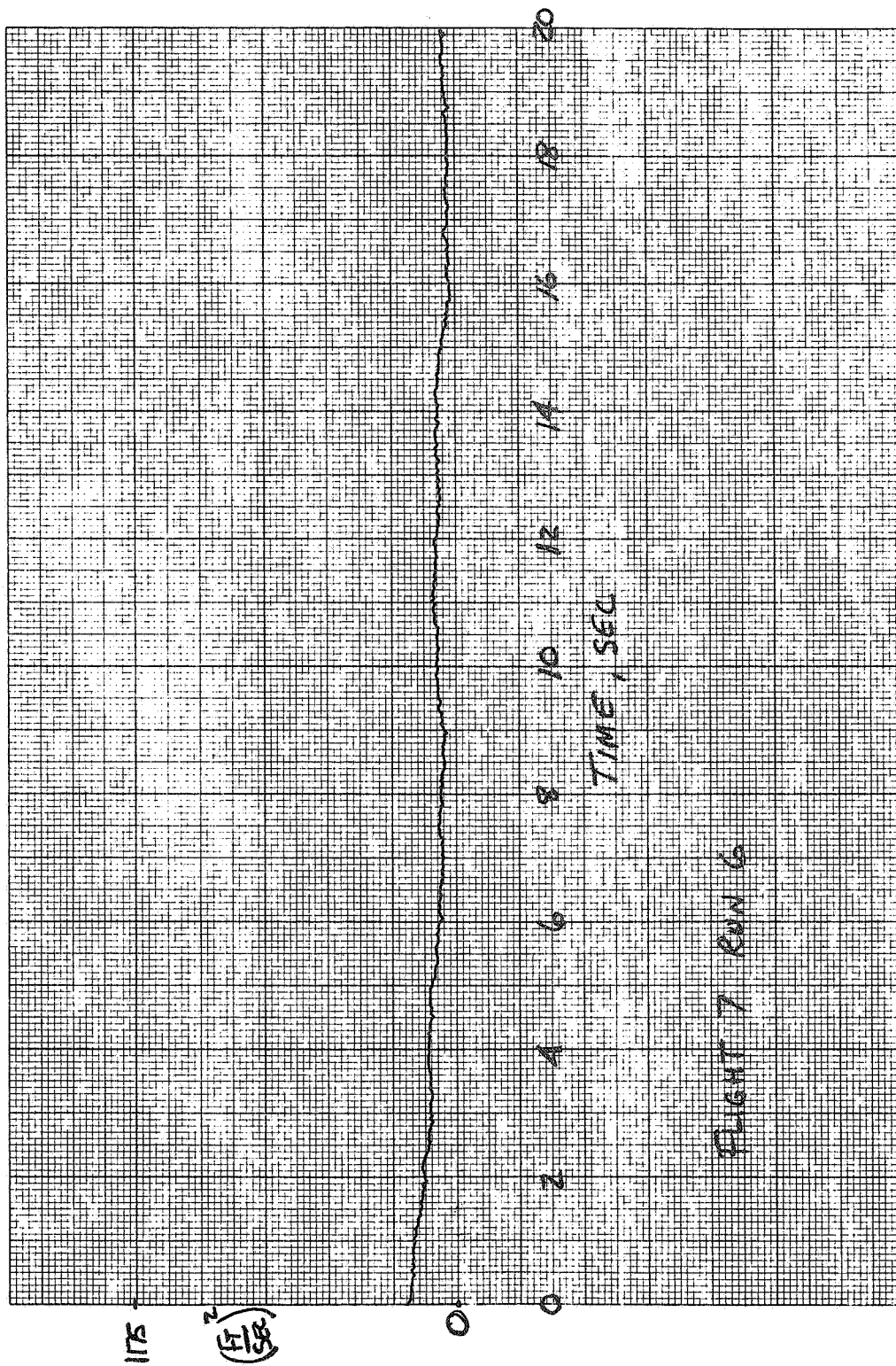


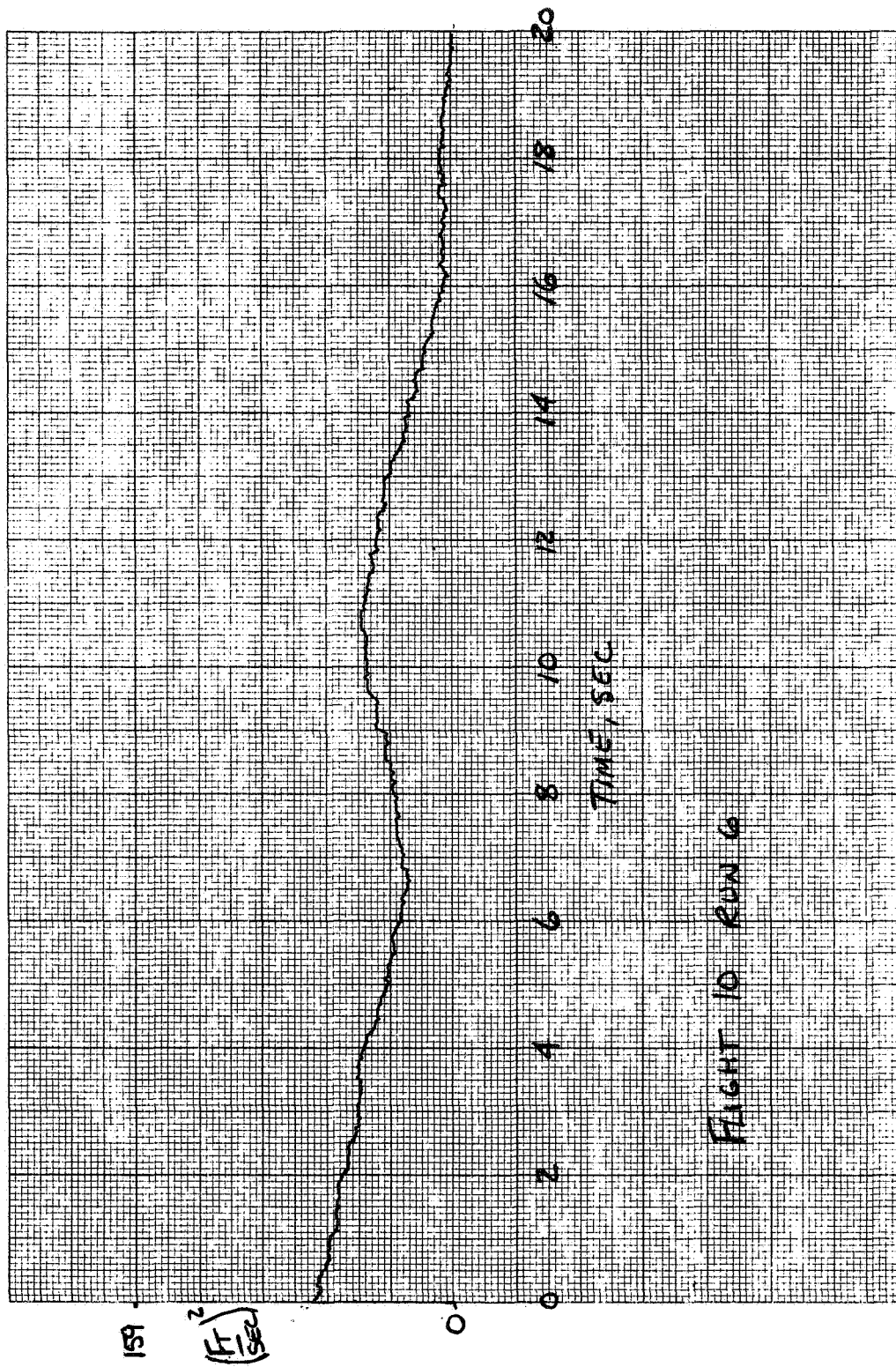


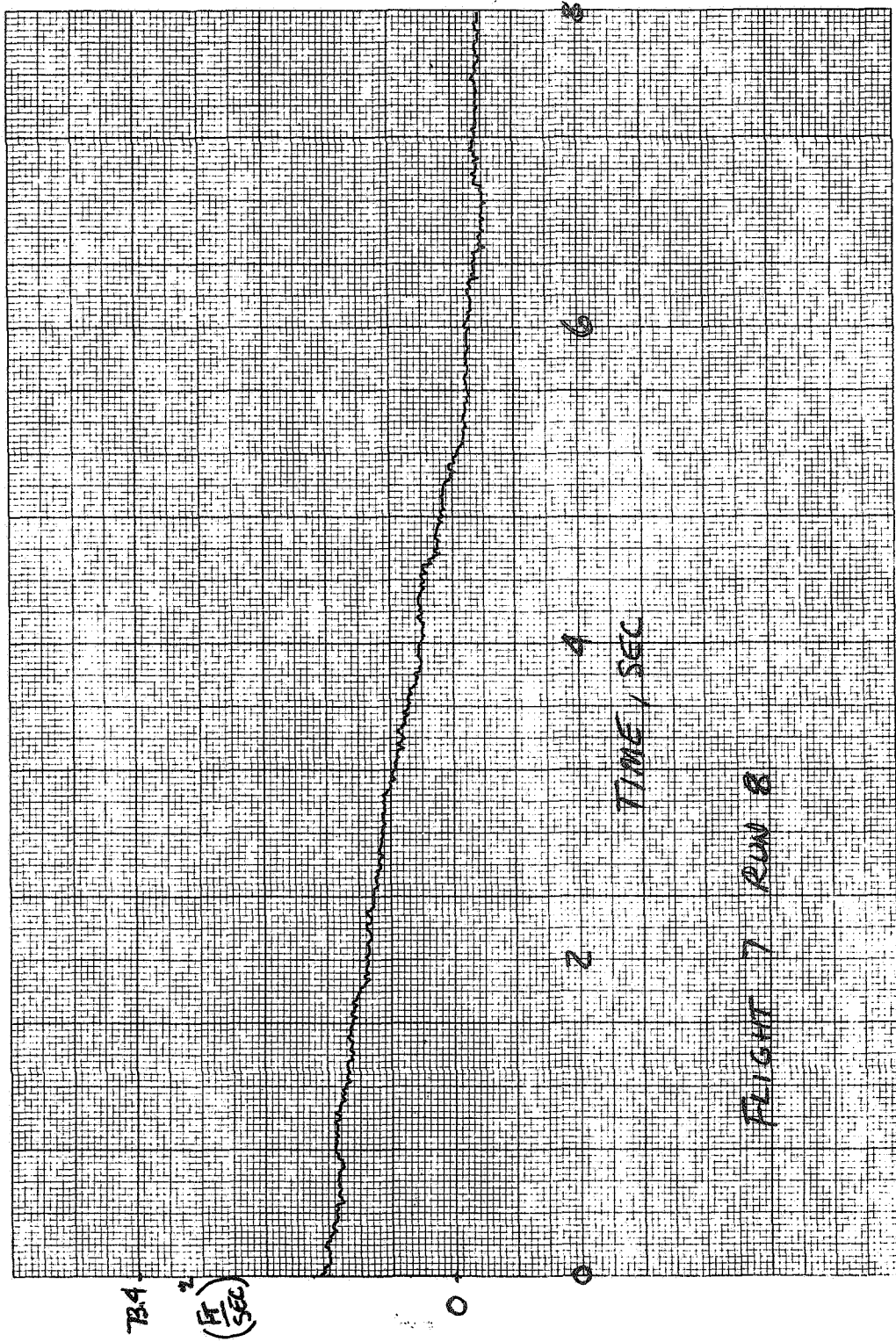
FLIGHT 7 RUN 4

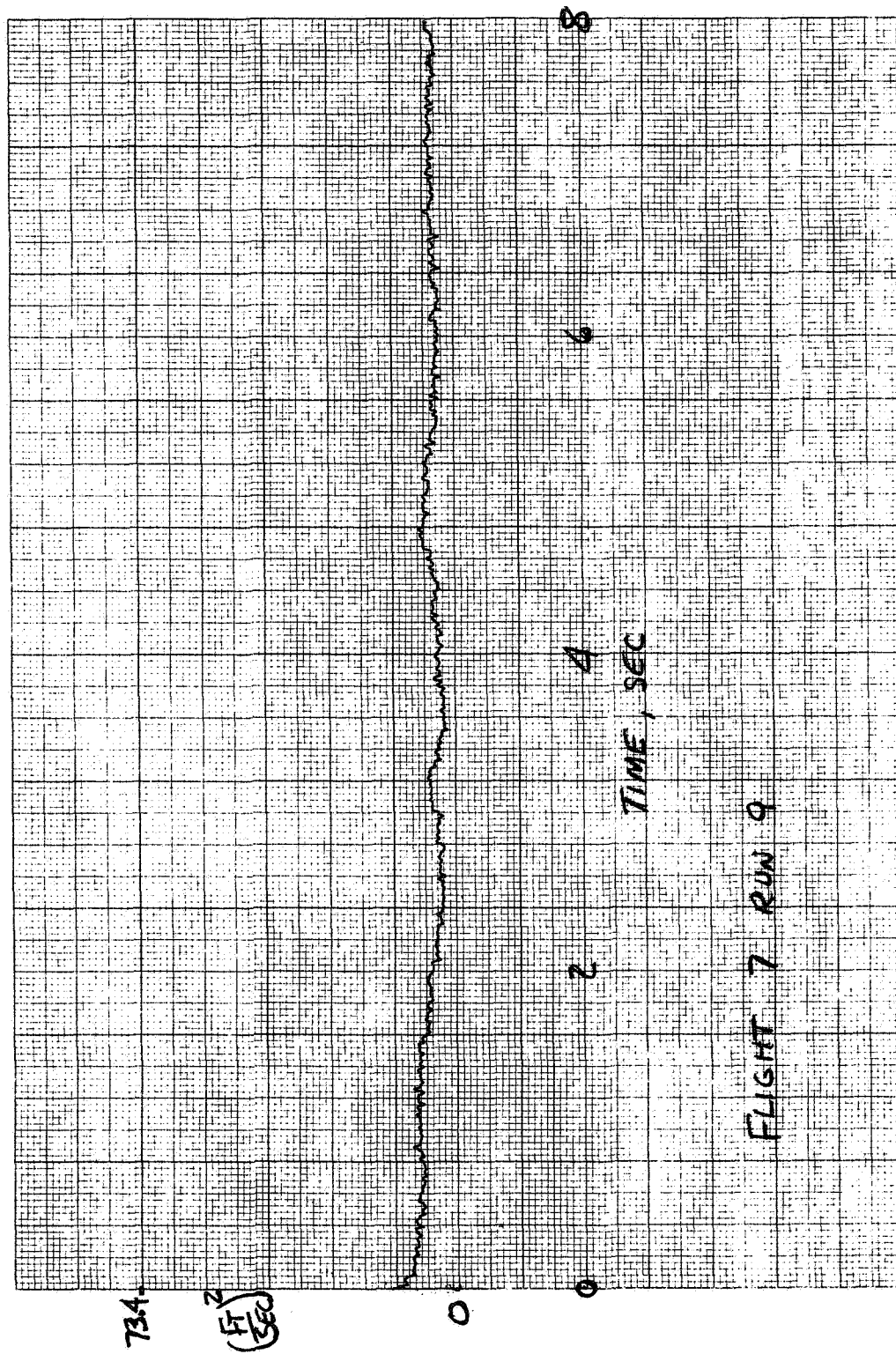


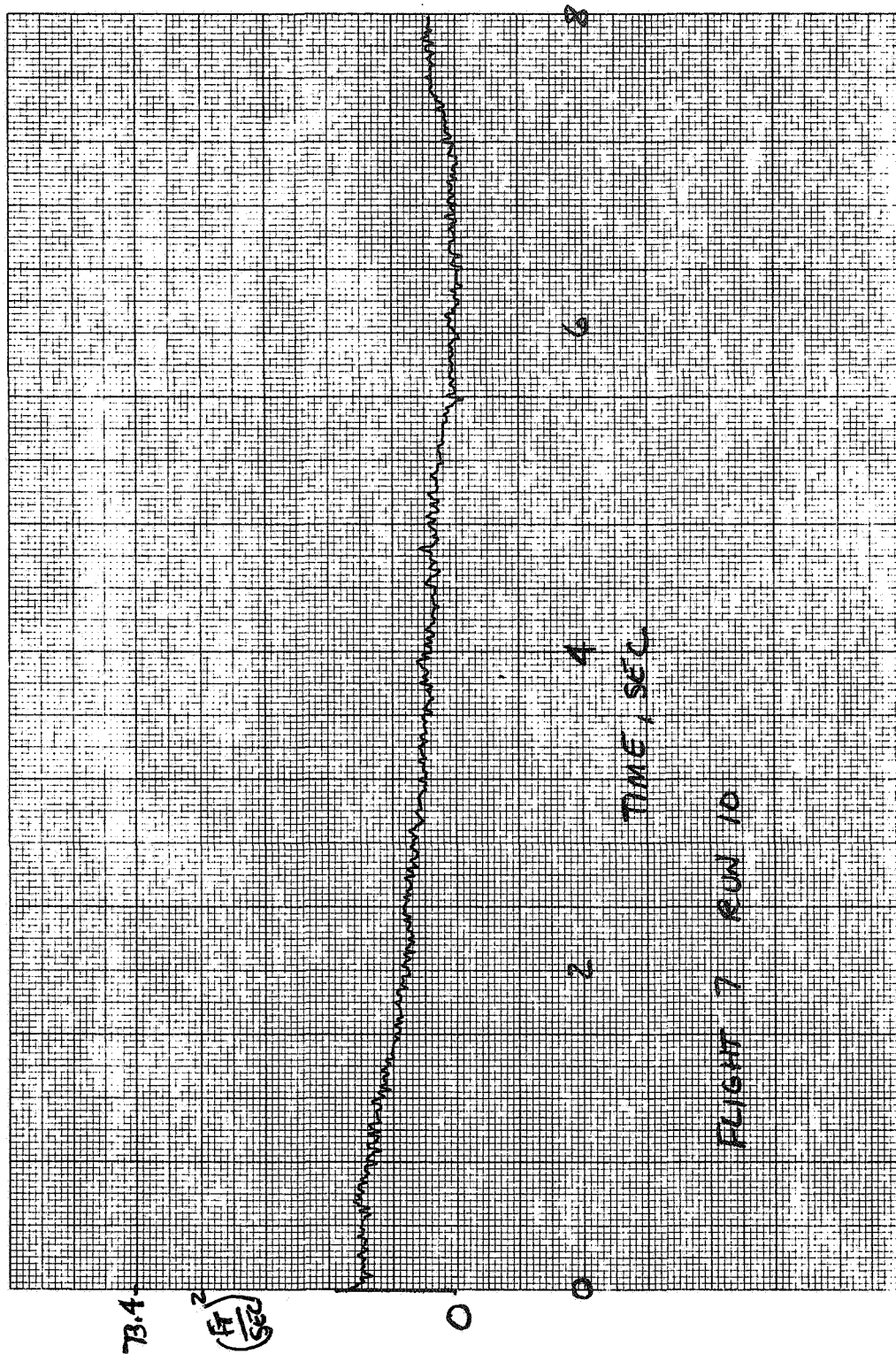


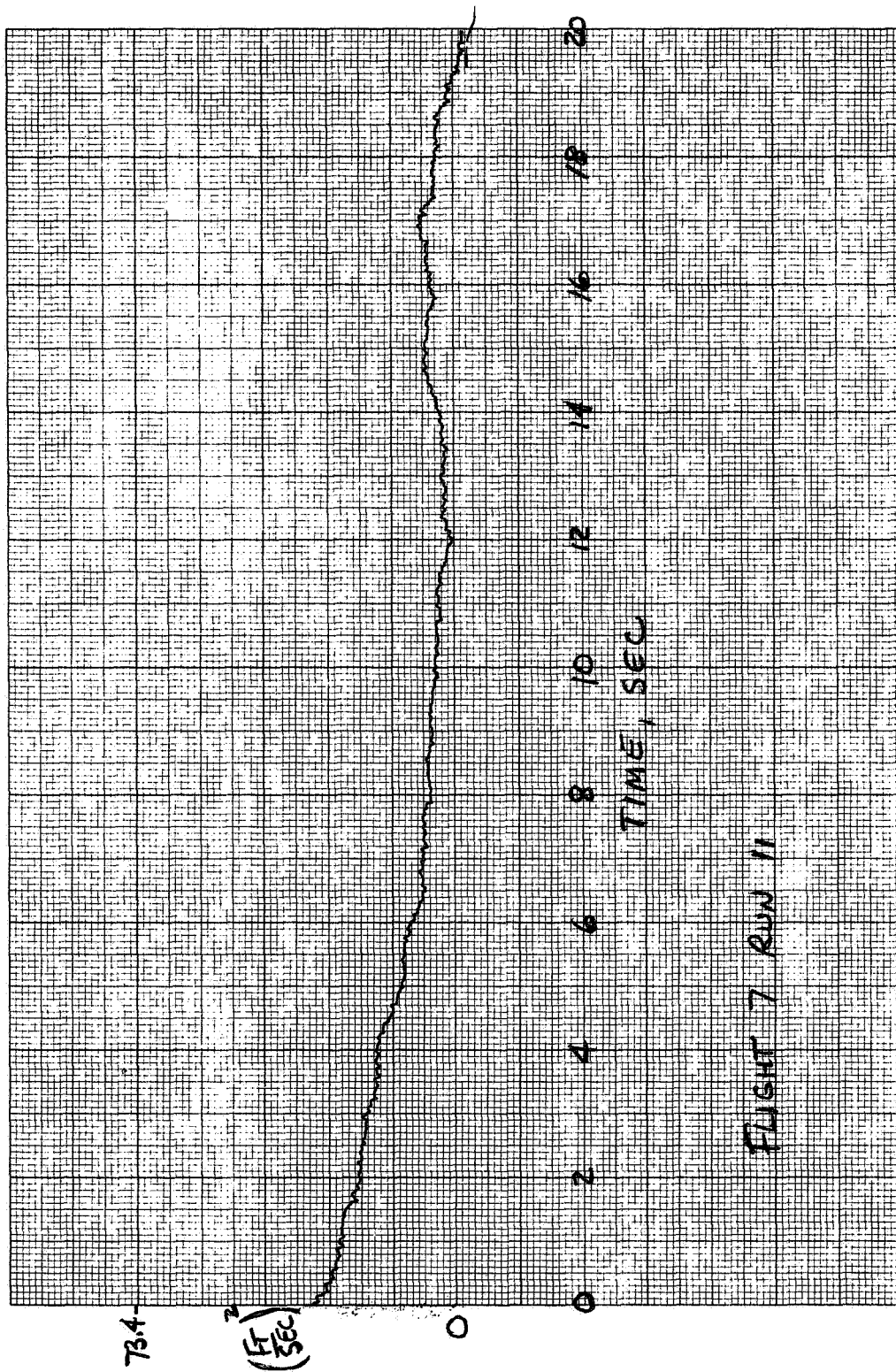


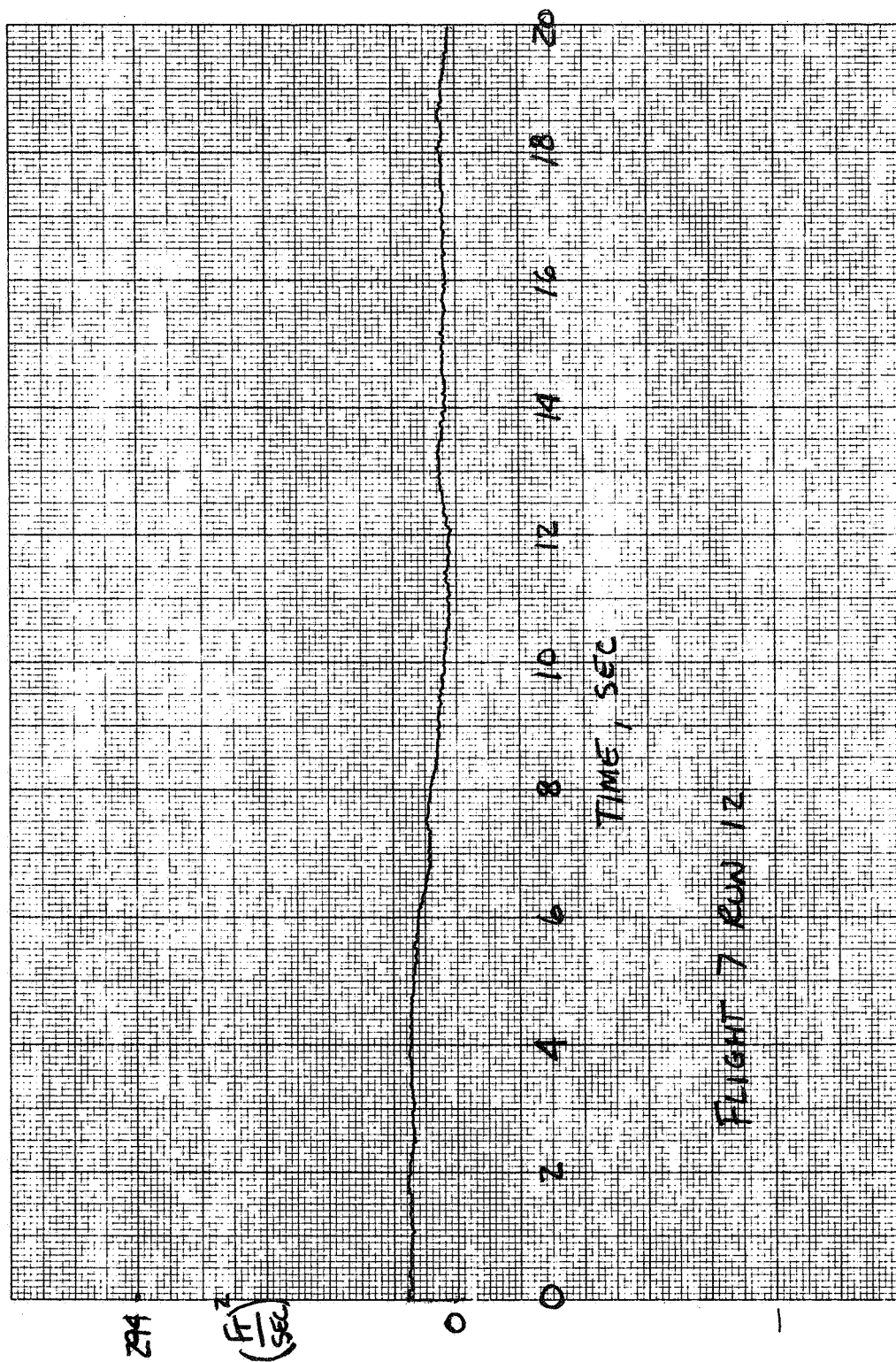


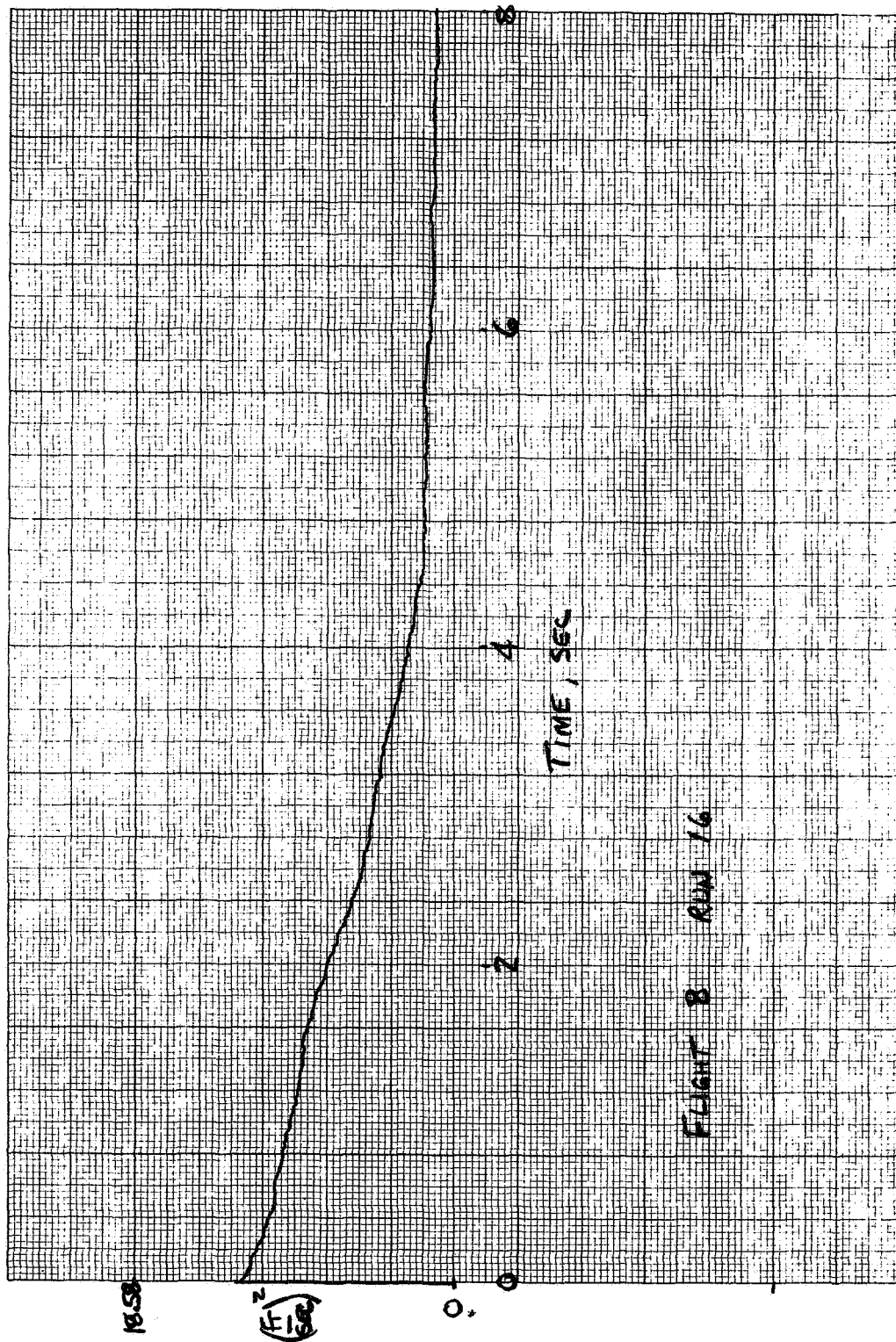




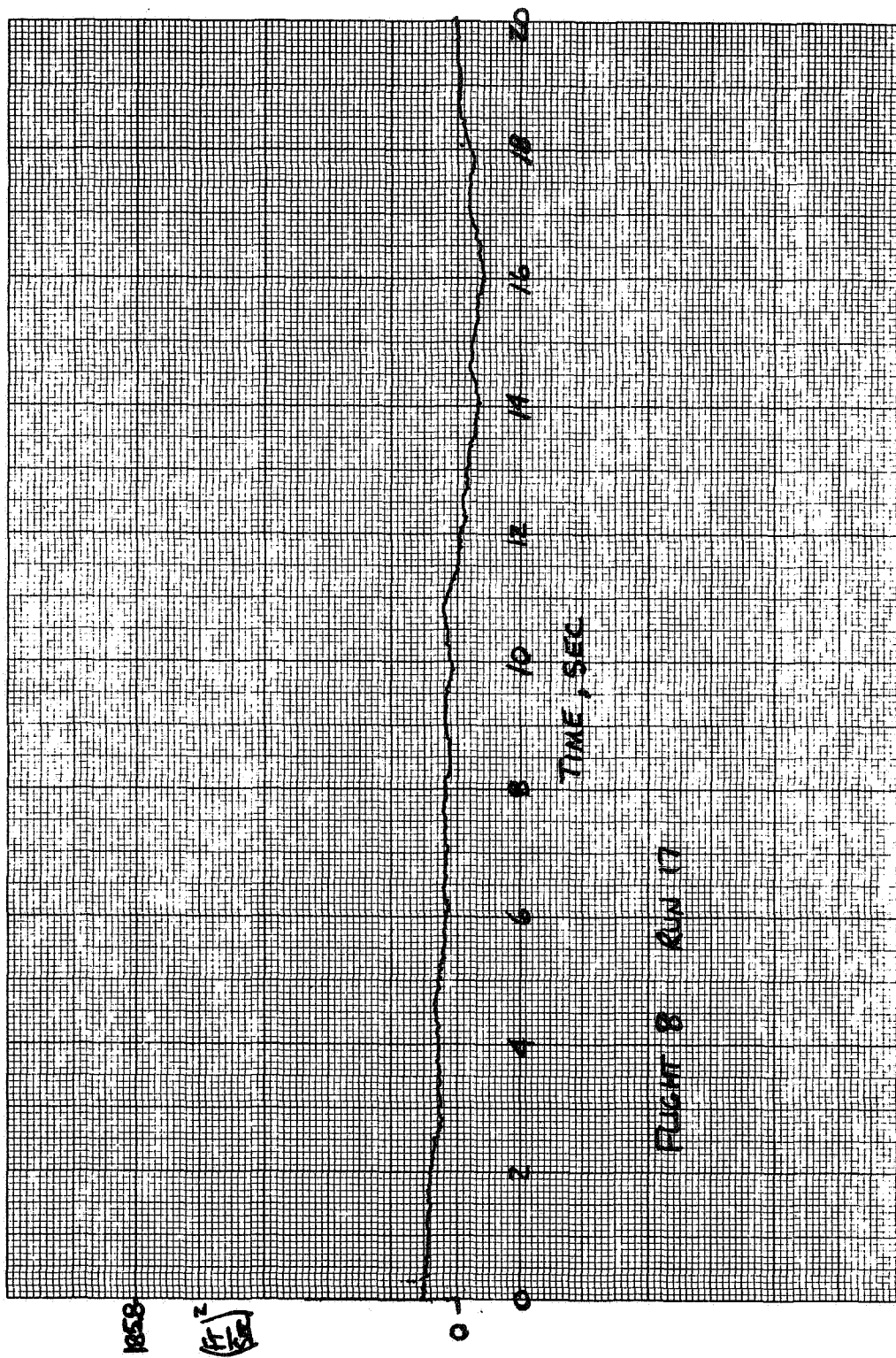




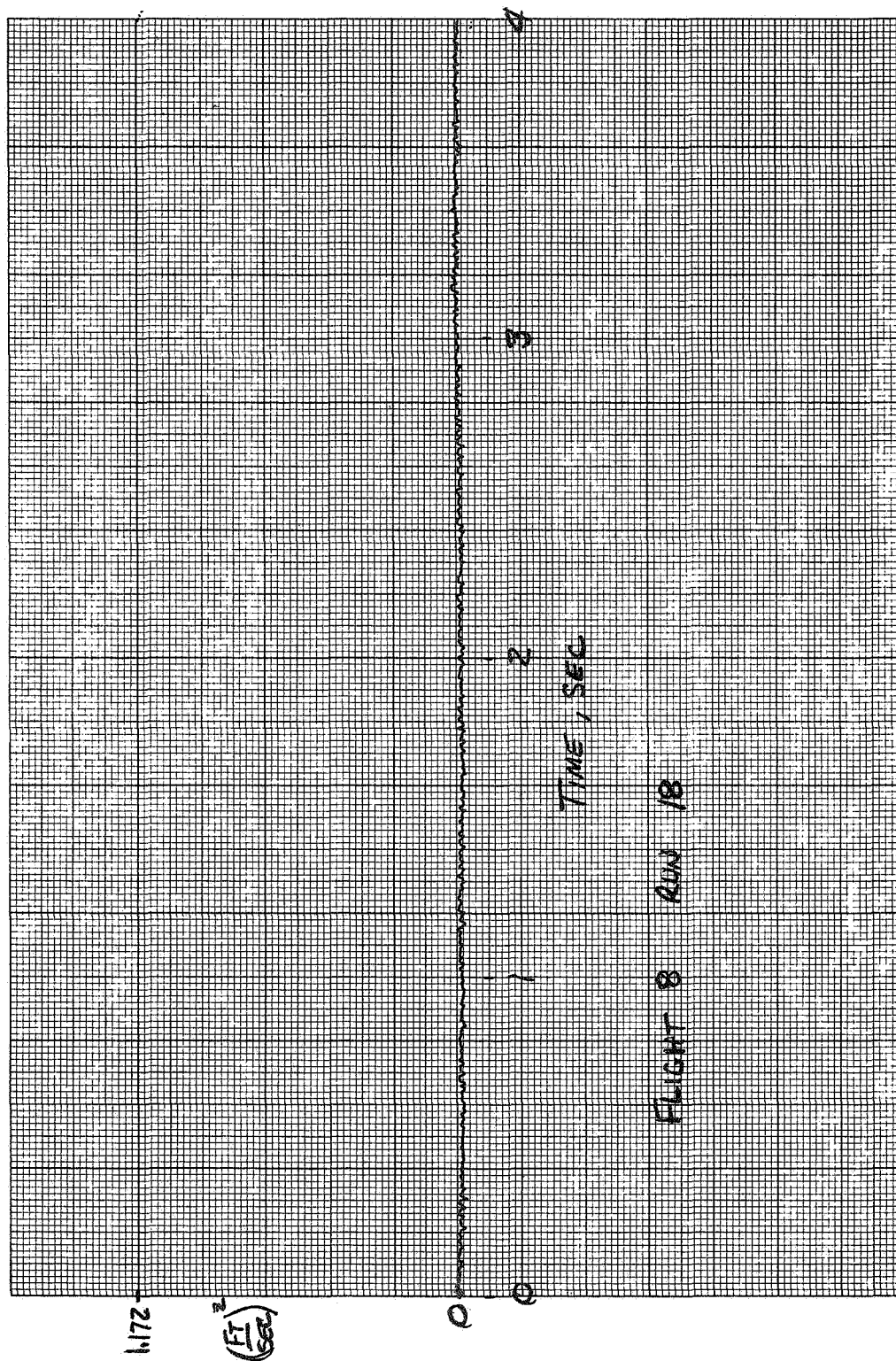


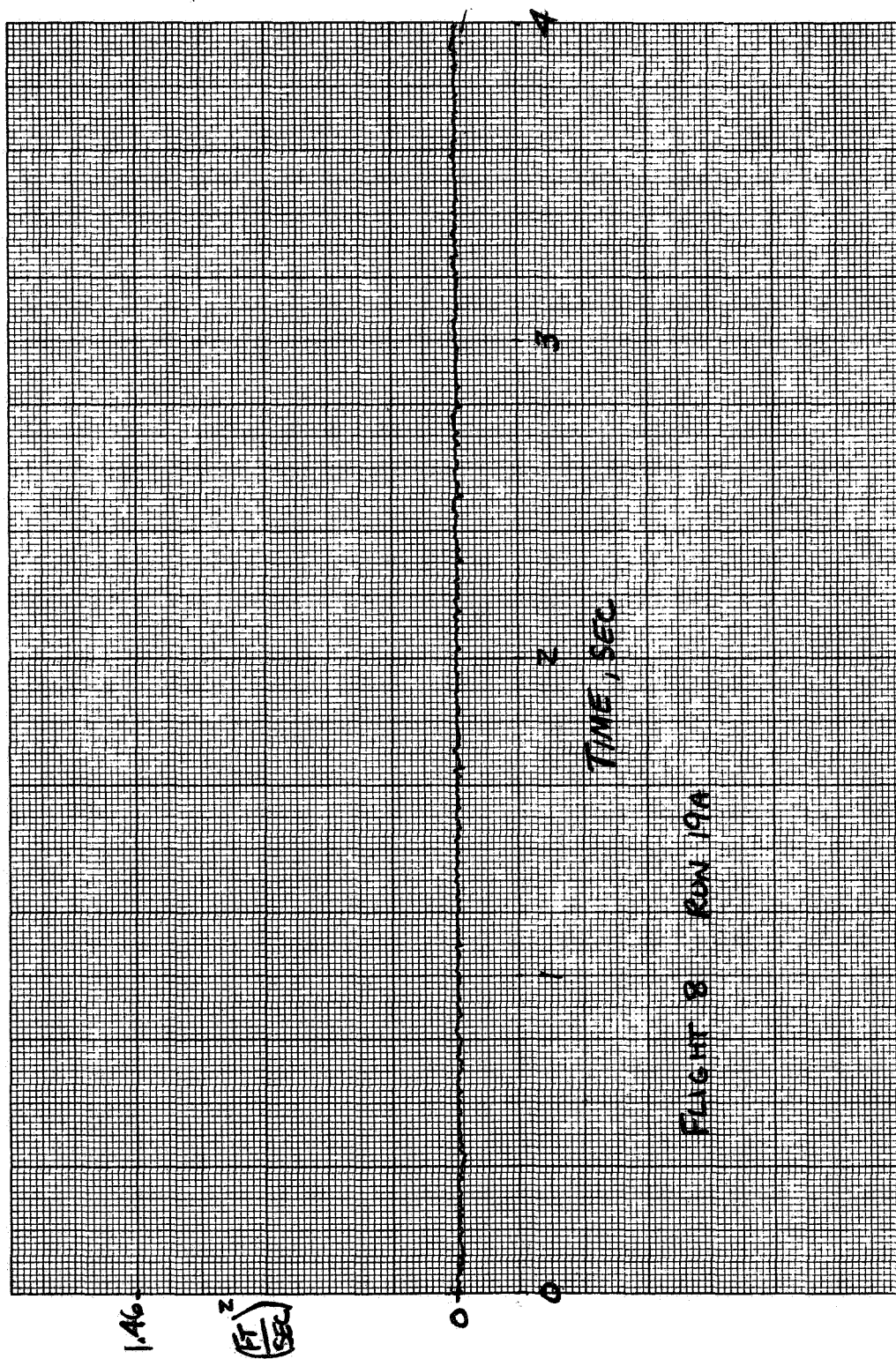


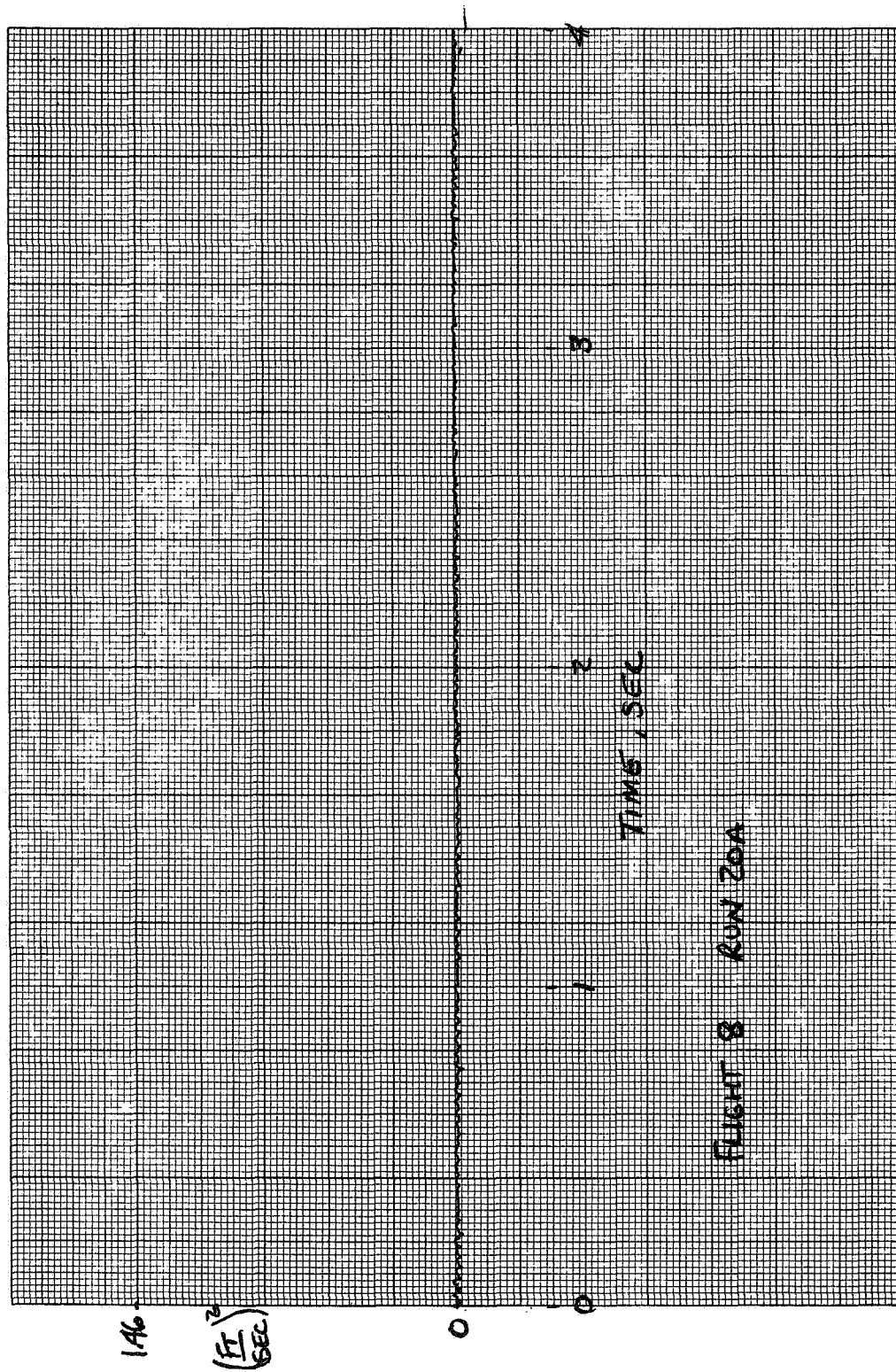
FLIGHT 8 RUN 16



FLIGHT 8 RUN 17







REFERENCES

1. Measurements of Aircraft Exterior Noise in the Field. ARP 796, Soc. Auto. Eng., Inc., June 15, 1965.
2. Hanson, D.B.: Study of Noise Sources in a Subsonic Fan Using Measured Blade Pressures and Acoustic Theory. NASA CR-2574, 1975.
3. Lowson, M.V. and Ollerhead, J.B.: A Theoretical Study of Helicopter Rotor Noise, J. Sound and Vib., Vol. 9, No. 2, 1969.
4. Barry, F.W. and Magliozi, B.: Noise Detectability Prediction Method for Low Tip Speed Propellers. AFAPL-TR-71-37. June 1971.
5. Magliozi, B. and Ganger, T.G.: Advanced V/STOL Propeller Technology, Vol. XIII - Far-Field Noise Investigation. AFFDL-TR-71-88, Vol. XIII, March, 1972.
6. Magliozi, B.: V/STOL Rotary Propulsion Systems Noise Prediction and Reduction. FAA-RD-76-49, May, 1976.
7. Lappe, V.O., "Low-Altitude Turbulence Model for Estimating Gust Loads on Aircraft". J. of Aircraft, Vol. 3, No. 1, Jan.-Feb., 1966. pp. 41-47.
8. D.B. Hanson, "Near Field Noise of High Tip Speed Propellers in Forward Flight", AIAA Paper No. 76-565, presented at 3rd Aerocoustics Conference, Palo Alto, California, July 1976.